Results of 1/4-Scale Experiments.
Vapor Simulant And Liquid Jet A Tests

Joseph E. Shepherd, J. Chris Krok
and Julian J. Lee
Explosion Dynamics Laboratory
California Institute of Technology
1200 E. California Blvd.
Pasadena, CA 91125
Order NTSB12-97-SP-0127

Larry L. Brown, Robert T. Lynch
and Timothy M. Samaras
Applied Research Associates, Inc.
Rocky Mountain Division
5941 S. Middlefield Rd., Suite 100
Littleton, CO 80123
Contract NTSB12-97-CB-0321

M. M. Birky
National Transportation Safety Board
490 L'Enfant Plaza, SW
Washington DC 20594

17 July 1998 **Revised January 28, 2000**
Explosion Dynamics Laboratory Report FM98-6

Prepared for and supported by the National Transportation Safety Board

Executive Summary

A quarter-scale engineering model of the center wing tank (CWT) of a 747-100 was constructed. This engineering model replicated the compartmentalization, passageways, and venting to the atmosphere. The model was designed to scale the fluid dynamical and combustion aspects of the explosion, not the structural failure of the beams or spars. The effect of structural failure on combustion was examined by using model beams and spars with deliberately engineered weak connections to the main tank structure. The model was filled with a simulant fuel (a mixture of propane and hydrogen) and ignited with a hot wire. The simulant fuel was chosen on the basis of laboratory testing to model the combustion characteristics (pressure rise and flame speed) of Jet A vapor created by a Jet A liquid layer at 50°C at an altitude of 13.8 kft.

A series of experiments was carried out in this model in order to: (a) investigate combustion in a CWT geometry; and (b) provide guidance to the TWA 800 crash investigation. The results of the experiments were observed with high-speed film, video, and still cameras, fast and slow pressure sensors, thermocouples, photodetectors, and motion sensors. A special pseudo-schlieren system was used to visualize flame propagation within the tank.

This report describes the test program, facility, instrumentation, the first 30 experiments, comparisons between experiments, and performance of the instrumentation; then examines the significance of these results to the TWA 800 crash investigation.

The key results of this study are:

Flame Motion The motion of flame was dominated by the effects of turbulence created by jetting through the passageways and vent stringers. A very rapid combustion event (lasting 10 to 20 ms) occurred once the flame traveled outside of the ignition bay and interacted with the turbulent flow. Most of the gas within the tank was burned during this rapid event.

Compartments The combustion time decreased with an increasing number of compartments (bays) within the tank. With six bays, combustion took only 100 to 150 ms to be completed from the time of ignition until the end of the rapid combustion phase. The total combustion event was three to four times shorter with compartments than without.

Venting Venting to the outside of the tank through the model vent stringers had a negligible effect on the combustion progress or on the peak pressure reached at the end of the burn.

Ignition Location Variation of the ignition location produced distinctive pressure loads on the structural components.

Liquid Fuel Lofting of a cold liquid fuel layer was produced by the combustion-induced gas motion. Although this spray of liquid eventually ignited and burned, it did not contribute to the pressure loading.

Structural Failure Structural failure resulted in flame acceleration, decreasing the overall combustion time.

TWA 800 Investigation The pressure loads were sufficiently high, up to 4 bar, and the combustion events were sufficiently short, that the forward portion (spanwise beam 3, front spar) of the CWT structure would fail as a direct consequence of the explosion. A combination of pressure loads was produced in some tests consistent with the TWA 800 wreckage. Replica tests, structural modeling, and sensitivity studies on fuel concentration are needed before any conclusions can be drawn about probable ignition locations.

Cargo Bay Tests with a simplified model of a half-full cargo bay indicated that repeated pressure waves with an amplitude of 1 bar or less are produced when an explosion scenario similar to TWA 800 is tested.

Future Testing Future studies should include replica tests, tests with Jet A vapor and warm liquid Jet A layers, and sensitivity tests to examine ignition location, fuel concentration, and vent area perturbations.

Summary Explosion tests in a 747-100 CWT model reveal that a very complex pattern of combustion occurs due the interaction of the flame and the flow-generated turbulence. A wide range of structural load patterns occur, depending on the location of the ignition source. Some of these load patterns are consistent with damage believed to be associated with the initial explosion event in TWA 800. Sensitivity of the loading to the ignition location indicates that narrowing down the ignition location in TWA 800 may be possible. However, the complexity of the combustion and structural failure processes in the actual center wing tank mandates extremely careful consideration of the uncertainties that enter into this process.

Acknowledgements

The contributions of many individuals made this test program possible. Some of them are explicitly acknowledged in this report but others worked behind the scenes.

At Caltech, Jamie Guthrie, Karen Cheetham, Marionne Epalle, Joe Haggerty, Ali Kiani, Larry Frazier, and Alan Goudy all made valuable contributions. Julian Lee was partially supported by a fellowship from FCAR of Quebec, Canada.

Don Jr. of Accurate Manufacturing (Burbank) built the tank in record time.

Bob Marchese of RPM Technical Services (Denver) guided the construction of the weak panels. Arnold Kerstein of the Gorrell Iron Works built the cargo bay model.

Rick Link of CDL (Halifax) did structural computations that helped us to develop the weak panel design.

Bob Guice and Mike Rictor of ARA pitched in at the test site; Sheila helped host the many visitors; and Vonda Brown did a great job with the photos. Paul Reining of the Denver Research Institute operated the forklift used to set up the facility, as well as the crane truck used to install the cargo bay.

The staff of Crosspoint Video Productions in Denver, CO was able to do wonders with our homegrown video.

Finally, we thank the TWA 800 crash investigation team members, both the NTSB and parties, for their advice and assistance with developing the test program.

Contents

List of Figures

List of Tables

Guides

stbd ..... starboard
SWB1 ..... Spanwise Beam 1
SWB2 ..... Spanwise Beam 2
SWB3 ..... Spanwise Beam 3
PR ..... Partial Rib

fwd ..... forward
RS ..... Rear Spar
MS ..... Middle Spar
FS ..... Forward Spar

Differential Pressure (ΔP) Relations

Stbd SWB1 = bay 6 − bay 4
Stbd MS = bay 4 − bay 2
SWB1 = bay 2 − bay 1
Aft PR = bay 5 − bay 6
Stbd Vent = bay 6 − bay 1

Port SWB1 = bay 5 − bay 3
Port MS = bay 3 − bay 2
SWB3 = bay 1 − bay 0
Fwd PR = bay 3 − bay 4
Port Vent = bay 3 − bay 1

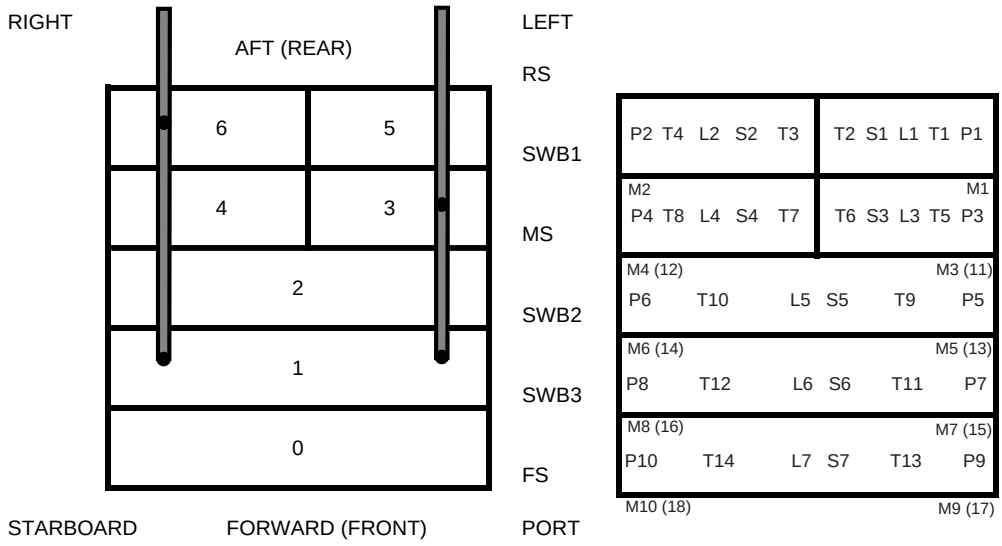

(a) (b)

Figure 1: Bay and transducer maps: (a) view looking down on the 1/4-scale facility showing bays, beams, spars, and vents; (b) view looking down on the 1/4-scale facility showing the instrument locations (schematic only, see Appendix A for precise coordinates). P – fast (PCB) pressure gauges, T – thermocouples, S – slow (Endevco) pressure gauges, L – light (photodiode) detectors, M – motion switches (numbers in parentheses represent locations on lower surface).

Table 1: Summary of 1997 Tests, by Number

Test	Date	Vent	Ign	Fuel	SWB1	MS	SWB2	SWB3	FS	Ribs	Comments
1	10-23	N	5	V	-	-	-	S	-	-	Baseline, electric match
2	10-29	N	5	V	-	S	-	S	-	-	Filament igniter, match backup
3	10-30	N	5	V	-	S	S	S	-	-	Filament igniter, match backup
4	10-31	Y	5	V	S	S	S	S	-	S	Filament igniters only in this test and later
5	11-03	Y	3	V	S	S	S	S	-	S	
6	11-04	Y	2	V	S	S	S	S	-	S	
7	11-04	Y	1	V	S	S	S	S	-	S	
8	11-05	Y	5	V& L	S	S	S	S	-	S	First test with liquid fuel
9	11-06	N	5	V	S	S	S	S	-	-	4 bay shot missed after Test 3
10	11-06	N	5	V	-	S	-	S	-	-	Redo of Test 2
11	11-07	N	5	V	-	-	-	S	-	-	Redo of Test 1 — baseline
12	11-07	P	5	V	-	S	-	S	-	-	Single hole midspar model, vents plugged
13	11-08	Y	5	V	S	S	S	W	-	S	First test of weak partition
14	11-13	Y	5	V	S	S	S(A)	S	-	S	First test of SWB2 access panel
15	11-15	Y	6R	V	S	S	S	S	-	S	Ignition location study
16	11-15	Y	1R	V	S	S	S	S	-	S	Ignition location study
17	11-17	Y	5	V	S	S	S(A)	W	W	S	Weak FS, weak SWB3, access panel in SWB2
18	11-19	Y	5	V	W	W	W	W	W	W	First all-weak panel test
19	11-21	Y	5	V& L	W	W	W	W	W	W	All-weak panel w/liquid
20	11-24	Y	2L	V& L	W	W	W	W	W	W	All-weak panel w/liquid
21	11-25	Y	1	V& L	W	W	W	W	W	W	All-weak panel w/liquid
22	12-03	Y	2Lo	V	S	S	S	W	W	S	6-mil Man Pan, part strong
23	12-05	Y	2Lo	V	S	S	S	W	W	S	Man Pan, 7.5% fuel
24	12-05	Y	2Lo	V	S	S	S	W	W	S	Man Pan, 6.5% fuel
25	12-06	N	5	V	S	S	S	S	N/A	S	Near redo of Test 4
26	12-06	Y	2Lo	V	S	S	S	S	N/A	S	6.5% fuel
27	12-07	Y	2Lo	V& L	S	S	S	W	W	S	Man Pan
28	12-08	Y	5	V& L	S	S	S	W	W	S	Man Pan
29	12-08	Y	1	V&L	S	S	S	W	W	S	Man Pan
30	12-17	Y	5	V& L	S	S	S	W	N/A	S	Man Pan, cargo bay

Julian Lee and Chris Krok prepare for Test 26.

Chapter 1

Introduction

1.1 Overview

The National Transportation Safety Board (NTSB) sponsored a testing program associated with the investigation into the TWA Flight 800 accident which occurred in July of 1996. California Institute of Technology (Caltech) and Applied Research Associates, Inc. (ARA) worked together with the NTSB to perform a study of combustion within a 1/4-scale model of a 747-100 Center Wing Tank (CWT). Tests were performed with the model to examine various ignition locations, vapor concentrations, the effect of a liquid fuel layer, and the failure of the internal partitions that represented the beams and spars within the tank.

The primary objective of the 1/4-scale testing was to gather data to help understand fuel-tank explosions and to investigate the effect of ignition location on the explosive process. Prior to the 1/4-scale testing, Caltech researchers performed laboratory testing at their Explosion Dynamics Laboratory (EDL) of fuel vapor pressure, flash point, flammability limits, and explosion pressure histories during controlled laboratory explosions of Jet A vapor and air (Shepherd et al. 1997a). Laboratory testing also included the determination of ignition energies required to ignite Jet A fuel vapor and the measurement of flame speeds in Jet A at various temperatures (Shepherd et al. 1998).

Laboratory testing was conducted in several pressure vessels of different sizes, all smaller than the 747-100 CWT and much simpler in construction. While this extensive laboratory testing provided essential information, it became clear that certain questions could only be answered through larger-scale testing. A 747 center wing tank consists of six compartments connected in a complex fashion by passageways and vent tubes. The ignition source and location are unknown. Lofting of liquid fuel, venting to the atmosphere, and failure of the structure are expected to play an important role in the course of the explosion. Prior to these tests, there was little experience with explosions in a tank with these features. Following discussions with parties to the investigation and experts on explosions, a test program (Shepherd et al. 1997b) was formulated to address these issues.

A 1/4-scale CWT test fixture was designed and fabricated by Caltech to provide a testing environment to study the phenomena associated with flame propagation in a multi-compartmented, vented tank and the coupling between the flame propagation and the resulting structural failure.

Detailed information about the motivation for the testing, relationship to the crash investigation goals, design process, scaling parameters and test series planning can be found in (Shepherd et al. 1997b). Key to the planning of the test series was the need to consider the requirements of the modeling effort that was conducted concurrently with the test program. These requirements dictated high-resolution photography of the combustion process and tank pressure, and temperature measurements crucial to the development of the combustion models. The modeling efforts were conducted by Sandia National Laboratories and Christian Michelson Research with input from Combustion Dynamics, Ltd.

The ARA-Caltech team provided the test site, instrumentation, and photo-instrumentation systems necessary to document the combustion process for various test configurations. In order to assess the performance of the combustion process and the resulting overpressures and temperatures associated with the explosions, it was necessary to implement an instrumentation suite for measurements that would document the entire combustion event.

Pressure transducers (dynamic and quasi-static) and thermocouples were used to document the pressure and temperature profiles versus time throughout the combustion process in each of the scaled CWT compartments (bays) for each test configuration. Light sensors were used to determine flame front arrival and motion sensors were positioned at multiple points on each of the failing/weak partitions to determine each partition's movement resulting from the combustion overpressures. Signal conditioning was used to condition the various sensor signatures to make them compatible with the recording media. Digital and analog recorders were used to capture the sensor signatures for "quick look" evaluations and for later data analysis and reporting.

Photo-instrumentation was used to provide the visualization necessary to understand the combustion process and to correlate the images with the electronic instrumentation recordings. Shadowgraph/pseudo-schlieren high-speed photographic systems were designed and deployed at the test site to document the vapor combustion process. Other high-speed cameras were fielded to document the flame propagation, panel ejection, and general test site overviews. Six high-resolution video cameras were used to provide test overview documentation and to monitor the combustion photography for safety procedures and test site operational requirements.

The first set of 1/4-scale CWT combustion experiments consisted of 30 tests which were conducted jointly by ARA and Caltech researchers. The tests were conducted at the ARA field test facility located approximately 30 miles southeast of Denver, Colorado. These tests consisted of four major test configurations. They were the ALPHA, BETA, GAMMA, and DELTA test series. The ALPHA baseline and validation test series was conducted, with no venting, using rigid partitions only (all-strong configuration), without or with partial ribs, and using the standard 8.4% by volume fuel vapor mixture (1.4% C_3H_8, 7% H_2, 91.6% air). The BETA test series also used an all-strong configuration, with standard fuel vapor (with liquid fuel added for one test) with full-up/all partition placement, and with different ignition source locations. The GAMMA test series consisted of a mixture of partition configurations: all-weak (using only failing partitions), all-strong, and combinations of weak and strong. In addition to the standard vapor simulant, some tests were run with a layer of Jet A, and others with reduced concentrations of vapor simulant. The single DELTA test was conducted to document the effects of the "cargo bay" volume. In this test, an additional steel tank was fitted to the

Table 1.1: Participants in quarter-scale testing.

Participant	**Responsibility**
National Transportation Safety Board	Funding, Schedule Requirements, Test Configurations, and Planning
California Institute of Technology, Explosion Dynamics Laboratory	Lead Technical Organization, Tank Design & Fabrication, Transducer Procurements, Fielding Assistance, Data Analysis, Reporting
Applied Research Associates, Inc. Rocky Mountain Division	Test Site, Instrumentation Design, Photography Design/Deployment, SOP Development, Site Plots, Video Editing/Film Conversions, Reporting, Site Maintenance
Sandia National Laboratories, Albuquerque	Modeling, Test Configurations, and Planning
Christian Michelson Research	Modeling, Test Configurations, and Planning
Combustion Dynamics, Ltd.	Consultation, Test Configurations, and Planning
Desert Research Institute	Consultation, Test Configurations, and Planning

1/4-scale test tank fixture. This test consisted of a part-strong partition configuration, standard fuel with Jet A liquid, and ignition in bay 5.

This report provides detailed information about the test facility, test site, and test system performance. We describe the design and fabrication of the 1/4-scale fuel tank, vapor fuel formulations, test site configuration, electronic and photographic instrumentation systems, and test operations. The results of individual tests are presented and issues particular to each event are described. The tests are then compared. We examine in detail the effect of parameters such as number of compartments, ignition location, liquid fuel, venting, and partition failure. The issues of data validity and test replication are discussed. We conclude by summarizing the results, examining the implications for the TWA 800 crash investigation and making recommendations for future work. In the appendices are provided a summary of test conditions, key results, and raw data plots of the quasi-static and dynamic pressures, temperatures, photometric signatures, and a discussion of daily test and event weather parameters.

1.2 Participants

The major participants and their respective project responsibilities for this experimental effort are listed in Table 1.1.

1.3 Test Plan

A detailed discussion of the objectives and test plan development can be found in the test plan document (Shepherd et al. 1997b). As part of the test plan process, a preliminary test matrix was developed.

The test matrix evolved as the testing proceeded. The results of testing were discussed in two major project meetings held in October and November, 1997. Participants at these meetings were representatives from NTSB, Caltech, ARA, Sandia National Laboratories (SNL), Christian Michelson Research (CMR), and Combustion Dynamics, Ltd. (CDL). The modeling and testing results proceeded in parallel. Discussion of the results of both programs led to significant revision of the original test matrix. The final test matrix that resulted from this process is shown in Table 1.2.

1.4 Project Management and Personnel

Caltech's and ARA's project responsibilities were performed under the direction of Joe Shepherd and Larry Brown, respectively. Under Caltech's and ARA's management structure, the Principal Investigators have full responsibility for the overall project. These duties included technical performance, adherence to test scheduling, development and monitoring of budgets, administration, and program level interfacing with NTSB personnel.

In a project of this scope and schedule, direct and timely communication between Caltech/ARA, the subcontractors, and the NTSB technical staff was essential. Dr. Merritt Birky and Dr. Vern Ellingstad were available for consultation for all of the test series and visited the test facility during this project to provide guidance and direction. Their input was important for the successful execution of the test series. Major issues that significantly affected the test schedule, budget, and technical quality were brought to the attention of the project managers and the appropriate NTSB personnel for resolution.

Other Caltech and ARA personnel who performed key roles in the success of this project were: Dr. Chris Krok, Dr. Julian Lee, and Pavel Svitek at Caltech; Tim Samaras, Bob Lynch, Peter Dzwilewski, and Sheila Becker at ARA. These personnel were instrumental in the areas of administration, design, fabrication, field preparations, testing, instrumentation, and data analysis.

The technical progress of this effort was monitored in several ways. In addition to NTSB visits, team project meetings took place in Colorado, and informal discussions between Caltech and ARA took place daily. The progress was maintained by internal reviews; and efforts were documented in working project log books.

Technical quality was maintained both through the internal Caltech/ARA review process, as well as through the comments and interaction of NTSB personnel. The draft report was reviewed by the NTSB. The final report and the internal documentation were reviewed and approved by the respective Division Managers before the documents were released. Joe Shepherd for Caltech and Peter Dzwilewski, Vice President of ARA and the Rocky Mountain Division Manager, performed the Corporate review of the final report.

1.5 Project Plan

The elements of the project plan, along with the as-tested schedule, are given in Fig. 1.1 and are discussed below.

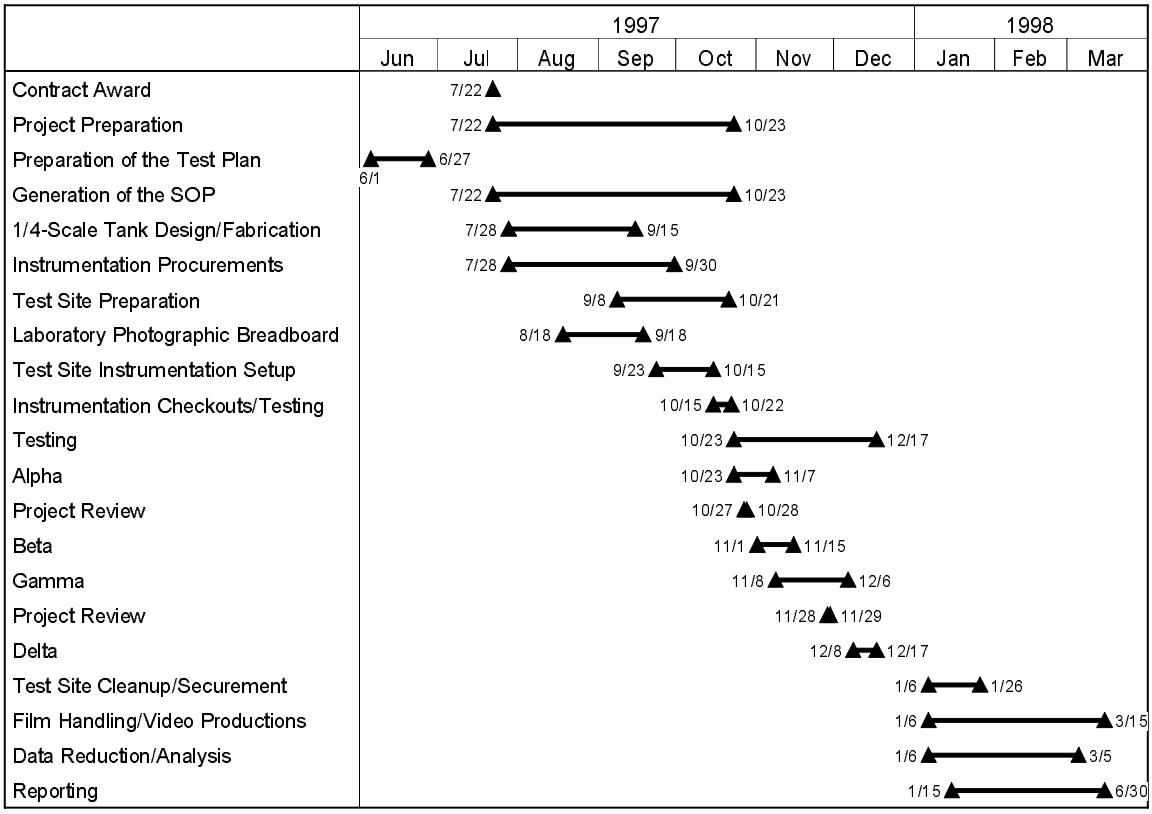

Figure 1.1: Project plan for fuel/air explosive testing.

Contract Award The contract award was received on 22 July 1997.

Project Preparation Preparations began immediately after award of the contract and included ordering the long-lead-time procurements for the tank fixture, optical, and instrumentation systems. The logistics required for this project were also planned during this time period

Preparation of the Test Plan Caltech delivered the Test Plan at the end of June which provided early direction, given the July contract start date. In addition, the two project review meetings conducted at the end of October and the end of November contributed greatly to the direction of the type and number of tests that were ultimately conducted.

Construction of the 1/4-Scale Model The 1/4-scale tank was designed at Caltech during June–August 1997 and constructed by Accurate Manufacturing in Burbank, California during

September 1997. The tank and other equipment was transported by Caltech to the ARA test site in early October, 1997 for installation and instrumentation preparations.

Instrumentation Development Caltech developed the instrument plan, procured and fabricated the instruments that were to be mounted on the tank. Special field-ready enclosures were provided for transducers to protect components and connectors from environmental and test conditions.

Generation of the SOP (Standard Operating Procedures) An SOP was generated to address the operational and safety requirements for this test series. The SOP format was comprehensive in detailing the general site operation and also specific in addressing the gas and liquid fuel handling, timing-and-firing procedures, and other test site issues. All site personnel were required to read and understand the SOP prior to conducting this test program. Each test was conducted in strict accordance with these procedures to ensure personnel safety, site safety and to maintain control of the test procedures.

Site Instrumentation ARA procured photographic supplies, storage medium, cabling/ connectors, site power, and other hardware/software items required to implement the test program.

Test Site Preparations Test site preparations included earth moving to provide a suitable, flat land area for location of the 1/4-scale test fixture and the supporting gas handling and instrumentation bunkers. The test site area was surface finished with river rock to allow operations in wet weather conditions. Camera bunkers, instrumentation vans, and a gas-handling structure were installed. Instrumentation and control cables were routed to their respective locations from the timing and firing instrumentation van.

Laboratory Photographic "Breadboard" The shadowgraph/pseudo-schlieren optical system was put together in a breadboard fashion to fine-tune the optical characteristics of the light source system used for documenting flame propagation through the bays in the 1/4-scale test fixture. Other checkouts of photographic systems were also performed during this phase of the project. Exposure checkouts and full-scale film runs were conducted in the ARA laboratories prior to field deployment.

Instrumentation Setup The laboratory-checked, instrumentation/photo-instrumentation systems were packed and transported to the ARA test facility for installation into the previously positioned bunkers and vans. Interconnecting cable terminations were completed for the control, firing, and instrumentation lines.

Checkouts/Testing This task included the checkouts and functioning of all the control, firing, and instrumentation systems. Transducers and other sensors were field tested to ensure

compliance with signal-to-noise ratios and operated to ascertain calibration validity. Photographic systems were checked with "full-up" film runs to determine the accuracy of timing and verification of exposure values for the up-coming test series.

Testing The testing program was conducted in four distinct phases, with some overlap contingent on commonality of test scenarios that resulted in non-consistent test numbering. The four test phases were as follows:

ALPHA The ALPHA test series varied the number of bays in the tank by varying the number of strong partitions. Configurations from one to six bays were tested. All tests used the standard fuel mixture with ignition in bay 5 and no venting.

BETA The BETA series used the all-strong partition configuration with all partitions installed. Tank venting was allowed with the standard fuel mixture and one test of the series included liquid Jet A on the bottom of the tank to simulate the nearly empty CWT conditions of the Flight 800 event. The ignition location was varied for this test series as documented in Table 1.2.

GAMMA The GAMMA series included a variety of all-weak, part-weak/part-strong, and all-strong partition configurations. With the exception of Test 25, tank venting was allowed. Standard and lower fuel vapor mixture tests and some tests with liquid Jet A were conducted. The ignition source locations were also varied for these tests.

DELTA The single DELTA test was designed and conducted to simulate the cargo bay volume forward of the CWT on Flight 800. An additional tank structure was attached to the 1/4-scale model and instrumented to document the pressures generated in the cargo bay.

Project Reviews The progress of the project and test planning was presented in the Project Review meetings conducted at the end of October and again at the end of November. Personnel from the organizational teams were in attendance for these meetings and significantly contributed to the overall quality and objectives of the program.

Online Status and Data Archive All members of the team were kept informed of the status and results of the experiments through a secure web site. Data from the tests were processed as soon as possible and made available through the web site in both graphical and data file formats.

Test Site Cleanup and Security The spent project materials were disposed of and the instrumentation and photo-instrumentation equipment was removed from the test site for safekeeping and maintenance during this task. Site security, power, and building structures are being maintained for possible future testing activity. Transducer post-calibrations were also performed during this time period.

Film Handling, Video Conversions, and Copying This phase of the project involved the compilation of the film and video records. Film splicing was performed and a high-resolution video master was produced and copies were made to provide working material for final report documentation and composite video production procedures. Video records were likewise edited into working copies and a master video tape was produced for the final report. The films from the 35- and 70-mm cameras were developed and selected prints generated for the report. The daily 35-mm documentary films and prints were assembled into photographic albums for documentation and future review.

Data Handling All recorded data from the instrumentation systems were backed up during the test series. The backup information was archived on ZIP disks for data reduction and analysis activities. The raw data were reduced to summary plots that included pressure, temperature, photodetectors, and the motion switches. In addition, test site daily weather and event time weather was plotted for inclusion into the report.

Data Analysis An extensive analysis of the data was carried out at Caltech. This involved first validating the data through detailed examination of individual records. The instrument results were then examined in conjunction with the video-tape records. Observation and interpretations were given for each test. The tests were then cross-plotted to find the effect of parameter variations. Finally, the results were examined in view of the goals of the accident investigation.

Reporting ARA and Caltech each wrote contributions for this document. Caltech assembled the document and published it.

Table 1.2: Test matrix for quarter-scale test series.

Test	Configuration	Ignition	Partitions	Vented	Fuel	Comments	Note
					ALPHA		
1	All strong	5	none	No	Standard[1]	Baseline (electric match)	c
11	All strong	5	none	No	Standard	Baseline test REPEAT	a
2	All strong	5	MS	No	Standard	2-compartment (match backup), data noise	c
10	All strong	5	MS	No	Standard	2-compartment REPEAT, 3 5/16-holes open in MS, stingers open	b,d
3	All strong	5	MS,SWB2	No	Standard	3-compartment (match backup)	c
9	All strong	5	MS, SWB2, SWB1	No	Standard	4-compartment, 3 5/16-in holes open in MS, jet fuel residue	b,d
12	All strong	5	MS with 2-in diam plugged hole		Standard	Validation test, 2-in hole in MS, stringers plugged	a,b
					BETA		
4	All strong	5	All[2]	Yes	Standard	Full-up	a,b
5	All strong	3	All[2]	Yes	Standard	Full-up, lost bay 1 pressure	a,d
6	All strong	2	All[2]	Yes	Standard	Full-up, bay 1 ignition through fuel manifold	a,f
7	All strong	1	All[2]	Yes	Standard	Full-up, aft PR failed late	a,e
8	All strong	5	All[2]	Yes	Standard w/liquid	Full-up	a
15	All strong	6R[3]	All[2]	Yes	Standard	Ignition location, aft PR failed, fwd PR damage	b,e
16	All strong	1R[3]	All[2]	Yes	Standard	Ignition location, aft PR failed, fwd PR damage	b,e
					GAMMA		
13	One weak	5	SWB3 weak	Yes	Standard	Test of CMR venting model	a
14	All strong	5	All strong with weak MP in SWB2	Yes	Standard	0.012-in MP	a
17	2 weak	5	Part[4]	Yes	Standard	0.012-in MP	a
18	All weak	5	All[2]	Yes	Standard	weak partitions	a
19	All weak	5	All[2]	Yes	Standard w/liquid	weak partitions, liquid lofting	a
20	All weak	2L	All[2]	Yes	Standard w/liquid	weak partitions	a
21	All weak	1	All[2]	Yes	Standard w/liquid	weak partitions	a
22	Part Strong	2L	Part[4]	Yes	Standard	0.006-in MP, fuel line ignition in bay 1	f
23	Part Strong	2L	Part[4]	Yes	Low 1	0.006-in MP, 7% total fuel, fuel line ignition in bay 1	f
24	Part Strong	2L	Part[4]	Yes	Low 2	0.006-in MP, 6.5% total fuel, plume in bay 1, aft PR fail?	d
27	Part Strong	2L	Part[4]	Yes	Standard w/liquid	0.006-in MP	a
29	Part Strong	1	Part[4]	Yes	Standard w/liquid	0.006-in MP, aft PR failed	e
28	Part Strong	5	Part[4]	Yes	Standard w/liquid	0.006-in MP	a
26	All Strong	2L	All	Yes	Low 2	model verification test	a
25	All Strong	5	All	No	Standard	"replica" (almost) of Test 5	a,b
					DELTA		
30	Part Strong	5	Part[4]	Yes	Standard w/liquid	With "cargo bay" mockup, 0.006-in MP	a

Notes:

1 Standard mixture is 1.4% C3H8, 7% H2, 91.6% air.

2 All partitions includes: SWB1, MS, SWB2, and both Partial Ribs.

3 Ignition location that simulate fuel probes: 1R, far right side next to SWB2 at top; 6R, far right next to SWB1 at top; 2L, Butt line, 2-in from bottom (compensator).

4 Part Strong has strong SWB1, MS, SWB2 and partial ribs. SWB3 and FS are weak, manufacturing access panel (MP) weak in SWB2.

a Data all valid, no known problems with test

b Tests selected for simulation comparisons

c Problems with data or test implementation, do not use data!

d Minor irregularities with data or setup

e Partial rib failure, may affect comparisons

f Ignition through fuel loading lines

Chapter 2

Test Site and Facility Description

2.1 Quarter-Scale Test Facility

The quarter-scale test facility is designed to be an engineering model that duplicates certain key features of the center wing tank, shown in Fig. 2.1. The model does not look exactly like a center wing tank and many features of the center wing tank are not included. The main purpose of the model is to have a facility in which the following issues may be investigated: ignition location; fuel type and amount; flame propagation; venting; the effect of structural failure of the beams and spars on combustion. For these issues, the most important features to model are compartmentalization of the center wing tank into bays, the flow passageways, and the venting. The precise way in which these features are scaled is described in detail in the test plan document (Shepherd et al. 1997b). Briefly, the volumes of the bays in the facility are 1/64 of the full-scale bays and the areas of the flow passageways and vent tubes are 1/16 of the corresponding full-scale features. The location of the passageways and vent tubes in the model are in approximately scaled locations. The fuel used in the model experiments was also scaled so that it had the same flame speed and combustion overpressure as the Jet A vapor-air mixture at the explosion altitude and a nominal tank temperature of 50°C.

Structurally, the 1/4-scale model is quite different that the actual wing tank. The model is basically a rectangular box with rigid top, bottom, back, and sides. Partitions are used to divide the tank into bays. These partitions can either be rigid (strong) or else are lightweight panels with deliberately weak connections designed to fail at a specified overpressure.

The construction of the tank was a design choice that was made due to the difficulty of structural scaling and to make the facility more useful for parametric testing. The difficulties of structural scaling are several. First, it is extremely expensive to make an accurate scale model of a highly stiffened, many jointed structure like the center wing tank. Second, the airplane itself plays a significant role in the structural response of the CWT. Third, such a structure would not be reuseable.

The only structural issue that was investigated in the present study was the effect of the failure of the beams and spars on the the combustion process. The goal of these tests was not to model the failure process, but to examine the effects of failure on combustion.

It is important to keep in mind the limited goals of the present study and the larger inves-

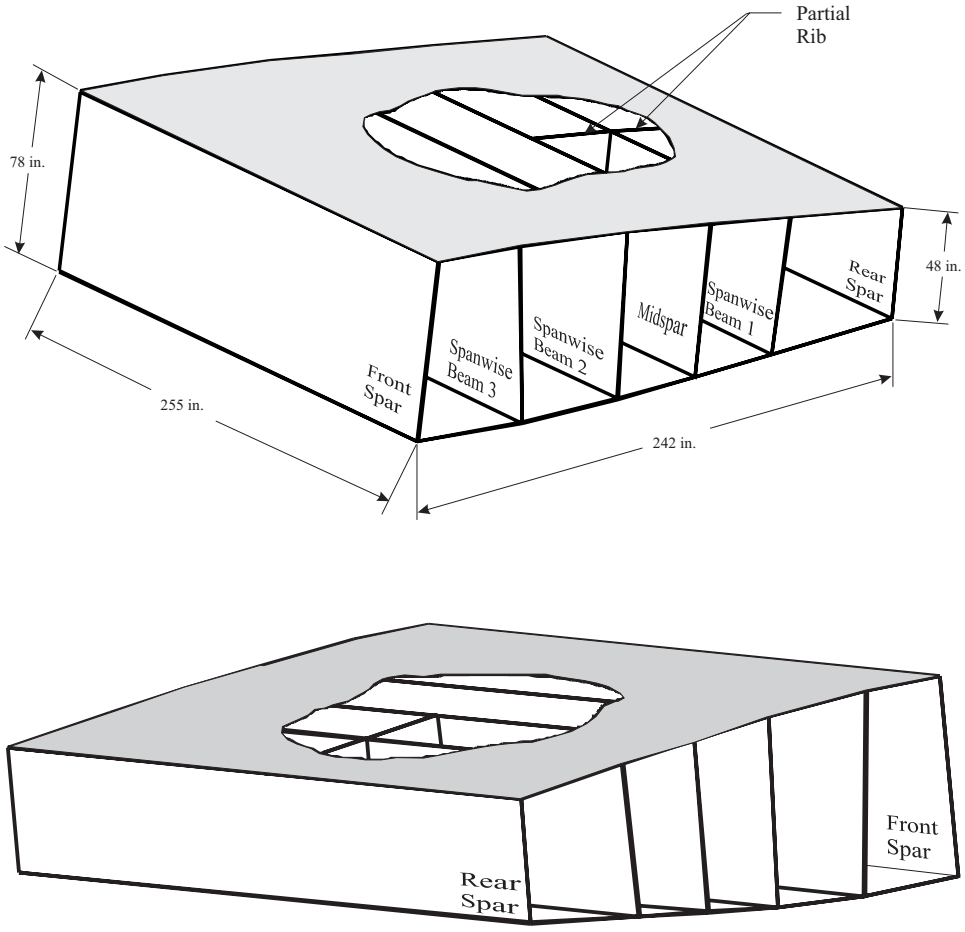

Figure 2.1: Perspective views of actual center wing tank.

tigation of which this is a part. For example, the present study was not carried out with Jet A vapor or spark ignition sources. Separate laboratory studies have been carried out on those issues. The present study does not attempt to create an ignition source using components found in a wing tank. Other investigative teams led by the NTSB have been testing actual components and investigating potential ignition sources.

2.1.1 The Tank Structure

The main structure of the model tank before any of the support hardware (fuel, instrumentation lines) was connected is shown in Fig. 2.5. The structure is built of standard A36 structural steel shapes, and has a maximum design pressure of 100 psi. The interior dimensions of the tank are 60 in $\times$ 60 in $\times$ 18 in. The top and bottom of the tank are constructed of 0.75-in thick plate, reinforced with cross-beams. The plate assemblies are welded to the main longitudinal beams, which in turn are welded to the four vertical columns. The rear spar, also made of 0.75-in plate, is welded in place. The columns and rear spar thus keep the top and bottom from separating under pressure. The columns also elevate the centerline of the tank to four feet. Smaller beams

on the top of the columns are used for hoisting partitions and windows. In practice, two people were always available for turnaround, and it was much quicker to lift the windows and frames into place by hand.

Figure 2.2: Model tank structure on flatbed at test site, awaiting unloading.

Figure 2.3: Unloading the tank from the truck.

The top, bottom, and rear walls of the tank are therefore part of the main structure. The sides of the tank are made of 1.25-in laminated polycarbonate, so one may see through the tank and view the combustion. To protect the windows from the heat of combustion and from being scratched by failing partitions, an additional piece of 0.125-in polycarbonate is placed

Figure 2.4: Tank being moved by forklift to test pad.

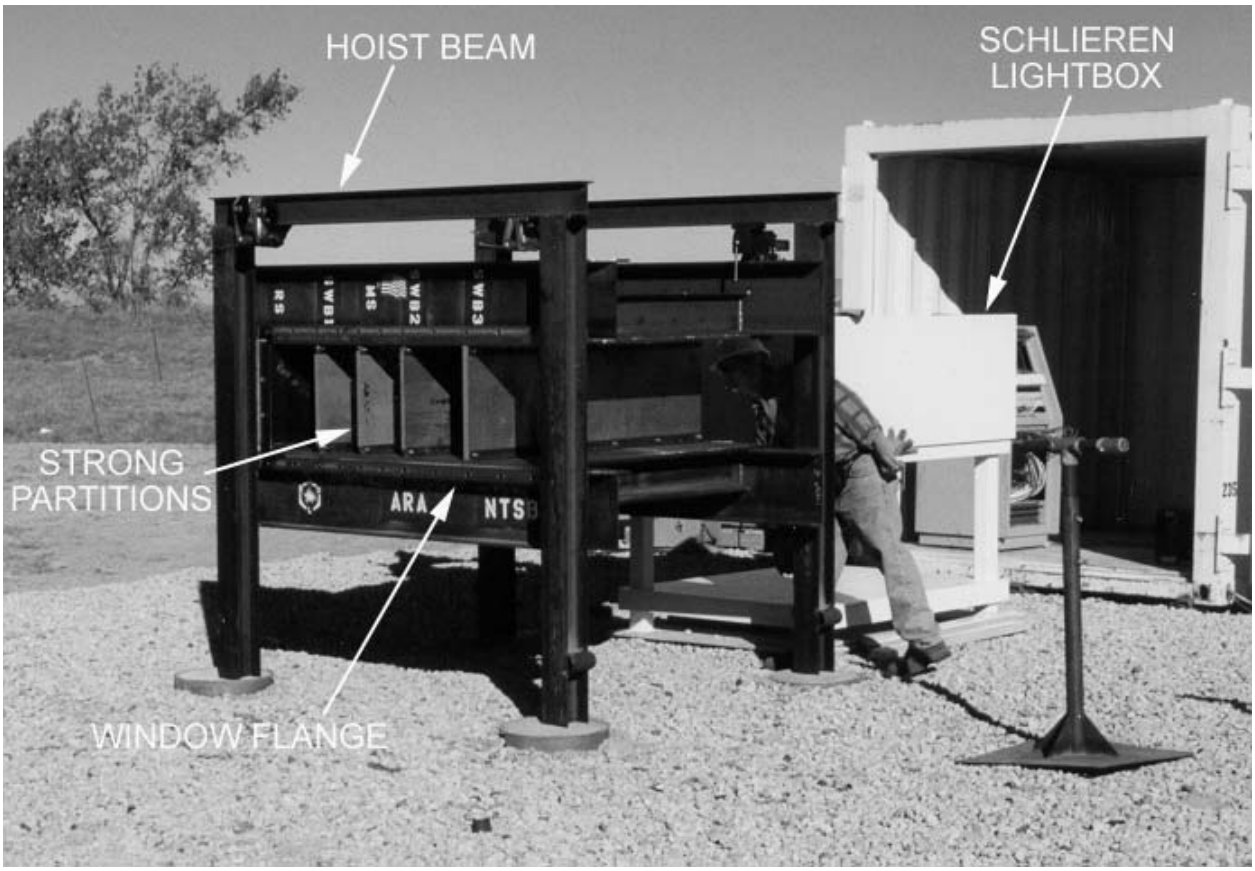

Figure 2.5: Tank in position on test pad, before installation of support hardware. Mike Rictor is checking alignment of multi-bay schlieren system.

inside the main window. The thinner pieces are referred to as sacrificial windows, and are typically discarded after each shot. With the main and sacrificial windows on the tank, the last

piece of the window assembly is the mounting frame. This frame is made of steel angle around the perimeter and vertical bars to retain the windows. The bars are located over the partition stations, so no viewing area is lost. (Drawings detailing the window frame design and sealing flange are available in Appendix C.)

During the initial stages of testing, different methods of sealing the windows to the tank were tried. First, RTV silicone was used. This worked well, but was difficult to clean off between shots. Long cure time in cold weather was also a problem. A silicone tape was also used, but was found to be not resiliant enough. A self-adhesive automotive trim tape was tried, but this was too thin to fill some gaps, and expensive as well. Finally, a tape made with a foam core and a rubber jacket was found in the McMaster-Carr catalog. The tape was 1/8-in thick, allowed compression, and was relatively inexpensive. This method of sealing the tank greatly reduced the turnaround time between tests, as there was no curing time. After the tests, the tape residue peeled off easily, although a heat gun was needed to soften the tape in cold weather.

Figure 2.6: Test facility with majority of support hardware attached.

2.1.2 Partitions

The center wing tank in a 747 is divided into seven sections, or bays, as shown in Figs. 2.1 and 2.8. Only bays 1 – 6 are used for fuel storage. Bay 0 is a dry bay since it does not contain any fuel. Thus, span-wise beam 3 (SWB3) is the forward tank pressure boundary. Span-wise beam 1 (SWB1), the mid-spar (MS), span-wise beam 2 (SWB2), and the partial ribs (PR) all have passageways as well as gaps around tubing passageways that allow fuel to flow and equilibrate

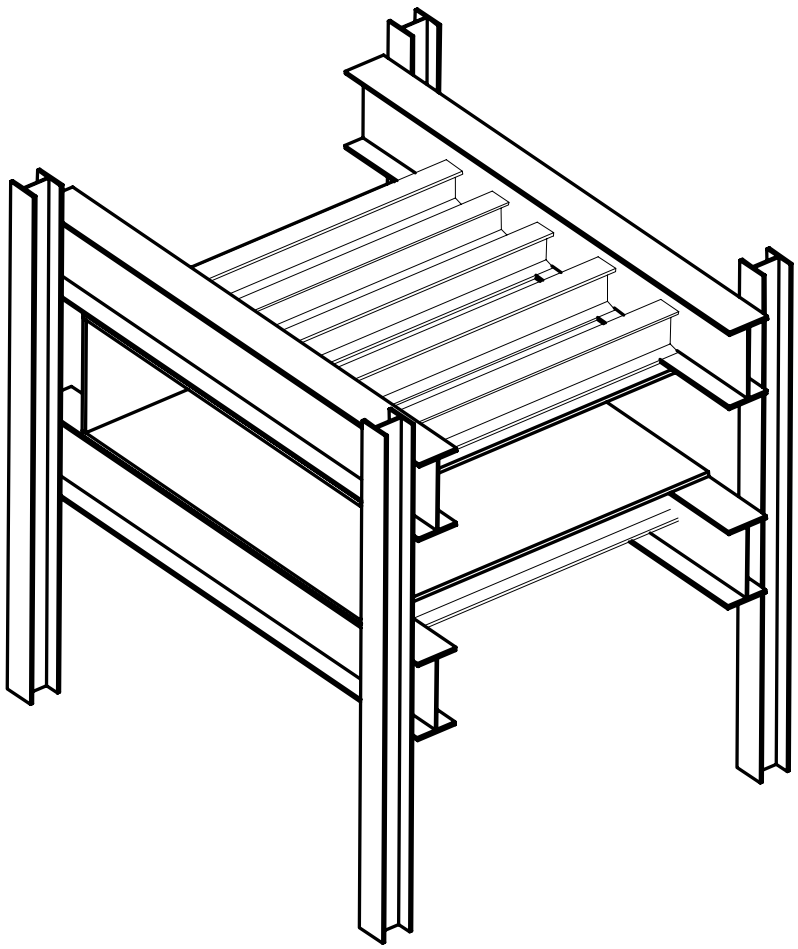

Figure 2.7: Schematic of tank construction (hoist beams omitted).

among the bays. The details of the passageways in the actual beams and spars are given in the test plan (Shepherd et al. 1997b). In the 1/4-scale model, the passageways are modeled by holes and corner cuts in the partitions (described in Appendix C). The total area associated with holes in each partition is given in Table 2.1. The partitions are removable, so various configurations can be studied.

Two types of partitions can be used in the tank model. Strong partitions are used when only flame propagation and pressure piling are studied. These partitions are constructed of 0.75-in aluminum (SWB3: 0.875 in), and are mounted to the top and bottom plates with steel angles and 1/2-in alloy steel cap screws and nuts (Fig. 2.9). SWB3 is sealed to the top and bottom of the tank with RTV silicone. Since SWB3 is the outer boundary of the system, the forward

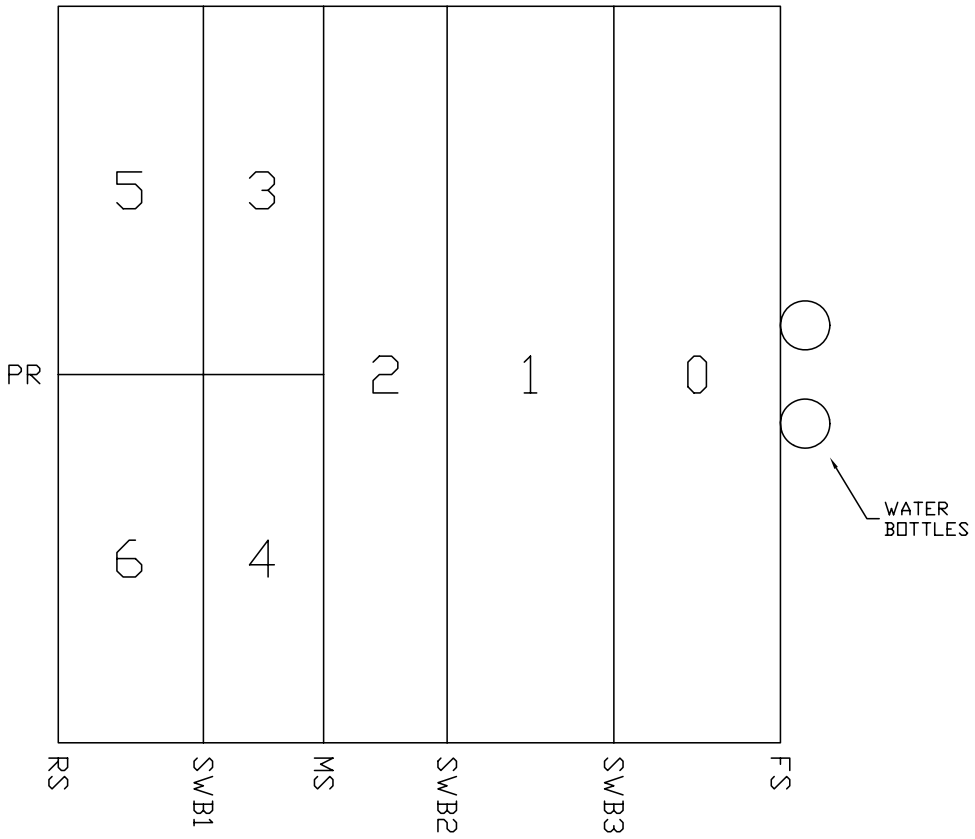

Figure 2.8: Numbering scheme of bays in quarter-scale facility.

Table 2.1: Total area of passageways between compartments of the 1/4-scale model.

Partition	Flow path	Scaled Flow Area (in^2)
Aft Partial rib	5-6	6.8
Forward Partial rib 2	3-4	2.8
SWB1 (L)	5-3	1.29
SWB1 (R)	6-4	1.64
MS (L)	3-2	1.58
MS (R)	4-2	1.51
SWB2	2-1	2.15
MP in SWB2	2-1	42

spar is not needed for strong partition tests. After the first few tests, the other partitions were sealed with RTV as well to prevent flow through the mounting brackets. In some tests, the partitions moved, and the sealant had to be re-applied. The ends of all partitions were sealed to the windows with foam tape. The PRs are made of 1/2-in polycarbonate to pass light for

the schlieren system. They are connected to the spars and beams with aluminum brackets. In practice, the strong PRs were not damaged by exposure to the gaseous flames, but were permanently tinted by soot in jet fuel tests.

Weak partitions were used to simulate beam or spar failure and to study the effects on the combustion process. The weak partitions are constructed of 0.090-in thick 6061 aluminum sheet, with the edges bent 90° to form mounting and sealing flanges. In weak partition tests, steel pipes are attached to the front of the forward spar to simulate the water bottles. The pipes are 4-in OD $\times$ 0.318-in wall, 15-in long. They weigh 15.6 lb each, slightly larger than the scaled weight of 14 lb. The partial ribs used with the weak partitions are made of 0.125-in thick polycarbonate.

The weak partitions were held onto the top and bottom plates of the tank with screws (alloy steel 10-24 socket-head cap screws), seven each on the top and bottom. These screws were modified to fail in shear when a pressure difference of 20 psi (1.38 bar) was applied to the partition. This corresponds to a shear load of 1540 lb on each screw. The first batch of screws were modified by reducing the diameter to 0.150 in (corresponding to the root diameter of the thread) over an 1/8-in wide section of the screw. This notch was centered at location 3/4 in from the head, so that it would be roughly centered at the edge of the plate to promote a clean break. The failure strength was verified using a simple lever and weight arrangement in the laboratory.

After running several weak partition tests, it was clear that a variety of mechanisms were responsible for failure; while many of the screws were breaking at the notch, in some cases the aluminum pulled over the nut, or the screw broke in a different location. So, when the first batch of screws was used up, unmodified socket-head cap screws were used for the last 3 – 4 tests. Typically, these were used on the forward spar, so SWB3 could be mounted consistently with the prevous tests. Since the forward spar appeared to fail from impact of SWB3, consistency in the failure pressure or mechanism was not considered essential.

In the part-strong test series, FS and SWB3 were weak panels. An opening was machined into SWB2 at the scaled location and size of the manufacturing panel (MP) on the right-hand side of the beam (see the drawing in Appendix C). A thin aluminum sheet was clamped over the hole to simulate the MP. The thickness of the sheet and a vertical knife edge (cutter bar) mounted on the front side determined the rupture pressure of the sheet. The MP used with tests 14 and 17 (0.012-in thick) appeared to have too high a rupture pressure (3.5 bar), so the thickness was reduced and a knife edge was added. Prior to carrying out the explosion tests, the MP rupture pressure was determined for two thicknesses with a simple field test.

Thicknesses of 0.006 in and 0.004 in were tested by covering the back side of the MP hole in SWB2 with a plate and connecting this to the compressed air supply. This formed a small pressure chamber. A pressure transducer was also mounted on the plate. The plate was mounted to the aft side of SWB2, while the diaphragm was mounted to the front, with a cutter bar. The cutter bar ran vertically between the center bolts on the diaphragm retainer frame. It was an 1/8-in thick steel bar with a sharpened edge. To record rupture pressure, the acquisition system was manually triggered, and at time zero the compressed air supply was connected to the chamber via the quick-disconnect at the maintenance connex. While the compressed air supply does not simulate the same rise time found in the experiments, it was adequate for the

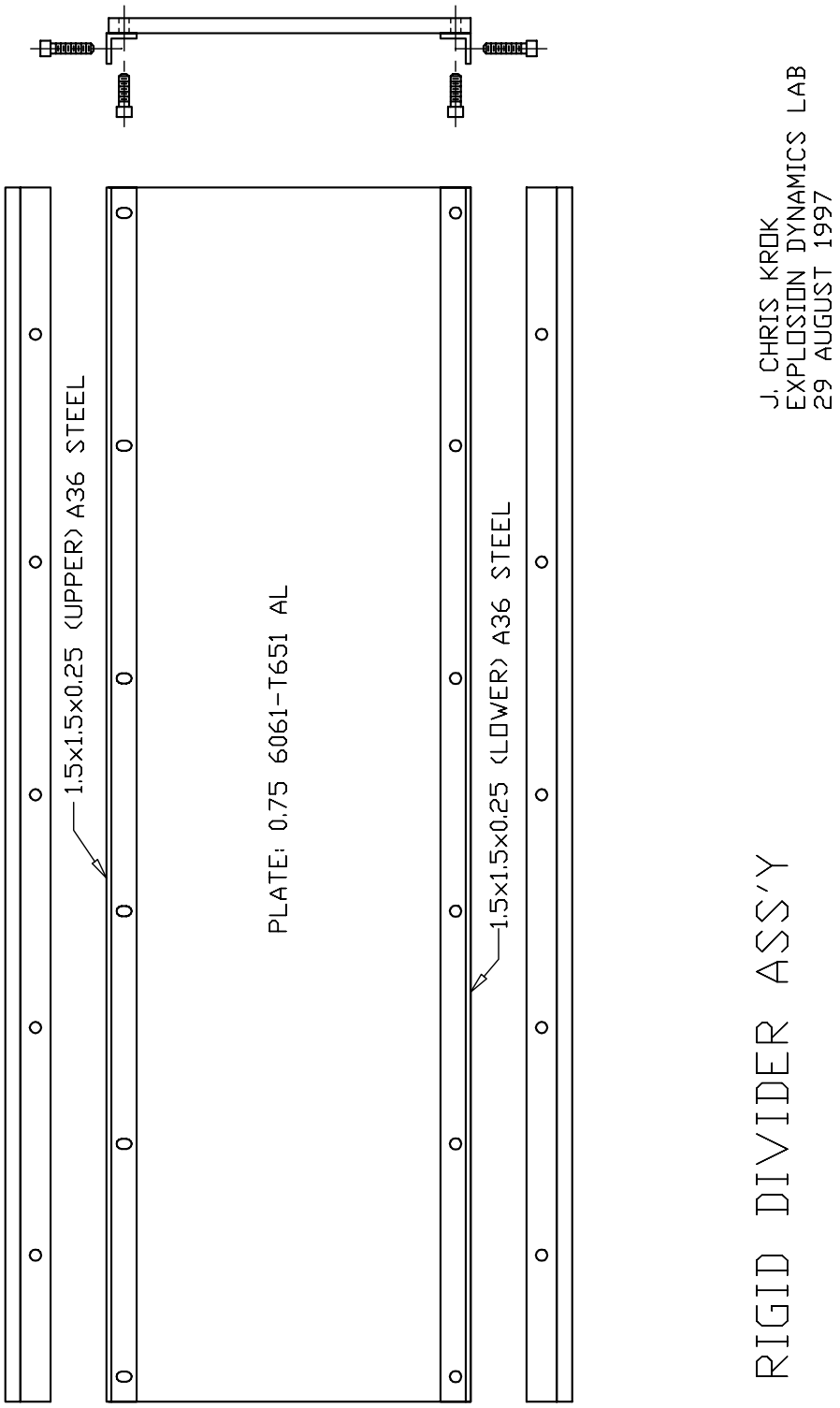

Figure 2.9: Construction of strong partitions.

purpose of determining the ruputure pressure. A test with the 0.012-in thick sheet and the cutter gave a failure pressure of 2.1 bar. Two tests were carried out with the 0.006-in thick sheet and the measured rupture pressures were 0.98 and 1.1 bar. The 0.006-in thick sheet and cutter were used in Tests 22 through 24, and 27 through 30.

2.1.3 Plumbing and Gas Handling

A schematic of the plumbing system is shown in Fig. 2.10. All valves are electropneumatic, operated by electrical signals from a mimic panel in the TCC (Test Command Center). Air pressure is supplied by a compressor at the maintenance connex.

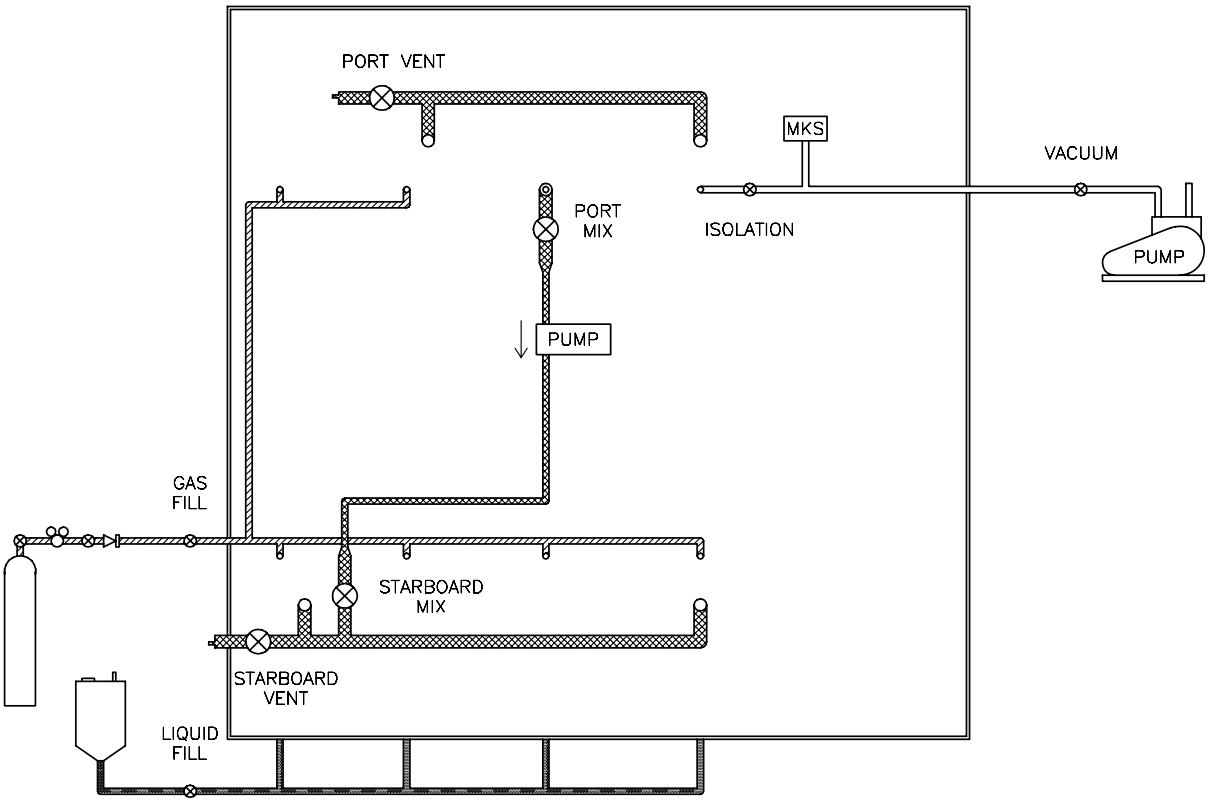

Figure 2.10: Plumbing schematic for the quarter-scale test facility.

The vent lines are constructed of 1-in OD tubing (0.84-in ID), and simulate the vent stringers that go from the CWT to the surge box near the wing tips of the airplane. The model vent stringers are scaled in diameter but not in length. To compensate for the shortness of the vent stringers, the flow resistance was increased by adding 0.437-in diameter orifices at the exit of each vent. This diameter was chosen based on computations of pressure drop in the full-scale stringer and the orifice. A schematic of the venting system is shown in Appendix C.

Ball valves in the vent exits allow them to be closed for gas filling and for certain tests. The starboard vent line also serves as a connection point for the circulation pump. The pump circulates and mixes the tank gas contents by drawing from the port side of bay 2, and pumps

into the aft end of the starboard vent, adjacent to bay 6. Gas pumped into the vent will primarily enter bay 6, but will also enter bay 1 through the vent line. The gas will flow through the passageways in the tank and return to bay 2. The gas was mixed for 15 minutes immediately prior to ignition.

Three sets of lines make up the fuel fill system. The vacuum line is used to evacuate the tank to the required pressure for fuel filling. The MKS pressure transducer in that line is used to measure atmospheric pressure and monitor pressure during gas filling. The gas fuel manifold is used to load the fuel vapor simulant mixture (16.7% C_3H_8, 83.3% H_2) into the tank. The premixed gas is supplied by a high pressure bottle and regulator set at 7 psi. The bottle is heated at the bottom and insulated in the middle to keep the propane from condensing and to produce convection currents to mix the gases. The gas enters the six bays through orifices which are sized to be roughly proportional to the bays to ensure a uniform filling time for all bays and reduce mixing time. The amount of gas introduced into the tank was determined by the method of partial pressures using the MKS pressure gauge.

The orifices feeding bays 1 and 2 have twice the area of those in the other bays, as these bays have no partial rib in the middle. The liquid fill manifold, on the underside of the tank, is used to load Jet A fuel when needed. This system consists of a 1-gallon reservoir and valve (vertical tube and valve on aft tank column, see Fig. 2.6), and fuel enters at four locations along the centerline of the tank. Bay pairs 3/4 and 5/6 each share a fuel line, and the fuel levels itself through the passageways in the panels. The fuel is drawn into the tank under partial vacuum to reduce loading time.

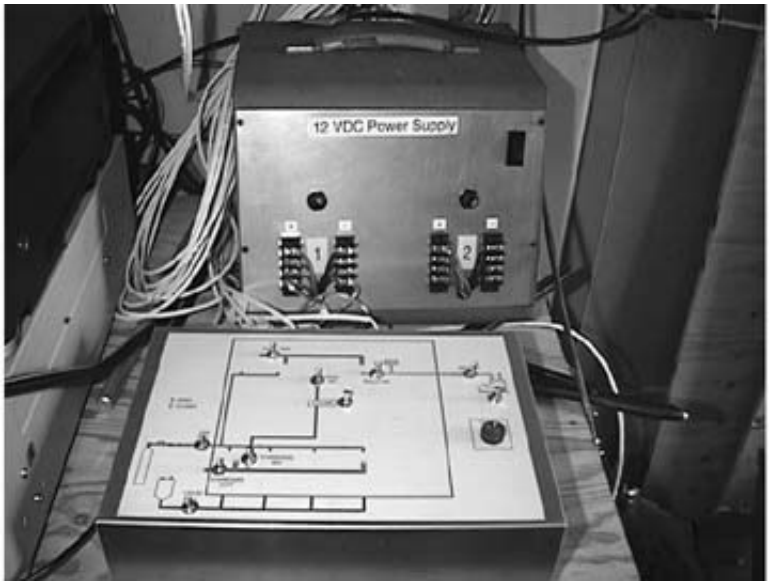

Figure 2.11: Valve control box of the quarter-scale test facility.

To indicate valve positions during filling and firing, semaphore assemblies were attached to the actuator shafts. These consist of red and green flags mounted on a vertical shaft at a 90° angle. The actuator motion is also 90°, so with proper alignment to a video camera, only one flag at a time will be seen in the monitor. The red flag has a two-letter abbreviation for the

valve name stenciled on it. Red indicates that the valve is open, green indicates closed. This convention is contrary to standard stoplight signals, but is used so that a red flag indicates an unsafe firing condition, with the exception of the vent valves which are opened after the tank is secured. In the tests, the semaphores were monitored with the west hilltop video camera.

In addition to the ball valves, two solenoid valves were used on the tank. These had no position indicator. The first allowed compressed air to flow into the jet fuel reservoir. Opening this valve with the jet fuel valve and vent valves would purge the tank with air in the event of a double misfire (both ignitors fail to ignite the mixture). The second valve was installed after test 19 to suppress post-shot pool fires in the tank. This valve was connected to a 7-gallon reservoir and the nitrogen bottle. The nitrogen regulator was set at 100 psi. Immediately after a shot with failing partitions and jet fuel, the control button was pressed to dispense nitrogen into the forward end of the tank. Despite a limited flow rate, combustion of the jet fuel within the tank could be extinguished.

2.2 Fuel-air mixture

Since the exact TWA-800 ullage conditions (composition, pressure, temperature) at the time of the explosion are difficult to reproduce in outdoor testing with vented tanks, a vapor fuel simulant was used instead of Jet A vapor. The mixtures used in these tests were chosen to mimic the properties of Jet A and approximate the environmental conditions measured in flight testing (Bower 1997) at 14 kft within the center wing tank of TWA 800.

The fuel simulant was blend of hydrogen and propane. Jet A was used for the fuel liquid in the cases where the liquid fuel layer on the tank floor was simulated. The fuel simulant was chosen on the basis of laboratory testing at Caltech comparing explosions of Jet A vapor in air at a simulated altitude of 14 kft with propane/hydrogen air mixtures at the simulated altitude of 5 kft at the test site (corresponding to a pressure of 0.83 atm).

The results of experiments on Jet A at a mass loading of 3 kg/m^3, temperatures between 40 and 60°C and initial pressure of 0.585 bar (appropriate to the TWA 800 CWT conditions) are discussed in Shepherd et al. 1997a, 1997b and 1998. The peak pressure rise varies between 2 and 4 bar for initial temperatures between 40 and 60°C. From these measurements and the previous considerations about the temperatures and fuel concentrations measured in the flight test, we selected the 50°C condition as being representative. In terms of Jet A vapor concentration, this case has a fuel-air mass ratio of 0.055 and a fuel mole fraction of 0.012.

Through repeated trials, a combination of fuels was found that approximately simulated the pressure-time characteristics of Jet A combustion in air at 0.585 bar and 50°C. The simulant was a mixture of propane and hydrogen, in a ratio of 1:5 by volume or 4.4:1 by mass. This combination was tested at a reduced pressure (0.83 bar) to correspond to the higher elevation of the Denver test site. A comparison between the combustion events in the simulant mixture (1.4% propane, 7% hydrogen and 91.6% air, pecentages by volume) and Jet A vapor-air mixture (50°C and mixed with air at 0.585 bar) is shown in Fig. 2.12.

Analysis of these pressure traces indicates that peak pressure rise is slighty larger for the simulant (ΔP_{max} = 3.65 bar) than for the Jet A (ΔP_{max} = 3.36 bar). However, the simulant has

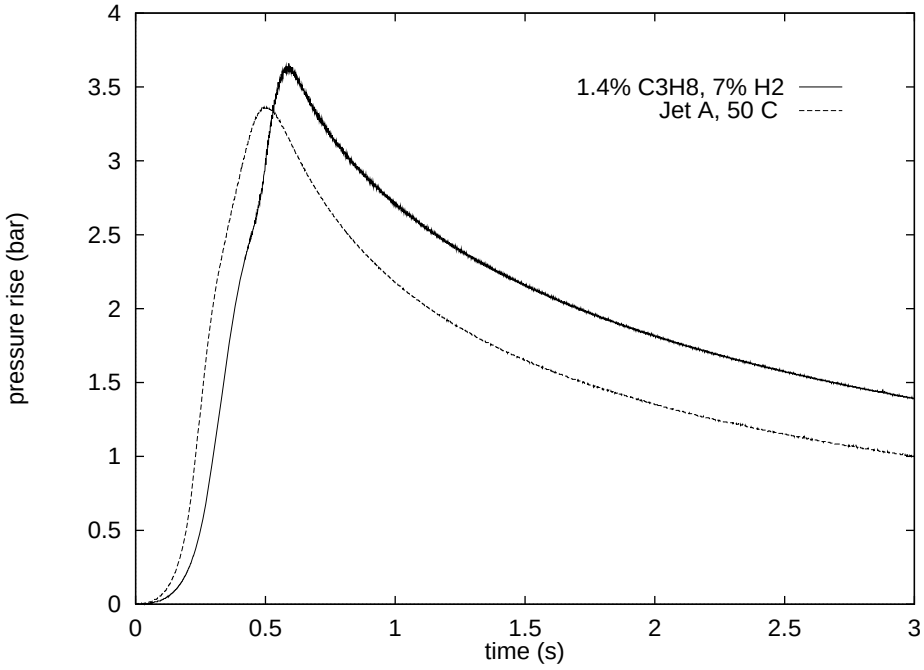

Figure 2.12: Comparison of combustion tests using LAX Jet A at 50°C mass loading of 3 kg/m^3 and 0.585 bar, and propane/hydrogen (1.4%/7%) at 25°C and 0.83 bar in the Hyjet Facility (1180 liters), both with spark ignition.

a slightly lower effective burning velocity (as determined by the $\Delta P^{1/3}$ analysis discussed in Shepherd et al. (1997)) of 52 cm/s as compared to 60 cm/s for the Jet A. Note that at 40°C, Jet A has an effective burning velocity of 15 to 18 cm/s and at 60°C, 66 cm/s. Peak pressure and flame speed also depend on initial temperature, these and other considerations about the fuel can be found in Section 8.

In addition to matching the peak pressure and flame speed, some considerations about the scaling of flame propagation are needed. Previous work on scale models of explosions (Mercx et al. 1995) indicate that small concentrations of oxygen or hydrogen may be required in order to increase the laminar burning velocity and prevent quenching. Separate laboratory experiments on quenching were carried out to show that the simulant mixture did not quench when passing through a 0.5-in diameter hole, the smallest size used to simulate the passageways through the beams, spar and partial ribs. However, quenching was observed with a 0.25-in diameter hole. These tests were carried out in the Hyjet facility, starting the flame in the 27-liter driver vessel which was connected at one end by the orifice to the 1180-liter main vessel.

2.3 Test Site Facilities

The ARA Field Test Facility was used to conduct the test series. This facility is operated by ARA and is located approximately 30 miles southeast of metropolitan Denver, Colorado. The controlled firing area consists of 55 acres which is enclosed within a security fence. The test

site is serviced with commercial power and is accessible via a paved road to the actual test arena. The test site enclosure is surrounded by pasture land with no inhabited structures within one mile.

Figure 2.13 shows the detailed plan view of the portion of the test site used for the 1/4-scale testing program. Note that the test fixture is isolated from the manned instrumentation van by an earthen berm and that several of the instrumentation bunkers are located on top of the berm to provide an elevated photographic view of the tests.

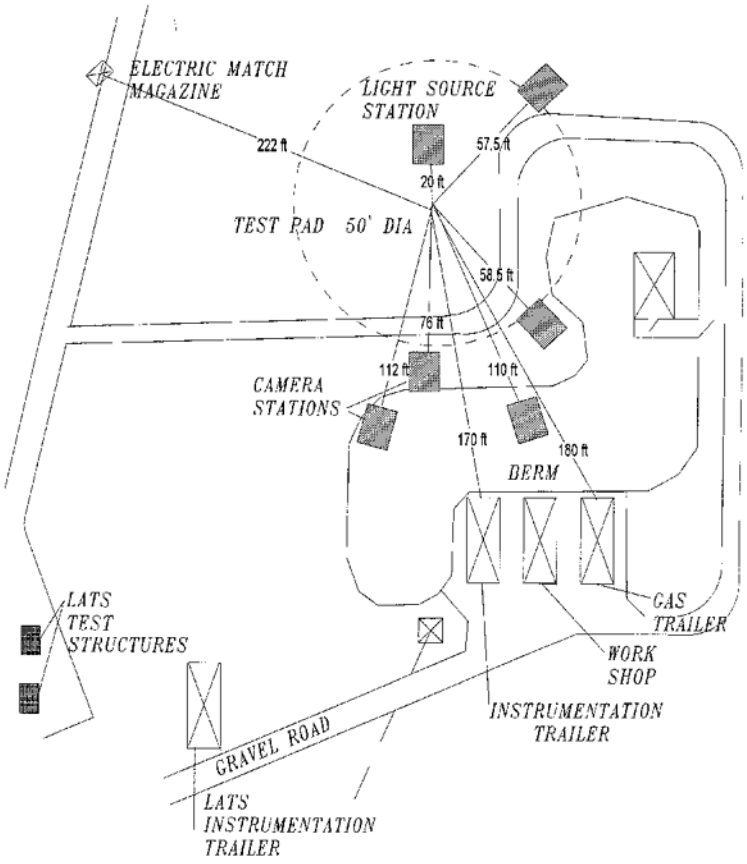

Figure 2.13: Plan view of ARA test site.

Figure 2.14 shows the location of the instrumentation van and two mobile housing structures (connex) which served for storage of the flammable materials and a general construction work area. The earthen berm seen in the background separates the instrumentation van from the 1/4-scale test fixture. Figures 2.15 and 2.16 show an overview of the general 1/4-scale test arena area. The test area is surrounded by photographic stations which are located to optimize the field-of-view for both the combustion process and general overview photography.

Figure 2.14: Instrumentation and storage structures.

Figure 2.15: Arena overview looking north.

Figure 2.16: Arena overview looking south.

2.4 Instrumentation and Photo-instrumentation Systems

2.4.1 Measurement Channels

The electronic measurements obtained by the 1/4-scale testing program to characterize the combustion process consisted of fourteen channels of temperature, seven channels of quasi-static pressure, ten channels of dynamic pressure, three channels of dynamic pressure located outside the tank, eighteen channels of motion detectors, and seven channels of photodetectors. This resulted in a total of 59 channels of electronic diagnostics. The photo-instrumentation used to document the combustion phenomena consisted of seven high-speed cameras, one 70-mm high-resolution camera, six video cameras, two timed 35-mm cameras, one 35-mm documentary camera, and one digital documentary camera. This resulted in eighteen channels of photo-instrumentation. In addition, pertinent test day weather information consisted of six channels of information relating to wind speed, wind direction, instrument van temperature, outdoor temperature, barometric pressure, and humidity. Therefore, a total of 83 channels of active diagnostics were used to characterize test performance. A brief review of the function of each type of measurement channel(s) is presented below.

Temperature (14 Channels) Used to measure the temperature in two places for each bay of the 1/4-scale test fixture.

Quasi-static Pressure (7 Channels) These pressure transducers were used to measure the quasi-static pressure of bays 0 – 6. The transducers were fitted with shields against heat and debris.

Dynamic Pressure (10 Channels) The dynamic pressure transducers were used to measure rapid pressure transients (shock or expansion waves) and were not fitted with extra thermal protection or debris shields. A layer of grease was used to provide limited thermal protection.

Free-field Incident Pressure (3 Channels) These pressure channels were used during some failing partition tests to document pressure waves propagating outside the tank.

Panel Motion Detectors (18 Channels) These break-switch sensors were positioned at each weak partition in the test fixture to measure the time of failure relative to event time zero.

Photodetectors (7 Channels) The photodetectors were positioned in each bay to monitor the visible and infrared radiation emitted by the movement of the combustion (flame) front through the various compartments.

High-speed Photography (7 Cameras) High-speed (400 fps) cameras (DBM) were used to provide the spatial resolution necessary to document the dynamic events associated with these

tests. Five cameras were used for the combustion photography and two cameras were used to capture panel ejection and fire ball characteristics.

70-mm High-resolution Photography (1 Camera) A 70-mm camera was positioned on the earthen berm above the test apparatus to provide high-resolution photography of the fire ball and panel ejection.

Video Cameras (6 Cameras) Two video cameras were used to provide real-time combustion monitoring for safety and light-source alignment. Three SVHS video cameras provided dynamic documentation of test performance, and one video camera was used for test documentation.

Timed 35-mm Cameras (2 Cameras) Two 35-mm cameras were timed to capture the first exposure, which occurred at event time zero, and successive frames at 4 frames and 8 frames per second, respectively. This provided very high-resolution pictures of panel motion and the fire ball, as well as general overview photography.

Documentary 35-mm Camera (1 Camera) A hand-held 35-mm camera was dedicated to the test program to provide full documentation of all pre-test activity and to provide post-event information.

Digital Documentation (1 Camera) A digital camera was used early in the program to generate pictures which could be sent to the various researchers via e-mail for assessing the site condition and progress.

2.4.2 Transducers

The transducers were all mounted on the top plate of the tank structure. The mounting pattern and coordinates of each gauge are specified in Appendix A of this document.

Photodetectors The photodetectors indicate arrival of the flame front by generating a signal based on flame luminosity. Each detector consists of a photo transistor that looks into the tank, protected by a transparent glass window 10 mm in diameter and 5 mm thick. This window was epoxied into a bored-through 1-in NPT stainless steel plug (Fig. 2.17). The photo transistor was mounted on top of the plug and wired to a BNC jack for connection to the instrumentation lines. The components were enclosed in an aluminum minibox.

Thermocouples The thermocouples were Omega type K, made from 0.005-in wire. Each thermocouple was mounted in a 0.125-in diameter two-hole ceramic tube that protruded 7 in into the tank. The thermocouple bead at the end of the tube was left bare to minimize the response time. The ceramic tube was mounted on the tank with a 1/8-in NPT compression

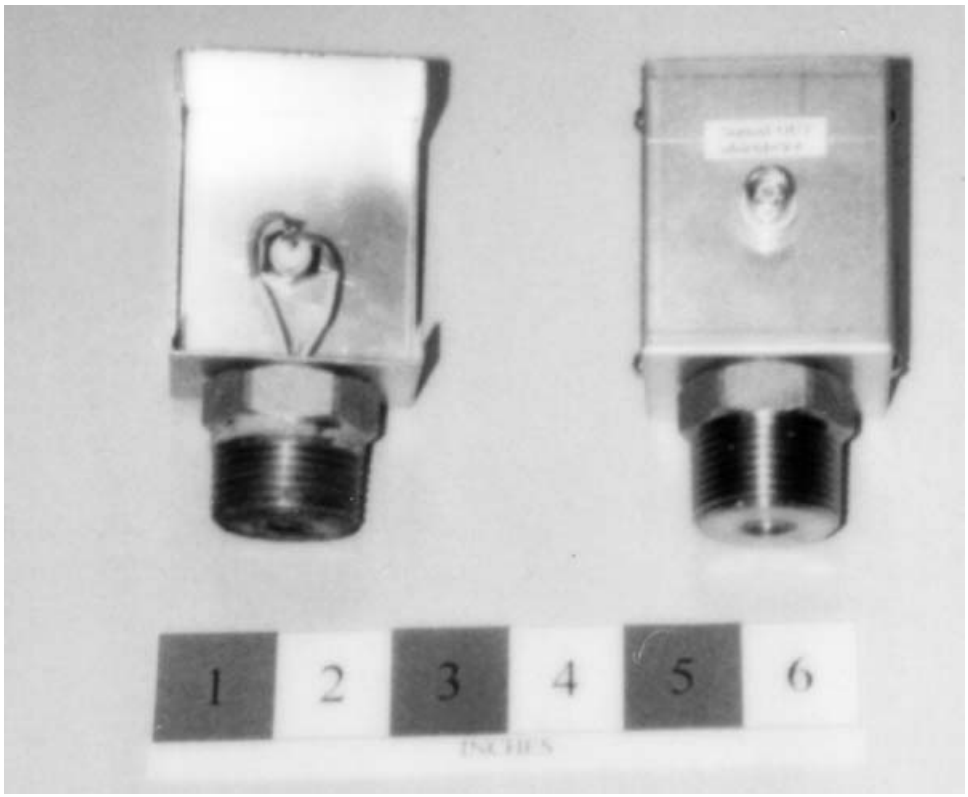

Figure 2.17: Photo detector assembly.

fitting as shown in Fig. 2.18. A teflon ferrule was used to seal the ceramic tube without crushing it.

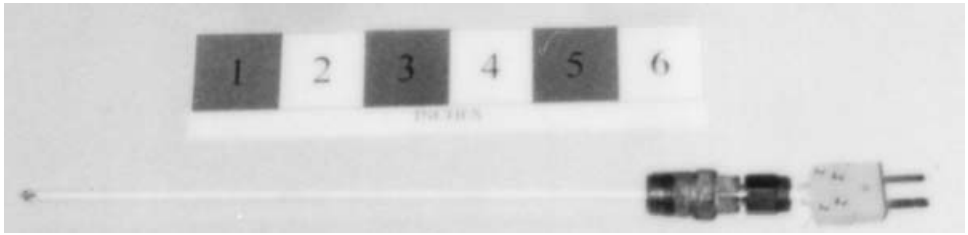

Figure 2.18: Thermocouple fixture.

Breakwire Motion Detectors The breakwire gauges consist of a thin strip of two-sided copper-clad circuit board as shown in Fig. 2.19. The strip is approximately 2 mm wide by 1.5 mm thick. A wire is soldered to the tip of the strip to provide electrical connection between the two sides. The detectors are mounted vertically, with the strip protruding into the tank. Four detectors are used for each weak partition (two on SWB1), i.e., one at each corner. The switch breaks readily when struck, signaling partition failure via a loss of continuity

(broken circuit). The installation time of these gauges was significantly shortened by the use of loudspeaker-type connectors to connect each gauge to its respective instrumentation wires.

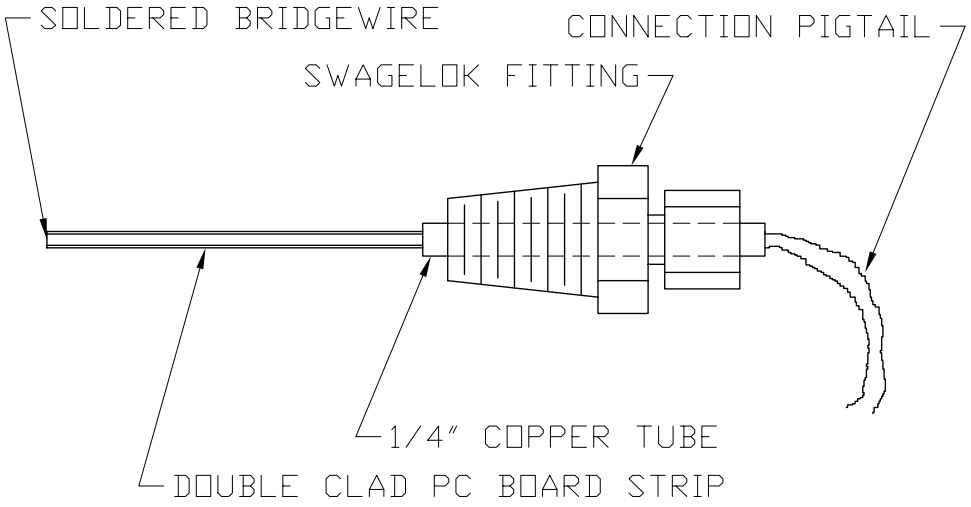

Figure 2.19: Breakwire assembly.

Dynamic Pressure Transducers The dynamic pressure transducers were PCB model 113A21, with a maximum pressure of 200 psi. They were mounted in protective housings (see gauge-Fig. 2.20), which contained Nylon isolators to prevent grounding of the transducer to the tank. The housing cap, which holds a Microdot-BNC feedthrough adapter, was also made of Nylon. To protect the diaphragms from thermal effects, a layer of silicon vacuum grease was smeared on each gauge before each test. This insulated the gauge for the first few hundred milliseconds of each test, which was enough to capture the peak pressure before the signal was affected. The transducers were calibrated at ARA after the test series, and some were found to behave significantly differently than the factory specification (see Appendix A).

In addition to the in-tank transducers, three PCB blast gauges (137A23, 50 psi) were set up outside the tank to record blast-wave pressures generated by failing partitions. Two placement configurations were used, but the signals were small in amplitude and difficult to interpret in both cases.

Static Pressure Transducers The static pressure transducers were Endevco type 8530B-200 (200 psi range), operated with 10 VDC excitation. These transducers are actually capable of high frequency response, but they are referred to as static transducers in this test program to indicate that they were scanned at a lower frequency (1 kHz) than the dynamic transducers. However, these transducers were the workhorse instruments in these tests and a substantial amount of the data analysis is based on the Endevco signals.

To protect the Endevcos from high combustion temperatures, the protective housings contained a sintered metal disk, or fritt, to quench combustion and absorb heat from the products. These also protect the gauge from flying debris. The housing assembly is shown in Fig. 2.21.

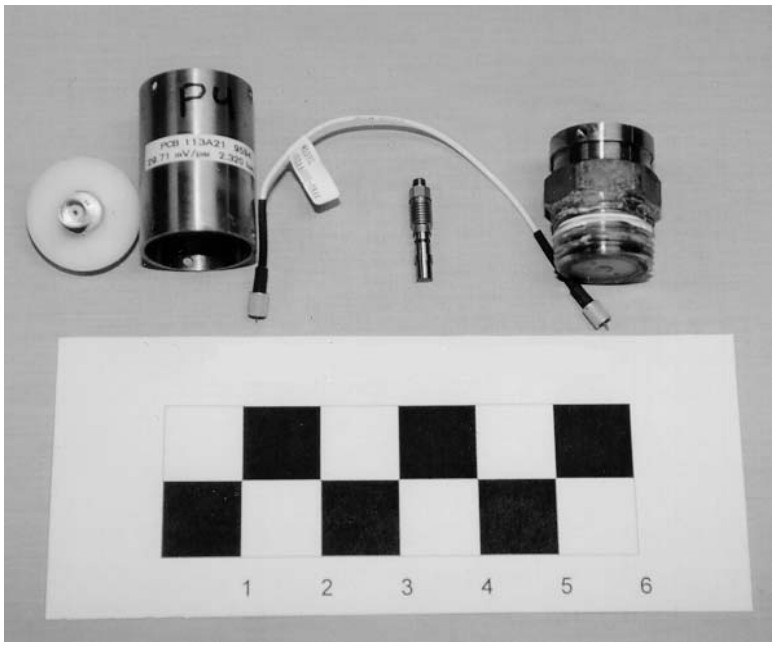

Figure 2.20: PCB dynamic pressure gauge with housing.

The gauge wires were connected to a female 9-pin D-sub connector mounted in the housing cap.

Figure 2.21: Endevco quasi-static pressure gauge with housing.

Ignitor The ignitor feedthrough was assembled from a Conax two-conductor feedthrough and a reducing bushing. Male quick-release tabs (0.25 in) were attached to the wires and potted in epoxy for connection of the match or filament. The hex nuts on the feedthrough were encased in PVC pipe to prevent them from being loosened by accident. The wires on the exterior side of the feedthrough were terminated with a 2-pin Molex connector so the firing line could be quickly connected or disconnected. Shorting plugs were also made for the feedthroughs. Inside the tank, a standard automotive light bulb socket was used to hold the bulb. The socket was attached to the feedthrough via a length of wire that placed the filament at the midpoint of the tank. After the bulb was inserted in the socket, the glass was broken off to expose the filament. For non-standard ignition locations (2Lo, 6R, 1R), longer wires were used to connect the socket, which was taped in the desired location.

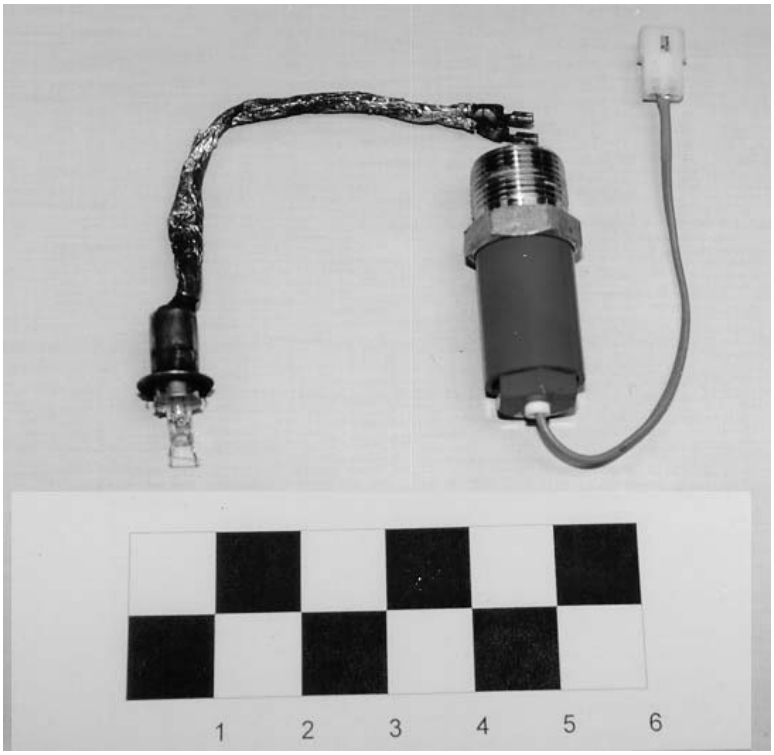

Figure 2.22: Ignitor feedthrough assembly with lamp socket.

2.5 Data Acquisition Systems

2.5.1 Signal Conditioning

Electronic Sequencer All of the event timing for the high-speed cameras, firing system, and the digitizers was controlled by a Bowen sequencer (Fig. 2.23). This sequencer has the ability to control ten channels of timing with a resolution capability of one microsecond. The outputs are selectable from either a pulse or a dry-relay closure.

The sequencer was manually started at T minus one minute (one minute to ignition); at T minus 30 seconds the firing system began charging and the motion detector debouncers were reset; at T minus 5 seconds the 400 fps cameras were activated; at T minus 3 seconds the 70-mm camera was started; and at T minus 0 the firing system and digitizers were triggered. The video cassette recorders were manually started at T minus 1 minute and stopped shortly after T minus 0. After event zero, the sequencer shut everything down at T plus 10 seconds.

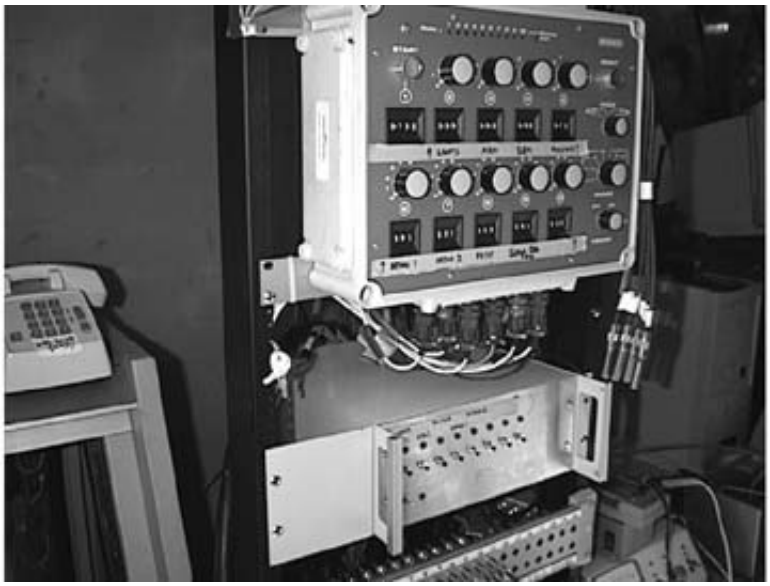

Figure 2.23: Electronic sequencer and interface unit.

Signal Conditioning Signal conditioning provided the interface from the suite of sensors to the digitizer which included excitation, amplification, and filtering. Each of the transducers used on the experiment utilized signal conditioning, as shown in Fig. 2.24.

Temperature The combustion temperature was measured by Type K thermocouples located inside the tank. The output of each thermocouple was connected to a thermocouple-to-millivolt converter unit manufactured by Omega Engineering (upper part of Fig. 2.25). These units provide cold junction compensation and linearization of the thermocouple signals. The output of these units was amplified, filtered, and sent to the instrumentation van via Ectron 563H amplifiers which increased the signal strength for transmission along the long cable lines back to the recording equipment. This was required to maintain desirable signal-to-noise ratios.

Pressure Two types of pressure measurements were made. The PCB piezo-electric gauges had the dynamic response necessary to accurately record shock waves and other rapid changes in pressure. ICP signal conditioning was used for these gauges, and was located in the instrumentation van. This system had a 100-kHz frequency response and visual indicators which showed if an open-circuit or short-circuit condition existed during the pre-test checkouts.

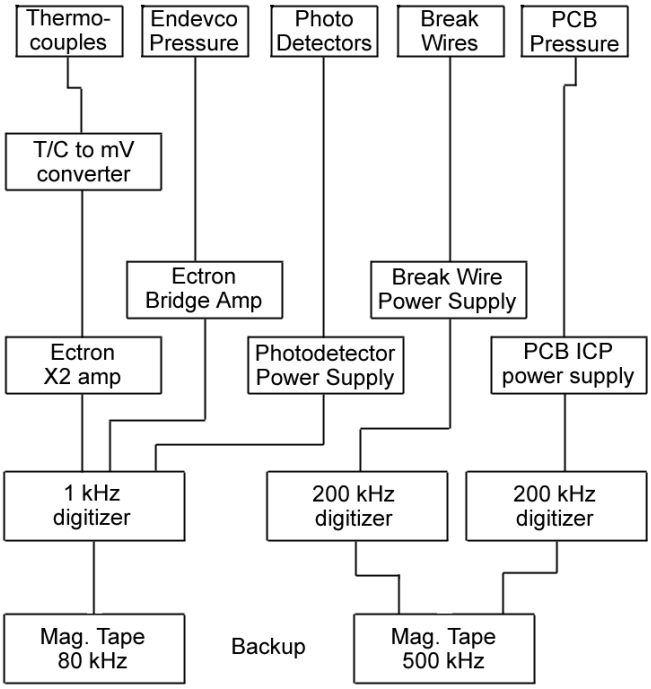

Figure 2.24: Diagram of transducer signal conditioning.

The other type of pressure transducer was the Endevco piezo-resistive, fully active, bridge transducer. This gauge was used to record the slow or "static" changes in pressure. This gauge required an excitation of ten volts (measured at the sensor). The Ectron 563H, 16-channel bridge amplifier provided the excitation, amplification, and the low-pass filtering (one kHz) required for the gauge to prevent aliasing errors in the digitizing process.

Photo Detector The signal conditioning unit for the photodetectors was located at the instrumentation trailer and provided power to the phototransistors that were mounted on the tank. The unit consisted of an impedance transformation circuit, which decreased the response time of the phototransistor used to detect the flame luminosity. The circuit is shown in Fig. 2.26. The PNP transistor presents the phototransistor emitter with a low-impedance constant voltage which greatly reduces propagation delays caused by internal capacitance. Since the objective was to measure the time of arrival of the flame front and relative size of the photodiode signal, no attempt was made to calibrate the signal output into photometric units.

Breakwires The breakwire signal conditioning unit was designed and developed by Caltech. It was located in the instrumentation trailer and provided power to the breakwires that detected the movement of the weak partitions. The conditioning unit consisted of a debouncing circuit

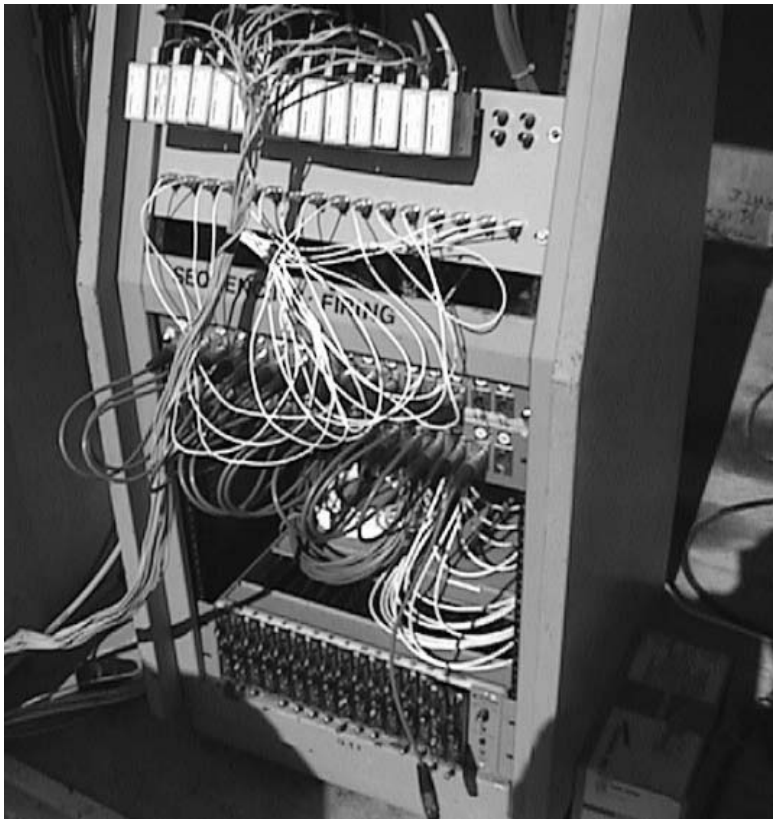

Figure 2.25: Thermocouple signal conditioning with patching.

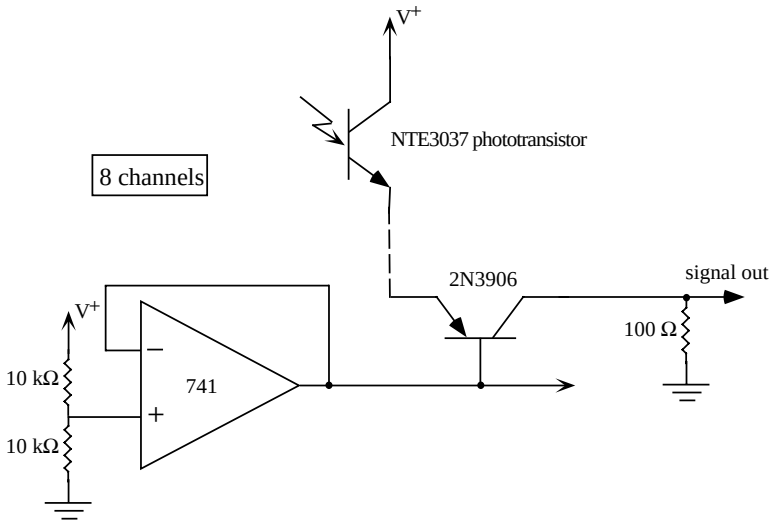

Figure 2.26: Photo-detector signal conditioning circuit.

that converted the continuity break from the breakwires into a step-function signal output. The conditioning circuit is shown in Fig. 2.27. A 7474 flip flop is connected as a latch that switches

to high when the detector circuit is broken.

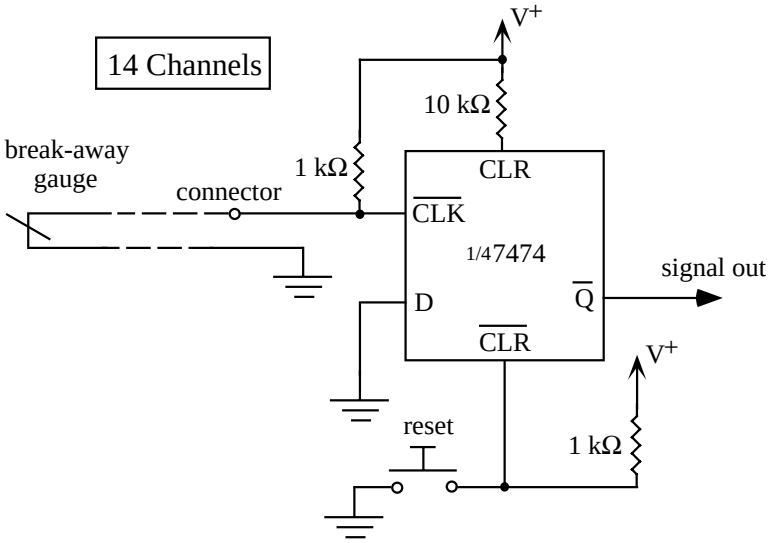

Figure 2.27: Breakwire gauge signal conditioning circuit.

2.5.2 Recording Systems

The recording systems comprised 83 discrete channels. A detailed description of the specific types of recording hardware and software is provided below.

Digital Recording This was accomplished by the use of 26 channels of high-speed digitizers (to 200 nanoseconds per point maximum for the tests, the digitizers operated at 5.0 microseconds per point), with 512 Kbytes of memory per channel, 12-bit analog-to-digital converters, and with the use of a 64-channel (not all channels utilized) digitizing system which digitized (12-bit) at the 1.0 millisecond per point rate, and had a 10-second usable record length, per channel. These two types of digital recording systems were controlled by PC-type computers using LabView software that had been previously modified to include setup configuration tables, selection of digitizing rates, memory allocation, and other menu-based macros which controlled the recording system's operational parameters. Through the PCs, "quick look" plots could be generated on laser-jet printers of all channels within 15 – 20 minutes after the event. This allowed for data review to assess the quality of the test information and the integrity of the sensors before the next scheduled test. Any anomalous behavior of the sensors would dictate repair or replacement before the next test was performed.

Analog Recording Two 14-track Honeywell 101 instrumentation grade tape recorders (one operating in the Wide Band Group II mode, DC-500 kHz, and the other in the Wide Band Group I mode, DC-80 kHz) were used to provide selected primary channel recording, and to provide backup recording for other critical measurement parameters. Post event, the recorded

analog sensor signatures were digitized with the digital systems described above for further data analysis and generation of the necessary hard copy for data review and analysis. The digital and analog recording systems are shown in Fig. 2.28.

Figure 2.28: Digital and analog recording systems.

Weather Recording The six channels of weather data were "data logged" in 24- to 48-hour periods. This data was subsequently downloaded into the digital recording computers for documentation of event time weather data and for continuous recording which provided a data base of test site climatic conditions (see Appendix D).

Patch Cable Interconnections Figure 2.29 shows the instrumentation van patch panels which interfaced the transducer, signal conditioning, and recording equipment. Each night, the patching was disconnected to prevent potential static and lightning voltage potentials from damaging the equipment.

2.5.3 Photo-instrumentation Systems

Test photography consisted of eighteen cameras that provided photographic coverage of the 1/4-scale tests. Each camera had a unique function that provided data or documentation for the testing. A description of this photography is detailed below.

High-speed Photography A total of seven high-speed cameras (DBM) were utilized in the photographic documentations of the fuel-tank tests. They consisted of intermittent pin-registered 16-mm cameras operating at 400 frames per second. The cameras were fitted with adjustable shutter mechanisms which allowed complete control of film emulsion exposure times. ARA

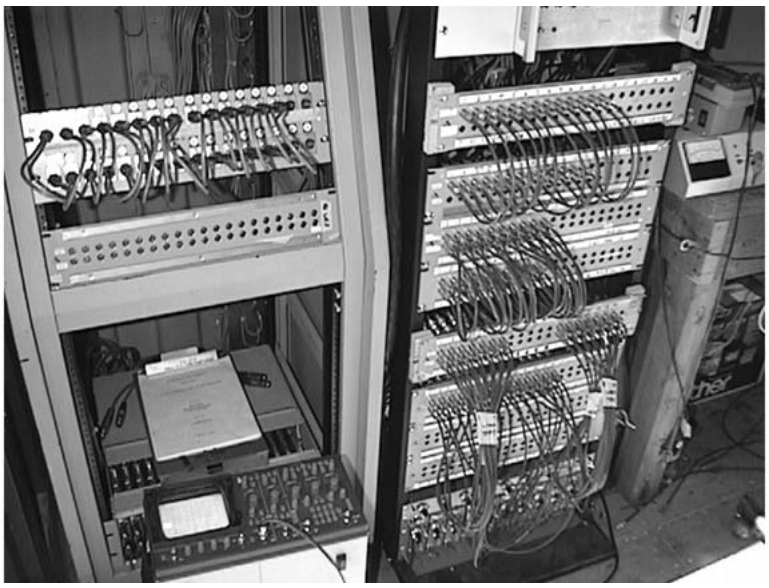

Figure 2.29: Patch panels.

chose VNF 2239 Ektachrome reversal film for the test series due to the slow ASA of 160, which resulted in high-resolution images.

High-speed Overview Cameras Two high-speed cameras provided overviews of the test chamber from two different angles. This provided information of partition failure as well as documentation of the fuel venting and combustion process when partition failure occurred. A high-speed camera is shown in Fig. 2.30.

Combustion Photography To document the flame propagation and fuel lofting inside the tank, ARA designed a special lighting system to photograph through the tank's Lexan windows. Laboratory tests showed that a shadowgraph or pseudo-schlieren system was needed so that small changes in gas density gradients could be detected. The prototype optical system consisted of an old-style carbon-arc lamp, 12-in fresnel lens, a "test chamber," and a 35-mm camera. Several heat sources were used to characterize the optional density resolution capability of the optical system. These heat sources included an open alcohol flame, a butane flame from a lighter, and a propane torch. One of the objectives was to obtain good depth of field across the length of the five-foot tank fixture. To do this, the lenses on the high-speed cameras had to be set at f:16 aperture or numerically higher. The camera was approximately 50 feet away from the test fixture. The test results proved that adequate lighting could be provided from an arc source, and that the pseudo-schlieren system design was adequate for the combustion documentation requirements.

Based upon the laboratory testing, the light source selected for the test series consisted of readily available sealed arc lamps which had rare earth metals to provide good color temperature balance for the daylight film. The source size of the lamp was about 0.3 inches, which pro-

Figure 2.30: Photo-instrumentation cameras: video camera (foreground), high-speed 400-fps DBM camera (background).

vided the small source (point source) necessary for optical imaging used in this photographic approach. The optical system was tested in the ARA laboratory with the camera distance set at 70 feet. The high-speed camera lens was set at f:32 using a neutral density filter of 1.9. These tests demonstrated that more than an adequate amount of illumination would be available for the upcoming test series. Again, an open alcohol flame and a propane torch were used for laboratory testing to demonstrate that adequate density resolution was achievable for combustion diagnostics.

The 1/4-scale tank was designed and configured for the combustion photography. The sides of the tank incorporated 1.25-in Lexan windows that were held in place with a removable steel framework. The interior side of the Lexan was protected by a 1/8-in expendable Lexan sheet that was replaced after every test due to the thermal and blast effects, and scraping caused by the movement of the partitions. These windows enabled a view through bays 1 to 6. The line-of-sight view through the tank bays resulted in grouping together bays 5 and 6, and 3 and 4. Therefore, there were four cameras, one each viewing bays 5/6, 3/4, 2, and 1. Each bay grouping had a separate light source, fresnel lens, and camera system to provide coverage of the flame front propagation.

A wooden bench was constructed to secure the light sources, along with a cover, to protect the equipment from normal test site climatic conditions. Figure 2.31 shows the light source configuration. An 8-ft by 10-ft portable building (connex) was used to house the light source power supplies. The high-speed cameras were mounted on a bench located approximately 60 ft from the test fixture (see Fig. 2.32). This equipment was also housed in an 8-ft by 10-ft connex. Optical alignment was crucial as the light source, high-speed cameras, and the center of the tank needed to be in perfect alignment due to the stringent optical requirements of the pseudo-schlieren system.

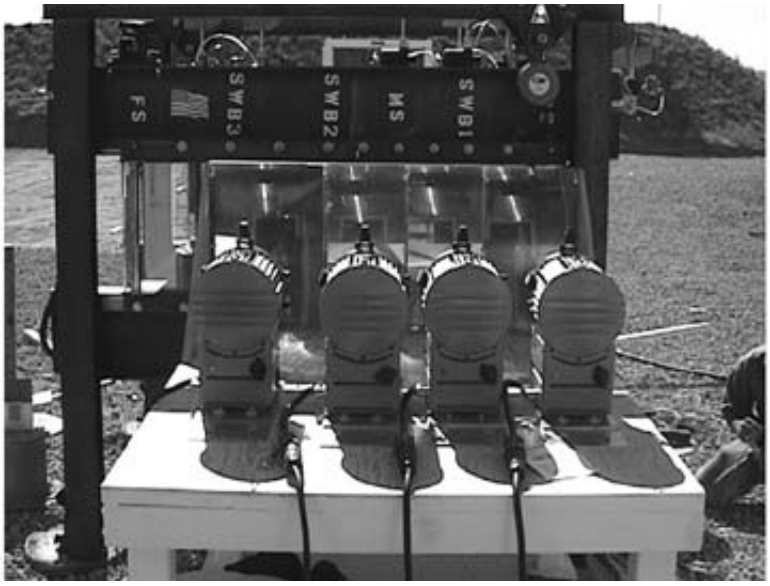

Figure 2.31: Combustion photography light sources, viewed from behind.

Figure 2.32: High-speed cameras for pseudo-schlieren combustion photography with beam splitters and video cameras.

To provide quick-look data, two high-resolution video cameras were installed in the combustion camera bunker. These cameras provided the same views as the high-speed cameras but at a greatly reduced framing rate. To get the same view as the high-speed cameras, glass beam splitters were used to divide the image into two optical paths. The video cameras and the beam splitters could be moved to any of the four locations to provide “quick looks” immediately after the shot. The video data from both cameras were recorded in the instrumentation trailer

on SVHS and 3/4-inch format video recorders.

A fifth high-speed camera was added at the beginning of Shot 20. This camera provided a full view of all bays for backup of the other four high-speed cameras. Different apertures were set depending on the test conditions to optimize the film records. This camera proved to be important during the fuel shots because the weak partitions can be viewed as they are being ejected from the test fixture.

Video Overview Cameras Three video cameras recorded the tests from different viewing angles (see Fig. 2.30). The effective shutter speed of these cameras was one-thousandth of a second. This provided a "quick look" after the test for safety assurance, and for rapid analysis of individual test results. The video signal was transmitted via cable to the instrumentation van where it was recorded on SVHS tape (Fig. 2.33). Panasonic AG-1980 SVHS recorders allowed stop-action viewing for a quick, detailed analysis. A fourth video camera was set up to get a close-up view of the tank during the fuel tests.

Figure 2.33: Video recording and monitoring equipment.

70-mm Photography A 70-mm motion picture camera was provided to generate high-resolution pictures of the test events. It operated at 20 frames per second, with an exposure time of 350 microseconds, to stop the action. Kodak Ektachrome 100 film was used for its small grain size and high-resolution prints. This camera cannot be viewed with a conventional projector as it is not a pin-registered camera, however, selected prints (made from negatives) provide very high resolution. Figure 2.34 shows an example of an image from this camera.

Timed SLRs Two Single Lens Reflex (SLR) cameras were used to provide very high-resolution images of the test event. Both SLR cameras were fitted with motor-wind drives which

Figure 2.34: Print from 70-mm motion-picture camera. Test 27.

allowed continuous framing rate capability after event time zero. The first frame for each of these cameras was timed for event time zero. One SLR camera ran at four frames per second, and the other operated at 8 frames per second. Kodak Royal Gold 100 was used for these cameras as well as Fuji Velvia slide film in some tests. All of the timed SLR photographs were assembled in an album for future reference of each test event. Figure 2.35 shows an example sequence.

Documentation Cameras Two hand-held cameras were used to document the 1/4-scale testing. One camera was a 35-mm film camera that provided documentation before and after each test and also for general test site documentation. These photographs were assembled in photo albums for reference for each test.

A digital camera was also used for documentation purposes because of its quick-look capability and also the ability to send electronic pictures over the internet for progress reports and clarification of test progress and technical issues. The images were also used in technical discussions during program review meetings.

Photographic Data Reduction One of the main intentions of the test series was the high-speed photo-documentation of the flame propagation inside the tank bays. To best visualize this process it was necessary to view all of the bays at the same time. Recall each of the com-

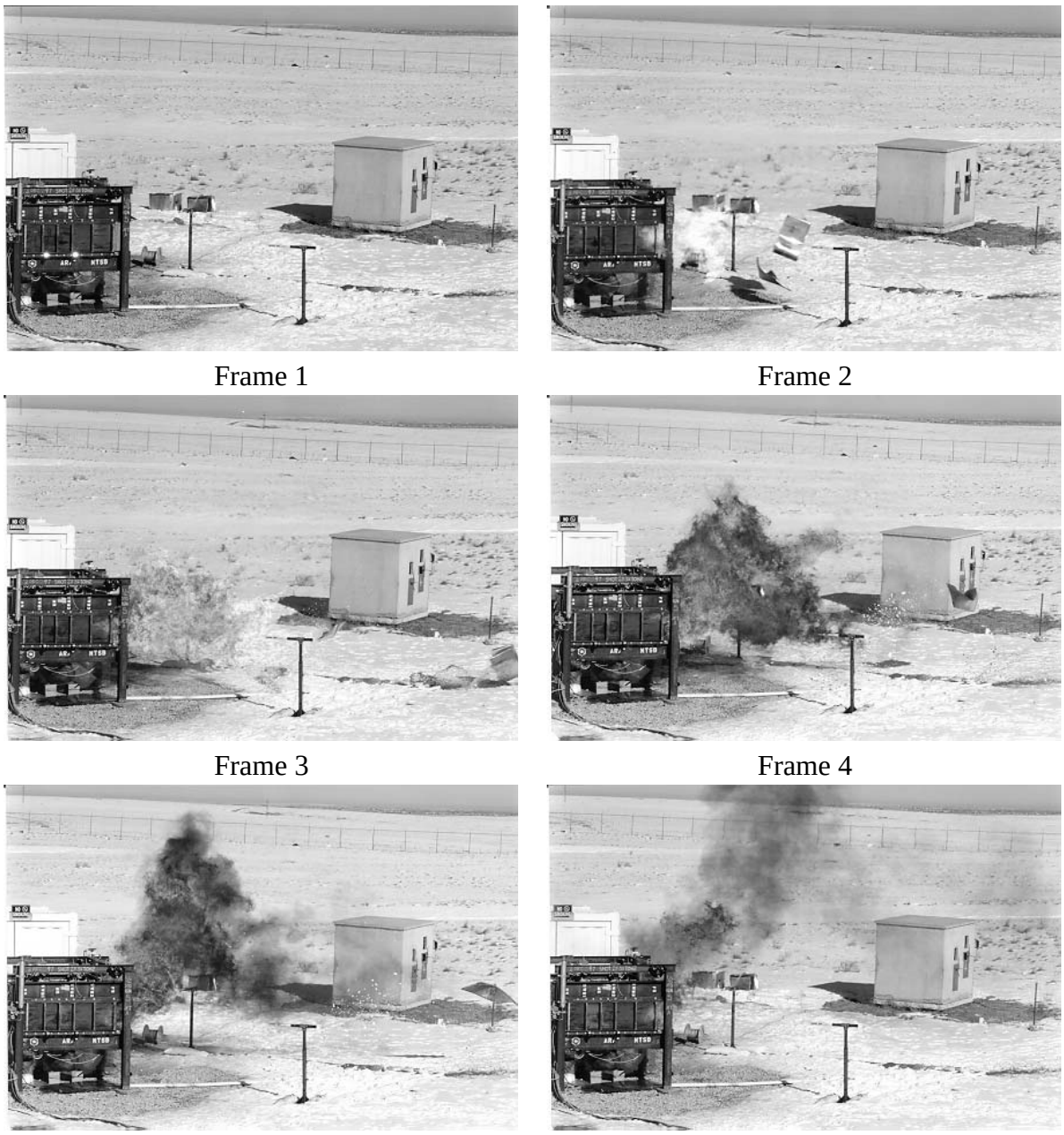

Figure 2.35: Timed frame sequence from 35-mm camera. Test 28.

partment groupings was photographed with individual cameras; thus the images from all four cameras needed to be compiled onto one medium. Video format was the medium chosen, as it provided high-quality format and allowed merging discrete records into a composite format.

A commercial video lab in the Denver area copied all of the 16-mm light source high-speed film to video. Once it was copied to video, it was then digitized and stored on a computer

hard drive. Using non-linear editing, all of the video sequences were assembled on one video frame. Adjustments such as slight differences in 16-mm film speed, event time zero, and slight variations in image size were made. The assembled video composite portrays the entire test fixture and all combustion bays, as if one camera photographed the entire fixture. Detailed combustion information could then be derived from viewing the flame propagation from one bay into the next.

2.6 Firing System

ARA designed and built an automated electronic firing system capable of delivering 15.8 joules of energy to the firing line. The unit has a 1400-microfarad capacitor that was charged to approximately 150 volts. A rapid discharge was obtained by an SCR firing circuit that was able to deliver the energy in less than 10 microseconds. The discharge characteristics are dependent on the looped inductance of the firing line and on the resistance of the electric match or filament ignition source used.

This system incorporated an arming key that effectively locks out the firing system during the arming process. This prevented unauthorized operation of the system while the experiments were being armed. The firing line also was shorted both at the instrumentation trailer and at the test fixture. The firing system was controlled by the firing sequencer and timer. The sequencer charged the firing system at T minus 30 seconds, and at T minus 0 seconds a firing pulse was sent to discharge the unit into the ignition source. The system was manually armed with the safety key to meet on-site safety requirements.

Due to the safety considerations given the gaseous mix, and the possibility of a failure of an electric match or a bulb filament, a second electric match or bulb filament was installed in another bay. Two separate firing lines were used.

After Test 1, it was concluded that the electric match was not a good candidate for an ignition source due to pyrotechnic fragments being launched at initiation. This created multiple sources of combustion which produced anomalous early-time combustion phenomena. A filament from a 12-volt bulb was used in subsequent tests to provide “point source” initiation. Comprehensive testing on this system proved that it was sufficient to reliably ignite the gas mixtures encountered in this test series. During Tests 2 and 3, an electric match was used for a backup. For Tests 4 through 30, an open filament was used as the backup ignition source.

2.7 Modifications

During the test program, various problems were encountered. Most of these were solved on the spot with simple modifications to the test facility or operating procedures. Two of the more significant problems are discussed below.

Sealing of Strong SWB3 During the first four tests, leakage of the combustion products around the sides of SWB3 was seen in the video footage. At first, this was attributed to the

choice of sealant, but we later discovered that the partition was moving forward under explosion pressures. The clamping force from the retainer bolts was inadequate. After Test 4, SWB3 was completely removed and cleaned of silicone to reduce lubrication effects. Then SWB3 was reinstalled, and three 1/4-in holes were drilled in the top and bottom angle brackets, and through the top and bottom plates. These provided a snug fit for 1/4-in socket-head cap screws which were used to provide additional shear resistance. The screws were long enough to place the full-diameter shoulder at the shear point, and alloy steel screws were used for the maximum possible strength. In Test 5, these were sheared off. Afterwards, SWB3 was tapped as far forward as possible with a mallet, the holes were re-drilled and two new ones were added in each bracket. These generally held, although the screws in the outboard holes were deformed over the course of testing. After SWB3 was secured in this manner, leakage was greatly reduced at the sides of the partition. The top and bottom seals were occasionally broken by motion of the outer edges of the panel, indicating the need for a stronger mounting bracket.

Blast Pressure Gauges Three blast pressure gauges were initially mounted along the centerline of the tank, facing the open end. The first gauge was 30 ft from the tank, and the other gauges were spaced at 5-ft intervals. In the first weak partition test (Test 17), we found that the blast wave signal was much smaller than anticipated. After some discussion, we decided that the FS may be deflecting the blast to the sides as it fails. For Test 18, the two farthest gauges were moved to 15 ft from the tank, at a 45°angle (one on each side). In addition, impact from the FS and the water bottles damaged the original gauge protection post, so this was replaced with a much stronger version that was partially buried for strength. Over the next few tests, blast wave pressures were still very weak and difficult to interpret, and the guard post (and water bottles) were repeatedly damaged, so the axial blast gauge was removed. The remaining off-axis gauges were found to be of limited use and were no longer recorded after the weak-partition tests were concluded.

Chapter 3

Test Operations

Test operations were carried out jointly by ARA and Caltech at ARA's test site. Activities were carefully coordinated in order to meet a tight schedule.

3.0.1 Overview

ARA prepared the test site infrastructure, photo-instrumentation, and data acquisition system between July and October, 1997. Caltech took delivery of the tank structure on October 14, completed the final preparations at Caltech, and transported the tank to Denver on October 16, 1997. The first test was carried out on October 23, 1997 and the last test was carried out on December 17, 1997 (see Table 1.2). It took four to five members of the team at the site to prepare for and carry out each test.

A test was carried out on the average about every three days. There were seven days when two tests were carried out in a single day. This was possible only when all-strong, vapor-fuel configurations were tested. Tests with Jet A liquid and weak partitions required substantially longer preparation and clean-up time. There were several weeks in which no testing was possible due to severe snow and cold at the test site. There was some development time associated with the manufacturing panel insert in SWB2, the weak panel construction method, and the cargo bay model. We had originally scheduled 8 weeks for 26 tests and the actual test period was 13 weeks for 30 tests.

As part of the preparations for the testing, ARA and Caltech both developed operating and safety procedures. A written SOP (Safe Operation Procedure) was in place by the time of the first test. Some modifications were made to accommodate changes in the ignition system and fuel loading but otherwise this SOP served for the entire test series.

A preliminary test matrix was also in place well ahead of the first test so that the conditions for first set of tests were fixed. The test matrix was modified following the October 27 and November 23 project reviews.

3.1 Test Team and Activities

The testing activity was a team effort led by Joe Shepherd of Caltech and Larry Brown of ARA. The Caltech members were Shepherd, Chris Krok, Julian Lee, and Pavel Svitek. The ARA members were Brown, Tim Samaras, Bob Lynch, and Peter Dzwilewski. The day-to-day operations of the test site were carried out by Tim Samaras, Larry Brown, Chris Krok, and Julian Lee with assistance from Pavel Svitek (Caltech) and Bob Lynch (ARA) on some tests.

The test team was responsible for the following activities:

1. Technical quality
2. Adherence to test schedules
3. Jet A simulant fuel development
4. Test fixture design and implementation
5. Instrumentation design, calibration, installation, operation, and maintenance
6. Optical designs
7. Design and implementation of photo-instrumentation systems
8. Test implementation
9. Documentation of test conditions
10. Quick-look data evaluations
11. Data processing and distribution
12. Data analysis
13. Reporting

The test matrix development and planning were carried out by the test team jointly with Merritt Birky, Vern Ellingstad, Dennis Crider, and Dan Bower of the NTSB. Numerical simulation and analysis were carried out by Mel Baer and Robert Gross of Sandia National Laboratory (SNL), Kees van Wingerden of Christian Michelson Research (CMR), and also Paul Thibault and Rick Link of Combustion Dynamics, Ltd (CDL). The test team, NTSB, and analysis groups met together twice in Denver to review the results and develop revised test plans.

3.2 Test Site Security and Safety

ARA was responsible for developing and maintaining security at the site. ARA also had the overall responsibility for safety.

3.2.1 Physical Security

Physical security measures protected the energetic materials (electric matches and explosive gas mixtures), instrumentation, photo-instrumentation, and the test fixture. The ARA Test Facility is remote from the Denver area and is, therefore, subject to possible intrusion. The 55-acre test facility is located approximately two miles off the main access road and is protected by two security gates. The site itself is surrounded by a security fence topped with concertina wire to discourage breaching activities. The test facility was further secured by padlocked and security-alarmed buildings. The electric matches were stored in an approved explosive bunker on the ARA test facility. Routine personnel visits to the test site during non-test times augmented the physical security of the site.

3.2.2 Safety

The primary safety concerns were with the handling of the electric matches and with the explosive gas mixtures, particularly when the test fixture was loaded prior to testing. ARA employees with Colorado Explosive Licenses handled all electric match experiments. All tests were conducted in strict accordance with established and approved Standard Operating Procedures (SOPs). In addition, all site personnel were required to understand and abide by the ARA General Safety Procedures established for the test site. First aid supplies, protective clothing and equipment, fire extinguishers, and warning lights were located at this facility. On active test days, a daily information meeting was conducted by site personnel prior to starting test preparations.

3.3 Test Procedures

3.3.1 Pre-Test Preparations

Pre-test preparations consisted of facility activation, construction and installation of test hardware, calibration of equipment, instrument checkouts (which included electronic and photographic systems), and predictions of peak pressure, temperatures, fireball, and fragmentation effects. The checkout procedures included dry runs of the firing sequence (with ignitors installed), triggering and functioning of the camera systems and also the signal conditioning and recording systems, and stimulating the transducers to determine operability. Depending on the test condition for each test, the fuel vapor and Jet A volumes were selected and prepared, the required partitions were installed, windows were installed and a leak check was performed.

Specific pre-test preparations for the different test conditions included setting the sensitivity level of the recording system for expected transducer outputs, selecting camera field-of-view, and adjusting exposure levels. The sensing systems were individually externally stimulated to produce an electrical output which was observed and verified by the recording systems. Likewise, the photographic systems and the video recorders were tested. In addition to standard checkouts at various times during the test program, calibration procedures were performed for the entire system in place. Selected transducers were pressurized to a known value (NIST

traceable) and the output voltage measured. A thermocouple calibrator unit was used to verify the accuracy of the temperature measurements. Only when all systems were checked for their operational readiness would the test countdown be initiated. The countdown included adhering to an SOP checklist of the ignitor installations, gas handling and loading operations, site assessment, and range clearance. Typically, these activities prior to the firing countdown would take 15–20 minutes, including a mixing period for the gas mixtures.

3.3.2 Countdown Procedure

In addition to the SOP used for each test scenario, a detailed instrumentation, mechanical, and gas handling checklist was used for all tests. This sequence of operations began with site clearance and energetic material loading preparations. The instrumentation components were systematically checked prior to gas loading and just prior to the 60-second countdown.

With all in readiness, the test site was again checked for unauthorized or unnecessary personnel and the fuels were loaded into the test fixture. During all pre-test activities dealing with the gas loading and pre-firing test procedures, the firing systems and the ignitor lines were shorted as a safety measure. The instrumentation van had direct and positive control of test site safety and could abort the timing and firing systems in the event of safety or performance-related problems.

A digital sequence timer was used to provide automatic control signals to the data recorders, camera systems, and the firing circuit (as described in Section 2.4). These systems were thoroughly tested during the dry runs preceding the loading of the energetic materials into the test fixture.

When all pre-firing checklists and responsibilities were completed, the energetic material handler authorized the instrumentation personnel to proceed with the test. At this point, all personnel were required to be in their designated locations in accordance with the SOP and the checklist procedures. The test sequence was then initiated.

At the point when the tank was sealed up and the igniters were installed, operations with the gas and liquid fuels were initiated. The following steps were carried out by the Caltech participants:

1. Zero MKS readout and read atmospheric pressure:
    a. Turn on vacuum pump.
    b. Open vacuum valve.
    c. Wait for readout to stabilize and zero meter.
    d. Close vacuum valve, open isolation valve and tank vents.
    e. Read atmospheric pressure.
2. Leak test tank:
    a. Calculate starting tank pressure for gas fill.
    b. Close vent valves, open isolation and vacuum valves.

c. Evacuate tank approximately to desired pressure.

d. After pressure settles, check for leak rate. Proceed if leak rate is < 0.5 Torr/min. Otherwise, attempt to fix leak.

3. Make final tank preparations:

a. Load 2.9 liters of Jet A into reservoir (if needed).

b. Connect firing lines.

c. Turn on sync strobes and schlieren lamps.

d. Check gas bottles (i.e., regulator setting, available gas).

4. Fill tank:

a. Recheck gauge zero and atmospheric pressure per above.

b. Recheck leak rate.

c. Record atmospheric data.

d. Open mixer valves.

e. Re-evacuate to start pressure.

f. While tank is at starting air pressure, open liquid fuel valve. End of liquid fill is shown either by increase in tank pressure rise rate or bubbling seen in schlieren video monitors.

g. Re-evacuate tank to gas fill start pressure.

h. Fill gaseous fuel by modulating gas fill valve.

i. When gas pressure comes to within 1 torr of desired value, mixing cycle may begin.

j. Mix for 15 minutes, adding fuel gas as needed to make final pressure corrections.

k. Turn off mixer, close all valves.

l. Open vent valves if required.

m. Ready to fire shot, turn control over to test condutor.

Post event, the gas and energetic material handlers assessed the “quick-look” data to provide assurance that combustion was achieved in all test fixture bays. This assessment also included evaluation of the video recordings which were used for site surveillance and event documentation. The energetic material handler inspected the test bed area for any unreacted energetic material and any other potentially unsafe conditions, such as fires or afterburning, and shorted the firing lines. Once test site conditions were determined to be safe, the facility was prepared for re-entry and radio communications to that effect were relayed to other on-site personnel so they could resume normal operations.

3.3.3 Post-Test Procedures

Quick-Look Data Review Immediately after each test, the instrumentation personnel performed data storage backup to prevent accidental loss of data and then automatically plotted the pressure and temperature test data for "quick-look" evaluation. If required, the data from the tape recorders was digitized, displayed, and plotted for evaluation of the analog sensor signatures. This process provided a basis for analyzing the preliminary results of the test, provided insight on whether all bays experienced combustion phenomenon, provided assurance that it was safe to re-enter the site area, and produced information on the relative performance of the sensor suites. This assessment also provided the basis for replacing transducers, changing transducer ranges, timing changes, and other instrumentation adjustments to enhance and optimize test results.

Photographic and Video Review Immediately after each test, the 16-mm high-speed camera film was prepared for overnight shipment to a film processing laboratory in Yuma, Arizona. Normal film turnaround time was three days. As soon as the film was received from processing, ARA and Caltech personnel performed a film review of test information to evaluate the combustion results and made exposure adjustments as necessary to compensate for test conditions.

Video records were reviewed post-event in the instrumentation van to assess their quality and adjustments were made as required. Video tape backups were made to archive the video information throughout the test series.

The 35- and 70-mm film records were processed in laboratories in the Denver area and were routinely reviewed for quality and completeness of documentation.

Chapter 4

Test System Performance

4.1 Overview

Overall, the test fixture, instrumentation, and photo-instrumentation performed extremely reliably and with very few system failures.

Out of thirty tests, there were four tests in which instrument data was lost in one or more channels. In one of these (Test 2), all seven channels of the Endevco data were contaminated by noise and in another (Test 6), all eight channels of the PCB data were lost due to no power to ICP units. Test 2 was repeated and the lost data were not essential in Test 6, since the PCB data were redundant in that test. In Test 5, one channel of Endevco data was lost, presumably due to a loose connection at the transducer. In Test 20, one channel of Endevco data was severely affected by loss of signal in the middle of the burn, again presumably due to a loose connector. Overall, out of thirty tests and a total of about 1,400 data records, less than 17 records were affected, sightly more than 1%. More details about the PCB performance and the affected data records are given in Appendix A and Chapter 6.

The photo-instrumentation systems performed well despite harsh weather conditions. However, four cameras had to be replaced during the test series due to mechanical malfunction. Since some problems with the cameras could only be diagnosed after the film returned from processing, there was some loss of information associated with these failures. A list of the specific cameras and tests affected are given in the Appendix A.

The performance of the major components of the test system will be briefly described in this section of the report.

4.2 Test Site

The ARA ordnance test site proved to be a serviceable and effective location for this series of tests. Although spartan, there were sufficient services and infrastructure to accomplish the job. Heavy equipment was available nearby to service the major testing requirements of site development, test fixture off loading/positioning, and installation of the simulated cargo bay on the test fixture for the last test (Test 30). The commercial on-site power was reliable. There

were no significant safety or security issues other than the occasional horseman near the fence and stray bunnies in the firing area.

The difficulties encountered were weather-related; the test series ran later into the fall than anticipated. Cold weather was nusiance for test preparation and at times made work outside impossible. Two major snow storms hit the test site area, which was unusual for the months during which the tests were conducted. Only a few test days were lost due to drifting snow covering the site and access road.

The test site was able to accommodate this test series and another scaled-rocket motor acoustic test series without any major conflicts. The remoteness of the test site provided virtually unlimited test schedule changes, and due to the large buffer area surrounding the 55-acre site, the tests were unaffected by noise, fragmentation, or fireball limitations.

4.3 Transducers

The transducer suite selected to document the 1/4-scale test fixture generally performed reliably and required minimal maintenance throughout the test series. Pressure was measured using Endevco and PCB transducers, flame-front time of arrival was measured using fine-wire thermocouple gauges and phototransistors, and weak partition failure was detected using motion switches. These transducers were previously described in more detail in Section 2.4.2.

The Endevco transducers used to measure the quasi-static pressure performed without failure throughout the test series. The thermal shields provided adequate protection for the transducers, and no maintenance or part replacement was required. Pressure calibration checks performed on the transducers before, during, and after the test series in the ARA laboratories showed a calibration shift of less than 2%. In one test (Test 2), the output signal from the gauges was contaminated by 120-Hz hum interference. This problem was attributed to a ground loop in the signal amplifiers and did not recur after it was corrected. In all other tests, the amount of baseline noise was low, and typically resulted in an uncertainty of approximately ± 0.03 bar. There were two tests in which signals from one gauge were either lost or intermittent due to loose connectors. The effects of flame-induced thermal shifts and frequency response are further discussed in Section 7

Internal PCB transducers were used to measure possible dynamic pressures from shocks and acoustic waves. No PCB gauge malfunction occurred during the tests but the data was lost in one test due to the ICP power supply not being turned on. These gauges were not thermally shielded using the same system as the Endevco gauges. Instead, a thin layer of vacuum grease was spread over the transducer head. While this minimal thermal shielding allowed for rapid response times, it did not protect the gauge from the thermal shifts which rendered the later part of the signal unusable. In three cases, the protection was completely inadequate and strong thermal effects are observed even in the initial portion of the traces. This is discussed in more detail in Section 7. Furthermore, the transducers appear to have suffered some calibration shift due to the thermal events. These calibration shifts were approximately 15% in the worst case (see Appendix A). The baseline noise on the signals from these gauges resulted in a low uncertainty of approximately ± 0.03 bar.

External PCB transducers were used to measure possible shock waves produced outside the test fixture by rapid venting of the combustion products in tests with weak partitions. Since they were not in direct contact with the combustion products, thermal shifts were negligible. Although they performed adequately, their signals were of limited use due to their small amplitude and their complexity. After initial tests, the signals from these gauges were not recorded for every test.

Photodetectors were used to measure the flame-front arrival at various points in the tank. These gauges operated reliably and without failure throughout the tests, requiring only occasional cleaning of dirt and soot from the glass window on the head of the gauge. Due to the unusual wiring arrangement, in which the shield of the BNC connectors was the positive supply voltage, care had to be taken to avoid contact between unconnected photodetector cables and the grounded metallic tank surface. The noise in the gauge signals was typically very low, at approximately 4 $\mathrm{mV_{rms}}$ compared to the typical maximum signal amplitude of 0.2 V to 2 V.

Fine-wire thermocouple gauges were also used to detect the arrival of the flame front at various points in the tank. These gauges were mounted in brittle ceramic tubes and were designed to break during tests so as not to interfere with the motion of the weak partitions. The thermocouples ceased to provide a signal when breakage occurred, and were replaced when necessary. The thermocouples performed reliably and broke cleanly when struck by the failed partition. The teflon ferules provided an adequate seal for the gauges but required replacement after being tightened and loosened approximately 5 – 10 times. Great care was required to avoid breaking the delicate gauges during installation. The signal noise typically caused an error of approximately $\pm 13\,^{\circ}\mathrm{C}$.

Motion detector switches were used to detect the moment of failure of a weak partition. Each switch was cleanly snapped off when struck by a moving partition, and a new set of motion switches was installed before each test involving weak partitions. However, the detectors were only designed to trigger when a partition moved forward. In some cases, the high-speed cameras showed partitions moving backward first. Also, when a switch remained intact after the initial explosion and a fire persisted in the tank for 5 to 10 seconds after the initial explosion, the switch was triggered by being subjected to intense heat even though it was not struck by a panel. The tips of the breakers consisted of a wire jumper soldered across the two sides of the circuit board strip; the solder melts under sustained heat and the jumper can fall off, sending a signal to the recording equipment. However, this can only occur if a switch is not struck by a panel during the initial explosion and subsequent sustained heat is applied to the switch over a long period of time, such as in the case of a post-explosion liquid fuel pool fire.

There is only one instance for which this is known to have happened. In Test 28, SWB3 managed to rotate over one of the bottom detectors and leave it completely intact. The subsequent fire in the tank was presumed to have melted the solder, causing the jumper wire at the end of the switch to fall off, causing that detector to produce a trigger signal. The signal was not recorded by the acquisition system however, because the time required for this exceptional type of trigger was longer than the recording time. Hence there does not appear to be any ambiguity as to whether a switch is truly triggered by a moving partition or by heat. The interpretation of the motion switch signals is further discussed in Section 5.4.1. The noise on the motion switch signals was negligible before trigger occurred due to the low-impedance short

circuit configuration of the gauge. It was typically ± 15 mV compared to the signal amplitude of about 4 V.

4.4 Signal Conditioning and Data Acquisition Performance

The signal conditioning systems operated without major malfunction throughout the tests. The thermocouple signal conditioning was installed in the gas handling connex, which was located approximately 10 feet from the test fixture. These gauges required the use of line drivers to meet the laboratory-comparable signal-to-noise ratios. The signal conditioning equipment for the remaining gauges was in the instrumentation van. All pressure, motion sensor, and flame detection signal conditioning performed well with little maintenance required, although a couple of signal amplifiers had to be replaced.

The digital and analog acquisition (recording) systems did not fail during the test series. The multiple computers controlling the acquisition systems performed post-event hard-copy and data archival procedures for each test. The three digital recording systems performed reliably and did not cause any test holds, missed-trigger conditions, or other problems that could have affected the test schedule. The ARA modified LabView software produced reliable configuration, calibration, quick look, and convenient hard-copy information.

4.5 Timing and Firing Performance

The timing system provided accurate and reliable timing and sequencing operations of the satellite instrumentation and photo-instrumentation systems that documented the test events. This system provided sequenced operation of the diagnostic systems from T minus 60 seconds, through event time zero, and through T plus 10 seconds.

The firing (fuel vapor ignition) system provided reliable operation of the electric matches and the ignition wires. A change was made from electric matches to ignition wires after the first test, and changes were made to the firing system. The firing power supply was modified and rigorously tested to ensure sufficient heating of the ignition wire with current limiting to prevent wire burnout. An excessive current could result in pieces of ignition wire scattered at ignition, causing undesirable multiple ignition sources, such as experienced with the early use of the electric matches.

During the test campaign there was never a failure of the first firing line. The only problem that surfaced was a sympathetic ignition of the backup electric match when the bulb filament was fired on Shot 2. Three tests conducted at the conclusion of the program proved that there was enough radiated electromagnetic energy from firing the primary bulb filament to induce sufficient current into the backup firing line to ignite the electric match due to the extremely low all-fire energy for these devices.

4.6 Photographic and Optical Performance

The photographic systems provided high-quality films, videos, and photographs of the combustion phenomena throughout the test. The pseudo-schlieren system was robust enough to withstand the rigors of the field environment. The light sources were found to be sensitive to vibrations, hence protective wood boxes were used to protect them against indirect blast wave overpressures during the weak partition tests. The sources were also turned on at the last possible moment in the test preparation sequence in order to alleviate over-heating. With these precautions, the system functioned reliably throughout the test series. The combustion photography demonstrated a high degree of optical density resolution sufficient to produce clear video composite production and reproduction. A listing of DBM camera performance in all tests is given in Table A.6 (p. 364).

The overview high-speed photography provided clear movies of the panel ejection during the weak partition tests. However, the amount of light was marginal during tests that were performed late in the day. Excessive wind was occasionally found to cause vibrations in the mirrors used to send the images to the cameras, but this problem was solved by tightening and reinforcing the mirror supports. The correct photographic field of views and aspect ratios were adjusted for all tests. Photography with the timed 35-mm cameras reliably generated high-resolution negatives which were useful for the Baltimore Public Hearing and for report generation. A compilation of dual sets of 35-mm pictures were arranged in photographic albums for test documentation and review. The video cameras were extremely useful in the "quick look" analysis of the data.

Four high-speed cameras suffered mechanical failures during this test series, possibly due to cold-weather operation. Backup cameras were fielded as mechanical problems occurred to maintain data returns. Additional cameras, high-speed and video, were used to produce additional photographic data in the event that other camera failures might occur.

Chapter 5

Data Analysis I: Individual Tests

Various methods were used to reduce and interpret the data. The first step was to plot and examine the quasi-static pressure data from the Endevco transducers. Based on this information, the apparent flame motion sequence was determined. This was then compared with schlieren information and time-of-arrival data from the photodetectors and thermocouples for confirmation and further insight. All of the data must be taken together in concert; for example, the schlieren system looks through two bays at once in the aft stations, so the film must be compared to other data to determine which bay is burning first. Likewise, pressure increases may be from combustion or venting from other bays. Other data can determine if a flame is present or not. The dynamic pressure data was added later to examine details of partition failure in the appropriate tests.

The static pressure data was also used to compute differential pressures across the partitions, partital ribs, and vents. Differential pressures are defined as positive if they act in the forward or starboard direction.

5.1 Time-of-Arrival Measurement

Photodetectors and thermocouples were used to determine the time of arrival of the flame at various points inside the test tank. The photodetectors provided a signal based on the luminosity of the flame when it arrived at the various points where the detectors were located on the the tank ceiling. Since the depth of the detector view was as long as the vertical tank height, the signals did not show a sharp rise when the detectors were triggered. If the flame front were flat and vertical, the photodetectors produced a sharper signal rise as the flame moved across the gauge window. Figure 5.1 shows a typical photodetector signal. The first peak at time zero was caused by the luminosity of the initiating filament. The subsequent arrival of the flame front at the detector window produced the second, larger peak. The level of luminosity varied greatly during the tests and the signal amplitude ranged from about 0.1 V to saturation of the signal conditioner at 0.5 V.

The time of arrival of the flame was determined by visual inspection of the photodetector signal as shown in Fig. 5.2. The signals from photodetectors L5 and L6 located in bays 2 and 1 respectively are shown with their corresponding time of arrival $L5_0$ and $L6_0$.

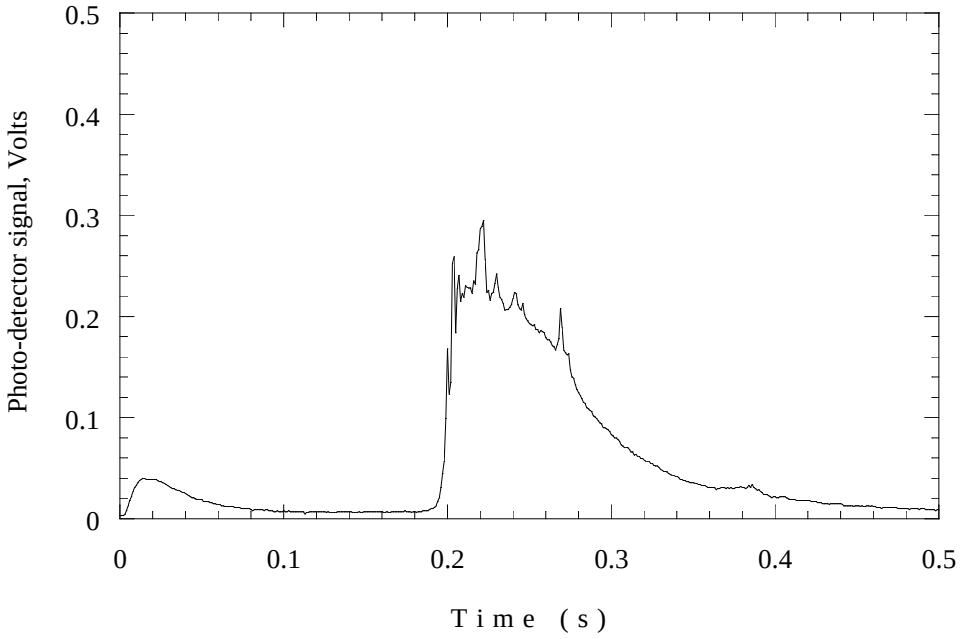

Figure 5.1: Photodetector signal in bay 2 for Test 6 with ignition in the bay.

The thermocouples produced a signal based on the flame temperature when the flame made contact with the transducer. A typical thermocouple signal is shown in Fig. 5.3. The maximum temperature indicated by the thermocouples varied between about 300°C and 1200°C. This will not be a true indication of peak flame temperature (estimated to be 1700°C) because the thermocouples take at least 20 to 40 ms to respond to a change in ambient gas temperature and the gas immediately begins cooling after the flame passes by. This lag time is simply due to the thermal mass of the thermocouple bead and the finite rate of heat transfer between the gas and the bead. Since the thermocouple signals were used only to determine the time of arrival of the flame, no attempt was made to quantitatively interpret the signal characteristics beyond the initial rise. In practice, it appeared that the thermocouples did not give a signal until the bay was nearly at its peak pressure, or burn completion. This is typically the case in the quicker burns, where the burn rate usually exceeds the response rate of the thermocouple.

The flame time of arrival at the thermocouple gauges was determined by visual inspection of the signal, similar to the procedure used for the photodetectors. Figure 5.4 shows the initial increases of T2 (bay 5), T3 (bay 6), and T10 (bay 2). The corresponding times of arrival for these thermocouples are shown as $T2_0$, $T3_0$, and $T10_0$. Since the thermocouples produce a signal at the moment of contact with the flame, the initial rise is sharper than for the photodetector signals and is easier to interpret. For this reason, the thermocouple data were primarily used in the analysis of the tests. In general, the thermocouples and photodiodes are usually in qualitative agreement (the order of ignition of the bays are the same) but not in quantitative agreement (the time-of-arrival values are different).

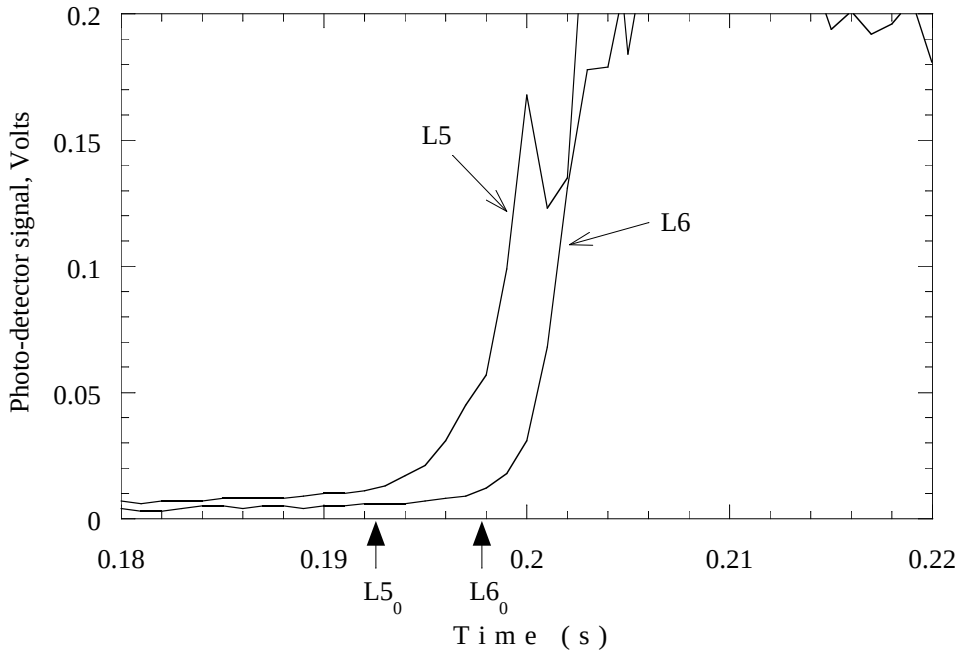

Figure 5.2: Two photodetector signals for Test 6, bay 2, with the corresponding time of arrival.

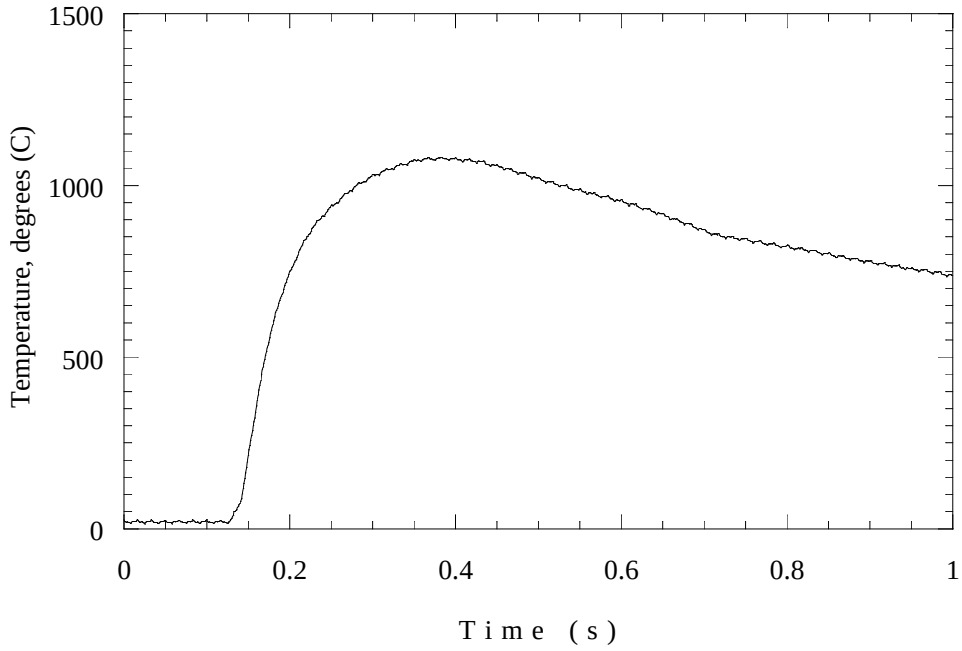

Figure 5.3: Thermocouple signal T3 for Test 4 in bay 6.

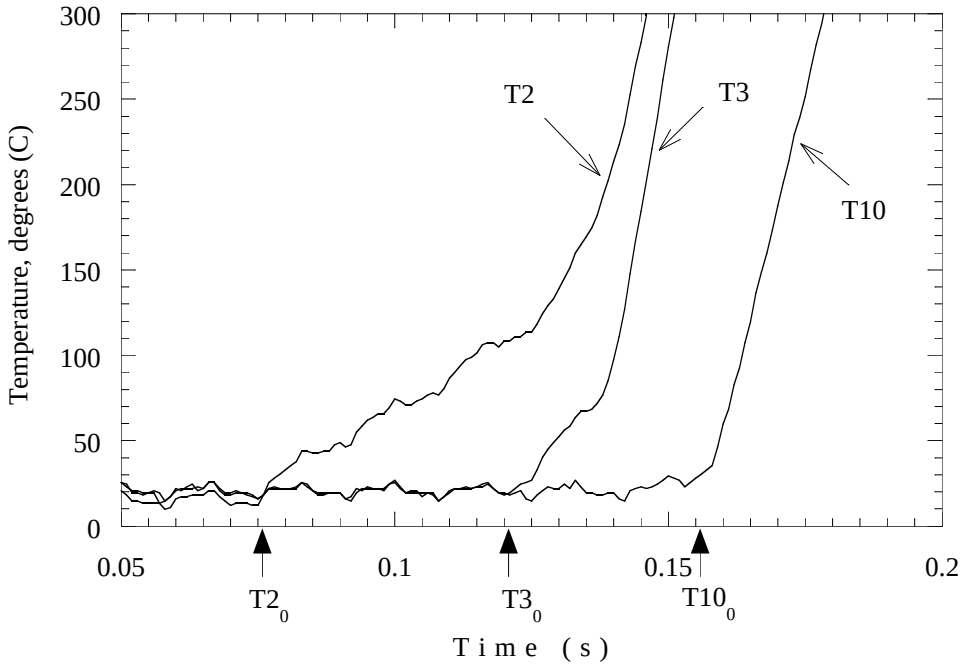

Figure 5.4: Thermocouple signals for Test 4 with their corresponding time of arrival.

5.2 ALPHA Test Series

The purpose of the ALPHA test series (Table 5.1) was to examine combustion in multi-compartment chambers. This test series began with a single compartment, bounded by RS and SWB3. Strong partitions were added one at a time to increase the number of compartments until the full 6-bay configuration was reached. The bay-5 ignition location was used in all tests. In addition, the vent stringers were closed to atmosphere, but allowed flow between their respective bays. The last test was a special test carried out for comparison with computer simulations. This was a 2-bay test, using a special midspar with only a 2-in diameter hole in the center. The vent connections were plugged for this test.

Table 5.1: ALPHA series tests. Primary ignitor in bay-5 location, 9-in from top (midpoint). Vents closed to atmosphere.

Test	Partitions	Bays	Primary Ign	Backup Ign	Comments
1	none	1	Match	Match	Baseline
11	none	1	Filament	Filament	Baseline repeat
2	MS	2	Filament	Match	
10	MS	2	Filament	Filament	Test 2 repeat
3	MS, SWB2	3	Filament	Match	
9	SWB1, MS, SWB2	4	Filament	Filament	
25	SWB1, MS, SWB2, PR	6	Filament	Filament	
12	Validation MS	2	Filament	Filament	Validation test

The original plans called for an electric match to be used as the ignition source. After the first test, Kees van Wingerden noted that this type of ignition source is distributed and not very repeatable. When we reviewed the film from the bay 5/6 schlieren camera, we found that this was indeed the case. Ignition of the electric match produced a burning spray of particulates that ignited a large volume of gas simultaneously, immediately producing a turbulent flame. This is very different than what is observed in the laboratory with a concentrated spark or hot surface.

After some trial and error, an alternative ignition method was developed that avoided these problems. We removed the glass envelope from a type 1156 automotive light bulb, and energized it with the firing system. Simple tests with photodiodes and visual observation indicated that the filament was rapidly heated to a sufficiently high temperature to use as an ignitor.

Initially, we did not know if this would be a reliable ignition source, so we continued using an electric match as backup. When we reviewed the schlieren movies, we found that the backup match was sympathetically firing when the fireset was discharged into the filament. This was later confirmed with independent tests of the ignition system. Although the backup firing line is shorted at the instrument trailer when the main line is in use, the match is connected at the tank in case of a misfire. There was apparently sufficient induction (the main and backup lines are run together) between the main and backup circuits to initiate the match when the fireset

Table 5.2: Time of arrival at the photodetector locations for the ALPHA test series. The missing time in Test 3 is due to a noisy signal.

Test	L1 (ms)	L2 (ms)	L3 (ms)	L4 (ms)	L5 (ms)	L6 (ms)
1	3	63	3	79	63	153
11	210	210	197	238	205	321
2	50	50	50	50	50	50
10	217	218	218	219	209	207
3	82	83	–	91	74	65
9	155	164	163	166	159	157
25	139	142	150	146	150	156
12	169	173	169	182	161	158

Table 5.3: Time of arrival at the thermocouple locations for the ALPHA test series. The missing time for Test 1 is due to a noisy signal.

Test	T1 (ms)	T2 (ms)	T3 (ms)	T4 (ms)	T5 (ms)	T6 (ms)	T7 (ms)	T8 (ms)	T9 (ms)	T10 (ms)	T11 (ms)	T12 (ms)
1	50	–	111	128	47	32	112	121	63	98	177	212
11	166	76	214	288	166	119	214	305	191	258	325	388
2	101	70	142	96	92	76	64	101	117	121	75	124
10	157	68	204	229	192	134	215	233	216	228	207	217
3	93	61	84	93	93	66	92	100	97	103	84	87
9	159	69	159	164	158	159	156	175	167	173	164	170
25	139	82	129	137	152	152	152	152	168	167	160	165
12	150	64	172	183	173	122	175	207	179	187	178	175

was discharged.

After gaining some confidence in the filament ignitor and carrying out laboratory tests, we used them in both the primary and backup systems from Test 4 on. Because of the accidental double ignition, tests 2 and 3 should be discarded from any comparative analysis. Test 11 is preferred to Test 1 as a baseline for the ALPHA series since it uses the filament ignition source rather than the match. A comparison is given below.

Table 5.4: Flame arrival times (ms), Test 1.

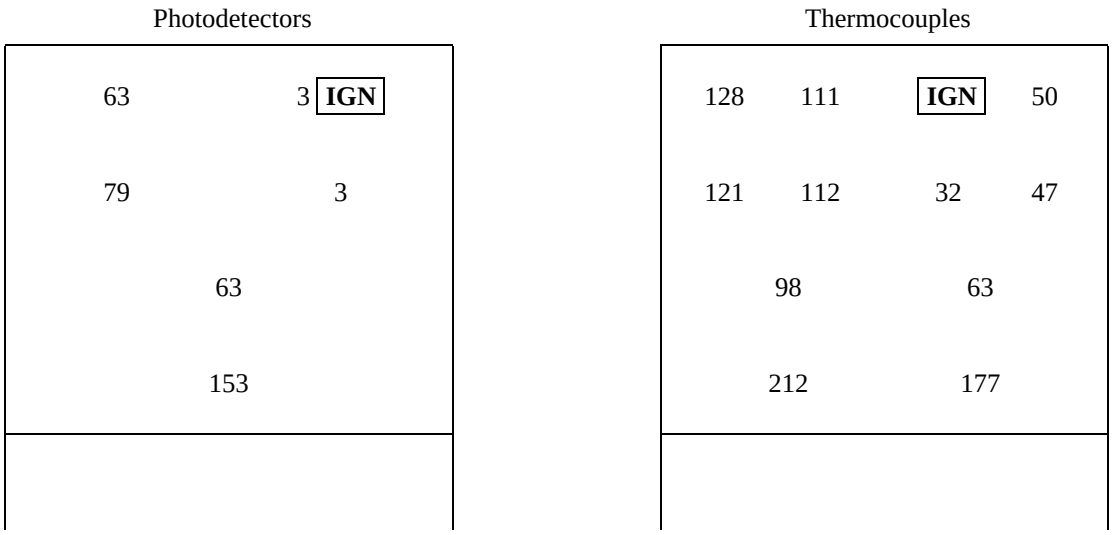

One-Compartment Configuration (Tests 1, 11) The one-compartment configuration was studied in Tests 1 and 11. Test 1 used an an electric match for ignition. An electric match consists of a bridgewire coated with a pyrotechnic composition and sealant. Upon initiation, the match bursts into fragments of burning pyrotechnics, providing multiple, distributed ignition sources. This resulted in a much faster burn than with filament ignition, as shown in Fig. 5.5. The pressure traces in Fig. 5.5 are taken from the bay 2 transducer, which is centrally located. Traces from different locations were essentially identical in the single-compartment test, indicating that the pressure was spatially uniform. Schlieren images from the forward bays showed a distorted, multiheaded flame front. Exterior video showed some leakage of combustion products through the side seals on SWB3.

After Test 1, a light-bulb filament (described above) was used as the ignition source. The bulb was fired with the same discharge system used for the match. The filament generates a smooth, spherical flame front. In Test 11, the flame begins showing small-scale turbulence by the time it reaches the bay 3/4 location, and larger scales are seen as the flame enters the bay 2 region. By the time the flame enters the bay 1 region, it has become nearly flat along the vertical direction. It is still curved along the spanwise axis, since the foremost point of the flame preceeds the edge of the flame that is in contact with the window. In Fig. 5.5, we see that the pressure builds smoothly at an increasing rate to a peak of 3.7 bar at 500 ms after ignition. Test 11 is the baseline test for the ALPHA series. Very little leakage occurred around SWB3 in this test.

While running Test 11, the liquid fuel valve was opened briefly to adjust air pressure in the tank. A small amount of fuel residue was left on the floor of the tank, but this appeared to be only a thin film approximately one foot square at the time of the test. Being such a thin layer, it is doubtful that this was lofted and burned during the test.

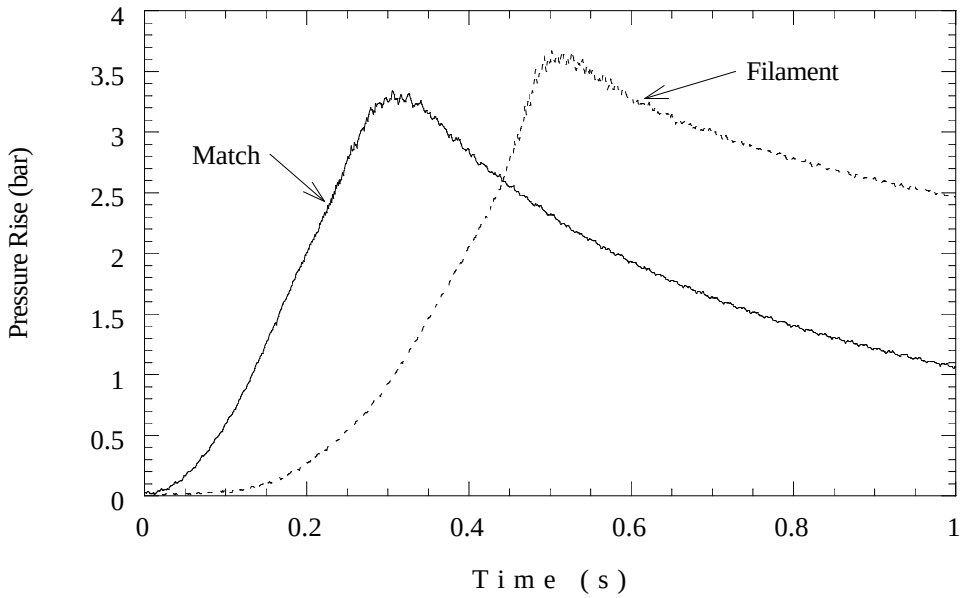

Figure 5.5: Comparison of electric match (Test 1) and filament (Test 11) ignition sources in one-compartment configurations. Bay 2 static pressure transducer was used for measurement.

Table 5.5: Flame arrival times (ms), Test 11.

Photodetectors		Thermocouples			
210	210 **IGN**	288	214	76 **IGN**	166
238	197	305	214	119	166
205		258		191	
321		388		325	

Two-Compartment Configuration (Tests 2, 10) The two-compartment configuration was studied in Tests 2 and 10. The two compartments were created by inserting the midspar in the one-compartment configuration. Test 02 was the first test to use the filament ignitor. However, an electric match was still used as a backup, and sympathetically ignited with the filament. The schlieren film in Test 2 showed that the filament initiated a slow, smooth flame front. This was quickly distorted and overcome by the flame ignited by the electric match. The bay 5/6 camera shows the filament flame getting blown aft as the much larger, turbulent flame enters from the bay 3/4 region. The video of the forward bays indicates that the flame first passed through the lower passageways of MS, riding on the jetting flow through the passages. This shot was fired after dark, but the external video picked up some burning particles exiting the forward end of the tank, indicating loss of the side seals on SWB3.

In addition to the dual ignition problem, static pressure data in Test 2 suffered a noise and crosstalk problem, making this data unusable. Thus, only Test 10 data will be presented here. In this test, the three 5/16-in holes in the MS used to attach the PRs were not plugged. However, no jets are visible coming from MS in the bay 2 schlieren films.

Figure 5.6 shows the static pressure traces from Test 10. Traces from the bay 2 and 3 transducers were chosen to represent the pressures in the two compartments. All of the traces for each bay were tightly overlain. Ignition occurs in the aft compartment, composed of bays 3 through 5. The pressure rise is very slow in these bays, and the flame initially burns laminarly. The pressure drives unburned mixture into the forward compartment through the vents and MS passageways, generating turbulence. The flow of unburned gas is shown by the gradual increase of pressure in bays 1 – 2. Once the flame enters the forward compartment, just after 200 ms, it rapidly engulfs the compartment, since the prexisting flow is turbulent. The pressure rise is much faster in the forward compartment, and flow reverses direction once the pressure exceeds that in the aft compartment. No pressure piling is evident in this test.

The pressure differential across the midspar is plotted in Fig. 5.7. There is a gradual pressurization of the aft compartment, followed by a reverse of the differential after 200 ms.

The schlieren films from this test (Fig. 5.8) show that the surface of the flame eventually becomes wrinkled as it grows to the size of the aft compartment. Ignition of the forward half of the tank clearly occurs through the vent stringers. The camera in bay 2 shows the approach of the initial flame front to the aft side of MS, but a much faster, turbulent flame enters from the right side and fills the forward compartment before the flame from the rear compartment gets there. The rapid combustion in the forward compartment generates a higher pressure, driving flow into the rear compartment. This generates turbulence and greatly accelerates the flame through the remainder of the unburnt gas. External footage showed very little leakage around SWB3.

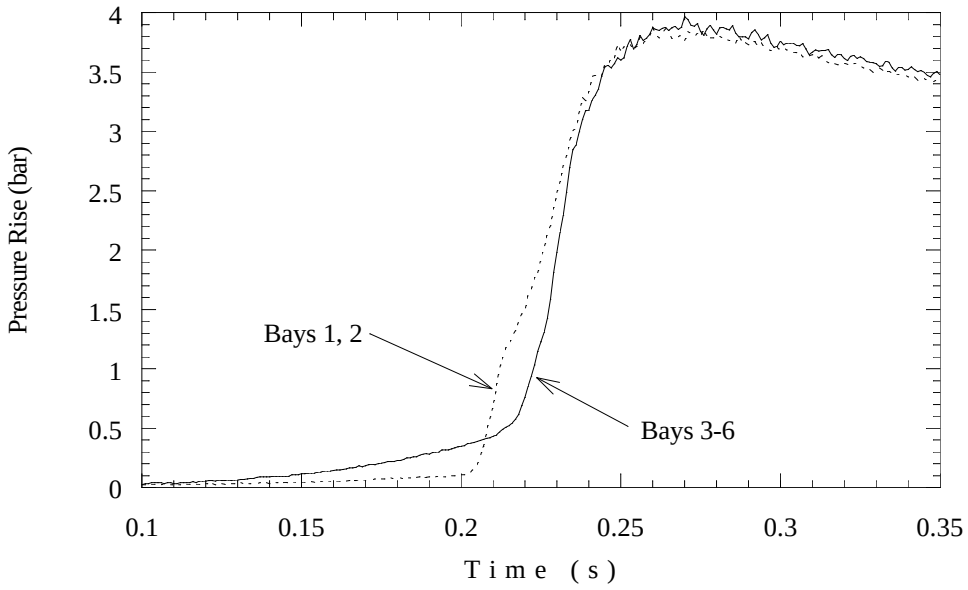

Figure 5.6: Static pressure traces from two-compartment configuration. Traces from bay 2 and bay 3 transducers shown. Test 10.

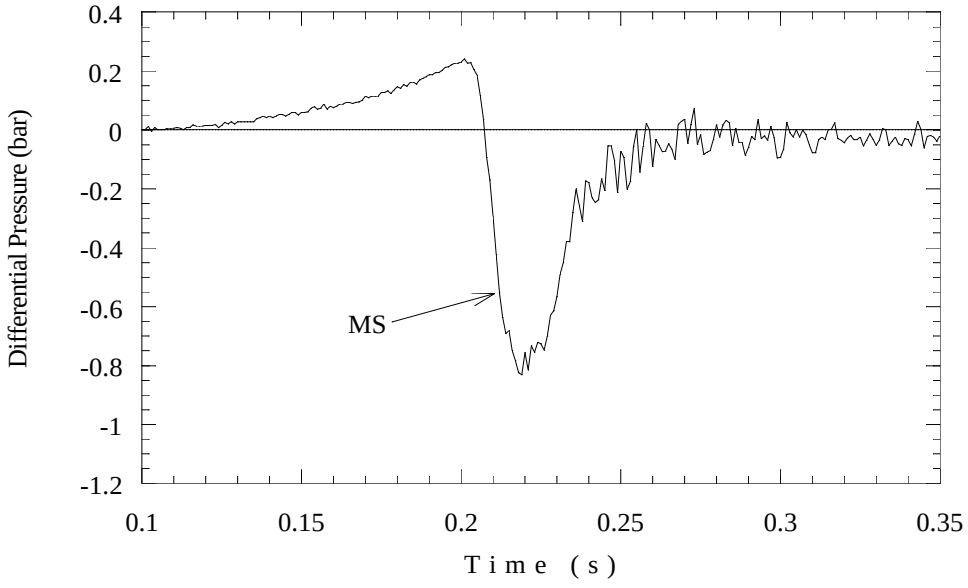

Figure 5.7: Differential pressure across midspar in two-compartment configuration. Test 10.

Table 5.6: Flame arrival times (ms), Test 10.

Photodetectors		Thermocouples			
218	217 **IGN**	229	204	68 **IGN**	157
219	218	233	215	134	192
209		228		216	
207		217		207	

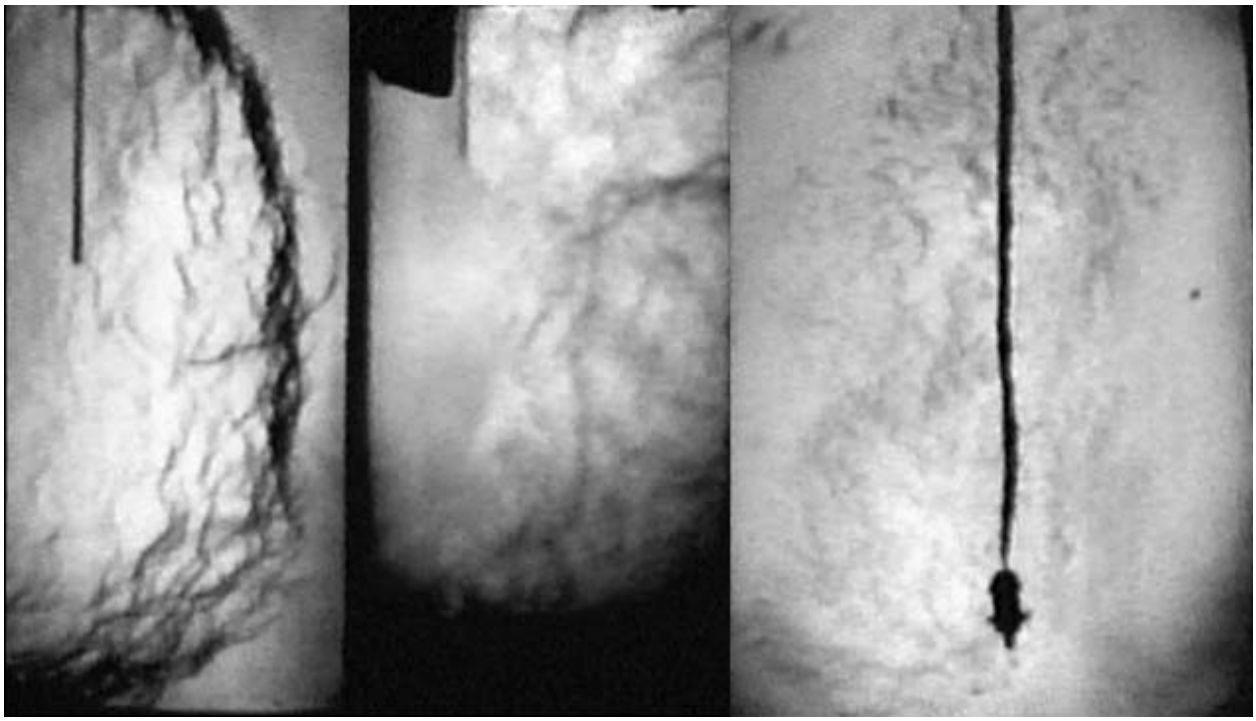

Figure 5.8: Composite of schlieren images from Test 10. (Bay camera 1 malfunctioned, so the image from the bay 5/6 location is missing from the left of the picture.) Note ignition of forward bays through vent stringers.

Three-Compartment Configuration (Test 3) The three-compartment configuration was created by adding spanwise beam 2 to the two-compartment configuration. This configuration was tested only once, and used the electric match for backup ignition. Unfortunately, sympathetic ignition occurred again, so this data is presented for reference purposes only, and can not be compared to other tests. Figure 5.9 shows the pressure traces from this test. Pressure rise in bays 3 – 6 is faster than in the two-compartment test, due to the dual-point ignition and scattering of the match composition (backup ignitor was in the bay 3 position). Bay 2 burns slightly faster when the flame enters it, but bay 1 shows similar behavior to the second compartment in the two-bay test, with slow initial pressurization due to gas flow followed by a rapid increase from turbulent combustion. In this test, reverse flow into bays 3 – 6 causes an overshoot in pressure, and a slight reverse pressure piling effect. This is shown in the pressure differentials in Fig. 5.10, where positive differentials occur over the midspar and the vents after 150 ms. The loading oscillates on MS and SWB2, in opposite phase.

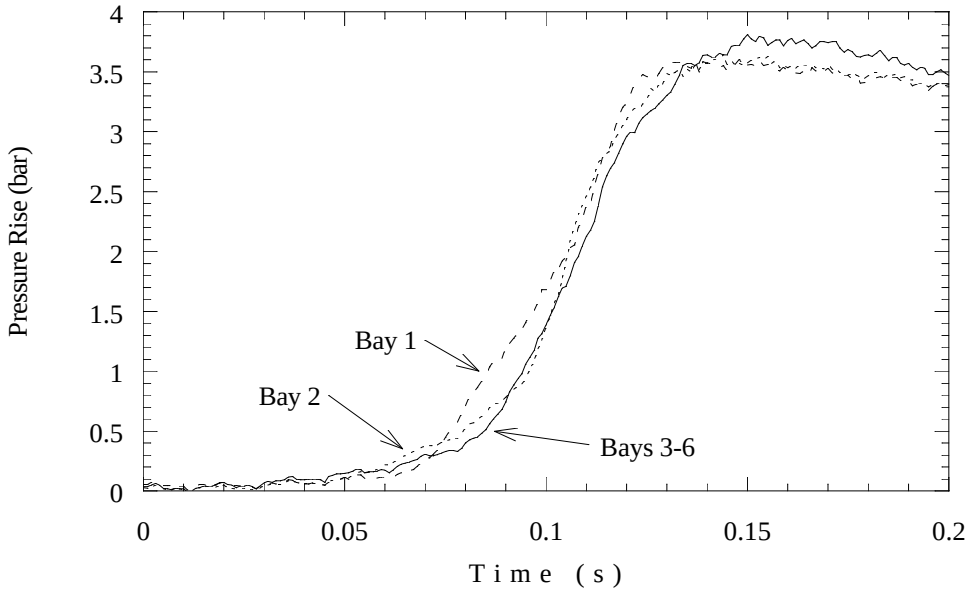

Figure 5.9: Pressure traces from three-compartment configuration. Sympathetic ignition of backup match occurred, so data is for reference only. Test 3.

The schlieren film from bays 5/6 shows a small, laminar flame ball surrounding the filament and then being engulfed by the large flame front from the electric match, as in Test 2. In this test, the flame front from the match was concentrated at the bottom of the tank. (The backup ignitor is mounted near the bottom of the tank in case a lean mixture creates a buoyancy driven flame.) Film from bay 2 shows the flame entering on a jet from one of the lower passageways in MS; the flame front impacts SWB2 and then proceeds rearward to fill bay 2. The external video showed leakage from both side seals on SWB3.

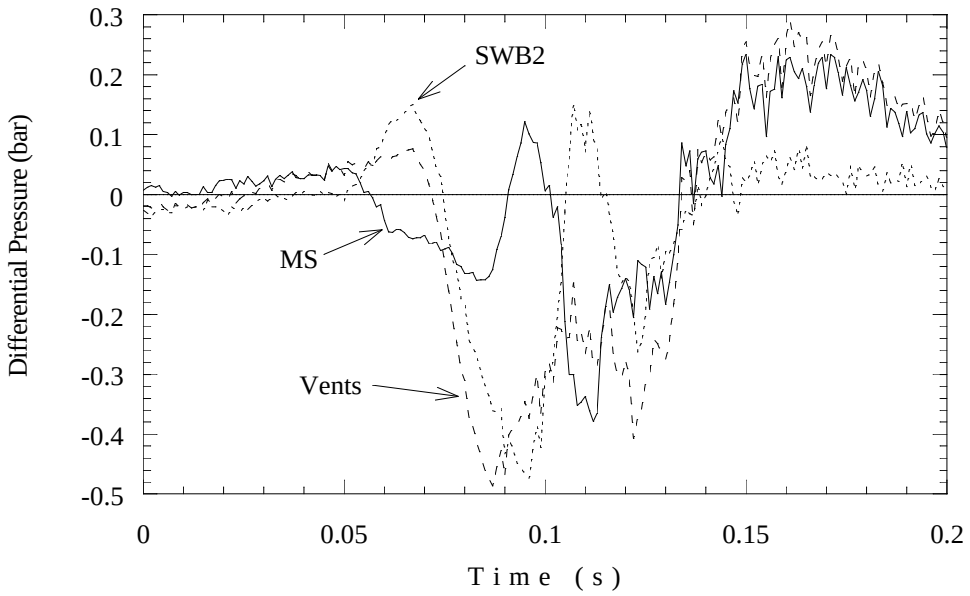

Figure 5.10: Differential pressures for three-compartment configuration. Sympathetic ignition of backup match occurred, so data is for reference only. Test 3.

Table 5.7: Flame arrival times (ms), Test 3.

Photodetectors		Thermocouples			
83	82 **IGN**	93	84	61 **IGN**	93
91		100	92	66	93
74		103		97	
65		87		84	

Four-Compartment Configuration (Test 9) Test 9 examined the four-compartment configuration. All of the strong partitions were installed, but no partial ribs were used. Note that the three 5/16-in holes in SWB1 and MS used to secure the PRs were not plugged, but this had no visible effect on the results. The holes are near the centers of the partitions, and with the ignition in bay 5, the flame reaches other, larger vents first that create the flame jet entering bays 3/4 (see schlieren discussion below). The pressure traces are shown in Fig. 5.11. Although ignition occurred in bay 5/6, the pressure trace for bays 3/4 exceeds that for bays 5/6 at 135 ms and is higher until about 162 ms.

This seems unusual, but this is the first time that SWB1 has been installed. In previous configurations, the partition closest to the ignitor was the MS, which was approximately 15 in from the point of ignition. SWB1 is only about 5 in from the ignitor, so it is possible for the flame to reach the partition and pass through the passageway early in the combustion process, when only a moderate amount of turbulence has been generated (compared to the earlier cases). Therefore, the flame enters bays 3/4 at about 135 ms, and burns somewhat faster. Bay 2 is ignited shortly thereafter, with a slightly faster pressure rise. The ignition delay is most pronounced in bay 1, where the pressure slowly rises until ignition occurs, and the pressure rises at a higher rate than in the previous bays. We also see the first evidence of pressure piling here, as the pressure in bay 1 peaks at a slightly higher value that that of the other bays.

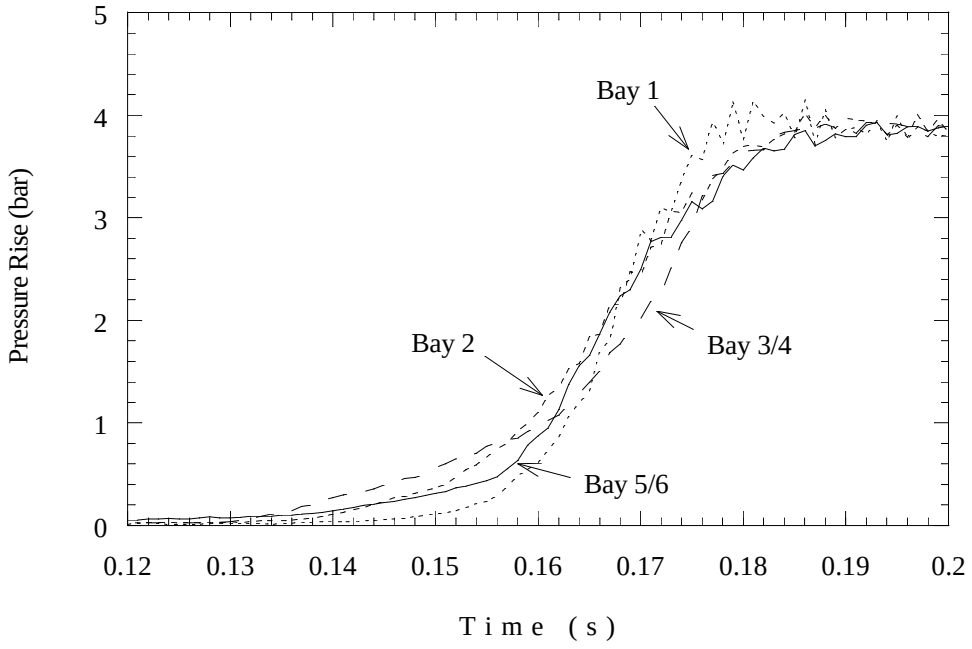

Figure 5.11: Pressure traces from four-compartment configuration. Test 9.

The differential pressures are shown in Figs. 5.12 and 5.13. In Fig. 5.12, we see that SWB1 initially has a slight positive pressure difference from the combustion occurring in the aftmost compartment. Once ignition occurs in bays 3/4, combustion is accelerated by the turbulence, increasing the rate of pressure rise. The greater pressure in bays 3/4 creates a positive pres-

sure difference on the MS, and a negative pressure difference on SWB1. Once combustion is initiated in bay 2, a negative pressure differential is developed on SWB2. Interestingly, the pressure increase in bays 3/4 slows, allowing the pressure in bays 5/6 to overtake it, and again puts positive pressure on SWB1. The vent pressures shown in Fig. 5.13 are as expected. Positive pressure gradients occur in the beginning, as combustion is initiated in the aft bays, and switch to negative once bay 1 is ignited.

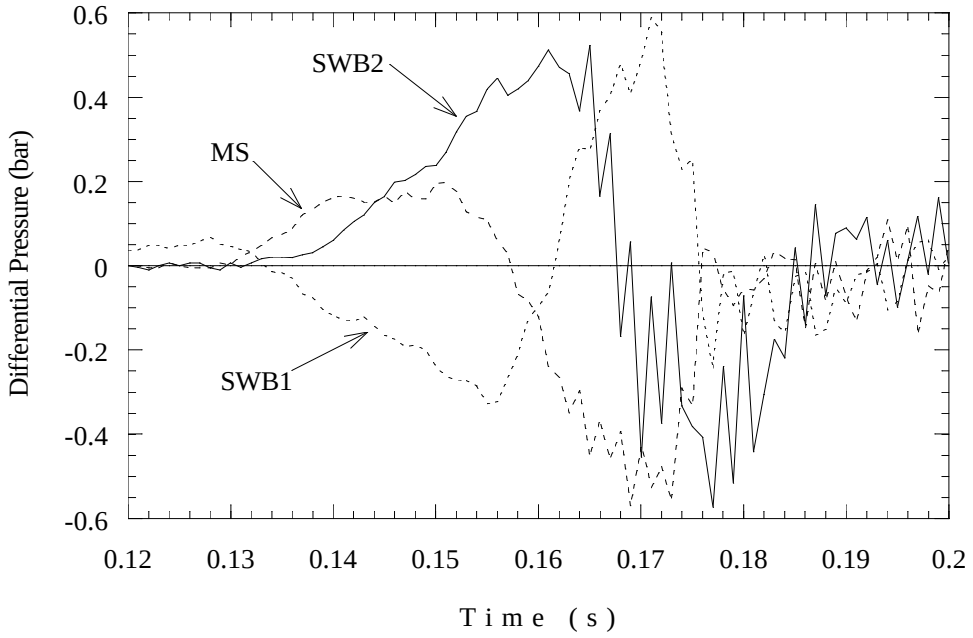

Figure 5.12: Differential pressure across partitions, four-compartment configuration. Test 9.

The schlieren films show that the flame propagates from bay 5 forward via the lower passageways in the partitions. Venting of pressure ahead of the flame, through the passageways, creates jets. The flame gets entrained in these jets, enters the next bay, and impacts the far partition before engulfing the rest of the bay. It does not appear that the vent stringers provide ignition to bay 1 in this test. In some of the bays, an opaque substance seemed to swirl in the products, and then dissipate. This appeared to be soot, and could have been generated by residual fuel from the previous test (Test 8 was the first test to use liquid Jet A). It doesn't appear to come out of the liquid fuel manifold, so it may come from under the partition brackets. The west hilltop video shows orange flames in some of the bays, confirming the presence of jet fuel. Bays 3 and 4 were filled with orange flame at one point. Orange flames in the other bays were very small. In addition, the video and DBM cameras at the SE station seemed to capture fuel spraying out from under the partition brackets. It appears that this fuel lofting occurs late in the event, so it will probably affect only the magnitude and duration of the peak pressures. The bay-to-bay communication and flame progression should be unaffected. Finally, the cameras indicated some leakage occurred around SWB3.

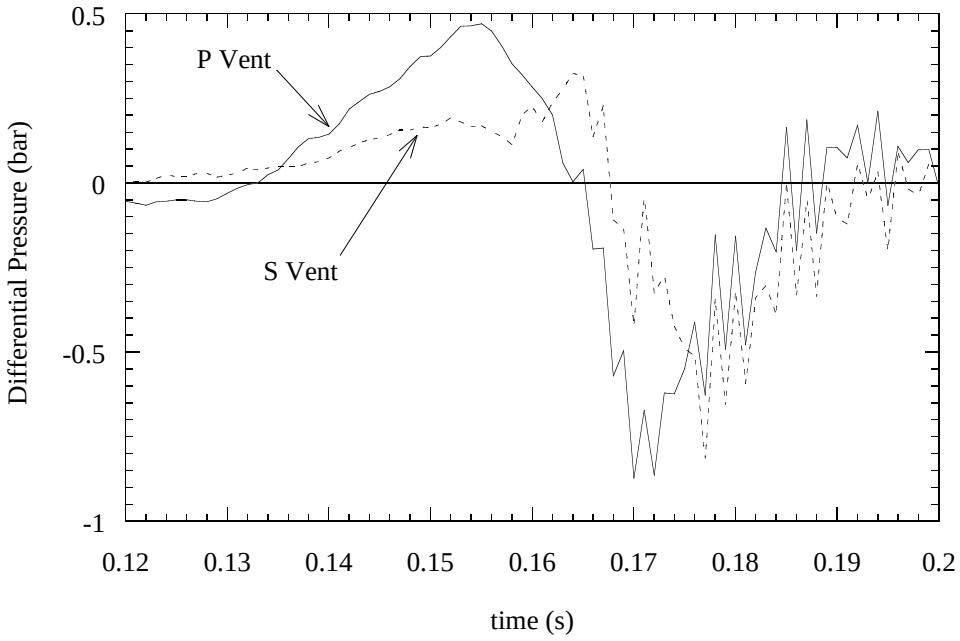

Figure 5.13: Differential pressure across vents, four-compartment configuration. Test 9.

Table 5.8: Flame arrival times (ms), Test 9.

Photodetectors		Thermocouples			
164	155 **IGN**	164	159	69 **IGN**	159
166	163	175	156	159	158
159		173		167	
157		170		164	

Six-Compartment Configuration (Test 25) Figures 5.14 – 5.20 show the results from the six-compartment ALPHA test. The six compartments correspond to the six bays in the CWT. Figure 5.14 shows the pressure in the ignition bay, bay 5, and the adjacent bays, bays 3 and 6. We see an interesting interplay between these bays, as venting and pressurization change the character of combustion from bay to bay. Bay 3 shows the highest rate of pressure rise, which may be the first indication of pressure piling. In Fig. 5.15, we add the trace from bay 4. Until 145 ms, the pressure rise is very slow, due only to venting from the other bays. Suddenly, ignition occurs and the pressure jumps above that of the other bays. The rapid combustion in bay 4 may be caused by dual ignition from bays 3 and 6 (see Fig. 5.16).

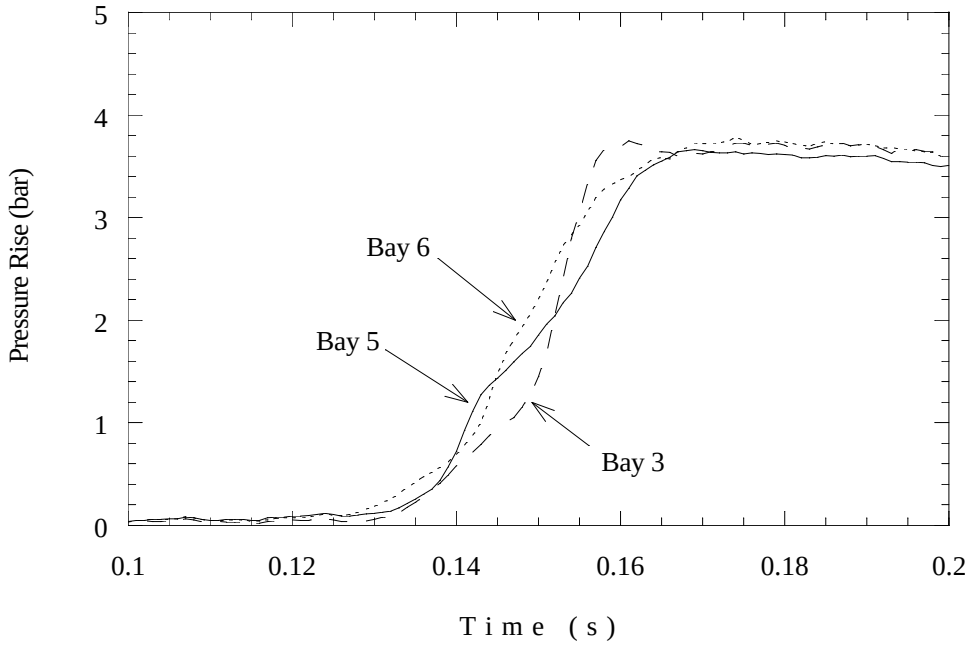

Figure 5.14: Pressure traces from six-bay configuration, bays 3, 5, and 6. Test 25.

Figure 5.17 shows the pressure traces from bays 1 and 2, with those from bays 4 and 5 as reference. Here, we see clear evidence of pressure piling. Bay 2 and bay 1 ignite sequentially, with increasing flame speeds and peak pressures (the peak in bay 1 isn't much higher than that in bay 2).

The pressure differentials across SWB1 and MS are shown in Fig. 5.18. The pressure is reasonably balanced from left to right on SWB1, although the starboard side shows the first increase. This indicates that the vent flow is adequate to equalize the pressure due to the slow initial combustion, but results in large pressure differences once turbulent combustion is initiated in bay 6. In addition, the flame enters bay 3, increasing pressure there and decreasing the differential across port SWB1. As the combustion progresses forward from bays 5 and 6 to bays 3 and 4, the pressure differential becomes positive on the MS, and changes to negative on SWB1. The pressure differential across SWB2 (Fig. 5.19) is large and positive from the rapid combustion in bay 2, and drops to a slight negative as bay 1 ignites and some pressure piling occurs. The vent stringers show the expected behavior, the initial combustion in the rear

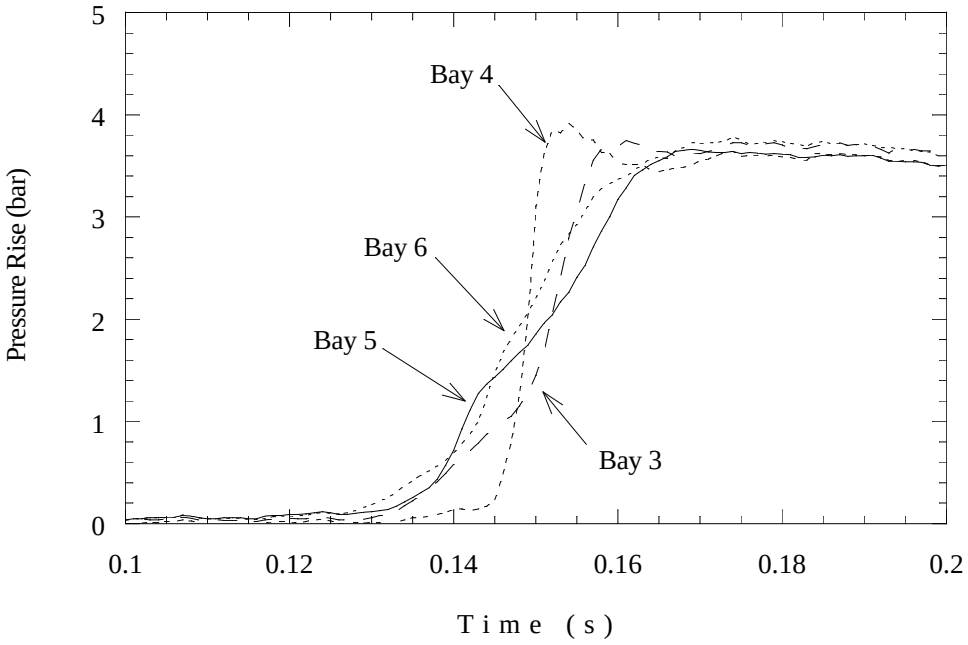

Figure 5.15: Pressure traces from six-bay configuration, bays 3/4. Test 25.

driving flow forward, followed by slight reverse flow as bay 1 ignites and the aft bays cool and depressurize.

Interesting changes in the pressures across the forward and aft PRs reflect the communication between the aft bays. The large negative spike on the forward PR results from the rapid pressure rise in bay 4, as shown in Fig. 5.15.

Bay camera 2 jammed in this test, so there is no schlieren film from bays 3/4. In bay 5, ignition produces a smooth, spherical flame that develops some wrinkles as it expands in the bay. Once it reaches the aft PR, the flame passes through one of the holes into bay 6, where venting from bay 5 has generated turbulence. As a result, the flame burns through bay 6 very quickly. In bay 2, the flame enters as a jet from one of the lower passageways in MS. This jet impinges on SWB2, and rapidly burns through the bay. Bay 1 ignites the same way, but burns faster than any of the other bays, aided by a second flame entering via the vent stringers. Combustion here is fast enough that one of the thermocouple probes breaks.

The exterior side view camera was misaligned, but the film does show that the flame entered bays 3/4 as a jet near the bottom of the bay, and propagated into the bay after reaching the MS. The other observation cameras only show minor leakage along the sides of SWB3.

Test 25 was nearly a replica of Test 4 (discussed in the BETA series section) except that the vents were closed in 25 and were open in 4. Comparison of these two tests is given in Chapter 6.

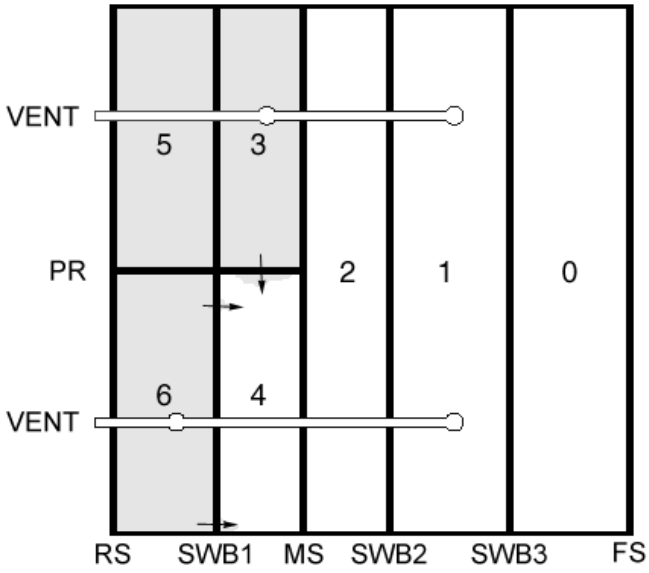

Figure 5.16: Possible dual ignition of bay 4 by bays 3 and 6, resulting in rapid pressure rise.

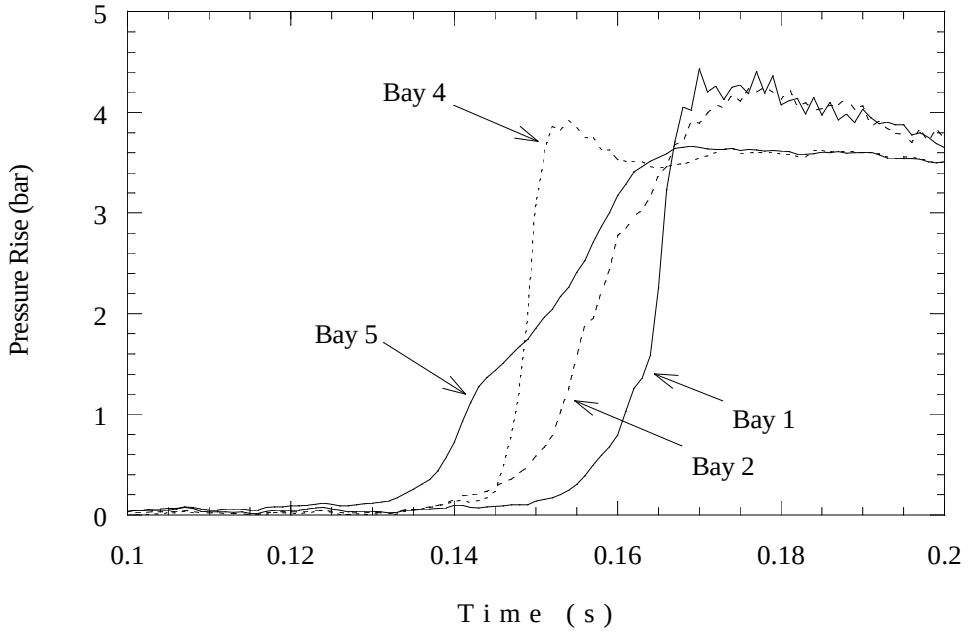

Figure 5.17: Pressure traces from six-bay configuration, bays 1, 2, 4, 5. Test 25.

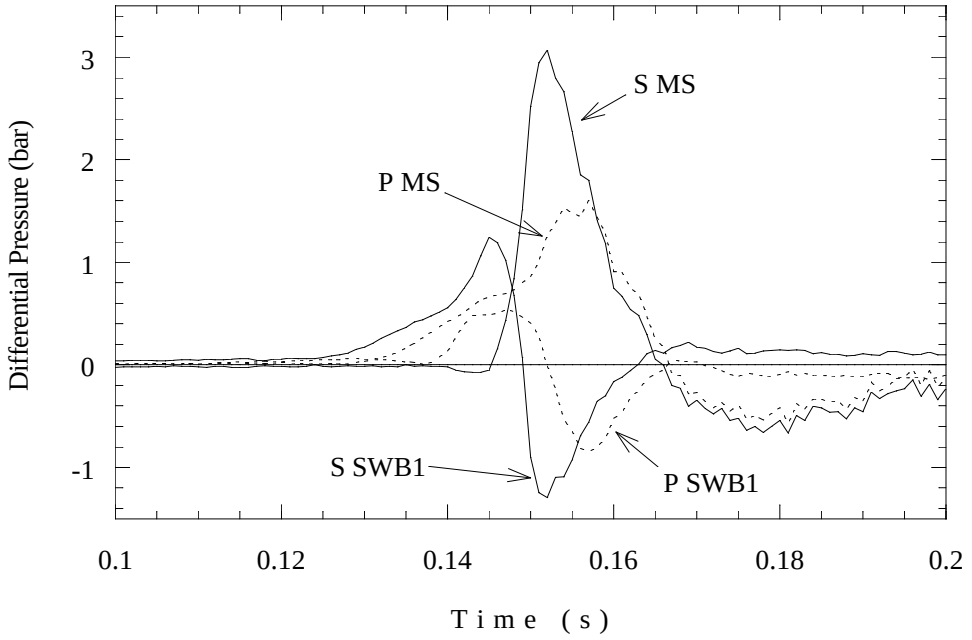

Figure 5.18: Pressure differentials across SWB1 and MS, six-bay configuration. Test 25.

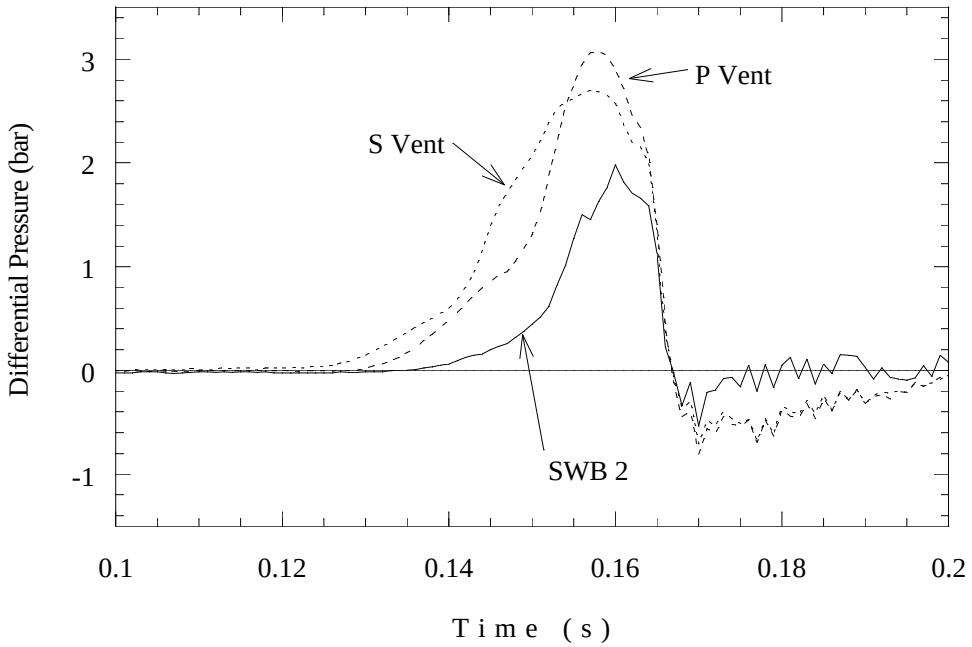

Figure 5.19: Pressure differentials across SWB2 and vent stringers, six-bay configuration. Test 25.

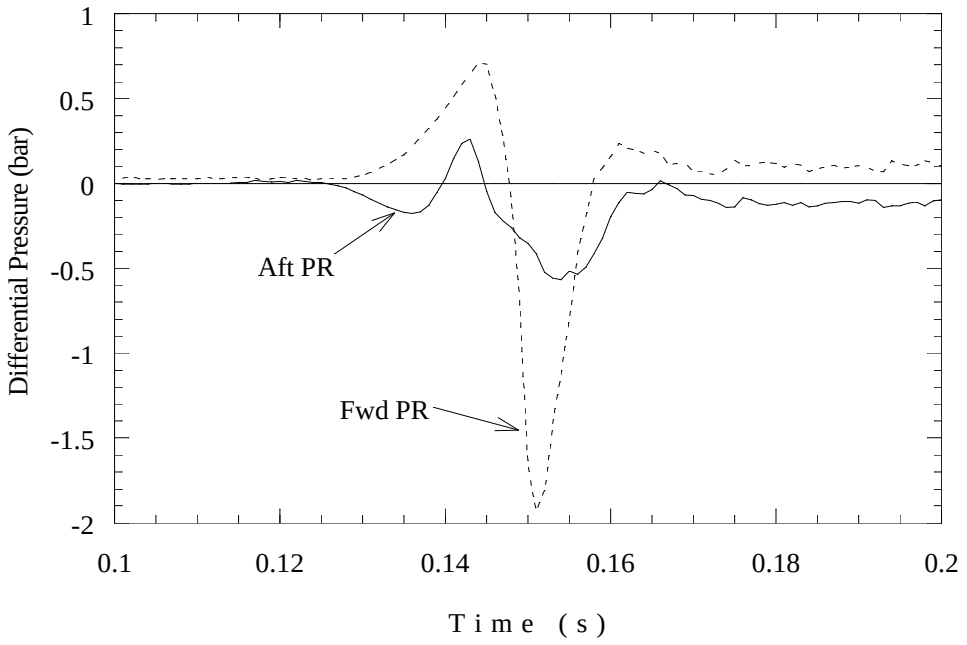

Figure 5.20: Pressure differentials across PRs, six-bay configuration. Test 25.

Table 5.9: Flame arrival times (ms), Test 25.

Photodetectors		Thermocouples			
142	139 **IGN**	137	129	82 **IGN**	139
146	150	152	152	152	152
150		167		168	
156		165		160	

Special Two-Compartment Test (Test 12) In light of the complex modeling problem presented by the 1/4-scale facility, we developed a simplified two-compartment test that can be more easily used to compare with computer simulations than the full tests. This configuration used a special MS that had only a single, 2-in (51-mm) diameter hole in the center to represent the sum of the other passageway areas. In addition, the vent lines were plugged to prevent flow through them. (Each vent line was only plugged at the forward end so the mixing system could still function. This path was closed by the valves during the test.) Ignition was in the bay 5 location.

The resulting pressure traces are shown in Fig. 5.21. The aft bays show the typical slow pressure rise, followed by ignition and a rapid rise in the forward bays. Interestingly, the peak shows *reverse* pressure piling in the aft bays, that is the peak pressure in the rear bays appears to be higher. This is reflected in the differential pressure across the MS (Fig. 5.22). The schlieren films showed the flame front following the venting flow out of the aft bays, and emerging into the forward bays carried by vortex at the head of the jet created by the flow through the hole in the MS.

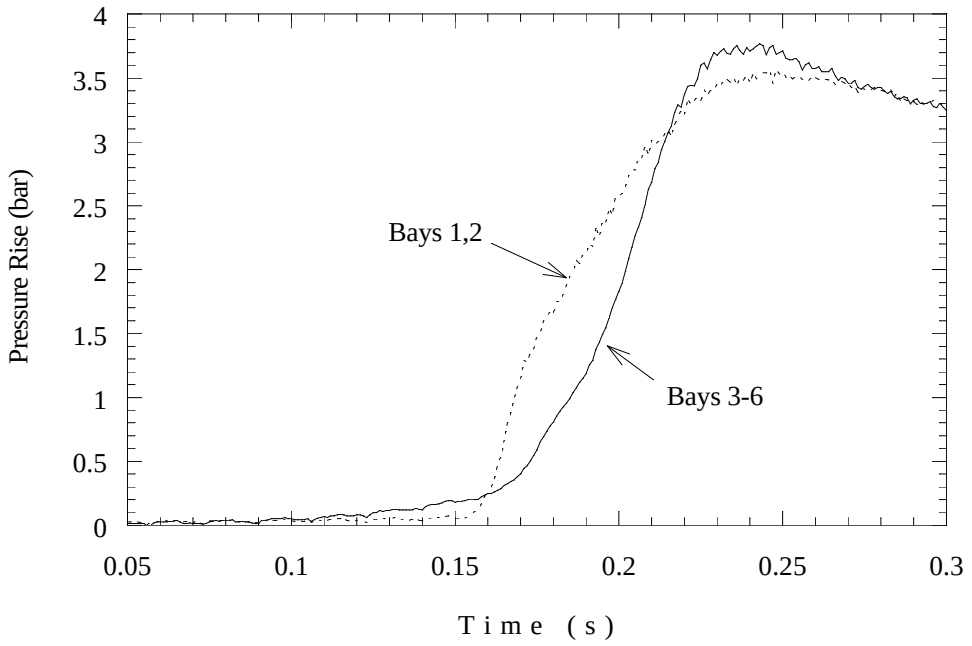

Figure 5.21: Pressure traces from two-compartment code validation configuration, with special MS and plugged vent stringers. Test 12.

The schlieren footage from Test 12 is simple, yet very interesting. The initial flame propagates and expands smoothly before it approaches MS. The expanding flame is driving flow of unburnt gas through the hole in MS, developing a jet in the forward half of the tank. The schlieren system isn't sensitive enough to resolve this. When the flame front gets halfway through the bay 3/4 region, the leading tip of the spherical flame reaches the jet flow area, and appears to get sucked through MS. The flame follows the path of the jet as it enters the forward bays, running straight to the wall, expanding to 1/3 – 1/2 of the bay height before impact. As

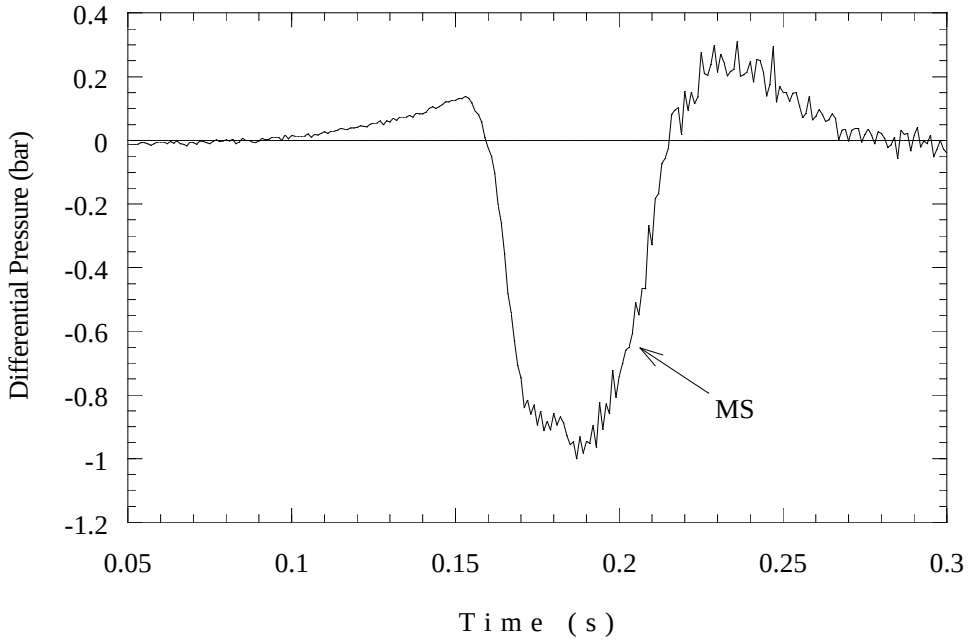

Figure 5.22: Differential pressure across MS from two-compartment code validation configuration. Test 12.

the flame reaches the wall, it is convected around the compartment by the large-scale turbulent vortex set up by the jetting. The pre-existing flowfield in the forward bays accelerates combustion so much that it burns out before the aft bays. The higher pressure generates reverse flow through the opening, generating turbulence and accelerating combustion in the aft bays. External video showed very little leakage past SWB3.

Table 5.10: Flame arrival times (ms), Test 12.

Photodetectors		Thermocouples			
173	169 **IGN**	183	172	64 **IGN**	150
182	169	207	175	122	173
161		187		179	
158		175		178	

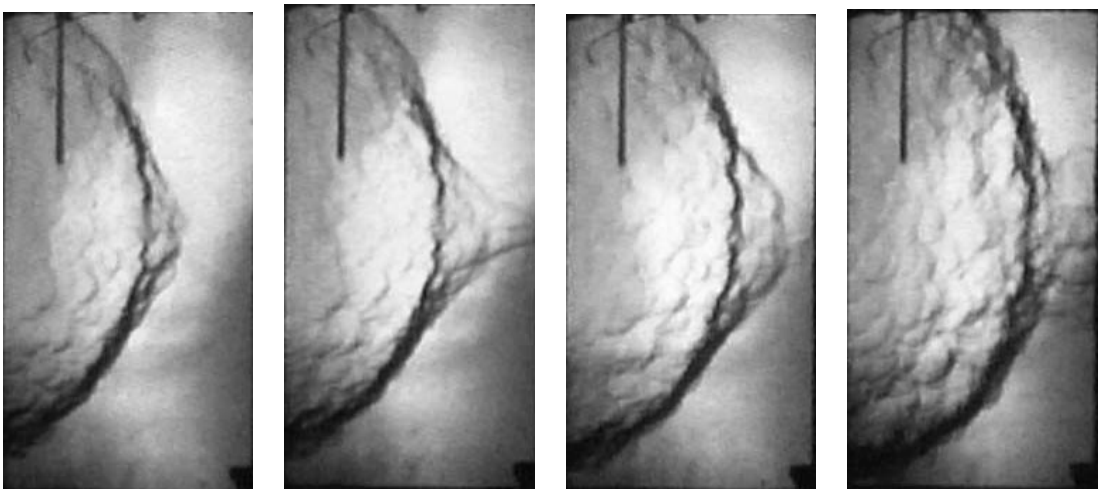

Figure 5.23: Sequence of schlieren images from bay 3/4 position showing growth of flame "nose" as it approaches passageway. Test 12.

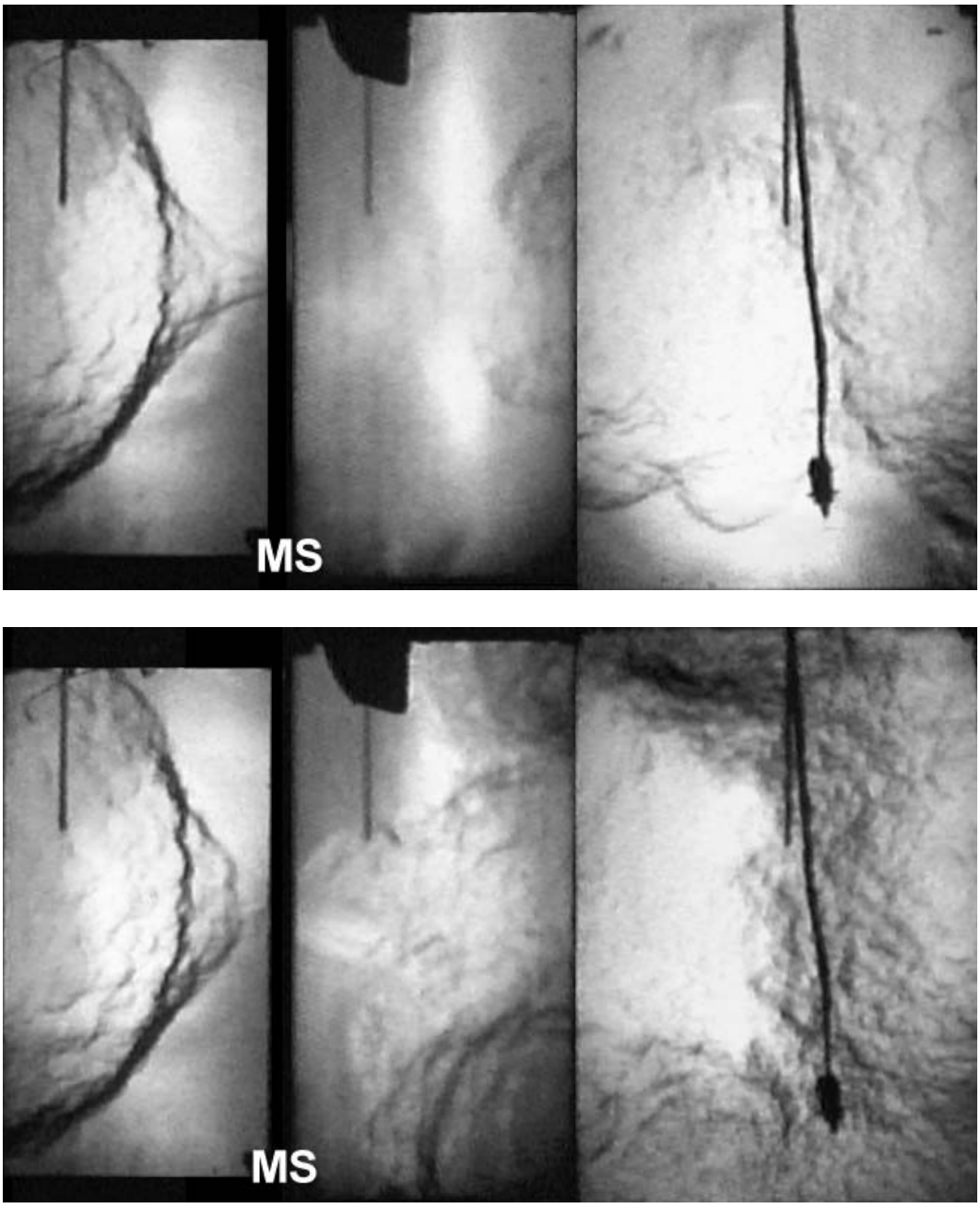

Figure 5.24: Sequence of composite schlieren images from Test 12, two-compartment configuration with special midspar. Note that the flame is so small that it cannot be resolved immediately downstream of the passageway in the first frame.

5.3 BETA Test Series

The BETA test series examined the effect of ignition location in the 6-bay, all-strong configuration. In these tests, the vent stringers were open to atmosphere, as in the TWA 800 configuration.

Table 5.11: BETA series tests. All tests use the six-bay, all-strong configuration, with vents open.

Test	Ignition	Comments	Test	Ignition	Comments
4	5		7	1	APR partial fail
8	5	With Jet A	15	6R	APR fail, FPR partial fail
5	3		16	1R	APR fail, FPR partial fail
6	2		26	2Lo	6.5% fuel

Ignition in Bay 5 (Test 4) Pressure traces from bay 5 ignition are shown in Figs. 5.25 – 5.30. This test differs from the six-bay test (25) of the ALPHA series in that the vent stringers are now open to atmosphere. In Fig. 5.25, we see the same inter-bay communication between bays 3, 5, and 6 that was evident in Test 25. Figure 5.26 indicates the delayed ignition and rapid combustion of bay 4, most likely due to multi-point ignition caused by flame propagation through several passageways.

Bay 2 ignites at about the same time as bay 4, as shown in Fig. 5.27. These bays were probably ignited by bay 3, which is adjacent to both. The rapid combustion of bay 3 could then ignite 2 and 4 at nearly the same time. The rapid combustion in 3 is due to turbulence generated by the venting of bay 5 into 3. Lastly, bay 1 is ignited by bay 2, with secondary ignition coming later from the vents. (This is shown in the schlieren films.) The rate of pressure rise in bay 1 is

Table 5.12: Time of arrival at the photodetector locations for the BETA test series. The missing times for Test 26 are due to a lack of luminosity.

Test	L1 (ms)	L2 (ms)	L3 (ms)	L4 (ms)	L5 (ms)	L6 (ms)
4	134	139	145	140	157	154
8	68	67	71	73	78	79
5	141	137	145	144	147	149
6	191	193	184	184	191	197
7	200	200	194	198	200	202
15	187	–	194	189	198	185
16	191	194	196	198	201	197
26	–	–	–	–	839	828

Table 5.13: Time of arrival at the thermocouple locations for the BETA test series. The missing time for Test 4 is due to a gauge malfunction.

Test	T1 (ms)	T2 (ms)	T3 (ms)	T4 (ms)	T5 (ms)	T6 (ms)	T7 (ms)	T8 (ms)	T9 (ms)	T10 (ms)	T11 (ms)	T12 (ms)
4	–	78	123	137	145	145	142	146	158	158	156	158
8	74	68	67	73	86	88	84	85	98	97	92	83
5	142	127	140	145	146	62	150	149	152	169	158	170
6	193	196	196	196	185	187	186	185	149	193	201	206
7	203	202	204	187	198	201	203	202	211	201	147	111
15	190	190	168	168	198	198	176	115	208	168	210	142
16	197	195	183	132	199	199	178	128	209	163	213	182
26	906	950	940	908	869	904	910	873	518	518	835	851

comparable to that in bay 4, which supports the idea of multipoint ignition. It is also possible that bay 1 had the highest level of turbulence and circulation before ignition, caused by the venting of the other bays into bay 1. This would also allow rapid burn completion and pressure rise. Pressure piling occurs in bays 2 and 1.

The differential pressures in Fig. 5.28 show that SWB1 and MS experience less loading of the port side, although the overall trend is consistent across each partition. The port side of SWB1 is particularly interesting, showing a long period with slight pressure, as the venting keeps up with combustion. This is followed by a small negative dip before going positive. When bay 3 ignites, the force changes direction to aft. The starboard side of SWB1 shows an early positive force, probably occurring when bay 6 is ignited, and undergoes rapid combustion. Bay 6 may vent back into bay 5, accelerating the combustion in bay 5 to completion and generating the positive pressure difference seen on the port side of SWB1.

The pressure across SWB2 is predominantly positive while bay 2 burns but before bay 1 ignites. When bay 1 ignites, the negative differential is of low magnitude, as the remainder of the tank is pressurized, so only the pressure piling in bay 1 can contribute to the rearward force. Pressures across the vents follow suit. Pressures across the partial ribs show much oscillation (Fig. 5.30), especially on the aft PR. The aft PR pressure differences are pronounced once bay 6 is ignited and undergoes turbulent combustion. The forward PR shows a positive differential pressure due to the combustion in bay 3, followed by a sharp negative spike when bay 4 ignites.

The schlieren film from bays 5/6 shows a smooth, spherically symmetric flame front propagating from the filament at ignition. The flame front remains smooth and seems to propagate at a constant velocity until it reaches one of the holes in the aft PR. At this point, the flame passes through the hole and ignites bay 6, which is immediately consumed via turbulent combustion. In the other bays, the flame jet always seems to come from the bottom passageways and impinges on the opposite spar before engulfing the rest of the compartment. This is especially clear in bay 1, where the jet has a longer distance to cross before it reachs SWB3. The jet shows very little lateral growth before reaching SWB3 and proceeding into the rest of bay 1. It appeared that a flame or products were also entering from the top vent connections, but this played a minor role compared to the bottom jet. External video showed blowout of the side

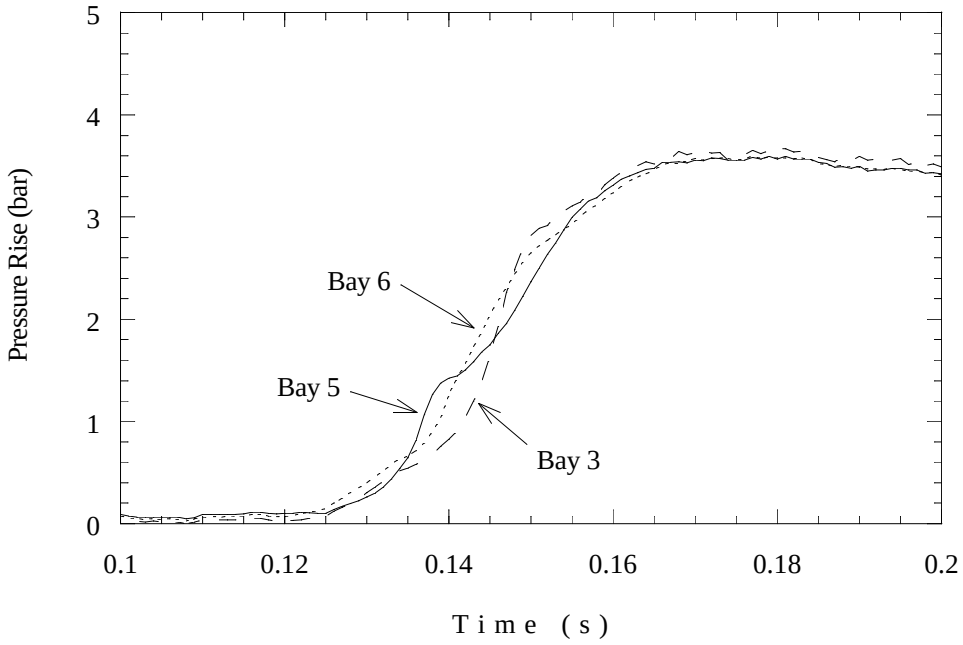

Figure 5.25: Pressure traces from bays 3, 5, 6, ignition in bay 5. Test 4.

seals on SWB3.

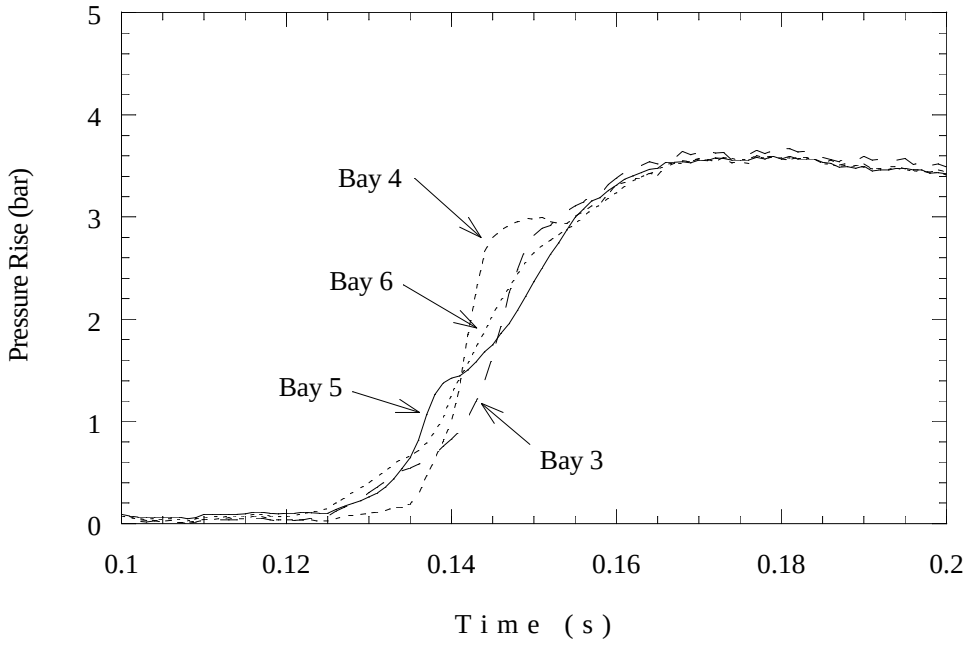

Figure 5.26: Pressure traces from bays 3 – 6, ignition in bay 5. Test 4.

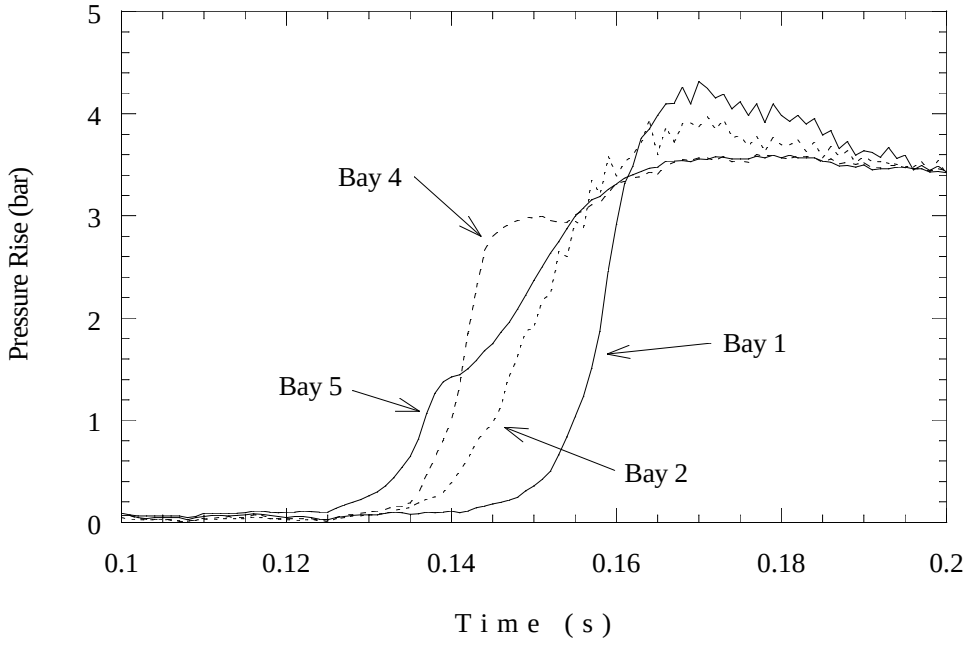

Figure 5.27: Pressure traces from bays 1, 2, 4, 5, ignition in bay 5. Test 4.

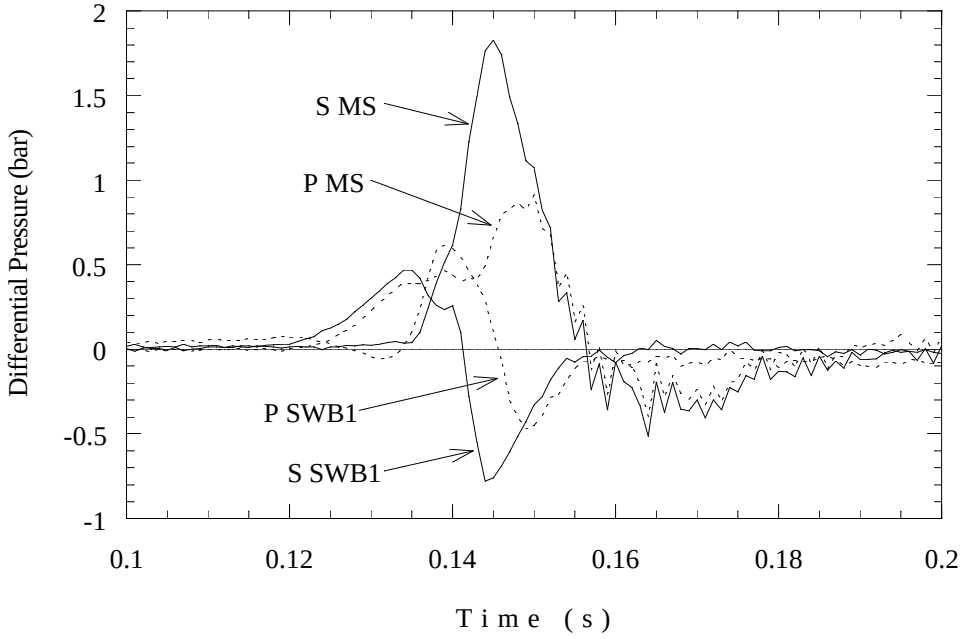

Figure 5.28: Differential pressures across SWB1 and MS, ignition in bay 5. Test 4.

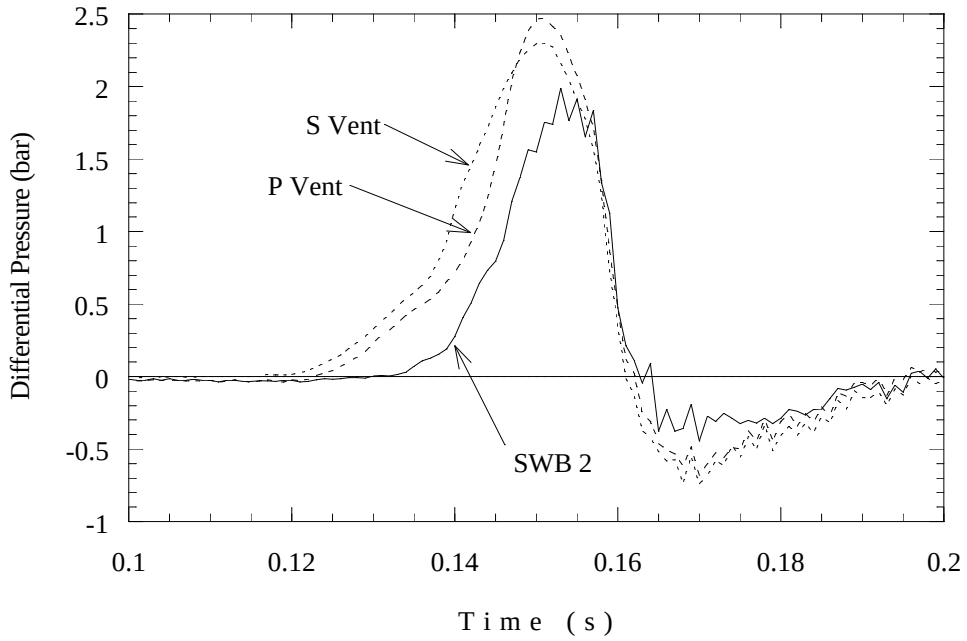

Figure 5.29: Differential pressures across SWB2 and vent stringers, ignition in bay 5. Test 4.

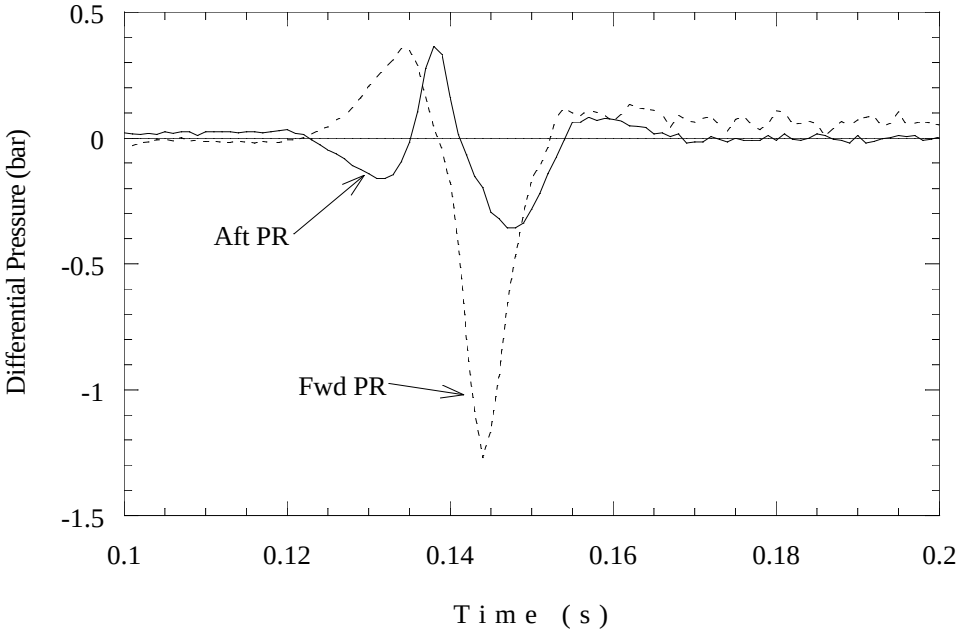

Figure 5.30: Differential pressures across PRs, ignition in bay 5. Test 4.

Table 5.14: Flame arrival times (ms). Test 4.

Photodetectors		Thermocouples	
139	134 **IGN**	137 123	78 **IGN**
140	145	146 142	145 145
157		158	158
154		158	156

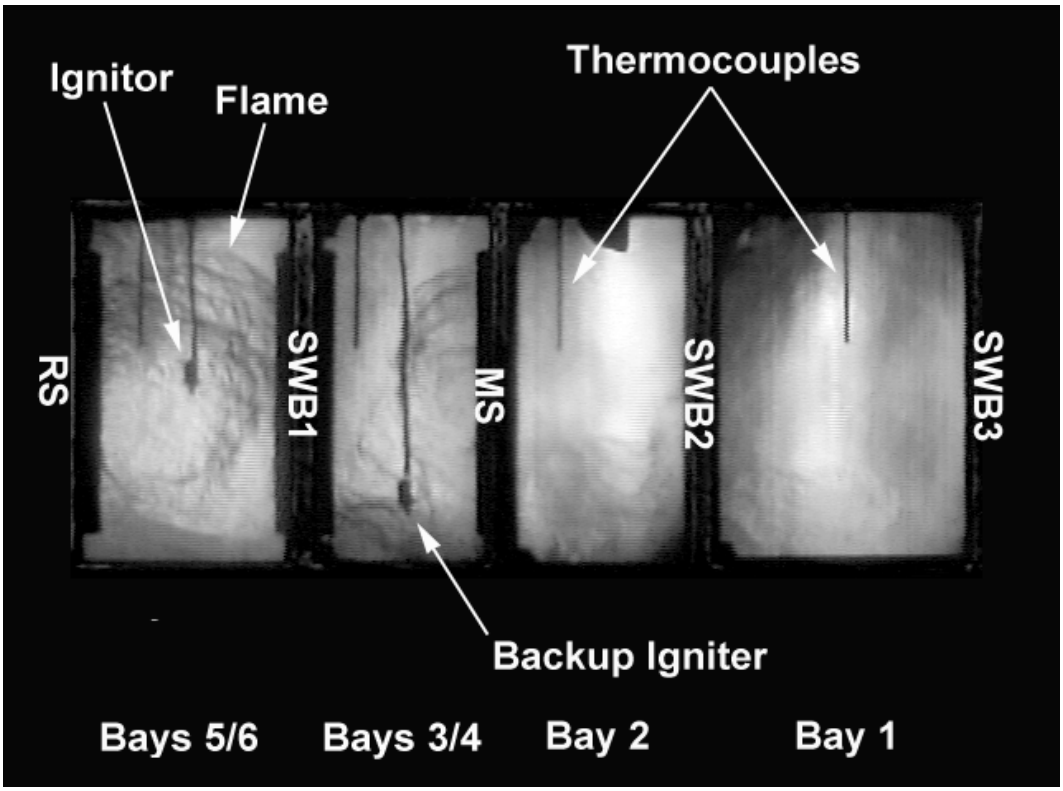

Figure 5.31: Sample composite schlieren image from Test 4, showing ignitors, thermocouples, and flame front.

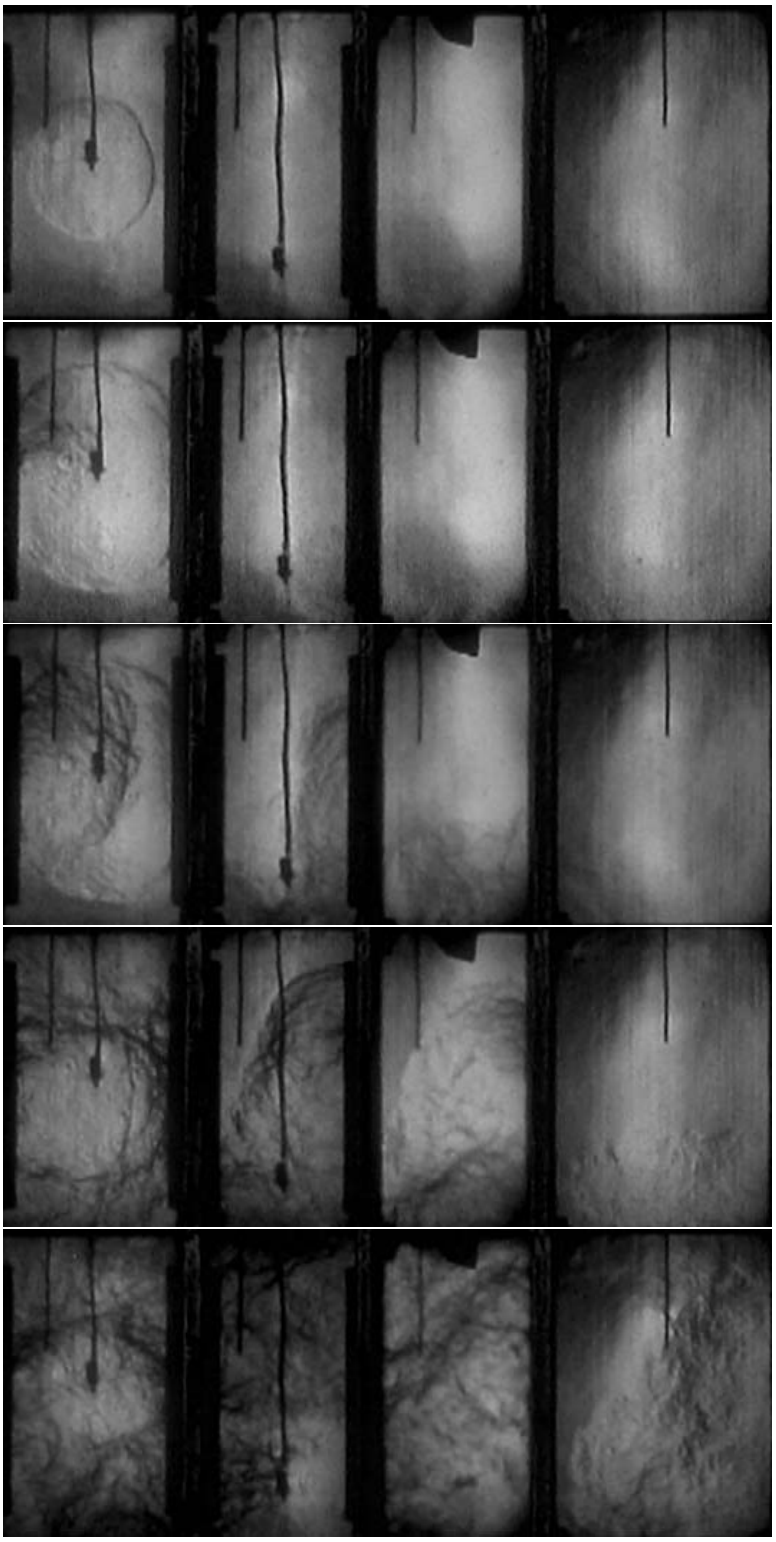

Figure 5.32: Sequence of composite schlieren images from Test 4. Frames are not equally spaced in time.

Ignition in Bay 5, with Cool Liquid Jet A Layer (Test 8) This was the first test to use a layer of Jet A in the bottom of the tank, in addition to the gaseous vapor simulant used in the previous tests. The test used 2.9 liters (about 2.3 kg, which is 1/64 of the 50 gallons estimated to have been in the CWT of TWA 800) of Jet A obtained from the local airport. If spread out uniformly over the bottom of the tank, this forms a layer about 0.05-in (1.2-mm) thick. During the test, lofting of the liquid was clearly visible in the video footage immediately after ignition (on the scale of the video framing rate). The tank was subsequently filled with an orange flame, whereas the gas-only flames were nearly invisible. Despite the obvious combustion of some portion of the Jet A, there was very little effect on the peak pressure. This is discussed in some detail in Chapter 6.

For the all-strong configuration, the Jet A combustion extinguished shortly after the gas phase combustion ended. Afterwards, soot covered the inside surfaces of the tank. In addition, there was a substantial fraction of the liquid fuel that was unburnt. This fuel coated all the interior surfaces of the tank. The fuel and soot were removed after each test with paper towels.

The pressure traces for this test are similar to those in Test 4, which had ignition in bay 5 and no liquid jet fuel layer. In Fig. 5.33, we see the interplay of pressures in bay 5 and the adjacent bays. Once bay 3 is ignited, the pressure rapidly increases and overshoots the pressures in bays 5 and 6. The trace from bay 4 is added in Fig. 5.34. We see that bay 4 is at nearly ambient pressure until it is ignited at about 80 ms. Once ignited, the bay 4 pressure rises much more rapidly than the other bays. This supports the notion of multiple ignition sources and high turbulence level in bay 4, as discussed for Test 4. Pressure piling is seen in bays 2 and 1 (Fig. 5.35), although they seem to ignite at the same time as bay 4. In fact, bay 2 ignites slightly sooner, and the flame may reach bay 1 through this route.

The differential pressures for this test are shown in Figs. 5.36 – 5.39. The starboard side of SWB1 experiences a large, positive differential pressure as bay 6 burns (Fig. 5.36). This is counteracted when bay 4 ignites, and the differential becomes negative. Likewise, on the port side, a small, positive differential pressure rise is created by the initial slow combustion in bay 5. Ignition of bay 3 drives the SWB1 pressure difference negative. The port side of MS shows a slower increase in pressure differential, as bay 2 ignites shortly after bay 3, and conteracts that pressurization from bay 3. The starboard side of MS shows a sharp jump from the rapid burn in bay 4. These traces coalesce and go negative as combustion proceeds in bay 2, slower but to a higher peak pressure due to the pressure piling effect.

SWB2 (Fig. 5.38) shows no large differential pressures since bay 1 and 2 pressures follow each other closely. The vent stringers follow the pressures of bays 3 and 6, with the starboard vent pressure rising first due to the earlier igntion of bay 6. In Fig. 5.39, the forward PR experiences a large excursion in differential pressure, while the aft PR pressures and changes are much smaller.

The pressure history across the forward PR is generated by the fast burn of bay 3 followed by the even faster burn of bay 4. The double-hump negative pressure difference across the aft PR results from the sequence of combustion events in bay 5. While pressure rise in bay 6 is fairly smooth (Fig. 5.33), that in bay 5 starts slow, accelerates, and slows again. This causes the pressure to lag behind that in bay 6 for most of the burn, creating the observed pressure history across the aft PR.

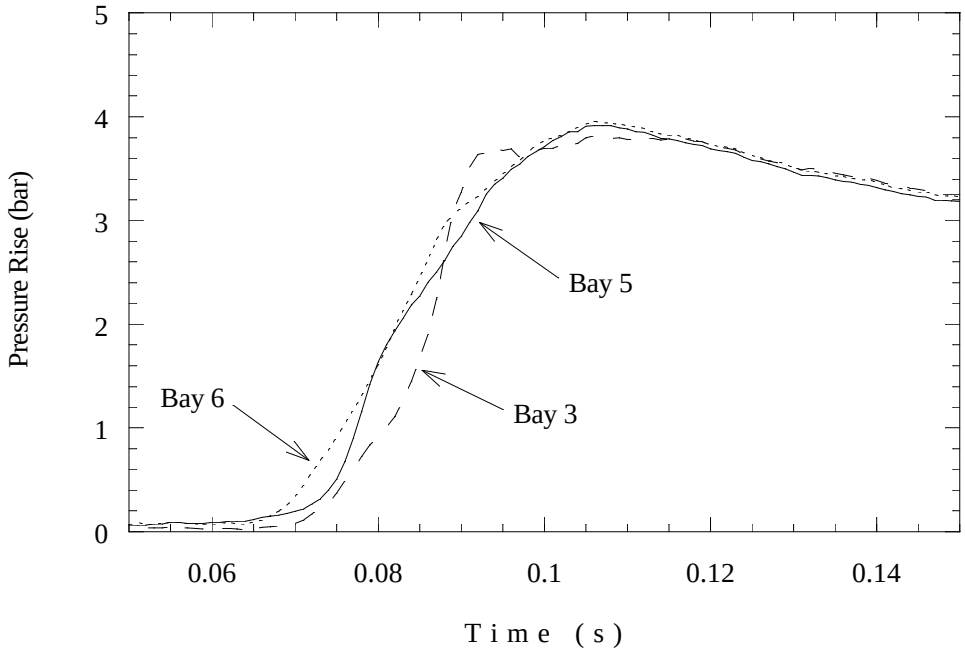

Figure 5.33: Pressure traces for bays 3, 5, 6, ignition in bay 5, with a cool liquid Jet A layer. Test 8.

The schlieren films could only record the early events of this test, as the view was rapidly blacked out by lofting and burning fuel and/or soot. In all bays, however, it is clear that combustion of the gaseous fuel begins before lofting and liquid fuel combustion in each bay. The film shows smooth ignition in bay 5, with the flame passing through the aft PR into bay 6, with rapid, turbulent combustion there. It appears that some fuel lofting does occur in bay 6, which may be caused by flow through the bottom passages in the aft PR. In bays 3 and 4, liquid lofting is clearly visible from the bottom corner passages. In the schlieren system, it is sometimes possible to see the events in adjacent bays since the camera field-of-view is often wider than the bay of interest. In bays 3 and 4, we see that lofting begins 2 or 3 frames before the initial flame in bay 5 reaches the partitions. It appears that the liquid fuel begins to burn shortly after the flame enters, as indicated by soot clouds that form and obscure the view. Bay 2 proceeds in the same fashion as bays 3 and 4. In bay 1, the flame enters via the vent connections, well before any flame is visible from the bottom passageways. This appears to be the primary source of ignition. Shortly after the flame enters, however, lofting is visible at the bottom of the compartment. As the flame jet from the vent stringer reaches the bottom of the compartment, it gets entrained into this flow and then engulfs bay 1.

The external footage showed a fair amount of leakage around SWB3, although this may have just been enhanced by the presence of soot and smoke in the gas. The NE DBM showed the leakage to be concentrated in the bottom starboard corner of SWB3, although there was leakage on both sides. The smoke also made an excellent tracer for flow out of the vent stringer exits (Fig. 5.41), which is not normally visible. Inside the tank, a white spray of lofting at the bottom starboard corner of SWB1 can be seen on the tape from the west hilltop video camera.

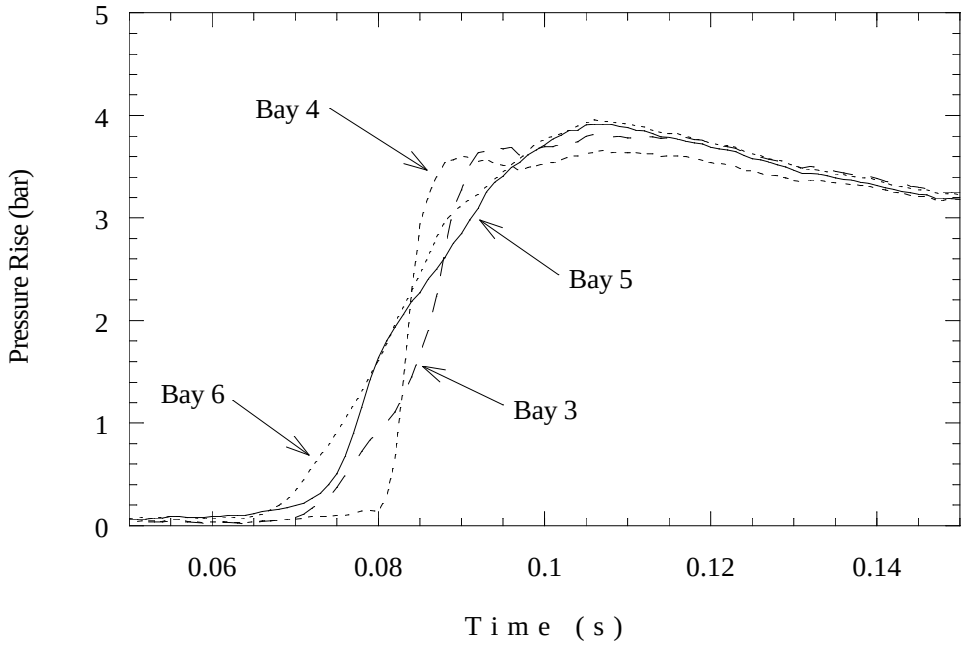

Figure 5.34: Pressure traces for bays 3 – 6, ignition in bay 5, with a cool liquid Jet A layer. Test 8.

This occurs within 1 – 2 frames of ignition, which is indicated by a glow from the filament. In the frame after lofting, an orange flame is visible that fills bay 5 and is already in bays 3 and 4. By the next frame, the orange flame is present throughout the tank. The orange flame persists for the longest time in bays 1 and 5/6. The lofting and subsequent flame is also visible in footage from the SE DBM. This camera is able to capture the lofting over a few more frames, and in all three forward compartments (along the starboard side). In bay 3, it appears that the liquid fuel ignites right at the region of lofting.

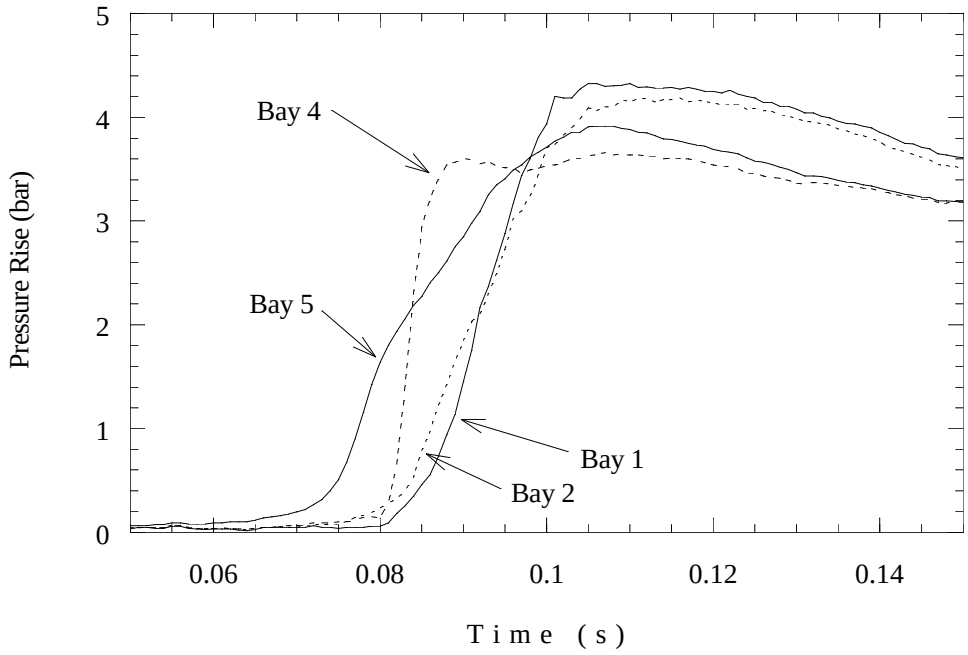

Figure 5.35: Pressure traces for bays 1, 2, 4, 5, ignition in bay 5, with a cool liquid Jet A layer. Test 8.

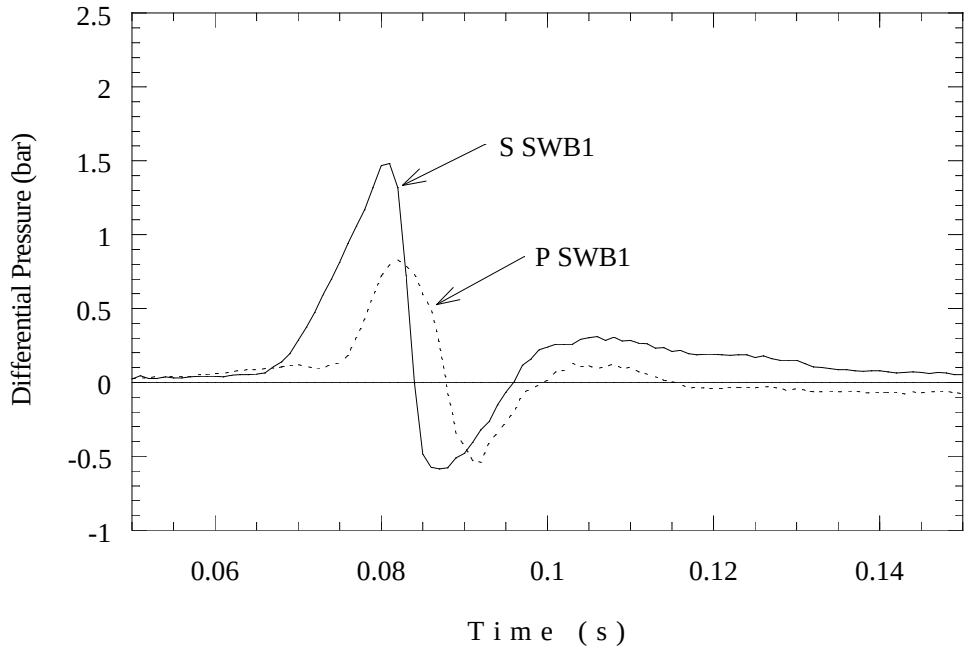

Figure 5.36: Differential pressure across SWB1, ignition in bay 5, with a cool liquid Jet A layer. Test 8.

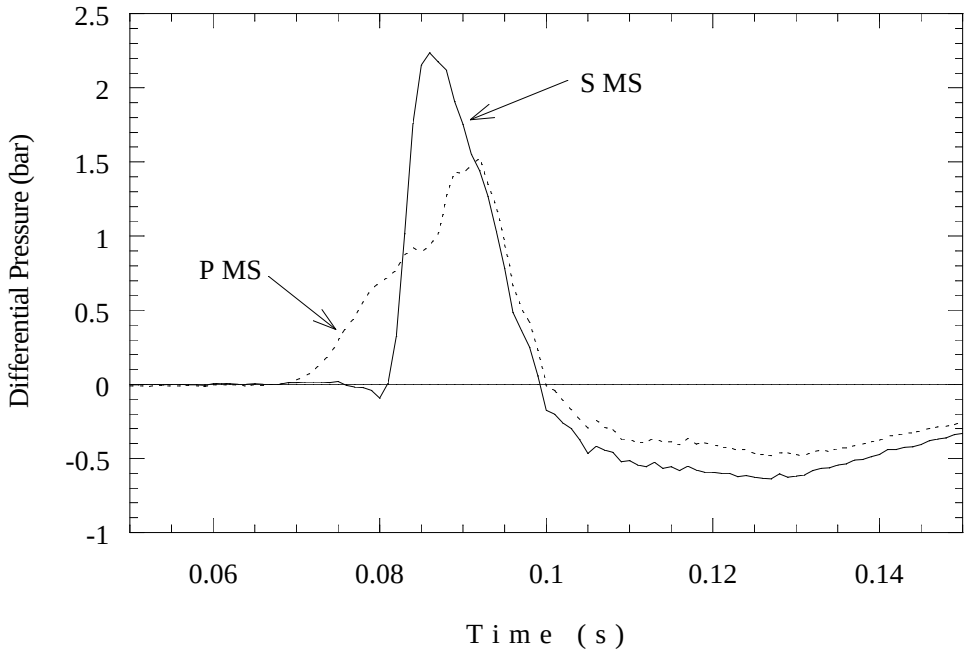

Figure 5.37: Differential pressure across MS, ignition in bay 5, with a cool liquid Jet A layer. Test 8.

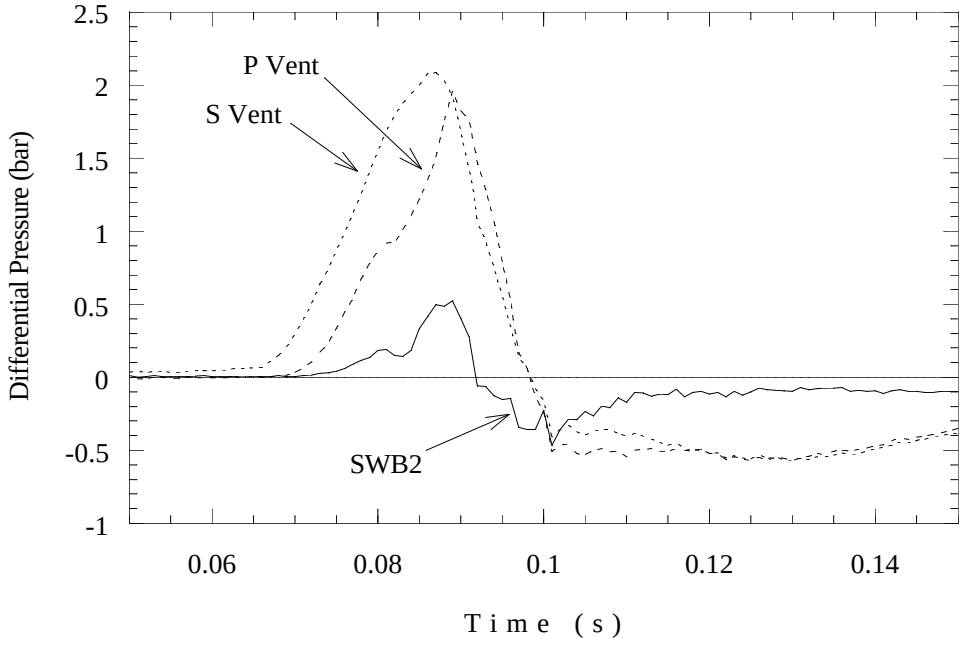

Figure 5.38: Differential pressures across SWB2 and vent stringers, ignition in bay 5, with a cool liquid Jet A layer. Test 8.

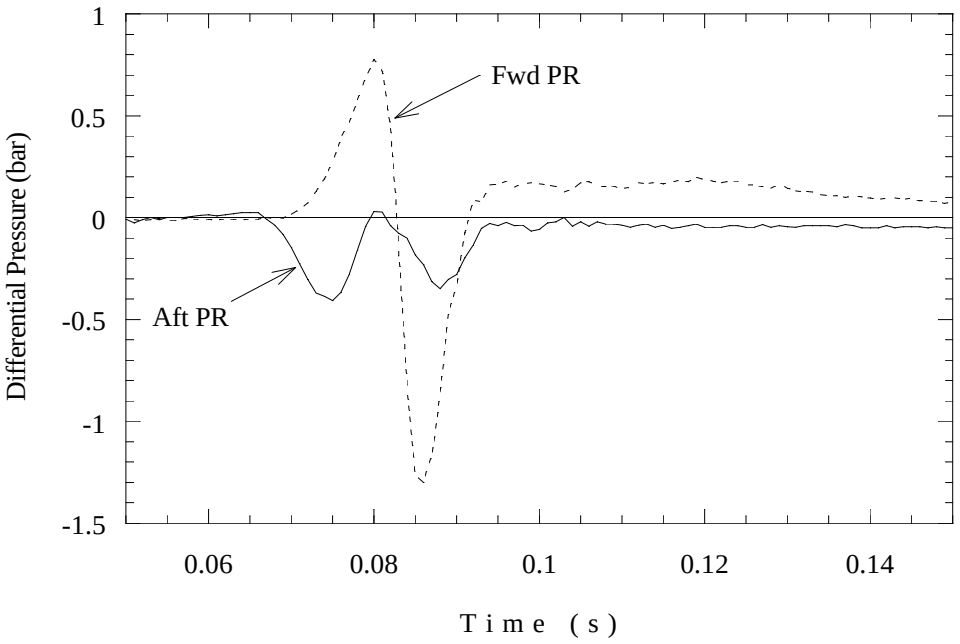

Figure 5.39: Differential pressures across PRs, ignition in bay 5, with a cool liquid Jet A layer. Test 8.

Table 5.15: Flame arrival times (ms), Test 8.

Photodetectors		Thermocouples			
67	68 **IGN**	73	67	68 **IGN**	74
73	71	85	84	88	86
78		97		98	
79		83		92	

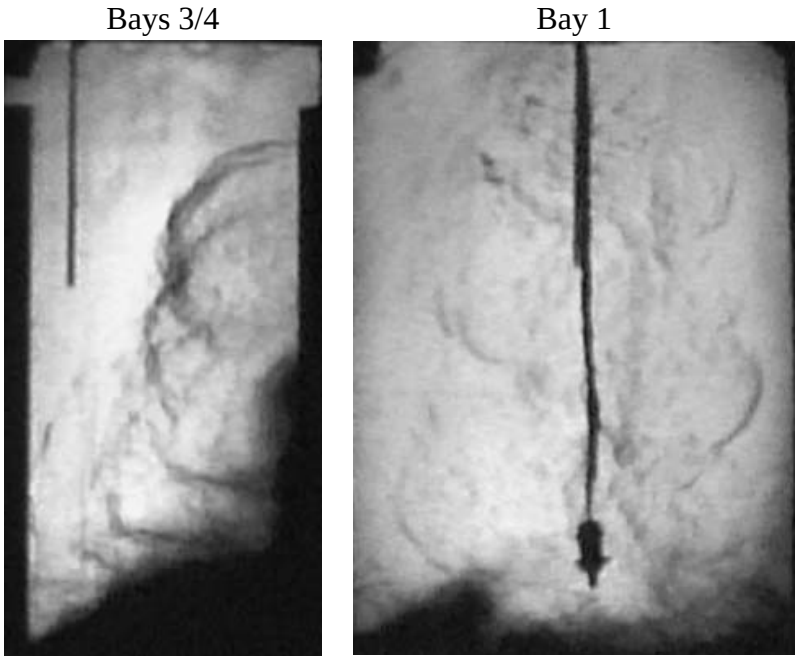

Figure 5.40: Fuel lofting in Test 8.

Figure 5.41: Venting of combustion products from vent stringers and leaks in SWB3. The soot acts as a tracer for the flows. Test 8.

Ignition in Bay 3 (Test 5) Pressure traces for ignition in bay 3 are shown in Figs. 5.42 – 5.45. In this test, the slow pressure transducer in bay 1 did not function, so pressure data is somewhat limited, especially with regard to differentials. Bay 3 has the typical slow pressure rise (Fig. 5.42), but bay 5 appears to ignite early, at about 120 ms. Bay 5 does not show the rapid pressure rise characteristic of turbulent combustion until after 140 ms. Bay 2 also ignites early, but doesn't show a change in slope until 150 ms. Bay 4 is the only one that shows immediate rapid combustion upon ignition, and it shows a rise rate comparable to that from dual ignition (previous discussion). Bays 2 and 5 are expected to be ignited earlier than 4, as the ignitor is closer to the boundaries of these bays than it is to bay 4. Examining bay 6 in Fig. 5.43, we see that it ignites shortly after bay 5, but quickly makes the transition to turbulent combustion.

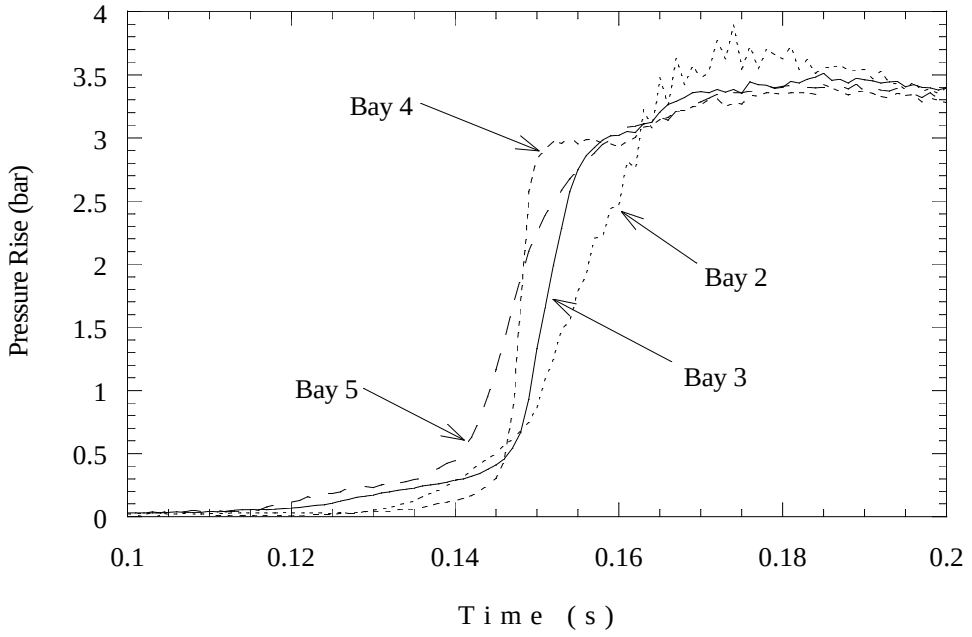

Figure 5.42: Pressure traces from bays 2 – 5, ignition in bay 3. Test 5.

In Fig. 5.44, the port side pressure differentials on SWB1 and MS lag the starboard ones. The starboard pressures also show the rapid pressure rise in bay 4, as the forces act outward from the bay. The port sides show no large negative differentials. The partial ribs, in Fig. 5.45, show primarily negative differentials. The forward PR shows a spike from the bay 4 pressure rise.

The schlieren films show that the flame starts smoothly in bay 3, then enters bays 2, 4, and 5 through the bottom passageways, initiating rapid turbulent combustion. In bay 1, the flame jet is clearly visible coming from one of the passageways above the bottom (i.e., not the corners). Just as the flame rolls around the top of the tank, flow from the vents is visible. It is engulfed by the main flame before we can see if it is a propagating flame. It appears that there was no leakage at the sides of SWB3.

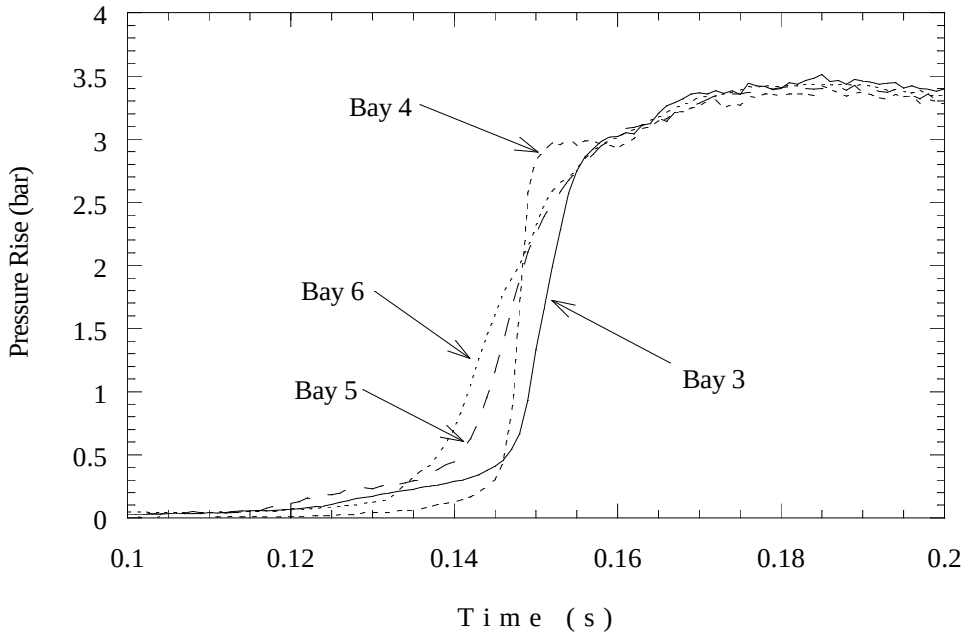

Figure 5.43: Pressure traces from bays 3 – 6, ignition in bay 3. Test 5.

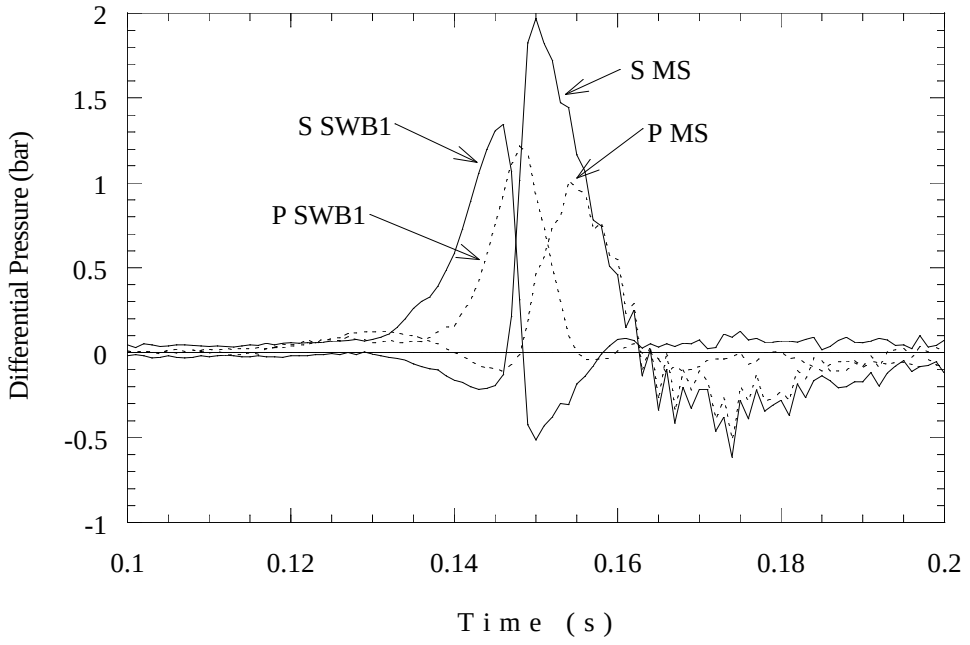

Figure 5.44: Differential pressure across SWB1 and MS, ignition in bay 3. Test 5.

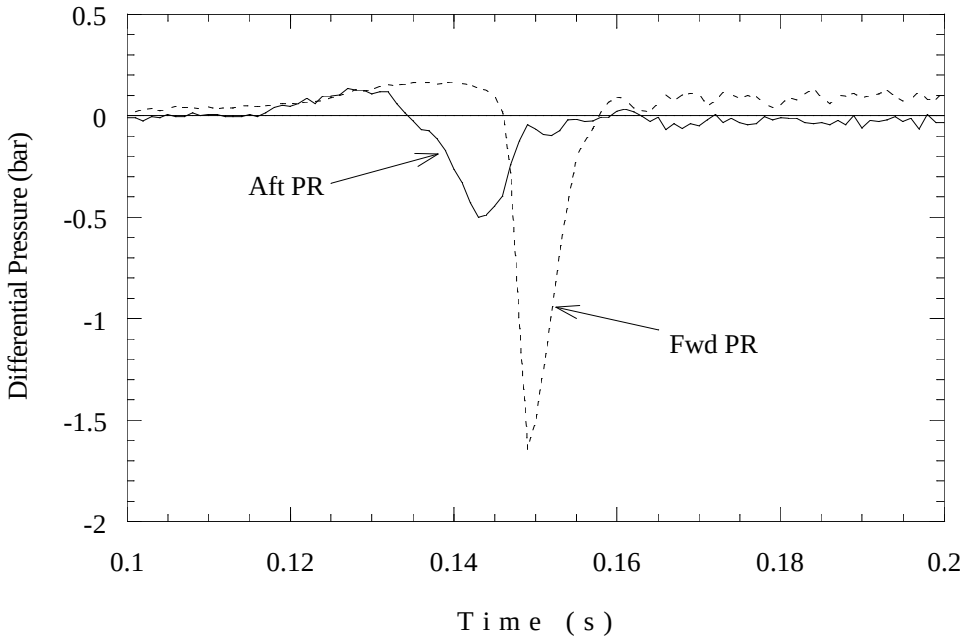

Figure 5.45: Differential pressure across PRs, ignition in bay 3. Test 5.

Table 5.16: Flame arrival times (ms), Test 5.

Photodetectors

137	141
144	145 **IGN**
147	
149	

Thermocouples

145 140	127 142
149 150	62 **IGN** 146
169	152
170	158

Ignition in Bay 2 (Test 6) In this test, the side seals on SWB2 appeared to fail with flow in the aft direction. Post-test inspection indicated that SWB1 and MS had moved forward. This movement loosened the bolt sealing washers, creating small leaks. The leaks were stopped by re-tightening the bolts. The flame is ignited in the center of the bay, and the vent stringers do not connect to that bay so that the flame can only propagate into the adjacent bays, 3/4 and 1. Figure 5.46 overlays the pressure traces for bays 3 and 4, and 5 and 6. This demonstrates that in this case the combustion process proceeds nearly simultaneously and at the same rate in the left and right bays at the aft end of the tank.

The pressure traces from all bays are shown in Fig. 5.47. The igniter is farther away from passageways in bay 2 than it was in previous locations, resulting in a long (about 180 ms) period prior to the onset of rapid combustion. As the flame enters subsequent bays, the rate of pressure rise is very similar. The flame enters bays 3 and 4 at 180 ms, and then 5 and 6 about 70 ms after. When ignition occurs in bays 5 and 6, the pressure in bay 2 also takes a sharp upturn. It is possible that turbulence has been generated there as a result of rapid combustion in other bays, and this accelerates the flame in bay 2. Surprisingly, bay 1 ignites last, resulting in pressure piling. Pressure piling also occurred in bays 5 and 6. Ignition in the center of the tank allows pressure piling to occur at both ends. It does not appear that flow through the vent stringers plays a role in bay 1 piling since there is no significant pressure rise in bay 1 before ignition.

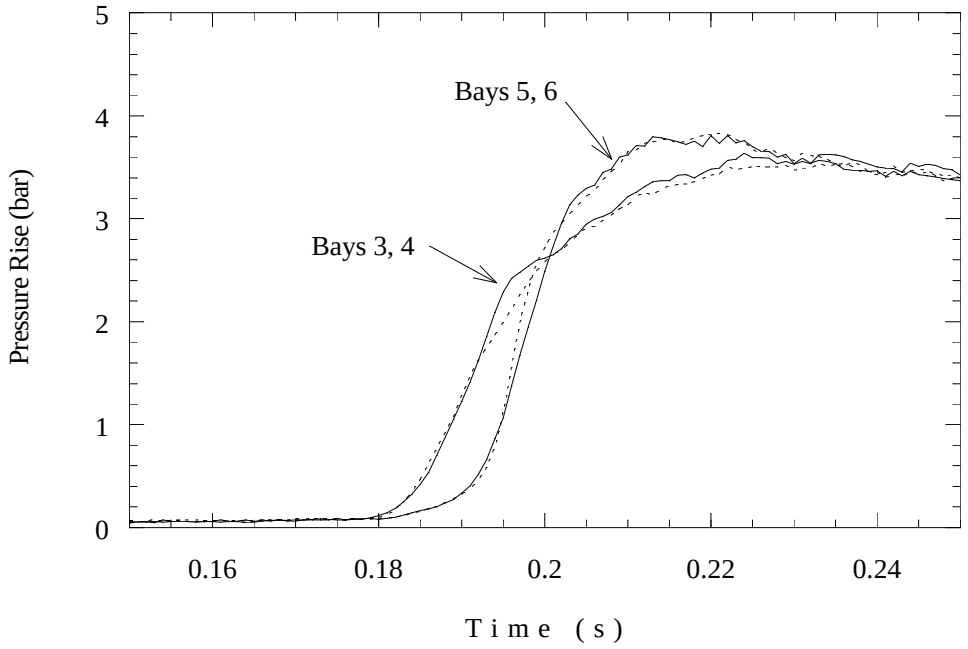

Figure 5.46: Pressure traces from bays 3 – 6, ignition in bay 2. Dashed lines indicate even-numbered bays. Test 6.

Figure 5.48 shows the right-left symmetry of the pressure loading — the port and starboard sides of SWB1 and MS follow each other closely — diverging only at and after the peak in the differential pressure. The pressure across the vent stringers, in Fig. 5.49, indicates the

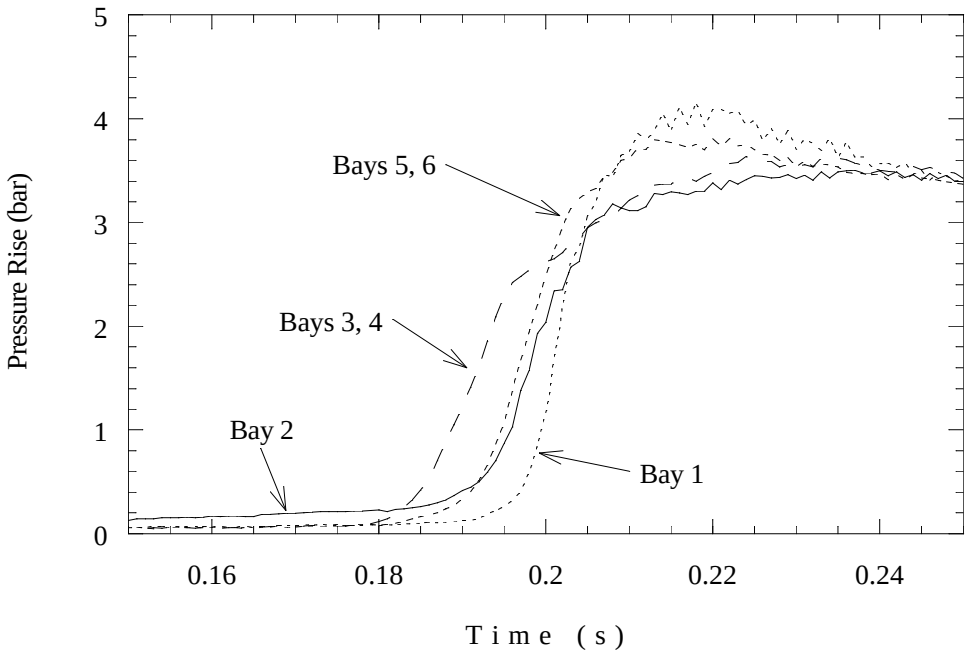

Figure 5.47: Pressure traces from bays 1, 2, 3, 5, ignition in bay 2. Test 6.

potential to pressurize bay 1, but the duration is too short for a significant amount of gas to flow into bay 1. In addition, the vent pressure differentials indicate the rearward progression of combustion, and the pressure rises across the port vent (connected to bay 3) before the starboard vent (connected to bay 6). SWB2 experiences a small pressure difference until the transition to rapid combustion in bay 2 at 180 ms. These differential pressures all become negative after bay 1 is ignited at 200 ms.

The differential pressures across the partial ribs are less than ± 0.4 bar, and occur in opposite directions (Fig. 5.50).

Schlieren films show that the flame starts smoothly in bay 2, and enters the other bays through the bottom passageways. When the flame reaches bays 5 and 6, combustion is very rapid, occurring over a few frames. It is not possible to distinguish between bays 5 and 6. It appears that combustion in bay 2 is accelerated by venting of the other bays. The original flame in bay 2 had already filled the cross section of the bay by that time, so it was not completely clear that unburnt mixture remained, but this is possible since the lateral extent of the bay is much greater than its cross-section. In bay 1, a flame jet is visible coming from the liquid fuel manifold before the main flame arrives (Fig. 5.51). The manifold flame does not seem to propagate far before it is overtaken by the main flame created by ignition from the passageways in SWB2. Minimal leakage occurred around SWB3. This may have been along the top, rather than at the side seals.

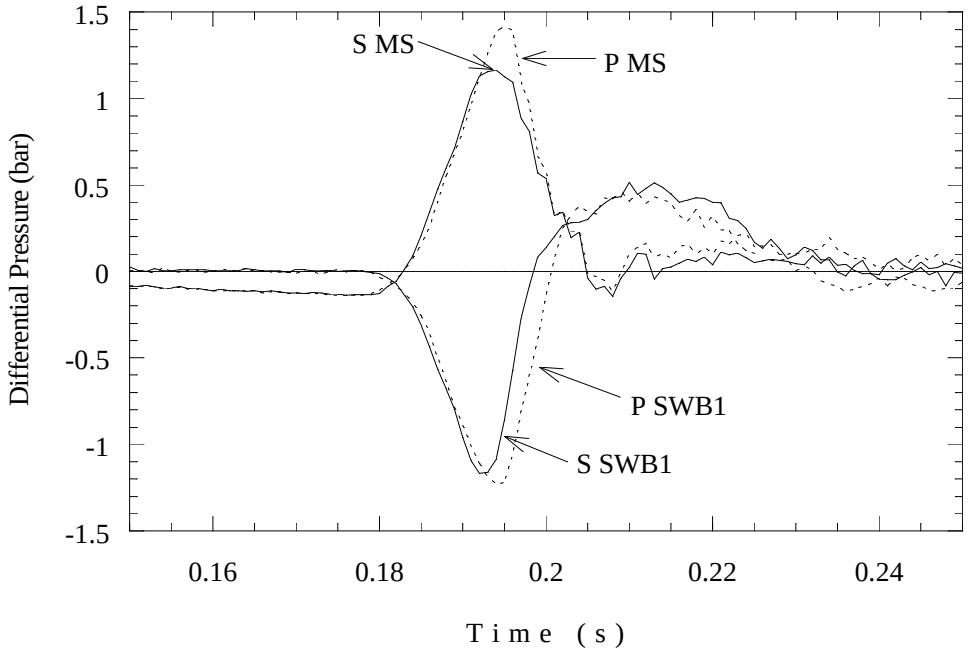

Figure 5.48: Differential pressure across SWB1 and MS, ignition in bay 2. Test 6.

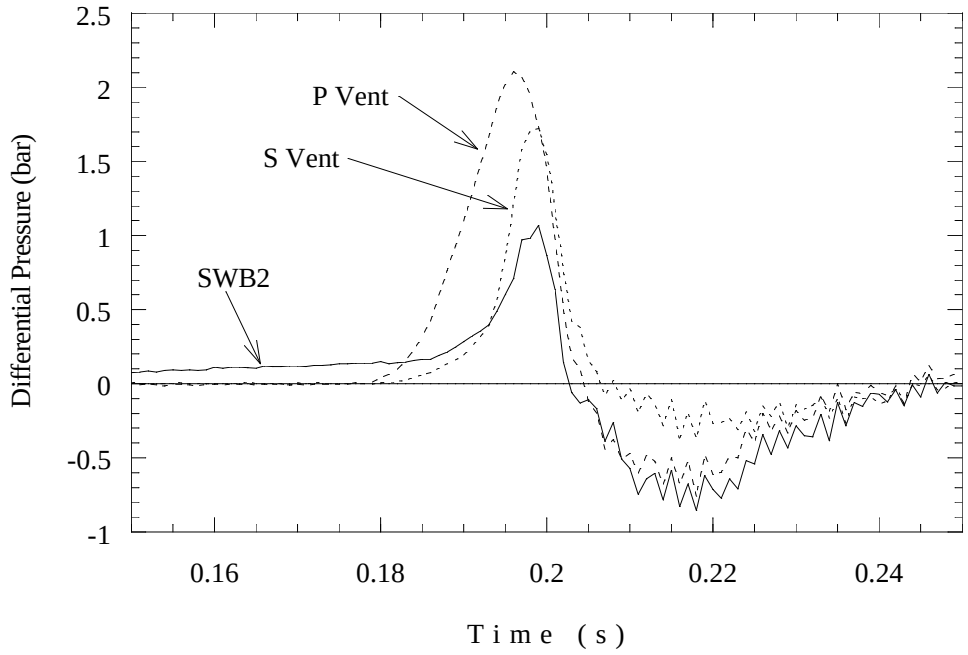

Figure 5.49: Differential pressure across SWB2 and vent stringers, ignition in bay 2. Test 6.

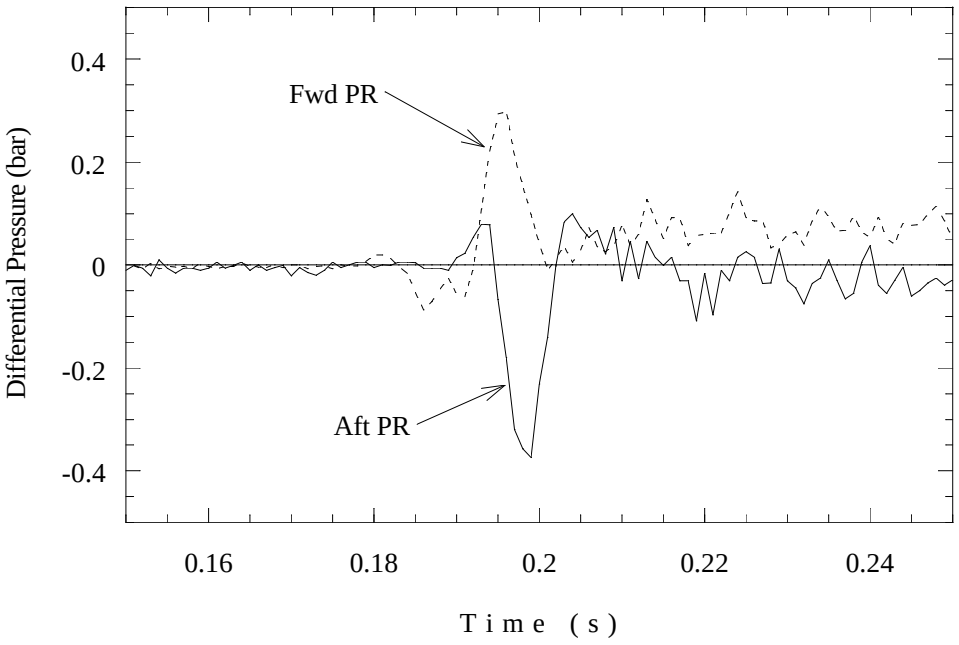

Figure 5.50: Differential pressure across PRs, ignition in bay 2. Test 6.

Table 5.17: Flame arrival times (ms), Test 6.

Photodetectors		Thermocouples			
193	191	196	196	196	193
184	184	185	186	187	185
191 **IGN**		193		149 **IGN**	
197		206		201	

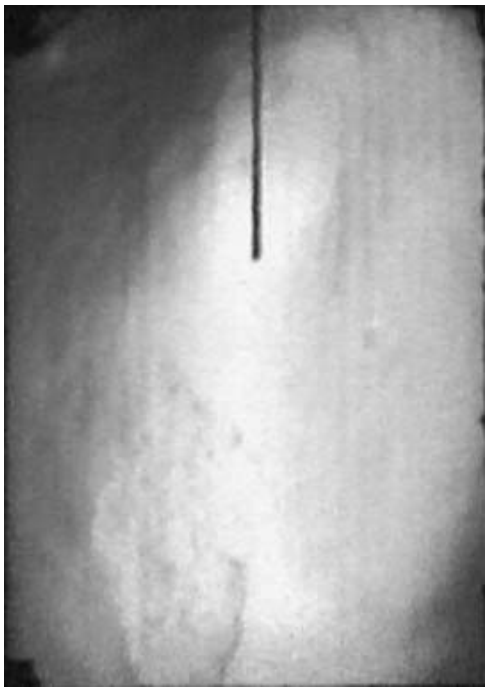

Figure 5.51: Ignition of bay 1 through jet fuel manifold in bottom of tank. Test 6.

Ignition in Bay 1 (Test 7) It should be noted that the aft PR underwent partial failure in this test, and this should be considered in analysis of the results. "Partial failure" means that the PR did not completely break free from its mounts. In this test, the forward end of the aft PR broke free of its bracket and bent during the burn. Polycarbonate allows a great deal of deformation before fracture and the PR returned to its original position after the pressure difference dropped. The aluminum brackets were responsible for the failure; the edges of the holes pulled around the 5/16-in bolts holding the brackets to SWB1. The bending motion damaged the side of the brackets attached to the PR, but they held. The bracket on RS was replaced with a heavier one after this test; this change eliminated this type of failure.

In this test, the lateral symmetry was not as strong as with bay 2 ignition. Figure 5.52 indicates that bays 3 and 4 were quite similar, but there is a clear difference between 5 and 6 at the onset of rapid combustion. Aside from bay 1, all of the bays had similar pressure traces, with the onset of rapid combustion occurring within 15 ms (Fig. 5.53) in all bays. The direct communication provided by the vent stringers from bay 1 to the rear bays may play a role in this coincidence. As pressure increases in bay 1, rearward flow is generated in the vents. When the flame enters the vents, it travels quickly to the rear bays. However, this does not explain why bay 6 ignites before bay 3, which is closer to bay 1. The thermocouple data (Table 5.18) confirms earlier ignition of the bays connected to the vent stringers.

Figures 5.54 and 5.55, and the thermocouple and photodiode data (Fig. 5.18), can all be used to determine the ignition order of the bays. The ignition sequence, after bay 1, appears to be 6, 3/4, and 2/5. It is interesting to note that bays 2 and 5 ignite at nearly the same time. The early ignition in bay 6 probably caused this.

Despite the small differences in ignition time, the steep slopes of the pressure traces created large differentials. The early ignition in bay 6 yields a positive force on the starboard side of SWB1 (Fig. 5.56), which goes negative when bay 4 ignites. The port side of SWB1 undergoes the opposite sequence, the pressure difference is initially negative when bay 3 ignites, and becomes positive when bay 5 ignites. There is greater lateral symmetry for the MS, Fig. 5.57, than for the other partitions.

As the vents and SWB2 (Fig. 5.58) all separate bay 1 from the aft portions of the tank, these pressure differentials fall closely together. The initial slow burn in bay 1 creates the gradual negative differential. Once bay 6 ignites, the pressure drop is reversed across the starboard vent, with the port vent and SWB2 following shortly thereafter as the flame reaches the other bays. It is interesting to note the decrease in slope in the starboard vent differential pressure prior to the rapid rise to the peak value.

Figure 5.59 shows the large pressure differential that caused the failure of the aft PR. Failure presumably occurred when the pressure reached 2.1 bar and rapidly dropped. This plot also shows the non-symmetrical behavior of this test compared to ignition in bay 2.

The schlieren films show combustion starting laminarly in bay 1 and the flame entering bay 2 through the bottom passageways. The flame enters bays 3 and 6 through the vents first. In bays 5 and 6, another flame front appears to enter from the bottom after the vent flame has propagated to the bottom of the tank; this may also be entrainment of the vent flame by jets flowing out of the passageways. The camera boresite was blocking the bottom of the bay 3/4 view, so that events in the bottom of those bays were not visible. In bay 1, after the initial flame

Table 5.18: Flame arrival times (ms), Test 7.

Photodetectors

200	200
198	194
200	
202 **IGN**	

Thermocouples

187	204	202	203
202	203	201	198
201		211	
111 **IGN**		147	

front fills the cross section, secondary flames are visible entering from the vent connections. It is not clear if these are actually flames or just hot products, since the flame had already passed through the vents.

After these flames enter bay 1, the turbulent flow generated by combustion in the other bays sweeps through bay 1 and brings combustion to completion. It is difficult to tell what causes partial failure of the aft PR. Possibly, the flame is initiated in bay 6 by the vent stringers, generating even more turbulence in bay 5. Once bay 5 ignites, it outpaces bay 6, creating the differential pressure which breaks the front end of the aft PR free and swings it starboard.

External video shows some leakage on the starboard side of SWB3. This occurs after the flame in bay 1 has been accelerated by combustion in the aft bays. An orange glow is visible when the flame reaches the aft bays, and this moves forward very rapidly (within one video frame).

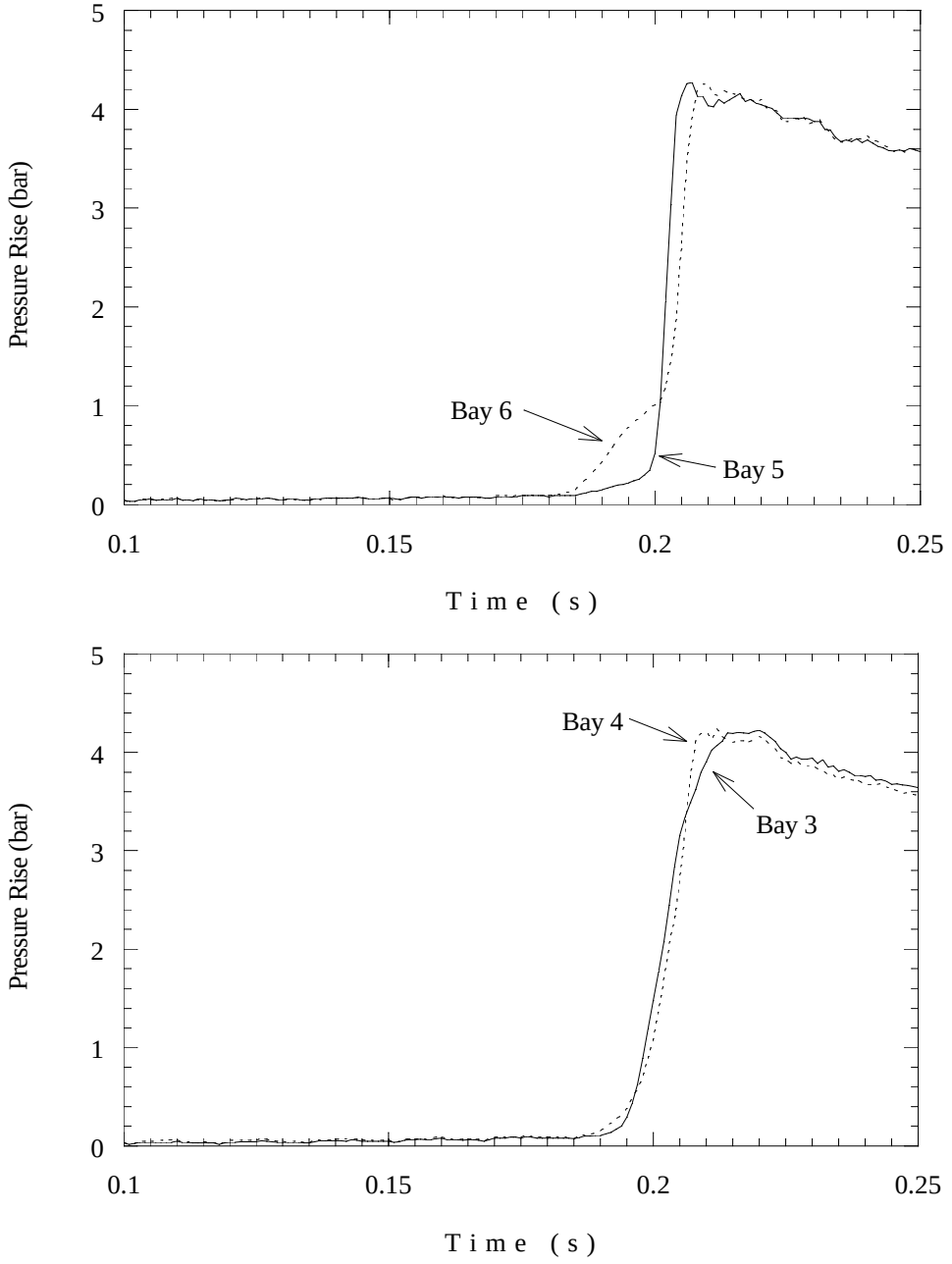

Figure 5.52: Comparison of bays 5, 6 and 3, 4, ignition in bay 1. Test 7.

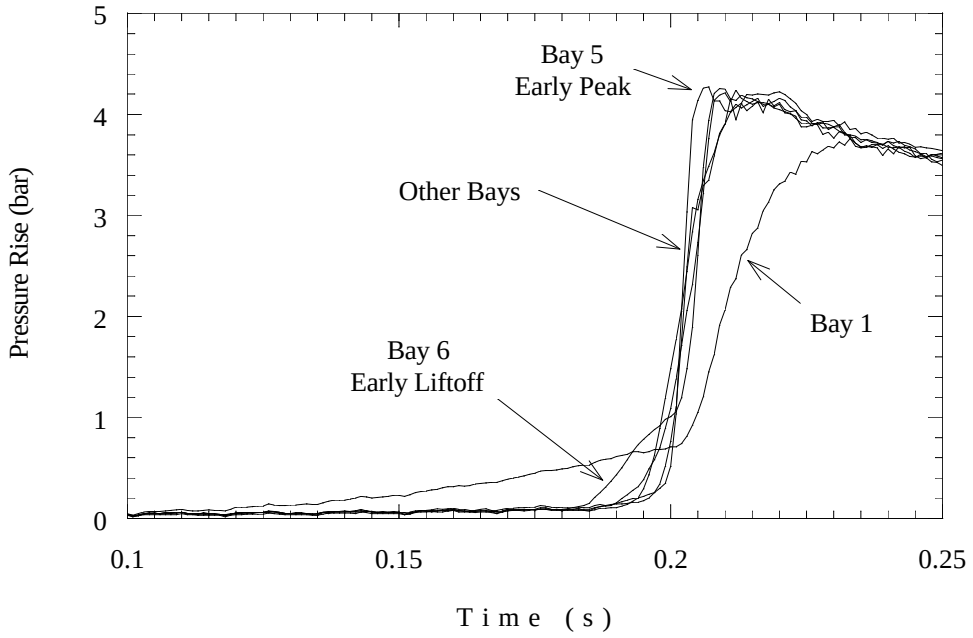

Figure 5.53: Pressure traces from all bays, ignition in bay 1. Note that bays 2 – 6 are all similar. Test 7.

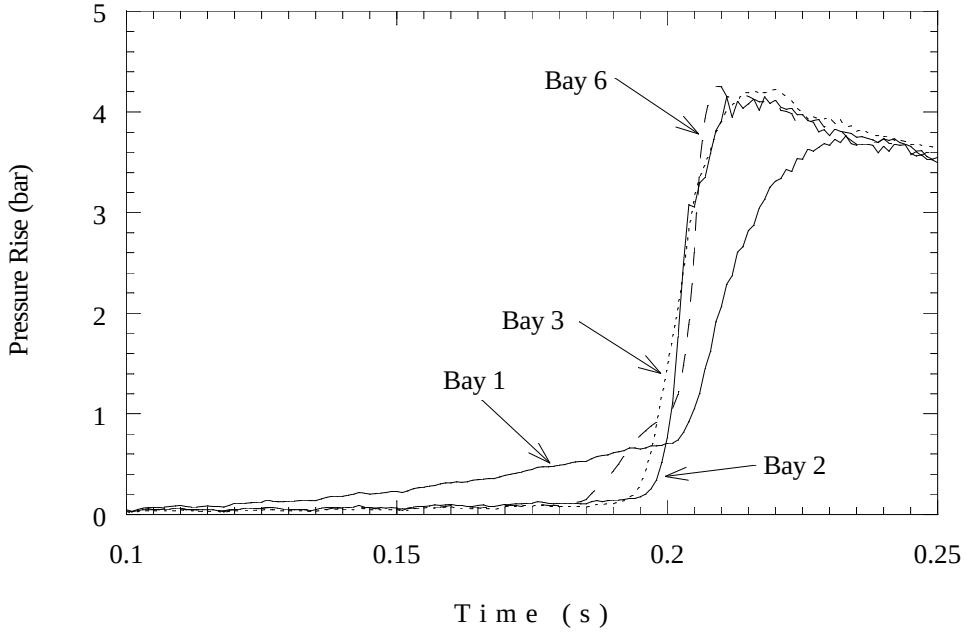

Figure 5.54: Pressure traces from bays 1, 2, 3, 6, ignition in bay 1. Test 7.

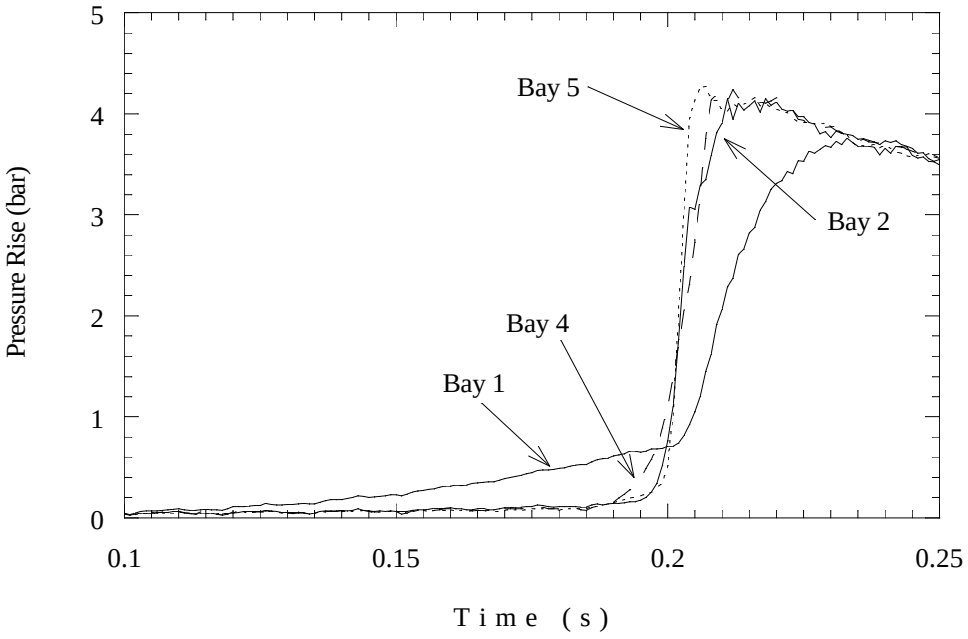

Figure 5.55: Pressure traces from bays 1, 2, 4, 5, ignition in bay 1. Test 7.

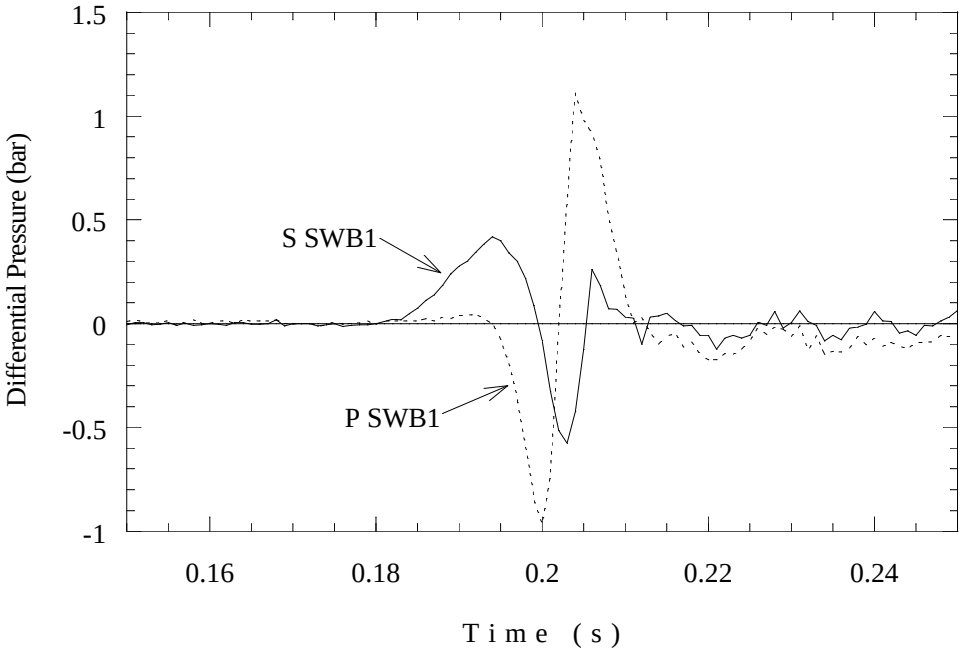

Figure 5.56: Differential pressure across SWB1, ignition in bay 1. Test 7.

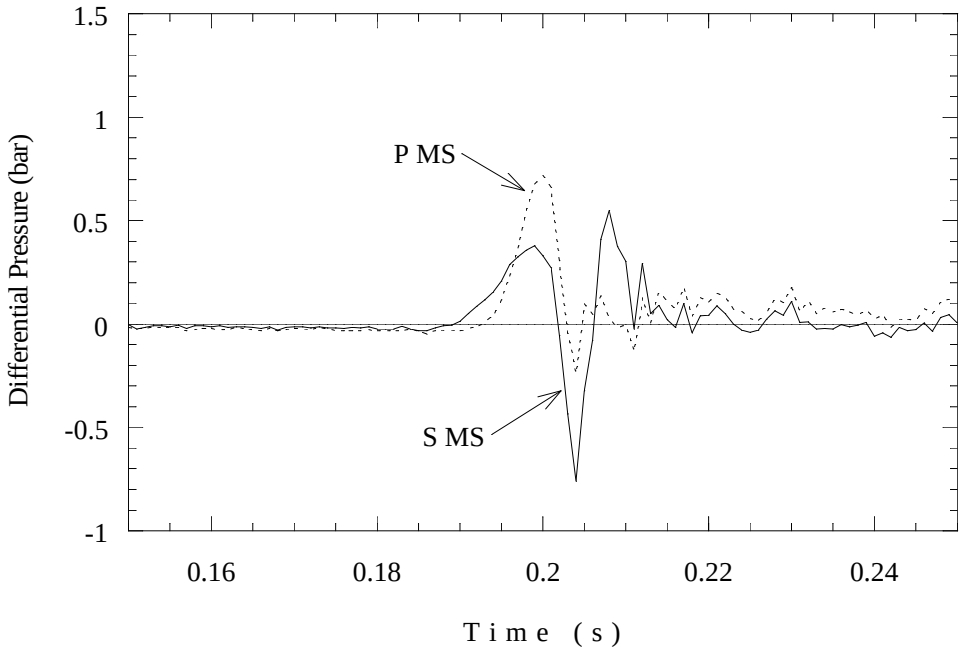

Figure 5.57: Differential pressure across MS, ignition in bay 1. Test 7.

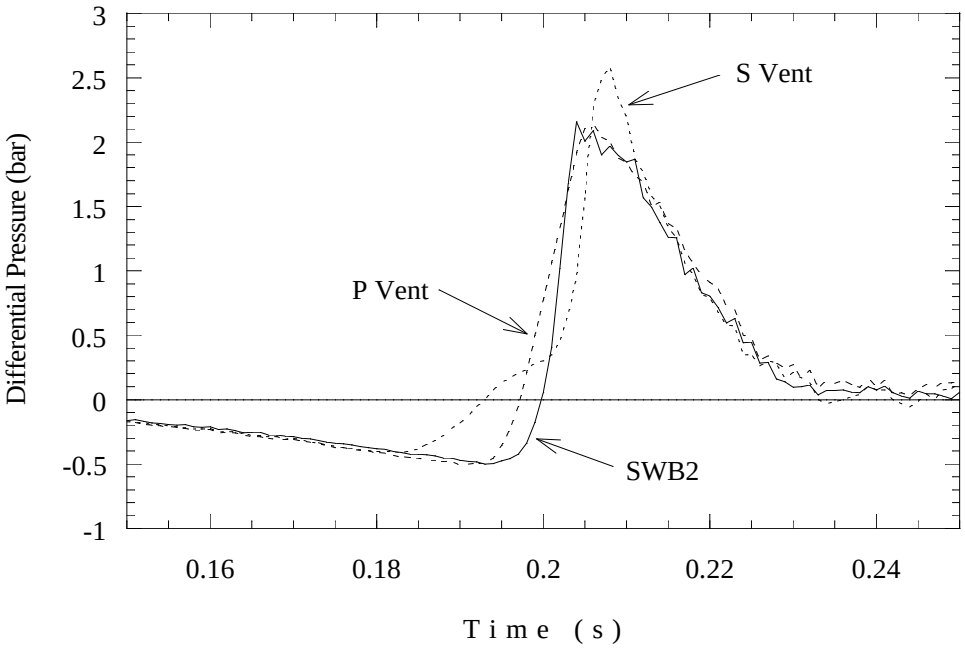

Figure 5.58: Differential pressure across SWB2 and vent stringers, ignition in bay 1. Test 7.

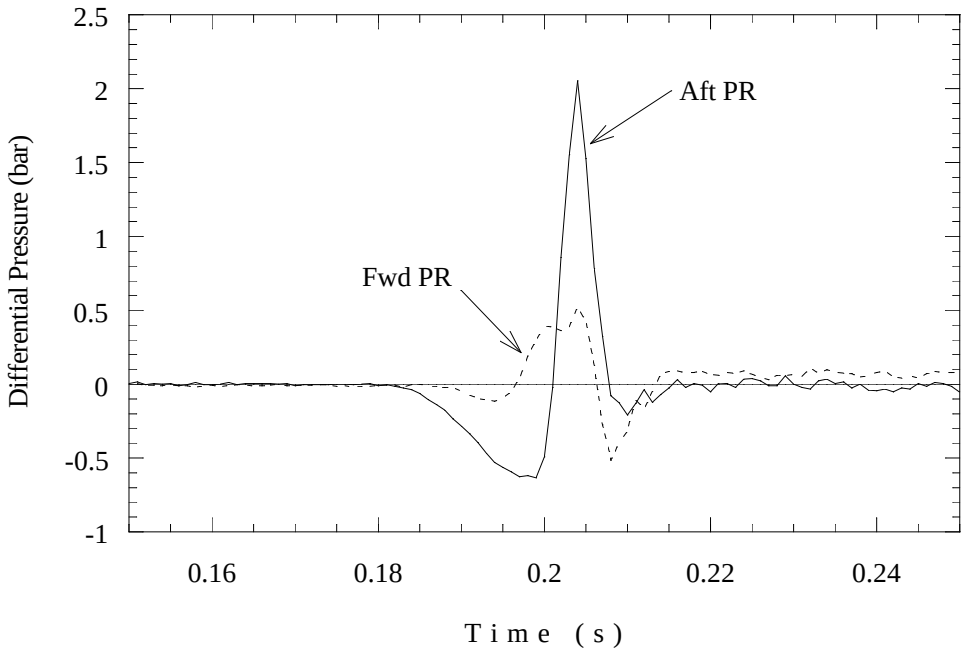

Figure 5.59: Differential pressure across PRs, ignition in bay 1. Test 7.

Ignition in Bay 6R (Test 15) The 6R ignition location is in bay 6, attached to the surface of SWB1 at a location 3 in from the starboard side and 2 in down from the top of the tank. This simulates a fuel probe location in the actual CWT. In this test, the forward PR failed at one end, and the aft PR failed completely by a combination of bolt failure and material fracture. Because of the failure of the partial rib, the geometry changed during the combustion event. This means that this test is not very useful for comparison with other tests or for numerical simulation unless the structural failure is also considered.

In addition to the PR failures, it also appeared that the outer edges of SWB1 swung forward and snapped back. The additional forces placed on the PRs by motion of SWB1 probably contributed to their failure. Some of the damage was quite extensive. The aft PR was actually fractured, whereas the aluminum bracket had failed in earlier tests. Some of the 10-32 screws were broken, too. Scuff marks in the rust on the top and bottom of the tank indicated that the edges of SWB1 and SWB2 deflected forward 0.75 to 1 in and returned. These marks could be from Test 14, but it looked like the buckling kinks in the SWB2 angle bracket were larger than they were before the test.

The pressure traces from bay 6 and the adjacent bays 4 and 5 are shown in Fig. 5.60. The flame enters bay 4 shortly after ignition because of the corner and vent stringer passages located near the ignitor. Thus, both bays undergo slow combustion at first, although there is some communication between them. Bay 5 shows a slow pressure rise from the combustion in 4 and 6, until it ignites at 185 ms and burns rapidly. Figure 5.61 adds the pressure trace from bay 3, which follows the early pressurization of bay 5 and ignites shortly after bay 5. Bay 3 experiences the highest pressure peak.

The pressure traces from bays 1 and 2 are shown in Fig. 5.62, with bays 4 and 6 for reference. In Fig. 5.61, we observe a slow initial pressure rise in bays 3 and 5 with pressures lower than in bays 6 and 4 until about 185 ms. This indicates that bays 3 and 5 were probably not ignited prior to that time, and were only being pressurized by outflow from bays 6 and 4. On the other hand, the early-time pressure in bays 1 and 2 closely follows the pressure in bay 6 until about 180 ms. Data from the thermocouples (Table 5.19) show that the flame runs up the starboard side of the tank very rapidly. Therefore we conclude that combustion begins in bays 2 and 1 shortly after the ignition in bay 6. The combustion is relatively slow and the peak pressures in bays 2 and 1 do not occur until about 230 ms, compared to 195 to 200 ms for the other bays.

This test produced differential pressures higher than those in any previous test, as much as 4 bar, shown in Figs. 5.63 – 5.65. The differential pressure across SWB1 and MS (Fig. 5.63) reflects the rapid combustion process in the aft bays. The starboard side of SWB1 has a small negative differential, arising from early pressure in bay 4. This becomes very large and positive as bay 6 transitions to turbulent combustion before bay 4.

The delay in transition to rapid combustion in bay 1 allows for high pressures across the vents, as shown in Fig. 5.64. The starboard vent differential rises first, as bay 6 begins to pressurize before bay 3, which is connected to the port vent. As the bay 3 pressure increases to its peak, exceeding the pressure in bay 6, the port vent differential pressure follows suit. The pressure across SWB2 is low by comparison, peaking at less than 1 bar. This is attributed to the slow rise and nearly equal values of bay 1 and 2 pressures.

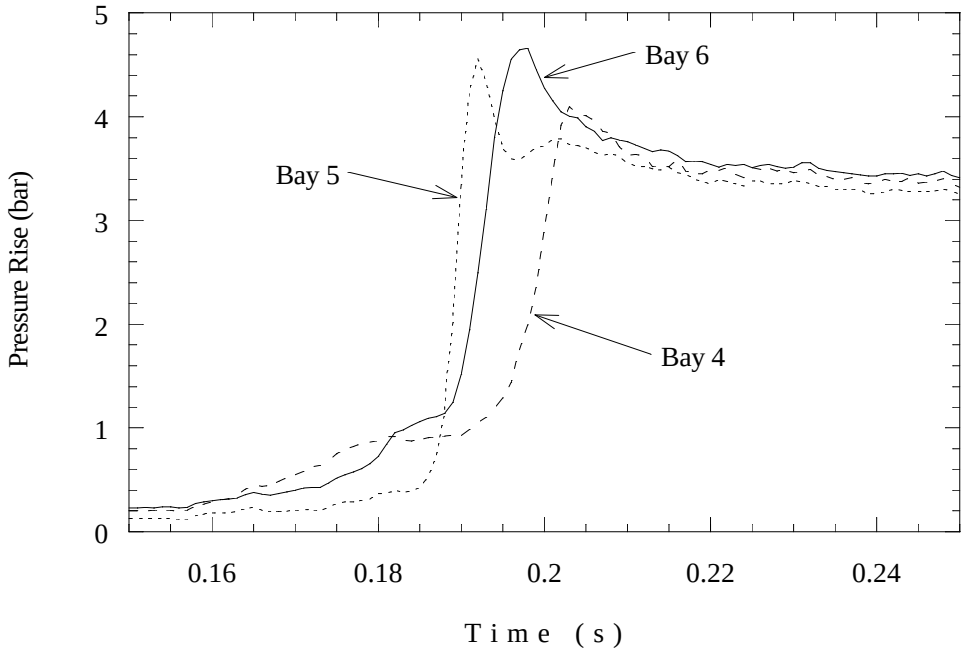

Figure 5.60: Pressure traces for bays 4, 5, 6, ignition in bay 6R. Test 15.

As stated above, both PRs suffered damage in this test. In Fig. 5.65, it appears that the forward PR failed at the peak pressure of 3 bar, although it remained attached at one end. The aft PR completely failed and was blown to the starboard, although the pressure differential shows a negative phase. This appears to last too long to be caused by flow from bay 5 after rupture of the PR, so perhaps the PR continued to divide the bays for a short time after it separated from the brackets. This would put the failure of the PRs at just before 200 ms.

Unfortunately, the schlieren system DBM covering bays 5 and 6 did not function correctly during this test. The bay 3/4 camera shows a laminar flame entering the top of bay 4 shortly after the timing strobe, through the passageway near the ignitor. When this flame makes it about two-thirds of the way towards the bottom of the bay, a turbulent flame suddenly forms at the bottom of the bay. It is unclear if this is in bay 3 or 4. At the same time, scattered light is visible from combustion in bay 2. Then, it appears that bay 3 is ignited and engulfed instantaneously. A few frames later, the forward PR fails. It actually flexes once, snaps back, and then flexes again and breaks free. As it breaks free, a reflection from the aft PR is also visible, showing that it too has broken free.

In bay 2, a flame jet enters from bay 3 or 4 via one of the top passageways. This jet reaches SWB2, spreads out and the flame burns down into the bay. Suddenly, the combustion accelerates further in bay 2, possibly associated with venting into bay 2 from bays 3 and 4. Reflected light from bays 3 and 4 show that this happens just as the forward PR is failing. The flame also enters bay 1 from one of the top passageways in SWB2, reaching SWB3 and then burning the entire bay. At one point, it appears that another flame enters vertically downward from one of the vent stringers, but it is difficult to tell for certain. As in the other bays, the combustion in bay 1 is violently accelerated near the end of the burn.

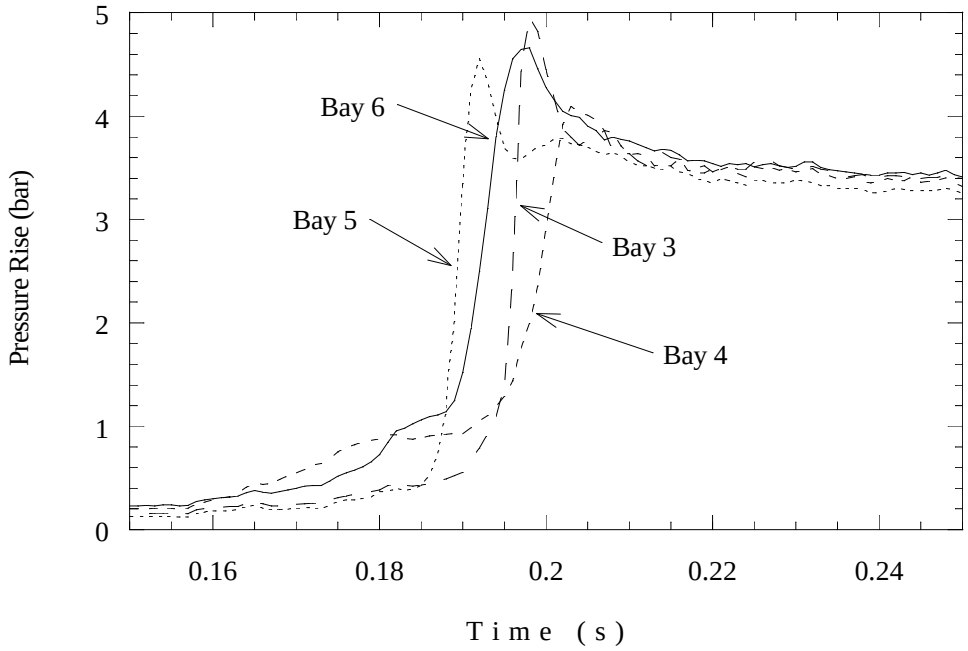

Figure 5.61: Pressure traces for bays 3 – 6, ignition in bay 6R. Test 15.

Exterior cameras showed very little evidence of leakage around SWB3.

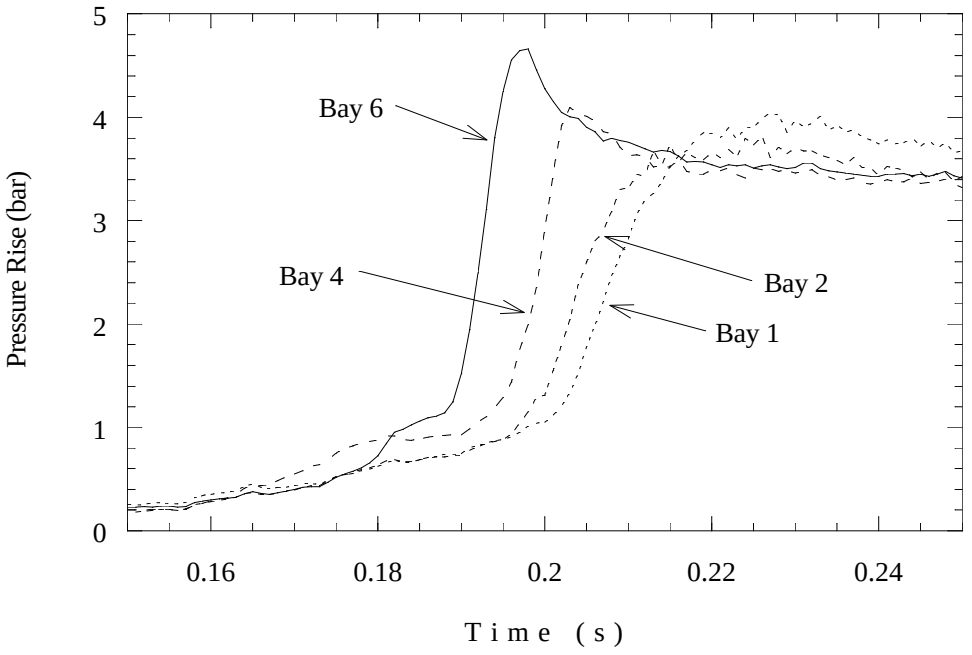

Figure 5.62: Pressure traces for bays 1, 2, 4, 6, ignition in bay 6R. Test 15.

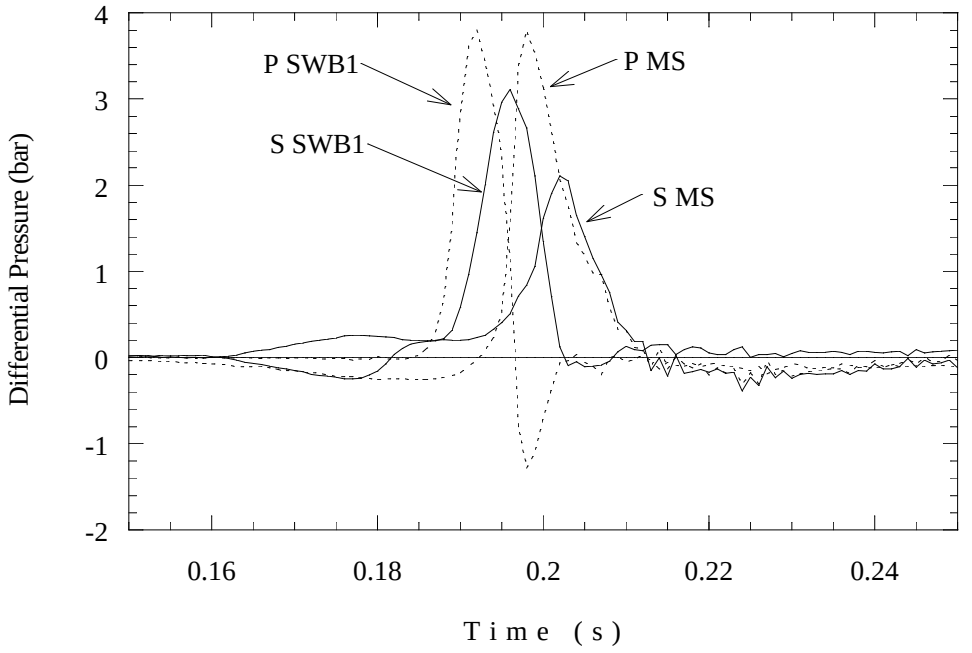

Figure 5.63: Differential pressure across SWB1 and MS, ignition in bay 6R. Test 15.

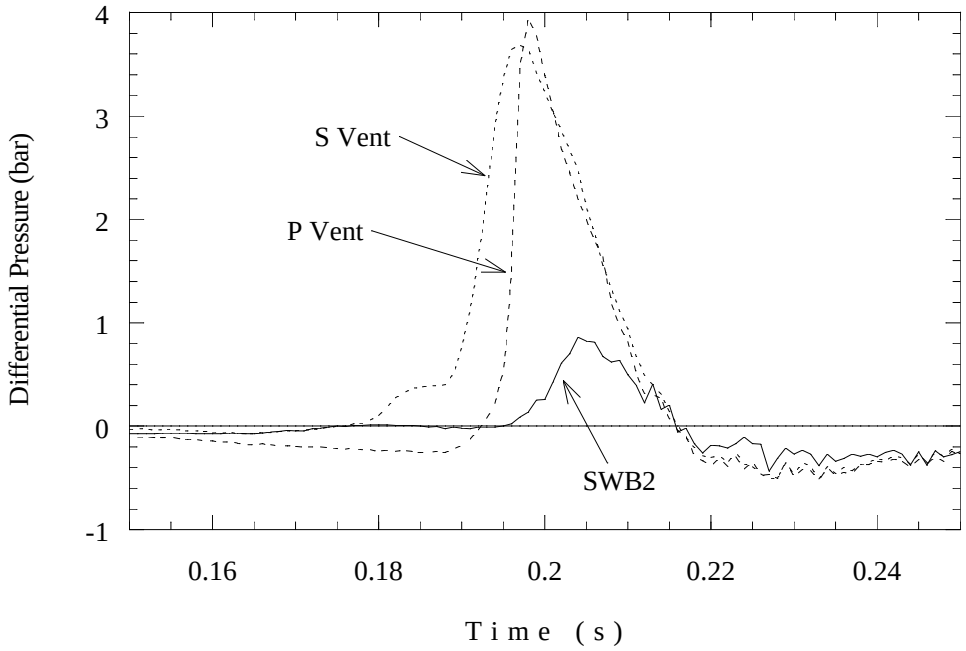

Figure 5.64: Differential pressure across SWB2 and vent stringers, ignition in bay 6R. Test 15.

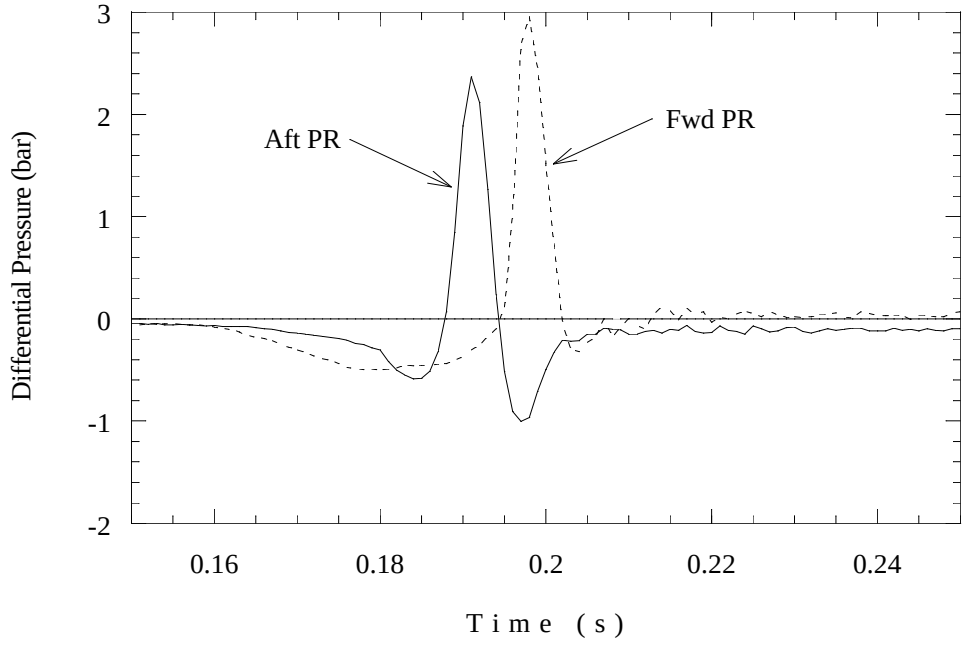

Figure 5.65: Differential pressure across PRs, ignition in bay 6R. Test 15.

Table 5.19: Flame arrival times (ms), Test 15.

Photodetectors

IGN	187
189	194
198	
185	

Thermocouples

168 **IGN** 168	190 190
115 176	198 198
168	208
142	210

Ignition in Bay 1R (Test 16) In this test, the partial ribs failed in the same manner as they did in the previous test (ignition 6R, Test 15). The forward PR broke free on one end, while the aft PR failed completely. The results of this test are thus not directly comparable with the other tests. Tests 14, 15 and 16 all resulted in damage to the interior of the tank.

Ignition location 1R is in bay 1, attached to SWB2, 3 in from the starboard side of the tank and 2 in from the top. This simulates a fuel probe location not addressed by the standard feedthrough locations. This location is close to flow holes in SWB2, and as a result, the flame enters bay 2 shortly after ignition. Figures 5.66 and 5.67 plot the pressures for all bays. Figure 5.67 shows the port sequence (bays 1, 2, 3, 5), while Fig. 5.66 shows the starboard sequence (bays 1, 2, 4, 6). From Fig. 5.66, we see that the flame moves rapidly along the starboard side of the tank, as all of the bays show the identical slow-combustion pressure rise up to 190 ms. This is confirmed by the thermocouple data (Table 5.20). The bays then begin transitioning to turbulent combustion in the reverse order of flame propagation, with bay 6 transitioning at 195 ms and bay 1 transitioning at about 205 ms. In contrast, Fig. 5.67 shows that bays 3 and 5, on the port side of the tank, show a shallower pressure rise that is probably associated with pressurization due to due flow from the other bays instead of combustion. Bay 5 is probably ignited directly into turbulent combustion, at about 190 ms. The resulting rapid pressure rise creates jetting back into the other bays, stirring them and causing transition to rapid combustion. Bays 3 and 6 are adjacent to bay 5, and both show a simultaneous change in pressure slope (see also Fig. 5.68). Bay 3 is undergoing its first combustion at this point, so it has a steeper slope and higher peak than bay 6, which has already consumed some of its reactants. Transition to rapid combustion then progresses forward through bays 4, 2, and 1.

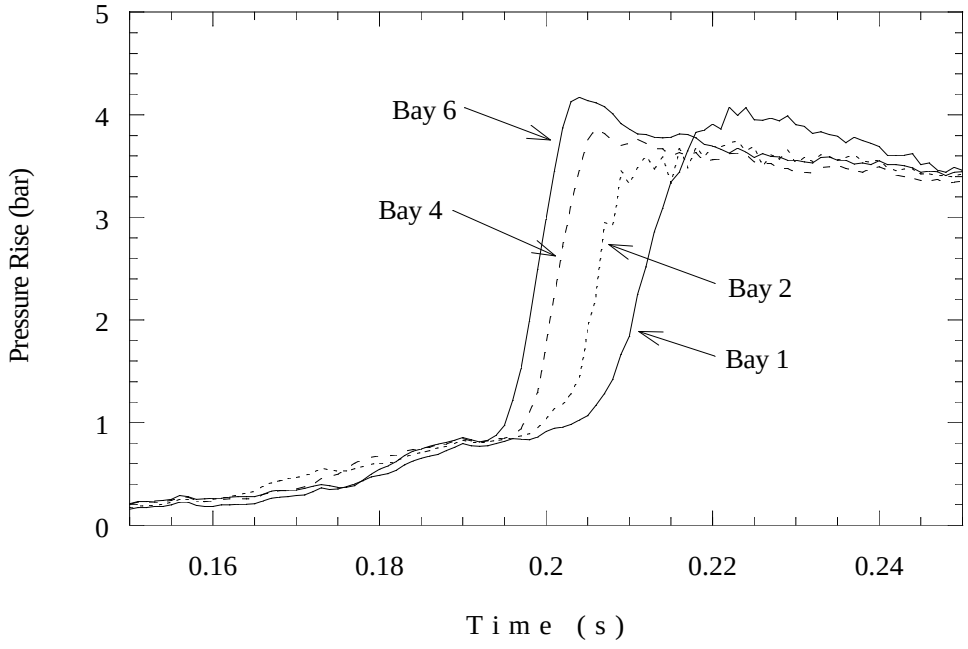

Figure 5.66: Pressure traces for bays 1, 2, 4, 6, ignition in bay 1R. Test 16.

The initiation of turbulent combustion in the port bays is shown also in the differential

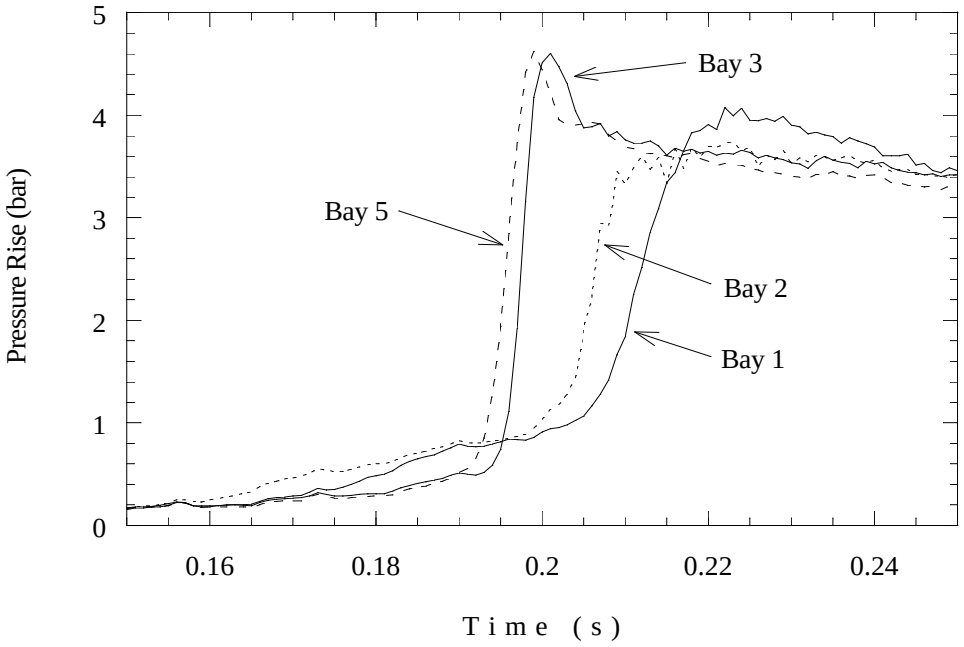

Figure 5.67: Pressure traces for bays 1, 2, 3, 5, ignition in bay 1R. Test 16.

pressures on SWB1 and MS in Figs. 5.69 and 5.70. The MS is a boundary of bay 2, and we see that there is a negative differential on the port side, as bay 3 has not been ignited. The starboard side has a minimal differential, as bay 4 was ignited early, and the pressure rise parallels that in bay 2. A large positive differential is generated when bay 3 is ignited under turbulent conditions, and the starboard side follows suit when bay 4 transitions to turbulence. SWB1 shows this to a lesser degree. The port side has zero differential until 190 ms, as no combustion is occurring on either the front or back. The starboard side begins to see a negative differential, but this returns to zero as bay 6 is ignited and the pressure rise keeps up with the other bays. Positive peaks occur with the transition to turbulence. The negative dip on the port side is a result of pressure piling in bay 3.

The differentials across SWB2 and the vents show the rapid propagation of the flame along the starboard side of the tank. The starboard vent shows no negative differential, indicating that bay 6 was ignited very quickly. The port vent initially has a negative pressure differential. The transition to rapid combustion drives all of these pressure differentials positive. SWB2 pressure differential becomes positive because because the transition progresses from rear to front.

Finally, Fig. 5.72 shows the lack of symmetry in the flame propagation via the pressure differentials across the partial ribs. The negative phase indicates combustion in the starboard side of the tank. The mixture in bays 3 and 5 become highly turbulent due to jetting from bays 4 and 6. When bays 3 and 5 are ignited, the pressure increases rapidly. The PRs probably failed near the peak pressure point. It is unknown why the aft PR trace shows a residual pressure difference after the main combustion event is over. The aft PR failed completely.

Bay cameras 1 and 3 failed in this test, so schlieren film is only available from bays 3/4 and

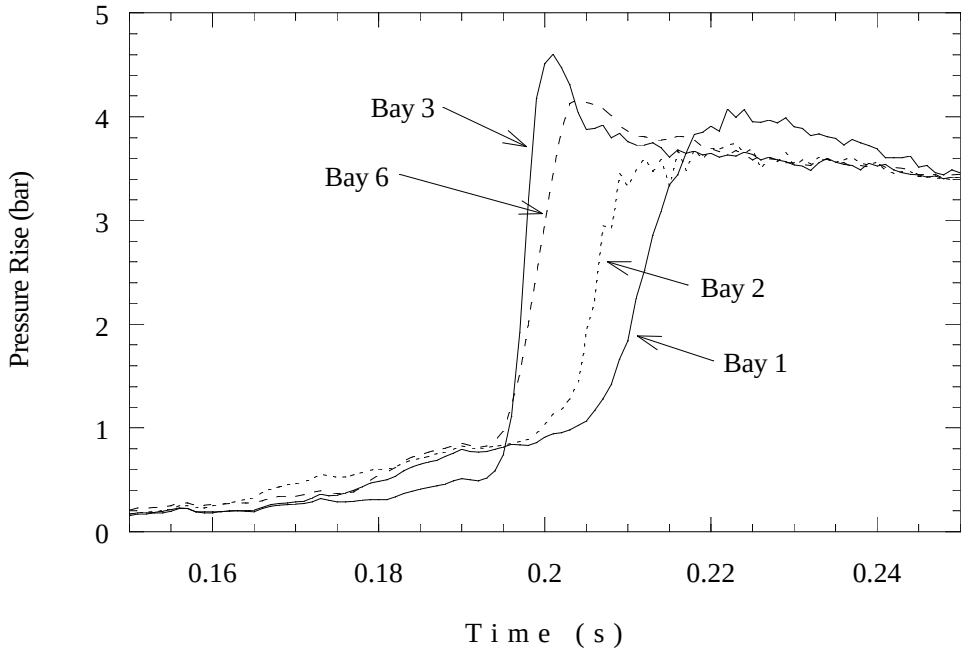

Figure 5.68: Pressure traces for bays 1, 2, 3, 6, ignition in bay 1R. Test 16.

1. In bay 1, the flame burns smoothly downward into the bay after ignition. Once it has filled the upper rear quadrant of the cross-section, some acceleration is seen, as if a jet were entering bay 1 through one of the upper passages in SWB2. Several frames later, another jet enters from one of the vent stringers and drives a flame front to the bottom of the compartment. Near the end of combustion, there is a sudden acceleration of the flame. In bays 3 and 4, the flame enters at the top, presumably from bay 2, but this is not clear in the film. It is also not clear whether the flame is entering bay 3 or 4, but the best guess would be bay 4, since ignition was on the right side of bay 1. The flame burns in a turbulent mode, but not very quickly, until the rapid acceleration at the end. This may represent the ignition of bay 3. The forward PR broke free on one end, but did not move much further in the film. One of the thermocouples was broken in this test.

External video cameras showed some leakage from the top of SWB3. The DBM at the SE station showed an dim orange glow at the end of the burn, starting in bay 6 and rapidly progressing through bays 1 and 2 (in that order). This should correspond to the rapid acceleration shown at the end of the burn in the schlieren films.

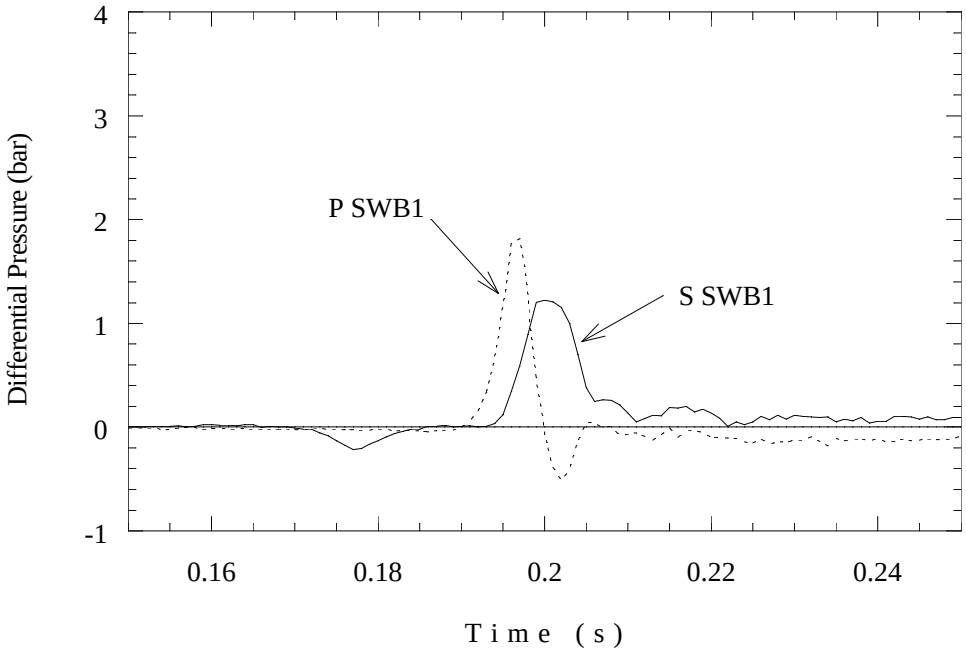

Figure 5.69: Differential pressure across SWB1, ignition in bay 1R. Test 16.

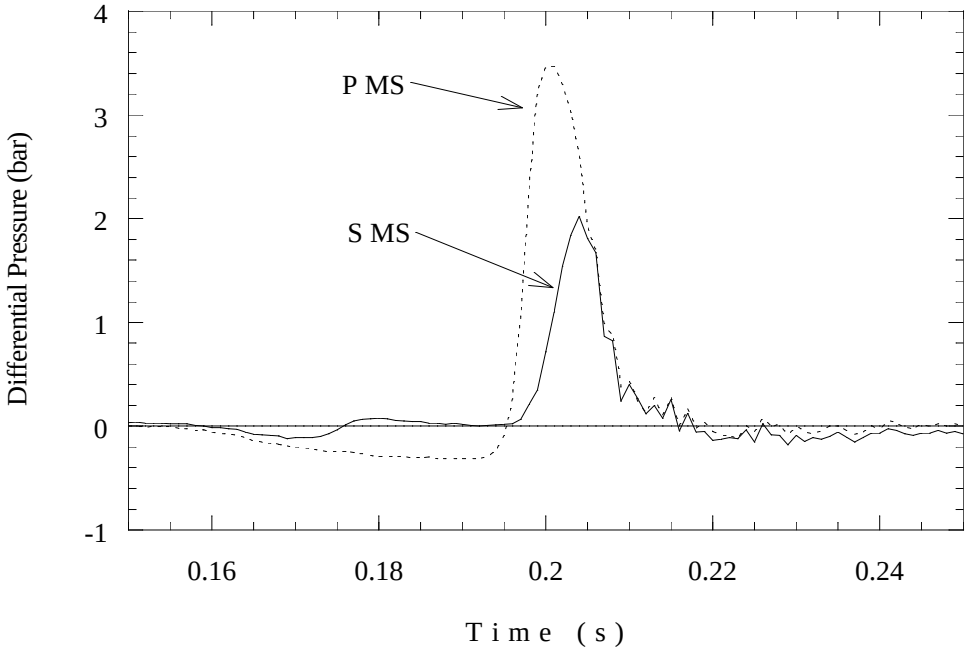

Figure 5.70: Differential pressure across MS, ignition in bay 1R. Test 16.

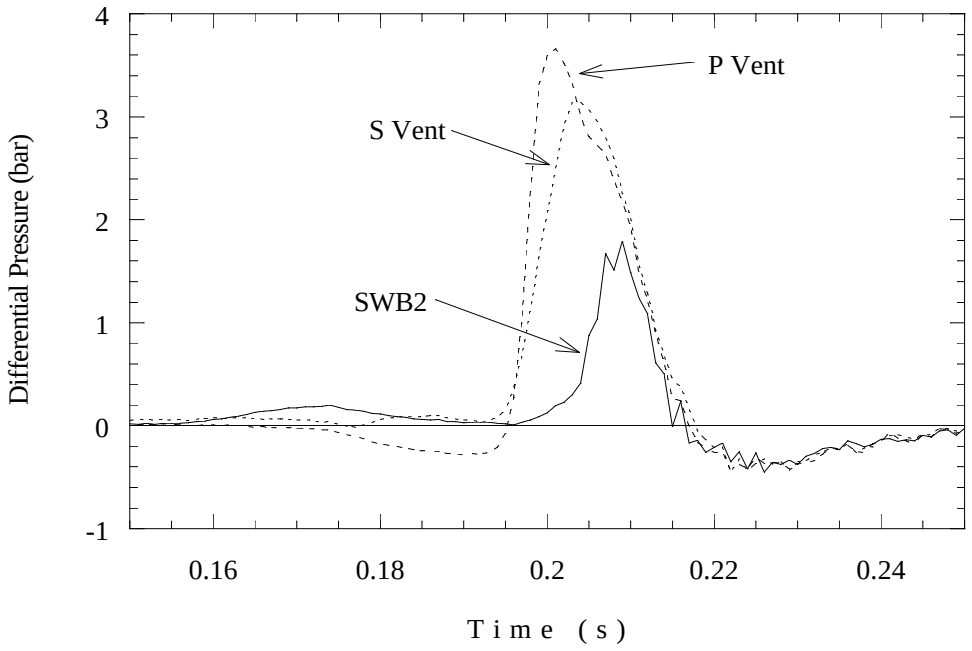

Figure 5.71: Differential pressure across SWB2 and vent stringers, ignition in bay 1R. Test 16.

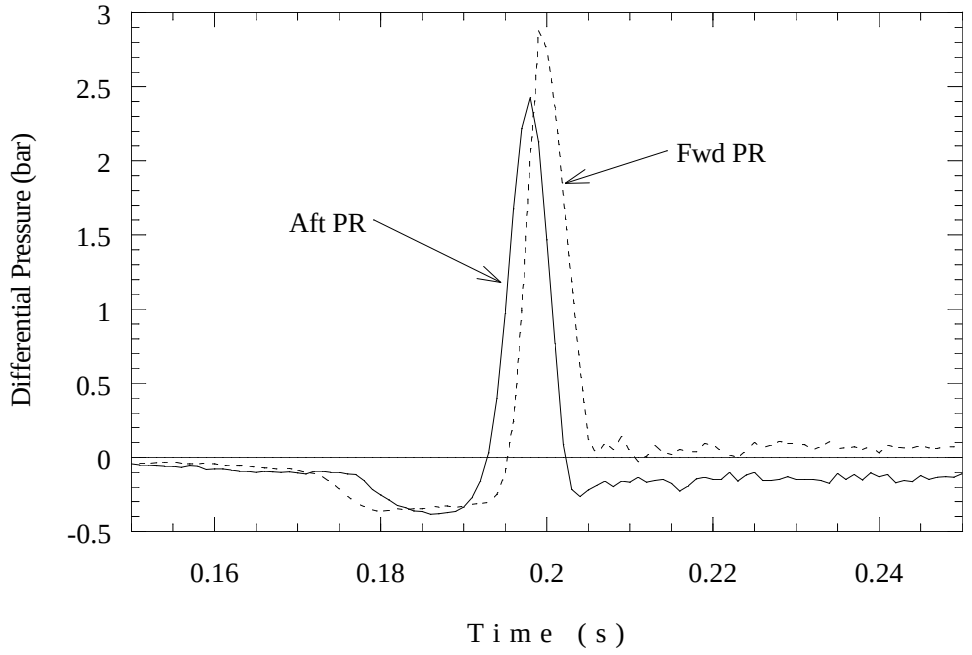

Figure 5.72: Differential pressure across PRs, ignition in bay 1R. Test 16.

Table 5.20: Flame arrival times (ms), Test 16.

Photodetectors		Thermocouples	
194	191	132 183	195 197
198	196	128 178	199 199
201		163	209
197 **IGN**		182 **IGN**	213

Ignition in Bay 2Lo, 6.5% Fuel (Test 26) The purpose of this test and two others (23 and 24) was to examine the effect of fuel concentration on the combustion phenomena. The actual fuel concentration in the CWT is uncertain due to the lack of exact knowledge about the distribution of liquid fuel, the temperatures within the tank, and the motion of the evaporated fuel.

During this test, a leak occurred in SWB3 when the tank was partially evacuated. Repeated attempts were made to seal the leak, which was about 2 torr per minute when the tank was evacuated to 91.6% of atmospheric pressure. Attempting to fix the leak occupied nearly a full day and was unsuccessful. It was decided to go ahead with the test and to compensate for the leak by decreasing the gas fill starting pressure. The tank was pumped to 0.5 torr less than the calculated pressure, and the fuel fill took 30 s to complete. If we assume the leak rate to be proportional to the difference in tank and atmospheric pressure, which is approximately true for small pressure differences, this would exactly compensate for the air contamination during a 30 s fill. Therefore, there is some uncertainty in the mixture but it is rather small, since the partial pressure of fuel added in this test was about 41 torr. The maximum error in the amount of fuel is about 1%, which implies that the fuel concentration in air is between 6.50% and 6.58% for this test.

As in the earlier bay 2 ignition test, the pressure rise is laterally symmetric in the aft bay pairs. The pressure traces in bays 3 and 4 were nearly identical, as were those in bays 5 and 6 (Fig. 5.73). The difference between the traces may simply be due to the slight offsets in the initial transducer zero level that always occur. Since the traces from each pair of aft bays are so similar, only one trace of each pair is shown together with the forward bays on Fig. 5.74.

This test had the lowest value of peak pressure rise, 1.3 bar, and the longest time to peak pressure, 0.9 s, of any test in the present series. Comparison with Test 6, which was the same configuration and used the standard fuel concentration, indicates the dramatic effect of lowering the fuel concentration. This is a consequence of the strong dependence of flame speed and peak pressure on fuel concentration. We observed in laboratory tests with a 6% mixture that buoyancy totally dominated the combustion event in a much smaller vessel. In Test 26, we suspect that combustion was incomplete in the aft bays. Evidence for this includes the schlieren observations, photodetector signals, thermocouple signals, and the substantial difference between the peak pressure and the AICC value or the results of Test 24. If all of the gas had burned in the tank, laboratory tests (see the discussion in Section 6.12) indicate that the peak pressure rise should have been (without any pressure piling effects) about 2.7 to 3 bar. If we neglect the effect of heat transfer and venting, the fraction of gas burned is proportional to fraction of the AICC pressure reached in the test. After correcting for heat transfer effects, which are substantial because of the long burn time, this data suggests that only 50% of the gas in the tank burned in Test 26.

In the present test, no transition to rapid combustion occurs until 800 ms after ignition and the rapid combustion event occurs over a period of about 100 ms. These times are approximately 5 times longer than observed with the standard fuel concentration. It appears that slow combustion proceeds throughout the vessel until sufficient turbulence is created in the forward bays to promote rapid combustion. Bay 1 is the first to transition to rapid combustion. Bay 1 then vents into bay 2, accelerating combustion there. Bay 2 possibly has a slightly lower peak pressure than bay 1 because the reactants were partially burned before transition to rapid

combustion occurred. Venting and turbulence generation progresses toward the rear of the tank after bays 1 and 2 burn. The aft bays reach lower peak pressures (about 0.9 bar peak pressure rise) than the foward bays (1.3 bar peak pressure rise). It is not clear how much of the pressure rise in the aft bays is due to combustion and how much is simply associated with pressurization created by venting the forward bays into the aft bays. The late plateau in pressure within bay 1 at 1050 ms is typical of buoyancy dominated combustion, but may also be associated with flow through the vent stringers.

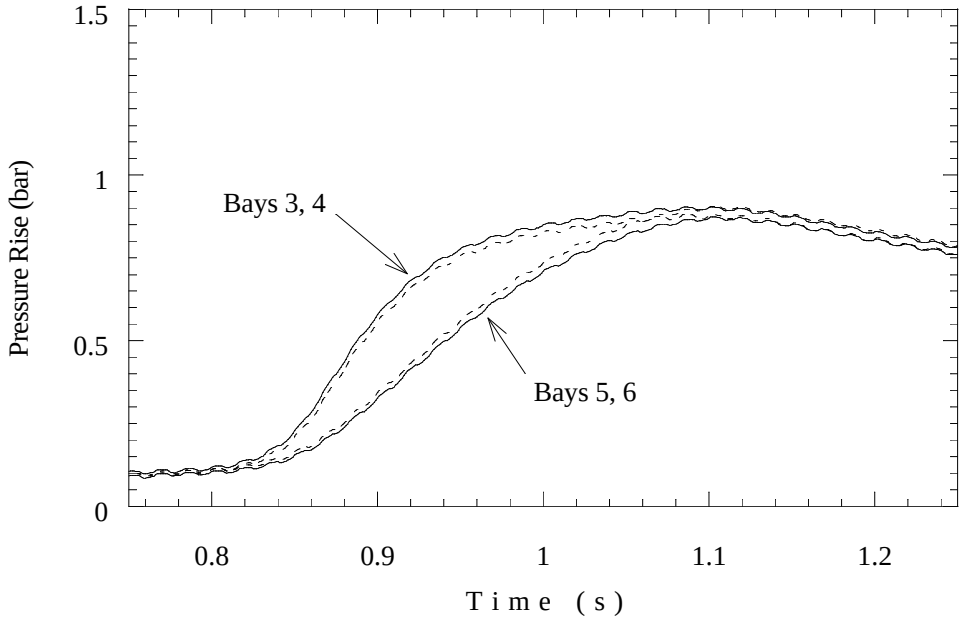

Figure 5.73: Pressure traces from bays 3 – 6. Dashed lines are even-numbered bays. Ignition in bay 2Lo, 6.5% fuel. Test 26.

The pressure differentials are shown in Figs. 5.75 and 5.76. The lateral symmetry of combustion in this test is again shown in Fig. 5.75, where the two sides of SWB1 are slightly offset and both sides of MS are indistinguishable. Both partitions experience force to the rear, since the transition to rapid combustion progresses from the front to the back of the tank. The pressure rises are slower and lower in amplitude in the aft bays than in the forward bays, so the differential across SWB1 is considerably lower than across the MS.

The differential pressure on the vents (Fig. 5.76) is negative due to the earlier transition to rapid combustion in bay 1 than in the aft bays. The pressure across SWB2 initially follows the vents, but then decreases as transition to rapid combustion occurs in bay 2. Differential pressures for the PRs are not shown, as they were always close to zero, and the signals were comparable to the noise level.

Bay camera 2 jammed in this test, so there is no schlieren information from bays 3/4. In bay 2, we see that the flame is carried upward by buoyancy while burning sideways toward SWB2. However, the flame generates enough flow that once the flame reaches the top of the tank it is carried down SWB2 and propagates towards the bottom of the tank. Before the flame reaches the bottom of bay 2, it appears that a jet enters from bay 1, through one of the lower

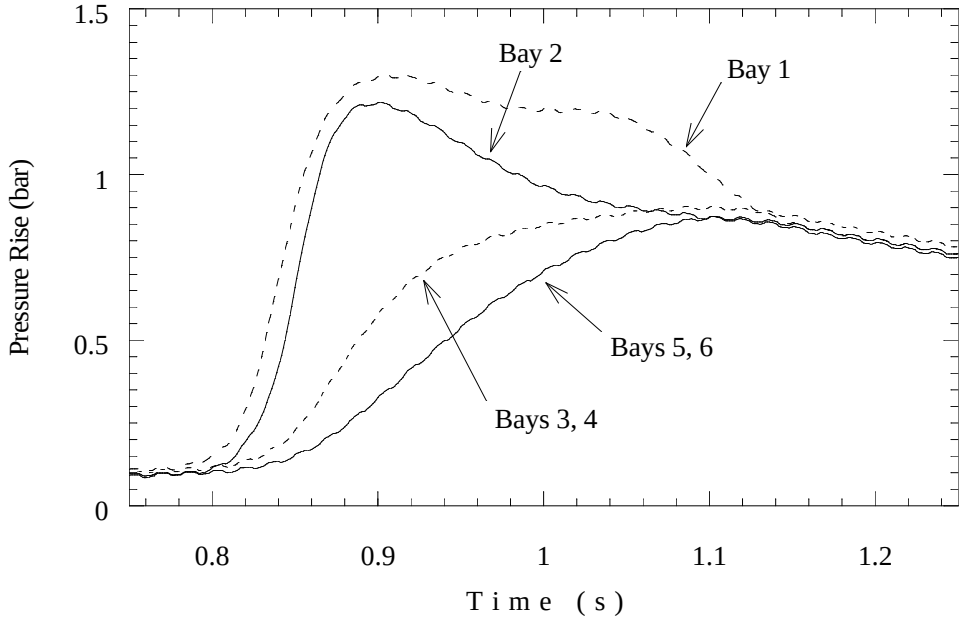

Figure 5.74: Pressure traces from all bays (3 and 5 representing 4 and 6, respectively) for ignition in bay 2Lo, 6.5% fuel. Test 26.

passageways in SWB2. This accelerates combustion in bay 2. In bay 1, combustion starts at the bottom and then independently at the top of the bay. In bays 5 and 6, there is no indication of combustion, although a dark mist appears on the aft PR. This may be jet fuel residue sprayed out of the jet fuel manifold.

This sequence of events is further confirmed by the thermocouple signals which show three distinct types of behavior (Fig. 5.77). In the ignition bay (bay 2), the temperature rises in a slow linear fashion suggesting a slow, laminar flame growth. At 800 ms, a turbulent flame with a much faster temperature rise appears in bay 1, apparently before the mixture in bay 2 has been completely consumed. At about 840 ms, the temperature in bay 2 suddenly begins to rise more quickly, indicating that the turbulent flame in bay 1 has jetted back into the ignition bay, turbulently stimulating the combustion of the remaining mixture. The peak temperatures indicated on the thermocouples in bays 1 and 2 are between 500 and 900°C, characteristic of lean combustion. On the other hand, the thermocouple signals in bays 3 – 6 show a slow rise in temperature barely exceeding 250°C. These temperatures are higher than the 100°C rise that would be predicted simply due to pressurization without combustion. This suggests that in the rear bays, there was a small amount of combustion and the pressurization was predominantly due to venting of the products from bays 1 and 2 into these bays without the ignition of the mixture.

The side-view camera shows the flame propagating in a way that would allow jets to go from bay 2 into bay 1, and then back from 1 into 2. Combustion is only dimly visible in bays 3/4, and it appears to occur after the events in bays 1 and 2. The observation cameras show no leakage past SWB3. The lack of visible combustion in bays 5/6 and 3/4 is consistent with the lack of photodetector signals (Table 5.21) from these bays. Note that this could also simply

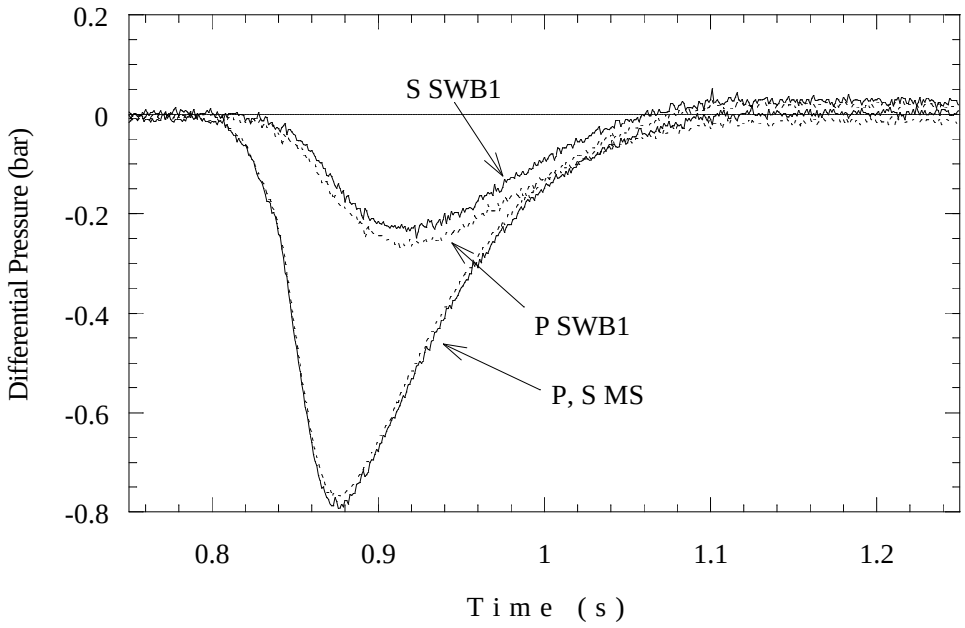

Figure 5.75: Differential pressure across SWB1 and MS, ignition in bay 2Lo, 6.5% fuel. Test 26.

be due to insufficient luminosity since flames in the lean simulant mixtures produce very little light in any case.

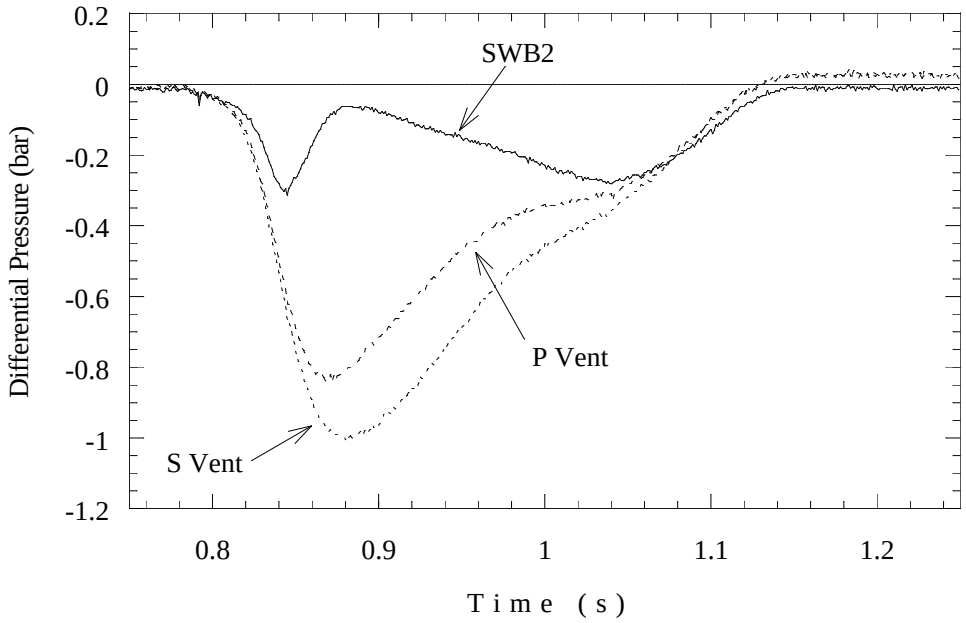

Figure 5.76: Differential pressure across SWB2 and vents, ignition in bay 2Lo, 6.5% fuel. Test 26.

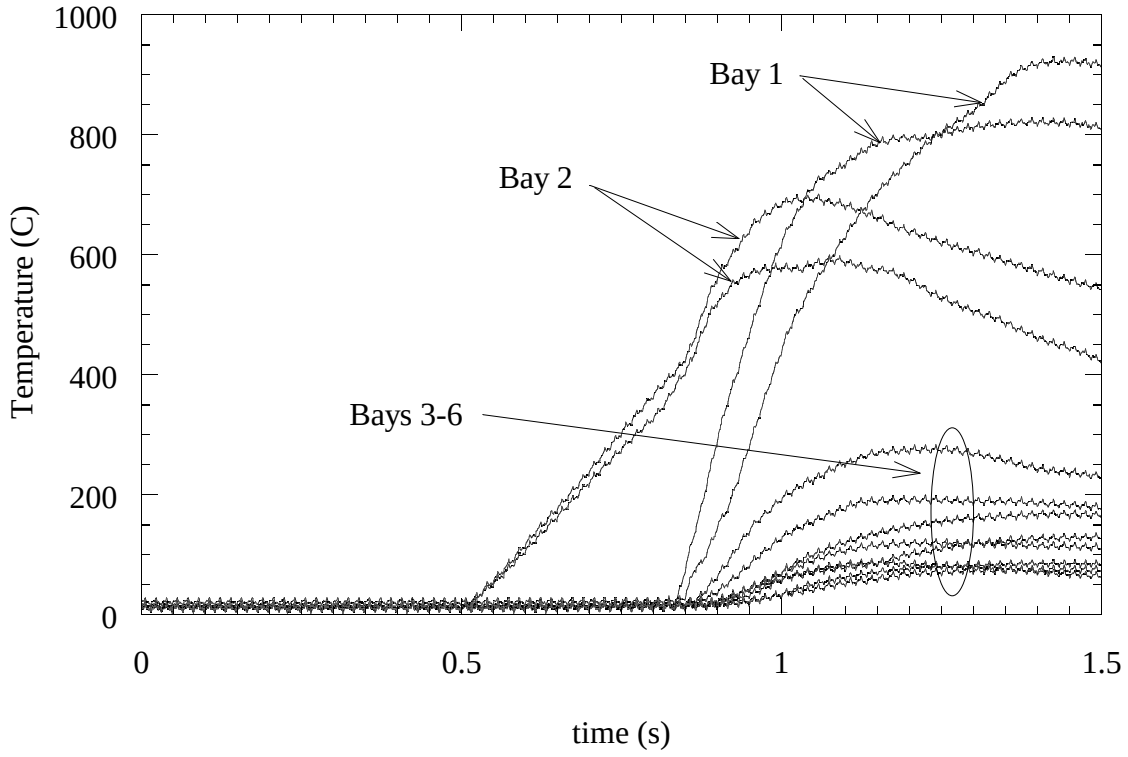

Figure 5.77: Thermocouple gauge signals for Test 26. The signals of the gauges in bays 1, 2, and 3 to 6 are indicated.

Table 5.21: Flame arrival times (ms), Test 26.

Photodetectors		Thermocouples	
		908 940	950 906
		873 910	904 869
839 **IGN**		518 **IGN**	518
828		851	835

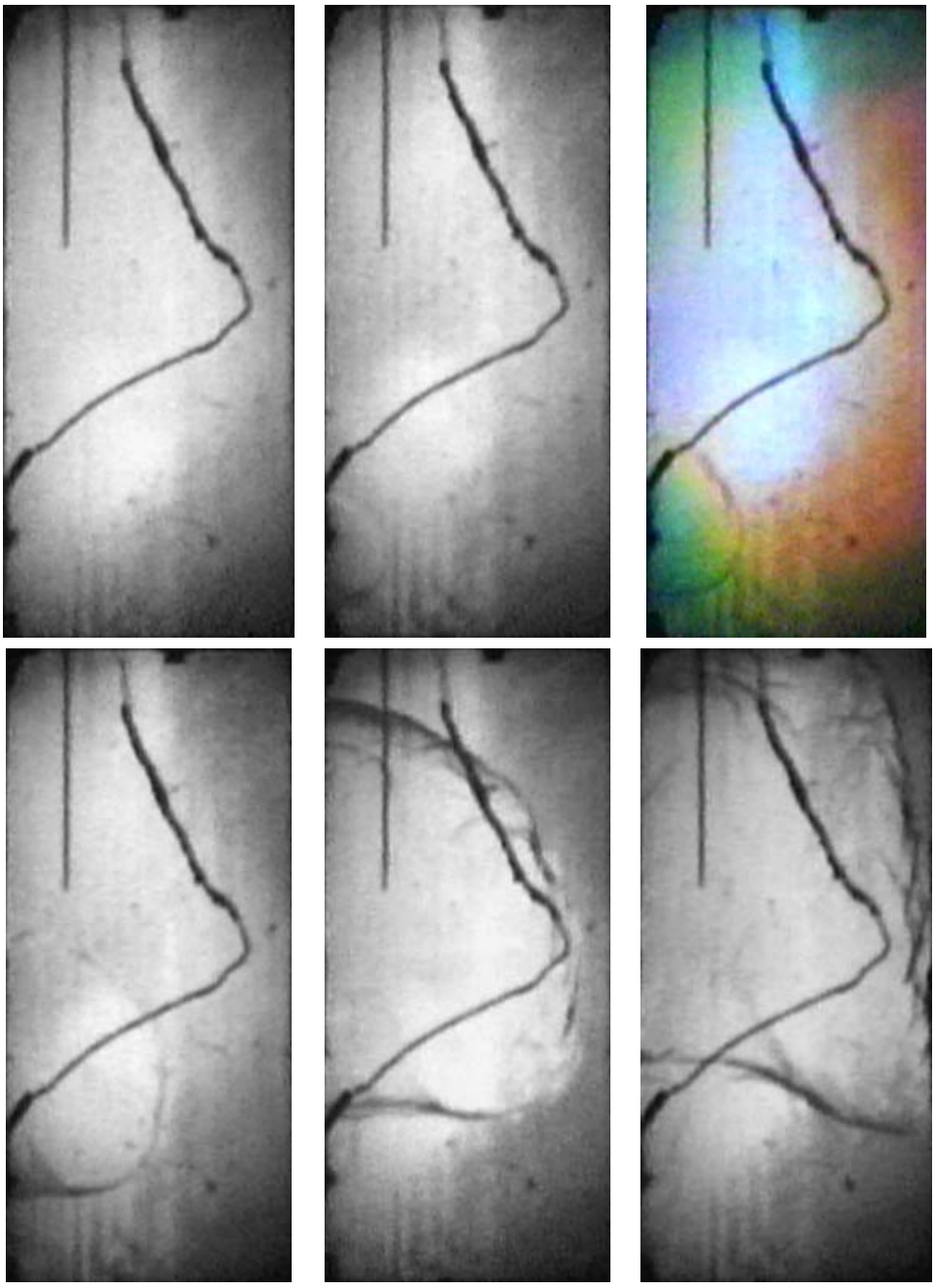

Figure 5.78: Schlieren sequence from bay 2 showing upward and sideways propagation of flame in 6.5% mixture of Test 26. (Continued in next figure.)

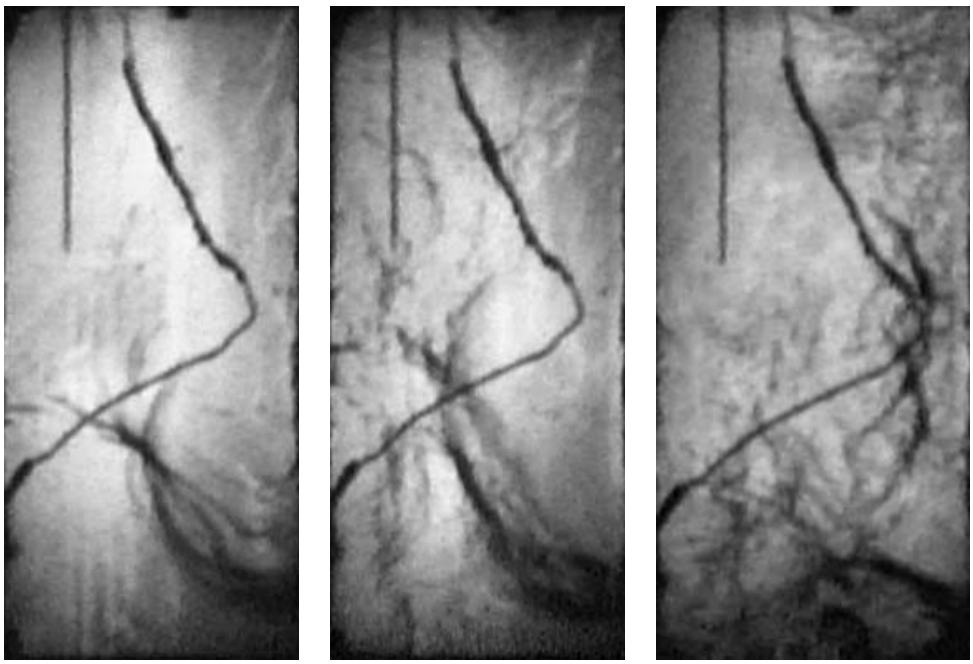

Figure 5.79: Continuation of Fig. 5.78.

5.4 GAMMA Test Series

All the tests in the GAMMA test series involved some degree of structural failure; configurations tested ranged from a weak MP in SWB2 to the all-weak configuration. These tests are subdivided into four groups, given in Table 5.22. The first subgroup covers Tests 13 and 14, which were used to test the failure pressure of the weak partitions and the MP, respectively. The second group includes the all-weak partition tests, with and without jet fuel. The third group includes the part-strong configuration with variable fuel concentration (6.5 – 8.4%) to study the effects of lower temperatures on combustion. The fourth group consisted of the part-strong configuration (weak FS, SWB3, and MP, other partitions strong) with jet fuel to study TWA 800 scenario. (One test was run without jet fuel for reference.) These tests looked at three ignition locations to see if any differences in the final results occurred.

5.4.1 Motion Detector Switch Signals

When weak partitions are used in a test, motion detectors or break switches are installed to record failure times, providing a non-ambiguous time of initial panel motion, as shown in Fig. 5.80. This signal was recorded from motion switch 8 during Test 19.

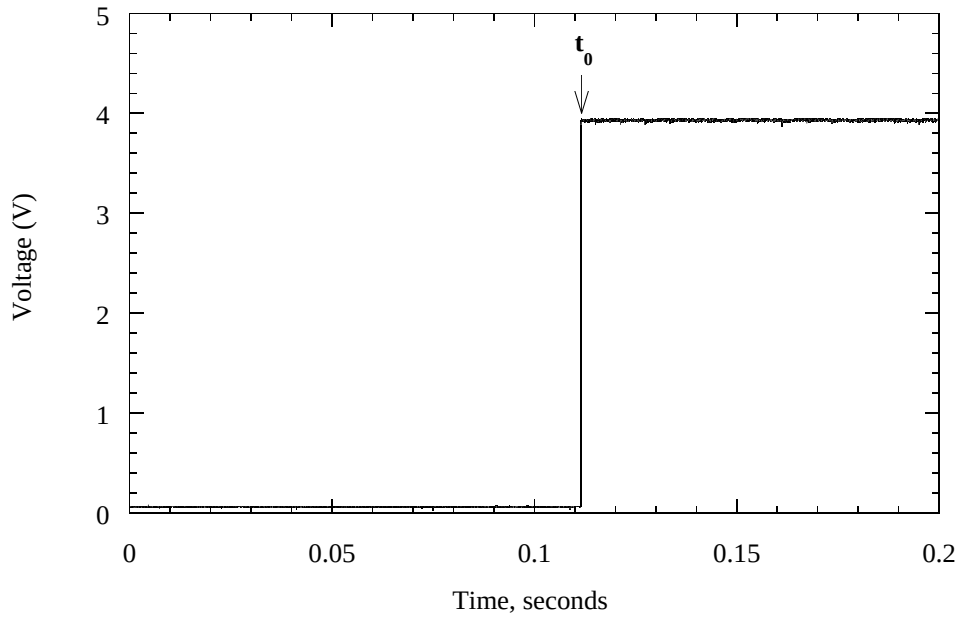

Figure 5.80: Typical motion detector signal showing the sharp transition to a higher voltage at the moment it is triggered (t_0).

There were a maximum of 18 motion switches that were used in the all-weak tests, one at each corner of FS, SWB3, SWB2, and MS, and also two at the upper corners of SWB1. A total of 8 motion switches plus a breakwire on the manufacturing panel were used on the part-strong tests. Because there were not enough fast digitizer channels available to record

all of the motion detectors, five signals had to be recorded on one of the analog tape backup drives. Unfortunately, no fiducial signal was available to synchronize this data with the signal recorded on the digital systems. The data was digitized from the tape at a later date. When these signals were compared to data from the digitizers, it was clear that there was a time offset in some tests.

The time offset was corrected by using data from the FS. Inspection of the high-speed film shows that the FS generally is projected directly outward and that all of the motion switches should be activated within 1 to 2 ms. Three of these switches were recorded digitally, and they were typically triggered over a 0.5- – 1-ms period. The fourth was recorded on the tape, and using the nominal timebase, gave a discrepancy of up to 13 ms in failure time. For the tests in which this was an issue (all-weak series 18 – 21), the analog tape data were corrected by averaging the failure times on the three digitized signals, and then taking the difference between this and the tape data. The tape values were then corrected by this amount. In the remainder of the tests, which were part strong, the tape values were not plotted. In Table 5.28 data recovered from the tape drives are shown in italics and the correction factor is given.

Table 5.22: GAMMA series tests.

Test	Ignition	Strong Partitions	Weak Partitions	Fuel	Comments
Special Purpose (5.4.2, p. 139)					
13	5	SWB1, MS, SWB2, MP	SWB3	8.4% gas	Weak partition test
14	5	SWB1, MS, SWB2, SWB3	MP	8.4% gas	Weak (12-mil) MP test
All Weak Partitions (5.4.3, p. 149)					
18	5	none	all	8.4% gas	Partition failure test
19	5	none	all	8.4% gas, Jet A	Lofting, failure
20	2Lo	none	all	8.4% gas, Jet A	Ign location
21	1	none	all	8.4% gas, Jet A	Ign location
Part Strong, Concentration Variation (5.4.4, p. 180)					
22	2Lo	SWB1, MS, SWB2	MP, SWB3, FS	8.4% gas	6-mil MP test
23	2Lo	SWB1, MS, SWB2	MP, SWB3, FS	7.5% gas	Low T simulation
24	2Lo	SWB1, MS, SWB2	MP, SWB3, FS	6.5% gas	Low T simulation
Part Strong, Ignition Location (5.4.5, p. 198)					
17	5	SWB1, MS, SWB2	MP, SWB3, FS	8.4% gas	TWA 800 scenario
28	5	SWB1, MS, SWB2	MP, SWB3, FS	8.4% gas, Jet A	TWA 800 scenario
27	2Lo	SWB1, MS, SWB2	MP, SWB3, FS	8.4% gas, Jet A	TWA 800 scenario
29	1	SWB1, MS, SWB2	MP, SWB3, FS	8.4% gas, Jet A	TWA 800 scenario

Table 5.23: Time of arrival at the photodetector locations for the GAMMA test series.

Test	L1 (ms)	L2 (ms)	L3 (ms)	L4 (ms)	L5 (ms)	L6 (ms)	L7 (ms)
13	108	104	104	107	113	120	128
14	128	128	173	166	180	184	–
17	123	116	119	118	127	129	144
18	95	89	85	92	100	102	108
19	99	94	87	96	99	109	113
20	104	103	104	92	105	111	117
21	120	114	115	115	115	116	125
22	185	186	183	178	187	198	198
23	260	259	256	253	260	262	269
24	498	498	414	411	416	432	438
27	129	135	132	133	135	139	148
28	98	96	95	99	105	103	117
29	162	146	155	151	157	161	161

Table 5.24: Time of arrival at the thermocouple locations for the GAMMA test series.

Test	T1 (ms)	T2 (ms)	T3 (ms)	T4 (ms)	T5 (ms)	T6 (ms)	T7 (ms)	T8 (ms)	T9 (ms)	T10 (ms)	T11 (ms)	T12 (ms)
13	109	65	100	106	120	122	113	117	124	126	125	127
14	127	72	117	125	174	174	170	168	183	185	187	185
17	123	70	114	122	133	134	125	128	141	144	–	145
18	97	67	86	91	–	111	102	105	108	111	109	103
19	101	65	95	98	114	114	105	128	113	110	114	113
20	112	107	108	112	107	109	100	100	108	98	122	–
21	126	124	122	114	118	120	121	121	120	121	85	64
22	188	182	187	188	174	162	184	189	179	179	189	184
23	260	249	264	262	237	240	253	257	230	240	264	264
24	420	448	448	432	376	401	417	414	337	374	435	433
27	141	136	141	145	127	125	138	139	139	135	145	156
28	101	62	91	94	113	115	112	110	126	126	122	110
29	165	165	163	150	164	163	165	162	160	162	114	92

Table 5.25: Motion-detector breakaway times.

	Top Left	Top Right	Bottom Left	Bottom Right
Test 13				
SWB3	125.0	124.0	126.0	124.0
Test 14				
MP	182.0			

5.4.2 Special Purpose Tests

Weak Partition Test (Test 13) This test was run to check the design of the weak partitions for failure mode and pressure. A weak partition was installed in the SWB3 station, while the other partitions were strong. No FS was used in this test. Ignition was in bay 5. When the test was run, we were quite surprised by the strength of the shock wave at the command trailer. SWB3 exited with sufficient velocity to damage the blast gauge guard. This guard consisted of a vertical, telescoping pipe welded to a flat base. The lower length of pipe had about a 2-in diameter, while the upper length had a 1.5-in diameter. The base was weighted with four 70-lb sandbags. When SWB3 hit the guard, it bent the upper length of pipe back by about 15 – 20° and flipped the guard over, throwing one of the sandbags about four feet in the air. After this test, a heavier guard post was installed. This guard was constructed of approximately 2×4-in rectangular steel tubing, buried 18 in in the ground, with a diagonal brace. Due to a patching problem, no data was recorded from the blast gauges in this test.

In Fig. 5.81, we see that bays 3 and 6 transition to rapid combustion at about 100 ms. Combustion in these bays then generates turbulence in bay 5, increasing its burn rate. The maximum pressure alternates between the bays, as in other bay 5 ignition tests. In Fig. 5.82, we see that bay 4 is the last of the aft bays to ignite. Pressure traces from the remainder of the bays are shown in Fig. 5.83. Bay 2 shows evidence of pressure piling after igniting at 105 ms, slightly exceeding 4 bar.

Bay 1 peaks at about 1.4 bar. The motion detector signals indicate that the panel begins to break at less than 0.8 bar, but the combustion continues to drive the pressure up in the time it takes the panel to fail completely. The pressure from bay 0 is shown also, falling under that for bay 1. It is shown here only for reference, as the FS was not installed. The panel appears to fail uniformly.

The differential pressure traces are shown in Figs. 5.84 – 5.86. Transition to rapid combustion in bays 3 and 4 results in higher differentials across MS than across SWB1. The pressures across SWB2 and the vents are even higher (Fig. 5.85), as they become the boundaries to atmosphere once SWB3 fails. Venting occurs through the vent connections to bay 1 and the passageways in SWB2. The pressures across the PRs are fairly low in this test, as the aft PR stays below $\pm$0.4 bar. The forward PR has a negative spike just before 120 ms, as bay 4 climbs to its peak pressure while the combustion in bay 3 is just starting.

Only two of the schlieren cameras functioned during this test, those in bays 1 and 2. In both bays, the flame enters via the lower passageways, impacts the far partition, and engulfs the bay.

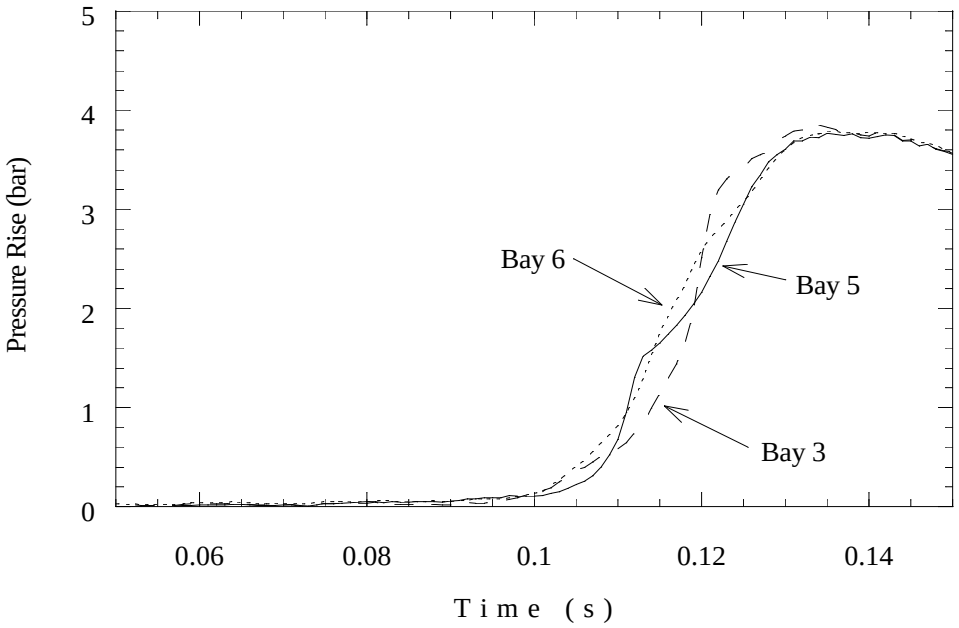

Figure 5.81: Pressure traces from bays 5, 3, 6, ignition in bay 5, weak SWB3. Test 13.

Bay 1 is a little more interesting in this case, as it is bordered by the weak SWB3. We can't actually see SWB3 depart, as it is out of the field of view. However, its failure can be inferred from other phenomena. First, the flame disappears before reaching the windows and quenching against them. Second, flow streaks appear on the left side of the frame where the SWB2 side seals give way once SWB3 fails and they become the border to atmospheric pressure. Finally, the fresnel lens creates alternating discoloration around the border of the field, after it is flexed by the blast wave.

The external video cameras aren't fast enough to view the moving panel. It is visible in a few frames only as a grey blur. Dust kicked up by the blast wave is also visible near the ground. The overcast skies caused the high-speed films to be underexposed, but they were still able to capture the flight of SWB3. The most interesting aspect of the film is the impact of SWB3 with the blast gauge protection post.

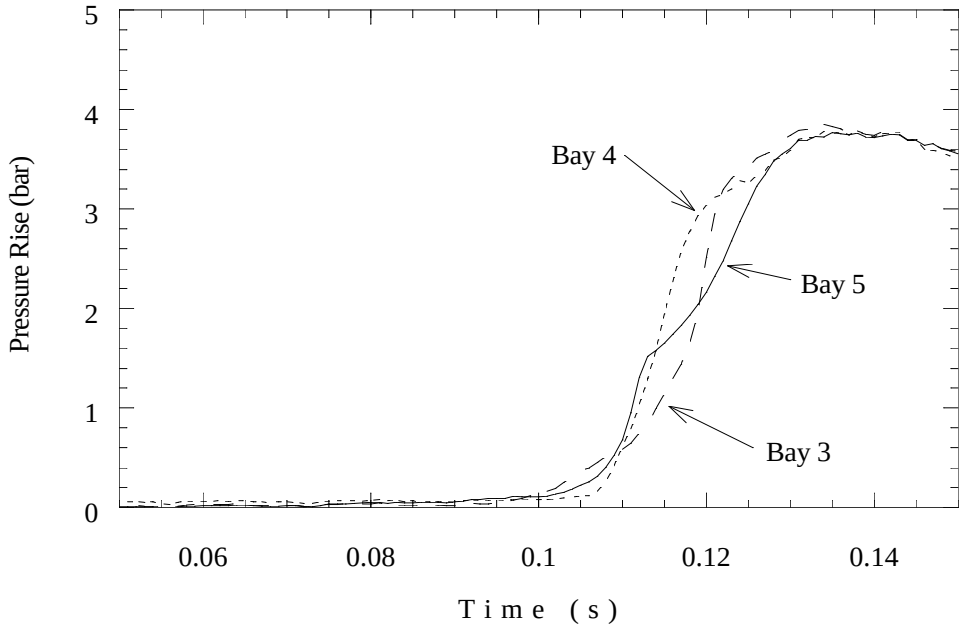

Figure 5.82: Pressure traces from bays 5, 3, 4, ignition in bay 5, weak SWB3. Test 13.

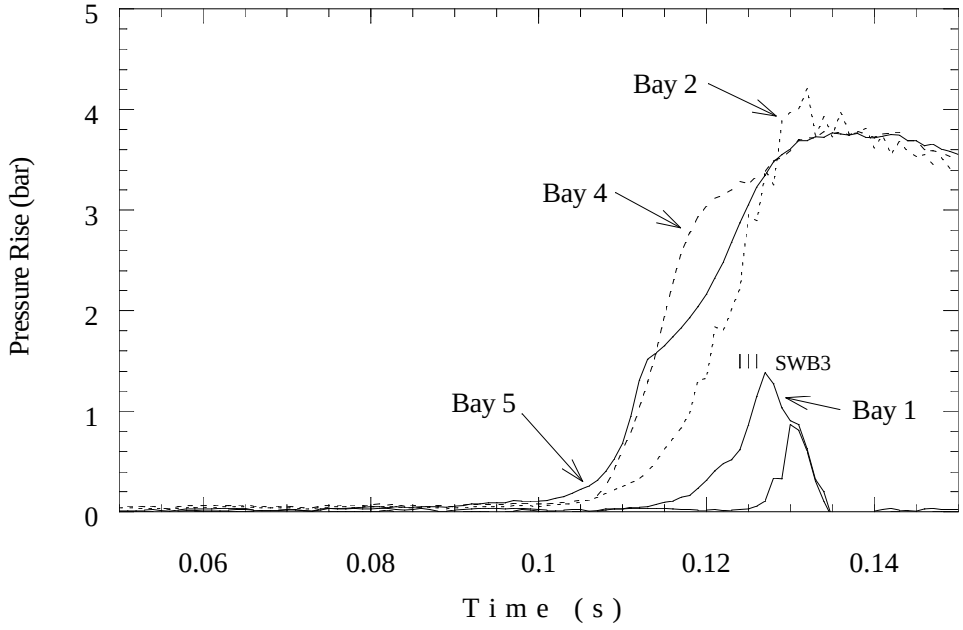

Figure 5.83: Pressure traces from bays 5, 4, 2, 1, with breakage indicators from SWB3. The trace under that for bay 1 is from bay 0, though no FS was used in this test. Test 13.

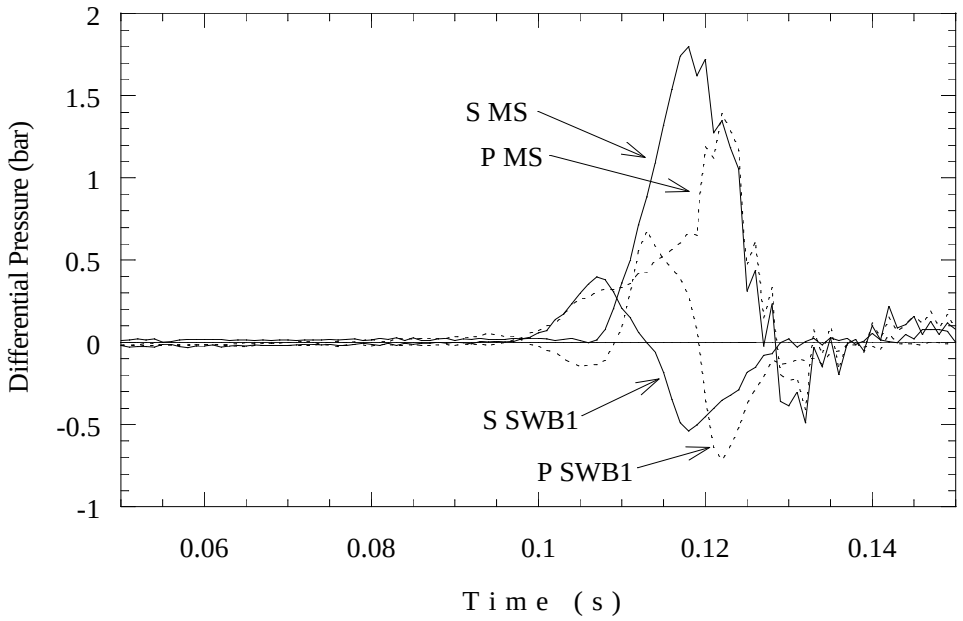

Figure 5.84: Differential pressure across SWB1 and MS, ignition in bay 5. Test 13.

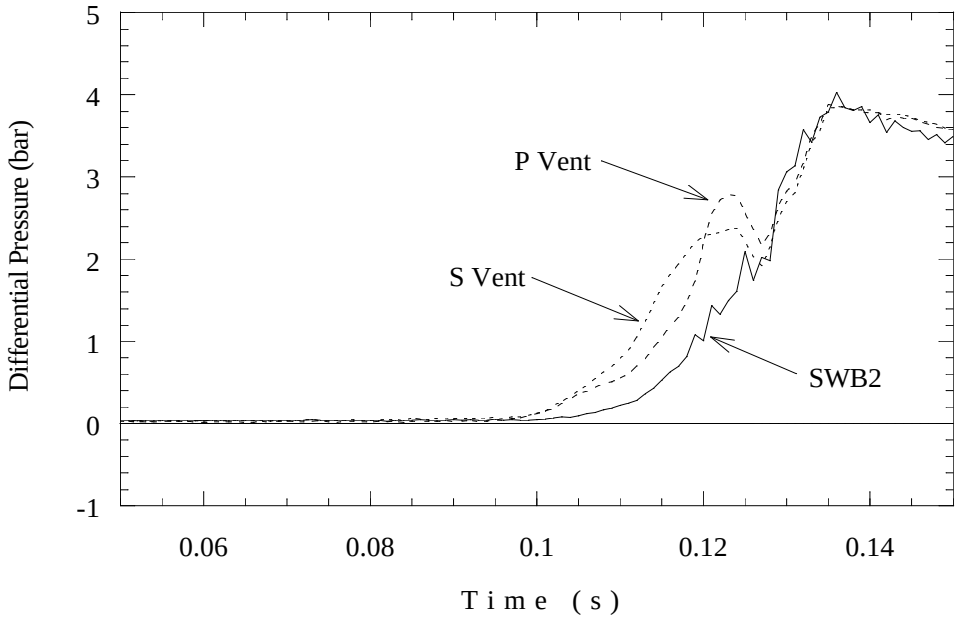

Figure 5.85: Differential pressure across SWB2 and vents. Test 13.

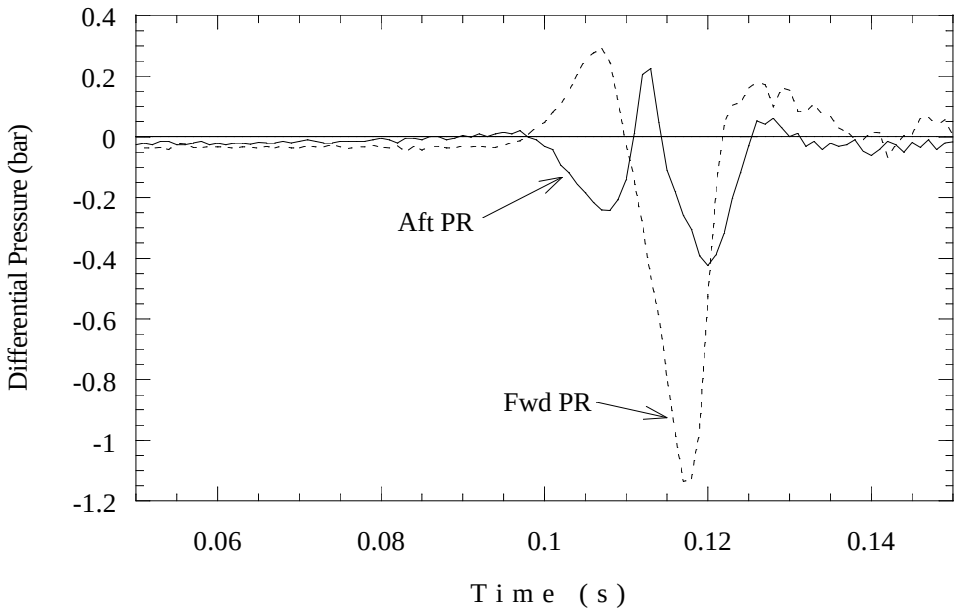

Figure 5.86: Differential pressure across PRs. Test 13.

Table 5.26: Flame arrival time (ms), Test 13.

Photodetectors		Thermocouples			
104	108 **IGN**	106	100	65 **IGN**	109
107	104	117	113	122	120
113		126		124	
120		127		125	
128					

Weak (12-mil) Manufacturing Panel Test (Test 14) This was the first test to use a diaphragm to represent the failure of the MP in SWB2. The rupture pressure was somewhat higher than desired, and later tests (after Test 17) used a diaphragm of 6-mil thickness with a cutter. Pressure traces are shown in Figs. 5.88 – 5.92. These pressure traces are very unusual, as there is a long delay before combustion is initiated in the forward bays. As this did not happen on any other 8.4% fuel tests, the results of this test are questionable.

This test generated some high local pressures, which damaged some of the partition brackets. The 1/4-in bolts holding in SWB3 were sheared, but the most interesting damage was to the angle steel on SWB2 and SWB1. The angles were actually buckled away from the aluminum plates, indicating that the ends of the plates had swung forward. The buckling is centered about the outermost vertical mounting bolts, where the holes created a stress concentration. Figure 5.87 shows the damage that was observed. The gap between the angle and the plate was as big as 1/4 in in some places. The aluminum plates also showed some residual deformation. In addition, the thermocouples on both sides of SWB2 were broken. The thermocouples in bay 1 were broken in multiple places; this could have resulted from the MP fragments passing through the bay, but it seems more likely that the breakage was from aerodynamic loads. This would have had to be the case for the thermocouples in bay 2. Finally, the brackets on the forward PR showed signs of having been damaged by tension.

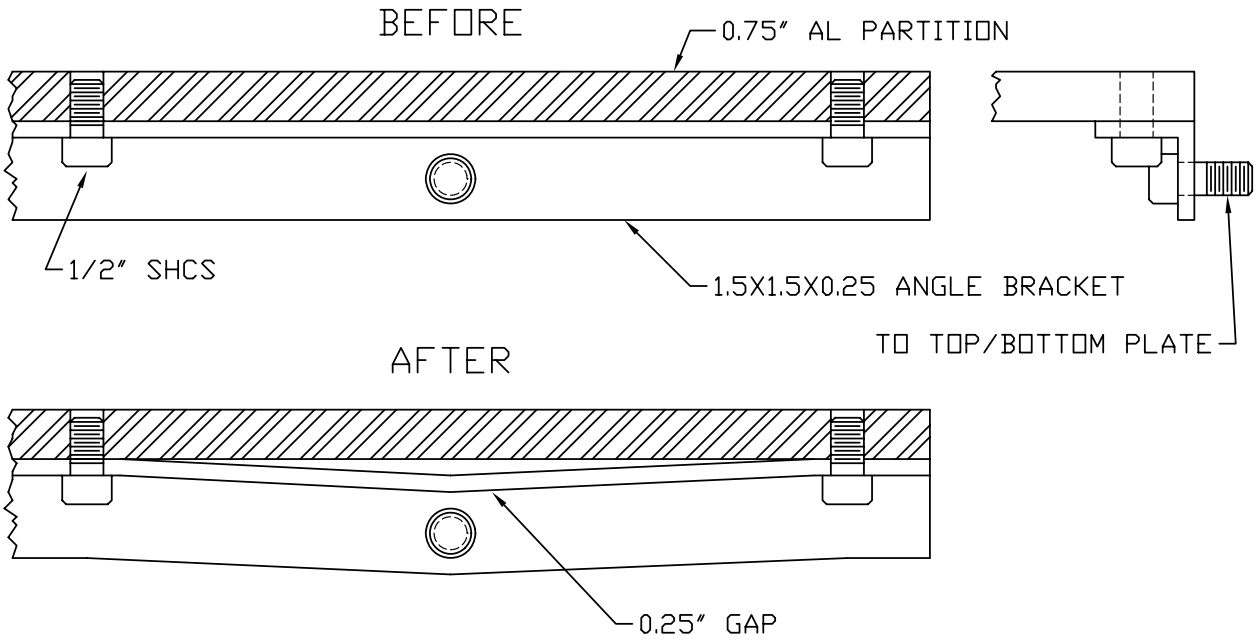

Figure 5.87: Damage to strong partition mounting brackets. View looking at top or bottom plate. Partition forced forward (toward bolts securing bracket to top/bottom plates), end of partition folded around last bolt.

Figure 5.88 shows pressure traces from the aft bays. The pressure histories are reasonably symmetric about the centerline. Ignition occurs in bay 5, and the flame quickly enters bay 6. Combustion does not occur in the forward bays until about 150 to 165 ms. Prior to this time,

the pressure rise in bays 3 and 4 is due only to venting through the passageways. The reason for the sudden ignition in bay 4 at 165 ms is not clear. Bay 3 ignites 10 ms later, and the pressure reaches a peak of nearly 5 bar. The slope of the traces indicates that these bays were ignited under turbulent conditions, due to venting from bays 5 and 6. It appears that the MP rupture does not affect the initiation of combustion in the aft bays.

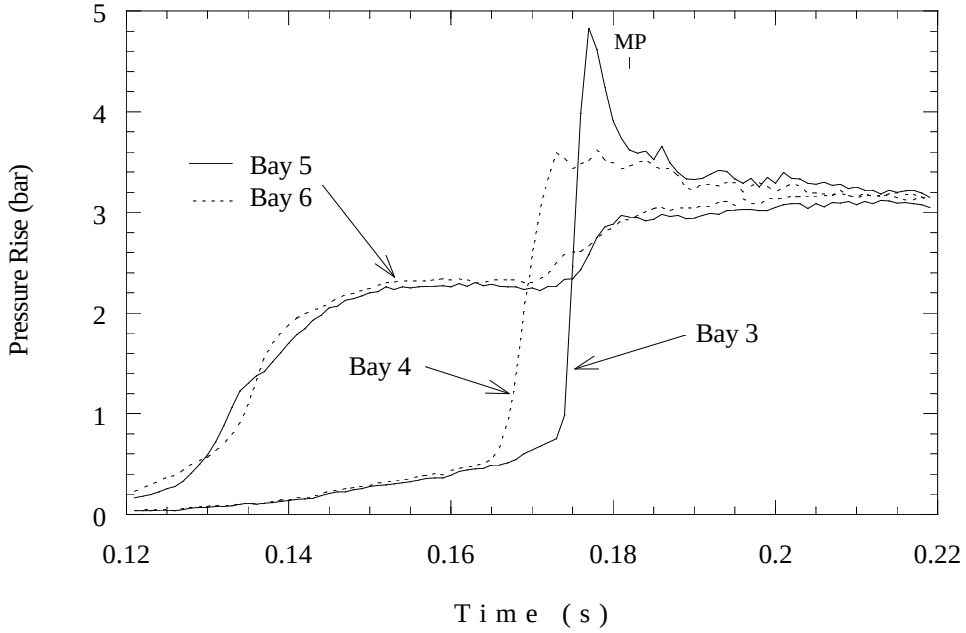

Figure 5.88: Pressure traces from bays 3 – 6, weak MP, ignition in bay 5. Test 14.

Figure 5.89 shows the pressure traces from bays 1 and 2, with those from 3 and 5 for reference. The flame proceeds forward sequentially, entering bay 2 at 180 ms and bay 1 at about 183 ms. While the bay 2 pressure trace does show a small kink coinciding with the MP rupture signal, we believe that the rupture actually occurred where the sharp peak is at 185 ms. MP rupture was recorded via a thin copper wire epoxied to the surface, wired to the partition motion detector circuit. This wire may have broken while the aluminum diaphragm was deforming, before the diaphragm fractured. The pressure in bay 2 drops sharply after the peak at 185 ms and then begins to rise again as bay 1 burns. Despite the large increase in flow area due to the MP rupture, the combustion in bay 1 is fast enough to prevent equalization between the two bays until about 195 ms. The MP area is 42 in^2 compared to the nominal passageway area of 2.15 in^2 in SWB2.

Differential pressures across SWB1 and MS are shown in Fig. 5.90. These are easily reconciled with the pressure traces. The rapid reversal of the differential pressure in bay 5 at 165 ms and bay 6 at 170 ms coincides with the ignition of bay 4, then bay 3.

The SWB2 differential pressure (Fig. 5.91) slowly rises as gas from the aft bays vents into bay 2, and then rapidly increases when the flame reaches bay 2. When the MP breaks, there is a sharp drop. The vent pressure differentials reflect the combustion sequence in the aft bays. The starboard vent differential pressure increases first while bay 6 burns. The port vent differential

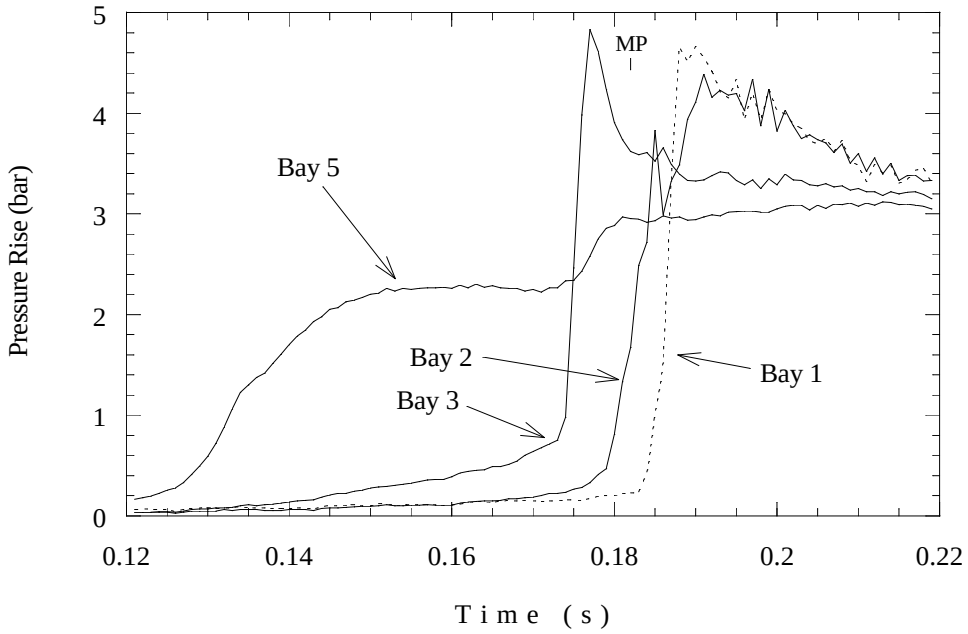

Figure 5.89: Pressure traces from bays 1 – 3, 5, weak MP, ignition in bay 5. Test 14.

pressure rapidly increases when bay 3 ignites at 172 ms. Ignition of bay 1 drives both pressure differentials negative until the aft bays equalize with bay 1.

The aft PR, in Fig. 5.92, shows very little pressure differential. The aft partial rib has the largest flow area (6.8 in^2) of any partition except when the MP in SWB2 is ruptured. Flow through the passageway serves to equalize the pressure quickly between bays 5 and 6; in addition rapid lateral flame motion results in nearly simultaneous combustion between bays 5 and 6. The flow area in the forward PR is smaller (2.8 in^2) than in the aft PR and there are usually large differences in ignition time of bays 3 and 4. This results in much larger pressure differentials across the forward partial rib than the aft.

The schlieren image of the flame in bays 3 and 4 was hard to make out. The camera on bays 5/6 failed. It appears that the flame entered one bay first, and other immediately after that. Combustion in bay 2 was rapid and violent, breaking one of the thermocouples. It is difficult to tell when this occurred relative to rupture of the MP, as the timing strobe is not visible in the video conversion of bay 1 footage. In bay 1, flow exits from the vent stringers before any other flame is visible, so this may be the ignition source. When the MP ruptures, the scattered debris and shockwave rip the ignitor from its feedthrough, and break both thermocouples. Other damage was also found in the tank, as described above. Exterior cameras show a small amount of leakage around SWB3.

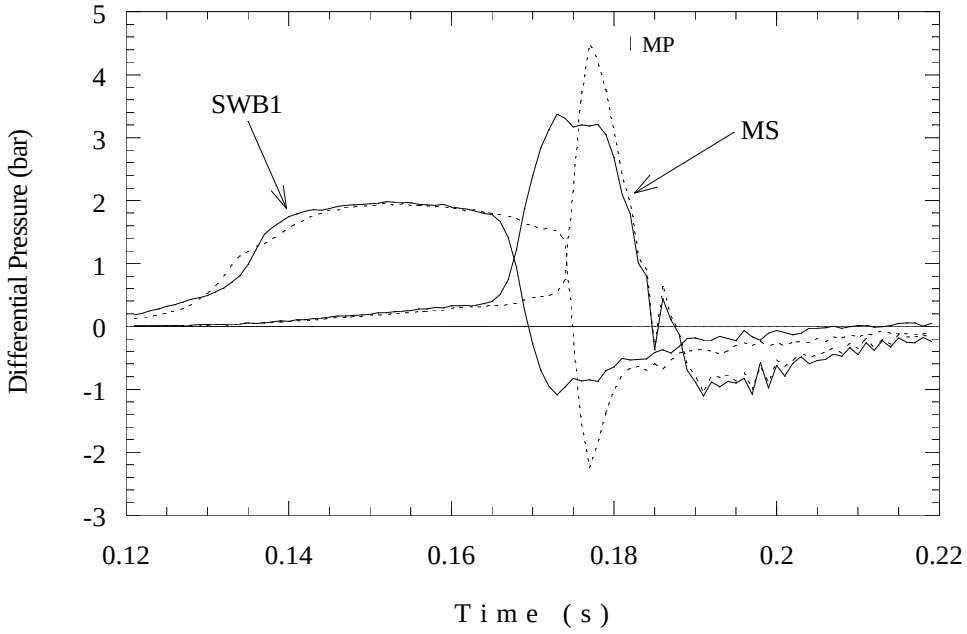

Figure 5.90: Differential pressure across SWB1 and MS, weak MP, ignition in bay 5. Dashed lines indicate port side of partition, solid lines indicate starboard. Test 14.

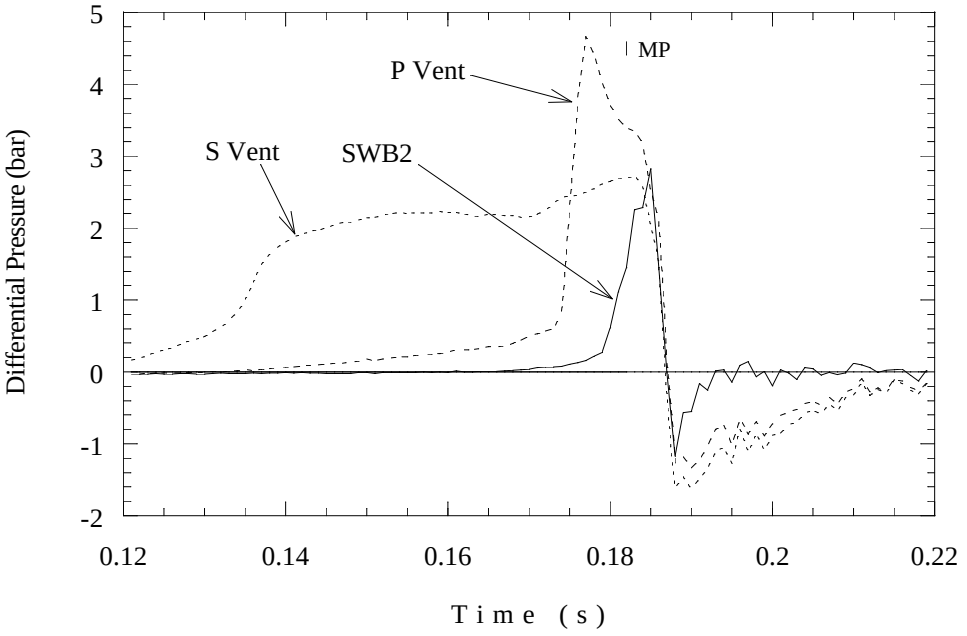

Figure 5.91: Differential pressure across SWB2 and vents, weak MP, ignition in bay 5. Test 14.

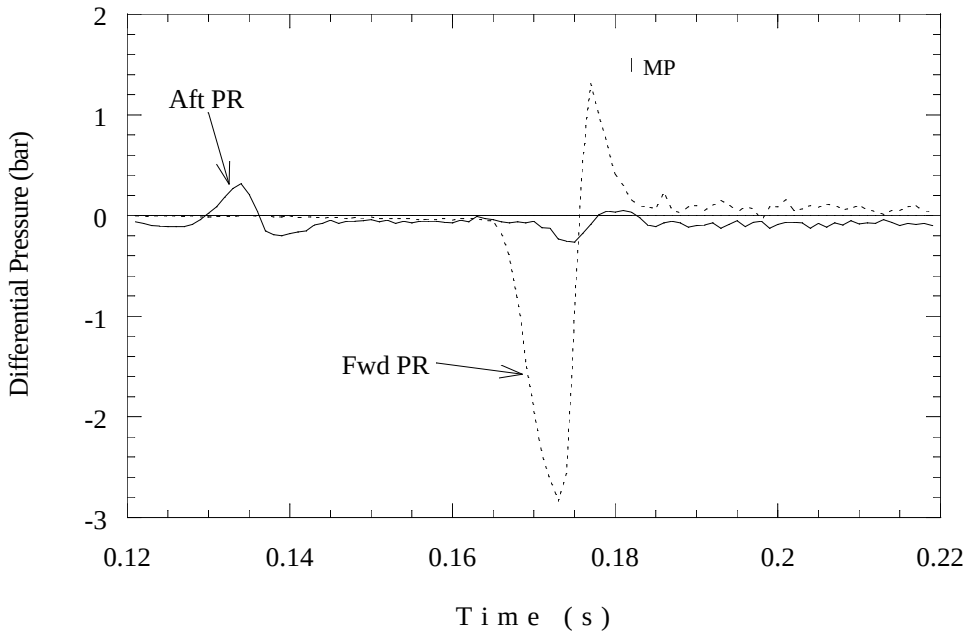

Figure 5.92: Differential pressures across PRs, weak MP, ignition in bay 5. Test 14.

Table 5.27: Flame arrival time (ms), Test 14.

Photodetectors		Thermocouples			
128	128 **IGN**	125	117	72 **IGN**	127
166	173	168	170	174	174
180		185		183	
184		185		187	

5.4.3 All-Weak Partition Tests

Ignition in Bay 5 (Test 18) This is the first test to use all weak panels to simulate the failure of SWB1, MS, SWB2, SWB3, and FS. The panels are observed to fail at a differential pressure between 1 and 2 bar, resulting in lower peak pressures in all bays as compared to the all-strong or part-strong tests. Panel failure occurs at the top and bottom where the panels are secured by screws. The nominal failure pressure was choosen to be 1.36 bar. This is a compromise that represents an average failure pressure for SWB2 as determined by Boeing computations (discussed in the Test Plan document, Shepherd et al. 1997b). Failure at this pressure was assured by shear failure of deliberately weakened retaining screws, as discussed in the Facility Section. However, this did not turn out to be the only failure mode. Failure modes were several: through shearing the screws, pulling the panel through the retaining nut, or prying the nut and body from the upper part of the screw.

All of the panels were blown out of the tank in Test 18, with only the aft PR remaining in the tank. SWB1 traveled the farthest, skipping 68 ft downrange. MS was folded in half (forward), probably while the middle of the partition was held in place by the forward PR.

The pressure traces are shown in Figs. 5.93 – 5.100. In Fig. 5.93, we see behavior typical of bay 5 ignition in the all-strong tests, except that the pressures now peak at about 2.5 bar rather than 4 bar. Note that the MS begins to fail earlier and complete failure takes 10 ms, as compared to 2 ms for SWB1 (Table 5.42). The pressure drop in bay 4 (Fig. 5.94) corresponds to the MS failing first on the starboard side.

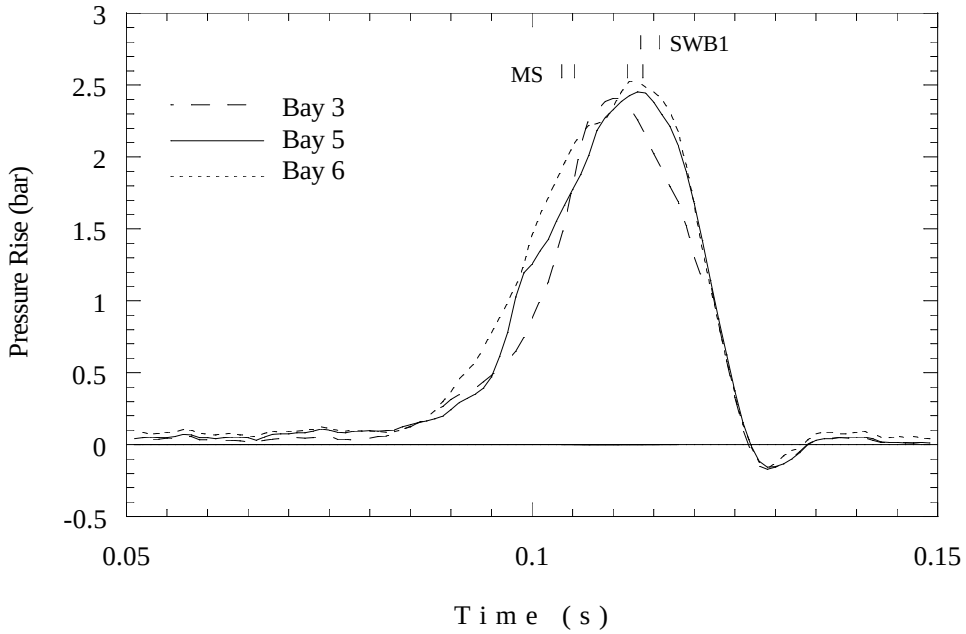

Figure 5.93: Pressure traces for bays 5, 3, 6, ignition in bay 5, all weak partitions. Markers indicate tripping of motion detectors. Test 18.

Figure 5.95 shows the pressures from the forward bays. Combustion appears to progress sequentially from back to front. Bay 0 contains no combustible mixture, so it does not show

Table 5.28: Motion detector breakaway times. Numbers in italics are from tape drives. MP only has one breakwire. N/R, not recorded. Tape drive values from some tests have been modified; see text.

	Top		Bottom	
	Port	Starboard	Port	Starboard
Test 18			*Correction: +5.52*	
SWB1	113.39	115.69	N/R	N/R
MS	111.73	103.68	*113.65*	*105.23*
SWB2	117.85	114.86	107.1	*106.47*
SWB3	106.24	107.14	107.1	*108.15*
FS	110.60	110.74	110.5	*110.61*
Test 19			*Correction: +13.25*	
SWB1	117.52	101.87	N/R	N/R
MS	125.73	106.47	*124.77*	*106.35*
SWB2	110.00	109.09	109.9	*108.66*
SWB3	111.63	111.52	111.7	*111.49*
FS	113.91	113.97	113.9	*113.93*
Test 20			*Correction: −5.92*	
SWB1	124.30	125.45	N/R	N/R
MS	113.11	122.38	*112.34*	*122.50*
SWB2	116.80	117.15	117.2	*117.08*
SWB3	117.38	117.51	117.8	*118.25*
FS	120.73	120.82	120.7	*120.75*
Test 21			*Correction: +3.50*	
SWB1	126.90	126.23	N/R	N/R
MS	125.96	125.31	*125.61*	*127.20*
SWB2	120.17	123.23	121.4	*129.92*
SWB3	122.19	121.61	123.7	*121.89*
FS	125.44	125.45	125.6	*125.50*

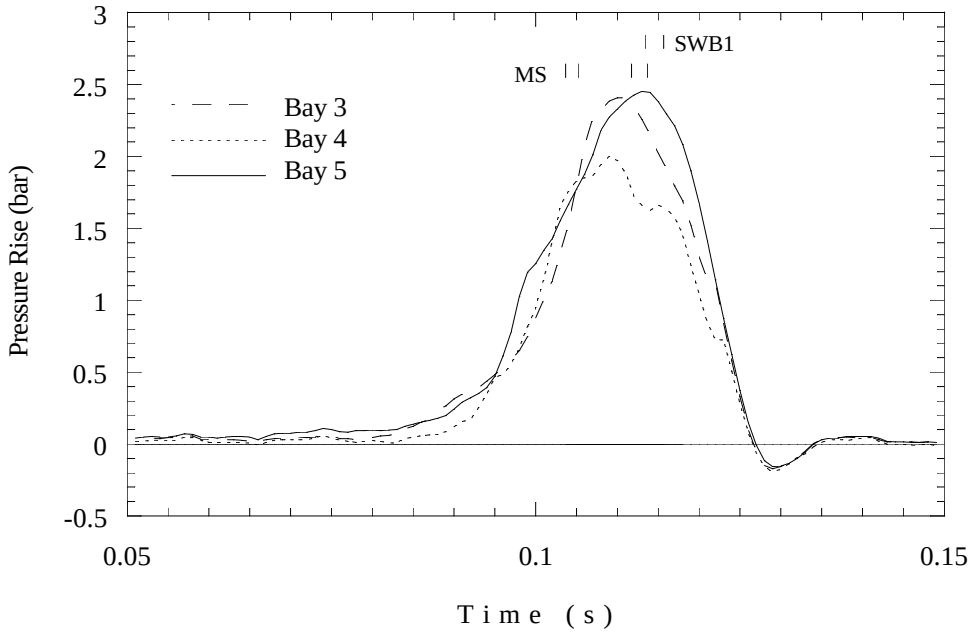

Figure 5.94: Pressure traces for bays 5, 3, 4, ignition in bay 5. Test 18.

a pressure signal until the rupture of SWB3, which occurs over a short period of time after 105 ms. The inertia of the gas and the pressurization of bays 0, 1, and 2 provide a confining action that enables higher peak pressures in the aft bays than in the forward bays. The negative phase at 130 ms is associated with the overexpansion caused by the gas motion emptying the tank after all the partitions have exited.

Differential pressures are shown in Figs. 5.96 – 5.100. Figure 5.96 shows SWB1 failing when the pressure difference reaches about 0.9 bar on the starboard side. This is somewhat lower than the nominal failure pressure of 1.36 bar. The MS begins to fail (0.8 bar differential pressure) on the starboard side at about 10 ms before SWB1 begins to fail. The port side of the MS fails next (1.0 bar differential pressure), but the differential pressure peaks later at about 120 ms.

SWB2 begins to fail at a low (0.5 bar) differential pressure (Fig. 5.98), but SWB3 fails at 1.1 bar, closer to the desired differential pressure. The pressure drops rapidly after SWB3 fails, as it is the boundary to atmosphere. SWB3 fails over a much shorter time span than the aft partitions.

Differential pressures across the vents are shown in Fig. 5.99. The pressure differential across the FS is simply the bay 0 pressure given in Fig. 5.95. The FS fails at nearly all corners simultaneously. Witness marks on SWB3 indicate that SWB3 typically impacts the FS and wraps itself (and FS) around the water bottles. The pressure rises sharply until FS fails, at which point the pressure makes a more gradual drop. The late spike in the trace for the FS is interesting. It may be a result of the late failure of the aft partitions. The vents are able to build up pressure, as the aft partitions fail later. The reason for the second peak at 120 ms is unclear; SWB3 has failed 5 ms earlier, so it is not due to the sudden drop in bay 0 pressure.

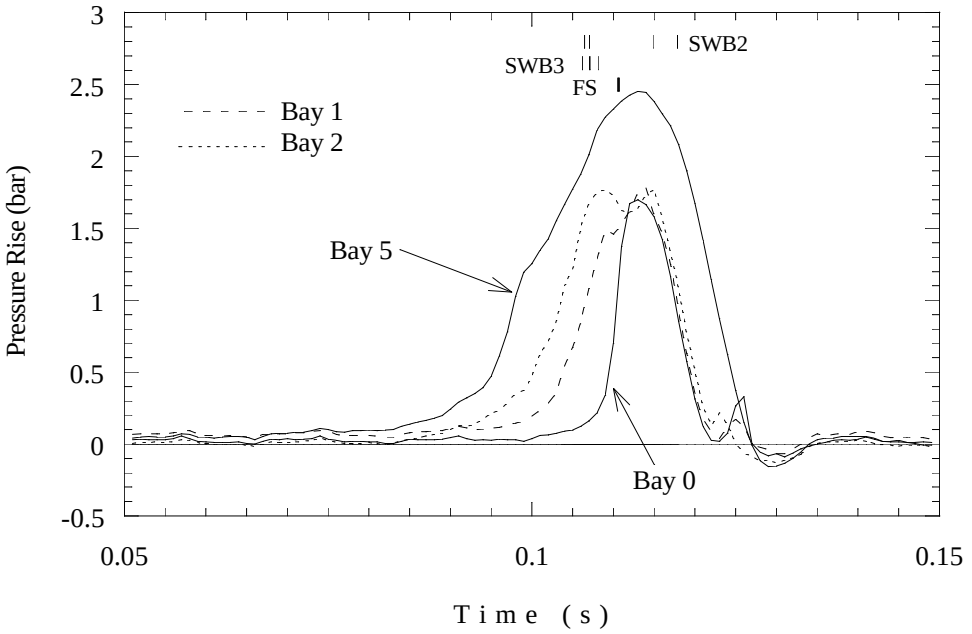

Figure 5.95: Pressure traces for bays 1, 2, 5, 0, ignition in bay 5. Test 18.

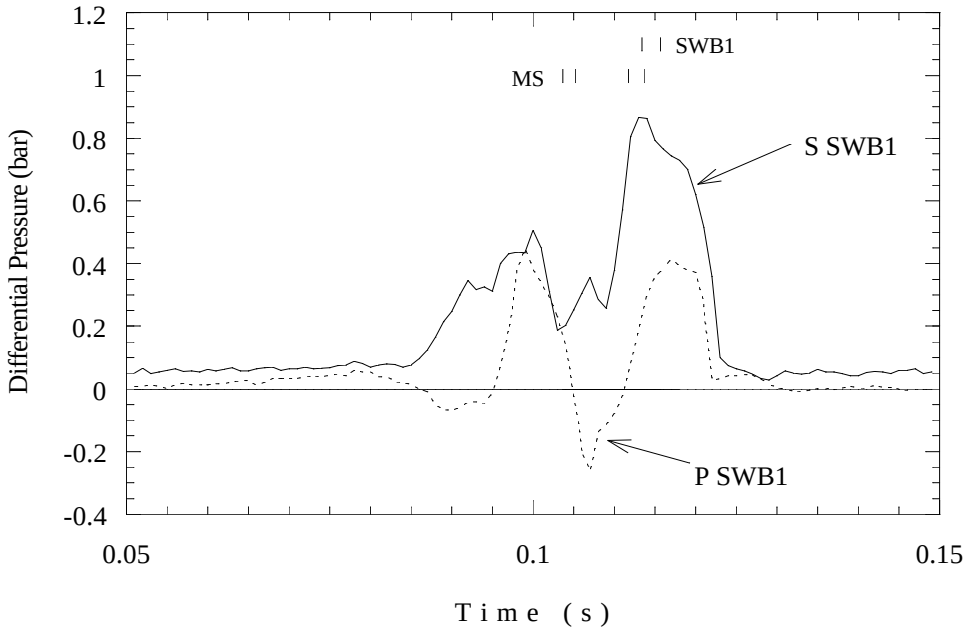

Figure 5.96: Differential pressures across SWB1. Test 18.

Differential pressures across the PRs are not very large, as the partitions fail before large pressures can build. The forward PR shows a positive pressure differential at 110 ms, which is consistant with the starboard side of MS failing and venting that compartment before the port side.

Bay camera 1 malfunctioned in this test, so there is no schlieren from bays 5 and 6. The

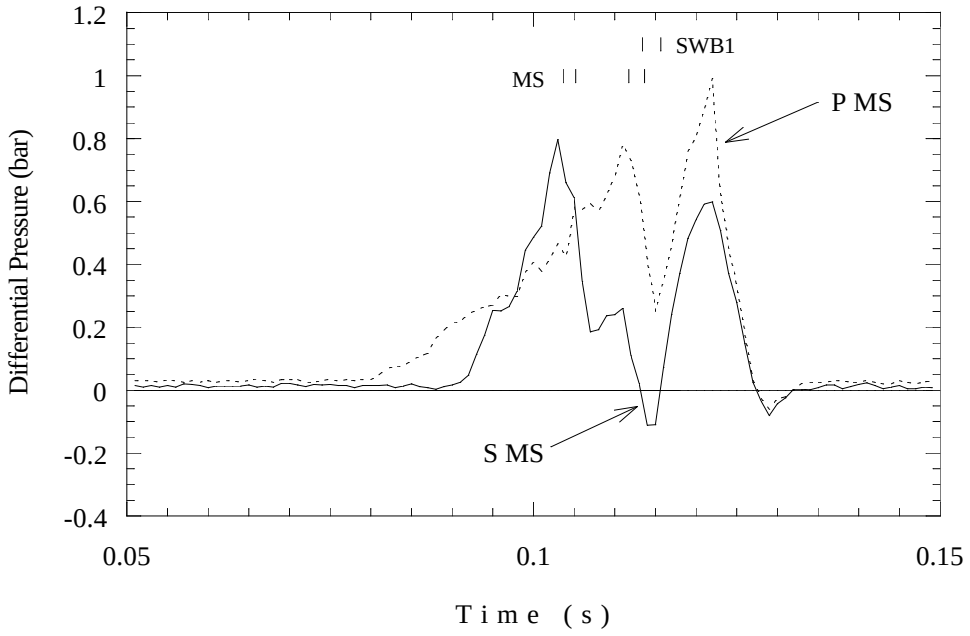

Figure 5.97: Differential pressure across MS. Test 18.

flame appears to enter bay 3 through the bottom passageways, jetting toward the MS, and propagating upward and into the bay. Ignition of bay 4 cannot be distinguished. Once the flame fills the cross-section of the frame, SWB1 bows forward a few inches, but snaps back. This may be the starboard side being pushed back into place by the increase in pressure associated with combustion in bay 4. As soon as SWB1 rebounds, it fails completely, and SWB1 proceeds past bay camera 2 with the aft PR forward bracket still attached.

In bay 2, the flame also enters at the bottom, but apparently through one of the passageways above the tank floor. This flame jet has a lower speed than usual, so instead of the flame reaching SWB2 and spreading along the partition into the bay, the flame immediately propagates upward into the bay. Before the flame fills the bay, the MS fails, and the view is blocked by the partitions until SWB1 passes. In bay 1, the flame enters through one of the passages above the floor. As the flame jet reaches SWB3 and begins spreading into the tank, another flame enters from the vent stringers. At the same time, SWB2 begins to bow forward. Before combustion in bay 1 is complete, SWB2 fails along the bottom edge and begins rotating upward. It still appears to be attached at the top when MS enters and sweeps it out of the tank. The view is obscured until the passage of SWB1.

Exterior footage from the cameras is underexposed because of the late firing time (1600 hrs). However, the action is still visible. The best footage is from the SE station film and video. It appears that SWB3 fails along the top first, and rotates forward towards FS. As FS fails, burning gas jets shoot up and forward from the top of FS. SWB3 and FS fold forward and wrap around the water bottles. It appears that SWB1 and MS actually pass under SWB2 on their way out of the tank. SWB2 remains relatively flat as it exits, but SWB1 and MS are folded forward. The folding results from the connection to RS via the PRs. The aft PR remained in

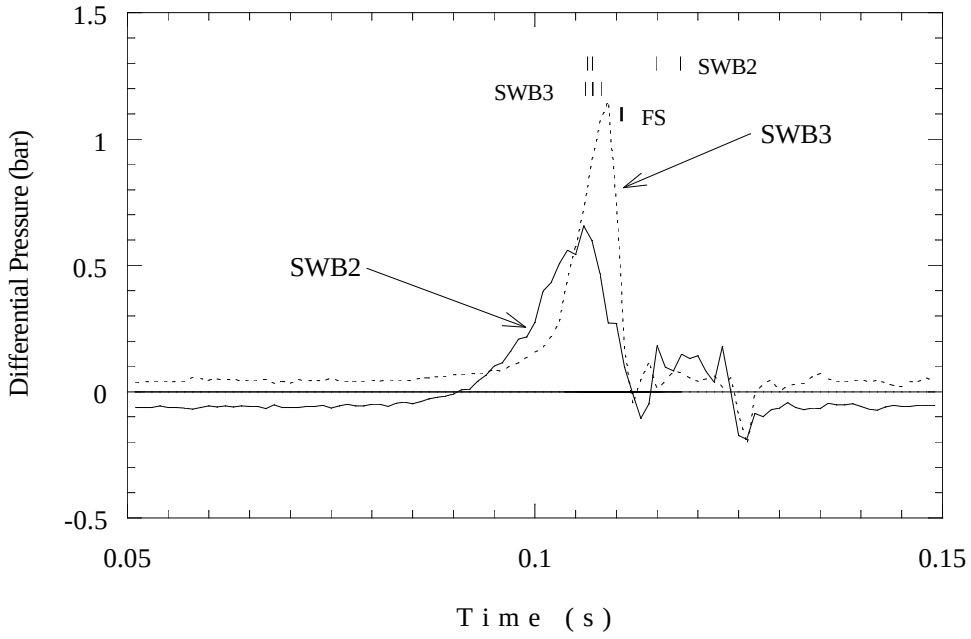

Figure 5.98: Differential pressure across SWB2 and SWB3. Test 18.

the tank during this test. After exiting the tank, the panels hit the blast gauge protector and were scattered about the field.

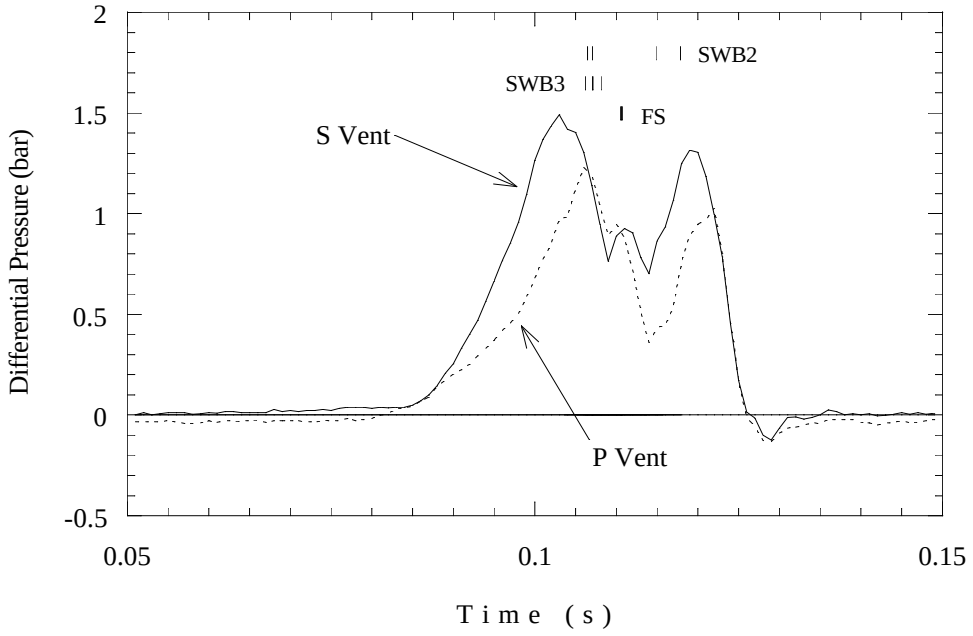

Figure 5.99: Differential pressure across vents. Test 18.

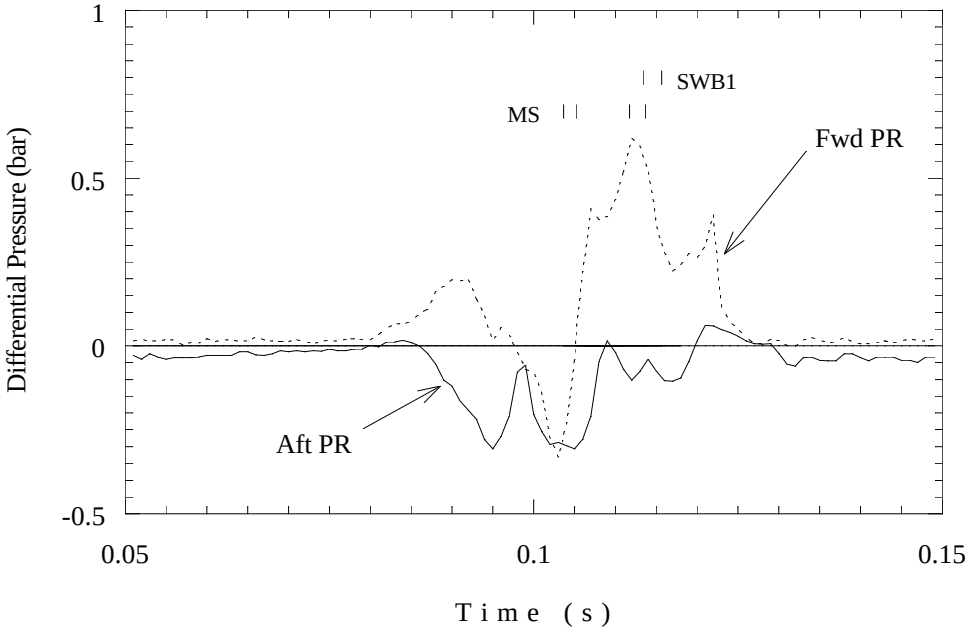

Figure 5.100: Differential pressure across PRs. Test 18.

Table 5.29: Flame arrival time (ms), Test 18.

Photodetectors		Thermocouples	
89	95 **IGN**	91 86	67 **IGN** 97
92	85	105 102	111
100		111	108
102		103	109
108			

Ignition in Bay 5, with Cold Liquid Jet A Layer (Test 19) This was the first of three tests to use a layer of cold Jet A with the all-weak configuration. As the panels exited the tank, the FS assembly impacted the gauge guard with the starboard water bottle. This stopped FS long enough for the port water bottle to tear free and travel 140 ft downrange. Despite the impact, which left a deep notch on one end of the starboard bottle, FS and the attached bottle ended up 96 ft from the tank. The gauge guard was nearly ripped out of the ground, and the diagonal brace broke off at the weld. Since no useful data was being obtained from the blast gauges, at this point the axial blast gauge and guard were removed.

Pressure traces are shown in Figs. 5.101 – 5.109. Note from the figures and Table 5.28 that the port sides of SWB1 and MS fail much later (20 ms for MS) than the starboard sides. In Fig. 5.101, we see the pressure traces for bay 5 and the adjacent bays, 3 and 6. Some of the typical interplay between bays 5 and 6 occurs, but partition failure begins before this can progress further. Figure 5.102 replaces the trace of bay 5 with that of bay 4, and we see that bay 4 still undergoes late ignition and rapid pressure rise, but this is cut short by failure of the port side of MS. Port side failure of SWB1 brings the traces of bays 4 and 6 together to some degree (note corresponding change in slope of bay 6 trace), but slight differences still occur until MS and SWB1 fail completely.

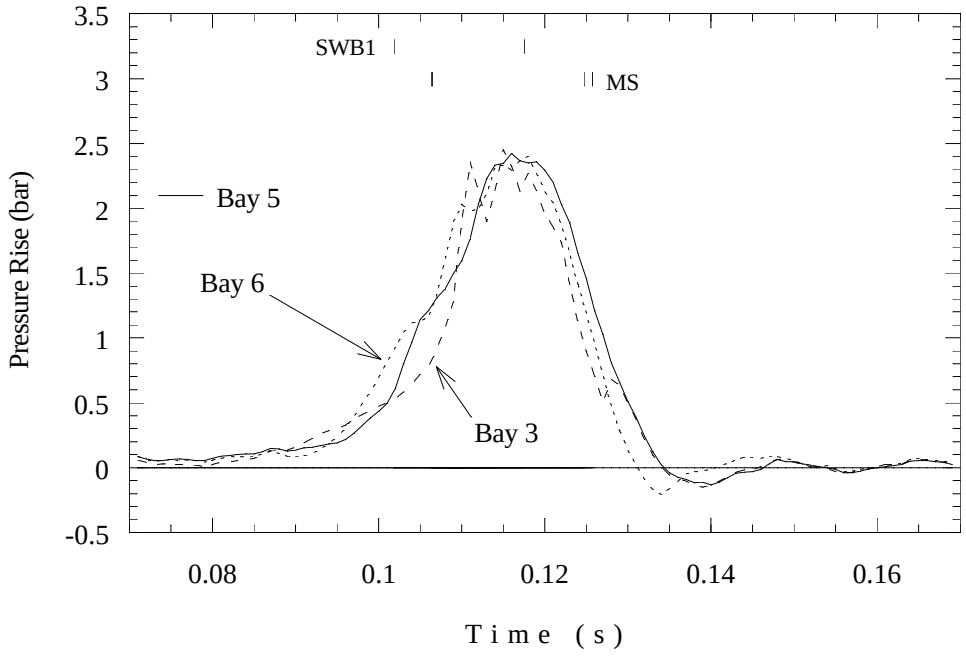

Figure 5.101: Pressure traces from bays 3, 5, 6, ignition in bay 5, with a cold liquid Jet A layer. Test 19.

Figure 5.103 shows the pressure in bays 1 and 2 with bay 5 for reference. Bays 2 and 1 ignite in sequence, and show an abrupt change in slope at about 110 ms. SWB3 fails when the bay 1 pressure is around 1 bar, but FS holds on for a short time longer, allowing the rapid pressure rise to peak at 3 bar. Bay 1 pressure drops immediately on the failure of FS, but halts at a brief plateau before continuing to zero. Bays 2 and 5 depressurize in sequence, as gas is

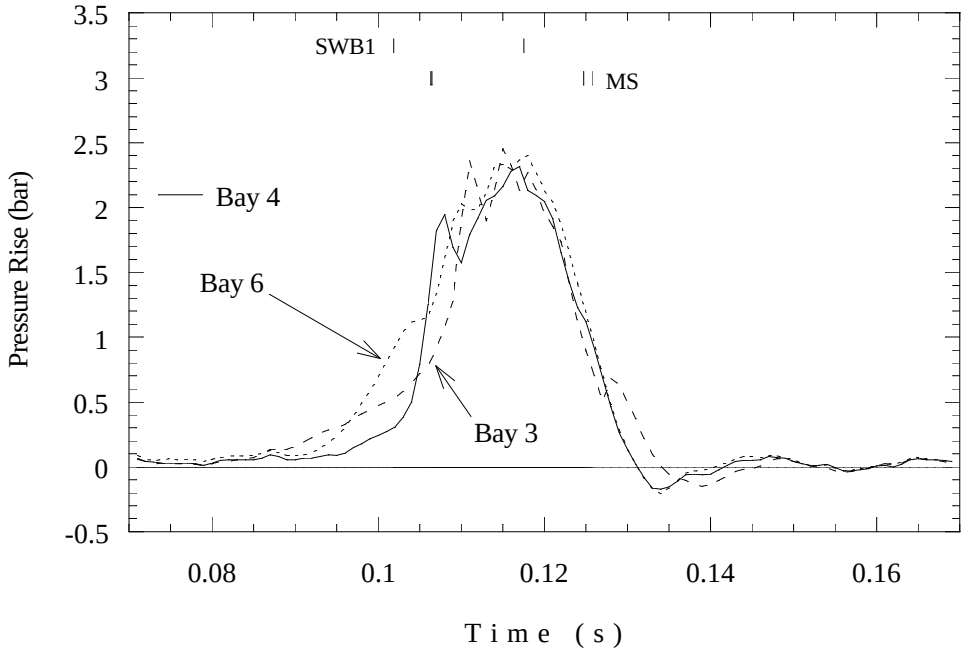

Figure 5.102: Pressure traces from bays 3, 4, 6, ignition in bay 5, with a cold liquid Jet A layer. Test 19.

vented from the open end of the tank. The pressures in the three forward bays are shown in Fig. 5.104, where we see that bay 0 pressurizes on failure of SWB1, and continues to increase after failure of FS. At 125 ms, a 0.5-bar pressure spike is visible in bay 0, probably the result of late failure of the port side of MS and SWB1.

Differential pressures across SWB1 and MS are shown in Figs. 5.105 and 5.106. The starboard side of SWB1 appears to fail with a differential pressure of less than one bar; the port side shows no large differentials when its failure is sensed. However, bottom sensors were not used on SWB1, so it is possible that the bottom of the partition failed earlier, reducing the pressure differentials, and later taking the top portion with it. The port side of MS also shows no large peaks directly associated with its failure, and both top and bottom were recorded. A 0.55-bar peak occurs shortly after indicated failure, so the motion detectors may have melted before they were actually tripped. The starboard side of MS, in contrast, shows a sharp peak of nearly 1.5 bar when failure occurs.

The failures of SWB2 and SWB3 are also clear, as shown in Fig. 5.107. SWB2 fails with a peak of 1.3 bar, and its failure generates a large amount of turbulence, as well as possible fuel lofting, yielding a very rapid pressure rise in bay 1 and a corresponding high failure pressure of 2.5 bar on SWB3. The late peak in differential pressure on SWB3 is probably due to the late failure of the port MS, but it is unclear why this would show up as a differential and not a static pressure. This may be caused by the passage of the aft partitions, which will retain some pressure behind them as they are ejected from the tank.

Figure 5.108 shows the similar patterns of behavior of the two vent stringers, and with all failure marks present, shows the aft-forward failure sequence. The MS and SWB1 both take

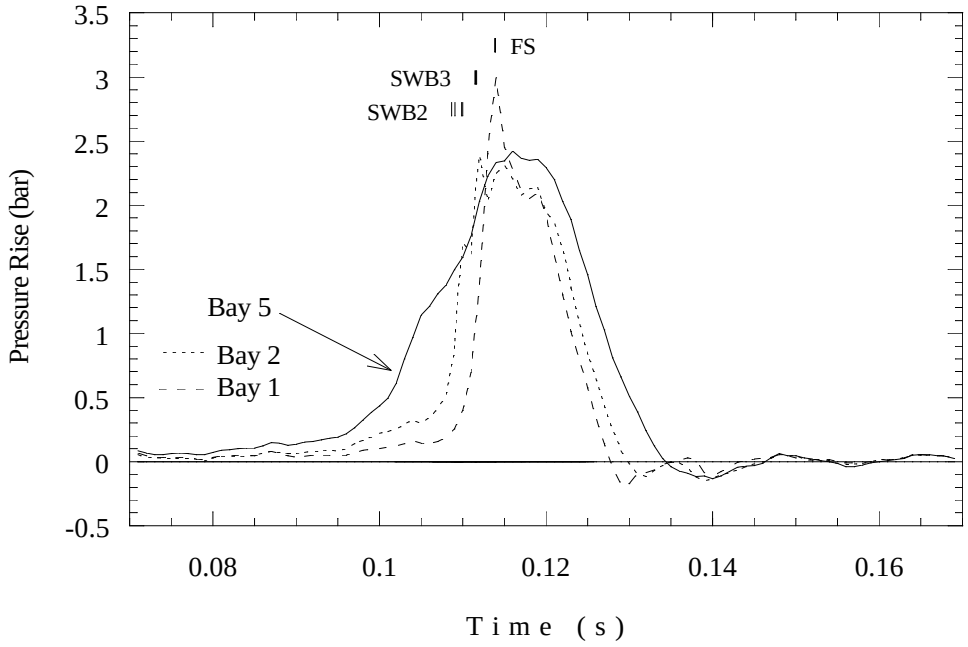

Figure 5.103: Pressure traces from bays 1, 2, 5, ignition in bay 5, with a cold liquid Jet A layer. Test 19.

a long time to fail on the port side and the second peak in differential pressure at 125 ms is attributable to the late failure of the MS. The PRs show small but sharply fluctuating pressure differentials over the course of the failure process. Pressure across the forward PR initially reflects the rapid combustion in bay 3, but failure of the starboard side of SWB1 generates turbulence in bay 4, accelerating combustion there and producing a rapid drop and negative differential pressure on the forward PR. By the time total failure has occurred in the aft bays, the differentials equilibrate. The PRs may have stayed intact, connecting SWB1 and MS, even after the partitions failed. This would account for the finite and equal pressure differential on both forward and aft PRs after 130 ms.

Bay cameras 2 and 3 malfunctioned in this test, so the schlieren footage is only available for bays 5/6 and 1. Ignition in bay 5 produces a smooth, spherical flame. When the flame reaches the aft PR, it enters bay 6 through one of the middle passageways. Bay 6 burns rapidly because of the turbulence set up by venting of bay 5. Once bay 6 is fully engulfed, lofting of the jet fuel obscures the view. By this time, it does not appear that SWB1 has failed. In bay 1, the flame enters through one of the passages above the floor of the tank. Fuel lofting from the corner vents begins at the same time. Shortly after the flame jet impinges on SWB3 and the flame begins spreading into the tank, another jet enters from the vent stringers. As these flames meet, and before the bay is fully engulfed, SWB2 begins to fail. The top and bottom fail at nearly the same time. MS is briefly visible passing through, but jet fuel and soot obscure the view thereafter.

Exterior footage shows a large fireball approximately 3 tank lengths long and 1 – 2 tanks high, or about 20-ft long by 12-ft high. The fireball is shown in a single closeup frame in

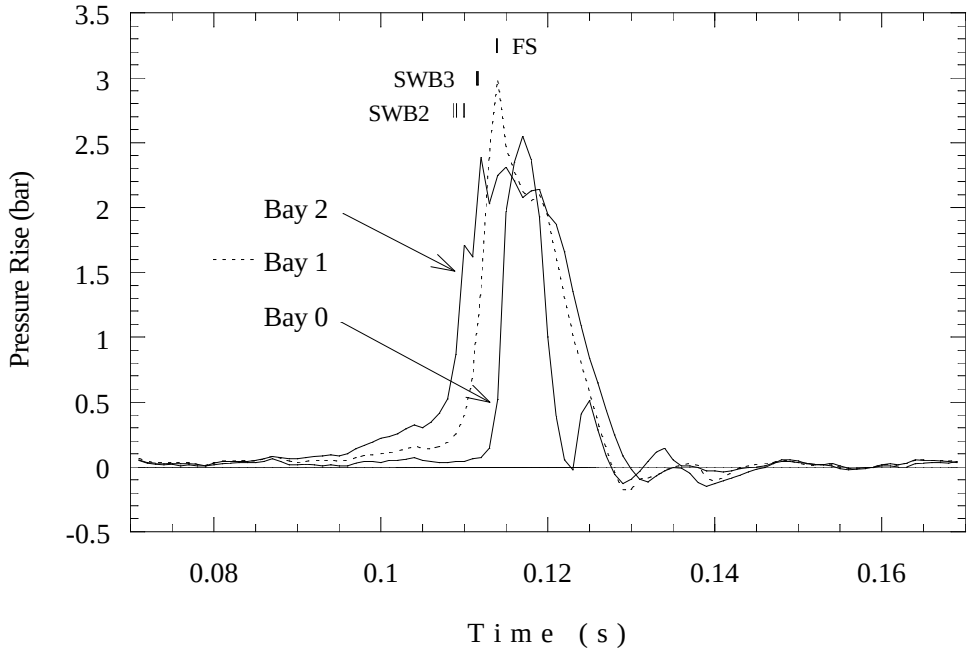

Figure 5.104: Pressure traces from bays 0 – 2, ignition in bay 5, with a cold liquid Jet A layer. Spike in bay 0 at 125 ms corresponds to failure of port side of MS. Test 19.

Fig. 5.110, and as a series of wide angle frames from the 8 fps Nikon in Fig. 5.111. The fireball engulfed the partitions as they were ejected, making it difficult to determine the grouping. One panel (SWB1) came out alone, after the others had apparently emerged together. This means that MS, SWB2 and SWB3 were all wrapped around the water bottles with FS. The blast gauge protector was torn from the ground and the weld to the reinforcing strut broken when the partitions impacted.

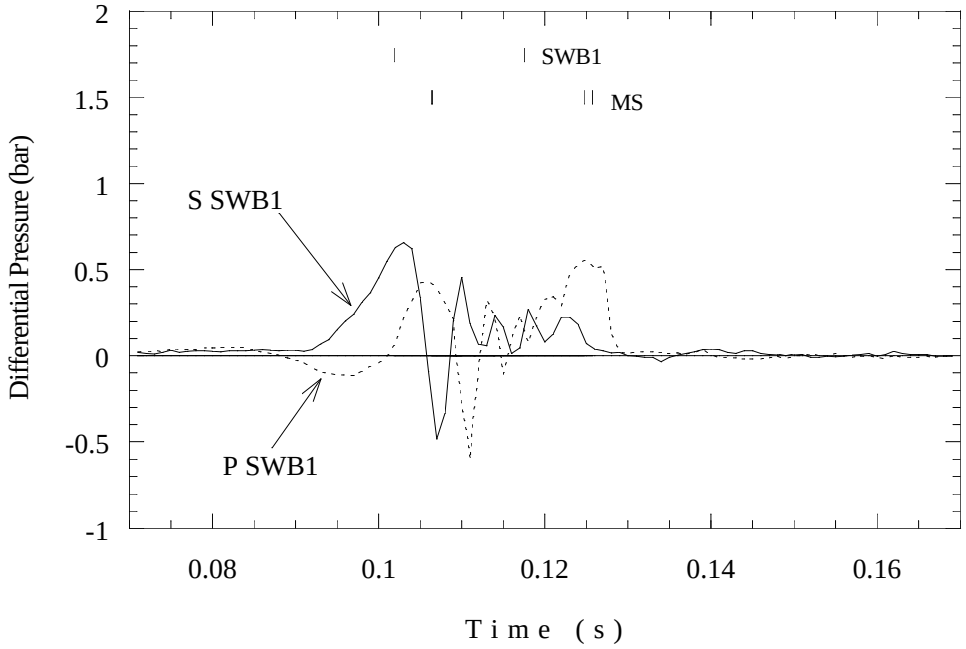

Figure 5.105: Differential pressure across SWB1, ignition in bay 5, with a cold liquid Jet A layer. Test 19.

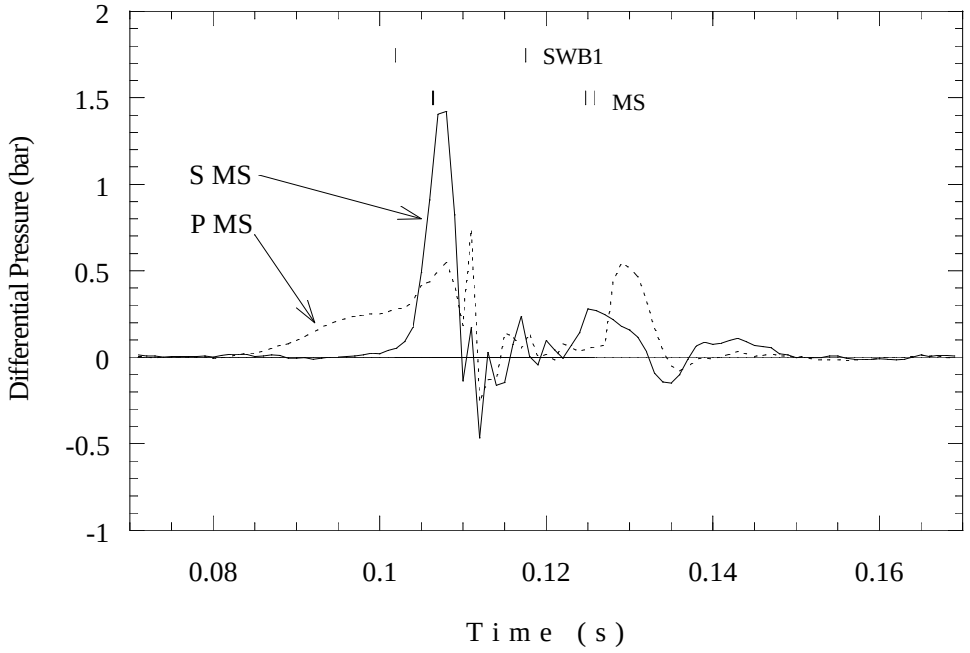

Figure 5.106: Differential pressure across MS, ignition in bay 5, with a cold liquid Jet A layer. Test 19.

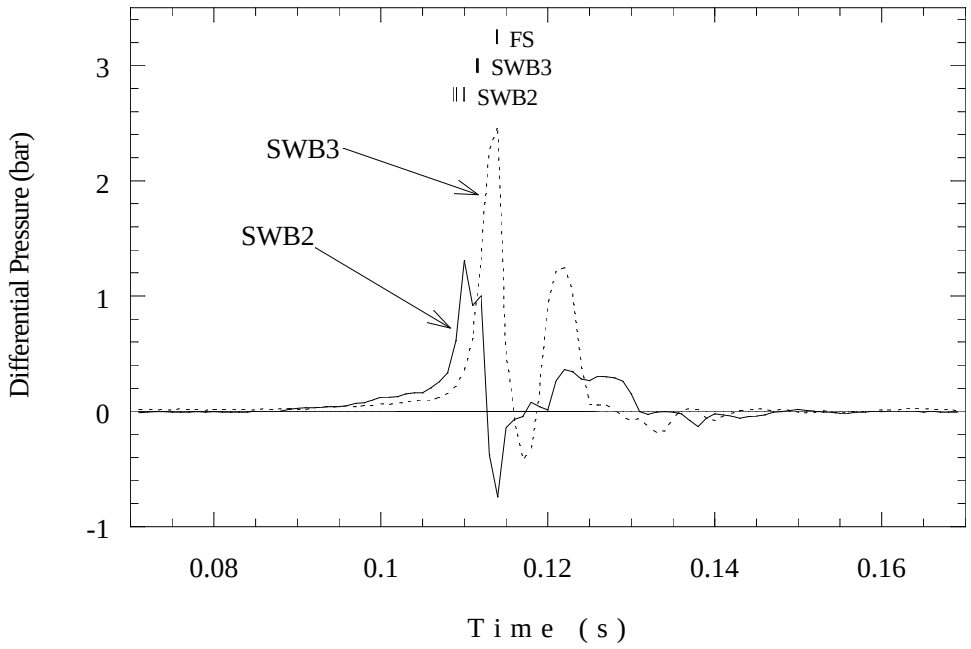

Figure 5.107: Differential pressure across SWB2 and SWB3, ignition in bay 5, with a cold liquid Jet A layer. Test 19.

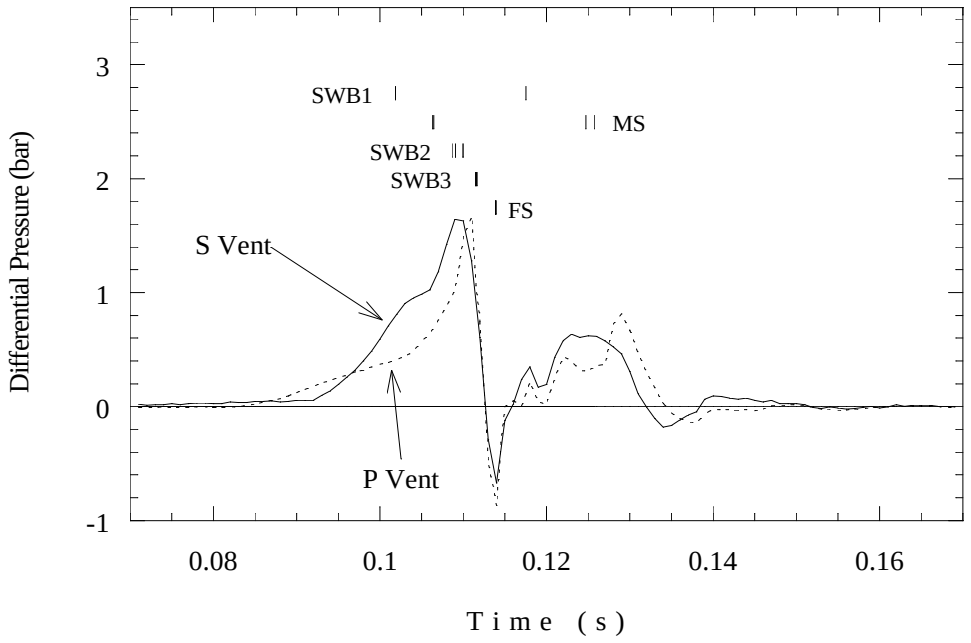

Figure 5.108: Differential pressure across vents, ignition in bay 5, with a cold liquid Jet A layer. Test 19.

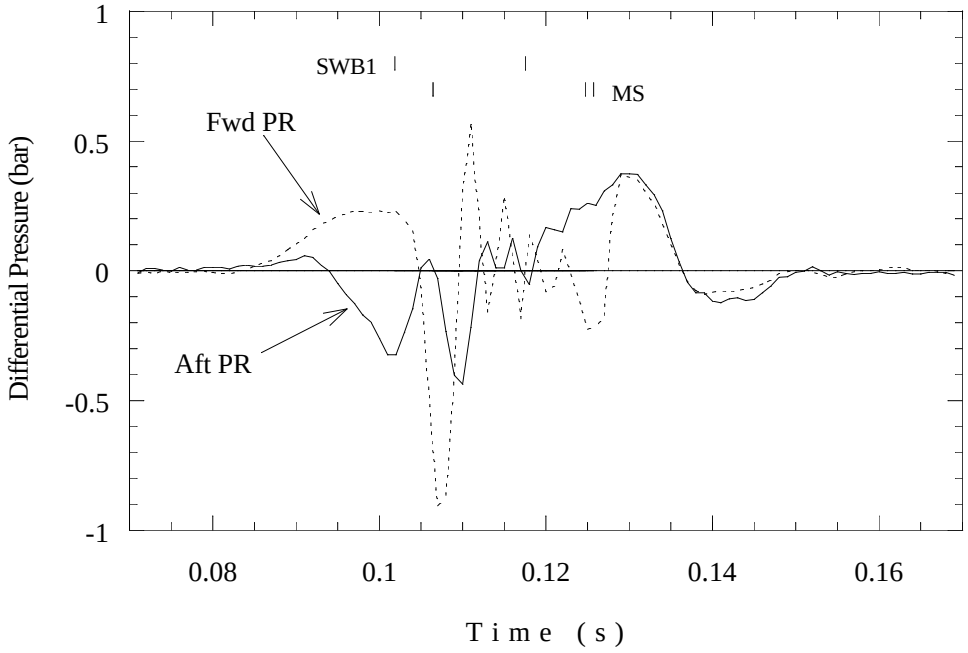

Figure 5.109: Differential pressure across PRs, ignition in bay 5, with a cold liquid Jet A layer. Test 19.

Table 5.30: Flame arrival time (ms), Test 19.

Photodetectors

94	99 **IGN**
96	87
99	
109	
113	

Thermocouples

98	95	65	101
128	105	114	114
110		113	
113		114	

Figure 5.110: Fireball from Test 19 at approximately its greatest extent.

Frame 1

Frame 2

Frame 3

Frame 4

Frame 5

Frame 6

Figure 5.111: Fireball sequence at 8 fps. Test 19.

Ignition in Bay 2Lo, with a Cold Liquid Jet A Layer (Test 20) In this test, the ignitor location was moved forward to 2Lo, the compensator location in bay 2. The FS, SWB3, and SWB2 were completely ejected from the tank. SWB1 and MS were folded forward but connected together by the forward PR, and remained partially within the tank near the open end; they were almost all of the way out, hanging by the center crease. Despite this, Test 20 holds the record for longest partition travel, with FS coming to rest at 207 ft, and one of the water bottles ending at 220 ft from the tank.

The associated pressure traces and partition failure signals are shown in Figs. 5.112 – 5.119. The proximity of the ignitor to passageways in the MS allows the flame to rapidly enter bays 3 and 4, as shown in Fig. 5.112. The video indicates that the flame enters bays 3 and 4 in a turbulent state, after some lofting has occurred. Venting of bays 3 and 4 into bay 2 generates turbulence, and accelerates the remainder of combustion, shown by the change in slope at 115 ms. It also appears that bay 3 ignites slightly before bay 4, possibly due to the lower MS passageway being located closer to the ignitor on that side of the tank. MS fails earlier on the port side than on the starboard, causing the pressure in bay 3 to dip slightly at 110 ms. Bay 4 remains intact for another 5 ms, resulting in a pressure peak of nearly 3 bar. Pressure in bay 2 increases until the failure of SWB2 and SWB3, and begins to drop after the FS fails.

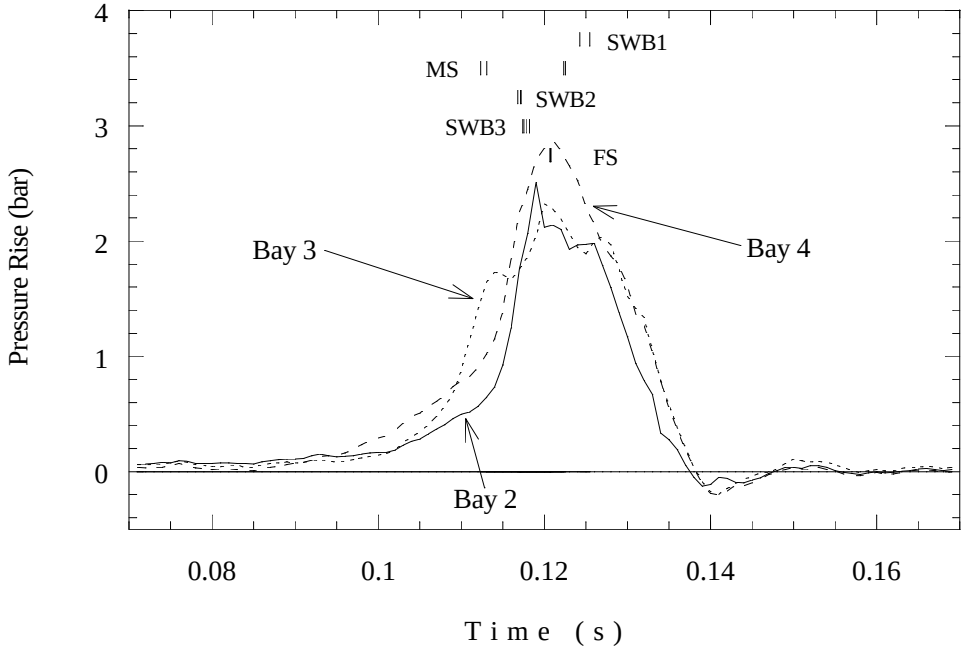

Figure 5.112: Pressure traces from bays 2 – 4, ignition in bay 2Lo, with a cold liquid Jet A layer. Test 20.

Bays 5 and 6 appear to ignite simultaneously with bay 3, as shown in Fig. 5.113. SWB1 was the last partition to fail in this test, resulting in higher peak pressures in the aft bays than in the forward bays. Bay 6 reaches the highest peak, with SWB1 probably supported on the starboard side by high pressure in bay 4. Both bays 5 and 6 vent rapidly after SWB1 fails.

Pressures in the forward bays are shown in Fig. 5.114. The pressure in bay 1 increases

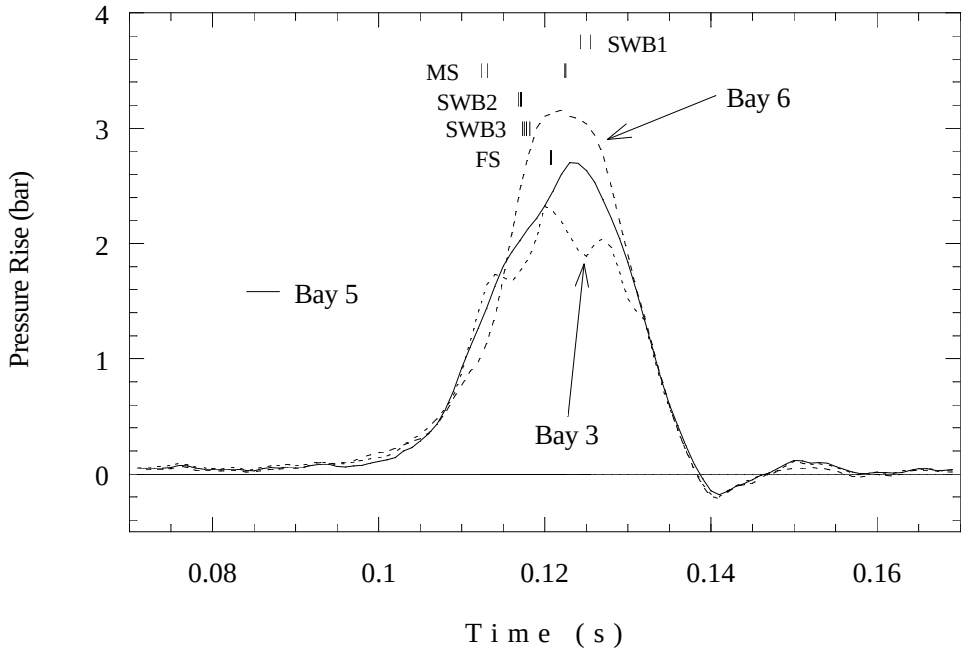

Figure 5.113: Pressure traces from bays 3, 5, 6, ignition in bay 2Lo, with a cold liquid Jet A layer. Test 20.

more slowly after SWB3 fails, but continues to increase due to the confinement by the FS. Failure of SWB3 causes pressurization of bay 0, which peaks and vents shortly after FS fails. Interestingly, bays 1 and 2 vent at a slower rate. There is also a late spike in the bay 0 pressure. This was probably caused by slow passage of one of the rear partitions. As mentioned above, SWB1 and MS were caught at the forward end of the tank and failed to exit completely. Once the panels reached the end of the tank, bay 0 vented at the same rate as bays 1 and 2.

Differential pressures across SWB1 and MS are shown in Figs. 5.115 and 5.116, respectively. We see that SWB1 experiences only moderate loads, and doesn't fail until the differential pressure reaches about 0.8 bar on both sides. This is lower than expected, but the forward PR is probably also pulling on SWB1, as MS failure is complete several ms earlier than SWB1. The 0.8-bar pressure difference is probably created by the venting of the forward portions of the tank. The MS port side fails at about 113 ms (peak pressure of 1 bar), followed by failure of the starboard side at 0.8 bar occurring at 122 ms. The rapid decrease in pressure difference on the port side is due to acceleration of combustion in bay 2 by the port MS rupture. The panel was probably still separating the bays, allowing some pressure differential to be maintained.

In Fig. 5.117, we see that SWB2 and SWB3 fail in rapid succession, almost simultaneously. The failures correspond to the peaks in the differential pressures observed at 117 ms. Note the second peak in SWB3 differential pressure at 129 ms. At the same time, the SWB2 pressure differential is zero, indicating that the SWB3 differential is associated with the passage of the aft partitions past this point.

Differential pressure across the vents is shown in Fig. 5.118. The port vent differential rapidly decreases at 113 ms when the port side of MS fails and pressure begins to equalize

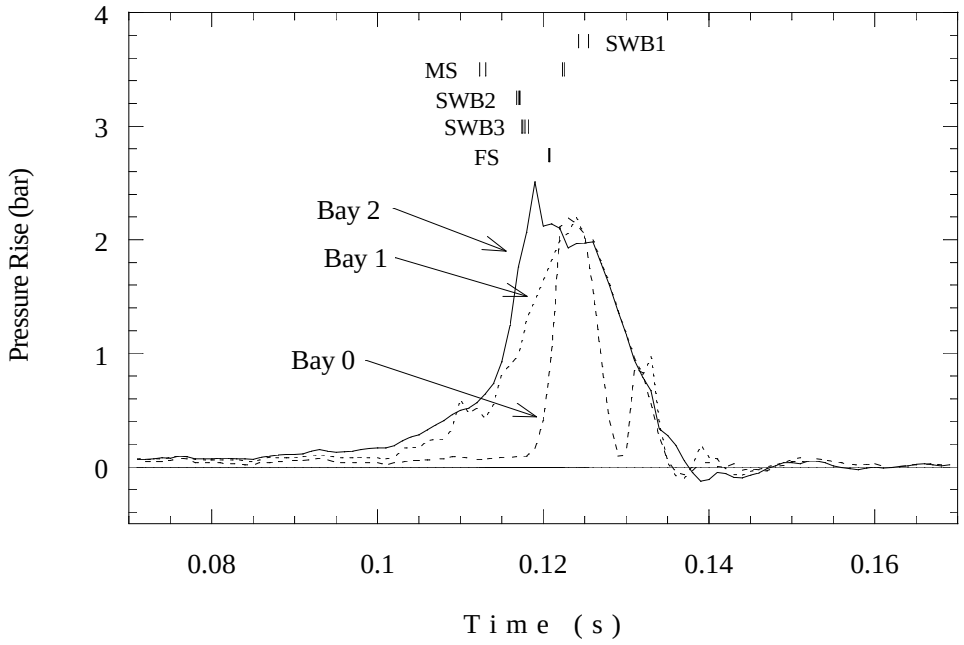

Figure 5.114: Pressure traces from bays 0 – 2, ignition in bay 2Lo, with a cold liquid Jet A layer. Test 20.

between bays 3 and 2. Failure of SWB2 results in the differential pressure rapidly decreasing. The starboard vent differential pressure peaks when SWB2 and SWB3 fail. Passage of the aft partitions is probably associated with the coincidence of the two traces after 130 ms. The differential pressures for the PRs are shown in Fig. 5.119. Both traces are similar, indicating lateral symmetry similar to that observed with bay 2 ignition in the all-strong case (Test 6).

All of the bay cameras functioned in this test. In bay 2, ignition produces a smooth flame that propagates out of the corner (between MS and the tank floor) and into the bay. When the flame has filled about three-quarters of the bay 2 cross-section, a jet enters the bay at the bottom and accelerates combustion in the bay. Some fuel lofting is visible in bay 2 under the jet. Before the flame can completely engulf the bay, the MS begins to fail and obscures the view.

Fuel lofting towards aft is visible in bays 3/4 quite early in the event, well ahead of the onset of rapid combustion in bay 2. However, the flame does not pass into bays 3/4 until much later. The flame proceeds upward and engulfs the bay. The view is obscured by jet fuel before the panels fail, though SWB1 can be seen passing the camera. Fuel lofting in bay 1 starts later than in bays 3/4. The flame enters at the bottom of bay 1 impinging on SWB3 and burning back into the bay. SWB2 slowly begins to fail as the jet impinges on SWB3, but gives way suddenly as the flame fills the bay. In the back of the tank, fuel begins to loft in bays 5/6 at approximately the same time as in bay 1. The flame enters at the bottom of bays 5/6 and burns upward, with the jet fuel behind it.

On the exterior, the side-view film camera was overexposed, but shows MS failing first, folding forward at the hinge created by the forward PR connection. SWB2 begins to bulge at

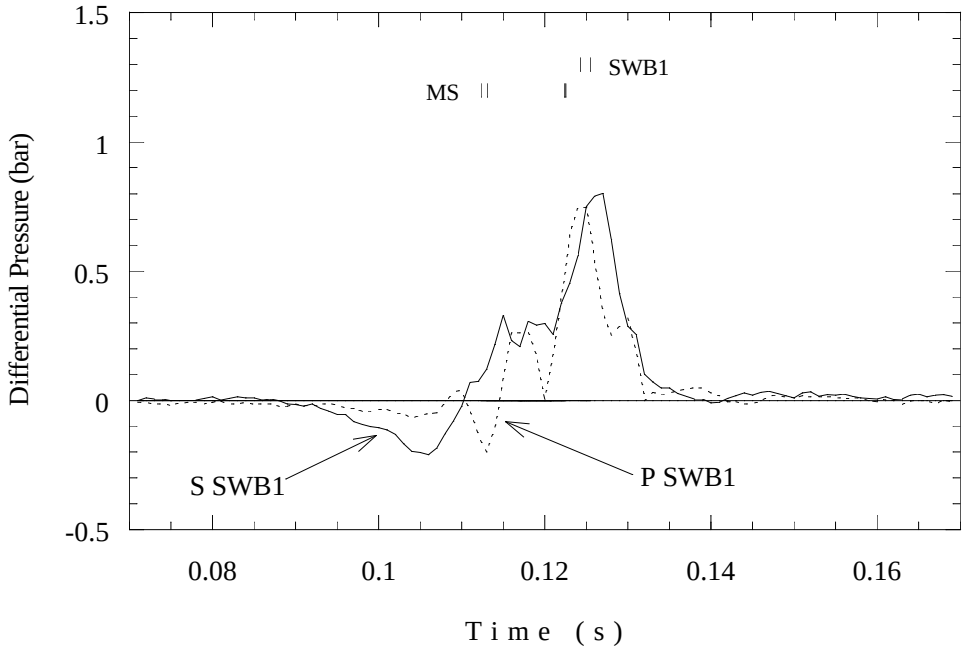

Figure 5.115: Differential pressure across SWB1, ignition in bay 2Lo, with a cold liquid Jet A layer. Test 20.

the same time, but remains in place until the ends of MS strike it. SWB3 fails at the same time as SWB2 but prior to the impact of SWB2. SWB1 folds forward and moves towards the exit of the tank shortly after SWB3 fails. This view also reveals a surprising amount of recoil movement by the tank.

All of the observational cameras produced good footage. The partitions are engulfed by the fireball as they exit, so it is difficult to determine grouping. It appears that SWB2, SWB3, and FS came out together, with the SE station camera showing SWB2 wrapping around SWB1 and FS after they have cleared the tank. SWB1 and MS stayed together and got caught at the open end of the tank, held in at the hinge point created by the PR connections. The west hilltop video camera captured a frame of panels exiting the fireball as a grey blur. (The gauge protector was removed for this test, so the partitions had an unobstructed path.)

The NE station video camera captured one frame just after the partitions exited the tank. Figure 5.120 shows the three partitions a few feet from the tank, the fireball about to overtake them. In the lead are spray clouds of jet fuel which are overtaken by fire in the next frame. Also visible is an airborne layer of dust along the ground, kicked up by the initial blast wave. This was also picked up by the NE and SE station cameras, but they are zoomed back a bit further and are not as sharp. The higher framing rate does show the flame engulfing the clouds of jet fuel.

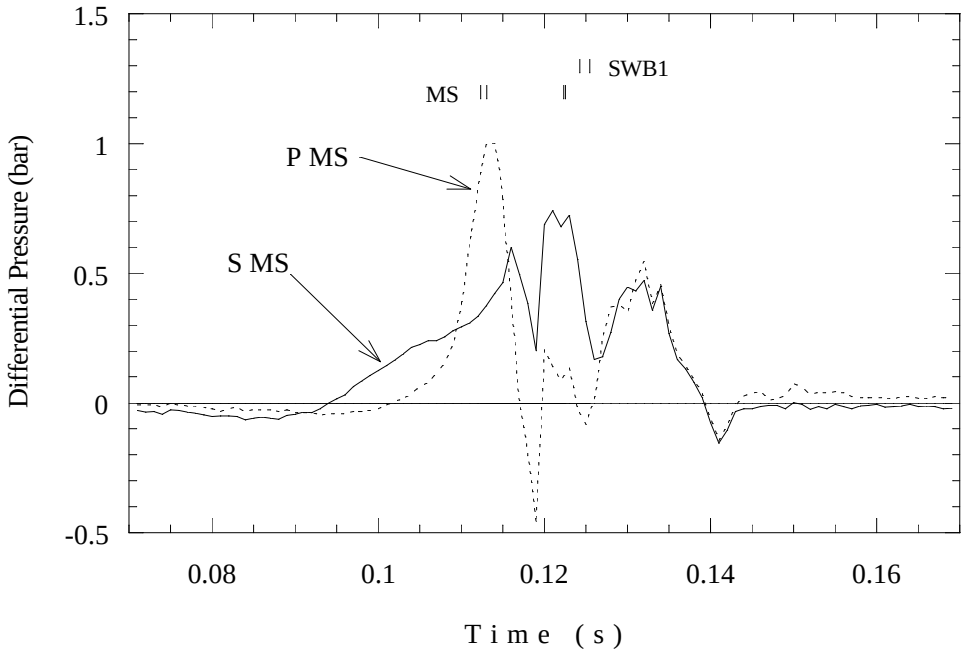

Figure 5.116: Differential pressure across MS, ignition in bay 2Lo, with a cold liquid Jet A layer. Test 20.

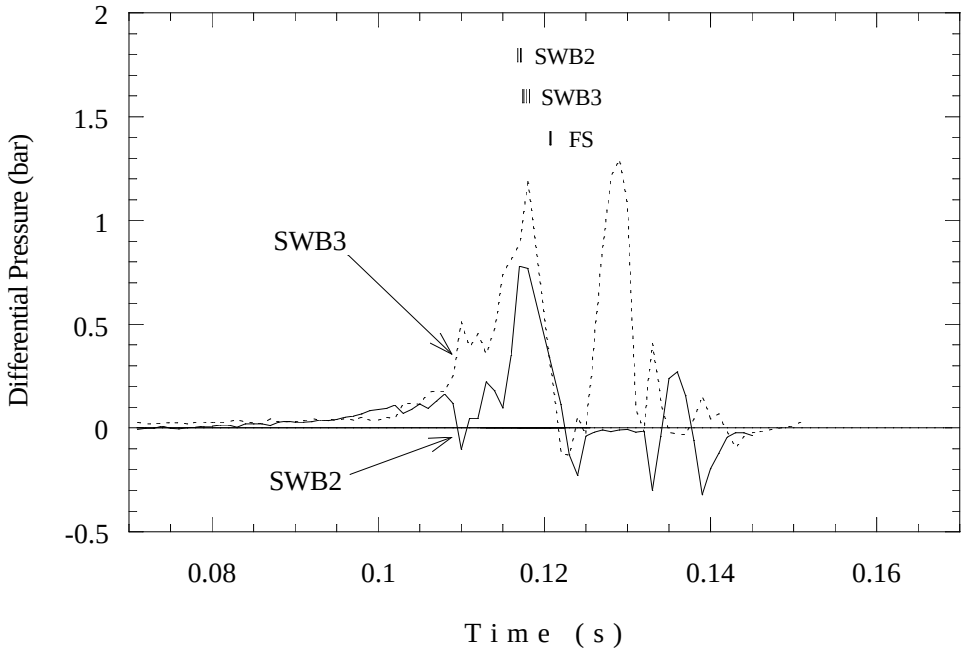

Figure 5.117: Differential pressure across SWB2 and SWB3, ignition in bay 2Lo, with a cold liquid Jet A layer. Test 20.

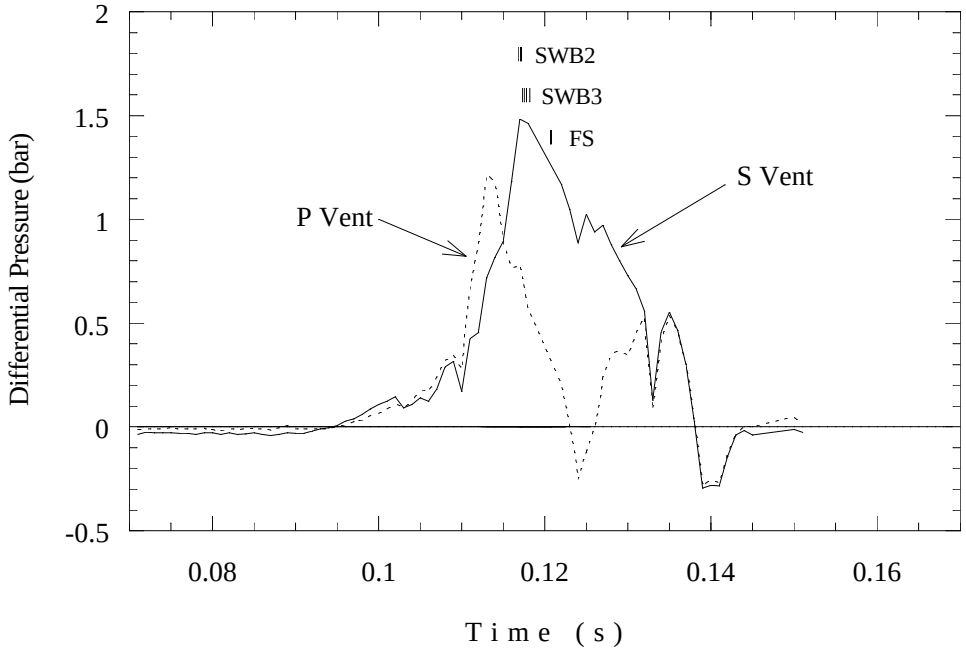

Figure 5.118: Differential pressure across vents, ignition in bay 2Lo, with a cold liquid Jet A layer. Test 20.

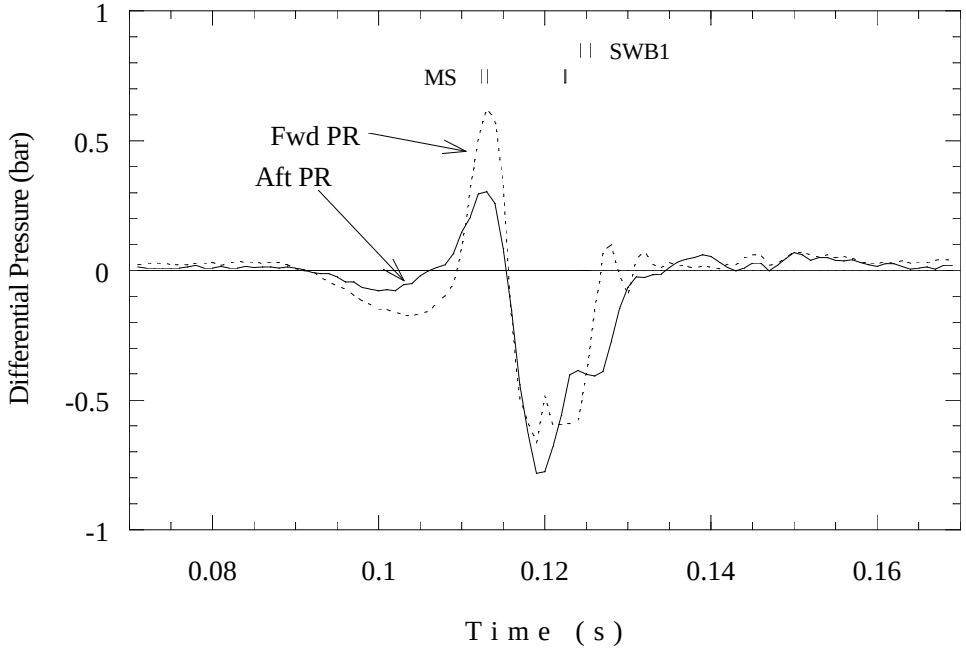

Figure 5.119: Differential pressure across PRs, ignition in bay 2Lo, with a cold liquid Jet A layer. Test 20.

Table 5.31: Flame arrival time (ms), Test 20.

Photodetectors

103	104
92	104
105 **IGN**	
111	
117	

Thermocouples

112	108	107	112
100	100	109	107
98 **IGN**		108	
		122	

Figure 5.120: Frame from SE video camera showing exit of panels surrounded by early fireball and led by jets of liquid fuel. Test 20.

Ignition in Bay 1, with a Cold Liquid Jet A Layer (Test 21) In this test, we see a different pattern of panel failure than in the previous tests, 19 and 20. SWB2 and SWB3 fail first, and the other panels fail nearly simultaneously after that. In fact, film footage indicates that the bottom of SWB2 actually failed *rearward* first, and then reversed direction as the aft bays burned. The motion detectors trip only on forward motion. After the test, we found that SWB1 remained in the tank, folded rearward, with both partial ribs attached to it (the aft PR had disconnected from RS). The shear bolts and tears in the mounting holes also showed that the ends of SWB1 had failed rearward. It was probably dragged forward a bit by MS before the forward PR detached. The longest travel in this test was by FS, which stopped 147 ft from the tank.

Figure 5.121 shows the pressure traces from bays 1, 3, and 6, covering the ignition location and the bays connected by the vent stringers. We see that bay 1 burns for some time before the aft bays ignite at 115 ms. Bay 1 begins to depressurize as SWB2 and SWB3 fail, but then the pressure continues to increase. This is probably caused by the aft partitions passing through the tank. Pressure piling in the aft bays is also shown in Fig. 5.121, as we see that bays 3 and 6 reach pressures of 3.2 and 4.5 bar, respectively. These bays can reach higher pressures because pressure in the forward bays supports the MS and SWB1 partitions. Bays 3 and 6 vent upon the failure of SWB1, MS, and FS.

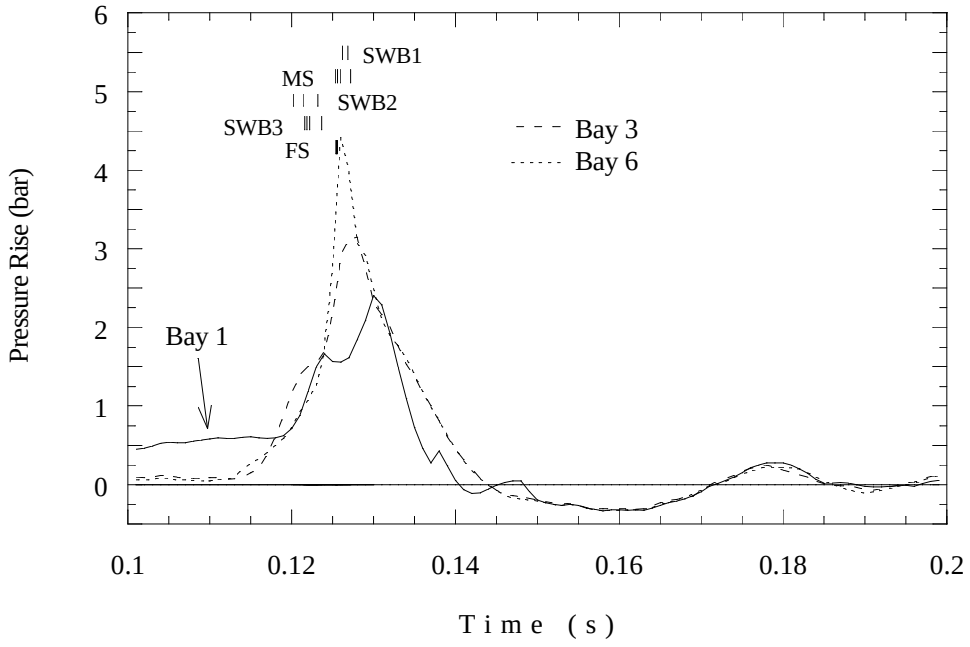

Figure 5.121: Pressure traces from bays 1, 3, 6, ignition in bay 1, with a cold liquid Jet A layer. Test 21.

In Fig. 5.122, we see that bays 4 and 5 also ignite at 115 ms. Pressure piling still occurs in the aft bays, but bay 5 only reaches a peak of 3.7 bar. It is unclear why bay 5 does not reach as high a peak pressure as does bay 6. It is interesting to note that all of these traces have similar peak profiles. Bays 4 and 5 follow the same venting profile as bays 3 and 6, maintaining pressure for a short period after partition failure because the aft partitions, torn loose, are still

stuck in the tank.

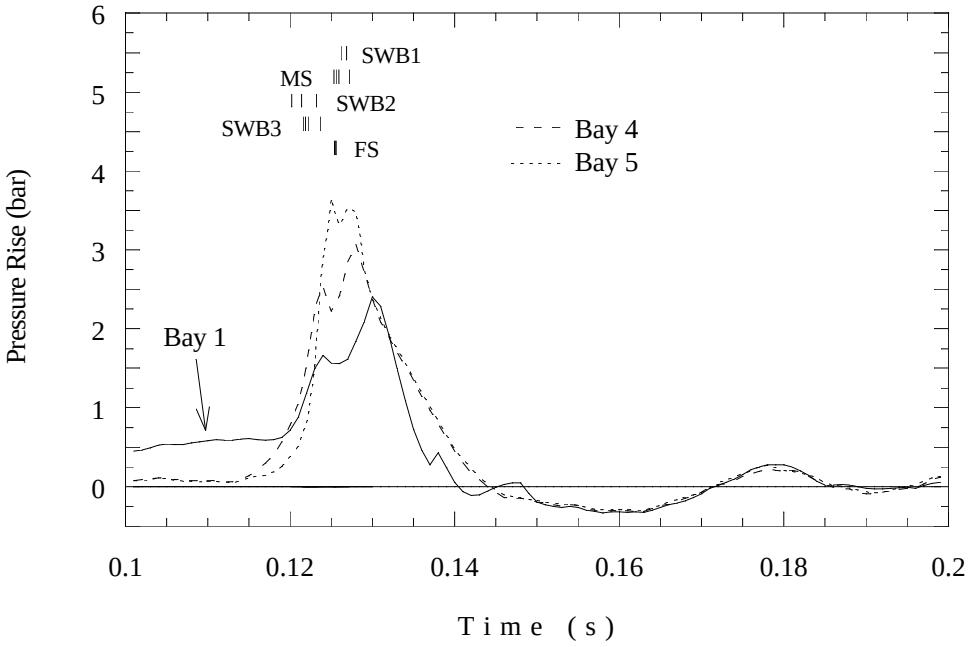

Figure 5.122: Pressure traces from bays 1, 4, 5, ignition in bay 1, with a cold liquid Jet A layer. Test 21.

The forward bay pressures are shown in Fig. 5.123. Bay 2 ignites about 2.5 ms before the aft bays ignite. Bay 2 burns rapidly on ignition, the pressure quickly surpassing that of bay 1. Bay 1 transitions to rapid combustion shortly after the onset of rapid combustion in bay 2. Bay 0 pressurizes upon the failure of SWB3, but pressure continues to increase for a short time after the failure of FS. There is a much longer negative pressure phase in this test than in the others with some oscillations in the tail of the signal. This is not registered by the bay 0 transducer because of its proximity to the open end of the tank.

Differential pressures across the aft partitions, SWB1 and MS, are shown in Figs. 5.124 and 5.125, respectively. Differential pressures across SWB1 indicate combustion proceeding from bay 3 to 4 followed by rapid combustion in bays 5 and 6. When SWB1 fails, the pressure differential drops to zero. The port side pressure difference decreases first, although the motion detector data shows nearly simultaneous failure of the top of the SWB1. It is possible that early failure occurred on the bottom, where no detectors were installed. The differentials on MS follow the same pattern. The late peak at 140 ms is probably due to SWB1 passing by on its way out of the tank.

The differential pressures on SWB2 and SWB3 are shown in Fig. 5.126. SWB2 initially experiences a rearward force from the combustion in bay 1, with a maximum amplitude of 0.4 bar. The films indicated that the bottom of SWB2 failed rearward first, which implies a very low failure pressure compared to the design value. As combustion is accelerated in bay 2, with possible contributions from liquid fuel lofting, the direction of force on SWB2 reverses and it fails in the forward direction in the same time frame as does SWB3. SWB3, being the initial

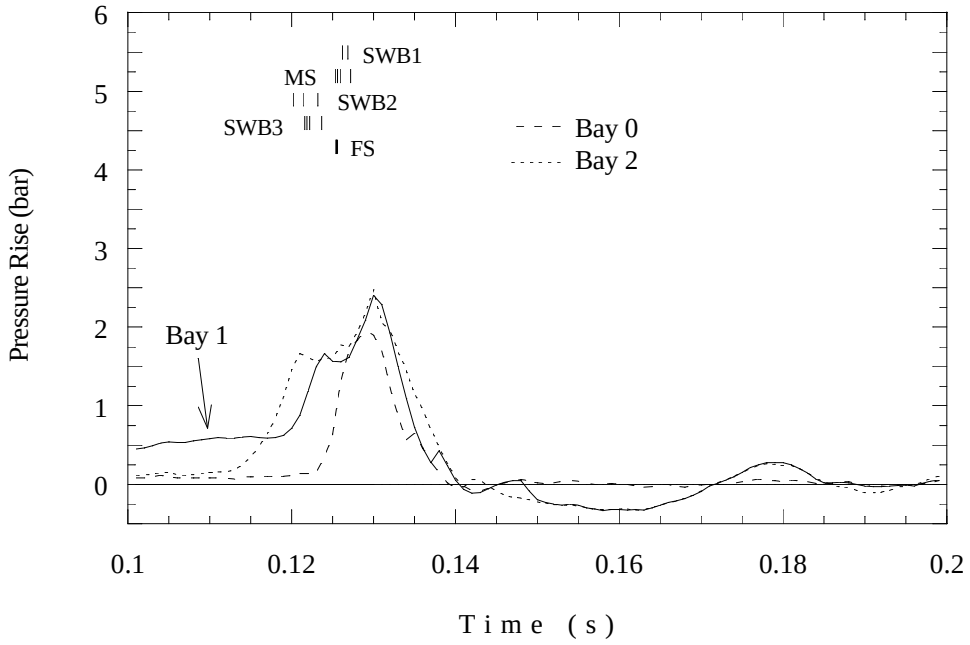

Figure 5.123: Pressure traces from bays 0 – 2, ignition in bay 1, with a cold liquid Jet A layer. Test 21.

tank boundary and adjacent to the ignition location, always experiences a positive pressure difference until failure of SWB3. In this test, the pressure difference was over 1.3 bar before complete failure of SWB3 occurred. The two subsequent peaks probably indicate passage of aft partitions through the SWB3 location.

Interpretation of the pressure differentials across the vents (Fig. 5.127) is straightforward. Combustion in bay 1 drives flow aft, with ignition and rapid combustion in the aft bays reversing the flow later on. The higher peak on the starboard vent reflects the higher peak pressure in bay 6. It is interesting that both vents show a secondary pulse after dropping to zero; no panel can pass the starboard vent, as it is in the aftmost bay. Possibly, combustion continues while the panels are vented, and after SWB1 and MS get caught within the tank, the blockage created by these panels creates a pressure differential across the vents.

The PR differentials, Fig. 5.128, show evidence of anti-symmetric combustion in the aft bays. The diagonal location of the vent stringers may contribute to this by providing anti-symmetric ignition locations.

All of the bay cameras funtioned in this test. The initial flame in bay 1 is very smooth and spherical. Shortly after the flame has filled bay 1, a jet enters from the vent stringers, immediately followed by fuel lofting on the tank floor, and forward motion of SWB2. As SWB2 is swept out of the tank, the view in bay 1 is obscured by soot. Fuel lofting initially occurs toward the rear of bay 2, since the flow is coming from bay 1. After lofting in bay 2 begins, SWB2 begins bowing towards aft, and subsequently fails and moves rearward. No gaseous flame is visible yet in bay 2 at the time SWB2 initially fails. Gaseous combustion appears to begin after the bottom of SWB2 reaches the MS station. As soon as SWB2 reaches

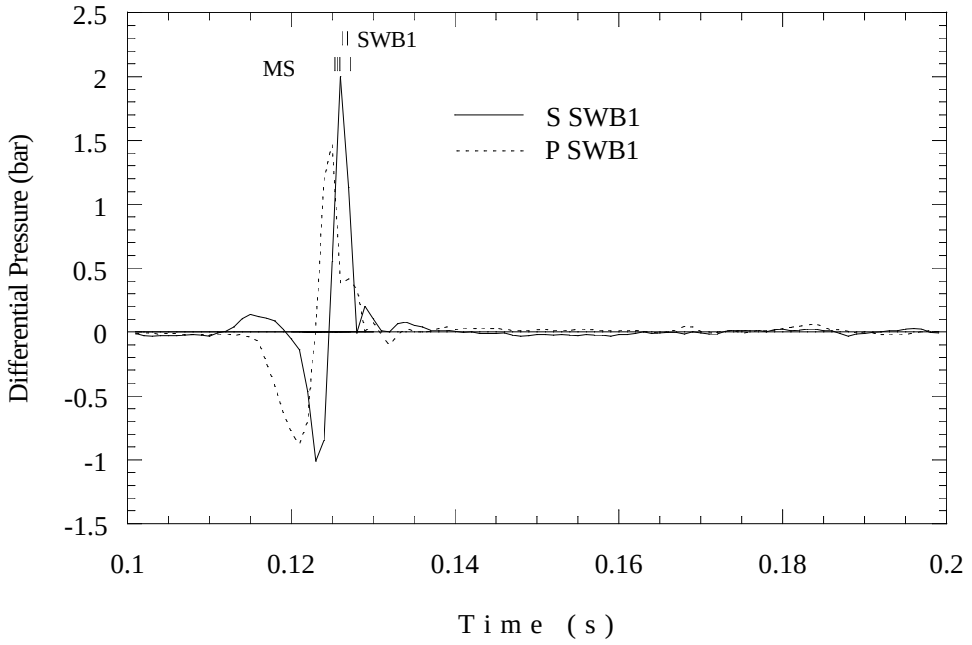

Figure 5.124: Differential pressure across SWB1, ignition in bay 1, with a cold liquid Jet A layer. Test 21.

the MS station, the motion is reversed and SWB2 is blown forward, out of the tank.

The timing strobe for bays 3 and 4 is not visible in the video conversion. However, it is clear that liquid fuel lofting occurs before arrival of the gaseous flame. When the flame arrives in bays 3/4, it enters through the bottom of MS. Within one frame (about 2.5 ms), the flame becomes a vertical plume reaching almost to the top of bays 3/4. The plume seems to be too broad to come from the liquid fuel manifold, and it doesn't appear to come from the vent stringer at the top of bay 3. The flame engulfs the bays, and the bottom of MS appears to fail rearward an inch or two before being blown forward. In bays 5 and 6, lofting occurs before the flame arrives in bay 6 via the vent stringer. The point at which the flame enters bay 5 is not visible, as SWB1 begins to fail rearward a few frames after the flame enters bay 6.

The exterior footage from the side view camera is somewhat obscured by the flame, but shows this order of events: The bottom of SWB2 fails rearward, and appears to collide with the bottom of MS, failing in the rearward direction as well. Both MS and SWB2 begin to move forward at the same time that SWB3 fails. While this is happening, the edges of SWB1 are blown backwards, but the forward PR connecting SWB1 to MS is pulling the center of SWB1 forward, forming the configuration that was found after the test. From the observation cameras, it appears that SWB2, SWB3, and FS exit as a unit, wrapped around the water bottles.

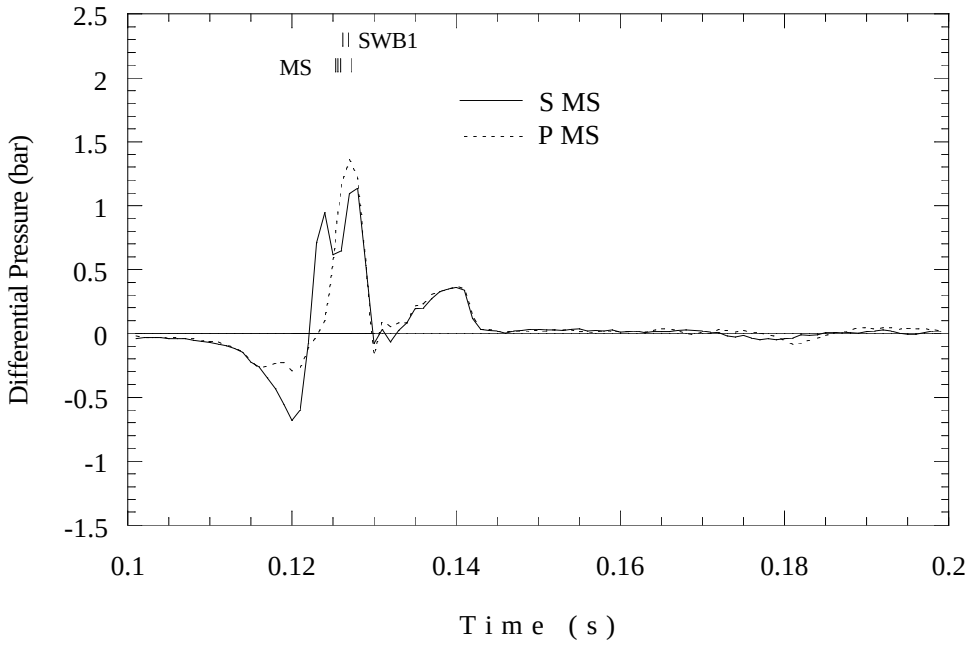

Figure 5.125: Differential pressure across MS, ignition in bay 1, with a cold liquid Jet A layer. Test 21.

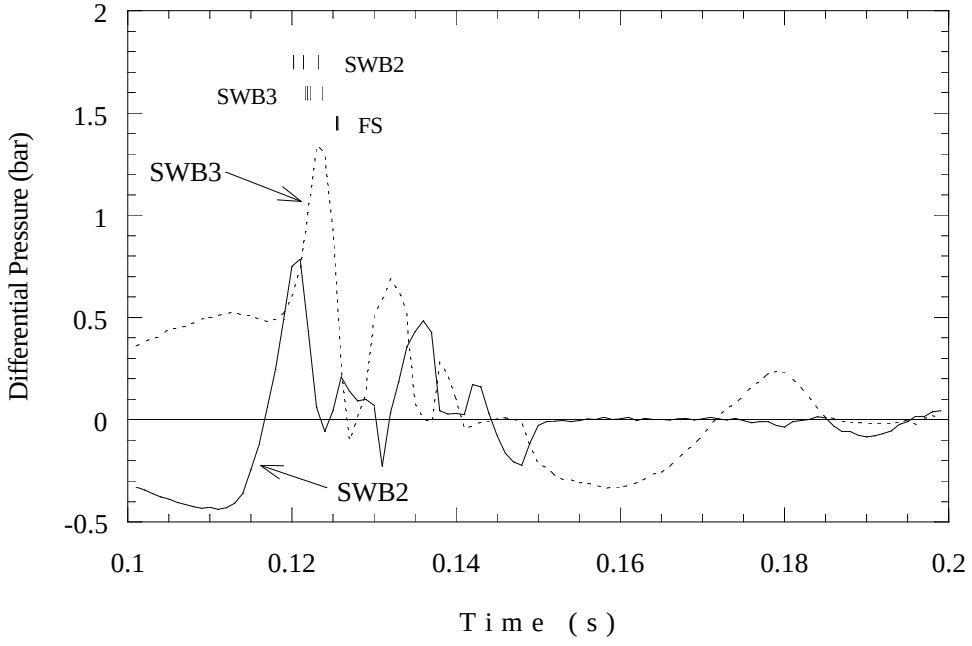

Figure 5.126: Differential pressure across SWB2 and SWB3, ignition in bay 1, with a cold liquid Jet A layer. Test 21.

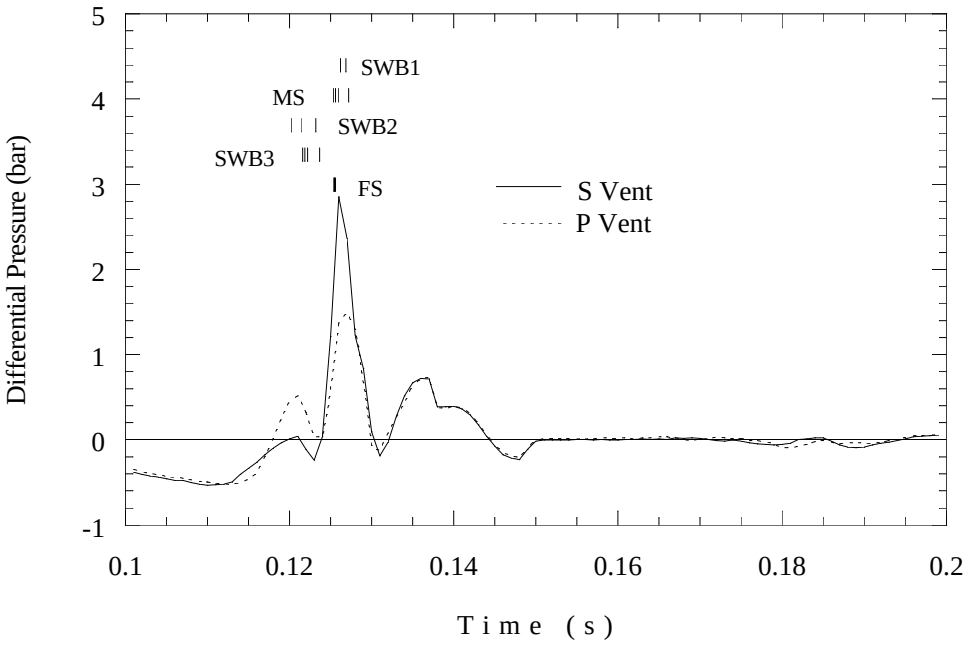

Figure 5.127: Differential pressure across vents, ignition in bay 1, with a cold liquid Jet A layer. Test 21.

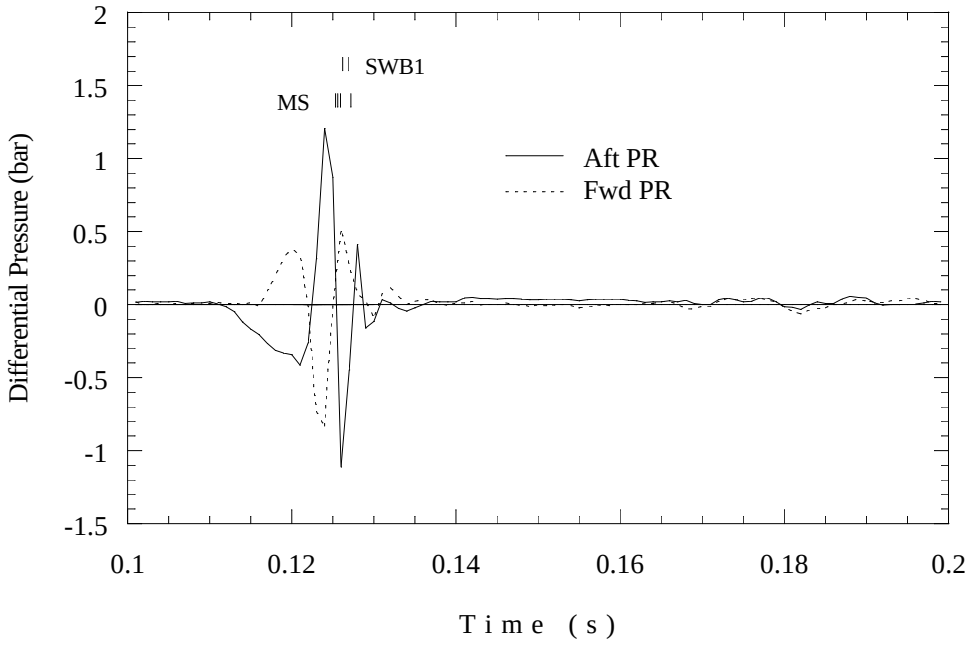

Figure 5.128: Differential pressure across PRs, ignition in bay 1, with a cold liquid Jet A layer. Test 21.

Table 5.32: Flame arrival time (ms), Test 21.

Photodetectors		Thermocouples			
114	120	114	122	124	126
115	115	121	121	120	118
115		121		120	
116 **IGN**		64 **IGN**		85	
125					

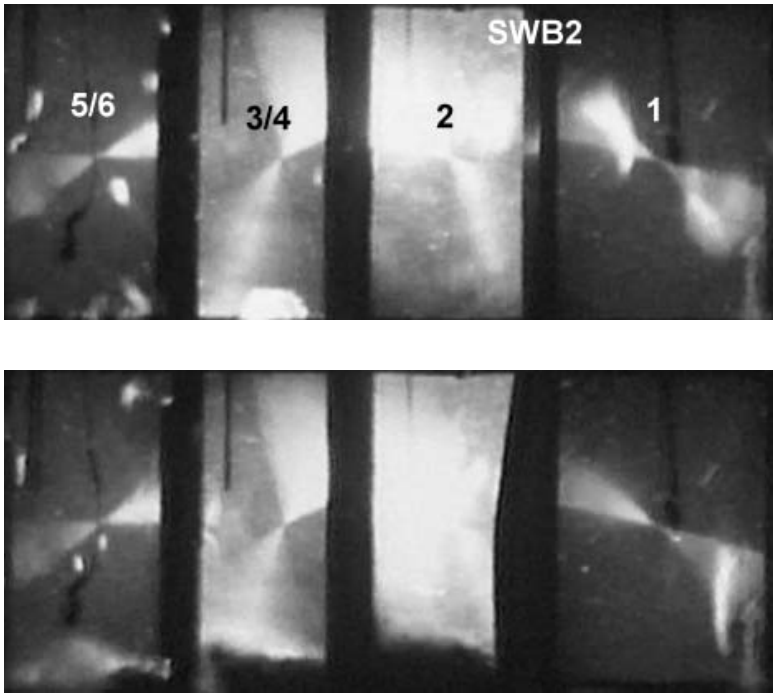

Figure 5.129: Lofting toward rear of fuel with ignition in bay 1 (Test 21). First frame is before ignition for reference. Note that SWB2 is failing rearward in second frame, accompanied by fuel lofting to the rear, indicated by the dark fan-like regions at the bottom surface.

5.4.4 Part Strong: Fuel Concentration Variation

These tests were carried out with the part-strong configuration and ignition in the 2Lo location. The times for the failure of SWB3 and FS are given in Table 5.33. The MP break times were not recorded in these tests.

Table 5.33: Motion detector breakaway times. Numbers in italics are from tape drives. MP only has one breakwire. N/R, not recorded.

	Top Left	Top Right	Bottom Left	Bottom Right
Test 22				
MP	N/R			
SWB3	192.41	192.42	200.2	*194.78*
FS	198.63	198.21	198.4	*189.58*
Test 23				
MP	N/R			
SWB3	264.9	264.5	274.2	*265.55*
FS	269.2	269.2	269.2	*260.97*
Test 24				
MP	N/R			
SWB3	433.6	433.3	434.0	*433.10*
FS	437.3	437.1	437.2	*436.89*

8.4% Gaseous Fuel (Test 22) This test was run with the standard concentration of gaseous fuel. During mixture filling, the liquid fill valve was opened for a short time to bleed in air. Some residual fuel bubbled out, leaving a film of fuel near the inlets about one square foot in area. These patches of liquid fuel did not appear to play any significant role during the explosion. The FS, with water bottles attached, stopped 48 ft from the tank; SWB3 only went 10 ft.

Pressure traces are shown in Figs. 5.130 – 5.135. The pressure traces in the aft bays (Fig. 5.130) exhibit lateral symmetry. Pressure piling occurs as the flame progresses from the front to the back. Bay 4 is the first aft bay to ignite, while bay 5 is the last aft bay to ignite. Bays 3 and 6 appear to ignite at the same time, but bay 6 burns faster. Figure 5.131 shows pressure traces from all of the forward bays, and also bays 3 and 5 (representing the aft bays). It appears that bays 2 and 1 ignite and accelerate at the same time. As bay 1 reaches about 1 bar, SWB3 begins to fail. Pressure in bay 1 dips and recovers as bay 0 (trace under bay 1) begins to pressurize, but FS then fails, and both bays vent. Rupture of the MP was not recorded, but probably occurred near 205 ms, when the pressure in bay 2 begins to drop.

Differential pressures across SWB1 and MS are shown in Fig. 5.132. The transition to rapid combustion can be observed in the starboard differentials at around 180 ms. At 205 ms, the pressure differential on MS rises when the rupture of the MP allows bay 2 to rapidly vent.

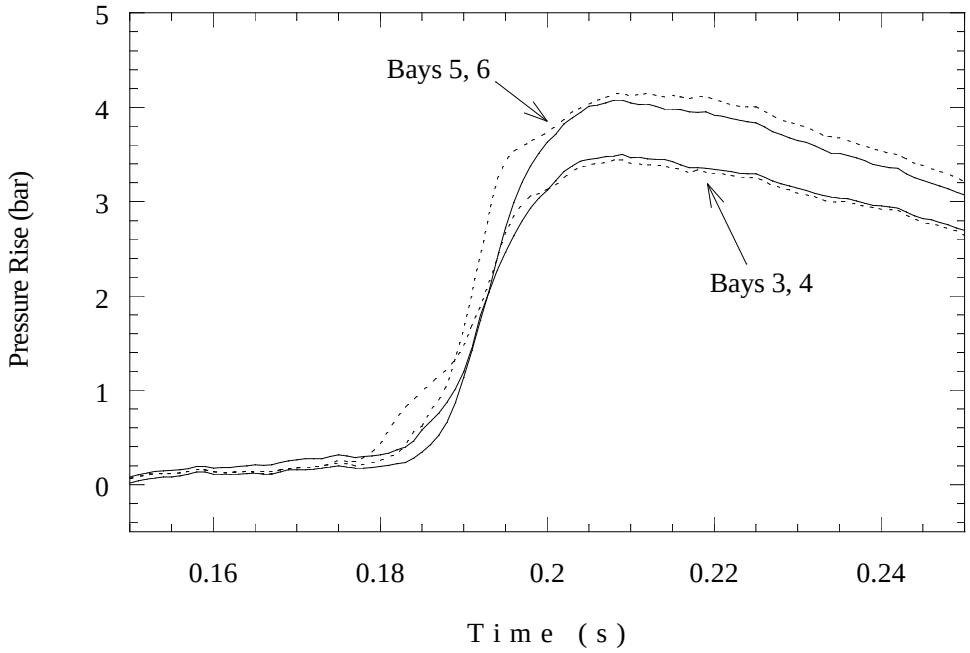

Figure 5.130: Pressure traces for bays 3 – 6, 8.4% fuel, ignition in 2Lo. Dashed lines indicate even-numbered bays. Early liftoff is in bay 4, late liftoff is in bay 5. Test 22.

Differentials across the forward partitions are shown in Fig. 5.133. SWB3 is the first partition to experience a forward force, with FS following after SWB3 fails. As bay 1 vents into bay 0, this also causes a pressure difference across SWB2. Once FS fails, the pressure across SWB2 jumps, and MP fails at just under 2 bar. Rapid venting of bay 2 through the MP opening occurs after 210 ms.

The vent stringer pressure differences are shown in Fig. 5.134. Bays 3 and 6 ignite at nearly the same time, but bay 6 has a greater rate of pressure rise, and this is reflected in the vent differentials (port vent connects to bay 3, starboard to bay 6). When SWB3 and FS fail, there is a dip in the pressure differential. Once both partitions fail and the forward bays vent, the vent pressure differentials reach maximum values.

The PR pressure differentials are modest as shown in Fig. 5.135. The rapid combustion in bay 6 results in the negative peak across the aft PR. Likewise, bay 4 has rapid burn, resulting in a negative pressure differential on the forward PR.

The bay cameras all functioned properly during this test. Ignition in bay 2 starts a smooth flame that propagates upward into the bay. When the flame has expanded to about three-fourths of the bay cross-section, a jet enters from a passageway above the floor in MS. This flame comes from either bay 3 or 4. This jet impinges on SWB2, and the flame fills the bay at a much faster rate than the initial one. After the burn has completed, a puff of smoke enters from the liquid fuel manifold, and a smear from the side seal on MS indicates that the MP has ruptured and the bay rapidly depressurized. In bays 3 and 4, a flame jet enters via one of the passages above the floor of the tank in MS. The jet impinges on SWB1 and the flame fills the bay. It is not possible to tell which bay is ignited first, or when the flame moves to the other bay,

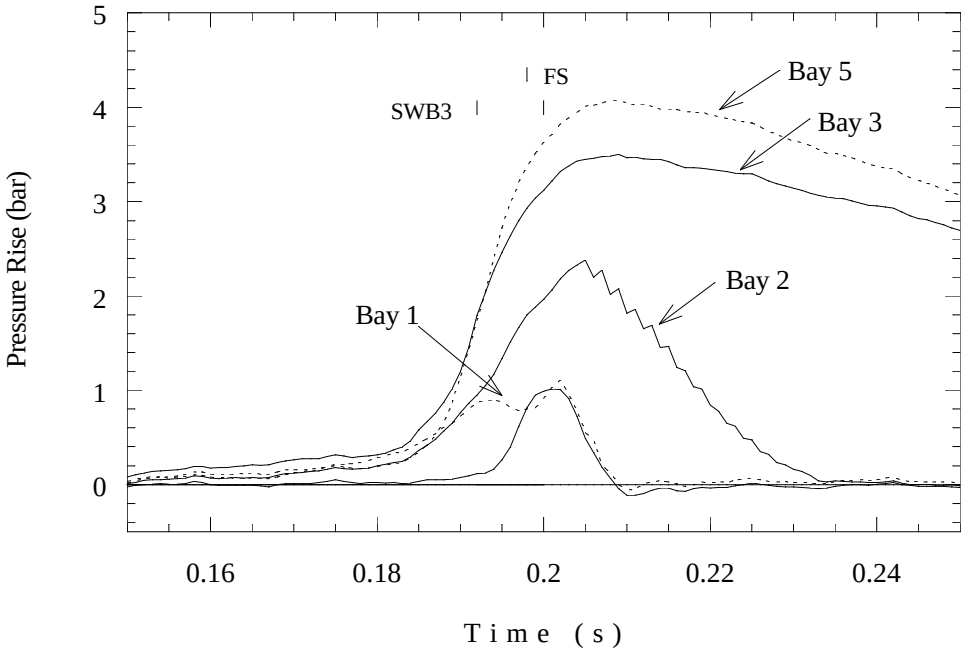

Figure 5.131: Pressure traces for bays 1 – 3, 5, 8.4% fuel. Test 22.

although this probably occurs with the rapid combustion near the end of the burn. In bay 1, the first flame comes from the liquid fuel manifold. When this has progressed halfway up the bay, a jet enters through a lower passageway in SWB2. This jet reaches SWB3 and expands into the bay. Shortly after bay 1 has been completely engulfed, the MP ruptures. Also, a small plume of smoke exits from the jet fuel manifold after MP rupture. In bays 5 and 6, the flame enters along the bottom of the tank and fills the bay after reaching RS. The other bay then ignites from the bottom and burns very rapidly. The flame may enter through the aft PR or through the MS. It is not possible to differentiate between bays 5 and 6 in this test. It also appears that a little bit of jet fuel residue (from the liquid layer of the previous test) from under the strong partition mounting brackets gets blown into the bays and ignited.

The side-view exterior camera shows the top of SWB3 failing first and rotating forward. When it reaches the FS, that fails as well. The flame progress seems to be bay 2, bays 3/4, bay 1, bays 5/6. The other exterior cameras show the FS wrapping around the water bottles as it exits, but SWB3 stays horizontal and doesn't fold around the FS.

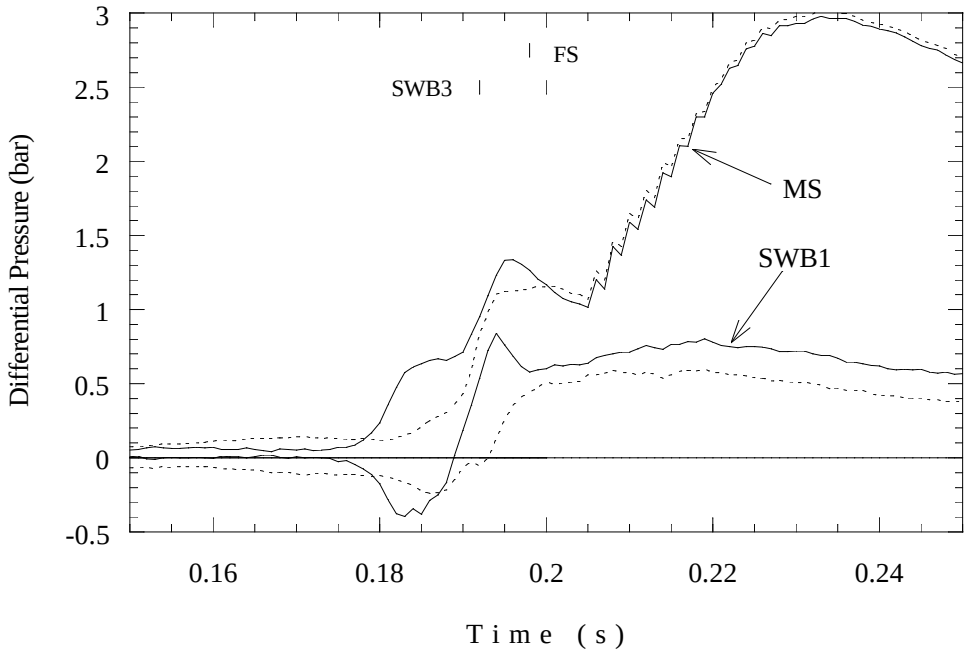

Figure 5.132: Differential pressure across SWB1 and MS, 8.4% fuel. Dashed lines for port side, solid lines for starboard. Test 22.

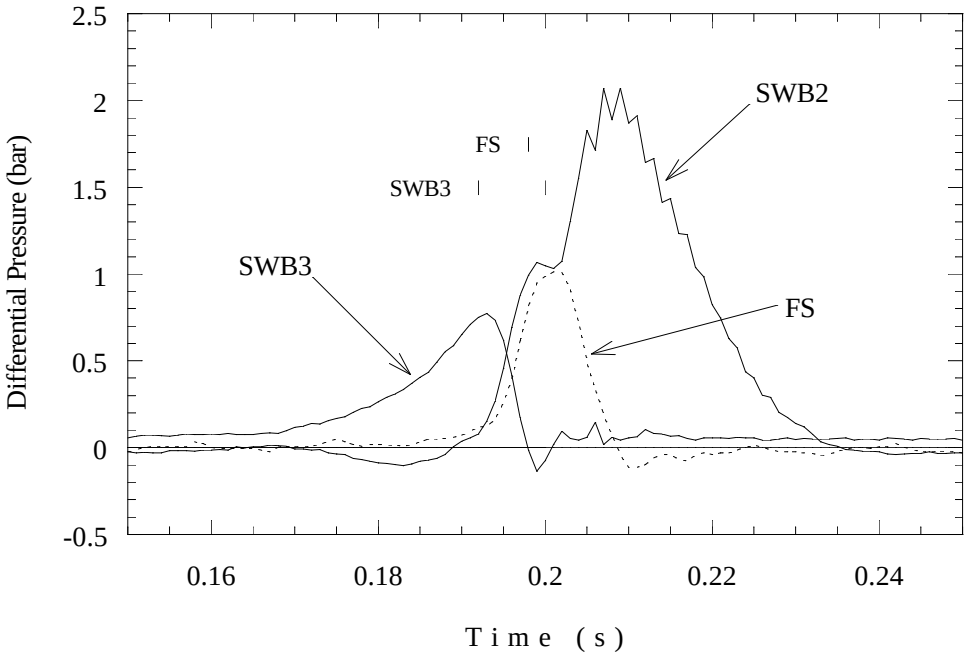

Figure 5.133: Differential pressures across SWB2, SWB3, and FS, 8.4% fuel. Test 22.

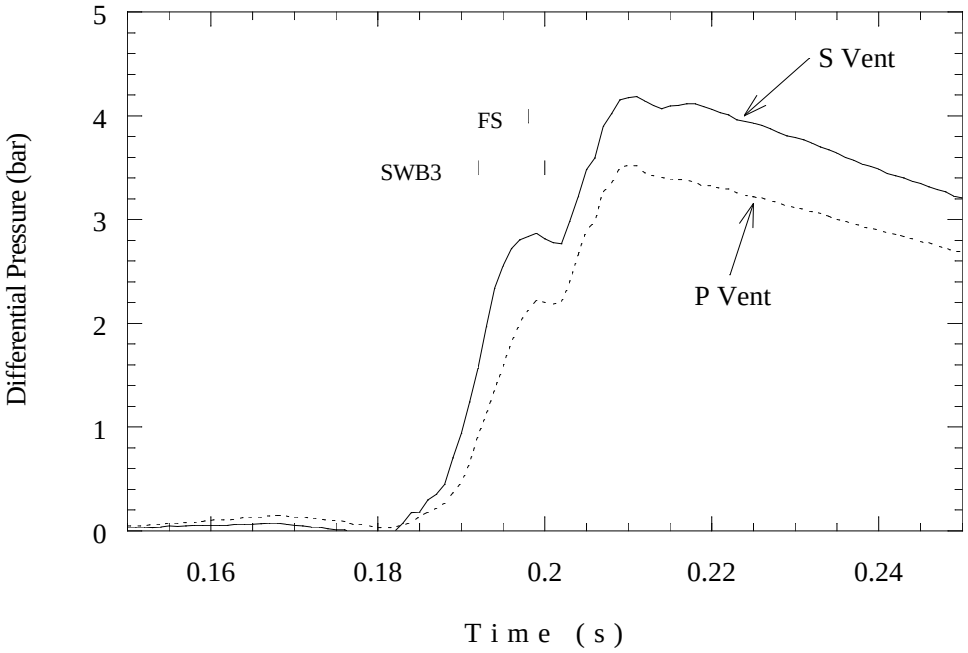

Figure 5.134: Differential pressure across vents, 8.4% fuel. Test 22.

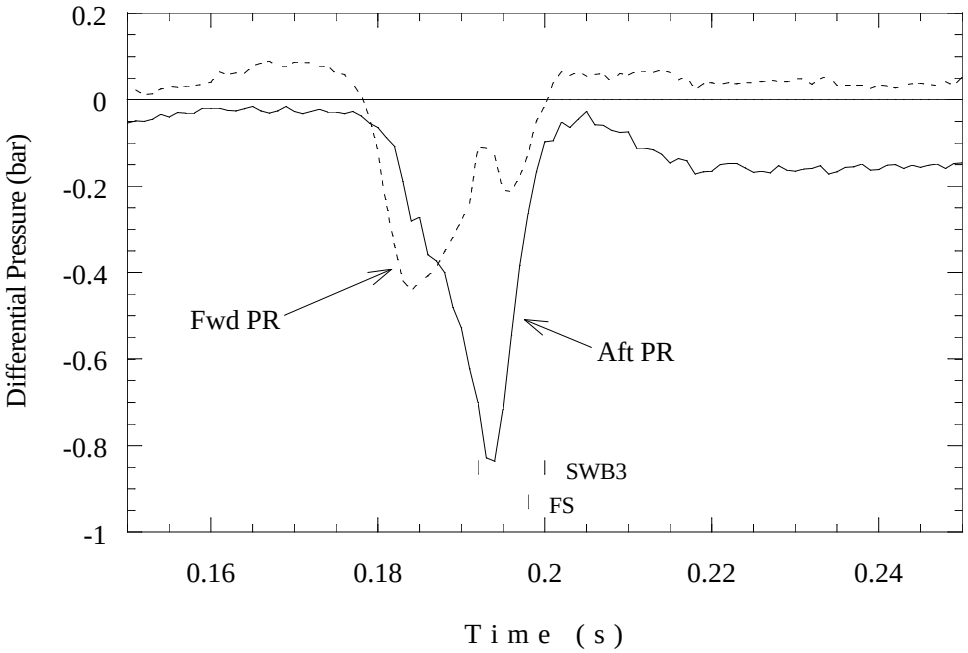

Figure 5.135: Differential pressure across PRs, 8.4% fuel. Test 22.

Table 5.34: Flame arrival times (ms), Test 22.

Photodetectors

186	185
178	183
187 **IGN**	
198	
198	

Thermocouples

188	187	182	188
189	184	162	174
179 **IGN**		179	
184		189	

7.5% Gaseous Fuel (Test 23) The fuel concentration was reduced to 7.5%. Based on laboratory tests and AICC computations, we expect the burn time to be increased and the peak pressure to be decreased by about 10% as compared to the standard concentration test. The event did take longer (0.27 s) as compared to the standard concentration test (0.2 s for Test 22). The peak pressure was about 4.1 bar (bay 6) in this test as compared to 4.4 bar (bay 5) in Test 22. Another major difference is the shorter distance the partitions traveled outside the tank. FS landed 36 ft away, and SWB3 just fell out of the tank.

Pressure traces for this test are shown in Figs. 5.136 – 5.141. Pressure traces from the aft bays are similar to those of Test 22 (see Fig. 5.130). In Fig. 5.136, we see that bay 3 shows the earliest ignition, though bay 4 undergoes turbulent combustion at 245 ms and overtakes bay 3 briefly before the traces coalesce. Bay 6 burns at a slightly faster rate than bay 5.

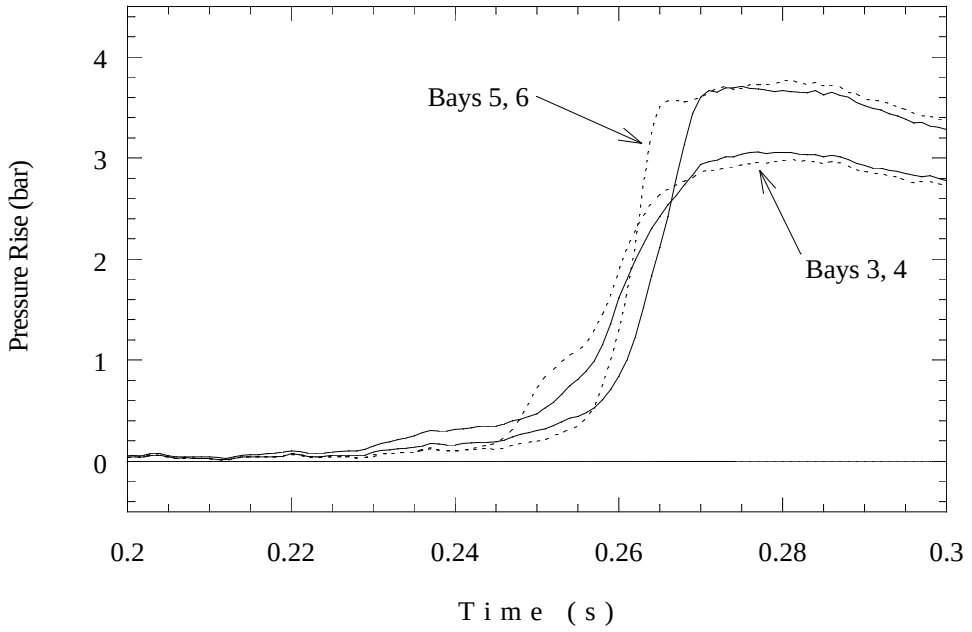

Figure 5.136: Pressure traces for bays 3 – 6, 7.5% fuel. Dashed lines indicate even-numbered bays. Test 23.

In the forward bays (Fig. 5.136), a pattern similar to that of Test 22 is seen, but bay 1 takes longer to ignite. When the bay 1 pressure reaches about 1 bar, SWB3 begins to fail. The FS fails at about 270 ms, prior to SWB3 completely failing.

The differential pressures across SWB1 and MS are plotted separately for clarity. The pressures across SWB1, Fig. 5.138, initially go negative, indicating ignition in bays 3 and 4 before bays 5 and 6. However, once bays 5 and 6 ignite, they burn at a faster rate than bays 3 and 4. This increased burning rate and pressure piling result in a reversal in the pressure differential at about 266 ms. Pressures across MS are of the same order in magnitude as those across SWB1, until rupture of the MP vents bay 2 and causes MS to be the main barrier to atmospheric pressure. The pressure differential on the MS is positive throughout the event; it appears that bays 3 and 4 ignited at the same time as bay 2 and burned as fast or faster than bay

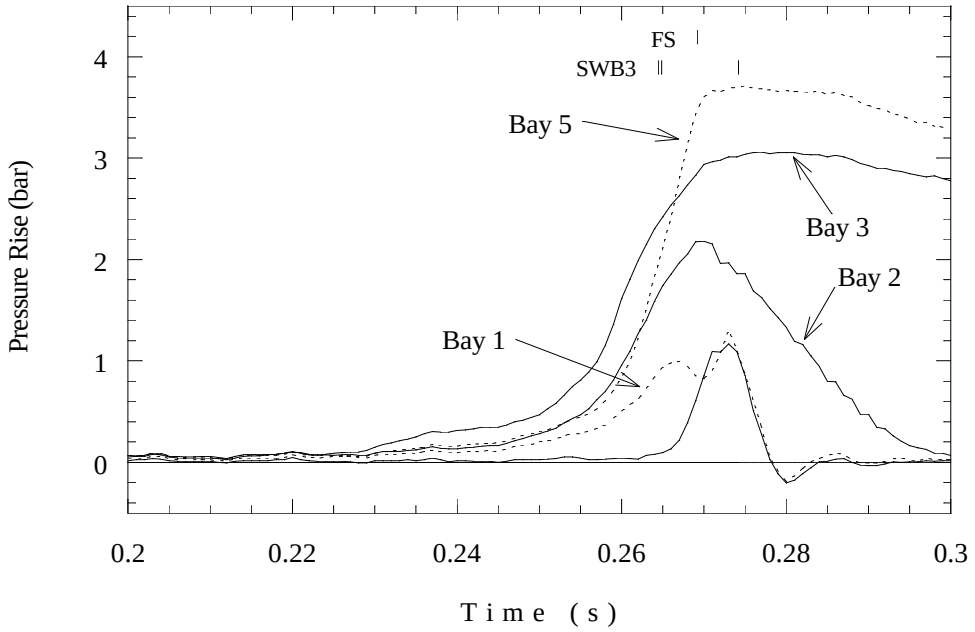

Figure 5.137: Pressure traces for bays 0 – 3, 5, 7.5% fuel. Bay 0 trace lies under that of bay 1. Test 23.

2.

The differential pressure across SWB2 in Fig. 5.140 shows an unusual double peak. This is caused by a late peak in the bay 1 pressure, immediately before the failure of FS. Once FS fails, the differential across SWB2 reaches its maximum value.

Differentials across the vents and PRs are shown in Fig. 5.141. The port vent shows a slow rise coincident with the forward PR, as slow combustion occurs in bay 3. When bay 6 ignites at 255 ms, it is already turbulent and burns rapidly to generate a positive pressure difference across the starboard vent (overtaking the port vent) and a negative pressure difference on the aft PR. A brief dip occurs in the vent differentials when the pressure peaks in the forward bays immediately before FS failure. After the forward partitions have failed, the vents reach their maximum differentials and vent the aft bays to atmosphere.

The bay cameras in this test all functioned normally. The schlieren footage from bay 2 shows that the flame in this mixture has a more rapid motion upward than downward or to the side, indicating that increased role of buoyancy for leaner mixtures. As the flame approaches the top of the tank, a flame jet enters from one of the passageways in MS above the floor. The jet impinges on SWB2, accelerating combustion in the bay, which burns to completion. The flame enters bay 3 or 4 through a lower passage in MS as a jet that impinges on SWB1. When the flame has traveled about three-quarters of the distance across bay 3/4, a second wave of much faster, more turbulent combustion can be seen. This is probably associated with motion perpendicular to the field of view, between bays 3 and 4.

In bay 1, the flame first enters as a jet through the jet fuel manifold. This flame is still fairly small when a jet from the main flame enters via a lower passageway in SWB2. This jet reaches SWB3 and then engulfs the bay, at which point SWB3 fails and the MP ruptures. A

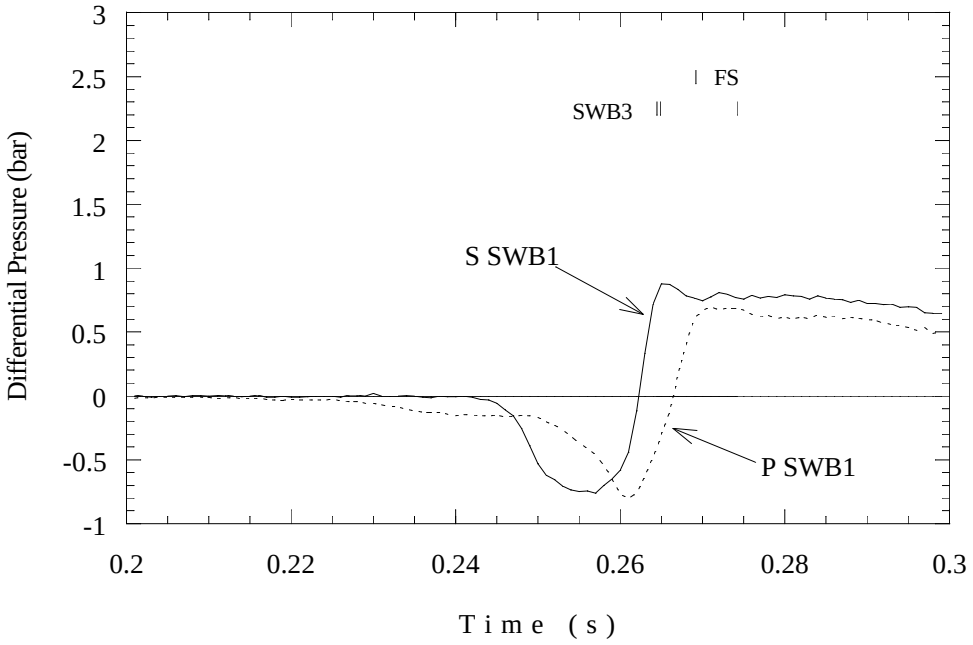

Figure 5.138: Differential pressure across SWB1, 7.5% fuel. Test 23.

puff of mist is visible coming from the jet fuel manifold after the panel failures. In bays 5 and 6, the flame seems to enter as a jet along the floor of the tank. It appears that both bays are ignited separately in rapid sequence, and one burns faster than the other, but this is difficult to determine. There could be two modes of combustion in one of the bays, with combustion in the other bay hidden by rapid combustion in the first.

The side-view camera shows that the flame proceeds to the rear of the tank first, going from bay 2 to 3/4 and 5/6 before igniting bay 1. Bay 1 ignition is almost simultaneous with bay 5/6 ignition. SWB3 fails first at the top, rotating into the FS and exiting horizontally without wrapping around the water bottles. The FS wraps around the water bottles before exiting. SWB3 lands right at the tank exit. As FS wraps around the water bottles, the NE station DBM showed that the ends of FS bent far enough to touch ech other and then sprang back a bit.

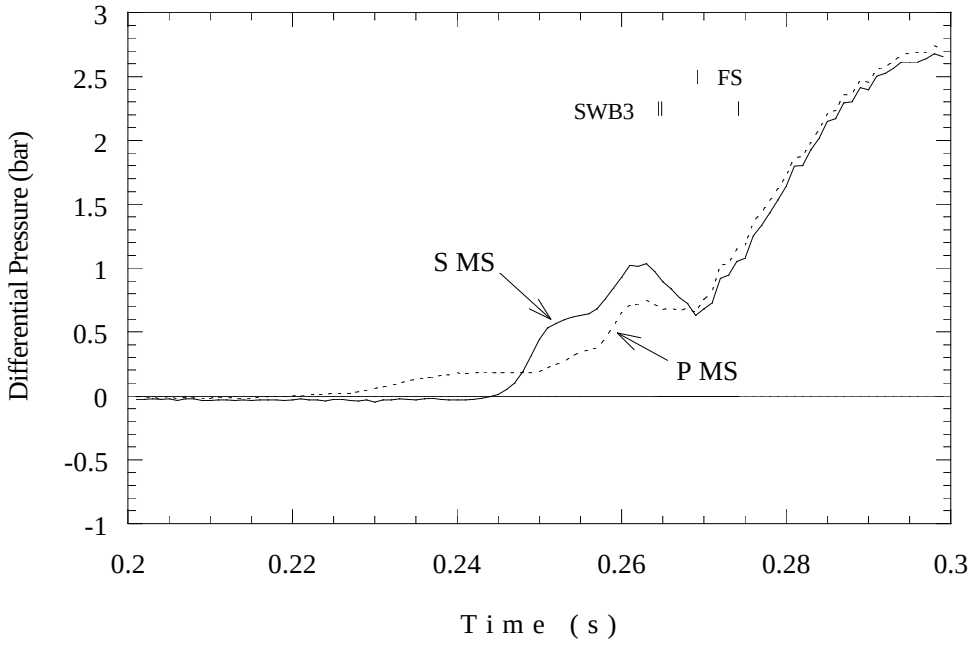

Figure 5.139: Differential pressure across MS, 7.5% fuel. Test 23.

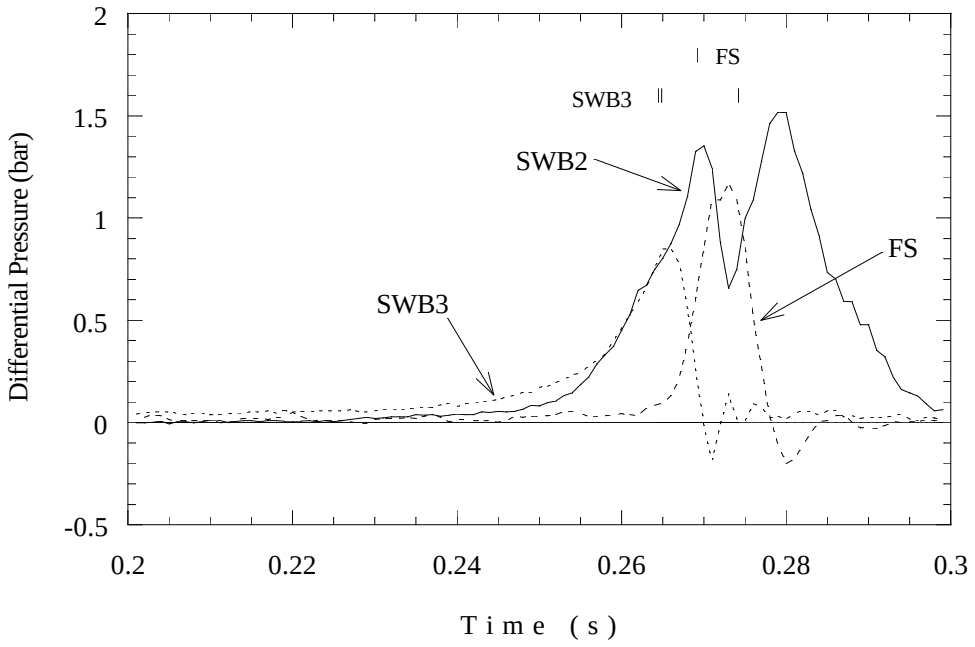

Figure 5.140: Differential pressure across SWB1, SWB2, and FS, 7.5% fuel. Test 23.

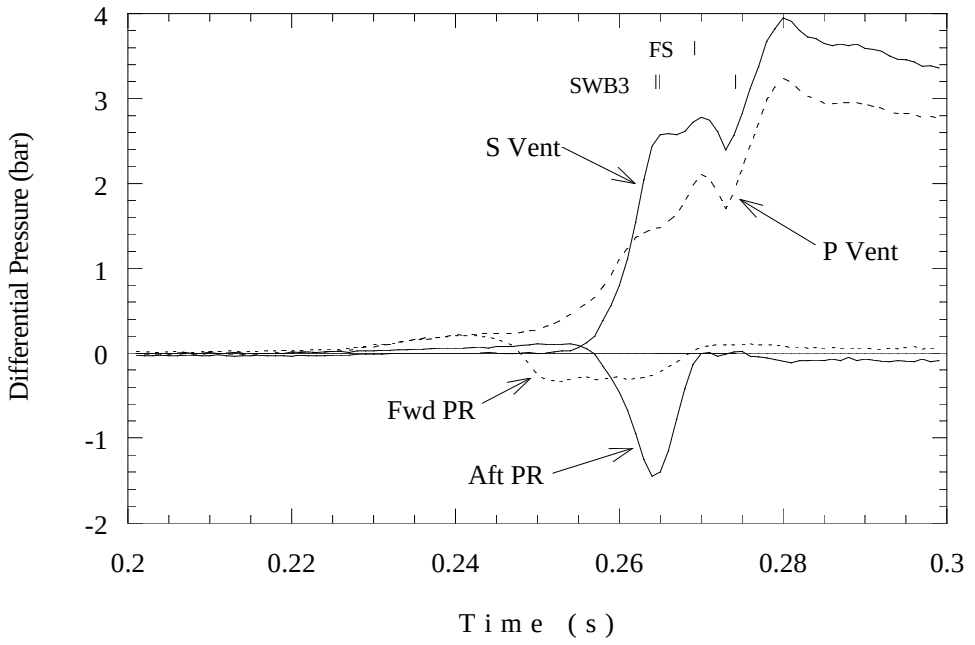

Figure 5.141: Differential pressure across vents and PRs, 7.5% fuel. Test 23.

Table 5.35: Flame arrival times (ms), Test 23.

Photodetectors

259	260
253	256
260 **IGN**	
262	
269	

Thermocouples

262	264	249	260
257	253	240	237
240 **IGN**		230	
264		264	

6.5% Gaseous Fuel (Test 24) This test used the leanest mixture of any test in the present series. In laboratory tests, 6% burned very slowly unless there was pre-existing turbulence in the vessel. A value of 6.5% was chosen for the present tests in order to make sure that some combustion would occur. From the laboratory tests and AICC computations, we expected the burn to be significantly longer and the peak pressure to be at least 20% lower than the standard composition. In spite of the trend observed in the previous tests and these expectations, there was a rapid combustion event late in Test 24 that produced a peak pressure of 4.7 bar and peak differential pressures of up to 3.8 bar. An usually loud shockwave was produced outside the vessel, and the explosion projected FS and the water bottles 86 ft downrange. It appears that the slow flame speed allowed substantially more time for turbulence generation and precompression in the other bays before ignition, resulting in higher pressures than in the standard concentration case.

The pressure traces (Figs. 5.142 – 5.148) for this test are very different than for any other test in this series. Note that the time scale in these plots covers 200 ms instead of the typical 100 ms. Figure 5.142, the pressure traces from the aft bays, shows that the burn was laterally symmetric. Bay 3 shows the earliest ignition, followed by ignition in bay 4 at 400 ms. At this time, combustion is accelerated in bay 3 and both bays burn at the same rate. Shortly after the first pressure peak at 420 ms, we see that SWB3 and FS fail.

Up until 420 ms, bays 5 and 6 show no sign of combustion, only pressurization from bays 3 and 4. The pressure at the beginning of the burn is about 0.8 bar due to this pressurization. Finally, at 490 ms, bays 5 and 6 ignite and rapid combustion results in a second, higher peak pressure in these bays. Bay 5 reaches a peak about 0.6 bar higher than that of bay 6. Evidence of the late burn in the aft bays is also visible in the video and photographs. Seal leakage occurred on the sides of SWB1, leaving streaks in the windows in bays 3 and 4. This late burn dramatically illustrates the strong dependence of the pressure loading on initial conditions near the lean flammability limit. In Test 26 (all-strong configuration with 6.5% fuel), bays 5 and 6 never ignited. In Test 24, the flame acceleration associated with partition failure may be a significant factor in inducing the late burn. Further testing with low-concentration mixtures is needed to clarify this situation.

Figure 5.143 shows the pressures from bays 1 and 2 together with bays 3 and 5. We see that the flame in bay 2 does appear to be accelerated by turbulence generated by the inflow from bays 3 and 4. Bay 1 doesn't begin to pressurize until the pressure in bay 2 begins to fall. Bay 1 reaches a pressure of 1.2 bar before SWB3 fails. Remarkably, bays 5 and 6 ignite at 500 ms, well after the other events. Confirmation of the burn is shown in the shallow pressurization of bays 3 and 4 and also the signals from the thermocouples and photodiodes, Table 5.36.

The pressure in bay 0 as compared to that in bays 1 and 2 is shown in Fig. 5.144.. Bay 0 pressurizes rapidly when SWB3 fails and reaches a sharp peak before FS fails as well. Shortly after the bay 0 peak, bay 2 shows a sharp change in pressure drop at 445 ms, accompanied by a kink in the other traces. This probably indicates rupture of the MP.

Despite the near-limit concentration, SWB1 and MS still experienced large differential pressures (Fig. 5.145). The pressure differential on SWB1 is negative while the forward bays are burning, then when bays 5 and 6 ignite at 500 ms, the pressure differential becomes large and positive.

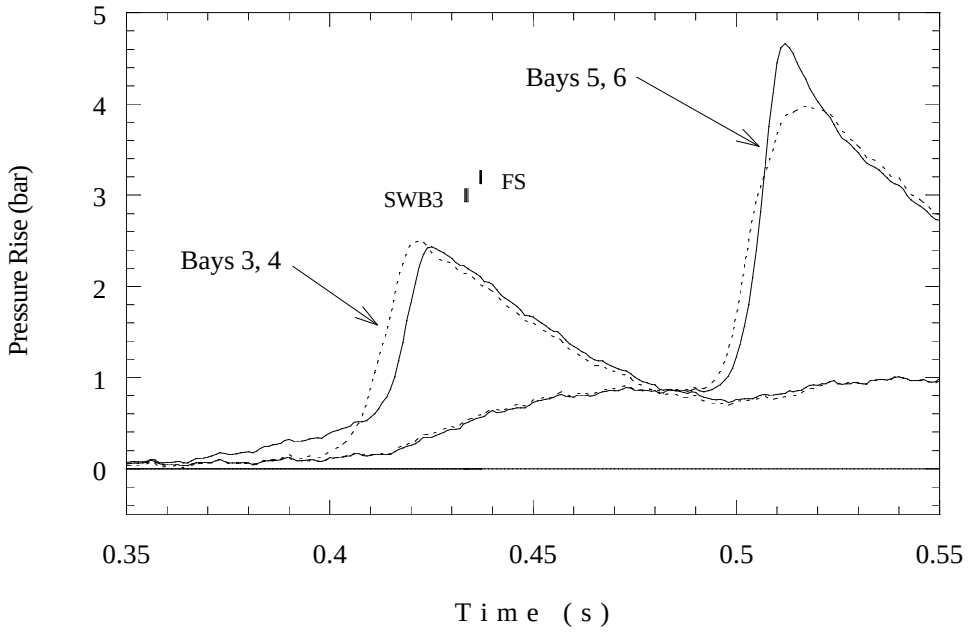

Figure 5.142: Pressure traces from bays 3 – 6, 6.5% fuel. Dashed lines indicate even-numbered bays. Trace with early liftoff is from bay 3; that with high peak is from bay 5. Test 24.

Differential pressures across SWB2 and SWB3 are shown in Fig. 5.146. SWB2 has a sharp valley at 440 ms, caused by combustion in bay 1 and pressurization of bay 0. When SWB3 fails, there is sharp negative spike, possibly the result of a reflected shock from the FS. After the partitions have failed, the SWB2 differential again rises and then falls as bay 2 vents.

The vent differentials, shown in Fig. 5.147, reflect the timing differences in combustion between the aft bays and bay 1. The port-vent differential pressure initially goes positive, indicating combustion in bay 3. The differential pressures in both vents show a sharp dip when bay 1 ignites at 430 ms. When bay 6 ignites at 500 ms, the starboard vent differential pressure increases rapidly to 4 bar.

Pressure across the forward PR, in Fig. 5.148, shows a slow burn in bay 3 followed by a rapid burn in bay 4. Venting from bay 4 into 3 probably accelerates combustion in bay 3. The aft PR shows the late-time sequential ignition and rapid combustion in bay 6 followed by bay 5.

Bay camera 2 jammed in this test, so there is no schlieren information for bays 3 and 4. The image in bay 2 is somewhat cropped at the corners, but the film clearly shows that the flame does not propagate downward. It burns primarily upward, but does have some sideways propagation. After the flame has reached the top of the bay, a jet enters through one of the lower passages in MS. The jet impinges on SWB2, and the flame accelerates through the bay. Judging by discoloration of light through the fresnel lenses, combustion is completed at the same time that the partitions fail. Bay 1 is unusual in this test. The film shows a jet entering bay 1 from one of the lower passageways in SWB2, but no combustion is immediately visible. Shortly after this jet starts, a jet is seen coming from the jet fuel manifold. This, too, appears

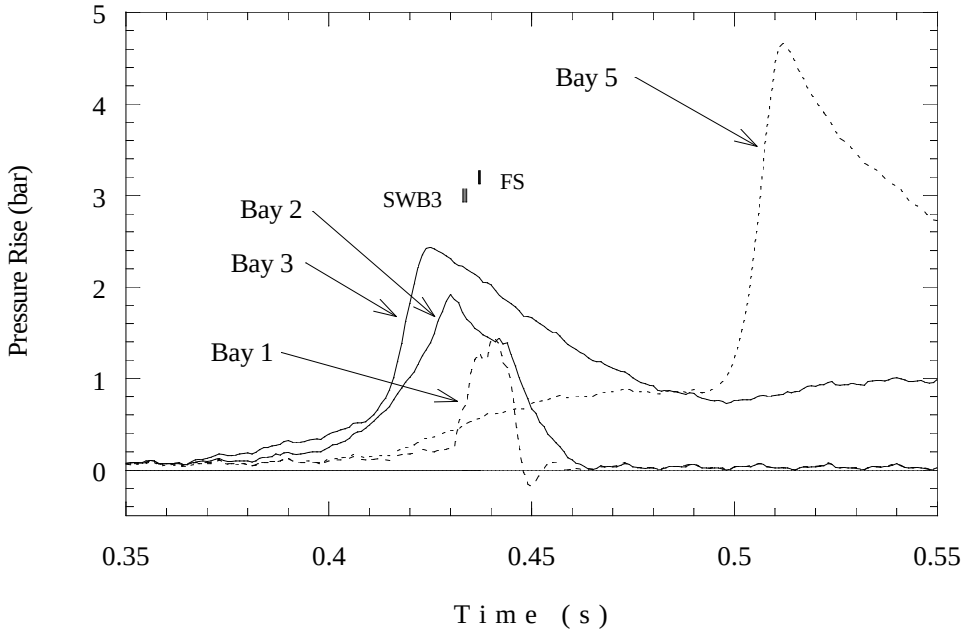

Figure 5.143: Pressure traces from bays 1 – 3, 5, 6.5% fuel. Test 24.

to be non-reacting. Suddenly, a flame enters from an unknown source, and the bay burns very rapidly. SWB3 and FS fail at that time, evidenced by the color change in the fresnel lens. The MP also ruptures at that time. This pre-pressurization may have caused a higher peak burn pressure and the more violent ejection of SWB3 and FS than occurred in the test with 7.5% fuel.

Unfortunately, the blastwave created upon partition failure caused the arc lamp serving bays 5 and 6 to shut down, and the later events in those bays were not captured. Only violent swirling is visible before the light goes out. The exterior side-view camera, however, does capture evidence of the burn. The flame is seen starting in bay 2, and propagating to bays 3/4 and then 1 before the arc light goes out. About 625 frames after ignition, black streaks begin to appear on the windows of bays 3/4. These indicate failure of the side seals on SWB1, because of the high pressure difference across the partition. This would not be caused by depressurization of the forward bays, because MS is acting as the barrier to atmosphere, so this is due to pressure in bays 3 and 4. In this test, both SWB3 and FS leave the tank together, wrapped around the water bottles.

There is a data reporting issue for this test. An e-mail message (from Krok to Shepherd) was sent stating that “the middle of the aft PR was blown out in the 2Lo, 6.5% all-strong test.” This would have been Test 26 (BETA series), but review of that data shows that PR failure did not occur. The message may have incorrectly mentioned all-strong when “part-strong” should have been used. This means that the message would actually be referring to Test 24. However, the test log sheets give no indication of failure in either Test 24 or 26. In both Test 24 and 26, the bay 5/6 schlieren visualization was terminated (film break, Test 26; lamp out, Test 24) before any PR failure was observed. Differential pressures across aft PR in Test 24 aren’t high

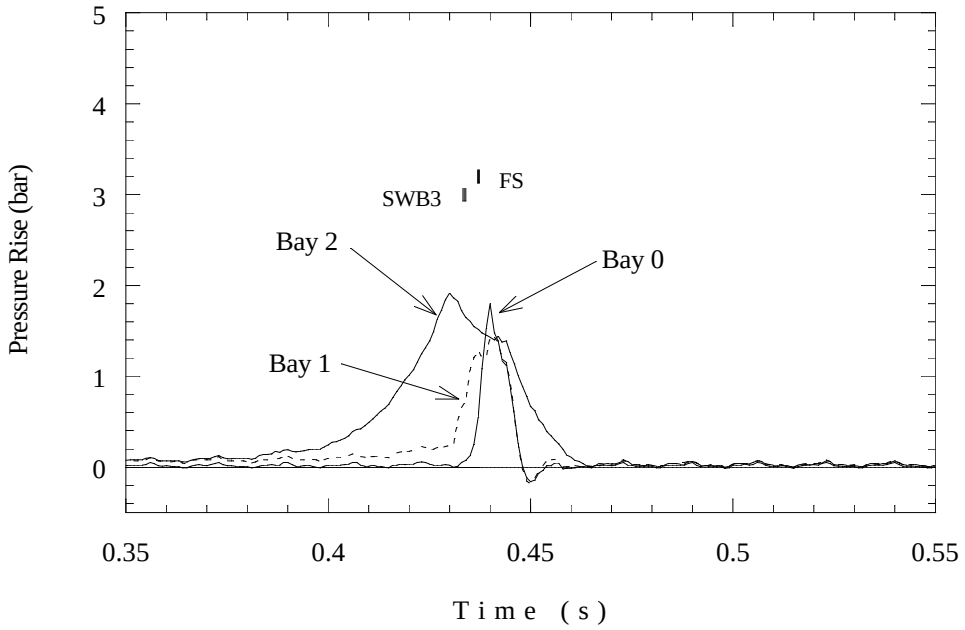

Figure 5.144: Pressure traces from bays 0 – 2, 6.5% fuel. Test 24.

enough alone to cause failure. It may be possible that the late burn in 5 and 6 put enough force on SWB1 to fail the aft PR in tension. The bay 3/4 schlieren camera shows side-seal leakage into bays 3 and 4 late in the test, and these seals generally only fail when the partition moves.

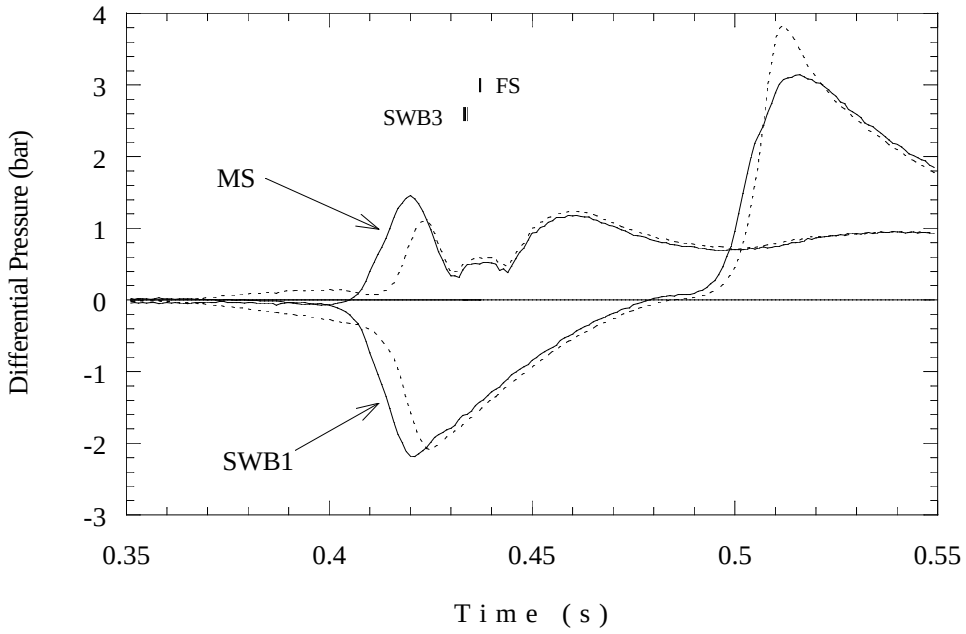

Figure 5.145: Differential pressure across SWB1 and MS, 6.5% fuel. Dashed lines indicate port side of panel. Test 24.

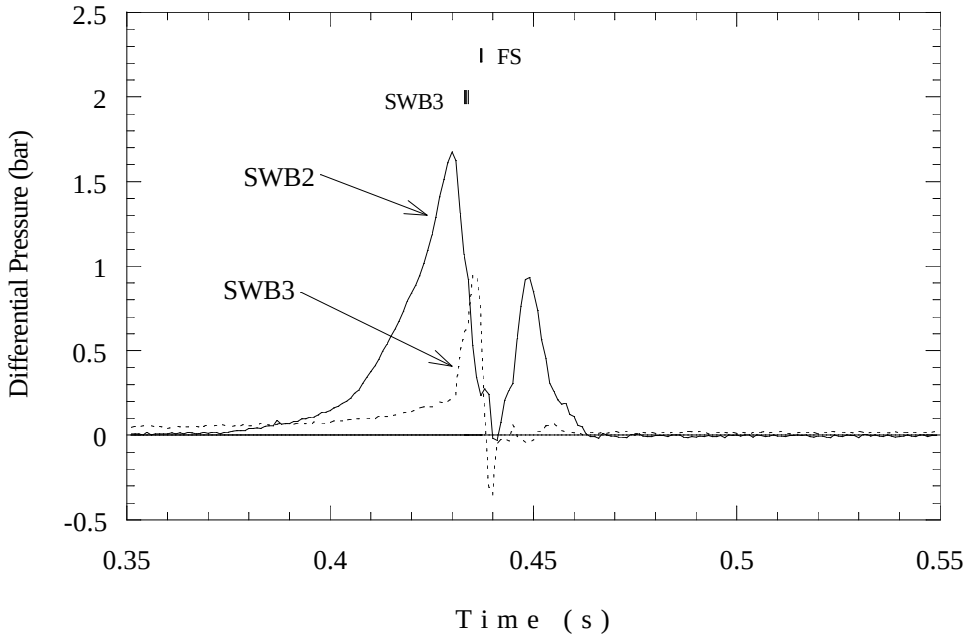

Figure 5.146: Differential pressure across SWB2 and SWB3, 6.5% fuel. Test 24.

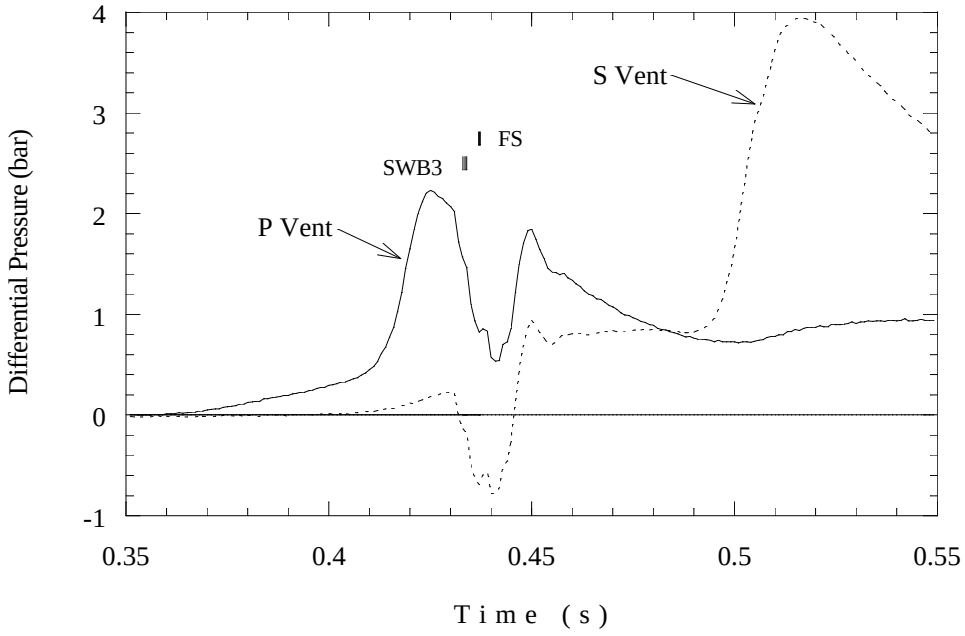

Figure 5.147: Differential pressure across vents, 6.5% fuel. Test 24.

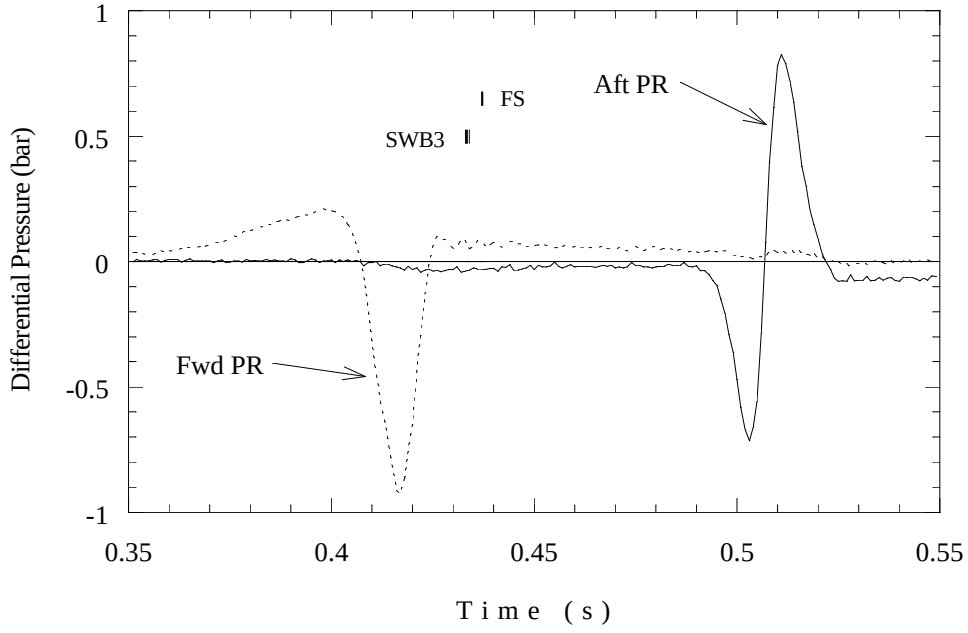

Figure 5.148: Differential pressure across PRs, 6.5% fuel. Test 24.

Table 5.36: Flame arrival times (ms), Test 24.

Photodetectors

498	498
411	414
416 **IGN**	
432	
438	

Thermocouples

432	448	448	420
414	417	401	376
374 **IGN**		337	
433		435	

5.4.5 Part Strong: Ignition Locations

This set of tests examines the part-strong configuration, in which only SWB3 and FS are weak, and a weak manufacturing panel is installed in SWB2. This configuration mimics a failure sequence that is postulated for TWA 800. The purpose of this series of tests was to examine the effect of ignition location on the loads produced on the beams and spars that remain within the tank during the explosion event. These results are examined Chapter 6 in the context of the crash investigation. The first test (Test 17) in this series is run with only vapor simulant and ignition in bay 5. The other tests in this series include a layer of cold liquid Jet A in the bottom of the tank, with ignition in bays 1, 2Lo, and 5. Motion-detector trip times are shown in Table 5.37 for all four tests.

Table 5.37: Motion-detector breakaway times. Numbers in italics are from tape drives. MP only has one breakwire. N/R, not recorded; N/S, no signal.

	Top Left	Top Right	Bottom Left	Bottom Right
Test 17				
MP	NR			
SWB3	139.46	136.33	*133.54*	*131.53*
FS	141.00	*136.97*	*137.55*	*137.04*
Test 27				
MP	151.60			
SWB3	144.58	144.79	145.6	*144.71*
FS	148.82	149.51	148.8	*148.64*
Test 28				
MP	121.72			
SWB3	114.68	115.78	117.9	*118.93*
FS	119.91	120.09	119.6	N/S
Test 29				
MP	160.20			
SWB3	152.06	152.56	170.7	*155.92*
FS	165.05	163.76	165.3	*147.23*

Ignition in Bay 5, no Jet A (Test 17) This test used a 0.012-in thick MP diaphragm, which was replaced in the later tests with one of 0.006-in thickness and a cutter, to give a lower rupture pressure. This was the first test to use multiple weak panels, as well as the FS water bottles. At the end of the test, the water bottles remained attached to FS and came to rest 75 ft from the tank. SWB3 only went about 20 ft, as it got caught on the blast gauge guard, allowing FS to continue downrange. The tank also slid back about 1/2 in, prompting installation of angle brackets on the legs so they could be bolted into the concrete pads. The concrete anchors still pulled loose in their holes, allowing the tank to rock, but they did prevent it from sliding back.

Pressure traces are shown in Figs. 5.149 – 5.156. In Fig. 5.149 we see the pressure in bay 5, the ignition bay, with the adjacent bays 3 and 6. Bays 5 and 6 show some cyclic pressurization. Combustion in bay 3 gets an early start but is outpaced by bays 5 and 6 until about 125 ms, when the flame in bay 3 accelerates, and the pressure overshoots that in the other bays. Bay 4, shown in Fig. 5.150, is the last of the aft bays to ignite, but then burns quickly.

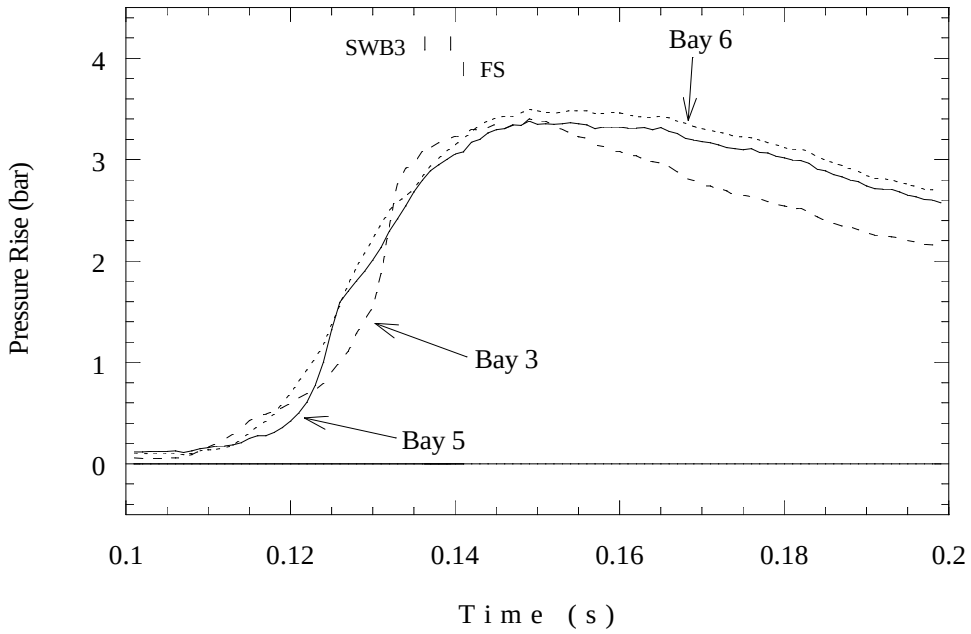

Figure 5.149: Pressure traces from bays 3, 5, 6, ignition in bay 5. Test 17.

In Fig. 5.151, we see that bays 2 and 1 ignite in sequence. Bay 2 pressurizes at a constant rate until the peak at 150 ms. The MP presumably ruptures near the peak pressure at 150 ms (the breakwire was not used in this test). The pressure in bay 1 continues to rise as SWB3 fails, and drops a short time after FS fails. The pressure in bay 0 is shown in Fig. 5.152, where we see that the pressure overshoots that in bay 1.

Bay 5 ignition produces asymmetrical combustion in the aft bays, as indicated by the differential pressures in Fig. 5.153. The divergence in the port-side traces at 110 ms indicate rapid combustion in bay 3, followed by combustion in bay 4. The differential pressures across SWB2 and SWB3 are shown in Fig. 5.154. The pressure across SWB2 dips when the pressure across SWB3 peaks, but then continues to rise. The MP presumably ruptures when the peak

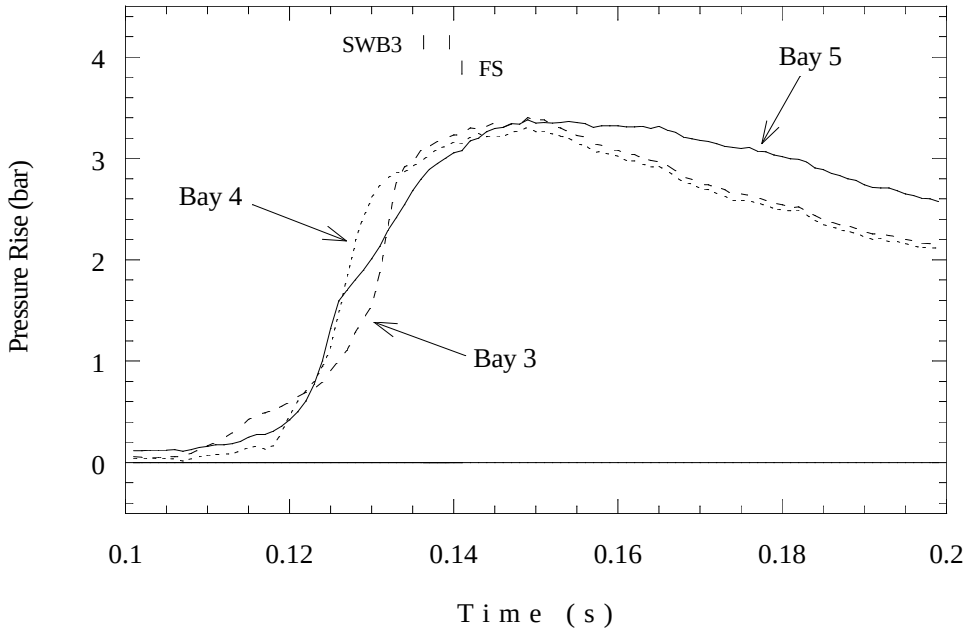

Figure 5.150: Pressure traces from bays 3 – 5, ignition in bay 5. Test 17.

pressure differential is reached at 150 ms. The SWB3 pressure differential continues to rise as the partition fails and then drops sharply when the last motion detector is tripped.

The pressure across the vents (Fig. 5.155) shows forward flow generated by combustion in the aft bays. Combustion in bay 1 eventually curbs the rise in differential pressure, but the failure of SWB3 and FS expose the forward ends of the vents to atmosphere, and another rise in the differential is seen. The port vent shows a lower differential after the peak because bay 3 also vents into bay 2, which is connected to atmosphere through the ruptured MP. Pressures across the PRs (Fig. 5.156) are small. Most notable is the sign change just after 120 ms that occurs in the pressure differential across the forward PR. This changes takes place when the flame passes from bay 3 to bay 4, burning faster in 4 than it had in 3.

Bay cameras 1 and 3 malfunctioned in this test, so schlieren is only available from bays 3/4 and 1. The flame enters bays 3 and 4 from the bottom; it is not possible to distinguish which bay is ignited first. We expect that bay 3 should ignite first since it is closest to bay 5. Ignition of bay 4 is also hard to see, but it appears that there is a rapid combustion event immediately after the flame fills bay 3. The flame also enters bay 1 through one of the lower passages (above floor level, not one of the corners). The jet reaches SWB3 and spreads into the compartment. Before the flame reaches the top, flow is visible from the vent stringers. The vent flame does not make much progress into bay 1 before the main flame reaches it. Just after the flame fills the compartment, it appears that gas begins moving out, indicating failure of SWB3. This is followed a few frames later by rupture of the MP.

Exterior footage shows that SWB3 impacts FS, and both fold forward around the water bottles. Because of the inertia of the water bottles, the panels exit at a much slower speed than in Test 13, for which only SWB3 was used. When the partitions collide with the new, stronger

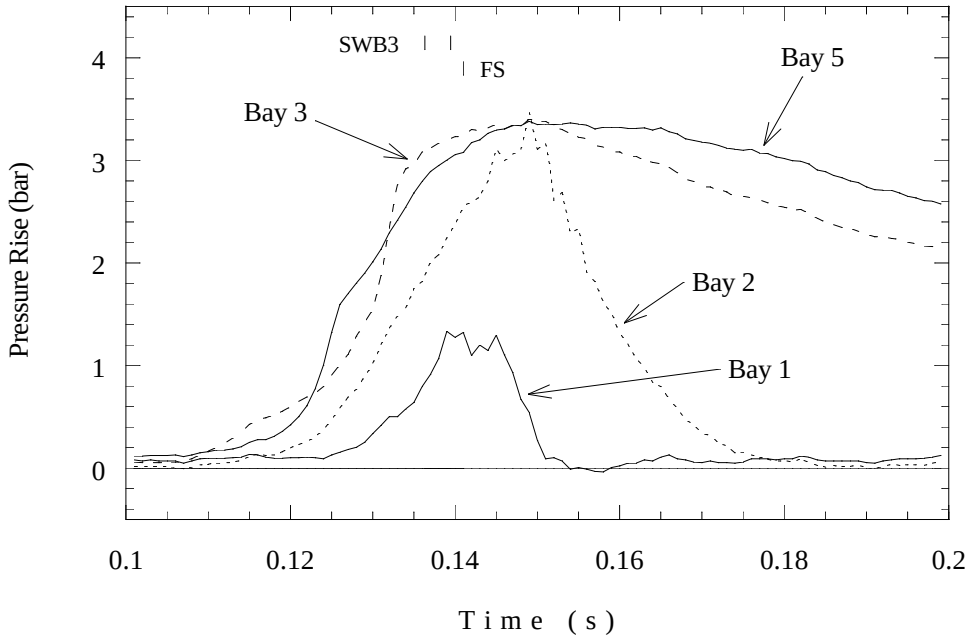

Figure 5.151: Pressure traces from bays 1 – 3, 5, ignition in bay 5. Test 17.

blast gauge protector, SWB3 gets tangled up on the protector while FS and the water bottles slide out and continue downrange. The gauge protector sustained damage from the impact. The MP ruptures and the pieces fly out past the two panels just as they are exiting the tank.

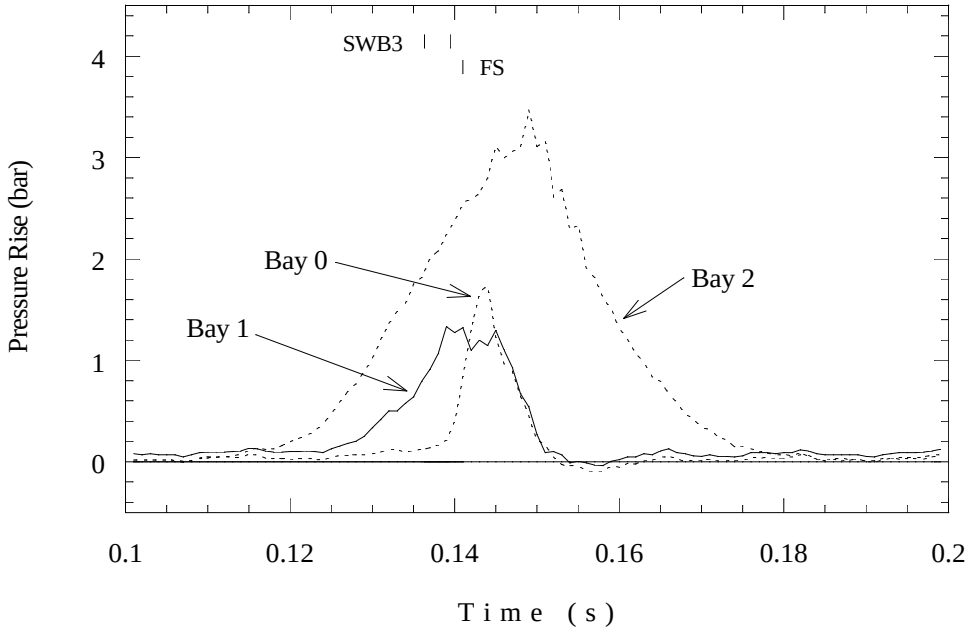

Figure 5.152: Pressure traces from bays 0 – 2, ignition in bay 5. Test 17.

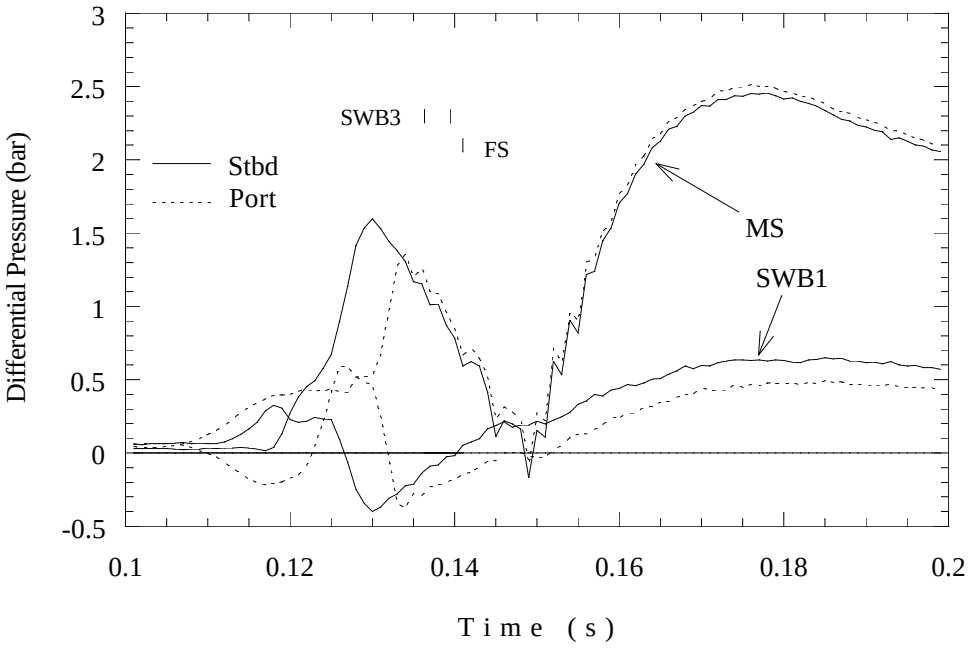

Figure 5.153: Differential pressure across SWB1 and MS, ignition in bay 5. Test 17.

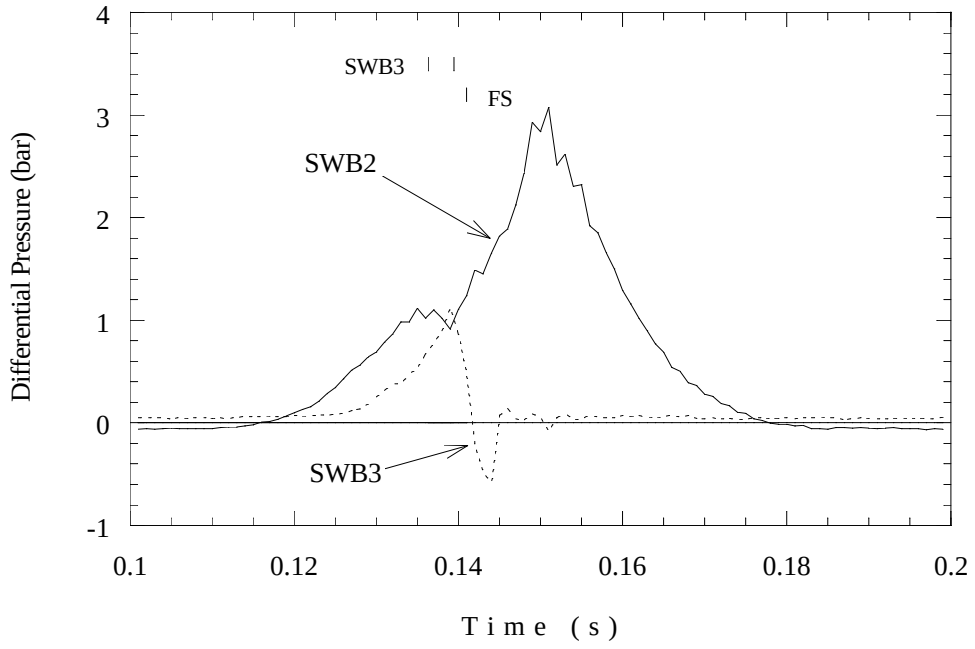

Figure 5.154: Differential pressure across SWB2 and SWB3, ignition in bay 5. Test 17.

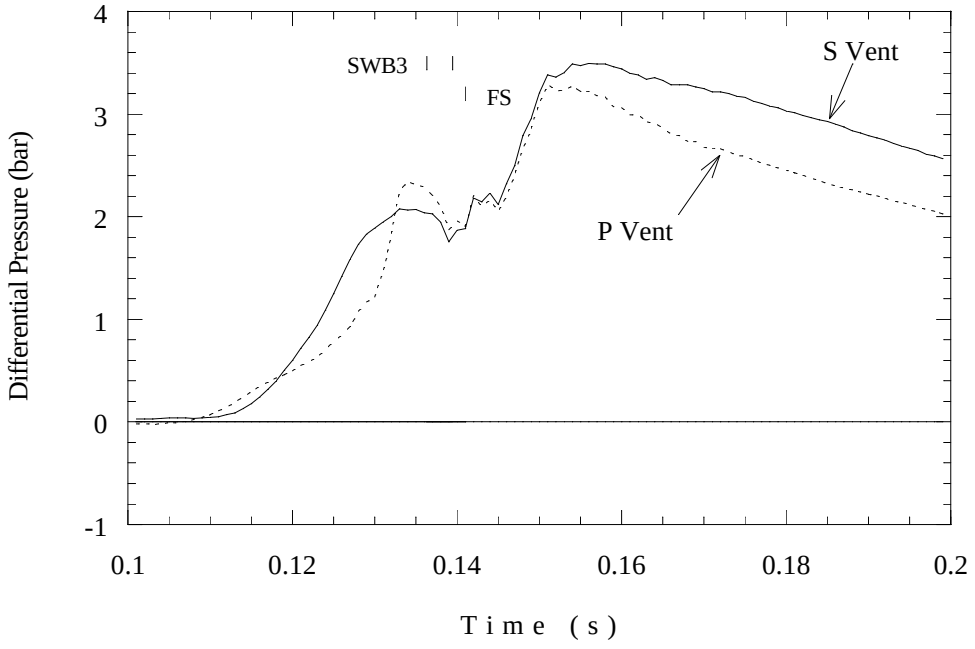

Figure 5.155: Differential pressure across vents, ignition in bay 5. Test 17.

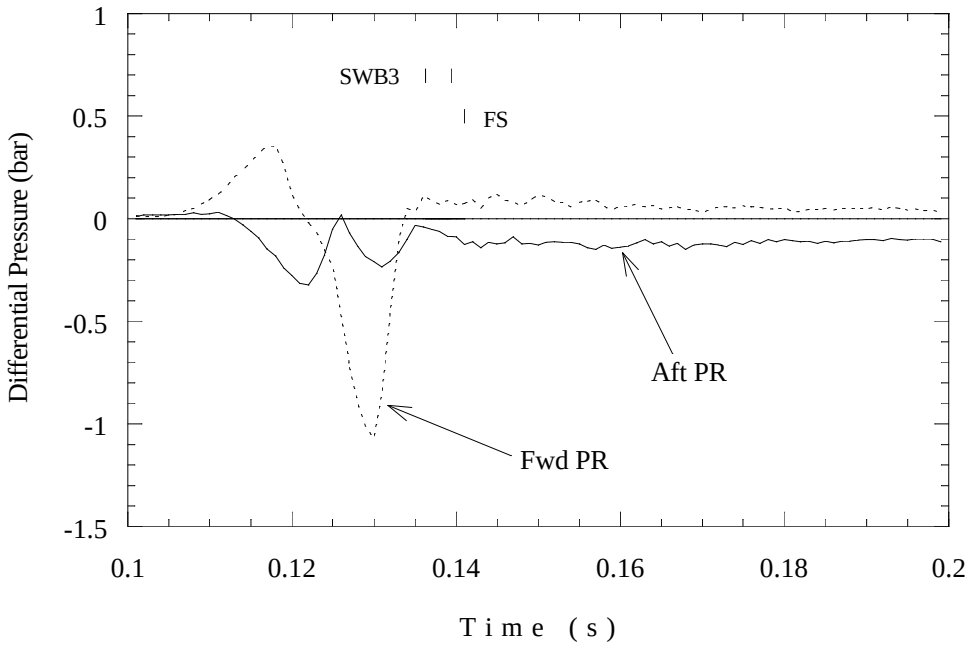

Figure 5.156: Differential pressure across PRs, ignition in bay 5. Test 17.

Table 5.38: Flame arrival times (ms), Test 17.

Photodetectors

116	123 **IGN**
118	119
127	
129	
144	

Thermocouples

122	114	70 **IGN**	123
128	125	134	133
144		141	
145			

Ignition in Bay 5, Cold Liquid Jet A Layer (Test 28) This test is a repeat of Test 17 with the addition of the liquid Jet A layer on the bottom of the tank. Although there are some quantitative differences, the tests are very similar qualitatively.

There was one anomaly in this test. SWB3 passed over the bottom right motion detector (M16) without tripping it. Later, the switch functioned when high temperatures melted the solder connection at the tip of the probe. Despite this malfunction, the indicated failure time was still close to that of the other switches on this panel. The FS assembly stopped 93 ft from the tank, and SWB3 landed at 42 ft.

Pressure traces are shown in Figs. 5.157 – 5.163. The aft bay traces (Fig. 5.157) are typical of bay 5 ignition and very similar to Test 17. There is an interplay between bays 5 and 6 associated with lateral venting and subsequent rapid pressurization of bays 3 and 4. Combustion in bay 4 was very rapid in this test in comparison to Test 17. The early failure of SWB3 and venting of bay 3 through the vent stringer may contribute to the lower peak pressure in bay 3 as compared to that in Test 17.

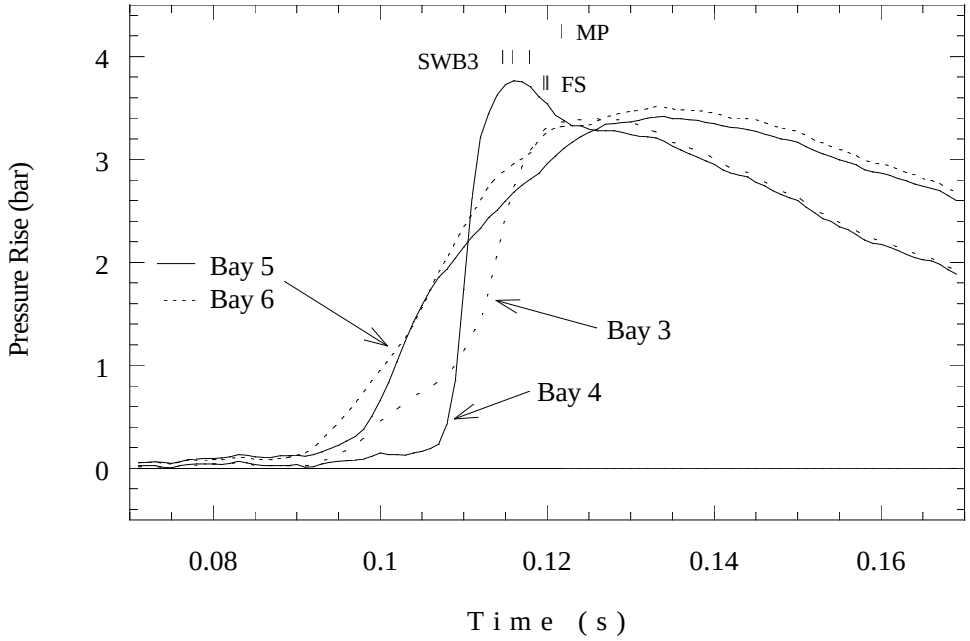

Figure 5.157: Pressure traces from bays 3 – 6, ignition in bay 5, layer of cold liquid Jet A. Test 28.

Pressure traces from bays 1 and 2 are shown in Fig. 5.158. These bays do not undergo rapid combustion until after the transition to rapid combustion in bay 4. Bay 2 peaks and immediately begins to drop after the MP rupture. Bay 1 reaches and sustains for 10 ms a peak of about 1.2 bar as SWB3 fails, which occurs over a period of 5 ms. The FS fails completely in less than 1 ms, probably after being struck by SWB3. Bay 0 is included in Fig. 5.159, and we see a sharp rise up to the failure point, with no significant negative pressure phase visible in bay 1 or 2.

Initially, the pressure difference on the starboard side of SWB1 is positive and increasing.

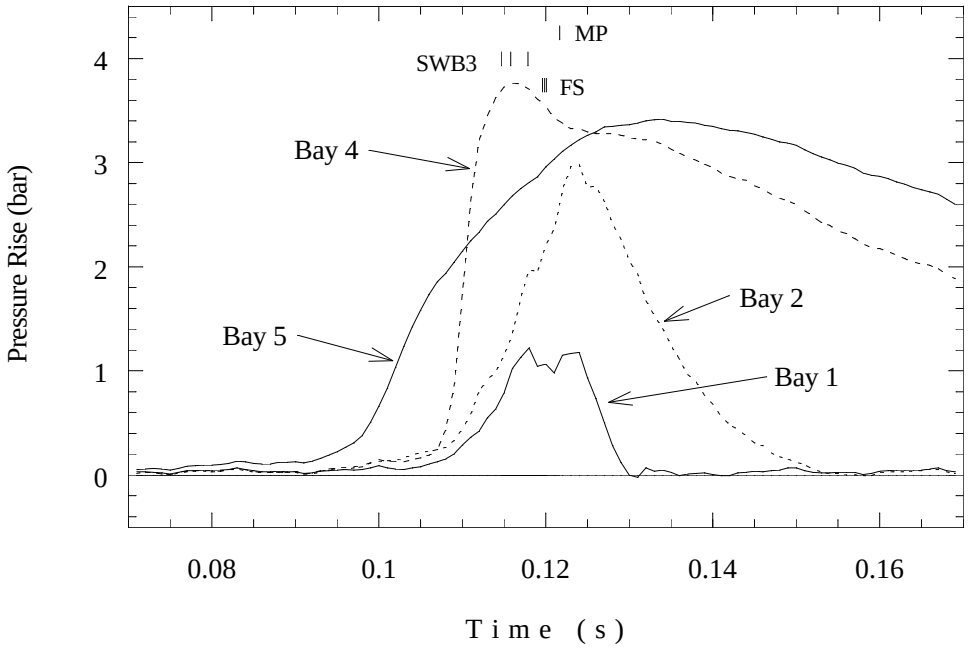

Figure 5.158: Pressure traces from bays 1, 2, 4, 5, ignition in bay 5, layer of cold liquid Jet A. Test 28.

As bay 6 begins to undergo rapid combustion (Fig. 5.160), the transition to a faster burn in bay 4 reverses this trend. The differential pressure on SWB2 (Fig. 5.161) increases rapidly until SWB3 ruptures. This rise is briefly interrupted when the MP ruptures and at 130 ms; venting through the MP begins to lower the pressure in bay 2. The failure of SWB3 takes about 5 ms and occurs at a differential pressure of about 1 bar .

The differential pressures on the vents (Fig. 5.162) and PRs (Fig. 5.163) are very similar to those in Test 17.

Only the exterior cameras were used in this test. The side-view camera shows jet fuel lofting and burning first in the four aft bays. The jet fuel ignites next in bay 1, where a vertical plume of flame indicates that fuel may be blowing out of the jet fuel manifold. This plume ignited from the top. Fuel in bay 2 was ignited immediately thereafter. SWB3 failed first along the top, and rotated enough that it did not wrap around FS and the water bottles as it exited. The fireball didn't appear to be much bigger than the tank in this test. The fireball is shown in Fig. 5.164, with its growth sequence captured by the 8 fps Nikon in Fig. 5.165. Contrast these to Figs. 5.110 and 5.111 (p. 164 and 165, respectively) to see how the fireball size compares between the part-strong and all-strong configurations.

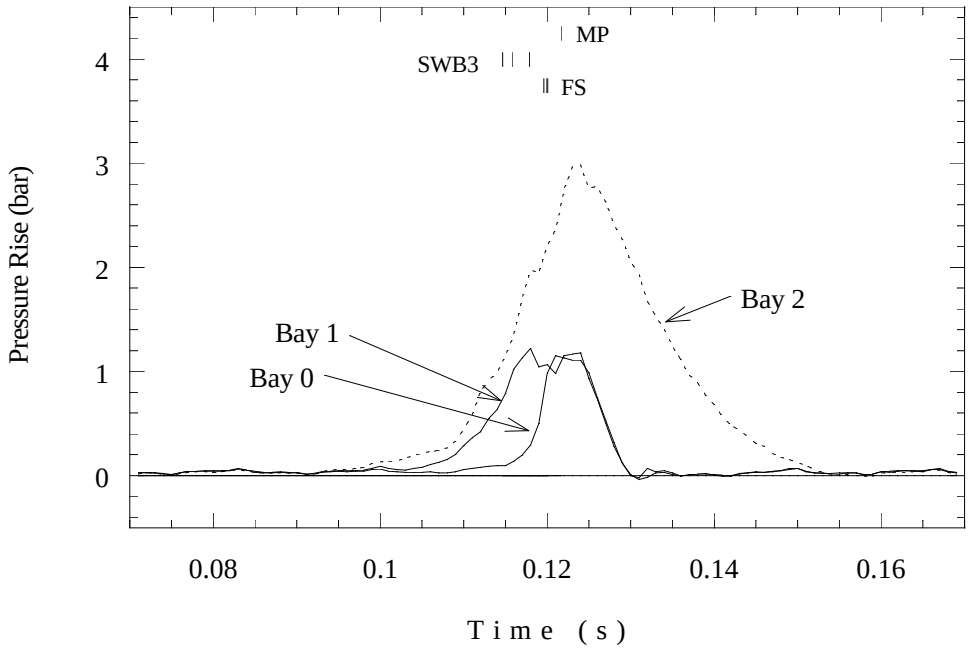

Figure 5.159: Pressure traces from bays 0 – 2, ignition in bay 5, layer of cold liquid Jet A. Test 28.

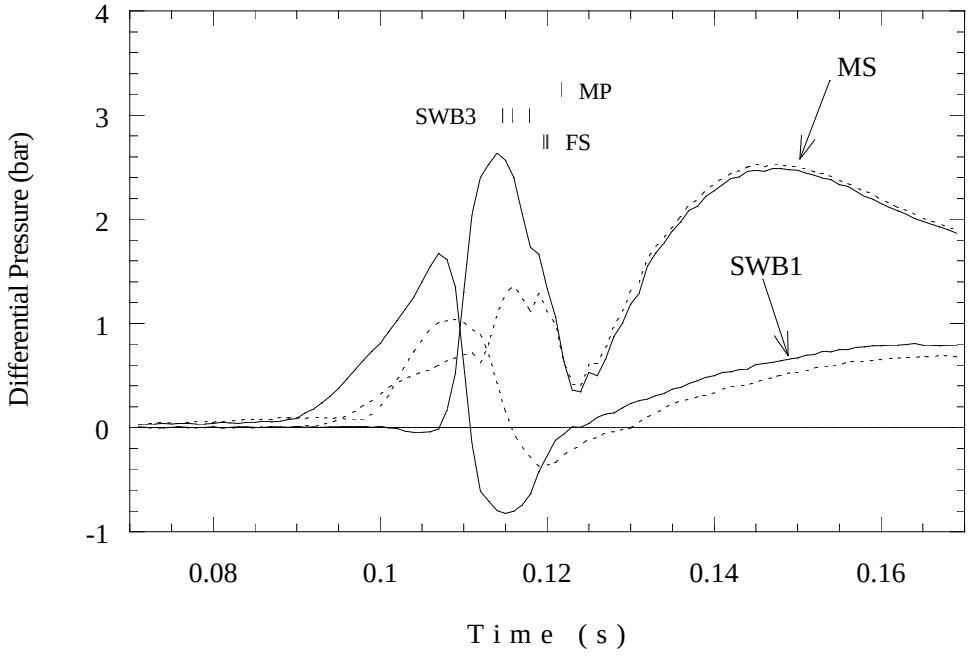

Figure 5.160: Differential pressure across MS and SWB1, ignition in bay 5, layer of cold liquid Jet A. Dashed lines indicate port side, solid lines indicate starboard side. Test 28.

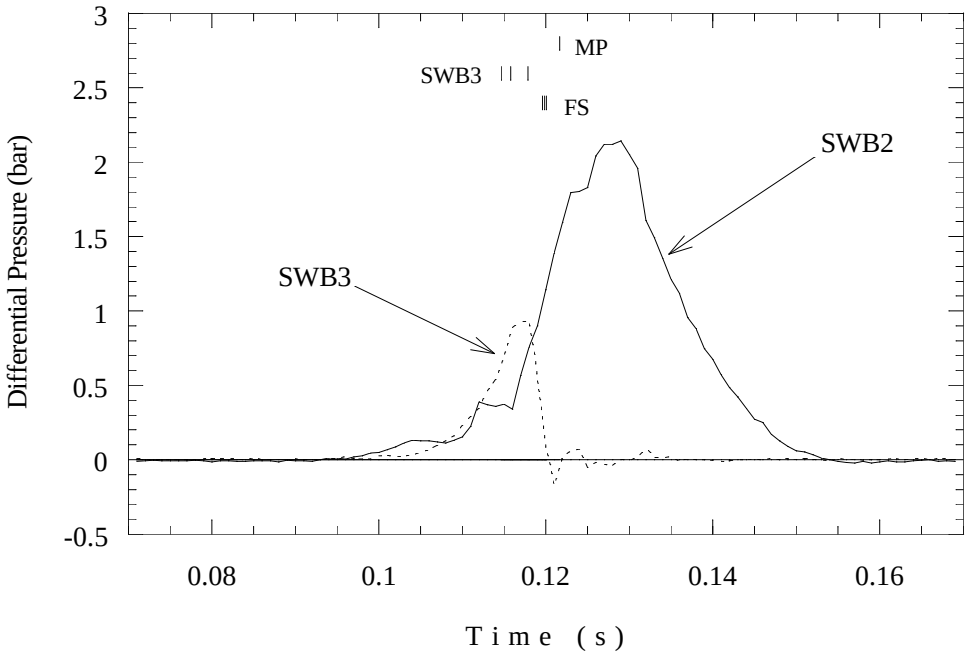

Figure 5.161: Differential pressure across SWB2 and SWB3, ignition in bay 5, layer of cold liquid Jet A. Test 28.

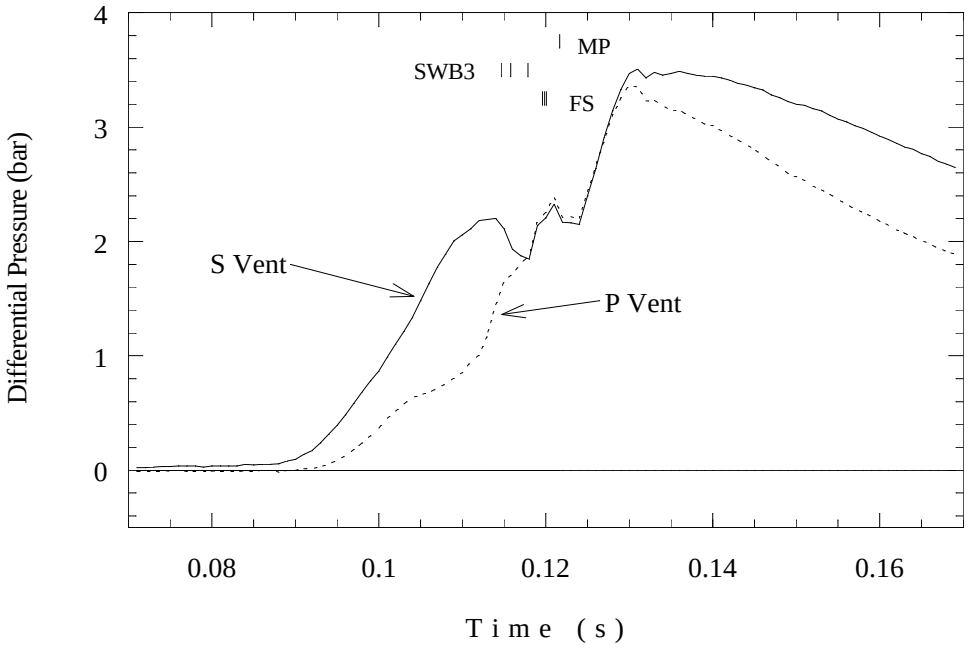

Figure 5.162: Differential pressure across vents, ignition in bay 5, layer of cold liquid Jet A. Test 28.

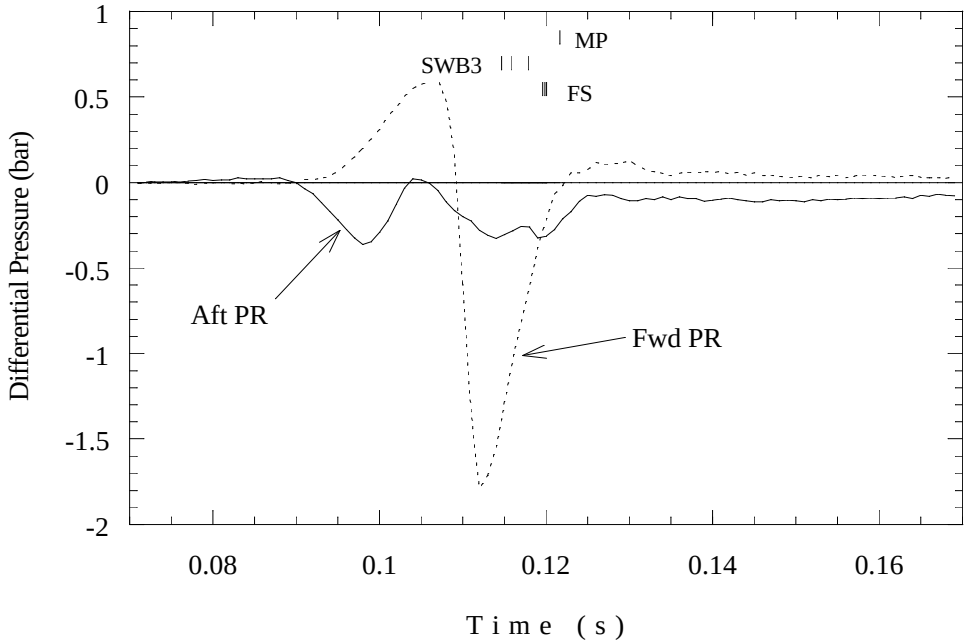

Figure 5.163: Differential pressure across PRs, ignition in bay 5, layer of cold liquid Jet A. Test 28.

Table 5.39: Flame arrival times (ms). Test 28.

Photodetectors

96	98 **IGN**
99	95
105	
103	
117	

Thermocouples

94	91	62 **IGN**	101
110	112	115	113
126		126	
110		122	

Figure 5.164: Fireball from Test 28 at approximately its greatest extent.

Frame 1

Frame 2

Frame 3

Frame 4

Frame 5

Frame 6

Figure 5.165: Fireball sequence at 8 fps. Test 28.

Ignition in Bay 2Lo, Cold Liquid Jet A Layer (Test 27) This test is a replica of Test 22 with the exception of a layer of cold liquid Jet A. The onset of rapid combustion occurred at about 140 ms, about 40 ms quicker than without Jet A. Once rapid combustion began, the resulting pressure and differential pressure histories were qualitatively very similar. The FS assembly came to rest 97 ft from the tank. SWB3 stopped at 64 ft. This is quite a bit farther than the partitions traveled in Test 22.

Pressure traces for this test are shown in Figs. 5.166 – 5.172. Bay 3 is the first to show a change in combustion rate, with an early but slow rise at 120 ms. Bays 4 – 6 show a slightly higher rate as combustion begins in those bays. Bays 3 – 6 transition to rapid combustion over the period of 133 – 140 ms. Figure 5.167 shows the trace from bays 1 and 2 with those of 3 and 5 for reference. Bay 2 transitions to rapid combustion shortly before bay 5 and reaches maximum pressure slightly after the MP ruptures at 152 ms. SWB3 fails early, at about 145 ms, and this enables bay 2 to empty directly to the atmosphere when the MP fails.

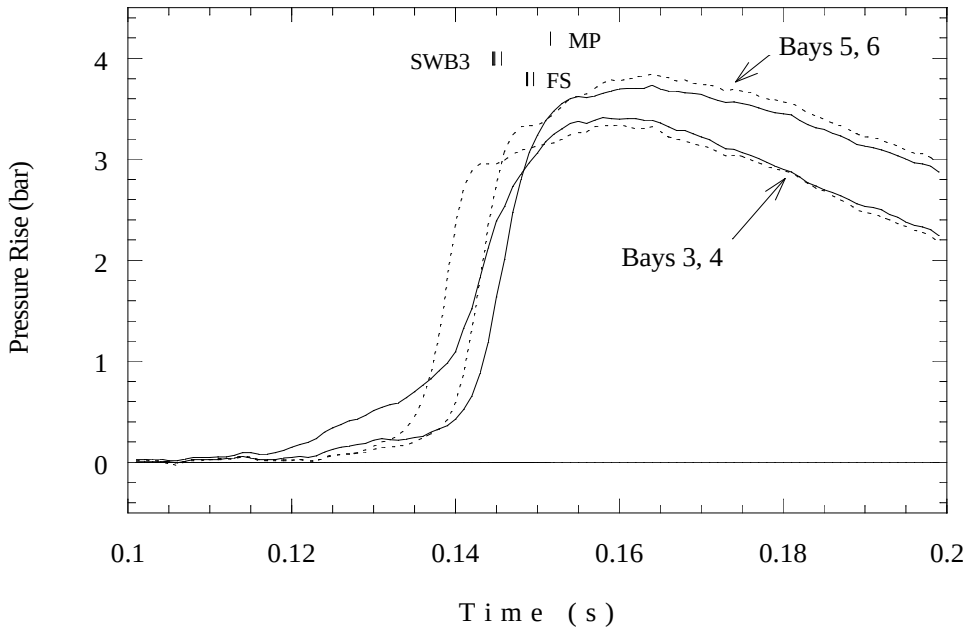

Figure 5.166: Static pressure traces from bays 3 – 6, ignition in bay 2Lo, cold liquid Jet A layer. Dashed lines indicate even-numbered bays. Test 27.

Figure 5.168 shows the pressure in bay 0, which rises sharply after SWB3 fails, and then drops once FS follows. A slight negative phase is visible after the bays vent.

The differential pressures across SWB1 and MS (Fig. 5.169) also show the lack of symmetry in this test. The transition to rapid combustion in bay 3 (140 ms) creates a local explosion on the starboard side of the tank, placing a forward force on MS and a rearward one on SWB1. The port side doesn't show this behavior, as bay 4 gets a slow start in combustion, resulting in a smaller rearward force on SWB1. The associated positive force on MS is not very big, as bay 2 has ignited and counteracts the bay 4 pressure. Once the MP ruptures, venting of bay 2 causes an increase in pressure differential across MS, and a much smaller increase across SWB1.

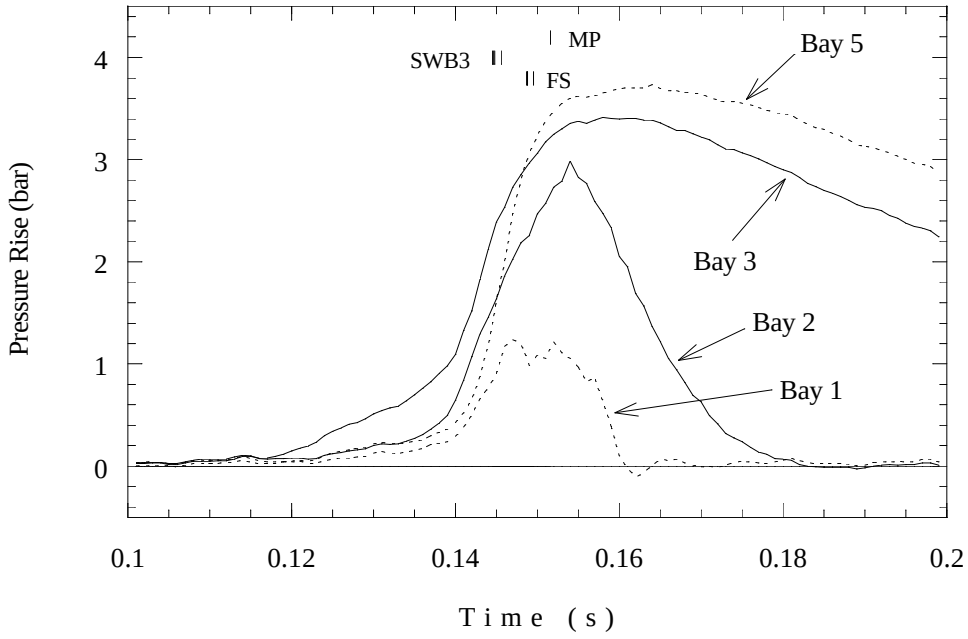

Figure 5.167: Pressure traces from bays 1 – 3, 5, ignition in bay 2Lo, cold liquid Jet A layer. Test 27.

In Fig. 5.170, the failure of SWB3 is observed to occur at a pressure difference of about 1 bar. It is interesting to note that bay 2 does not depressurize immediately upon rupture of the MP, but the pressure is maintained for about 10 ms. This may be due to continuing combustion in bay 2 after the MP rupture. The differential pressures on the vents (Fig 5.171) are similar to those observed in other tests.

The pressures across the PRs (Fig. 5.172) again show the asymmetry in this test, which is unusual for ignition in bay 2 (central or 2Lo). The peaks indicate rapid pressure rises in bays 4 and 6, before 3 and 4 can catch up and equalize the pressure. Once the panels fail, the venting serves to equalize pressures, with the slight negative differential pressure on the aft PR due to the connection of bay 6 to bay 1 via the vent stringer.

Only the exterior cameras were used in this test. The side-view camera shows the jet fuel igniting simultaneously in all bays aft of bay 1, with the largest initial flame in bays 3 and 4. The jet fuel in bay 1 ignites two or three frames later. SWB3 fails slightly earlier at the top than at the bottom, and the initial flame is directed upward as FS fails. The observation cameras show SWB3 and FS exiting together, wrapped around the water bottles. The fireball is considerably smaller in this test than in the all-weak partition tests.

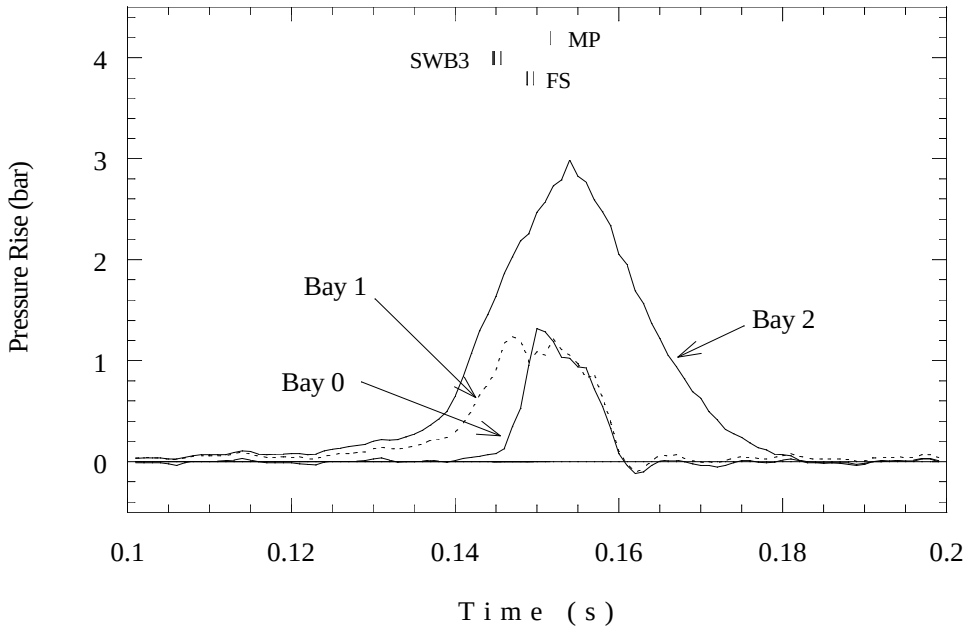

Figure 5.168: Pressure traces from bays 0 – 2, ignition in bay 2Lo, cold liquid Jet A layer. Test 27.

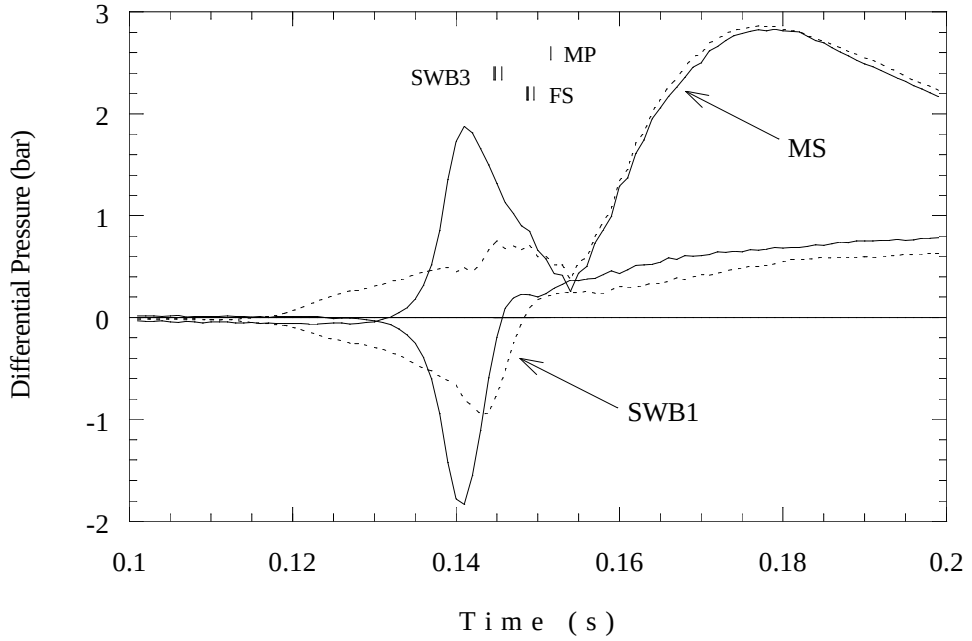

Figure 5.169: Differential pressure across SWB1 and MS, ignition in bay 2Lo, cold liquid Jet A layer. Dashed lines indicate port side of partition. Test 27.

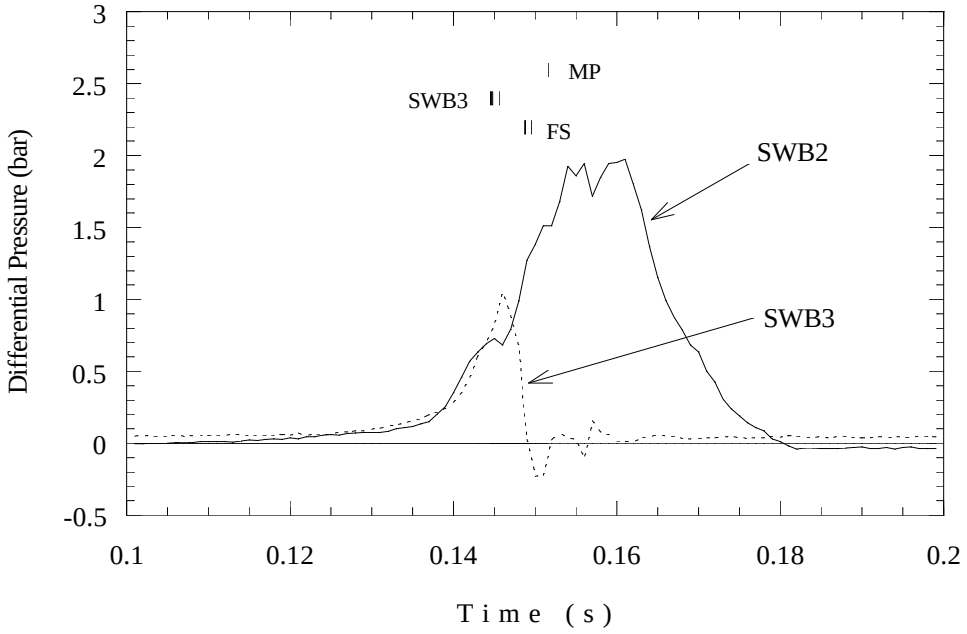

Figure 5.170: Differential pressure across SWB2 and SWB3, ignition in bay 2Lo, cold liquid Jet A layer. Test 27.

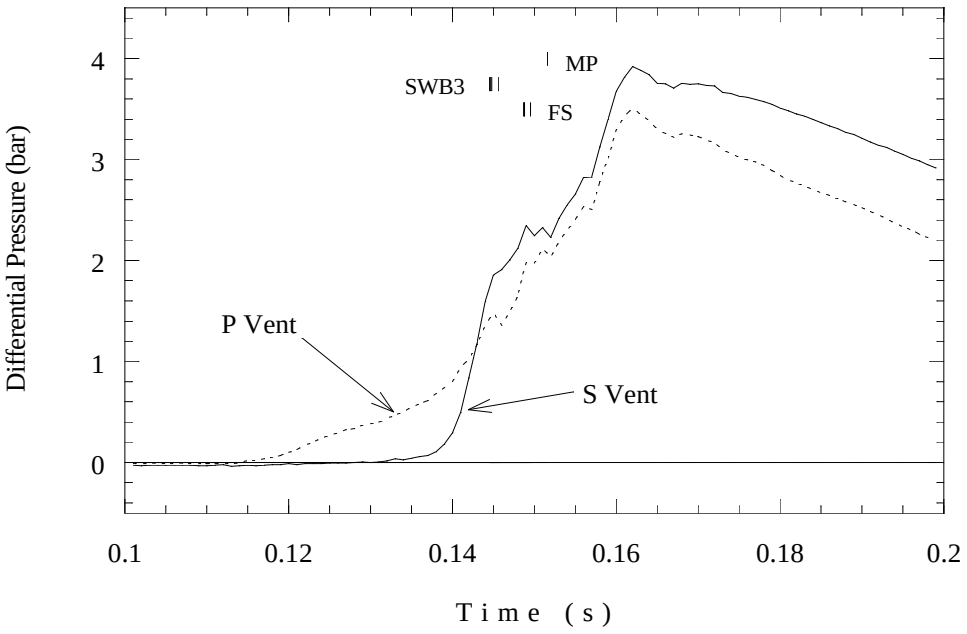

Figure 5.171: Differential pressure across vents, ignition in bay 2Lo, cold liquid Jet A layer. Test 27.

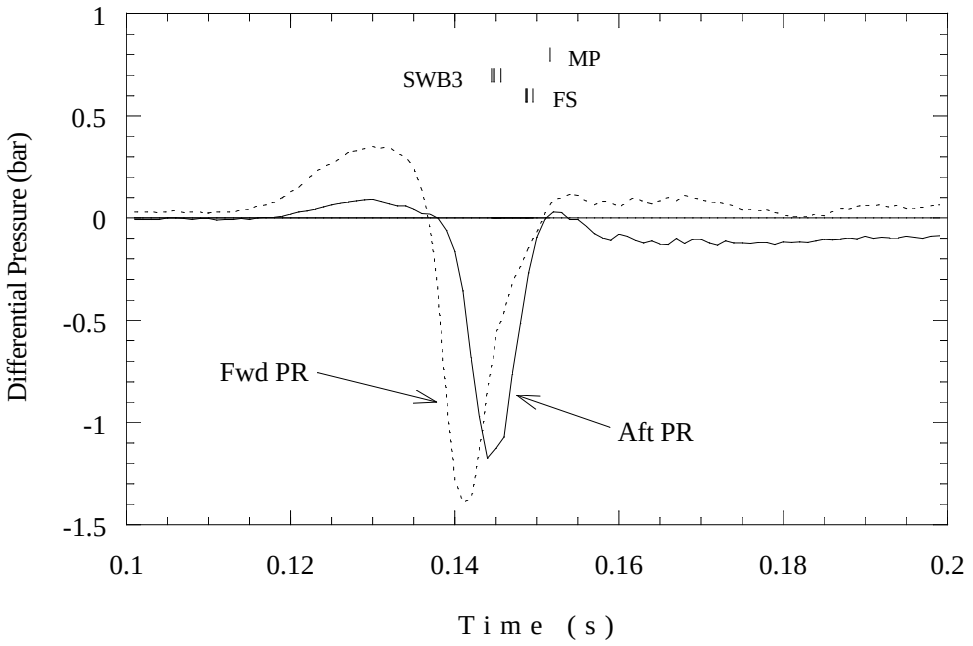

Figure 5.172: Differential pressure across PRs, ignition in bay 2Lo, cold liquid Jet A layer. Test 27.

Table 5.40: Flame arrival times (ms), Test 27.

Photodetectors

135	129
133	132
135 **IGN**	
139	
148	

Thermocouples

145	141	136	141
139	138	125	127
135 **IGN**		139	
156		145	

Ignition in Bay 1, Cold Liquid Jet A Layer (Test 29) This test used the standard vapor concentration, the part-strong configuration, ignition in Bay 1, and a cold liquid Jet A layer. There was no comparable test in the present series without the Jet A layer. Test 21 is the corresponding all-weak test and Test 7 is a similar all-strong test, except without Jet A.

In this test, the aft PR broke, so the data may not be directly comparable to other tests. It should have occurred late enough in the test to allow use of the early data, however. A similar failure occurred in Test 7. Another anomaly was that the signal from the bottom left of SWB3 lags far behind the other signals from SWB3. There is no time zero ambiguity since all signals were recorded on the same digitizer. It is possible that the panel skipped over the trip switch, and the contact was later broken by melting of the solder. However this was not recorded in the test notes. The FS assembly came to rest 72 ft from the tank, and SWB3 only went 14 ft. Usually, SWB3 is wrapped around FS and the water bottles, but in this test, the outer portions of SWB3 were bent backwards instead of forwards. There were no witness marks to indicate contact of SWB3 and FS.

The pressure traces are shown in Figs. 5.173 – 5.181. Figure 5.173 shows the pressure traces from bay 1 and bays 2, 3, and 6, which communicate directly with bay 1, via either SWB2 or the vent stringers. The pressure in bay 1 increases gradually and for a long period of time before the other bays start to pressurize. It appears that the other bays ignite under turbulent conditions, since the pressure increases prior to rapid combustion are small.

The pressure in bay 6, connected by the starboard vent stringer to bay 1, undergoes several rate changes; an initial rise at 147 ms, a decrease in rate at 158 ms when SWB3 begins to fail, and an increase in rate at 165 ms when FS fails. Bays 2 and 3 pressurize nearly simultaneously until the FS fails. The MP ruptures early, before the FS fails. The failure of the MP may have been prematurely induced by the pressure decrease in bay 1 associated with the venting into bay 0 after SWB3 fails and the pressure in bay 1 decreases to a low at 160 ms. The bay 1 pressure rises until the FS fails and bay 1 peaks at 1.5 bar. This is also demonstrated in Fig. 5.175, where we see that the bay 0 and 1 pressure traces coalesce shortly before 160 ms. The pressure histories in the aft bays (Figs. 5.174 and 5.176) are similar to those observed in Test 7.

The differential pressure across SWB1, Fig. 5.177, shows a slight increase on the starboard side as bay 6 begins to burn, but both pressure differentials quickly go negative as rapid combustion is initiated in bays 3 and 4. Pressure across MS is much more uniform (Fig. 5.178); the maximum at 190 ms is due to venting of bay 2 through the manufacturing panel.

In Fig. 5.179, we see that the pressure across SWB2 starts negative as the pressure slowly builds in bay 1. As soon as SWB3 begins to fail, the pressure difference begins to rise and peaks when FS fails. There is a slight kink in the curve when the MP fails. The trace for SWB3 confirms that the partition fails early, since the pressure difference drops to zero at the time of SWB3 failure.

The pressures across the vents (Fig. 5.180) show that the initial flow is toward the rear, caused by combustion in bay 1. The differential pressures across the vents rapidly increase to large positive values as the aft bays ignite. When FS fails, the vent stringers vent the aft bays to atmosphere. The PRs, Fig. 5.181, show moderate differentials. The forward PR experiences a small spike in force when bay 3 ignites, and the aft PR experiences a larger excursion as

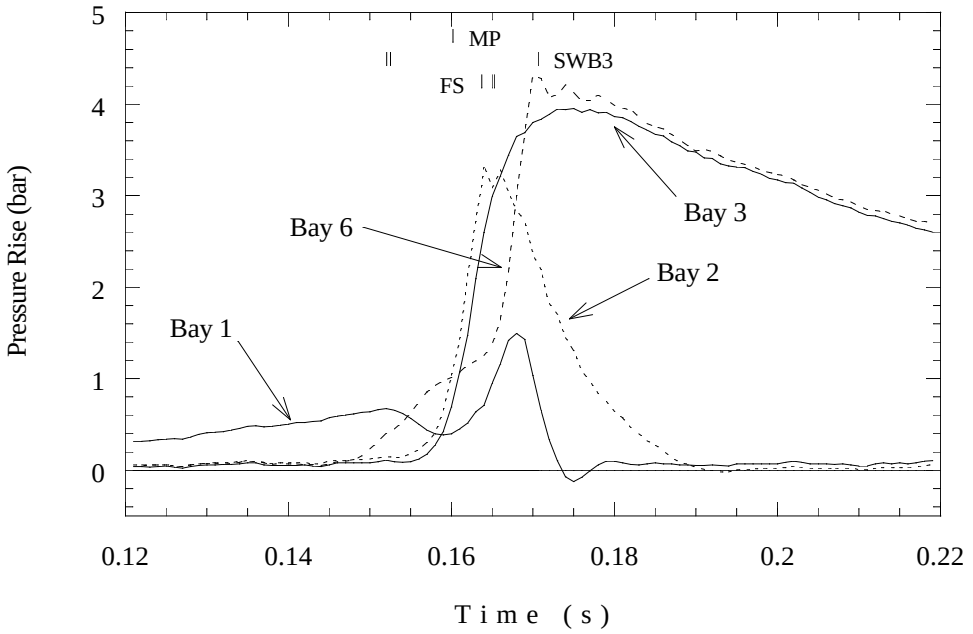

Figure 5.173: Pressure traces from bays 1 – 3, 6, ignition in bay 1, cold liquid Jet A layer. Test 29.

combustion proceeds from bay 5 to bay 6, where combustion is faster.

Only the observation cameras were used during this test. The late hour of this test (1615 hrs) caused exposure problems with the DBM cameras. The side-view camera shows the jet fuel igniting first in bays 5/6, in a vertical plume that may be generated by the vents or by the jet fuel manifold. The fuel in bays 3/4 ignites next, in a diagonal plume from the bottom passages. The flame in bay 2 is ignited at multiple points. By the time the fuel in bay 1 is burning, SWB3 has already failed. It appears to fail first at the top and rotate into FS. SWB3 does not wrap around FS.

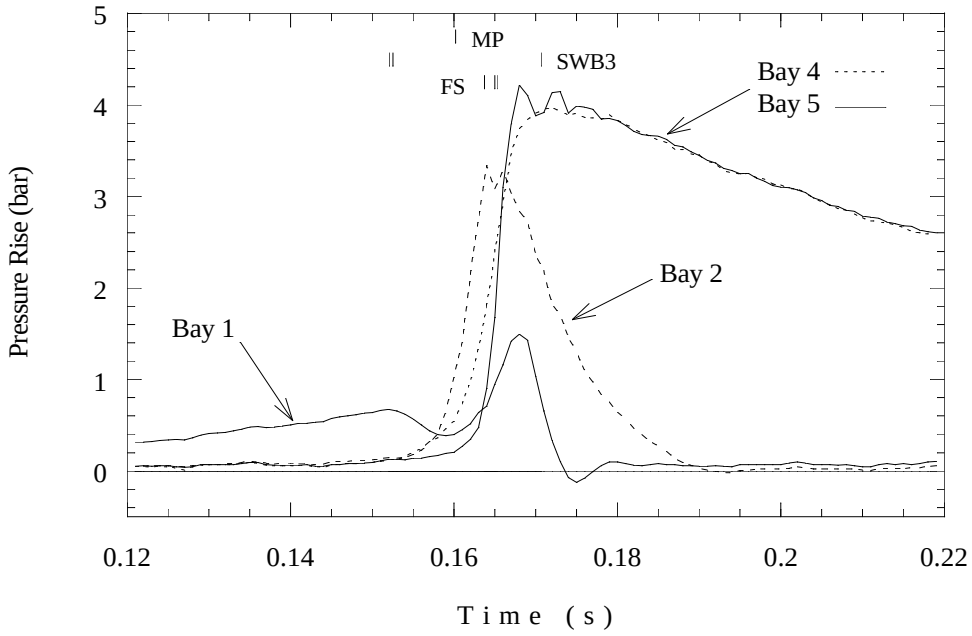

Figure 5.174: Pressure traces from bays 1, 2, 4, 5, ignition in bay 1, cold liquid Jet A layer. Test 29.

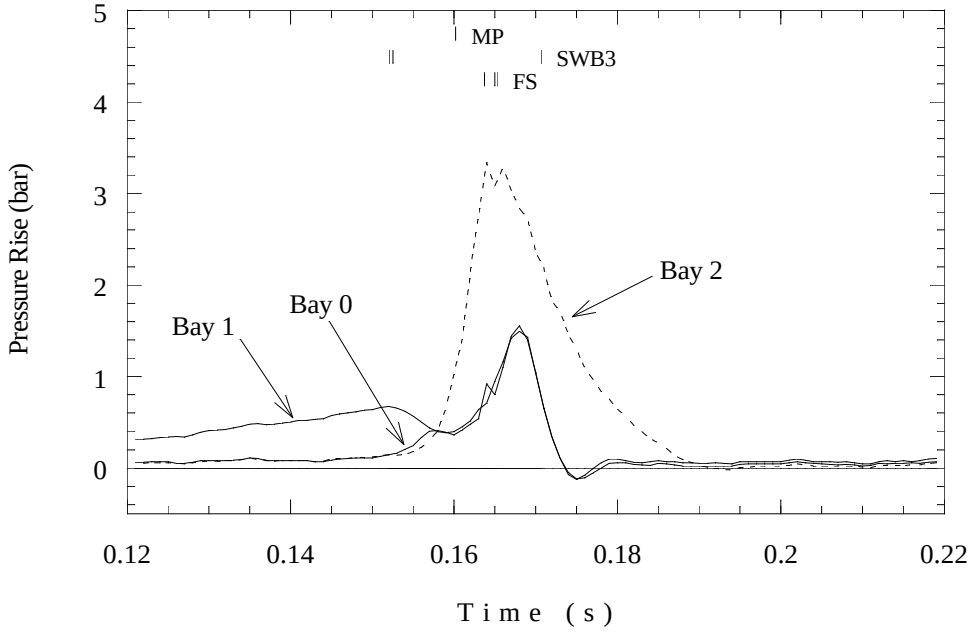

Figure 5.175: Pressure traces from bays 0 – 2, ignition in bay 1, cold liquid Jet A layer. Test 29.

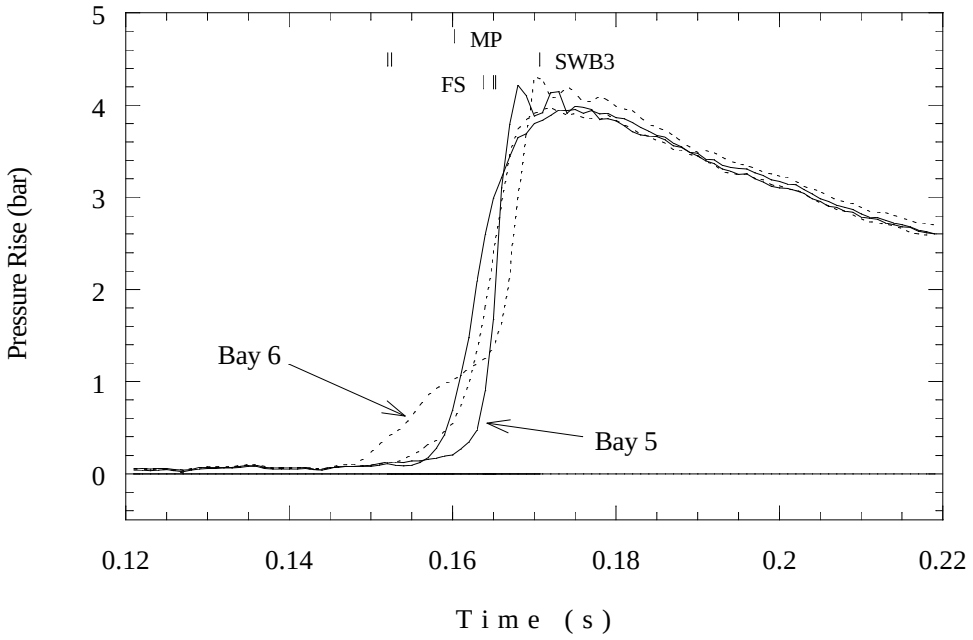

Figure 5.176: Pressure traces from bays 3 – 6, ignition in bay 1, cold liquid Jet A layer. Test 29.

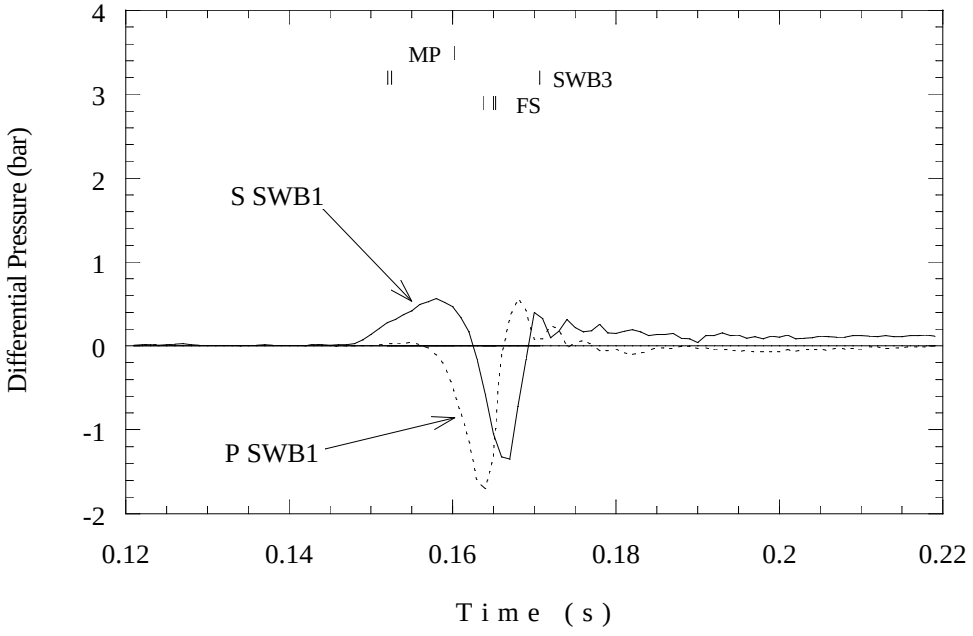

Figure 5.177: Differential pressure across SWB1, ignition in bay 1, cold liquid Jet A layer. Test 29.

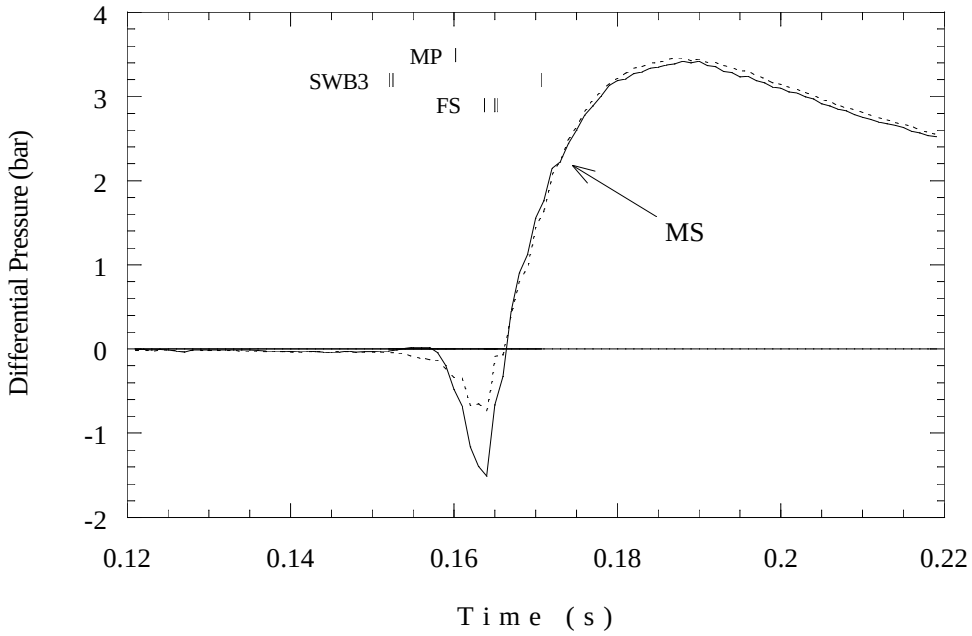

Figure 5.178: Differential pressure across MS, ignition in bay 1, cold liquid Jet A layer. Dashed line indicates port side. Test 29.

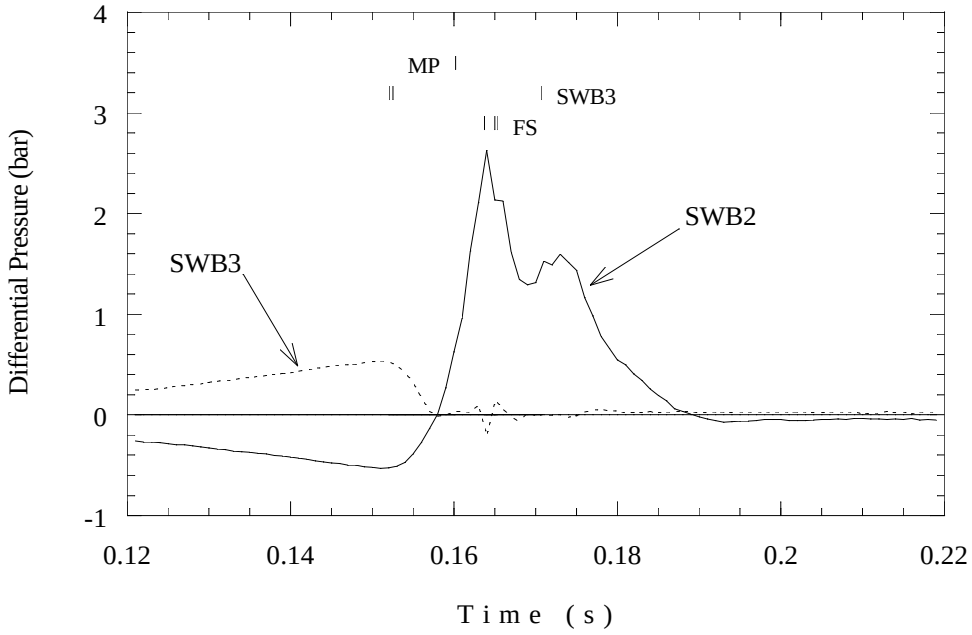

Figure 5.179: Differential pressure across SWB2 and SWB3, ignition in bay 1, cold liquid Jet A layer. Test 29.

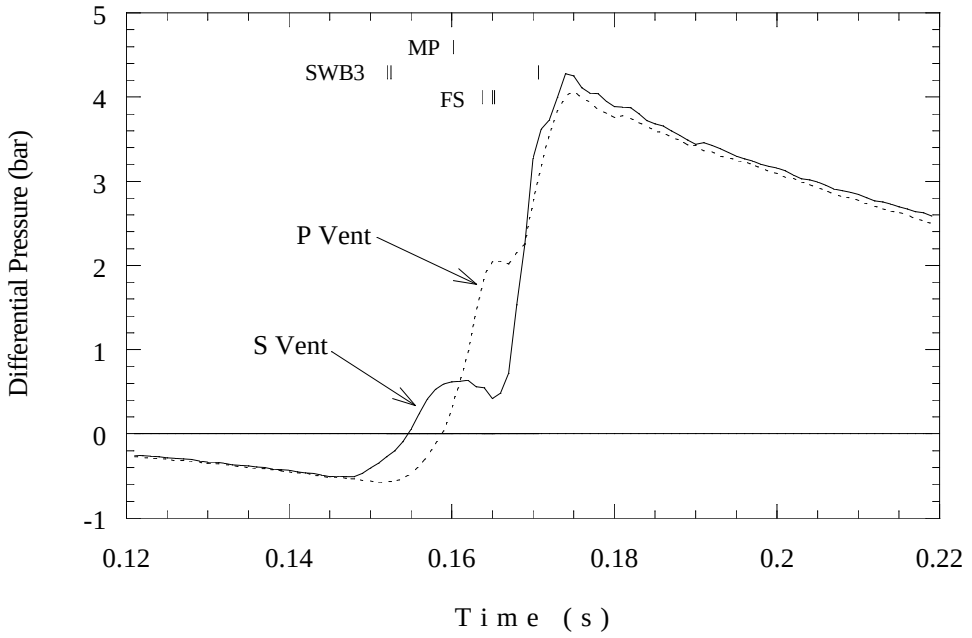

Figure 5.180: Differential pressure across vents, ignition in bay 1, cold liquid Jet A layer. Test 29.

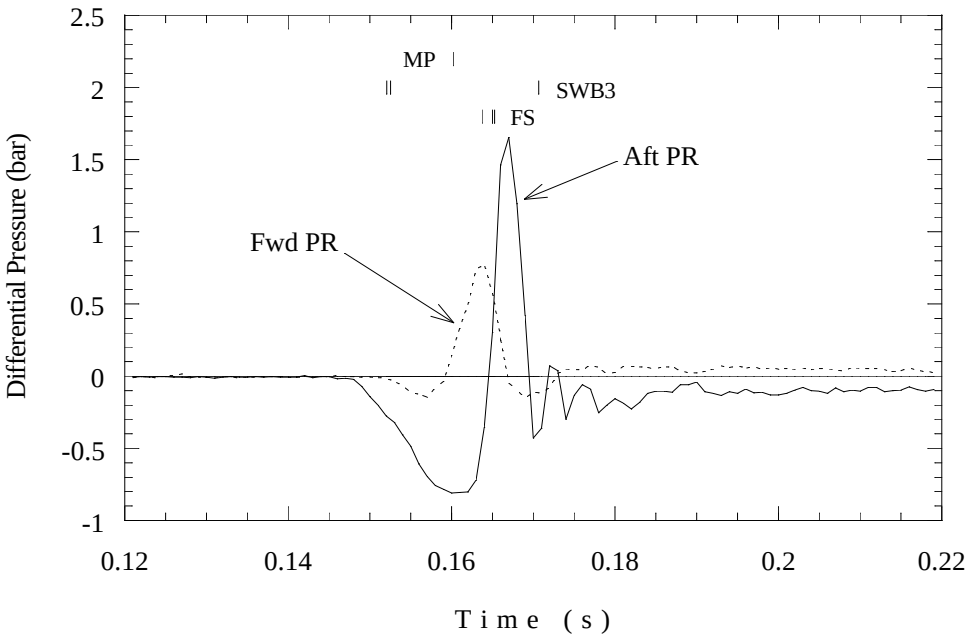

Figure 5.181: Differential pressure across PRs, ignition in bay 1, cold liquid Jet A layer. Test 29.

Table 5.41: Flame arrival times (ms), Test 29.

Photodetectors

146	162
151	155
157	
161 **IGN**	
161	

Thermocouples

150	163	165	165
162	165	163	164
162		160	
92 **IGN**		114	

5.5 DELTA Test (Test 30)

Test 30 was carried out with a scale-model cargo bay attached to the front of the tank. The part-strong configuration was used except that the FS was omitted. Ignition was in bay 5 with the standard (8.4%) fuel concentration and a layer of cold liquid Jet A.

In all of the previous tests, the end of the fuel tank was open to atmosphere, allowing any ejected jet fuel and combustion products to expand freely. This resulted in a fireball and shockwaves in the atmosphere, but did not give an indication of what the pressure would be in the cargo bay. To examine this issue, a steel box was added to the forward end of the tank to simulate the open volume of the cargo bay (i.e., excluding cargo containers).

The open volume of the cargo bay in the 747-100 was estimated by assuming that the cargo bay was half-full of cargo containers (the situation in TWA 800). The total volume was computed by approximating the cargo bay as extending from station 520 to 980 (Boeing reference coordinates) with a cross section identical to the CWT tank, i.e., approximately 6 ft $\times$ 20 ft. This roughly approximates the lower portion of the fuselage beneath the cabin floor. A closer estimate would require accounting for the details of the cargo bay construction. For the purposes of evaluating the pressure wave and enhanced pressurization due to liquid Jet A combustion, the present estimate was considered adequate. A total volume of 4560 ft^3 was computed in this fashion. If half of this volume (2280 ft^3) is considered as free, then a 1/4-scale model cargo bay should have a volume of 35.6 ft^3, slightly smaller than the total volume (37.5 ft^3) of the 1/4-scale tank (this includes the CWT). The actual volume used was 43.3 ft^3.

Table 5.42: Motion detector breakaway times. MP only has one breakwire. N/R, not recorded.

	Top Left	Top Right	Bottom Left	Bottom Right
Test 30				
MP	110.77			
SWB3	105.17	105.63	N/R	N/R

The cargo bay was constructed of 0.5-in thick steel sides, and one end was closed with a 0.075-in thick steel sheet, which we expected would remain intact until the pressure difference reached 20 to 30 psi. The inside dimensions of the cargo bay box were 57.75 in wide by 18 in tall, with an overall length of 72 in. The open end was slid into the "socket" created by the main beams, so the cargo bay would be open to the FS, as shown in Fig. 5.182. Because of fillet welds conecting the tank top and bottom plates to the main beams, it was not possible to butt the cargo bay up against the top and bottom plates of the center tank and create a tight seal. A gap of about 0.25 in remained. This was filled with three layers of the foam tape that was also used on the windows. The windows overlapped the sides of the cargo bay by 0.5 in, so the foam tape was used there in the same manner as it was on the sides of the tank. The forward end of the cargo bay was supported by a simple truss and adjustable jacks to provide leveling. The cargo bay was retained by four steel load chains looped around the vertical posts supporting the tank model. The chains were rated to 15,000 lbs tensile strength, and were

tightened by ratcheting load binders with a capacity of 9,000 lbs. These ratings would allow the system to withstand a 30 psi load, which was the maximum expected pressure on the end plate prior to failure.

Table 5.43: Time-of-arrival at the photodetector locations for the DELTA test series.

Test	L1 (ms)	L2 (ms)	L3 (ms)	L4 (ms)	L5 (ms)	L6 (ms)	L7 (ms)
30	88	86	87	95	96	93	109

For instrumentation, the cargo bay was outfitted with two static and four dynamic pressure gauges. These were relocated from the aft portions of the tank in such a way that there would be at least one pressure gauge remaining in each bay. That is, in the half-bays (3 – 6), where there is only one dynamic gauge, only one gauge was removed. The gauge numbers used and their location in the cargo bay is shown in Fig. 5.183.

In earlier tests, substantial damage was caused by the collision of the FS, and particularly the water bottles, with objects outside the tank. This raised concerns for this test since the water bottles might tear through the thin end plate of the cargo bay before fuel-air combustion was completed. Several alternatives were considered, including using disintegrating, sand-filled bottles that would provide a blunt impact force, versus the sharp corners of the pipes. In the end, we decided to eliminate the FS and water bottles altogether. We were also concerned that SWB3 would move forward flat, like a piston, preventing adequate lofting. This was prevented by removing the plugs and motion switches from the bottom plate mounting holes and inserting the 1/2-in cap screws that were used to mount the strong partitions. These would temporarily restrain the bottom of SWB3, causing the top to rotate forward as it had during TWA 800. This worked well in the test.

The end of the cargo bay did not rupture during the test. Two small dents were visible in the end plate, from the impact of SWB3. After the test, the top and bottom plates were observed to have permanent deflections of about 3 in. Post-test photos are shown in Figs. 5.184 and 5.185.

The slow pressure traces from this test are shown in Figs. 5.186 – 5.188. Some bays are not represented since slow gauges from bays 3 (gauge S3) and 5 (gauge S1) were moved to the cargo bay. Although there were PCB gauges in those bays, there were significant thermal effects on these signals and the traces are unreliable. Therefore, pressure data is not presented for these bays. Because of this missing data, differential pressures will not be calculated for this test. Note that with the exception of the missing FS, the configuration of the tank is the

Table 5.44: Time-of-arrival data for the thermocouple locations for the DELTA test series.

Test	T1 (ms)	T2 (ms)	T3 (ms)	T4 (ms)	T5 (ms)	T6 (ms)	T7 (ms)	T8 (ms)	T9 (ms)	T10 (ms)	T11 (ms)	T12 (ms)
30	91	55	82	86	100	106	100	100	118	118	110	-

Figure 5.182: Setup of cargo bay for Test 30.

same as Test 28. Up until the point where SWB3 ruptures at 105 ms, the pressures in the two tests should be similar. Inspection of the results of Test 28 indicates that this is reasonable as long as a difference of about 10 ms in the onset of rapid combustion is accounted for.

Figure 5.186 shows traces from bays 2, 4, and 6. The pressure traces are typical of bay 5 ignition, with a slow, smooth rise in bay 6, followed by delayed ignition and a sharp jump in bay 4 pressure. Bay 2 reaches a peak of 2.4 bar, while the MP ruptures shortly before this, at about 110 ms. The peak pressure in bay 2 is lower in this test than in Test 28, probably due to the lack of confinement associated with the missing FS.

Pressures from bays 0 and 1 are shown in Fig. 5.187. SWB3 fails at 105 ms, shortly before the pressure in bay 1 reaches a peak of 1.2 – 1.3 bar. Failure of SWB3 results in the pressure traces from bays 1 and 0 coalescing at 110 ms. The rupture of SBW3 sends pressure waves into bay 0 and the model cargo bay. These waves reverberate within the tank and cargo bay, thus pressurizing the cargo bay. In Fig. 5.188, the time and pressure scales have been expanded to show the shockwaves. These waves are not well resolved by the Endevco gauges due to the slow rate of recording and the thermal protection system. Very well-defined shockwaves are visible on the PCB traces. The timing of the pressure pulses indicates that it takes about 6 ms for the waves to travel from bay 0 to the end of the cargo bay, corresponding to the speed of sound in the air, about 330 m/s. The peak pressures on the Endevcos reach 1.3 bar, with an average of about 0.9 bar.

Inspection of the PCB data (Figs. 5.189 and 5.190) indicates that a precursor shock with an amplitude of about 0.5 bar initially travels forward into the cargo bay (see PCB No. 05 and

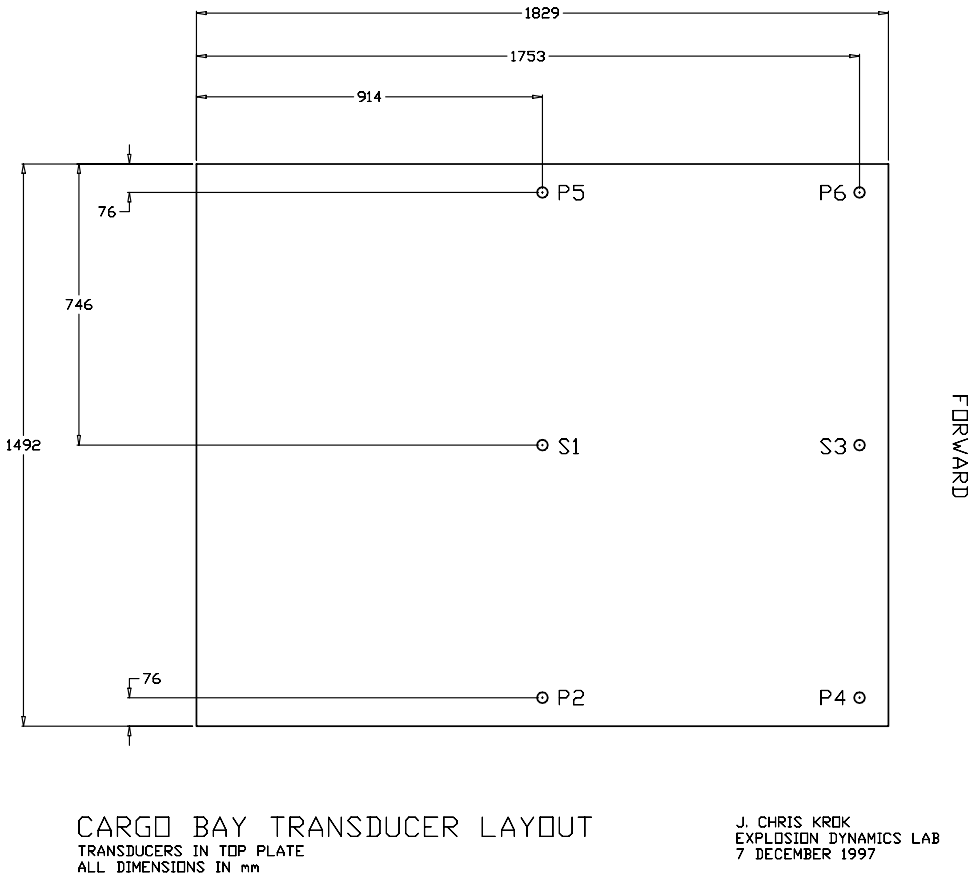

Figure 5.183: Gauge numbers and locations in top plate of cargo bay. Test 30.

No. 02 traces). After this wave reflects, the amplitude approximately doubles to about 1.0 bar. Since PCB gauges No. 06 and 04 are very close to the end wall, the incident and reflected waves cannot be distinguished and only a single 1 bar amplitude wave is seen initially. The series of shock waves associated with the reverberation within the tank are clearly visible on the PCB traces. Note that the peak amplitude is fairly constant despite the venting out of the gap between the cargo bay and tank.

All cameras were operational during this test. Upon ignition in bay 5, we see the typical smooth flame growth followed by rapid, turbulent combustion in bay 6 once the flame passes through the large hole in the aft PR. Fuel lofting is also visible, caused by venting of bay 5 through the bottom passages in the aft PR. As the gaseous fuel in bay 6 burns to completion, the liquid is lofted and burned, obscuring the view. In bays 3 and 4, fuel lofting begins about 24 frames after ignition, as the flame in bay 5 approaches SWB1. This lofting is probably in bay 3. The flame first appears at 41 frames after ignition, rapidly engulfing the bay. It is not possible to determine when the flame passes from one bay to the other. The gas fuel combustion is very rapid, and the jet fuel combustion immediately obscures the view. In bay 2, fuel lofting begins only a few frames before the flame enters the bay at the bottom. This bay is also rapidly engulfed and blocked by fuel combustion. Bay 1 events are interesting during this test. Lofting

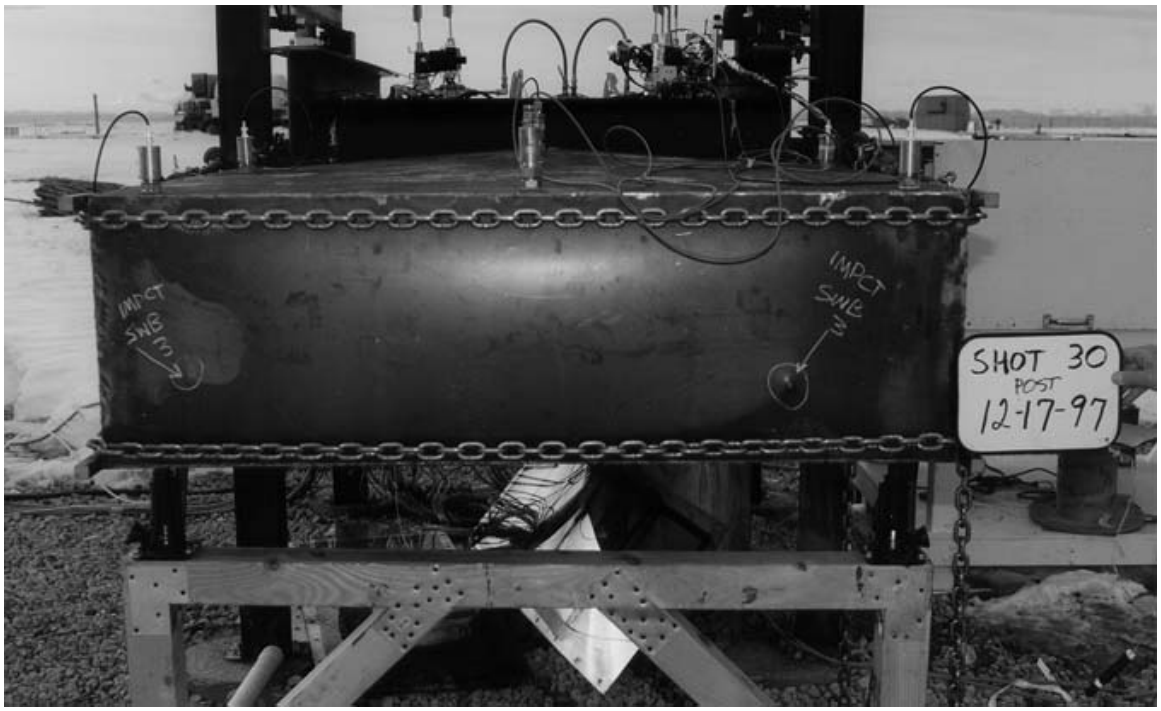

Figure 5.184: End of cargo bay after Test 30. Note that the end plate is bulged, and two dents are present from impact of SWB3. The top and bottom plates of the cargo bay are bulged out approximately 3 in at the centers of the open end.

begins concurrently with entry of the flame from a lower or bottom passageway in SWB2. In the next frame, a dark jet is seen shooting out of one of the vent stringers. In frame 3, the dark material is gone, but a gaseous flame is left in its place. In frame 4, another dark jet enters from the vents, presumably from the opposite side. Any flame from this jet is obscured by the first one. The bay is then engulfed in flame, but the jet fuel is still within the bottom few inches of the bay. By frame 10, the MP is ruptured, and fuel lofting begins in earnest. Judging by the motion of the MP pieces, SWB3 has also failed, and this contributes to lofting in bay 1. The bay is then obscured.

The exterior side-view camera was zoomed out to include the cargo bay in its field of view, so it is harder to see details in the fuel tank. The whole tank is involved and SWB3 is failing by 41 frames after ignition. Lofting begins in bay 3 one frame before it appears in bay 6, and begins in bay 2 a frame after that. As for the dark jets from the vent stringers in bay 1, the first one does not show any self-luminous flame from jet fuel. The second one does, but this may be coincidental with the gaseous flame initiated by the first jet. (Flames from the gaseous fuel are not typically self-luminous; the jet fuel produces an orange flame under these conditions.)

SWB3 fails first at the top and rotates forward, indicating that the bottom “trip” bolts worked as planned. Shortly after the failure of SWB3, the top and bottom plates of the cargo bay snap outward from the pressure, throwing the transducer cables on the top plate in the air. Since the open end is not reinforced, this unfortunately breaks the seal between the cargo bay

Figure 5.185: Interior of cargo bay after Test 30 (starboard window removed). SWB3 rebounded from the far end and came to rest back in the fuel tank.

and the tank. A tongue of fire forms under the cargo bay, probably from jet fuel that remained on the floor of the tank and was blown out of the bottom opening. This lower flame turns into a flame jet, and is joined by one of equal strength on the top surface. The flames extend several feet beyond the end of the cargo bay, as seen in Fig. 5.191 (taken by one of the Nikon cameras). Fortunately, the flames were of short duration, and the transducers were in protective housings, so they were not damaged. (The flame jet lasted for less than 2 seconds.) The jet also blows the airborne transducer cables forward.

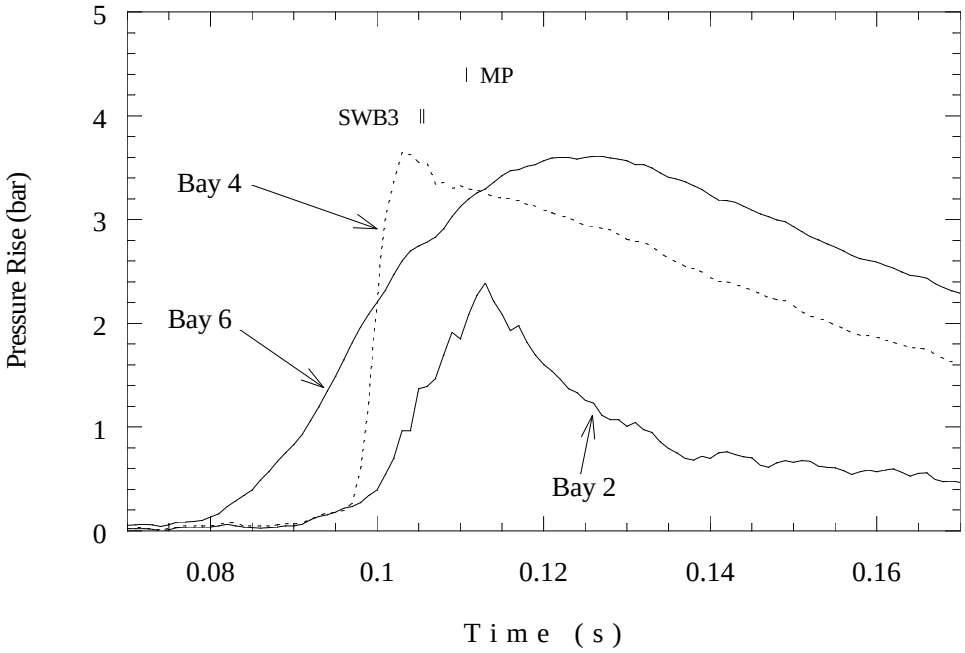

Figure 5.186: Pressure traces from bays 2, 4, 6, cargo bay test. Test 30.

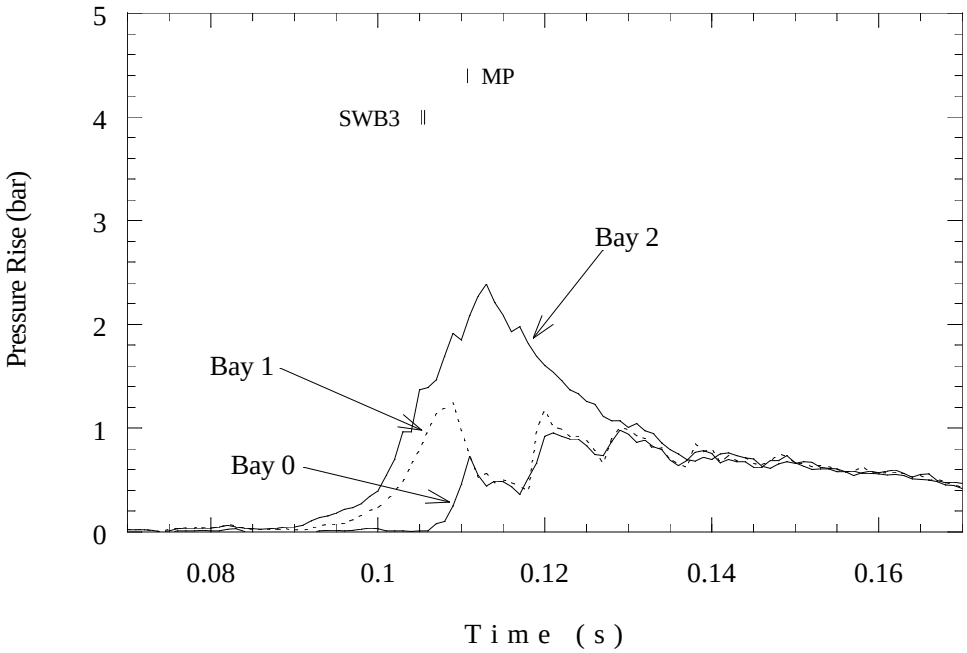

Figure 5.187: Pressure traces from bays 0 – 2, cargo bay test. Test 30.

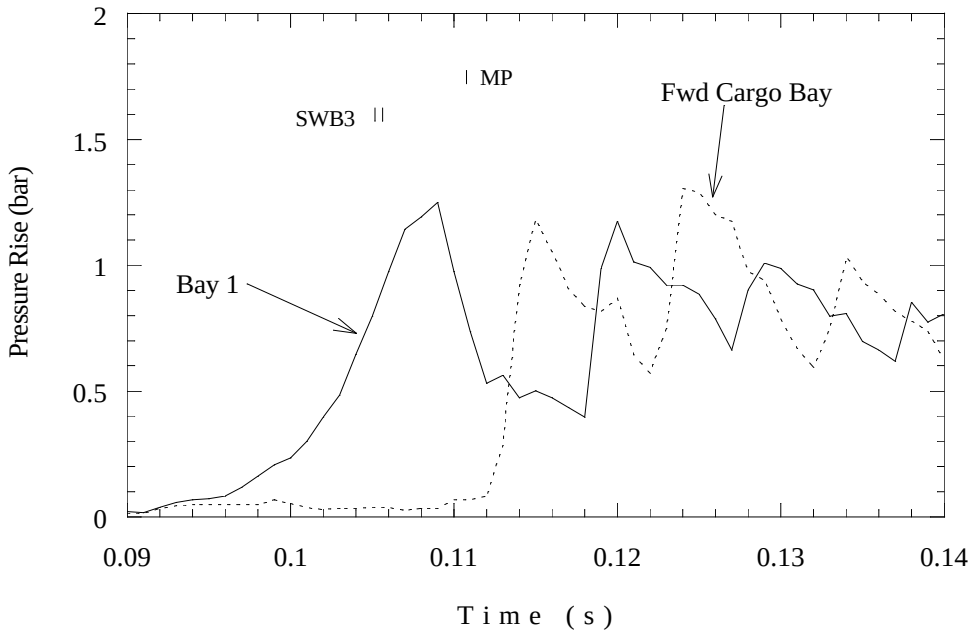

Figure 5.188: Pressure traces from bay 1 and forward end of cargo bay, showing wave reverberations. Note that both axes are expanded on this plot for clarity. Test 30.

Table 5.45: Flame arrival times (ms), Test 30.

Photodetectors		Thermocouples			
86	88 **IGN**	86	82	55 **IGN**	91
95	87	100	100	106	100
96		118		118	
93				110	
109					

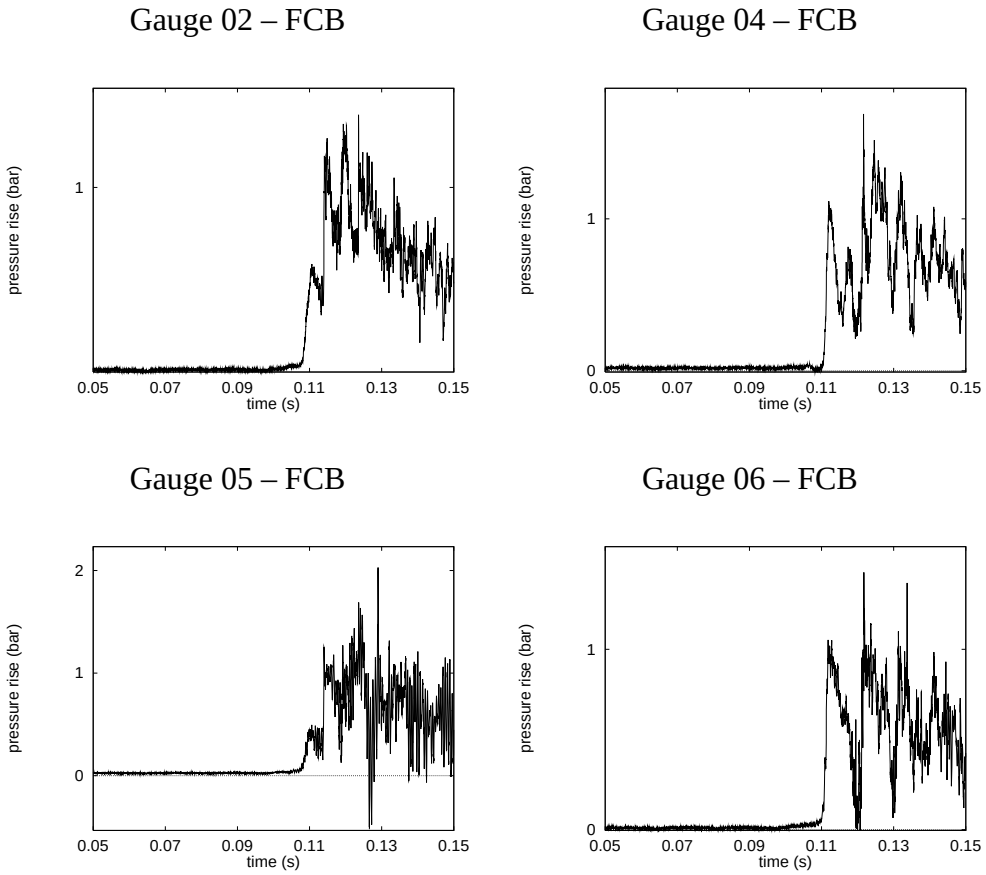

Figure 5.189: Signals from PCB gauges 2, 4, 5, and 6, all located in the foreward cargo bay (FCB) model. Test 30.

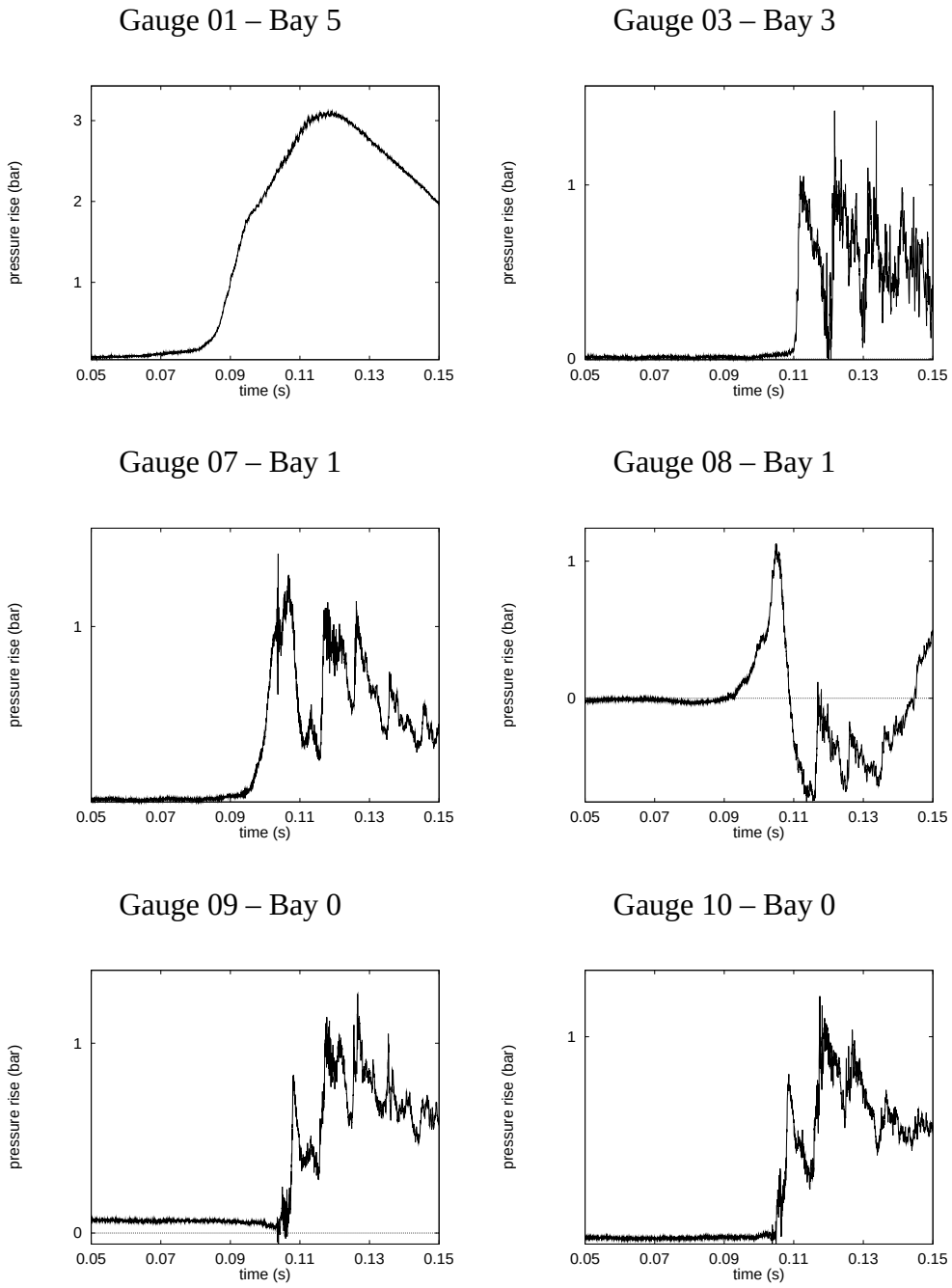

Figure 5.190: Signals from PCB gauges 1, 3, 7 – 10; all located inside the tank model. Test 30.

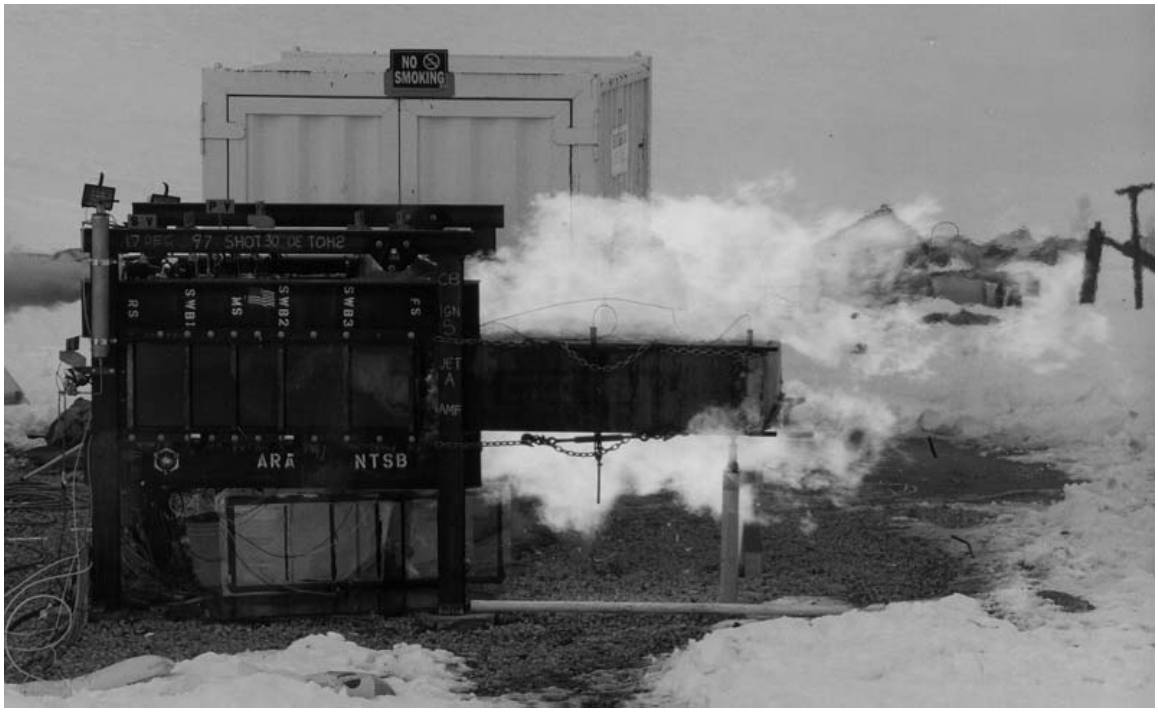

Figure 5.191: Flame jets exiting gaps created by deformation of top and bottom of cargo bay. Test 30.

Chapter 6

Data Analysis II: Comparisons

In this chapter, results from different tests are compared. We examine the effect of various parameters: different facilities; the number of compartments; the role of venting during combustion; ignition location; partition failure; liquid fuel; cargo bay.

6.1 1/4-Scale Tests vs. HYJET Simulant Tests

The HYJET series of tests used a hydrogen/propane mixture to simulate the combustible fuel vapor produced by evaporation of Jet A at 50°C. This simulant mixture was developed in the HYJET facility at Caltech and those tests are discussed in the test plan report (Shepherd et al. 1997b). The simulant was chosen so that tests could be run at nominal Denver, Colorado atmospheric conditions ($T = 25\,\mathrm{deg C}$, $P = 843$ mbar), and simulate the combustion of jet fuel vapor at 50°C and 14 kft altitude (585 mbar). Comparison of pressure traces from HYJET experiments with the simulant mixture in the 1/4-scale facility (Test 11) is shown in Fig. 6.1. Excellent agreement is seen in peak pressures and burn rates (proportional to the slope of the pressure-time curve), with some variation between the traces near the end of the burn (0.4 to 0.5 s). The variations are due to the differences in internal geometry of the vessels, which affects the shape of the flames. Despite different ignition systems and geometeries in the two facilities, the pressure traces are very similar. A longer-time-scale plot illustrating the cooling of the combustion products is shown in Fig. 6.2. The cooling time constants for the two facilities are very similar since the volumes and surface-to-volume ratios for these particular configurations are similar.

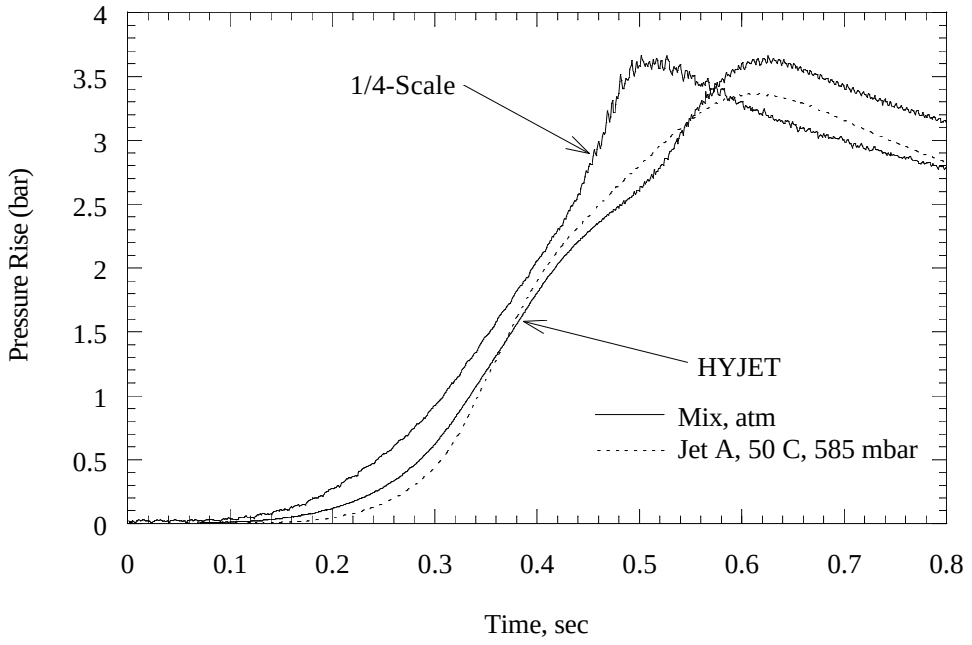

Figure 6.1: Comparison of pressure traces for explosions in the 1/4-scale (1 bay, Test 11) and HYJET facilities. The HYJET simulant test was run at 25°C and 843 mbar (run 484), while the Jet A test was at 50°C and 585 mbar (run 470).

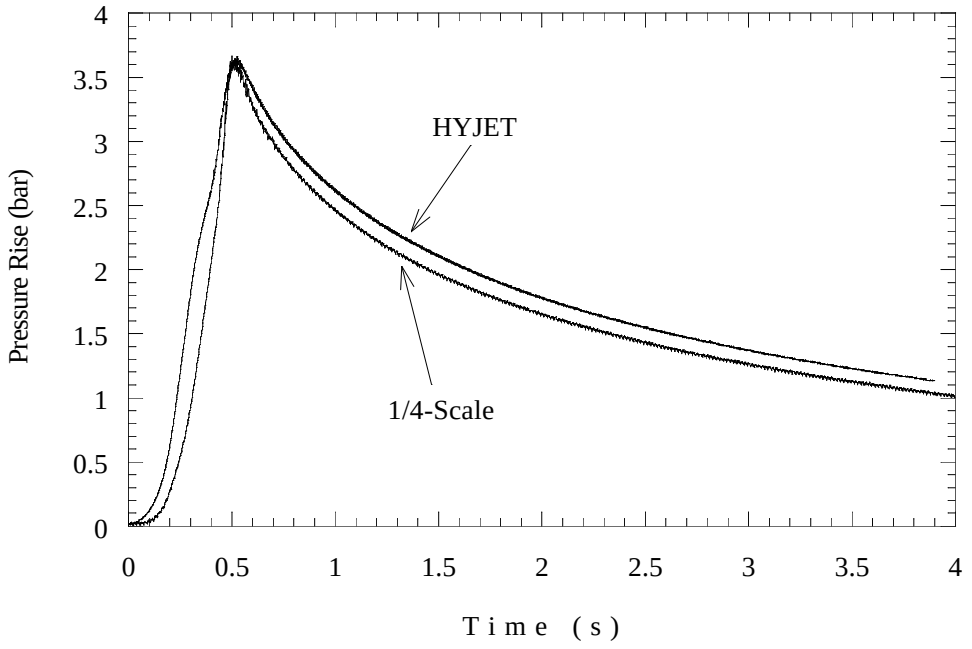

Figure 6.2: Comparison of 1/4-scale and HYJET pressures during the burn and cooldown processes. The trace from HYJET has been shifted to the left by 100 ms in order to compensate for timing differences in the data acquisition systems.

6.2 Ignitors: Match vs. Filament

(Comparisons of Tests 1 and 11.) The first three tests (1, 2, and 3) used an electric match as the ignitor. Schlieren photography of the first test showed that the match fragmented into a number of pieces, creating a large, distributed ignition source. This resulted in a faster pressure rise than a single-point ignitor like an electrical spark or hot wire would provide (Fig. 6.3). In addition, the size of the ignition source was not reproducible so that tests carried out with match ignition were difficult to compare.[1] Furthermore, the matches were classified as pyrotechnic devices and required special handling precautions.

For these reasons, the electric match was replaced with a filament from a Type 1156 automotive tail-light bulb, the glass envelop of the bulb having been removed prior to the test. We continued to use the same electrical circuit as used with the matches. Discharge of the charged capacitor into the bare filament produced a rapid temperature rise that quickly ignited the mixture. Timing tests indicated that the delay from capacitor discharge until ignition was minimal, less than 100 μs. Separate tests at Caltech (Kunz 1998) on ignition of both the simulant mixture and Jet A vapor showed that reliable ignition was accomplished in this fashion. The pressure time curves from spark and filament ignition were comparable.[2] Visual observation in each of the 1/4-scale experiments demonstrated that the filament ignited the mixture reliably and always created a small laminar flame ball, as shown in Fig. 6.4. Starting with Test 4, the filament was used in all subsequent tests for both the main and backup ignitor.

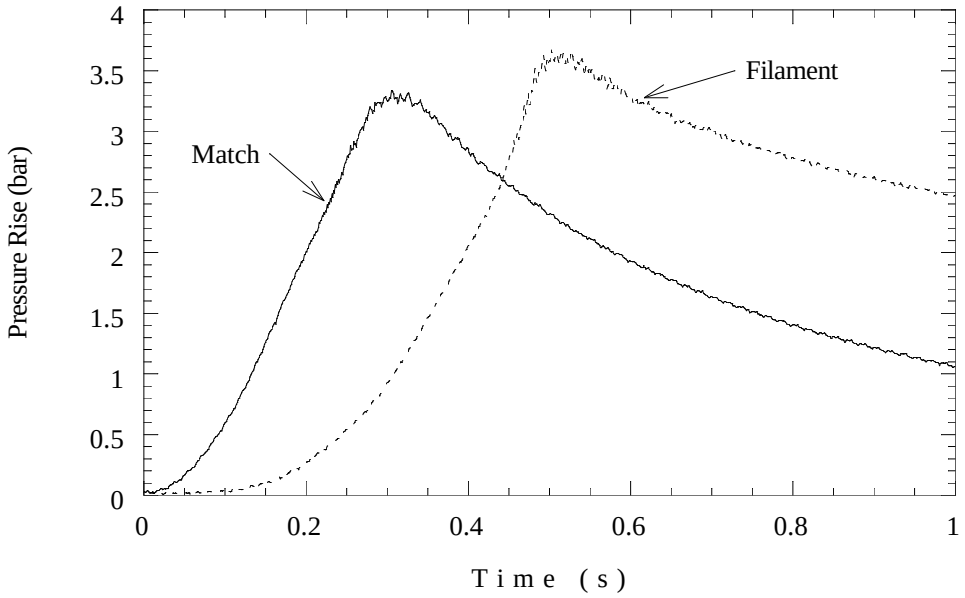

Figure 6.3: Comparison of pressure traces from match (Test 1) and filament (Test 11) ignition, one bay.

[1] We thank Kees van Wijngerden of CMR for pointing out this issue and discussing the experiences at CMR with match ignition.

[2] We thank Oliver Kunz and Ulrich Pfahl of Caltech for carrying out these tests on short notice.

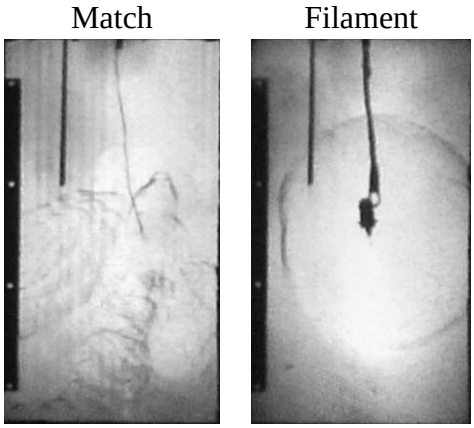

Figure 6.4: Schlieren images of match and filament ignition.

6.3 Number of Compartments

(Comparisons of Tests 11, 10, 9, and 25.) This section summarizes the results of the ALPHA test series, in which the number of bays was increased from 1 to 6 by adding partitions. Ignition was in bay 5 for this set of tests. Figure 6.5 compares the bays with the highest peak pressure from each configuration. The three-bay configuration is not included, as the sympathetic dual ignition[3] in Test 3 rendered the comparison invalid. We see that, as a container is compartmentalized, the burn rate and peak pressure increase with increasing number of compartments or bays.

All instruments and visual observations demonstrate that it is the turbulence generated by flow through the passageways that causes the increase in burn rate with the number of compartments. Clearly the most dramatic effects result from the addition of a single partition. The time at which the peak pressure occurs drops from 0.5 to 0.25 s but more significantly the peak rate of pressure rise increases by a factor of 50. Addition of two more partitions further increases rate of pressure increase slightly and further decreases the time to peak pressure. In the two-bay test, the time and value of the peak pressure was the same in both bays; with four bays, the highest peak pressure occurred in bay 1, 0.1 bar higher and 10 ms earlier than the others.

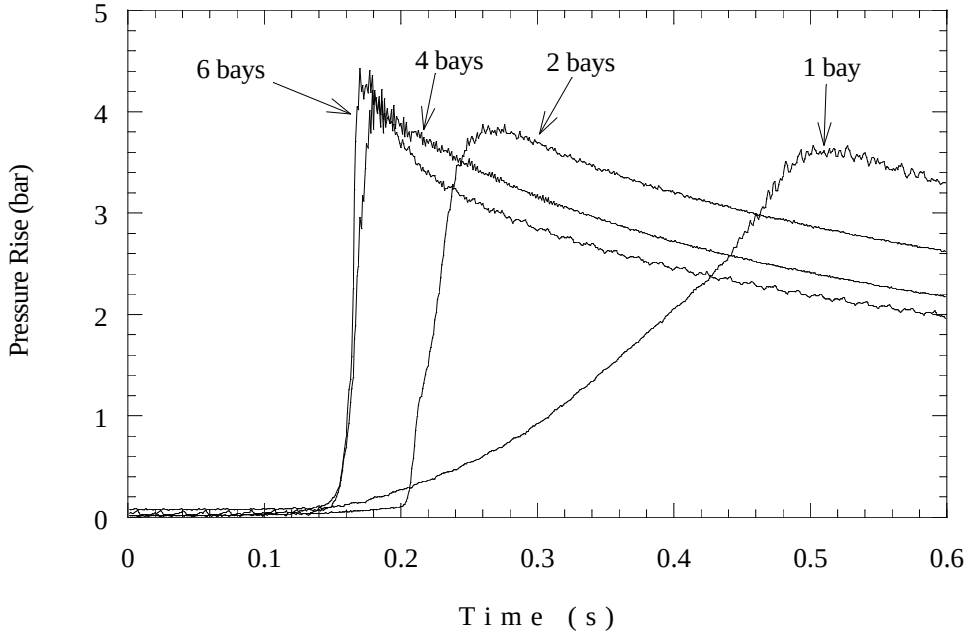

Figure 6.5: Effect of number of bays on pressure history. For each configuration, the bay with the highest peak pressure was chosen to represent the configuration.

There are only minor differences between the peak pressure plot for the four- and six-bay tests. This is not unexpected since the six-bay configuration is created by subdividing the

[3] A match backup ignitor was used in this test and the electrical transient created when the filament was heated also initiated the match. Visual observation and separate electrical tests confirmed this effect.

back two bays by inserting the partial rib models. While this does introduce some additional flow passageways, it apparently does not significantly affect time to peak pressure. The peak pressure for the four- and six-bay cases with ignition in bay 5 occurred at 0.16 to 0.18 s. While 0.16 s was a nominal burn time for the six-bay configuration, this value is influenced by igniter location and other factors such as motion of the model beams and spars.

In the four-bay test, the bay farthest from the ignitor had the highest pressure, and it peaked *first*. In the six-bay test, the highest pressures were found farthest from the ignitor, but they peaked later than the other pressures. Another feature of the of six-bay configuration was the pattern of combustion in the back four bays. Bay 4, which is diagonally across from the bay 5 ignitor, generally showed the highest peaks and quickest burns of the aft bays.

6.4 Single vs. Multi-Hole MS

(Comparisons of Tests 12 and 10.) In the ALPHA series, two tests were run in the two-bay configuration: Test 10 used the standard MS, while Test 12 used a special MS that would be easy to model and could be used to validate numerical simulations. The special MS had a single 2-in diameter hole in the center, which yields a total flow area equal to the summation of the passage areas in the standard MS. In addition, the vent stringers were plugged, so the hole in the MS was the only flow path from one compartment to the next.

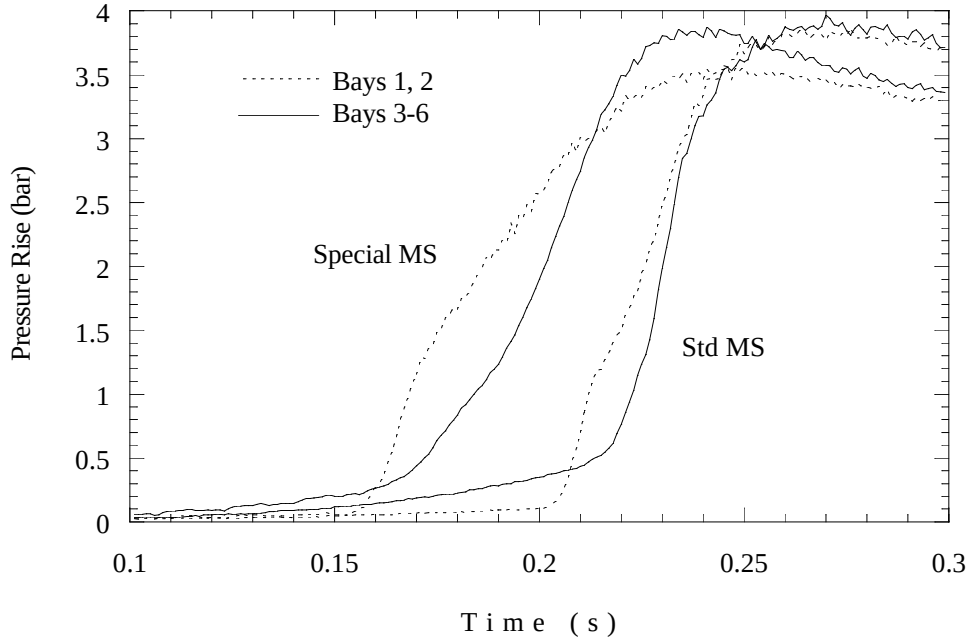

Figure 6.6: Comparison of two-bay tests, standard MS vs. special validation MS.

It is not clear why the pressure rise occurs earlier for Test 12 than for Test 10, but this may be due to the higher mixture temperature in Test 12 (32°C vs. 25°C). Another possibility is that there are greater flow losses through some of the holes in the standard midspar than in the single-hole midspar.

Aside from the 40-ms offset in the pressure traces, the tests are quite similar. Both show a long, slow initial burn in the ignition bay, followed by rapid combustion in the forward bay once it is ignited. With the special MS, the aft bay pressure overshoots the forward bay pressure. With the standard MS, both bays equalize before they reach peak pressure. With the special MS, the aft bay pressure has a higher peak value (comparable to values reached with the standard MS) than the forward bay. The forward bay was also ignited differently in the tests. In test 10, the flame traveled through the vent stringers (presumably the port vent stringer, as this is closer to the ignitor). In Test 12, the only flow path was through the center hole.

The following Test 12 observations were obtained by viewing the video transcriptions of the high-speed camera records. It was difficult to synchronize the film with the pressure trace using the fiducial flash since the video frames do not correspond exactly to the camera frames.

For this reason, the comments are more qualitative than quantitative.

Camera 1 (Bays 5 and 6) — not working

Camera 2 (Bay 3 and 4)

The flame appears to propagate with a hemispherical front containing weak cellular instability. A teat appears where the flow is elongating the flame as it is sucked into the hole. Just after the flame goes through the hole, the flame becomes very turbulent downstream and then also upstream. This might be due to the back flow through the hole which happens at about 160 ms, only about 5 – 10 ms after the flame reaches bay 2. The flame in bays 3 and 4 appears to come to a stop and then rapid turbulent burning occurs.

Camera 3 (Bay 2)

The flame appears to jump from the hole in the MS to the front of bay 2/1 almost as soon as it reaches the hole. The flame then burns back from bay 1 toward the hole. Streaming from bay 2 through the hole into bays 3 and 4 is visible within 5 – 10 ms, even before the flame has burned completely back to the hole. The flame is either laminar (unlikely) or else completely burned out in bays 2 and 3 at approximately 185 ms (within 15 – 20 ms after the flame passes through the hole) and the flow is quite turbulent in bays 3 and 4.

Camera 4 (Bay 1)

Center of the film is slightly overexposed. Passage of combustion through the center of the tank is barely visible. Within 5 – 8 ms, rapid turbulent combustion propagates from the front of bay 1 back toward the MS. This burns out within 25 ms.

The second crossover (between forward and aft traces) in pressure (210 ms) appears to be due to flow backward, the combustion complete at this point.

6.5 Vented vs. Unvented

(Comparisons of Tests 4 and 25.) These two tests were intended to be replica tests (repeat tests with all conditions duplicated as closely as possible) except that the vent stringer exits were open to atmosphere in Test 4, while they were closed in Test 25. Both tests were identical otherwise, using the six-bay, all-strong configuration with ignition in bay 5.

The pressure traces from each test are compared in Fig. 6.7. In four of the bays (1, 2, 5, 6), the pressure traces are nearly identical, only arriving a few milliseconds later in the unvented test. In bays 3 and 4, the unvented test shows a slightly higher peak pressure than the vented test. It may be possible that the venting gas attenuates the peak pressures in these bays, but this should also yield lower pressures in bays 5 and especially 6, where one of the vent stringers connects. It is more likely that the rapid rise in bays 3 and 4 is strongly dependent on the timing of the flame propagation.

In general, we conclude that the gas vented to the atmosphere has little or no effect on either the timing of the combustion events or values of the peak pressures. The effect of venting is apparent on a much longer time scale (seconds) after the combustion is complete. Simple estimates of the venting rate using choked flow indicate a maximum flow rate (at the peak pressure) of about 0.2 kg/s, indicating that at most 0.5% of the mass of the tank would be vented during a 0.02-s combustion transient.

The differential pressures (Fig. 6.8) are very sensitive to timing, and the variation in bays 3 and 4 between the two tests result in larger mismatch between differential pressures involving those bays. However, while the amplitudes and timing are different in the two tests, the pressure histories are qualitatively similar. For the differential pressures that do not involve these bays, the results of the two tests are much closer.

These two tests can also be used to get an indication of the reproducibility of these very complex combustion events. To that end, a quantitative comparison of these two tests has been carried out. It is important to keep in mind that Tests 25 and 4 are not exact replicas, so it is premature to judge if the differences are systematic or intrinsic variability. Additional simulations with the vents open or closed, all other parameters remaining constant, would be very valuable in determining how much of this variability is due to vent configuration. Replica experiments are proposed as part of a second series of tests.

6.5.1 Quantitative Comparison Between Tests 4 and 25

Characteristic peak values were extracted from the data files for each test and are compared in Tables 6.1 and 6.2. In Table 6.1 two comparisons are tabulated. The difference in the value of the measured peak pressures (using the Endevco gauges) is given as $P_{25,max}$ - $P_{04,max}$, expressed as a percentage. The difference in the time at which the peak pressure occurs is given as $t_{max,25}$ - $t_{max,04}$, expressed in ms.

In Table 6.2, six comparisons are made based on peak differential pressures and impulses. The differential pressures are computed by taking the difference between pressures in adjacent bays as described in the table. Reported are:

1. The difference between peak positive values of the differential pressures for the two tests, expressed as a percentage.

$$\delta\Delta P_{max} = \Delta P_{max,25} - \Delta P_{max,04}$$

2. The difference between the peak negative values of the differential pressures for the two tests, expressed as a percentage.

$$\delta\Delta P_{min} = \Delta P_{min,25} - \Delta P_{min,04}$$

3. The difference in the time of occurrence of the peak pressures (both positive and negative) for the two tests, expressed in ms.

$$\delta t_{max} = t_{max,25} - t_{max,04} \qquad \delta t_{min} = t_{min,25} - t_{min,04}$$

4. The difference in the peak differential impulse between the two tests, expressed as a percentage

$$\delta I_{max} = I_{max,25} - I_{max,04}$$

where the impulse I is defined as the time integral of the differential pressure.

$$I = \int_0^t \Delta P dt$$

Note that the peak impulses reported in the table are simply the largest value obtained within the initial 200-ms analysis period. Even larger values are possible at later times.

5. The difference in the time of occurrence of the peak differential impulses, expressed in ms.

$$\delta t_{I,max} = t_{I_{max},25} - t_{I_{max},04}$$

The following general conclusions can be reached from these comparisons. The peak pressures are reproduced within 10% and the time of occurrence of the peak pressure is reproduced within 20 ms. Although the qualitative features of each pressure differential are replicated in the two tests, there is a substantial amount of variability in the quantitative measures. The values of the peak (max or min) differential pressure can be as much as 90% different between the two tests. The time of occurence of the peak differentials can differ as much as 17 ms. The impulse during the 200-ms period can differ by up to 72%.

These differences should be viewed in the context of previous work on explosoins. This particular explosion is created by a turbulent combustion event in a multi-chambered vessel. It is well known that such events have some intrinsic variability and are not strictly reproducible. In terms of past experience, the pressure histories in Tests 25 and 4 compare very favorably

Table 6.1: Test 4 vs. 25. Comparison of Endevco peak pressure and time-to-peak pressure.

Bay	$P_{25} - P_{04}$ (%)	$t_{25} - t_{04}$ (ms)
6	5	-3
5	2	-12
4	9	-23
3	2	-19
2	7	7
1	3	0

Table 6.2: Test 4 vs. 25. Comparison of Endevco pressure differentials and impulses based on pressure differentials.

Bay	$\delta\Delta P_{max}$ (%)	δt_{max} (ms)	$\delta\Delta P_{min}$ (%)	δt_{min} (ms)	δI_{max} (%)	$\delta t_{I,max}$ (ms)
6-4	90	10	50	8	59	8
5-3	-13	8	58	8	25	6
4-2	51	7	25	17	47	10
3-2	55	7	35	17	55	10
2-1	0	7	19	0	-14	2
1-0	3	0	N/A	N/A	-10	N/A
PR 5-6	-33	5	45	6	-72	4
PR 3-4	66	10	42	7	47	9

and the replica test results would be considered adequate for the purposes of understanding the explosion phenomenology. What has not been done in the past is to quantify the amount of variability observed in the results of replica tests. Since the variability in the results translates to uncertainty in the predicted failure pattern of the CWT, it is important in this program to better quantify the test-to-test variability.

Another important issue is the wide range of possibilities we currently have for fuel distribution and temperature in TWA 800. If we find large differences in test results for which we made only a small change (vent stringers open to the atmosphere vs. closed), this suggests that varying the fuel concentration between compartments should also be carefully examined.

These issues are addressed further in the Chapter 9.

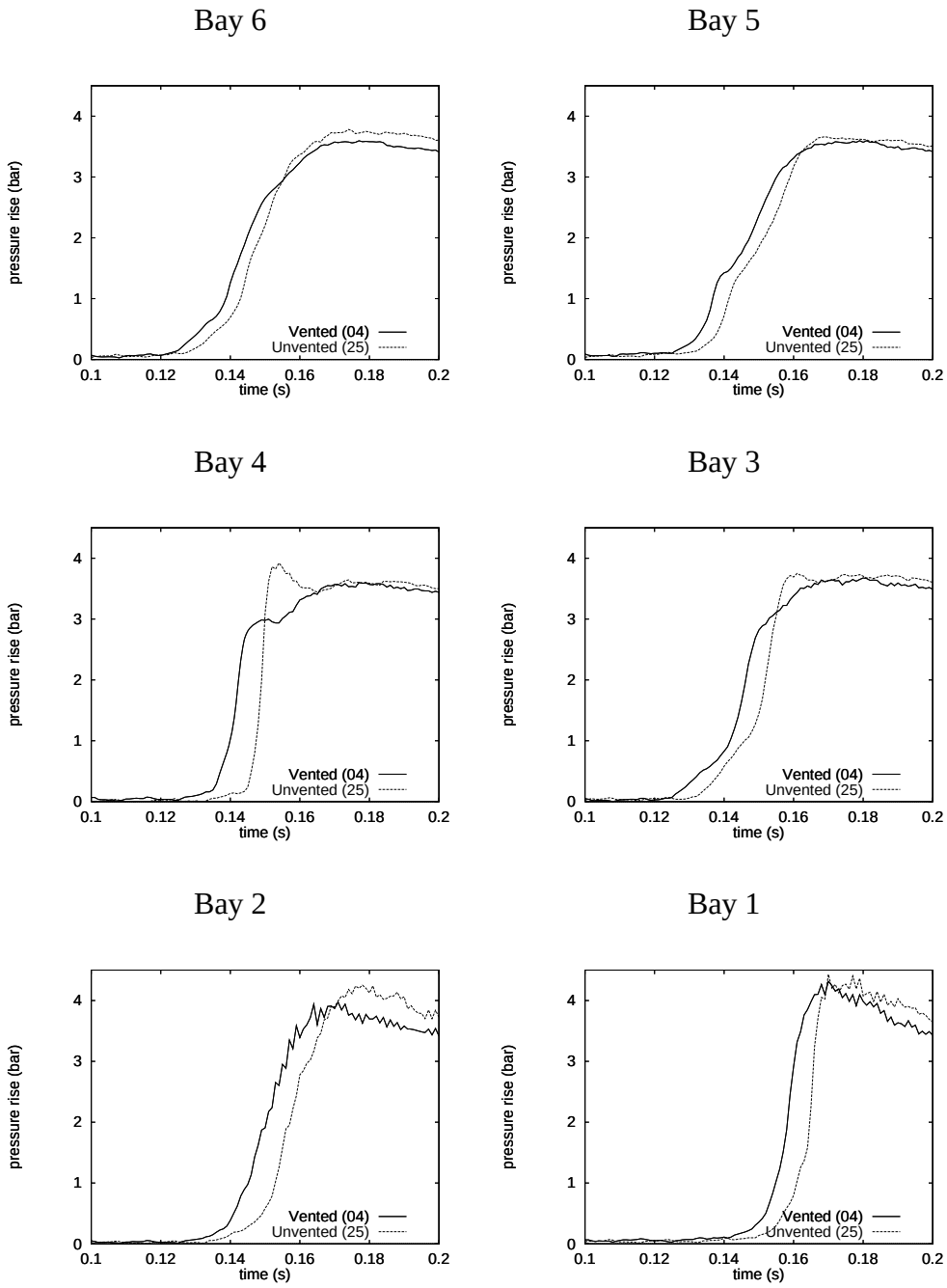

Figure 6.7: Comparison of individual pressure traces, vented (Test 4) vs. unvented (Test 25), ignition in bay 5.

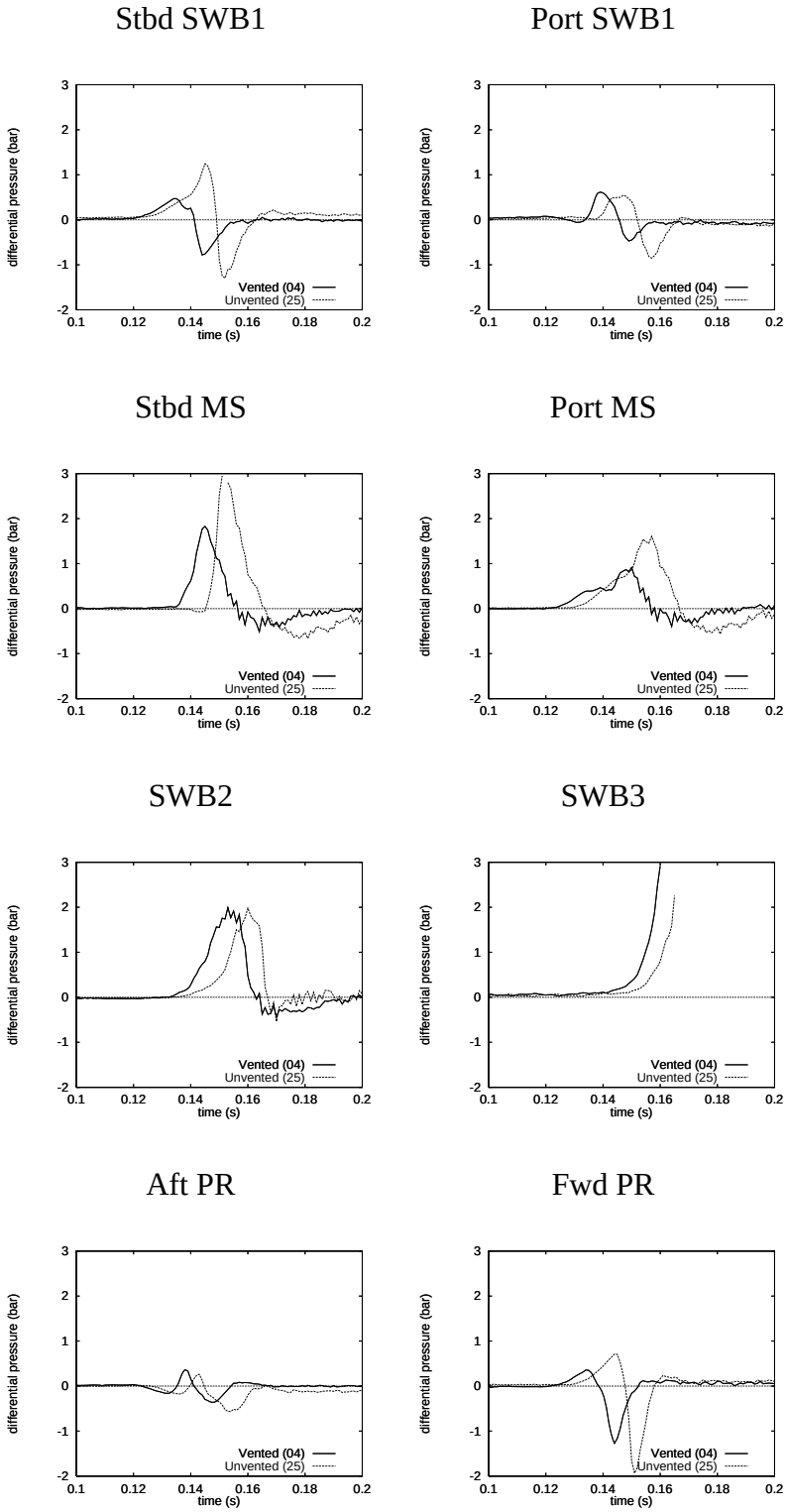

Figure 6.8: Comparison of differential pressures, vented (Test 4) vs. unvented (Test 25), ignition in bay 5.

6.6 Ignition Source Location

One of key goals of the present study was to examine the effect of ignitor location on combustion propagation and the resulting variations in pressure loading on the structural components.

A common phenomenon observed in many tests is the increase in peak pressure associated with pressurization of a bay prior to combustion. Pressurization prior to combustion occurs because of a net inflow of mass associated with flow through the passageways between compartments. When combustion occurs in a pressurized bay, the peak pressure will be higher than for a similar combustion event in a bay that is at the starting pressure. In general, this effect is progressive with distance from the ignitor and is often described as "pressure piling" since the pressure appears to accumulate or pile-up as the flame travels through the tank. For example, thermochemical computations predict that an initial pressure increase of 30% in a bay will result in a peak pressure after combustion that is 1.2 bar higher than for an unpressurized bay. In many of the present tests, pressure piling occurred in the bays farthest from the ignitor. In several all-strong tests, the spread in peak pressures between bays was as large as 0.9 bar.

In the all-strong tests, pressure piling and differences in communication between bays resulted in a distinctive pattern of differential pressures. Placing the ignitor near a passageway also promoted rapid travel of the flame to other bays. In tests with weak partitions, the sequence of partition failure did depend on the ignition location. In the all-weak tests, a substantial reduction of the peak pressure in all bays was caused by the venting process.

Caution is in order when interpreting the results of these tests. Failure of particular partitions in the 1/4-scale model does not necessarily imply failure of the corresponding full-scale structural components. This is due to the differences between the structure of 1/4-scale model and the actual TWA 800 center wing tank. For example, failure of the partial ribs was observed in some tests, however this would not be expected to occur in full-scale CWT with the same peak pressures. This is because the connections to the partial ribs were weaker in the 1/4-scale model than in the actual CWT. Likewise, SWB1 and MS are substantially weaker in the 1/4-scale model than in the full-scale CWT. Because of these factors and other structural issues, the measured pressure differentials must be interpreted using structural analysis in order to make any inference about the failure of the actual tank structure. In addition, there are a number of other considerations such as fuel distribution and temperature that must be addressed either through numerical simulation or modeling.

6.6.1 All Strong

(Comparisons of Tests 4, 5, 6, 7, 15, and 16.) Changes in the ignition location clearly affected the results of these tests, although in all tests, the pressure across SWB3 was 3.7 – 4.2 bar, i.e., enough to cause it to fail. Pressure piling occurred in bays away from the point of ignition. For example, ignition in bay 5 caused piling in bays 1 and 2, while ignition in bay 2 caused piling in bays 5 and 6 and 1. A summary of the peak differential pressures in these tests is shown in Fig. 6.9. Note in particular that ignition in bay 2 appears to produce the lowest overall peak pressure differentials.

The following paragraphs summarize the features of each test. Pressures and pressure

differentials for each test are compared with Test 4 (ignition in bay 5) in Figs. 6.10 – 6.19.

Bay 5 Ignition (Test 4) One unique feature is a rapid pressure rise at about 150 ms in bays 4 and 3. Pressure piling occurs in bays 1 and 2. The highest differential pressure is on the starboard MS, caused by the rapid combustion in bay 4. SWB2 and SWB3 also see large pressure differentials. The peak pressure across SWB3 is 4.2 bar. Following the start of combustion in bay 5, the apparent sequence of combustion within the bays is: 3, 6, 4, 2, and 1.

Bay 3 Ignition (Test 5) There is no static pressure data from bay 1. There was a rapid pressure rise in bay 4, as with ignition in bay 5. No pressure piling was evident in bays 5 and 6, although there is evidence of rapid combustion in bay 5. The initial pressure increases are slower, as if some of the bays are ignited early and burn in laminar fashion before transitioning to turbulence. After bay 3, the apparent ignition sequence is: 5, 6, 2, and 4. There is pressure piling in bay 2, so it probably occurs in bay 1 as well. The peak pressure in bay 2 is about 3.8 bar. Pressure differentials across MS and SWB1 were higher in this test than with ignition in bay 5.

Bay 2 Ignition (Test 6) Pressures in the pairs of aft bays (5/6 and 3/4) increased in a nearly identical fashion. Bays 3 and 4 have nearly the same peak pressure as bay 2, but pressure piling occurs in bays 5, 6, and 1. After bay 2, the apparent ignition sequence is: 3 and 4, 5 and 6, 1. The differential pressure across SWB2 was only about 1 bar in this test. Combustion in bays 3 and 4 created opposing differentials on the enclosing partitions: $+1.25$ bar on MS, and -1.25 bar on SWB1. The peak pressure across SWB3 was 4 bar.

Bay 1 Ignition (Test 7) The PRs failed during this and the following tests, but failure may have been late enough (after the burn) so that PRs can be treated as intact for the purposes of analysis and modeling. Pressures in the aft bay pairs increased in a similar fashion, although early ignition occurred in bay 6, probably due to the vent stringer connection to bay 1. Bay 1 exhibits a long, slow burn, followed by a sudden acceleration and ignition of the other bays at about 200 ms with a rapid combustion transient (5 – 10 ms duration). The highest peak pressure was 4.3 bar in bay 5. Bay 1 reaches only 3.7 bar, which is also the pressure across SWB3. The rapid combustion in the aft bays causes large differential pressures, even though ignition times are very close for each bay. The pressure difference on the port side of SWB1 swings from -1 to 1.25 bar, SWB2 experiences a peak differential of 2.1 bar, and the aft PR reaches over 2 bar (at which point it fails).

Bay 6R Ignition (Test 15) Pressure piling occurred in bays 3, 4, 5, and 6. Bay 3 had the highest pressure in this test, nearly 5 bar. Bays 6 and 5 reached 4.6 bar. It appears that all of the bays on the starboard side (1, 2, 4, and 6) ignited early, since all followed the pressure rise rate of bay 6. This is confirmed by the thermocouple data. The pressure in bays 3 and 5 remained low until about 190 ms, then increased rapidly. The other bays showed slow initial burns with transitions to turbulent combustion in the following order: 6, 4, 2, 1. (Bay 4 exhibited

some small variations prior to the main acceleration event.) Pressure differentials were high everywhere except on SWB2, which peaked at only 1 bar. Differential pressures on parts of MS and SWB1 ranged from 2 to 4 bar, and the PRs experienced 2.5 – 3 bar, resulting in their failure. The peak pressure across SWB3 was 4 bar.

Bay 1R Ignition (Test 16) The flame appears to run along the starboard side of the tank, igniting bays 2, 4, and 6 early in the event. This was confirmed by the thermocouples. Bays 3 and 5 lag behind and ignite directly into turbulent combustion later. The starboard bays transitioned to turbulent combustion in the following order: 6, 4, 2, 1. The highest peak pressures were 4.6 bar in bays 3 and 5. Some pressure piling does occur in bay 1, with a peak of about 4 bar. This is one of two cases in which pressure piling occurred in the bay of first ignition; this also occurred for Bay 6R. The port MS reached a differential pressure of 3.5 bar, highest of the aft partitions. SWB2 differential pressure reached 1.8 bar, and SWB3 reached 4 bar. Pressure differentials across the PRs reached 2.5 – 3 bar, causing them to fail as in the previous test (Test 15).

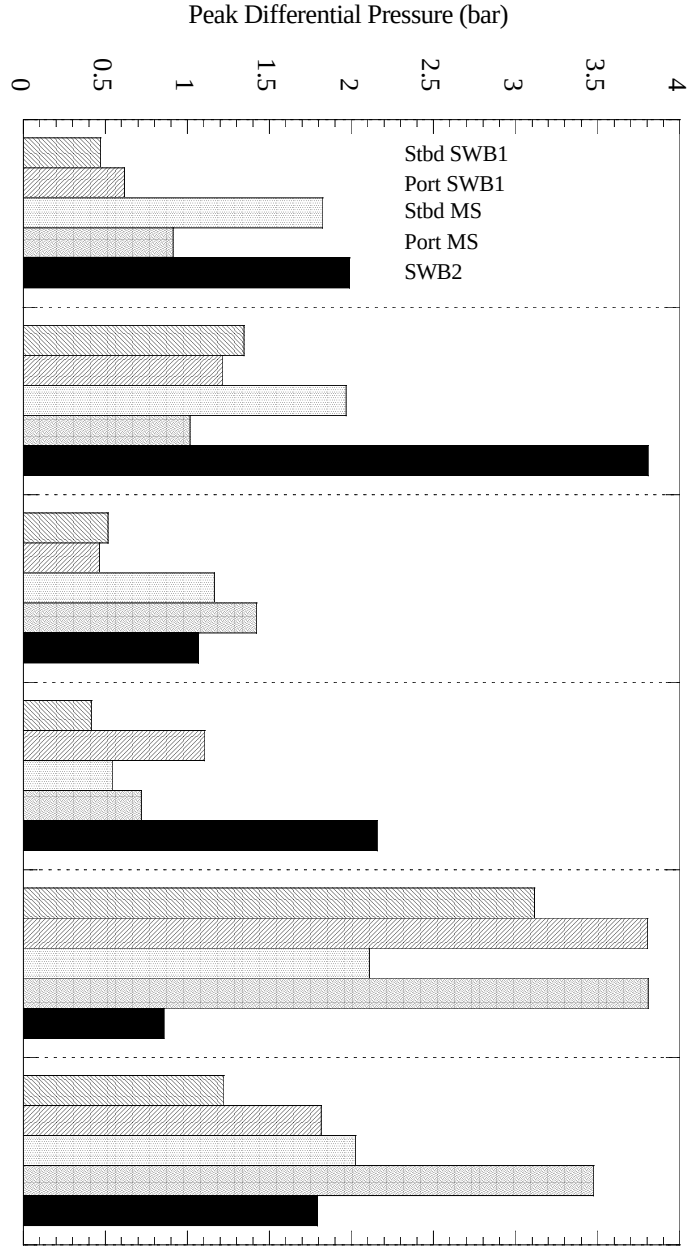

Figure 6.9: Comparison of differential pressures for ignition locations used in the all-strong configuration (BETA series Tests 5, 6, 7, 15, 16). Only the positive peak values are shown here, see the data in Appendix B for tabulated postive and negative peak values.

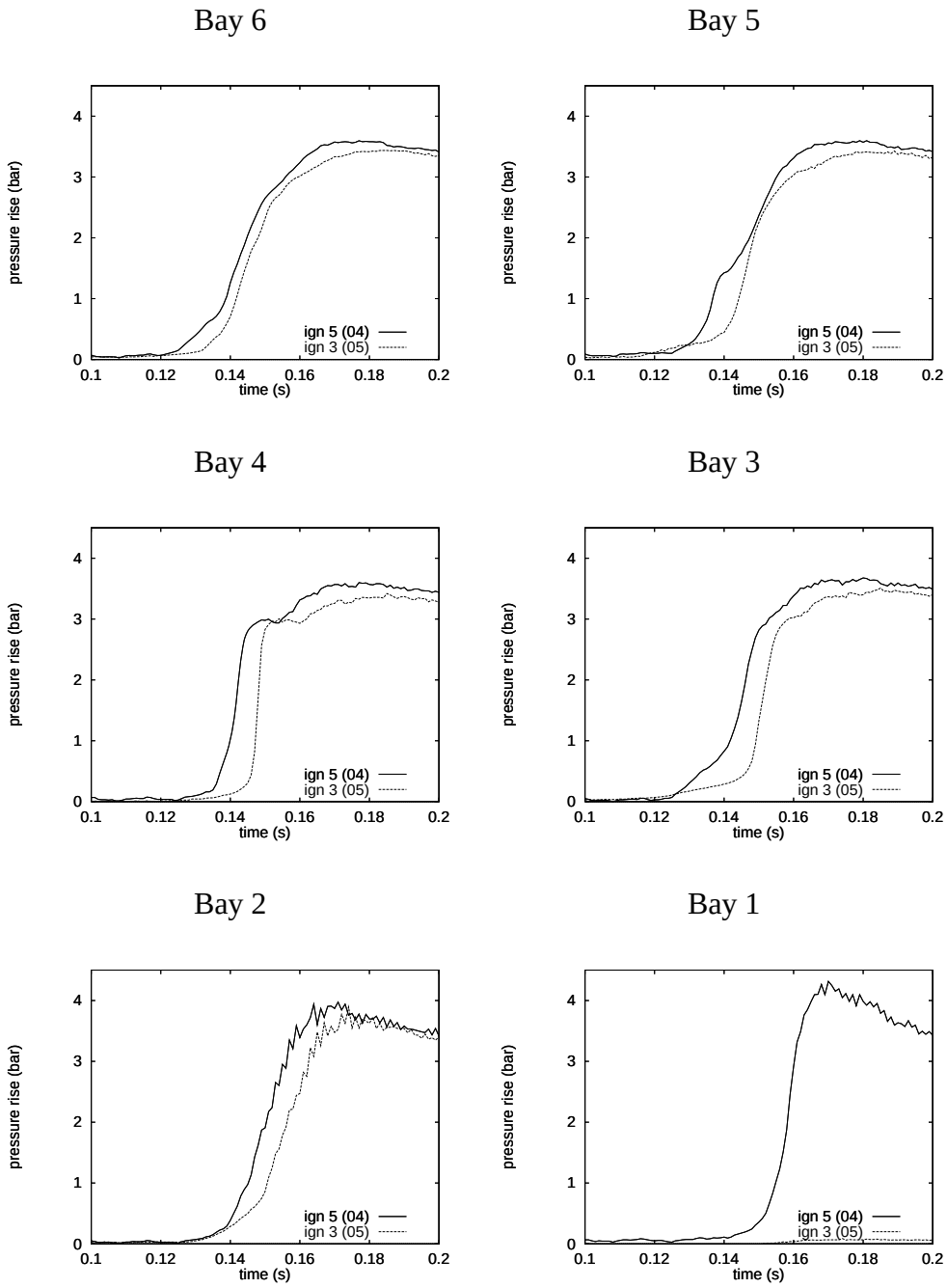

Figure 6.10: Comparison of individual pressure traces, ignition in bay 3 vs. reference ignition in bay 5.

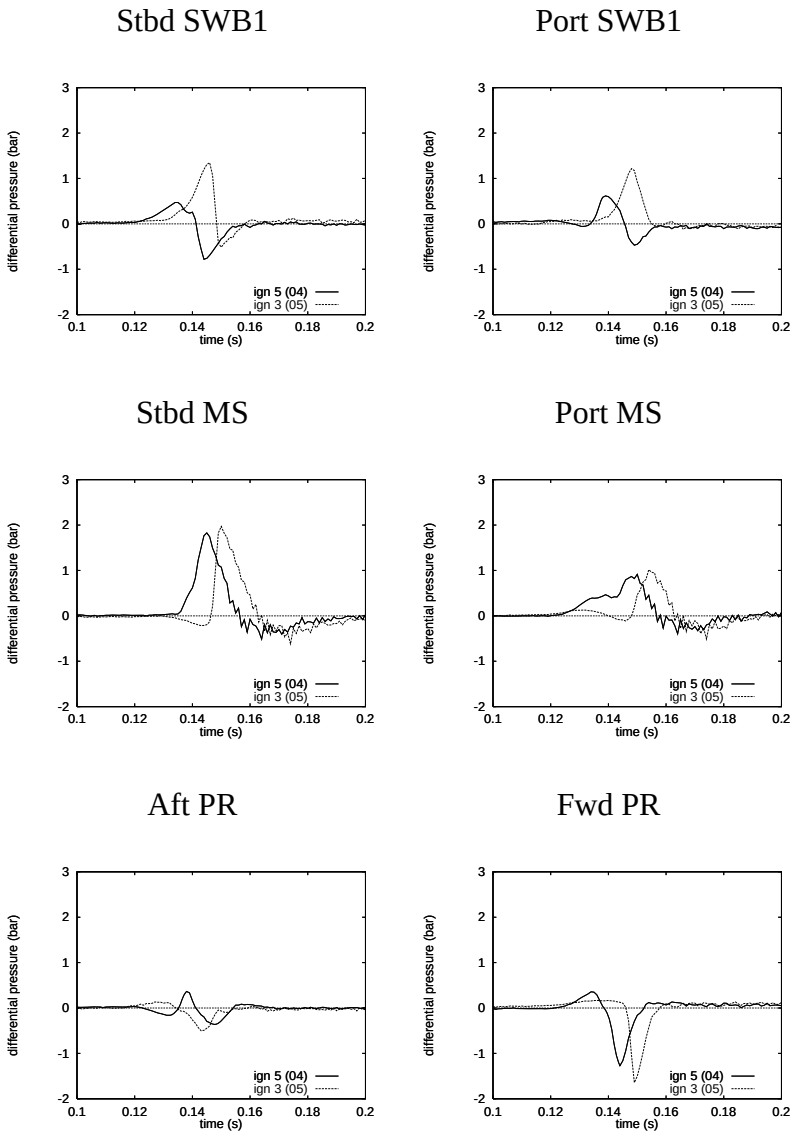

Figure 6.11: Comparison of differential pressures: all-strong, ignition in bay 3 vs. reference ignition in bay 5.

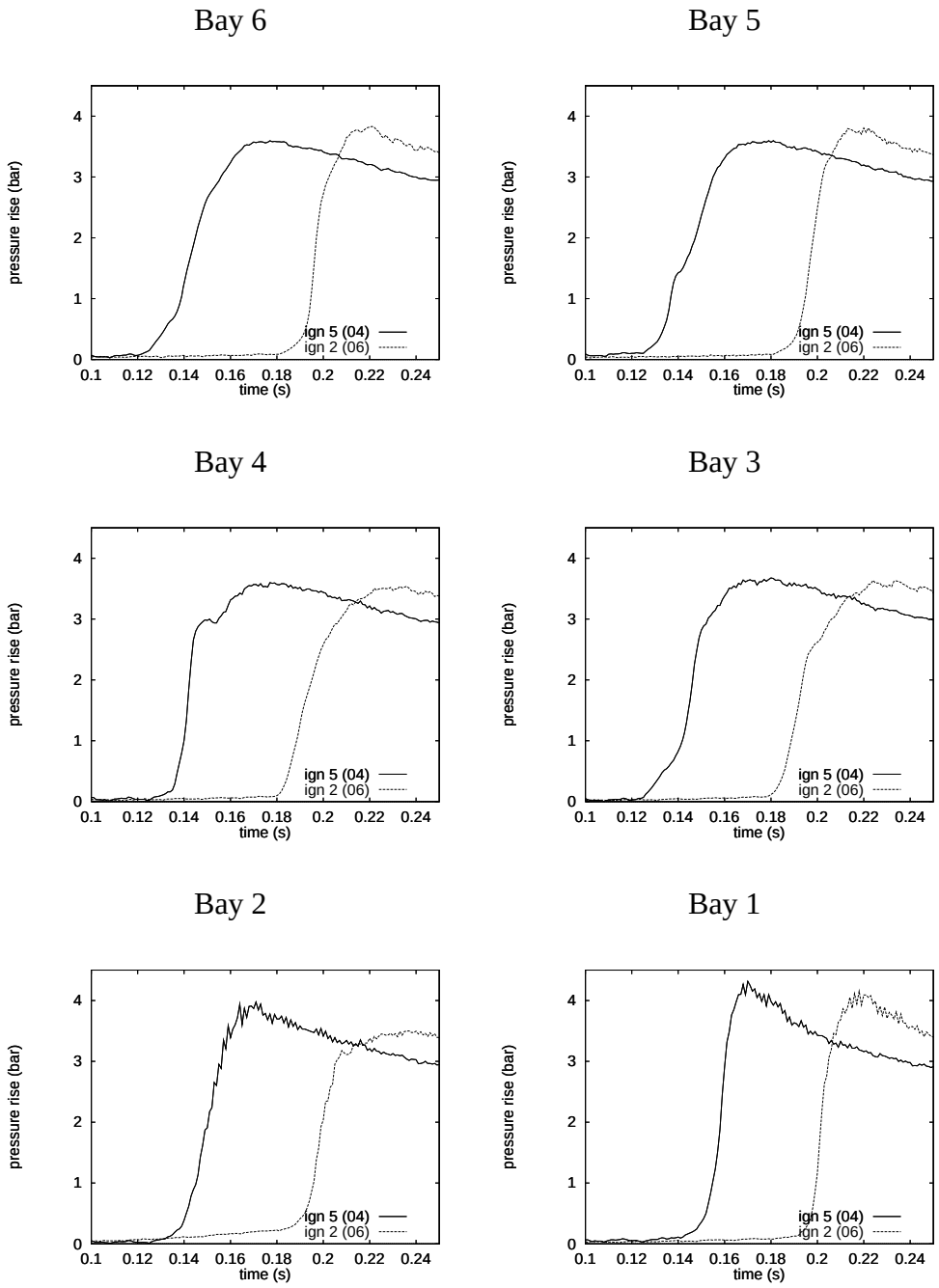

Figure 6.12: Comparison of individual pressure traces, ignition in bay 2 vs. reference ignition in bay 5.

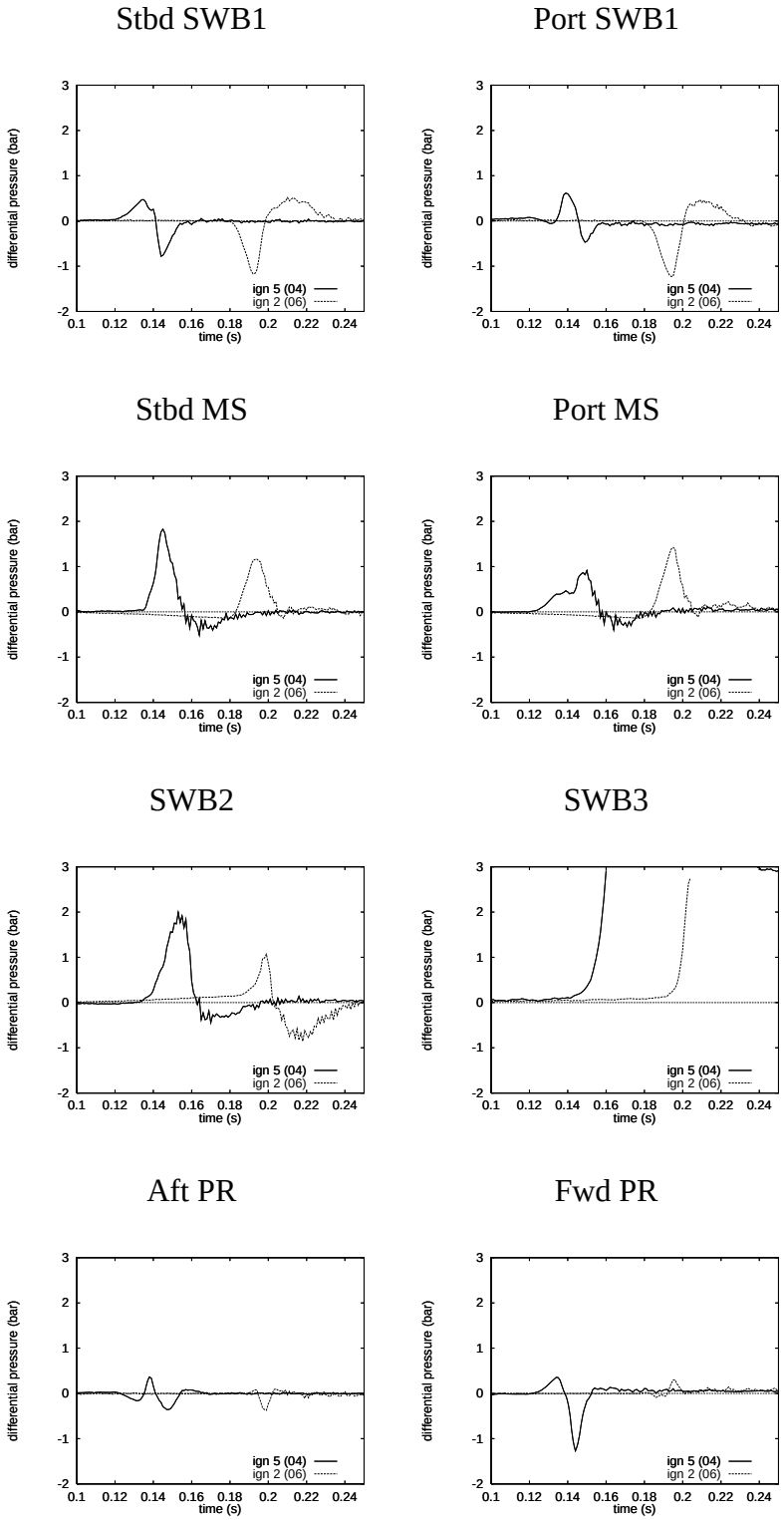

Figure 6.13: Comparison of differential pressures: all-strong, ignition in bay 2 vs. reference ignition in bay 5.

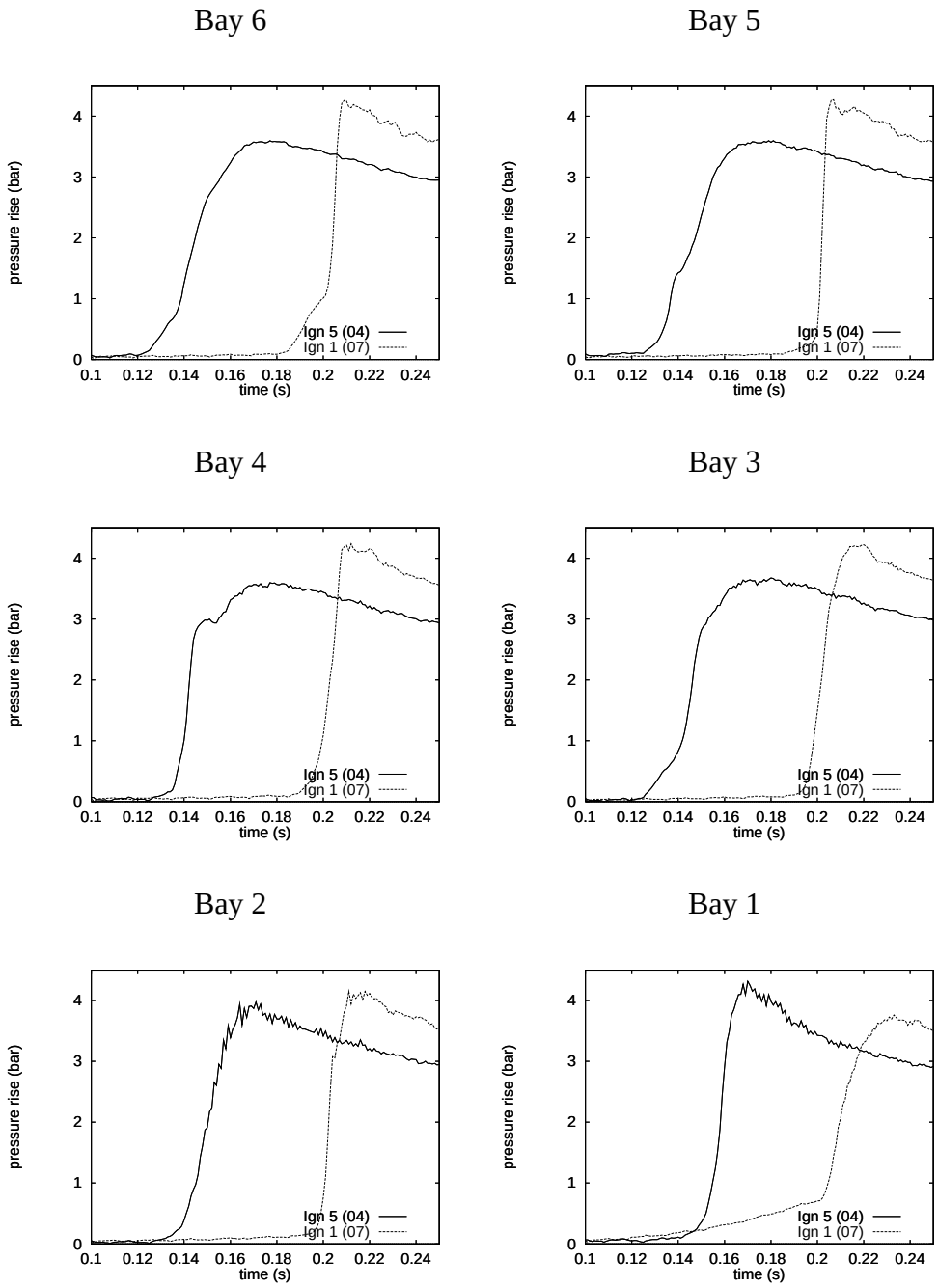

Figure 6.14: Comparison of individual pressure traces, ignition in bay 1 vs. reference ignition in bay 5.

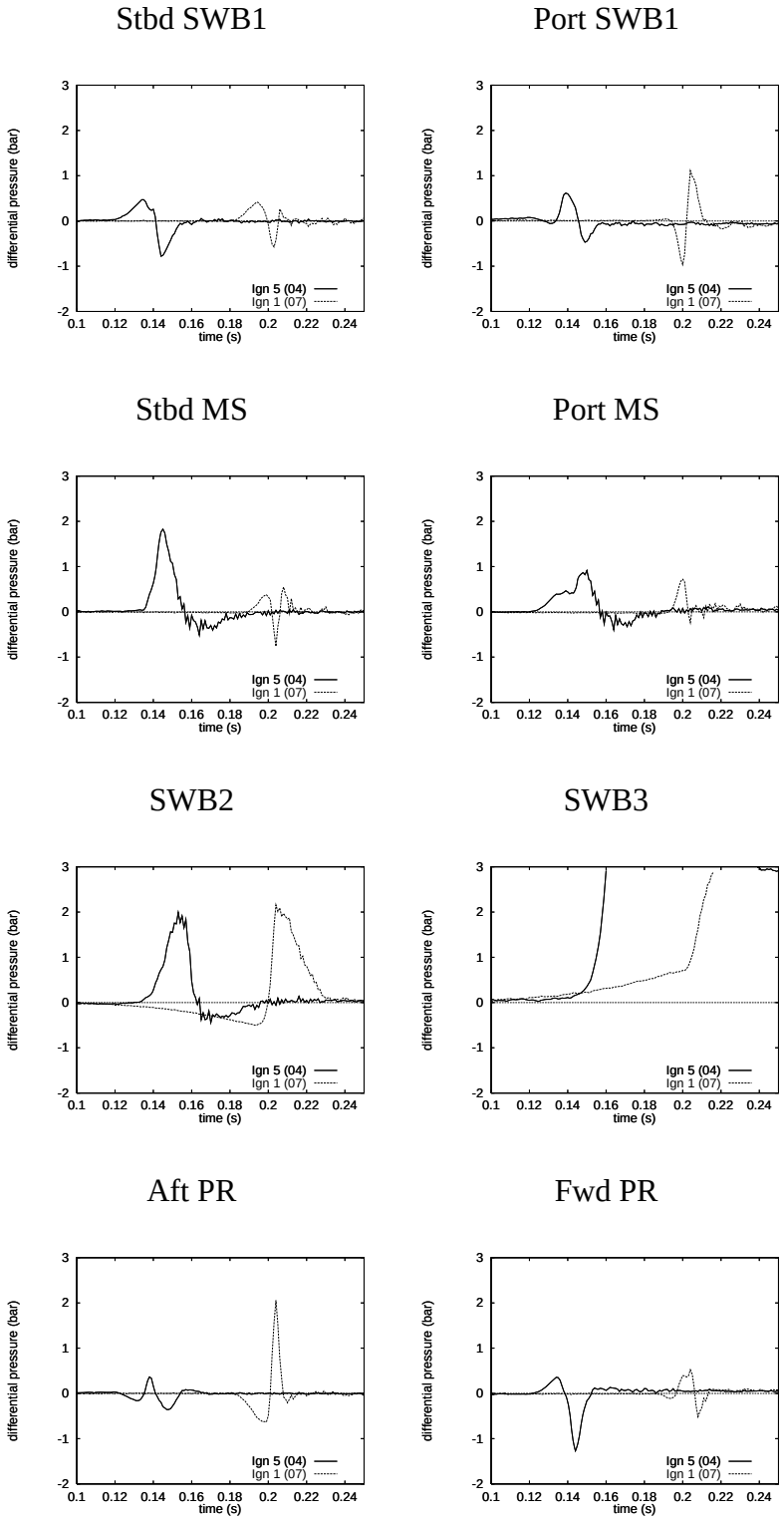

Figure 6.15: Comparison of differential pressures: all-strong, ignition in bay 1 vs. reference ignition in bay 5.

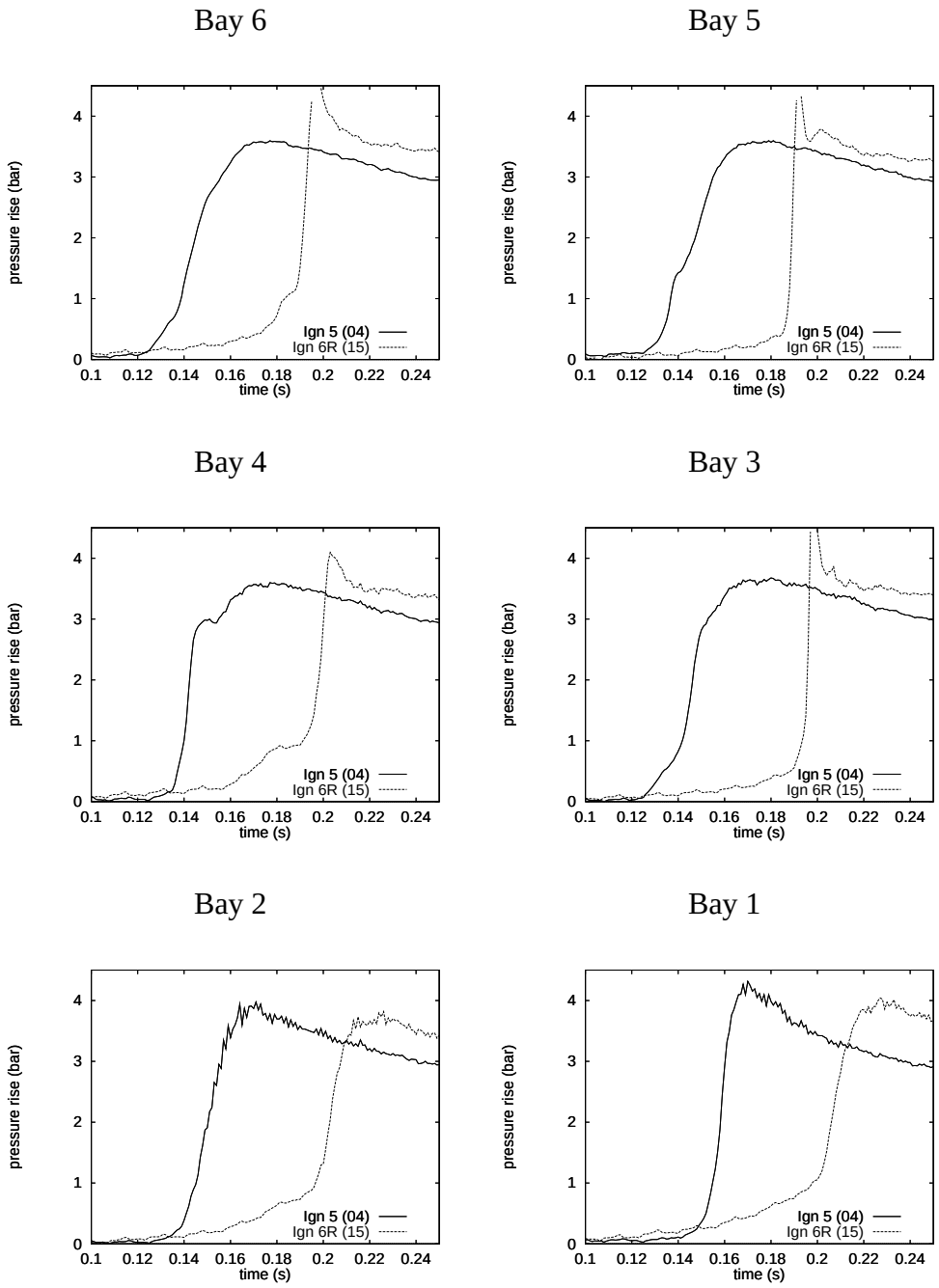

Figure 6.16: Comparison of individual pressure traces, ignition in bay 6R vs. reference ignition in bay 5.

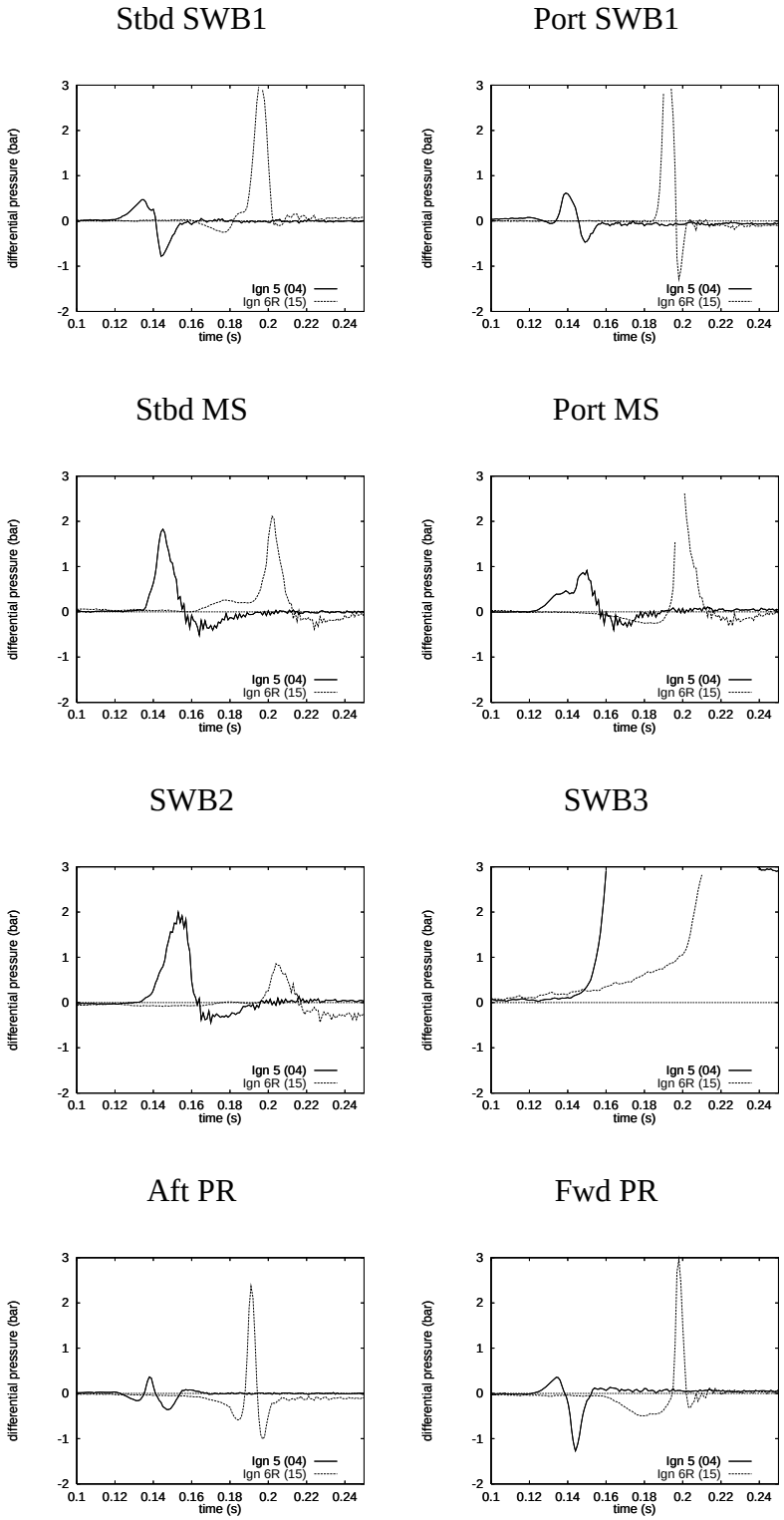

Figure 6.17: Comparison of differential pressures: all-strong, ignition in bay 6R vs. reference ignition in bay 5.

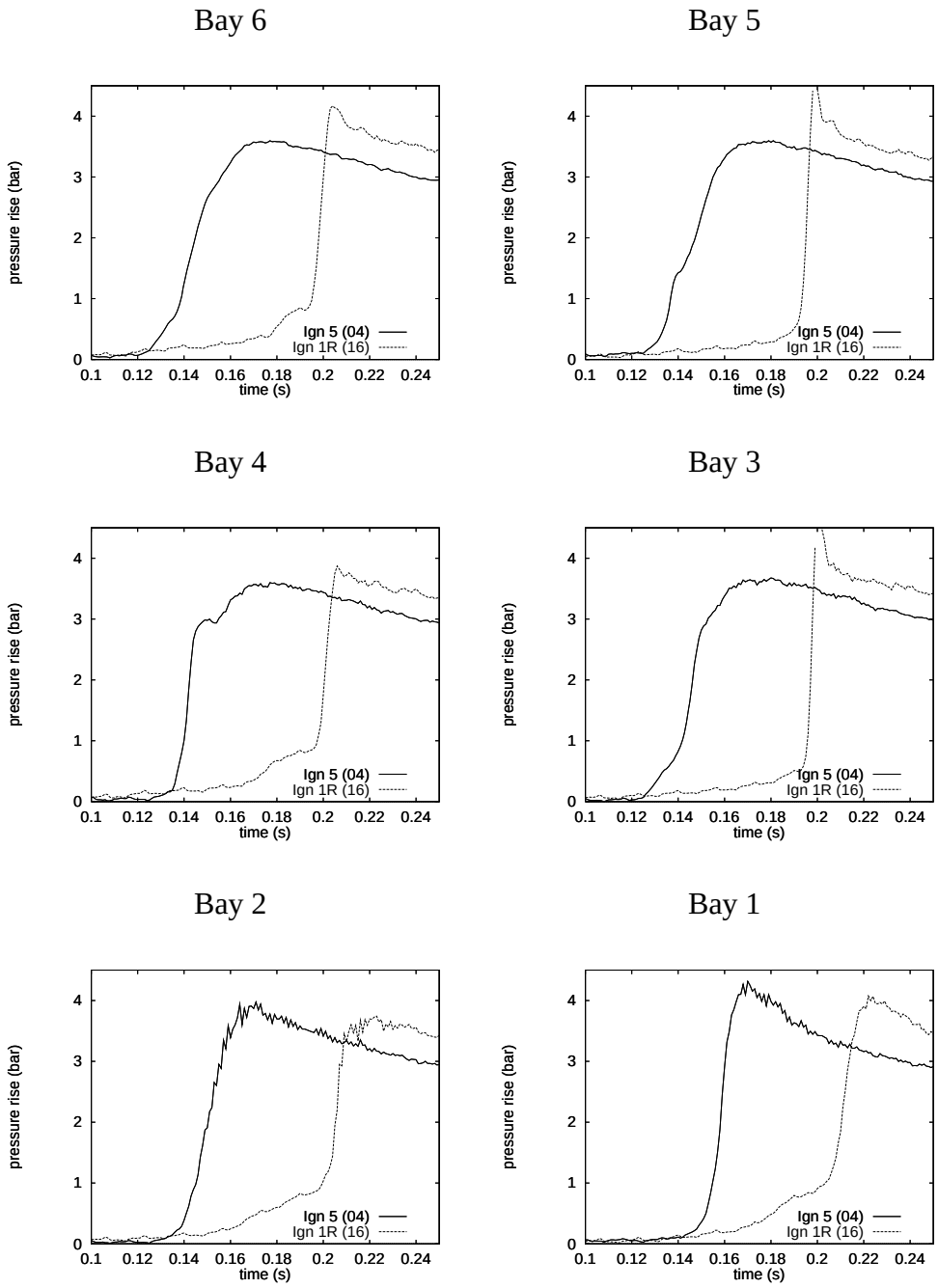

Figure 6.18: Comparison of individual pressure traces, ignition in bay 1R vs. reference ignition in bay 5.

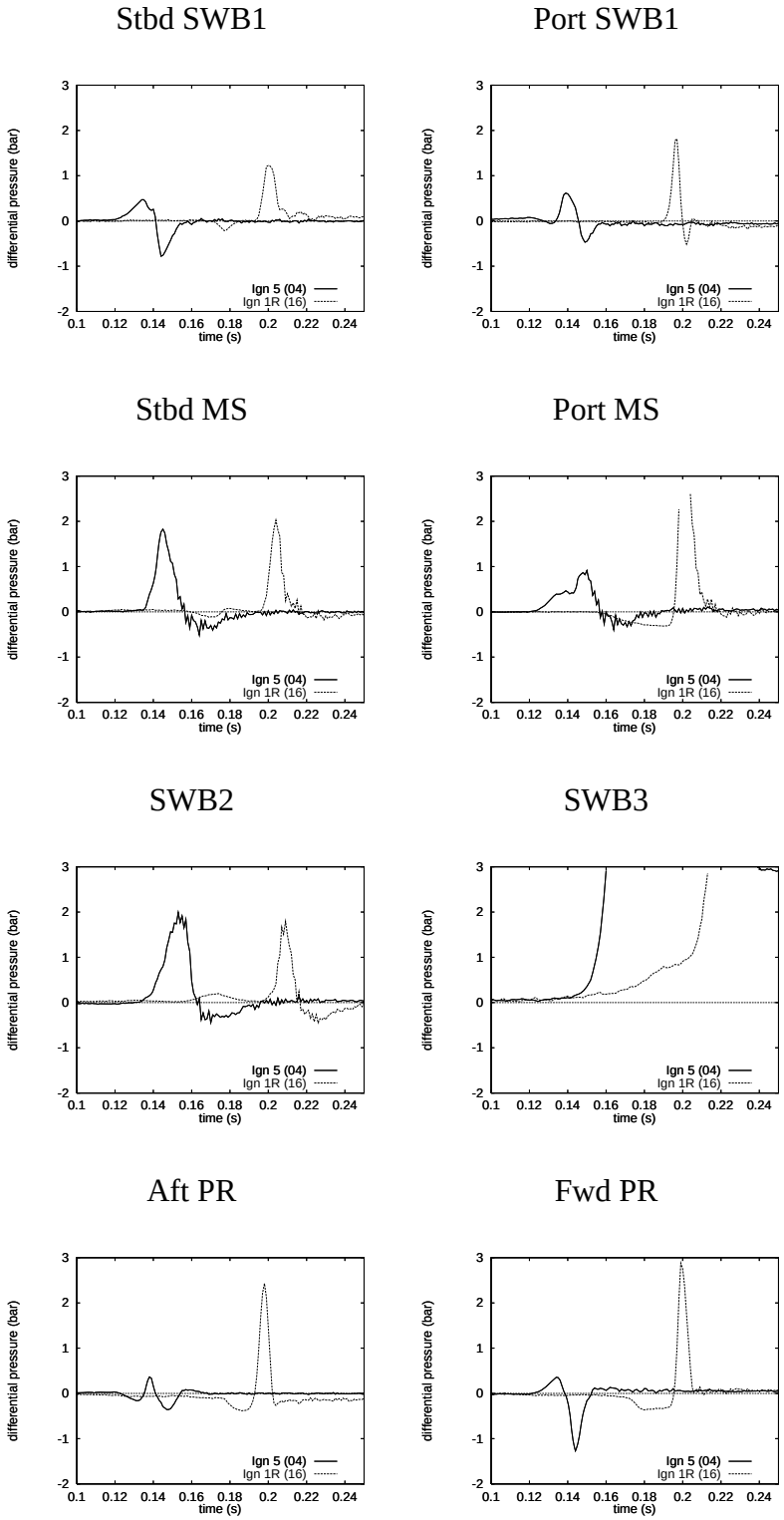

Figure 6.19: Comparison of differential pressures: all-strong, ignition in bay 1R vs. reference ignition in bay 5.

6.6.2 Part Strong (With Jet A)

(Comparisons of Tests 27, 28, and 29.) Ignition in bay 5 or 2Lo results in a rapid pressure rise in bay 4 similar to that observed in the dry tests. The onset of the pressure rise appears to occur about 30 to 40 ms earlier in tests with liquid. In tests with ignition in bay 2Lo or 5, the MP appears to fail after SWB3 and FS get ejected; SWB3 fails over a short period of time, and FS fails uniformly. With ignition in bay 1, the slow pressure rise there caused one corner of SWB3 to fail early, pressurizing bay 0. The subsequent pressure rise was fast enough for FS to fail fairly uniformly and the MP ruptured towards the back of the tank while SWB3 was failing.

In these tests, pressure piling occurs in the bays away from the ignitor. The failure of the weak partitions SWB3 and FS, and also the MP in SWB2 does not allow piling to occur in bays 1 and 2, but the peak pressures in the aft bays are clearly higher when the ignitor is moved forward. A summary of the peak differential pressures is shown in Fig. 6.20. The differences are not as marked as in the all-strong cases.

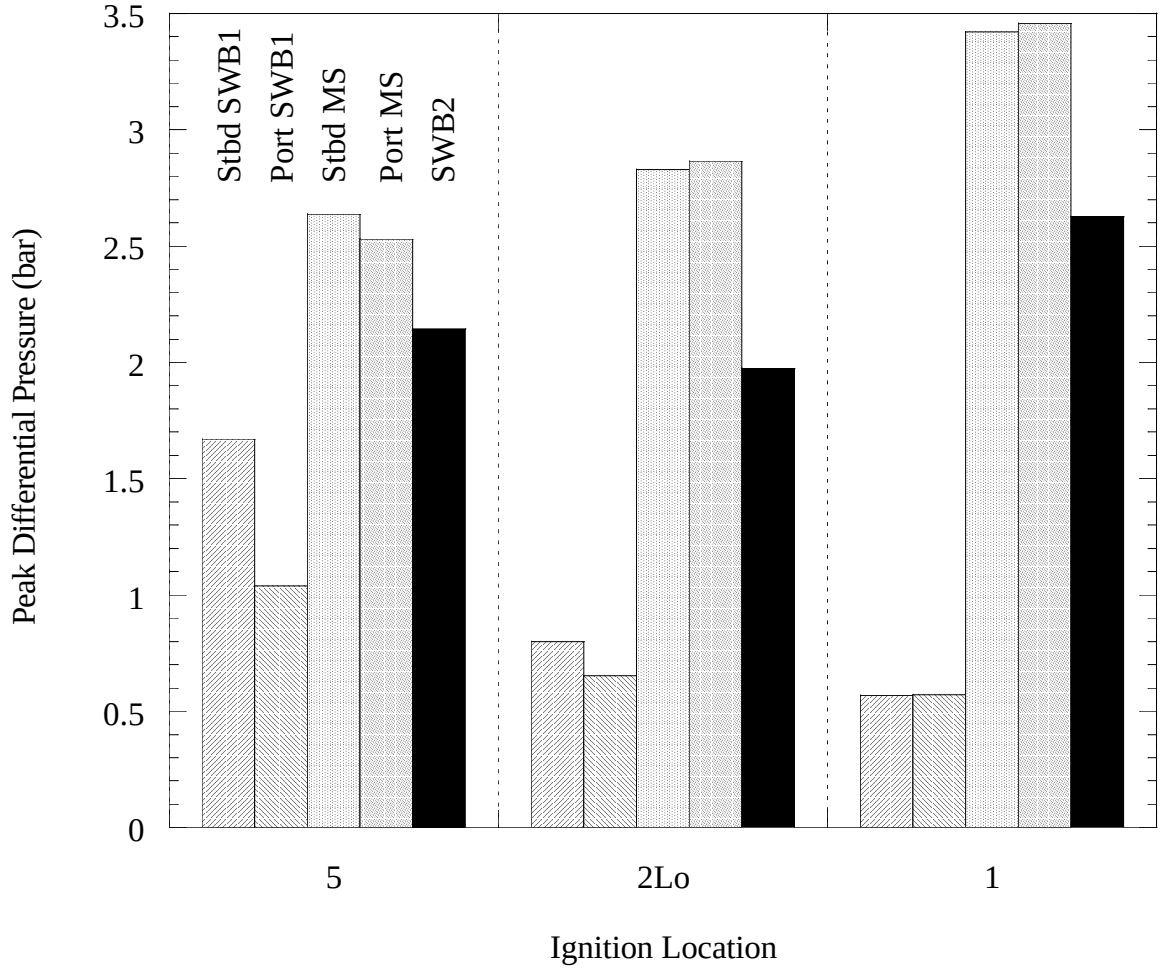

Figure 6.20: Comparison of peak differential pressures for different ignition locations in part-strong configuration (Tests 27, 28, and 29). Only the positive peak values are shown here, see the data in Appendix B for tabulated postive and negative peak values.

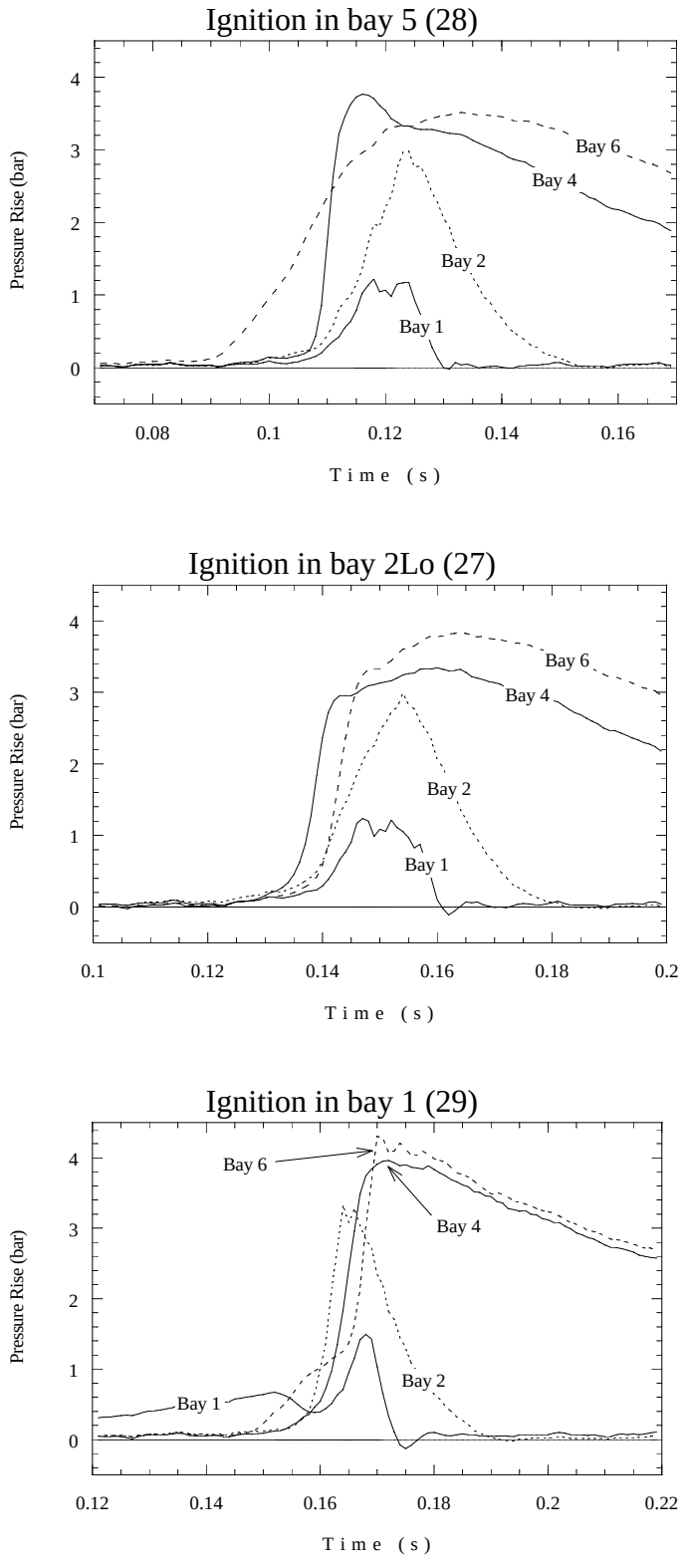

Figure 6.21: Pressure histories for all bays (except 3) for three ignition locations: bay 5 (Test 28), bay 2Lo (Test 27), and bay 1 (Test 29). Part-strong tests with liquid Jet A layer.

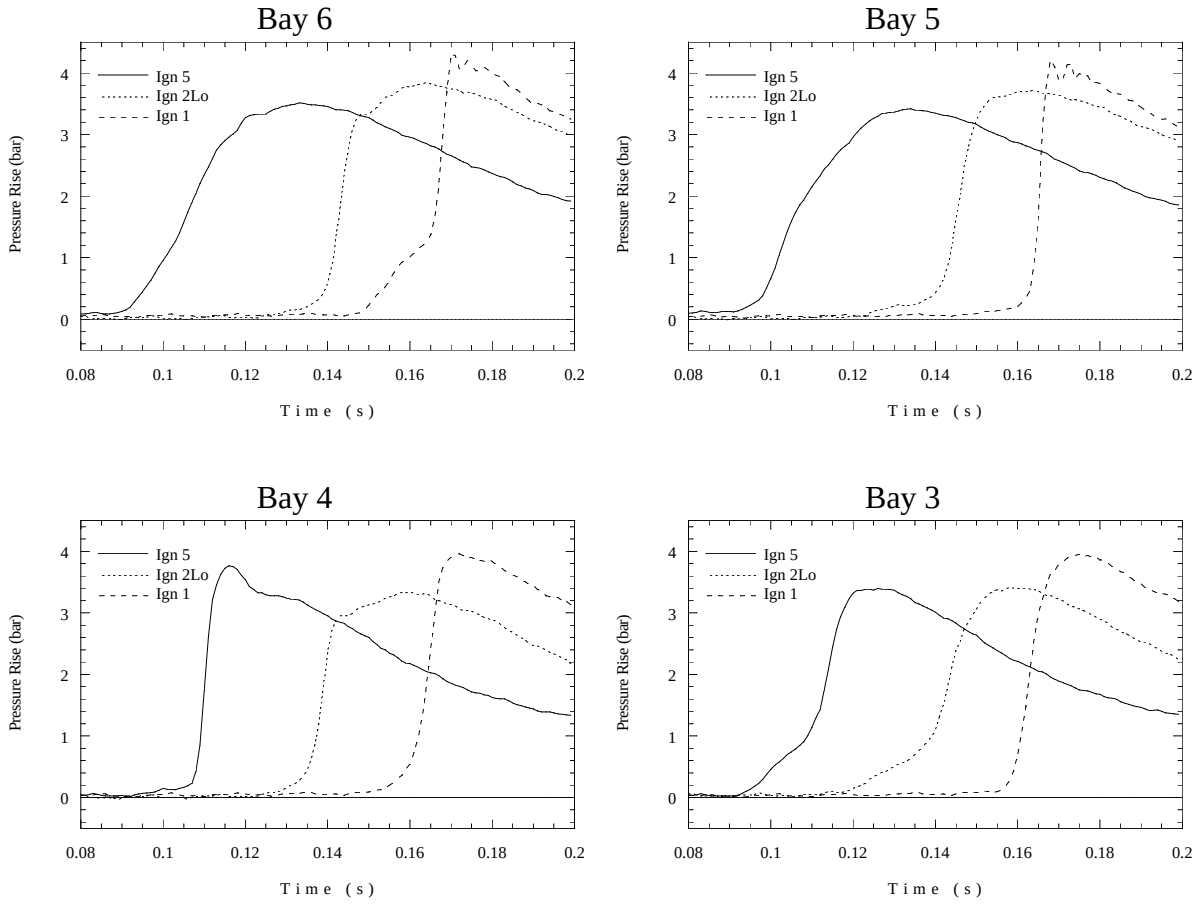

Figure 6.22: Comparison of pressure traces in bays 6, 5, 4, and 3 for three ignition locations: bay 5 (Test 28), bay 2Lo (Test 27), and bay 1 (Test 29) in part-strong tests with liquid Jet A layer. Part 1 of 2.

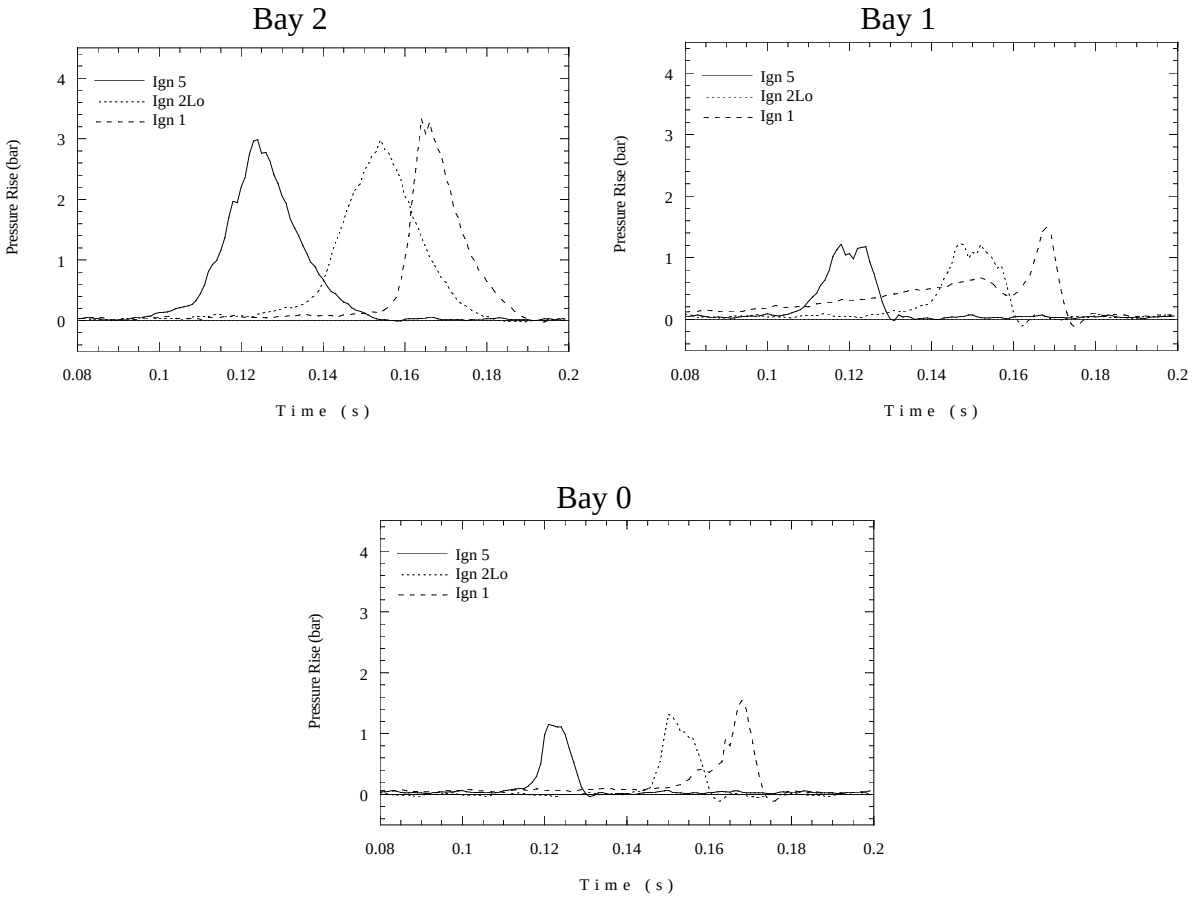

Figure 6.23: Comparison of pressure traces in bays 2, 1, and 0 for three ignition locations: bay 5 (Test 28), bay 2Lo (Test 27), and bay 1 (Test 29) in part-strong tests with liquid Jet A layer. Part 2 of 2.

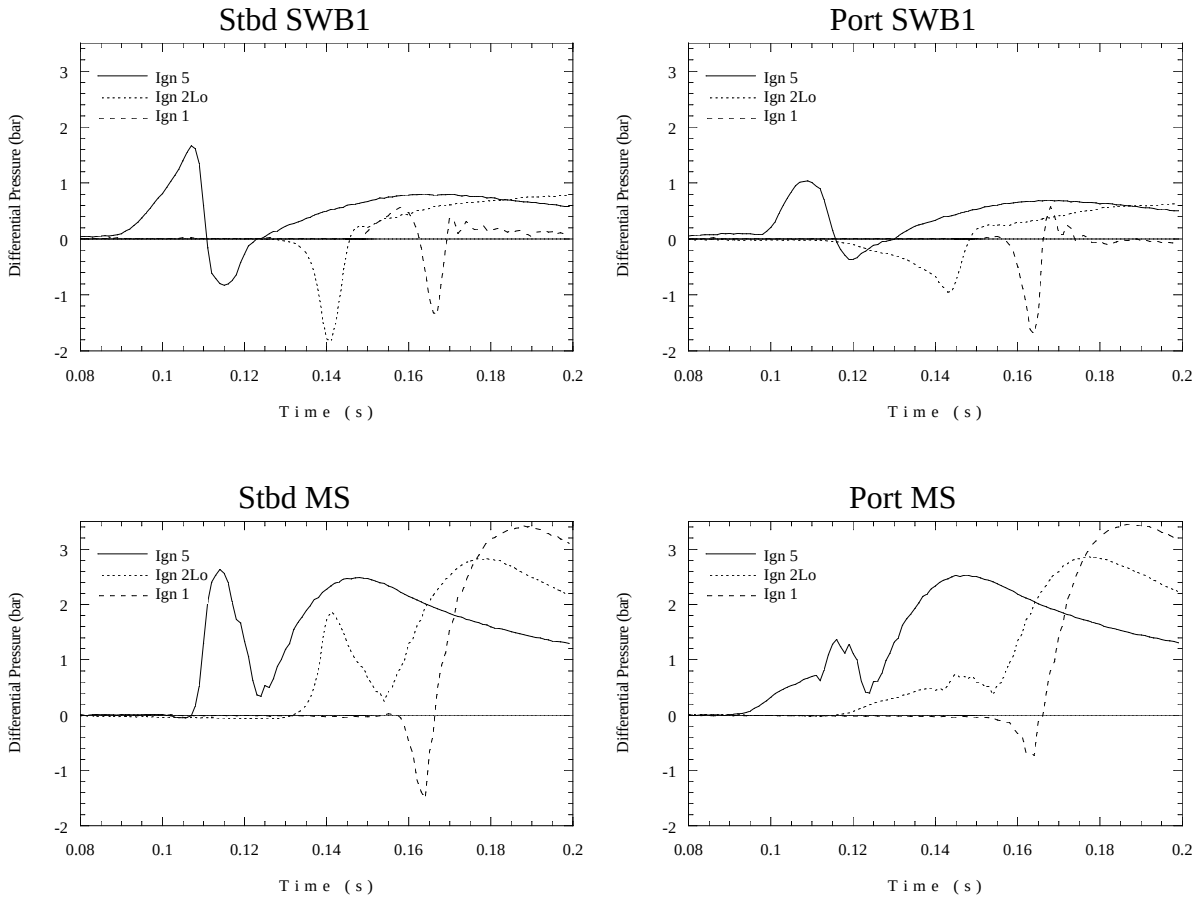

Figure 6.24: Comparison of differential pressures for SWB1 and MS for three ignition locations: bay 5 (Test 28), bay 2Lo (Test 27), and bay 1 (Test 29) in part-strong tests with liquid Jet A layer. Part 1 of 2.

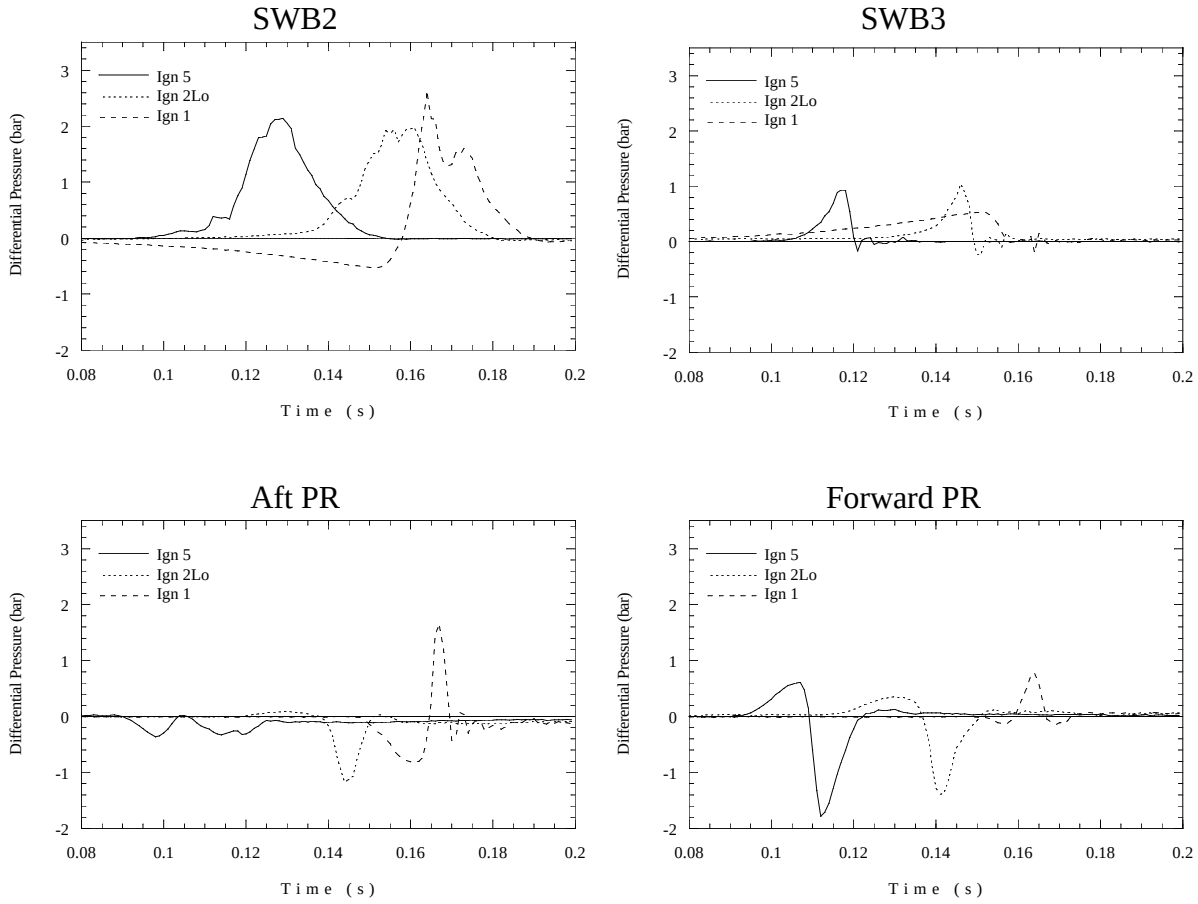

Figure 6.25: Comparison of differential pressures for SWB2, SWB3 and PRs for three ignition locations: bay 5 (Test 28), bay 2Lo (Test 27), and bay 1 (Test 29) in part-strong tests with liquid Jet A layer. Part 2 of 2.

6.6.3 All Weak (With Jet A)

(Comparisons of Tests 19, 20, and 21.) The most notable effect of ignition location on the all-weak tests was the resulting pattern of structural failure. Each test was only performed once and further testing would be required to confirm that these differences are truly systematic. In general, the further back the ignitor is located, the more partitions are expelled from the tank. In Test 19, ignition in bay 5, all of the panels except SWB1 were thrown clear of the tank (SWB1 was expelled in Test 18, which was identical to 19 but without Jet A). In Test 20 with ignition in position 2Lo, SWB1, and MS remained within the forward portion of the tank. In Test 21, ignition in bay 1, SWB1 and MS remained in the aft end of the tank. SWB1 was bent and failed towards the aft end of the tank, and the bay cameras showed SWB2 failing aftward first, and then moving forward.

As the ignitor is moved forward, pressure piling occurs in the aft bays. Even though all of the partitions are weak, failure is not instantaneous for all partitions, but is progressive. This results in higher pressures at the back of the tank than at the front in some cases. Ignition in the aft end of the tank was still able to generate turbulence and rapid combustion in the forward end. Ignition in bay 5 generated rapid enough combustion in bay 1 that the differential across SWB3 reached 2.5 bar before that partition failed. Figure 6.26 summarizes the peak differential pressures found in these tests. On the whole, these values are substantially smaller than those obtained in the all-strong tests.

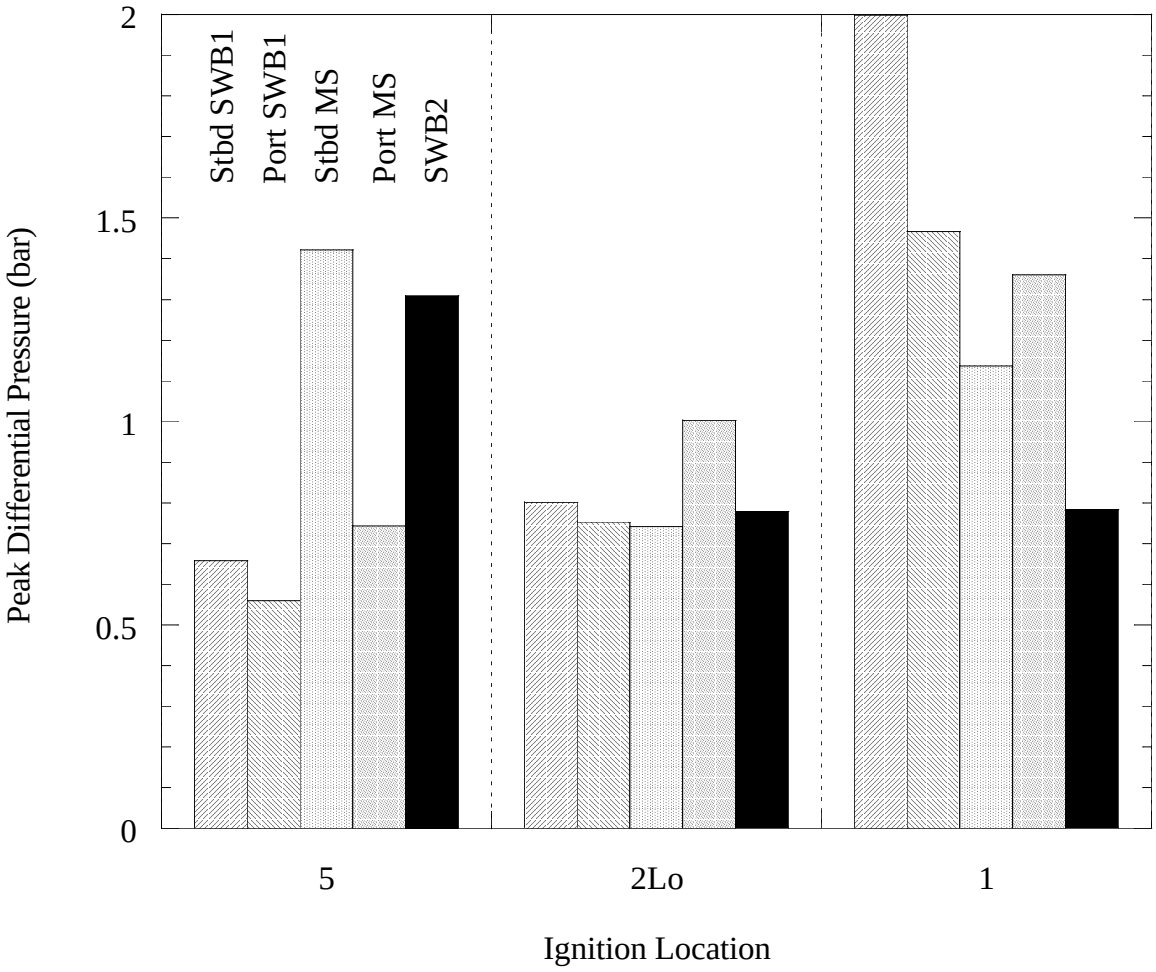

Figure 6.26: Comparison of peak differential pressures for different ignition locations in all-weak configuration (Tests 19, 20, and 21). Only the positive peak values are shown here, see the data in Appendix B for tabulated postive and negative peak values.

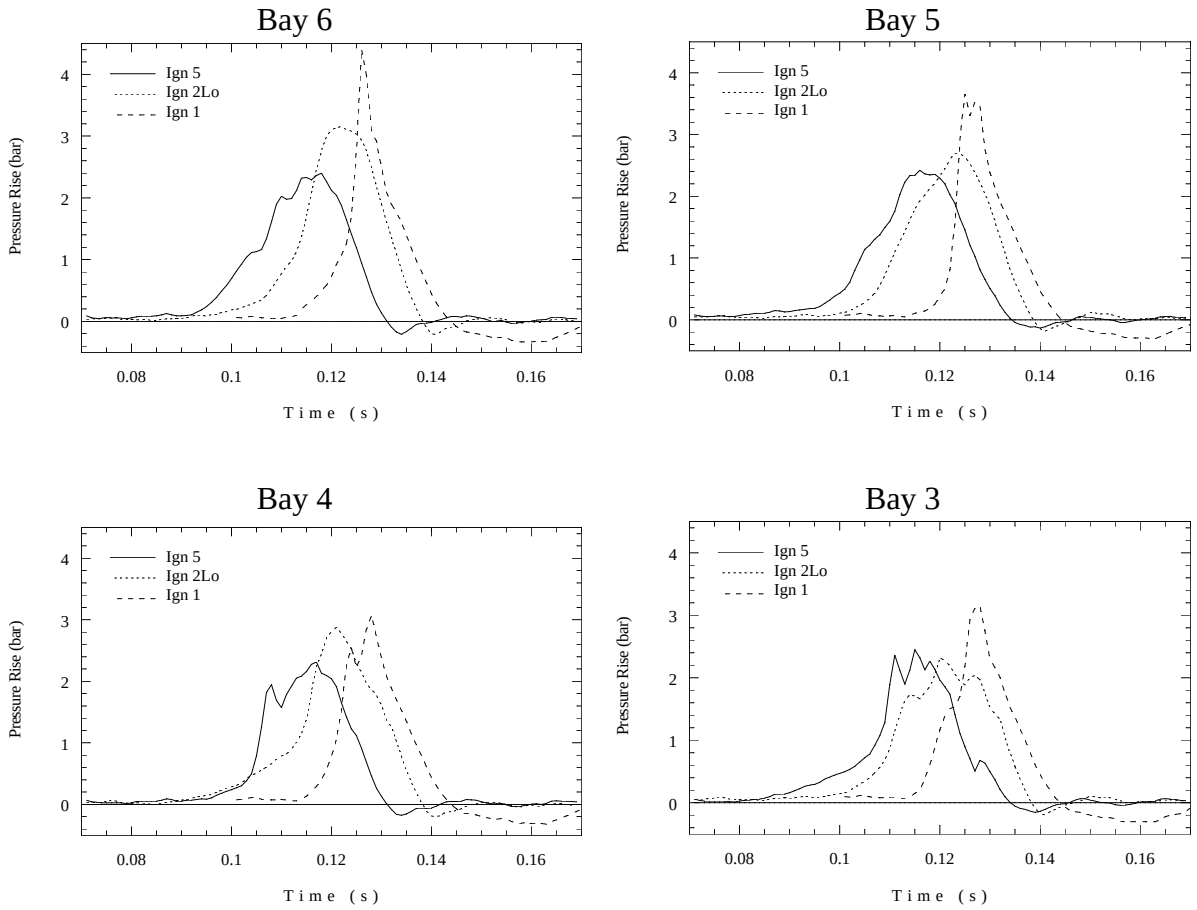

Figure 6.27: Comparison of pressure histories in bays 6, 5, 4, and 3 for three ignition locations: bay 5 (Test 19), bay 2Lo (Test 20), bay 1 (Test 21) in all-weak tests with a cold liquid Jet A layer. Part 1 of 2.

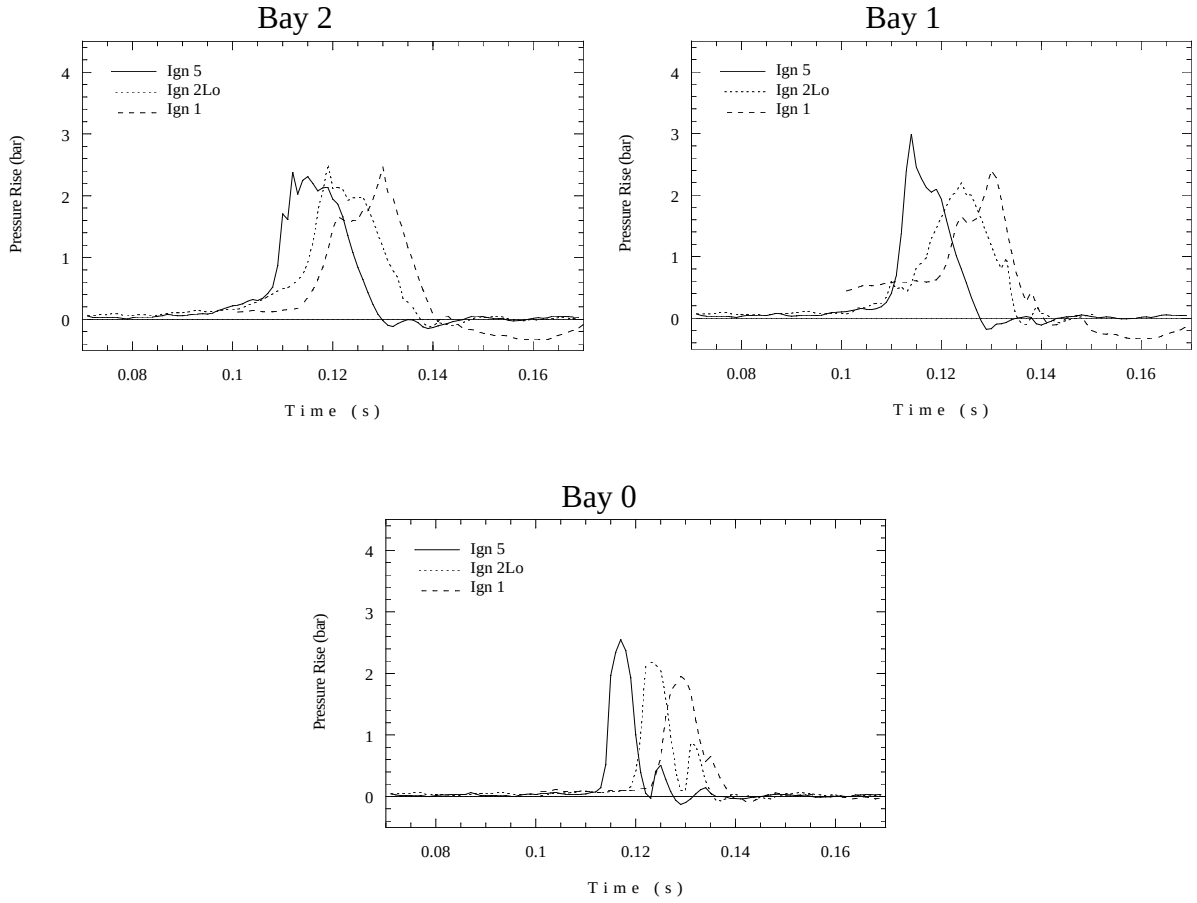

Figure 6.28: Comparison of pressure histories in bays 2, 1, and 0 for three ignition locations: bay 5 (Test 19), bay 2Lo (Test 20), bay 1 (Test 21) in all-weak tests with a cold liquid Jet A layer. Part 2 of 2.

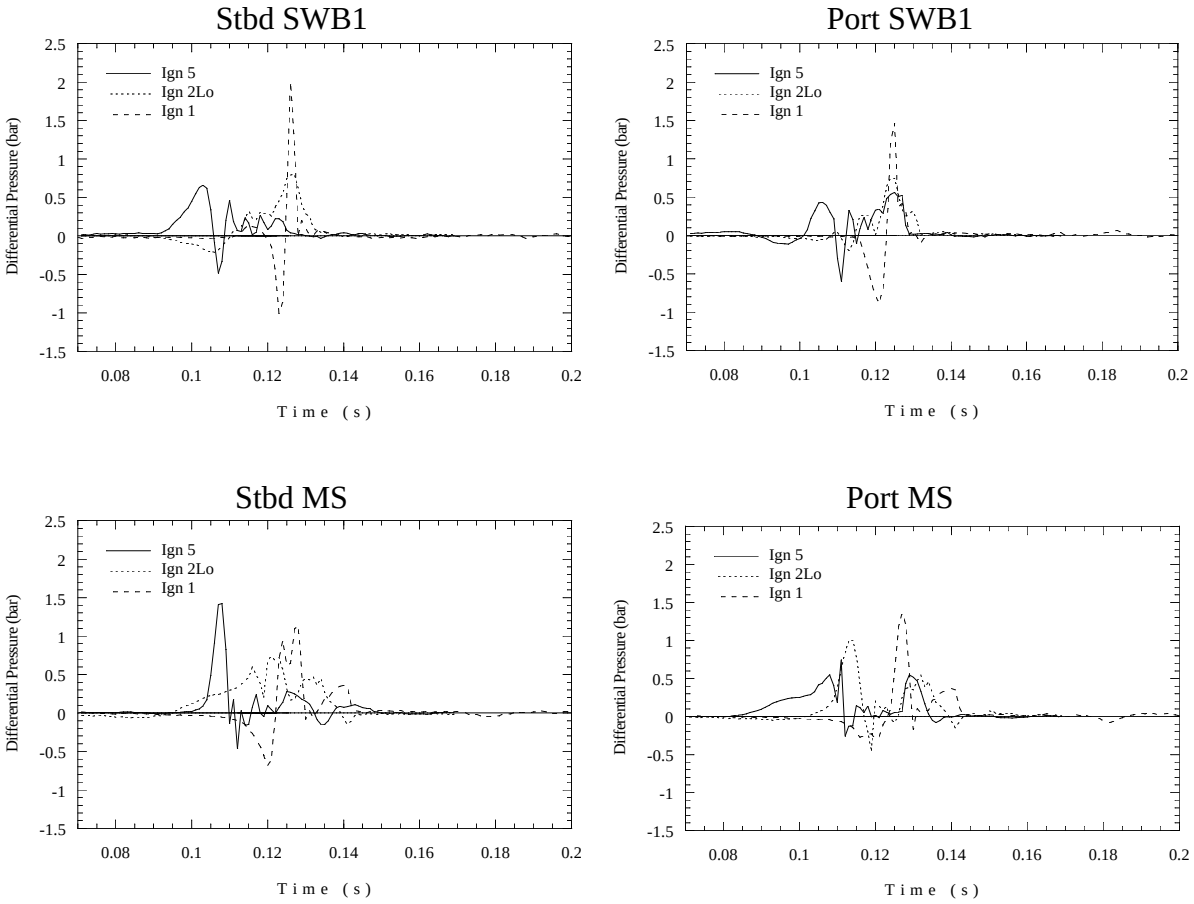

Figure 6.29: Comparison of differential pressure on SWB1 and MS for three ignition locations: bay 5 (Test 19), bay 2Lo (Test 20), bay 1 (Test 21) in all-weak tests with a cold liquid Jet A layer. Part 1 of 2.

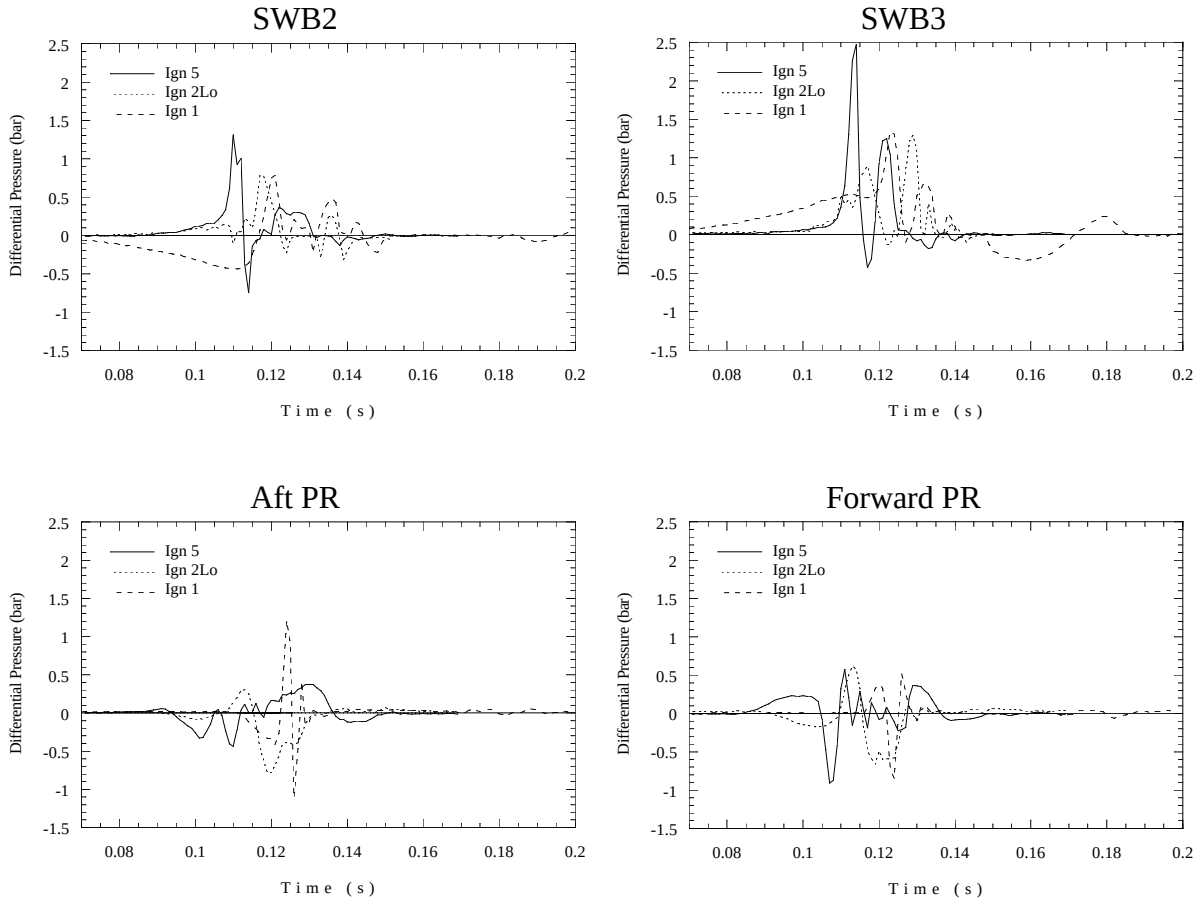

Figure 6.30: Comparison of differential pressure on SWB2, SWB3, and PRs for three ignition locations: bay 5 (Test 19), bay 2Lo (Test 20), bay 1 (Test 21) in all-weak tests with a cold liquid Jet A layer. Part 2 of 2.

6.7 Fuel Concentration

(Comparisons of Tests 22, 23, and 24.) In these tests, the total fuel concentration was 8.4% (Test 22), 7.5% (Test 23), and 6.5% (Test 24) for the part-strong configuration with ignition in bay 2Lo. Laboratory testing indicated that the lean limit for this fuel is about 6%, so these tests span the range of lean combustion behavior in which buoyancy plays a key role in flame propagation.

As the fuel concentration was decreased, the peak pressures generally decreased (Fig. 6.32) as expected just from energy content. However, the partitions were ejected the farthest in Test 24, the lowest fuel concentration, 6.5%. In this test, a severe pressure piling in the aft portion of the tank was observed. Bays 5 and 6 did not ignite until well after the burns were over in the other bays. During that time, the bays were pressurized to about 1 bar by the venting of bays 3 and 4. This higher initial pressure resulted in a peak pressure of over 4.8 bar when bays 5 and 6 finally ignited and burned. This late burn will not be shown in most comparison plots so that greater detail in the early stages of combustion may be compared. This late burn is a result of near-limit behavior of the system. In Test 26, which also used 6.5% fuel but was in the all-strong configuration, buoyancy was even more apparent with substantial periods of upward propagation of the flame. The peak pressure rise was only about 1 bar and bays 5 and 6 apparently never ignited in Test 26. A summary of the peak differential pressures for Tests 22, 23, and 24 is shown in Fig. 6.31.

In Figs. 6.33 and 6.34, pressure comparisons are shown for each bay. In the rear of the tank, bays 6, 5, 4, and 3, the initial (prior to 0.4 s) peak pressure decreases with increasing fuel concentration. The initial pressure peaks in the forward bays, 2, 1, and 0 either are independent of fuel concentration or in the case of bay 0, is highest for the lowest concentration.

The late (0.4 to 0.55 s) aft explosion event in Test 24 apparently resulted in the farther projection of partitions with 6.5% fuel as compared to 8.4% fuel. Test 23 (7.5%) resulted in the shortest projection of the partitions.

The differential pressures are compared in Fig. 6.35. In these plots, the differential pressures involving the aft bays are plotted for an extra 100 ms, to show the burn in these bays.

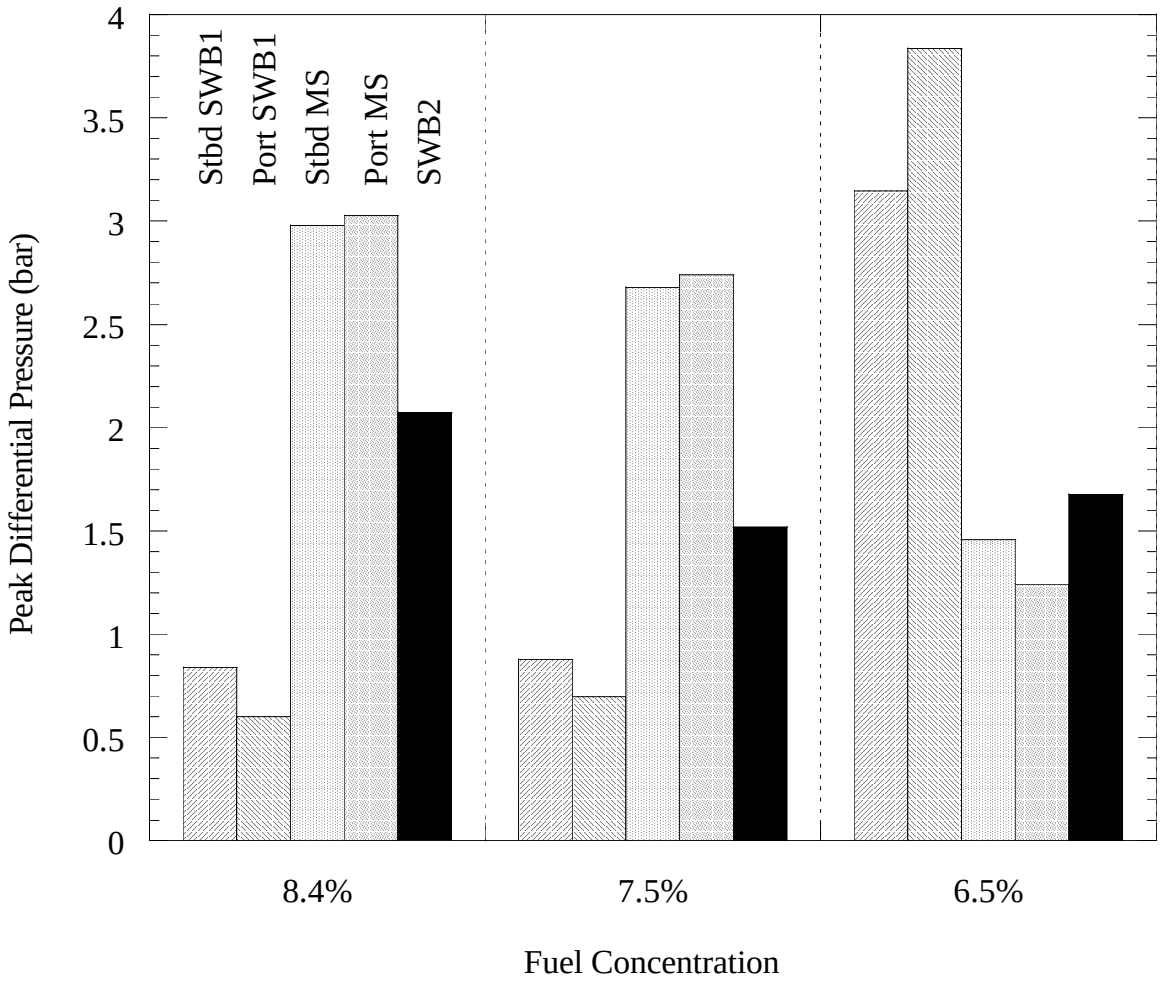

Figure 6.31: Comparison of peak differential pressures for fuel concentrations of 8.4% (Test 22), 7.5% (Test 23), and 6.5% (Test 24). Only the positive peak values are shown here, see the data in Appendix B for tabulated postive and negative peak values.

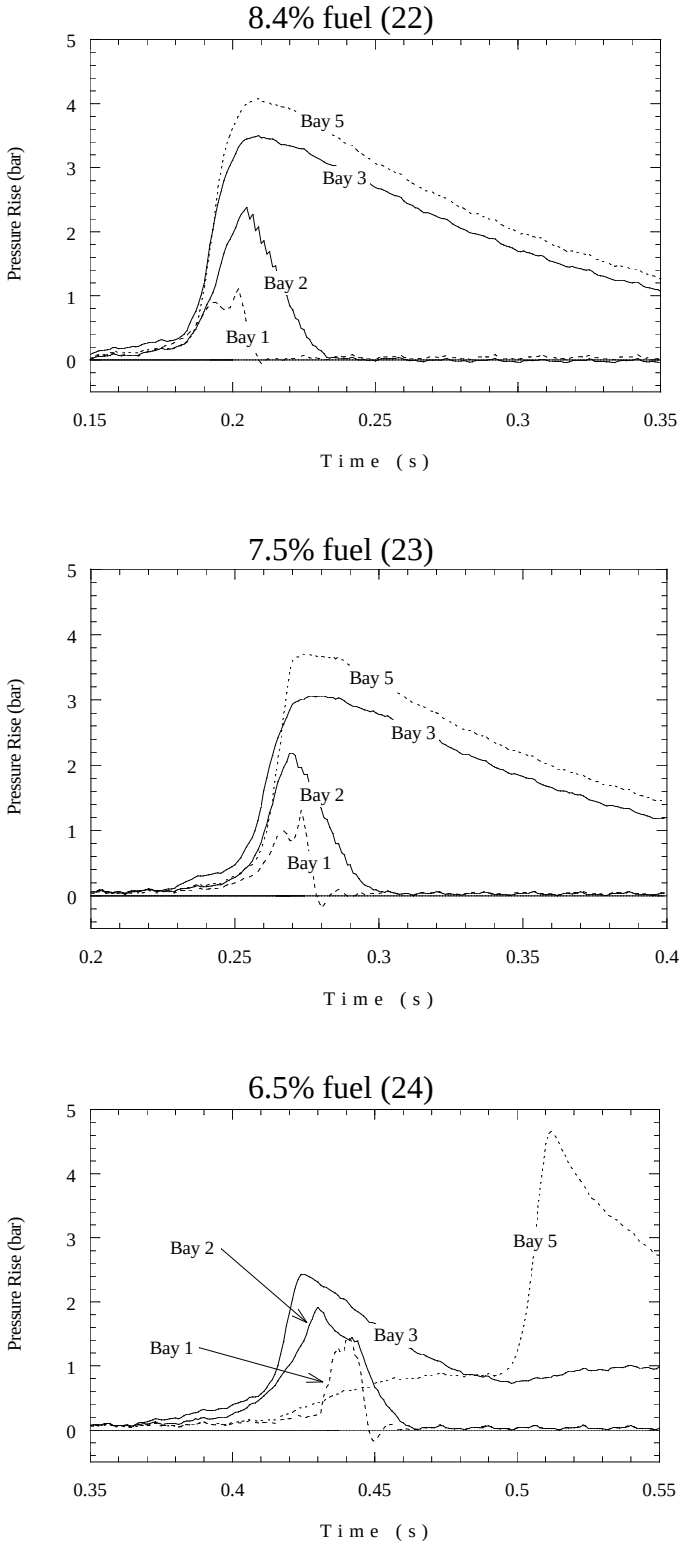

Figure 6.32: Pressure traces for bays 1, 2, 3, and 5 in part-strong tests with fuel concentrations of 8.4% (Test 22), 7.5% (Test 23), and 6.5% (Test 24).

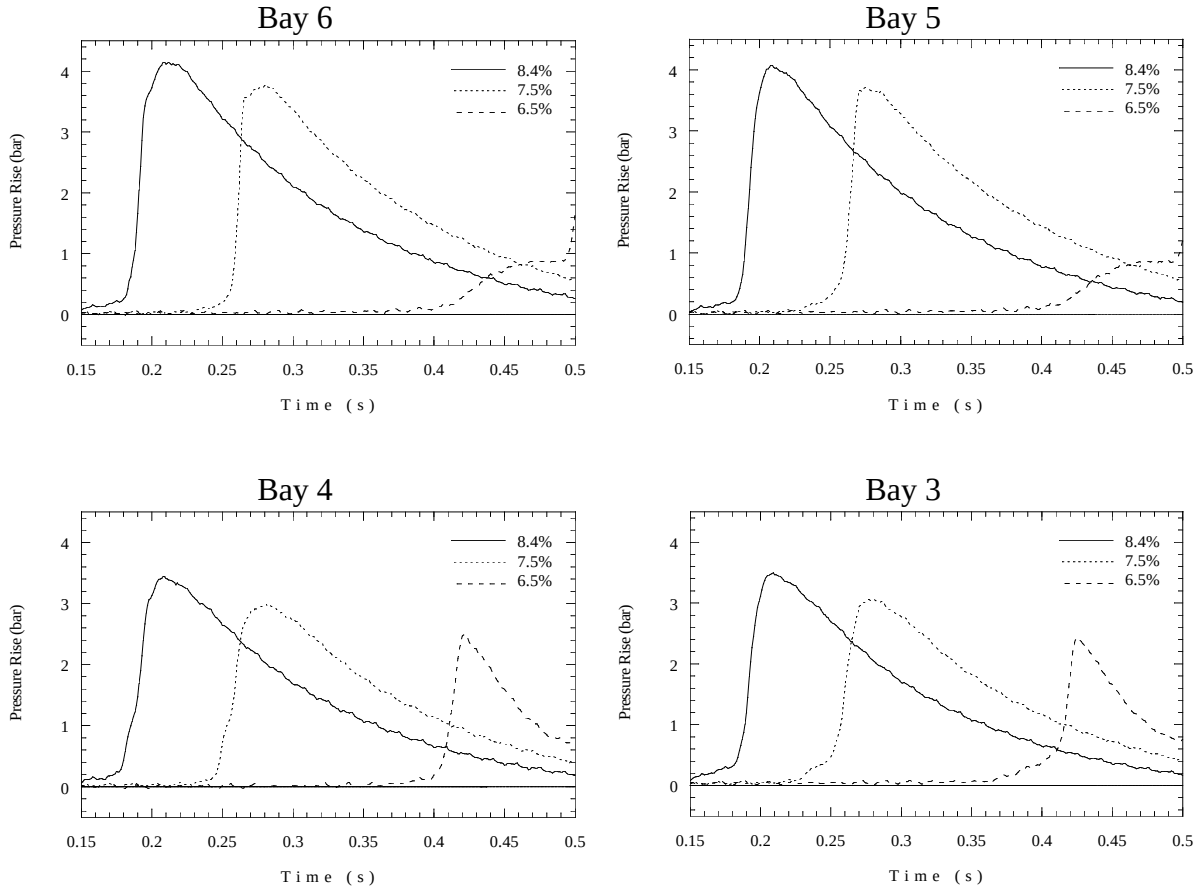

Figure 6.33: Comparison of pressure traces for bays 6, 5, 4, and 3, in part-strong tests with fuel concentrations of 8.4% (Test 22), 7.5% (Test 23), and 6.5% (Test 24). Part 1 of 2.

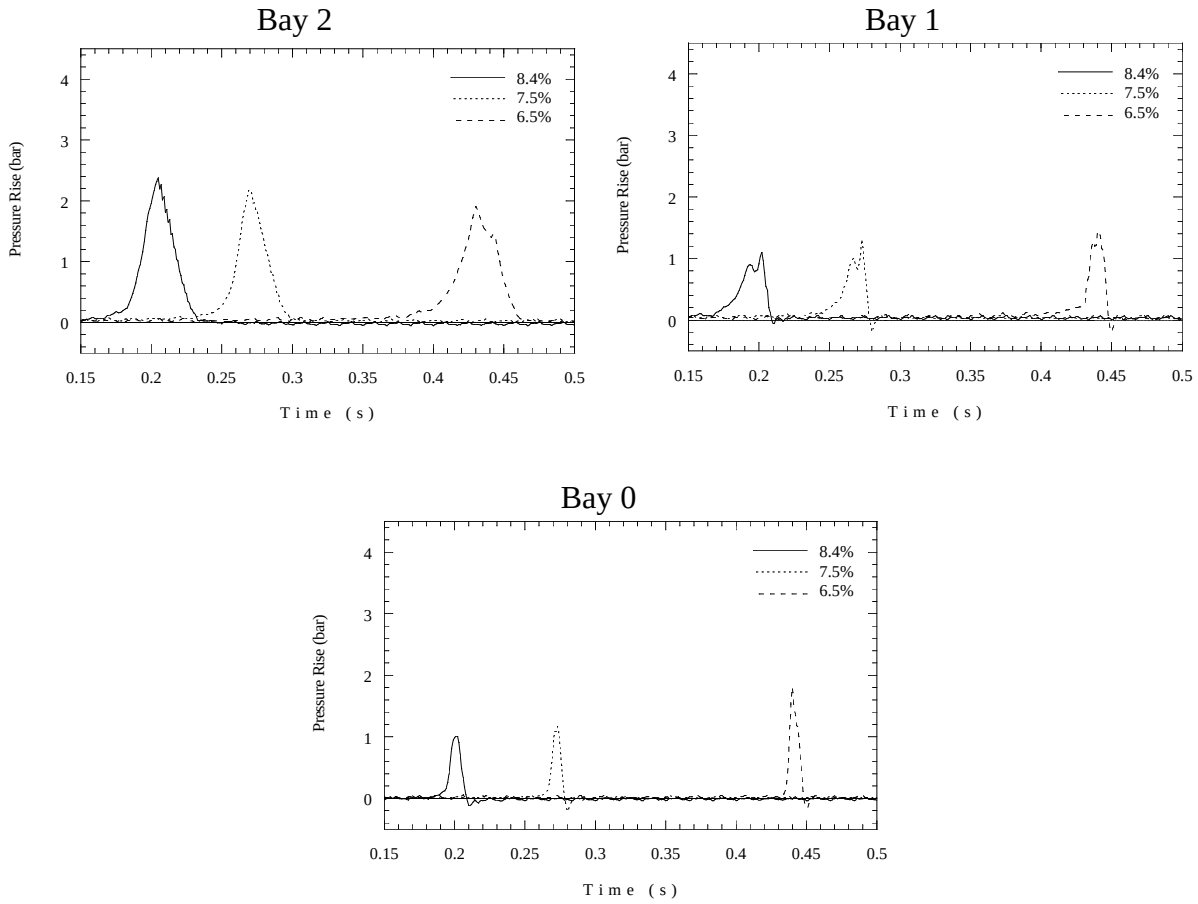

Figure 6.34: Comparison of pressure traces for bays 2, 1, and 0 in part-strong tests with fuel concentrations of 8.4% (Test 22), 7.5% (Test 23), and 6.5% (Test 24). Part 2 of 2.

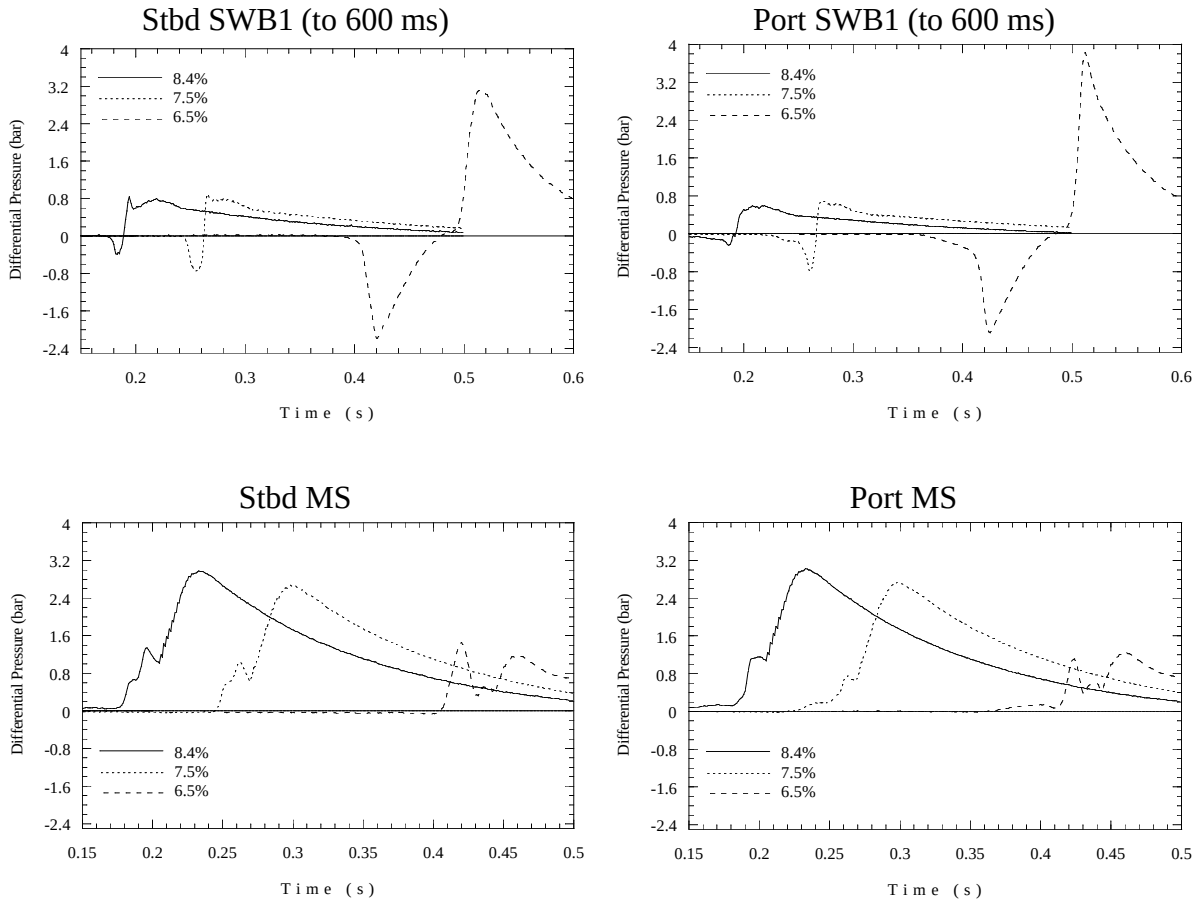

Figure 6.35: Comparison of differential pressures for SWB1 and MS. Part-strong tests with fuel concentrations of 8.4% (Test 22), 7.5% (Test 23), and 6.5% (Test 24). Part 1 of 2.

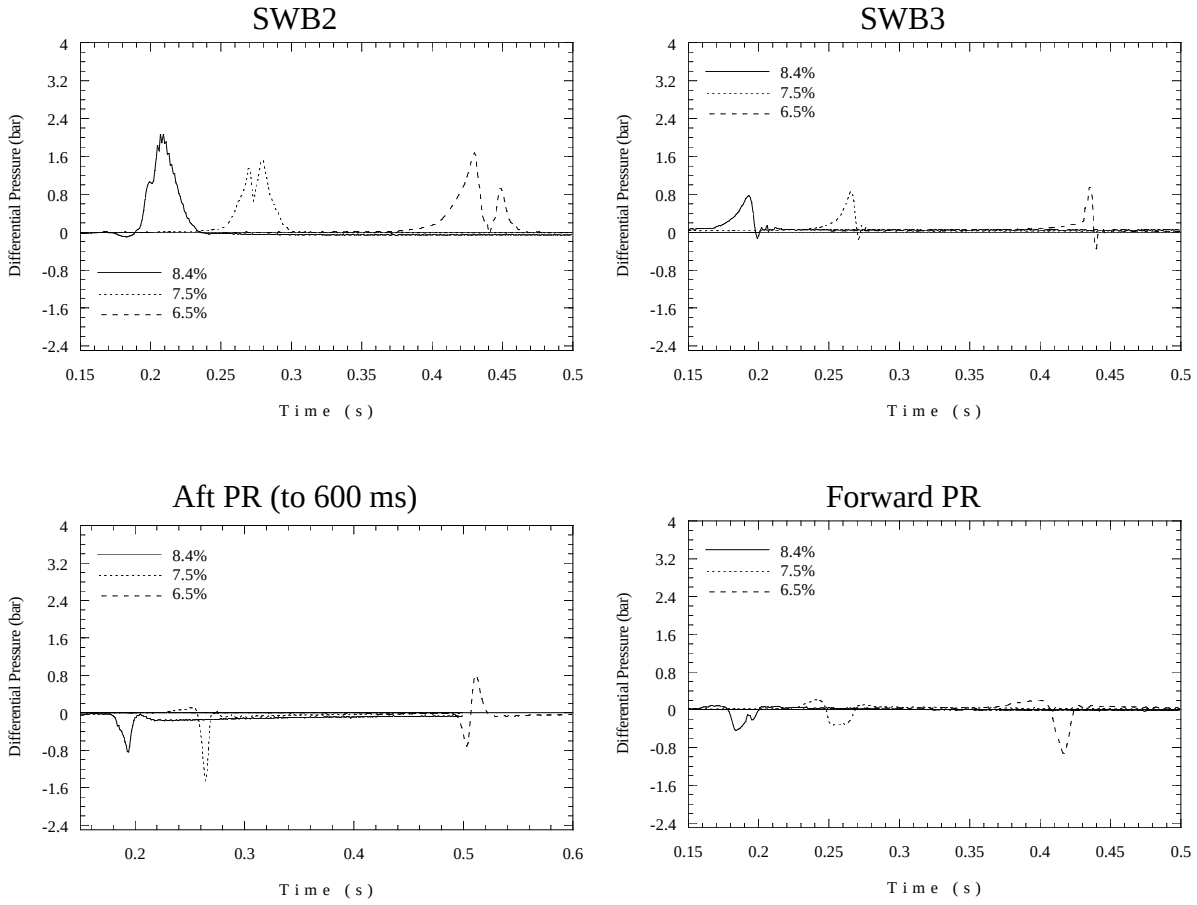

Figure 6.36: Comparison of differential pressures for SWB2, SWB3, and PRs. Part-strong tests with fuel concentrations of 8.4% (Test 22), 7.5% (Test 23), and 6.5% (Test 24). Part 2 of 2.

6.8 Partition Failure

(Comparisons of Tests 4, 17, and 18.) In this section we contrast the results from three tests with the same ignitor location and fuel concentration but with differing ranges of partition failure. The initial portions of the pressure transient are similar for all of these cases, but shifted to earlier times when the partitions fail. With no failure (Test 4), 25 ms elapsed from start of pressure rise to the peak in bay 4. For failure of only FS, SWB3, and MP (Test 17), the duration of the event was 30 ms from start of pressure rise to the peak in bay 4. For the all-weak case (Test 17), about 23 ms elapsed from the start of pressure rise to the first failure of SWB3. In general, partition failure reduces the peak pressures by a factor of about two. The late, rapid pressure rise in bay 4 caused by bay 5 ignition is barely visible in the all-weak tests. In addition, the forward partitions fail before pressure piling is seen in the forward bays. Figure 6.37 shows the peak differential pressures from these tests.

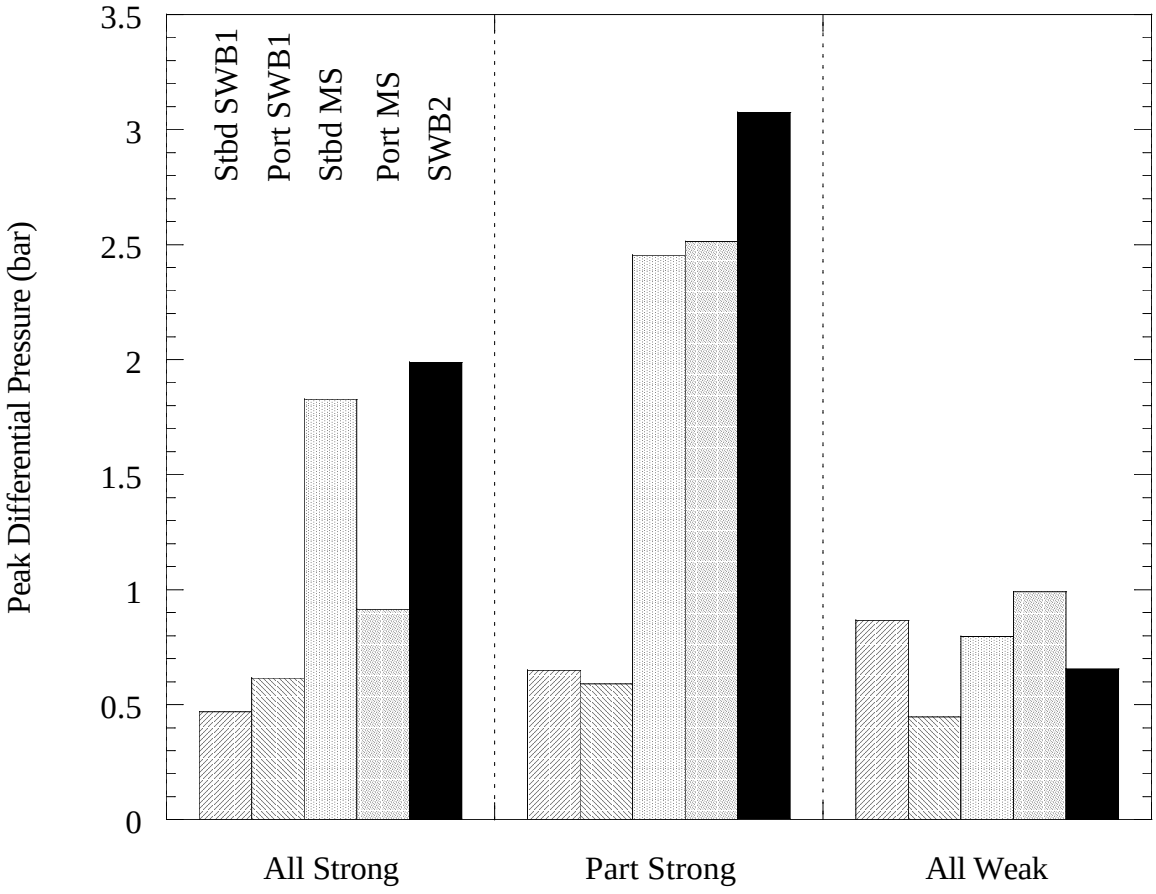

Figure 6.37: Comparison of peak differential pressures for different structural configurations, Test 4 (all-strong), Test 17 (part-strong), and Test 18 (all-weak). Ignition in bay 5 for all tests. Only the positive peak values are shown here, see the data in Appendix B for tabulated postive and negative peak values.

Partition failures result in sequential load transfer as the forward partitions fail and the

next one in line becomes the boundary to atmospheric pressure. The initial differentials are similar in the all-strong and part-strong cases, Tests 4 and 17. Once SWB3 and FS fail in Test 17, SWB2 is the barrier to atmosphere. In Test 17, SWB2 experiences a greater differential pressure than in Test 4, but this is quickly alleviated by rupture of the manufacturing panel. That shifts the pressure boundary back to the MS. In Fig. 5.153 (p. 202), we see that the MS differential jumps up as it becomes the forward boundary. The differential across SWB1 also goes up slightly, as bays 3 and 4 are venting faster than 5 and 6. Likewise, the vent stringers see a jump once SWB3 fails. Prior to failure, the differentials across the port MS and the forward PR are similar until failure begins.

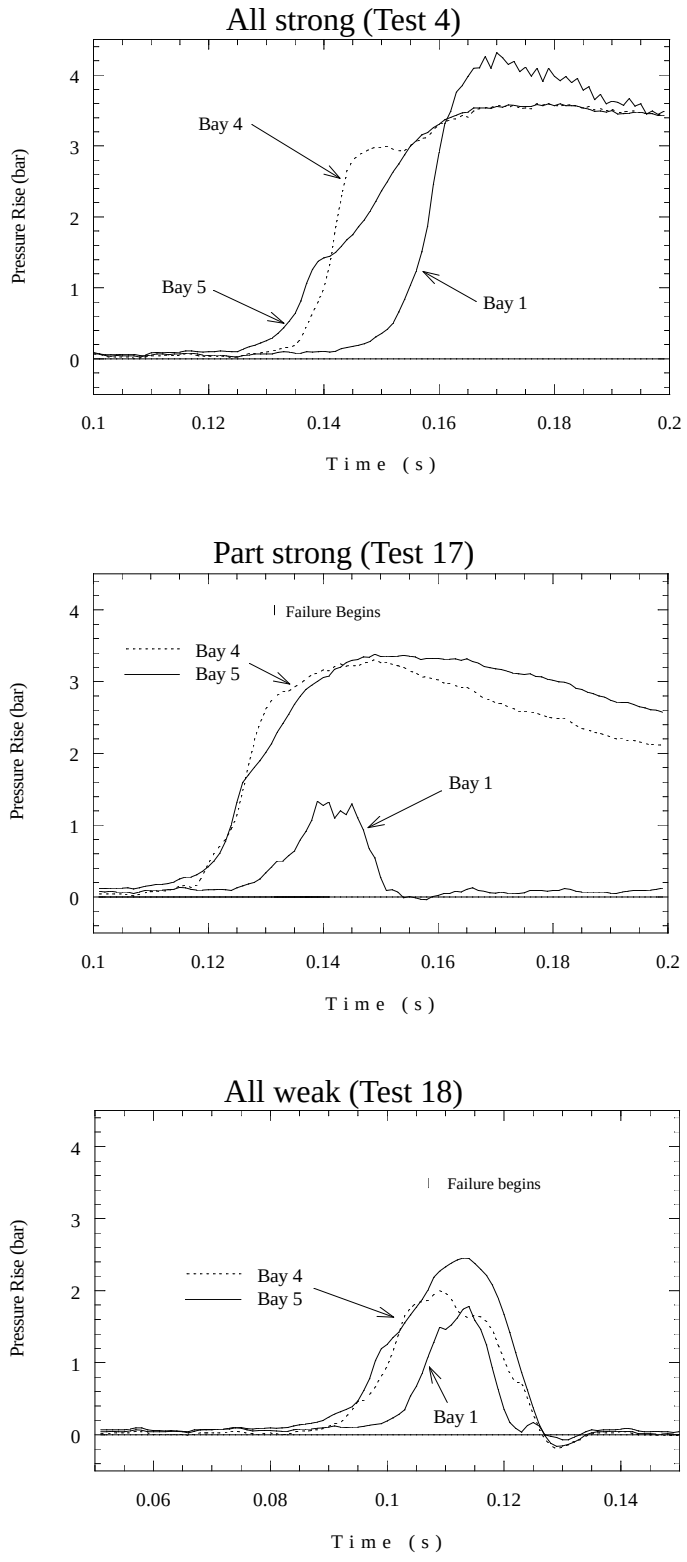

Figure 6.38: Pressure traces for three strutural configurations, Tests 4, 17, and 18. Ignition in bay 5 for all tests.

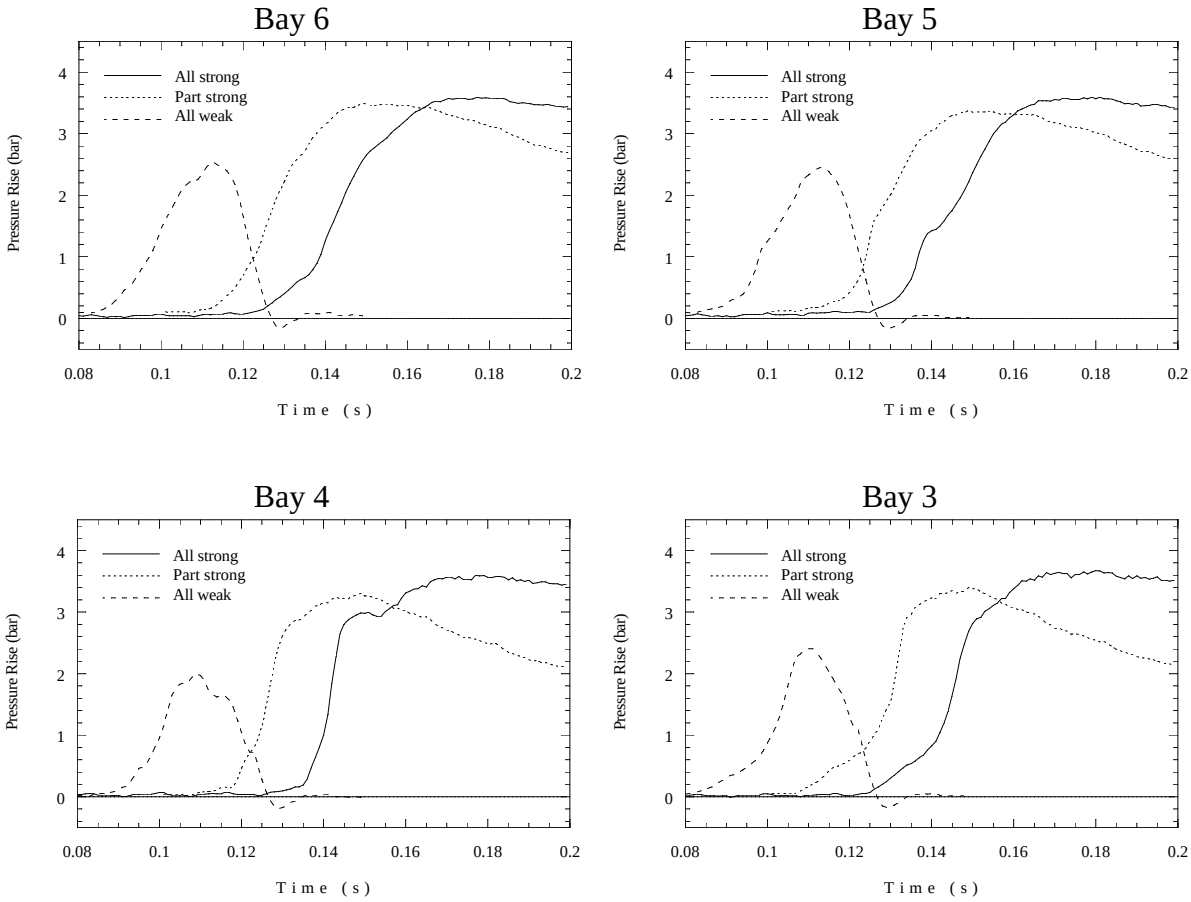

Figure 6.39: Comparison of pressure traces in bays 6, 5, 4, and 3 for three structural configurations, Tests 4 (all-strong), 17 (part-strong), and 18 (all-weak). Ignition in bay 5 for all tests.

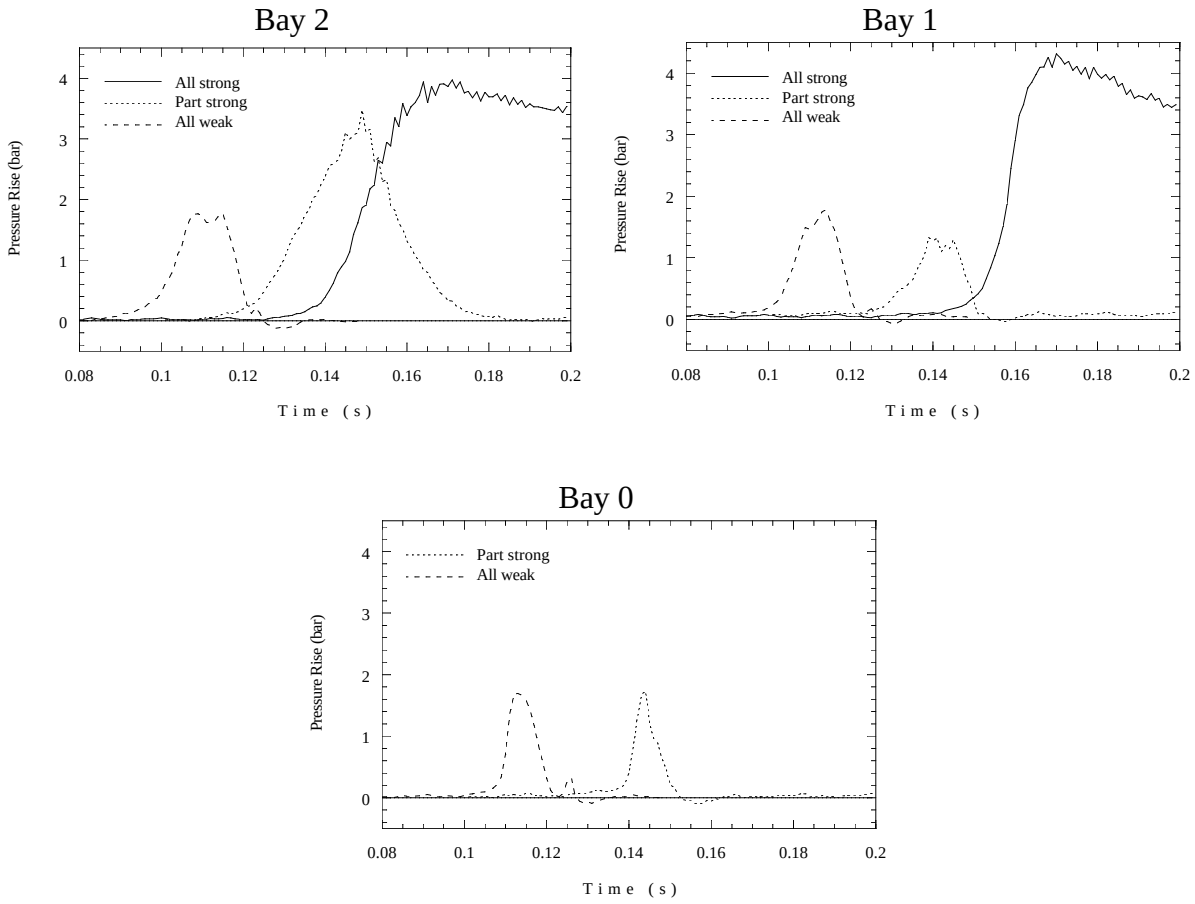

Figure 6.40: Comparison of pressure traces in bays 2, 1, and 0 for three strutural configurations, Tests 4 (all-strong), 17 (part-strong), and 18 (all-weak). Ignition in bay 5 for all tests.

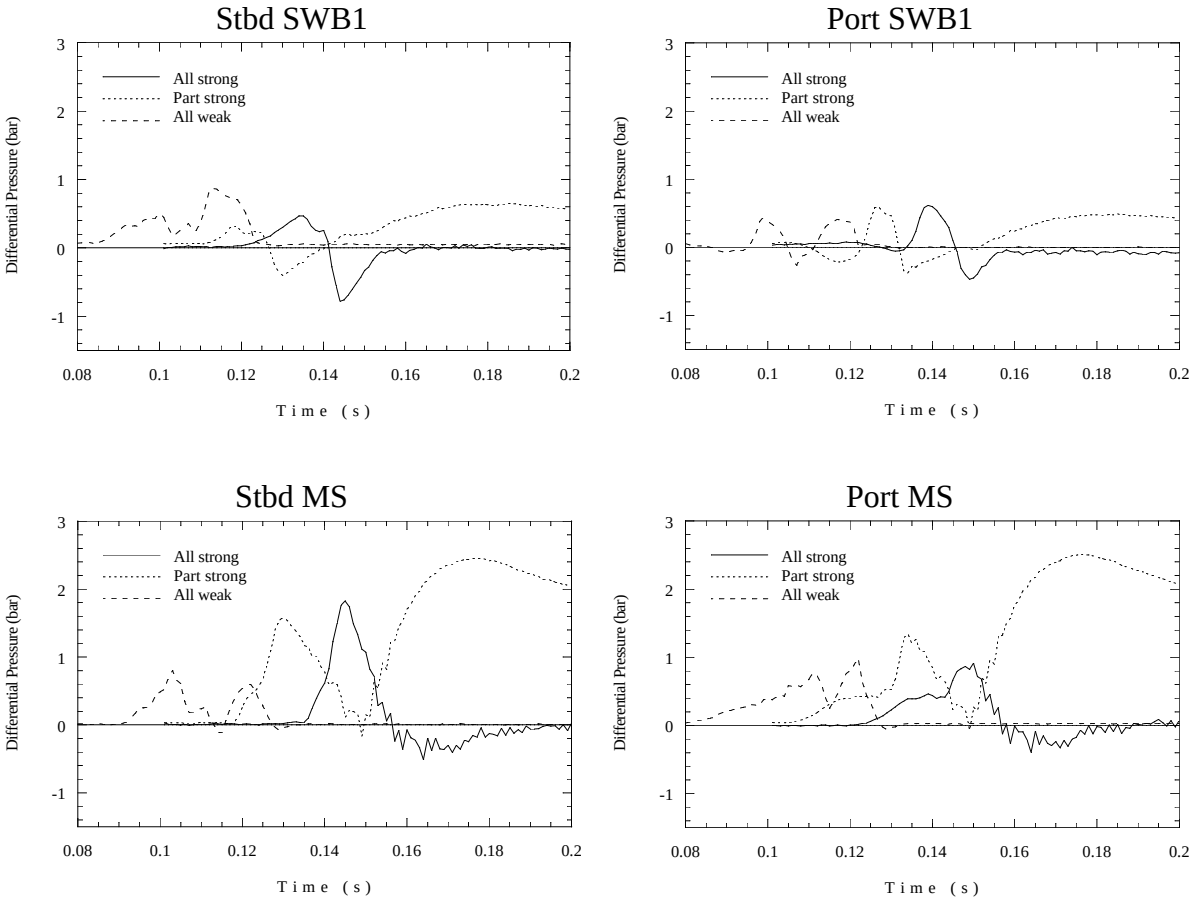

Figure 6.41: Comparison of differential pressures across SWB1 and MS for three strutural configurations, Tests 4 (all-strong), 17 (part-strong), and 18 (all-weak). Ignition in bay 5 for all tests.

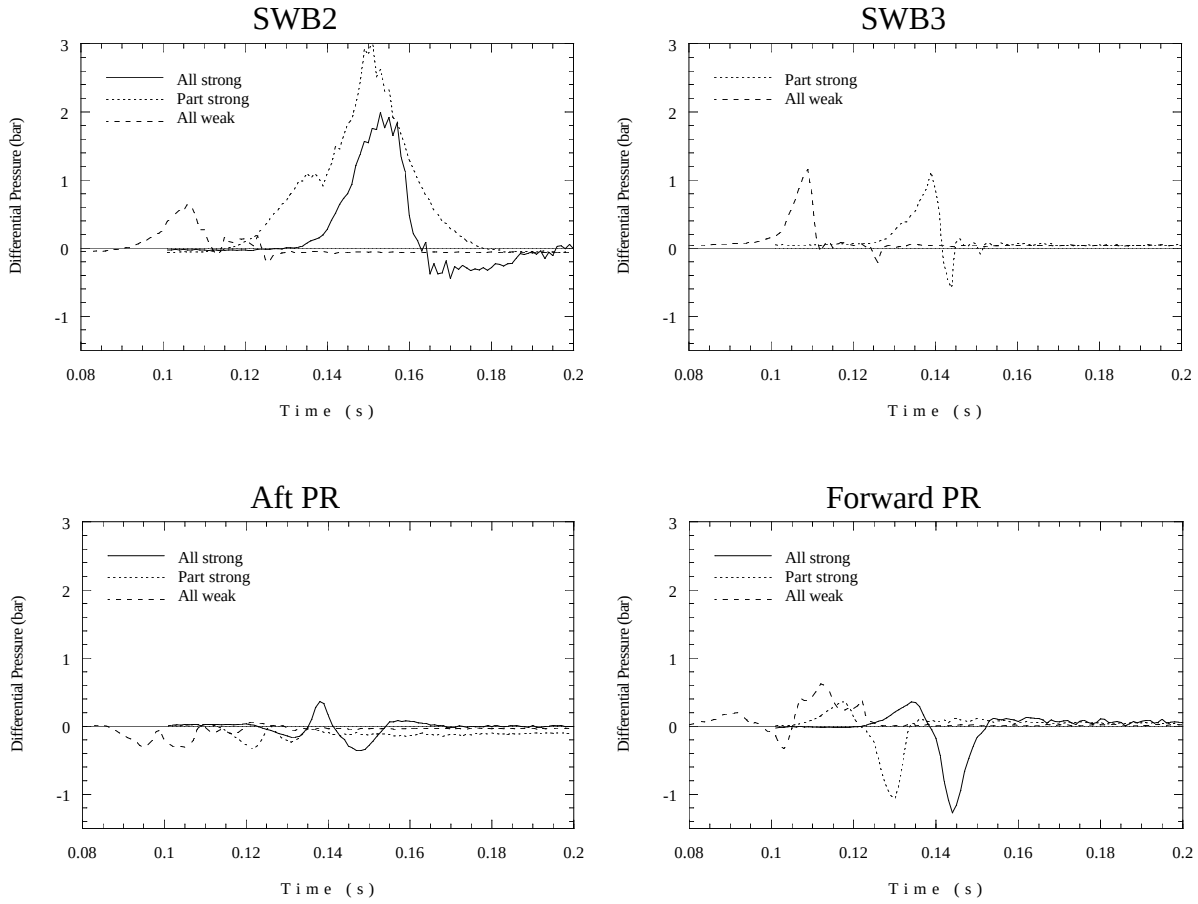

Figure 6.42: Comparison of differential pressures across SWB2, SWB3, and PRs for three strutural configurations, Tests 4 (all-strong), 17 (part-strong), and 18 (all-weak). Ignition in bay 5 for all tests.

6.9 Effect of Cold Liquid Jet A Layers

(Comparisons of Tests 4 vs. 8, 17 vs. 28, and 18 vs. 19.) This section compares wet (with a cold liquid Jet A layer and gaseous simulant) and dry (gaseous simulant only) tests in the all-strong, part-strong, and all-weak configurations with ignition in bay 5. The bay cameras indicate that the jet fuel ignition occurred after the gaseous fuel combustion was well underway in all cases. The effect of the liquid layer on the vapor combustion was pronounced in some cases but not evident in others. In the all-strong (4 vs. 8) and part-strong (17 vs. 28) configurations, the presence of a Jet A liquid layer apparently causes the rapid portion of the burn to occur 20 to 60 ms earlier. In the all-weak configuration (18 vs. 19), there are no obvious systematic differences between the two tests. There is one other set of part-strong comparison tests, 22 vs. 27, (not discussed in this section) with a different ignition location, 2Lo. Test 22 unfortunately had jet ignition through the fuel manifold, which may invalidate the comparison. Onset of the rapid burning phase is 45 ms earlier in Test 27 (vapor and liquid Jet A) than in Test 22 (vapor simulant only). Until further replica testing is carried out, it is not clear if these time differences are significant or simply reflect the intrinsic variability in the results of these tests.

Once the rapid combustion phase does start, the pressure signals were qualitatively very similar in the wet and dry cases. The magnitudes of the peak differential pressures (Fig. 6.43) are not identical due to the instrinsic variability in the results of these tests, but there are no obvious systematic differences.

6.9.1 All-Strong Configuration

(Comparison of Tests 4 and 8.) The combustion event happens 58 ms earlier in Test 8 (wet) than in Test 4 (dry), but this could be due partially to the tank temperature difference: 12°C for Test 4, 22°C for Test 8. The peak pressure in bay 1 is only 0.1 bar higher in Test 8 than in Test 4. The pressure rises began over a range of 15 ms for Test 8 vs. 17 ms in Test 4. The pressure in bay 1 rises much faster in Test 8 than in Test 4. The peak pressures in bays 1 and 2, and also the MS differential pressure, are higher and persist longer in Test 8 than in Test 4. In Test 8, the peak pressure in bays 3 and 4 are 0.7 bar higher than in Test 4. Positive differential pressures across SWB1 are much higher in Test 8 than in Test 4. However, in Test 8 the rapid ignition in bay 1 results in a lower differential pressure across SWB2 than in Test 4.

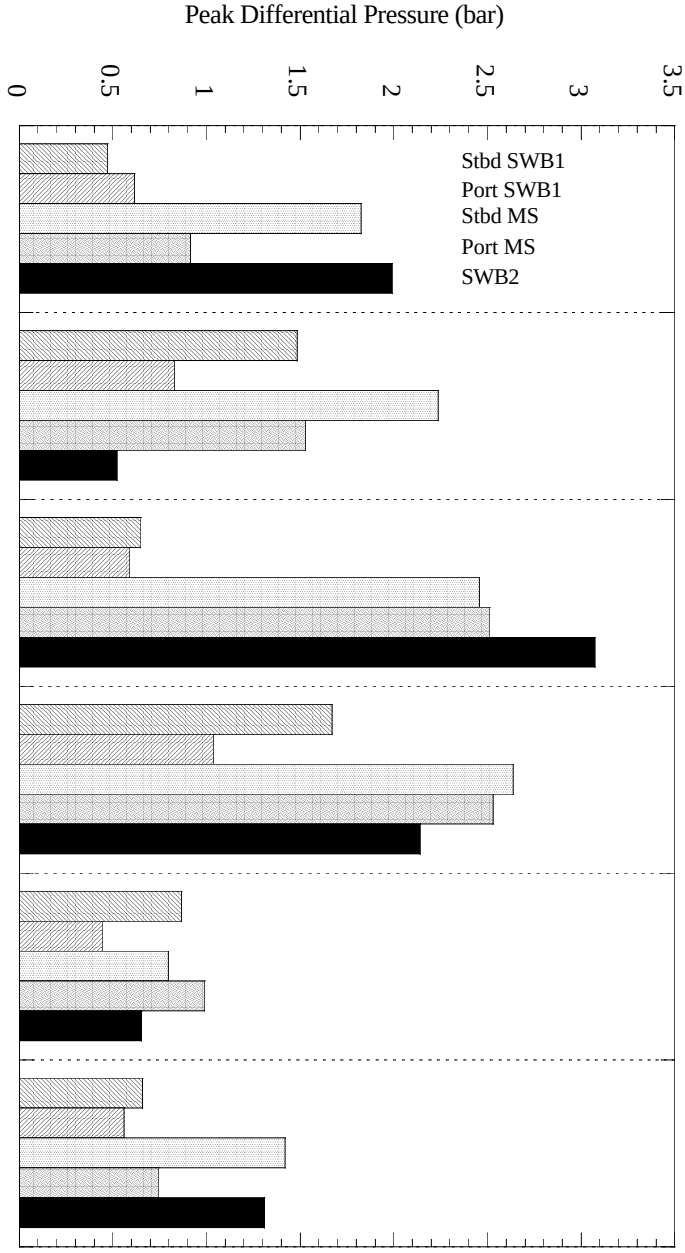

Figure 6.43: Comparison of peak differential pressures with and without Jet A for all structural configurations. All strong: Test 4 (dry) vs. Test 8 (wet); part strong: Test 17 (dry) vs. Test 28 (wet); weak: Test 18 (dry) vs. Test 19 (wet). Only the positive peak values are shown here, see the data in Appendix B for tabulated postive and negative peak values.

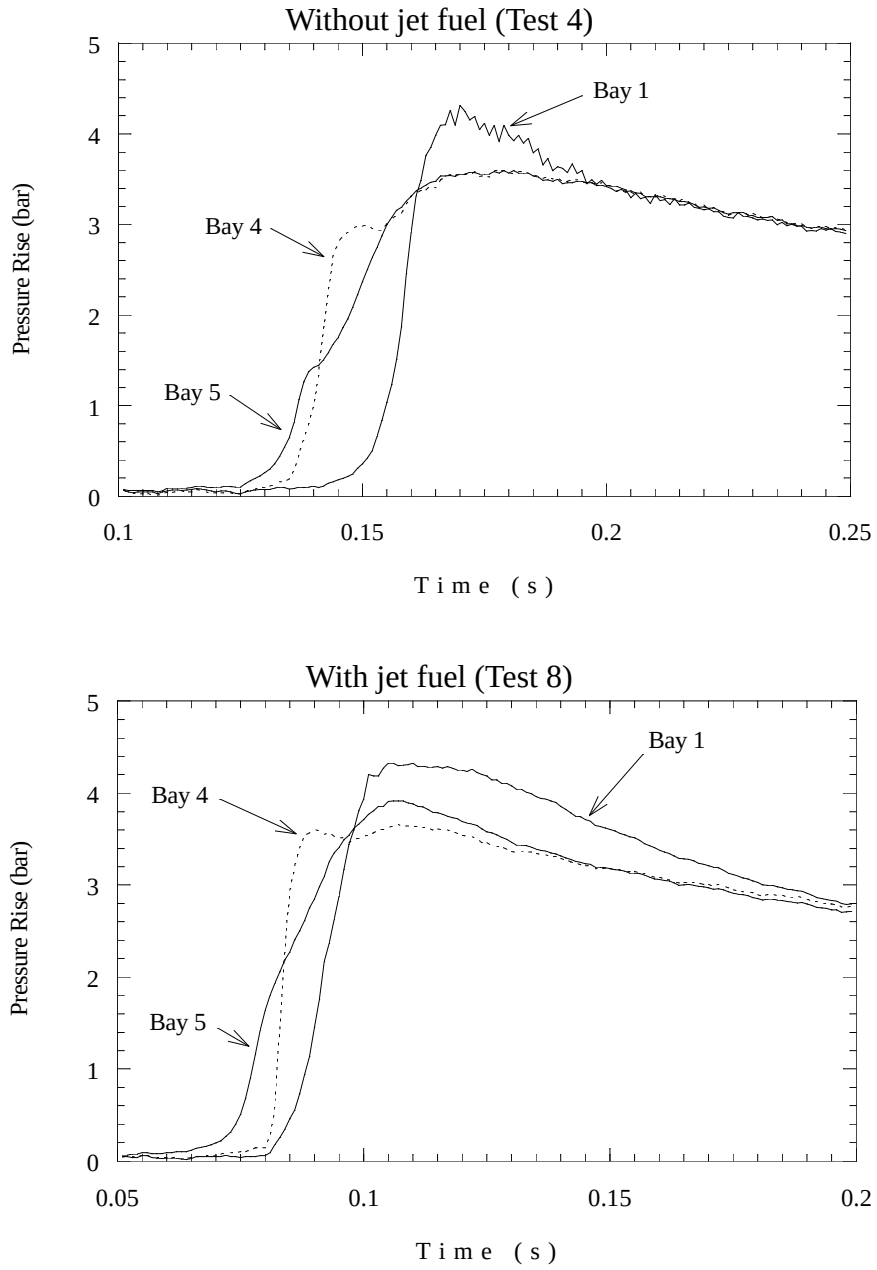

Figure 6.44: Comparison of pressures in bays 5, 4, and 1 for all-strong tests with (Test 8) and without (Test 4) a layer of cold liquid Jet A.

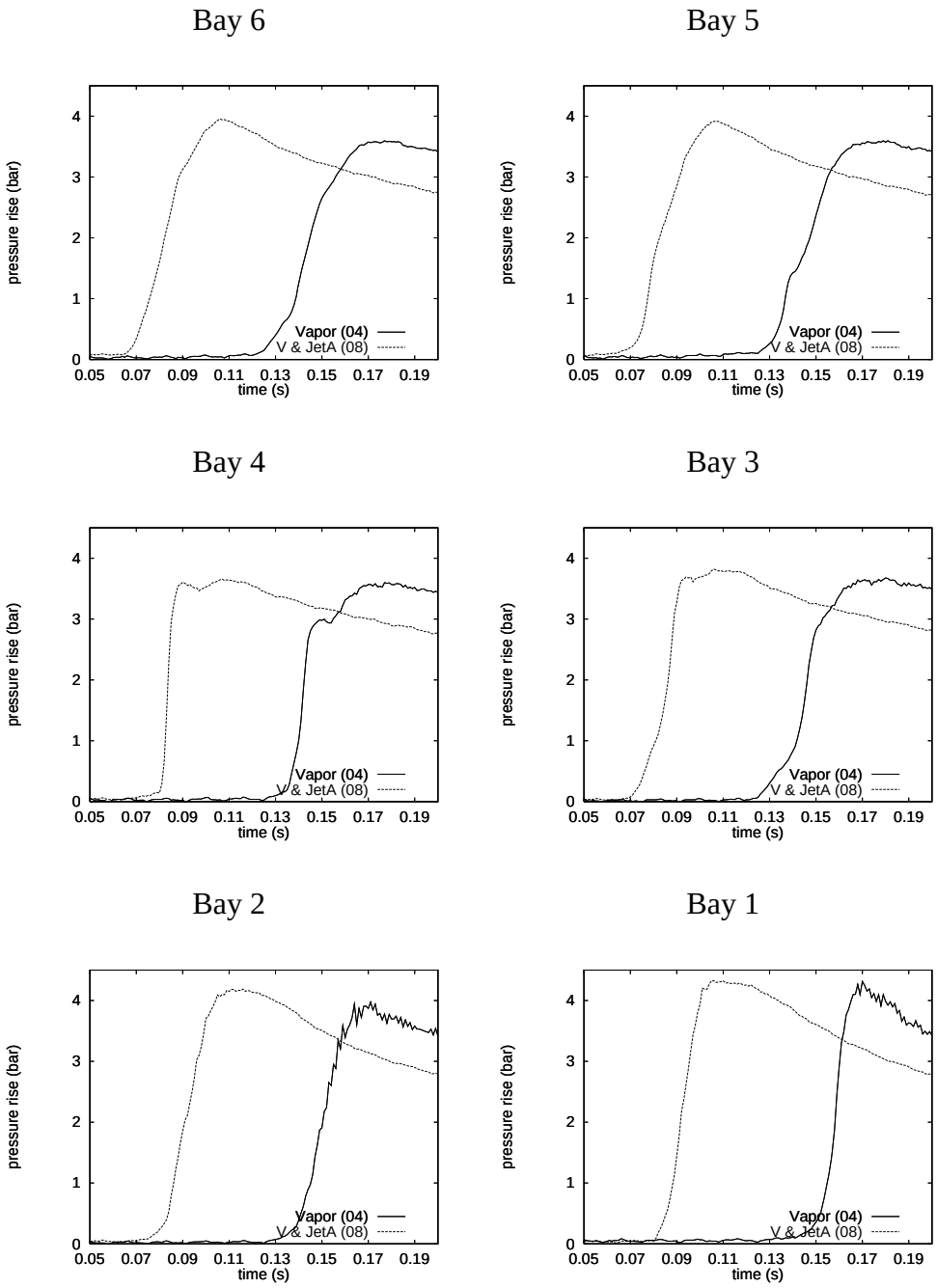

Figure 6.45: Comparison of individual pressure traces: all-strong, with (Test 8) and without (Test 4) cold liquid Jet A layers, ignition in bay 5.

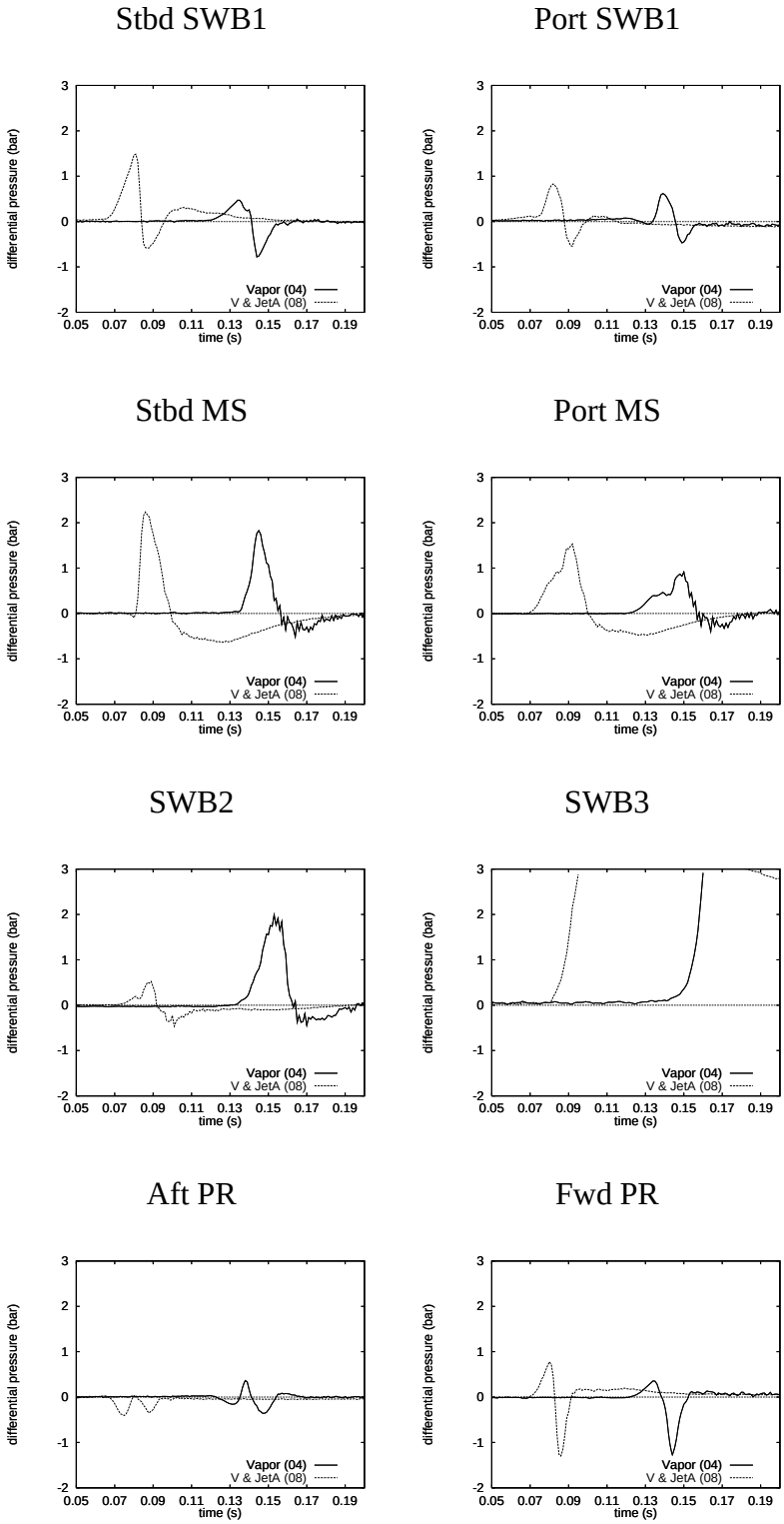

Figure 6.46: Comparison of differential pressures: all-strong, with (Test 8) and without (Test 4) cold liquid Jet A layers, ignition in bay 5.

6.9.2 Part-Strong Configuration

(Comparisons of Tests 17 and 28.) The pressure rise starts earlier by 17 ms when Jet A is present (Test 28). The bay 4 ignition process appears more rapid with the Jet A (Test 28) than without (Test 17). As remarked in the previous section, this may just be test-to-test variation. The initial temperatures were: 17°C(Test 17) and 10°C(Test 28). The bay 1 pressure trace is nearly identical in both cases, indicating the dominance of failure effects in determining the forward bay pressure histories. The pressure in bay 2 decays slightly slower in Test 17 than in Test 28. The peak pressure in bay 2 in Test 17 was about 0.4 bar higher. The bay 4 peak pressure in Test 28 was 0.4 bar higher than the peak pressure in Test 17.

The pressure differentials were similar in both tests, with the main differences caused by timing and the more rapid bay 4 pressure rise in Test 28. This is responsible for the big differences on starboard SWB1 and MS between the two tests. The differential pressure on SWB2 was about 1 bar higher in Test 17 than in Test 28. A similar effect was observed in the all-strong comparisons (see Section 6.6.1).

In Test 8, we saw that the gaseous fuel burned before the lofted Jet A. Perhaps this is the reason for smaller differences between wet and dry tests when weak partitions are present. The failure occurs before the lofted fuel gets ignited, so the majority of lofting and combustion occurs outside the tank, or after the partitions have failed. After the failure, only bays 3 – 6 can maintain high pressures, but lofting is not as severe in these bays (especially in bays 5 and 6).

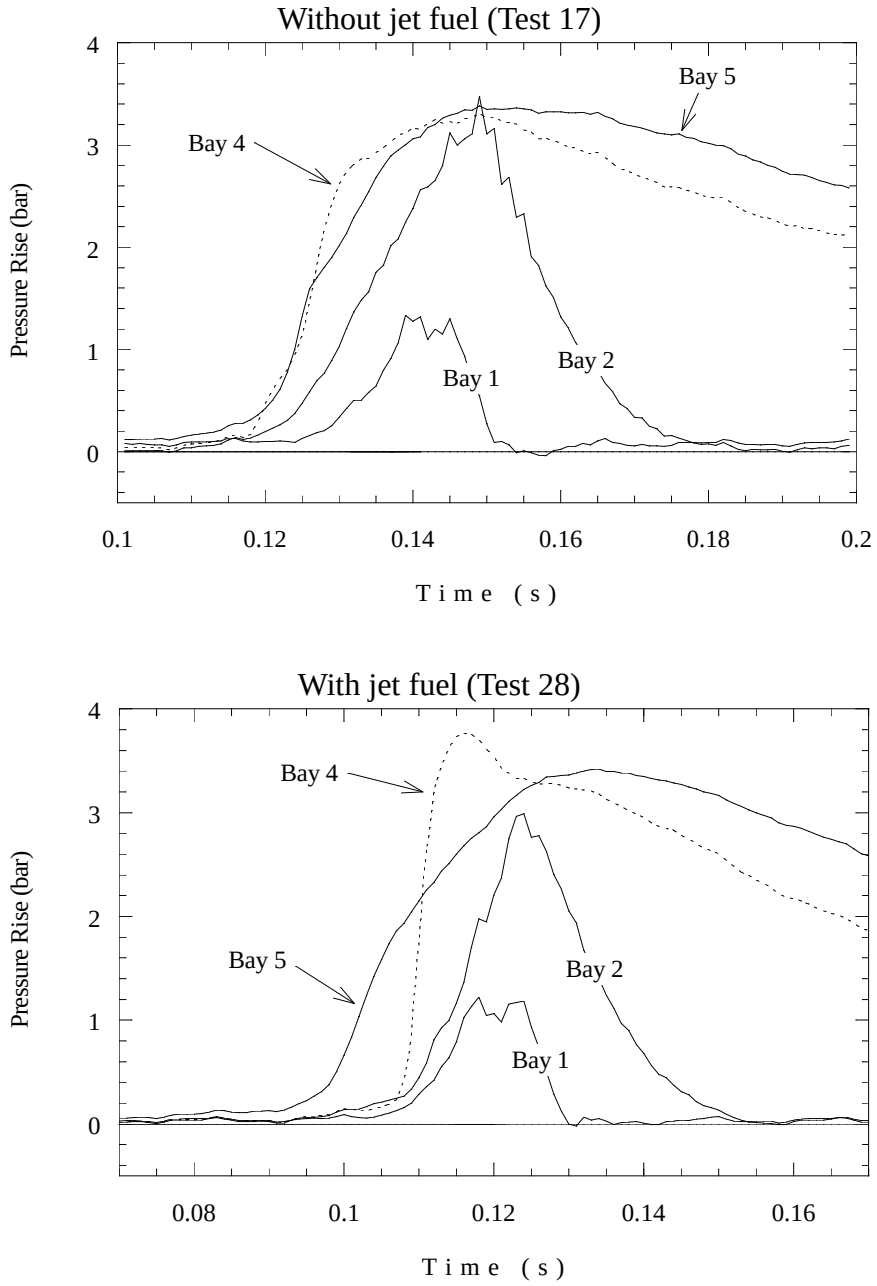

Figure 6.47: Pressure traces for bays 1, 2, 4, and 5 for part-strong tests with (Test 28) and without (Test 17) cold liquid Jet A layers.

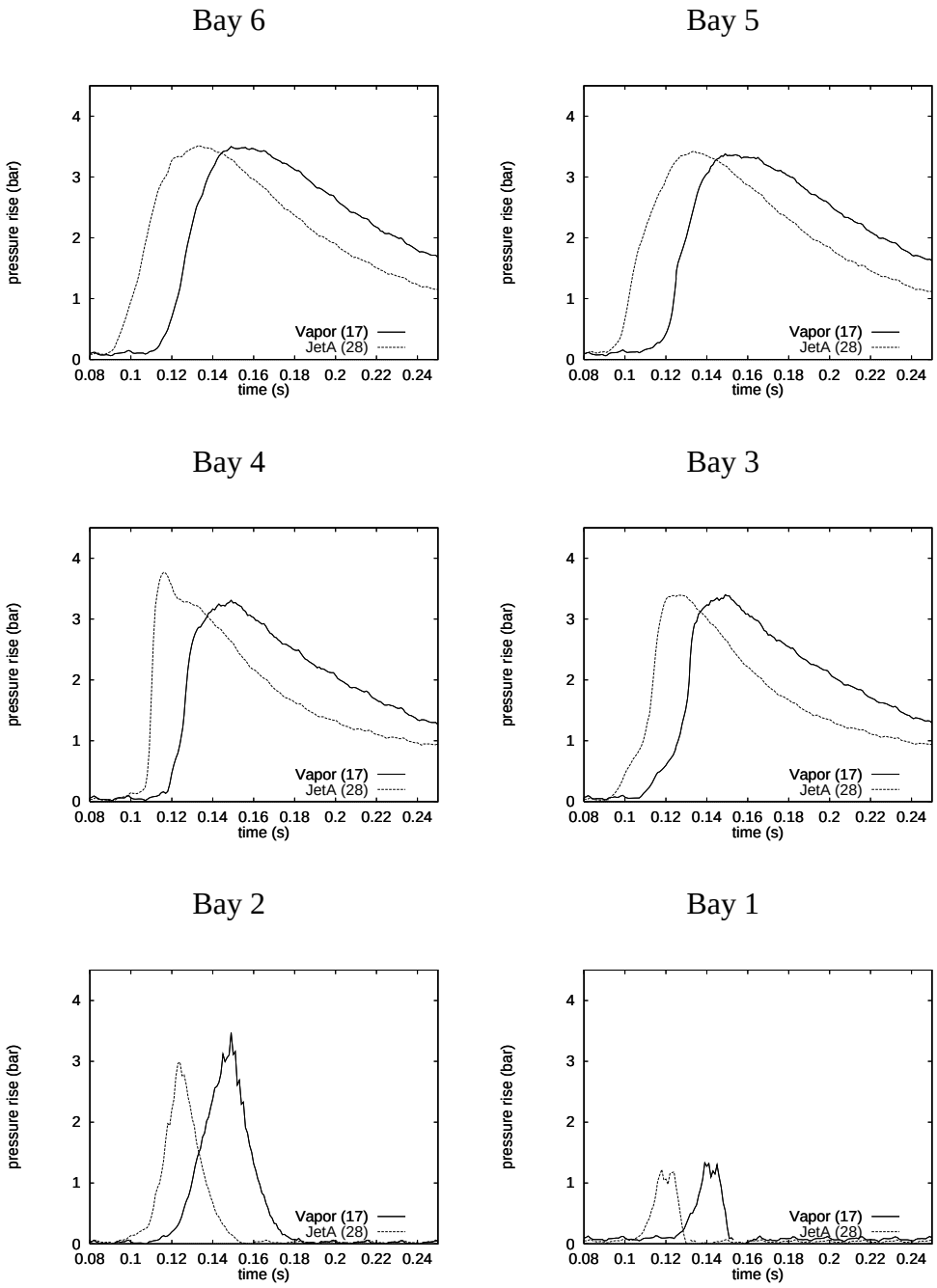

Figure 6.48: Comparison of individual pressure traces for each bay in the part-strong configuration with (Test 28) and without (Test 17) cold liquid Jet A layers, ignition in bay 5.

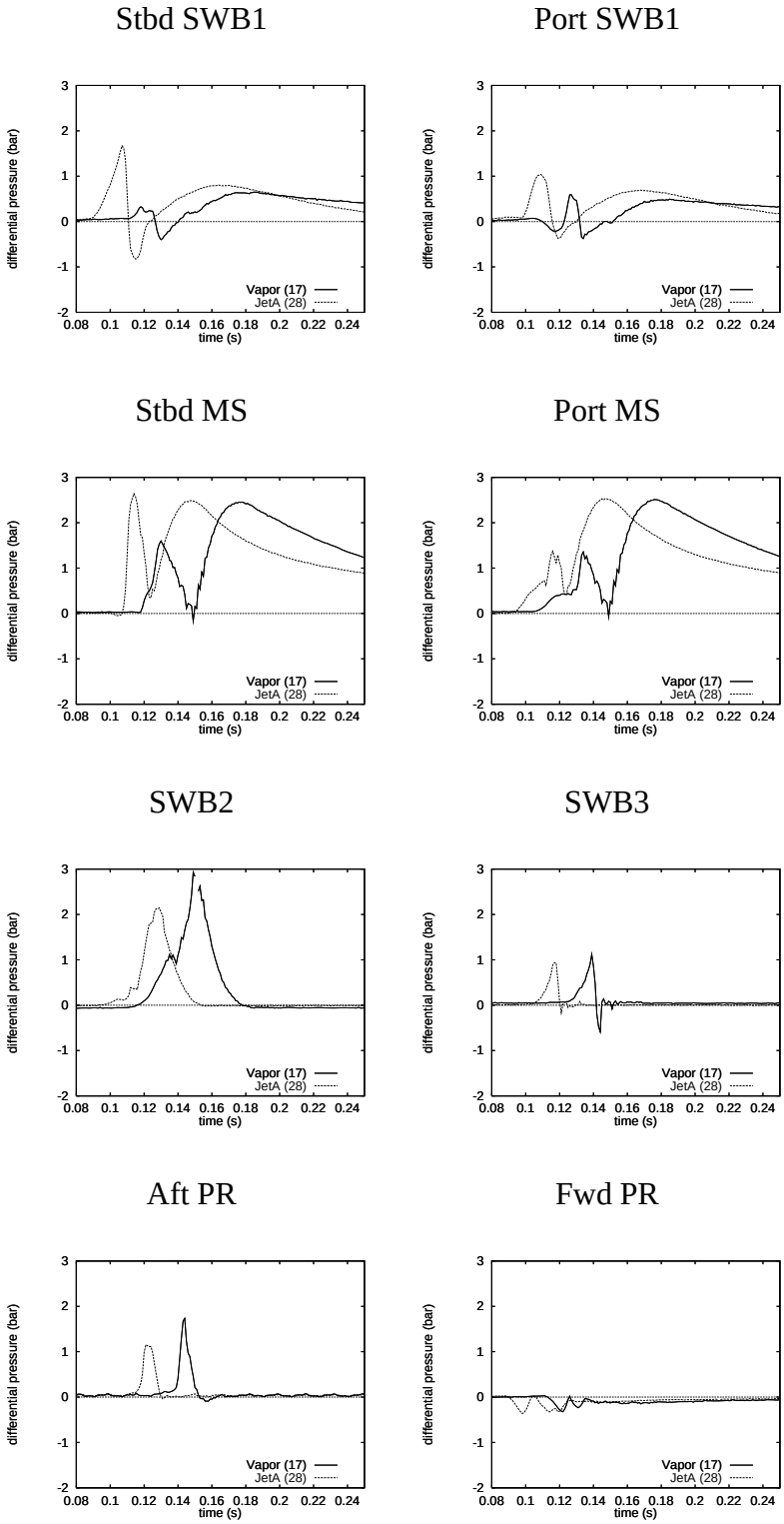

Figure 6.49: Comparison of differential pressures, part-strong configuration with (Test 28) and without (Test 17) cold liquid Jet A layers, ignition in bay 5.

6.9.3 All-Weak Configuration

(Comparisons of Tests 18 and 19.) The pressure traces in the aft bays (3 – 6) are nearly identical in these two tests. Slightly higher peak and differential pressures are observed in bays 0, 1, and 2 with the Jet A layer (Test 19) than without (Test 18). The differential pressures in the two tests are very different, perhaps due to test-to-test variations in failure characteristics of the panels. Only the aft PR differential pressure is comparable in the two tests.

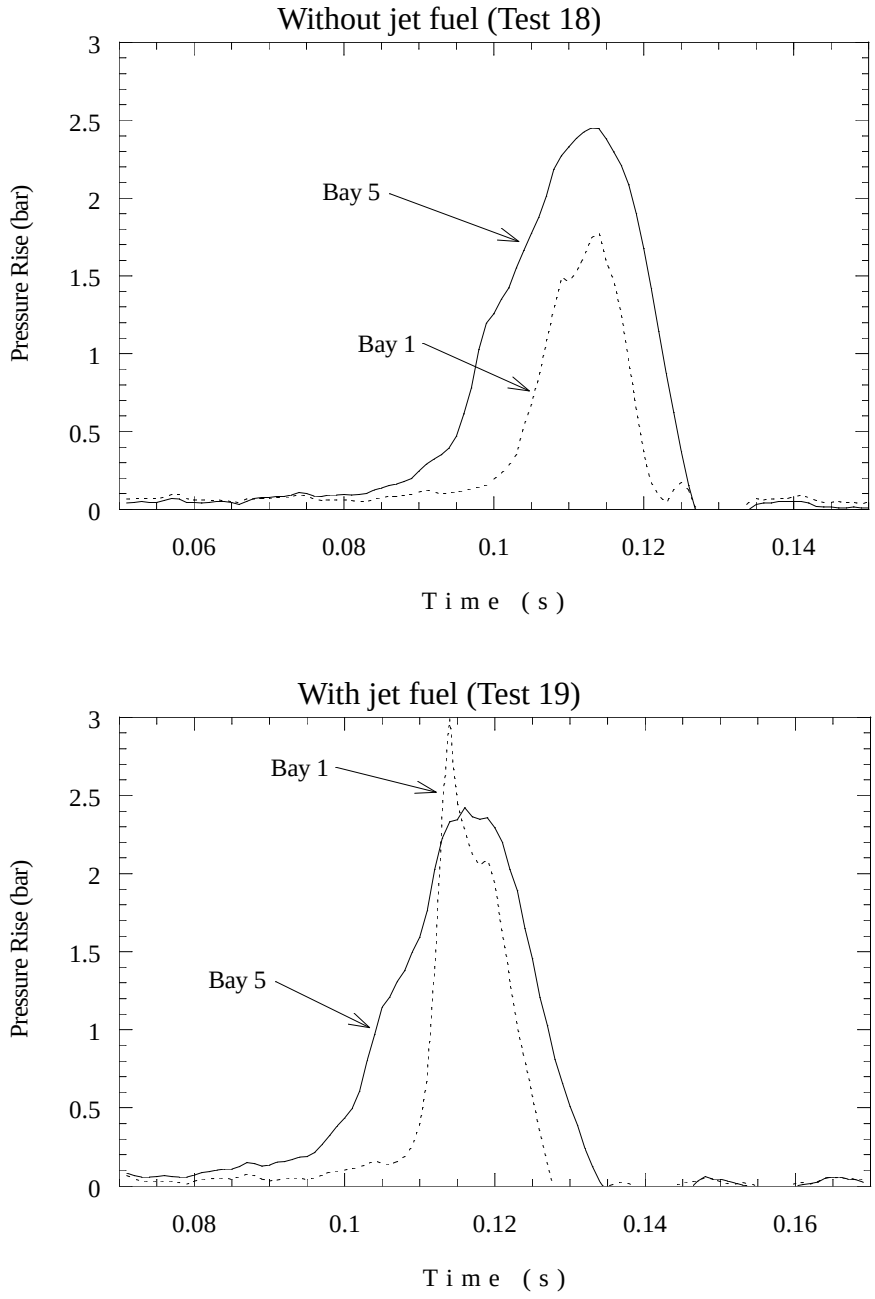

Figure 6.50: Pressure traces for bays 1 and 5 for all-weak tests with (test 19) and without (18) a cold liquid Jet A layer.

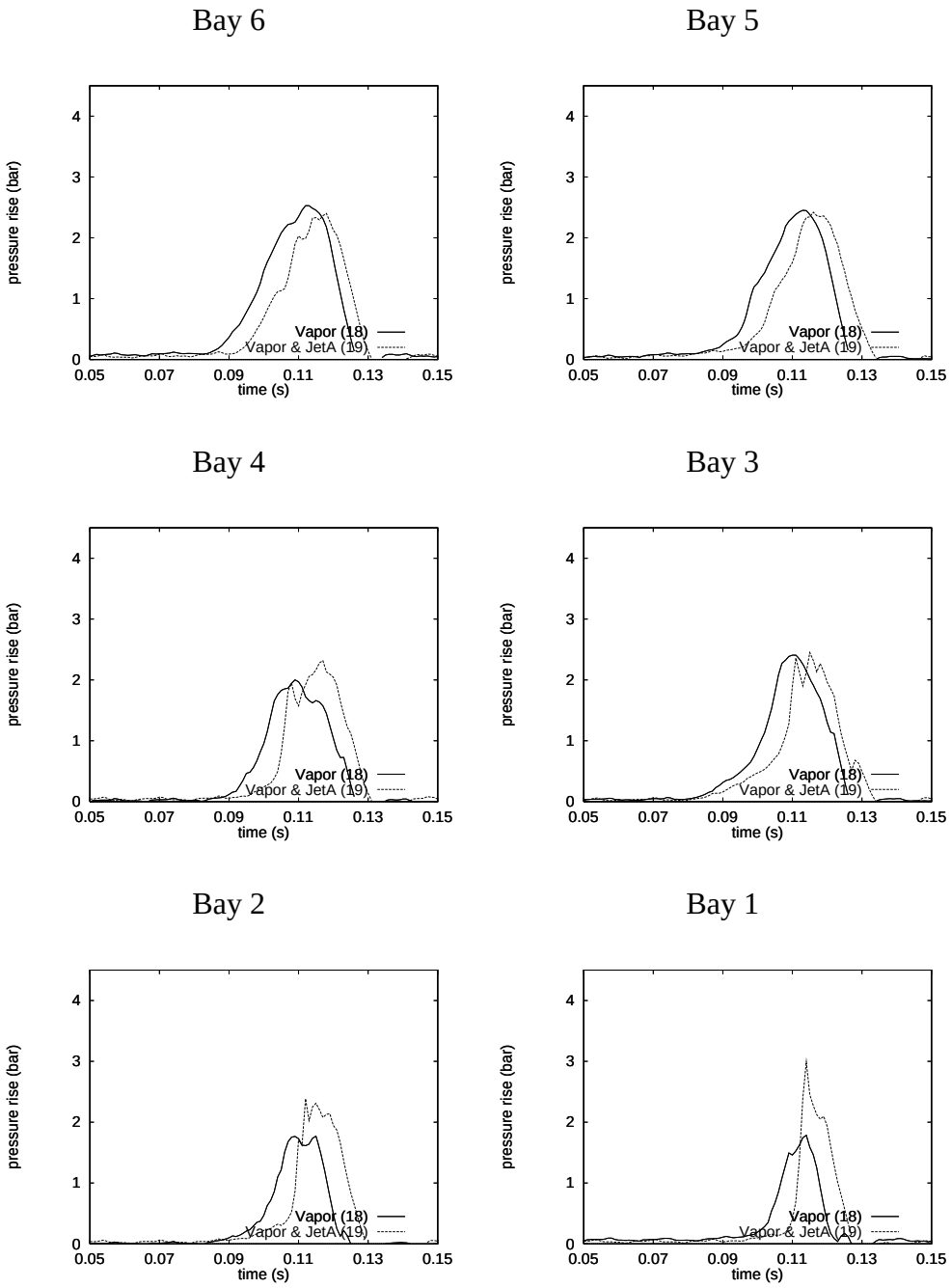

Figure 6.51: Comparison of pressure traces for all bays in the all-weak tests with (Test 19) and without (Test 18) cold liquid Jet A layers.

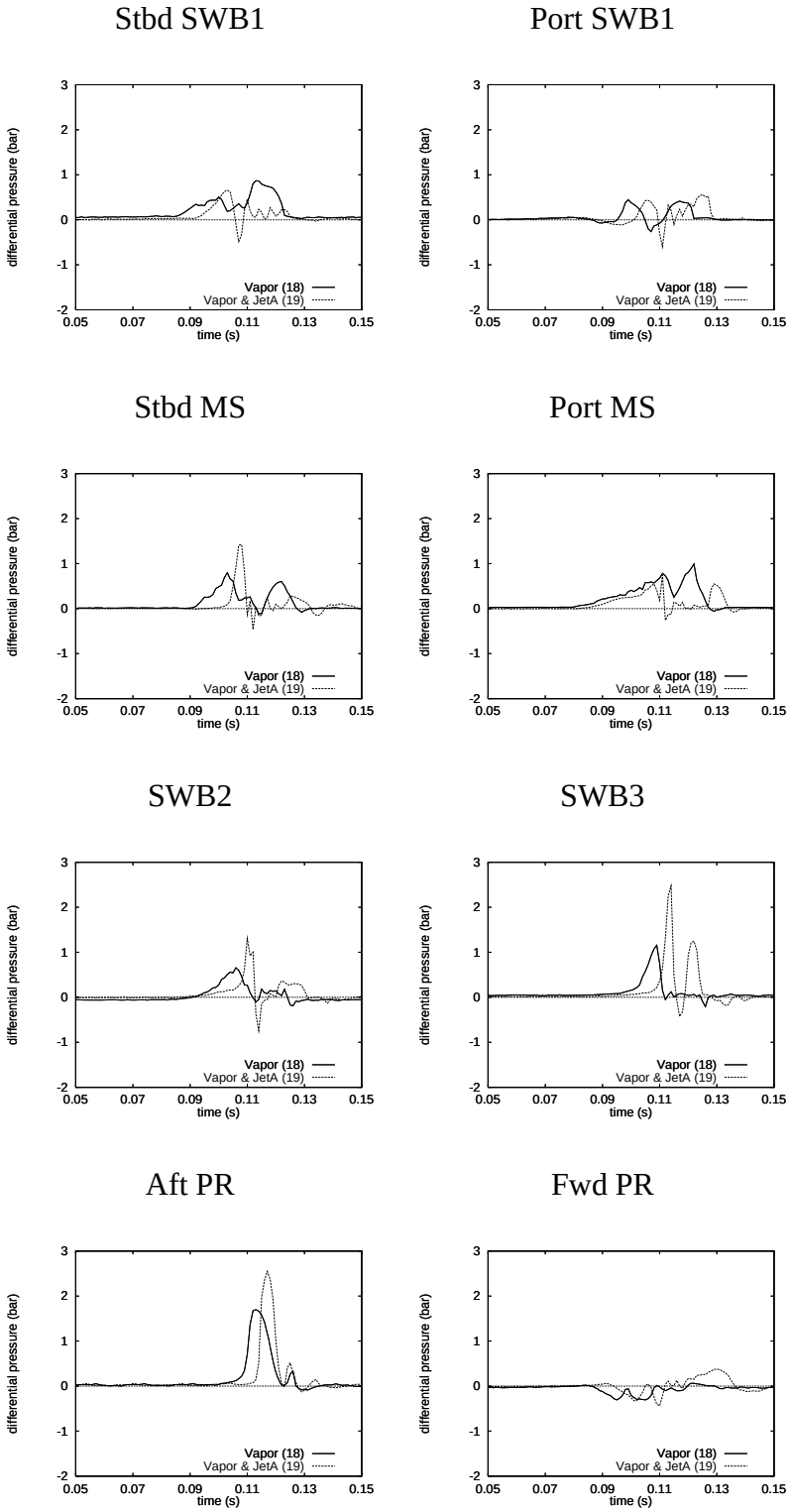

Figure 6.52: Comparison of differential pressures in the all-weak tests with (Test 19) and without (Test 18) cold liquid Jet A layers.

6.10 Cargo-Bay Configuration

(Comparisons of Tests 28 and 30.) The cargo-bay configuration (Test 30) is compared with part-strong configuration (Test 28) in Fig. 6.53. Both tests used the part-strong partition arrangement, had a cold layer of liquid Jet A, and ignition in bay 5. In Test 30, the FS was not installed in order to avoid impact damage to the transducers at the end of the mock cargo bay. There is a modest influence of the cargo bay model on the combustion process within the tank. In general, the magnitudes of the peak pressure and peak differential pressures are comparable in the two cases. Accounting for a time shift of about 10 ms, the pressure histories are both qualitatively and quantitatively comparable.

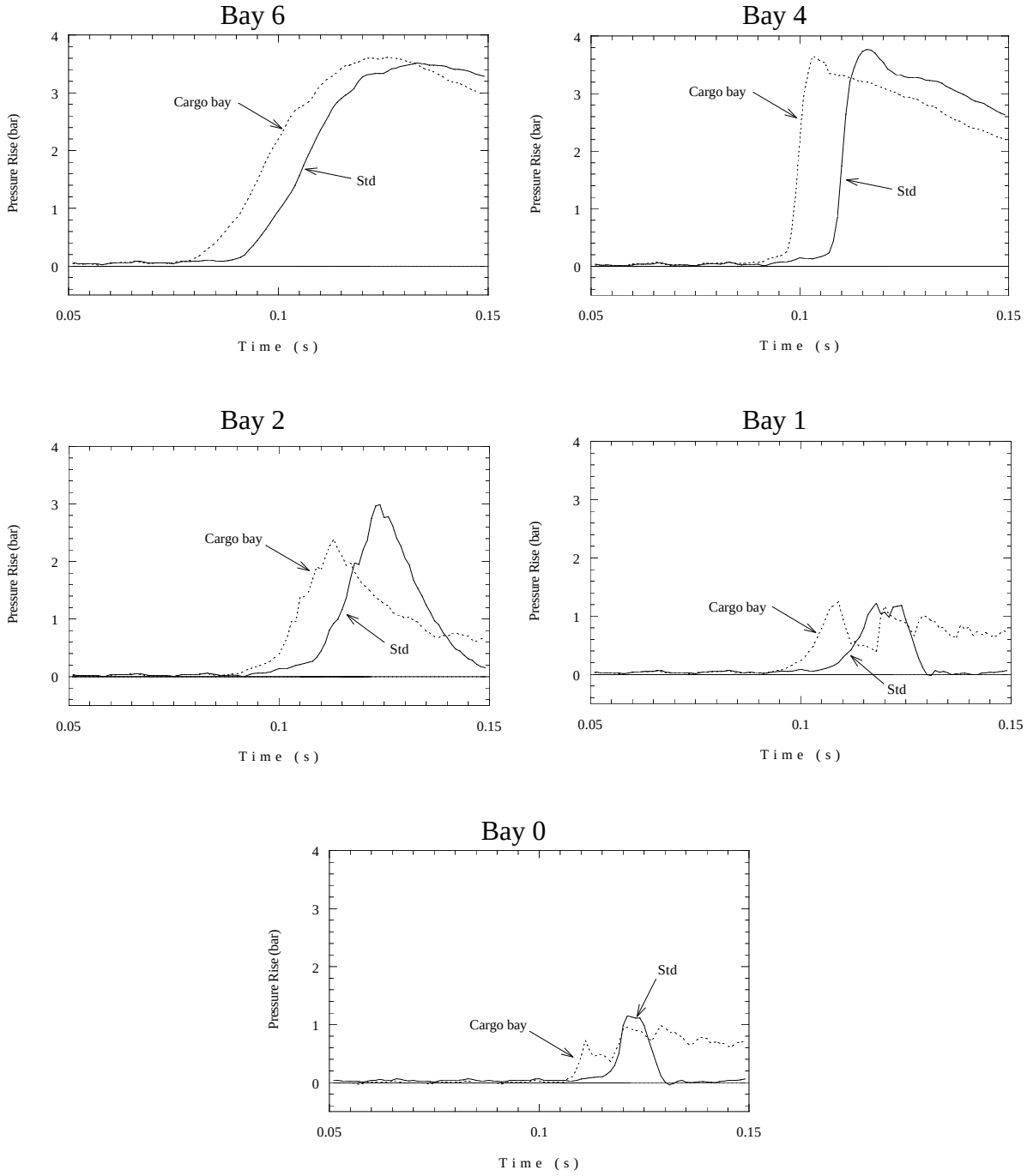

Figure 6.53: Comparison of pressures, cargo-bay configuration (Test 30) vs. standard part-strong configuration (Test 28). Ignition in bay 5, with cold liquid Jet A layer. Note that FS was not installed in the cargo bay test.

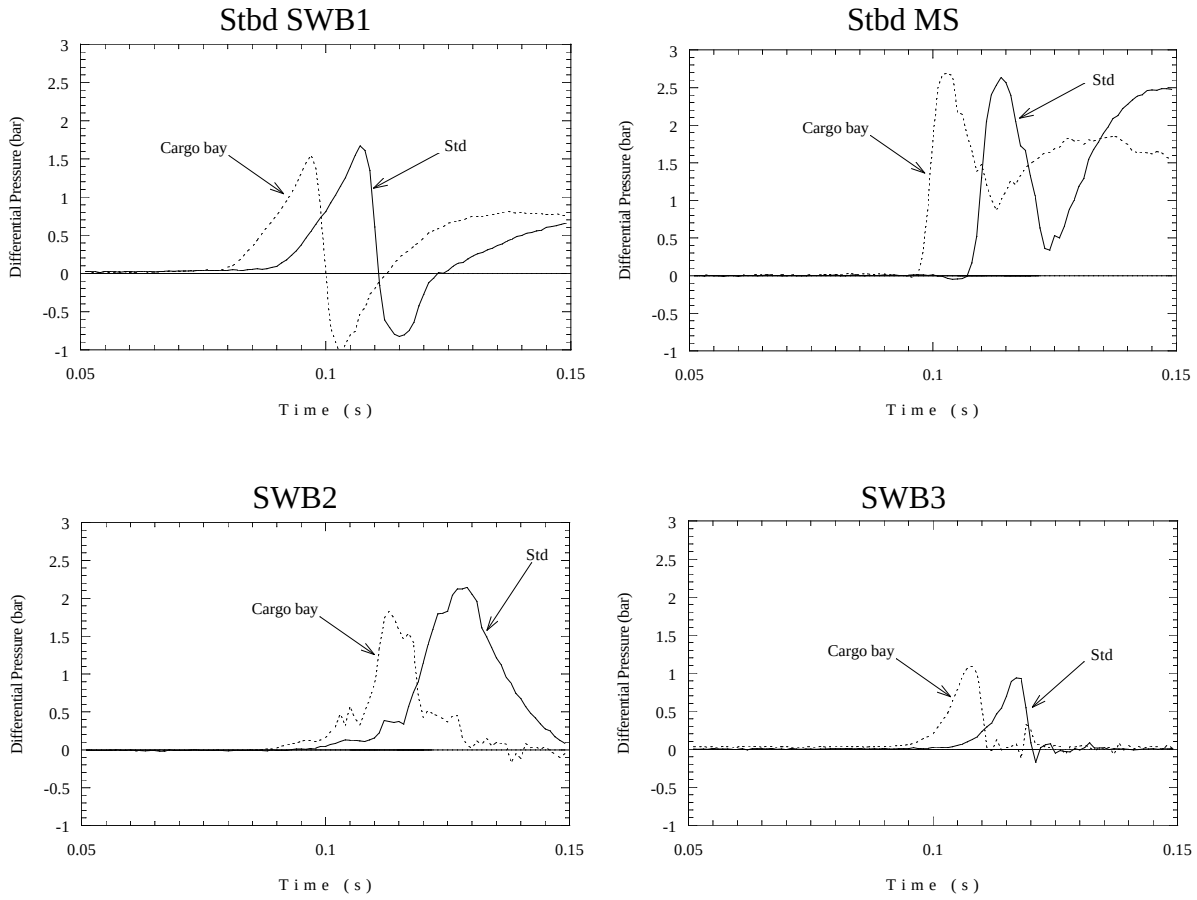

Figure 6.54: Comparison of differential pressures, cargo-bay configuration (Test 30) vs. standard part-strong configuration (Test 28). Ignition in bay 5, with cold liquid Jet A layer. Note that FS was not installed in the cargo bay test. Some differentials are missing because slow pressure transducers were moved into cargo bay from aft tank locations.

Chapter 7

Pressure Measurements

Two types of pressure measurements were made during these tests. The slow or static system consisted of a set of strain-gauge type (Endevco) gauges with a thermal protection system. The fast or dynamic system consisted of a set of piezoelectric (PCB) gauges with only a thin grease layer for thermal protection. The two instrument systems were chosen in order to record both rapid and slow pressure changes throughout the flame-propagation and partition-failure events. Both types of gauges have different operating characteristics which must be kept in mind when comparing the pressure traces.

Table 7.1: Frequency response of the pressure transducers as specified by the manufacturer.

Transducer type	Model	Upper frequency limit (MHz)	Lower frequency limit (Hz)
Fast or Dynamic	PCB 113A21	≥ 1	100 *
Slow or Static	Endevco 8530B-200	0.15	0

* for 1% accuracy

7.0.1 Frequency Response

The PCB gauges are referred to as “dynamic” gauges because they are insensitive to pressure variations of a sufficiently low frequency. The main application of these gauges in explosion research is to record the fast pressure changes associated with shock waves or detonations. However, these gauges can also produce useful data for much lower frequency signals, as obtained in the present tests, but some care must be take in signal interpretation.

The limitation in the present tests on the upper frequency response of the dynamic pressure measurement was the sampling rate chosen. The choice of sampling rate is based on the amount of time that must be recorded; the amount of memory available per channel; and the frequency of the phenomena being measured. The response time of the transducer itself is much faster than the sampling rate used (Table 7.1), therefore the sampling rate determines the upper frequency limit. The acquisition system cannot reproduce signal frequencies higher than

half the sampling frequency, hence the sampling rate places an upper bound on the frequency response of the pressure measurement system. The sampling rate for the dynamic gauges was 200 kHz, placing an upper frequency limit of 100-kHz pressure signals. The dynamic pressure measurement system therefore could not resolve pressure variations shorter than 10 μs. The data acquisition systems were capable of sampling much faster, up to 5 MHz, but the recording time would have had to have been shortened proportionately.

The low frequency response of the dynamic pressure gauges was determined by the time constant of the electronic circuitry associated with the FET amplifier located at the transducer. The time constant of the present arrangement was greater than or equal to one second. To maintain an accuracy of 1% or better in the pressure measurement, the period of the pressure signal must be shorter than 1% of the time constant, i.e., 10 ms. Theoretically, the lowest frequency pressure variation that can be accurately resolved is therefore 100 Hz. In actual practice, useful data can be obtained for much lower frequencies, possibly as low as 10 Hz. In the present tests, the discrepancy between the static and dynamic pressure gauges is generally of the order of 5% for signal frequencies of approximately 20 Hz, or a period of 50 ms. For transients longer than 50 ms, the dynamic pressure transducers will become increasingly inaccurate. A more serious drawback of using the PCB gauges over a long time period in a combustion experiment is the production of artifacts in the signal created by the heating of the sensitive element in the gauge.

The term "static" is applied to the Endevco gauges because they generate a true reading of static pressure. However, these are sophisticated instruments that can record pressure signals with frequency content up to 150 kHz. In the present tests, the actual upper frequency limit is affected by two factors: the sampling rate of the data acquisition system and the mounting method of the gauge. The static gauge signals were sampled at 1 kHz, so the upper frequency limit of the acquisition system was 500 Hz. In other words, the static pressure measurement system could not resolve pressure variations shorter than 2 ms due to the acquisition system. The transducer response is also limited by two pieces of porous sintered metal mounted in front of the transducer head to protect it from heat. The degree of high-frequency filtering from this mounting arrangement is not known precisely, but the effects can be evaluated experimentally by comparing the signals with those from the dynamic pressure gauges which were not mounted with sintered metal plates.

7.0.2 Resolution of Pressure Waves

The upper frequency limit of the static pressure gauges causes rapid pressure pulses to not be resolved. If the duration of a pressure pulse is much shorter than the response time of the static pressure measurement system (approximately 2 ms), then the pulse will not be recorded. Rapid pressure variations can result from various compression and expansion waves and in extreme cases, shockwaves. These wave phenomena can cause strong pressure peaks and oscillatory behavior that will not show in the static pressure signals. Figure 7.1 shows pressure oscillations of approximately 400 Hz caused by the rupture of a weak manufacturing panel in an otherwise all-strong configuration (Section 5.4.2). The oscillations only appear in the dynamic pressure trace and not in the static pressure trace.

It should be noted that in the present plots of the dynamic gauge signals, the raw data

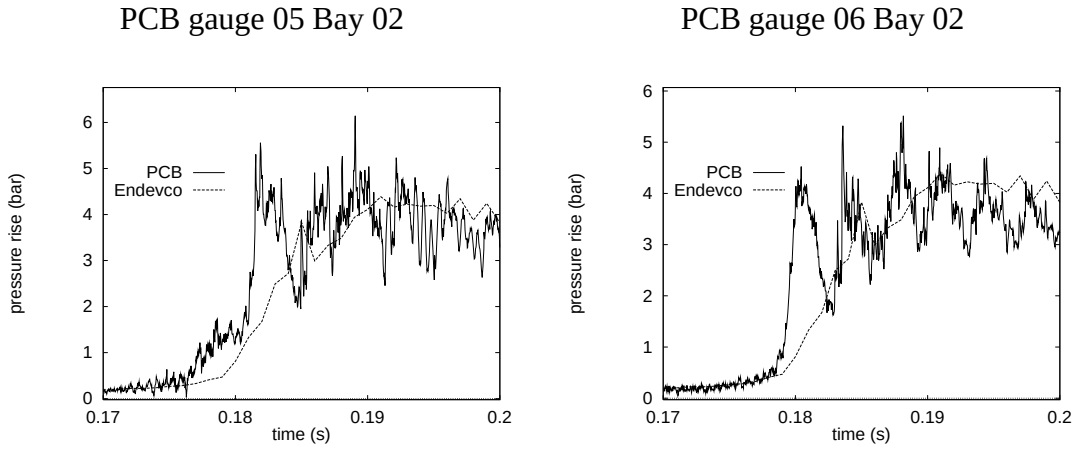

Figure 7.1: Oscillatory pressure behavior for Test 14, bay 2 recorded by (a) port side and (b) starboard side dynamic (PCB) gauges compared to the single static (Endevco) gauge in the bay.

from the acquisition system was processed with a 5-point moving average, then decimated so that only every 5th point remained. This was done to reduce the 10-Mbyte data files to a manageable size without changing the visual appearance of the plots.

Figure 7.2 shows examples of rapid pressure pulses in Test 19. At the leading edge of both dynamic pressure traces there is a sharp spike (shockwave) that is not observed in the static gauge signals. Note that the peak pressure given by the dynamic gauge is much higher (4 bar) than the peak pressure indicated by the static pressure signal (2.5 bar). Note also that this is an extreme case and the significance of such high pressures to structural response must be evaluated in view of the very short duration of the pulse.

In some tests, wave effects within a single bay produced differences in the port side and starboard side dynamic gauges. These effects were not resolved by the single, centrally located static gauge, as shown in Fig. 7.3. The double peak recorded by the starboard side dynamic gauge (Fig. 7.3b) does not appear in the port side gauge signal (Fig. 7.3a). The static gauge signal shows a single pressure peak with a peak pressure approximately the same as that of the dynamic gauge signals.

7.0.3 Time Lag

Another consequence of the limited frequency response of the static pressure gauges is that there can be a time lag between the true pressure and the recorded pressure. This is manifested as an lag or phase shift between the pressure as recorded by the PCB and the Endevco gauges. This time lag is a direct result of the signal filtering that occurs in the static pressure gauges. This effect is illustrated in Fig. 7.4 where a square pulse with rapid rising and falling edges is filtered through a system with a low upper frequency limit. A time lag develops in the filtered

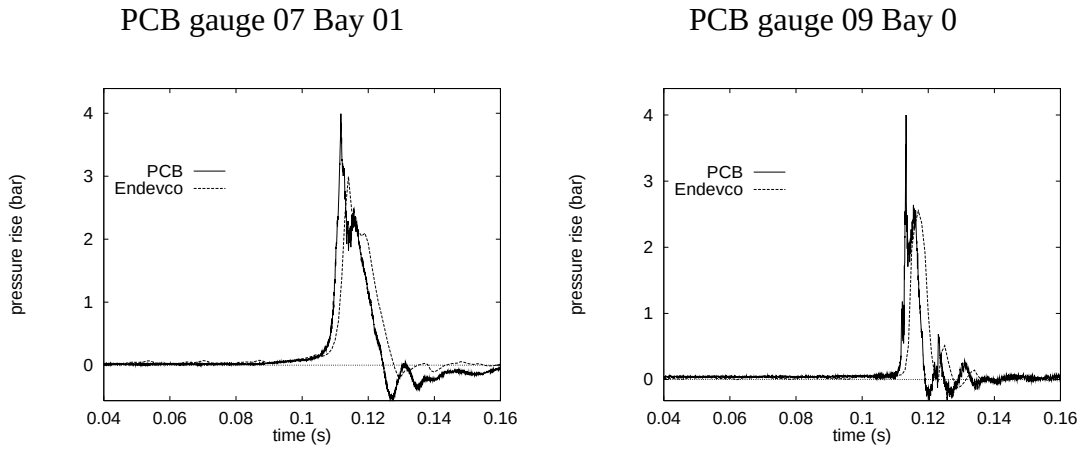

Figure 7.2: Rapid pressure pulses for Test 19, bays 0 and 1, recorded by dynamic (PCB) gauges on the port side, compared to the Endevco gauge signals.

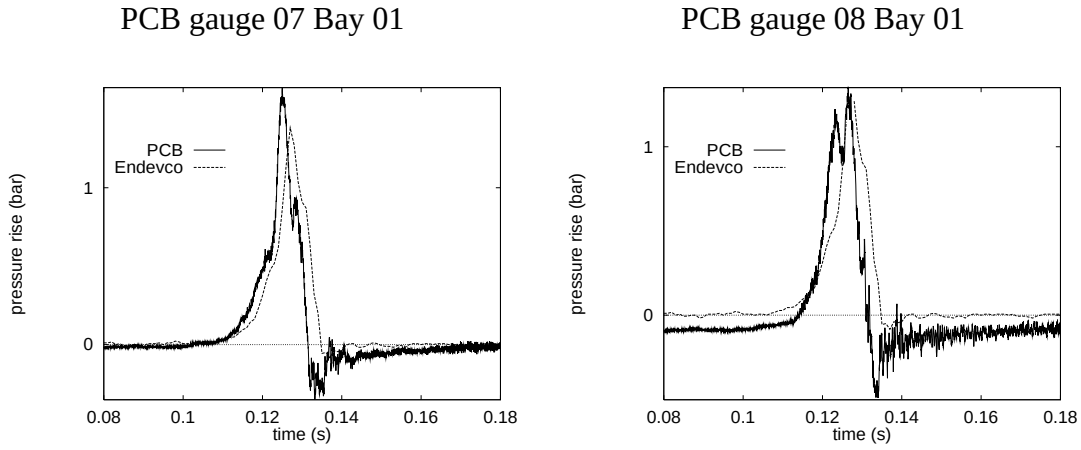

Figure 7.3: Rapid pressure pulses for Test 13, bay 1, recorded by dynamic (PCB) gauges on (a) the port side and (b) the starboard side, compared to the Endevco gauge signals.

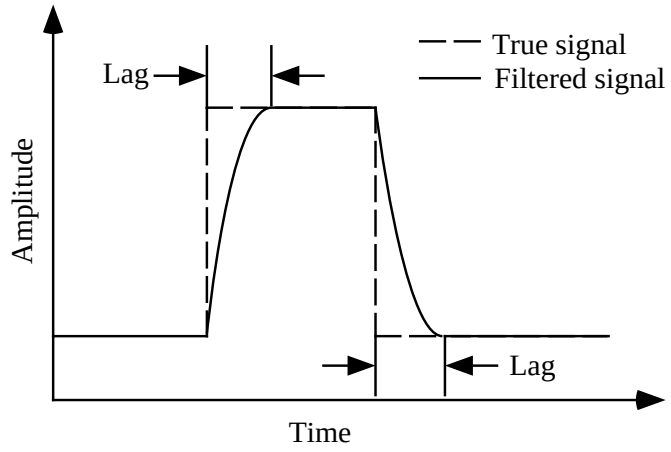

Figure 7.4: Illustration of the time lag resulting from a system with a low frequency response.

signal during the rising and falling edges of the signal. This time lag depends on the upper frequency limit of the filtering system, and as the limit decreases, the time lag increases.

Figure 7.5 shows this time-lag effect in pressure signals from Test 29. Although the features of the pressure history in bay 1 are fairly well represented in both the static and dynamic gauges, the static gauge signals typically lag behind the dynamic gauge signal by up to 2 to 3 ms. In this particular test, the time lag produces a roughly uniform shift of the static gauge signal in time.

In certain cases, the duration of a pressure pulse can be altered by time lag. If the rising edge of the pressure pulse is slow, both the static and dynamic gauges can follow the pressure variation and accurately represent it. However if the falling edge is rapid, there will be a time lag in the static gauge signal compared to the dynamic gauge signal. This situation is shown in Fig. 7.6, where the static gauge signal slightly lengthens the duration of the pressure pulse due to the time lag.

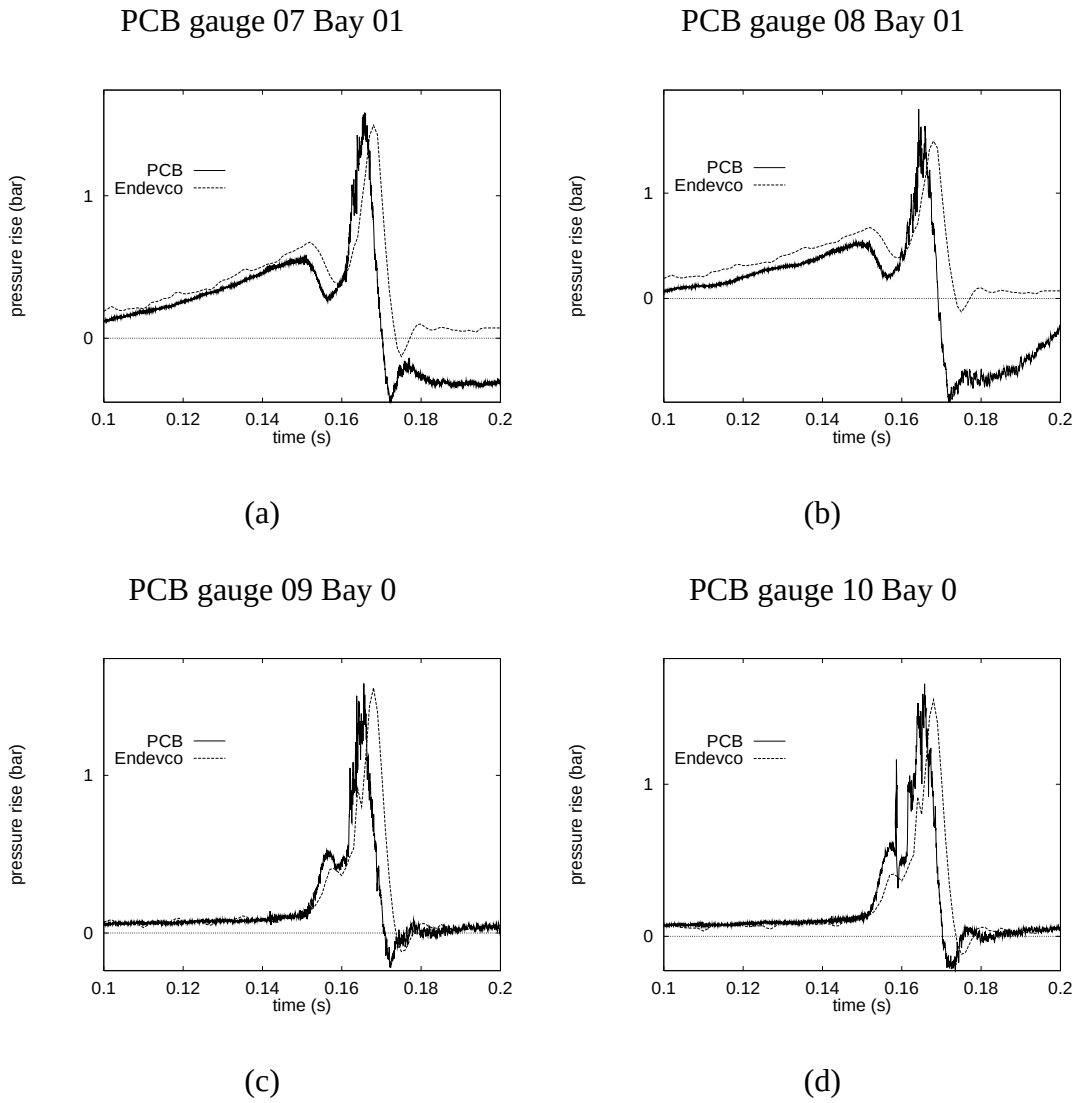

Figure 7.5: Dynamic (PCB) and static (Endevco) gauge pressure pulses showing the phase shift in the static gauge signal as compared to the dynamic gauge signal for Test 29: bay 1 on the (a) port side and (b) starboard side; and for bay 0 on the (c) port side and (d) starboard side.

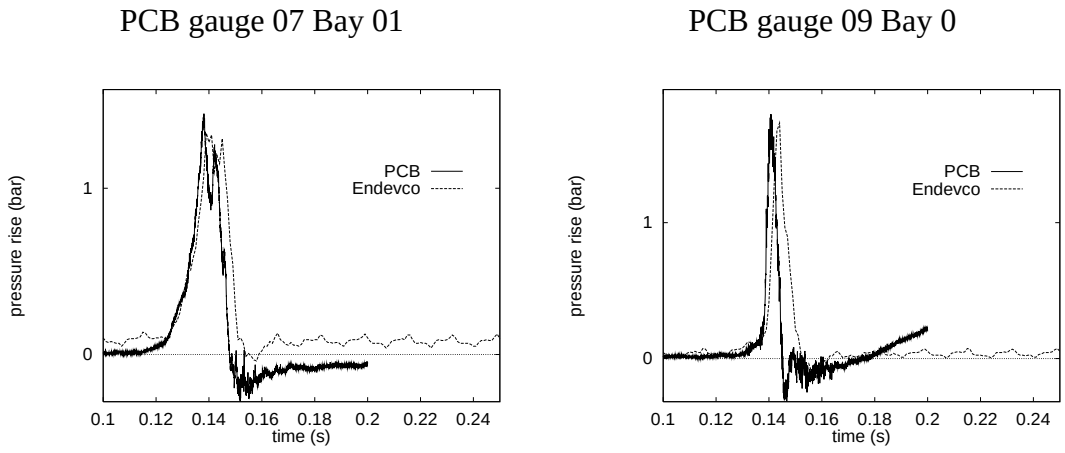

Figure 7.6: Pressure pulse widening shown for Test 17, bays 0 and 1, recorded by dynamic (PCB) and static (Endevco) gauges on (a) the port side and (b) the starboard side.

7.0.4 Differential Pressures

In the previous sections, we have shown that the limited frequency response can result in the failure to record short pulses and can also alter the pulse duration due to time lag. The inability of the static gauges to resolve certain features in the pressure signal can result in a discrepancy in the pressure differential between two bays when obtained from the dynamic or static gauge signals. This may be important when considering the impulse and pressure that causes a partition to fail.

Figure 7.7 shows the pressure difference across SWB2 and SWB3 for Test 29. These results were computed using the pressure traces from both the dynamic and static pressure gauges. For the pressure differences across SWB2, i.e., between bays 1 and 2, the static gauge trace clearly lags behind the dynamic gauge trace by 2 to 3 ms in the initial rising part of the signal, but the peak values of the pressure differences is the same for both gauges. Following the peak, the static and dynamic traces diverge from each other, especially for the port side signals. This may be due to temperature effects on the dynamic gauges or strong lateral pressure waves.

We also note that the pressure differential trace from the starboard side dynamic gauge (Fig. 7.7b) more closely matches the trace from the centrally located static gauges than the port side dynamic gauges (Fig. 7.7a). This indicates that the discrepancy between the static and dynamic signals on the port side may be due to wave effects. For the pressure differences across SWB3, i.e., between bays 0 and 1, the static and dynamic pressure differentials are exactly matched during the slow initial rise from 0.100 s to 0.150 s. During the sharp drop between 0.150 s and 0.155 s, the static trace lags behind the dynamic one by about 3 ms. The dynamic trace subsequently falls about 0.3 to 0.5 bar below the static traces, most likely due to temperature effects in the dynamic gauges.

A slight pulse widening, as observed in the static pressure signal of Test 17, can also influence the pressure differential. Figure 7.8 shows the pressure differentials across SWB2 and SWB3 obtained with the static and dynamic pressure traces. Since the pressure variations in bays 1 and 2 are relatively slow, they are equally well resolved by both the dynamic and static gauges. Consequently, the dynamic and static pressure differentials across SWB2 (Figs. 7.8a and 7.8b) match closely in terms of peak pressure and general features of the signal. In bays 0 and 1, there is a pulse widening effect in the static pressure signal (Fig. 7.6). As a result, there is discrepancy between the static and dynamic pressure differentials across SWB3, as can be seen in Figs. 7.8c and 7.8d. The initial pressure rise up to 0.135 s is fairly well matched between the static and dynamic signals. Then a time lag of about 3 ms develops in the static signal. After 0.142 s, certain variations in the dynamic signal are not well reproduced by the static signal.

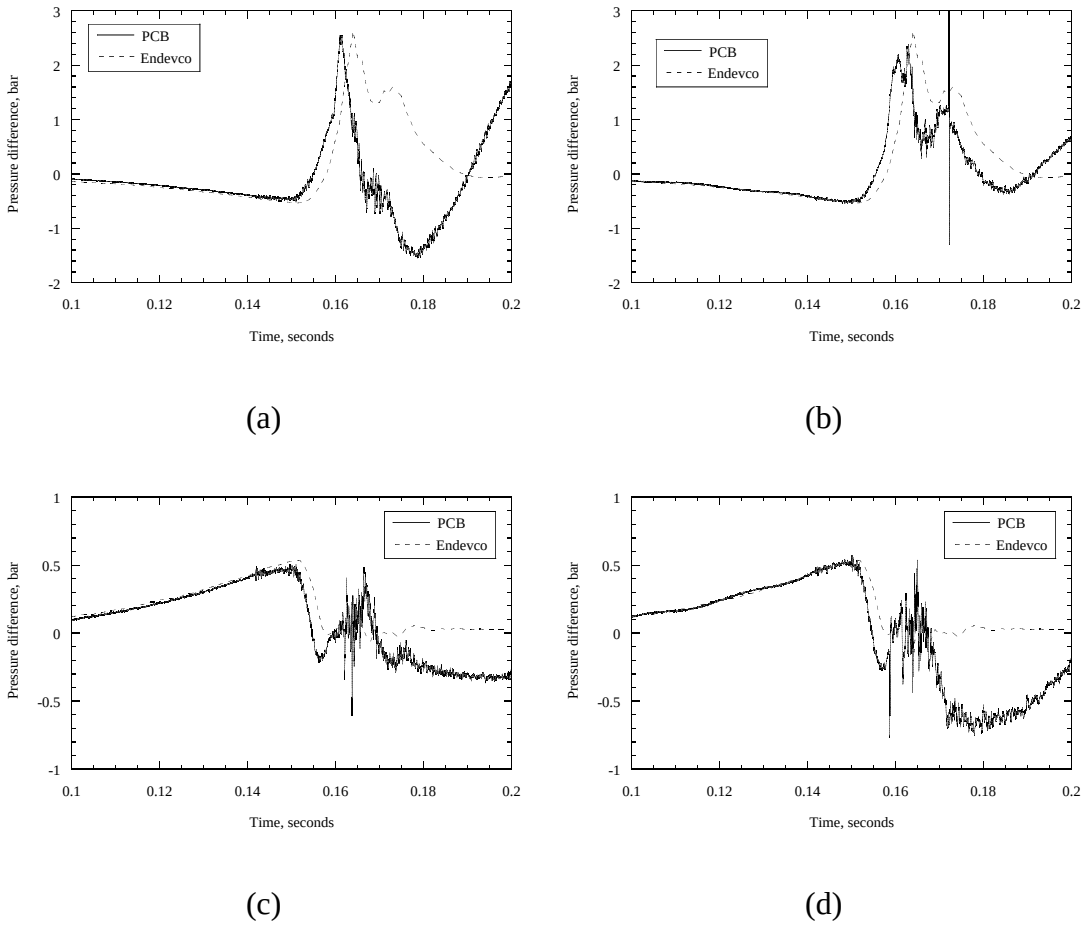

Figure 7.7: Pressure differentials obtained from static (Endevco) and dynamic (PCB) signals for Test 29 between bays 1 and 2 on the (a) port side and (b) the starboard side; and also between bays 0 and 1 on the (c) port side and (d) the starboard side.

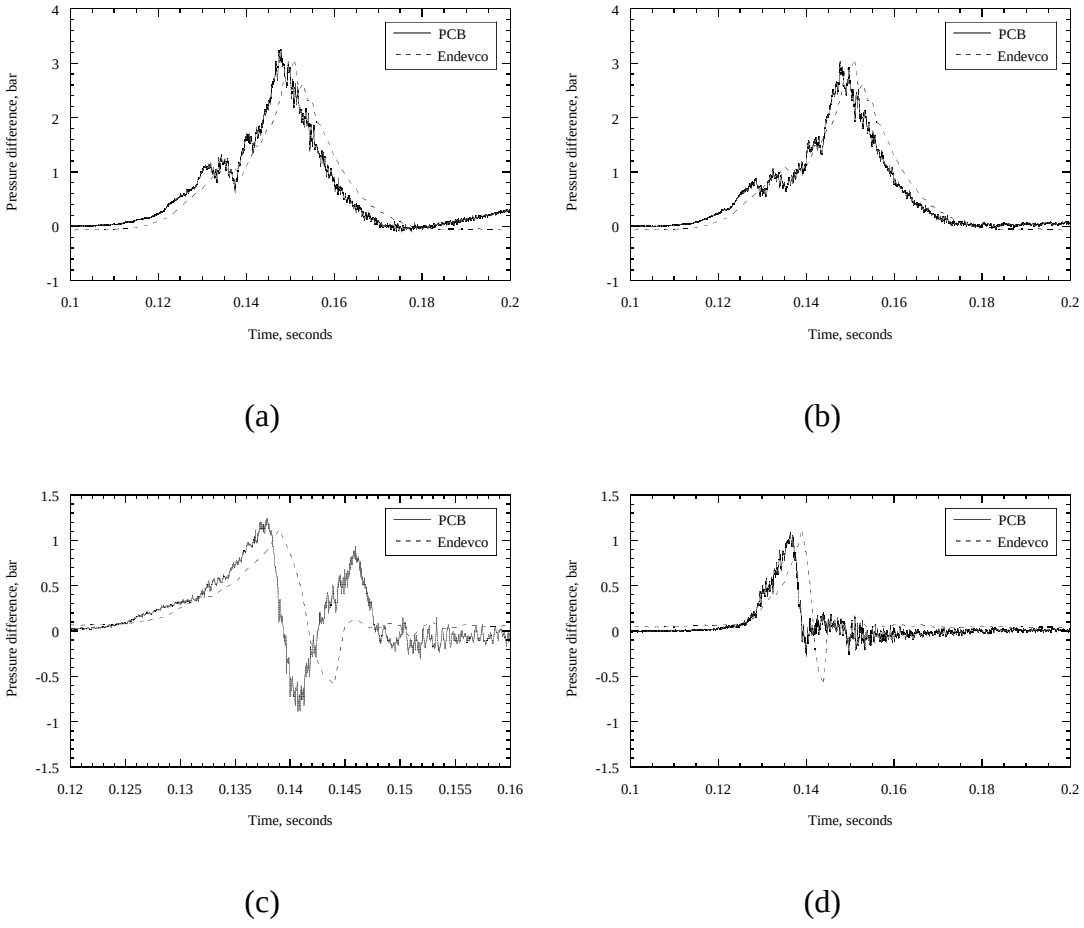

Figure 7.8: Pressure differentials obtained from static (Endevco) and dynamic (PCB) signals for Test 17 between bays 1 and 2 on the (a) port side and (b) the starboard side; and also between bays 0 and 1 on the (c) port side and (d) the starboard side.

7.0.5 Thermal Effects

Pressure gauges are usually very sensitive to thermal loads on the gauge's sensitive surface. Although both static and dynamic types of gauges can operate over a wide range of ambient temperatures (e.g., -73°C to 135°C for the dynamic gauges used in the present measurements), contact between the combustion products (1000 to 2000°C) and the gauge surface produces substantial thermal stresses in the senstive element and correspondingly large artifacts in the output signal.

To minimize this effect, the pressure gauges were protected against excessive heating by the combustion products. The static gauges were mounted with two porous sintered metal discs in front of the sensitive element. This mounting arrangement was found in laboratory tests to effectively eliminate temperature effects for event durations of up to 4 s. Hence for the duration of the flame propagation in the present 1/4-scale experiments, the static pressure measurements were essentially immune to temperature effects. The dynamic gauges were protected from heat by applying a 2- to 3-mm layer of silicon-based vacuum grease to the head. However, this technique only provided a limited amount of heat protection, and thermal effects were observed to influence the dynamic pressure signals after a certain time of contact with the combustion products.

Figure 7.9 shows a dynamic pressure trace compared to a static pressure trace in the same bay. The traces initially agree quite well until about 0.180 s, when thermal effects begin to change the pressure reading of the dynamic pressure trace. After 0.180 s, the static pressure gauge signals continue to rise to about 1 bar higher than the dynamic gauge signals. After about 0.200 s, the dynamic gauge signals are dominated by temperature effects as they rise to more than 7 bar. This is a particularly extreme example of how excessive heating can cause the dynamic gauge signals to indicate a pressure that is much higher or lower than the true pressure. Once temperature effects appear, the dynamic gauge signals are no longer reliable. In general, the only way to check this is through redundant measurements with heat-protected gauges.

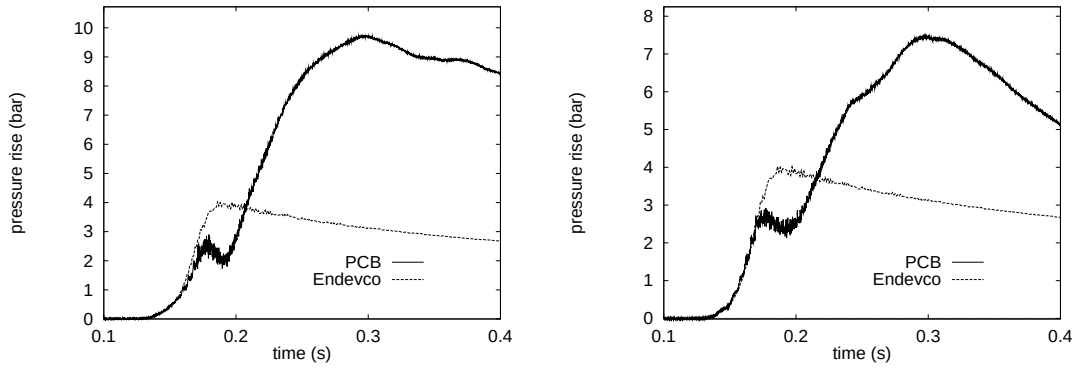

Figure 7.9: Thermal effects on a dynamic gauge as compared to a static gauge for pressure measurements during Test 9 in bay 2 for the (a) port side and (b) starboard side dynaimc gauges.

7.0.6 General Agreement Between Dynamic and Static Pressure Gauges

The performance of the PCB and Endevco gauges has been examined in detail for each test by overlaying the traces. The results of this study are given in Table 7.2. The Endevco gauges performed exceptionally well. Complete and noise-free data sets were obtained in 25 out of 30 tests. Only in one test (Test 2) was the data completely unusable. In the other four tests, there was either a single bad signal or some noise which could be removed by careful processing.

On the other hand, the PCB gauges had a number of artifacts in the signals associated with thermal (temperature) effects and noise spikes. These artifacts and other issues are given in Table 7.2. We have determined the performance of the PCBs during the time period up to the occurrence of peak pressure by visual inspection of comparative traces (PCB vs Endevco). The data have been divided into the following categories:

1. Excellent: 100% of gauges agree within 5-10%; 18 tests were in this category.
2. Good: 80% or more of the gauges agree within 5-10%; 3 tests were in this category.
3. Fair: 50% or more of the gauges agree within 5-10%; 3 tests were in this category.
4. Poor: Less than 50% of the gauges agree or else there are obvious problems with missing or noisy signals for a majority of the gauges; 6 tests were in this category.

After the burn period, the PCBs often showed some evidence of thermal effects and time constant influence. Since the portion of the signal during the burn period is much more important than the longer period associated with product cooling, we did not consider this to be reason to disqualify a signal. For tests in which fast waves occurred, it is important to examine the PCB signals in order to properly resolve these waves. Note that the ARA raw data given in the Appendices is not on a time scale that enables the reproduction of these fast transients or else the data has been decimated or filtered before plotting. It is necessary to examine the original digital data in order to get an appreciation for the wave signatures in those cases.

In general, there were many tests in which the dynamic and static pressure traces agreed very well during the combustion phase of the experiments and even afterwards. These were cases in which wave and thermal effects were relatively small. Wave effects were small in all-strong configurations where no partition or panel failure occured. In some tests there were very strong thermal effects because the PCB gauges were not properly coated with grease. In other tests, burning of liquid Jet A may have increased the thermal load on the gauge.

Dynamic vs. Static Pressure Gauges (Test 4) Since Test 4 serves as a baseline for many of our comparisons, we chose this test to make detailed comparisons between the two type of pressure gauges. Figures 7.10 and 7.11 contrast the PCB and Endevco signals and also the pressure differentials across each structural component.

In bays 3 and 4, the static and dynamic pressure signals are nearly identical (Figs. 7.10c and 7.11d). In the other bays, the static pressure signals are consistently 0.2 to 0.5 bar higher than the dynamic pressure signals after the burn was over. This could be due to temperature effects. During the burn, the agreement is much better.

The agreement of dynamic and static pressure traces during the burn is demonstrated in Figs. 7.12 and 7.13 by comparing the pressure differentials computed from the two different sets of gauges. There is a much higher frequency content in the PCB signals but that, as discussed above, is to be expected. Allowing for the higher frequency content and the lag in the Endevco signals, the overall agreement between the computed pressure differentials is excellent. This gives a high degree of confidence in the validity of the data. Similar comparisons are possible for many of the tests cataloged as “excellent” in Table 7.2.

Table 7.2: Evaluation of Pressure Signal Quality

Test	1	2	3	4	5	6	7	8	9	10	11	12	13	14	15	16	17	18	19	20	21	22	23	24	25	26	27	28	29	30
Dynamic (PCB) Pressure Gauges																														
Excellent				X	X		X					X	X	X	X		X	X	X	X	X	X	X	X	X	X	X			
Good										X						X														X
Fair								X			X																	X		
Poor	X	X	X			X			X																				X	
Fast Waves													X	X			X	X	X	X	X	X	X	X			X	X	X	X
Temperature	D	X	X		X		X	X	D		X			X	X	X	X		X								X	X	D	X
Lost Data						E																			A					
Noise																		N1	N2	N3										N4
Special																													B	C
Static (Endevco) Pressure Gauges																														
Missing data					F																									
Noisy Signals		G																		I						H				
Other	J																													

Notes:
A - Bay 1, PCB P08 no signal.
B - Bay 0, 1, 2 PCB signals are fine for waves. Other signals have temperature artifacts.
C - Some gauges were moved, not possible to compare all signals.
D - No protective grease, data invalid after flame arrival.
E - No PCB data at all, power supply not turned on.
N1 - Noise spikes in Gauge 8.
N2 - Noise spikes in Gauge 4.
N3 - Noise spikes in Gauge 6.
N4 - Noise spikes in Gauge 6.

F - Bay 1 Endevco, no signal.
G - Large amplitude (0.5 bar) 60-Hz noise on all signals. Not usable.
H - Small amplitude ($\pm$0.06 bar) 60-Hz noise. Data usable.
I - Bay 1 Endevco intermittent signal between 0.12 and 0.13 s.
J - Bay 5 Endevco gain or calibration factor off by a factor of 2.

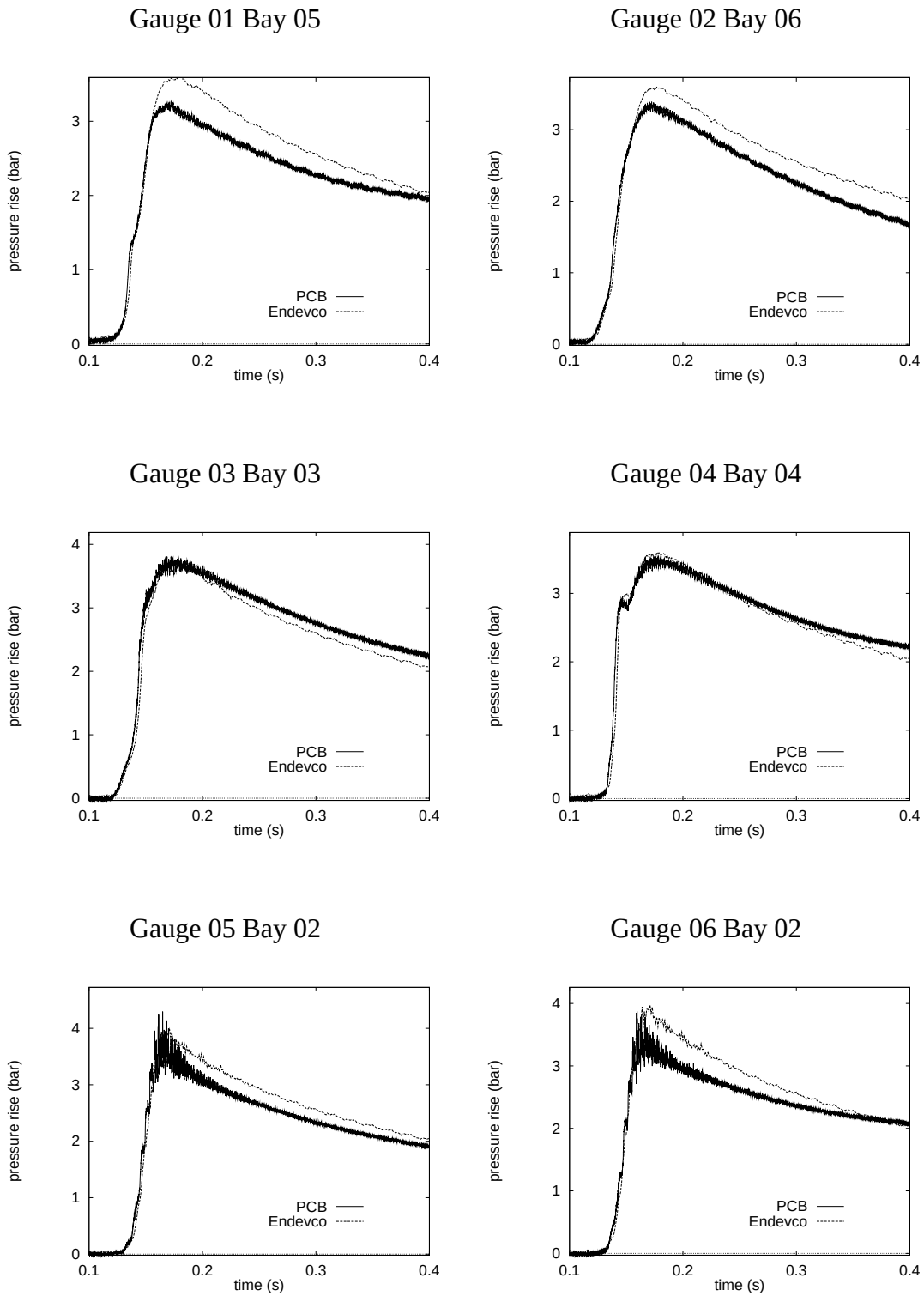

Figure 7.10: Static and dynamic pressure traces for Test 4.

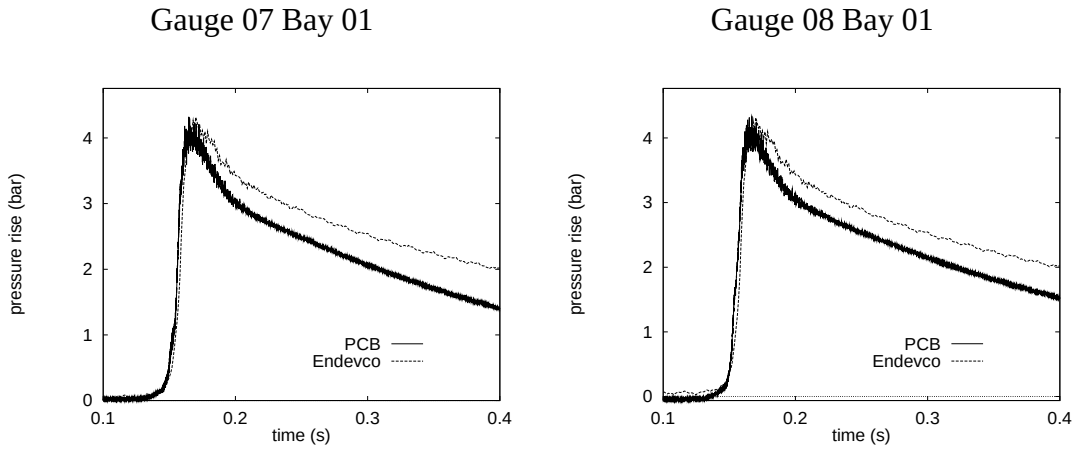

Figure 7.11: Static and dynamic pressure traces for Test 4 (cont.).

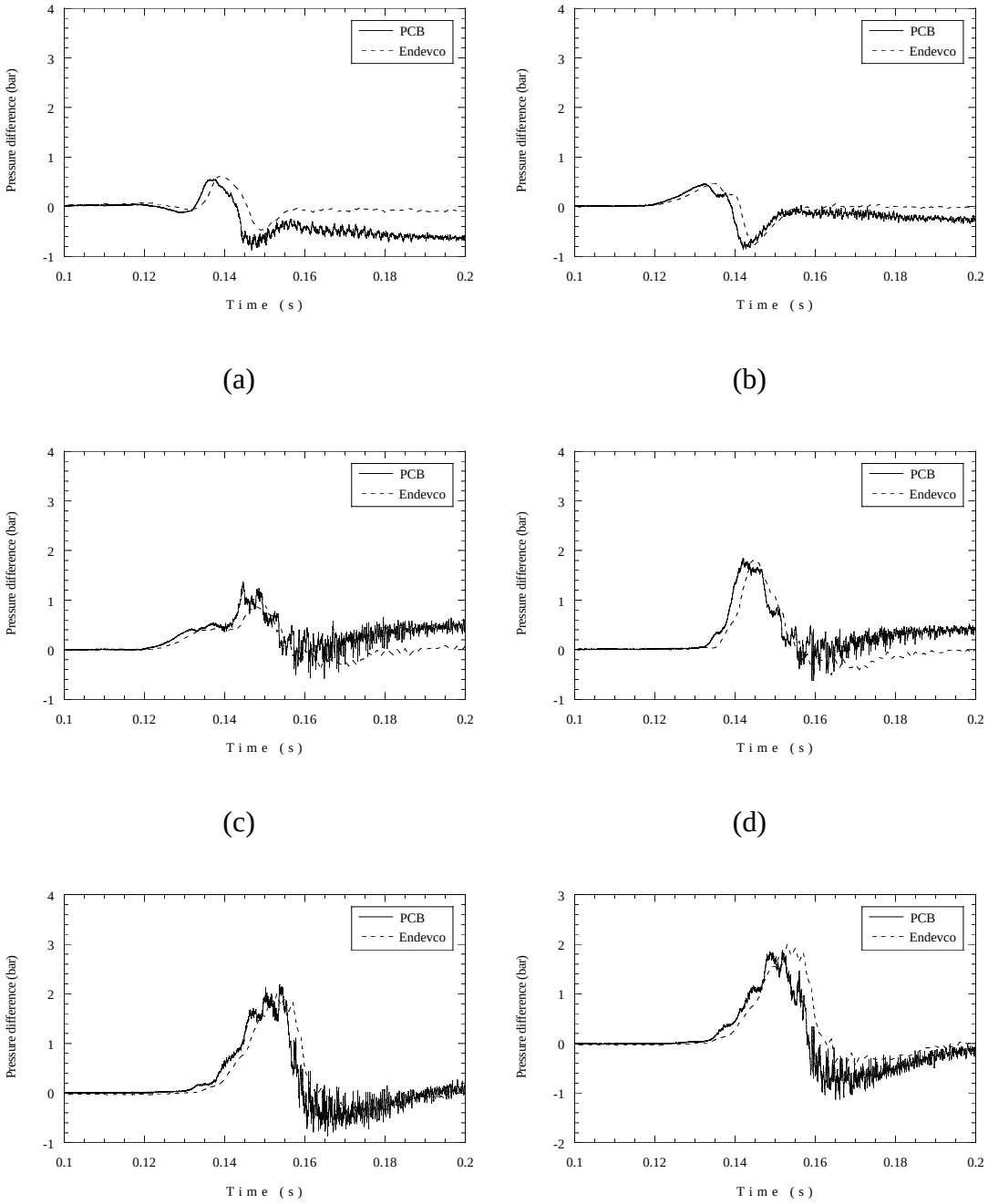

Figure 7.12: Pressure differentials for Test 4 obtained from static and dynamic pressure traces across (a) SWB1 on the port side, (b) SWB1 on the starboard side, (c) MS on the port side, (d) MS on the starboard side, (e) SWB2 on the port side, and (f) SWB2 on the starboard side.

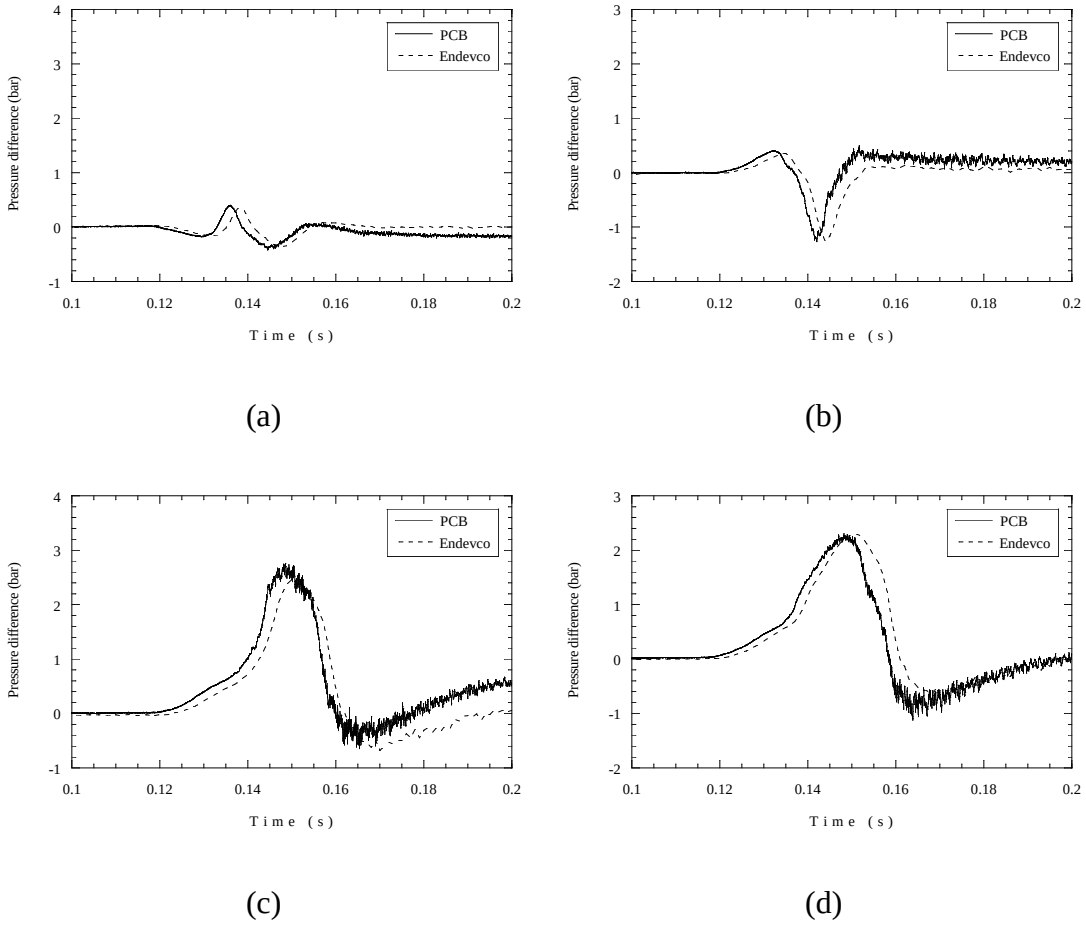

Figure 7.13: Pressure differentials for Test 4 obtained from static and dynamic pressure traces (a) across the aft partial rib, (b) across the front partial rib, (c) between the port side stringer vent extremities, and (d) between the starboard side vent extremities.

Chapter 8

Fuel Considerations

As discused in Section 2.2, a simulant fuel was used in the present series of experiments instead of Jet A. A nominal vapor fuel concentration of 8.4% (7% H_2 and 1.4% C_3H_8, i.e., a ratio of H_2:C_3H_8 of 5:1 by volume or 1:4.4 by mass) was used in the present experiments. However, there were some variations on this. In seven experiments, a cold Jet A liquid layer was added to simulate the residual fuel on the CWT floor. In one experiment, the vapor concentration was lowered to 7.5% and in two, 6.5%. Furthermore, since the experiment was performed outdoors with no temperature control, the initial temperature ranged between 0 and 32°C.

All of these factors can cause substantial variations in combustion properties. We examined these issues using laboratory experiments and chemical equilibrium estimates to determine the effect of fuel concentration and temperature on the combustion process. In addition, we examined several other fuel-related issues: hot filament vs spark ignition; comparison of simulant fuels with Jet A combustion at 40°C; and, the potential for initiation of detonation in the simulant mixture.

8.1 Comparison of Jet A and Simulant Fuel

Laboratory experiments were carried out with Jet A in both a 1.8-liter and 1180-liter vessels at Caltech. These experiments . The experiments in the 1180-liter vessel were used to develop the simulant fuel and are described in detail in Shepherd et al. (1997) and Shepherd et al. (1998). Tests in the 1.8-liter vessel are described in (Shepherd et al. 1998) and (Lee and Shepherd 1999).

The most important factor in determining the combustion parameters is the amount of Jet A vapor, which is primariy determined by the fuel temperature (Shepherd et al. 1997). Surface and air temperatures were measured in the TWA 800 emulation flight test (Bower 1997) and the range of values obtained at 14 kft are given in Table 8.1. Based on these values a nominal temperature of 50°C was used for both Jet A liquid and the fuel vapor-air mixture. Results from a test at that condition and the corresponding simulant mixture were shown previously in Section 2.2, Fig. 2.12. Experiments were also carried out at both 40°C and 60°C to examine the effect of initial temperature. The parameters and results of those tests are given in Table 8.2.

The results of experiments at 40°C are given in Fig. 8.1 and for 50°C in Fig. 8.2.

Table 8.1: Range of temperatures measured in TWA 800 emulation flight test (Bower 1997)

.

Bay	T (°C)
Air Temperatures	
1 (right)	40-43
1 (center)	46-49
1 (left)	38-43
2 (right)	38-43
2 (center)	46-49
2 (left)	38-43
3	46-54
4	40-46
5	43-49
6	40-43
Surface Temperatures	
1	54
2	46-54
3	38-54
4	NA
5	49-60
6	49-54

Table 8.2: Tests carried out in the 1180-liter vessel (Hyjet) with Jet A.

Test	Fuel	T_o (C)	P_o (bar)	ΔP_{max} (bar)	S_u (cm/s)
466	Jet A (LAX)	40.1	0.585	1.9	7.5-10
464	Jet A (LAX)	40.8	0.585	2.1	10-13
586	Jet A (ARCO)	40.0	0.585	2.2	14-19
587	Jet A (ARCO)	40.1	0.585	2.3	10-14
470	Jet A (El Monte)	49.4	0.585	3.4	36-48
584	Jet A (ARCO)	49.3	0.585	3.5	43-58
588	Jet A (El Monte)	50.7	0.585	3.7	43-58
468	Jet A (LAX)	46.4	0.585	3.13	NA
487	Jet A (LAX)	59.6	0.585	4.48	64-68

8.2 Ignition System Tests

As discussed in Section 5.2, the ignition system described in Sections 2.6 and 2.4.2 was chosen for reliability and to minimize ignitor effects that were observed when using electric match

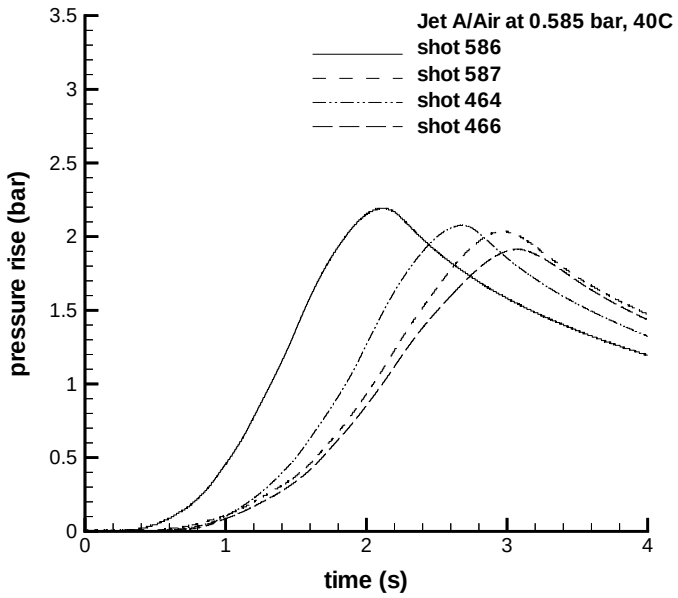

Figure 8.1: Pressure traces from four tests in Hyjet (1180-liter vessel) at 40°C, 0.585 bar and various sources of Jet A.

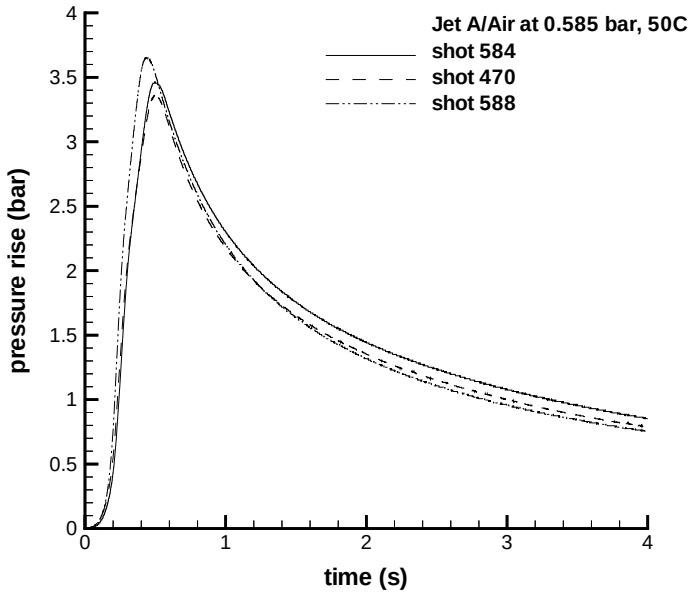

Figure 8.2: Pressure traces from three tests in Hyjet (1180-liter vessel) at 50°C, 0.585 bar and various sources of Jet A.

ignition. Briefly, the ignition system consisted of a bare light bulb filament that was rapidly heated by discharging a 1400 μF capacitor charged to 150 V into the filament. The circuit parameters were chosen so that the filament did not break and no molten fragments or sparks were formed. Minimum ignition conditions were not studied as part of the 1/4-scale tests but examined in separate laboratory tests described in Shepherd et al. (1998) and Lee and Shepherd (1999).

This was confirmed by visual observation and continuity measurements on test filaments. Measurements with a photodiode indicated that the filament reached its peak temperature in less than 10 μs. Heat transfer from the very hot filament to the surrounding fuel vapor-air mixture initiates the combustion.

Since all of the previous laboratory testing had been carried out with spark ignition, comparison tests were made using the light bulb filament and the spark source. The results of these tests are given in Table 8.4. Note that the peak pressures obtained with two ignition systems are essentially identical for the 7.0% and 8.4% cases in the 407-l vessel. Results in the 11.25-l vessel show more variability since much smaller amounts of gas are involved and the gas composition is subject to greater uncertainty than in the larger vessels. For the 6% case, buoyancy plays a very important role in the flame development and the results are very different for the two ignition systems since one set of tests were performed with a fan running in the test vessel and the other under quiescent conditions.

Selected video frames from two visualization tests are shown in Figs. 8.4 and 8.3. In Fig. 8.4, the filament is visible at the bottom of the first frame and is obscured in subsequent frames due to the video camera saturating from the light emitted by the glowing filament. The spark is a very short duration and is not captured in the video recording process. Once the flame has grown slightly larger than the size of the filament or the spark, the development appears to be almost identical for the two cases. This is further confirmed by comparison of the pressure traces for hot filament and spark ignition, as shown in Fig. 8.5.

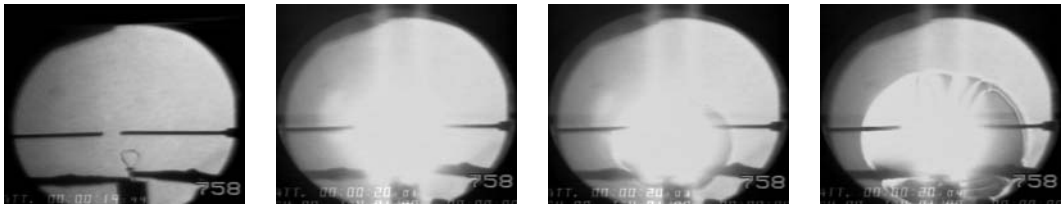

Figure 8.3: Four images from an ignition test (758) using the hot filament ignitor with 8.4% simulant in air at 0.815 bar in 11.25-liter vessel.

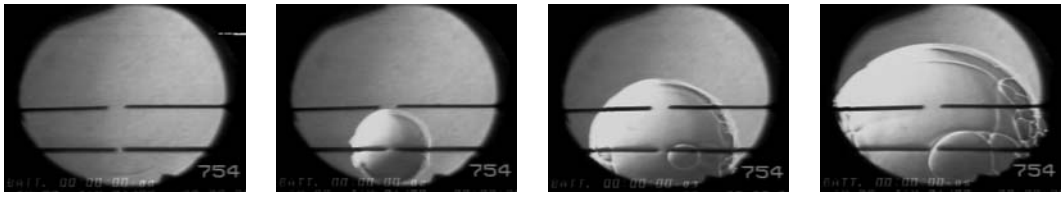

Figure 8.4: Four images from an ignition test (754) using the spark ignitor with 8.4% simulant in air at 0.815 bar in 11.25-liter vessel.

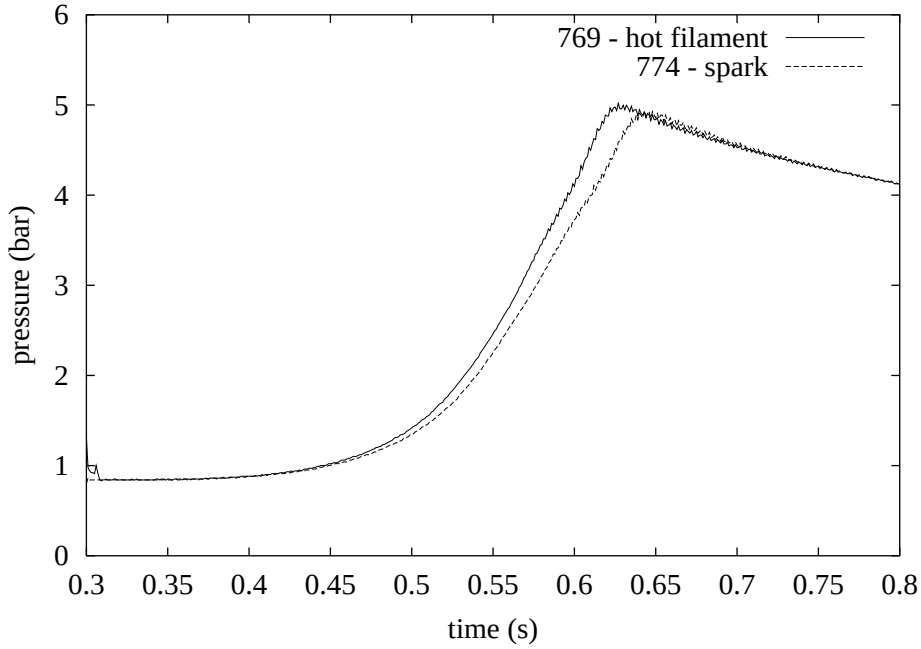

Figure 8.5: Comparison of pressure signals for two ignitors, spark (774) and hot filament (769), 8.4% simulant in air at 0.815 bar, 407-l vessel.

8.3 Initial Concentration Effects

A series of numerical computations was carried out to estimate the effect of varying the fuel concentration. The ratio of hydrogen to propane was kept fixed at 5:1 for all of these simulations, since that is how the experiments were carried out. These computations assumed adiabatic, isochoric (constant-volume) complete combustion (AICC) and were carried out using the STANJAN (Reynolds 1986) chemical equilibrium code with a complete set of major and minor combustion products. The results are given in Table 8.3 for nominal initial conditions of 295 K and 0.83 atm.

Laboratory experiments were carried out with simulant fuel to also examine the effect of varying the fuel concentration and the results of selected tests are given in Table 8.4. These tests were peformed in 1180-l, 407-l, and 11.25-l vessels, all located in the Explosion Dynamics Laboratory at Caltech. The results of tests at three concentrations in the 1180-liter vessel are plotted in Fig. 8.6.

These tests demonstrated the ability to initiate flames with both spark and filament sources with concentrations between 6 and 8.4% fuel. The downward propagation limit was found to be between 6% and 7%. Flames initiated in 6% fuel burned very slowly and buoyancy prevented downward propagation in the small vessels if the mixture was initially quiescent. However, in larger vessels or if the flame was initiated in a turbulent flow, relatively complete combustion resulted. Pressure traces obtained with filament and spark ignition at the same concentration were nearly identical for the 8.4% fuel cases.

For tests 956 through 963, the video and pressure data were analyzed to determine the ef-

Table 8.3: Effect of fuel concentration on computed peak pressure (AICC). Initial conditions: 0.83 atm, 295 K.

Fuel fraction	Fuel-air mass ratio	Equivalence ratio	C_3H_8	H_2	Air	O_2	N_2	P_{AICC} (bar)
1			0.167	0.833				
0.14	0.051	0.97	0.023	0.117	0.860	0.181	0.679	7.41
0.13	0.047	0.89	0.022	0.108	0.870	0.183	0.687	7.25
0.12	0.043	0.81	0.020	0.100	0.880	0.185	0.695	6.86
0.11	0.039	0.74	0.018	0.092	0.890	0.187	0.703	6.51
0.10	0.035	0.66	0.017	0.083	0.900	0.189	0.711	6.23
0.09	0.031	0.59	0.015	0.075	0.910	0.191	0.719	5.79
0.08	0.027	0.52	0.013	0.067	0.920	0.193	0.727	5.30
0.07	0.023	0.45	0.012	0.058	0.930	0.195	0.735	4.95
0.06	0.020	0.38	0.010	0.050	0.940	0.197	0.743	4.41
Standard								
0.084	0.029	0.55	0.014	0.07	0.916	0.192	0.724	5.60

fective burning speed. Pressure data alone was analyzed for the other tests. The analysis of the video data is discussed in (Ross and Shepherd 1996) and the pressure data is discussed in Shepherd et al. (1997a). Measurements (Kunz 1998) have been previously made for a number of fuels including propane and hydrogen. Comparison of these data with other researchers' measurements of flame speed indicate that the pressure reduction technique is reasonably reliable away from the lean limit but the video technique works better for very lean flames. In general, the values obtained from either technique are similar to the "laminar burning speed" that is measured using burners or the "two-kernel" method.

A graphical comparison of flame speed results is shown in Fig. 8.8. The results from the 11.25-l vessel are systematically lower than in the other vessels. The burning speeds (27 to 42 cm/s) for the 8.4% simulant are in the same range as those (35 to 60 cm/s) obtained for Jet A at 40 to 50°C using the pressure reduction method Shepherd et al. (1997a). Eliminating the lower values obtained from the 11.25-l vessel, a value of 38-42 cm/s is consistent with all other experiments at a concentration of 8.4%. This includes the 1/4-scale experiment number 11, which gives a value of 39 cm/s when analyzed using the t-cubed method. The peak pressure rise is compared with the computed AICC values in Fig. 8.7. The decrement of approximately 1 bar between AICC and measured peak pressures is due to heat transfer during the burn. These results are consistent with data obtained for other hydrocarbons.

8.3.1 Uncertainty

There are several sources of uncertainty in the fuel composition, all small. The MKS pressure gauge used to measure the partial pressures of air and air-fuel mixture within the tank has a quoted accuracy of $\pm$ 0.1 torr (0.13 mbar). The gauge compensates for temperature variations between 0 and 150°C. The fuel mixture had slight variations from the specified composition.

Table 8.4: Laboratory tests of simulant ignition. All tests tests carried out at an initial temperature of 20 to 25°C. Initial pressure was either 0.83 or 0.815 bar as indicated.

Vessel Size (liter)	Test No.	Ignitor	Fuel (%)	P_{max} (bar)	S_{video} (cm/s)	S_{t^3} (cm/s)
		$P_\circ$ = 0.83 bar				
1180	484	spark	8.4	4.49	-	38
1180	493	spark	8.4	4.76	-	41
407	770	filament	6.0	1.2	-	-
407	772	spark	6.0	3.0*	-	-
407	773	spark	6.0	3.3*	-	-
407	771	filament	7.0	4.1	-	-
407	775	spark	7.0	4.0	-	-
407	774	spark	8.4	4.9	-	41.6
407	769	filament	8.4	5.0	-	42.0
11.25	754	spark	8.4	4.88	-	-
11.25	758	hot filament	8.4	4.17	-	-
		$P_\circ$ = 0.815 bar				
1180	518	spark	6.5	3.34	-	8.6
1180	519	spark	7.5	4.11	-	20.4
1180	520	spark	6.5	3.28	-	8.7
1180	521	spark	7.5	3.89	-	21.1
11.25	956	spark	6.5	0.86	5.5	13.3
11.25	957	spark	6.5	1.58	7.6	12.6
11.25	958	spark	6.5	1.51	7.1	11.6
11.25	959	spark	7.5	3.15	14.4	16.5
11.25	960	spark	7.5	3.18	14.9	16.1
11.25	961	spark	8.4	3.61	21.1	25.5
11.25	962	spark	8.4	3.65	22.1	27.0
11.25	963	spark	10.0	4.35	34.7	43.9

*Pressure value is for turbulent combustion.

The mixture was certified (analyzed by GC) by the supplier, and the results are given in Appendix A. The mole fraction of propane was 16.71% in the first bottle and 16.81% in the

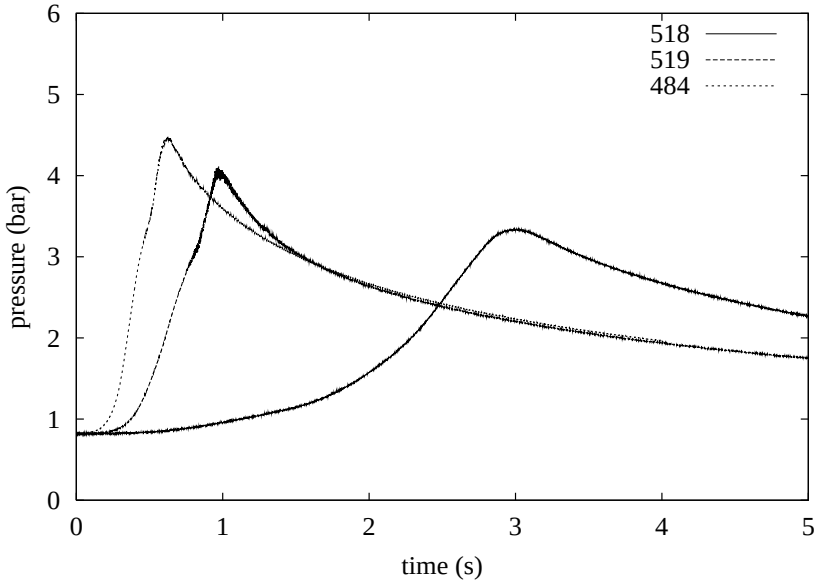

Figure 8.6: Pressure histories of selected simulant mixtures measured in laboratory tests in a 1180-liter vessel at 295 K and 0.815-0.83 bar.

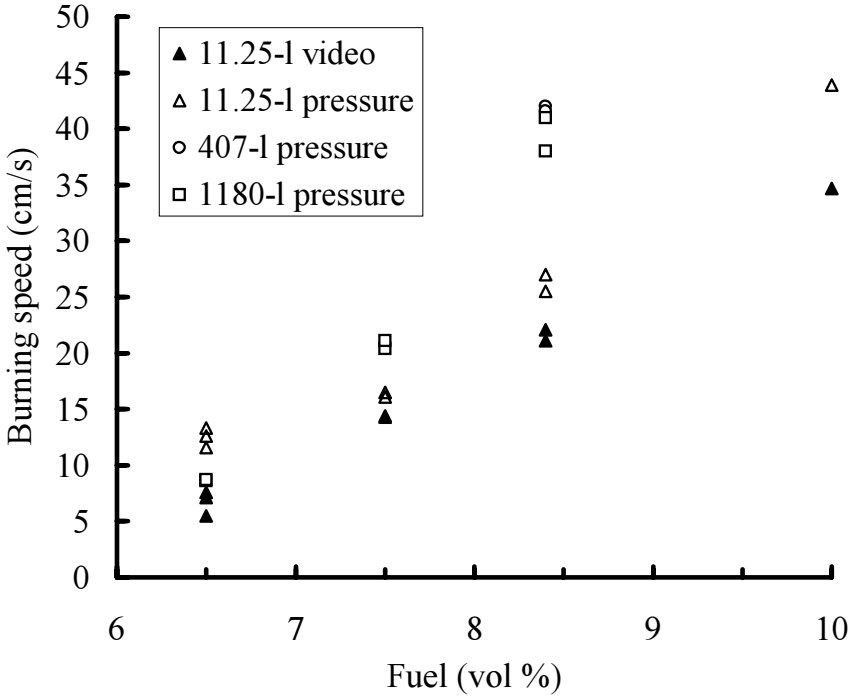

Figure 8.7: Burning speeds of simulant mixtures measured in laboratory tests in 11.25-liter vessel at 295 K and 0.815 bar.

second bottle. Since the pressure inside the tank was lowered before the fuel was introduced,

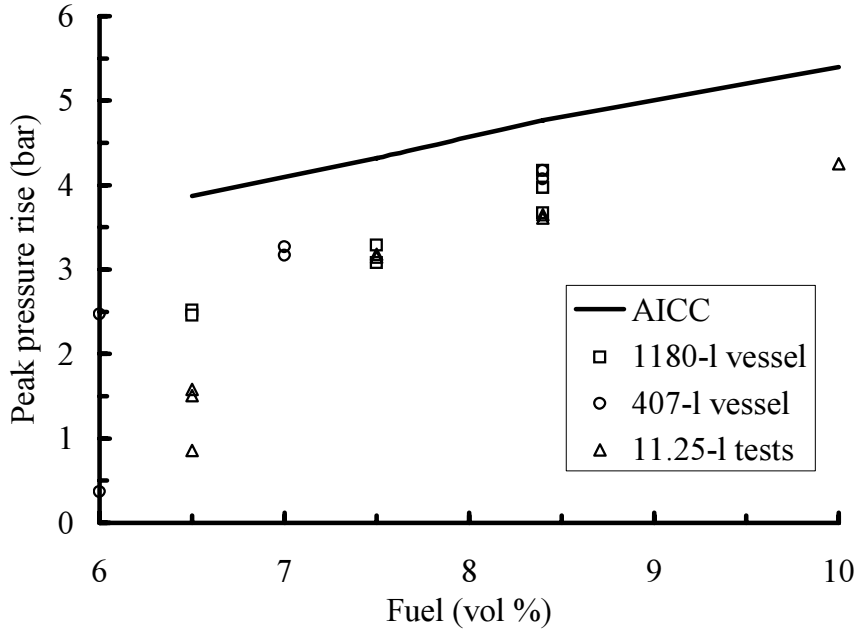

Figure 8.8: Peak pressure of simulant mixtures measured in laboratory tests in a 11.25-liter vessel at 295 K and 0.815 bar.

air would leak into the tank during the fill process. The typical maximum leak rate was less than 0.5 torr/min. In the 30 seconds required to fill the tank, this means that approximately 0.125 torr (0.164 mbar) of air would enter the tank along with the fuel mixture. The rate at which air enters the tank will decrease as the tank is filled and the pressure difference goes to zero; this was accounted for by assuming a linear dependence of leak rate on pressure difference. The air temperature within the tank was slightly nonuniform due to solar heating of the top of the tank.

Considering all these factors, the fuel partial pressure may be in error by as much as $\pm$ 0.4 torr (0.5 mbar). The standard fuel amount corresponds to a partial pressure of 52 torr (68.5 mbar) in a nominal ambient atmospheric pressure of 619 torr (815 mbar) so that the estimated fuel amount (by mole) is 8.40% $\pm$ 0.06. AICC estimates indicate that the peak pressure will be uncertain by about 0.2% due to the fill uncertainty. The mixture in bottle 2 is predicted to have an AICC pressure about 0.87% lower than bottle 1. Bottle 1 was used from Test 1 through Test 21, then bottle 2 was used for Tests 22 and higher. The switch was made over the Thanksgiving break and bottle 2 was heated during that time in order to mix it.

8.4 Initial Temperature

The experiments were carried out over a wide range of initial temperatures since the tank was subjected to ambient weather conditions. Previous experience with outdoor testing has shown that this environmental factor produces a very substantial variation in the peak pressure. This is because the density of the gaseous fuel and air increase as the temperature decreases. For a given volume, the total mass of explosive and therefore the peak pressure will increase as the temperature decreases. AICC computations were carried out for the nominal mixture concentration over a range in initial temperatures at a fixed atmospheric pressure and the results are given in Table 8.5.

The results of the temperature effect computations are compared with the experimental peak pressures in Fig. 8.9. The peak pressure values shown are the maximum values found after examining all the bays in each 1/4-scale experiment. The data are divided into various cases depending on the fuel type and structural configuration. Focusing on the vapor-only, all-strong configurations, a clear correlation between initial temperature and peak pressure emerges. The thin dashed line is a linear correlation of that data, and is parallel to the calculated trend. This similar trend of decreasing pressure with increasing initial temperature indicates that the experimental pressures indeed show a temperature effect. Also, the experimental peak pressures are approximately 1 bar lower than the calculated values. This decrement is due to heat transfer during the burn, which is consistent with experimental results (Kunz 1998) obtained in the laboratory in closed vessels for a wide range of hydrocarbon fuels.

Table 8.5: Effect of initial temperature on computed peak pressure (AICC) for the nominal vapor fuel (8.4%) at an initial pressure of 0.83 bar.

T (°C)	P_{AICC} (bar)
-15	6.32
-10	6.22
-5	6.11
0	6.01
5	5.91
10	5.82
15	5.72
20	5.64
25	5.55
30	5.47

8.5 Jet A Vapor Contamination

For tests in which liquid Jet A fuel was introduced into the tank, there is an issue of evaporated Jet A contaminating the nominal gaseous fuel simulant in the tank ullage. The Jet A vapors

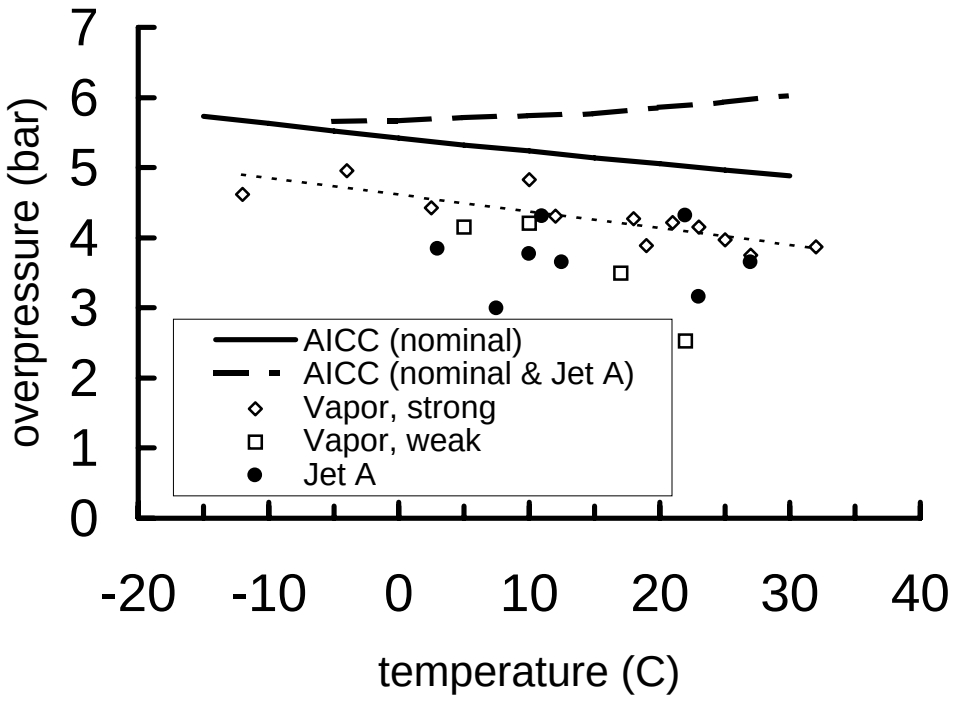

Figure 8.9: Comparison of experimental peak pressure with AICC computations with and without Jet A vapor. Unlabeled dashed line is a linear correlation to simulant-only tests with all strong configuration.

would contribute to the total amount of fuel in the gaseous fuel-air mixture. As a result, the mixture would be richer and the combustion properties such as the peak pressure and the flame speed would be slightly increased.

Amount of Evaporated Jet A To evaluate the effect of the Jet A vapor contamination, the partial pressure of the vapor was estimated using experimental vapor pressure curves obtained recently at the Caltech Explosion Dynamics Laboratory Shepherd et al. (1997a). We used the vapor pressure curve for Jet A at a mass-volume ratio of 3 kg/m^3 for our calculation since this was the same mass-volume ratio used throughout the 1/4-scale tests with liquid fuel, i.e., 2.9 liters (2.3 kg) in the 0.77 m^3 tank. The resulting Jet A vapor contamination amounts for all the tests with liquid fuel are shown in Table 8.6.

The contamination is expressed in two ways, mole and mass fraction. The mole fraction as percent of Jet A in the entire fuel-air mixture appears in the “Jet A (%)” column, and varies from 0.18% at 3°C to 0.41% at 27°C. The relative percentage of Jet A vapor in the total fuel vapor is given in the “Jet A in fuel” column, and varies between 2.1% to 4.7% by mole. The fraction by mass is higher since the Jet A vapor is much heavier than the simulant mixture. The mass fraction of simulant in air and Jet A vapor in air are given in the last two columns.

Table 8.6: Composition of fuel-air mixture in the tank for each test with Jet A vapor contamination.

Test	T (°C)	$P_{ambient}$ (torr)	$P_{simulant}$ (torr)	P_{JetA} (torr)	Simulant (%)	Jet A (%)	Jet A in fuel (%)	M_{sim}/M_a	M_{tf}/M_a
8	22	622.8	52.3	2.2	8.4	0.35	4.0	0.026	0.043
19	7.5	612.9	51.5	1.3	8.4	0.22	2.5	0.026	0.037
20	23	618.7	52.0	2.2	8.4	0.36	4.1	0.026	0.044
21	27	615.6	51.7	2.5	8.4	0.41	4.7	0.026	0.046
27	3	608.0	51.1	1.1	8.4	0.18	2.1	0.026	0.035
28	10	606.1	50.9	1.5	8.4	0.24	2.8	0.026	0.038
29	11	604.6	50.8	1.5	8.4	0.25	2.9	0.026	0.038
30	12.5	615.0	51.7	1.6	8.4	0.26	3.0	0.026	0.039

8.5.1 Estimated combustion pressure

In order to examine the effect of Jet A contamination on the combustion pressure, we used the estimated maximum amounts of Jet A vapor from Table 8.6 to calculate the AICC pressure. The composition of the vapor was based on the results of Woodrow and Seiber (1997) and approximated to be C_9H_{16}, which has a molar mass of 124 g/mol. The enthalpy of formation was chosen to be -6124 kJ/mole, which results in a heat of combustion of about 42 MJ/kg, typical of kerosene-type fuels. The results of AICC computations with (bold solid line) and without (bold dashed line) Jet A vapor are shown in Fig. 8.9. At a temperature of 0°C, the Jet A vapor is predicted to increase the peak explosion pressure about 0.5 bar. Since the vapor pressure increases with increasing temperature, the effect is higher at 30°C, and the Jet A vapor is predicted to increase the peak pressure by 1.4 bar.

However, the effects of Jet A vapor contamination are not apparent in the experimental results over the range of temperatures encountered during the tests (3°C to 27°C). There appear to have been certain factors that inhibited the evaporation of the liquid Jet A in the tank. The most influential factor is likely the lack of mixing of the liquid fuel. In laboratory tests at Caltech (Shepherd et al. 1997a), mixing was found to greatly decrease the time required for Jet A to evaporate and reach equilibrium at a given temperature. Since the evaporating vapor must first diffuse through the liquid before escaping the liquid surface, lack of mixing can lengthen the equilibration time by several orders of magnitude. In the 1/4-scale tests, the Jet A was quiescent. Moreover, there was a relatively short time delay of approximately 15 minutes between the introduction of the liquid Jet A into the tank and the actual ignition of the test mixture. It is therefore probable that only a very small amount of Jet A evaporated, thus minimizing the effects of contamination.

Another factor that could account for the apparent lack of Jet A vapor contamination is uncertainty in the the estimation of the liquid fuel temperature. The initial temperatures recorded before ignition of the test mixture were taken in the ullage of the tank. The ullage temperature was typically a few degrees higher than the ambient temperature (Table A.2) due to solar heat-

ing of the top of the tank. The bottom plate of the tank on which the liquid fuel rested was not exposed to the sun, and was probably closer to the ambient temperature than the ullage temperature. Hence the temperatures used to estimate the partial pressures of the Jet A in Table 8.6 likely represent a slight overestimate.

8.6 Detonation Cell Width

When a mixture is ignited by a spark, the resulting flame may accelerate to a detonation if certain critical conditions exist. This never happened in the present experiments, as only low-speed flames were created. However, we felt it was important to understand the margin between deflagration and detonation for the simulant mixtures. To that end, experiments were carried out to measure the detonation cell width for simulant mixtures at various concentrations, approaching the nominal concentration from above. These measurements were carried out[1] in the Caltech detonation tube and followed the methods described in Akbar et al. (1997). The results of these experiments are given in Table 8.7 and Fig. 8.10.

Table 8.7: Measured detonation cell widths for propane-hydrogen mixtures.

Fuel Amount (%)	Equivalence ratio	Cell Width (mm)	Range $+/-$ (mm)
16.8	1.0	31.9	8
15.1	0.9	44.8	18
13.4	0.8	49.8	12
11.8	0.7	63.8	26
10.1	0.6	93.8	44
8.4	0.5	*	–

*Detonation could not be initiated.

Note that the results are given in Fig. 8.10 as a function of equivalence ratio rather than fuel concentrations. The relationship between the equivalence ratio of these fuel-air mixtures is given in Table 8.7. Also note that the nominal simulant mixture has an equivalence ratio of 0.5. An equivalence ratio of 0.6 was the lowest value for which we were able to obtain data in the detonation tube at Caltech. The cell width for the simulant mixture is, not surprisingly, intermediate between the values for propane and hydrogen at the same equivalence ratio.

Since the cell width increases very rapidly as the equivalence ratio decreases, we estimate that the cell width for the nominal simulant mixture (ϕ = 0.5) is between 150 and 300 mm. These values are comparable to the transverse dimensions of the bays indicating that although detonation would be possible, it would be extremely difficult to initiate. Based on these measurements and the observations in the tests, we concluded that detonation of the simulant mixture is not an issue in the 1/4-scale experiments.

[1] M. Kaneshige of Caltech performed these experiments.

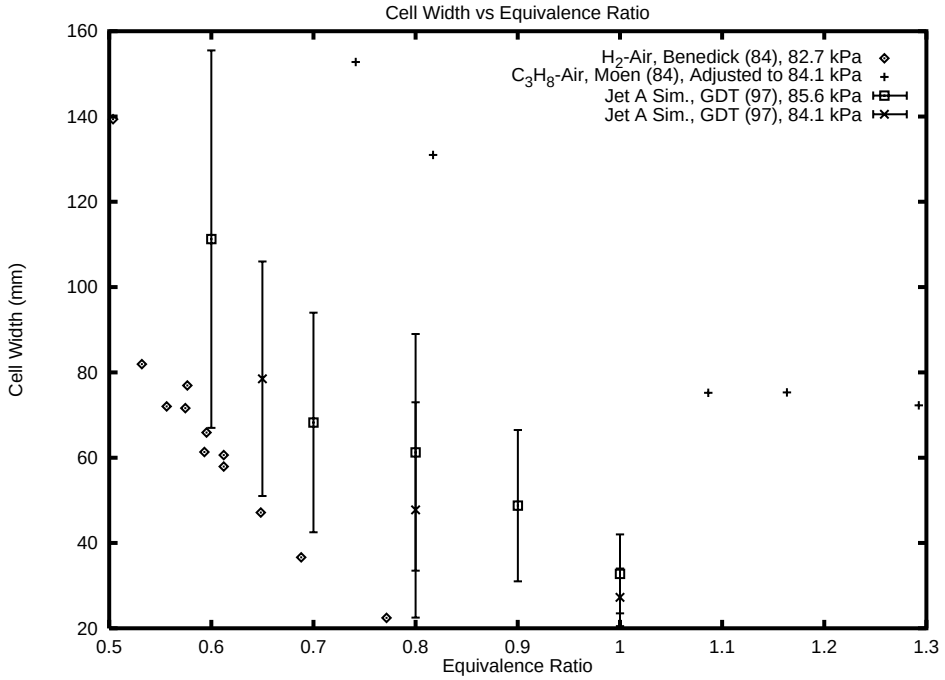

Figure 8.10: Detonation-cell widths in lean hydrogen, propane, and propane-hydrogen simulant mixtures.

Chapter 9

Summary and Recommendations

A quarter-scale engineering model of the center wing tank (CWT) of a 747-100 was constructed. This engineering model replicated the compartmentalization, passageways, and venting to the atmosphere. The model was designed to scale the fluid dynamical and combustion aspects of the explosion, not the structural failure of the beams or spars. The effect of structural failure on combustion was examined by using model beams and spars with deliberately engineered weak connections to the main tank structure.

A series of experiments was carried out in this model with two main objectives in mind:

1. Investigate combustion in a CWT geometry.

   These tests have provided the first data about flame propagation in a 747 center-wing-tank geometry. The effect of flame acceleration by turbulence dominates the combustion event once the ignition has progressed beyond a certain stage. Data have been obtained which can be directly compared to the numerical simulations.

2. Provide guidance to the TWA 800 crash investigation.

   Test were carried out for various ignition source locations. The results of these tests demonstrate the pressure loads produced by ignition sources in various locations. These pressure loads can in turn be used to estimate the types of structural failure that would have resulted from an explosion starting in a specific location in the CWT. By comparing observed and predicted structural failure, the ignition source location may be narrowed down. In actual practice, there are a number of issues that must be addressed, such as numerical simulation of both structural response and full-scale explosions, in order to complete this process.

Note that the quarter-scale tests do not directly address the question of what the ignition source was or the combustion characteristics of Jet A vapor. Ignition sources are under investigation by other teams within the NTSB. The combustion (Shepherd et al. 1997b) and ignition characteristics (Shepherd et al. 1998) of Jet A vapor were determined in separate laboratory tests carried out prior to the the quarter-scale experiment. Before carrying out the present

experiments, it was determined that Jet A vapor under the conditions of the TWA 800 accident would have been present in sufficient quantity within the center wing tank to have been flammable under a wide range of ignition sources.

Thirty experiments were successfully carried out with Jet A vapor simulant with combustion characteristics appropriate to Jet A vapor at 50°C and a mass loading of 3 kg/m^3 in air at 13.8 kft. Of these tests, seven used a cold liquid Jet A layer to examine the effect of liquid fuel dispersion on the combustion process. Four tests were carried out with all weak partitions that were completely ejected from the tank after the pressure difference had increased to about 20 psi. Seven tests were carried out with a partition configuration (failure of FS, SWB3, and MP in SWB2) that mimics a failure scenario considered by the accident sequence group. One test was carried out with a model cargo bay structure. Sixteen tests were carried out with all strong (no failures) partitions.

9.1 Test Results

The main test results were:

1. Combustion is very significantly accelerated when the flame encounters the turbulence produced by flow in the passageways.
2. The combustion event is complete in about 150 to 200 ms. In a full-scale CWT, this would correspond to 600 to 800 ms.
3. The majority of the gas is burned during a short period lasting between 10 and 20 ms at the end of the event. In a full-scale CWT, this corresponds to 40 to 80 ms in duration.
4. The internal beams (SWB1, SWB2) and the midspar (MS) can experience forces during the explosion in both the forward and rearward directions.
5. In tests without structural failure (all strong), the peak pressures were about 80% of the ideal (adiabatic, constant volume) value.
6. Venting of gas through the vent stringers into the atmosphere has a negligible effect on the combustion event.
7. Structural failure accelerates the combustion event.
8. A cold Jet A liquid layer on the bottom of the tank serves to accelerate the flame slightly but does not contribute to the peak pressure.
9. Variations in fuel concentration have a strong influence on the combustion event.
10. An effect of ignition source location is observed, but further work is needed to relate this to the observed damage pattern in TWA 800.

Specific factors are now examined in detail.

9.1.1 Flame Propagation

1. The turbulence caused by the passageways in the tank greatly accelerates the flame propagation.

2. The flame propagates slowly until it reaches the vicinity of the passageways leading to the adjacent bays.

3. Slow flame propagation in the ignition bay accounts for 90% of the total burn time, and the pressure rise is small during this period. Once the flame reaches the turbulent regions produced by flow through the passageways and vents, the flame quickly moves through the entire tank and the peak pressure is reached within 10 to 20 ms. Nearly all of the pressure rise occurs during this short period.

4. The differential pressures that create the structural loads on the beams and spars all occur during the sharp increase in pressure that takes place at the end of the burn. Both positive and negative differential pressures can be created on the internal beams and the midspar. The duration of these loads would be between 40 and 80 ms in the full-scale CWT.

5. When two bays are connected by a vent tube, a flame in one bay can propagate through the vent tube and ignite the mixture in the other bay.

6. Ignition near a passageway (such as in the 1R or 6R location) allows the flame to immediately run along a series of in-line passageways before propagating into the bays.

7. In a multi-chamber configuration, the peak pressure increases with increasing distance from the ignition location. This is known as “pressure piling” and has been observed previously in connection with combustion in multi-compartment geometries. As a result, the spread in peak pressures between different bays can be up to 1 bar.

8. Different ignition locations produce distinct characteristic pressure history signatures in each bay. However, it is not clear if the observed characteristics are sufficiently different in all cases to produce distinct patterns of structural damage. The relationship between structural damage and ignition location is the subject of continued study.

9.1.2 Partition Failure

It is important to emphasize that the partition failure in the 1/4-scale model does not replicate the structural failure in the full-scale tank. The partitions in the model have equal failure pressures, about 20 psi overpressure, and all fail by shear or tearing of the fasteners connecting the partitions to the rigid upper and lower surfaces. In the actual tank, the MS, SWB1, and the PRs are all much stronger than FS, SWB3, and SWB2. The upper and lower surfaces of the actual CWT will deflect during an explosion. The failure of the CWT is an extremely complex process which we are not attempting to model. The purpose of the weak partitions is to examine how the combustion event is affected by failure of the beams and spars.

1. If the ignition source is located in the aft portion of the tank, partition failure can reduce or suppress the “pressure piling” through rapid venting of the tank contents.

2. If the ignition source is located in the forward portion of the tank, pressure piling can occur in the aft bays of the tank.

3. In these tests, failure pressure is reached regardless of ignition location, and weak partitions always failed. However, only three levels of fuel concentration were examined in the present tests and no nonuniform fuel distributions were examined. Furthermore, the partitions were all set to fail at a single pressure difference, about 20 psi, and the aft partitititions (SWB1, MS) are substantially stronger than the forward partitions in the actual tank.

4. More partitions are expelled from the tank as the ignitor is moved aft. When ignition occurs in the rear bays, all the partitions are expelled. When ignition occurs in the forward bays (1 or 2), the aft partitions remain in the tank.

5. SWB1, MS, and SWB2 can initially fail in both forward and aft directions depending on the ignition location. However, the failure pressures of the 1/4-scale weak panels are significantly lower than that of the full-scale structure in many cases. As discussed subsequently, extrapolation of the 1/4-scale results indicates that the full-scale motion of these partitions would preferentially occur in the forward direction with the notable exception of the maintenance doors in SWB1.

6. Failure of the manufacturing panel in SWB2 occurs after the failure of SWB3. This is, however, a consequence of the relative strength of the MP as compared to SWB3 in the 1/4-scale model. In the accident explosion, the failure of the MP in SWB2 is believed to have been significantly influenced by the stress state produced by the failure of the other portions of the structure.

7. The partial ribs broke in several 1/4-scale all-strong tests. This failure was due to a weak or fatigued angle bracket connecting the Lexan sheet to the spars or SWB1, or to secondary stress due to the motion of SWB1 or MS during the explosion event. Failure of the PRs is not believed to be significant factor in the actual CWT early event failure.

9.1.3 Liquid Fuel

An important limitation of the present tests is that the facility was not heated and the Jet A layers were substantially colder those in the actual CWT of TWA 800. The characteristics of the spray cloud produced by fuel lofting and the ignition delay times of cold Jet A could be significantly different than hot Jet A. All of the conclusions drawn below should be viewed in this context and may have to be revised if and when tests with hot Jet A layers are carried out.

1. Flow speeds in the passageways are sufficiently high to cause liquid fuel lofting.

2. The liquid becomes involved in the combustion process later in the event since it must be lofted, dispersed, and then ignited. A substantial amount of the liquid remains unburnt on the interior surfaces of the tank at the conclusion of each test.

3. The presence of cold Jet A liquid was correlated with an earlier (20 to 60 ms sooner) onset of the rapid pressure rise in the strong and part-strong tests. However, the pressure history during the rapid rise phase was similar with and without Jet A. No noticeable effect was observed in the all-weak tests.

4. The presence of cold liquid Jet A slightly reduces the peak pressures and increases the duration of the burn in all-strong tests, relative to the vapor-only tests.

5. The cold Jet A liquid did not have time to evaporate and contribute vapor fuel in the present tests.

9.1.4 Fuel Concentration

The results obtained by lowering fuel concentration are mixed and contradictory. Further testing is needed.

1. In one test (Test 26, all-strong, ignition in bay 2Lo) with reduced fuel concentration (6.5%), the combustion event took substantially longer, about five times as long as the baseline case. Flame acceleration due to turbulence was observed, but there was no rapid pressure transient such as was observed in the standard-concentration tests or Test 24.

2. In another test (Test 24, part-strong, ignition in bay 2Lo) with the same concentration (6.5%), substantial pressure piling occurred when rapid flame acceleration set in after SWB3 and the FS failed. Peak pressures in Test 24 were three to four times higher than in Test 26.

9.2 Implications for the TWA 800 Crash Investigation

The present results cannot be directly compared to the TWA 800 explosion event. Following are some key differences between the 1/4-scale model tests and an explosion in an actual CWT that prevent such a direct comparison.

1. **Fuel**

   The fuel used in the 1/4-scale testing to date is a uniformly distributed vapor simulant. The actual fuel was vapor evaporated from nonuniformly distributed and heated Jet A liquid.

2. **Structural Response**

   The CWT tank and adjacent airplane structure have been modeled only at the very crudest level by the 1/4-scale facility.

3. **Size and Geometry**

   The actual CWT is four times larger than our model and contains many features that are not in the model.

4. **Initiation**

   The method of combustion initiation in the TWA 800 event is still unknown and only one type of initiator has been used in the experiments.

Despite these limitations, the 1/4-scale facility has provided some essential data on explosions in a CWT-like geometry. In order to go further with this information and apply it to understanding the event in TWA 800, several steps need to be taken:

1. Estimate the structural response times for various components of the center wing tank. This will enable a more rational evaluation of the failure criteria. It is known that both peak pressure and impulse play a role in structural failure depending on the ratio of structural response times to pressure loading characteristic times. At present the structural response times are unknown.

2. Assess the performance of numerical simulations of flame propagation against the data provided by the present tests.[1]

3. Develop a thermal model that can be used to approximate the distribution of temperature on the bottom of the tank.

4. Obtain a better estimate of the liquid and vapor fuel distribution within the tank. This requires using the thermal model as input to a convection and mass transport computation.

5. Evaluate the unique structural failure signatures that are provided by the wreckage.

6. Determine the feasibility of carrying out simulations of the explosion within the CWT tank with various ignition locations and obtaining reliable structural loads.

7. Evaluate the level of effort required to do the computational mechanics simulations of the CWT. Determine if these computations have to be coupled directly to the flame propagation simulation or if uncoupled simulations will be adequate.

8. Determine if larger-scale experiments are needed to complement the numerical simulation of CWT explosions.

After these steps are taken, then the present data can be used together with numerical simulations to examine the influence of the ignition source location on predicted structural damage. By comparing the predicted and actual damage, the ignition source location may be localized within the tank.

[1] These studies are in progress at CMR and SNL.

At each step in this process, a very careful evaluation of the unknown factors and their impact on the accuracy of the simulations and findings must be made. One key part of this evaluation is the comparison of the experimental results with numerical simulations of flame propagation.

9.2.1 Observations on Present Results

We can make some general observations about the structural loads that were produced in the 1/4-scale experiment. It is well known that the entire loading history is significant in evaluating structural response. Fortunately, there is a simple characterization of the loading paths that can be used to readily summarize the loading history. The standard approach is to characterize the load by the peak differential pressure and the total impulse on each structural member of interest. As mentioned earlier, the total impulse is obtained by integrating the time history of the differential pressure.

Although peak pressure/maximum impulse is an extremely useful representation of the loading, it is approximate. When the fundamental frequency of structural response is comparable to the loading frequency, the details of the pressure history must be considered. For external blast problems, two equivalent approaches, dynamic load factors and pressure-impulse diagrams, have been extensively applied to these problems. The present case, failure due to internal pressurization of a multi-compartment vessel, is a more complex problem than blast loading. Further consideration of the structural failure issues is outside the scope of this portion of the investigation.

The peak pressure differentials can be compared with failure pressures that were estimated previously by Boeing as part of the accident investigation. In the limit of very slow pressurization compared to the response time of the structure, no failure will occur unless the peak differential pressure exceeds the failure pressure. If the load is applied very rapidly compared to the structural response time, then a critical impulse must be exceeded in addition to exceeding the peak pressure. For very short impulses, the peak pressure can be quite high compared to the static failure pressure before failure occurs. Since we do not have estimates of the structural response times, there is no way to estimate the impulse failure threshold. However, the impulses have been computed for each pressure differential and the peak positive and negative magnitudes are given in Appendix B.

The peak pressures (positive and negative) on the SWB1, MS, and SWB2 for selected tests are summarized in Figs. 9.3,9.2, and 9.4. The tests used for the summarized analysis of the differential pressure are tabulated in Table 9.1. Six of these tests were carried out with the nominal vapor fuel concentration and the all-strong configuration. The other six were carried out with all-weak or part-strong configurations and a layer of liquid Jet A.

Also shown in Table 9.1 is the sequence in which the differential pressure maxima and minima occurred on each partition. In these tests, the differential pressures contain a positive pressure maximum and a negative pressure minimum. The pressure maximum indicates a pressure against the partition in the forward direction. The pressure minimum indicates a pressure on the partition in the aft direction. When the pressure maximum occurs before the pressure minimum, this suggests that the partition should have a tendency to fail in the forward

direction. When the pressure minimum occurs before the pressure maximum, it is possible that the partition fails in the aft direction. However, one must interpret this data with care, since the partition failure depends not only on the direction of the pressure difference, but on the magnitude and impulse of the pressure pulse.

Table 9.1: Tabulated tests used for the analysis of the dependence of the differential pressure on ignition location. For the differential peak pressure sequence, "+" indicates that the pressure maximum occurred first, and "−" indicates that the pressure minimum occurred first.

	Test number	Ignition location (bay)	Differential peak pressure sequence				
			SWB1		MS		SWB2
			Starboard	Port	Starboard	Port	
ALL-STRONG	4	5	+	+	+	+	+
	5	3	+	+	+	+	+
	6	2	−	−	+	+	+
	7	1	+	−	−†	+	−
	15	6R	−	+	+	−	+
	16	1R	−	+	+	−	+
PART-STRONG	28*	5	+	+	+	+	+
	29*	1	+	−	−	−	−
	27*	2Lo	−	−	+	+	+
ALL-WEAK	19*	5	+	+	+	+	+
	21*	1	−	−	−	−	−
	20*	2Lo	−	−	+	+	+

* Layer of liquid Jet A in the tank during test.

† Positive peak followed by a negative peak followed by a larger positive peak.

The peak pressure differentials observed for each beam and spar of the example tests are now discussed and compared with the estimated failure pressures. The failure estimates were developed by Boeing and are currently (July 1998) under revision. There are a number of assumptions and simplifications that were used to develop these estimates. Both the numbers and the conclusions regarding failure should be used cautiously. An extensive effort is in progress by other investigators to sharpen these estimates and make a comprehensive evaluation of the damage signatures and damage criteria. The following discussion gives only a preliminary indication of how the 1/4-scale results can be used.

Rear Spar Differential failure pressure was estimated by Boeing to be 3.7 bar (55 psi). The rear spar is believed not to have failed due to the initial explosion. The measured peak differential pressure straddled this value, either higher or lower depending on the test configuration. On the surface, this indicates that rear spar failure might occur in some cases. However, the flight test thermal and gas sampling data indicate that our use of compositions appropriate to

a 50°C environment within the tank overestimate the amount of fuel vapor that was actually present in TWA 800.

The CWT ullage temperature (Bower 1997) at 14 kft was between 40 and 50°C and the measured (Sagebiel 1997) fuel-air mass ratio was about 0.05, corresponding to a partial pressure of fuel of about 6.5 mbar. The vapor pressure of Jet A (3 kg/m^3) at 40°C is 6 mbar and at 50°C, 10 mbar (Woodrow and Seiber 1997). This indicates that less fuel should be used to simulate the TWA 800 event than the nominal mixture used in the 1/4-scale tests. If there is less fuel, then the peak pressures may be less than the failure pressure of the RS. Laboratory tests on Jet A vapor indicate that the maximum explosion pressure rise at 40°C is about 3 bar (44 psi). Test 23 (part strong) with 7.5% total fuel had a peak pressure of about 3.7 – 3.8 bar on the RS but there was clear evidence of pressure piling in the aft bays in this test. Test 24 (part strong) with 6.5% total fuel had a peak pressure difference of 4 – 4.7 bar on the rear spar but a very unusual delayed explosion event occurred in this test and there was substantial pressure piling. Test 26 (all strong) with 6.5% total fuel had a peak pressure difference of 1.1 bar. Due to the effects of pressure piling, further testing will be required in order to put an upper bound on the fuel concentration that will not fail the RS.

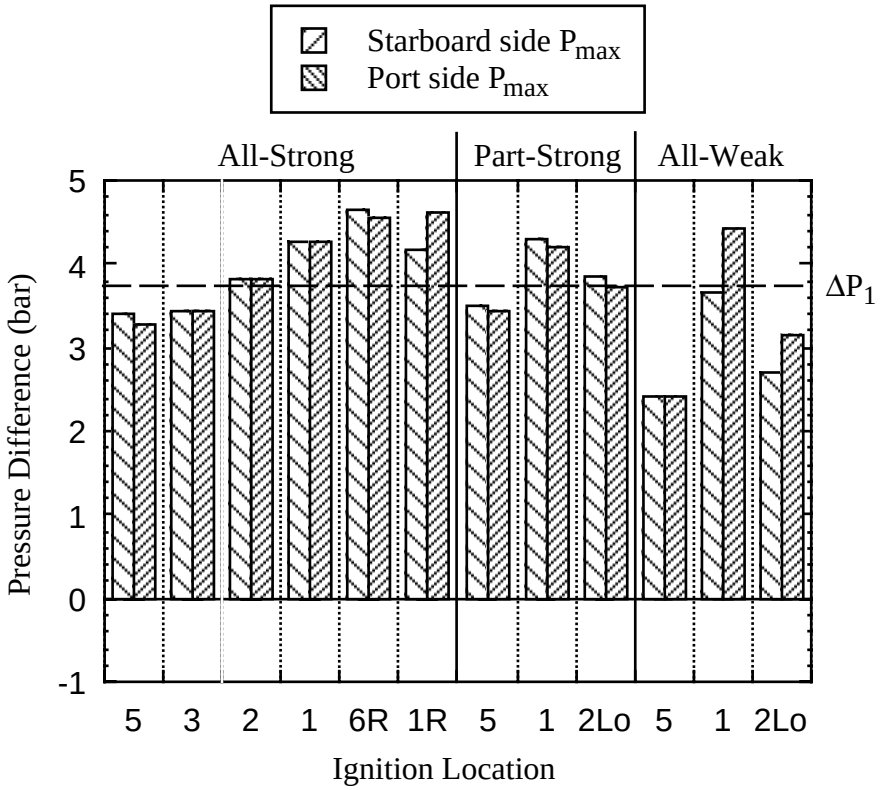

Figure 9.1: Summary of peak differential pressure on RS for selected tests given in Table 9.1.

SWB1 Differential failure pressure for SWB1 is estimated by Boeing to be about 3.3 bar. SWB1 is believed not to have failed due to the initial explosion. The measured peak differential

pressure is substantially less than the failure pressure in all cases except for Test 15, all-strong, ignition in 6R. The maintenance doors would fail in the aft direction in five of the twelve cases examined. The maintenance doors would fail in the forward direction in threee cases and there would be no failure at all in four cases. The maintenance doors are believed to have failed in the aft direction as a result of the initial explosion. The force on SWB1 is mixed, i.e., both forward and rearward.

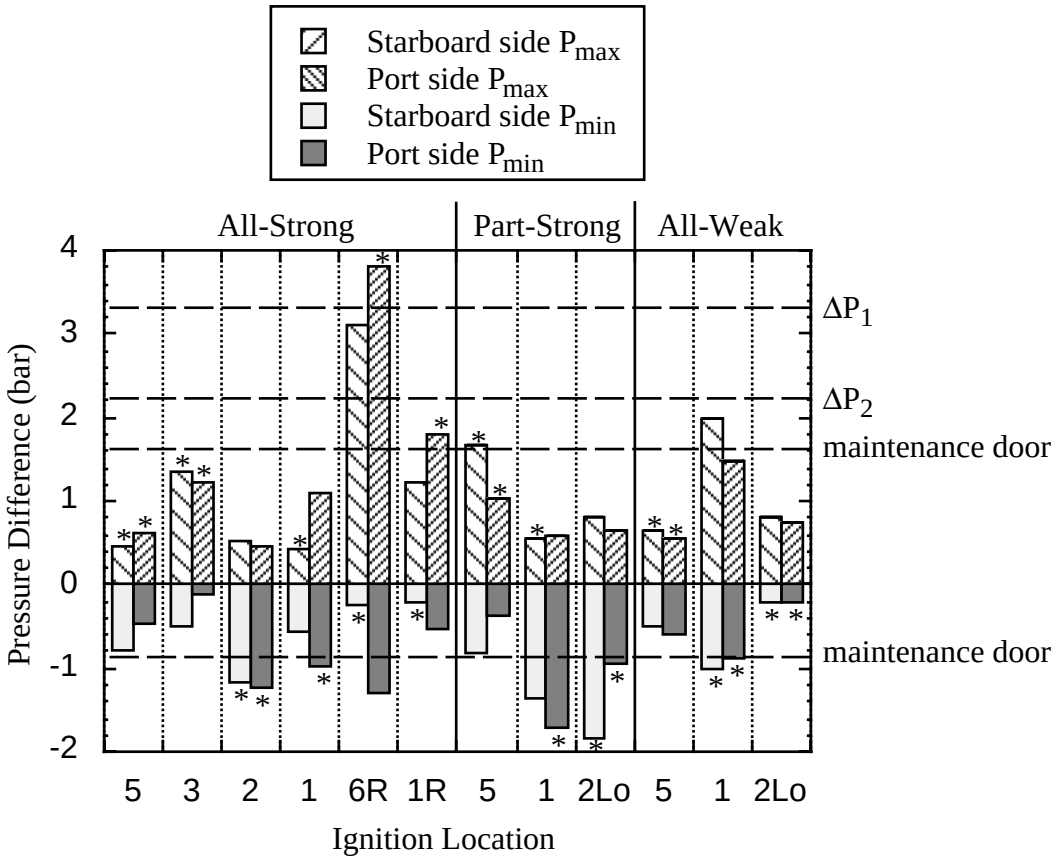

Figure 9.2: Summary of peak differential pressure on SWB1 for selected tests given in Table 9.1. The pressure peak that occurred first is indicated by an asterisk.

MS The failure pressure for the MS is estimated by Boeing to be about 2.2 bar. The observed peak pressures are higher than this in five out of the twelve cases examined. The failure pressure for the maintenance doors is about 1.6 bar (both directions). At least one door would fail forward in nine cases, aft in one case, and no failure in two cases. The doors are believed not to have failed due to the initial explosion. The force on the MS is predominately in the forward direction.

SWB2 The failure pressure for SWB2 is estimated by Boeing to be about 1.4 bar if SWB3 is intact and 1.3 if SWB3 has failed. The observed peak pressures are higher than failure in eight

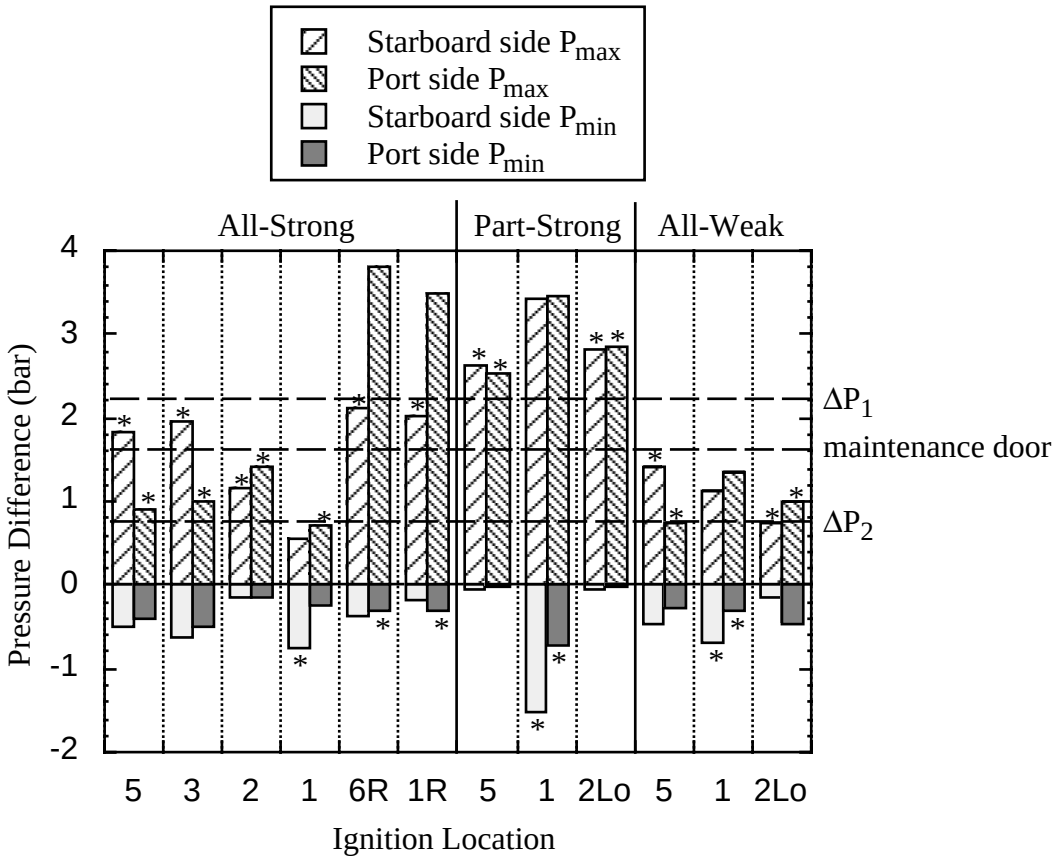

Figure 9.3: Summary of peak differential pressure on the MS for selected tests given in Table 9.1. The pressure peak that occurred first is indicated by an asterisk.

out of the twelve cases examined. The status of SWB2 is questionable, but some fraction of it was believed not to have failed due to the initial explosion.

The failure pressure for the maintenance door is about 1.5 bar (forward) and 1.6 bar (aftward). The door would fail forward in eight cases, aft in zero cases, and no failure in four cases. The door is believed not to have failed due to the initial explosion. The manufacturing panel is believed to have failed, but the timing is unclear and this may have occurred later in the event. Boeing estimated a residual strength (after shearing due to keel beam motion) of about 0.82 bar. MP failure would have occurred in eleven out of twelve cases. The force on SWB2 is predominately in the forward direction.

SWB3 The failure differential pressure of SWB3 is estimated by Boeing to be 1.4 bar. In all tests except those with 6% total fuel, the peak pressure on the front spar exceeded this value by at least a factor of two and in some cases, three. In order to get a lower bound on the fuel concentration that will result in failing SWB3, further tests with parametric variation of fuel concentration are needed.

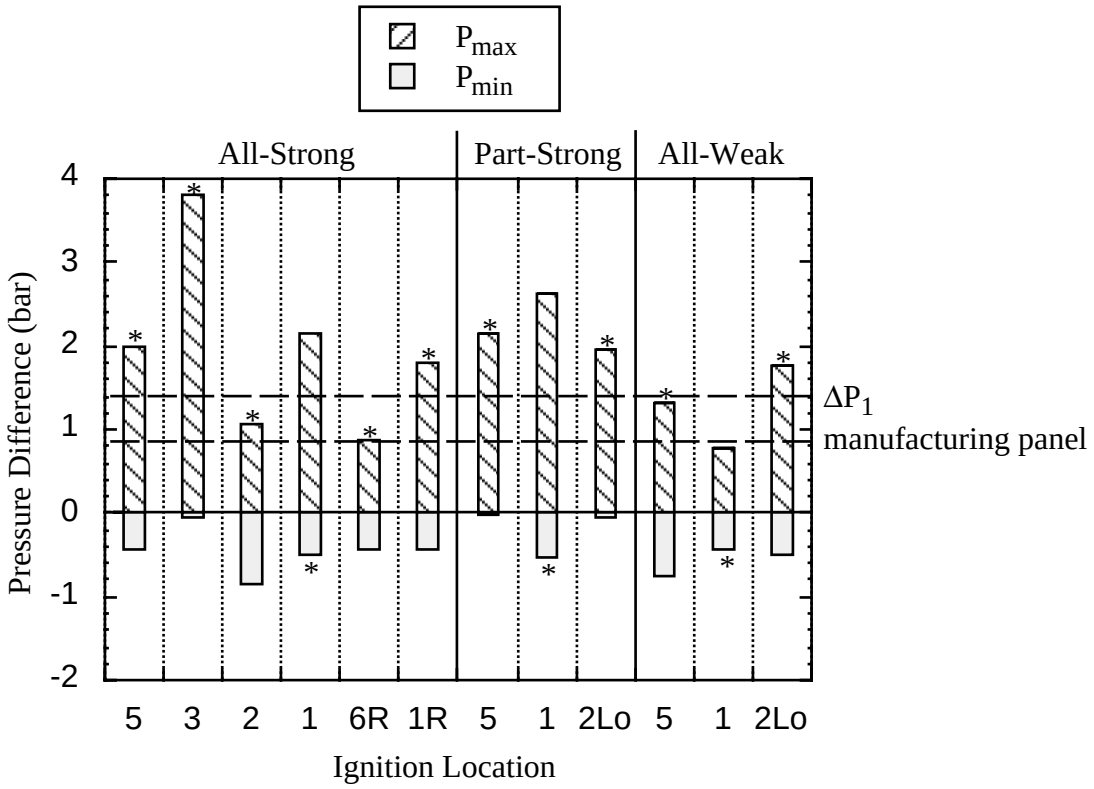

Figure 9.4: Summary of peak differential pressure on SWB2 for selected tests given in Table 9.1. The pressure peak that occurred first is indicated by an asterisk.

FS One key issue for TWA 800 is: Was the FS failure due to overpressure or due to impact by SWB3? In the present testing, 3 – 4 ms elapsed between SWB3 and FS failure. There were pressure pulses produced in bay 0, but it is not clear if these precede or lag the actual failure. The structure and failure mechanism in these tests is sufficiently different from the actual CWT that this issue cannot be resolved using the present data.

All-Strong Tests A case can be made that an ignition source in bay 2 would produce a combination of loading that would be most consistent with the observed damage. However, as the next discussion shows, the failure of SWB3 and the FS appear to completely invalidate that conclusion.

Part-Strong Tests The part-strong tests were performed because this situation was thought to best approximate the failure sequence in TWA 800. However, the results of our tests indicate that failure of both SWB2 and MS would have occurred. This contradicts the assumptions in the part-strong model and raises questions about the consistency of the fuel concentration and structural failure modeling. Clearly, further testing is needed with lower fuel concentrations in order to clarify this situation. In addition, our model of structural failure may simply be too naive.

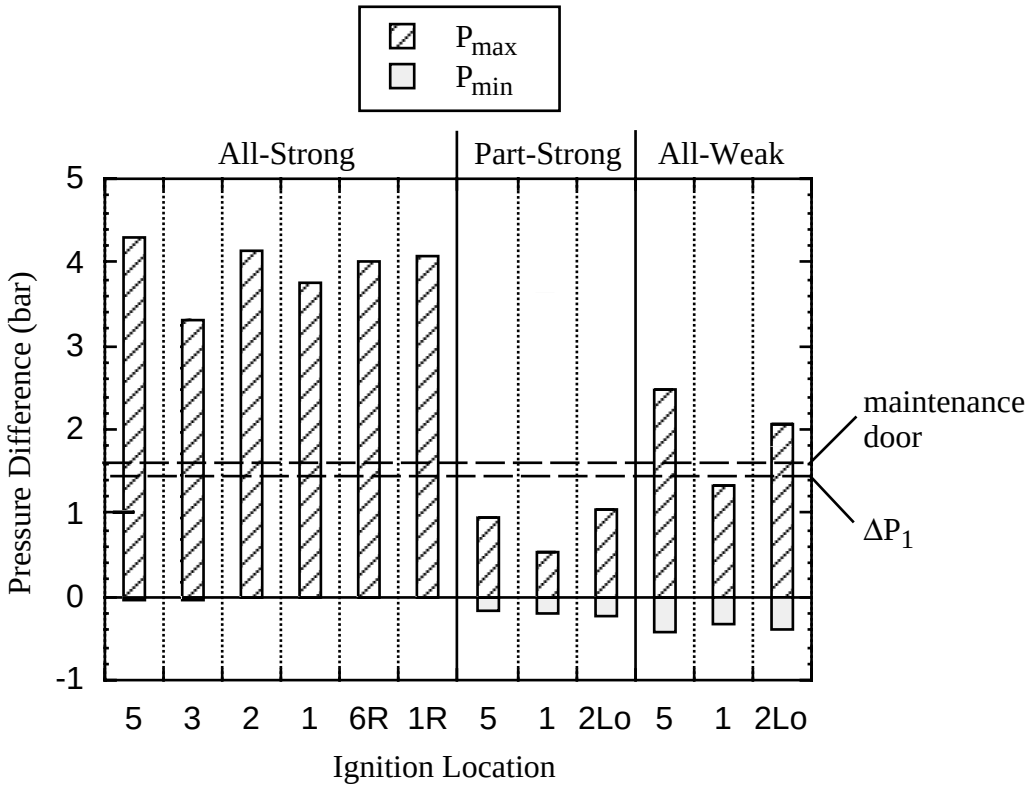

Figure 9.5: Summary of peak differential pressure on SWB3 for selected tests given in Table 9.1.

All-Weak Tests The all-weak case appears to be in complete contradiction to the observed damage pattern. However, what these results do indicate is that *partial* failure of the rear beams and spars (or else just failure of the doors) may play a role in explaining the observed damage. The bulging of the upper wing skin could also play a role. Sensitivity studies examining the role of increasing the flow area in SWB1 and the MS (i.e., to simulate flow areas created by cracks and openings) would be useful in clarifying the extent of these effects.

Cargo Bay Test A single cargo bay test was carried out. Shockwaves with an amplitude of about 1 bar were observed reverberating within the tank. The average pressurization associated with these waves was about 0.9 bar above ambient. There was no obvious build-up in average pressure during the time period that those data were recorded. Since no comparative tests were carried out without liquid Jet A, no conclusions could be drawn regarding the role of liquid lofting and cargo bay pressurization.

9.3 Testing vs. Numerical Simulations

One purpose of the present testing was to create a database for comparison with numerical simulations. Numerical simulations can explore a much larger range of parameters faster and

more cheaply than field tests can. However, before the results of simulations can be used with confidence, they must be verified through detailed comparison with appropriate experimental data. This is referred to as "code validation" by the numerical simulation community.

Unfortunately, due to the lack of replica tests in the database, rigorous validation is not possible at this time. Further evaluation of the intrinsic uncertainties in the experimental results are needed in order to carry out a validation study. Despite this issue, it is still vital to assess the ability of numerical simulations to adequately reproduce the essential features observed in the experiments. This can best be done through careful comparison of simulation and test results. Consideration of each test indicated that the following set are suitable for comparisons: 10, 9, 12, 4, 5, 6, 7, 15, 16, 25. Since the main goal is to compare experiments against vapor-phase models of combustion, the following criteria were used to select tests for comparison studies: all-strong configurations with no failures of any partitions; vapor-phase fuel only; single-point ignition using a filament; no obvious ignition through the fuel manifold.

The following irregularities should be noted:

1. Tests 7, 15, and 16 had partial rib failures.

2. Tests 9 and 10 have three additional 5/16-in holes in the MS.

3. Test 6 had clear ignition through the fuel manifold.

4. Flow through the liquid fuel manifold may be an issue for all of the tests.

9.3.1 Intrinsic Variability

The present experiment is an example of turbulent combustion in a complex geometry. All experiments with turbulent flows have the essential feature that instantaneous properties consist of a mean component plus some random fluctuations. This creates an instrinsic variability in the results of testing with seemingly identical configurations. This variability is independent of the systematic or uncontrolled variation associated with initial conditions, failure of seals, or other hardware or procedural problems.

The conventional way to analyze turbulent flows is by averaging, either time averaging in a given experiment or ensemble averaging over a series of experiments. Models are then compared to the statistical properties of the experimental results, including mean velocity, turbulent kinetic energy, various cross-correlations, etc. Comparison usually progresses from lower-order statistics (mean properties) to higher-order (fluctuations and derivatives) as the models and experiments become more sophisticated. By comparing simulation results against averaged experimental data, the effects of intrinsic variability can be minimized.

In the present case, the only possibility is ensemble averaging (averaging the results of multiple tests with the same configuration) but this is not realistic since the experiments are too time-consuming to obtain a significant sample size. In the present test program, each test was designed to examine a different parameter and repeat tests were not performed. Therefore, we are unable to rigorously assess the amount of intrinsic variability. The closest we can come to this is the comparison between Tests 4 and 25, which is promising but far from definitive.

Until the experiments have been sufficiently replicated and the variability has been quantified, it is difficult to assess the result of such comparisons. For this reason, it is important to do additional testing that will provide some data on the reproducibility of the experimental results. Such replica testing is recommended for the next phase of this project.

A related issue is the sensitivity of the experimental results to small changes in hardware or procedure. This could be examined through a parametric test program, but it is not clear if systematic variations could be distinguished from the intrinsic statistical fluctuations. Another way to address this issue is to carry out a series of numerical simulations to determine the consequence of small changes in the configuration. Important parameters that need to be studied include ignition location, passageway area, and fuel concentration.

9.3.2 Comparison of Models and Experiments

At the simplest level, the experimental pressure-time histories in each bay should be compared with the model results. The data of greatest interest are the pressure differences and impulses across the various spanwise beams and spars. These quantities are the most significant in producing the structural loads that will ultimately determine which components of the structure fail and how.

The slow pressure data (Endevco transducers) appear to be the most reliable for comparison with models. Comparisons between the fast and slow pressure transducer results indicate that in many cases the two agree very well if the high-frequency content in the fast transducers is filtered out or ignored. However, the pressure rise times in some cases are only 5 – 10 ms so that pressure waves (1 – 3 ms transit times across the compartment) are now beginning to play a role in determining the pressure differentials. This means that arrival-time differences of a few ms can make a substantial difference in the outcome. It is probably unreasonable to expect that either model or experiment will perform with sub-millisecond resolution or accuracy for this scale of experiment.

The issue of frequency content in the pressure signals must be examined in the context of structural response. If the characteristic frequencies of the structure are sufficiently low, then it will be possible to ignore the high-frequency content or approximate shockwaves as impulsive loads. Further work on the structural response of the CWT is therefore needed in order to develop criteria for evaluating the performance of models.

9.3.3 Extrapolation to Full Scale

The naive extrapolation to full scale is simply to use all of the observations (pressure and pressure difference histories, flame motion, and partition motion) directly from the 1/4-scale experiment and to multiply the time scale by a factor of four. There are no scaling factors for pressure or velocity, since these should be approximately the same in the scale model and the actual tank.

While this is adequate for rough estimates, there are a number of ways in which the 1/4-scale model is not similar to the full-scale center wing tank:

1. **Geometry** The 1/4-scale tank is rectangular, there are no stiffeners, and the vent passageways are not all in the scaled postions.

2. **Scale** Turbulence and buoyancy effects will be different in the full-scale vs. the 1/4-scale facility.

3. **Vapor Fuel** The simulant fuel was chosen to match the burning velocity and peak pressure of Jet A vapor at the explosion altitude. While this is the starting point for similarity, other features such as the strain-rate dependence, extinction strain, and Lewis number are not matched.

4. **Liquid Fuel** The behavior of the cold liquid Jet A layer in the 1/4-scale model is probably not representative of a warm layer in full scale. There is much more time available in full scale than in 1/4-scale for dispersion, evaporation and droplet combustion. This means that liquid fuel may play a disproportionately larger role in an actual CWT explosion than in a scale model.

These differences need to be considered both in extrapolation of data and in modeling. The best technique for extrapolation will be model simulations that have been validated on the sub-scale experiments.

9.4 Future Testing

There are three main recommendations for future testing:

1. **Testing with Jet A Vapor** This is needed in order to (a) address the differences in combustion characteristics between the simulant mixture and Jet A vapor and (b) examine the dispersion and combustion of warm Jet A liquid layers vs. the cold layers used in the present test series.

   Operating with Jet A vapor will require heating the facility and operating at sub-atmospheric pressure. The Jet A vapor will be produced simply by introducing a scaled amount of warm Jet A liquid and allowing it to evaporate and mix with the air in the tank. Experience gained in the first series of tests indicates that this will be feasible. Tests should be made at 40 and 50°C with various locations for the ignition source. The Jet A should be introduced as liquid and allowed to evaporate and come to equilibrium prior to ignition.

   The Jet A used in these tests should be characterized by laboratory testing to obtain flashpoint, the liquid and vapor composition, vapor pressure, and ignition energy. In order to compare the tests with numerical simulation and previous vapor testing, the all-strong configuration is more useful than the part-strong or weak configurations.

   Note that if Jet A vapor is used, then the pressure differences across SWB3 and the vent stringers will be slightly less than the accident event values since the ambient pressure at the test site is about 0.23 bar higher than at the explosion altitude. However, this is not

expected to make a large difference in the results since SWB3 fails at a differential pressure of 1.4 bar and the flow out of the vent stringers does not appear to play a significant role in the combustion event. If the difference in pressure is a concern, the strength of SWB3 and the size of the restriction orifices in the vents could be adjusted to compensate for this difference.

2. **Replication Testing** Replication tests should be performed using the vapor simulant in order to further characterize the repeatability of the results obtained in the first test series. The following tests are canditates for replication: 4, 6, and 7 (repeat 7 twice to check PR failure). In addition, two to three tests should be carried out with the all-strong configuration, ignition in Bay 2Lo.

   Selected tests should be carried out with the liquid fill pipes plugged, otherwise replicating existing or planned tests with open fill pipes, in order to examine the issue of flame communication through the liquid fuel manifold.

3. **Fuel Concentration** Flight-test results and the observed damages suggest that the actual fuel concentration was less than assumed in the present tests. Further testing with more realistic fuel concentrations — with either Jet A at 40°C or else lower concentrations of simulant fuel — is needed to clarify the effect of partition failure and ignition location.

9.5 Recommended Facility Improvements

As in every test program, not all problems are evident at the design stage, and operation of the facility reveals possible improvements. The facility performed remarkably well given the limited amount of time available and the lack of testing before field set-up. Following are recommendations for future tests:

Bay Communication through Jet Fuel Manifold Plug jet fuel manifold holes for gas-only tests. It may ultimately be necessary to put a valve on each one (all controlled by the same signal), but the presence of liquid in the jet fuel tests should considerably restrict flow through the manifold.

Partition Mounting Make stronger mounts for the strong partitions. Instead of $1.5\times1.5\times1/4$ angle steel, a solid 1.5×1.5 steel bar would probably work better. In addition, the mounting holes need to be fixed to reduce slop. This is only really necessary on SWB3. The best solution would be to drill and tap the holes in the top and bottom tank plates from 3/8 NPT to the next larger fine-thread bolt size. This would probably be around 3/4 in or larger. Drill the mounting brackets for this size bolt, and use SHCS bolted in from the inside to mount the partitions. For sealing, the bolt should extend 1.5 diameters beyond the plate, so a sealing washer and nut can be used. (On SWB3, seals are not needed for strong partition tests, as the gas boundary is aft of the bolt holes.) When weak partitions are used, the holes can be sealed by threading in a short SHCS from the outside with a rubber-faced sealing washer. A thread adapter will be needed

for use of the breakaway switches, but this is easily made. For the other partitions, 3/8 NPT thread bushings could be drilled out to a 1/2-in hole to match the bolts. These would tighten up the holes and protect the pipe threads during the test. The only problem is that these will interfere with use of the sealing washers. An alternate proposition is to tap the insides of these with 1/2-20 threads and permanently install them in the pipe threads, and proceed as above. The bushing hexes would be ground off after installation.

Motion Switches The main drawback of the present motion switches is their inability to detect backward motion of the partitions. A new switch design should be capable of detecting panel motion in either direction.

Cameras The cameras worked well overall, but a few comments can be made. The side-view camera was an excellent idea and should be retained in the future. It should be mounted further off-axis so it can view the tank in natural light and does not have to be shuttered for the schlieren system. Looking at these films, it appears that the four bay cameras can be replaced by two cameras servicing two bays each. It may also be possible to use mirrors and direct the images from all four bays into one camera. In addition, a faster framing rate would be useful for the side-view and schlieren cameras. A Hycam running at 2 – 4 kfps should be adequate. The DBM cameras work well for the observation positions, but perhaps an additional Hycam focused right on the end of the tank to view partition exit would be useful.

Mixing "Wet" and "Dry" Tests In Test 9, we found that jet fuel residue left under the strong partition brackets from the previous test was blown out and burned. At present, there is no way to tell what effect this had on the results. To prevent this from happening in the future, all shots with gas only ("dry") should be grouped and run separately from the "wet" tests whenever possible.

Ignition Location Ignition location should be carefully measured in each test since small variations (less than 1 inch) are predicted by numerical simulation (CMR) to make substantial differences in the differential pressures.

Jet A Tests Heating capability and insulation should be integrated into the facility in order to carry out tests with Jet A . The sealing of SWB3 for both strong and weak partitions should be improved so that the tank can be kept at 0.6 bar for 1 – 2 hours with an acceptable leakage rate. What is acceptable is a matter of judgement, but 3 to 5 mbar/hour is a good target.

Data Recording The motion-sensor signals should be recorded on a single set of high-speed digitizers so that there are no time offset discrepancies with the tape recordings.

Cargo Bay If further tests are carried out with the model cargo bay, the following changes are suggested: (1) improve the sealing between the cargo bay and tank models; (2) perform

comparative tests with and without Jet A layers; (3) recompute the volume of the full-scale cargo bay, correct for all inaccessible volume, and construct a more realistic model.

Weak Partitions If further weak partition tests are carried out, the mounting system and failure points should be redesigned for more consistent failure pressure.

Bibliography

Akbar, R., M. Kaneshige, E. Schultz, and J. Shepherd (1997, July). Detonations in H_2-N_2O-CH_4-NH_3-O_2-N_2 mixtures. Technical Report FM97-3, GALCIT, California Institute of Technology.

Bower, D. (1997, November). Flight test chairman's factual report. Accident DCA-96-Ma-070, NTSB Docket SA-516 Exhibit 23, National Transportation Safety Board.

Kunz, O. (1998, March). Combustion characteristics of hydrogen- and hydrocarbon-air mixtures in closed vessels. Technical Report FM98-4, GALCIT, California Institute of Technology.

Lee, J. J. and J. E. Shepherd (1999, December). Spark Ignition Measurements in Jet A: part II. Explosion Dynamics Laboratory Report FM99-7, California Institute of Technology.

Mercx, W. P. M., D. M. Johnson, and J. Puttock (1995). Validation of scaling techniques for experimental vapor cloud explosions. *Process Safety Progress 14*(2), 120–130.

Reynolds, W. C. (1986, January). *The Element Potential Method for Chemical Equilibrium Analysis: Implementation in the Interactive Program STANJAN* (3rd ed.). Dept. of Mechanical Engineering: Stanford University, Stanford, CA.

Ross, M. and J. Shepherd (1996, July). Lean combustion characteristics of hydrogen-nitrous oxide-ammonia mixtures in air. Technical Report FM96-4, GALCIT. Graduate Aeronautical Laboratories Report to Los Alamos National Laboratory, Parts I and II.

Sagebiel, J. C. (1997, November). Sampling and analysis of vapors from the center wing tank of a test Boeing 747-100 aircraft. Final report for NTSB, Desert Research Institute.

Shepherd, J. E., J. C. Krok, and J. J. Lee (1997, June). Jet A explosion experiments: Laboratory testing. Explosion Dynamics Laboratory Report FM97-5, California Institute of Technology.

Shepherd, J. E., J. C. Krok, J. J. Lee, and M. M. Birky (1997, June). Jet A explosions – field test plan 1/4-scale experiments. Explosion Dynamics Laboratory Report FM97-17, California Institute of Technology.

Shepherd, J. E., J. J. Lee, and J. C. Krok (1998, June). Spark ignition measurements in Jet A. Explosion Dynamics Laboratory Report FM97-9, California Institute of Technology.

Woodrow, J. E. and J. N. Seiber (1997, November). The laboratory characterization of jet fuel vapors under simulated flight conditions. Final report for NTSB, Order No. NTSB12-97-SP-0255, University of Nevada, Reno, Nevada.

Appendix A

Reference Tables

A.1 Shot Locator Index

The following index can be used to locate the page number of a particular test.

A.2 Transducers

Before the test series began, the Endevco transducers were calibrated at Caltech. The pressure gauge had not been calibrated, and all of the values are high. Thus, the manufacturer's values were used for data acquisition. The PCB transducers were not calibrated before the tests because dynamic calibration equipment was not available. After the test series, all transducers were calibrated by ARA. ARA used a test rig that was recently calibrated and certified to NIST standards. The results show that the Endevco gauges remained true, aided by the thermal/debris protection system. The PCBs, however, showed some variations.

Table A.1: Comparison of pre- and post-test gauge calibrations. All values in mV/psi.

Serial Number	Manufacturer Calibration	Pre-test (CIT) Calibration	Post-test (ARA) Calibration
PCB Gages			
9593	29.51		30.27
9597	29.11		25.25
9595	30.52		26.27
9590	29.37		28.20
9594	29.71		29.08
9596	30.06		25.72
9572	29.93		27.79
9592	28.90		25.99
Endevco Gages			
10140	1.65	1.84	1.62
10320	1.63	1.82	1.62
10241	1.49	1.68	1.49
10322	1.69	1.88	1.69
10321	1.62	1.83	1.62
10327	1.34	1.50	1.33
10148	1.71	1.90	1.71

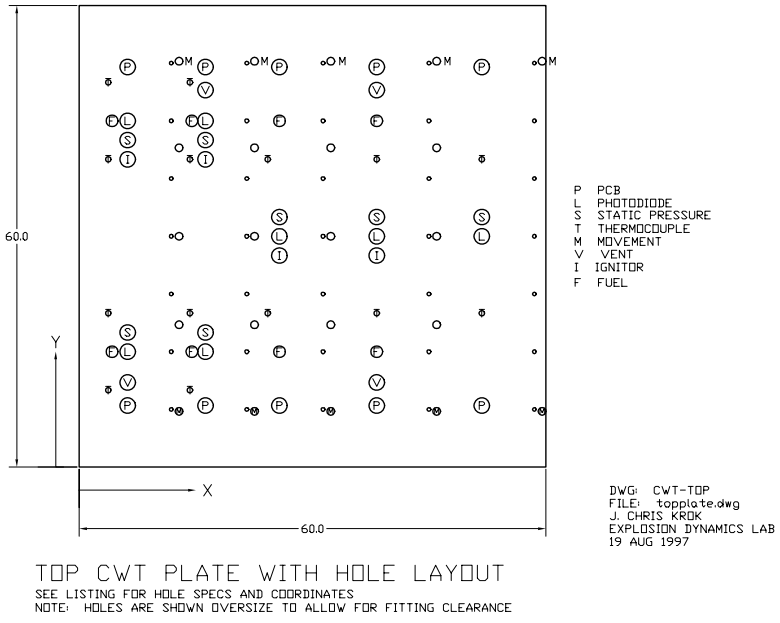

Figure A.1: Transducer layout on top surface of the tank. See tables for dimensions.

Table A.2: Transducer locations (inch). Gauge numbers given in parentheses refer to motion detectors on the bottom surface of the tank.

Gauge	Location	X	Y	Gauge	Location	X	Y
Breakaway Detectors							
M1	SWB1	12.1	52.75	M2	SWB1	12.1	7.25
M3 (11)	MS	21.8	52.75	M4 (12)	MS	21.8	7.25
M5 (13)	SWB2	31.6	52.75	M6 (14)	SWB2	31.6	7.25
M7 (15)	SWB3	45.2	52.75	M8 (16)	SWB3	45.2	7.25
M9 (17)	FS	58.75	52.75	M10 (18)	FS	58.75	7.25
PCB Mounts							
P1	Bay 5L	5.5	52.0	P2	Bay 6R	5.5	8.0
P3	Bay 3L	15.5	52.0	P4	Bay 4R	15.5	8.0
P5	Bay 2L	25.0	52.0	P6	Bay 2R	25.0	8.0
P7	Bay 1L	37.5	52.0	P8	Bay 1R	37.5	8.0
P9	Bay 0L	51.0	52.0	P10	Bay 0R	51.0	8.0
Thermocouples; 6.75” from top of tank							
T1	Bay 5L	3.0	50.0	T2	Bay 5R	3.0	40.0
T3	Bay 6L	3.0	20.0	T4	Bay 6R	3.0	10.0
T5	Bay 3L	13.5	50.0	T6	Bay 3R	13.5	40.0
T7	Bay 4L	13.5	20.0	T8	Bay 4R	13.5	10.0
T9	Bay 2L	23.5	40.0	T10	Bay 2R	23.5	20.0
T11	Bay 1L	37.5	40.0	T12	Bay 1R	37.5	20.0
T13	Bay 0L	51.0	40.0	T14	Bay 0R	51.0	20.0
Static Pressure							
S1	Bay 5	5.5	42.5	S2	Bay 6	5.5	17.5
S3	Bay 3	15.5	42.5	S4	Bay 4	15.5	17.5
S5	Bay 2	25.0	32.5	S6	Bay 1	37.5	32.5
S7	Bay 0	51.0	32.5				
Photodiodes							
L1	Bay 5	5.5	45.0	L2	Bay 6	5.5	15.0
L3	Bay 3	15.5	45.0	L4	Bay 4	15.5	15.0
L5	Bay 2	25.0	30.0	L6	Bay 1	37.5	30.0
L7	Bay 0	51.0	30.0				
Vents							
V1	Bay 6R	5.5	11.0	V1	Bay 1R	37.5	11.0
V2	Bay 3L	15.5	49.0	V2	Bay 1	37.5	49.0

Table A.3: Transducer locations (mm). Gauge numbers given in parentheses refer to motion detectors on the bottom surface of the tank.

Gauge	Location	X	Y	Gauge	Location	X	Y
Breakaway Detectors							
M1	SWB1	307	1340	M2	SWB1	307	184
M3 (11)	MS	554	1340	M4 (12)	MS	554	184
M5 (13)	SWB2	803	1340	M6 (14)	SWB2	803	184
M7 (15)	SWB3	1148	1340	M8 (16)	SWB3	1148	184
M9 (17)	FS	1492	1340	M10 (18)	FS	1492	184
PCB Mounts							
P1	Bay 5L	140	1321	P2	Bay 6R	140	203
P3	Bay 3L	394	1321	P4	Bay 4R	394	203
P5	Bay 2L	635	1321	P6	Bay 2R	635	203
P7	Bay 1L	953	1321	P8	Bay 1R	953	203
P9	Bay 0L	1295	1321	P10	Bay 0R	1295	203
Thermocouples; 171 mm from top of tank							
T1	Bay 5L	76	1270	T2	Bay 5R	76	1016
T3	Bay 6L	76	508	T4	Bay 6R	76	254
T5	Bay 3L	343	1270	T6	Bay 3R	343	1016
T7	Bay 4L	343	508	T8	Bay 4R	343	254
T9	Bay 2L	597	1016	T10	Bay 2R	597	508
T11	Bay 1L	953	1016	T12	Bay 1R	953	508
T13	Bay 0L	1295	1016	T14	Bay 0R	1295	508
Static Pressure							
S1	Bay 5	140	1080	S2	Bay 6	140	445
S3	Bay 3	394	1080	S4	Bay 4	394	445
S5	Bay 2	635	826	S6	Bay 1	953	826
S7	Bay 0	1295	826				
Photodiodes							
L1	Bay 5	140	1143	L2	Bay 6	140	381
L3	Bay 3	394	1143	L4	Bay 4	394	381
L5	Bay 2	635	762	L6	Bay 1	953	762
L7	Bay 0	1295	762				
Vents							
V1	Bay 6R	140	279	V1	Bay 1R	953	279
V2	Bay 3L	394	1245	V2	Bay 1	953	1245

Table A.4: Ignition locations.

	inch			mm		
Location	X	Y	Z	X	Y	Z
Bay 6R	10.6	3.5	2 from top	269	89	51 from top
Bay 5	5.5	40.0	9 from top	140	1016	229 from top
Bay 3	15.5	40.0	9 from top	394	1016	229 from top
Bay 2	25.0	27.5	9 from top	635	699	229 from top
Bay 2Lo	21.1	26.0	2 from bottom	535	660	51 from bottom
Bay 1	37.5	27.5	9 from top	953	699	229 from top
Bay 1R	43.6	3.5	2 from top	1107	89	51 from top

Table A.5: Partition locations. Partition thicknesses given below are for strong partitions. Weak partitions are all 0.090 in (2.3 mm). Location can be taken as the same for both. The location is given as the distance from the forward face of RS to the aft face of the partition.

	inch		mm	
Partition	Location	Thickness	Location	Thickness
SWB1	10.6	0.75	269	19
MS	20.3	0.75	516	19
SWB2	30.1	0.75	765	19
SWB3	43.6	0.875	1107	22
FS	57.5	N/A	1461	N/A

A.3 DBM Camera Performance

Table A.6: Performance of DBM cameras during the test series. N/U, not used; B/S, boresite not retracted; F/E, framing error.

Test	Baycam 1 (Bays 5/6)	Baycam 2 (Bays 3/4)	Baycam 3 (Bay 2)	Baycam 4 (Bay 1)	Side view camera	NE station	SE station
01	OK	OK	jam	OK		N/U	N/U
02	All baycams OK					N/U	N/U
03	OK	OK	OK	jam		N/U	OK
04	All baycams OK					OK	OK
05	All baycams OK					OK	film break
06	OK	half B/S	OK	OK		OK	OK
07	OK	half B/S	OK	OK		OK	OK
08	All baycams OK					OK	OK
Timing sync strobes installed							
09	All baycams OK					OK	OK
10	OK	OK	half boresite	OK		OK	OK
11	OK	OK	half boresite	OK		OK	OK
12	F/E	OK	OK	OK		OK	OK
13	F/E	B/S?	OK	OK		OK	OK
14	F/E	OK	OK	OK		OK	OK
15	F/E	OK	OK	OK		OK	jam
16	F/E	jam	OK	OK		OK	OK
17	F/E	OK	jam	OK		OK	OK
18	F/E	OK	OK	OK		OK	OK
19	OK	boresite	jam	OK		OK	OK
Side-view camera installed							
20	focus	OK	OK	OK	OK	OK	OK
21	All baycams OK				OK	film break	OK
22	All baycams OK				OK	film break	OK
23	All baycams OK				OK	OK	OK
24	OK	jam	OK	OK	OK	OK	OK
25	OK	jam	OK	OK	misalign	N/U	N/U
26	OK	jam	OK	OK	OK	N/U	N/U
27	Baycams not used				OK	OK	OK
28	Baycams not used				OK	focus	OK
29	Baycams not used				dark	dark	dark
30	All baycams OK				OK	OK	OK

A.4 Test Data Status

The test configuration, initial conditions, fuel type and concentration, and status of data are given in the following tables. The tests have been rearranged according to type of partitions.

There were various irregularities and unusual situations noted during the tests. For the purposes of determining the status of the data, codes A – F were assigned to each test according to the table below.

Code	Condition
A	Data all valid, no problems with test
B	Test selected for comparisons with simulations
C	Problems with data or test implementation, do not use for comparison
D	Minor irregularites with data or setup
E	Partial rib failure, may affect the comparisons
F	Ignition through the liquid fuel loading lines

A.5 Test and Ambient Temperatures

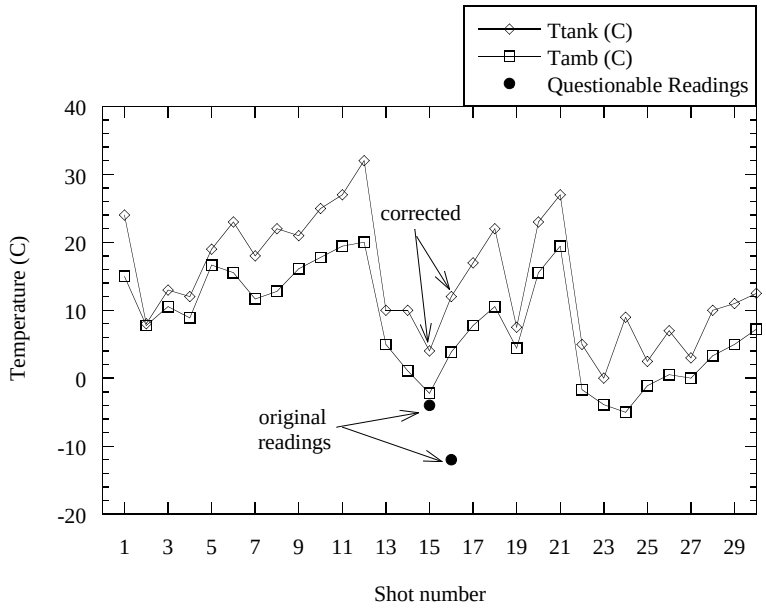

Figure A.2: Correlation between temperature in the tank and the ambient air temperature. The original temperature readings in the tank for Tests 15 and 16 are -4°C and -12°C respectively. These readings are believed to have an erroneous sign, and the corrected temperatures of 4°C and 12°C are found to correlate well with temperatures in the tank for the other tests.

Table A.7: ALPHA test series. All strong, vents closed, standard vapor fuel mixture, ignition in bay 5.

Test	Type	Status	T, °C	P, torr	Video start	Remarks
01	1-bay	C	24	608.0	0:00:32	Match ignition
11	1-bay	A,B	27	617.0	0:30:55	Repeat of Test 1 with filament ignition
02	2-bay	C	8	614.1	0:02:56	Filament with match backup, noise in data
03	3-bay	C	13	613.2	0:05:30	Filament with match backup
10	2-bay	D,B	25	620.4	0:27:39	3 5/16-in holes in MS open
09	4-bay	D,B	21	621.3	0:24:21	Jet A residue under partitions; 3 5/16-in holes in SWB1, MS open
25	6-bay	A,B	2.5	613.9	1:15:37	Near replica of Test 4, vents open
12	2-bay	A,B	32	616.0	0:34:08	1 2-in-diam. hole in MS, stringers plugged

Table A.8: BETA test series. All strong, six-bay, vents open.

Test	Igniter	Status	T, °C	P, torr	Video start	Remarks
04	5	A,B	12	619.9	0:07:47	Leak rate 1 torr/min
08	5, Jet A	A	22	622.8	0:20:49	First test with liquid Jet A
05	3	D,B	19	618.3	0:11:09	Bay 1 static pressure gauge data lost
06	2	F,B	22.5	617.1	0:14:02	Bay 1 ignition through fuel manifold
07	1	E,B	18	618.7	0:17:15	Aft PR fail at 205 ms
15	6R	E,B	4*	619.7	0:42:31	Aft PR fail, fwd PR damage at 190 ms
16	1R	E,B	12*	620.1	0:45:44	Aft PR fail, fwd PR damage at 197 ms
26	2Lo	A,B	7	612.5	1:18:00	6.5% fuel, SWB3 leakage on fill (compensated)

* Temperature corrected for a suspected error in the sign of the original temperature readings (Figure A.2)

Table A.9: GAMMA, DELTA test series. Six-bay, vents open, weak and part-strong partitions

Test	Igniter	Status	T, °C	P, torr	Video start	Remarks
Special purpose						
13	5	A	10	617.0	0:37:01	Weak SWB3 test, for CMR venting model comparison
14	5	A	10	608.5	0:39:18	0.012-in thick MP test, unusual burn in Bays 5 and 6
All weak						
18	5	A	22	614.3	0:51:15	All partitions ejected
19	5, Jet A	A	7.5	612.8	0:54:09	SWB1 held in by aft PR
20	2Lo, Jet A	A	23	618.7	0:57:58	SWB1, MS held up at edge of tank
21	1, Jet A	A	27	615.6	1:02:16	SWB1, MS stayed in; vertical plume in 3/4, too big for manifold
Flight 800 (part strong) configuration, variable concentration, ignition in 2Lo						
22	8.4%	F	5	614.7	1:05:41	Bay 1 ignition through fuel manifold
23	7.5%	F	0	619.0	1:08:49	Bay 1 ignition through fuel manifold
24	6.5%	C	9	617.8	1:12:20	Plume in bay 1, no ign; late burn in 5/6, possible aft PR failure
Flight 800 configuration, ignition location study						
17	5	A	17	618.6	0:48:57	0.012-in thick MP
27	2Lo, Jet A	A	3	607.9	1:21:37	0.006-in thick MP
28	5, Jet A	A	10	606.1	1:24:52	0.006-in thick MP
29	1, Jet A	E	11	604.6	1:28:00	Aft PR failure, possible jet fuel plume in bays 5/6
DELTA test: cargo bay						
30	5, Jet A	A	12.5	615.0	1:30:49	Venting from cargo bay, deformation at juncture

Table A.10: Gas bottle information.

	Bottle 1	Bottle 2
Start date	21 Oct 1997?	26 Nov 1997
Propane	16.71%	16.81%
Hydrogen	Balance	Balance
Pressure	520 psi	520 psi
Volume STP	52 cu ft	52 cu ft
Control No.	22-09-52	22-09-52
Cylinder No.	Z2979-P	AS-18745

A.6 Simulant Fuel Information

The simulant fuel was purchased from Matheson in Cucamonga, CA. The nominal composition of the bottle was 83.3% hydrogen and 16.7% propane. Each bottle was certified and supplied with an analysis. The certification information is given below. When delivered, each bottle contained approximately 54.6 ft^3 and had a pressure of about 520 psia.

One concern during the testing was the propane might condense and contents would become stratified. When the bottle is filled, the gas is mixed by putting the bottle on rollers for about 45 min. If the temperature drops below the staturation temperature, the propane will condense. For a full bottle, this happens at about 45 to 50 °F. In order to avoid this, the bottle was heated at the bottom and wrapped with insulation. No evidence of stratification was observed in any tests.

A.7 Video Tape

The film from the DBM cameras was transferred to video and edited in sequence onto a single video tape containing records from all tests. The tape also contains the records from the VHS video cameras that were used.

The order of the views are:

1. Bays 5/6 schlieren DBM
2. Bays 3/4 schlieren DBM
3. Bay 2 schlieren DBM
4. Bay 1 schlieren DBM
5. Side-view DBM
6. West hilltop video

7. NE video
8. SE video
9. NE DBM
10. SE DBM

Results from a given test can be located on the tape by using the index in Table A.11.

Table A.11: Video Tape Log. Times are elapsed time from the beginning of the tape.

Shot	Time (hr:min:sec)	Test	Time (hr:min:sec)	Shot	Time (hr:min:sec)
1	0:00:32	11	0:30:55	21	1:02:16
2	0:02:56	12	0:34:08	22	1:05:41
3	0:05:30	13	0:37:01	23	1:08:49
4	0:07:47	14	0:39:18	24	1:12:20
5	0:11:09	15	0:42:31	25	1:15:37
6	0:14:02	16	0:45:44	26	1:18:00
7	0:17:15	17	0:48:57	27	1:21:37
8	0:20:49	18	0:51:15	28	1:24:52
9	0:24:21	19	0:54:09	29	1:28:00
10	0:27:39	20	0:57:58	30	1:30:49

Appendix B

Tabulated Data

B.1 Endevco Peak Pressure Data

Test 04

Bay	P_{max} (bar)	t_{max} (s)	P_{min} (bar)	t_{min} (s)
6	3.595	0.177	−0.072	3.997
5	3.596	0.181	−0.061	3.998
4	3.600	0.177	−0.081	3.997
3	3.677	0.180	−0.084	3.997
2	3.975	0.171	−0.076	3.997
1	4.314	0.170	−0.050	3.997

Test 05

Bay	P_{max} (bar)	t_{max} (s)	P_{min} (bar)	t_{min} (s)
6	3.436	0.187	−0.113	3.613
5	3.427	0.189	−0.082	3.996
4	3.420	0.185	−0.124	3.946
3	3.510	0.185	−0.103	3.982
2	3.894	0.174	−0.096	3.996
1	Data not valid			

Test 06

Bay	P_{max} (bar)	t_{max} (s)	P_{min} (bar)	t_{min} (s)
6	3.831	0.221	0.015	−0.053
5	3.805	0.222	0.010	0.036
4	3.538	0.236	−0.006	−0.220
3	3.637	0.224	−0.005	−0.036
2	3.501	0.237	0.005	−0.203
1	4.153	0.218	−0.006	−0.136

Test 07

Bay	P_{max} (bar)	t_{max} (s)	P_{min} (bar)	t_{min} (s)
6	4.257	0.209	0.015	0.068
5	4.270	0.207	0.015	0.035
4	4.238	0.212	0.012	0.084
3	4.223	0.220	0.000	−0.216
2	4.151	0.218	0.010	0.051
1	3.762	0.233	−0.017	0.001

Test 08

Bay	P_{max} (bar)	t_{max} (s)	P_{min} (bar)	t_{min} (s)
6	3.954	0.106	0.010	−0.136
5	3.917	0.107	−0.005	−0.236
4	3.656	0.107	0.006	0.014
3	3.820	0.106	0.000	−0.070
2	4.187	0.116	0.015	−0.003
1	4.325	0.110	0.011	0.047

Test 09

Bay	P_{max} (bar)	t_{max} (s)	P_{min} (bar)	t_{min} (s)
6	3.970	0.193	0.021	−0.058
5	3.928	0.195	−0.010	−0.009
4	3.935	0.193	−0.012	−0.126
3	4.056	0.192	−0.005	−0.037
2	4.020	0.186	0.005	−0.036
1	4.220	0.186	0.067	0.047

Test 10

Bay	P_{max} (bar)	t_{max} (s)	P_{min} (bar)	t_{min} (s)
6	3.929	0.272	0.026	0.031
5	3.836	0.271	−0.005	−0.222
4	3.867	0.273	−0.012	−0.108
3	3.967	0.270	0.000	0.016
2	3.879	0.260	0.005	0.047
1	3.896	0.267	0.056	0.039

Test 11

Bay	P_{max} (bar)	t_{max} (s)	P_{min} (bar)	t_{min} (s)
6	3.729	0.508	0.015	−0.026
5	3.626	0.514	−0.005	−0.242
4	3.644	0.515	−0.012	0.041
3	3.731	0.493	0.010	0.041
2	3.667	0.502	0.005	0.024
1	3.746	0.525	0.084	0.057

Test 12

Bay	P_{max} (bar)	t_{max} (s)	P_{min} (bar)	t_{min} (s)
6	3.872	0.243	0.046	0.039
5	3.785	0.238	0.010	0.056
4	3.767	0.243	−0.012	0.006
3	3.874	0.241	0.000	−0.194
2	3.566	0.248	0.005	0.056
1	3.645	0.248	0.078	−0.027

Test 13

Bay	P_{max} (bar)	t_{max} (s)	P_{min} (bar)	t_{min} (s)
6	3.790	0.136	−0.051	1.024
5	3.769	0.135	−0.077	0.941
4	3.786	0.138	−0.025	1.007
3	3.854	0.134	−0.054	1.007
2	4.207	0.132	−0.030	0.940
1	1.382	0.127	−0.084	0.137

Test 14

Bay	P_{max} (bar)	t_{max} (s)	P_{min} (bar)	t_{min} (s)
6	3.195	0.215	0.016	−0.007
5	3.121	0.213	0.036	0.026
4	3.619	0.178	0.006	0.026
3	4.829	0.177	0.000	0.009
2	4.388	0.191	0.010	0.059
1	4.665	0.190	0.033	0.059

Test 15

Bay	P_{max} (bar)	t_{max} (s)	P_{min} (bar)	t_{min} (s)
6	4.660	0.198	0.037	−0.044
5	4.561	0.192	−0.036	−0.094
4	4.096	0.203	0.025	−0.094
3	4.957	0.198	0.010	0.073
2	3.818	0.226	−0.015	−0.211
1	4.041	0.227	0.045	0.023

Test 16

Bay	P_{max} (bar)	t_{max} (s)	P_{min} (bar)	t_{min} (s)
6	4.168	0.204	0.021	0.098
5	4.622	0.199	0.000	−0.119
4	3.873	0.206	0.012	0.048
3	4.602	0.201	0.015	0.048
2	3.743	0.223	0.010	0.031
1	4.075	0.222	−0.017	−0.019

Test 17

Bay	P_{max} (bar)	t_{max} (s)	P_{min} (bar)	t_{min} (s)
6	3.501	0.149	−0.011	0.775
5	3.381	0.149	−0.015	0.825
4	3.309	0.149	−0.031	0.942
3	3.401	0.149	−0.010	0.858
2	3.475	0.149	−0.020	3.279
1	1.332	0.139	−0.039	0.158

Test 18

Bay	P_{max} (bar)	t_{max} (s)	P_{min} (bar)	t_{min} (s)
6	2.528	0.113	−0.164	0.129
5	2.452	0.113	−0.158	0.129
4	2.001	0.109	−0.192	0.129
3	2.407	0.111	−0.172	0.129
2	1.771	0.115	−0.131	0.130
1	1.784	0.114	−0.067	0.131

Test 19

Bay	P_{max} (bar)	t_{max} (s)	P_{min} (bar)	t_{min} (s)
6	2.401	0.118	−0.206	0.134
5	2.421	0.116	−0.133	0.140
4	2.317	0.117	−0.174	0.134
3	2.451	0.115	−0.153	0.139
2	2.386	0.112	−0.151	0.139
1	2.993	0.114	−0.178	0.129

Test 20

Bay	P_{max} (bar)	t_{max} (s)	P_{min} (bar)	t_{min} (s)
6	2.702	0.123	−0.179	0.141
5	3.158	0.122	−0.212	0.141
4	2.323	0.120	−0.197	0.141
3	2.881	0.121	−0.204	0.141
2	2.507	0.119	−0.126	0.139
1	Data not valid.			

Test 21

Bay	P_{max} (bar)	t_{max} (s)	P_{min} (bar)	t_{min} (s)
6	3.652	0.125	−0.301	0.163
5	4.416	0.126	−0.328	0.160
4	3.145	0.128	−0.310	0.162
3	3.073	0.128	−0.316	0.163
2	2.472	0.130	−0.328	0.162
1	2.402	0.130	−0.334	0.158

Test 22

Bay	P_{max} (bar)	t_{max} (s)	P_{min} (bar)	t_{min} (s)
6	4.152	0.209	−0.011	0.868
5	4.076	0.209	−0.107	0.810
4	3.445	0.208	−0.006	0.918
3	3.500	0.209	−0.010	0.985
2	2.381	0.205	−0.055	1.001
1	1.104	0.202	−0.056	0.210

Test 23

Bay	P_{max} (bar)	t_{max} (s)	P_{min} (bar)	t_{min} (s)
6	3.776	0.281	−0.042	1.063
5	3.713	0.275	−0.046	0.863
4	2.993	0.281	−0.050	0.963
3	3.062	0.277	−0.030	0.896
2	2.184	0.270	−0.005	1.864
1	1.310	0.273	−0.184	0.280

Test 24

Bay	P_{max} (bar)	t_{max} (s)	P_{min} (bar)	t_{min} (s)
6	3.977	0.517	−0.037	1.233
5	4.663	0.512	−0.031	1.333
4	2.497	0.422	−0.056	1.316
3	2.432	0.425	−0.020	1.166
2	1.917	0.430	−0.005	1.968
1	1.449	0.440	−0.184	0.450

Test 25

Bay	P_{max} (bar)	t_{max} (s)	P_{min} (bar)	t_{min} (s)
6	3.782	0.174	−0.005	0.032
5	3.662	0.169	−0.015	−0.051
4	3.922	0.154	−0.037	0.049
3	3.751	0.161	0.000	0.049
2	4.252	0.178	−0.010	0.049
1	4.431	0.170	0.006	0.032

Test 26

Bay	P_{max} (bar)	t_{max} (s)	P_{min} (bar)	t_{min} (s)
6	0.936	1.108	−0.016	−0.136
5	0.899	1.108	−0.031	0.050
4	0.886	1.108	−0.043	0.415
3	0.935	1.091	−0.005	−0.203
2	1.251	0.891	−0.020	0.131
1	1.332	0.907	−0.006	−0.086

Test 27

Bay	P_{max} (bar)	t_{max} (s)	P_{min} (bar)	t_{min} (s)
6	3.845	0.164	−0.037	1.308
5	3.734	0.164	−0.036	1.191
4	3.346	0.160	−0.050	1.842
3	3.416	0.158	−0.015	1.191
2	2.986	0.154	−0.035	1.725
1	1.237	0.147	−0.111	0.162

Test 28

Bay	P_{max} (bar)	t_{max} (s)	P_{min} (bar)	t_{min} (s)
6	3.517	0.133	−0.005	0.993
5	3.422	0.134	−0.020	1.080
4	3.767	0.116	−0.019	1.160
3	3.396	0.126	−0.015	1.293
2	2.986	0.124	−0.005	1.811
1	1.221	0.118	−0.022	0.131

Test 29

Bay	P_{max} (bar)	t_{max} (s)	P_{min} (bar)	t_{min} (s)
6	4.311	0.170	0.005	1.045
5	4.219	0.168	−0.005	1.296
4	3.966	0.172	−0.012	1.780
3	3.953	0.175	−0.015	1.262
2	3.334	0.164	−0.020	0.194
1	1.494	0.168	−0.128	0.175

Test 30

Bay	P_{max} (bar)	t_{max} (s)	P_{min} (bar)	t_{min} (s)
6	3.612	0.126	−0.011	1.977
4	3.650	0.103	−0.019	1.076
2	2.391	0.113	−0.010	1.810
1	1.249	0.109	−0.006	−0.126
0	0.980	0.129	−0.029	1.994
mid CB	1.093	0.122	−0.026	1.366

B.2 Endevco Pressure Differential and Impulse Data

Test 04

Bays	ΔP_{max} (bar)	t_{max} (s)	ΔP_{min} (bar)	t_{min} (s)	I_{max} (bar-ms)	$t_{I,max}$ (s)
Stbd SWB1 (6-4)	0.470	0.135	−0.781	0.144	6.671	0.141
Port SWB1 (5-3)	0.616	0.139	−0.470	0.149	5.528	0.145
Stbd MS (4-2)	1.827	0.145	−0.513	0.164	17.909	0.156
Port MS (3-2)	0.913	0.150	−0.396	0.164	14.376	0.156
SWB2 (2-1)	1.990	0.153	−0.445	0.170	27.855	0.164
SWB3 (1-0)	4.314	0.170	−0.050	3.997	163.123	0.199
Aft PR (5-6)	0.364	0.138	−0.357	0.148	0.575	0.122
Fwd PR (3-4)	0.356	0.134	−1.270	0.144	3.495	0.138

Test 05

Bays	ΔP_{max} (bar)	t_{max} (s)	ΔP_{min} (bar)	t_{min} (s)	I_{max} (bar-ms)	$t_{I,max}$ (s)
Stbd SWB1 (6-4)	1.345	0.146	−0.514	0.150	9.465	0.148
Port SWB1 (5-3)	1.216	0.148	−0.122	0.166	9.605	0.154
Stbd MS (4-2)	1.969	0.150	−0.616	0.174	15.975	0.162
Port MS (3-2)	1.015	0.154	−0.512	0.174	10.650	0.162
SWB2 (2-1)	Data not valid.					
SWB3 (1-0)	Data not valid.					
Aft PR (5-6)	0.133	0.127	−0.501	0.143	1.654	0.134
Fwd PR (3-4)	0.167	0.136	−1.642	0.149	2.876	0.145

Test 06

Bays	ΔP_{max} (bar)	t_{max} (s)	ΔP_{min} (bar)	t_{min} (s)	I_{max} (bar-ms)	$t_{I,max}$ (s)
Stbd SWB1 (6-4)	0.517	0.210	−1.168	0.192	0.015	−0.212
Port SWB1 (5-3)	0.466	0.209	−1.229	0.194	0.008	−0.235
Stbd MS (4-2)	1.165	0.194	−0.142	0.208	9.865	0.237
Port MS (3-2)	1.421	0.195	−0.138	0.178	14.183	0.249
SWB2 (2-1)	1.069	0.199	−0.854	0.218	14.818	0.202
SWB3 (1-0)	4.153	0.218	−0.006	−0.136	184.065	0.249
Aft PR (5-6)	0.099	0.204	−0.374	0.199	0.184	0.194
Fwd PR (3-4)	0.297	0.196	−0.088	0.186	4.525	0.249

Test 07

Bays	ΔP_{max} (bar)	t_{max} (s)	ΔP_{min} (bar)	t_{min} (s)	I_{max} (bar-ms)	$t_{I,max}$ (s)
Stbd SWB1 (6-4)	0.417	0.194	−0.575	0.203	4.393	0.199
Port SWB1 (5-3)	1.108	0.204	−0.966	0.200	1.542	0.212
Stbd MS (4-2)	0.548	0.208	−0.760	0.204	2.002	0.232
Port MS (3-2)	0.720	0.200	−0.237	0.204	6.389	0.249
SWB2 (2-1)	2.157	0.204	−0.502	0.193	11.360	0.248
SWB3 (1-0)	3.762	0.233	−0.017	0.001	173.457	0.249
Aft PR (5-6)	2.055	0.204	−0.633	0.199	0.968	0.207
Fwd PR (3-4)	0.523	0.204	−0.516	0.208	4.671	0.249

Test 08

Bays	ΔP_{max} (bar)	t_{max} (s)	ΔP_{min} (bar)	t_{min} (s)	I_{max} (bar-ms)	$t_{I,max}$ (s)
Stbd SWB1 (6-4)	1.484	0.081	−0.586	0.087	16.297	0.166
Port SWB1 (5-3)	0.829	0.082	−0.542	0.092	9.180	0.087
Stbd MS (4-2)	2.236	0.086	−0.636	0.127	23.344	0.099
Port MS (3-2)	1.529	0.092	−0.482	0.127	22.657	0.100
SWB2 (2-1)	0.523	0.089	−0.465	0.101	4.321	0.091
SWB3 (1-0)	4.325	0.110	0.011	0.047	389.709	0.199
Aft PR (5-6)	0.029	0.080	−0.407	0.075	1.154	0.067
Fwd PR (3-4)	0.777	0.080	−1.300	0.086	9.854	0.199

Test 09

Bays	ΔP_{max} (bar)	t_{max} (s)	ΔP_{min} (bar)	t_{min} (s)	I_{max} (bar-ms)	$t_{I,max}$ (s)
Stbd SWB1 (6-4)	0.619	0.171	−0.298	0.155	1.839	0.175
Port SWB1 (5-3)	0.197	0.151	−0.570	0.169	3.466	0.157
Stbd MS (4-2)	0.464	0.165	−0.633	0.177	9.242	0.167
Port MS (3-2)	4.220	0.186	0.067	0.047	129.423	0.199
SWB2 (2-1)	0.471	0.155	−0.873	0.170	10.948	0.165
SWB3 (1-0)	0.324	0.164	−0.813	0.177	8.635	0.167
Aft PR (5-6)	0.000	0.999	0.000	0.999	0.000	0.199
Fwd PR (3-4)	0.000	0.999	0.000	0.999	0.000	0.199

Test 10

Bays	ΔP_{max} (bar)	t_{max} (s)	ΔP_{min} (bar)	t_{min} (s)	I_{max} (bar-ms)	$t_{I,max}$ (s)
Back-Front (Stbd MS (4-2))	0.241	0.201	−0.831	0.219	10.384	0.207

Test 12

Bays	ΔP_{max} (bar)	t_{max} (s)	ΔP_{min} (bar)	t_{min} (s)	I_{max} (bar-ms)	$t_{I,max}$ (s)
Back-Front (Stbd MS (4-2))	0.310	0.236	−1.001	0.187	5.181	0.159

Test 13

Bays	ΔP_{max} (bar)	t_{max} (s)	ΔP_{min} (bar)	t_{min} (s)	I_{max} (bar-ms)	$t_{I,max}$ (s)
Stbd SWB1 (6-4)	0.398	0.107	−0.540	0.118	4.534	0.113
Port SWB1 (5-3)	0.680	0.113	−0.717	0.122	4.552	0.119
Stbd MS (4-2)	1.797	0.118	−0.489	0.132	22.322	0.179
Port MS (3-2)	1.393	0.122	−0.407	0.132	22.628	0.179
SWB2 (2-1)	4.025	0.136	−0.021	0.969	185.573	0.179
SWB3 (1-0)	1.382	0.127	−0.084	0.137	11.805	0.134
Aft PR (5-6)	0.224	0.113	−0.424	0.120	0.330	0.099
Fwd PR (3-4)	0.292	0.107	−1.136	0.117	2.563	0.110

Test 14

Bays	ΔP_{max} (bar)	t_{max} (s)	ΔP_{min} (bar)	t_{min} (s)	I_{max} (bar-ms)	$t_{I,max}$ (s)
Stbd SWB1 (6-4)	1.979	0.152	−1.092	0.173	66.950	0.169
Port SWB1 (5-3)	1.963	0.152	−2.250	0.177	74.883	0.174
Stbd MS (4-2)	3.372	0.173	−1.104	0.191	49.907	0.187
Port MS (3-2)	4.501	0.177	−1.051	0.191	38.312	0.187
SWB2 (2-1)	2.820	0.185	−1.174	0.188	15.144	0.187
SWB3 (1-0)	4.665	0.190	0.033	0.059	222.062	0.249
Aft PR (5-6)	0.316	0.134	−0.263	0.175	0.474	0.116
Fwd PR (3-4)	1.316	0.177	−2.841	0.173	0.102	0.098

Test 15

Bays	ΔP_{max} (bar)	t_{max} (s)	ΔP_{min} (bar)	t_{min} (s)	I_{max} (bar-ms)	$t_{I,max}$ (s)
Stbd SWB1 (6-4)	3.116	0.196	−0.249	0.176	24.640	0.249
Port SWB1 (5-3)	3.803	0.192	−1.285	0.198	23.299	0.196
Stbd MS (4-2)	2.111	0.202	−0.384	0.224	19.654	0.212
Port MS (3-2)	3.807	0.198	−0.308	0.224	18.647	0.212
SWB2 (2-1)	0.859	0.204	−0.434	0.227	12.816	0.217
SWB3 (1-0)	4.041	0.227	0.045	0.023	189.532	0.249
Aft PR (5-6)	2.367	0.191	−1.006	0.197	1.679	0.194
Fwd PR (3-4)	2.962	0.198	−0.496	0.180	1.463	0.249

Test 16

Bays	ΔP_{max} (bar)	t_{max} (s)	ΔP_{min} (bar)	t_{min} (s)	I_{max} (bar-ms)	$t_{I,max}$ (s)
Stbd SWB1 (6-4)	1.224	0.200	−0.215	0.177	12.363	0.249
Port SWB1 (5-3)	1.814	0.197	−0.516	0.202	7.418	0.199
Stbd MS (4-2)	2.026	0.204	−0.181	0.229	14.319	0.217
Port MS (3-2)	3.475	0.200	−0.315	0.190	21.212	0.219
SWB2 (2-1)	1.794	0.209	−0.450	0.226	16.124	0.216
SWB3 (1-0)	4.075	0.222	−0.017	−0.019	177.653	0.249
Aft PR (5-6)	2.429	0.198	−0.384	0.186	5.112	0.202
Fwd PR (3-4)	2.879	0.199	−0.365	0.180	9.194	0.249

Test 17

Bays	ΔP_{max} (bar)	t_{max} (s)	ΔP_{min} (bar)	t_{min} (s)	I_{max} (bar-ms)	$t_{I,max}$ (s)
Stbd SWB1 (6-4)	0.651	0.185	−0.400	0.130	50.061	0.249
Port SWB1 (5-3)	0.590	0.126	−0.375	0.134	36.973	0.249
Stbd MS (4-2)	2.455	0.178	−0.166	0.149	199.506	0.249
Port MS (3-2)	2.512	0.176	−0.074	0.149	200.222	0.249
SWB2 (2-1)	3.074	0.151	−0.083	0.633	67.573	0.247
SWB3 (1-0)	1.120	0.139	−0.585	0.144	7.681	0.141
Aft PR (5-6)	1.733	0.144	−0.089	0.158	11.036	0.152
Fwd PR (3-4)	0.031	0.111	−0.323	0.122	0.942	0.113

Test 18

Bays	ΔP_{max} (bar)	t_{max} (s)	ΔP_{min} (bar)	t_{min} (s)	I_{max} (bar-ms)	$t_{I,max}$ (s)
Stbd SWB1 (6-4)	0.867	0.113	0.028	0.129	14.408	0.126
Port SWB1 (5-3)	0.447	0.099	−0.262	0.107	5.732	0.145
Stbd MS (4-2)	0.796	0.103	−0.112	0.114	11.199	0.127
Port MS (3-2)	0.991	0.122	−0.061	0.129	17.420	0.127
SWB2 (2-1)	0.655	0.106	−0.189	0.126	9.244	0.124
SWB3 (1-0)	1.154	0.109	−0.207	0.126	6.864	0.122
Aft PR (5-6)	1.698	0.113	−0.089	0.131	14.599	0.126
Fwd PR (3-4)	0.061	0.121	−0.307	0.105	0.740	0.087

Test 19

Bays	ΔP_{max} (bar)	t_{max} (s)	ΔP_{min} (bar)	t_{min} (s)	I_{max} (bar-ms)	$t_{I,max}$ (s)
Stbd SWB1 (6-4)	0.658	0.103	−0.484	0.107	7.206	0.148
Port SWB1 (5-3)	0.560	0.125	−0.601	0.111	6.467	0.140
Stbd MS (4-2)	1.421	0.108	−0.465	0.112	6.661	0.149
Port MS (3-2)	0.744	0.111	−0.260	0.112	9.461	0.134
SWB2 (2-1)	1.309	0.110	−0.743	0.114	8.324	0.135
SWB3 (1-0)	2.476	0.114	−0.426	0.117	12.744	0.128
Aft PR (5-6)	2.550	0.117	−0.128	0.129	15.012	0.127
Fwd PR (3-4)	0.373	0.130	−0.437	0.110	2.836	0.136

Test 20

Bays	ΔP_{max} (bar)	t_{max} (s)	ΔP_{min} (bar)	t_{min} (s)	I_{max} (bar-ms)	$t_{I,max}$ (s)
Stbd SWB1 (6-4)	0.801	0.127	−0.210	0.106	5.063	0.149
Port SWB1 (5-3)	0.753	0.124	−0.199	0.113	5.124	0.149
Stbd MS (4-2)	0.742	0.121	−0.154	0.141	12.939	0.139
Port MS (3-2)	1.002	0.114	−0.464	0.119	6.933	0.139
SWB2 (2-1)	Data not valid					
SWB3 (1-0)	Data not valid					
Aft PR (5-6)	2.190	0.123	−0.069	0.137	15.892	0.135
Fwd PR (3-4)	0.303	0.113	−0.782	0.119	0.611	0.115

Test 21

Bays	ΔP_{max} (bar)	t_{max} (s)	ΔP_{min} (bar)	t_{min} (s)	I_{max} (bar-ms)	$t_{I,max}$ (s)
Stbd SWB1 (6-4)	1.999	0.126	−1.009	0.123	3.063	0.200
Port SWB1 (5-3)	1.467	0.125	−0.887	0.121	0.266	0.188
Stbd MS (4-2)	1.136	0.128	−0.682	0.120	2.309	0.170
Port MS (3-2)	1.361	0.127	−0.292	0.120	3.036	0.167
SWB2 (2-1)	0.784	0.121	−0.440	0.111	0.001	0.011
SWB3 (1-0)	1.346	0.123	−0.334	0.158	25.653	0.140
Aft PR (5-6)	1.959	0.129	−0.094	0.143	18.198	0.138
Fwd PR (3-4)	1.208	0.124	−1.111	0.126	0.006	0.014

Test 22

Bays	ΔP_{max} (bar)	t_{max} (s)	ΔP_{min} (bar)	t_{min} (s)	I_{max} (bar-ms)	$t_{I,max}$ (s)
Stbd SWB1 (6-4)	0.839	0.194	−0.395	0.183	60.323	0.299
Port SWB1 (5-3)	0.601	0.219	−0.240	0.186	46.108	0.299
Stbd MS (4-2)	2.978	0.233	0.042	0.752	229.298	0.299
Port MS (3-2)	3.027	0.233	0.030	0.865	231.381	0.299
SWB2 (2-1)	2.073	0.209	−0.110	0.093	45.536	0.299
SWB3 (1-0)	0.774	0.193	−0.136	0.199	10.502	0.259
Aft PR (5-6)	1.014	0.201	−0.113	0.211	10.860	0.208
Fwd PR (3-4)	−0.015	0.165	−0.836	0.194	1.615	0.180

Test 23

Bays	ΔP_{max} (bar)	t_{max} (s)	ΔP_{min} (bar)	t_{min} (s)	I_{max} (bar-ms)	$t_{I,max}$ (s)
Stbd SWB1 (6-4)	0.877	0.265	−0.762	0.257	18.169	0.299
Port SWB1 (5-3)	0.699	0.271	−0.800	0.261	9.895	0.299
Stbd MS (4-2)	2.679	0.298	−0.048	0.230	72.397	0.299
Port MS (3-2)	2.739	0.298	−0.020	0.743	71.683	0.299
SWB2 (2-1)	1.517	0.279	−0.022	0.688	35.299	0.299
SWB3 (1-0)	0.848	0.266	−0.184	0.271	11.090	0.294
Aft PR (5-6)	1.171	0.273	−0.202	0.280	8.992	0.278
Fwd PR (3-4)	0.112	0.254	−1.450	0.264	2.127	0.256

Test 24

Bays	ΔP_{max} (bar)	t_{max} (s)	ΔP_{min} (bar)	t_{min} (s)	I_{max} (bar-ms)	$t_{I,max}$ (s)
Stbd SWB1 (6-4)	3.147	0.516	−2.184	0.421	109.550	0.599
Port SWB1 (5-3)	3.836	0.512	−2.090	0.425	108.480	0.599
Stbd MS (4-2)	1.458	0.420	−0.073	0.398	167.248	0.599
Port MS (3-2)	1.243	0.461	−0.020	0.995	162.867	0.599
SWB2 (2-1)	1.677	0.430	−0.030	0.441	38.754	0.463
SWB3 (1-0)	0.953	0.436	−0.353	0.440	9.846	0.438
Aft PR (5-6)	1.802	0.440	−0.158	0.450	12.480	0.447
Fwd PR (3-4)	0.825	0.511	−0.714	0.503	0.005	0.268

Test 25

Bays	ΔP_{max} (bar)	t_{max} (s)	ΔP_{min} (bar)	t_{min} (s)	I_{max} (bar-ms)	$t_{I,max}$ (s)
Stbd SWB1 (6-4)	1.246	0.145	−1.295	0.152	12.291	0.149
Port SWB1 (5-3)	0.541	0.147	−0.852	0.157	7.091	0.151
Stbd MS (4-2)	3.073	0.152	−0.660	0.181	28.767	0.166
Port MS (3-2)	1.607	0.157	−0.565	0.181	25.172	0.166
SWB2 (2-1)	1.982	0.160	−0.537	0.170	24.175	0.166
SWB3 (1-0)	4.431	0.170	0.006	0.032	147.377	0.199
Aft PR (5-6)	0.262	0.143	−0.567	0.154	0.270	0.126
Fwd PR (3-4)	0.709	0.144	−1.936	0.151	5.657	0.147

Test 26

Bays	ΔP_{max} (bar)	t_{max} (s)	ΔP_{min} (bar)	t_{min} (s)	I_{max} (bar-ms)	$t_{I,max}$ (s)
Stbd SWB1 (6-4)	0.081	1.101	−0.219	0.923	0.013	0.266
Port SWB1 (5-3)	0.008	0.642	−0.277	0.916	0.081	0.439
Stbd MS (4-2)	−0.003	1.125	−0.813	0.876	0.179	0.440
Port MS (3-2)	0.043	1.101	−0.756	0.872	0.025	0.258
SWB2 (2-1)	−0.002	1.217	−0.314	0.845	1.759	0.786
SWB3 (1-0)	1.332	0.907	0.006	0.348	407.301	1.199
Aft PR (5-6)	0.013	0.591	−0.042	1.122	0.062	0.438
Fwd PR (3-4)	0.083	1.101	0.022	0.640	5.271	1.199

Test 27

Bays	ΔP_{max} (bar)	t_{max} (s)	ΔP_{min} (bar)	t_{min} (s)	I_{max} (bar-ms)	$t_{I,max}$ (s)
Stbd SWB1 (6-4)	0.799	0.205	−1.837	0.141	17.959	0.199
Port SWB1 (5-3)	0.653	0.205	−0.953	0.143	11.168	0.199
Stbd MS (4-2)	2.830	0.179	−0.065	0.122	118.717	0.199
Port MS (3-2)	2.866	0.177	−0.022	0.113	114.954	0.199
SWB2 (2-1)	1.974	0.161	−0.046	0.666	45.811	0.196
SWB3 (1-0)	1.048	0.146	−0.232	0.150	7.459	0.148
Aft PR (5-6)	1.319	0.150	−0.118	0.162	11.791	0.160
Fwd PR (3-4)	0.093	0.130	−1.174	0.144	1.075	0.138

Test 28

Bays	ΔP_{max} (bar)	t_{max} (s)	ΔP_{min} (bar)	t_{min} (s)	I_{max} (bar-ms)	$t_{I,max}$ (s)
Stbd SWB1 (6-4)	1.669	0.107	−0.826	0.115	43.154	0.179
Port SWB1 (5-3)	1.039	0.109	−0.369	0.119	35.779	0.179
Stbd MS (4-2)	2.637	0.114	−0.048	0.104	132.365	0.179
Port MS (3-2)	2.530	0.147	−0.020	0.745	129.685	0.179
SWB2 (2-1)	2.142	0.129	−0.027	0.551	41.462	0.175
SWB3 (1-0)	0.935	0.117	−0.171	0.121	6.489	0.120
Aft PR (5-6)	1.152	0.121	−0.039	0.131	9.281	0.129
Fwd PR (3-4)	0.028	0.088	−0.362	0.098	0.668	0.090

Test 29

Bays	ΔP_{max} (bar)	t_{max} (s)	ΔP_{min} (bar)	t_{min} (s)	I_{max} (bar-ms)	$t_{I,max}$ (s)
Stbd SWB1 (6-4)	0.567	0.158	-1.347	0.167	4.611	0.162
Port SWB1 (5-3)	0.572	0.168	-1.700	0.164	0.015	0.021
Stbd MS (4-2)	3.422	0.188	-1.506	0.164	85.133	0.199
Port MS (3-2)	3.458	0.188	-0.735	0.164	89.178	0.199
SWB2 (2-1)	2.626	0.164	-0.532	0.151	16.134	0.191
SWB3 (1-0)	0.535	0.151	-0.208	0.164	17.671	0.163
Aft PR (5-6)	1.555	0.168	-0.118	0.175	14.485	0.173
Fwd PR (3-4)	1.653	0.167	-0.811	0.160	0.015	0.011

Appendix C

Design Drawings

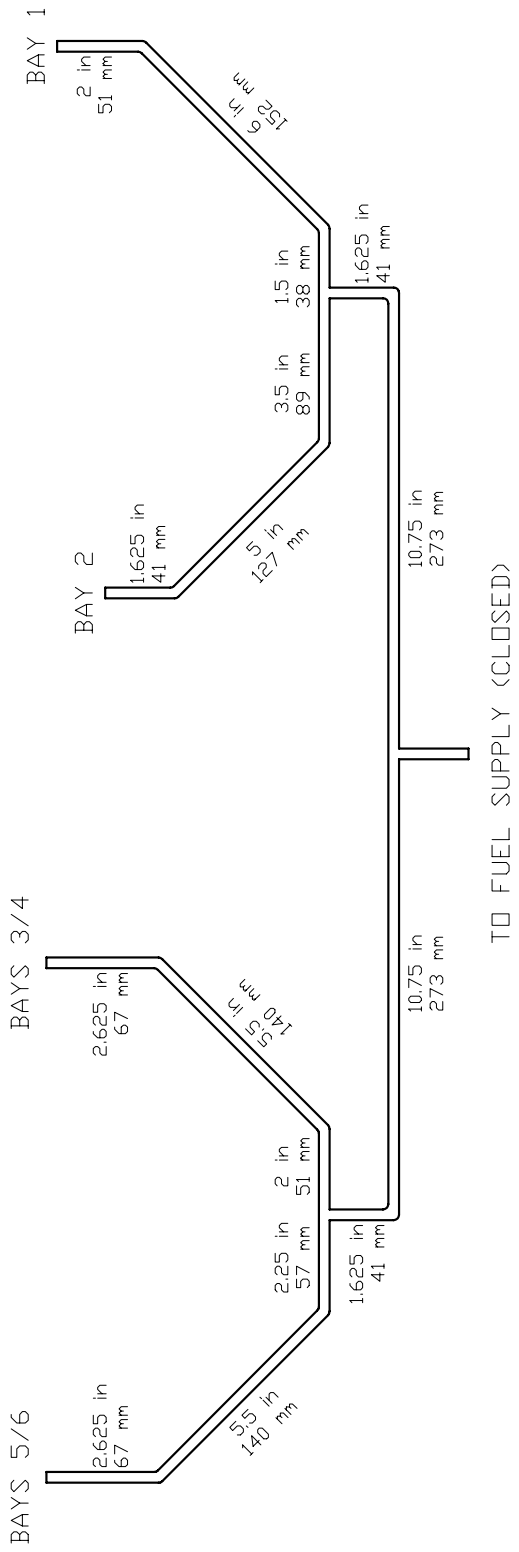

JET FUEL MANIFOLD AS-BUILT DIMENSIONS
TUBING ID: 0.180 IN / 4.6 MM

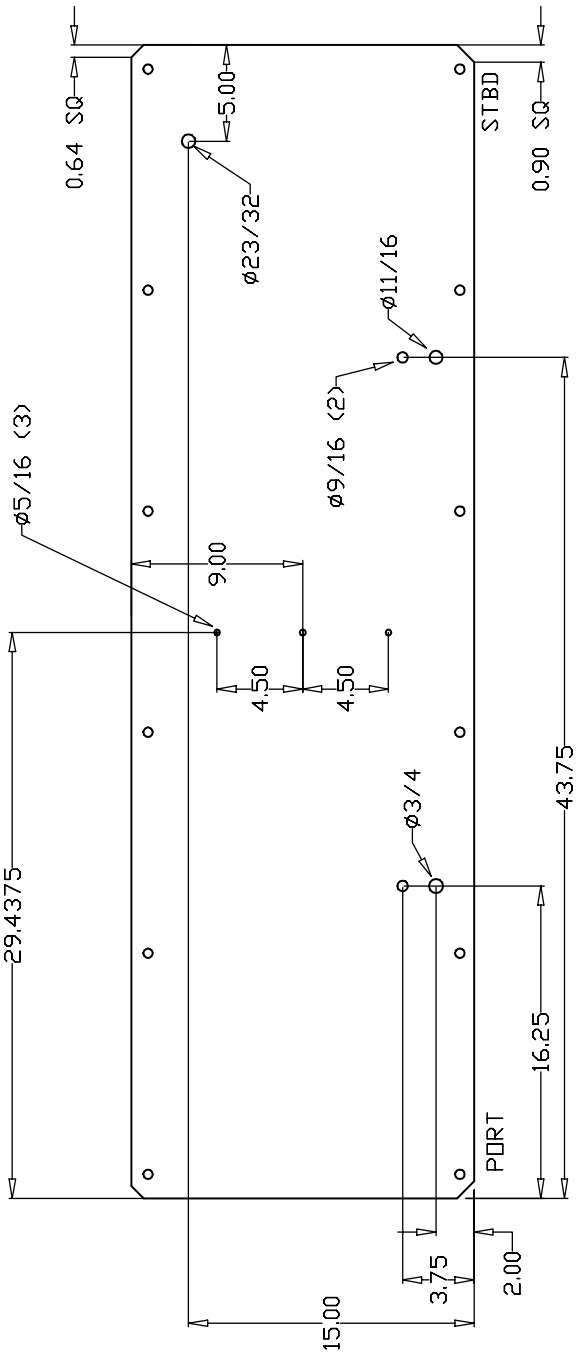

SPANWISE BEAM 1 DETAILS

J. CHRIS KROK
EXPLOSION DYNAMICS LAB
29 AUGUST 1997

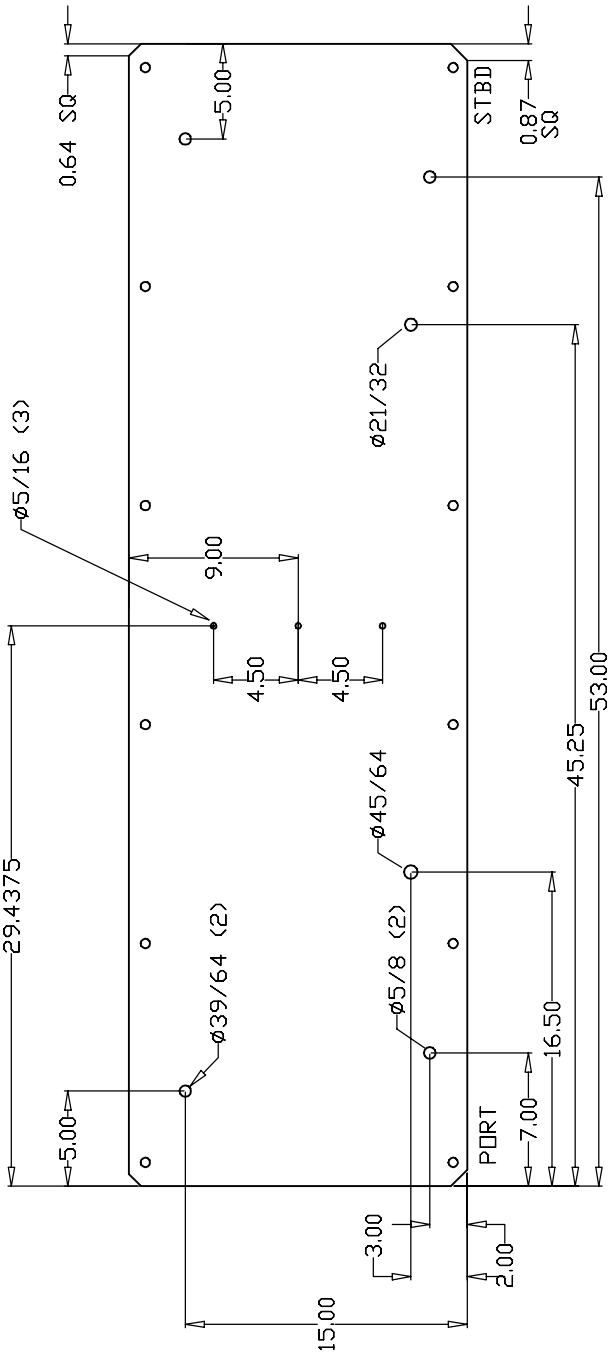
0.64 SQ
5.00
STBD
0.87 SQ
ø21/32
ø5/16 (3)
9.00
4.50
4.50
53.00
45.25
ø45/64
29.4375
ø39/64 (2)
ø5/8 (2)
16.50
5.00
PORT
7.00
3.00
2.00
15.00
MIDSPAR: DETAILS
J. CHRIS KROK
EXPLOSION DYNAMICS LAB
29 SEPTEMBER 1997

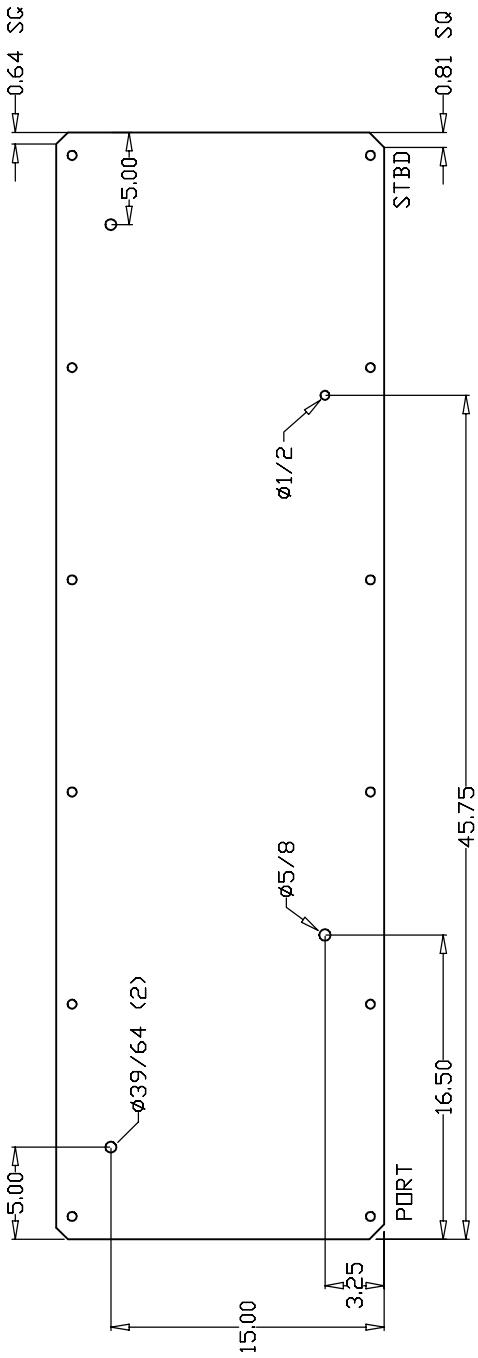

SPANWISE BEAM 2: DETAILS

J. CHRIS KROK
EXPLOSION DYNAMICS LAB
29 SEPTEMBER 1997

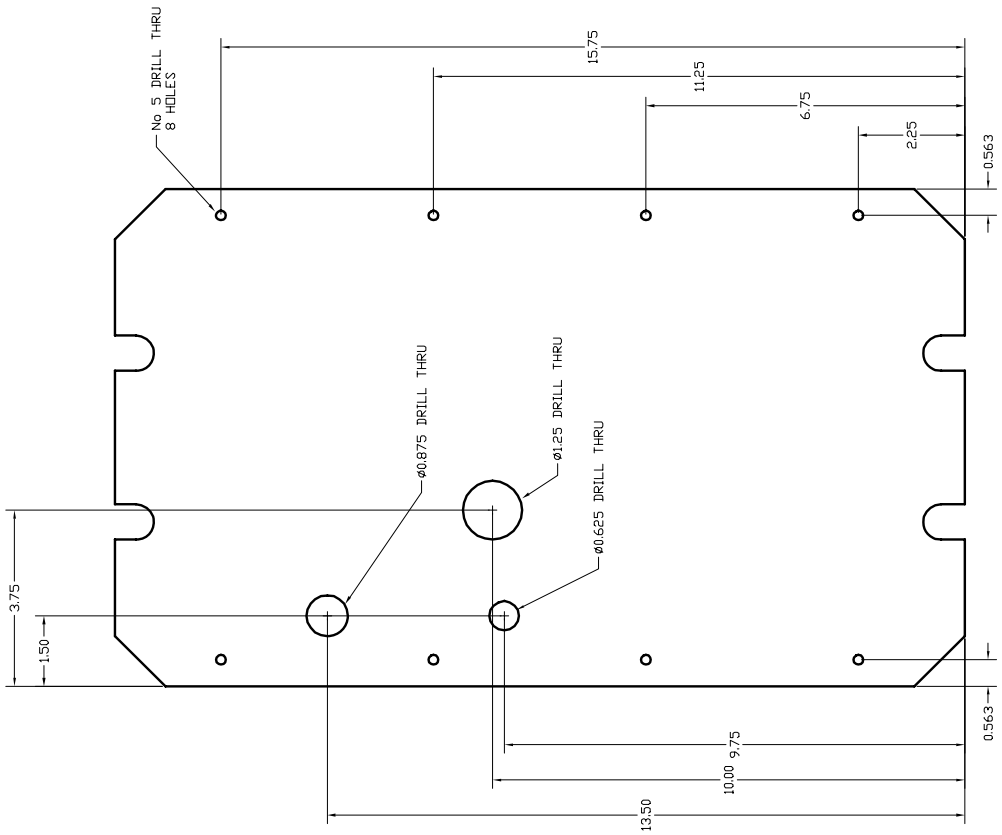

REAR PARTIAL RIB HOLE DIMENSIONS

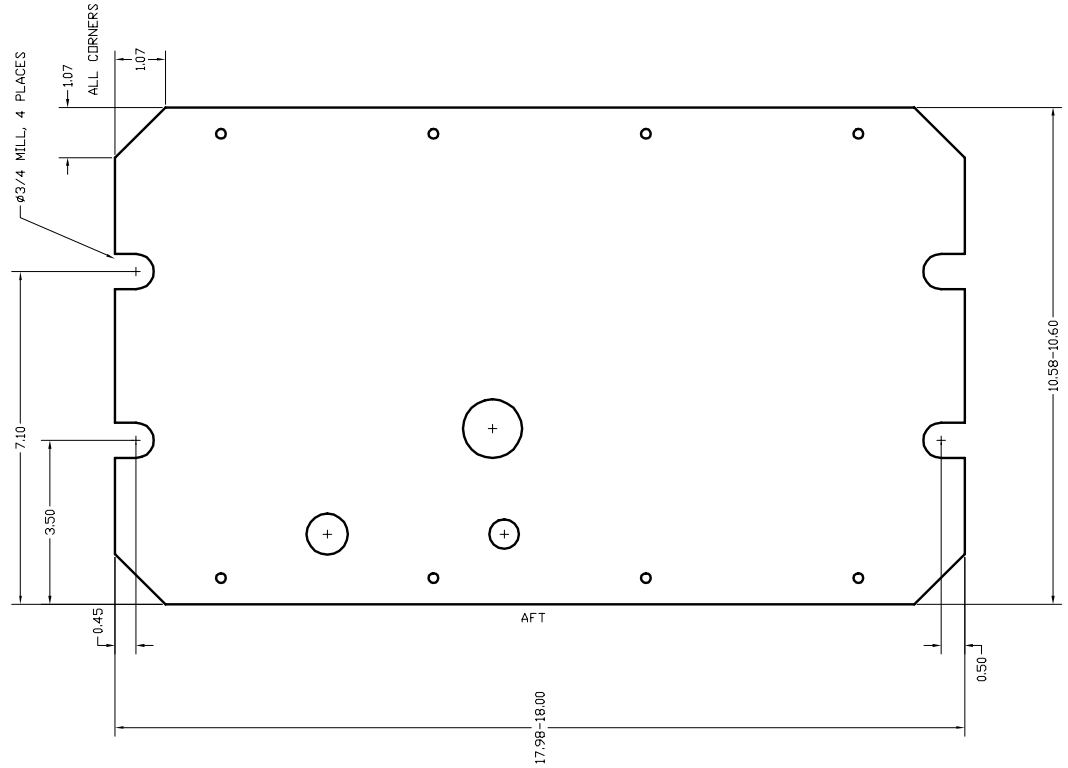

REAR PARTIAL RIB

EXPLOSION DYNAMICS LABORATORY
J. CHRIS KROK
25 SEPTEMBER 1997
FILE: aft-rib.dwg

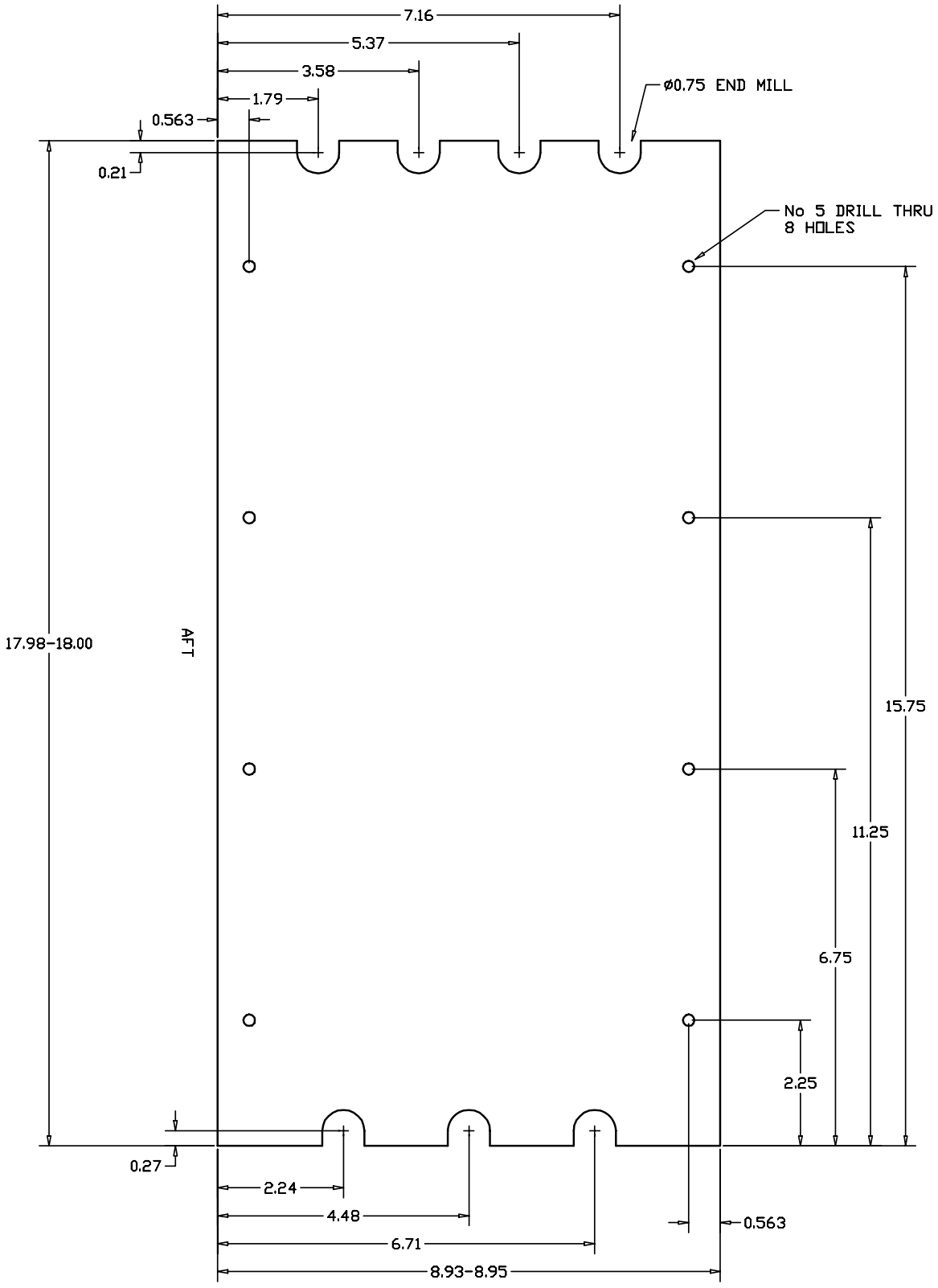

FORWARD PARTIAL RIB

EXPLOSION DYNAMICS LABORATORY
J. CHRIS KROK
25 SEPTEMBER 1997
FILE: forerib.dwg

SIDE VIEW

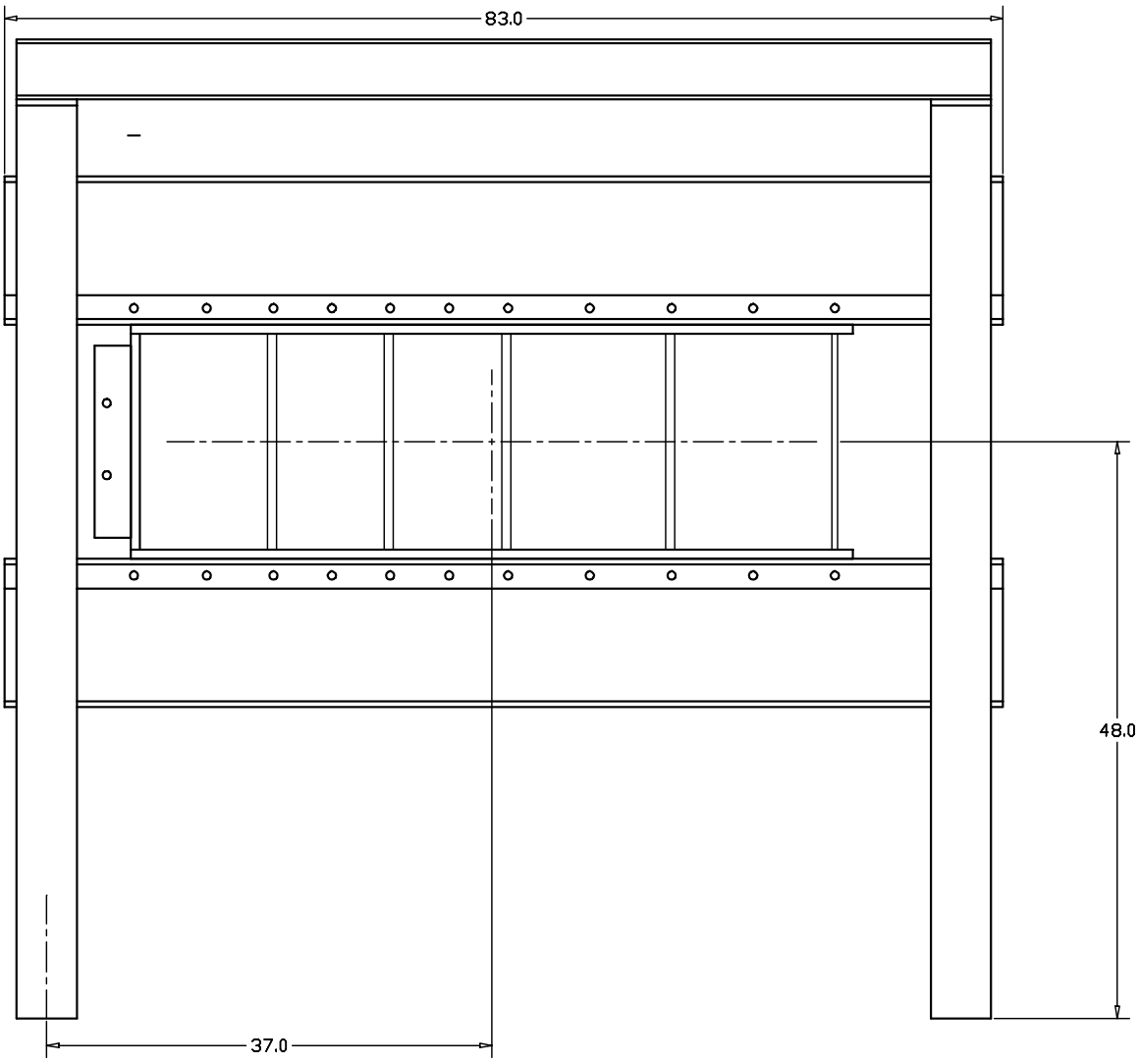

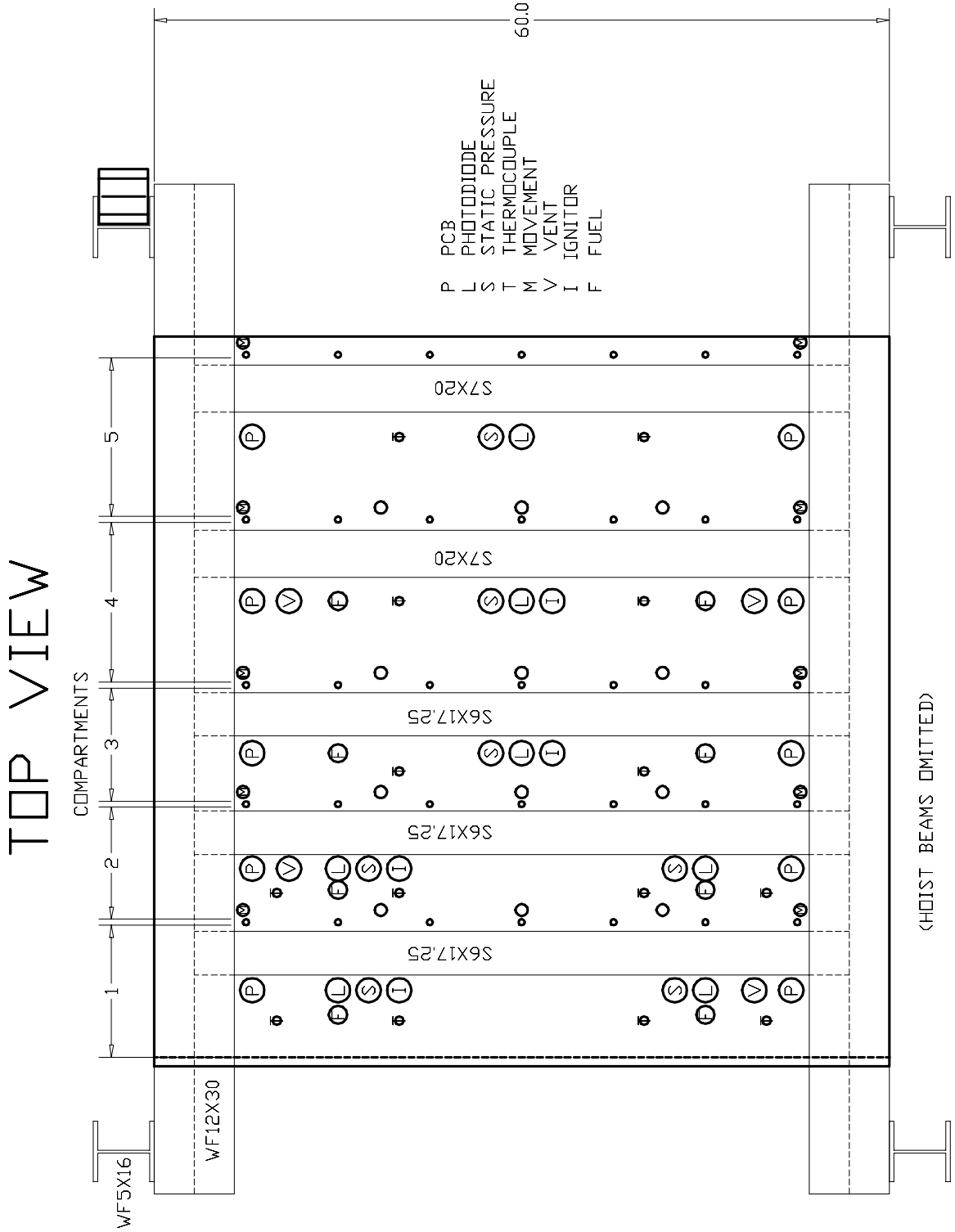
TOP VIEW
60.0
P PCB
L PHOTODIODE
S STATIC PRESSURE
T THERMOCOUPLE
M MOVEMENT
V VENT
I IGNITOR
F FUEL
S7X20
S7X20
S6X17.25
S6X17.25
S6X17.25
COMPARTMENTS
1
2
3
4
5
WF12X30
WF5X16
(HOIST BEAMS OMITTED)

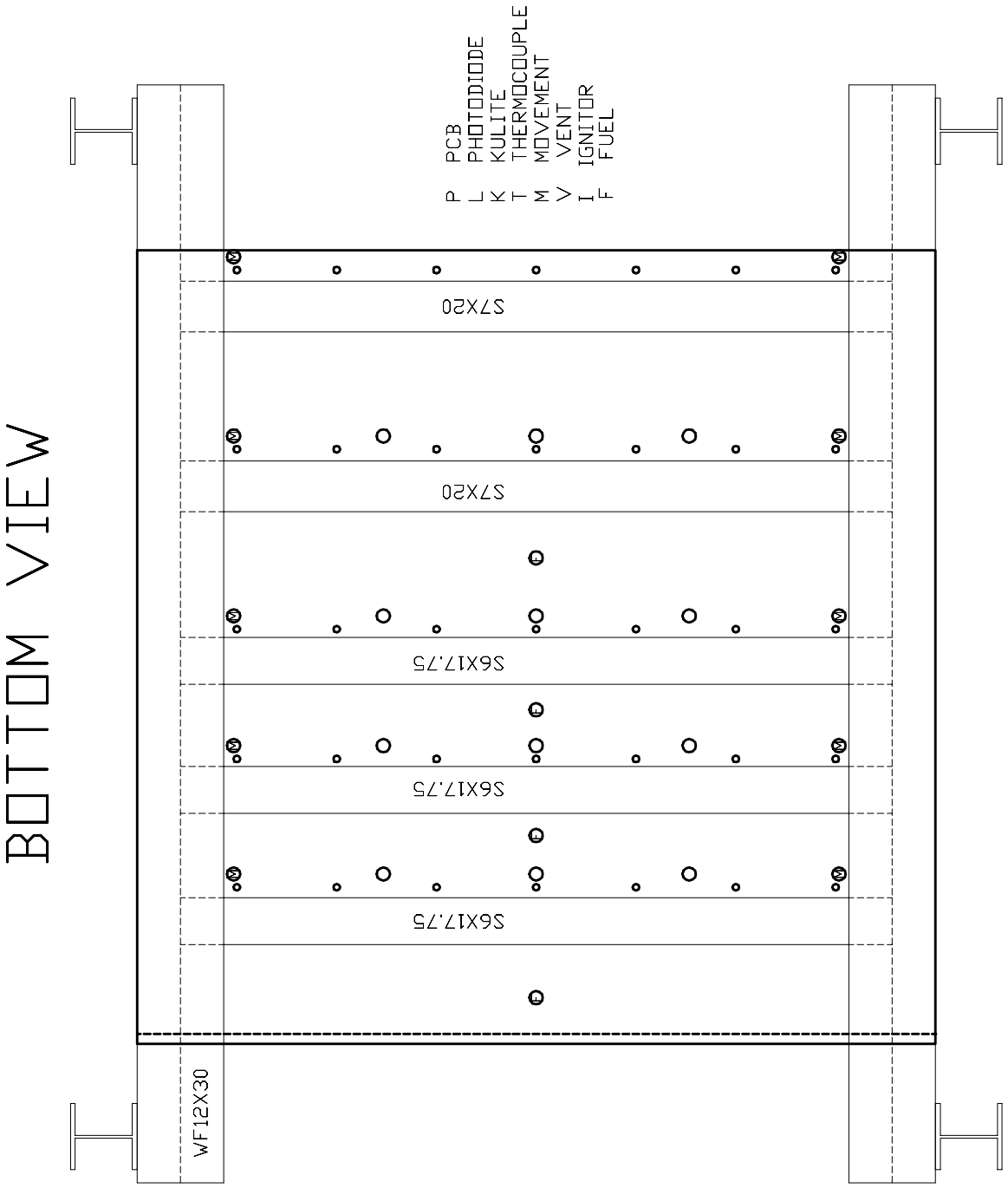
BOTTOM VIEW
P PCB
L PHOTODIODE
K KULITE
T THERMOCOUPLE
M MOVEMENT
V VENT
I IGNITOR
F FUEL
S7X20
S7X20
S6X17.75
S6X17.75
S6X17.75
WF12X30

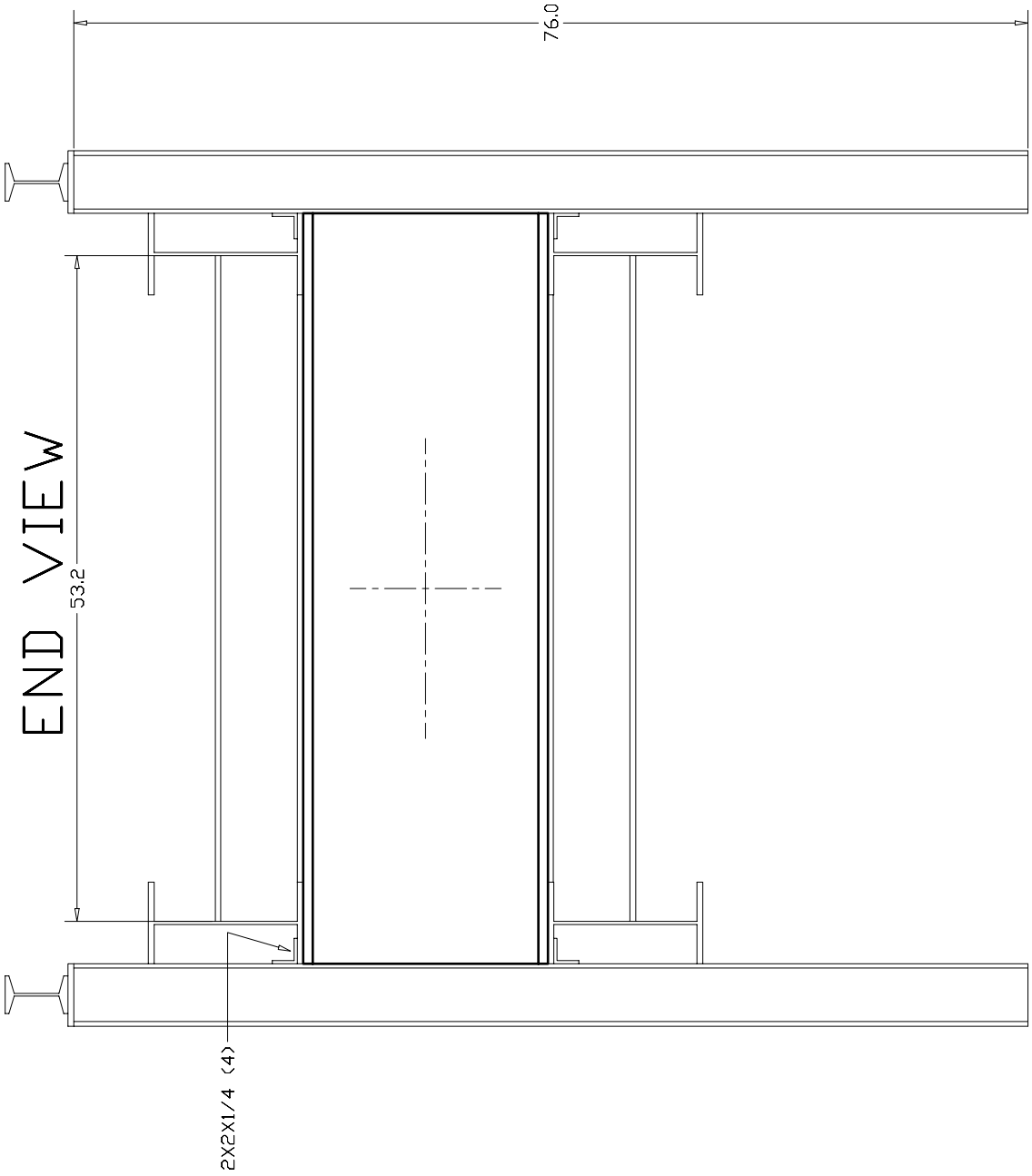
76.0
END VIEW
53.2
2X2X1/4 (4)

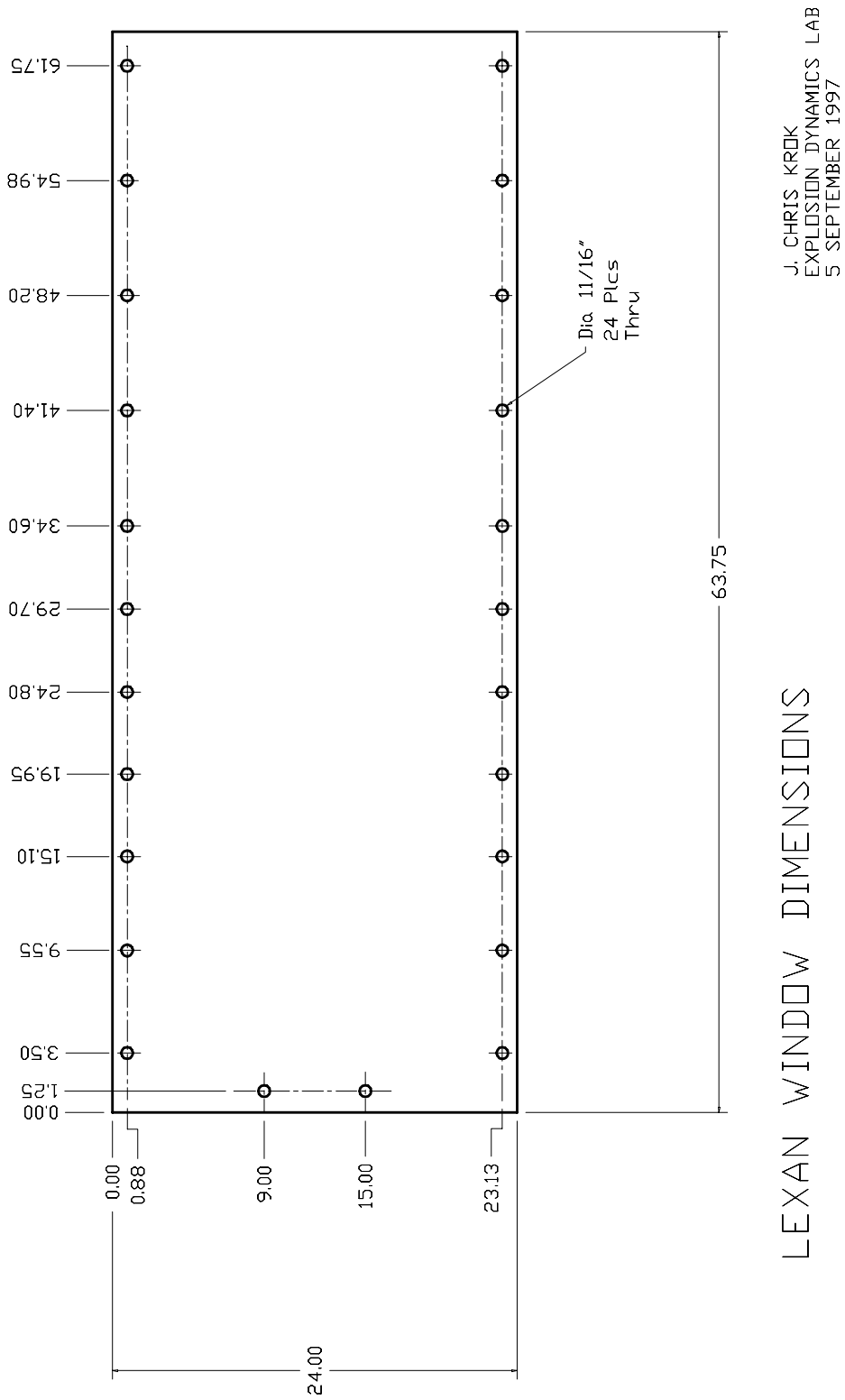
LEXAN WINDOW DIMENSIONS
J. CHRIS KROK
EXPLOSION DYNAMICS LAB
5 SEPTEMBER 1997
Dia. 11/16"
24 Plcs
Thru
63.75
24.00
0.00
0.88
9.00
15.00
23.13
0.00
1.25
3.50
9.55
15.10
19.95
24.80
29.70
34.60
41.40
48.20
54.98
61.75

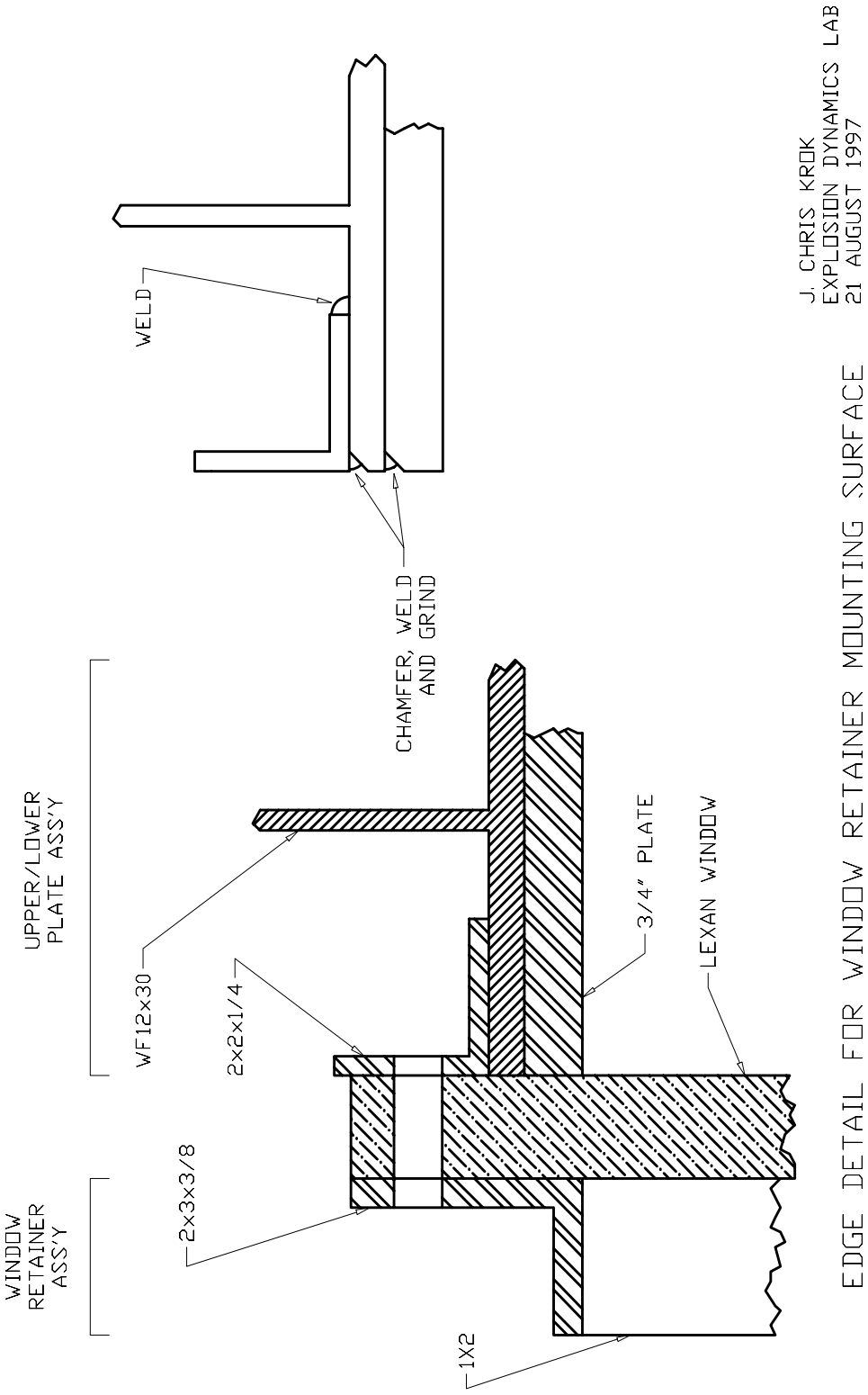
WELD
CHAMFER, WELD AND GRIND
UPPER/LOWER PLATE ASS'Y
WF12×30
2×2×1/4
3/4" PLATE
LEXAN WINDOW
WINDOW RETAINER ASS'Y
2×3×3/8
1X2
EDGE DETAIL FOR WINDOW RETAINER MOUNTING SURFACE
J. CHRIS KROK
EXPLOSION DYNAMICS LAB
21 AUGUST 1997

MANUFACTURING PANEL RETAINER
MAT'L" 0.25 STEEL PLATE

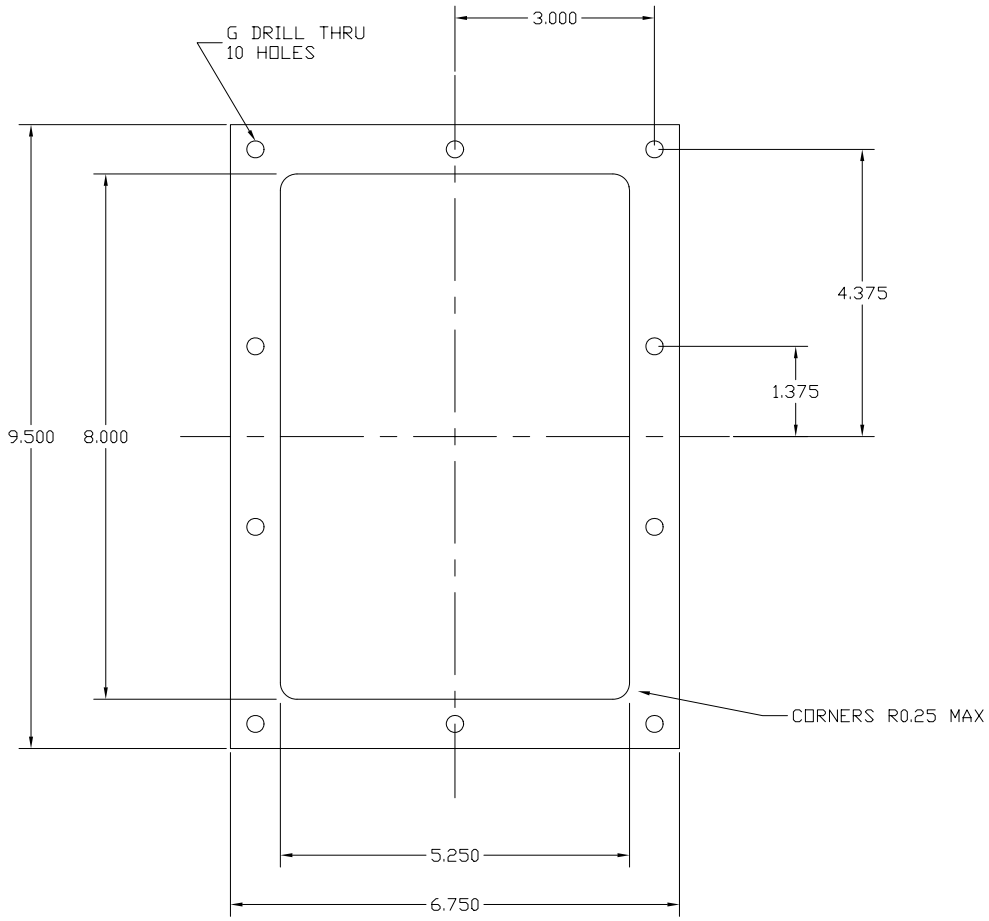

PANELS: SAME DIMENSIONS AS RETAINER,
NO CENTER HOLE
MAT'L:
1 PC 0.25 STEEL
10 PCS AL SHEET

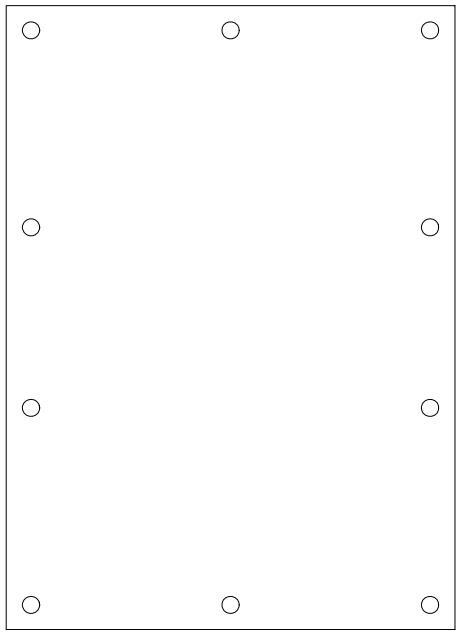

J. CHRIS KROK
EXPLOSION DYNAMICS LAB
9 NOVEMBER 1997

MANUFACTURING PANELS AND RETAINER

ALL DIMENSIONS INCHES ±0.005

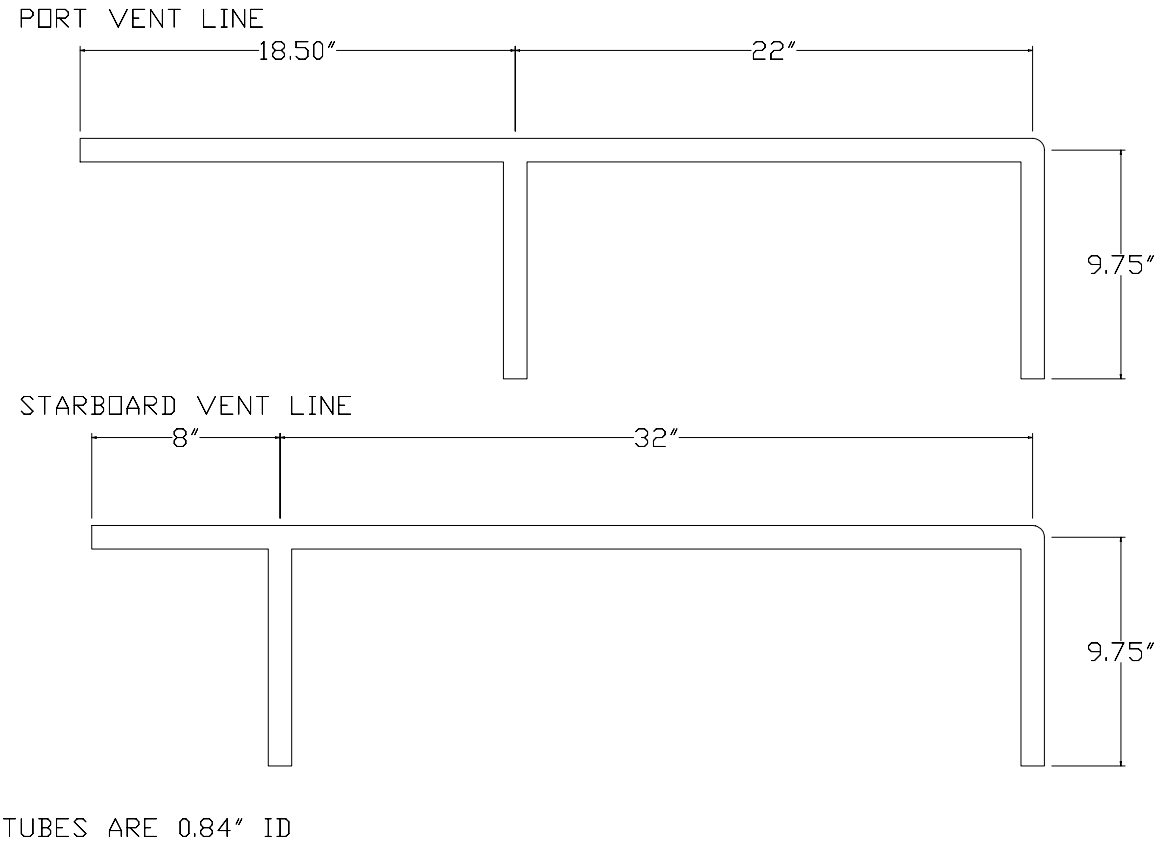

TUBES ARE 0.84″ ID

Appendix D

Raw Data Plots

D.1 Weather

TEST #	DATE	TIME	TEMP. (F)	BARO. ("HG)	RH %	WIND (MPH)	WIND DIR.	
1	23-Oct	17:05	59	29.73	21	0		0
2	29-Oct	17:34	46	29.87	44	4	S	
3	31-Oct	10:15	51	29.82	50	10	S	
4	1-Nov	12:16	48	30.1	38	19	SW	
5	3-Nov	12:24	62	30.08	24	7	SSW	
6	4-Nov	11:17	60	30.04	26	11	NNW	
7	4-Nov	14:52	53	30.07	36	7	NNW	
8	5-Nov	13:26	55	30.22	38	4	ESE	
9	6-Nov	11:29	61	30.18	31	7	ENE	
10	6-Nov	14:42	64	30.16	27	11	E	
11	7-Nov	12:17	67	30.02	23	7	NW	
12	7-Nov	15:43	68	30	24	2	NNE	
13	8-Nov	15:09	41	30.05	71	6	NNE	
14	13-Nov	13:53	34	29.65	63	0		0
15	15-Nov	12:44	28	30.1	44	3	S	
16	15-Nov	15:40	39	30.11	26	2	WSW	
17	17-Nov	13:49	46	30.05	34	1	NNE	
18	19-Nov	15:55	51	29.88	42	5	ESE	
19	21-Nov	13:45	40	29.86	45	4	NNW	
20	24-Nov	13:14	60	30.09	22	0		0
21	25-Nov	15:17	67	29.98	24	11	W	
22	3-Dec	13:38	29	29.97	61	7	SSW	
23	5-Dec	10:48	25	30.1	65	3	W	
24	5-Dec	16:01	23	30.07	64	5	S	
25	6-Dec	11:17	30	29.92	54	4	ESE	
26	6-Dec	16:11	33	29.85	56	2	E	
27	7-Dec	11:24	32	29.68	58	7	WSW	
28	8-Dec	11:01	38	29.59	54	6	SSW	
29	8-Dec	15:47	41	29.53	54	3	E	
30	17-Dec	13:37	45	29.94	48	8	SSE	

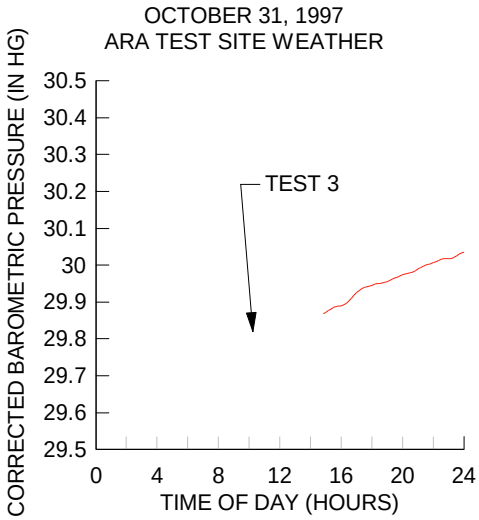
OCTOBER 31, 1997
ARA TEST SITE WEATHER
CORRECTED BAROMETRIC PRESSURE (IN HG)
30.5
30.4
30.3
30.2
30.1
30
29.9
29.8
29.7
29.6
29.5
TEST 3
0
4
8
12
16
20
24
TIME OF DAY (HOURS)

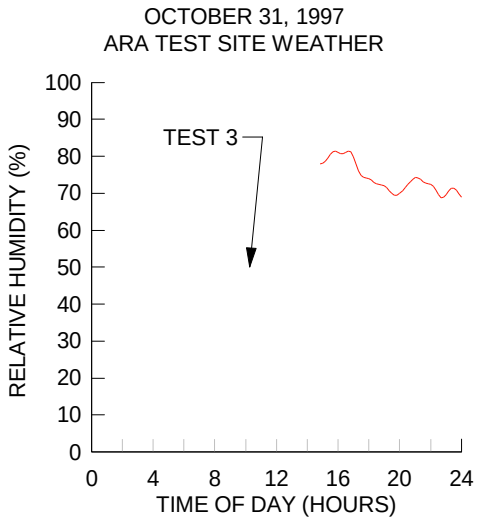
OCTOBER 31, 1997
ARA TEST SITE WEATHER
RELATIVE HUMIDITY (%)
100
90
80
70
60
50
40
30
20
10
0
TEST 3
0
4
8
12
16
20
24
TIME OF DAY (HOURS)

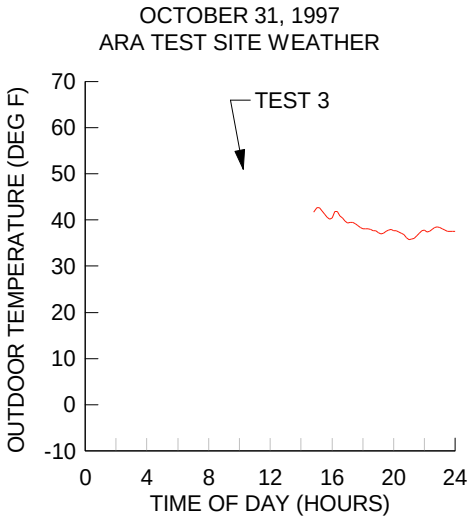
OCTOBER 31, 1997
ARA TEST SITE WEATHER
OUTDOOR TEMPERATURE (DEG F)
70
60
50
40
30
20
10
0
-10
TEST 3
0
4
8
12
16
20
24
TIME OF DAY (HOURS)

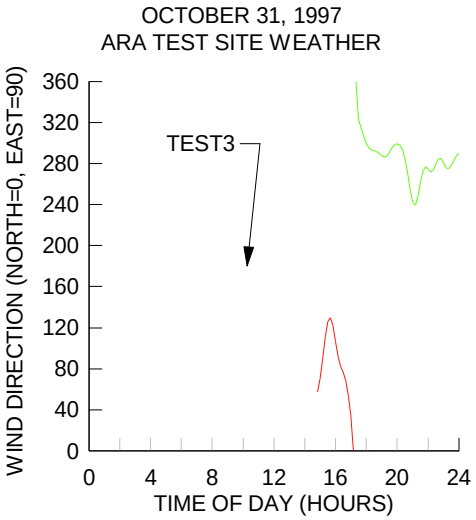
OCTOBER 31, 1997
ARA TEST SITE WEATHER
WIND DIRECTION (NORTH=0, EAST=90)
360
320
280
240
200
160
120
80
40
0
TEST3
0
4
8
12
16
20
24
TIME OF DAY (HOURS)

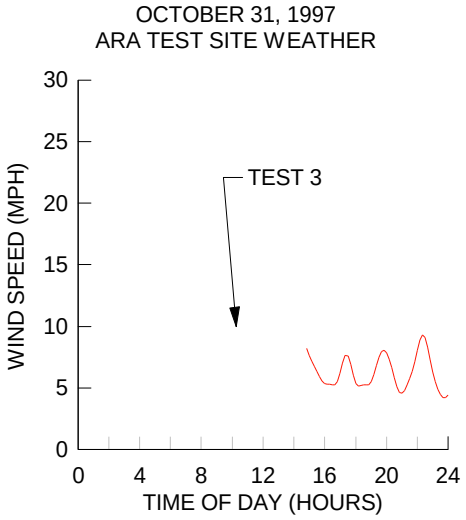
OCTOBER 31, 1997
ARA TEST SITE WEATHER
WIND SPEED (MPH)
30
25
20
15
10
5
0
TEST 3
0
4
8
12
16
20
24
TIME OF DAY (HOURS)

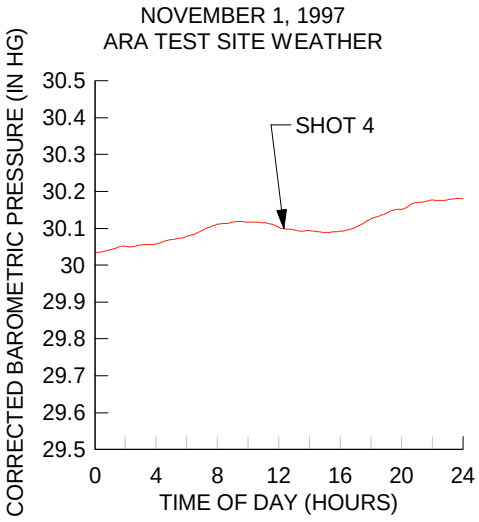
NOVEMBER 1, 1997
ARA TEST SITE WEATHER
CORRECTED BAROMETRIC PRESSURE (IN HG)
30.5
30.4
30.3
30.2
30.1
30
29.9
29.8
29.7
29.6
29.5
SHOT 4
0
4
8
12
16
20
24
TIME OF DAY (HOURS)

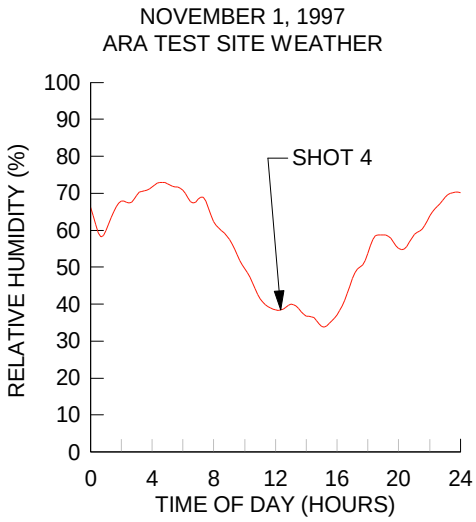
NOVEMBER 1, 1997
ARA TEST SITE WEATHER
RELATIVE HUMIDITY (%)
100
90
80
70
60
50
40
30
20
10
0
SHOT 4
0
4
8
12
16
20
24
TIME OF DAY (HOURS)

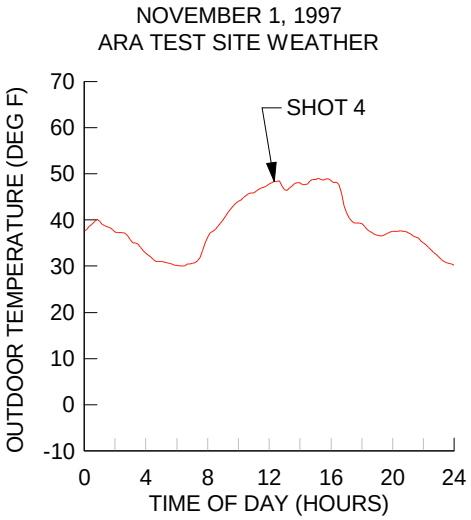
NOVEMBER 1, 1997
ARA TEST SITE WEATHER
OUTDOOR TEMPERATURE (DEG F)
70
60
50
40
30
20
10
0
-10
SHOT 4
0
4
8
12
16
20
24
TIME OF DAY (HOURS)

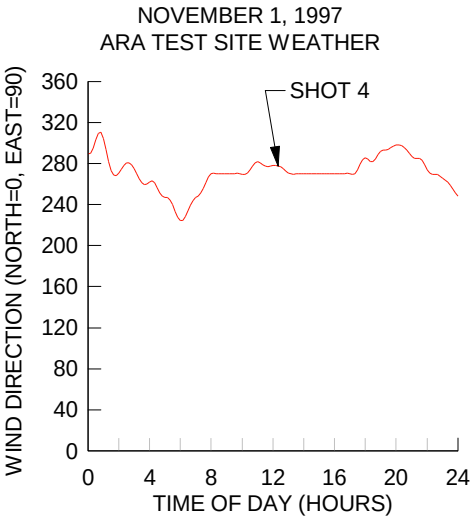
NOVEMBER 1, 1997
ARA TEST SITE WEATHER
WIND DIRECTION (NORTH=0, EAST=90)
360
320
280
240
200
160
120
80
40
0
SHOT 4
0
4
8
12
16
20
24
TIME OF DAY (HOURS)

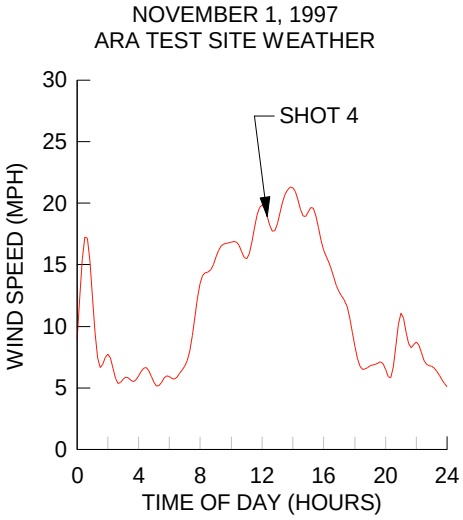
NOVEMBER 1, 1997
ARA TEST SITE WEATHER
WIND SPEED (MPH)
30
25
20
15
10
5
0
SHOT 4
0
4
8
12
16
20
24
TIME OF DAY (HOURS)

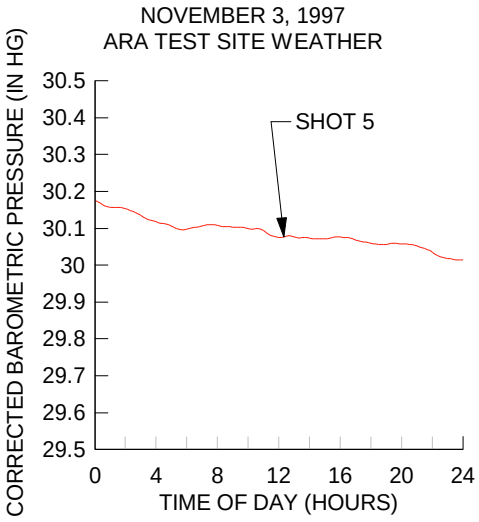
NOVEMBER 3, 1997
ARA TEST SITE WEATHER
CORRECTED BAROMETRIC PRESSURE (IN HG)
30.5
30.4
30.3
30.2
30.1
30
29.9
29.8
29.7
29.6
29.5
SHOT 5
0
4
8
12
16
20
24
TIME OF DAY (HOURS)

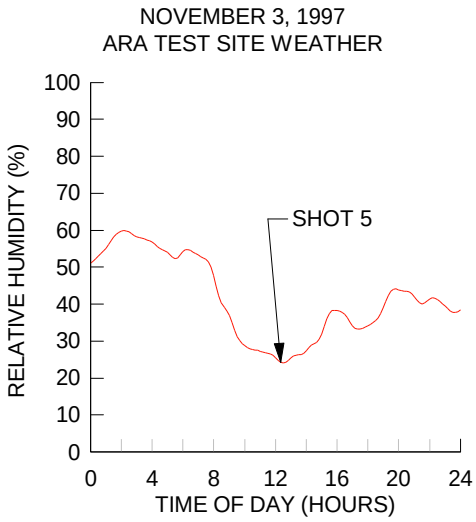
NOVEMBER 3, 1997
ARA TEST SITE WEATHER
RELATIVE HUMIDITY (%)
100
90
80
70
60
50
40
30
20
10
0
SHOT 5
0
4
8
12
16
20
24
TIME OF DAY (HOURS)

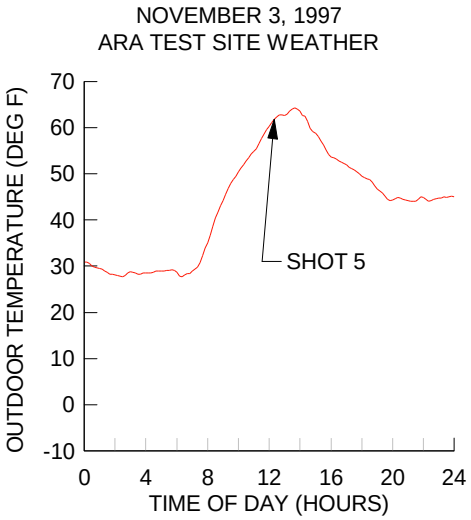
NOVEMBER 3, 1997
ARA TEST SITE WEATHER
OUTDOOR TEMPERATURE (DEG F)
70
60
50
40
30
20
10
0
-10
SHOT 5
0
4
8
12
16
20
24
TIME OF DAY (HOURS)

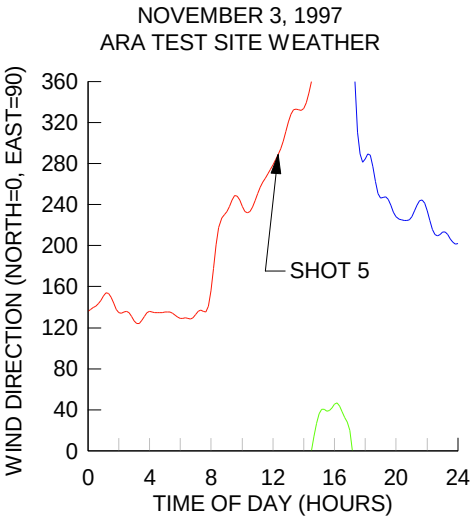
NOVEMBER 3, 1997
ARA TEST SITE WEATHER
WIND DIRECTION (NORTH=0, EAST=90)
360
320
280
240
200
160
120
80
40
0
SHOT 5
0
4
8
12
16
20
24
TIME OF DAY (HOURS)

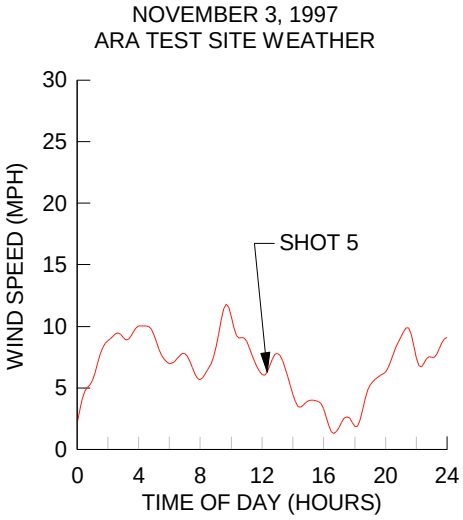
NOVEMBER 3, 1997
ARA TEST SITE WEATHER
WIND SPEED (MPH)
30
25
20
15
10
5
0
SHOT 5
0
4
8
12
16
20
24
TIME OF DAY (HOURS)

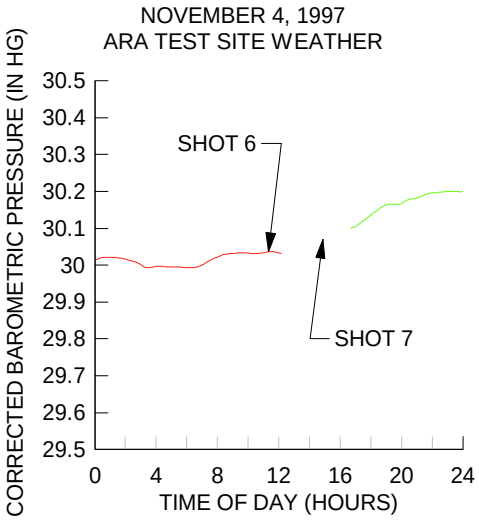
NOVEMBER 4, 1997
ARA TEST SITE WEATHER
CORRECTED BAROMETRIC PRESSURE (IN HG)
30.5
30.4
30.3
30.2
30.1
30
29.9
29.8
29.7
29.6
29.5
SHOT 6
SHOT 7
0
4
8
12
16
20
24
TIME OF DAY (HOURS)

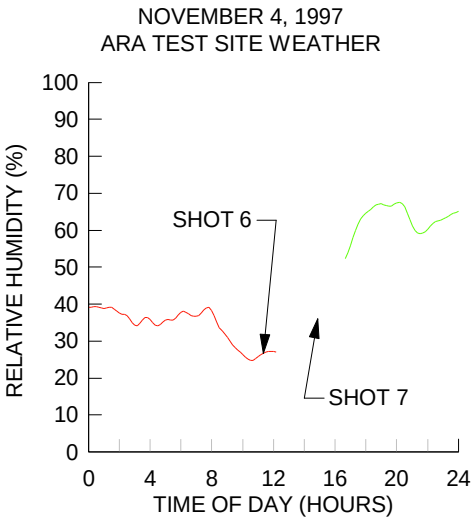
NOVEMBER 4, 1997
ARA TEST SITE WEATHER
RELATIVE HUMIDITY (%)
100
90
80
70
60
50
40
30
20
10
0
SHOT 6
SHOT 7
0
4
8
12
16
20
24
TIME OF DAY (HOURS)

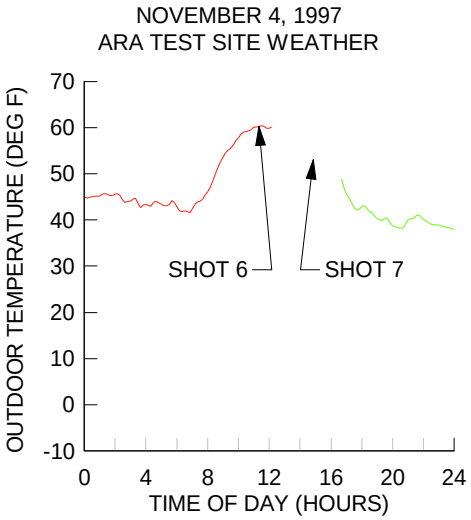
NOVEMBER 4, 1997
ARA TEST SITE WEATHER
OUTDOOR TEMPERATURE (DEG F)
70
60
50
40
30
20
10
0
-10
SHOT 6
SHOT 7
0
4
8
12
16
20
24
TIME OF DAY (HOURS)

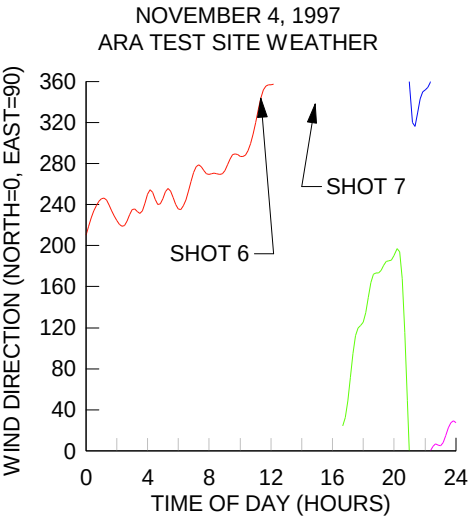
NOVEMBER 4, 1997
ARA TEST SITE WEATHER
WIND DIRECTION (NORTH=0, EAST=90)
360
320
280
240
200
160
120
80
40
0
SHOT 7
SHOT 6
0
4
8
12
16
20
24
TIME OF DAY (HOURS)

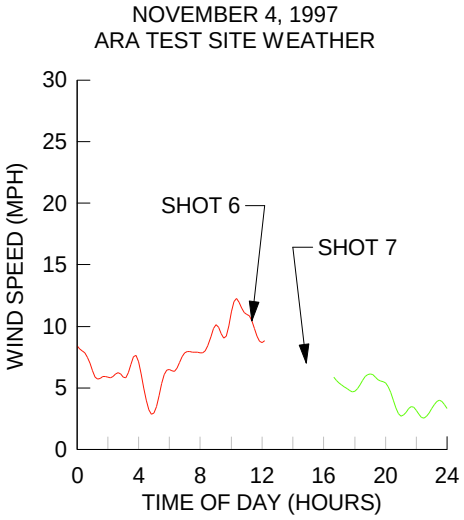
NOVEMBER 4, 1997
ARA TEST SITE WEATHER
WIND SPEED (MPH)
30
25
20
15
10
5
0
SHOT 6
SHOT 7
0
4
8
12
16
20
24
TIME OF DAY (HOURS)

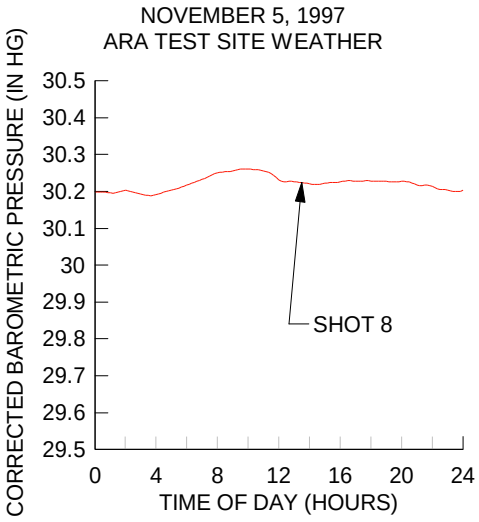
NOVEMBER 5, 1997
ARA TEST SITE WEATHER
CORRECTED BAROMETRIC PRESSURE (IN HG)
30.5
30.4
30.3
30.2
30.1
30
29.9
29.8
29.7
29.6
29.5
SHOT 8
0
4
8
12
16
20
24
TIME OF DAY (HOURS)

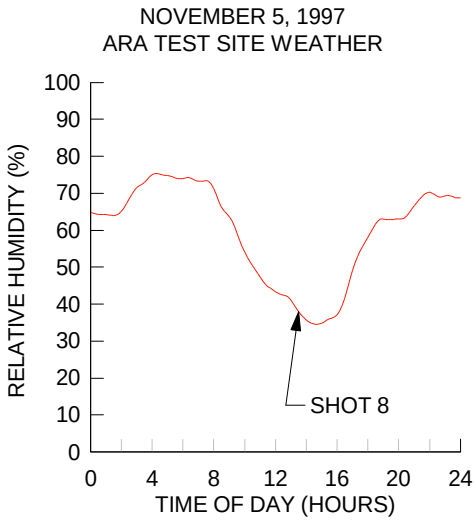
NOVEMBER 5, 1997
ARA TEST SITE WEATHER
RELATIVE HUMIDITY (%)
100
90
80
70
60
50
40
30
20
10
0
SHOT 8
0
4
8
12
16
20
24
TIME OF DAY (HOURS)

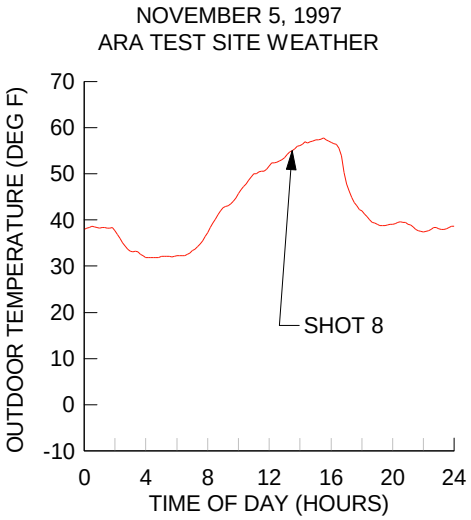
NOVEMBER 5, 1997
ARA TEST SITE WEATHER
OUTDOOR TEMPERATURE (DEG F)
70
60
50
40
30
20
10
0
-10
SHOT 8
0
4
8
12
16
20
24
TIME OF DAY (HOURS)

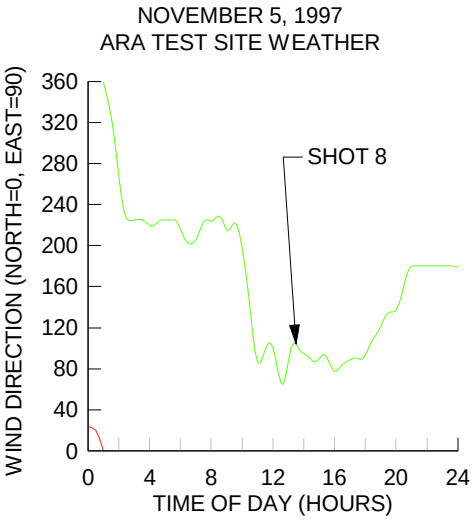
NOVEMBER 5, 1997
ARA TEST SITE WEATHER
WIND DIRECTION (NORTH=0, EAST=90)
360
320
280
240
200
160
120
80
40
0
SHOT 8
0
4
8
12
16
20
24
TIME OF DAY (HOURS)

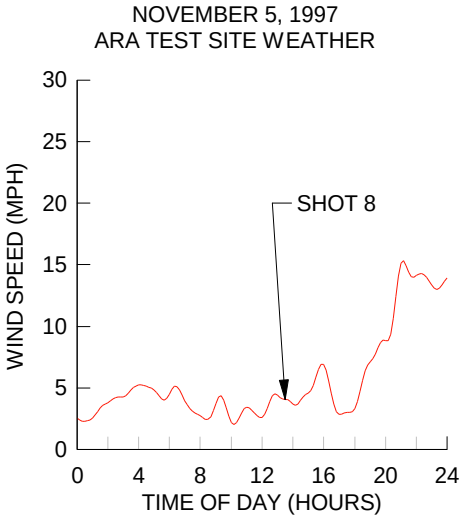
NOVEMBER 5, 1997
ARA TEST SITE WEATHER
WIND SPEED (MPH)
30
25
20
15
10
5
0
SHOT 8
0
4
8
12
16
20
24
TIME OF DAY (HOURS)

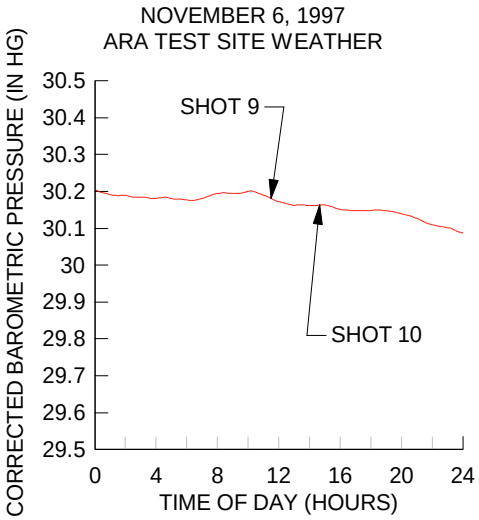
NOVEMBER 6, 1997
ARA TEST SITE WEATHER
CORRECTED BAROMETRIC PRESSURE (IN HG)
30.5
30.4
30.3
30.2
30.1
30
29.9
29.8
29.7
29.6
29.5
SHOT 9
SHOT 10
0
4
8
12
16
20
24
TIME OF DAY (HOURS)

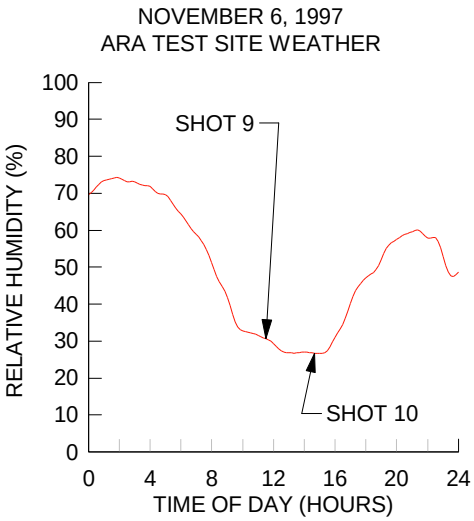
NOVEMBER 6, 1997
ARA TEST SITE WEATHER
RELATIVE HUMIDITY (%)
100
90
80
70
60
50
40
30
20
10
0
SHOT 9
SHOT 10
0
4
8
12
16
20
24
TIME OF DAY (HOURS)

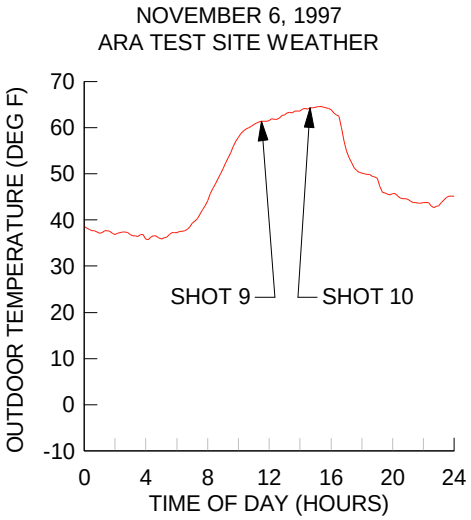
NOVEMBER 6, 1997
ARA TEST SITE WEATHER
OUTDOOR TEMPERATURE (DEG F)
70
60
50
40
30
20
10
0
-10
SHOT 9
SHOT 10
0
4
8
12
16
20
24
TIME OF DAY (HOURS)

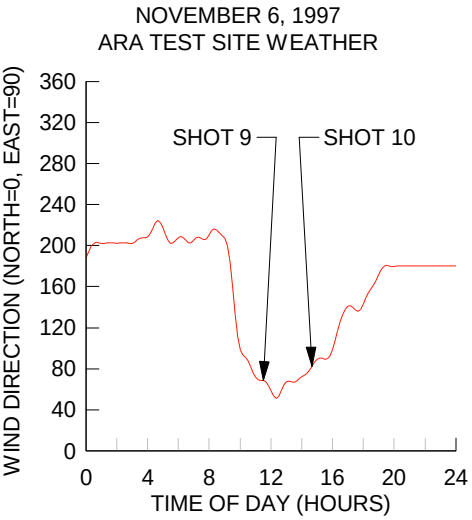
NOVEMBER 6, 1997
ARA TEST SITE WEATHER
WIND DIRECTION (NORTH=0, EAST=90)
360
320
280
240
200
160
120
80
40
0
SHOT 9
SHOT 10
0
4
8
12
16
20
24
TIME OF DAY (HOURS)

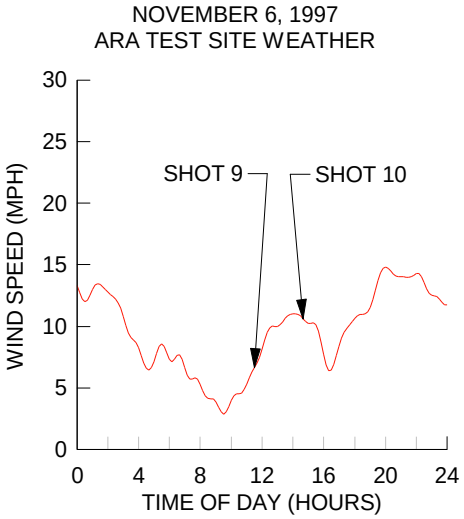
NOVEMBER 6, 1997
ARA TEST SITE WEATHER
WIND SPEED (MPH)
30
25
20
15
10
5
0
SHOT 9
SHOT 10
0
4
8
12
16
20
24
TIME OF DAY (HOURS)

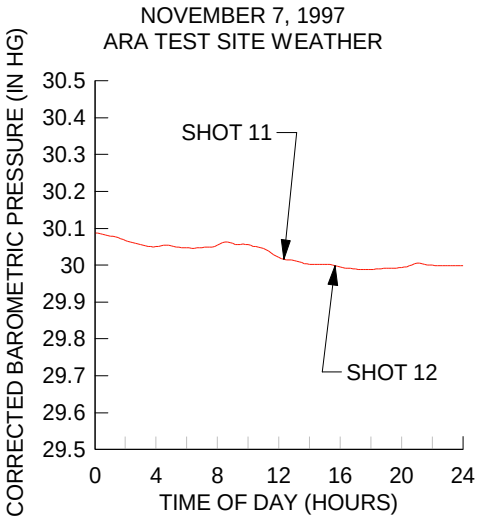
NOVEMBER 7, 1997
ARA TEST SITE WEATHER
CORRECTED BAROMETRIC PRESSURE (IN HG)
30.5
30.4
30.3
30.2
30.1
30
29.9
29.8
29.7
29.6
29.5
SHOT 11
SHOT 12
0
4
8
12
16
20
24
TIME OF DAY (HOURS)

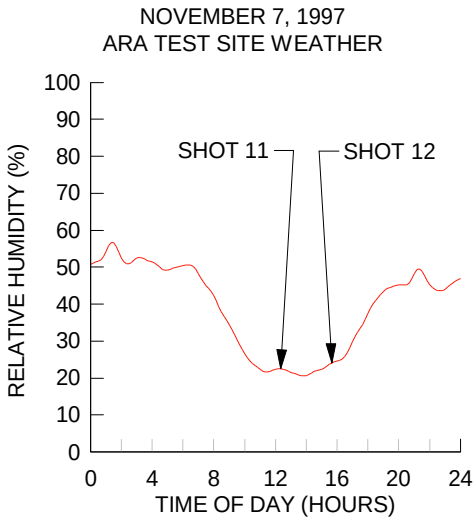
NOVEMBER 7, 1997
ARA TEST SITE WEATHER
RELATIVE HUMIDITY (%)
100
90
80
70
60
50
40
30
20
10
0
SHOT 11
SHOT 12
0
4
8
12
16
20
24
TIME OF DAY (HOURS)

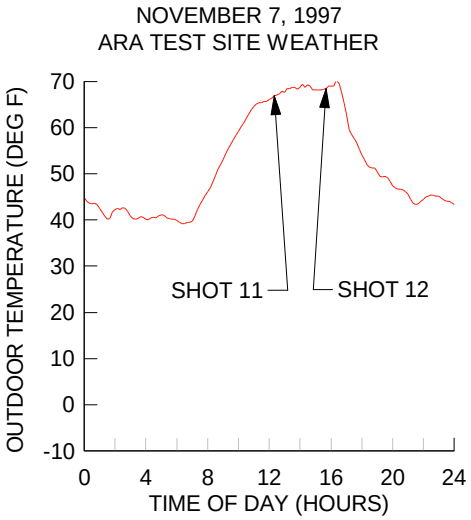
NOVEMBER 7, 1997
ARA TEST SITE WEATHER
OUTDOOR TEMPERATURE (DEG F)
70
60
50
40
30
20
10
0
-10
SHOT 11
SHOT 12
0
4
8
12
16
20
24
TIME OF DAY (HOURS)

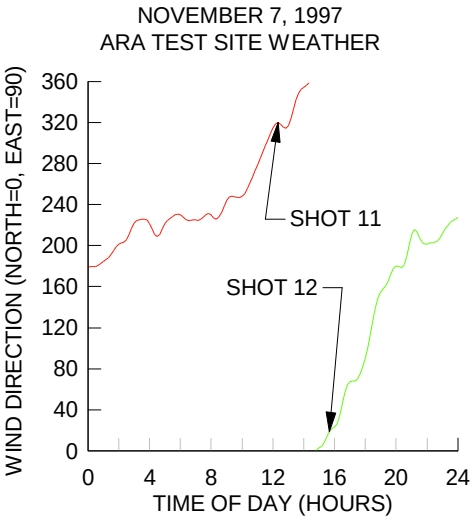
NOVEMBER 7, 1997
ARA TEST SITE WEATHER
WIND DIRECTION (NORTH=0, EAST=90)
360
320
280
240
200
160
120
80
40
0
SHOT 11
SHOT 12
0
4
8
12
16
20
24
TIME OF DAY (HOURS)

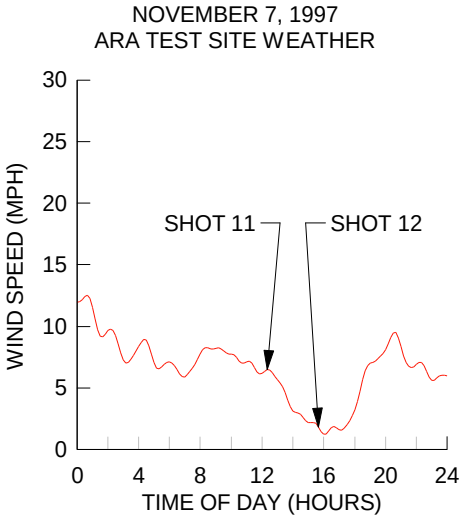
NOVEMBER 7, 1997
ARA TEST SITE WEATHER
WIND SPEED (MPH)
30
25
20
15
10
5
0
SHOT 11
SHOT 12
0
4
8
12
16
20
24
TIME OF DAY (HOURS)

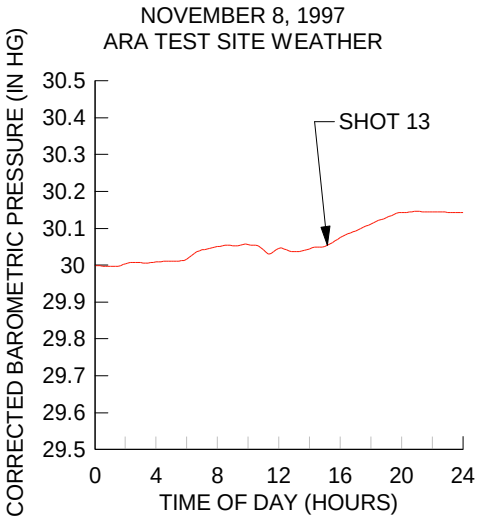
NOVEMBER 8, 1997
ARA TEST SITE WEATHER
CORRECTED BAROMETRIC PRESSURE (IN HG)
30.5
30.4
30.3
30.2
30.1
30
29.9
29.8
29.7
29.6
29.5
SHOT 13
0
4
8
12
16
20
24
TIME OF DAY (HOURS)

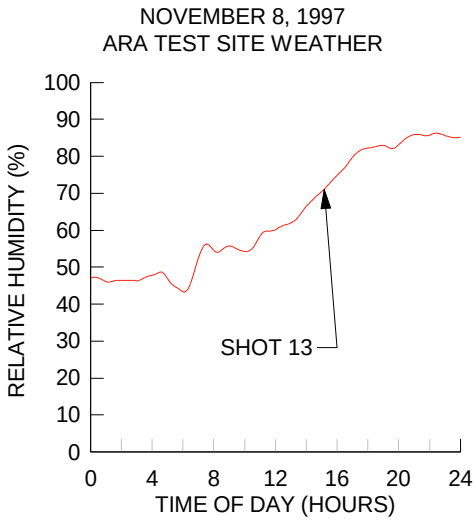
NOVEMBER 8, 1997
ARA TEST SITE WEATHER
RELATIVE HUMIDITY (%)
100
90
80
70
60
50
40
30
20
10
0
SHOT 13
0
4
8
12
16
20
24
TIME OF DAY (HOURS)

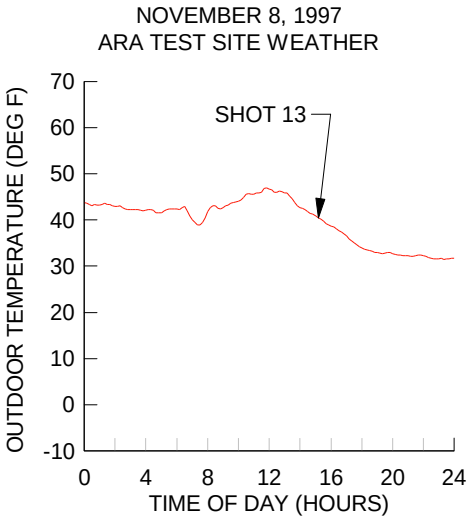
NOVEMBER 8, 1997
ARA TEST SITE WEATHER
OUTDOOR TEMPERATURE (DEG F)
70
60
50
40
30
20
10
0
-10
SHOT 13
0
4
8
12
16
20
24
TIME OF DAY (HOURS)

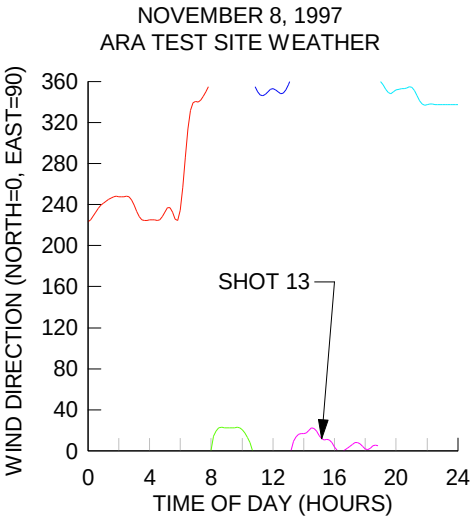
NOVEMBER 8, 1997
ARA TEST SITE WEATHER
WIND DIRECTION (NORTH=0, EAST=90)
360
320
280
240
200
160
120
80
40
0
SHOT 13
0
4
8
12
16
20
24
TIME OF DAY (HOURS)

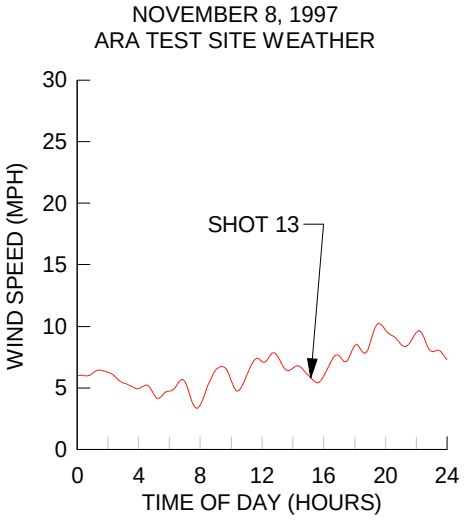
NOVEMBER 8, 1997
ARA TEST SITE WEATHER
WIND SPEED (MPH)
30
25
20
15
10
5
0
SHOT 13
0
4
8
12
16
20
24
TIME OF DAY (HOURS)

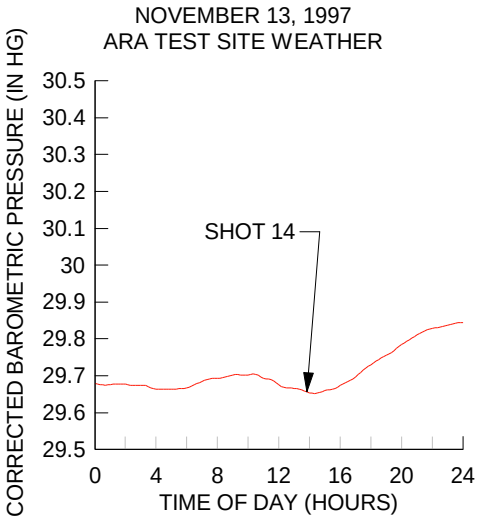
NOVEMBER 13, 1997
ARA TEST SITE WEATHER
CORRECTED BAROMETRIC PRESSURE (IN HG)
30.5
30.4
30.3
30.2
30.1
30
29.9
29.8
29.7
29.6
29.5
SHOT 14
0
4
8
12
16
20
24
TIME OF DAY (HOURS)

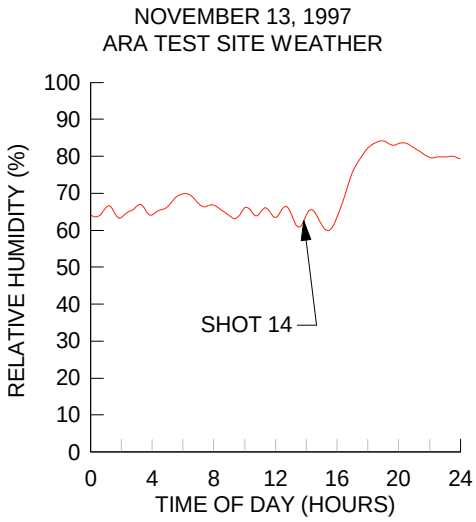
NOVEMBER 13, 1997
ARA TEST SITE WEATHER
RELATIVE HUMIDITY (%)
100
90
80
70
60
50
40
30
20
10
0
SHOT 14
0
4
8
12
16
20
24
TIME OF DAY (HOURS)

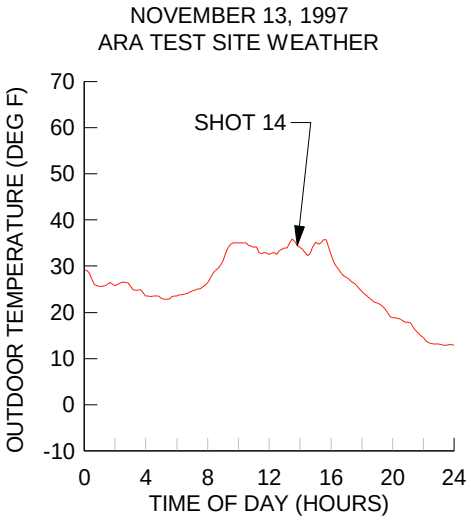
NOVEMBER 13, 1997
ARA TEST SITE WEATHER
OUTDOOR TEMPERATURE (DEG F)
70
60
50
40
30
20
10
0
-10
SHOT 14
0
4
8
12
16
20
24
TIME OF DAY (HOURS)

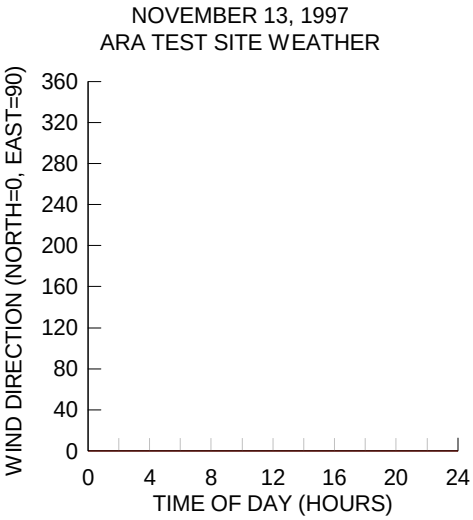
NOVEMBER 13, 1997
ARA TEST SITE WEATHER
WIND DIRECTION (NORTH=0, EAST=90)
360
320
280
240
200
160
120
80
40
0
0
4
8
12
16
20
24
TIME OF DAY (HOURS)

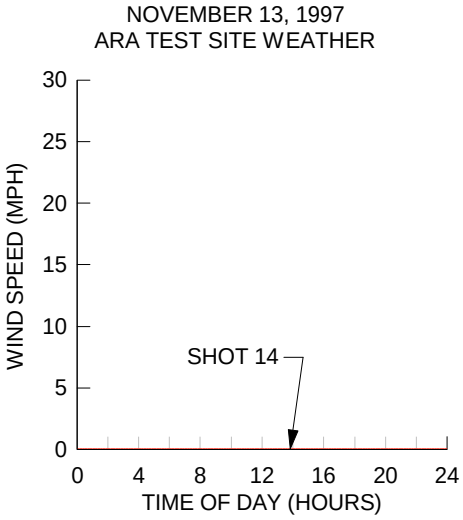
NOVEMBER 13, 1997
ARA TEST SITE WEATHER
WIND SPEED (MPH)
30
25
20
15
10
5
0
SHOT 14
0
4
8
12
16
20
24
TIME OF DAY (HOURS)

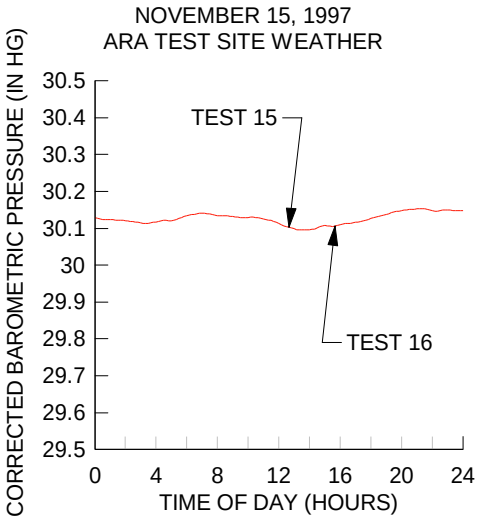
NOVEMBER 15, 1997
ARA TEST SITE WEATHER
CORRECTED BAROMETRIC PRESSURE (IN HG)
30.5
30.4
30.3
30.2
30.1
30
29.9
29.8
29.7
29.6
29.5
TEST 15
TEST 16
0
4
8
12
16
20
24
TIME OF DAY (HOURS)

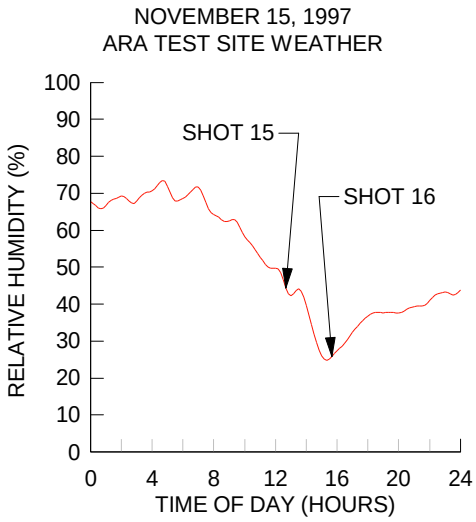
NOVEMBER 15, 1997
ARA TEST SITE WEATHER
RELATIVE HUMIDITY (%)
100
90
80
70
60
50
40
30
20
10
0
SHOT 15
SHOT 16
0
4
8
12
16
20
24
TIME OF DAY (HOURS)

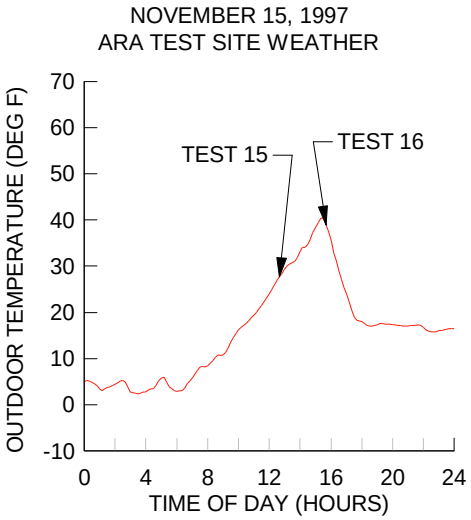
NOVEMBER 15, 1997
ARA TEST SITE WEATHER
OUTDOOR TEMPERATURE (DEG F)
70
60
50
40
30
20
10
0
-10
TEST 15
TEST 16
0
4
8
12
16
20
24
TIME OF DAY (HOURS)

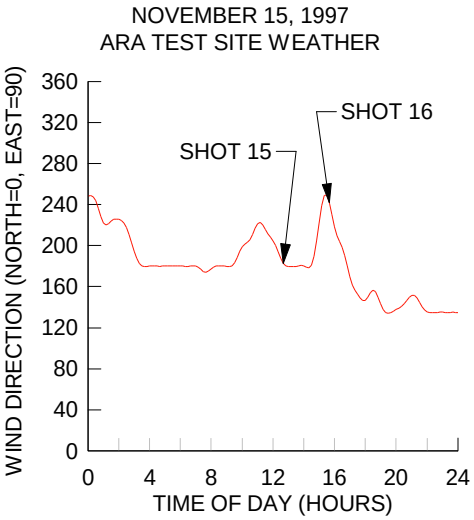
NOVEMBER 15, 1997
ARA TEST SITE WEATHER
WIND DIRECTION (NORTH=0, EAST=90)
360
320
280
240
200
160
120
80
40
0
SHOT 15
SHOT 16
0
4
8
12
16
20
24
TIME OF DAY (HOURS)

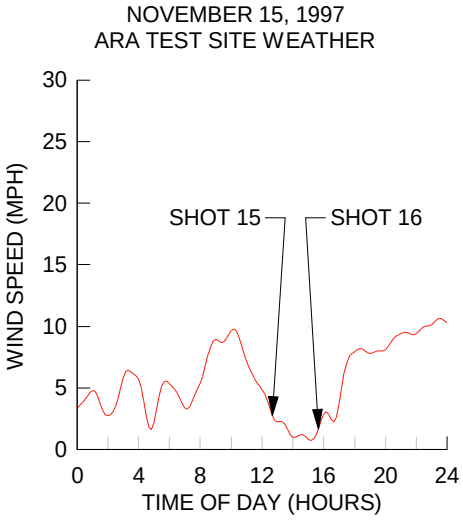
NOVEMBER 15, 1997
ARA TEST SITE WEATHER
WIND SPEED (MPH)
30
25
20
15
10
5
0
SHOT 15
SHOT 16
0
4
8
12
16
20
24
TIME OF DAY (HOURS)

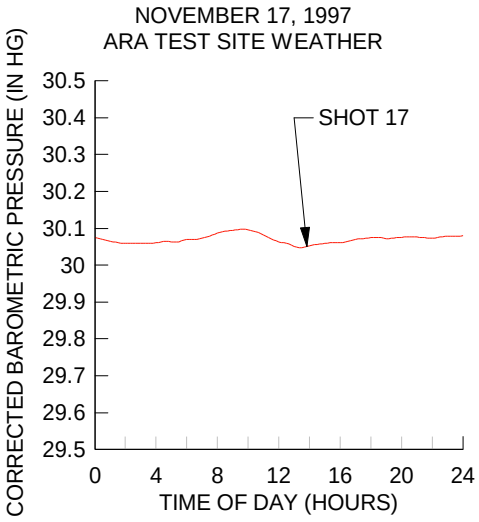
NOVEMBER 17, 1997
ARA TEST SITE WEATHER
CORRECTED BAROMETRIC PRESSURE (IN HG)
30.5
30.4
30.3
30.2
30.1
30
29.9
29.8
29.7
29.6
29.5
SHOT 17
0
4
8
12
16
20
24
TIME OF DAY (HOURS)

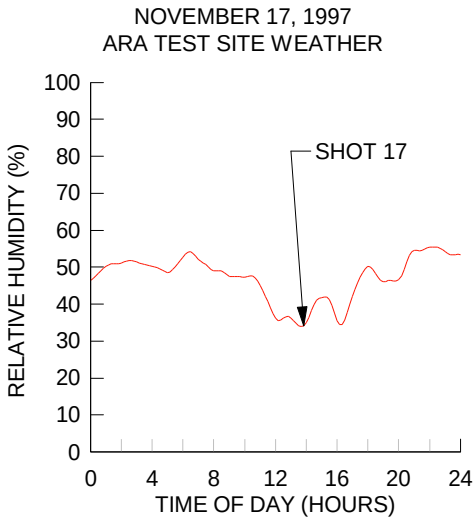
NOVEMBER 17, 1997
ARA TEST SITE WEATHER
RELATIVE HUMIDITY (%)
100
90
80
70
60
50
40
30
20
10
0
SHOT 17
0
4
8
12
16
20
24
TIME OF DAY (HOURS)

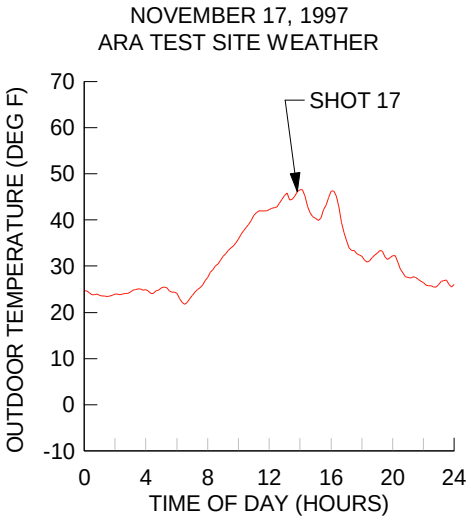
NOVEMBER 17, 1997
ARA TEST SITE WEATHER
OUTDOOR TEMPERATURE (DEG F)
70
60
50
40
30
20
10
0
-10
SHOT 17
0
4
8
12
16
20
24
TIME OF DAY (HOURS)

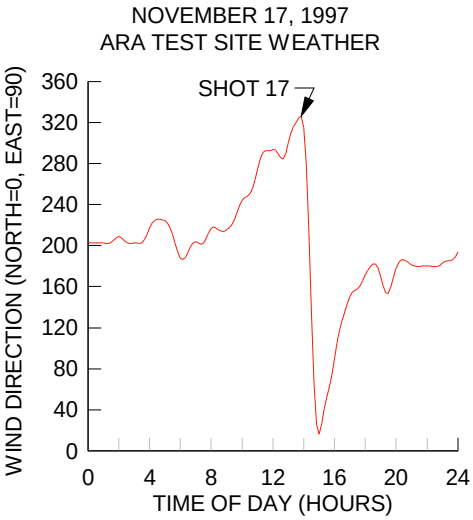
NOVEMBER 17, 1997
ARA TEST SITE WEATHER
WIND DIRECTION (NORTH=0, EAST=90)
360
320
280
240
200
160
120
80
40
0
SHOT 17
0
4
8
12
16
20
24
TIME OF DAY (HOURS)

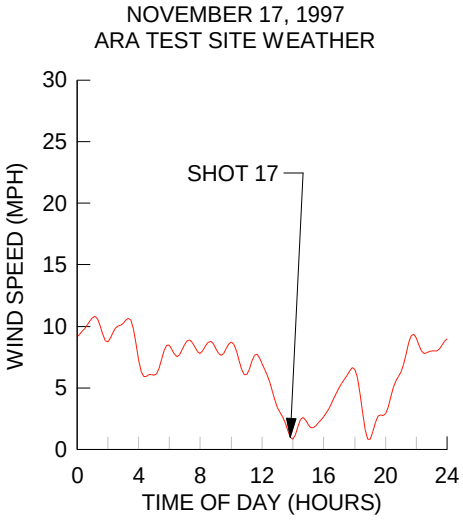
NOVEMBER 17, 1997
ARA TEST SITE WEATHER
WIND SPEED (MPH)
30
25
20
15
10
5
0
SHOT 17
0
4
8
12
16
20
24
TIME OF DAY (HOURS)

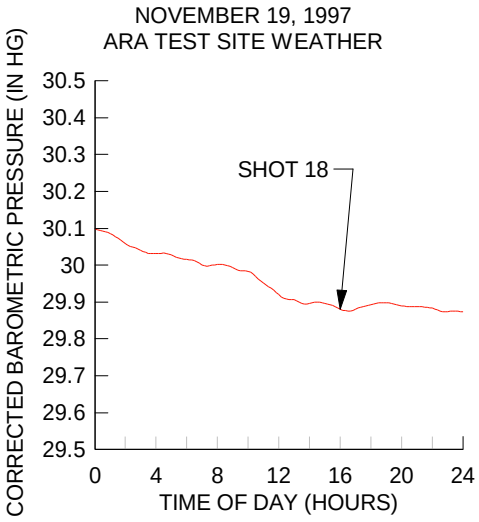
NOVEMBER 19, 1997
ARA TEST SITE WEATHER
CORRECTED BAROMETRIC PRESSURE (IN HG)
30.5
30.4
30.3
30.2
30.1
30
29.9
29.8
29.7
29.6
29.5
SHOT 18
0
4
8
12
16
20
24
TIME OF DAY (HOURS)

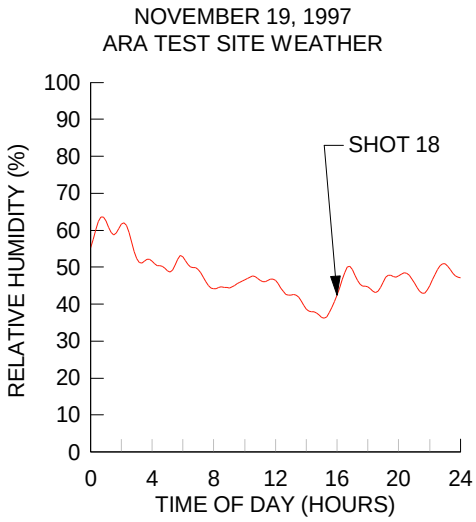
NOVEMBER 19, 1997
ARA TEST SITE WEATHER
RELATIVE HUMIDITY (%)
100
90
80
70
60
50
40
30
20
10
0
SHOT 18
0
4
8
12
16
20
24
TIME OF DAY (HOURS)

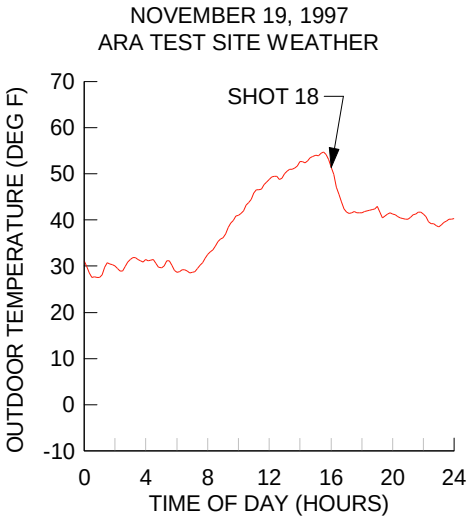
NOVEMBER 19, 1997
ARA TEST SITE WEATHER
OUTDOOR TEMPERATURE (DEG F)
70
60
50
40
30
20
10
0
-10
SHOT 18
0
4
8
12
16
20
24
TIME OF DAY (HOURS)

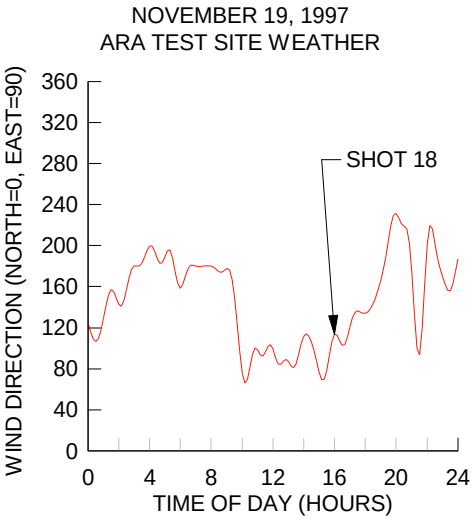
NOVEMBER 19, 1997
ARA TEST SITE WEATHER
WIND DIRECTION (NORTH=0, EAST=90)
360
320
280
240
200
160
120
80
40
0
SHOT 18
0
4
8
12
16
20
24
TIME OF DAY (HOURS)

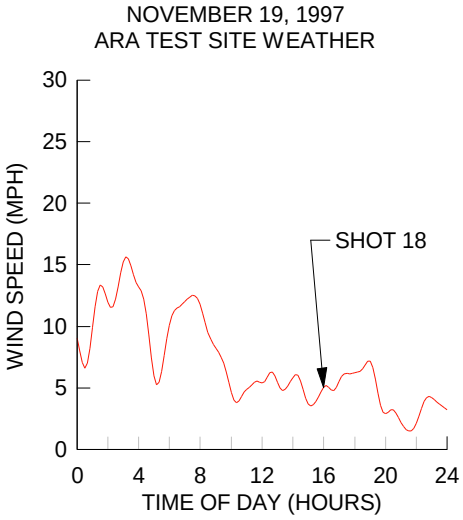
NOVEMBER 19, 1997
ARA TEST SITE WEATHER
WIND SPEED (MPH)
30
25
20
15
10
5
0
SHOT 18
0
4
8
12
16
20
24
TIME OF DAY (HOURS)

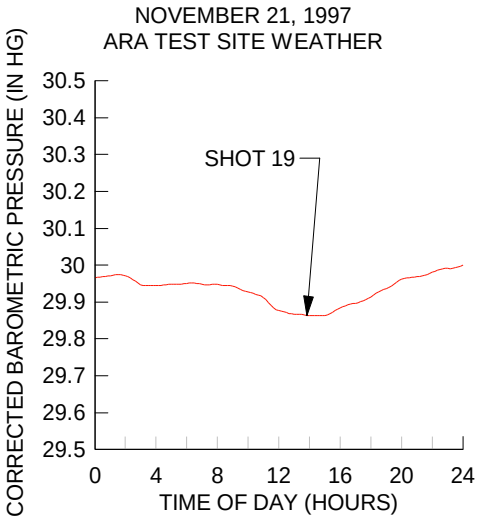
NOVEMBER 21, 1997
ARA TEST SITE WEATHER
CORRECTED BAROMETRIC PRESSURE (IN HG)
30.5
30.4
30.3
30.2
30.1
30
29.9
29.8
29.7
29.6
29.5
SHOT 19
0
4
8
12
16
20
24
TIME OF DAY (HOURS)

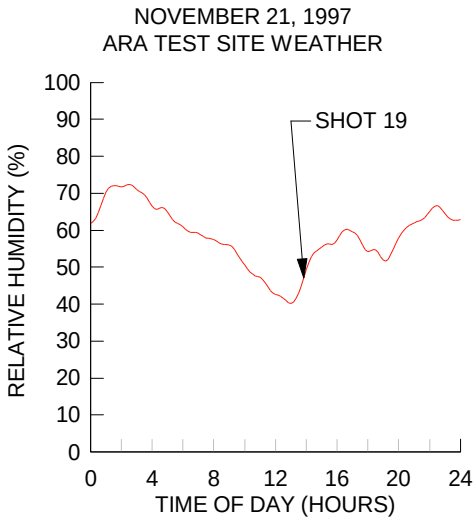
NOVEMBER 21, 1997
ARA TEST SITE WEATHER
RELATIVE HUMIDITY (%)
100
90
80
70
60
50
40
30
20
10
0
SHOT 19
0
4
8
12
16
20
24
TIME OF DAY (HOURS)

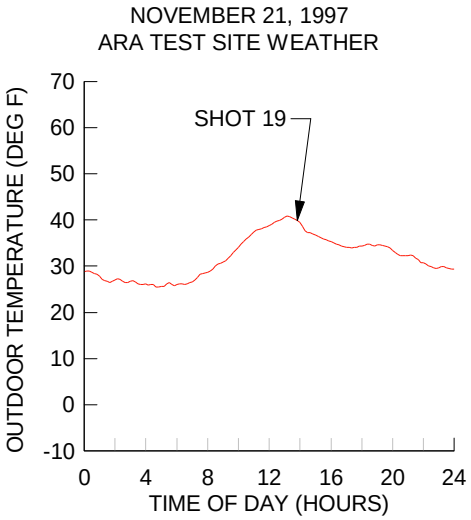
NOVEMBER 21, 1997
ARA TEST SITE WEATHER
OUTDOOR TEMPERATURE (DEG F)
70
60
50
40
30
20
10
0
-10
SHOT 19
0
4
8
12
16
20
24
TIME OF DAY (HOURS)

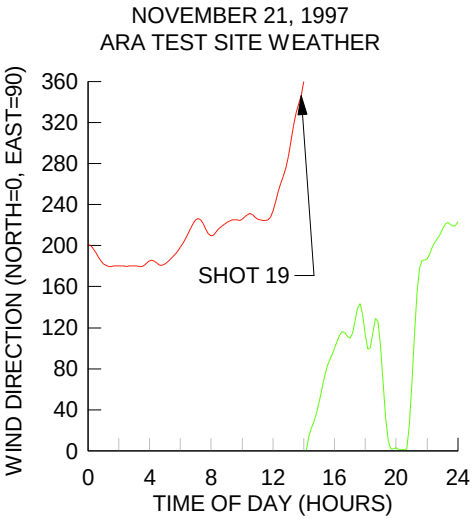
NOVEMBER 21, 1997
ARA TEST SITE WEATHER
WIND DIRECTION (NORTH=0, EAST=90)
360
320
280
240
200
160
120
80
40
0
SHOT 19
0
4
8
12
16
20
24
TIME OF DAY (HOURS)

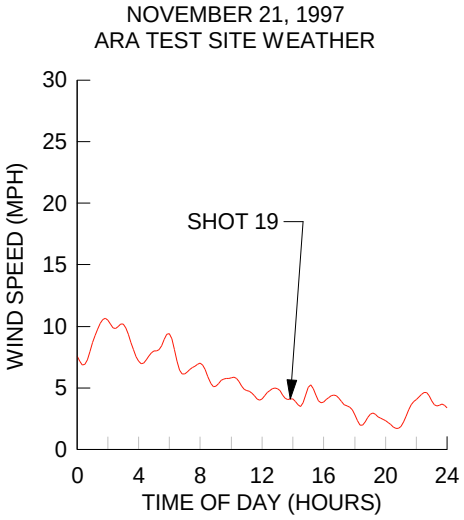
NOVEMBER 21, 1997
ARA TEST SITE WEATHER
WIND SPEED (MPH)
30
25
20
15
10
5
0
SHOT 19
0
4
8
12
16
20
24
TIME OF DAY (HOURS)

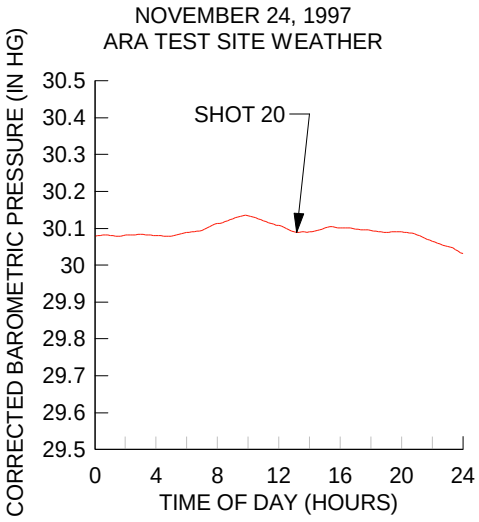
NOVEMBER 24, 1997
ARA TEST SITE WEATHER
CORRECTED BAROMETRIC PRESSURE (IN HG)
30.5
30.4
30.3
30.2
30.1
30
29.9
29.8
29.7
29.6
29.5
SHOT 20
0
4
8
12
16
20
24
TIME OF DAY (HOURS)

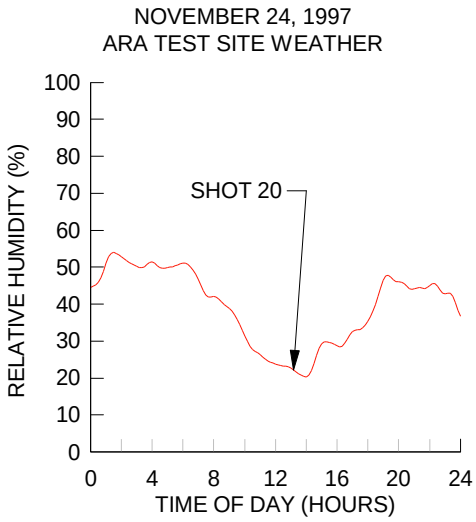
NOVEMBER 24, 1997
ARA TEST SITE WEATHER
RELATIVE HUMIDITY (%)
100
90
80
70
60
50
40
30
20
10
0
SHOT 20
0
4
8
12
16
20
24
TIME OF DAY (HOURS)

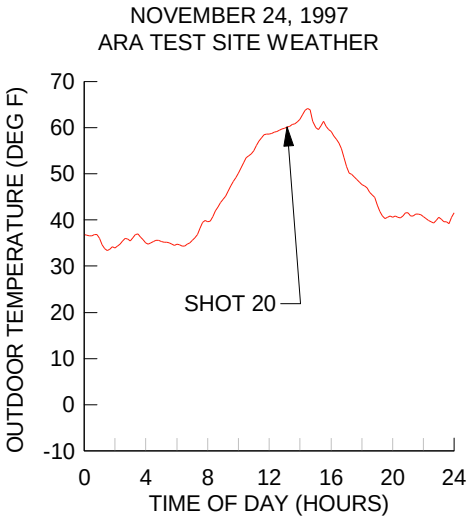
NOVEMBER 24, 1997
ARA TEST SITE WEATHER
OUTDOOR TEMPERATURE (DEG F)
70
60
50
40
30
20
10
0
-10
SHOT 20
0
4
8
12
16
20
24
TIME OF DAY (HOURS)

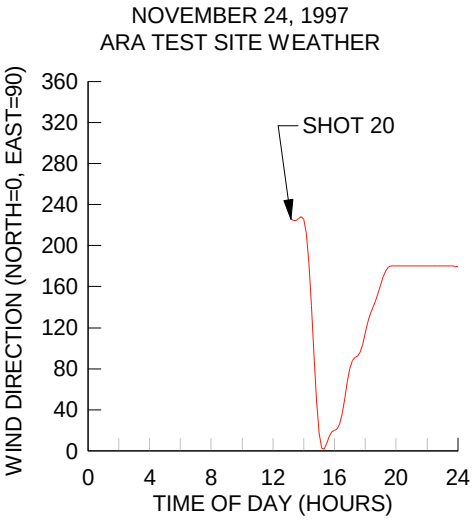
NOVEMBER 24, 1997
ARA TEST SITE WEATHER
WIND DIRECTION (NORTH=0, EAST=90)
360
320
280
240
200
160
120
80
40
0
SHOT 20
0
4
8
12
16
20
24
TIME OF DAY (HOURS)

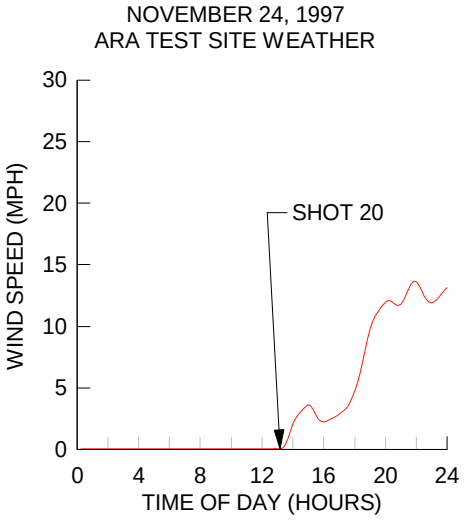
NOVEMBER 24, 1997
ARA TEST SITE WEATHER
WIND SPEED (MPH)
30
25
20
15
10
5
0
SHOT 20
0
4
8
12
16
20
24
TIME OF DAY (HOURS)

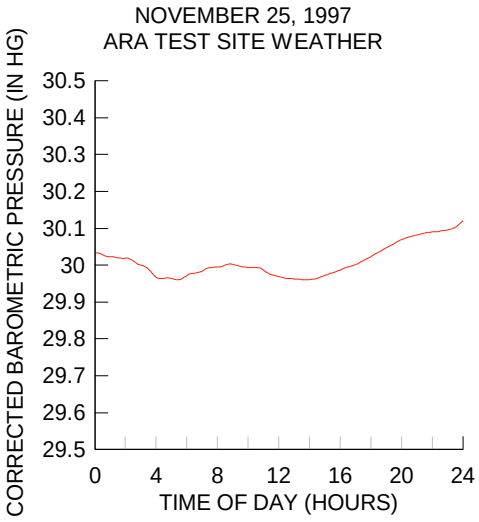
NOVEMBER 25, 1997
ARA TEST SITE WEATHER
CORRECTED BAROMETRIC PRESSURE (IN HG)
30.5
30.4
30.3
30.2
30.1
30
29.9
29.8
29.7
29.6
29.5
0
4
8
12
16
20
24
TIME OF DAY (HOURS)

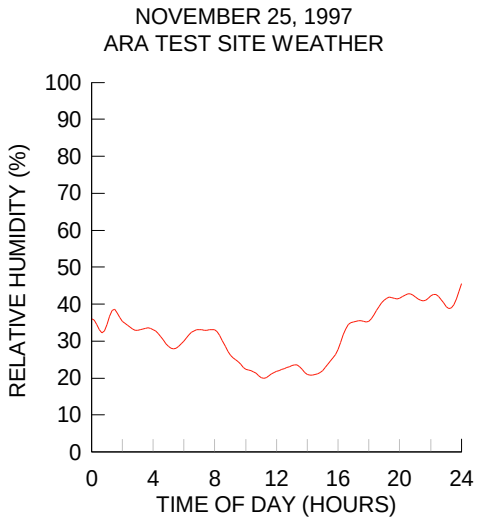
NOVEMBER 25, 1997
ARA TEST SITE WEATHER
RELATIVE HUMIDITY (%)
100
90
80
70
60
50
40
30
20
10
0
0
4
8
12
16
20
24
TIME OF DAY (HOURS)

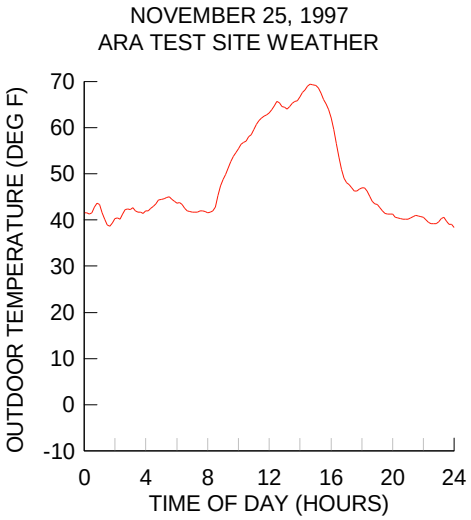
NOVEMBER 25, 1997
ARA TEST SITE WEATHER
OUTDOOR TEMPERATURE (DEG F)
70
60
50
40
30
20
10
0
-10
0
4
8
12
16
20
24
TIME OF DAY (HOURS)

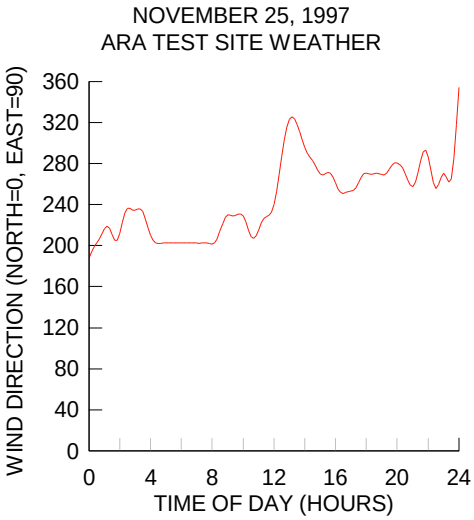
NOVEMBER 25, 1997
ARA TEST SITE WEATHER
WIND DIRECTION (NORTH=0, EAST=90)
360
320
280
240
200
160
120
80
40
0
0
4
8
12
16
20
24
TIME OF DAY (HOURS)

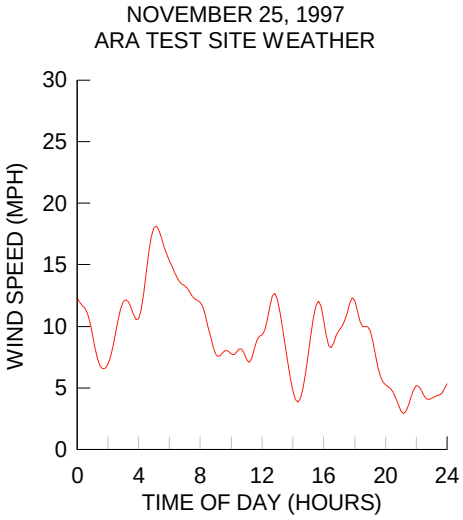
NOVEMBER 25, 1997
ARA TEST SITE WEATHER
WIND SPEED (MPH)
30
25
20
15
10
5
0
0
4
8
12
16
20
24
TIME OF DAY (HOURS)

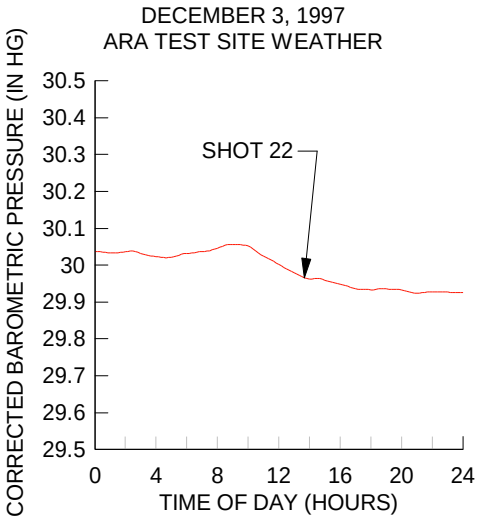
DECEMBER 3, 1997
ARA TEST SITE WEATHER
CORRECTED BAROMETRIC PRESSURE (IN HG)
30.5
30.4
30.3
30.2
30.1
30
29.9
29.8
29.7
29.6
29.5
SHOT 22
0
4
8
12
16
20
24
TIME OF DAY (HOURS)

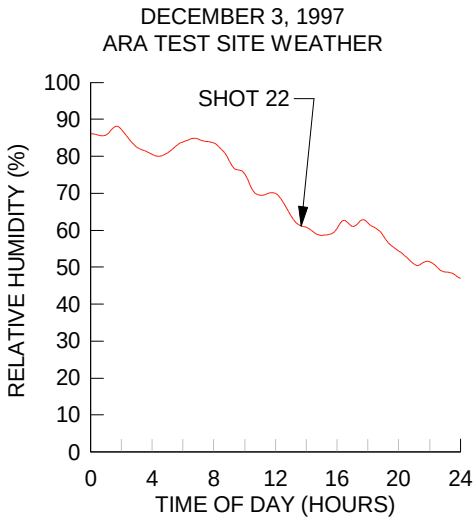
DECEMBER 3, 1997
ARA TEST SITE WEATHER
RELATIVE HUMIDITY (%)
100
90
80
70
60
50
40
30
20
10
0
SHOT 22
0
4
8
12
16
20
24
TIME OF DAY (HOURS)

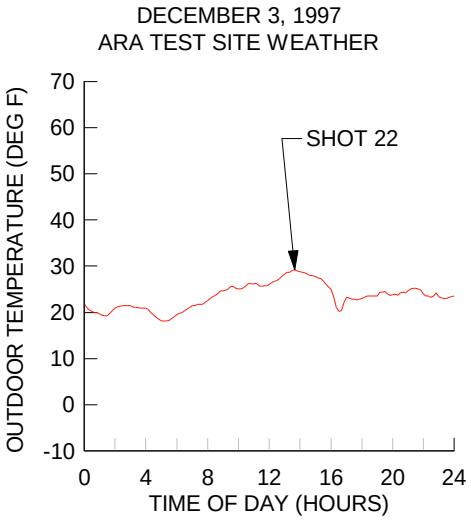
DECEMBER 3, 1997
ARA TEST SITE WEATHER
OUTDOOR TEMPERATURE (DEG F)
70
60
50
40
30
20
10
0
-10
SHOT 22
0
4
8
12
16
20
24
TIME OF DAY (HOURS)

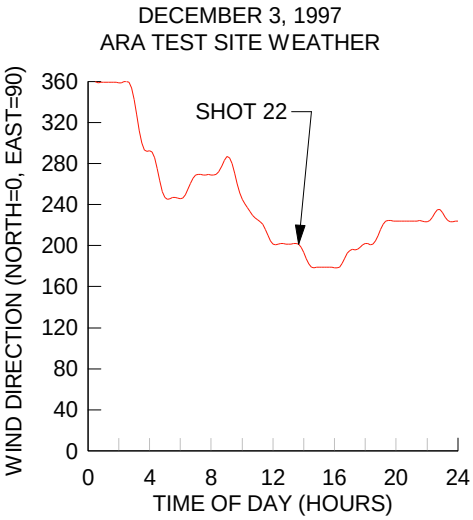
DECEMBER 3, 1997
ARA TEST SITE WEATHER
WIND DIRECTION (NORTH=0, EAST=90)
360
320
280
240
200
160
120
80
40
0
SHOT 22
0
4
8
12
16
20
24
TIME OF DAY (HOURS)

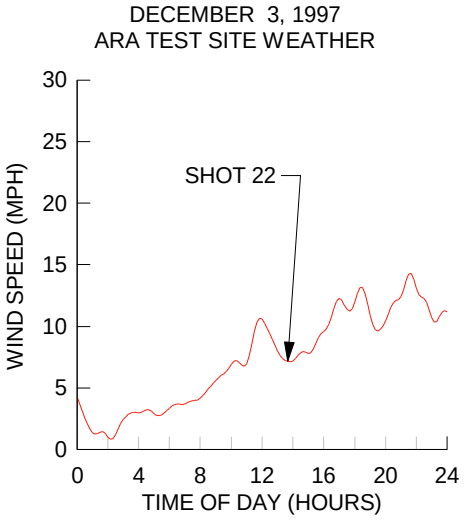
DECEMBER 3, 1997
ARA TEST SITE WEATHER
WIND SPEED (MPH)
30
25
20
15
10
5
0
SHOT 22
0
4
8
12
16
20
24
TIME OF DAY (HOURS)

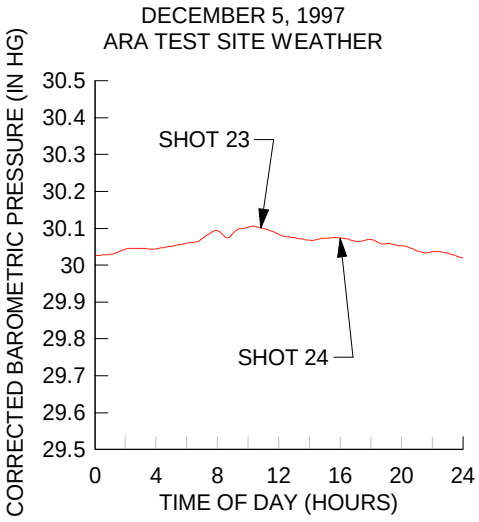
DECEMBER 5, 1997
ARA TEST SITE WEATHER
CORRECTED BAROMETRIC PRESSURE (IN HG)
30.5
30.4
30.3
30.2
30.1
30
29.9
29.8
29.7
29.6
29.5
SHOT 23
SHOT 24
0
4
8
12
16
20
24
TIME OF DAY (HOURS)

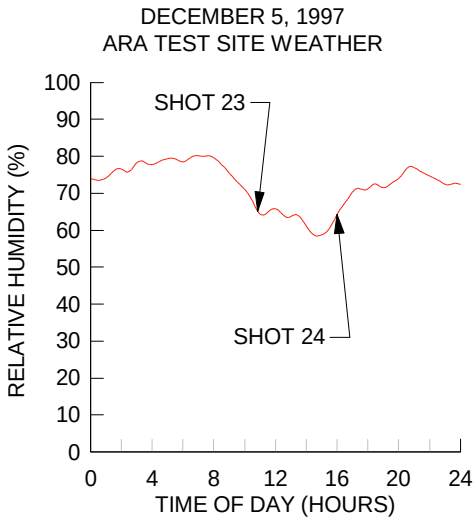
DECEMBER 5, 1997
ARA TEST SITE WEATHER
RELATIVE HUMIDITY (%)
100
90
80
70
60
50
40
30
20
10
0
SHOT 23
SHOT 24
0
4
8
12
16
20
24
TIME OF DAY (HOURS)

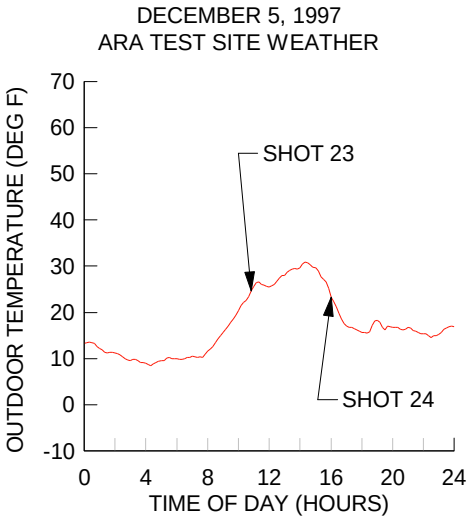
DECEMBER 5, 1997
ARA TEST SITE WEATHER
OUTDOOR TEMPERATURE (DEG F)
70
60
50
40
30
20
10
0
-10
SHOT 23
SHOT 24
0
4
8
12
16
20
24
TIME OF DAY (HOURS)

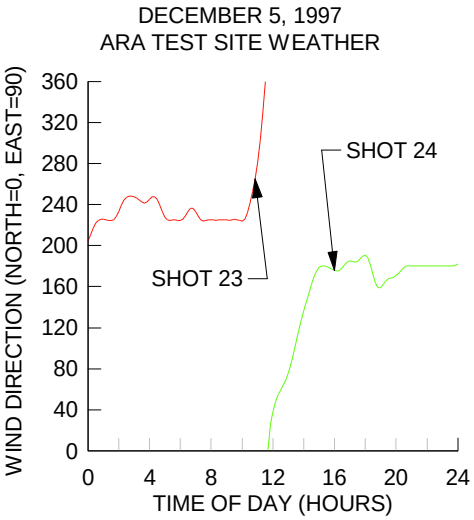
DECEMBER 5, 1997
ARA TEST SITE WEATHER
WIND DIRECTION (NORTH=0, EAST=90)
360
320
280
240
200
160
120
80
40
0
SHOT 24
SHOT 23
0
4
8
12
16
20
24
TIME OF DAY (HOURS)

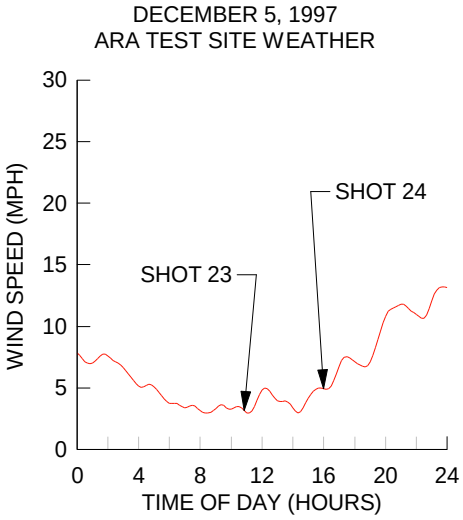
DECEMBER 5, 1997
ARA TEST SITE WEATHER
WIND SPEED (MPH)
30
25
20
15
10
5
0
SHOT 24
SHOT 23
0
4
8
12
16
20
24
TIME OF DAY (HOURS)

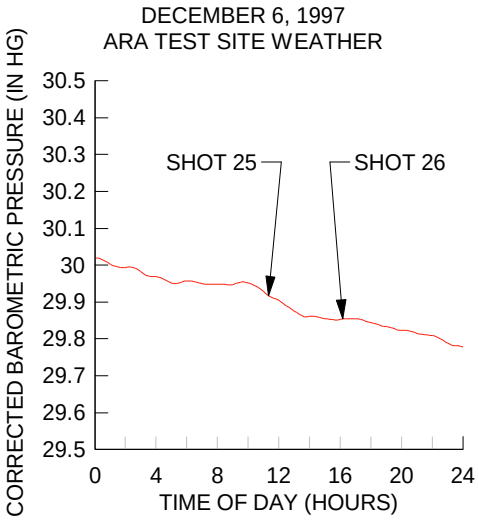
DECEMBER 6, 1997
ARA TEST SITE WEATHER
CORRECTED BAROMETRIC PRESSURE (IN HG)
30.5
30.4
30.3
30.2
30.1
30
29.9
29.8
29.7
29.6
29.5
SHOT 25
SHOT 26
0
4
8
12
16
20
24
TIME OF DAY (HOURS)

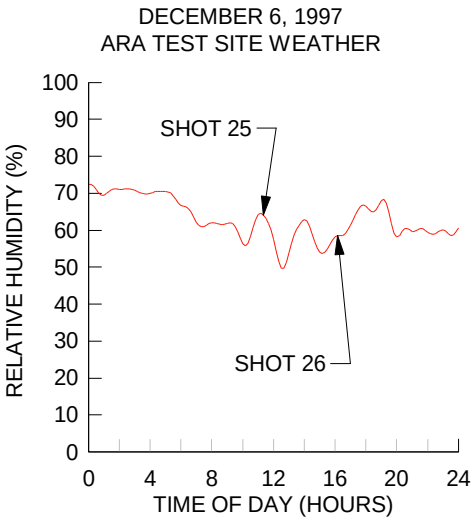
DECEMBER 6, 1997
ARA TEST SITE WEATHER
RELATIVE HUMIDITY (%)
100
90
80
70
60
50
40
30
20
10
0
SHOT 25
SHOT 26
0
4
8
12
16
20
24
TIME OF DAY (HOURS)

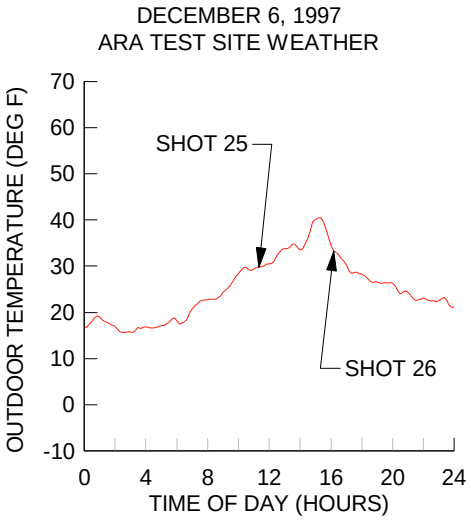
DECEMBER 6, 1997
ARA TEST SITE WEATHER
OUTDOOR TEMPERATURE (DEG F)
70
60
50
40
30
20
10
0
-10
SHOT 25
SHOT 26
0
4
8
12
16
20
24
TIME OF DAY (HOURS)

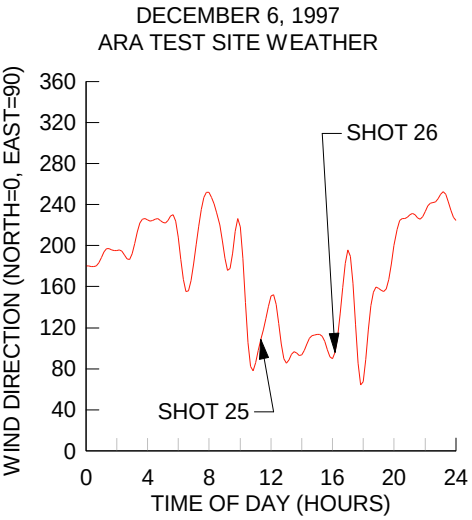
DECEMBER 6, 1997
ARA TEST SITE WEATHER
WIND DIRECTION (NORTH=0, EAST=90)
360
320
280
240
200
160
120
80
40
0
SHOT 26
SHOT 25
0
4
8
12
16
20
24
TIME OF DAY (HOURS)

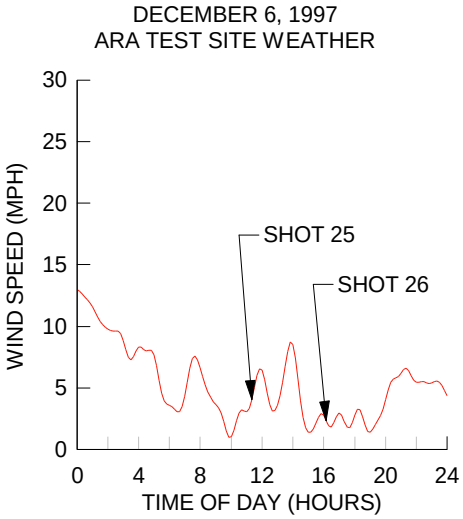
DECEMBER 6, 1997
ARA TEST SITE WEATHER
WIND SPEED (MPH)
30
25
20
15
10
5
0
SHOT 25
SHOT 26
0
4
8
12
16
20
24
TIME OF DAY (HOURS)

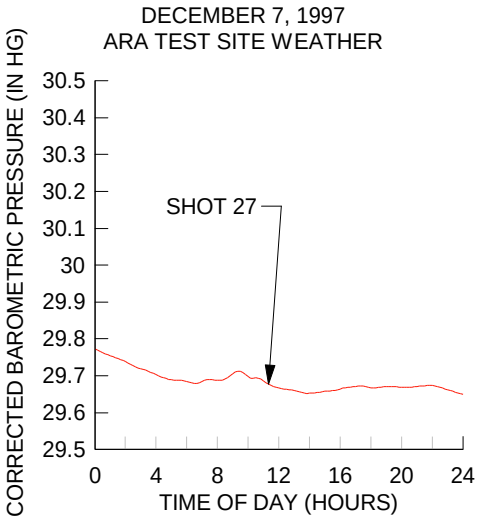
DECEMBER 7, 1997
ARA TEST SITE WEATHER
CORRECTED BAROMETRIC PRESSURE (IN HG)
30.5
30.4
30.3
30.2
30.1
30
29.9
29.8
29.7
29.6
29.5
SHOT 27
0
4
8
12
16
20
24
TIME OF DAY (HOURS)

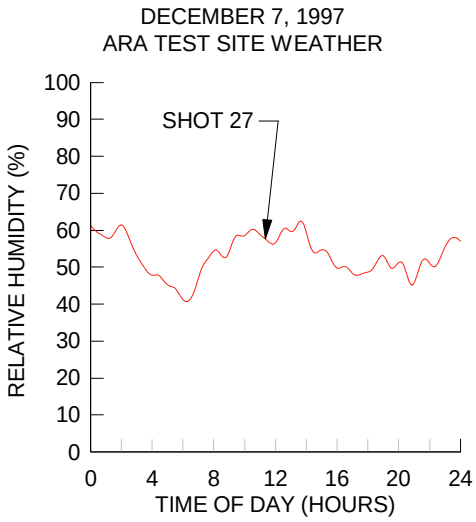
DECEMBER 7, 1997
ARA TEST SITE WEATHER
RELATIVE HUMIDITY (%)
100
90
80
70
60
50
40
30
20
10
0
SHOT 27
0
4
8
12
16
20
24
TIME OF DAY (HOURS)

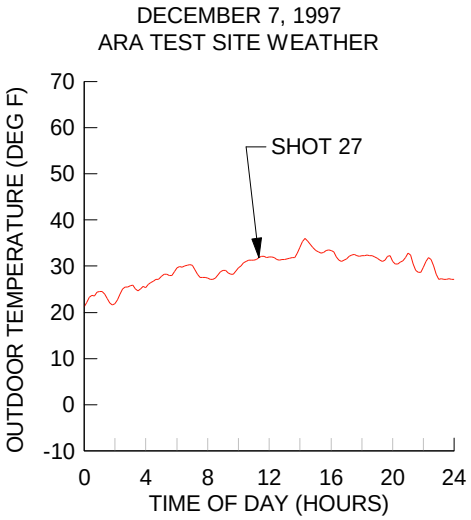
DECEMBER 7, 1997
ARA TEST SITE WEATHER
OUTDOOR TEMPERATURE (DEG F)
70
60
50
40
30
20
10
0
-10
SHOT 27
0
4
8
12
16
20
24
TIME OF DAY (HOURS)

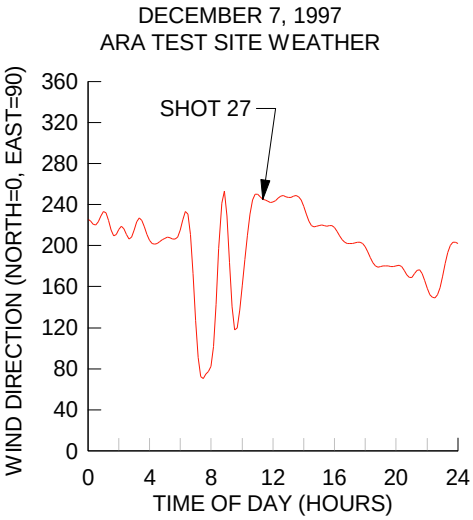
DECEMBER 7, 1997
ARA TEST SITE WEATHER
WIND DIRECTION (NORTH=0, EAST=90)
360
320
280
240
200
160
120
80
40
0
SHOT 27
0
4
8
12
16
20
24
TIME OF DAY (HOURS)

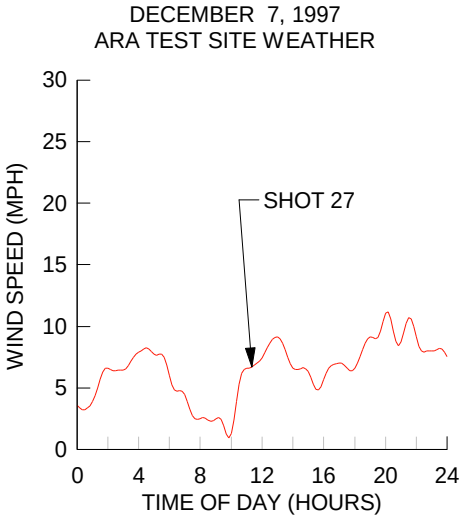
DECEMBER 7, 1997
ARA TEST SITE WEATHER
WIND SPEED (MPH)
30
25
20
15
10
5
0
SHOT 27
0
4
8
12
16
20
24
TIME OF DAY (HOURS)

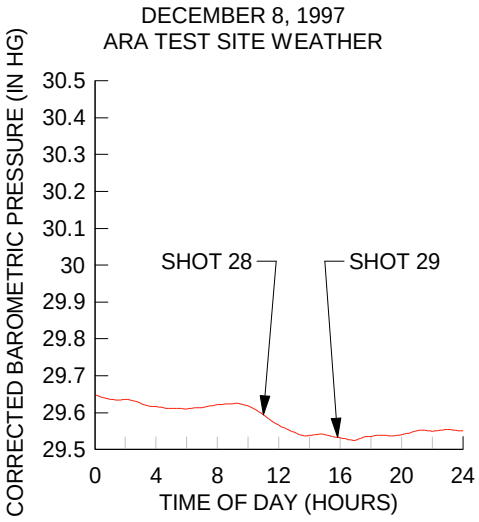
DECEMBER 8, 1997
ARA TEST SITE WEATHER
CORRECTED BAROMETRIC PRESSURE (IN HG)
30.5
30.4
30.3
30.2
30.1
30
29.9
29.8
29.7
29.6
29.5
SHOT 28
SHOT 29
0
4
8
12
16
20
24
TIME OF DAY (HOURS)

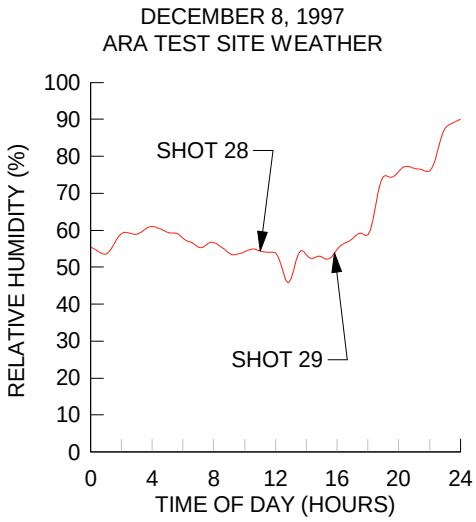
DECEMBER 8, 1997
ARA TEST SITE WEATHER
RELATIVE HUMIDITY (%)
100
90
80
70
60
50
40
30
20
10
0
SHOT 28
SHOT 29
0
4
8
12
16
20
24
TIME OF DAY (HOURS)

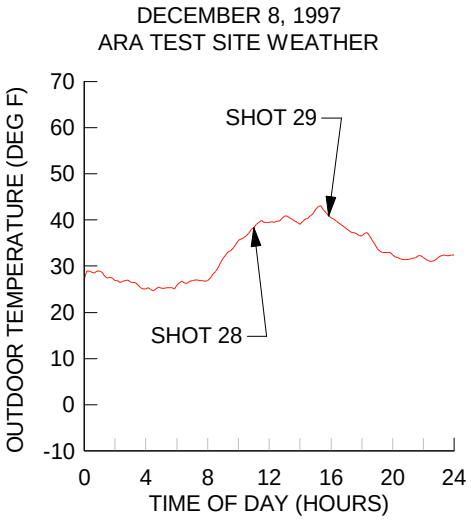
DECEMBER 8, 1997
ARA TEST SITE WEATHER
OUTDOOR TEMPERATURE (DEG F)
70
60
50
40
30
20
10
0
-10
SHOT 29
SHOT 28
0
4
8
12
16
20
24
TIME OF DAY (HOURS)

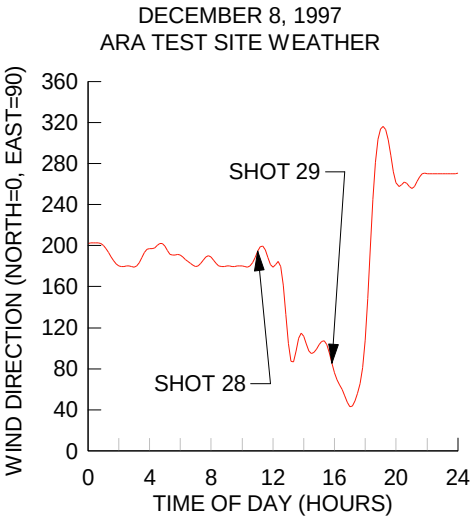
DECEMBER 8, 1997
ARA TEST SITE WEATHER
WIND DIRECTION (NORTH=0, EAST=90)
360
320
280
240
200
160
120
80
40
0
SHOT 29
SHOT 28
0
4
8
12
16
20
24
TIME OF DAY (HOURS)

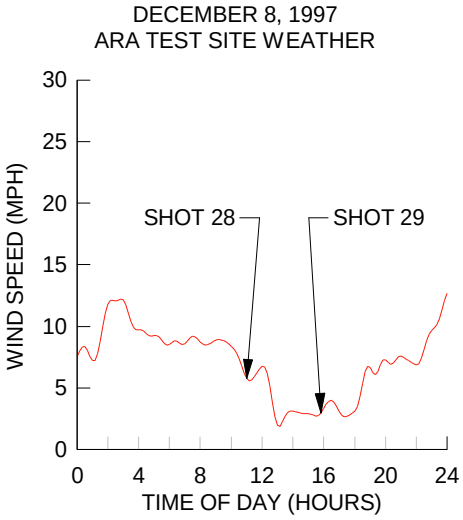
DECEMBER 8, 1997
ARA TEST SITE WEATHER
WIND SPEED (MPH)
30
25
20
15
10
5
0
SHOT 28
SHOT 29
0
4
8
12
16
20
24
TIME OF DAY (HOURS)

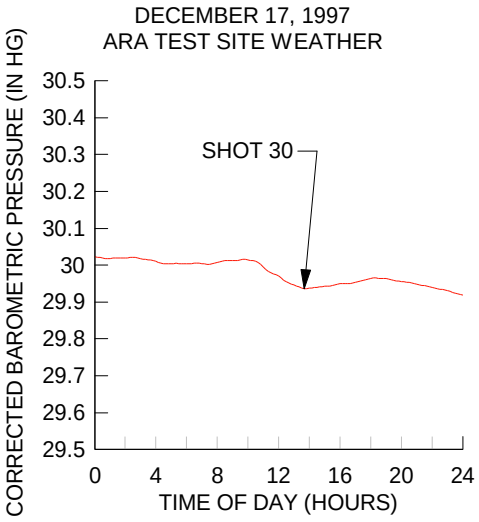
DECEMBER 17, 1997
ARA TEST SITE WEATHER
CORRECTED BAROMETRIC PRESSURE (IN HG)
30.5
30.4
30.3
30.2
30.1
30
29.9
29.8
29.7
29.6
29.5
SHOT 30
0
4
8
12
16
20
24
TIME OF DAY (HOURS)

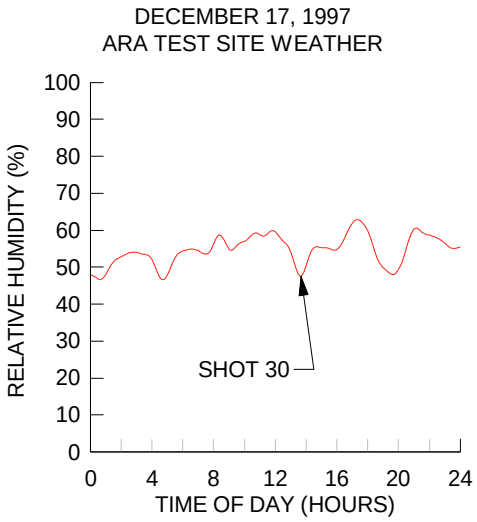
DECEMBER 17, 1997
ARA TEST SITE WEATHER
RELATIVE HUMIDITY (%)
100
90
80
70
60
50
40
30
20
10
0
SHOT 30
0
4
8
12
16
20
24
TIME OF DAY (HOURS)

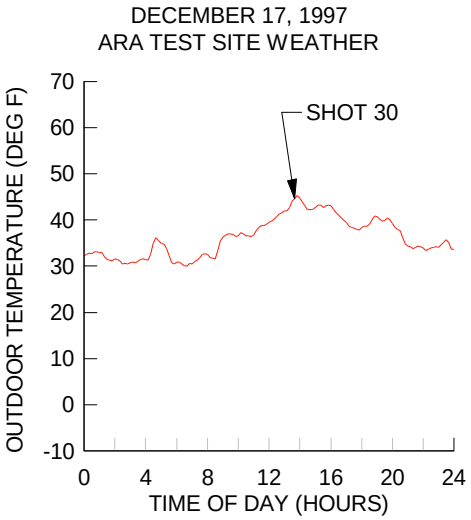
DECEMBER 17, 1997
ARA TEST SITE WEATHER
OUTDOOR TEMPERATURE (DEG F)
70
60
50
40
30
20
10
0
-10
SHOT 30
0
4
8
12
16
20
24
TIME OF DAY (HOURS)

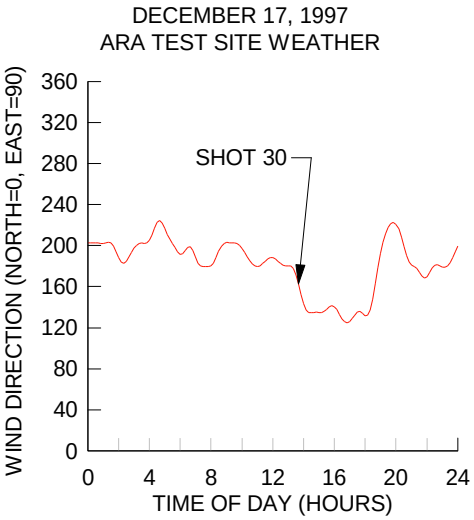
DECEMBER 17, 1997
ARA TEST SITE WEATHER
WIND DIRECTION (NORTH=0, EAST=90)
360
320
280
240
200
160
120
80
40
0
SHOT 30
0
4
8
12
16
20
24
TIME OF DAY (HOURS)

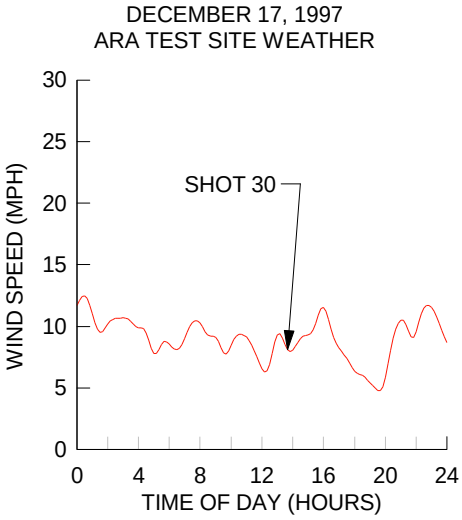
DECEMBER 17, 1997
ARA TEST SITE WEATHER
WIND SPEED (MPH)
30
25
20
15
10
5
0
SHOT 30
0
4
8
12
16
20
24
TIME OF DAY (HOURS)

D.2 External Pressure

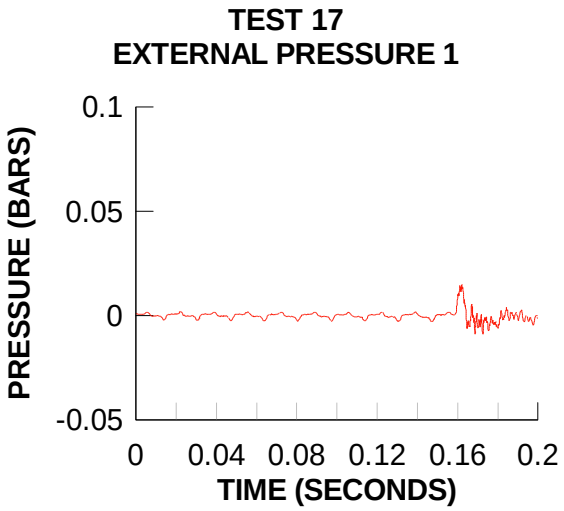
TEST 17
EXTERNAL PRESSURE 1
PRESSURE (BARS)
0.1
0.05
0
-0.05
0
0.04
0.08
0.12
0.16
0.2
TIME (SECONDS)

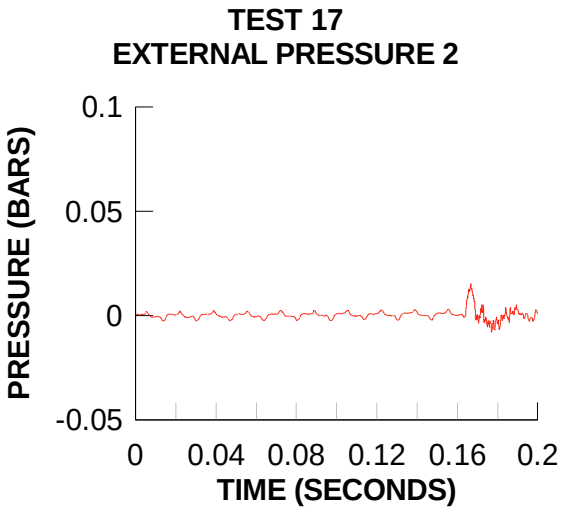
TEST 17
EXTERNAL PRESSURE 2
PRESSURE (BARS)
0.1
0.05
0
-0.05
0
0.04
0.08
0.12
0.16
0.2
TIME (SECONDS)

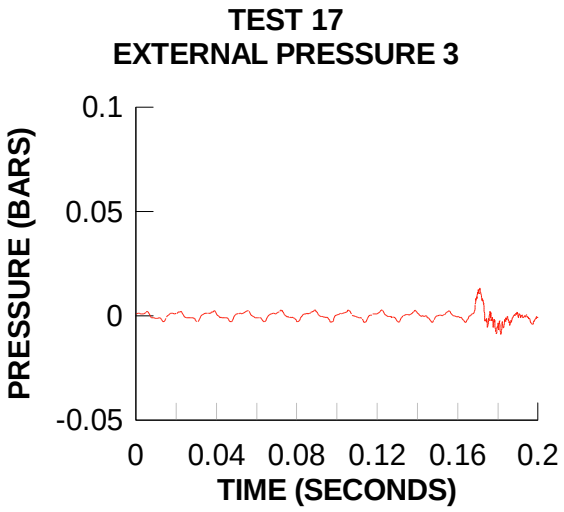
TEST 17
EXTERNAL PRESSURE 3
PRESSURE (BARS)
0.1
0.05
0
-0.05
0
0.04
0.08
0.12
0.16
0.2
TIME (SECONDS)

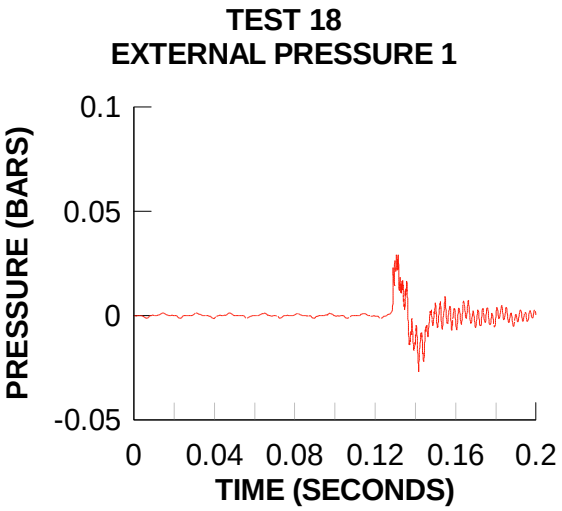
TEST 18
EXTERNAL PRESSURE 1
PRESSURE (BARS)
0.1
0.05
0
-0.05
0
0.04
0.08
0.12
0.16
0.2
TIME (SECONDS)

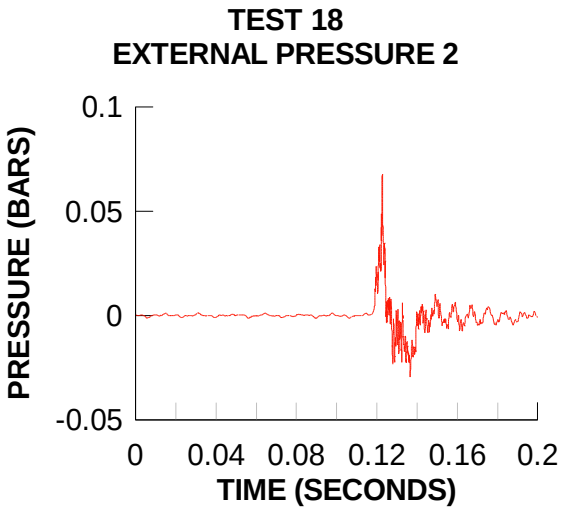
TEST 18
EXTERNAL PRESSURE 2
PRESSURE (BARS)
0.1
0.05
0
-0.05
0
0.04
0.08
0.12
0.16
0.2
TIME (SECONDS)

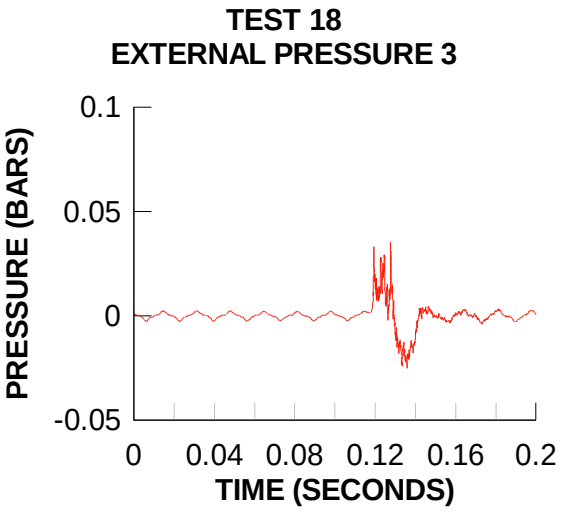
TEST 18
EXTERNAL PRESSURE 3
PRESSURE (BARS)
0.1
0.05
0
-0.05
0
0.04
0.08
0.12
0.16
0.2
TIME (SECONDS)

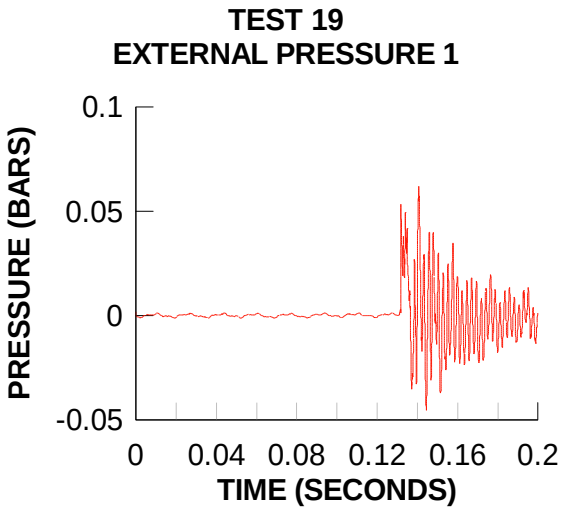
TEST 19
EXTERNAL PRESSURE 1
PRESSURE (BARS)
0.1
0.05
0
-0.05
0
0.04
0.08
0.12
0.16
0.2
TIME (SECONDS)

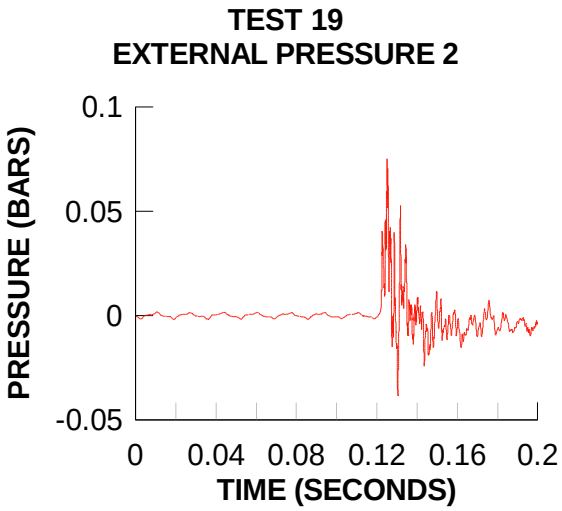
TEST 19
EXTERNAL PRESSURE 2
PRESSURE (BARS)
0.1
0.05
0
-0.05
0
0.04
0.08
0.12
0.16
0.2
TIME (SECONDS)

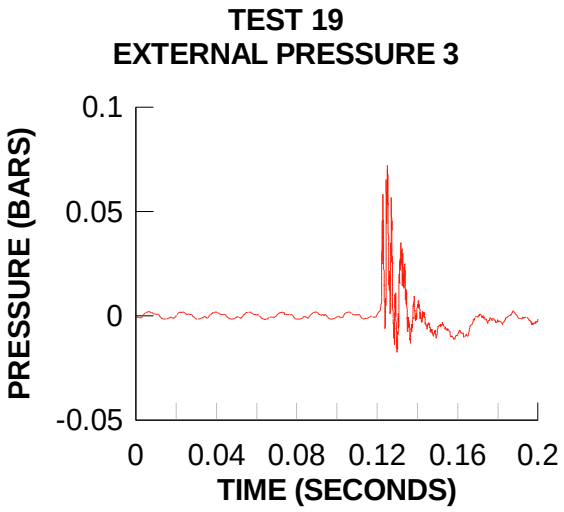
TEST 19
EXTERNAL PRESSURE 3
PRESSURE (BARS)
0.1
0.05
0
-0.05
0
0.04
0.08
0.12
0.16
0.2
TIME (SECONDS)

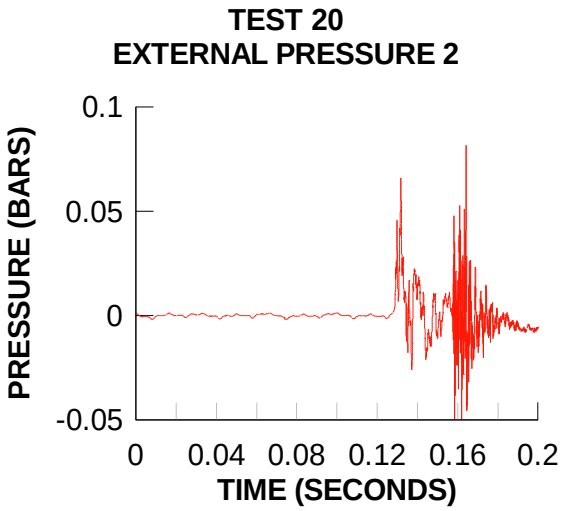
TEST 20
EXTERNAL PRESSURE 2
PRESSURE (BARS)
0.1
0.05
0
-0.05
0
0.04
0.08
0.12
0.16
0.2
TIME (SECONDS)

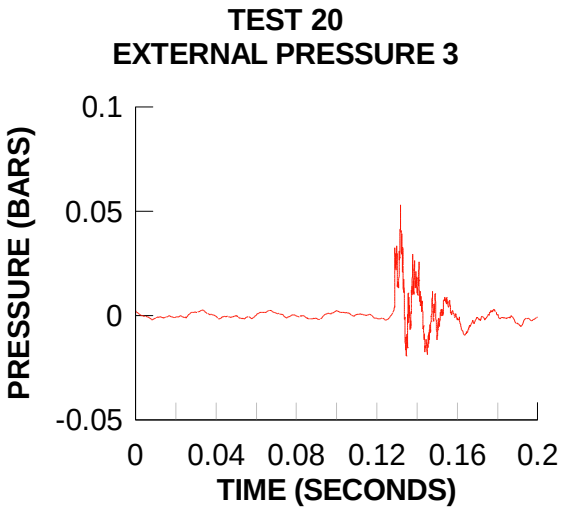
TEST 20
EXTERNAL PRESSURE 3
PRESSURE (BARS)
0.1
0.05
0
-0.05
0
0.04
0.08
0.12
0.16
0.2
TIME (SECONDS)

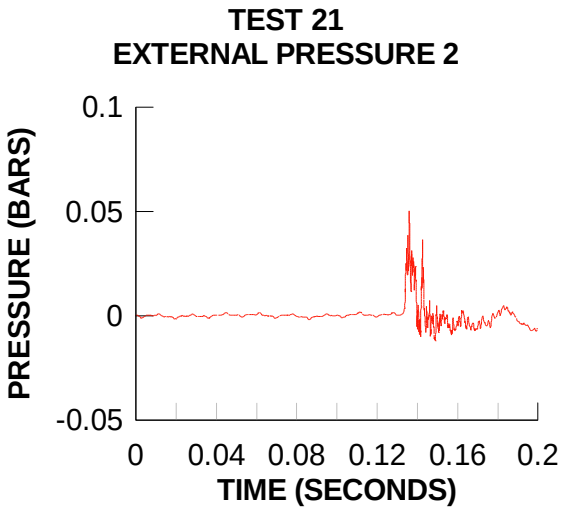
TEST 21
EXTERNAL PRESSURE 2
PRESSURE (BARS)
0.1
0.05
0
-0.05
0
0.04
0.08
0.12
0.16
0.2
TIME (SECONDS)

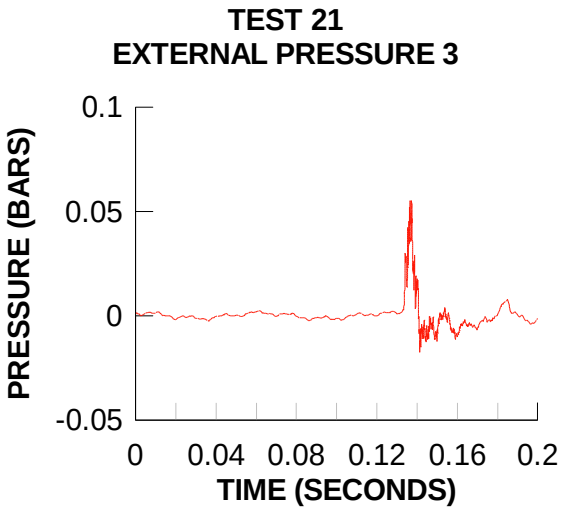
TEST 21
EXTERNAL PRESSURE 3
PRESSURE (BARS)
0.1
0.05
0
-0.05
0
0.04
0.08
0.12
0.16
0.2
TIME (SECONDS)

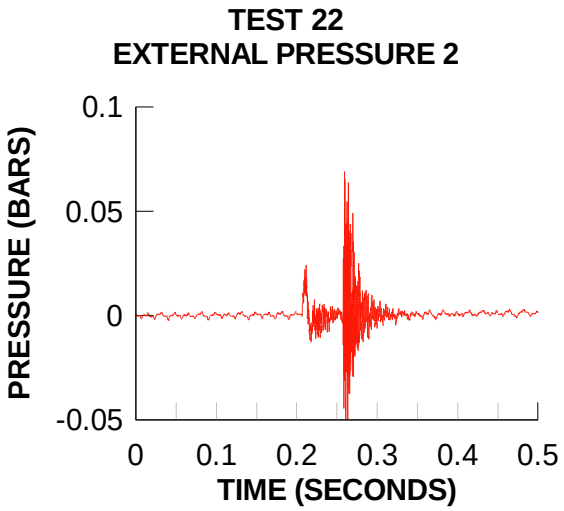
TEST 22
EXTERNAL PRESSURE 2
PRESSURE (BARS)
0.1
0.05
0
-0.05
0
0.1
0.2
0.3
0.4
0.5
TIME (SECONDS)

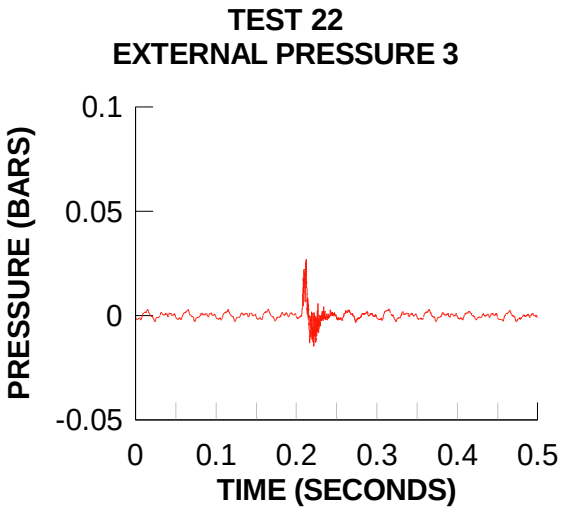
TEST 22
EXTERNAL PRESSURE 3
PRESSURE (BARS)
0.1
0.05
0
-0.05
0
0.1
0.2
0.3
0.4
0.5
TIME (SECONDS)

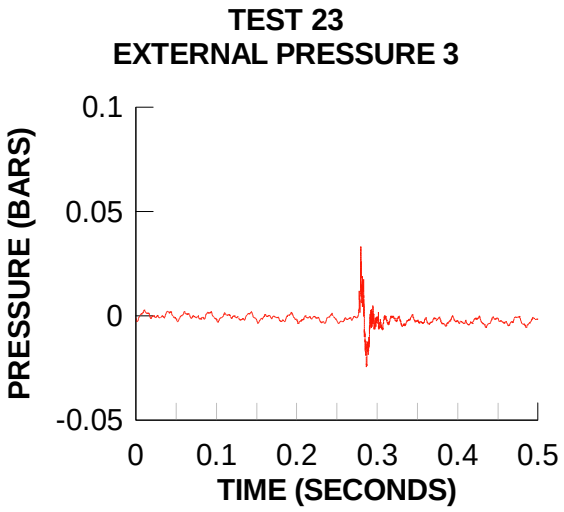
TEST 23
EXTERNAL PRESSURE 3
PRESSURE (BARS)
0.1
0.05
0
-0.05
0
0.1
0.2
0.3
0.4
0.5
TIME (SECONDS)

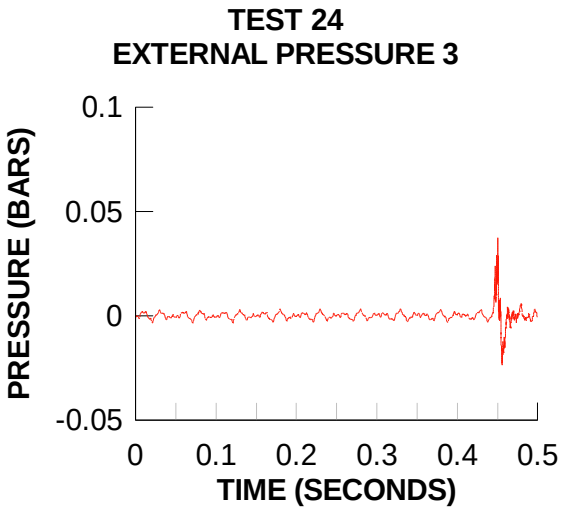
TEST 24
EXTERNAL PRESSURE 3
PRESSURE (BARS)
0.1
0.05
0
-0.05
0
0.1
0.2
0.3
0.4
0.5
TIME (SECONDS)

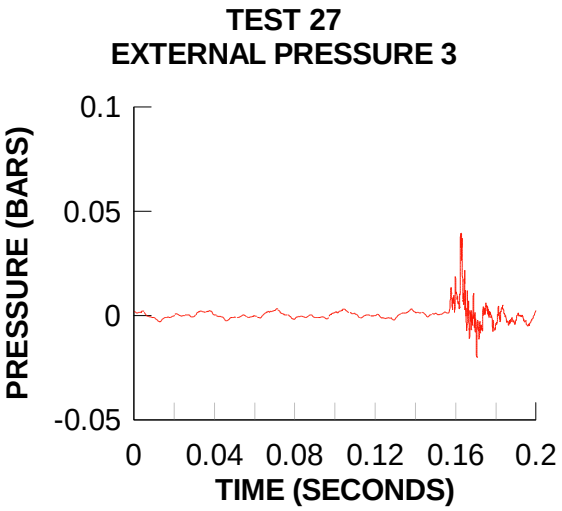
TEST 27
EXTERNAL PRESSURE 3
PRESSURE (BARS)
0.1
0.05
0
-0.05
0
0.04
0.08
0.12
0.16
0.2
TIME (SECONDS)

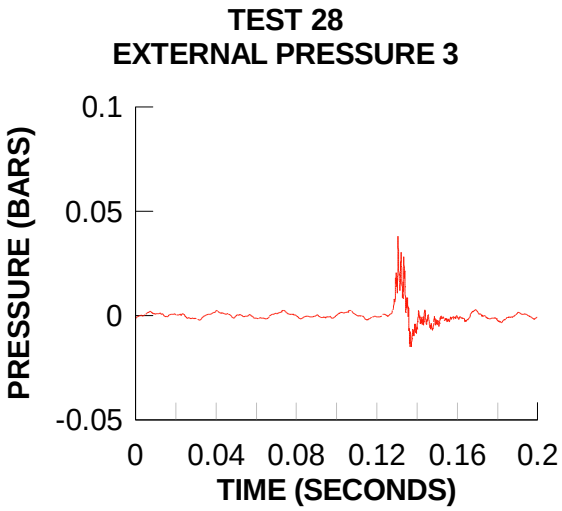
TEST 28
EXTERNAL PRESSURE 3
PRESSURE (BARS)
0.1
0.05
0
-0.05
0
0.04
0.08
0.12
0.16
0.2
TIME (SECONDS)

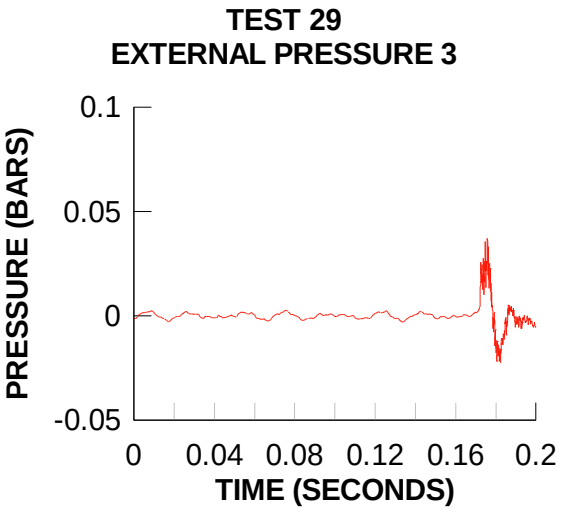
TEST 29
EXTERNAL PRESSURE 3
PRESSURE (BARS)
0.1
0.05
0
-0.05
0
0.04
0.08
0.12
0.16
0.2
TIME (SECONDS)

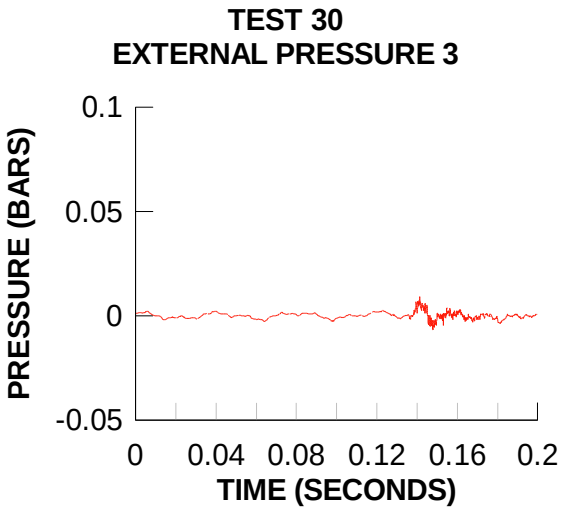
TEST 30
EXTERNAL PRESSURE 3
PRESSURE (BARS)
0.1
0.05
0
-0.05
0
0.04
0.08
0.12
0.16
0.2
TIME (SECONDS)

D.3 Thermocouples

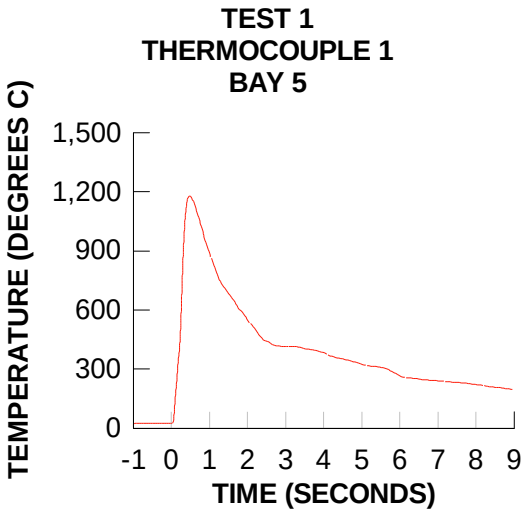
TEST 1
THERMOCOUPLE 1
BAY 5
TEMPERATURE (DEGREES C)
1,500
1,200
900
600
300
0
-1 0 1 2 3 4 5 6 7 8 9
TIME (SECONDS)

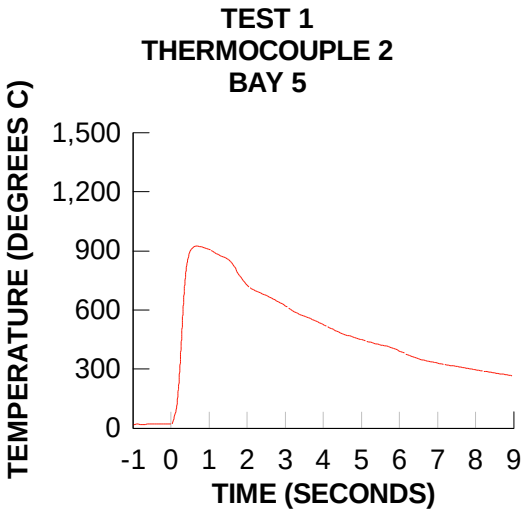
TEST 1
THERMOCOUPLE 2
BAY 5
TEMPERATURE (DEGREES C)
1,500
1,200
900
600
300
0
-1 0 1 2 3 4 5 6 7 8 9
TIME (SECONDS)

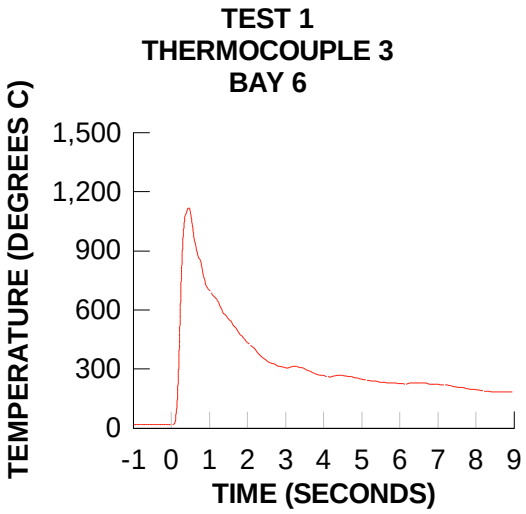
TEST 1
THERMOCOUPLE 3
BAY 6
TEMPERATURE (DEGREES C)
1,500
1,200
900
600
300
0
-1 0 1 2 3 4 5 6 7 8 9
TIME (SECONDS)

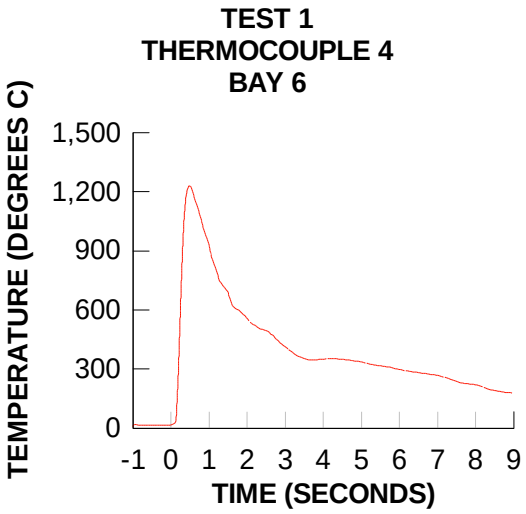
TEST 1
THERMOCOUPLE 4
BAY 6
TEMPERATURE (DEGREES C)
1,500
1,200
900
600
300
0
-1 0 1 2 3 4 5 6 7 8 9
TIME (SECONDS)

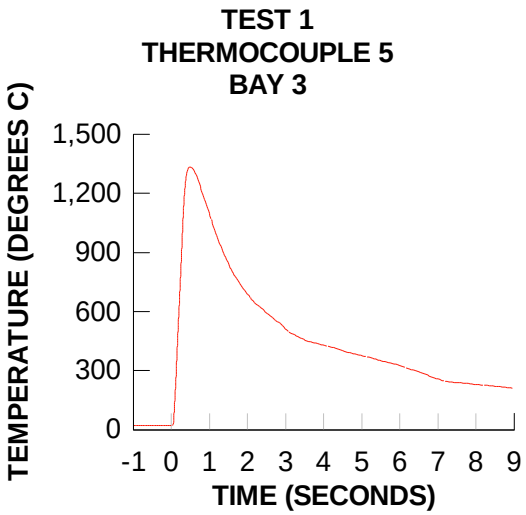
TEST 1
THERMOCOUPLE 5
BAY 3
TEMPERATURE (DEGREES C)
1,500
1,200
900
600
300
0
-1 0 1 2 3 4 5 6 7 8 9
TIME (SECONDS)

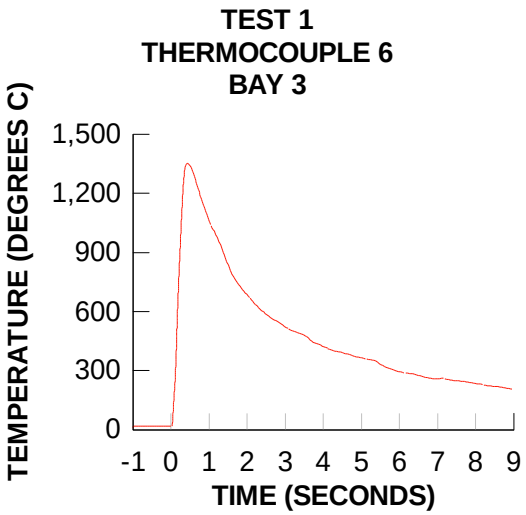
TEST 1
THERMOCOUPLE 6
BAY 3
TEMPERATURE (DEGREES C)
1,500
1,200
900
600
300
0
-1 0 1 2 3 4 5 6 7 8 9
TIME (SECONDS)

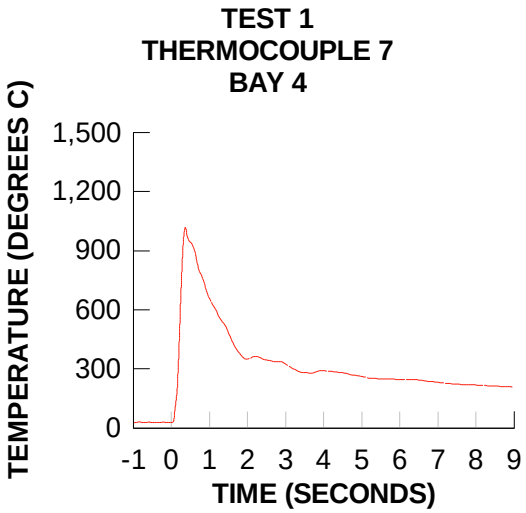
TEST 1
THERMOCOUPLE 7
BAY 4
TEMPERATURE (DEGREES C)
1,500
1,200
900
600
300
0
-1 0 1 2 3 4 5 6 7 8 9
TIME (SECONDS)

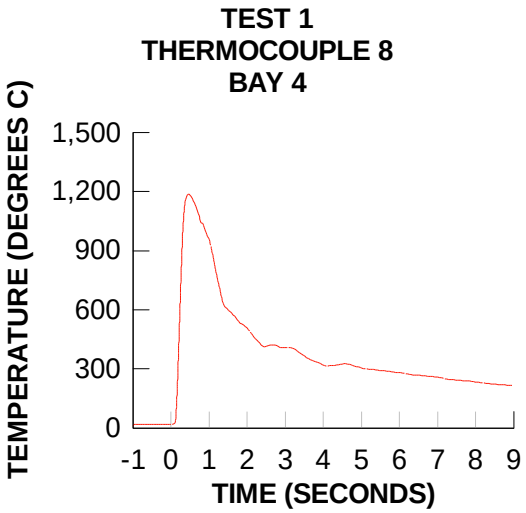
TEST 1
THERMOCOUPLE 8
BAY 4
TEMPERATURE (DEGREES C)
1,500
1,200
900
600
300
0
-1 0 1 2 3 4 5 6 7 8 9
TIME (SECONDS)

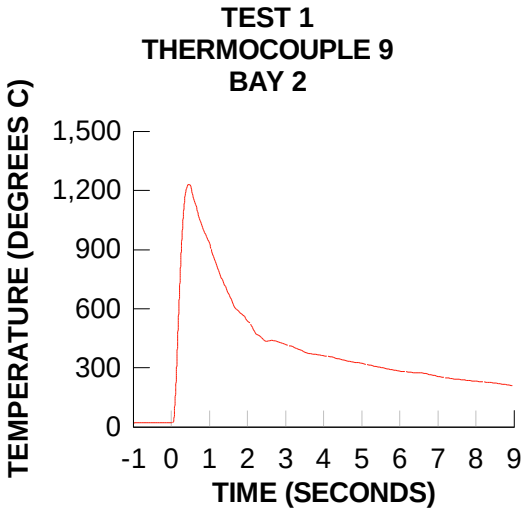
TEST 1
THERMOCOUPLE 9
BAY 2
TEMPERATURE (DEGREES C)
1,500
1,200
900
600
300
0
-1 0 1 2 3 4 5 6 7 8 9
TIME (SECONDS)

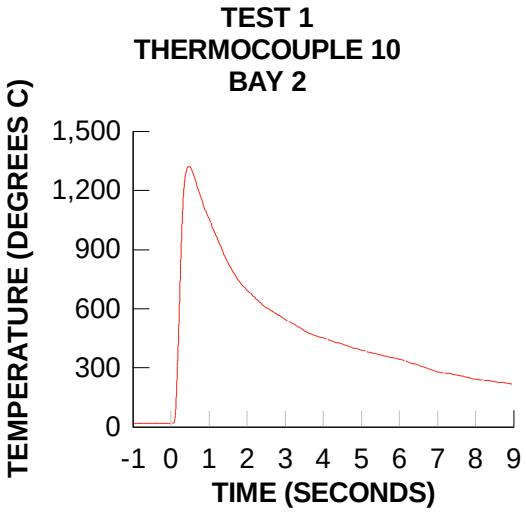
TEST 1
THERMOCOUPLE 10
BAY 2
TEMPERATURE (DEGREES C)
1,500
1,200
900
600
300
0
-1 0 1 2 3 4 5 6 7 8 9
TIME (SECONDS)

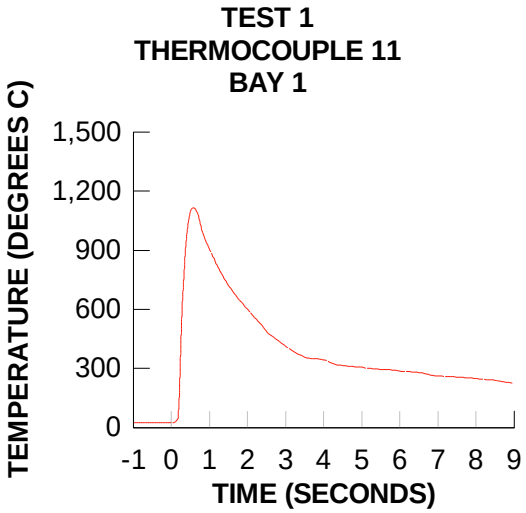
TEST 1
THERMOCOUPLE 11
BAY 1
TEMPERATURE (DEGREES C)
1,500
1,200
900
600
300
0
-1 0 1 2 3 4 5 6 7 8 9
TIME (SECONDS)

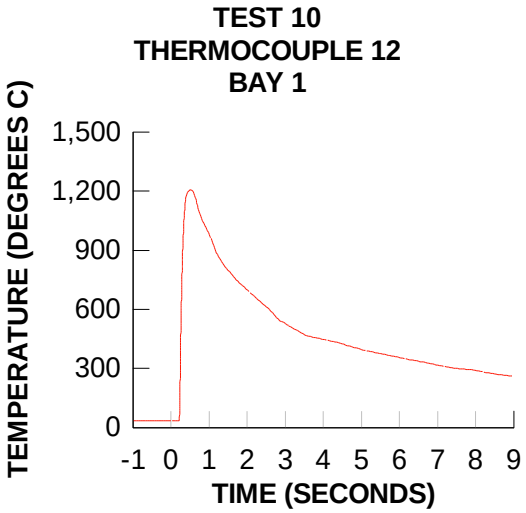
TEST 10
THERMOCOUPLE 12
BAY 1
TEMPERATURE (DEGREES C)
1,500
1,200
900
600
300
0
-1 0 1 2 3 4 5 6 7 8 9
TIME (SECONDS)

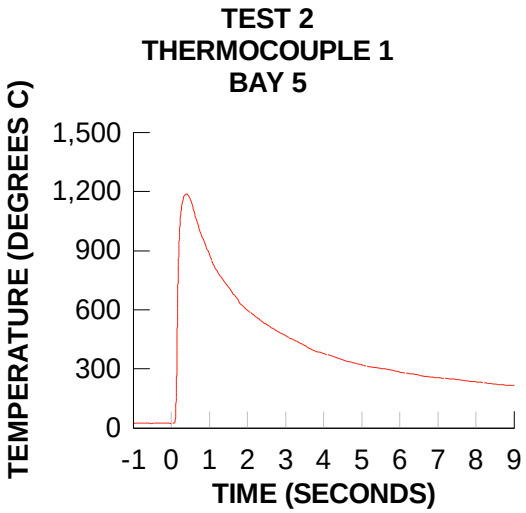
TEST 2
THERMOCOUPLE 1
BAY 5
TEMPERATURE (DEGREES C)
1,500
1,200
900
600
300
0
-1 0 1 2 3 4 5 6 7 8 9
TIME (SECONDS)

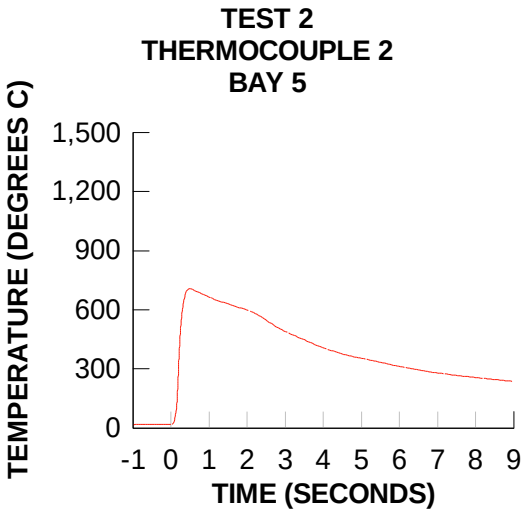
TEST 2
THERMOCOUPLE 2
BAY 5
TEMPERATURE (DEGREES C)
1,500
1,200
900
600
300
0
-1 0 1 2 3 4 5 6 7 8 9
TIME (SECONDS)

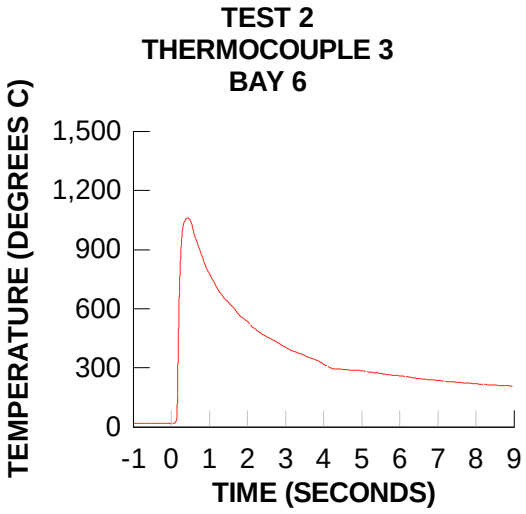
TEST 2
THERMOCOUPLE 3
BAY 6
TEMPERATURE (DEGREES C)
1,500
1,200
900
600
300
0
-1 0 1 2 3 4 5 6 7 8 9
TIME (SECONDS)

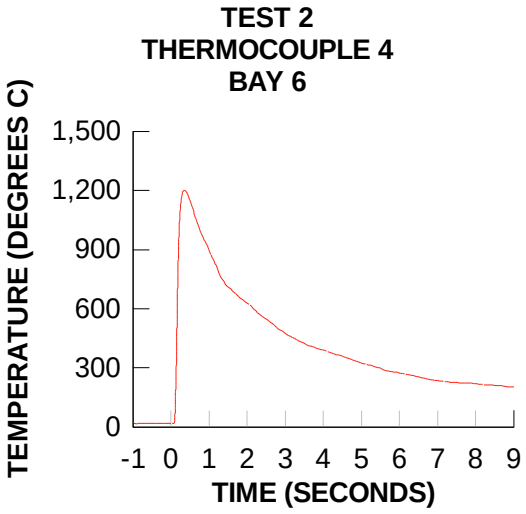
TEST 2
THERMOCOUPLE 4
BAY 6
TEMPERATURE (DEGREES C)
1,500
1,200
900
600
300
0
-1 0 1 2 3 4 5 6 7 8 9
TIME (SECONDS)

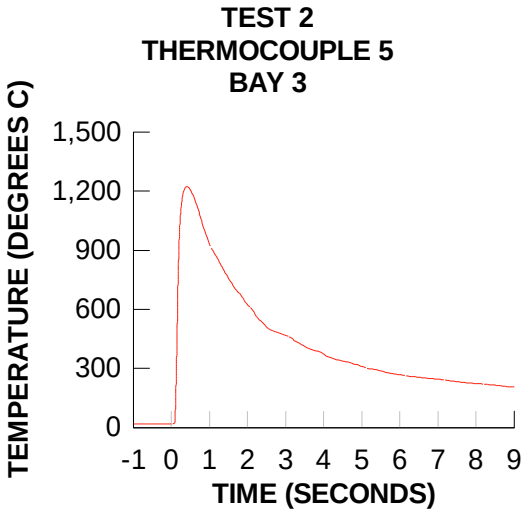
TEST 2
THERMOCOUPLE 5
BAY 3
TEMPERATURE (DEGREES C)
1,500
1,200
900
600
300
0
-1 0 1 2 3 4 5 6 7 8 9
TIME (SECONDS)

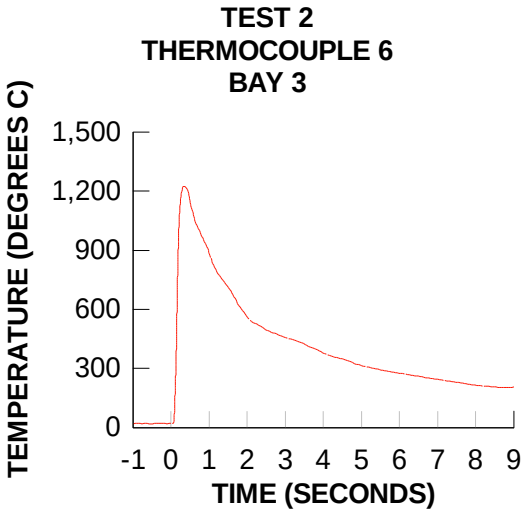
TEST 2
THERMOCOUPLE 6
BAY 3
TEMPERATURE (DEGREES C)
1,500
1,200
900
600
300
0
-1 0 1 2 3 4 5 6 7 8 9
TIME (SECONDS)

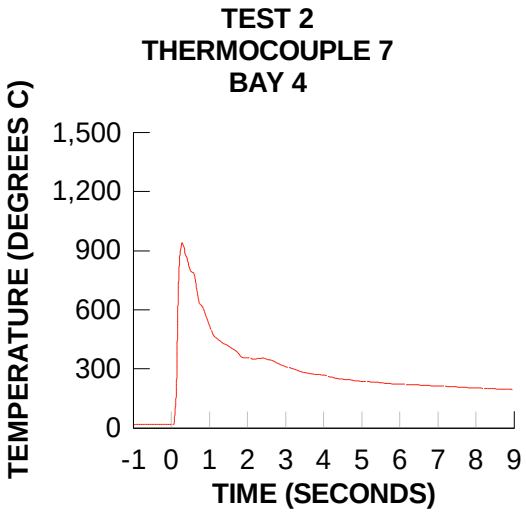
TEST 2
THERMOCOUPLE 7
BAY 4
TEMPERATURE (DEGREES C)
1,500
1,200
900
600
300
0
-1 0 1 2 3 4 5 6 7 8 9
TIME (SECONDS)

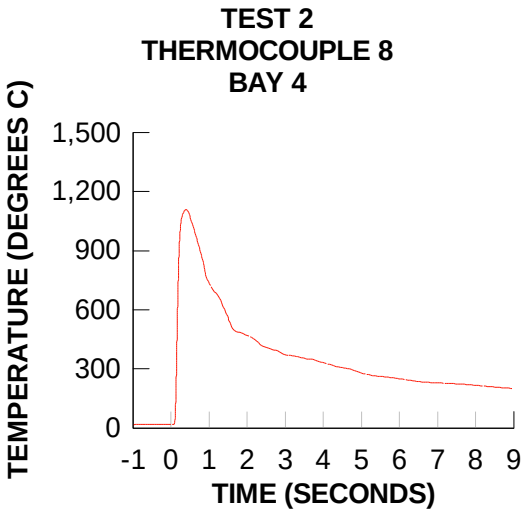
TEST 2
THERMOCOUPLE 8
BAY 4
TEMPERATURE (DEGREES C)
1,500
1,200
900
600
300
0
-1 0 1 2 3 4 5 6 7 8 9
TIME (SECONDS)

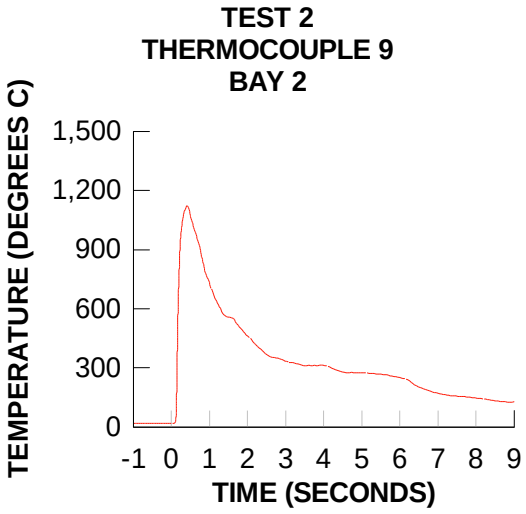
TEST 2
THERMOCOUPLE 9
BAY 2
TEMPERATURE (DEGREES C)
1,500
1,200
900
600
300
0
-1 0 1 2 3 4 5 6 7 8 9
TIME (SECONDS)

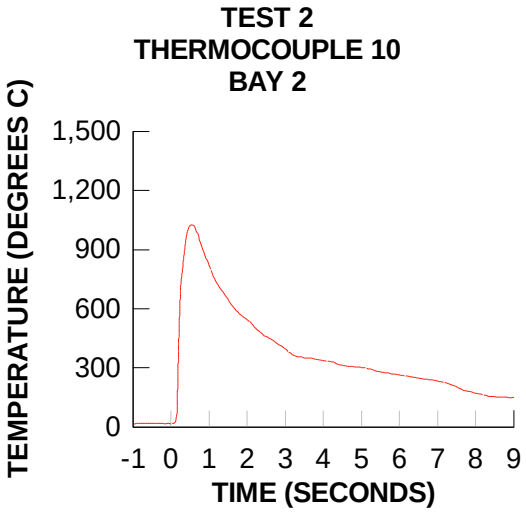
TEST 2
THERMOCOUPLE 10
BAY 2
TEMPERATURE (DEGREES C)
1,500
1,200
900
600
300
0
-1 0 1 2 3 4 5 6 7 8 9
TIME (SECONDS)

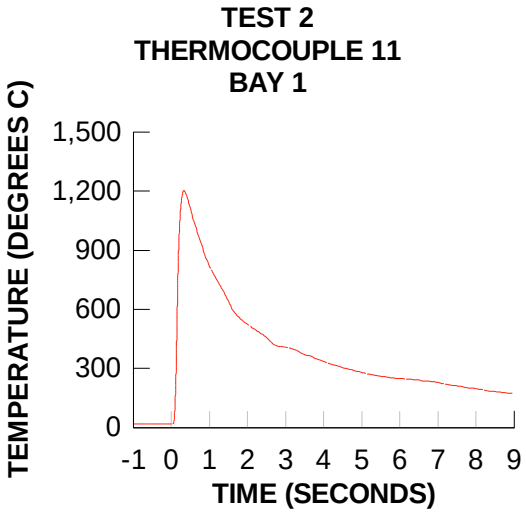
TEST 2
THERMOCOUPLE 11
BAY 1
TEMPERATURE (DEGREES C)
1,500
1,200
900
600
300
0
-1 0 1 2 3 4 5 6 7 8 9
TIME (SECONDS)

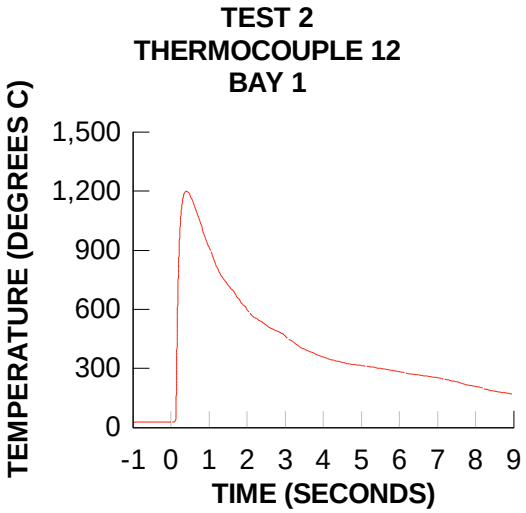
TEST 2
THERMOCOUPLE 12
BAY 1
TEMPERATURE (DEGREES C)
1,500
1,200
900
600
300
0
-1 0 1 2 3 4 5 6 7 8 9
TIME (SECONDS)

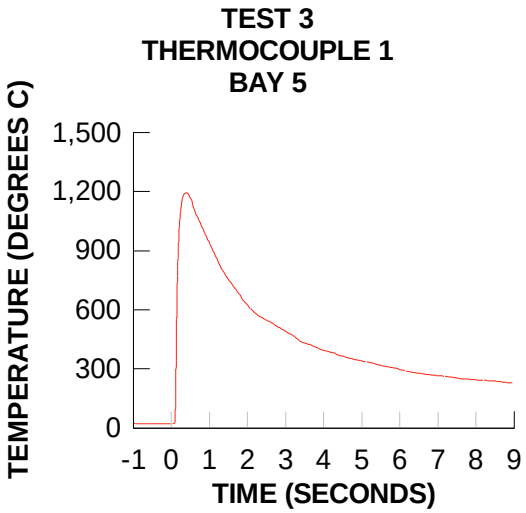
TEST 3
THERMOCOUPLE 1
BAY 5
TEMPERATURE (DEGREES C)
1,500
1,200
900
600
300
0
-1 0 1 2 3 4 5 6 7 8 9
TIME (SECONDS)

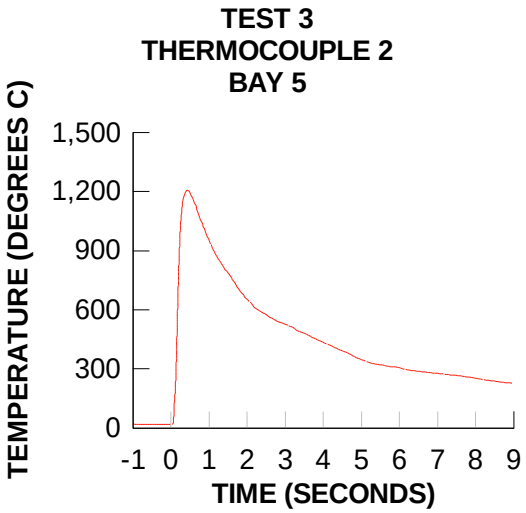
TEST 3
THERMOCOUPLE 2
BAY 5
TEMPERATURE (DEGREES C)
1,500
1,200
900
600
300
0
-1 0 1 2 3 4 5 6 7 8 9
TIME (SECONDS)

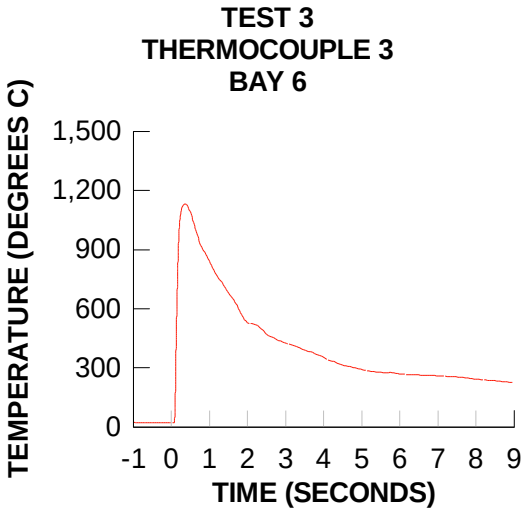
TEST 3
THERMOCOUPLE 3
BAY 6
TEMPERATURE (DEGREES C)
1,500
1,200
900
600
300
0
-1 0 1 2 3 4 5 6 7 8 9
TIME (SECONDS)

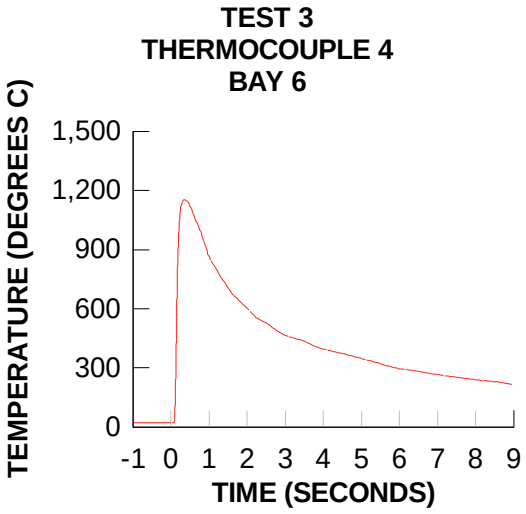
TEST 3
THERMOCOUPLE 4
BAY 6
TEMPERATURE (DEGREES C)
1,500
1,200
900
600
300
0
-1 0 1 2 3 4 5 6 7 8 9
TIME (SECONDS)

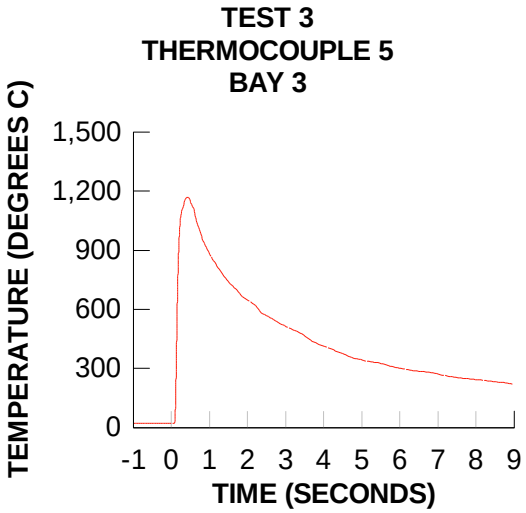
TEST 3
THERMOCOUPLE 5
BAY 3
TEMPERATURE (DEGREES C)
1,500
1,200
900
600
300
0
-1 0 1 2 3 4 5 6 7 8 9
TIME (SECONDS)

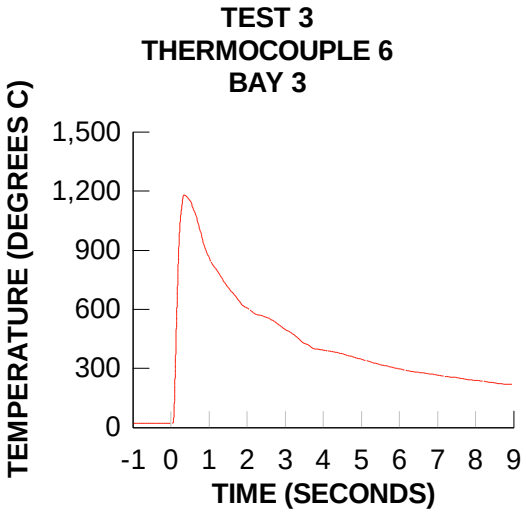
TEST 3
THERMOCOUPLE 6
BAY 3
TEMPERATURE (DEGREES C)
1,500
1,200
900
600
300
0
-1 0 1 2 3 4 5 6 7 8 9
TIME (SECONDS)

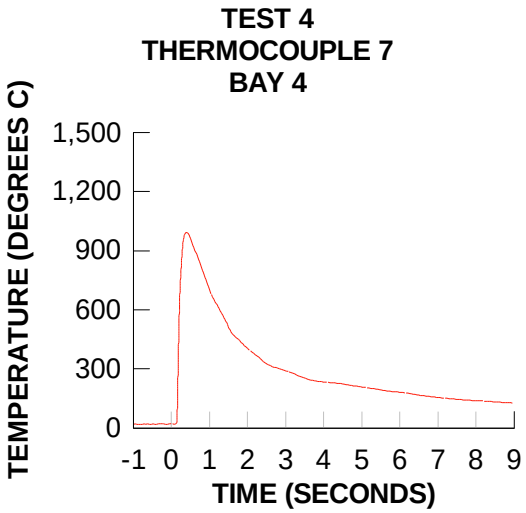
TEST 4
THERMOCOUPLE 7
BAY 4
TEMPERATURE (DEGREES C)
1,500
1,200
900
600
300
0
-1 0 1 2 3 4 5 6 7 8 9
TIME (SECONDS)

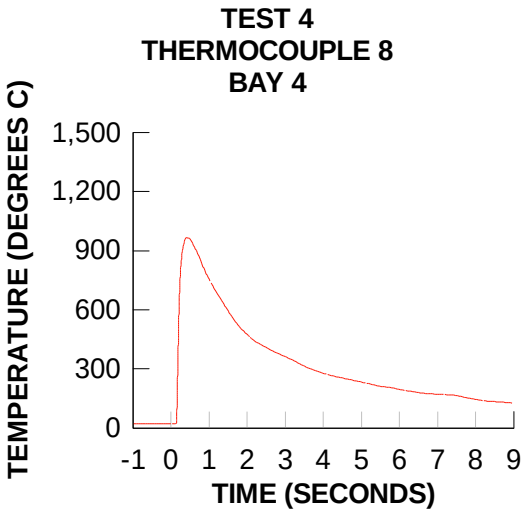
TEST 4
THERMOCOUPLE 8
BAY 4
TEMPERATURE (DEGREES C)
1,500
1,200
900
600
300
0
-1 0 1 2 3 4 5 6 7 8 9
TIME (SECONDS)

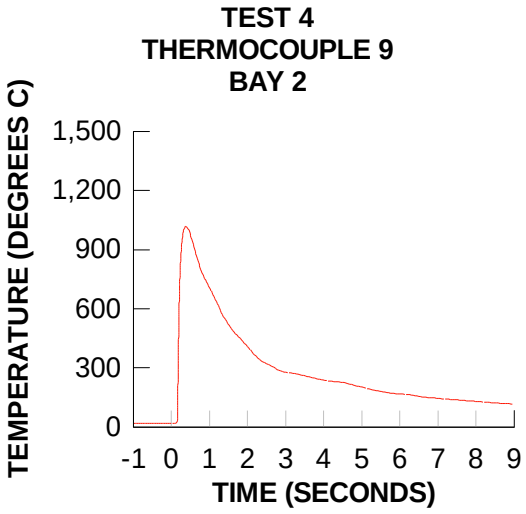
TEST 4
THERMOCOUPLE 9
BAY 2
TEMPERATURE (DEGREES C)
1,500
1,200
900
600
300
0
-1 0 1 2 3 4 5 6 7 8 9
TIME (SECONDS)

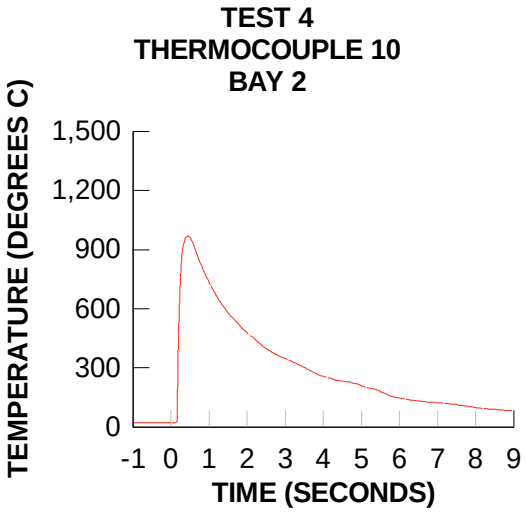
TEST 4
THERMOCOUPLE 10
BAY 2
TEMPERATURE (DEGREES C)
1,500
1,200
900
600
300
0
-1 0 1 2 3 4 5 6 7 8 9
TIME (SECONDS)

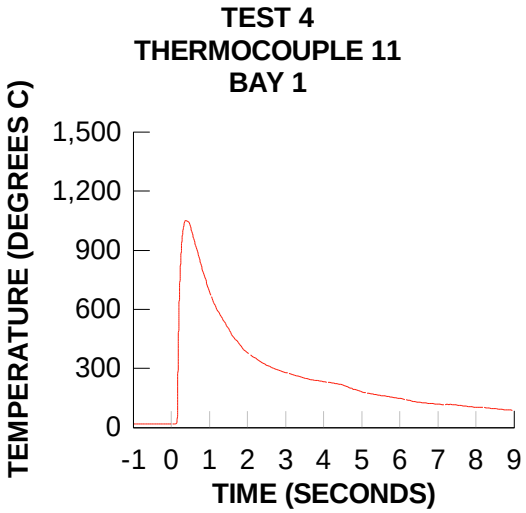
TEST 4
THERMOCOUPLE 11
BAY 1
TEMPERATURE (DEGREES C)
1,500
1,200
900
600
300
0
-1 0 1 2 3 4 5 6 7 8 9
TIME (SECONDS)

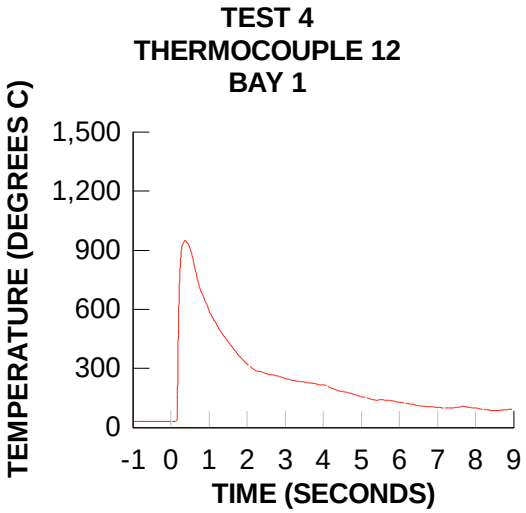
TEST 4
THERMOCOUPLE 12
BAY 1
TEMPERATURE (DEGREES C)
1,500
1,200
900
600
300
0
-1 0 1 2 3 4 5 6 7 8 9
TIME (SECONDS)

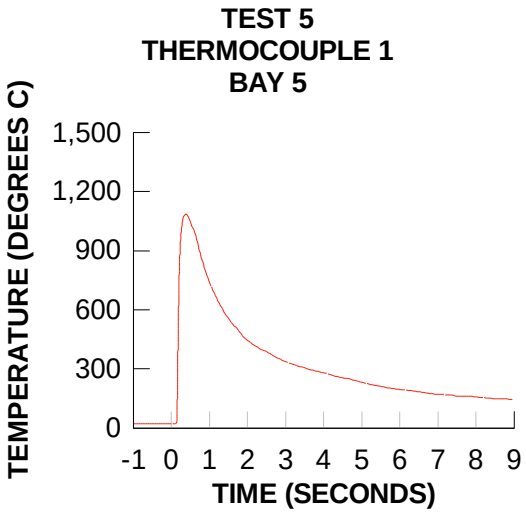
TEST 5
THERMOCOUPLE 1
BAY 5
TEMPERATURE (DEGREES C)
1,500
1,200
900
600
300
0
-1 0 1 2 3 4 5 6 7 8 9
TIME (SECONDS)

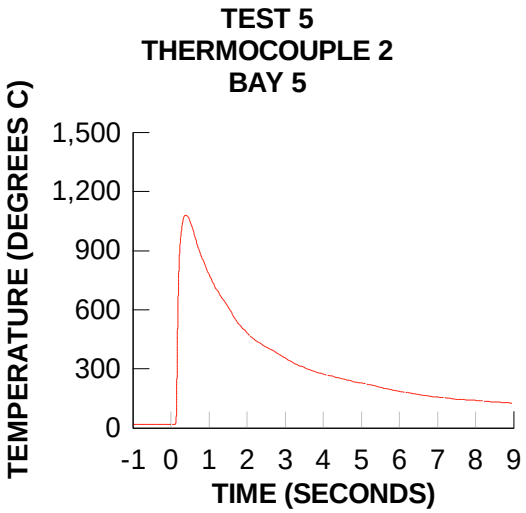
TEST 5
THERMOCOUPLE 2
BAY 5
TEMPERATURE (DEGREES C)
1,500
1,200
900
600
300
0
-1 0 1 2 3 4 5 6 7 8 9
TIME (SECONDS)

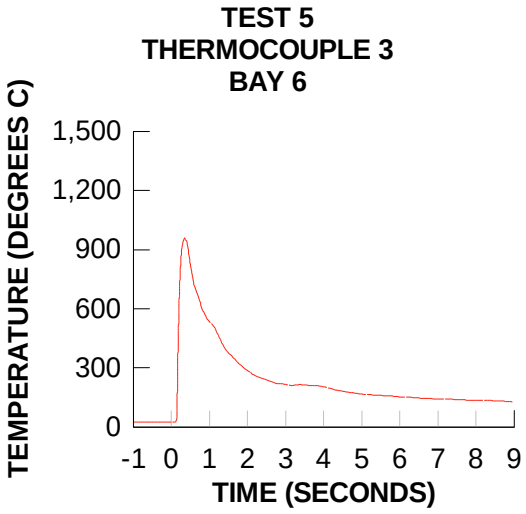
TEST 5
THERMOCOUPLE 3
BAY 6
TEMPERATURE (DEGREES C)
1,500
1,200
900
600
300
0
-1 0 1 2 3 4 5 6 7 8 9
TIME (SECONDS)

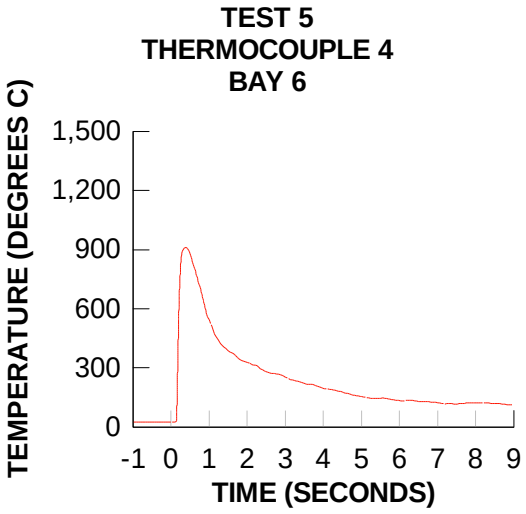
TEST 5
THERMOCOUPLE 4
BAY 6
TEMPERATURE (DEGREES C)
1,500
1,200
900
600
300
0
-1 0 1 2 3 4 5 6 7 8 9
TIME (SECONDS)

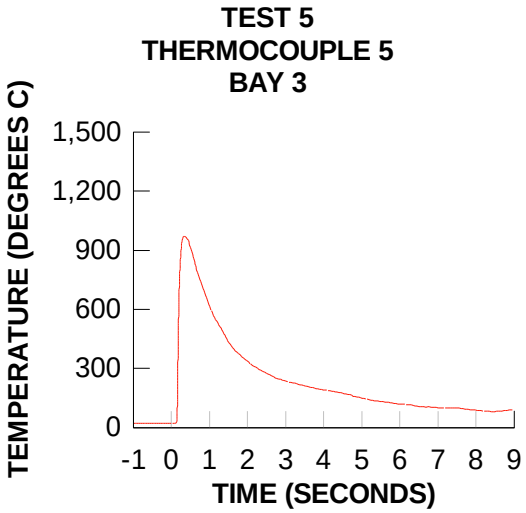
TEST 5
THERMOCOUPLE 5
BAY 3
TEMPERATURE (DEGREES C)
1,500
1,200
900
600
300
0
-1 0 1 2 3 4 5 6 7 8 9
TIME (SECONDS)

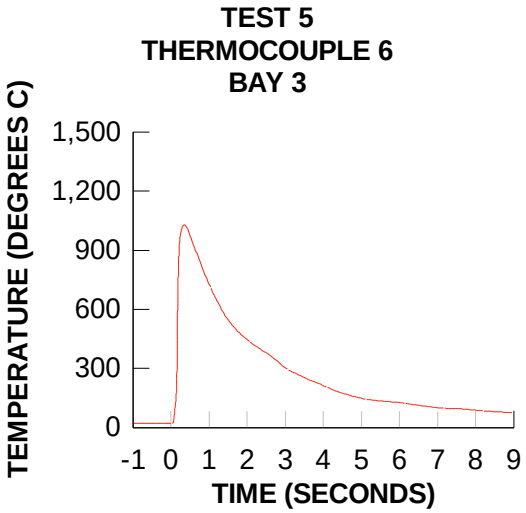
TEST 5
THERMOCOUPLE 6
BAY 3
TEMPERATURE (DEGREES C)
1,500
1,200
900
600
300
0
-1 0 1 2 3 4 5 6 7 8 9
TIME (SECONDS)

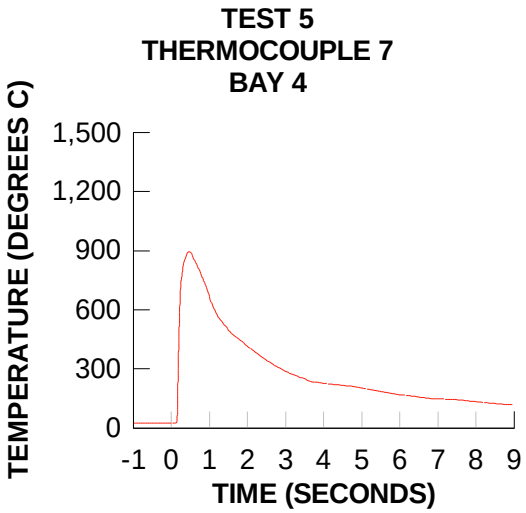
TEST 5
THERMOCOUPLE 7
BAY 4
TEMPERATURE (DEGREES C)
1,500
1,200
900
600
300
0
-1 0 1 2 3 4 5 6 7 8 9
TIME (SECONDS)

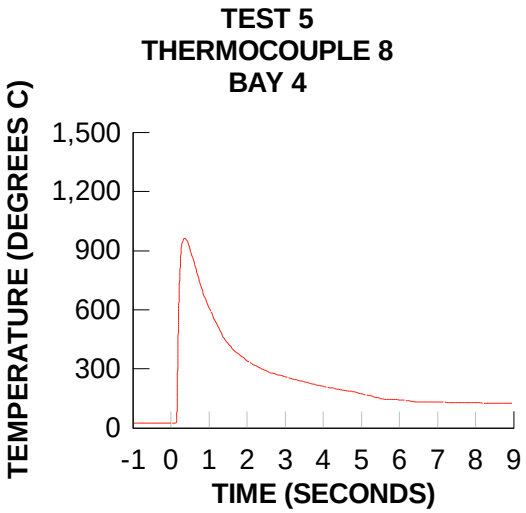
TEST 5
THERMOCOUPLE 8
BAY 4
TEMPERATURE (DEGREES C)
1,500
1,200
900
600
300
0
-1 0 1 2 3 4 5 6 7 8 9
TIME (SECONDS)

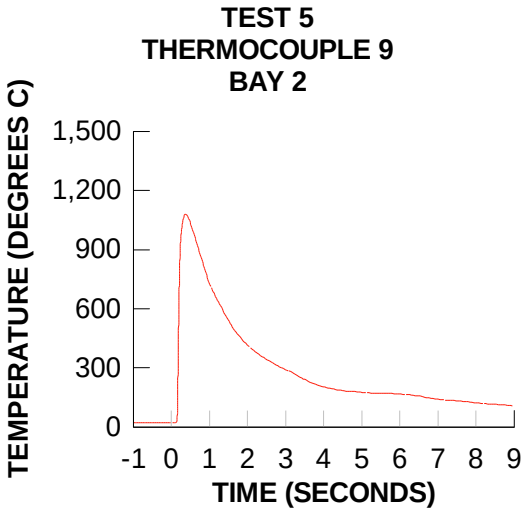
TEST 5
THERMOCOUPLE 9
BAY 2
TEMPERATURE (DEGREES C)
1,500
1,200
900
600
300
0
-1 0 1 2 3 4 5 6 7 8 9
TIME (SECONDS)

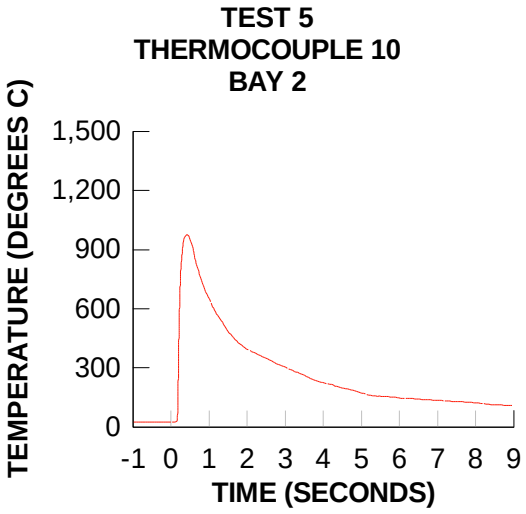
TEST 5
THERMOCOUPLE 10
BAY 2
TEMPERATURE (DEGREES C)
1,500
1,200
900
600
300
0
-1 0 1 2 3 4 5 6 7 8 9
TIME (SECONDS)

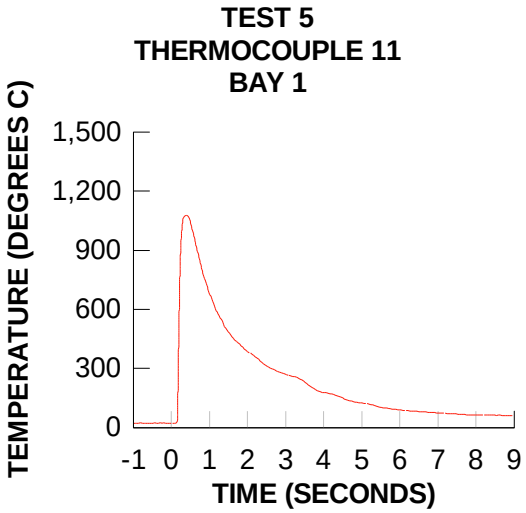
TEST 5
THERMOCOUPLE 11
BAY 1
TEMPERATURE (DEGREES C)
1,500
1,200
900
600
300
0
-1 0 1 2 3 4 5 6 7 8 9
TIME (SECONDS)

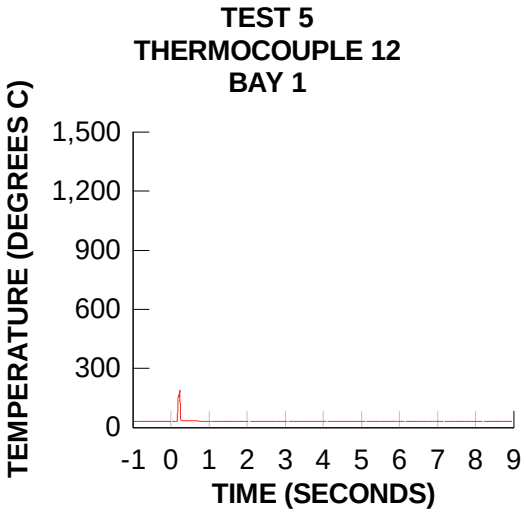
TEST 5
THERMOCOUPLE 12
BAY 1
TEMPERATURE (DEGREES C)
1,500
1,200
900
600
300
0
-1 0 1 2 3 4 5 6 7 8 9
TIME (SECONDS)

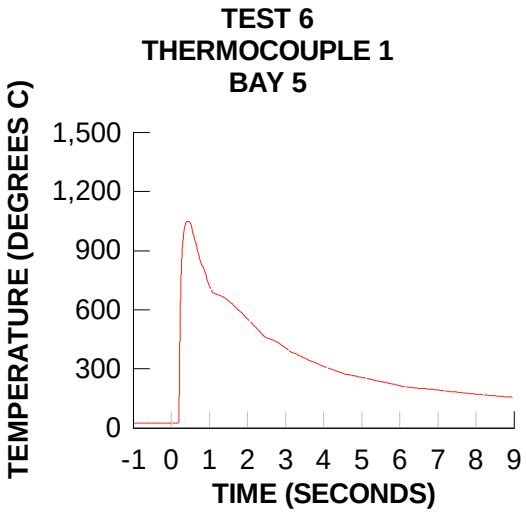
TEST 6
THERMOCOUPLE 1
BAY 5
TEMPERATURE (DEGREES C)
1,500
1,200
900
600
300
0
-1 0 1 2 3 4 5 6 7 8 9
TIME (SECONDS)

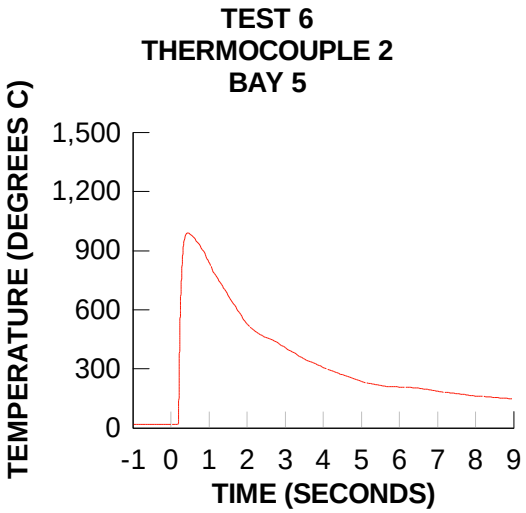
TEST 6
THERMOCOUPLE 2
BAY 5
TEMPERATURE (DEGREES C)
1,500
1,200
900
600
300
0
-1 0 1 2 3 4 5 6 7 8 9
TIME (SECONDS)

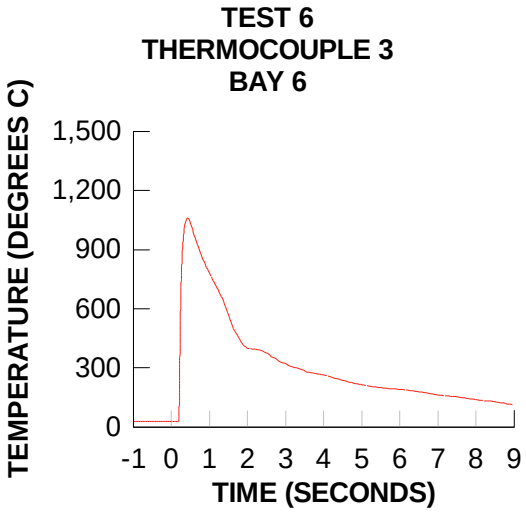
TEST 6
THERMOCOUPLE 3
BAY 6
TEMPERATURE (DEGREES C)
1,500
1,200
900
600
300
0
-1 0 1 2 3 4 5 6 7 8 9
TIME (SECONDS)

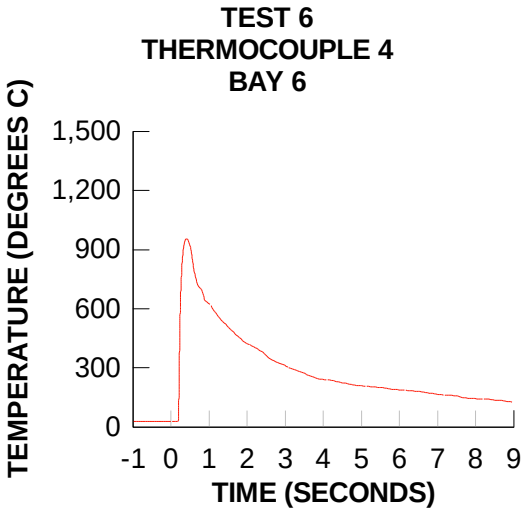
TEST 6
THERMOCOUPLE 4
BAY 6
TEMPERATURE (DEGREES C)
1,500
1,200
900
600
300
0
-1 0 1 2 3 4 5 6 7 8 9
TIME (SECONDS)

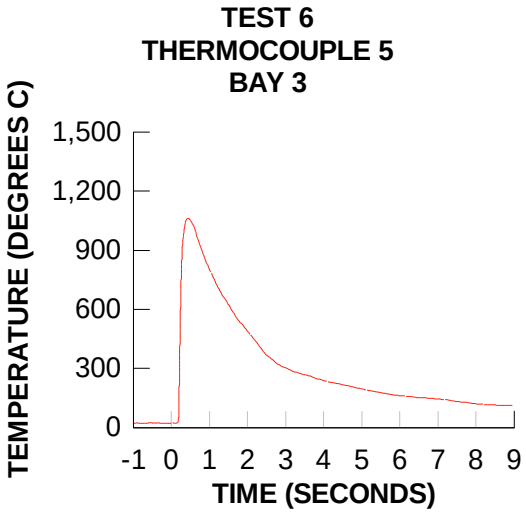
TEST 6
THERMOCOUPLE 5
BAY 3
TEMPERATURE (DEGREES C)
1,500
1,200
900
600
300
0
-1 0 1 2 3 4 5 6 7 8 9
TIME (SECONDS)

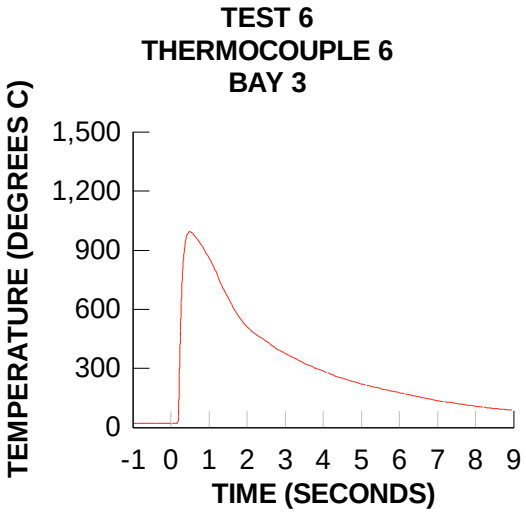
TEST 6
THERMOCOUPLE 6
BAY 3
TEMPERATURE (DEGREES C)
1,500
1,200
900
600
300
0
-1 0 1 2 3 4 5 6 7 8 9
TIME (SECONDS)

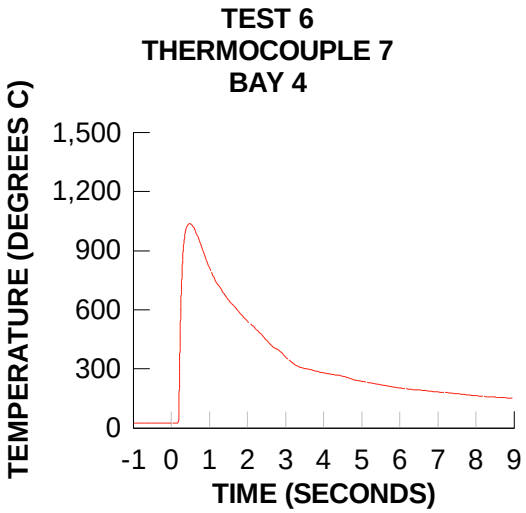
TEST 6
THERMOCOUPLE 7
BAY 4
TEMPERATURE (DEGREES C)
1,500
1,200
900
600
300
0
-1 0 1 2 3 4 5 6 7 8 9
TIME (SECONDS)

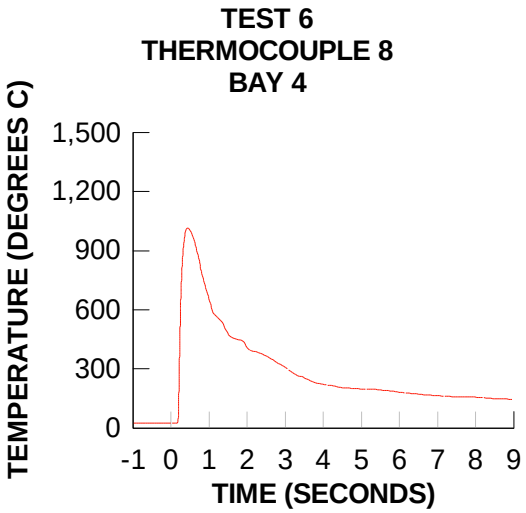
TEST 6
THERMOCOUPLE 8
BAY 4
TEMPERATURE (DEGREES C)
1,500
1,200
900
600
300
0
-1 0 1 2 3 4 5 6 7 8 9
TIME (SECONDS)

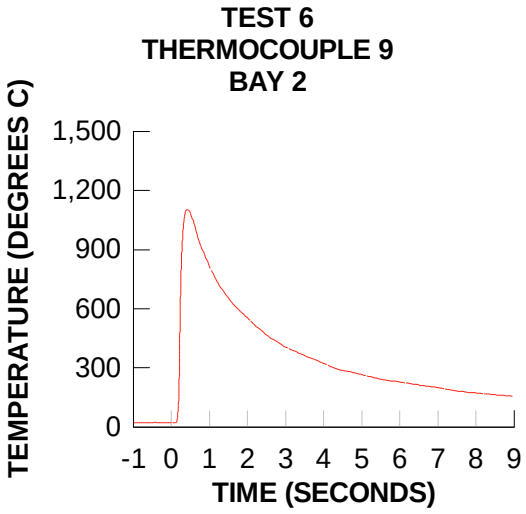
TEST 6
THERMOCOUPLE 9
BAY 2
TEMPERATURE (DEGREES C)
1,500
1,200
900
600
300
0
-1 0 1 2 3 4 5 6 7 8 9
TIME (SECONDS)

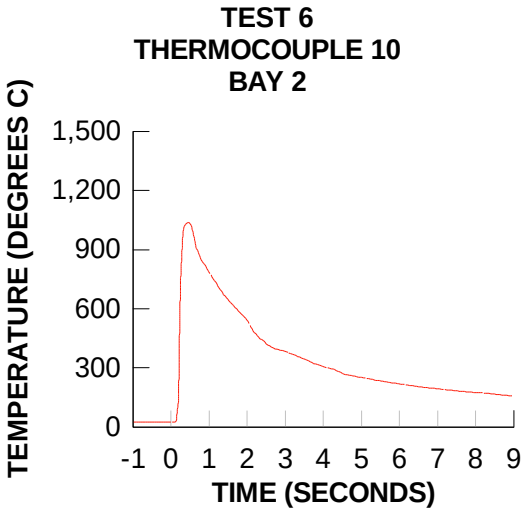
TEST 6
THERMOCOUPLE 10
BAY 2
TEMPERATURE (DEGREES C)
1,500
1,200
900
600
300
0
-1 0 1 2 3 4 5 6 7 8 9
TIME (SECONDS)

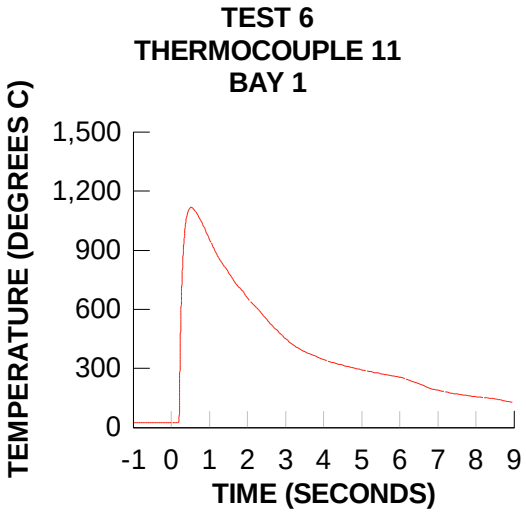
TEST 6
THERMOCOUPLE 11
BAY 1
TEMPERATURE (DEGREES C)
1,500
1,200
900
600
300
0
-1 0 1 2 3 4 5 6 7 8 9
TIME (SECONDS)

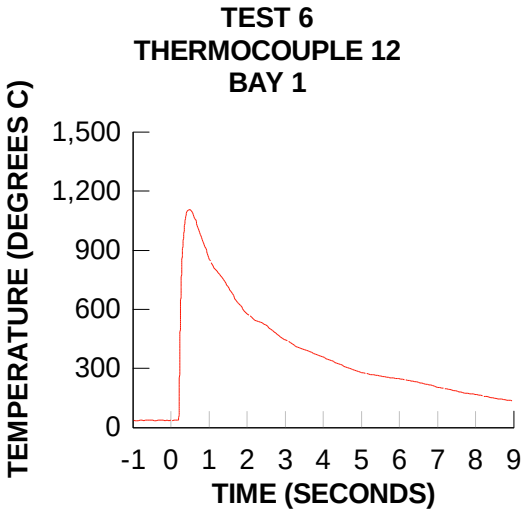
TEST 6
THERMOCOUPLE 12
BAY 1
TEMPERATURE (DEGREES C)
1,500
1,200
900
600
300
0
-1 0 1 2 3 4 5 6 7 8 9
TIME (SECONDS)

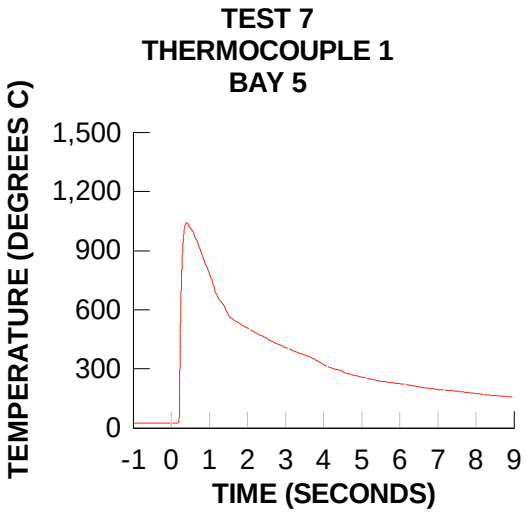
TEST 7
THERMOCOUPLE 1
BAY 5
TEMPERATURE (DEGREES C)
1,500
1,200
900
600
300
0
-1 0 1 2 3 4 5 6 7 8 9
TIME (SECONDS)

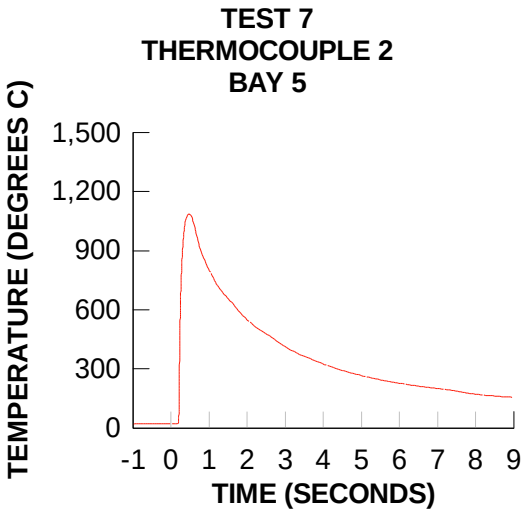
TEST 7
THERMOCOUPLE 2
BAY 5
TEMPERATURE (DEGREES C)
1,500
1,200
900
600
300
0
-1 0 1 2 3 4 5 6 7 8 9
TIME (SECONDS)

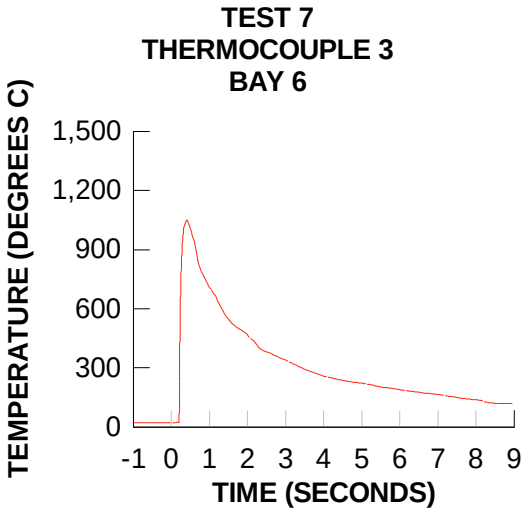
TEST 7
THERMOCOUPLE 3
BAY 6
TEMPERATURE (DEGREES C)
1,500
1,200
900
600
300
0
-1 0 1 2 3 4 5 6 7 8 9
TIME (SECONDS)

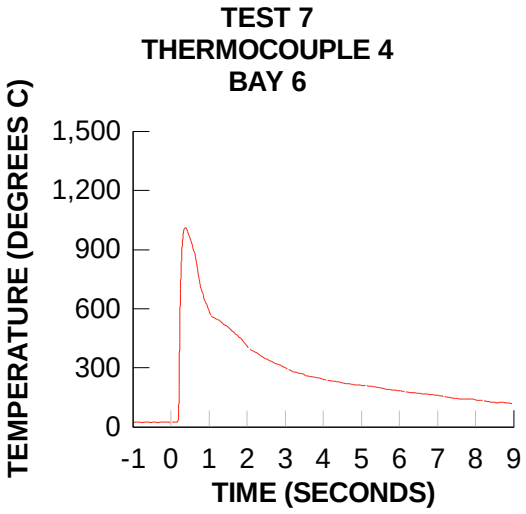
TEST 7
THERMOCOUPLE 4
BAY 6
TEMPERATURE (DEGREES C)
1,500
1,200
900
600
300
0
-1 0 1 2 3 4 5 6 7 8 9
TIME (SECONDS)

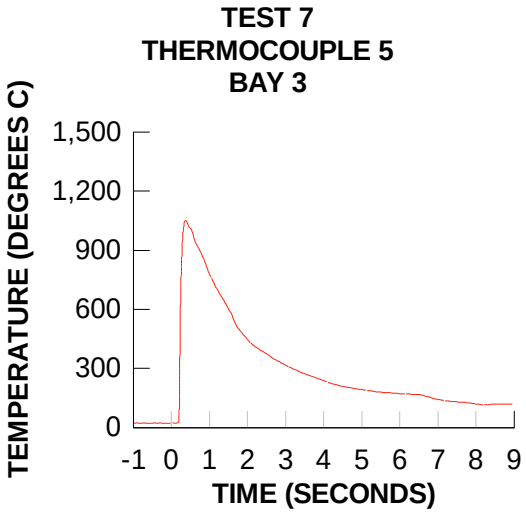
TEST 7
THERMOCOUPLE 5
BAY 3
TEMPERATURE (DEGREES C)
1,500
1,200
900
600
300
0
-1 0 1 2 3 4 5 6 7 8 9
TIME (SECONDS)

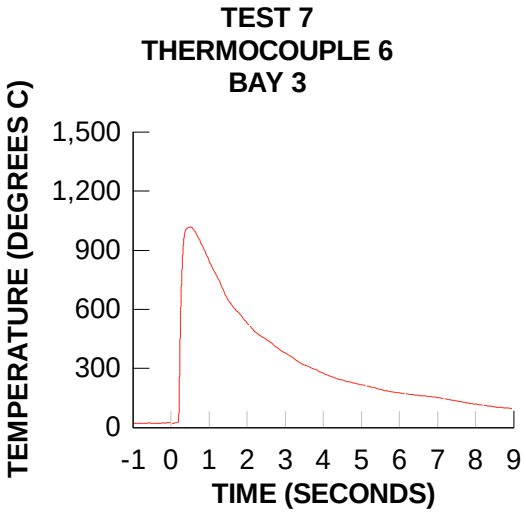
TEST 7
THERMOCOUPLE 6
BAY 3
TEMPERATURE (DEGREES C)
1,500
1,200
900
600
300
0
-1 0 1 2 3 4 5 6 7 8 9
TIME (SECONDS)

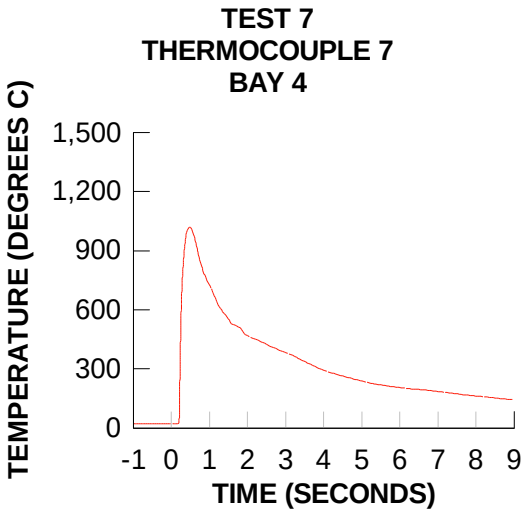
TEST 7
THERMOCOUPLE 7
BAY 4
TEMPERATURE (DEGREES C)
1,500
1,200
900
600
300
0
-1 0 1 2 3 4 5 6 7 8 9
TIME (SECONDS)

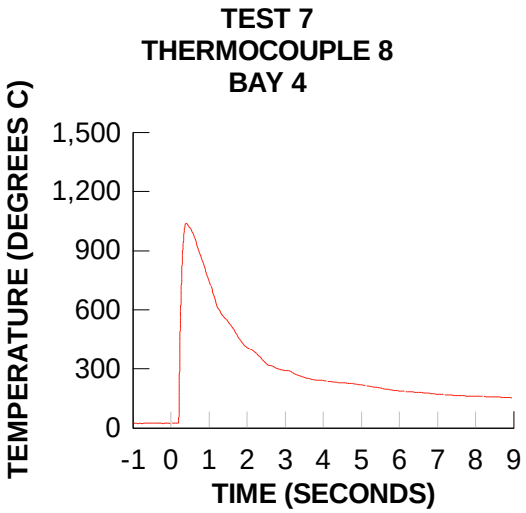
TEST 7
THERMOCOUPLE 8
BAY 4
TEMPERATURE (DEGREES C)
1,500
1,200
900
600
300
0
-1 0 1 2 3 4 5 6 7 8 9
TIME (SECONDS)

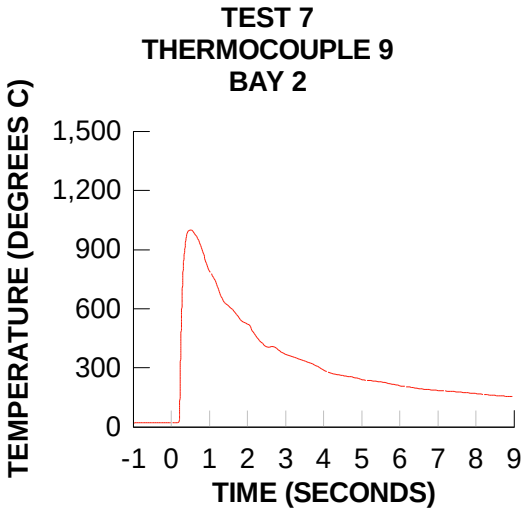
TEST 7
THERMOCOUPLE 9
BAY 2
TEMPERATURE (DEGREES C)
1,500
1,200
900
600
300
0
-1 0 1 2 3 4 5 6 7 8 9
TIME (SECONDS)

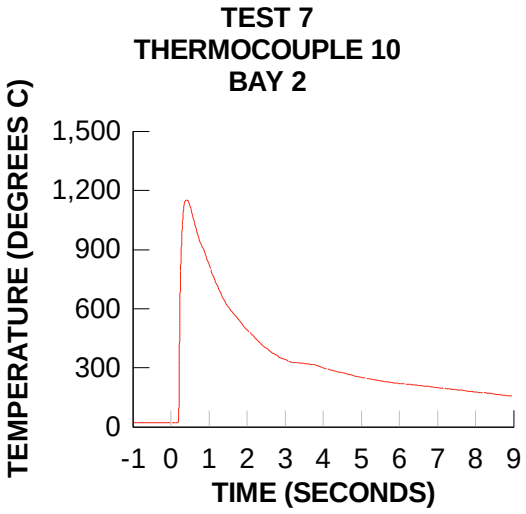
TEST 7
THERMOCOUPLE 10
BAY 2
TEMPERATURE (DEGREES C)
1,500
1,200
900
600
300
0
-1 0 1 2 3 4 5 6 7 8 9
TIME (SECONDS)

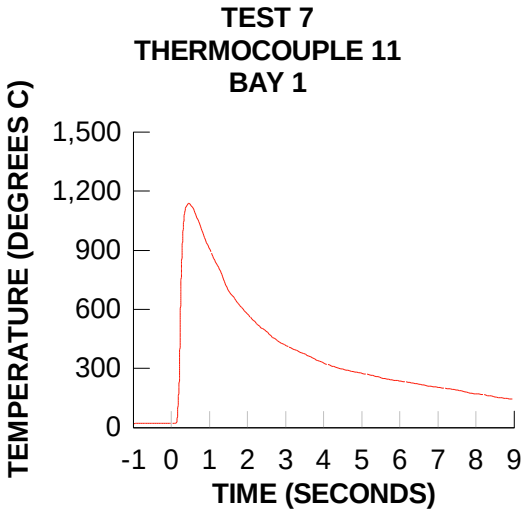
TEST 7
THERMOCOUPLE 11
BAY 1
TEMPERATURE (DEGREES C)
1,500
1,200
900
600
300
0
-1 0 1 2 3 4 5 6 7 8 9
TIME (SECONDS)

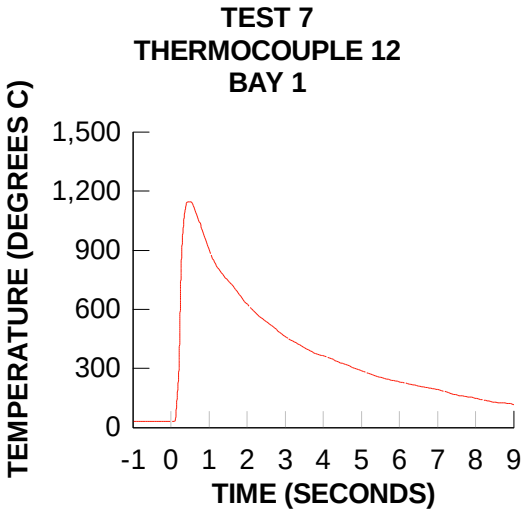
TEST 7
THERMOCOUPLE 12
BAY 1
TEMPERATURE (DEGREES C)
1,500
1,200
900
600
300
0
-1 0 1 2 3 4 5 6 7 8 9
TIME (SECONDS)

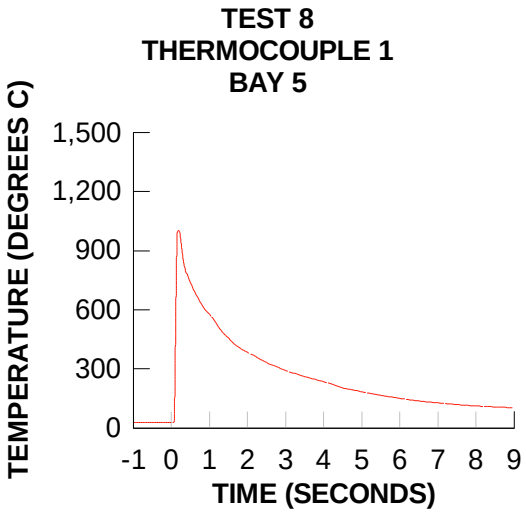
TEST 8
THERMOCOUPLE 1
BAY 5
TEMPERATURE (DEGREES C)
1,500
1,200
900
600
300
0
-1 0 1 2 3 4 5 6 7 8 9
TIME (SECONDS)

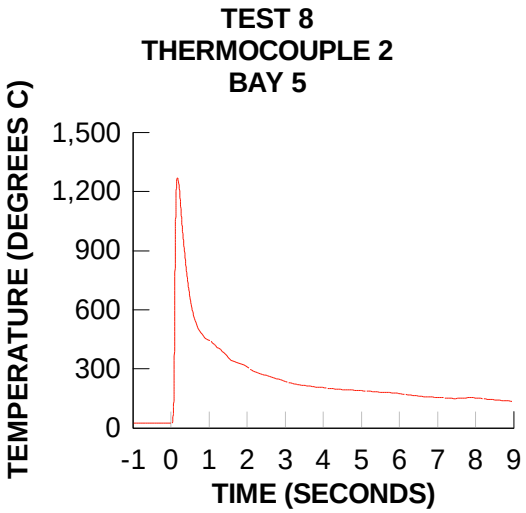
TEST 8
THERMOCOUPLE 2
BAY 5
TEMPERATURE (DEGREES C)
1,500
1,200
900
600
300
0
-1 0 1 2 3 4 5 6 7 8 9
TIME (SECONDS)

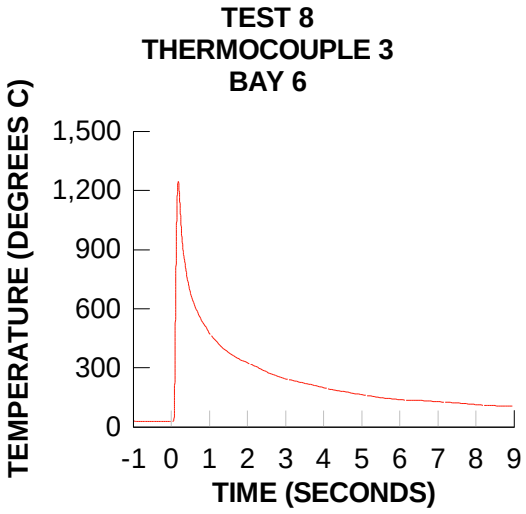
TEST 8
THERMOCOUPLE 3
BAY 6
TEMPERATURE (DEGREES C)
1,500
1,200
900
600
300
0
-1 0 1 2 3 4 5 6 7 8 9
TIME (SECONDS)

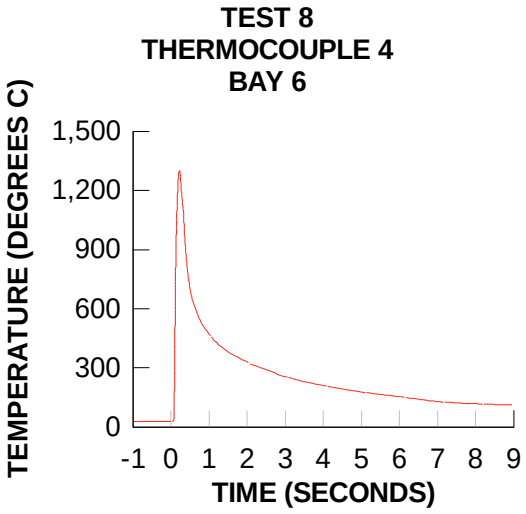
TEST 8
THERMOCOUPLE 4
BAY 6
TEMPERATURE (DEGREES C)
1,500
1,200
900
600
300
0
-1 0 1 2 3 4 5 6 7 8 9
TIME (SECONDS)

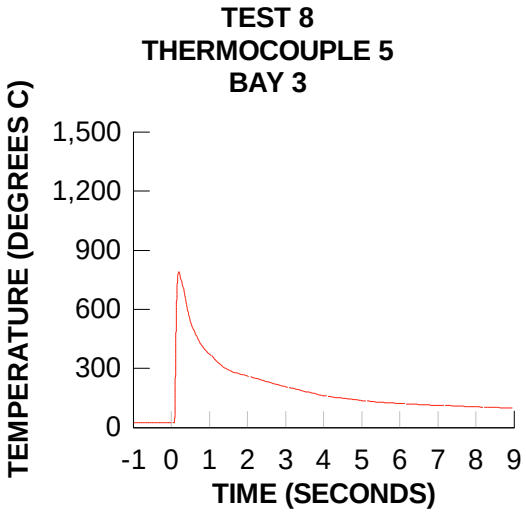
TEST 8
THERMOCOUPLE 5
BAY 3
TEMPERATURE (DEGREES C)
1,500
1,200
900
600
300
0
-1 0 1 2 3 4 5 6 7 8 9
TIME (SECONDS)

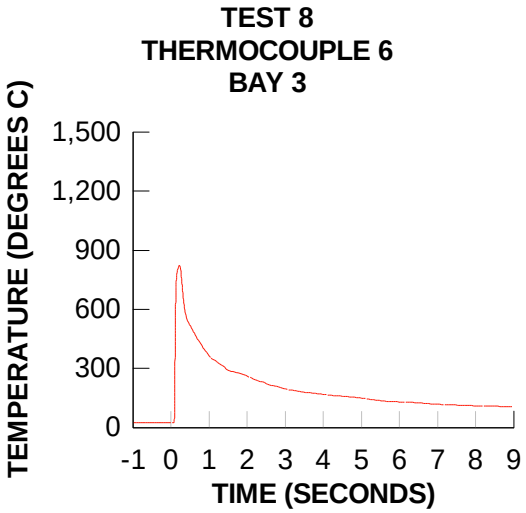
TEST 8
THERMOCOUPLE 6
BAY 3
TEMPERATURE (DEGREES C)
1,500
1,200
900
600
300
0
-1 0 1 2 3 4 5 6 7 8 9
TIME (SECONDS)

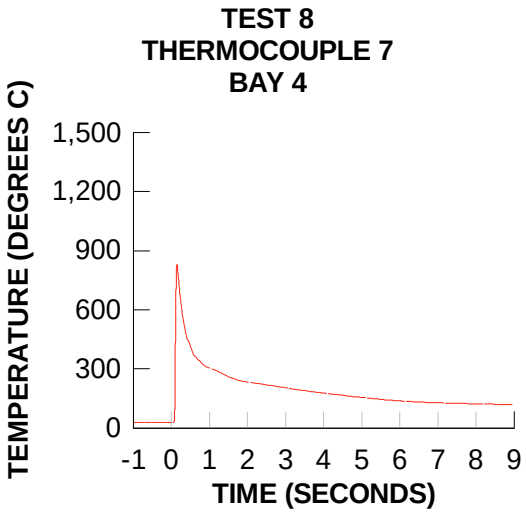
TEST 8
THERMOCOUPLE 7
BAY 4
TEMPERATURE (DEGREES C)
1,500
1,200
900
600
300
0
-1 0 1 2 3 4 5 6 7 8 9
TIME (SECONDS)

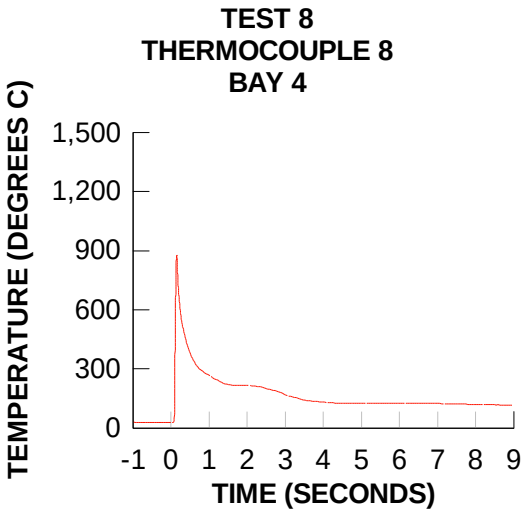
TEST 8
THERMOCOUPLE 8
BAY 4
TEMPERATURE (DEGREES C)
1,500
1,200
900
600
300
0
-1 0 1 2 3 4 5 6 7 8 9
TIME (SECONDS)

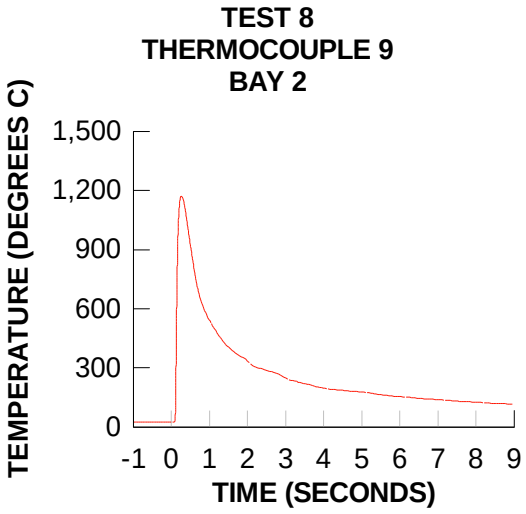
TEST 8
THERMOCOUPLE 9
BAY 2
TEMPERATURE (DEGREES C)
1,500
1,200
900
600
300
0
-1 0 1 2 3 4 5 6 7 8 9
TIME (SECONDS)

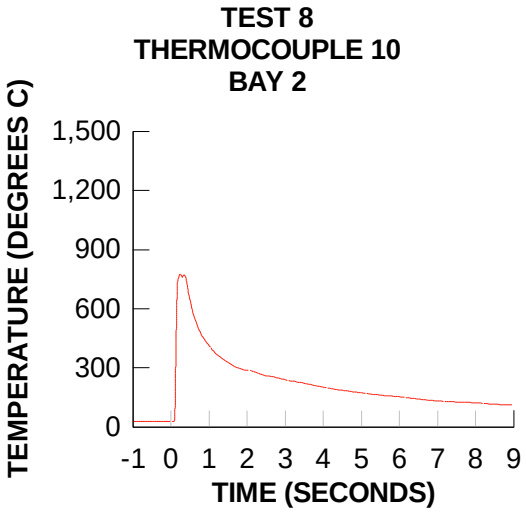
TEST 8
THERMOCOUPLE 10
BAY 2
TEMPERATURE (DEGREES C)
1,500
1,200
900
600
300
0
-1 0 1 2 3 4 5 6 7 8 9
TIME (SECONDS)

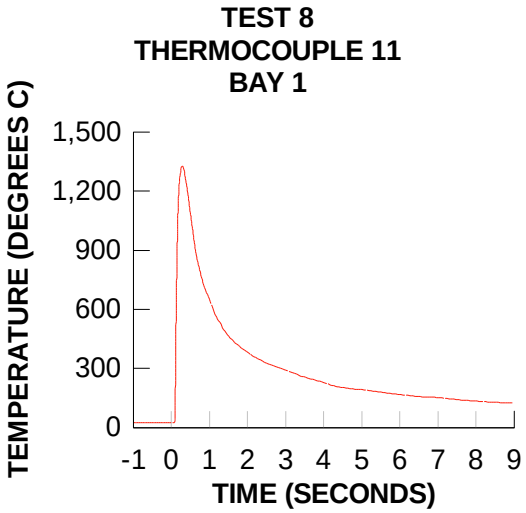
TEST 8
THERMOCOUPLE 11
BAY 1
TEMPERATURE (DEGREES C)
1,500
1,200
900
600
300
0
-1 0 1 2 3 4 5 6 7 8 9
TIME (SECONDS)

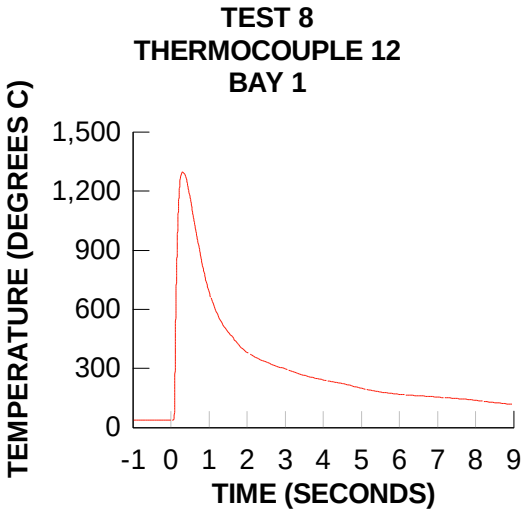
TEST 8
THERMOCOUPLE 12
BAY 1
TEMPERATURE (DEGREES C)
1,500
1,200
900
600
300
0
-1 0 1 2 3 4 5 6 7 8 9
TIME (SECONDS)

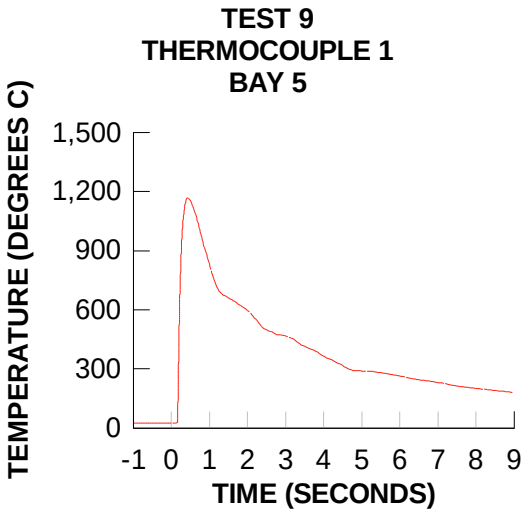
TEST 9
THERMOCOUPLE 1
BAY 5
TEMPERATURE (DEGREES C)
1,500
1,200
900
600
300
0
-1 0 1 2 3 4 5 6 7 8 9
TIME (SECONDS)

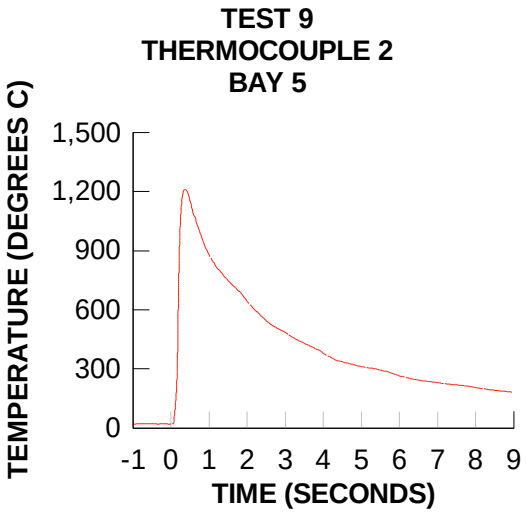
TEST 9
THERMOCOUPLE 2
BAY 5
TEMPERATURE (DEGREES C)
1,500
1,200
900
600
300
0
-1 0 1 2 3 4 5 6 7 8 9
TIME (SECONDS)

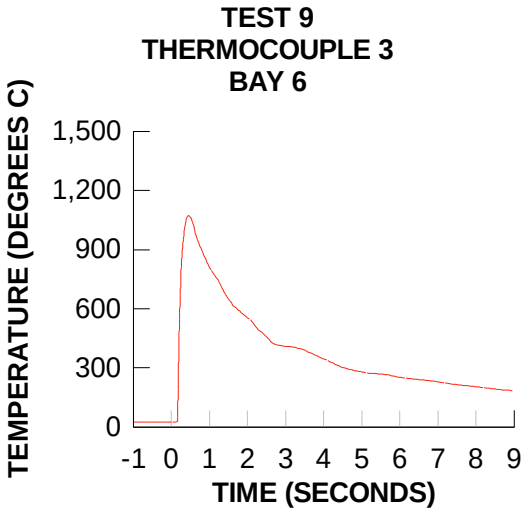
TEST 9
THERMOCOUPLE 3
BAY 6
TEMPERATURE (DEGREES C)
1,500
1,200
900
600
300
0
-1 0 1 2 3 4 5 6 7 8 9
TIME (SECONDS)

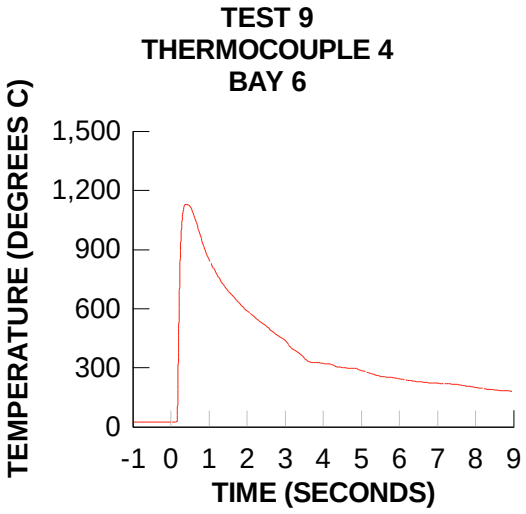
TEST 9
THERMOCOUPLE 4
BAY 6
TEMPERATURE (DEGREES C)
1,500
1,200
900
600
300
0
-1 0 1 2 3 4 5 6 7 8 9
TIME (SECONDS)

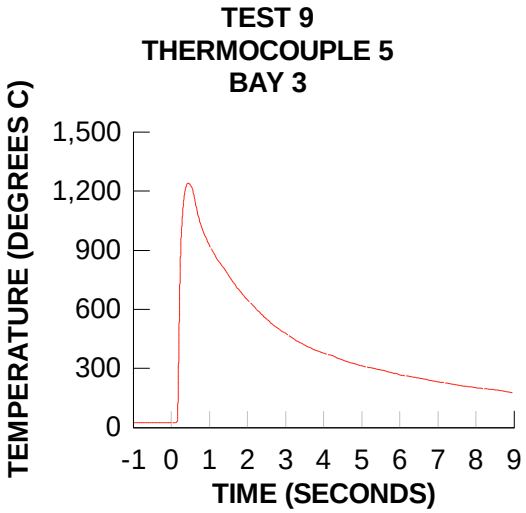
TEST 9
THERMOCOUPLE 5
BAY 3
TEMPERATURE (DEGREES C)
1,500
1,200
900
600
300
0
-1 0 1 2 3 4 5 6 7 8 9
TIME (SECONDS)

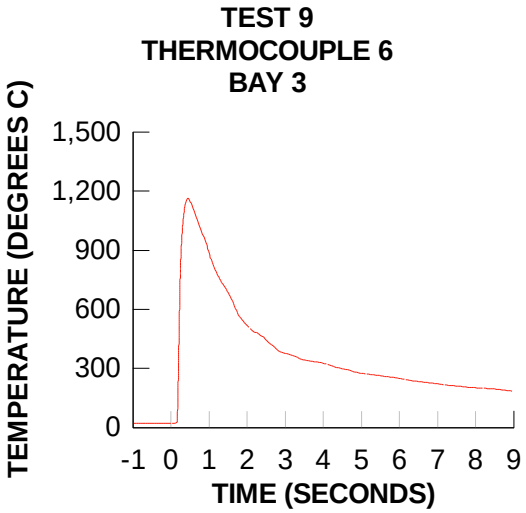
TEST 9
THERMOCOUPLE 6
BAY 3
TEMPERATURE (DEGREES C)
1,500
1,200
900
600
300
0
-1 0 1 2 3 4 5 6 7 8 9
TIME (SECONDS)

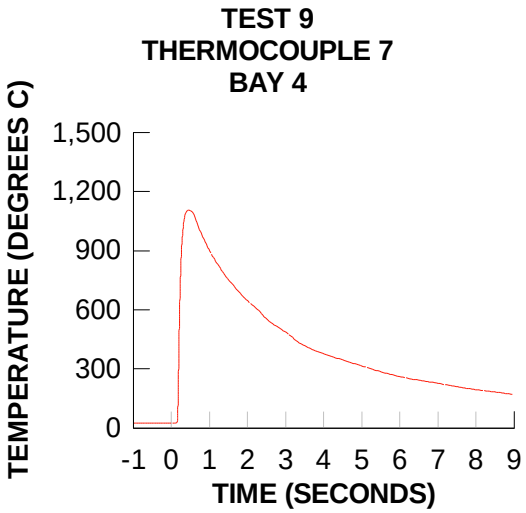
TEST 9
THERMOCOUPLE 7
BAY 4
TEMPERATURE (DEGREES C)
1,500
1,200
900
600
300
0
-1 0 1 2 3 4 5 6 7 8 9
TIME (SECONDS)

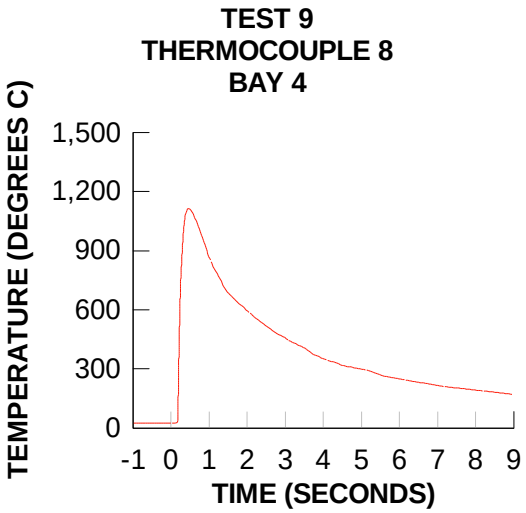
TEST 9
THERMOCOUPLE 8
BAY 4
TEMPERATURE (DEGREES C)
1,500
1,200
900
600
300
0
-1 0 1 2 3 4 5 6 7 8 9
TIME (SECONDS)

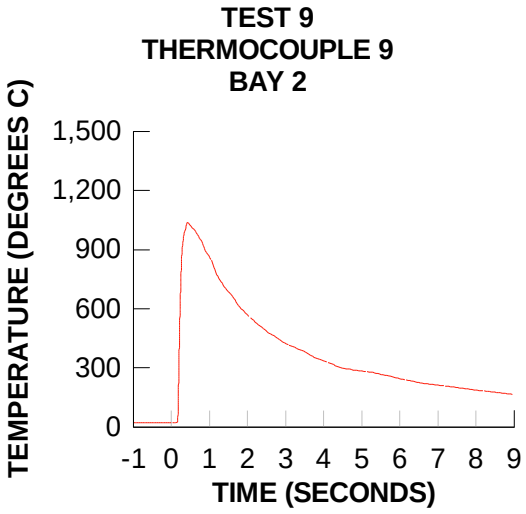
TEST 9
THERMOCOUPLE 9
BAY 2
TEMPERATURE (DEGREES C)
1,500
1,200
900
600
300
0
-1 0 1 2 3 4 5 6 7 8 9
TIME (SECONDS)

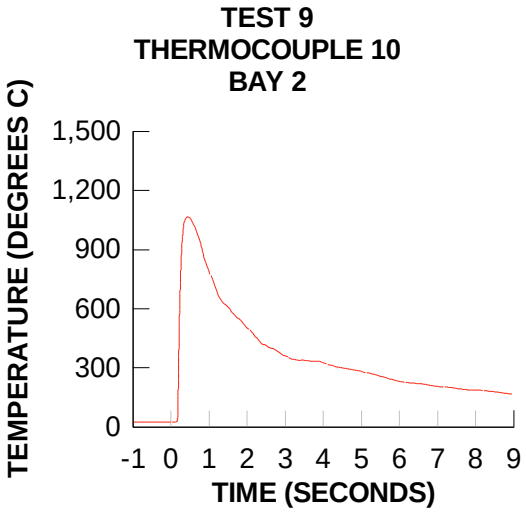
TEST 9
THERMOCOUPLE 10
BAY 2
TEMPERATURE (DEGREES C)
1,500
1,200
900
600
300
0
-1 0 1 2 3 4 5 6 7 8 9
TIME (SECONDS)

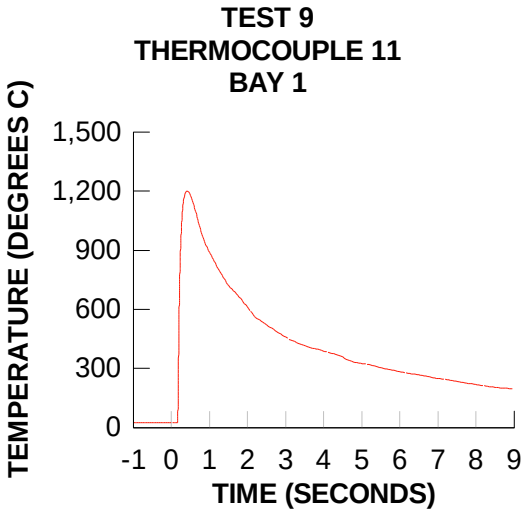
TEST 9
THERMOCOUPLE 11
BAY 1
TEMPERATURE (DEGREES C)
1,500
1,200
900
600
300
0
-1 0 1 2 3 4 5 6 7 8 9
TIME (SECONDS)

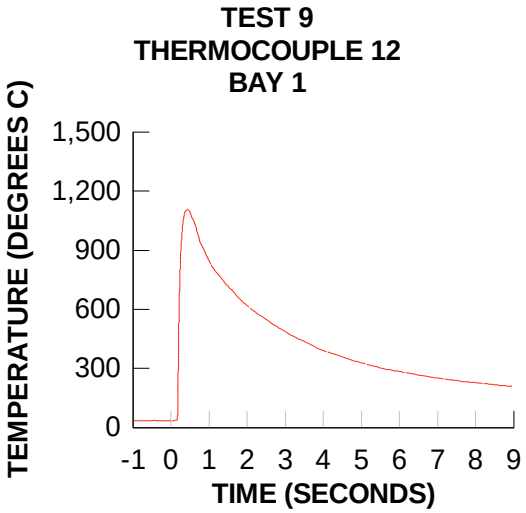
TEST 9
THERMOCOUPLE 12
BAY 1
TEMPERATURE (DEGREES C)
1,500
1,200
900
600
300
0
-1 0 1 2 3 4 5 6 7 8 9
TIME (SECONDS)

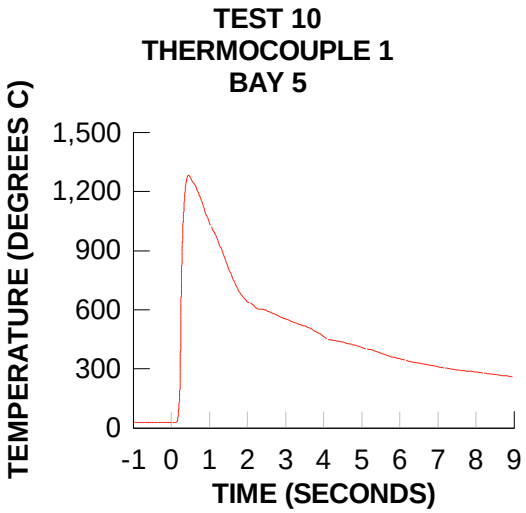
TEST 10
THERMOCOUPLE 1
BAY 5
TEMPERATURE (DEGREES C)
1,500
1,200
900
600
300
0
-1 0 1 2 3 4 5 6 7 8 9
TIME (SECONDS)

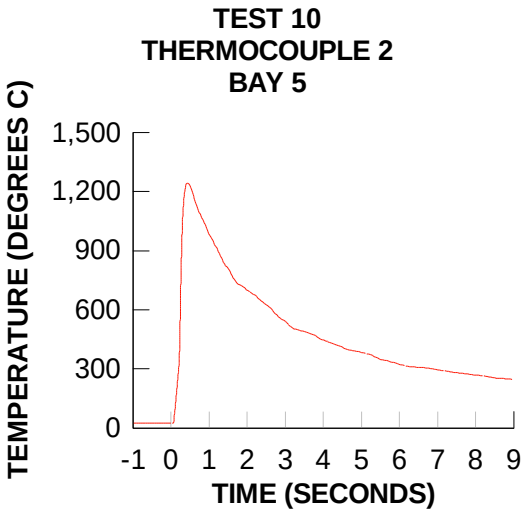
TEST 10
THERMOCOUPLE 2
BAY 5
TEMPERATURE (DEGREES C)
1,500
1,200
900
600
300
0
-1 0 1 2 3 4 5 6 7 8 9
TIME (SECONDS)

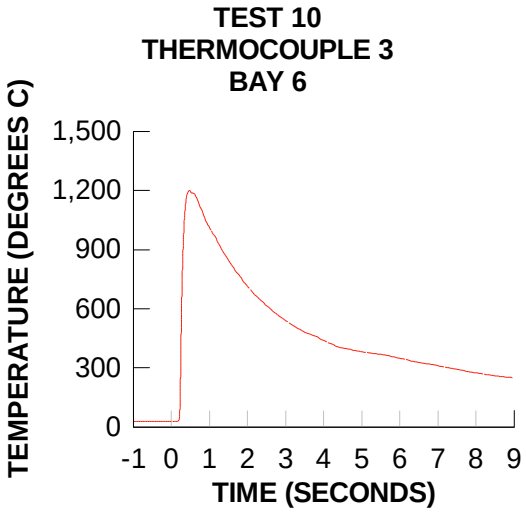
TEST 10
THERMOCOUPLE 3
BAY 6
TEMPERATURE (DEGREES C)
1,500
1,200
900
600
300
0
-1 0 1 2 3 4 5 6 7 8 9
TIME (SECONDS)

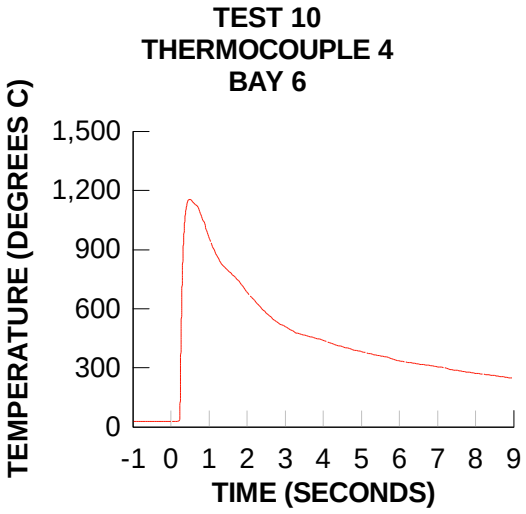
TEST 10
THERMOCOUPLE 4
BAY 6
TEMPERATURE (DEGREES C)
1,500
1,200
900
600
300
0
-1 0 1 2 3 4 5 6 7 8 9
TIME (SECONDS)

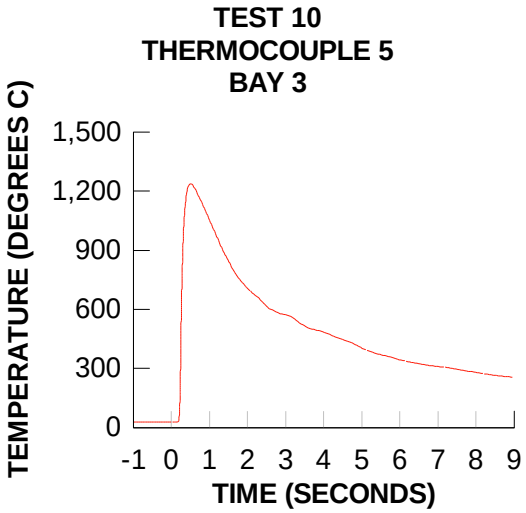
TEST 10
THERMOCOUPLE 5
BAY 3
TEMPERATURE (DEGREES C)
1,500
1,200
900
600
300
0
-1 0 1 2 3 4 5 6 7 8 9
TIME (SECONDS)

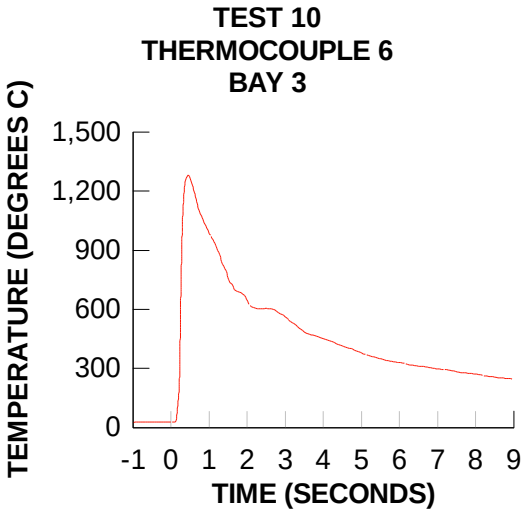
TEST 10
THERMOCOUPLE 6
BAY 3
TEMPERATURE (DEGREES C)
1,500
1,200
900
600
300
0
-1 0 1 2 3 4 5 6 7 8 9
TIME (SECONDS)

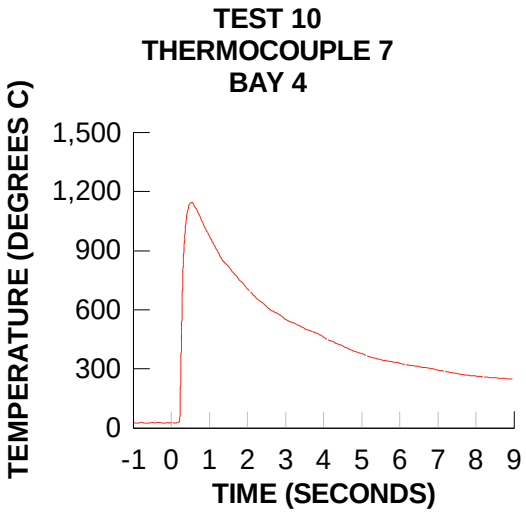
TEST 10
THERMOCOUPLE 7
BAY 4
TEMPERATURE (DEGREES C)
1,500
1,200
900
600
300
0
-1 0 1 2 3 4 5 6 7 8 9
TIME (SECONDS)

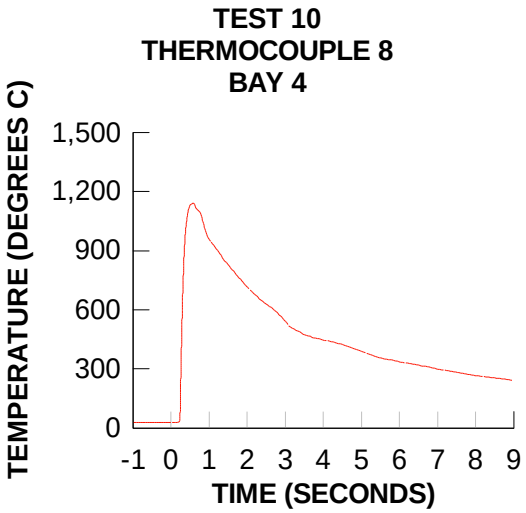
TEST 10
THERMOCOUPLE 8
BAY 4
TEMPERATURE (DEGREES C)
1,500
1,200
900
600
300
0
-1 0 1 2 3 4 5 6 7 8 9
TIME (SECONDS)

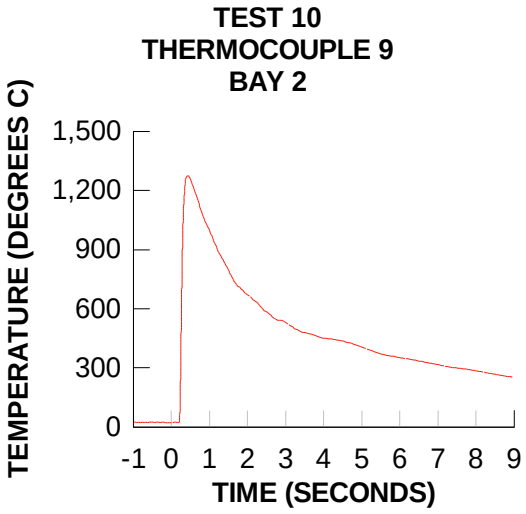
TEST 10
THERMOCOUPLE 9
BAY 2
TEMPERATURE (DEGREES C)
1,500
1,200
900
600
300
0
-1 0 1 2 3 4 5 6 7 8 9
TIME (SECONDS)

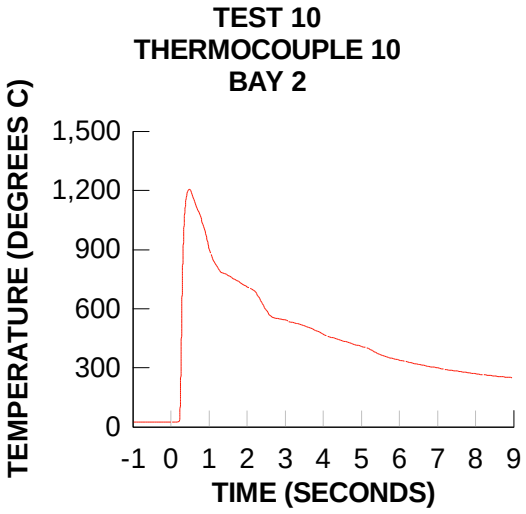
TEST 10
THERMOCOUPLE 10
BAY 2
TEMPERATURE (DEGREES C)
1,500
1,200
900
600
300
0
-1 0 1 2 3 4 5 6 7 8 9
TIME (SECONDS)

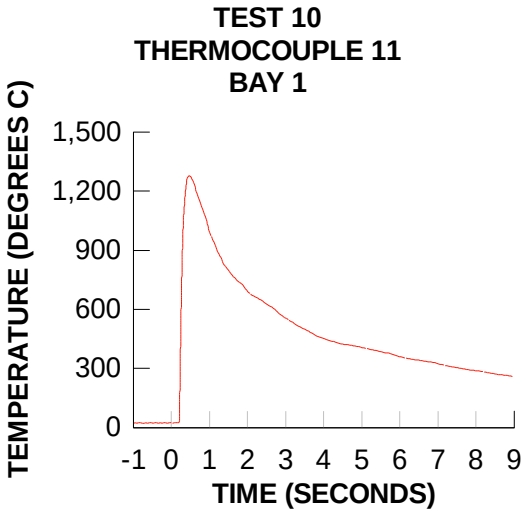
TEST 10
THERMOCOUPLE 11
BAY 1
TEMPERATURE (DEGREES C)
1,500
1,200
900
600
300
0
-1 0 1 2 3 4 5 6 7 8 9
TIME (SECONDS)

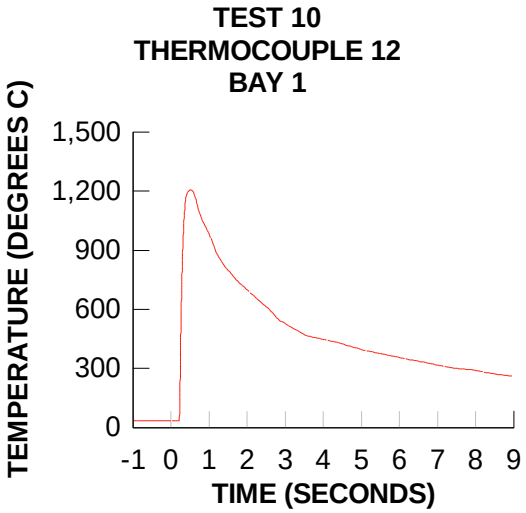
TEST 10
THERMOCOUPLE 12
BAY 1
TEMPERATURE (DEGREES C)
1,500
1,200
900
600
300
0
-1 0 1 2 3 4 5 6 7 8 9
TIME (SECONDS)

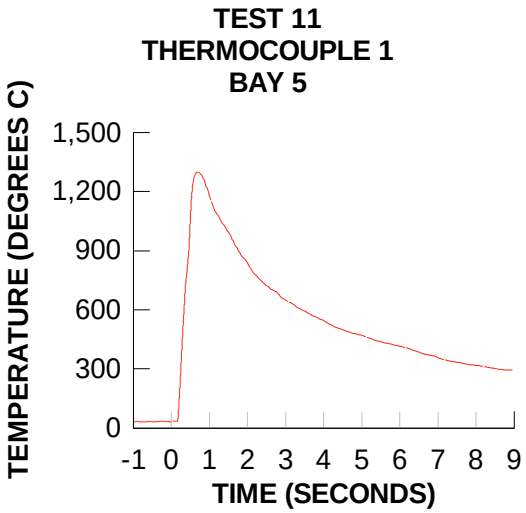
TEST 11
THERMOCOUPLE 1
BAY 5
TEMPERATURE (DEGREES C)
1,500
1,200
900
600
300
0
-1 0 1 2 3 4 5 6 7 8 9
TIME (SECONDS)

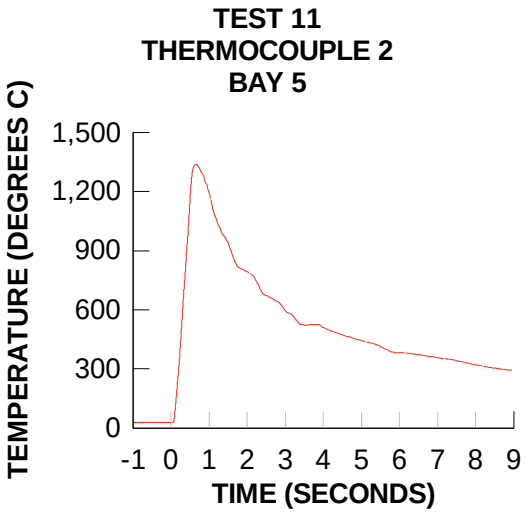
TEST 11
THERMOCOUPLE 2
BAY 5
TEMPERATURE (DEGREES C)
1,500
1,200
900
600
300
0
-1 0 1 2 3 4 5 6 7 8 9
TIME (SECONDS)

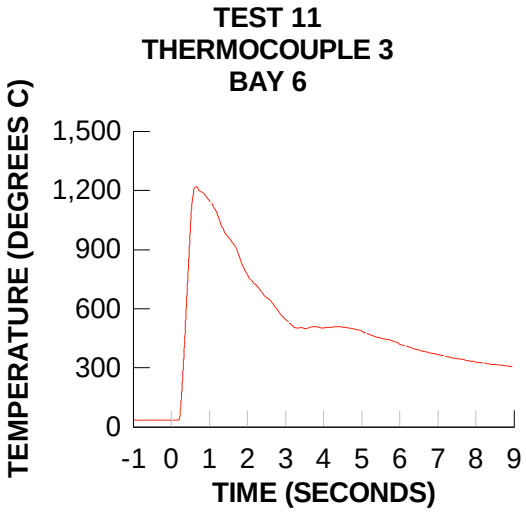
TEST 11
THERMOCOUPLE 3
BAY 6
TEMPERATURE (DEGREES C)
1,500
1,200
900
600
300
0
-1 0 1 2 3 4 5 6 7 8 9
TIME (SECONDS)

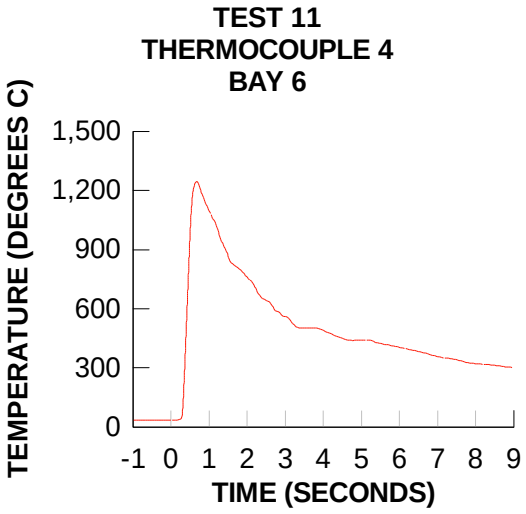
TEST 11
THERMOCOUPLE 4
BAY 6
TEMPERATURE (DEGREES C)
1,500
1,200
900
600
300
0
-1 0 1 2 3 4 5 6 7 8 9
TIME (SECONDS)

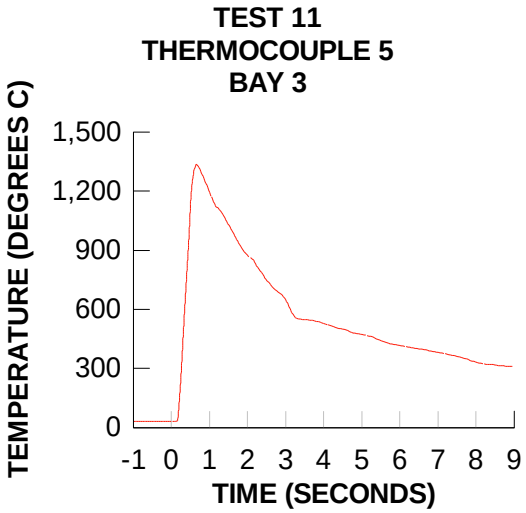
TEST 11
THERMOCOUPLE 5
BAY 3
TEMPERATURE (DEGREES C)
1,500
1,200
900
600
300
0
-1 0 1 2 3 4 5 6 7 8 9
TIME (SECONDS)

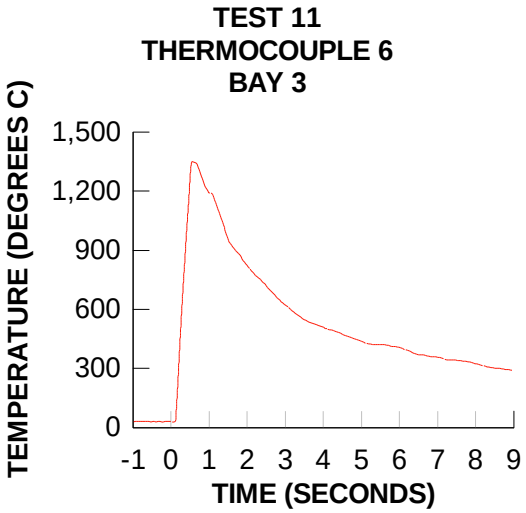
TEST 11
THERMOCOUPLE 6
BAY 3
TEMPERATURE (DEGREES C)
1,500
1,200
900
600
300
0
-1 0 1 2 3 4 5 6 7 8 9
TIME (SECONDS)

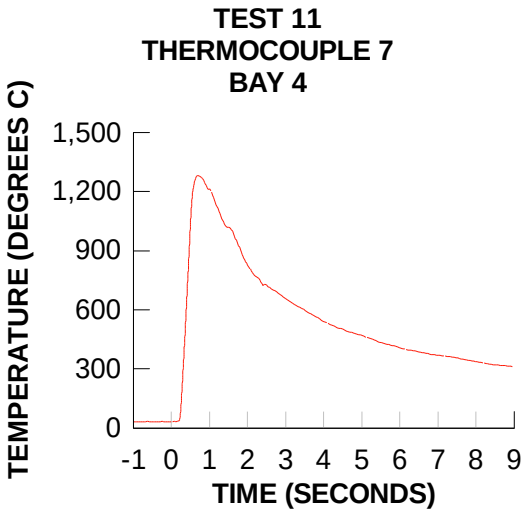
TEST 11
THERMOCOUPLE 7
BAY 4
TEMPERATURE (DEGREES C)
1,500
1,200
900
600
300
0
-1 0 1 2 3 4 5 6 7 8 9
TIME (SECONDS)

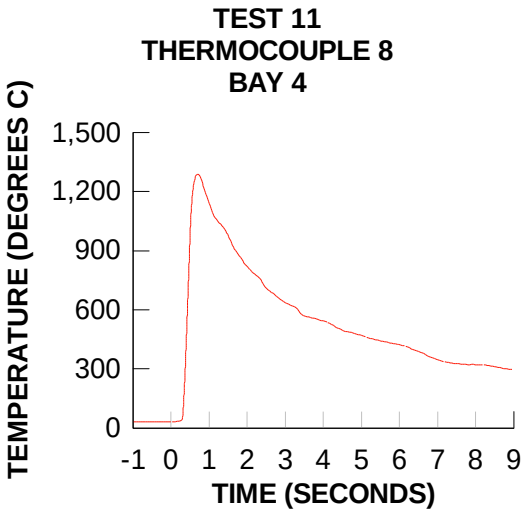
TEST 11
THERMOCOUPLE 8
BAY 4
TEMPERATURE (DEGREES C)
1,500
1,200
900
600
300
0
-1 0 1 2 3 4 5 6 7 8 9
TIME (SECONDS)

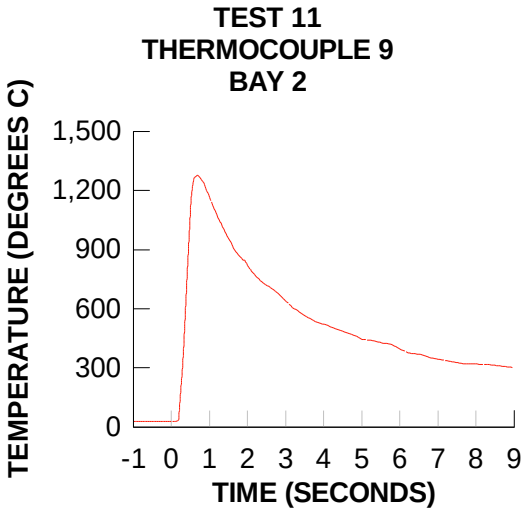
TEST 11
THERMOCOUPLE 9
BAY 2
TEMPERATURE (DEGREES C)
1,500
1,200
900
600
300
0
-1 0 1 2 3 4 5 6 7 8 9
TIME (SECONDS)

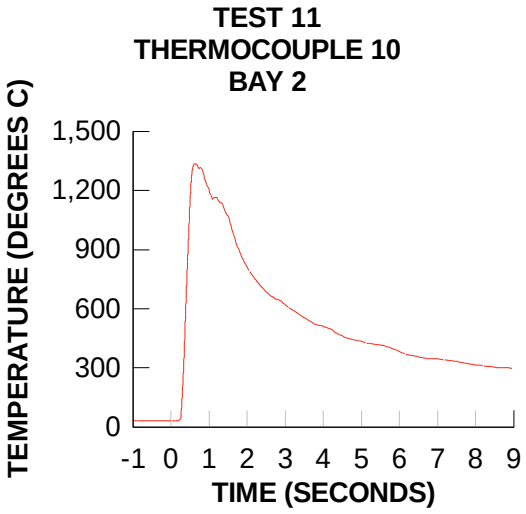
TEST 11
THERMOCOUPLE 10
BAY 2
TEMPERATURE (DEGREES C)
1,500
1,200
900
600
300
0
-1 0 1 2 3 4 5 6 7 8 9
TIME (SECONDS)

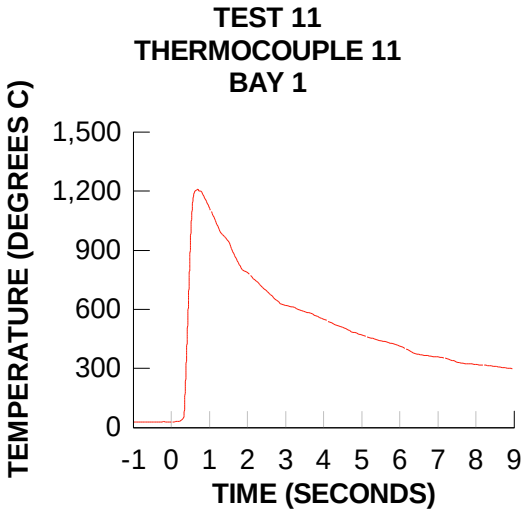
TEST 11
THERMOCOUPLE 11
BAY 1
TEMPERATURE (DEGREES C)
1,500
1,200
900
600
300
0
-1 0 1 2 3 4 5 6 7 8 9
TIME (SECONDS)

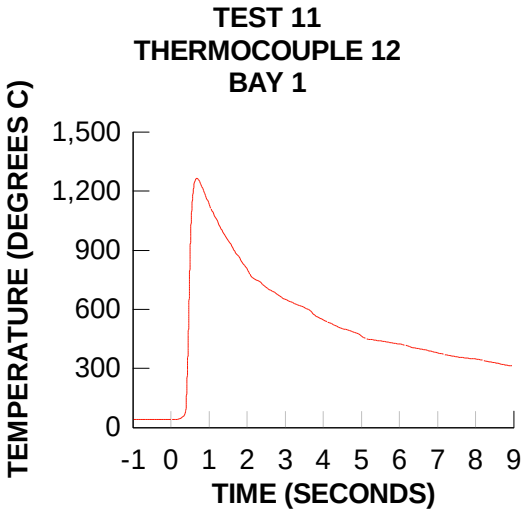
TEST 11
THERMOCOUPLE 12
BAY 1
TEMPERATURE (DEGREES C)
1,500
1,200
900
600
300
0
-1 0 1 2 3 4 5 6 7 8 9
TIME (SECONDS)

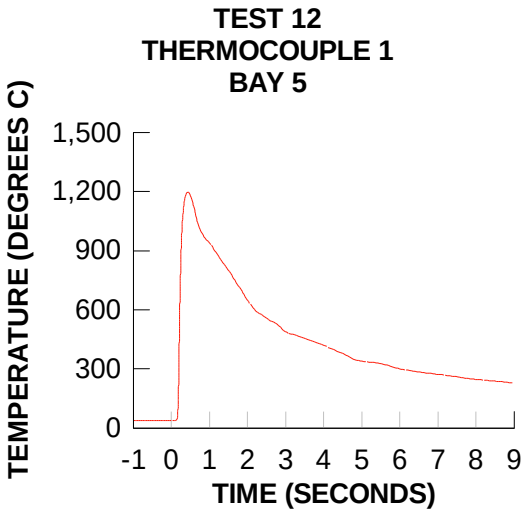
TEST 12
THERMOCOUPLE 1
BAY 5
TEMPERATURE (DEGREES C)
1,500
1,200
900
600
300
0
-1 0 1 2 3 4 5 6 7 8 9
TIME (SECONDS)

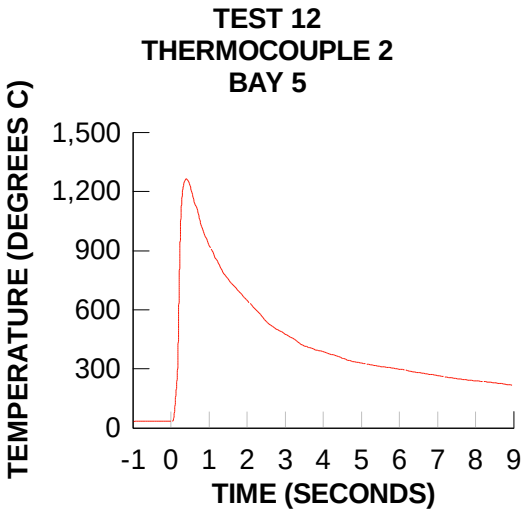
TEST 12
THERMOCOUPLE 2
BAY 5
TEMPERATURE (DEGREES C)
1,500
1,200
900
600
300
0
-1 0 1 2 3 4 5 6 7 8 9
TIME (SECONDS)

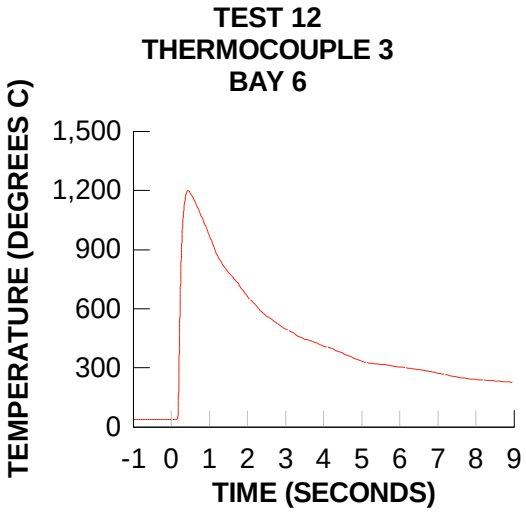
TEST 12
THERMOCOUPLE 3
BAY 6
TEMPERATURE (DEGREES C)
1,500
1,200
900
600
300
0
-1 0 1 2 3 4 5 6 7 8 9
TIME (SECONDS)

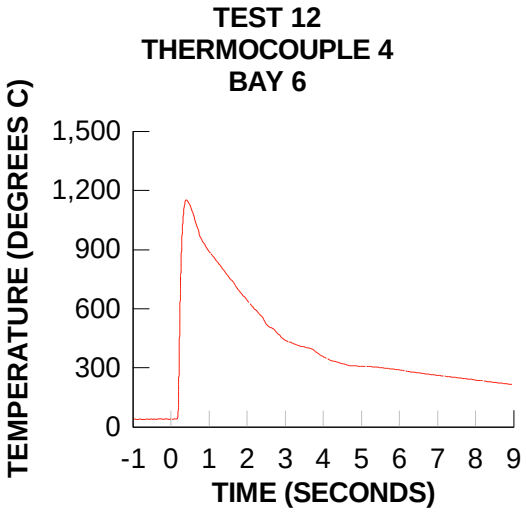
TEST 12
THERMOCOUPLE 4
BAY 6
TEMPERATURE (DEGREES C)
1,500
1,200
900
600
300
0
-1 0 1 2 3 4 5 6 7 8 9
TIME (SECONDS)

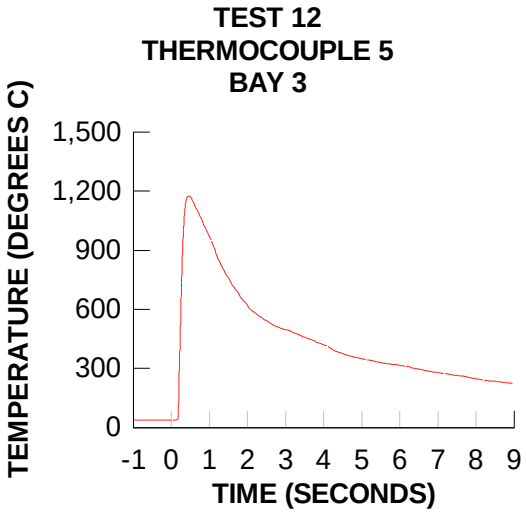
TEST 12
THERMOCOUPLE 5
BAY 3
TEMPERATURE (DEGREES C)
1,500
1,200
900
600
300
0
-1 0 1 2 3 4 5 6 7 8 9
TIME (SECONDS)

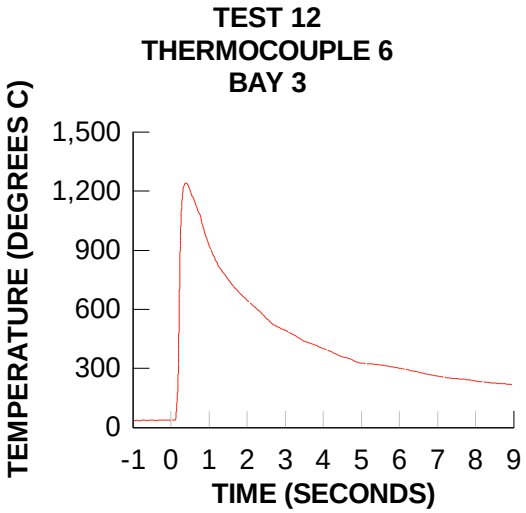
TEST 12
THERMOCOUPLE 6
BAY 3
TEMPERATURE (DEGREES C)
1,500
1,200
900
600
300
0
-1 0 1 2 3 4 5 6 7 8 9
TIME (SECONDS)

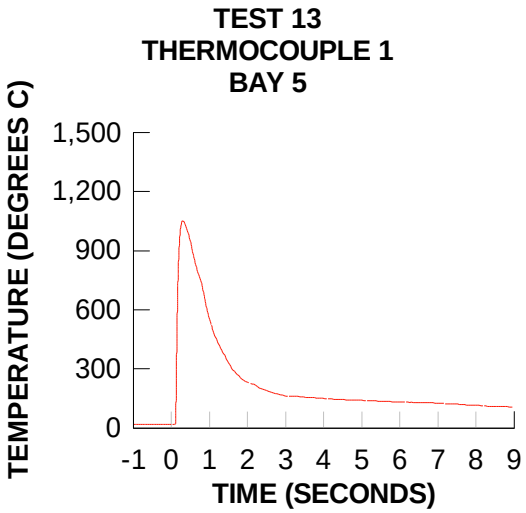
TEST 13
THERMOCOUPLE 1
BAY 5
TEMPERATURE (DEGREES C)
1,500
1,200
900
600
300
0
-1 0 1 2 3 4 5 6 7 8 9
TIME (SECONDS)

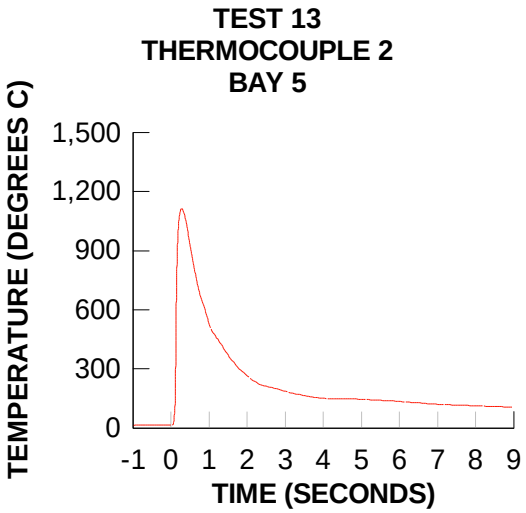
TEST 13
THERMOCOUPLE 2
BAY 5
TEMPERATURE (DEGREES C)
1,500
1,200
900
600
300
0
-1 0 1 2 3 4 5 6 7 8 9
TIME (SECONDS)

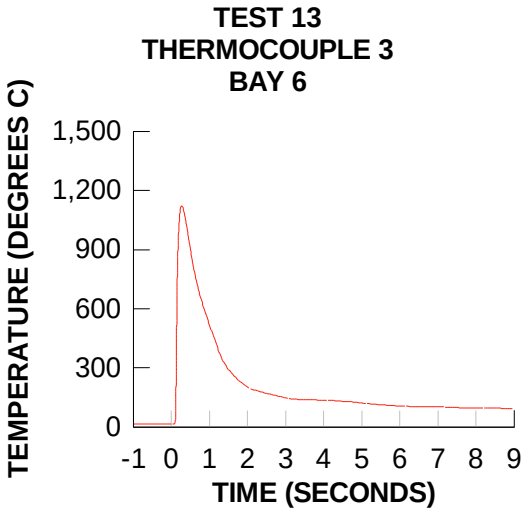
TEST 13
THERMOCOUPLE 3
BAY 6
TEMPERATURE (DEGREES C)
1,500
1,200
900
600
300
0
-1 0 1 2 3 4 5 6 7 8 9
TIME (SECONDS)

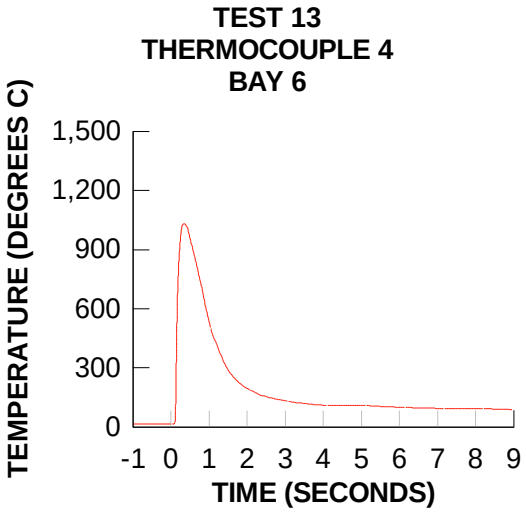
TEST 13
THERMOCOUPLE 4
BAY 6
TEMPERATURE (DEGREES C)
1,500
1,200
900
600
300
0
-1 0 1 2 3 4 5 6 7 8 9
TIME (SECONDS)

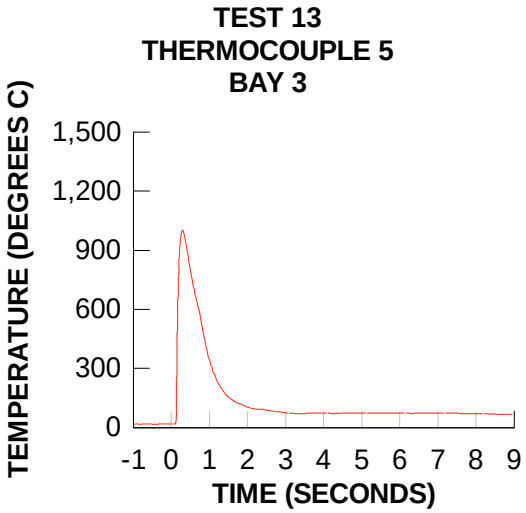
TEST 13
THERMOCOUPLE 5
BAY 3
TEMPERATURE (DEGREES C)
1,500
1,200
900
600
300
0
-1 0 1 2 3 4 5 6 7 8 9
TIME (SECONDS)

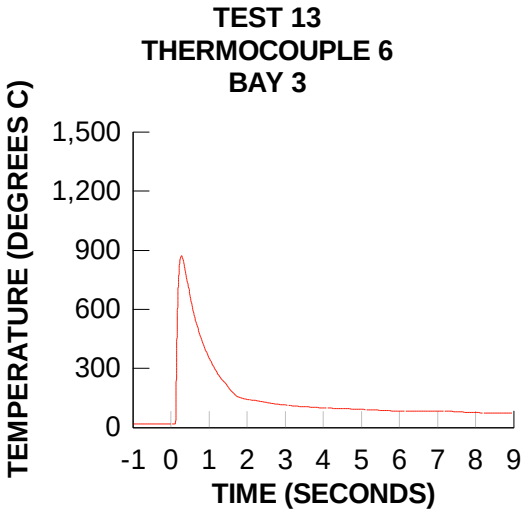
TEST 13
THERMOCOUPLE 6
BAY 3
TEMPERATURE (DEGREES C)
1,500
1,200
900
600
300
0
-1 0 1 2 3 4 5 6 7 8 9
TIME (SECONDS)

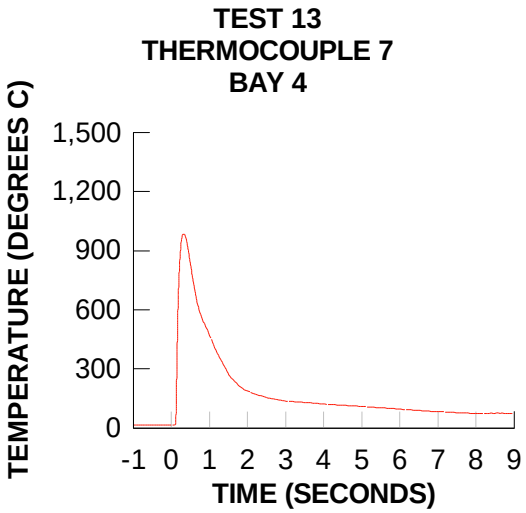
TEST 13
THERMOCOUPLE 7
BAY 4
TEMPERATURE (DEGREES C)
1,500
1,200
900
600
300
0
-1 0 1 2 3 4 5 6 7 8 9
TIME (SECONDS)

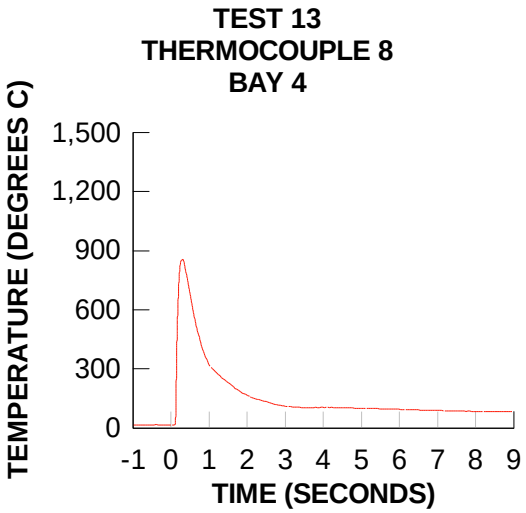
TEST 13
THERMOCOUPLE 8
BAY 4
TEMPERATURE (DEGREES C)
1,500
1,200
900
600
300
0
-1 0 1 2 3 4 5 6 7 8 9
TIME (SECONDS)

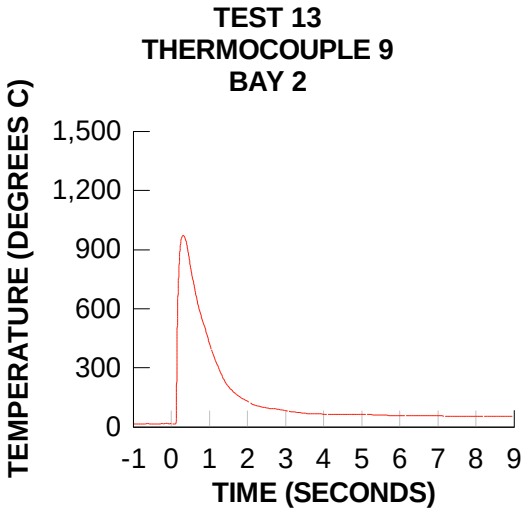
TEST 13
THERMOCOUPLE 9
BAY 2
TEMPERATURE (DEGREES C)
1,500
1,200
900
600
300
0
-1 0 1 2 3 4 5 6 7 8 9
TIME (SECONDS)

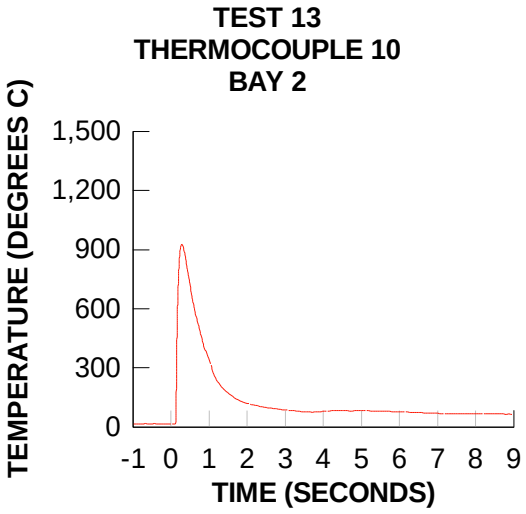
TEST 13
THERMOCOUPLE 10
BAY 2
TEMPERATURE (DEGREES C)
1,500
1,200
900
600
300
0
-1 0 1 2 3 4 5 6 7 8 9
TIME (SECONDS)

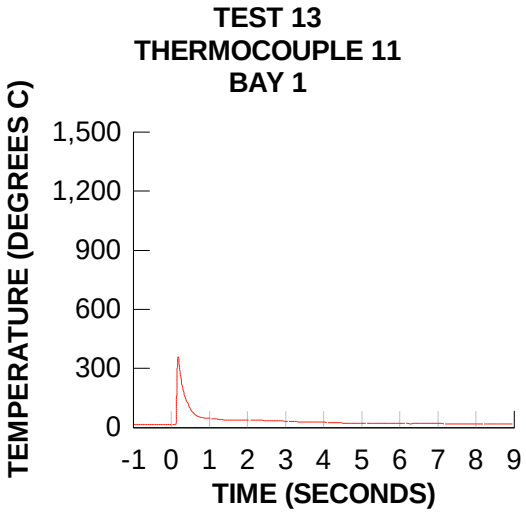
TEST 13
THERMOCOUPLE 11
BAY 1
TEMPERATURE (DEGREES C)
1,500
1,200
900
600
300
0
-1 0 1 2 3 4 5 6 7 8 9
TIME (SECONDS)

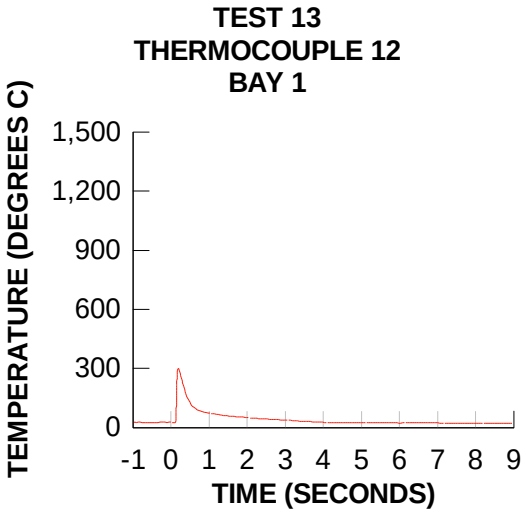
TEST 13
THERMOCOUPLE 12
BAY 1
TEMPERATURE (DEGREES C)
1,500
1,200
900
600
300
0
-1 0 1 2 3 4 5 6 7 8 9
TIME (SECONDS)

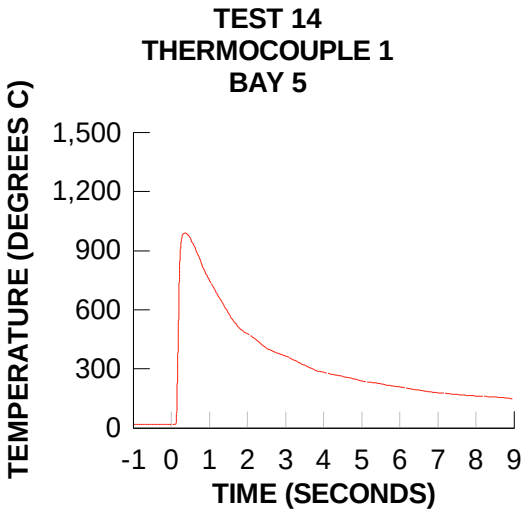
TEST 14
THERMOCOUPLE 1
BAY 5
TEMPERATURE (DEGREES C)
1,500
1,200
900
600
300
0
-1 0 1 2 3 4 5 6 7 8 9
TIME (SECONDS)

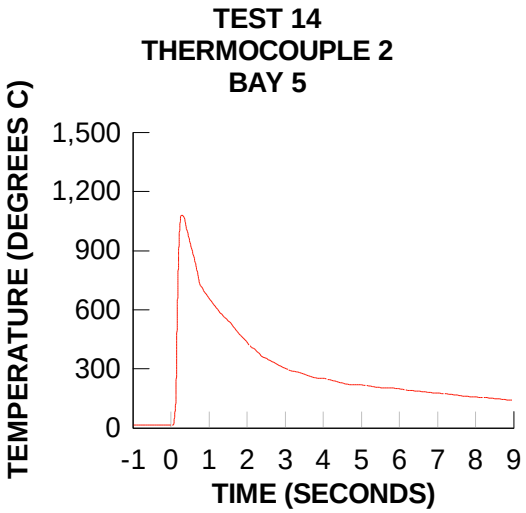
TEST 14
THERMOCOUPLE 2
BAY 5
TEMPERATURE (DEGREES C)
1,500
1,200
900
600
300
0
-1 0 1 2 3 4 5 6 7 8 9
TIME (SECONDS)

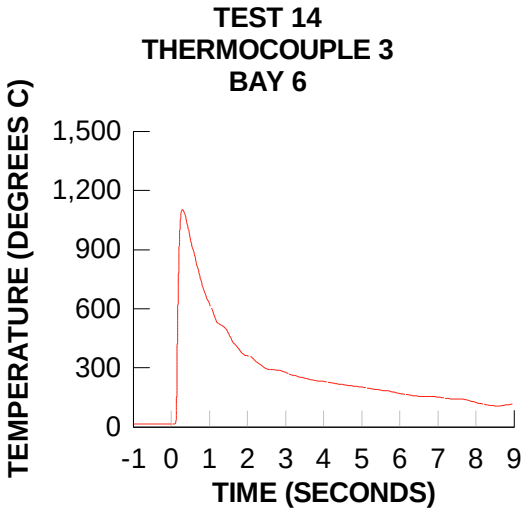
TEST 14
THERMOCOUPLE 3
BAY 6
TEMPERATURE (DEGREES C)
1,500
1,200
900
600
300
0
-1 0 1 2 3 4 5 6 7 8 9
TIME (SECONDS)

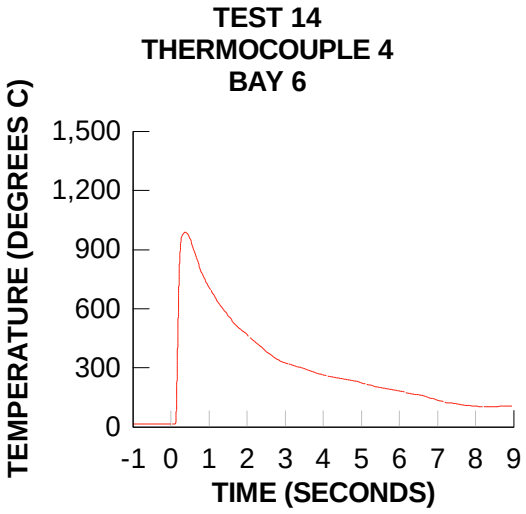
TEST 14
THERMOCOUPLE 4
BAY 6
TEMPERATURE (DEGREES C)
1,500
1,200
900
600
300
0
-1 0 1 2 3 4 5 6 7 8 9
TIME (SECONDS)

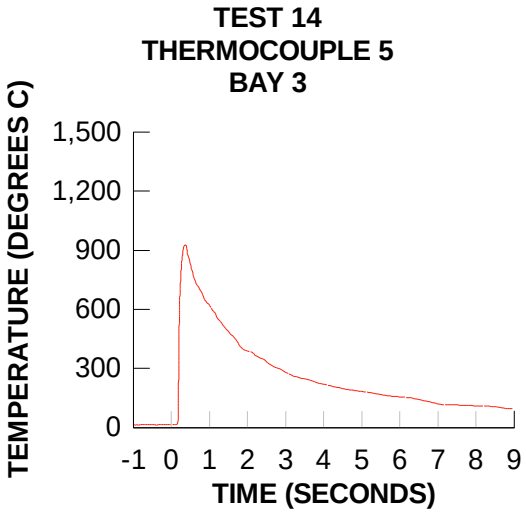
TEST 14
THERMOCOUPLE 5
BAY 3
TEMPERATURE (DEGREES C)
1,500
1,200
900
600
300
0
-1 0 1 2 3 4 5 6 7 8 9
TIME (SECONDS)

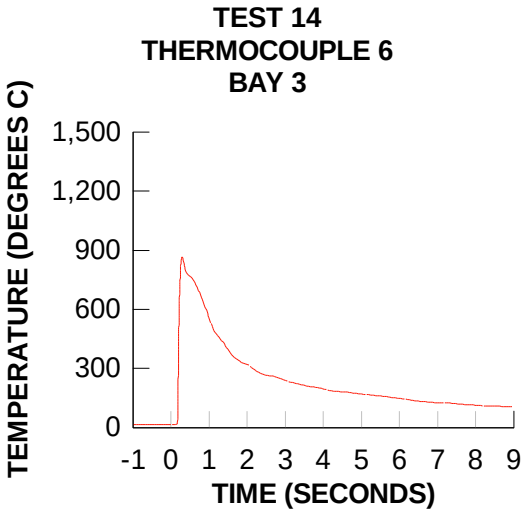
TEST 14
THERMOCOUPLE 6
BAY 3
TEMPERATURE (DEGREES C)
1,500
1,200
900
600
300
0
-1 0 1 2 3 4 5 6 7 8 9
TIME (SECONDS)

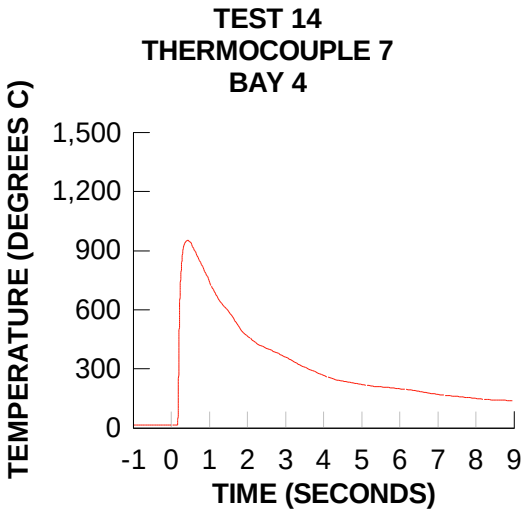
TEST 14
THERMOCOUPLE 7
BAY 4
TEMPERATURE (DEGREES C)
1,500
1,200
900
600
300
0
-1 0 1 2 3 4 5 6 7 8 9
TIME (SECONDS)

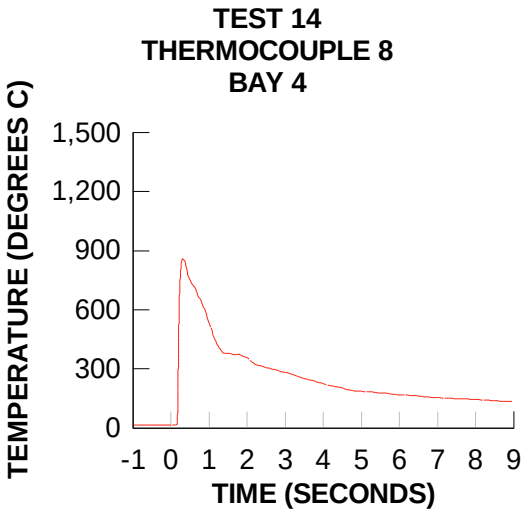
TEST 14
THERMOCOUPLE 8
BAY 4
TEMPERATURE (DEGREES C)
1,500
1,200
900
600
300
0
-1 0 1 2 3 4 5 6 7 8 9
TIME (SECONDS)

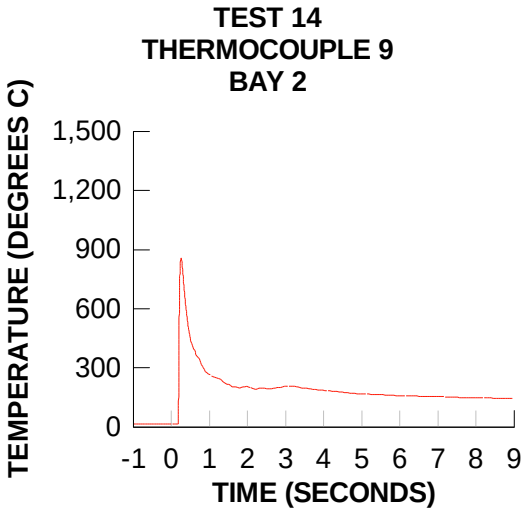
TEST 14
THERMOCOUPLE 9
BAY 2
TEMPERATURE (DEGREES C)
1,500
1,200
900
600
300
0
-1 0 1 2 3 4 5 6 7 8 9
TIME (SECONDS)

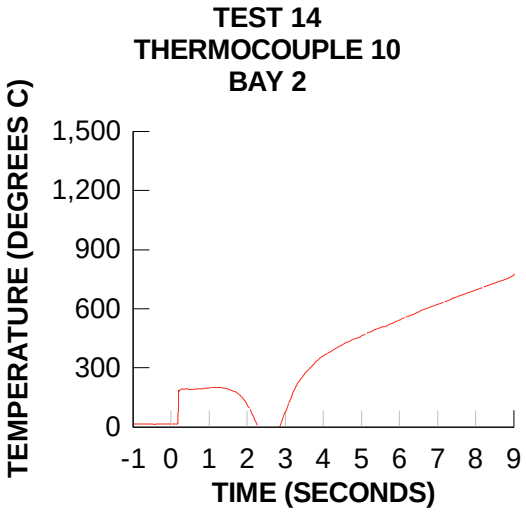
TEST 14
THERMOCOUPLE 10
BAY 2
TEMPERATURE (DEGREES C)
1,500
1,200
900
600
300
0
-1 0 1 2 3 4 5 6 7 8 9
TIME (SECONDS)

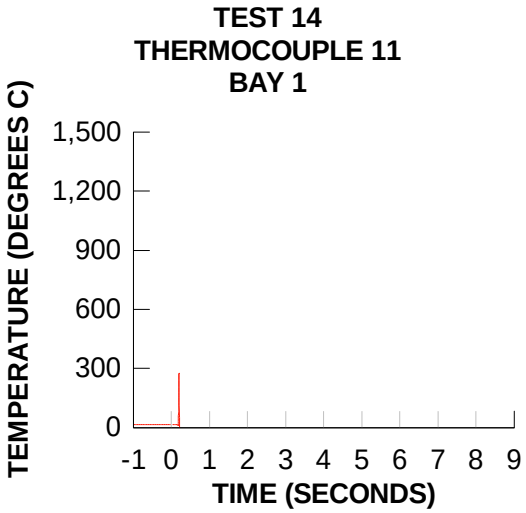
TEST 14
THERMOCOUPLE 11
BAY 1
TEMPERATURE (DEGREES C)
1,500
1,200
900
600
300
0
-1 0 1 2 3 4 5 6 7 8 9
TIME (SECONDS)

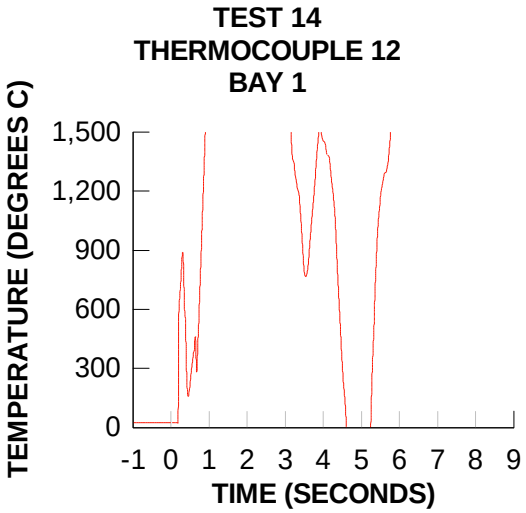
TEST 14
THERMOCOUPLE 12
BAY 1
TEMPERATURE (DEGREES C)
1,500
1,200
900
600
300
0
-1 0 1 2 3 4 5 6 7 8 9
TIME (SECONDS)

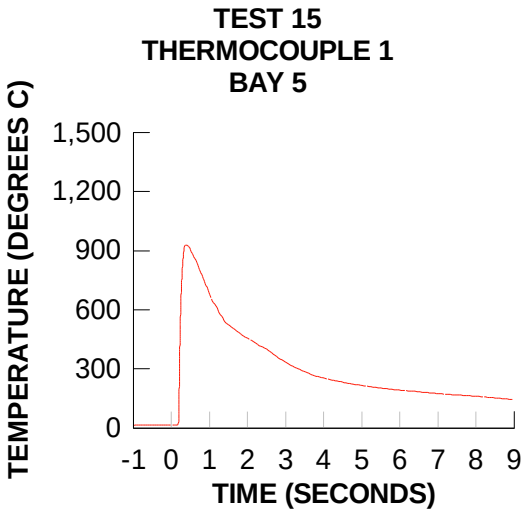
TEST 15
THERMOCOUPLE 1
BAY 5
TEMPERATURE (DEGREES C)
1,500
1,200
900
600
300
0
-1 0 1 2 3 4 5 6 7 8 9
TIME (SECONDS)

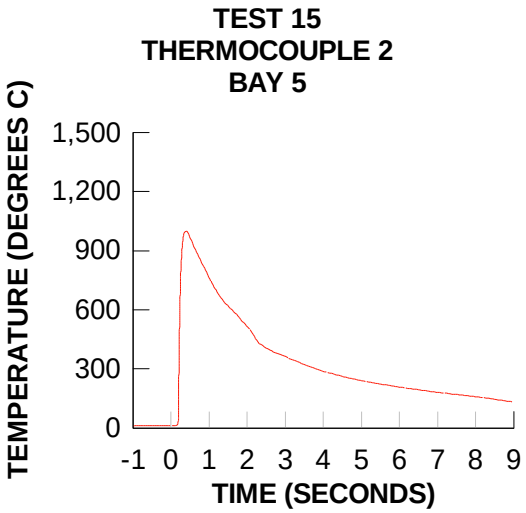
TEST 15
THERMOCOUPLE 2
BAY 5
TEMPERATURE (DEGREES C)
1,500
1,200
900
600
300
0
-1 0 1 2 3 4 5 6 7 8 9
TIME (SECONDS)

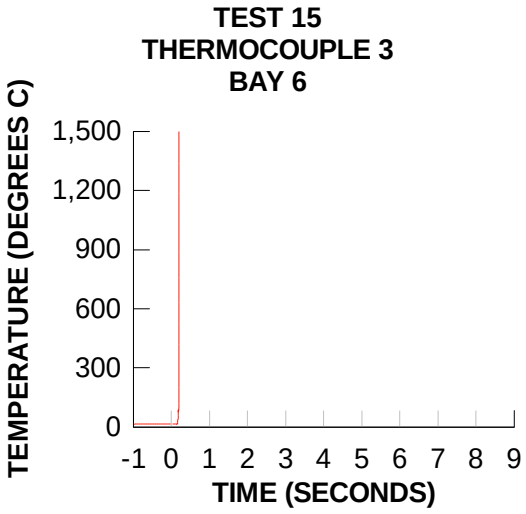
TEST 15
THERMOCOUPLE 3
BAY 6
TEMPERATURE (DEGREES C)
1,500
1,200
900
600
300
0
-1 0 1 2 3 4 5 6 7 8 9
TIME (SECONDS)

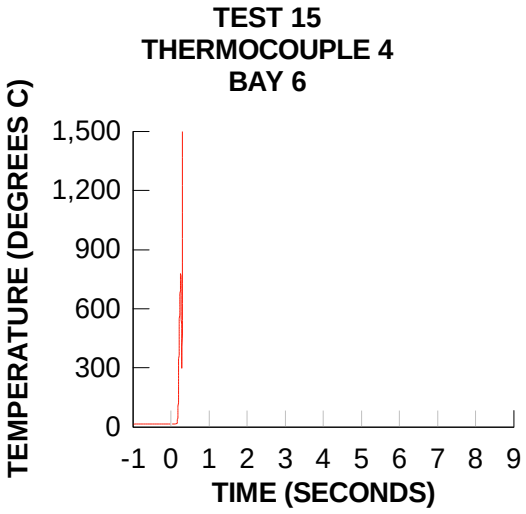
TEST 15
THERMOCOUPLE 4
BAY 6
TEMPERATURE (DEGREES C)
1,500
1,200
900
600
300
0
-1 0 1 2 3 4 5 6 7 8 9
TIME (SECONDS)

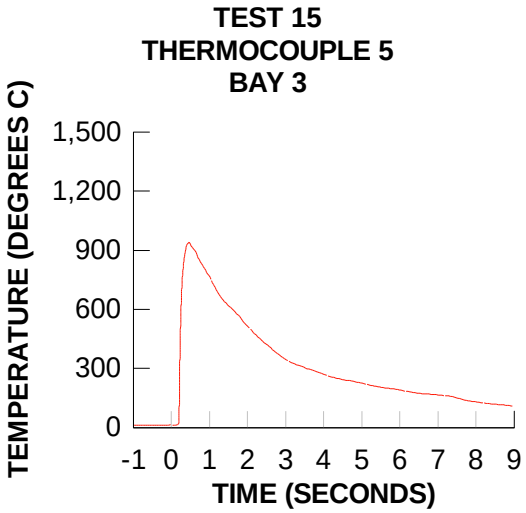
TEST 15
THERMOCOUPLE 5
BAY 3
TEMPERATURE (DEGREES C)
1,500
1,200
900
600
300
0
-1 0 1 2 3 4 5 6 7 8 9
TIME (SECONDS)

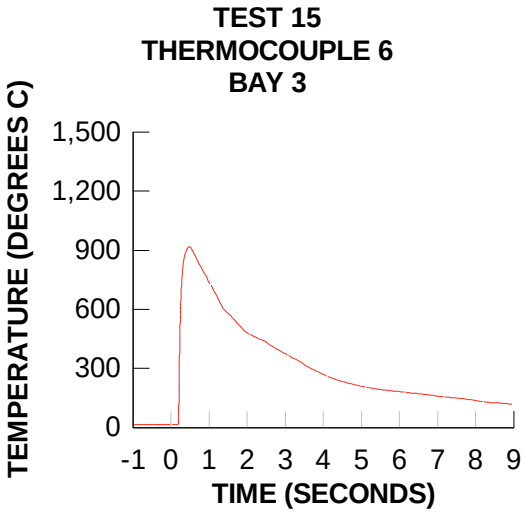
TEST 15
THERMOCOUPLE 6
BAY 3
TEMPERATURE (DEGREES C)
1,500
1,200
900
600
300
0
-1 0 1 2 3 4 5 6 7 8 9
TIME (SECONDS)

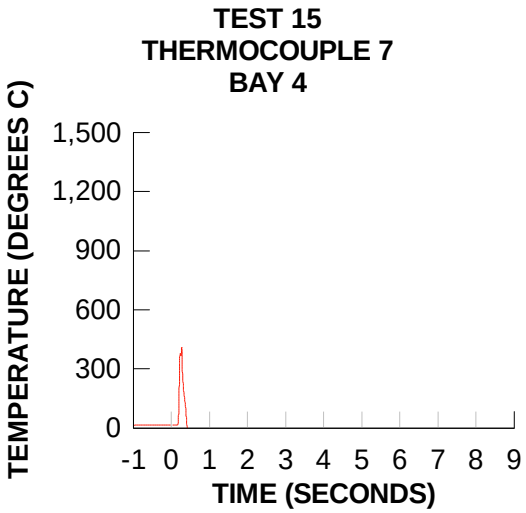
TEST 15
THERMOCOUPLE 7
BAY 4
TEMPERATURE (DEGREES C)
1,500
1,200
900
600
300
0
-1 0 1 2 3 4 5 6 7 8 9
TIME (SECONDS)

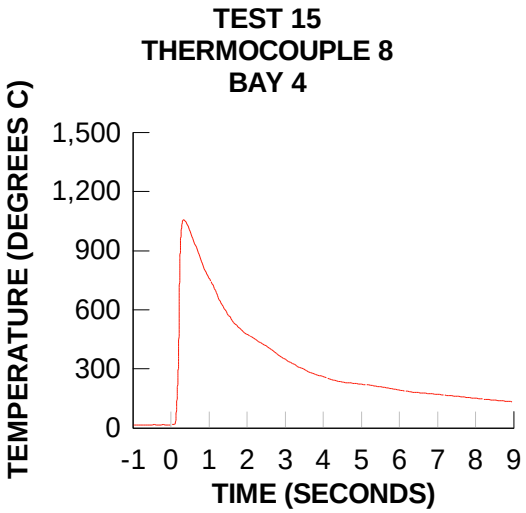
TEST 15
THERMOCOUPLE 8
BAY 4
TEMPERATURE (DEGREES C)
1,500
1,200
900
600
300
0
-1 0 1 2 3 4 5 6 7 8 9
TIME (SECONDS)

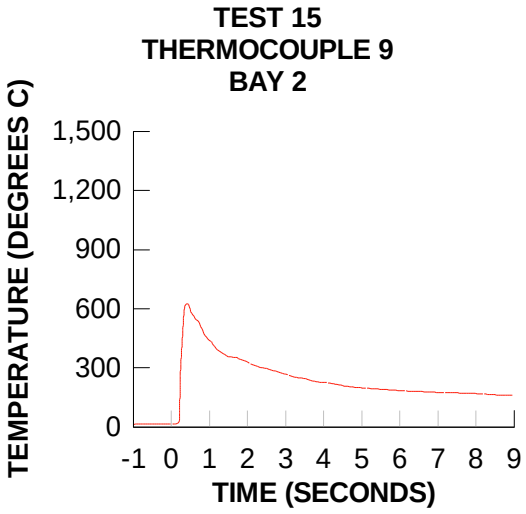
TEST 15
THERMOCOUPLE 9
BAY 2
TEMPERATURE (DEGREES C)
1,500
1,200
900
600
300
0
-1 0 1 2 3 4 5 6 7 8 9
TIME (SECONDS)

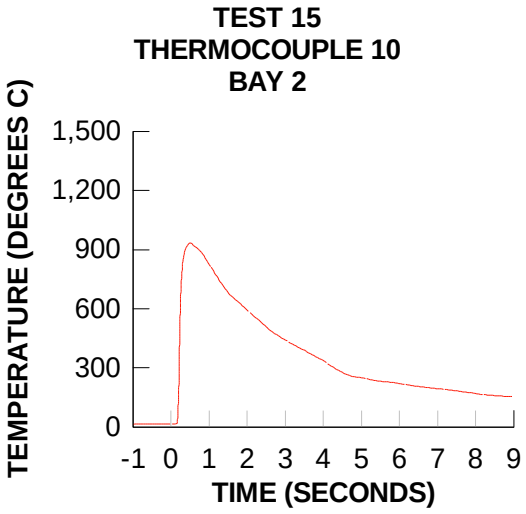
TEST 15
THERMOCOUPLE 10
BAY 2
TEMPERATURE (DEGREES C)
1,500
1,200
900
600
300
0
-1 0 1 2 3 4 5 6 7 8 9
TIME (SECONDS)

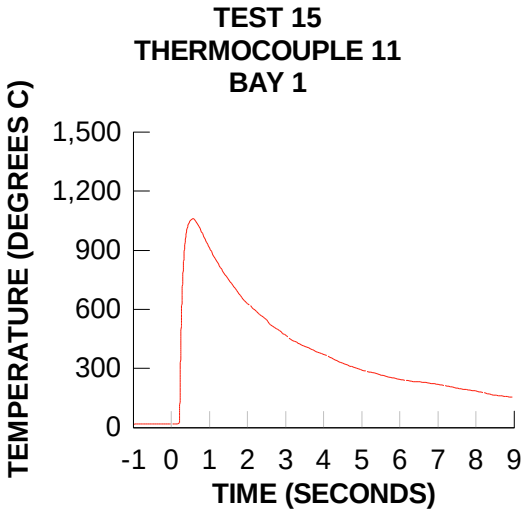
TEST 15
THERMOCOUPLE 11
BAY 1
TEMPERATURE (DEGREES C)
1,500
1,200
900
600
300
0
-1 0 1 2 3 4 5 6 7 8 9
TIME (SECONDS)

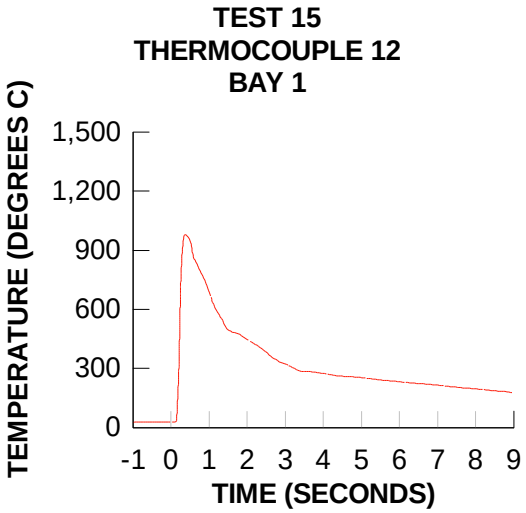
TEST 15
THERMOCOUPLE 12
BAY 1
TEMPERATURE (DEGREES C)
1,500
1,200
900
600
300
0
-1 0 1 2 3 4 5 6 7 8 9
TIME (SECONDS)

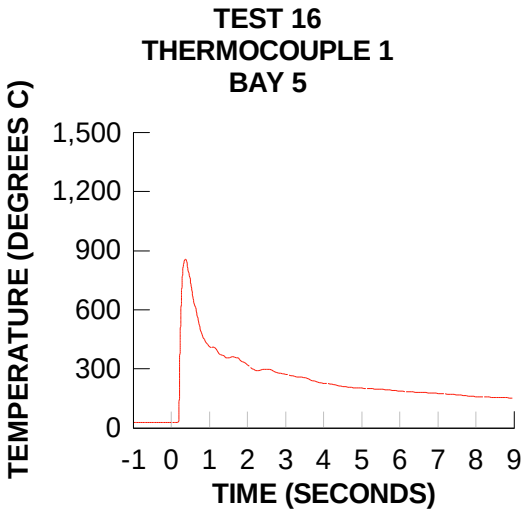
TEST 16
THERMOCOUPLE 1
BAY 5
TEMPERATURE (DEGREES C)
1,500
1,200
900
600
300
0
-1 0 1 2 3 4 5 6 7 8 9
TIME (SECONDS)

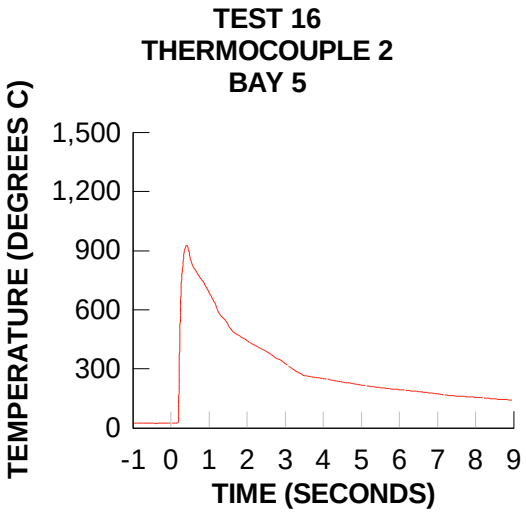
TEST 16
THERMOCOUPLE 2
BAY 5
TEMPERATURE (DEGREES C)
1,500
1,200
900
600
300
0
-1 0 1 2 3 4 5 6 7 8 9
TIME (SECONDS)

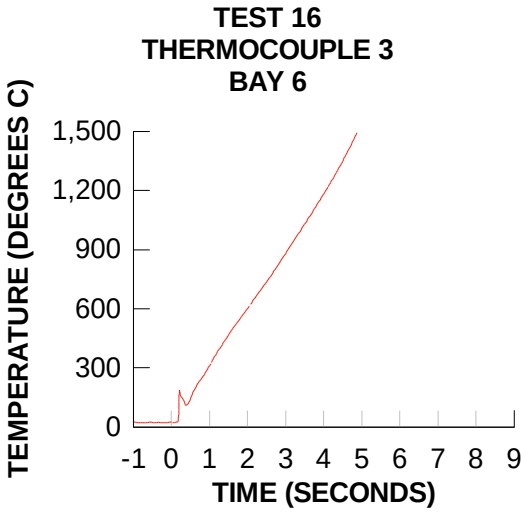
TEST 16
THERMOCOUPLE 3
BAY 6
TEMPERATURE (DEGREES C)
1,500
1,200
900
600
300
0
-1 0 1 2 3 4 5 6 7 8 9
TIME (SECONDS)

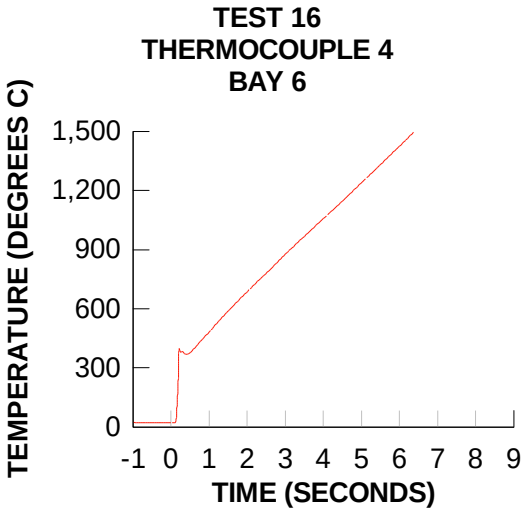
TEST 16
THERMOCOUPLE 4
BAY 6
TEMPERATURE (DEGREES C)
1,500
1,200
900
600
300
0
-1 0 1 2 3 4 5 6 7 8 9
TIME (SECONDS)

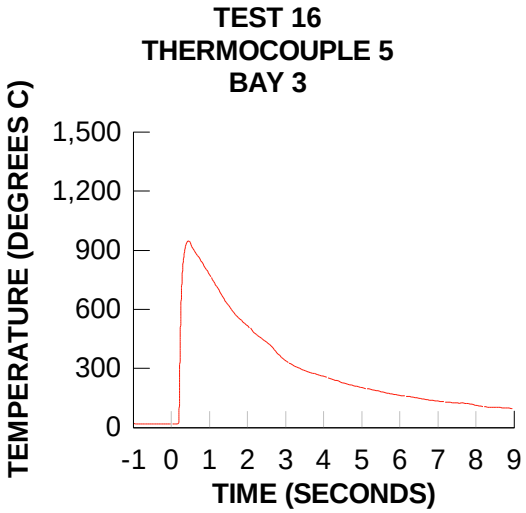
TEST 16
THERMOCOUPLE 5
BAY 3
TEMPERATURE (DEGREES C)
1,500
1,200
900
600
300
0
-1 0 1 2 3 4 5 6 7 8 9
TIME (SECONDS)

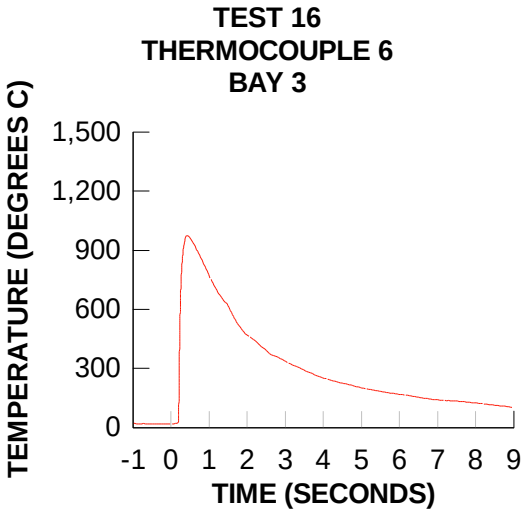
TEST 16
THERMOCOUPLE 6
BAY 3
TEMPERATURE (DEGREES C)
1,500
1,200
900
600
300
0
-1 0 1 2 3 4 5 6 7 8 9
TIME (SECONDS)

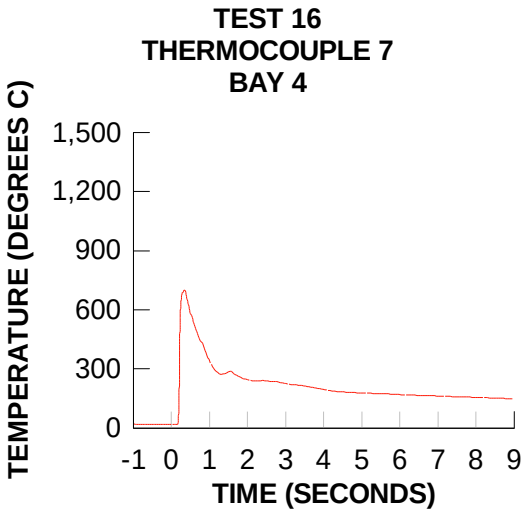
TEST 16
THERMOCOUPLE 7
BAY 4
TEMPERATURE (DEGREES C)
1,500
1,200
900
600
300
0
-1 0 1 2 3 4 5 6 7 8 9
TIME (SECONDS)

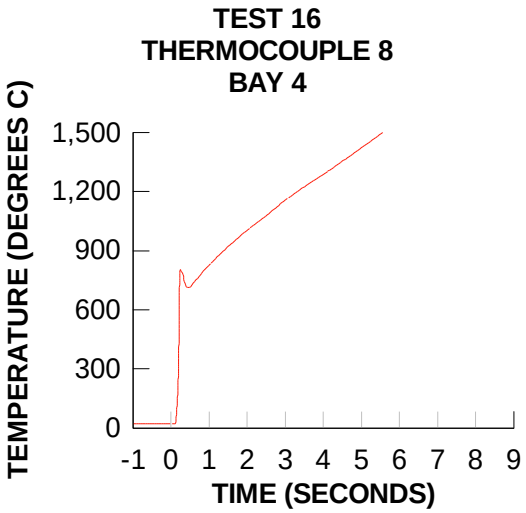
TEST 16
THERMOCOUPLE 8
BAY 4
TEMPERATURE (DEGREES C)
1,500
1,200
900
600
300
0
-1 0 1 2 3 4 5 6 7 8 9
TIME (SECONDS)

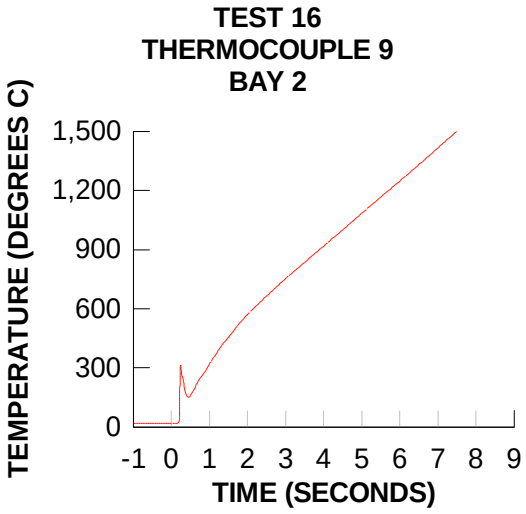
TEST 16
THERMOCOUPLE 9
BAY 2
TEMPERATURE (DEGREES C)
1,500
1,200
900
600
300
0
-1 0 1 2 3 4 5 6 7 8 9
TIME (SECONDS)

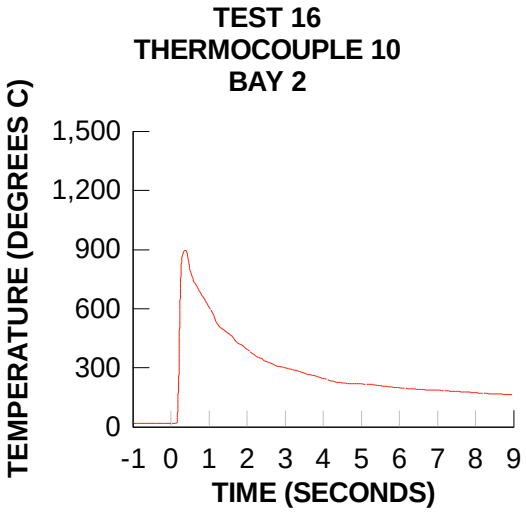
TEST 16
THERMOCOUPLE 10
BAY 2
TEMPERATURE (DEGREES C)
1,500
1,200
900
600
300
0
-1 0 1 2 3 4 5 6 7 8 9
TIME (SECONDS)

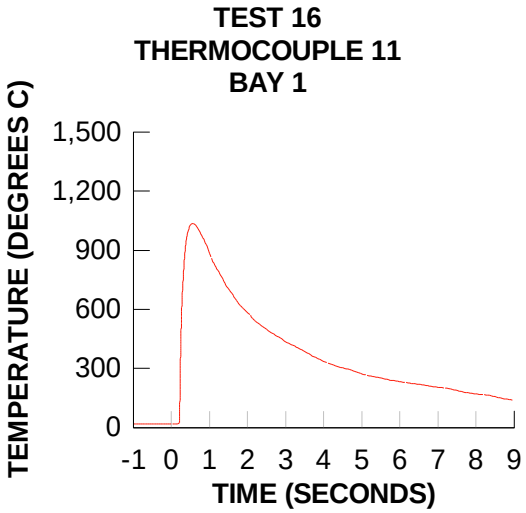
TEST 16
THERMOCOUPLE 11
BAY 1
TEMPERATURE (DEGREES C)
1,500
1,200
900
600
300
0
-1 0 1 2 3 4 5 6 7 8 9
TIME (SECONDS)

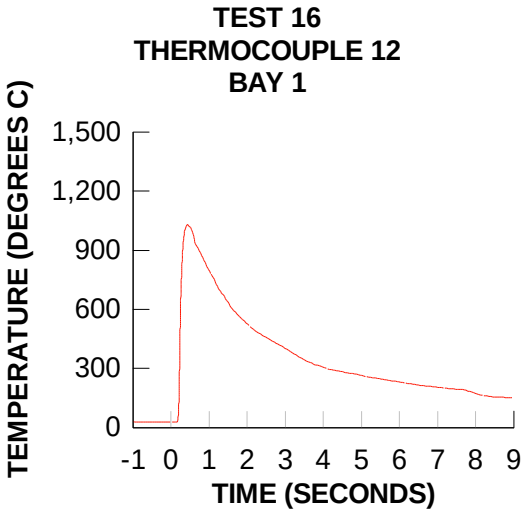
TEST 16
THERMOCOUPLE 12
BAY 1
TEMPERATURE (DEGREES C)
1,500
1,200
900
600
300
0
-1 0 1 2 3 4 5 6 7 8 9
TIME (SECONDS)

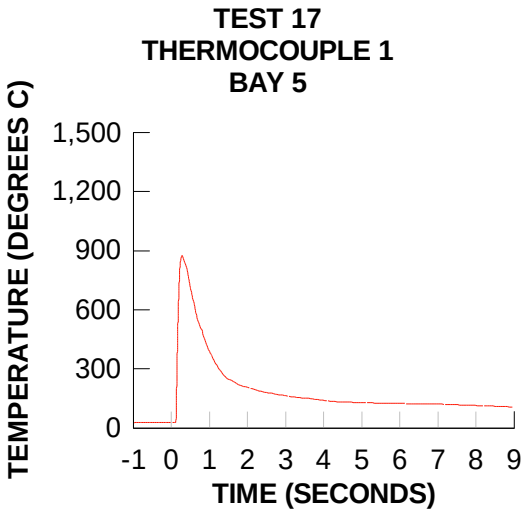
TEST 17
THERMOCOUPLE 1
BAY 5
TEMPERATURE (DEGREES C)
1,500
1,200
900
600
300
0
-1 0 1 2 3 4 5 6 7 8 9
TIME (SECONDS)

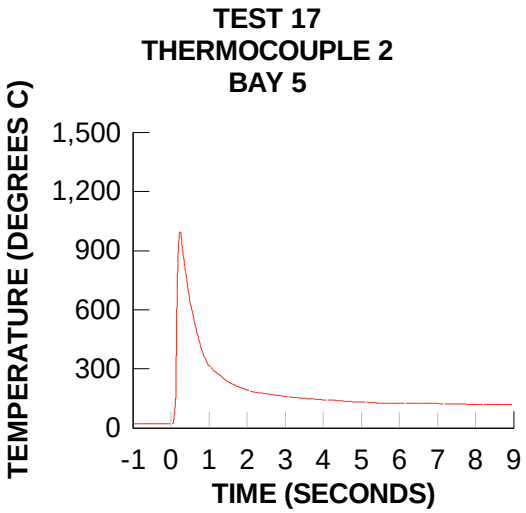
TEST 17
THERMOCOUPLE 2
BAY 5
TEMPERATURE (DEGREES C)
1,500
1,200
900
600
300
0
-1 0 1 2 3 4 5 6 7 8 9
TIME (SECONDS)

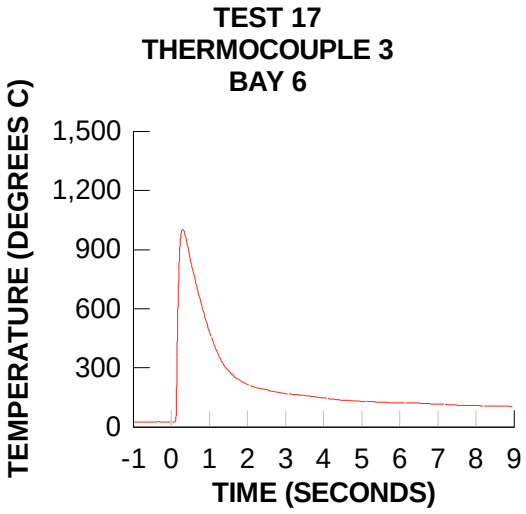
TEST 17
THERMOCOUPLE 3
BAY 6
TEMPERATURE (DEGREES C)
1,500
1,200
900
600
300
0
-1 0 1 2 3 4 5 6 7 8 9
TIME (SECONDS)

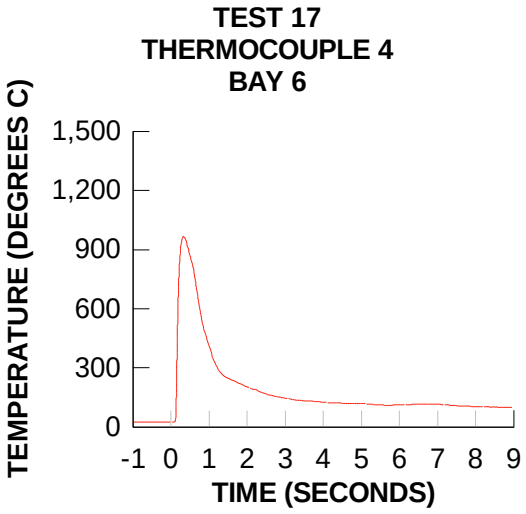
TEST 17
THERMOCOUPLE 4
BAY 6
TEMPERATURE (DEGREES C)
1,500
1,200
900
600
300
0
-1 0 1 2 3 4 5 6 7 8 9
TIME (SECONDS)

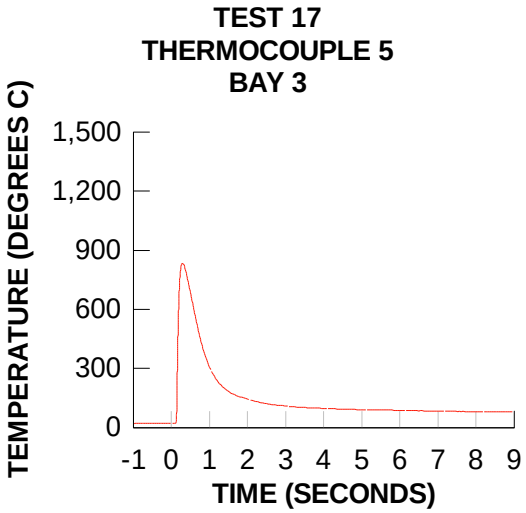
TEST 17
THERMOCOUPLE 5
BAY 3
TEMPERATURE (DEGREES C)
1,500
1,200
900
600
300
0
-1 0 1 2 3 4 5 6 7 8 9
TIME (SECONDS)

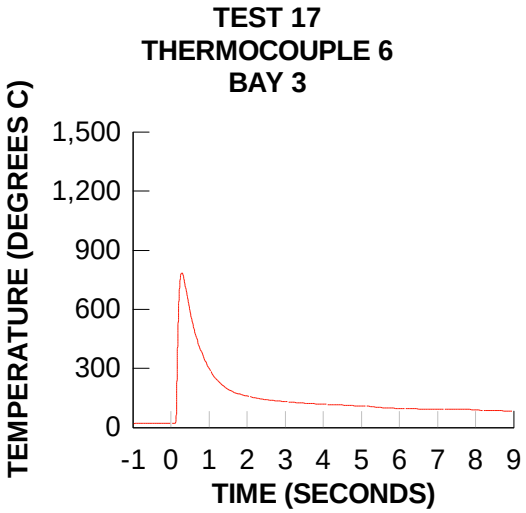
TEST 17
THERMOCOUPLE 6
BAY 3
TEMPERATURE (DEGREES C)
1,500
1,200
900
600
300
0
-1 0 1 2 3 4 5 6 7 8 9
TIME (SECONDS)

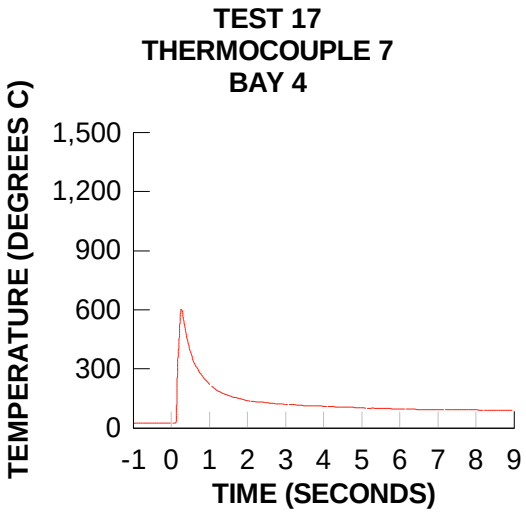
TEST 17
THERMOCOUPLE 7
BAY 4
TEMPERATURE (DEGREES C)
1,500
1,200
900
600
300
0
-1 0 1 2 3 4 5 6 7 8 9
TIME (SECONDS)

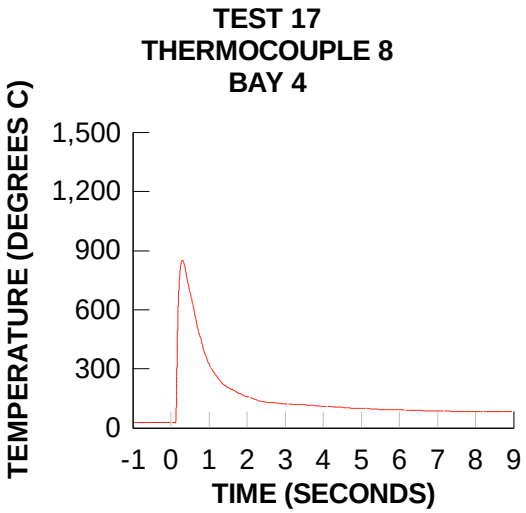
TEST 17
THERMOCOUPLE 8
BAY 4
TEMPERATURE (DEGREES C)
1,500
1,200
900
600
300
0
-1 0 1 2 3 4 5 6 7 8 9
TIME (SECONDS)

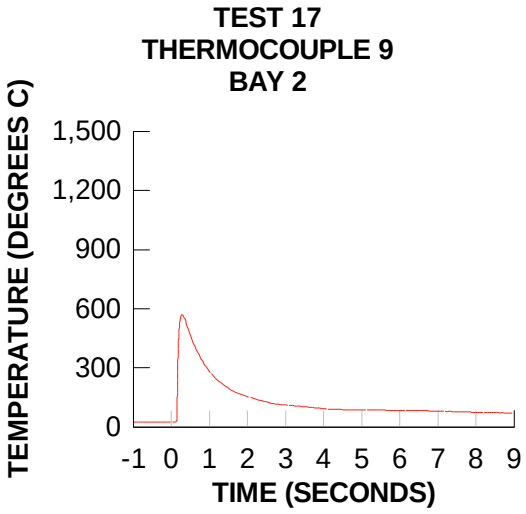
TEST 17
THERMOCOUPLE 9
BAY 2
TEMPERATURE (DEGREES C)
1,500
1,200
900
600
300
0
-1 0 1 2 3 4 5 6 7 8 9
TIME (SECONDS)

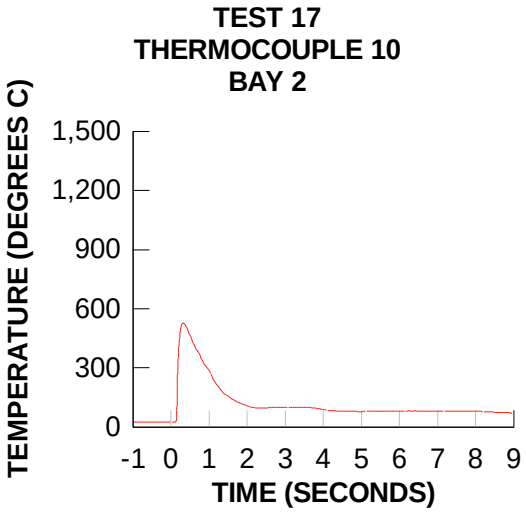
TEST 17
THERMOCOUPLE 10
BAY 2
TEMPERATURE (DEGREES C)
1,500
1,200
900
600
300
0
-1 0 1 2 3 4 5 6 7 8 9
TIME (SECONDS)

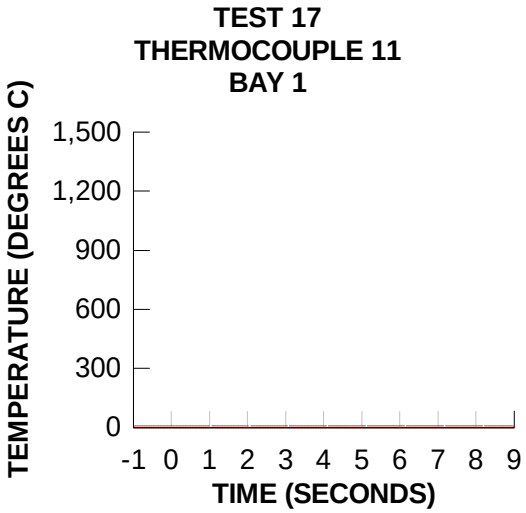
TEST 17
THERMOCOUPLE 11
BAY 1
TEMPERATURE (DEGREES C)
1,500
1,200
900
600
300
0
-1 0 1 2 3 4 5 6 7 8 9
TIME (SECONDS)

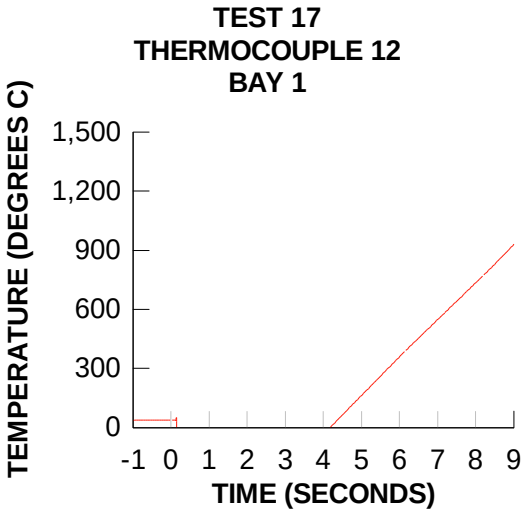
TEST 17
THERMOCOUPLE 12
BAY 1
TEMPERATURE (DEGREES C)
1,500
1,200
900
600
300
0
-1 0 1 2 3 4 5 6 7 8 9
TIME (SECONDS)

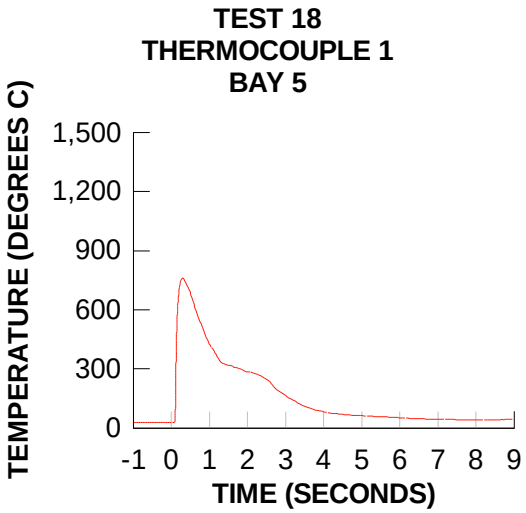
TEST 18
THERMOCOUPLE 1
BAY 5
TEMPERATURE (DEGREES C)
1,500
1,200
900
600
300
0
-1 0 1 2 3 4 5 6 7 8 9
TIME (SECONDS)

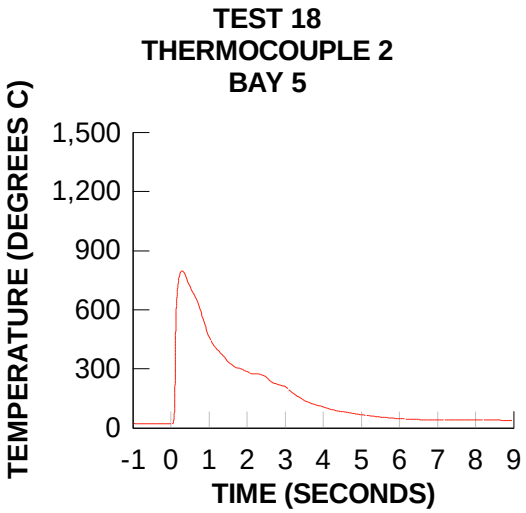
TEST 18
THERMOCOUPLE 2
BAY 5
TEMPERATURE (DEGREES C)
1,500
1,200
900
600
300
0
-1 0 1 2 3 4 5 6 7 8 9
TIME (SECONDS)

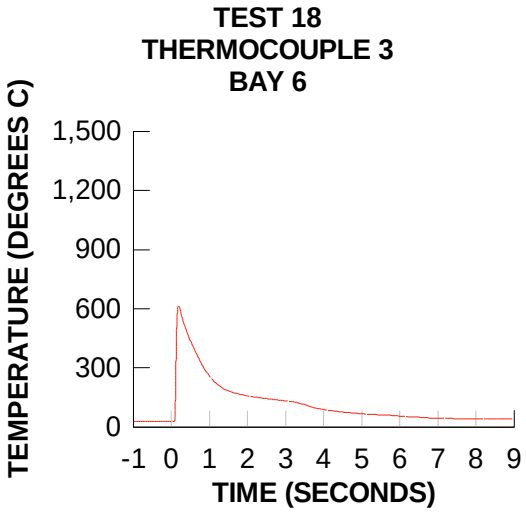
TEST 18
THERMOCOUPLE 3
BAY 6
TEMPERATURE (DEGREES C)
1,500
1,200
900
600
300
0
-1 0 1 2 3 4 5 6 7 8 9
TIME (SECONDS)

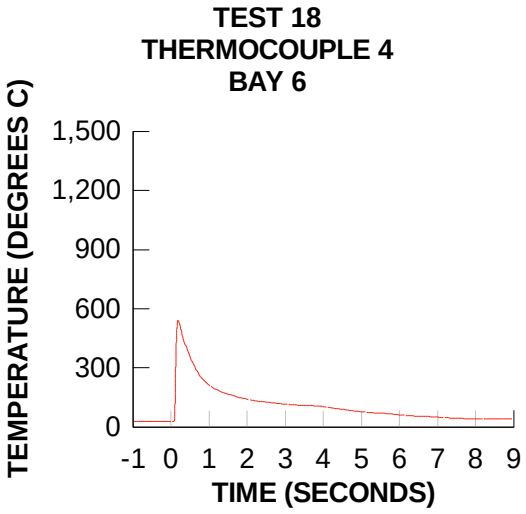
TEST 18
THERMOCOUPLE 4
BAY 6
TEMPERATURE (DEGREES C)
1,500
1,200
900
600
300
0
-1 0 1 2 3 4 5 6 7 8 9
TIME (SECONDS)

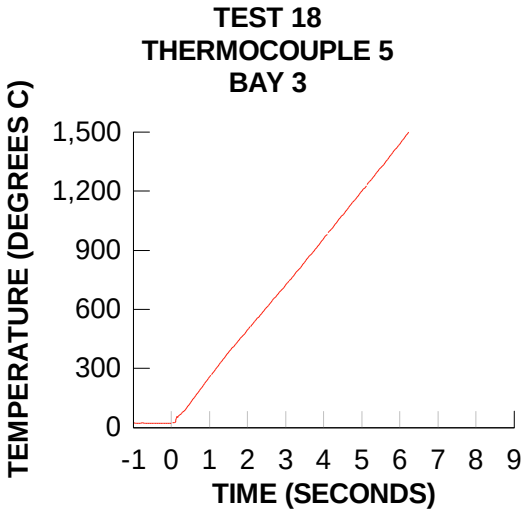
TEST 18
THERMOCOUPLE 5
BAY 3
TEMPERATURE (DEGREES C)
1,500
1,200
900
600
300
0
-1 0 1 2 3 4 5 6 7 8 9
TIME (SECONDS)

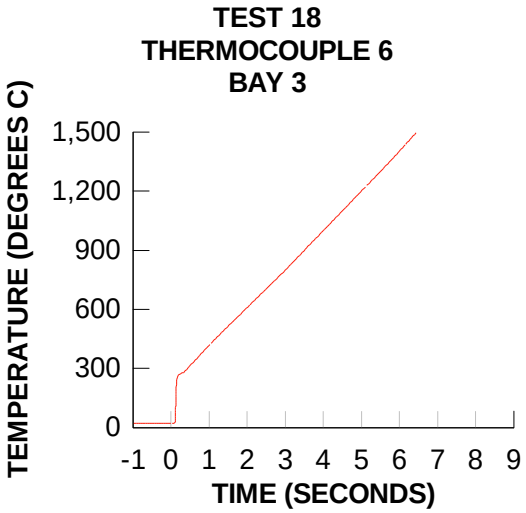
TEST 18
THERMOCOUPLE 6
BAY 3
TEMPERATURE (DEGREES C)
1,500
1,200
900
600
300
0
-1 0 1 2 3 4 5 6 7 8 9
TIME (SECONDS)

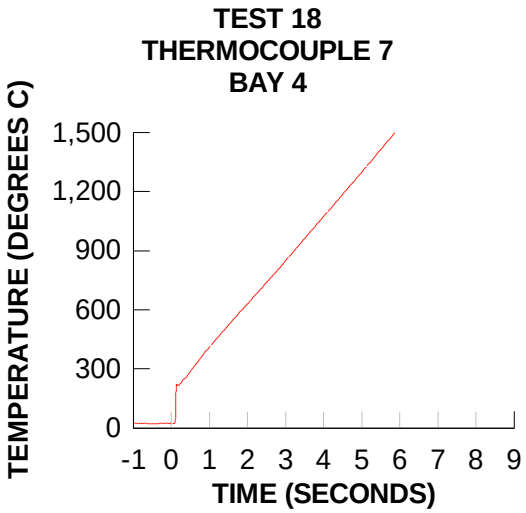
TEST 18
THERMOCOUPLE 7
BAY 4
TEMPERATURE (DEGREES C)
1,500
1,200
900
600
300
0
-1 0 1 2 3 4 5 6 7 8 9
TIME (SECONDS)

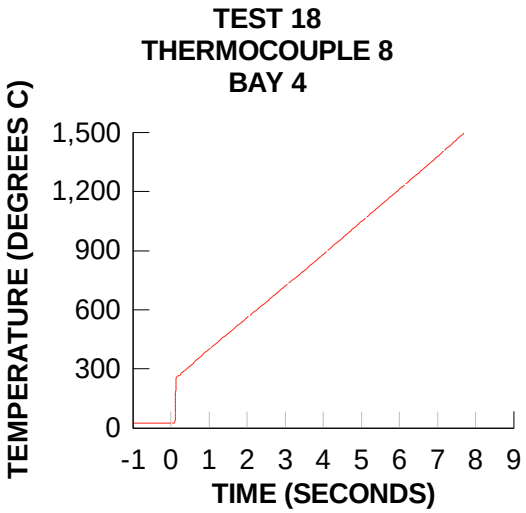
TEST 18
THERMOCOUPLE 8
BAY 4
TEMPERATURE (DEGREES C)
1,500
1,200
900
600
300
0
-1 0 1 2 3 4 5 6 7 8 9
TIME (SECONDS)

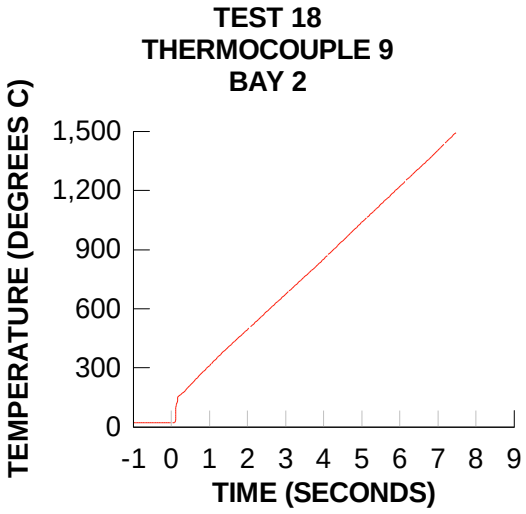
TEST 18
THERMOCOUPLE 9
BAY 2
TEMPERATURE (DEGREES C)
1,500
1,200
900
600
300
0
-1 0 1 2 3 4 5 6 7 8 9
TIME (SECONDS)

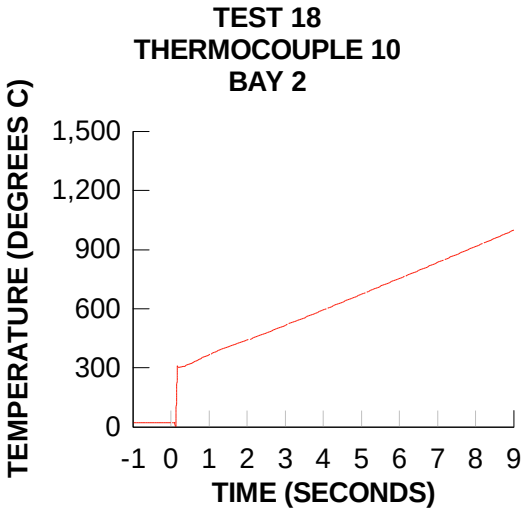
TEST 18
THERMOCOUPLE 10
BAY 2
TEMPERATURE (DEGREES C)
1,500
1,200
900
600
300
0
-1 0 1 2 3 4 5 6 7 8 9
TIME (SECONDS)

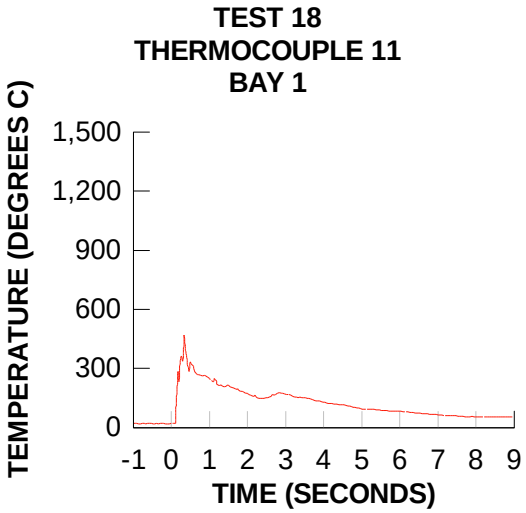
TEST 18
THERMOCOUPLE 11
BAY 1
TEMPERATURE (DEGREES C)
1,500
1,200
900
600
300
0
-1 0 1 2 3 4 5 6 7 8 9
TIME (SECONDS)

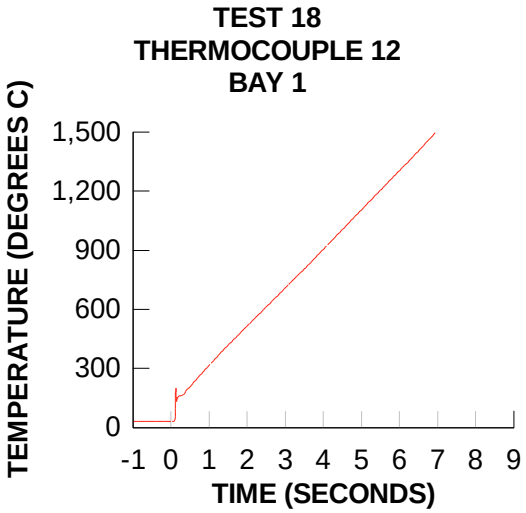
TEST 18
THERMOCOUPLE 12
BAY 1
TEMPERATURE (DEGREES C)
1,500
1,200
900
600
300
0
-1 0 1 2 3 4 5 6 7 8 9
TIME (SECONDS)

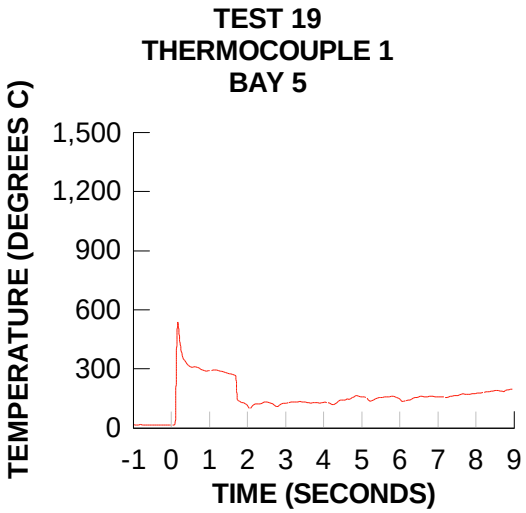
TEST 19
THERMOCOUPLE 1
BAY 5
TEMPERATURE (DEGREES C)
1,500
1,200
900
600
300
0
-1 0 1 2 3 4 5 6 7 8 9
TIME (SECONDS)

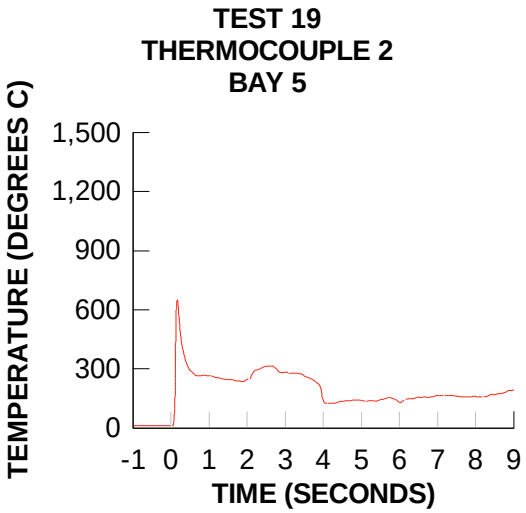
TEST 19
THERMOCOUPLE 2
BAY 5
TEMPERATURE (DEGREES C)
1,500
1,200
900
600
300
0
-1 0 1 2 3 4 5 6 7 8 9
TIME (SECONDS)

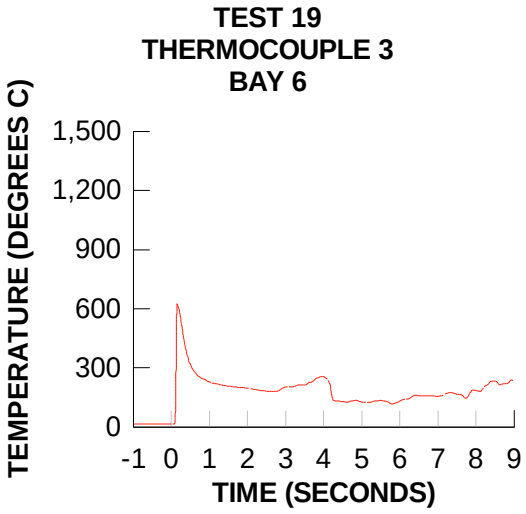
TEST 19
THERMOCOUPLE 3
BAY 6
TEMPERATURE (DEGREES C)
1,500
1,200
900
600
300
0
-1 0 1 2 3 4 5 6 7 8 9
TIME (SECONDS)

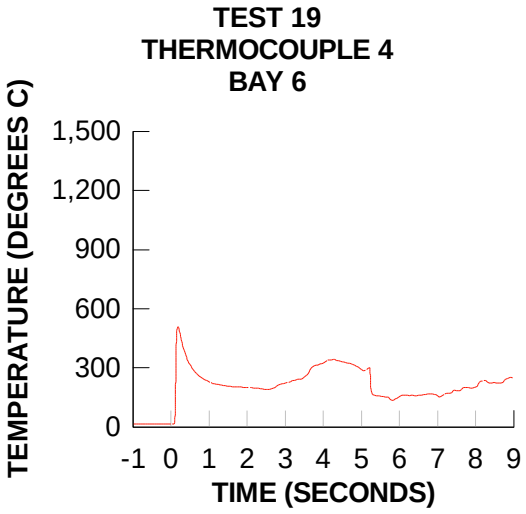
TEST 19
THERMOCOUPLE 4
BAY 6
TEMPERATURE (DEGREES C)
1,500
1,200
900
600
300
0
-1 0 1 2 3 4 5 6 7 8 9
TIME (SECONDS)

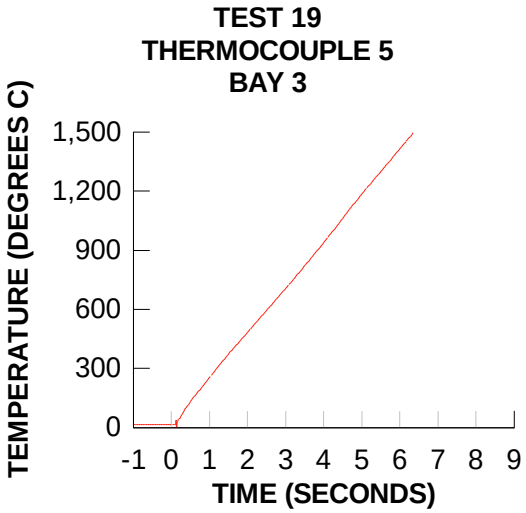
TEST 19
THERMOCOUPLE 5
BAY 3
TEMPERATURE (DEGREES C)
1,500
1,200
900
600
300
0
-1 0 1 2 3 4 5 6 7 8 9
TIME (SECONDS)

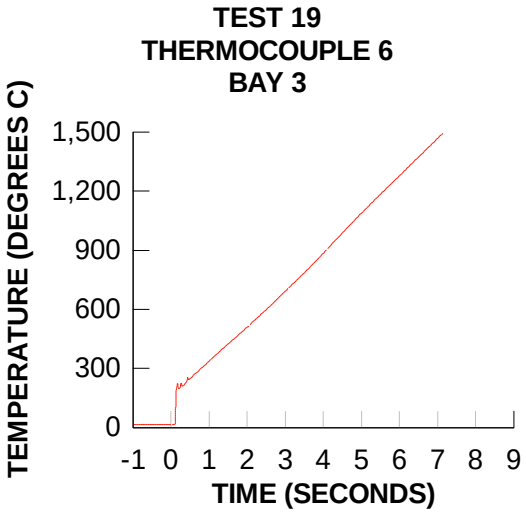
TEST 19
THERMOCOUPLE 6
BAY 3
TEMPERATURE (DEGREES C)
1,500
1,200
900
600
300
0
-1 0 1 2 3 4 5 6 7 8 9
TIME (SECONDS)

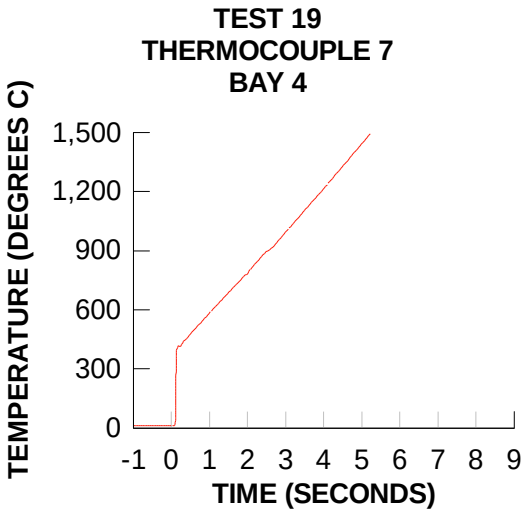
TEST 19
THERMOCOUPLE 7
BAY 4
TEMPERATURE (DEGREES C)
1,500
1,200
900
600
300
0
-1 0 1 2 3 4 5 6 7 8 9
TIME (SECONDS)

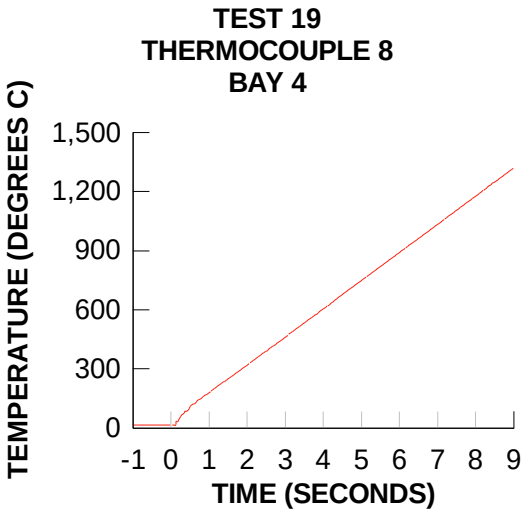
TEST 19
THERMOCOUPLE 8
BAY 4
TEMPERATURE (DEGREES C)
1,500
1,200
900
600
300
0
-1 0 1 2 3 4 5 6 7 8 9
TIME (SECONDS)

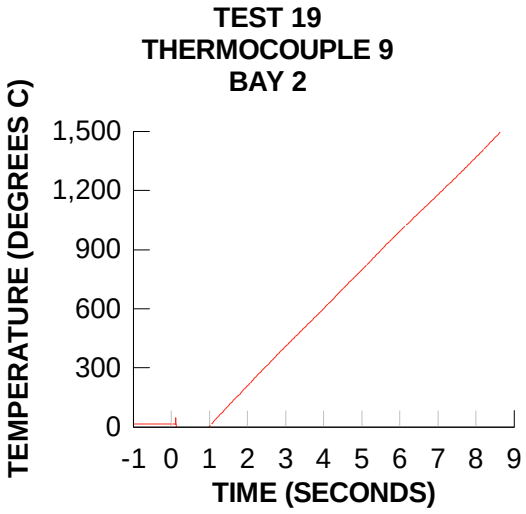
TEST 19
THERMOCOUPLE 9
BAY 2
TEMPERATURE (DEGREES C)
1,500
1,200
900
600
300
0
-1 0 1 2 3 4 5 6 7 8 9
TIME (SECONDS)

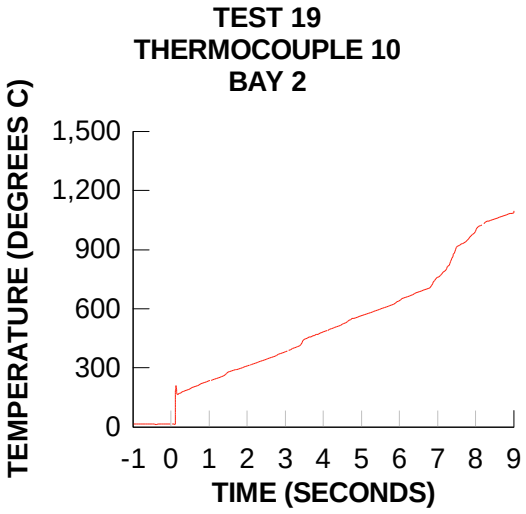
TEST 19
THERMOCOUPLE 10
BAY 2
TEMPERATURE (DEGREES C)
1,500
1,200
900
600
300
0
-1 0 1 2 3 4 5 6 7 8 9
TIME (SECONDS)

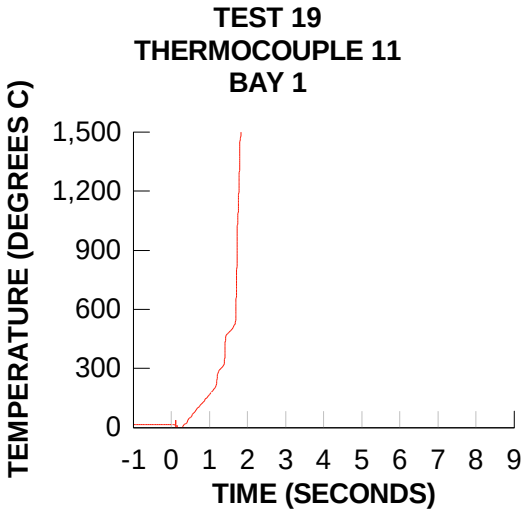
TEST 19
THERMOCOUPLE 11
BAY 1
TEMPERATURE (DEGREES C)
1,500
1,200
900
600
300
0
-1 0 1 2 3 4 5 6 7 8 9
TIME (SECONDS)

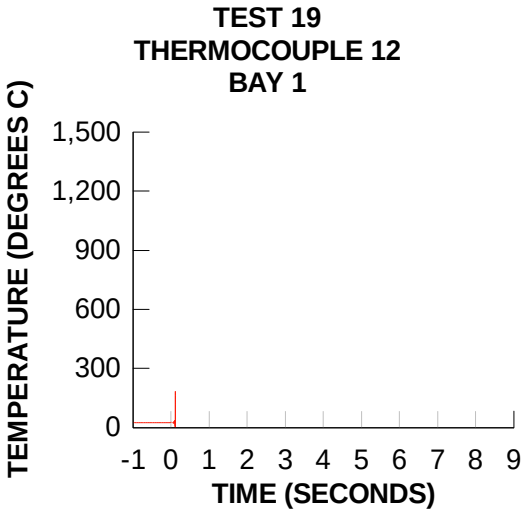
TEST 19
THERMOCOUPLE 12
BAY 1
TEMPERATURE (DEGREES C)
1,500
1,200
900
600
300
0
-1 0 1 2 3 4 5 6 7 8 9
TIME (SECONDS)

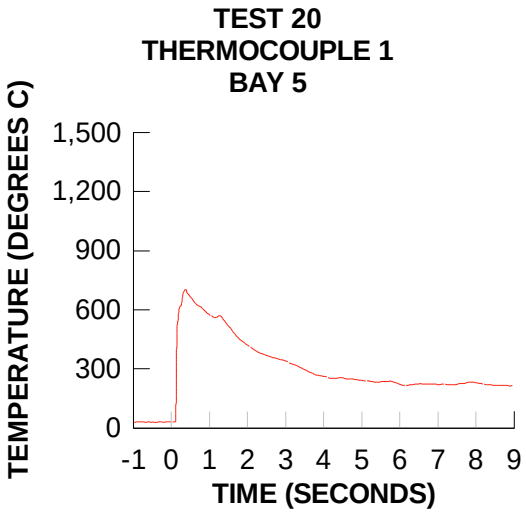
TEST 20
THERMOCOUPLE 1
BAY 5
TEMPERATURE (DEGREES C)
1,500
1,200
900
600
300
0
-1 0 1 2 3 4 5 6 7 8 9
TIME (SECONDS)

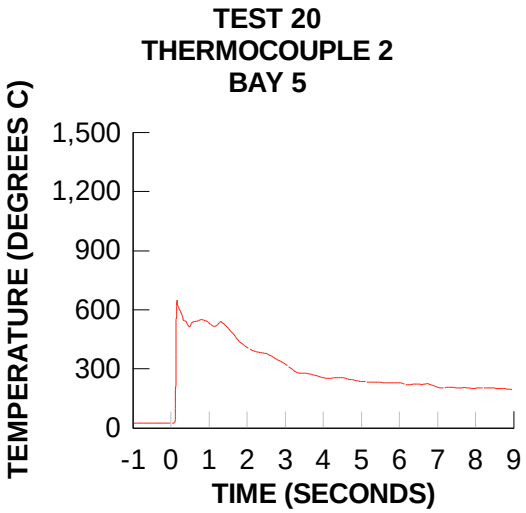
TEST 20
THERMOCOUPLE 2
BAY 5
TEMPERATURE (DEGREES C)
1,500
1,200
900
600
300
0
-1 0 1 2 3 4 5 6 7 8 9
TIME (SECONDS)

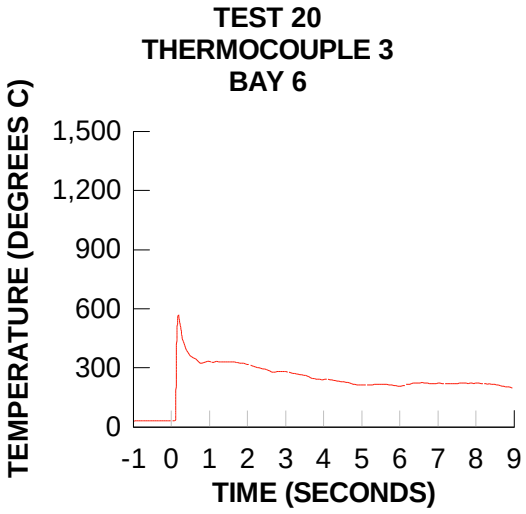
TEST 20
THERMOCOUPLE 3
BAY 6
TEMPERATURE (DEGREES C)
1,500
1,200
900
600
300
0
-1 0 1 2 3 4 5 6 7 8 9
TIME (SECONDS)

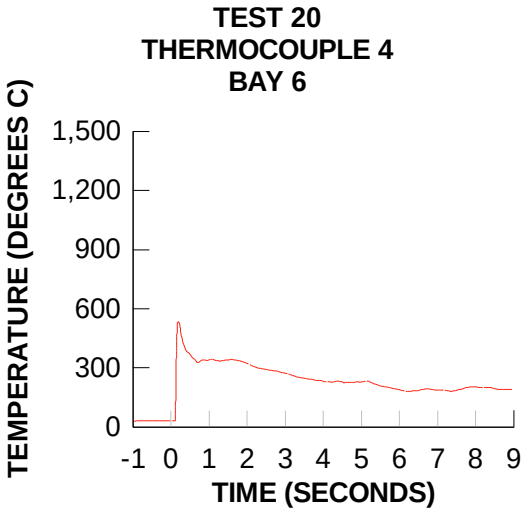
TEST 20
THERMOCOUPLE 4
BAY 6
TEMPERATURE (DEGREES C)
1,500
1,200
900
600
300
0
-1 0 1 2 3 4 5 6 7 8 9
TIME (SECONDS)

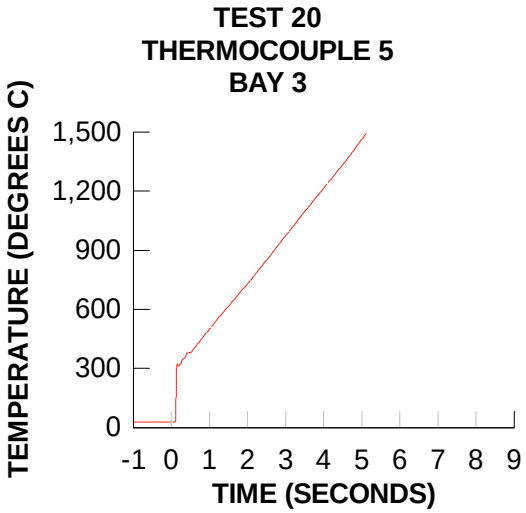
TEST 20
THERMOCOUPLE 5
BAY 3
TEMPERATURE (DEGREES C)
1,500
1,200
900
600
300
0
-1 0 1 2 3 4 5 6 7 8 9
TIME (SECONDS)

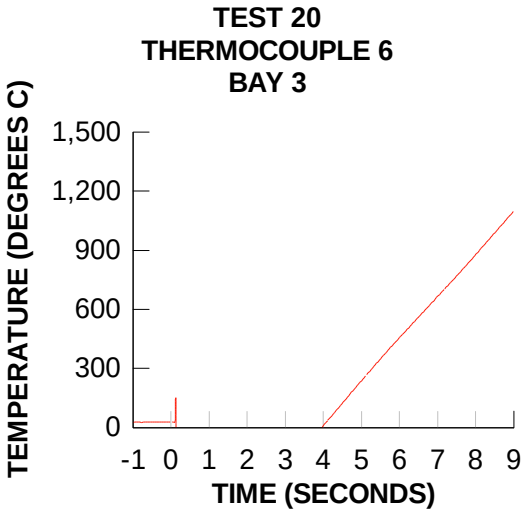
TEST 20
THERMOCOUPLE 6
BAY 3
TEMPERATURE (DEGREES C)
1,500
1,200
900
600
300
0
-1 0 1 2 3 4 5 6 7 8 9
TIME (SECONDS)

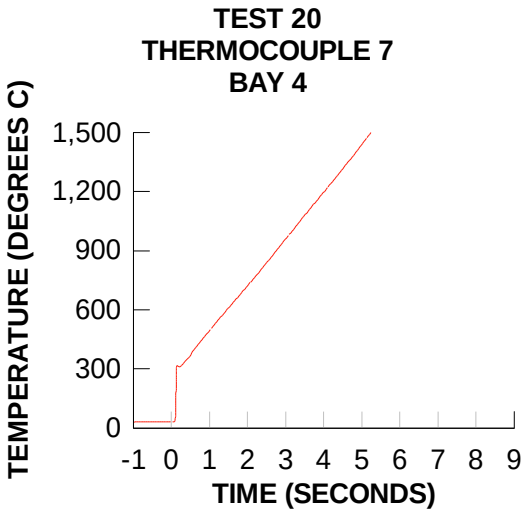
TEST 20
THERMOCOUPLE 7
BAY 4
TEMPERATURE (DEGREES C)
1,500
1,200
900
600
300
0
-1 0 1 2 3 4 5 6 7 8 9
TIME (SECONDS)

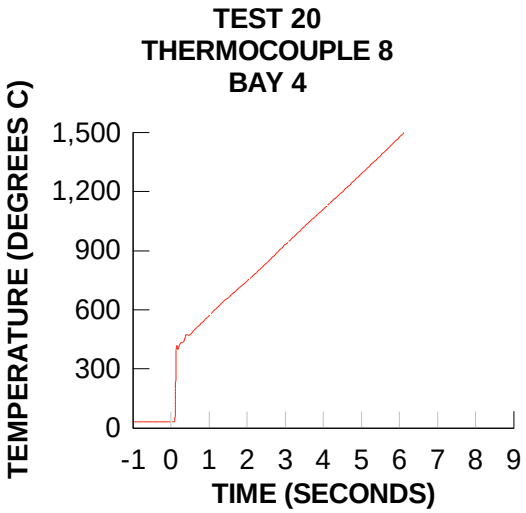
TEST 20
THERMOCOUPLE 8
BAY 4
TEMPERATURE (DEGREES C)
1,500
1,200
900
600
300
0
-1 0 1 2 3 4 5 6 7 8 9
TIME (SECONDS)

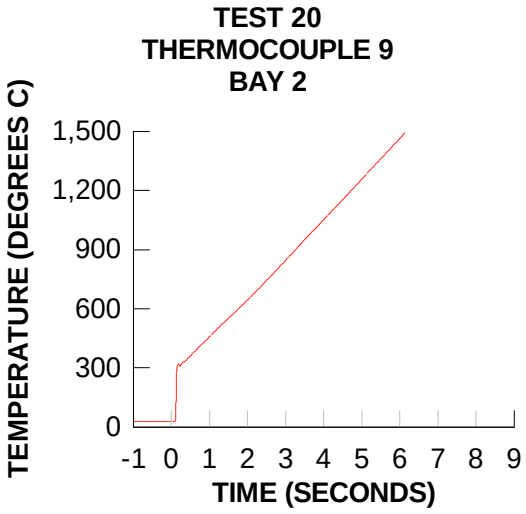
TEST 20
THERMOCOUPLE 9
BAY 2
TEMPERATURE (DEGREES C)
1,500
1,200
900
600
300
0
-1 0 1 2 3 4 5 6 7 8 9
TIME (SECONDS)

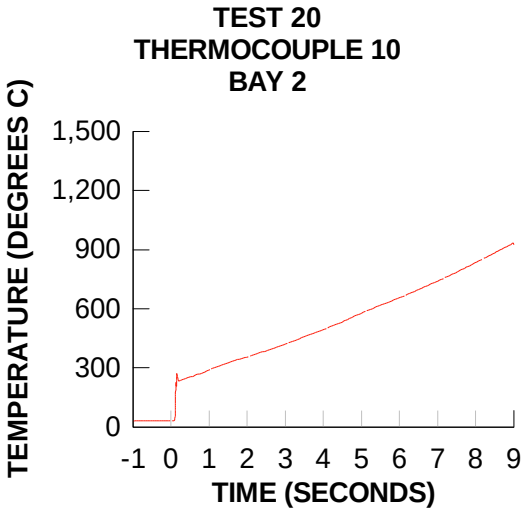
TEST 20
THERMOCOUPLE 10
BAY 2
TEMPERATURE (DEGREES C)
1,500
1,200
900
600
300
0
-1 0 1 2 3 4 5 6 7 8 9
TIME (SECONDS)

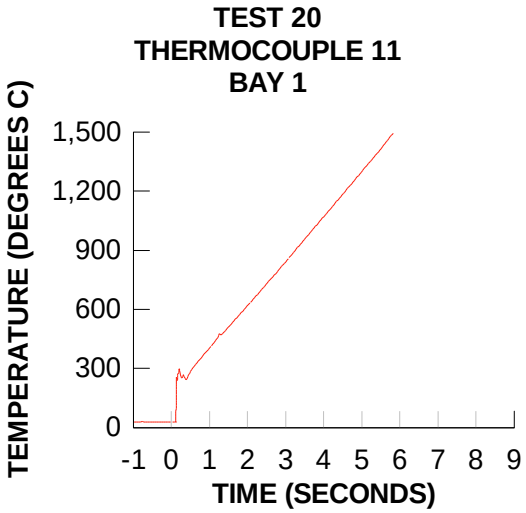
TEST 20
THERMOCOUPLE 11
BAY 1
TEMPERATURE (DEGREES C)
1,500
1,200
900
600
300
0
-1 0 1 2 3 4 5 6 7 8 9
TIME (SECONDS)

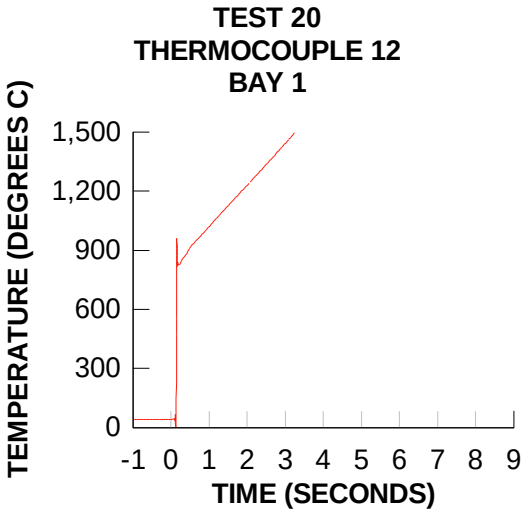
TEST 20
THERMOCOUPLE 12
BAY 1
TEMPERATURE (DEGREES C)
1,500
1,200
900
600
300
0
-1 0 1 2 3 4 5 6 7 8 9
TIME (SECONDS)

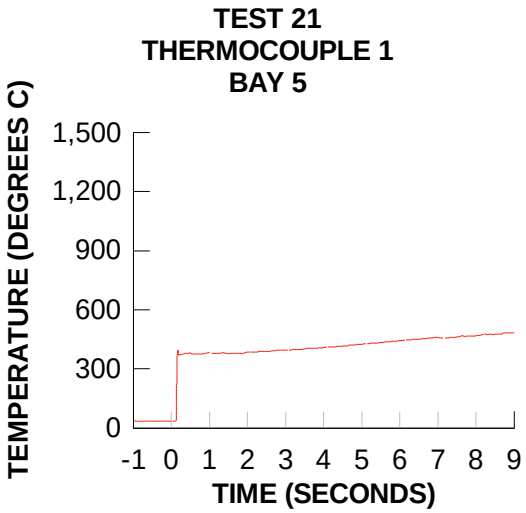
TEST 21
THERMOCOUPLE 1
BAY 5
TEMPERATURE (DEGREES C)
1,500
1,200
900
600
300
0
-1 0 1 2 3 4 5 6 7 8 9
TIME (SECONDS)

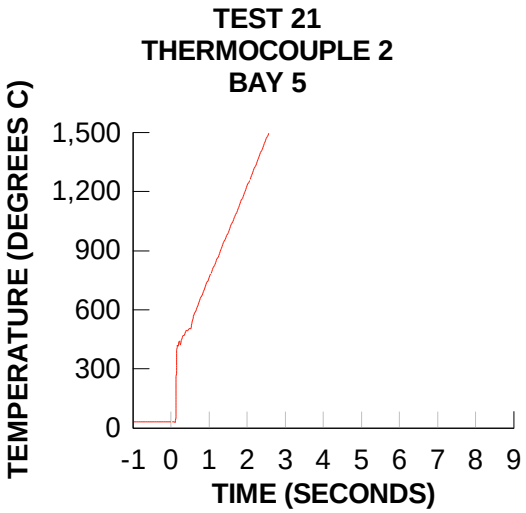
TEST 21
THERMOCOUPLE 2
BAY 5
TEMPERATURE (DEGREES C)
1,500
1,200
900
600
300
0
-1 0 1 2 3 4 5 6 7 8 9
TIME (SECONDS)

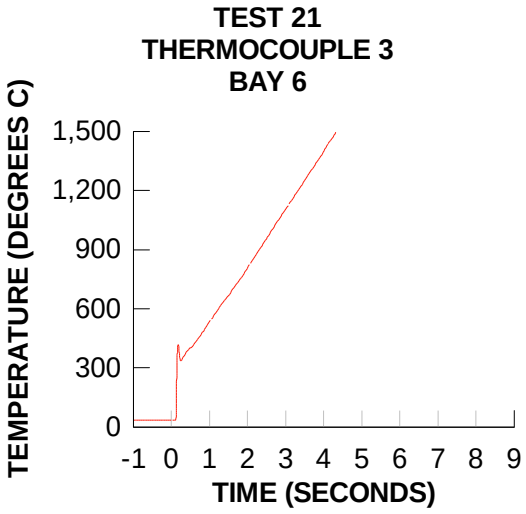
TEST 21
THERMOCOUPLE 3
BAY 6
TEMPERATURE (DEGREES C)
1,500
1,200
900
600
300
0
-1 0 1 2 3 4 5 6 7 8 9
TIME (SECONDS)

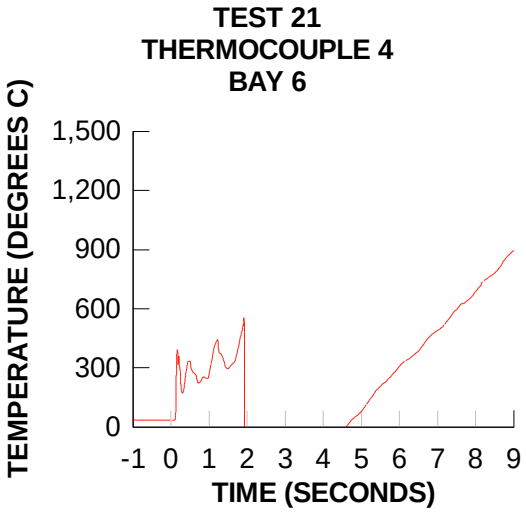
TEST 21
THERMOCOUPLE 4
BAY 6
TEMPERATURE (DEGREES C)
1,500
1,200
900
600
300
0
-1 0 1 2 3 4 5 6 7 8 9
TIME (SECONDS)

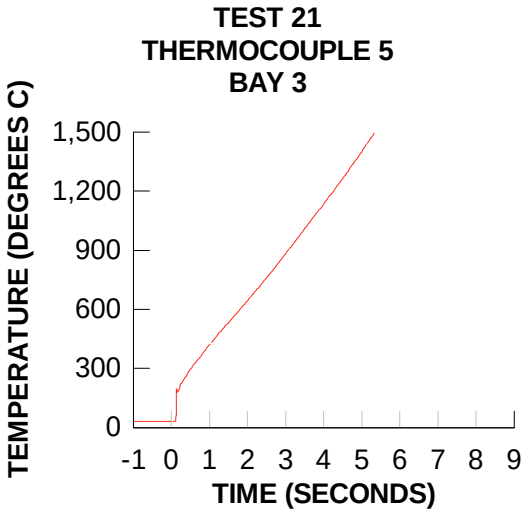
TEST 21
THERMOCOUPLE 5
BAY 3
TEMPERATURE (DEGREES C)
1,500
1,200
900
600
300
0
-1 0 1 2 3 4 5 6 7 8 9
TIME (SECONDS)

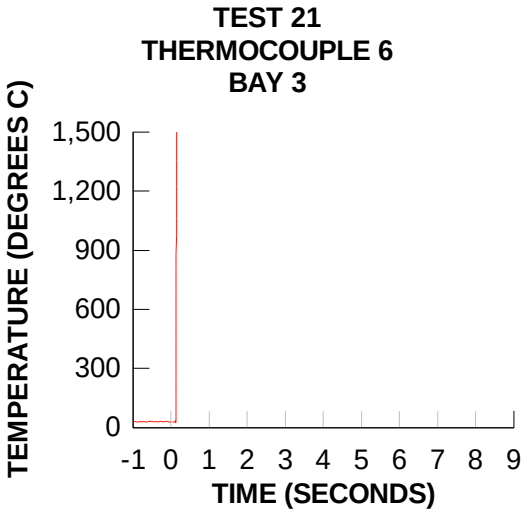
TEST 21
THERMOCOUPLE 6
BAY 3
TEMPERATURE (DEGREES C)
1,500
1,200
900
600
300
0
-1 0 1 2 3 4 5 6 7 8 9
TIME (SECONDS)

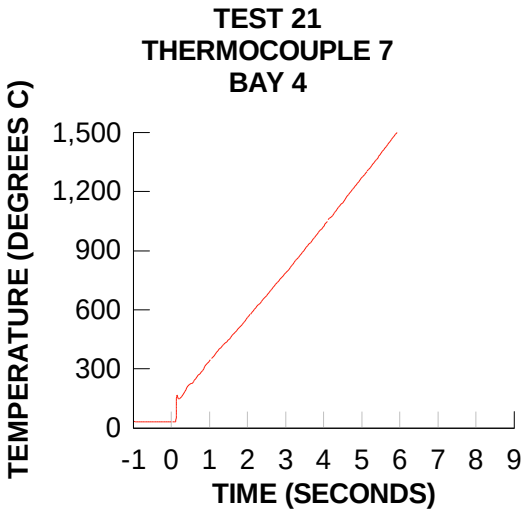
TEST 21
THERMOCOUPLE 7
BAY 4
TEMPERATURE (DEGREES C)
1,500
1,200
900
600
300
0
-1 0 1 2 3 4 5 6 7 8 9
TIME (SECONDS)

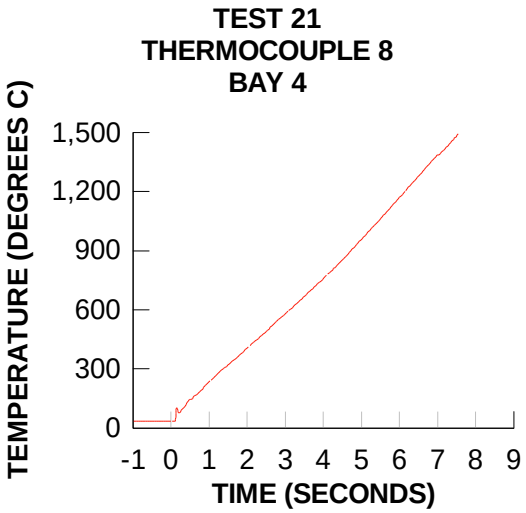
TEST 21
THERMOCOUPLE 8
BAY 4
TEMPERATURE (DEGREES C)
1,500
1,200
900
600
300
0
-1 0 1 2 3 4 5 6 7 8 9
TIME (SECONDS)

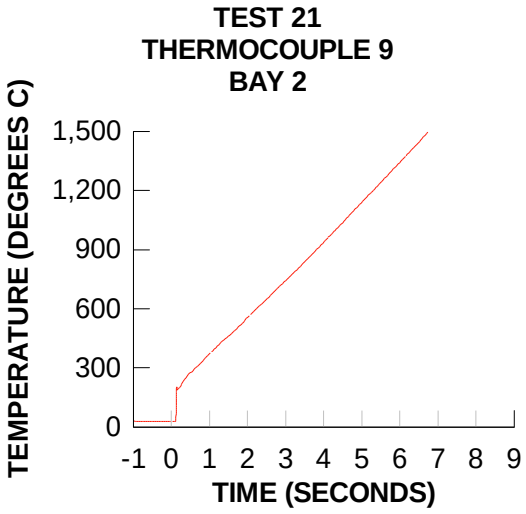
TEST 21
THERMOCOUPLE 9
BAY 2
TEMPERATURE (DEGREES C)
1,500
1,200
900
600
300
0
-1 0 1 2 3 4 5 6 7 8 9
TIME (SECONDS)

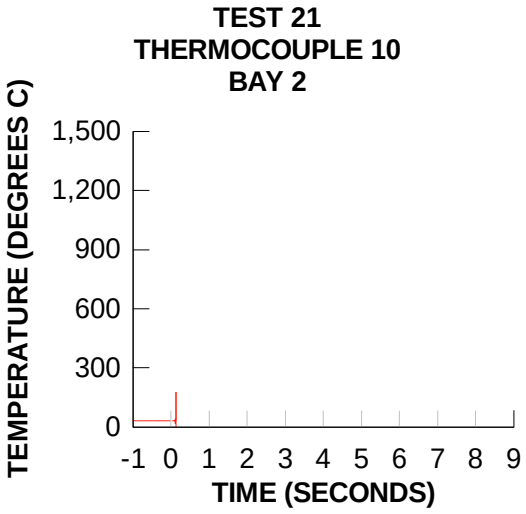
TEST 21
THERMOCOUPLE 10
BAY 2
TEMPERATURE (DEGREES C)
1,500
1,200
900
600
300
0
-1 0 1 2 3 4 5 6 7 8 9
TIME (SECONDS)

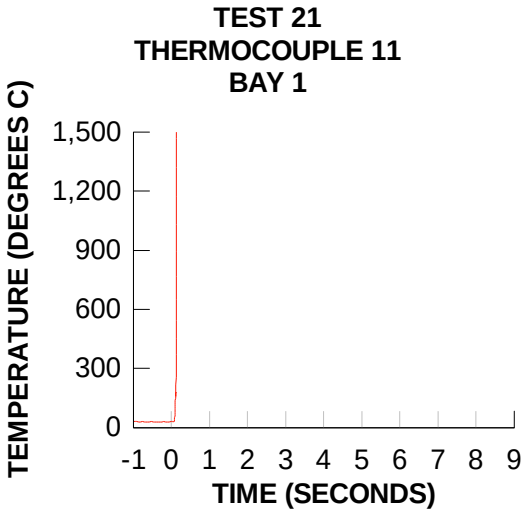
TEST 21
THERMOCOUPLE 11
BAY 1
TEMPERATURE (DEGREES C)
1,500
1,200
900
600
300
0
-1 0 1 2 3 4 5 6 7 8 9
TIME (SECONDS)

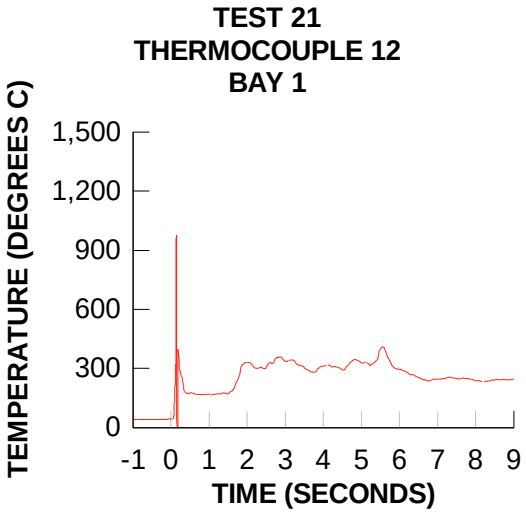
TEST 21
THERMOCOUPLE 12
BAY 1
TEMPERATURE (DEGREES C)
1,500
1,200
900
600
300
0
-1 0 1 2 3 4 5 6 7 8 9
TIME (SECONDS)

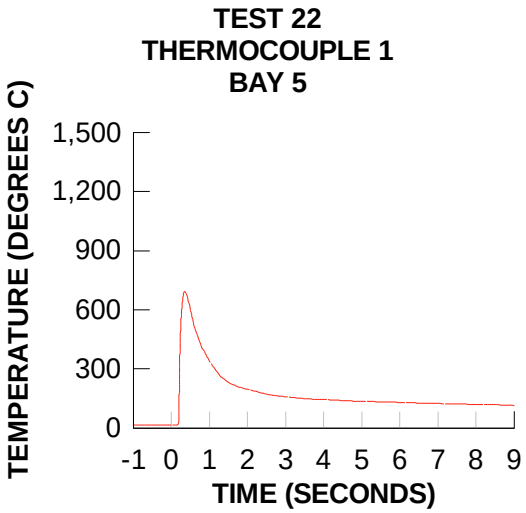
TEST 22
THERMOCOUPLE 1
BAY 5
TEMPERATURE (DEGREES C)
1,500
1,200
900
600
300
0
-1 0 1 2 3 4 5 6 7 8 9
TIME (SECONDS)

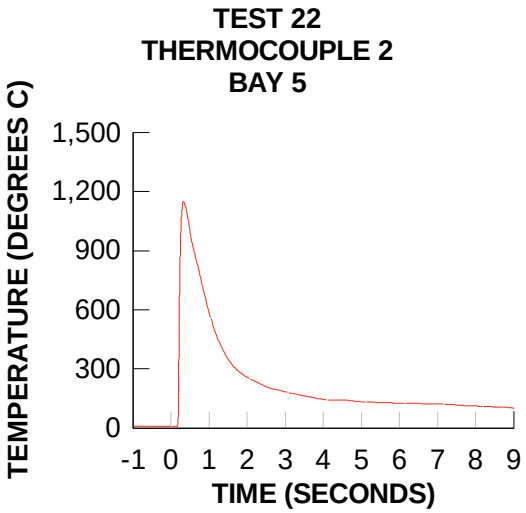
TEST 22
THERMOCOUPLE 2
BAY 5
TEMPERATURE (DEGREES C)
1,500
1,200
900
600
300
0
-1 0 1 2 3 4 5 6 7 8 9
TIME (SECONDS)

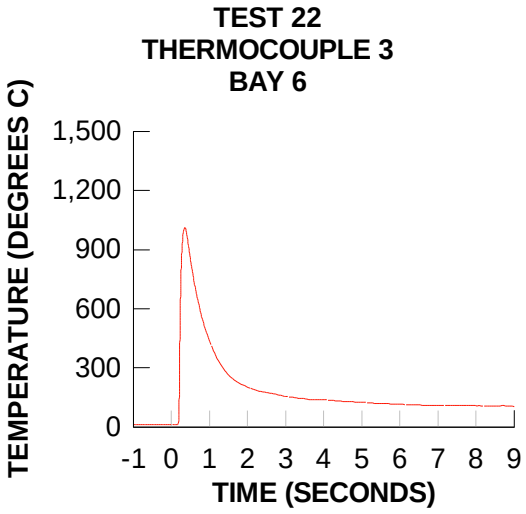
TEST 22
THERMOCOUPLE 3
BAY 6
TEMPERATURE (DEGREES C)
1,500
1,200
900
600
300
0
-1 0 1 2 3 4 5 6 7 8 9
TIME (SECONDS)

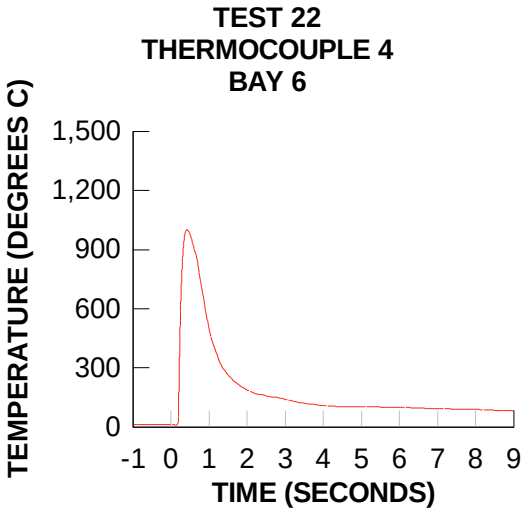
TEST 22
THERMOCOUPLE 4
BAY 6
TEMPERATURE (DEGREES C)
1,500
1,200
900
600
300
0
-1 0 1 2 3 4 5 6 7 8 9
TIME (SECONDS)

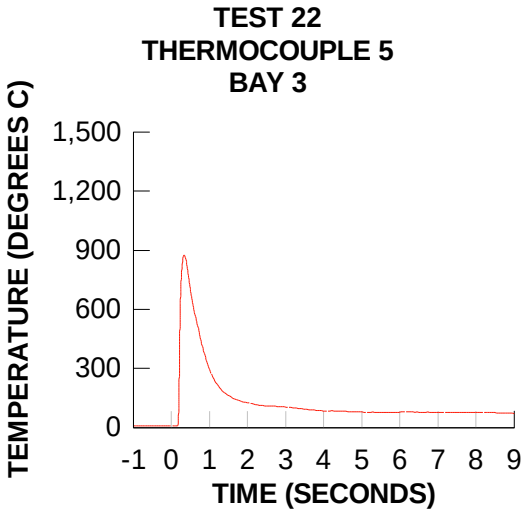
TEST 22
THERMOCOUPLE 5
BAY 3
TEMPERATURE (DEGREES C)
1,500
1,200
900
600
300
0
-1 0 1 2 3 4 5 6 7 8 9
TIME (SECONDS)

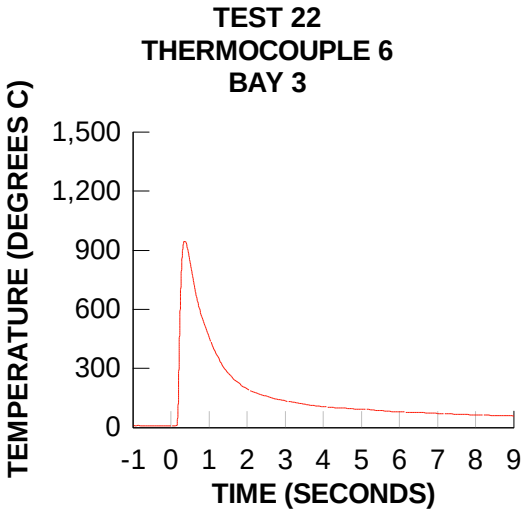
TEST 22
THERMOCOUPLE 6
BAY 3
TEMPERATURE (DEGREES C)
1,500
1,200
900
600
300
0
-1 0 1 2 3 4 5 6 7 8 9
TIME (SECONDS)

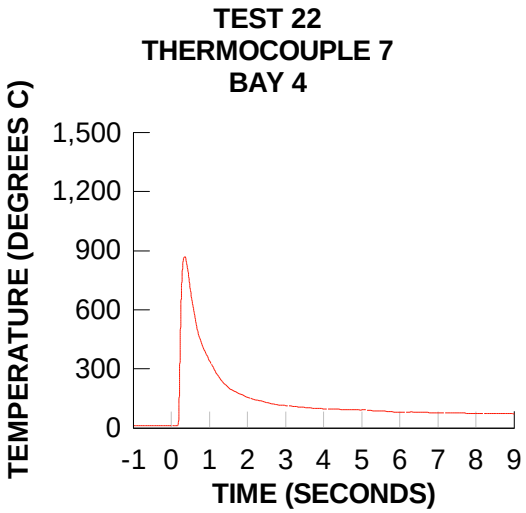
TEST 22
THERMOCOUPLE 7
BAY 4
TEMPERATURE (DEGREES C)
1,500
1,200
900
600
300
0
-1 0 1 2 3 4 5 6 7 8 9
TIME (SECONDS)

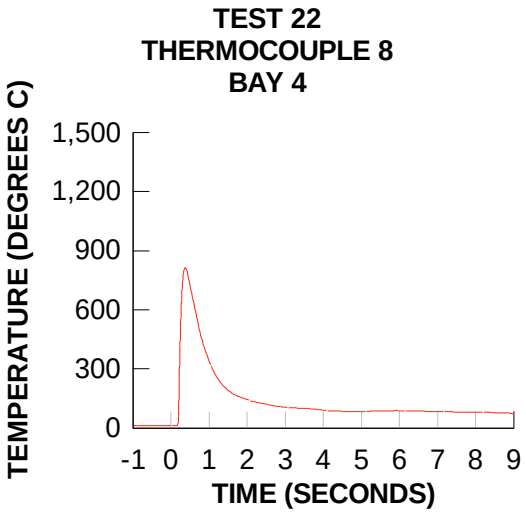
TEST 22
THERMOCOUPLE 8
BAY 4
TEMPERATURE (DEGREES C)
1,500
1,200
900
600
300
0
-1 0 1 2 3 4 5 6 7 8 9
TIME (SECONDS)

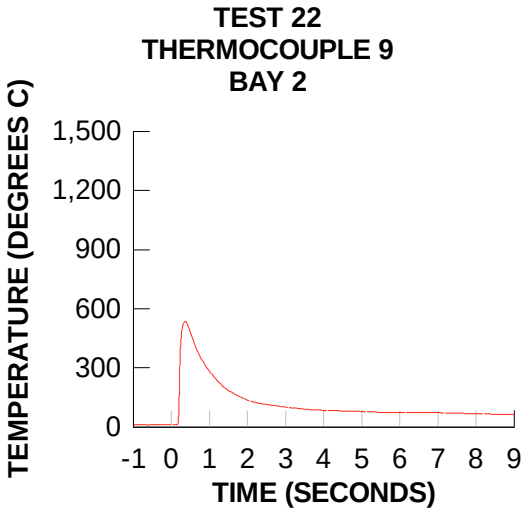
TEST 22
THERMOCOUPLE 9
BAY 2
TEMPERATURE (DEGREES C)
1,500
1,200
900
600
300
0
-1 0 1 2 3 4 5 6 7 8 9
TIME (SECONDS)

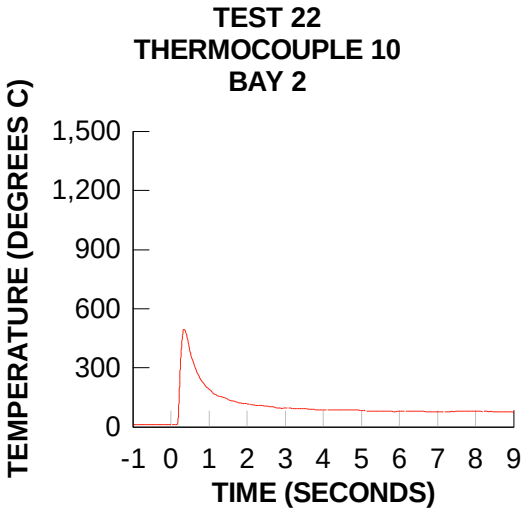
TEST 22
THERMOCOUPLE 10
BAY 2
TEMPERATURE (DEGREES C)
1,500
1,200
900
600
300
0
-1 0 1 2 3 4 5 6 7 8 9
TIME (SECONDS)

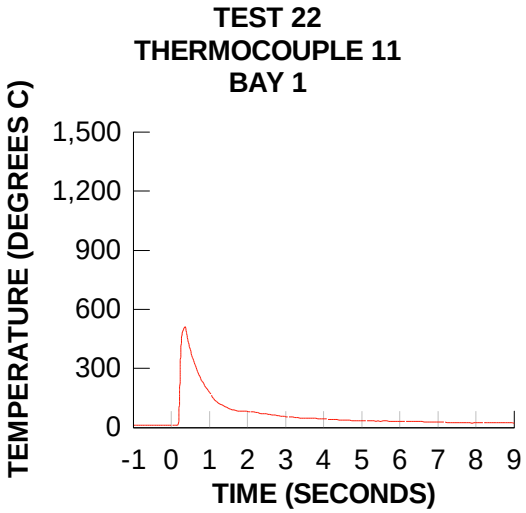
TEST 22
THERMOCOUPLE 11
BAY 1
TEMPERATURE (DEGREES C)
1,500
1,200
900
600
300
0
-1 0 1 2 3 4 5 6 7 8 9
TIME (SECONDS)

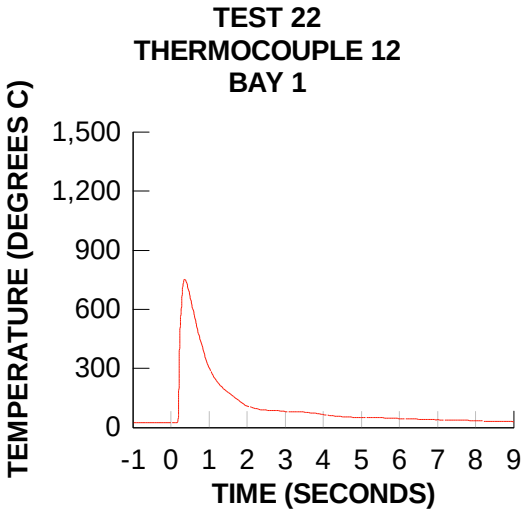
TEST 22
THERMOCOUPLE 12
BAY 1
TEMPERATURE (DEGREES C)
1,500
1,200
900
600
300
0
-1 0 1 2 3 4 5 6 7 8 9
TIME (SECONDS)

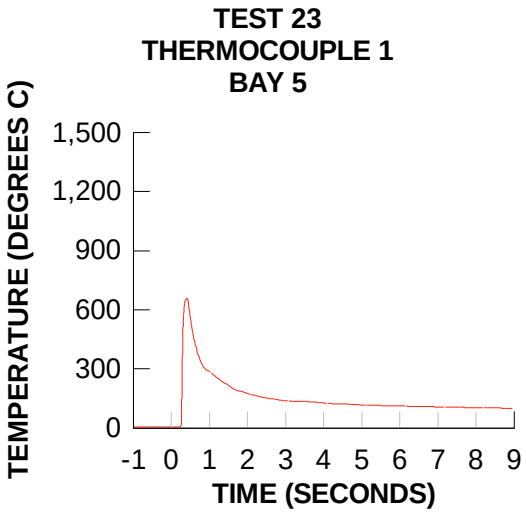
TEST 23
THERMOCOUPLE 1
BAY 5
TEMPERATURE (DEGREES C)
1,500
1,200
900
600
300
0
-1 0 1 2 3 4 5 6 7 8 9
TIME (SECONDS)

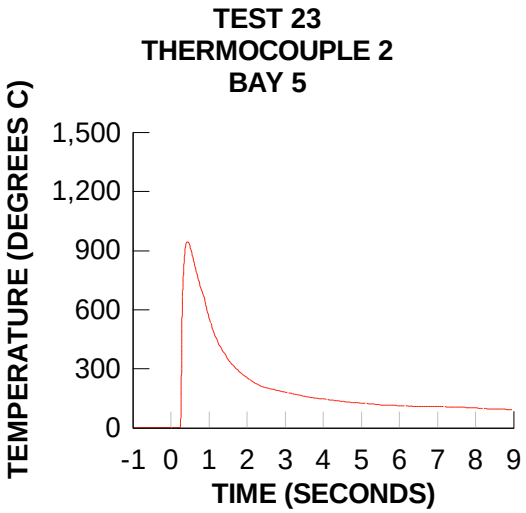
TEST 23
THERMOCOUPLE 2
BAY 5
TEMPERATURE (DEGREES C)
1,500
1,200
900
600
300
0
-1 0 1 2 3 4 5 6 7 8 9
TIME (SECONDS)

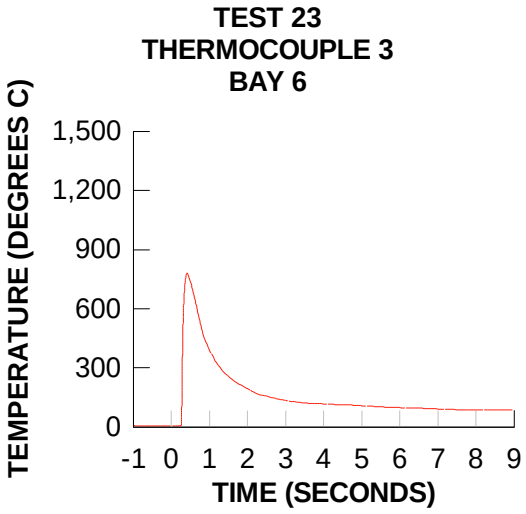
TEST 23
THERMOCOUPLE 3
BAY 6
TEMPERATURE (DEGREES C)
1,500
1,200
900
600
300
0
-1 0 1 2 3 4 5 6 7 8 9
TIME (SECONDS)

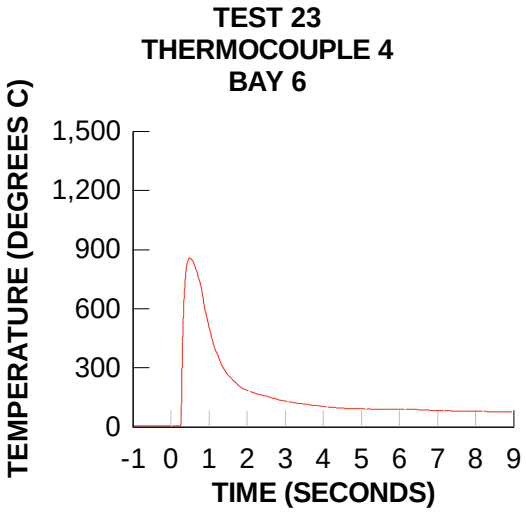
TEST 23
THERMOCOUPLE 4
BAY 6
TEMPERATURE (DEGREES C)
1,500
1,200
900
600
300
0
-1 0 1 2 3 4 5 6 7 8 9
TIME (SECONDS)

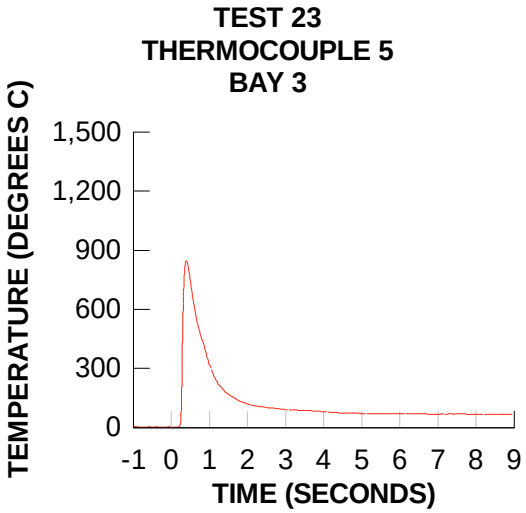
TEST 23
THERMOCOUPLE 5
BAY 3
TEMPERATURE (DEGREES C)
1,500
1,200
900
600
300
0
-1 0 1 2 3 4 5 6 7 8 9
TIME (SECONDS)

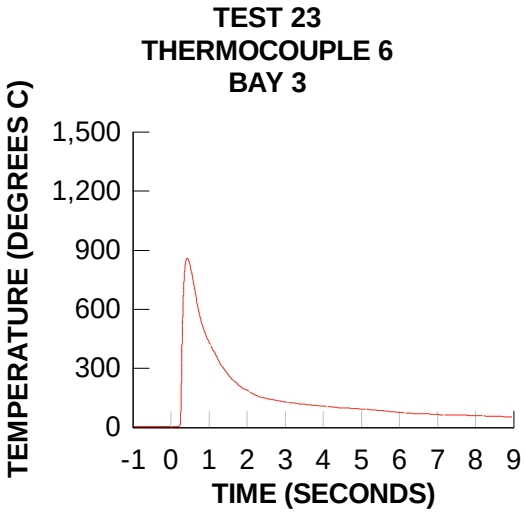
TEST 23
THERMOCOUPLE 6
BAY 3
TEMPERATURE (DEGREES C)
1,500
1,200
900
600
300
0
-1 0 1 2 3 4 5 6 7 8 9
TIME (SECONDS)

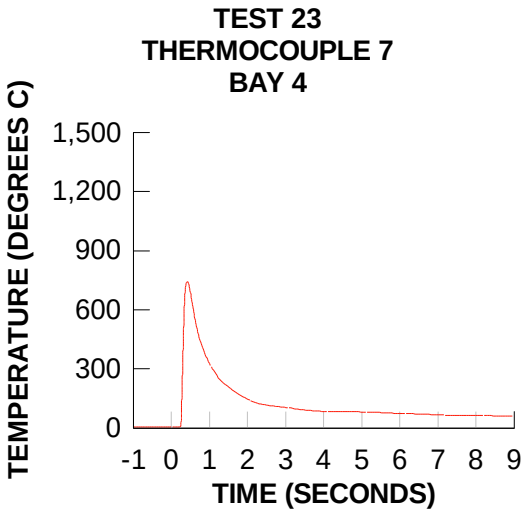
TEST 23
THERMOCOUPLE 7
BAY 4
TEMPERATURE (DEGREES C)
1,500
1,200
900
600
300
0
-1 0 1 2 3 4 5 6 7 8 9
TIME (SECONDS)

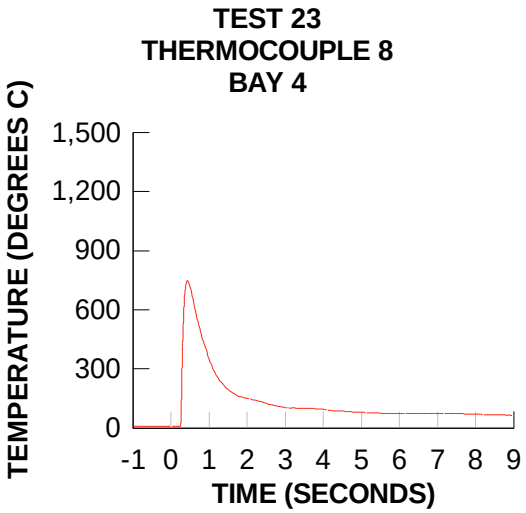
TEST 23
THERMOCOUPLE 8
BAY 4
TEMPERATURE (DEGREES C)
1,500
1,200
900
600
300
0
-1 0 1 2 3 4 5 6 7 8 9
TIME (SECONDS)

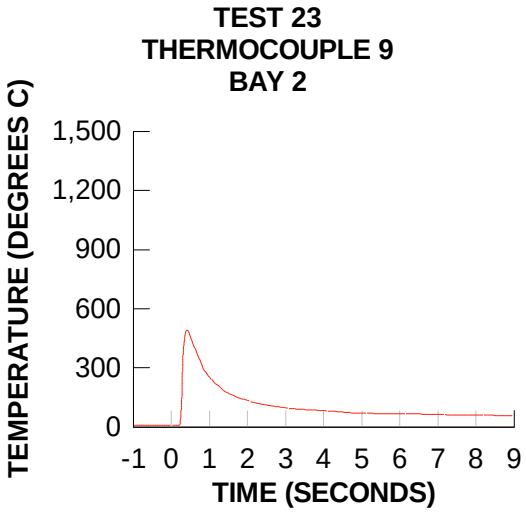
TEST 23
THERMOCOUPLE 9
BAY 2
TEMPERATURE (DEGREES C)
1,500
1,200
900
600
300
0
-1 0 1 2 3 4 5 6 7 8 9
TIME (SECONDS)

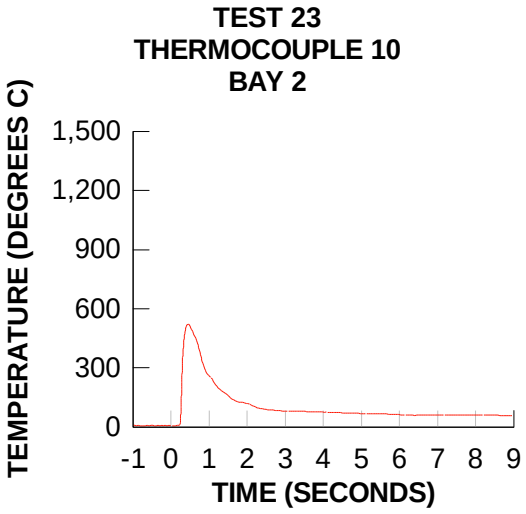
TEST 23
THERMOCOUPLE 10
BAY 2
TEMPERATURE (DEGREES C)
1,500
1,200
900
600
300
0
-1 0 1 2 3 4 5 6 7 8 9
TIME (SECONDS)

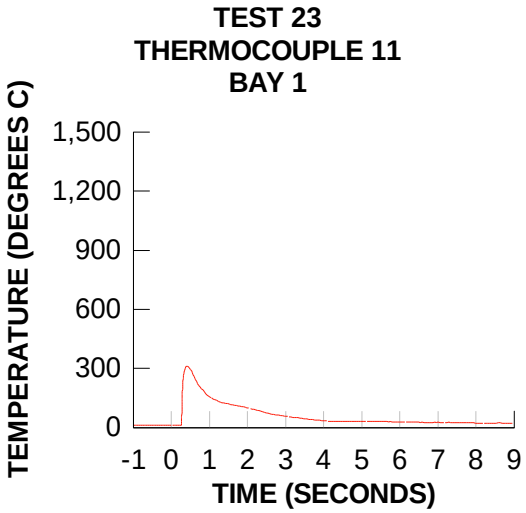
TEST 23
THERMOCOUPLE 11
BAY 1
TEMPERATURE (DEGREES C)
1,500
1,200
900
600
300
0
-1 0 1 2 3 4 5 6 7 8 9
TIME (SECONDS)

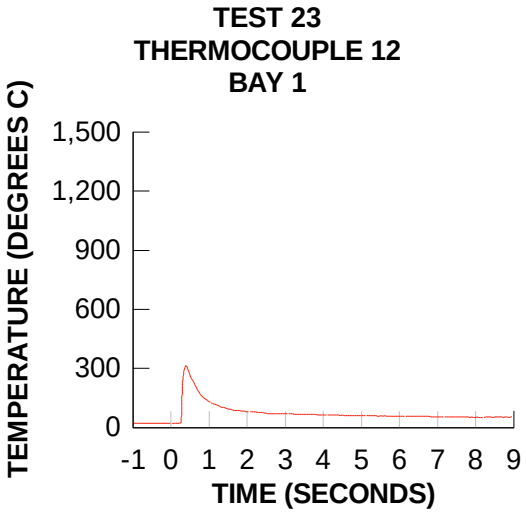
TEST 23
THERMOCOUPLE 12
BAY 1
TEMPERATURE (DEGREES C)
1,500
1,200
900
600
300
0
-1 0 1 2 3 4 5 6 7 8 9
TIME (SECONDS)

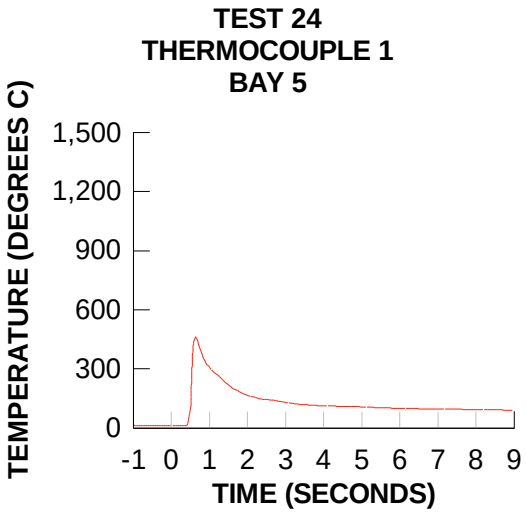
TEST 24
THERMOCOUPLE 1
BAY 5
TEMPERATURE (DEGREES C)
1,500
1,200
900
600
300
0
-1 0 1 2 3 4 5 6 7 8 9
TIME (SECONDS)

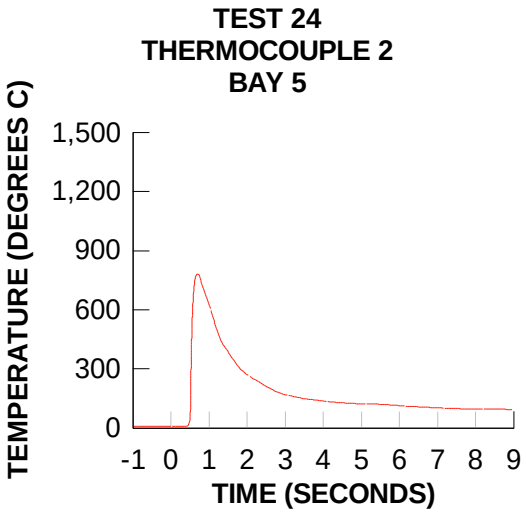
TEST 24
THERMOCOUPLE 2
BAY 5
TEMPERATURE (DEGREES C)
1,500
1,200
900
600
300
0
-1 0 1 2 3 4 5 6 7 8 9
TIME (SECONDS)

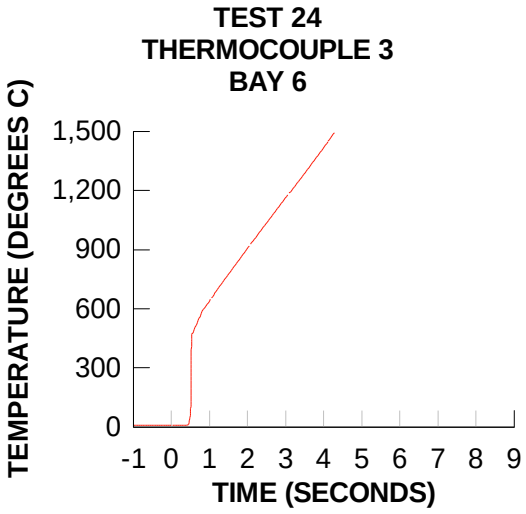
TEST 24
THERMOCOUPLE 3
BAY 6
TEMPERATURE (DEGREES C)
1,500
1,200
900
600
300
0
-1 0 1 2 3 4 5 6 7 8 9
TIME (SECONDS)

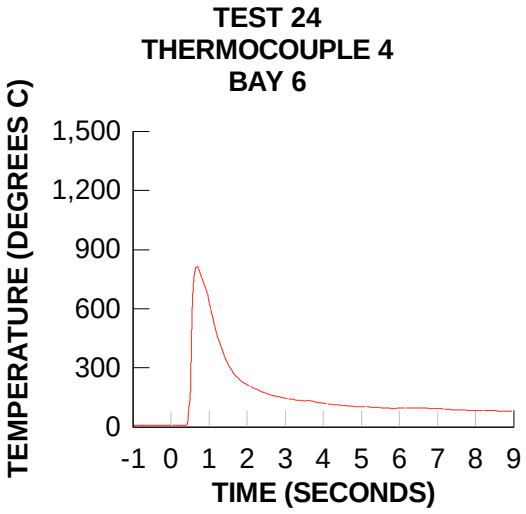
TEST 24
THERMOCOUPLE 4
BAY 6
TEMPERATURE (DEGREES C)
1,500
1,200
900
600
300
0
-1 0 1 2 3 4 5 6 7 8 9
TIME (SECONDS)

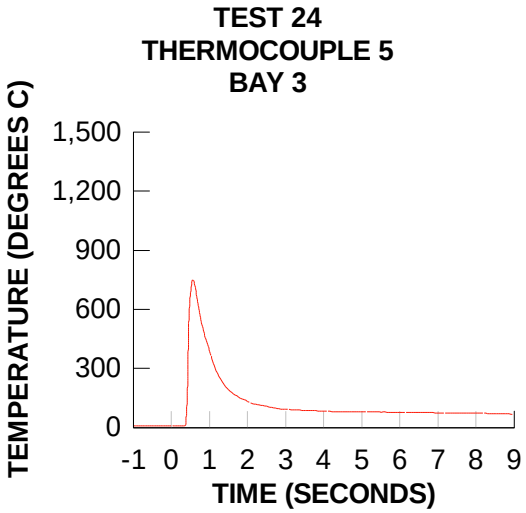
TEST 24
THERMOCOUPLE 5
BAY 3
TEMPERATURE (DEGREES C)
1,500
1,200
900
600
300
0
-1 0 1 2 3 4 5 6 7 8 9
TIME (SECONDS)

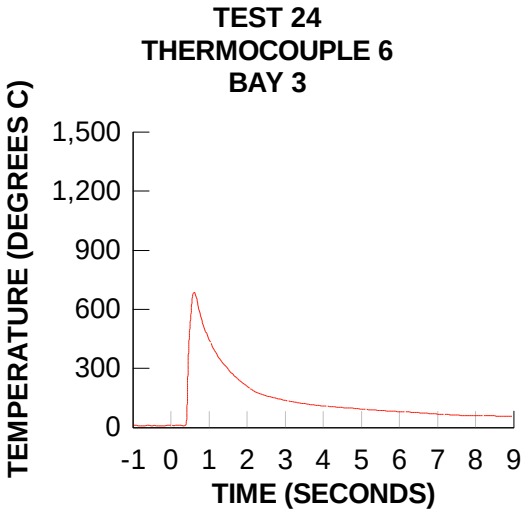
TEST 24
THERMOCOUPLE 6
BAY 3
TEMPERATURE (DEGREES C)
1,500
1,200
900
600
300
0
-1 0 1 2 3 4 5 6 7 8 9
TIME (SECONDS)

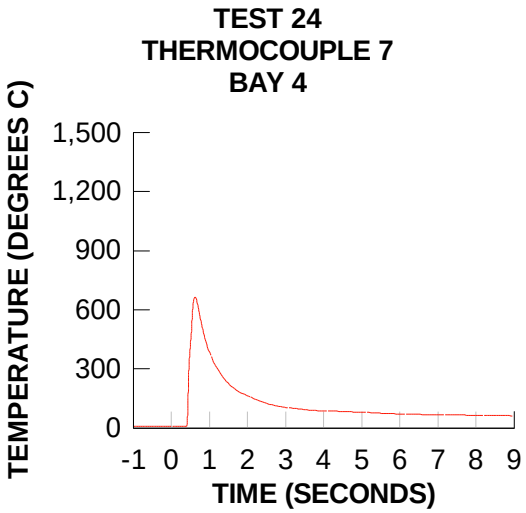
TEST 24
THERMOCOUPLE 7
BAY 4
TEMPERATURE (DEGREES C)
1,500
1,200
900
600
300
0
-1 0 1 2 3 4 5 6 7 8 9
TIME (SECONDS)

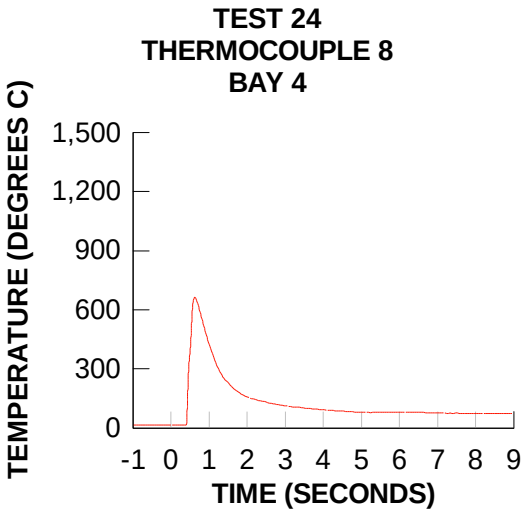
TEST 24
THERMOCOUPLE 8
BAY 4
TEMPERATURE (DEGREES C)
1,500
1,200
900
600
300
0
-1 0 1 2 3 4 5 6 7 8 9
TIME (SECONDS)

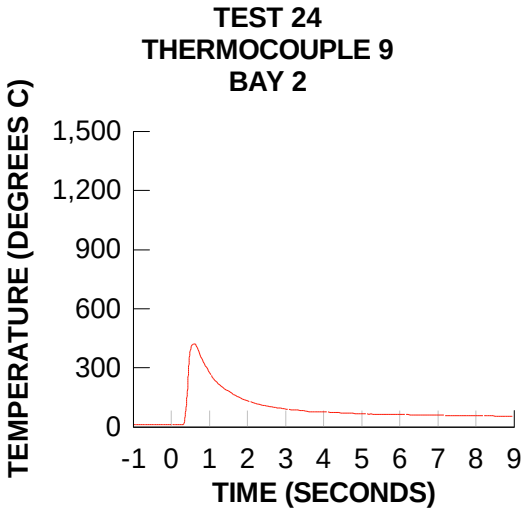
TEST 24
THERMOCOUPLE 9
BAY 2
TEMPERATURE (DEGREES C)
1,500
1,200
900
600
300
0
-1 0 1 2 3 4 5 6 7 8 9
TIME (SECONDS)

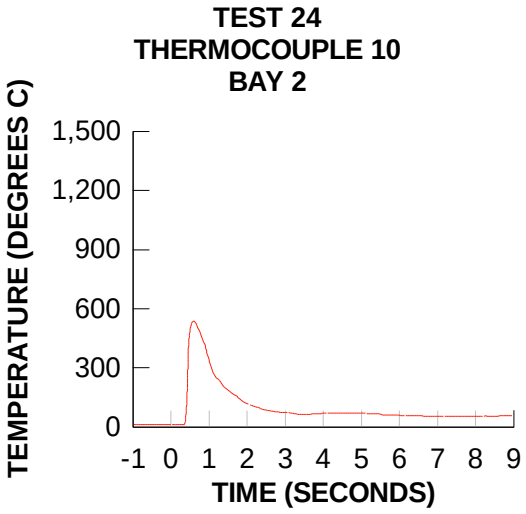
TEST 24
THERMOCOUPLE 10
BAY 2
TEMPERATURE (DEGREES C)
1,500
1,200
900
600
300
0
-1 0 1 2 3 4 5 6 7 8 9
TIME (SECONDS)

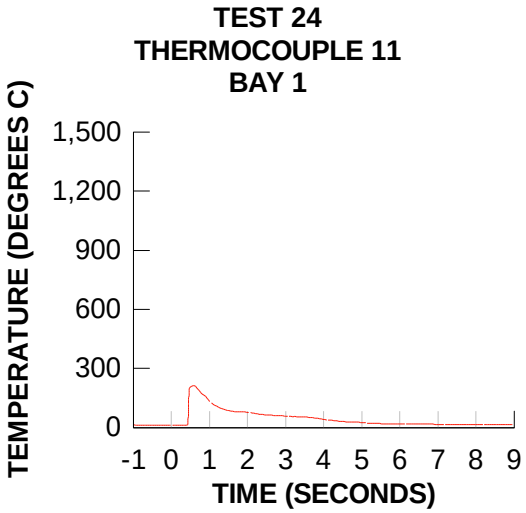
TEST 24
THERMOCOUPLE 11
BAY 1
TEMPERATURE (DEGREES C)
1,500
1,200
900
600
300
0
-1 0 1 2 3 4 5 6 7 8 9
TIME (SECONDS)

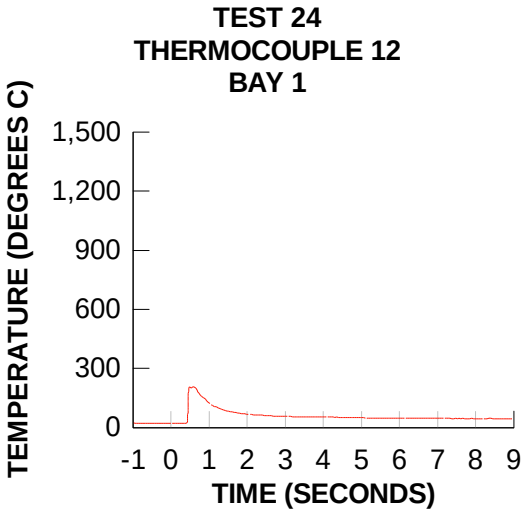
TEST 24
THERMOCOUPLE 12
BAY 1
TEMPERATURE (DEGREES C)
1,500
1,200
900
600
300
0
-1 0 1 2 3 4 5 6 7 8 9
TIME (SECONDS)

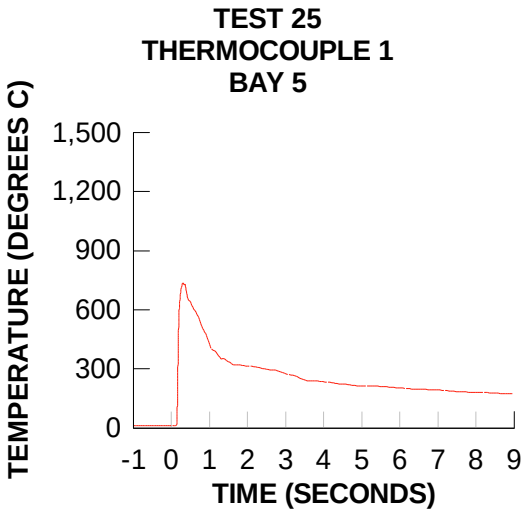
TEST 25
THERMOCOUPLE 1
BAY 5
TEMPERATURE (DEGREES C)
1,500
1,200
900
600
300
0
-1 0 1 2 3 4 5 6 7 8 9
TIME (SECONDS)

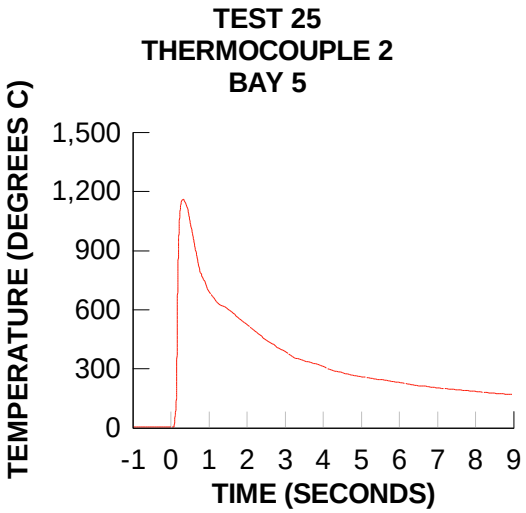
TEST 25
THERMOCOUPLE 2
BAY 5
TEMPERATURE (DEGREES C)
1,500
1,200
900
600
300
0
-1 0 1 2 3 4 5 6 7 8 9
TIME (SECONDS)

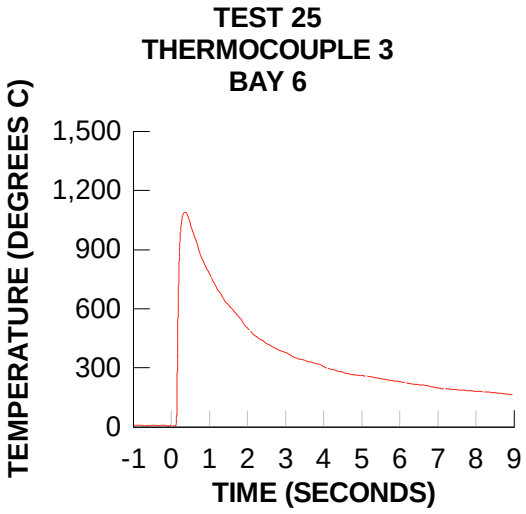
TEST 25
THERMOCOUPLE 3
BAY 6
TEMPERATURE (DEGREES C)
1,500
1,200
900
600
300
0
-1 0 1 2 3 4 5 6 7 8 9
TIME (SECONDS)

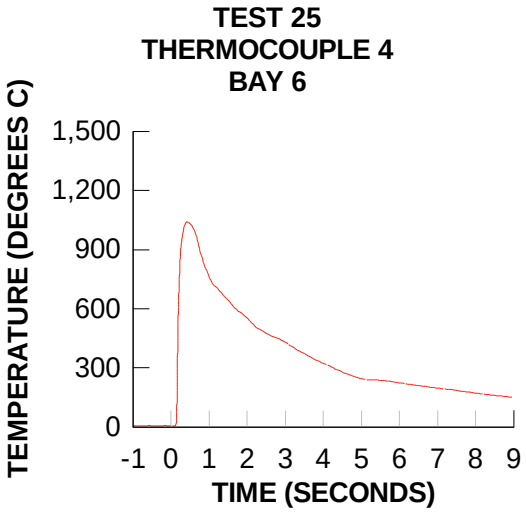
TEST 25
THERMOCOUPLE 4
BAY 6
TEMPERATURE (DEGREES C)
1,500
1,200
900
600
300
0
-1 0 1 2 3 4 5 6 7 8 9
TIME (SECONDS)

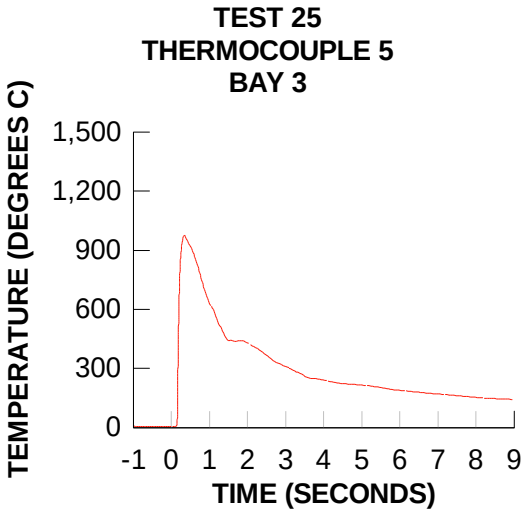
TEST 25
THERMOCOUPLE 5
BAY 3
TEMPERATURE (DEGREES C)
1,500
1,200
900
600
300
0
-1 0 1 2 3 4 5 6 7 8 9
TIME (SECONDS)

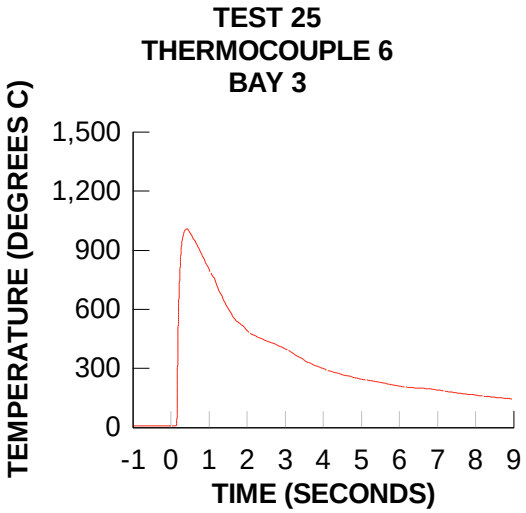
TEST 25
THERMOCOUPLE 6
BAY 3
TEMPERATURE (DEGREES C)
1,500
1,200
900
600
300
0
-1 0 1 2 3 4 5 6 7 8 9
TIME (SECONDS)

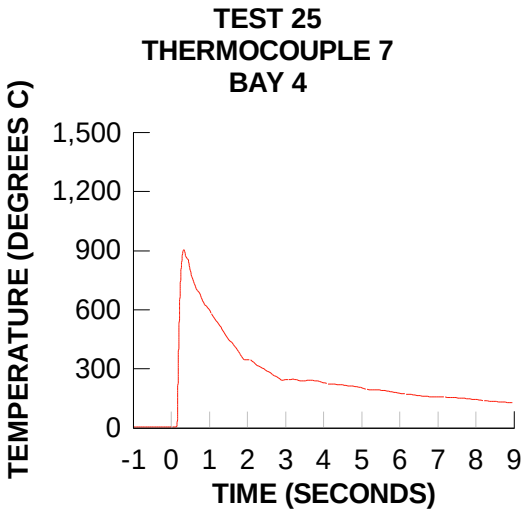
TEST 25
THERMOCOUPLE 7
BAY 4
TEMPERATURE (DEGREES C)
1,500
1,200
900
600
300
0
-1 0 1 2 3 4 5 6 7 8 9
TIME (SECONDS)

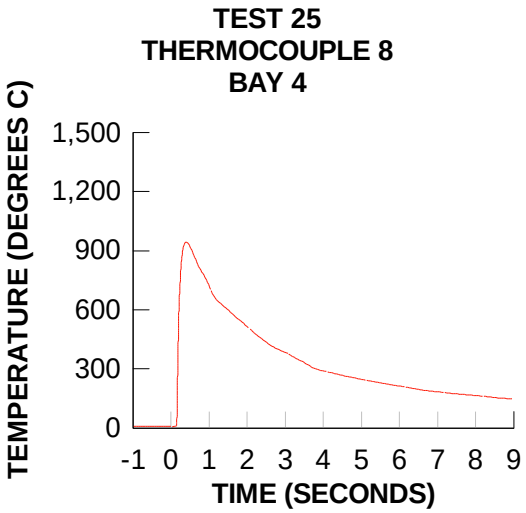
TEST 25
THERMOCOUPLE 8
BAY 4
TEMPERATURE (DEGREES C)
1,500
1,200
900
600
300
0
-1 0 1 2 3 4 5 6 7 8 9
TIME (SECONDS)

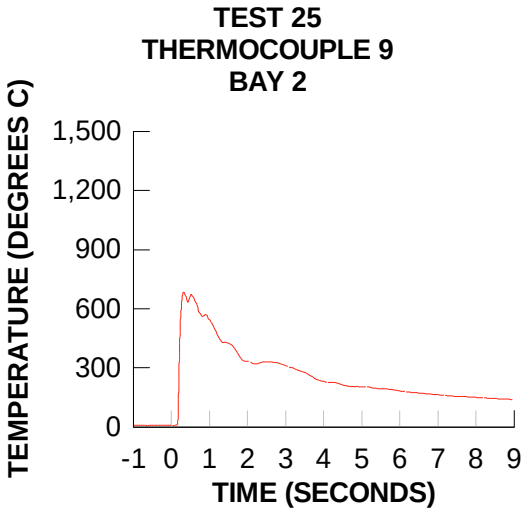
TEST 25
THERMOCOUPLE 9
BAY 2
TEMPERATURE (DEGREES C)
1,500
1,200
900
600
300
0
-1 0 1 2 3 4 5 6 7 8 9
TIME (SECONDS)

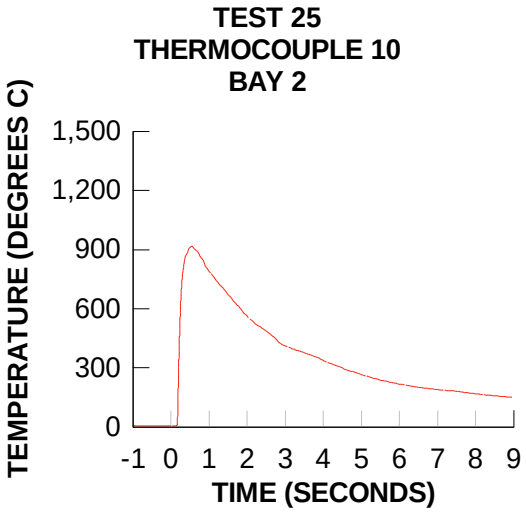
TEST 25
THERMOCOUPLE 10
BAY 2
TEMPERATURE (DEGREES C)
1,500
1,200
900
600
300
0
-1 0 1 2 3 4 5 6 7 8 9
TIME (SECONDS)

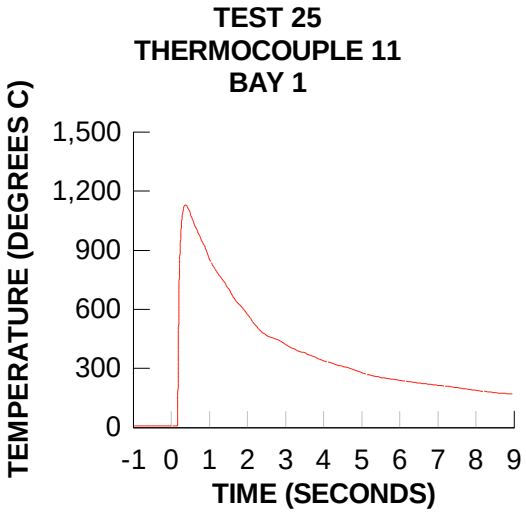
TEST 25
THERMOCOUPLE 11
BAY 1
TEMPERATURE (DEGREES C)
1,500
1,200
900
600
300
0
-1 0 1 2 3 4 5 6 7 8 9
TIME (SECONDS)

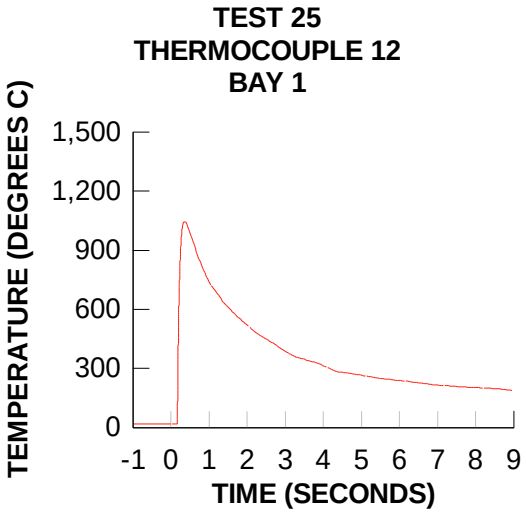
TEST 25
THERMOCOUPLE 12
BAY 1
TEMPERATURE (DEGREES C)
1,500
1,200
900
600
300
0
-1 0 1 2 3 4 5 6 7 8 9
TIME (SECONDS)

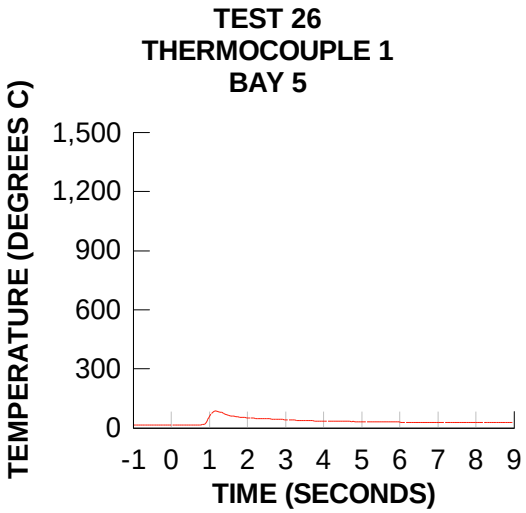
TEST 26
THERMOCOUPLE 1
BAY 5
TEMPERATURE (DEGREES C)
1,500
1,200
900
600
300
0
-1 0 1 2 3 4 5 6 7 8 9
TIME (SECONDS)

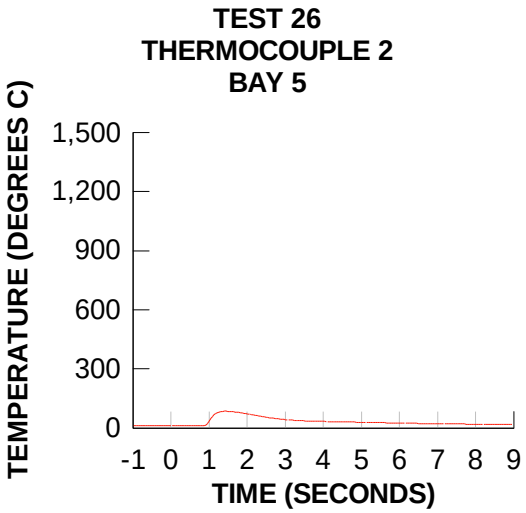
TEST 26
THERMOCOUPLE 2
BAY 5
TEMPERATURE (DEGREES C)
1,500
1,200
900
600
300
0
-1 0 1 2 3 4 5 6 7 8 9
TIME (SECONDS)

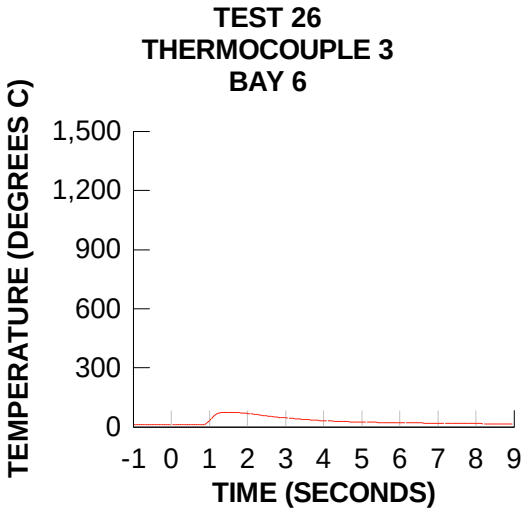
TEST 26
THERMOCOUPLE 3
BAY 6
TEMPERATURE (DEGREES C)
1,500
1,200
900
600
300
0
-1 0 1 2 3 4 5 6 7 8 9
TIME (SECONDS)

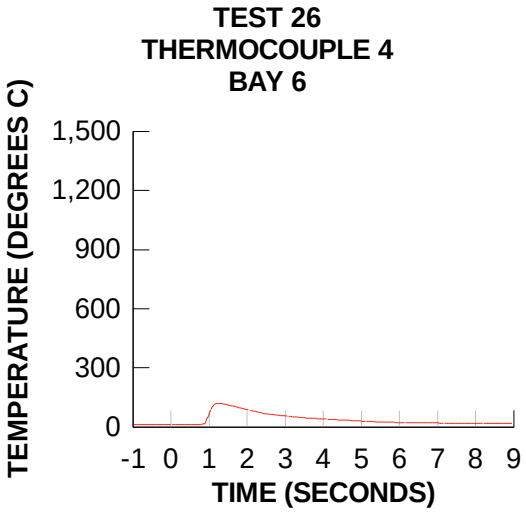
TEST 26
THERMOCOUPLE 4
BAY 6
TEMPERATURE (DEGREES C)
1,500
1,200
900
600
300
0
-1 0 1 2 3 4 5 6 7 8 9
TIME (SECONDS)

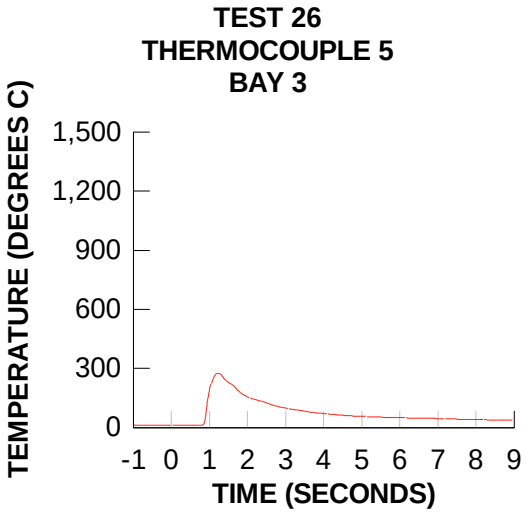
TEST 26
THERMOCOUPLE 5
BAY 3
TEMPERATURE (DEGREES C)
1,500
1,200
900
600
300
0
-1 0 1 2 3 4 5 6 7 8 9
TIME (SECONDS)

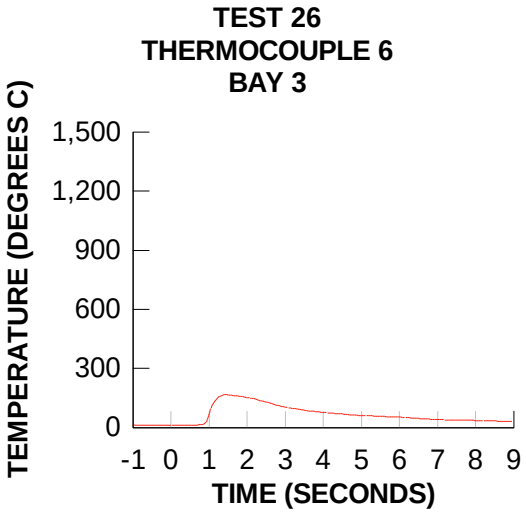
TEST 26
THERMOCOUPLE 6
BAY 3
TEMPERATURE (DEGREES C)
1,500
1,200
900
600
300
0
-1 0 1 2 3 4 5 6 7 8 9
TIME (SECONDS)

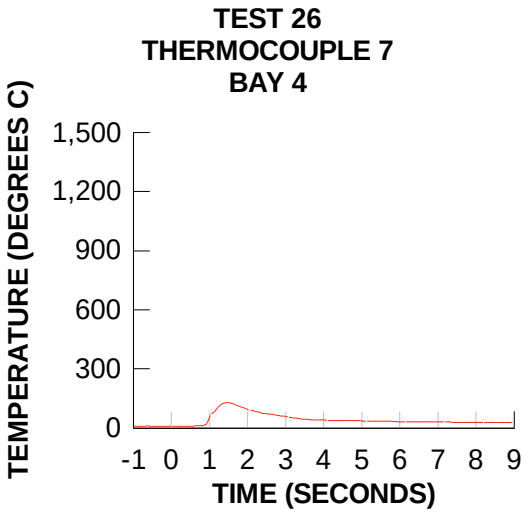
TEST 26
THERMOCOUPLE 7
BAY 4
TEMPERATURE (DEGREES C)
1,500
1,200
900
600
300
0
-1 0 1 2 3 4 5 6 7 8 9
TIME (SECONDS)

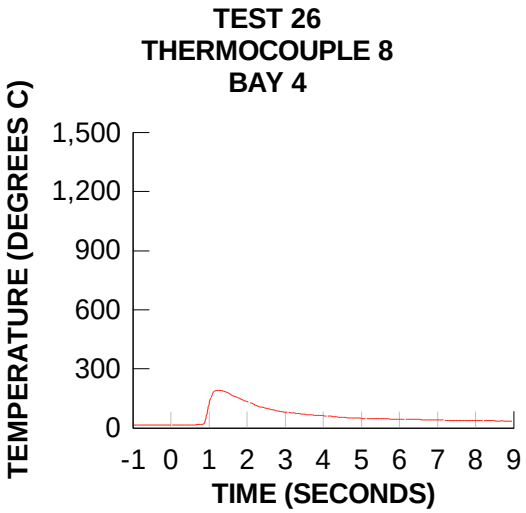
TEST 26
THERMOCOUPLE 8
BAY 4
TEMPERATURE (DEGREES C)
1,500
1,200
900
600
300
0
-1 0 1 2 3 4 5 6 7 8 9
TIME (SECONDS)

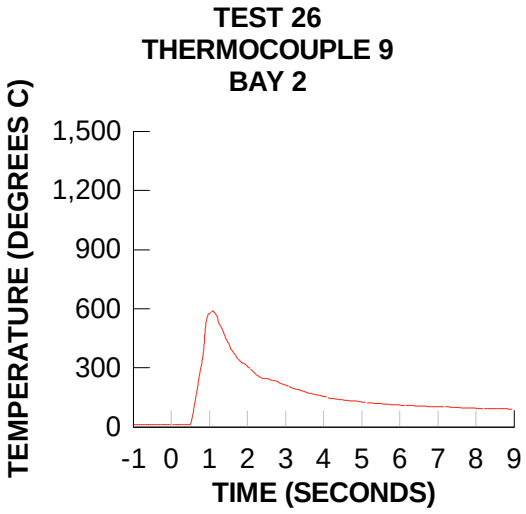
TEST 26
THERMOCOUPLE 9
BAY 2
TEMPERATURE (DEGREES C)
1,500
1,200
900
600
300
0
-1 0 1 2 3 4 5 6 7 8 9
TIME (SECONDS)

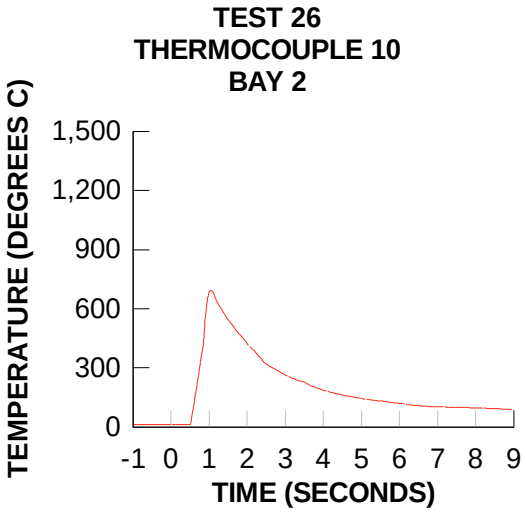
TEST 26
THERMOCOUPLE 10
BAY 2
TEMPERATURE (DEGREES C)
1,500
1,200
900
600
300
0
-1 0 1 2 3 4 5 6 7 8 9
TIME (SECONDS)

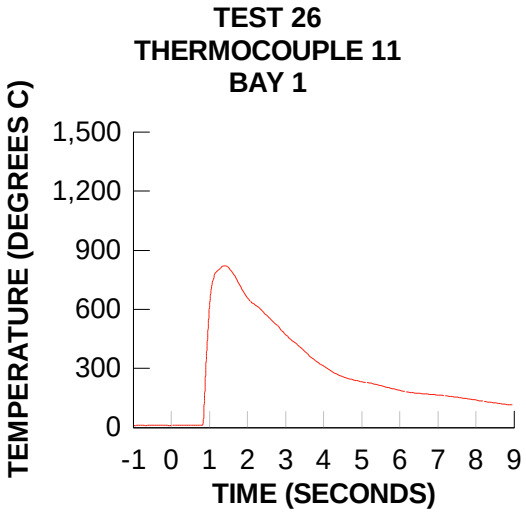
TEST 26
THERMOCOUPLE 11
BAY 1
TEMPERATURE (DEGREES C)
1,500
1,200
900
600
300
0
-1 0 1 2 3 4 5 6 7 8 9
TIME (SECONDS)

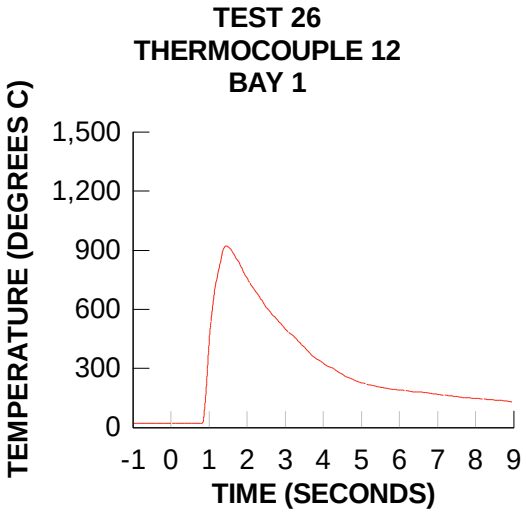
TEST 26
THERMOCOUPLE 12
BAY 1
TEMPERATURE (DEGREES C)
1,500
1,200
900
600
300
0
-1 0 1 2 3 4 5 6 7 8 9
TIME (SECONDS)

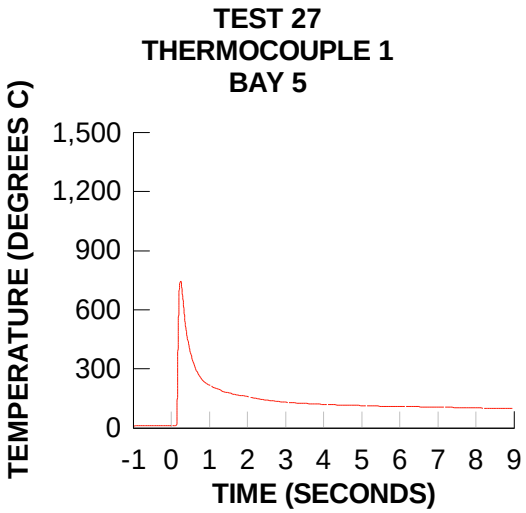
TEST 27
THERMOCOUPLE 1
BAY 5
TEMPERATURE (DEGREES C)
1,500
1,200
900
600
300
0
-1 0 1 2 3 4 5 6 7 8 9
TIME (SECONDS)

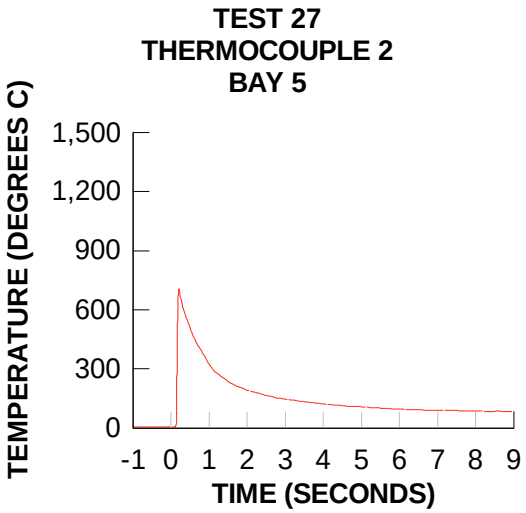
TEST 27
THERMOCOUPLE 2
BAY 5
TEMPERATURE (DEGREES C)
1,500
1,200
900
600
300
0
-1 0 1 2 3 4 5 6 7 8 9
TIME (SECONDS)

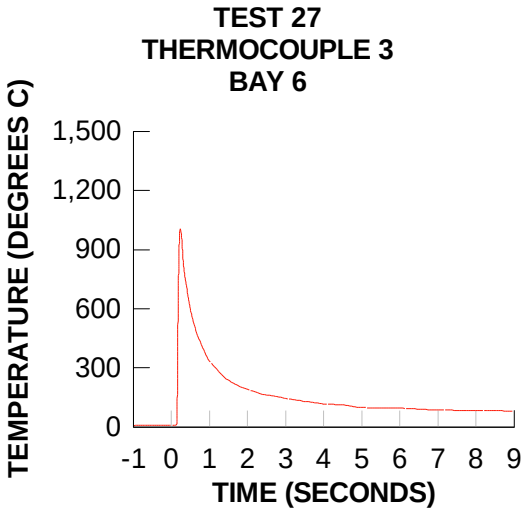
TEST 27
THERMOCOUPLE 3
BAY 6
TEMPERATURE (DEGREES C)
1,500
1,200
900
600
300
0
-1 0 1 2 3 4 5 6 7 8 9
TIME (SECONDS)

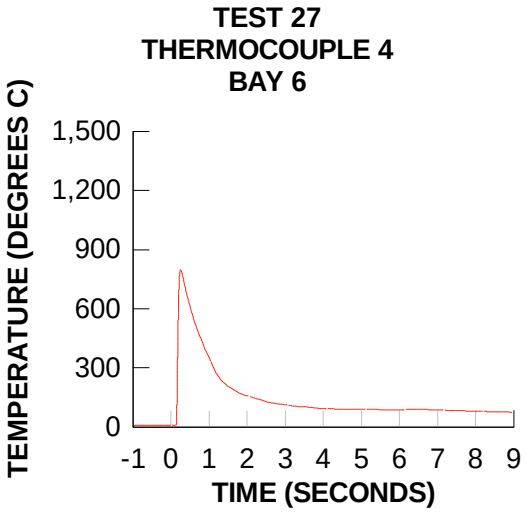
TEST 27
THERMOCOUPLE 4
BAY 6
TEMPERATURE (DEGREES C)
1,500
1,200
900
600
300
0
-1 0 1 2 3 4 5 6 7 8 9
TIME (SECONDS)

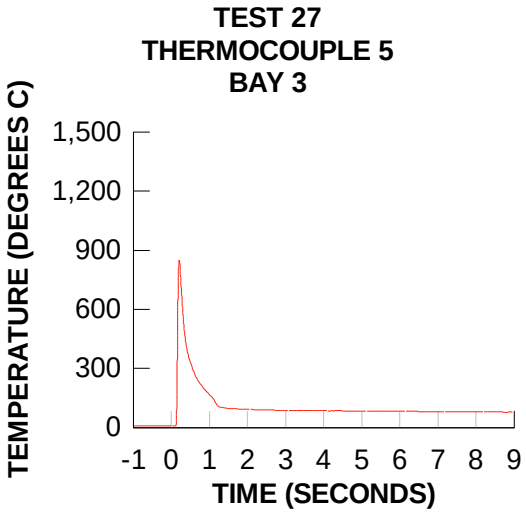
TEST 27
THERMOCOUPLE 5
BAY 3
TEMPERATURE (DEGREES C)
1,500
1,200
900
600
300
0
-1 0 1 2 3 4 5 6 7 8 9
TIME (SECONDS)

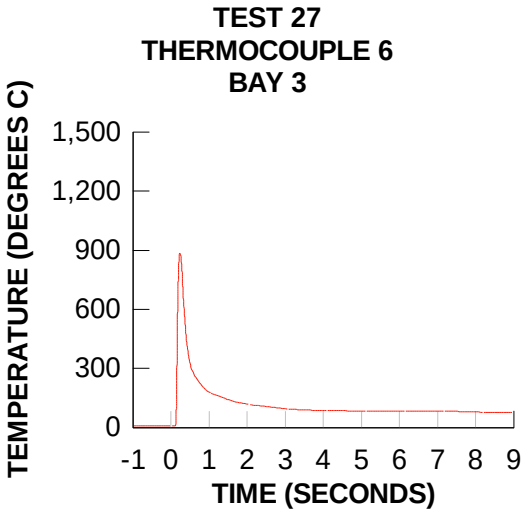
TEST 27
THERMOCOUPLE 6
BAY 3
TEMPERATURE (DEGREES C)
1,500
1,200
900
600
300
0
-1 0 1 2 3 4 5 6 7 8 9
TIME (SECONDS)

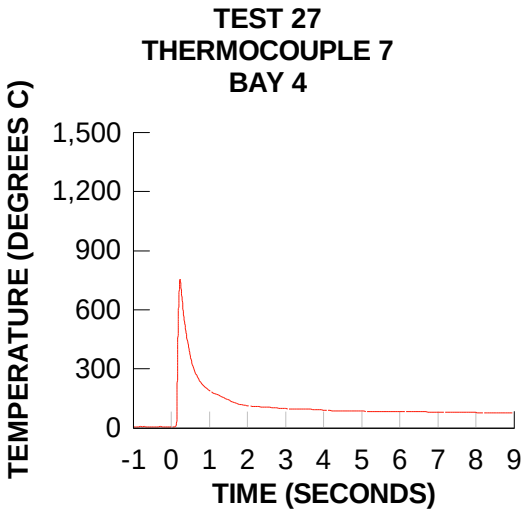
TEST 27
THERMOCOUPLE 7
BAY 4
TEMPERATURE (DEGREES C)
1,500
1,200
900
600
300
0
-1 0 1 2 3 4 5 6 7 8 9
TIME (SECONDS)

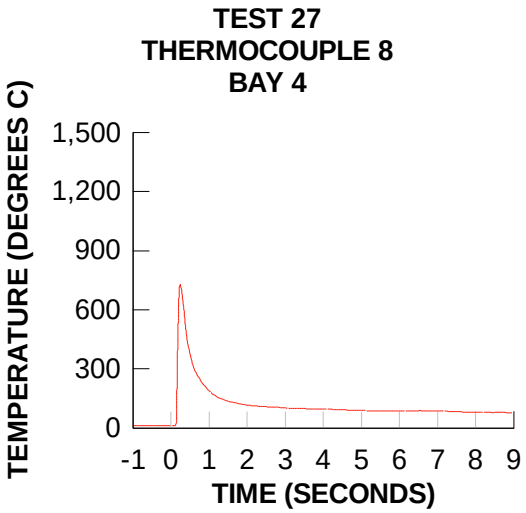
TEST 27
THERMOCOUPLE 8
BAY 4
TEMPERATURE (DEGREES C)
1,500
1,200
900
600
300
0
-1 0 1 2 3 4 5 6 7 8 9
TIME (SECONDS)

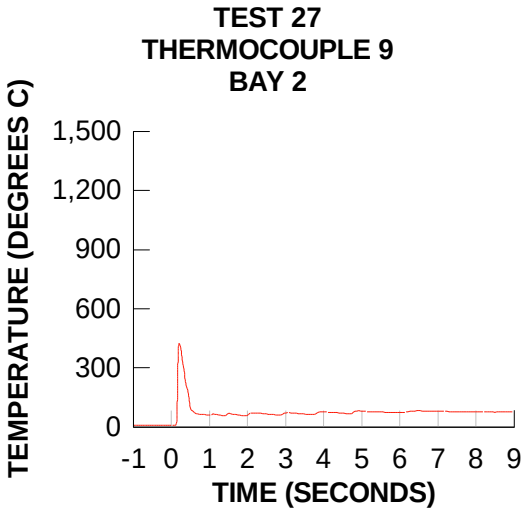
TEST 27
THERMOCOUPLE 9
BAY 2
TEMPERATURE (DEGREES C)
1,500
1,200
900
600
300
0
-1 0 1 2 3 4 5 6 7 8 9
TIME (SECONDS)

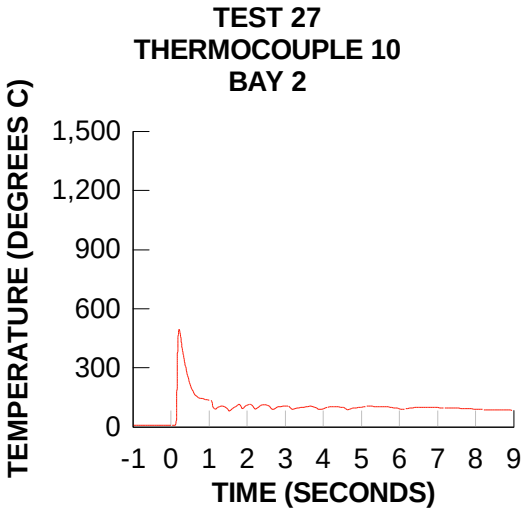
TEST 27
THERMOCOUPLE 10
BAY 2
TEMPERATURE (DEGREES C)
1,500
1,200
900
600
300
0
-1 0 1 2 3 4 5 6 7 8 9
TIME (SECONDS)

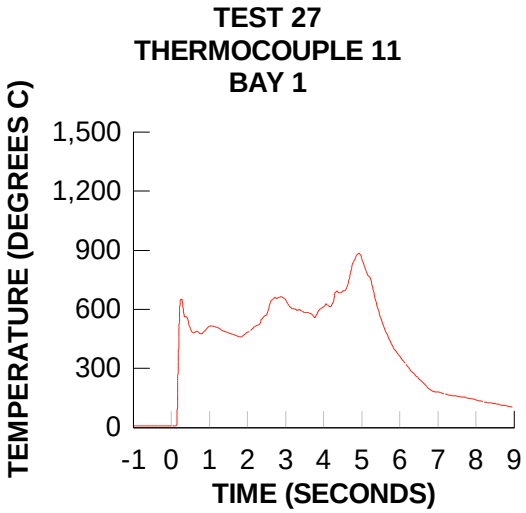
TEST 27
THERMOCOUPLE 11
BAY 1
TEMPERATURE (DEGREES C)
1,500
1,200
900
600
300
0
-1 0 1 2 3 4 5 6 7 8 9
TIME (SECONDS)

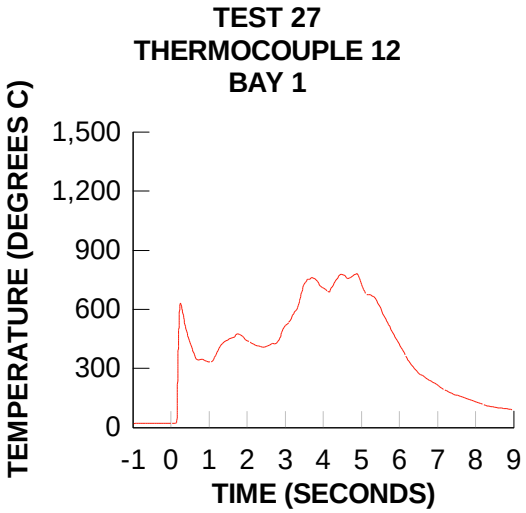
TEST 27
THERMOCOUPLE 12
BAY 1
TEMPERATURE (DEGREES C)
1,500
1,200
900
600
300
0
-1 0 1 2 3 4 5 6 7 8 9
TIME (SECONDS)

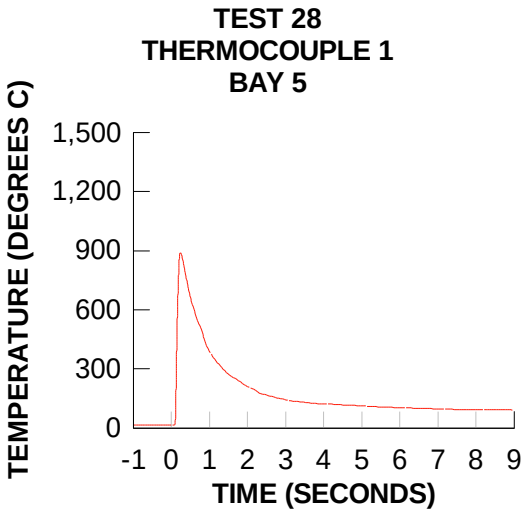
TEST 28
THERMOCOUPLE 1
BAY 5
TEMPERATURE (DEGREES C)
1,500
1,200
900
600
300
0
-1 0 1 2 3 4 5 6 7 8 9
TIME (SECONDS)

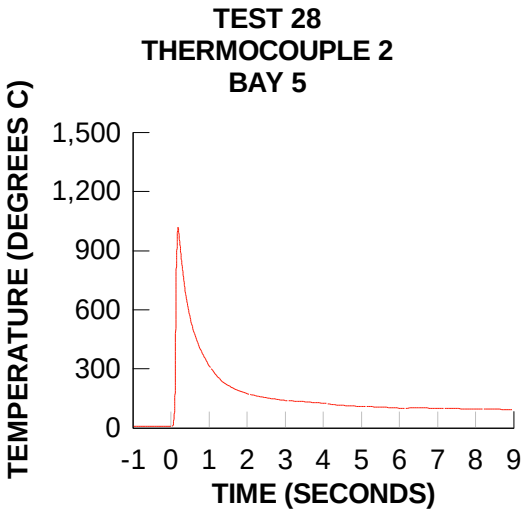
TEST 28
THERMOCOUPLE 2
BAY 5
TEMPERATURE (DEGREES C)
1,500
1,200
900
600
300
0
-1 0 1 2 3 4 5 6 7 8 9
TIME (SECONDS)

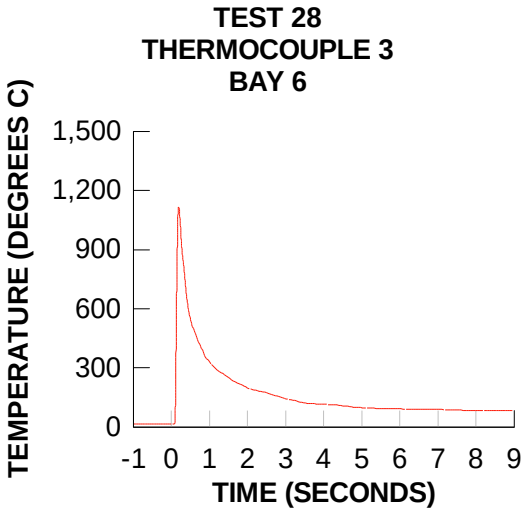
TEST 28
THERMOCOUPLE 3
BAY 6
TEMPERATURE (DEGREES C)
1,500
1,200
900
600
300
0
-1 0 1 2 3 4 5 6 7 8 9
TIME (SECONDS)

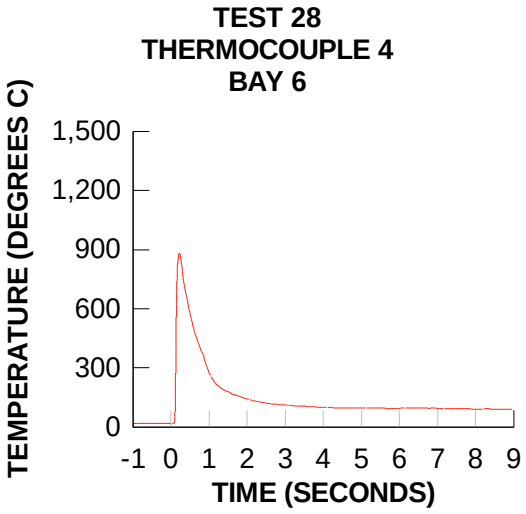
TEST 28
THERMOCOUPLE 4
BAY 6
TEMPERATURE (DEGREES C)
1,500
1,200
900
600
300
0
-1 0 1 2 3 4 5 6 7 8 9
TIME (SECONDS)

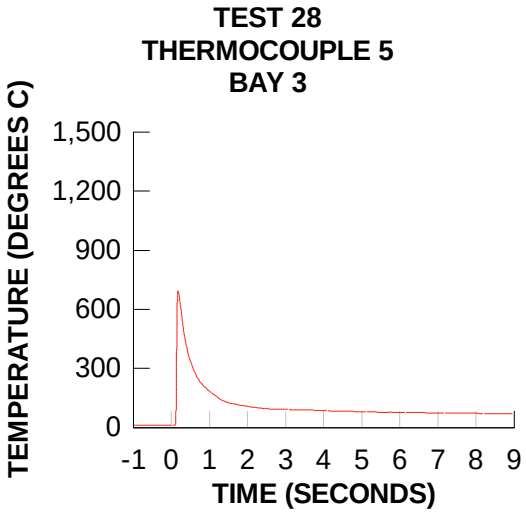
TEST 28
THERMOCOUPLE 5
BAY 3
TEMPERATURE (DEGREES C)
1,500
1,200
900
600
300
0
-1 0 1 2 3 4 5 6 7 8 9
TIME (SECONDS)

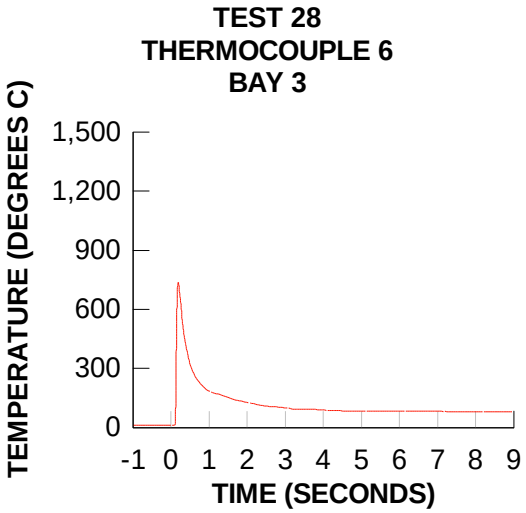
TEST 28
THERMOCOUPLE 6
BAY 3
TEMPERATURE (DEGREES C)
1,500
1,200
900
600
300
0
-1 0 1 2 3 4 5 6 7 8 9
TIME (SECONDS)

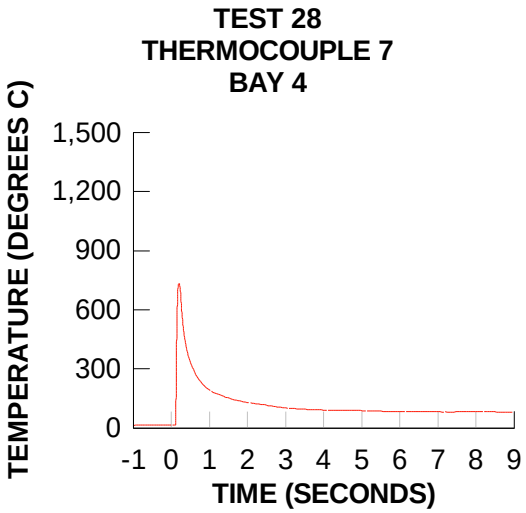
TEST 28
THERMOCOUPLE 7
BAY 4
TEMPERATURE (DEGREES C)
1,500
1,200
900
600
300
0
-1 0 1 2 3 4 5 6 7 8 9
TIME (SECONDS)

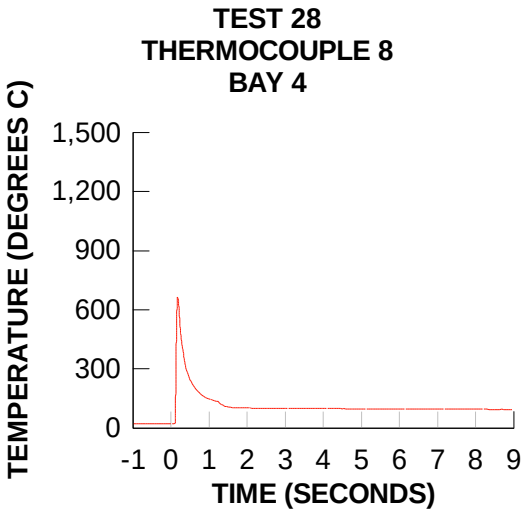
TEST 28
THERMOCOUPLE 8
BAY 4
TEMPERATURE (DEGREES C)
1,500
1,200
900
600
300
0
-1 0 1 2 3 4 5 6 7 8 9
TIME (SECONDS)

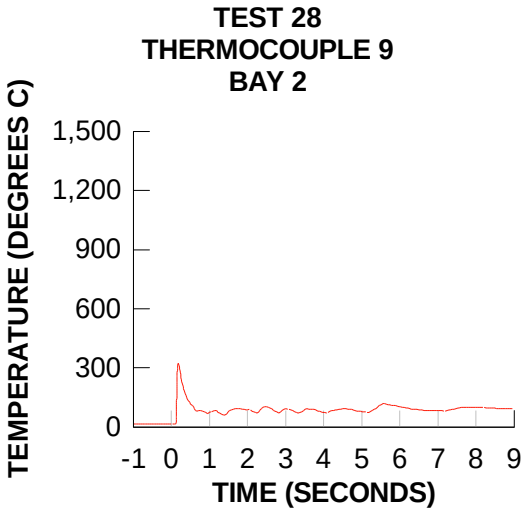
TEST 28
THERMOCOUPLE 9
BAY 2
TEMPERATURE (DEGREES C)
1,500
1,200
900
600
300
0
-1 0 1 2 3 4 5 6 7 8 9
TIME (SECONDS)

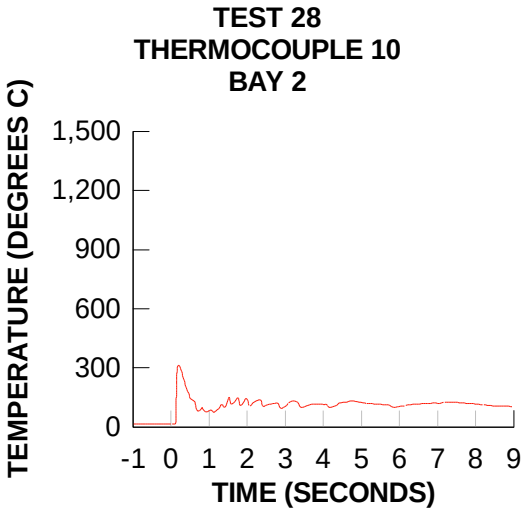
TEST 28
THERMOCOUPLE 10
BAY 2
TEMPERATURE (DEGREES C)
1,500
1,200
900
600
300
0
-1 0 1 2 3 4 5 6 7 8 9
TIME (SECONDS)

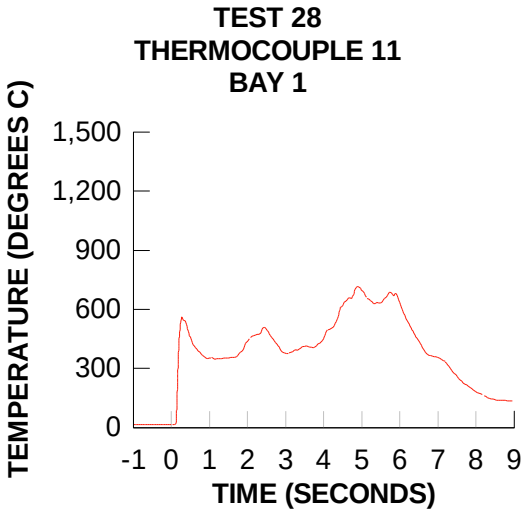
TEST 28
THERMOCOUPLE 11
BAY 1
TEMPERATURE (DEGREES C)
1,500
1,200
900
600
300
0
-1 0 1 2 3 4 5 6 7 8 9
TIME (SECONDS)

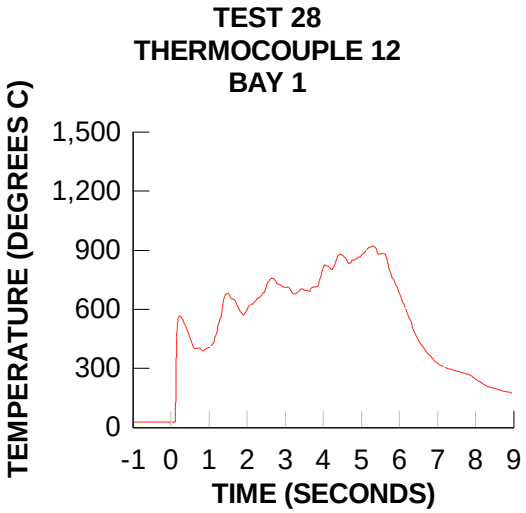
TEST 28
THERMOCOUPLE 12
BAY 1
TEMPERATURE (DEGREES C)
1,500
1,200
900
600
300
0
-1 0 1 2 3 4 5 6 7 8 9
TIME (SECONDS)

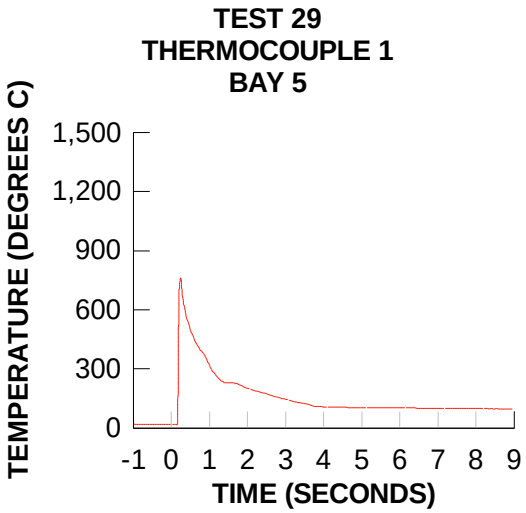
TEST 29
THERMOCOUPLE 1
BAY 5
TEMPERATURE (DEGREES C)
1,500
1,200
900
600
300
0
-1 0 1 2 3 4 5 6 7 8 9
TIME (SECONDS)

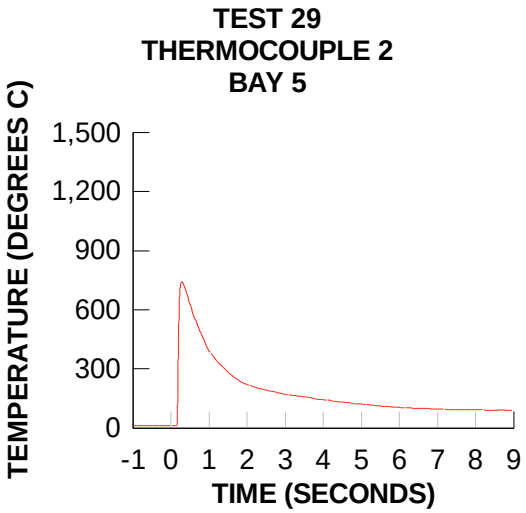
TEST 29
THERMOCOUPLE 2
BAY 5
TEMPERATURE (DEGREES C)
1,500
1,200
900
600
300
0
-1 0 1 2 3 4 5 6 7 8 9
TIME (SECONDS)

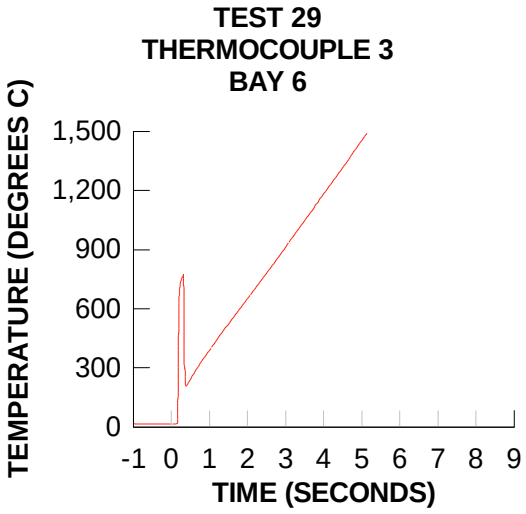
TEST 29
THERMOCOUPLE 3
BAY 6
TEMPERATURE (DEGREES C)
1,500
1,200
900
600
300
0
-1 0 1 2 3 4 5 6 7 8 9
TIME (SECONDS)

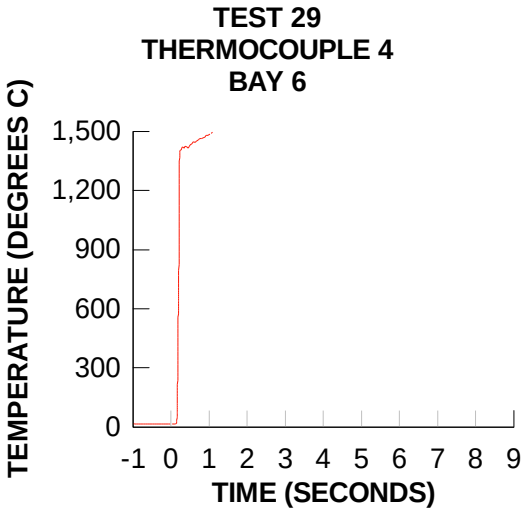
TEST 29
THERMOCOUPLE 4
BAY 6
TEMPERATURE (DEGREES C)
1,500
1,200
900
600
300
0
-1 0 1 2 3 4 5 6 7 8 9
TIME (SECONDS)

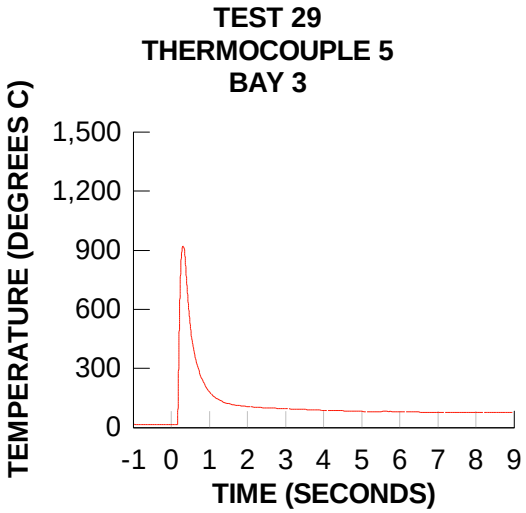
TEST 29
THERMOCOUPLE 5
BAY 3
TEMPERATURE (DEGREES C)
1,500
1,200
900
600
300
0
-1 0 1 2 3 4 5 6 7 8 9
TIME (SECONDS)

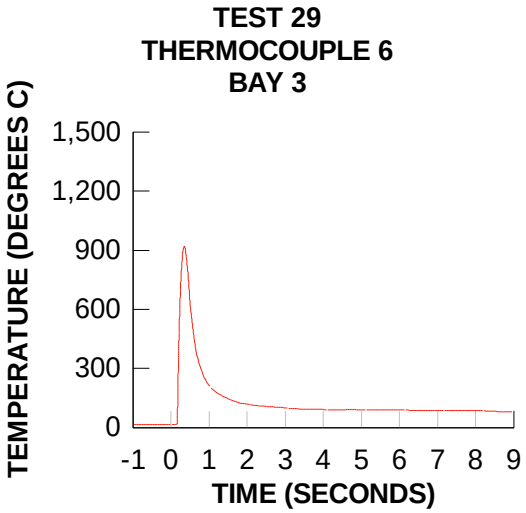
TEST 29
THERMOCOUPLE 6
BAY 3
TEMPERATURE (DEGREES C)
1,500
1,200
900
600
300
0
-1 0 1 2 3 4 5 6 7 8 9
TIME (SECONDS)

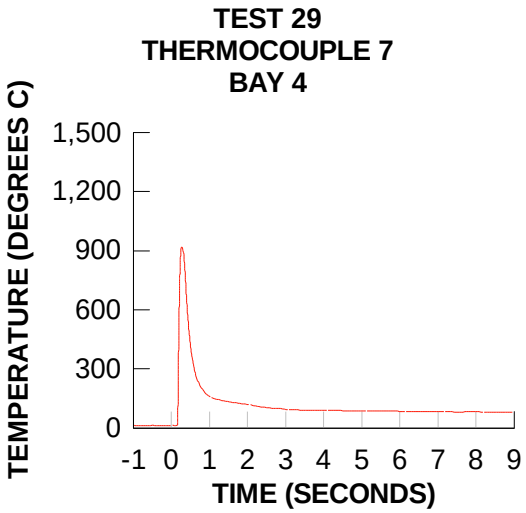
TEST 29
THERMOCOUPLE 7
BAY 4
TEMPERATURE (DEGREES C)
1,500
1,200
900
600
300
0
-1 0 1 2 3 4 5 6 7 8 9
TIME (SECONDS)

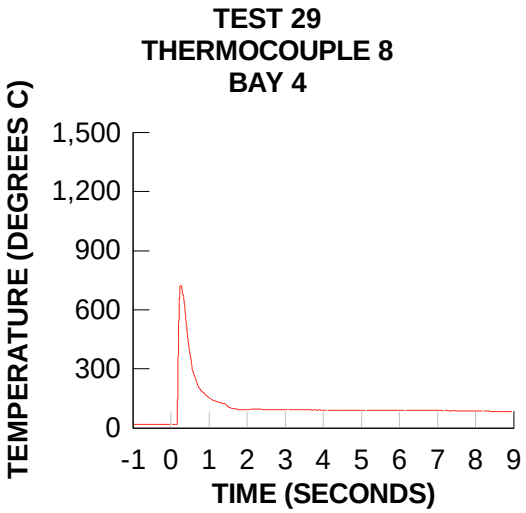
TEST 29
THERMOCOUPLE 8
BAY 4
TEMPERATURE (DEGREES C)
1,500
1,200
900
600
300
0
-1 0 1 2 3 4 5 6 7 8 9
TIME (SECONDS)

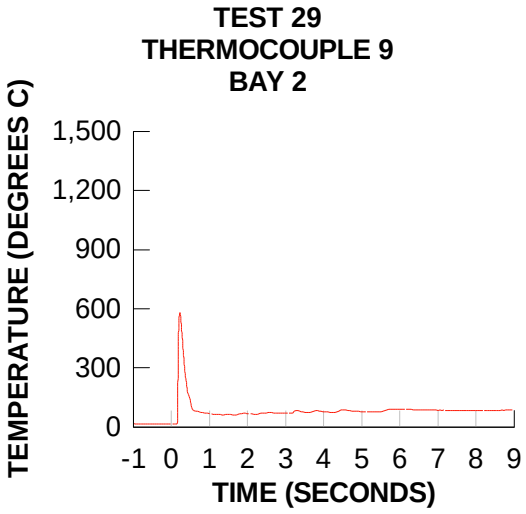
TEST 29
THERMOCOUPLE 9
BAY 2
TEMPERATURE (DEGREES C)
1,500
1,200
900
600
300
0
-1 0 1 2 3 4 5 6 7 8 9
TIME (SECONDS)

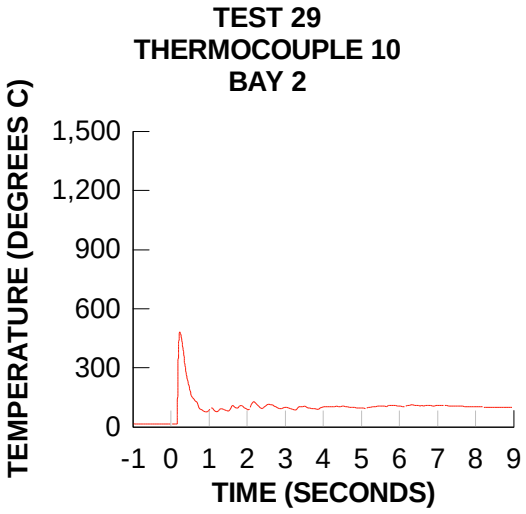
TEST 29
THERMOCOUPLE 10
BAY 2
TEMPERATURE (DEGREES C)
1,500
1,200
900
600
300
0
-1 0 1 2 3 4 5 6 7 8 9
TIME (SECONDS)

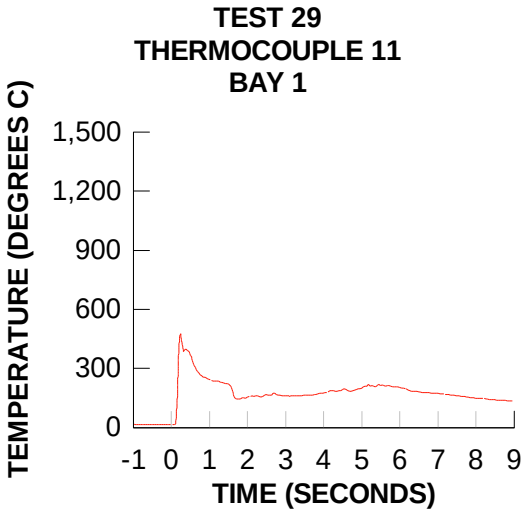
TEST 29
THERMOCOUPLE 11
BAY 1
TEMPERATURE (DEGREES C)
1,500
1,200
900
600
300
0
-1 0 1 2 3 4 5 6 7 8 9
TIME (SECONDS)

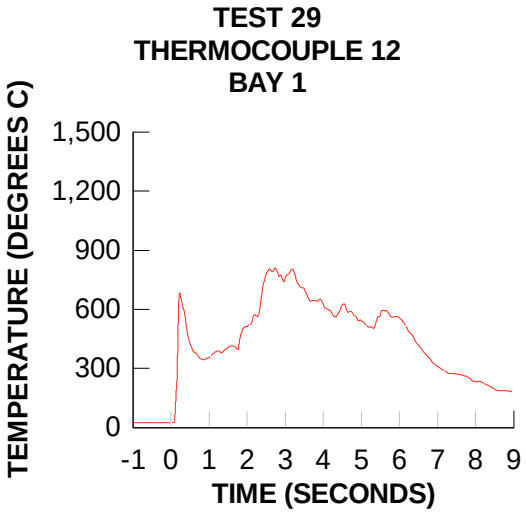
TEST 29
THERMOCOUPLE 12
BAY 1
TEMPERATURE (DEGREES C)
1,500
1,200
900
600
300
0
-1 0 1 2 3 4 5 6 7 8 9
TIME (SECONDS)

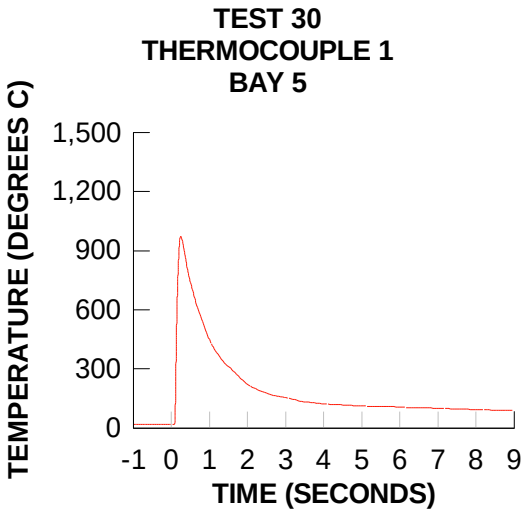
TEST 30
THERMOCOUPLE 1
BAY 5
TEMPERATURE (DEGREES C)
1,500
1,200
900
600
300
0
-1 0 1 2 3 4 5 6 7 8 9
TIME (SECONDS)

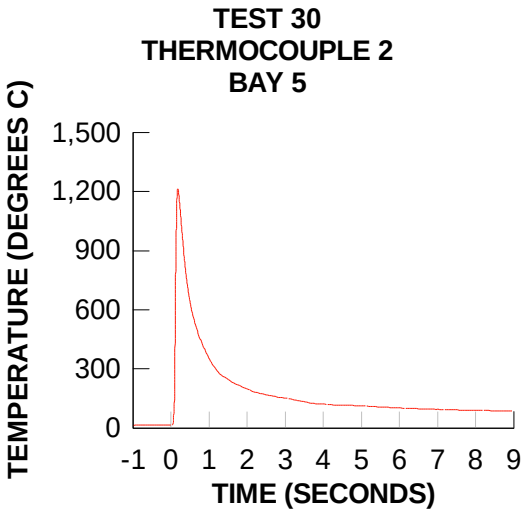
TEST 30
THERMOCOUPLE 2
BAY 5
TEMPERATURE (DEGREES C)
1,500
1,200
900
600
300
0
-1 0 1 2 3 4 5 6 7 8 9
TIME (SECONDS)

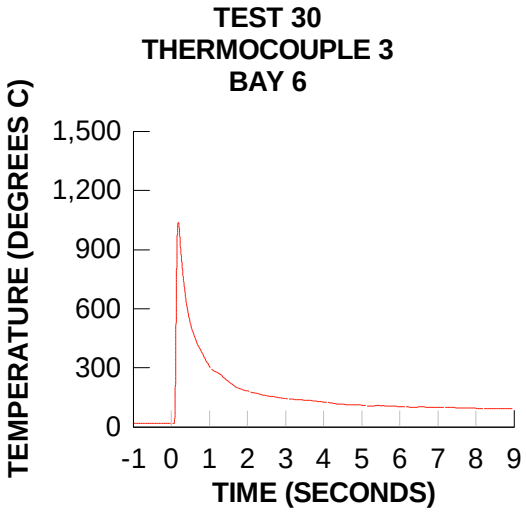
TEST 30
THERMOCOUPLE 3
BAY 6
TEMPERATURE (DEGREES C)
1,500
1,200
900
600
300
0
-1 0 1 2 3 4 5 6 7 8 9
TIME (SECONDS)

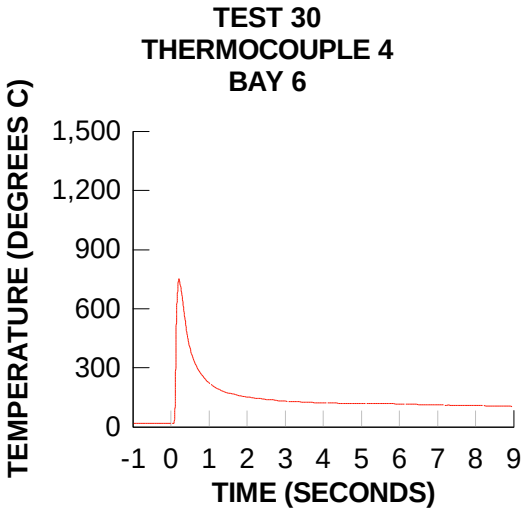
TEST 30
THERMOCOUPLE 4
BAY 6
TEMPERATURE (DEGREES C)
1,500
1,200
900
600
300
0
-1 0 1 2 3 4 5 6 7 8 9
TIME (SECONDS)

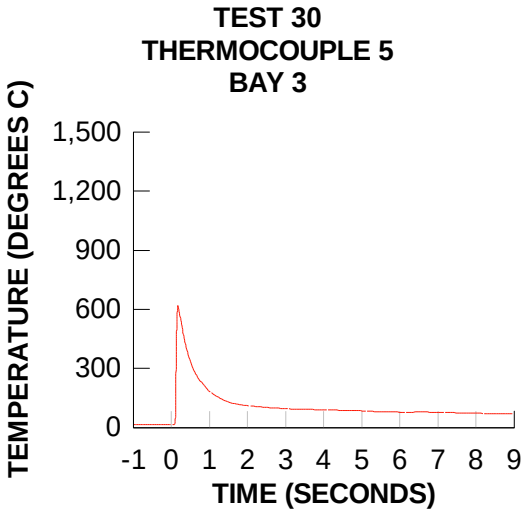
TEST 30
THERMOCOUPLE 5
BAY 3
TEMPERATURE (DEGREES C)
1,500
1,200
900
600
300
0
-1 0 1 2 3 4 5 6 7 8 9
TIME (SECONDS)

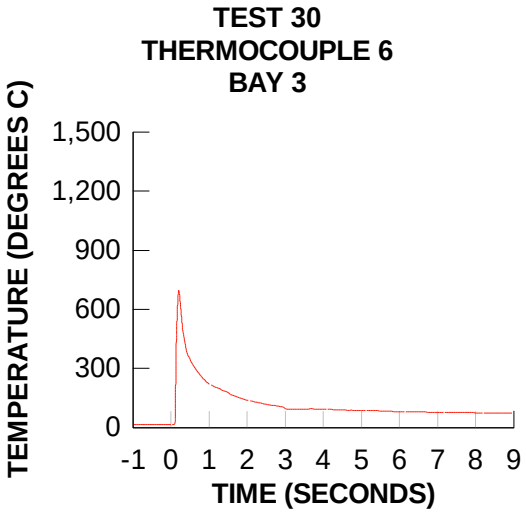
TEST 30
THERMOCOUPLE 6
BAY 3
TEMPERATURE (DEGREES C)
1,500
1,200
900
600
300
0
-1 0 1 2 3 4 5 6 7 8 9
TIME (SECONDS)

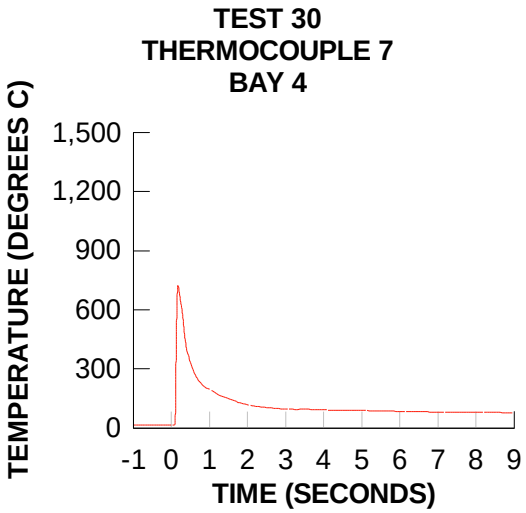
TEST 30
THERMOCOUPLE 7
BAY 4
TEMPERATURE (DEGREES C)
1,500
1,200
900
600
300
0
-1 0 1 2 3 4 5 6 7 8 9
TIME (SECONDS)

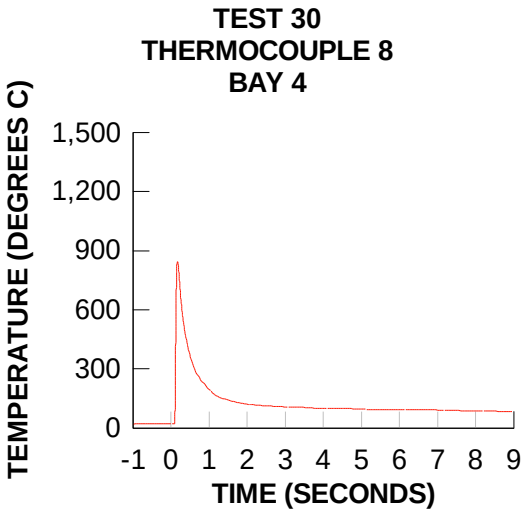
TEST 30
THERMOCOUPLE 8
BAY 4
TEMPERATURE (DEGREES C)
1,500
1,200
900
600
300
0
-1 0 1 2 3 4 5 6 7 8 9
TIME (SECONDS)

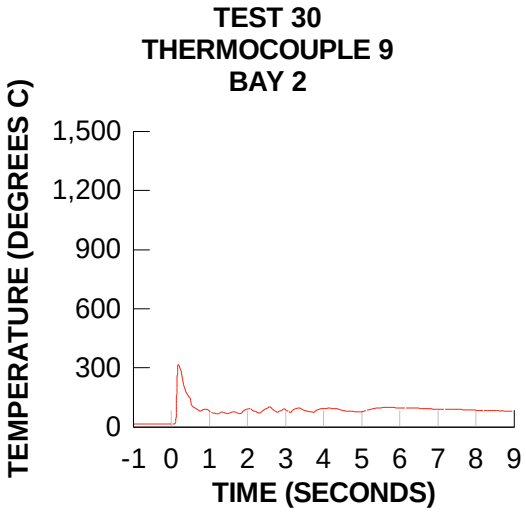
TEST 30
THERMOCOUPLE 9
BAY 2
TEMPERATURE (DEGREES C)
1,500
1,200
900
600
300
0
-1 0 1 2 3 4 5 6 7 8 9
TIME (SECONDS)

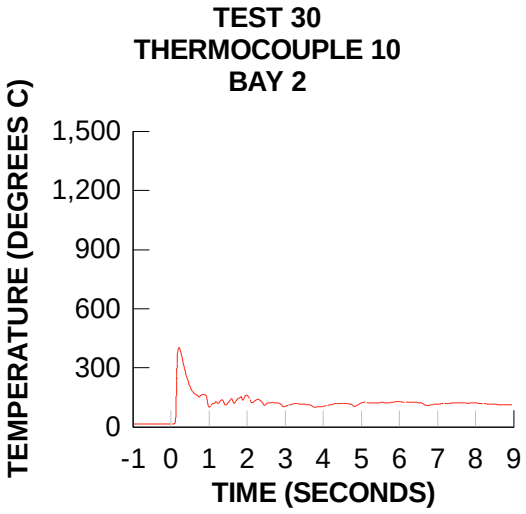
TEST 30
THERMOCOUPLE 10
BAY 2
TEMPERATURE (DEGREES C)
1,500
1,200
900
600
300
0
-1 0 1 2 3 4 5 6 7 8 9
TIME (SECONDS)

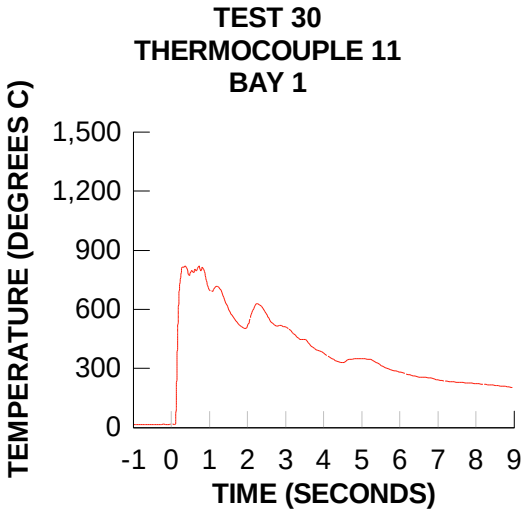
TEST 30
THERMOCOUPLE 11
BAY 1
TEMPERATURE (DEGREES C)
1,500
1,200
900
600
300
0
-1 0 1 2 3 4 5 6 7 8 9
TIME (SECONDS)

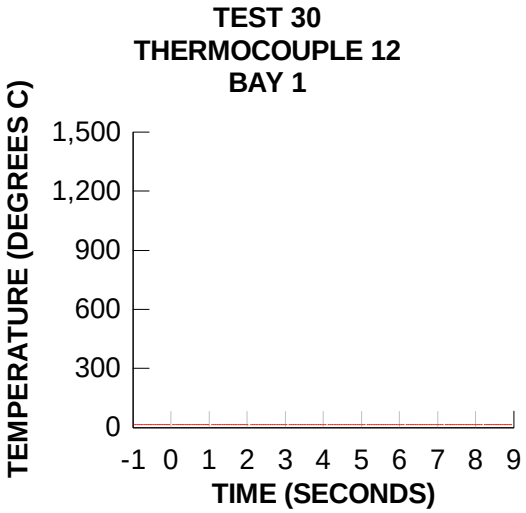
TEST 30
THERMOCOUPLE 12
BAY 1
TEMPERATURE (DEGREES C)
1,500
1,200
900
600
300
0
-1 0 1 2 3 4 5 6 7 8 9
TIME (SECONDS)

D.4 Endevco (Static) Pressure

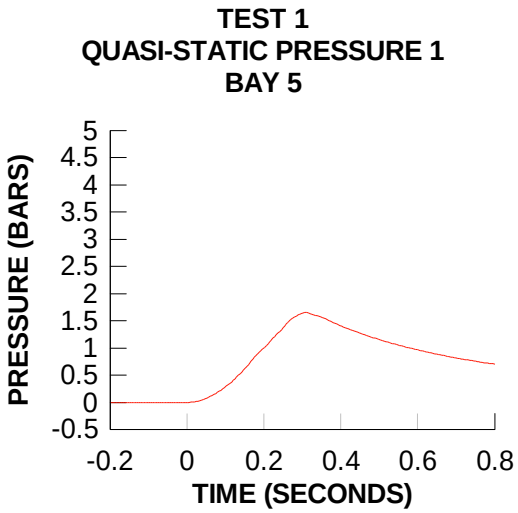
TEST 1
QUASI-STATIC PRESSURE 1
BAY 5
PRESSURE (BARS)
TIME (SECONDS)

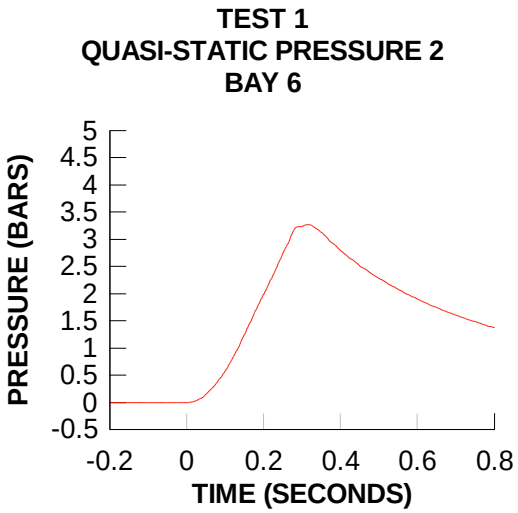
TEST 1
QUASI-STATIC PRESSURE 2
BAY 6
PRESSURE (BARS)
TIME (SECONDS)

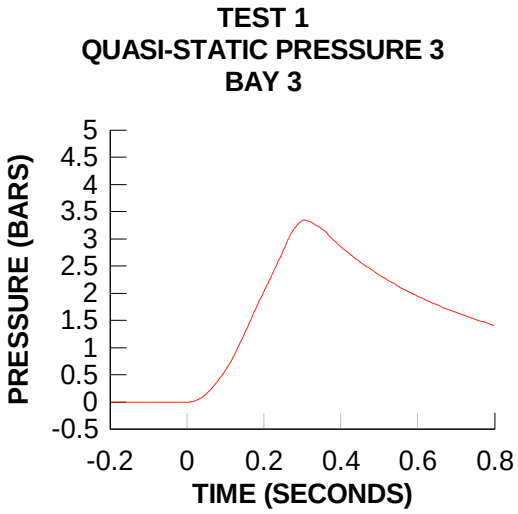
TEST 1
QUASI-STATIC PRESSURE 3
BAY 3
PRESSURE (BARS)
TIME (SECONDS)

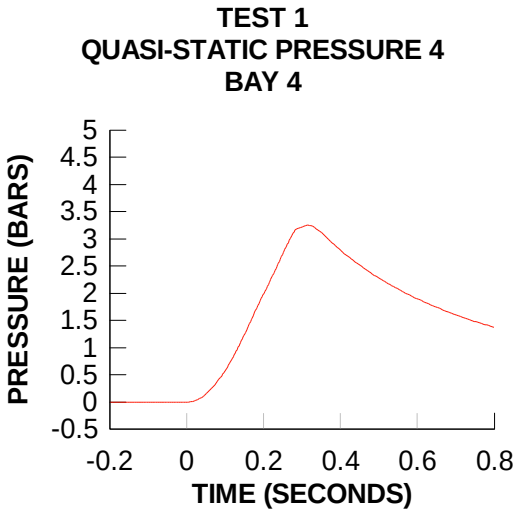
TEST 1
QUASI-STATIC PRESSURE 4
BAY 4
PRESSURE (BARS)
TIME (SECONDS)

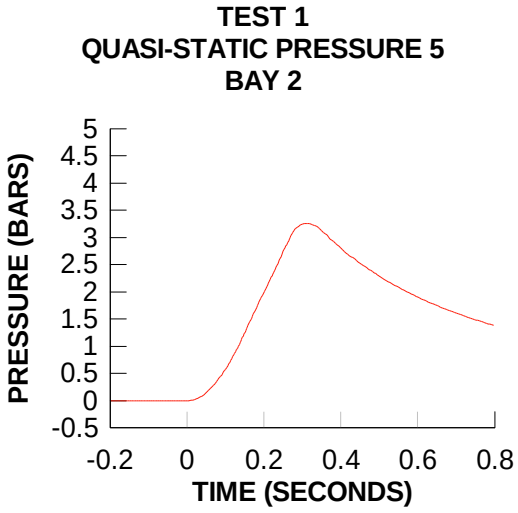
TEST 1
QUASI-STATIC PRESSURE 5
BAY 2
PRESSURE (BARS)
TIME (SECONDS)

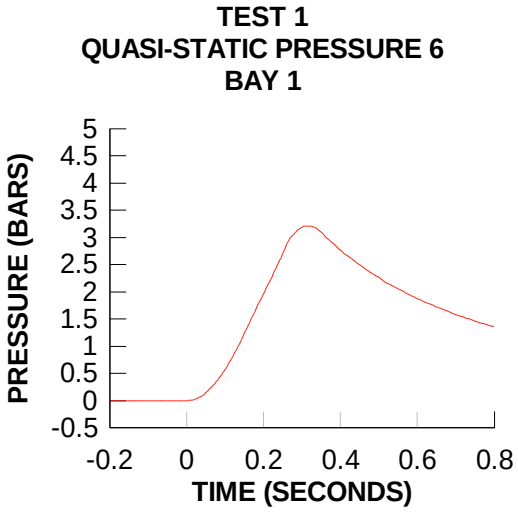
TEST 1
QUASI-STATIC PRESSURE 6
BAY 1
PRESSURE (BARS)
TIME (SECONDS)

TEST 2
QUASI-STATIC PRESSURE 1
BAY 5

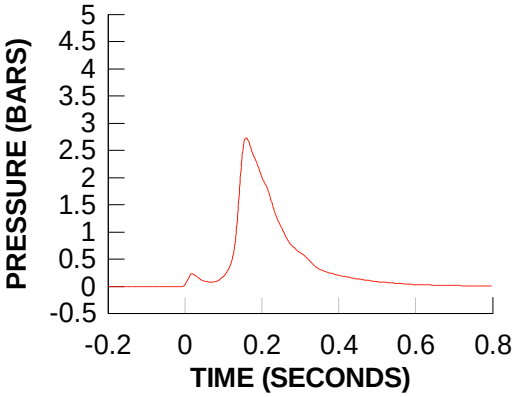

TEST 2
QUASI-STATIC PRESSURE 2
BAY 6

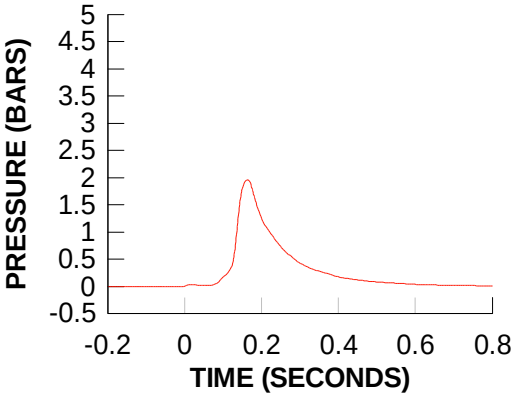

TEST 2
QUASI-STATIC PRESSURE 3
BAY 3

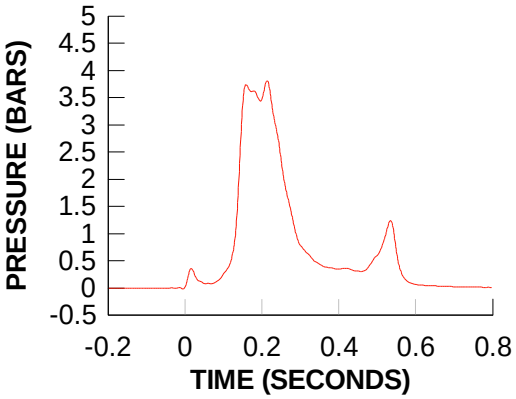

TEST 2
QUASI-STATIC PRESSURE 4
BAY 4

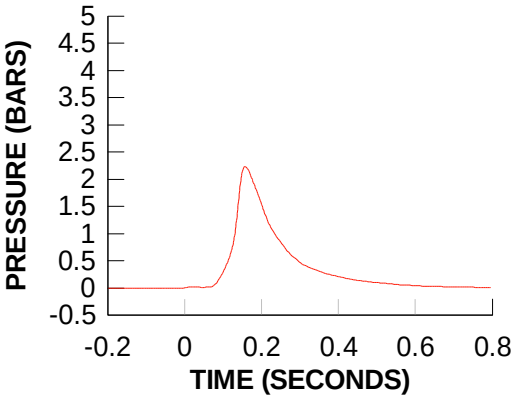

TEST 2
QUASI-STATIC PRESSURE 5
BAY 2

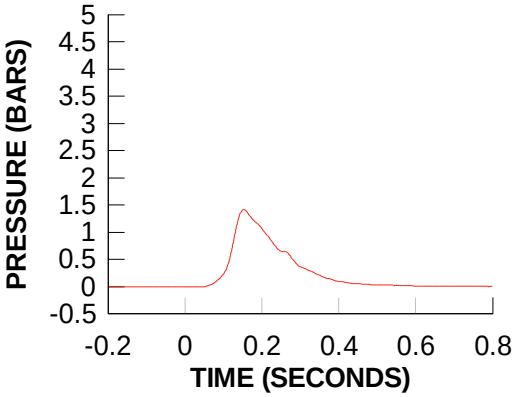

TEST 2
QUASI-STATIC PRESSURE 6
BAY 1

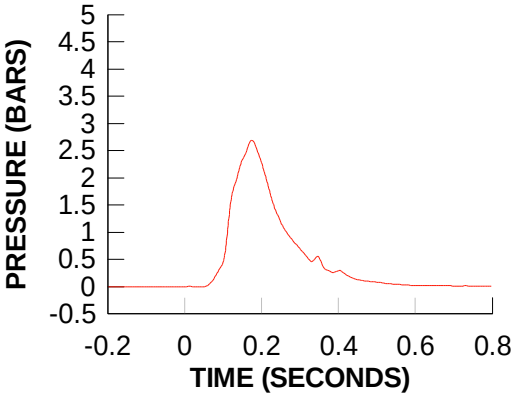

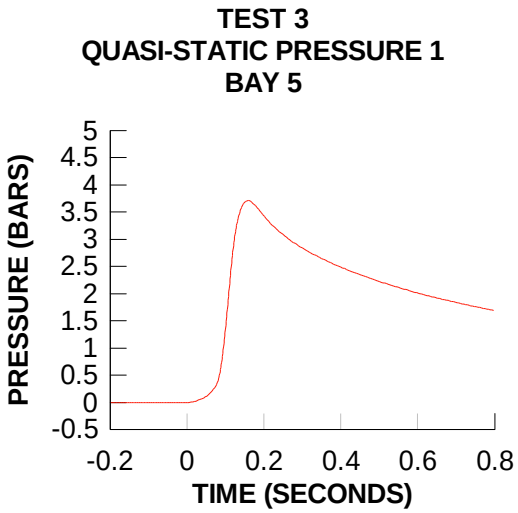
TEST 3
QUASI-STATIC PRESSURE 1
BAY 5
PRESSURE (BARS)
TIME (SECONDS)

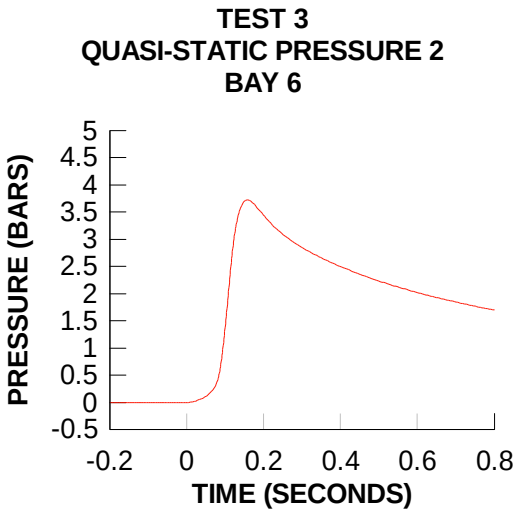
TEST 3
QUASI-STATIC PRESSURE 2
BAY 6
PRESSURE (BARS)
TIME (SECONDS)

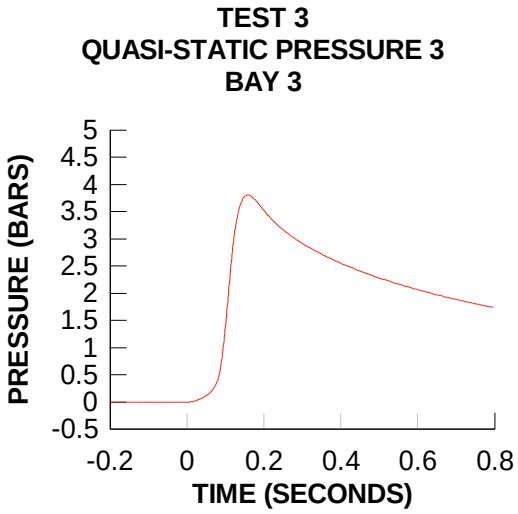
TEST 3
QUASI-STATIC PRESSURE 3
BAY 3
PRESSURE (BARS)
TIME (SECONDS)

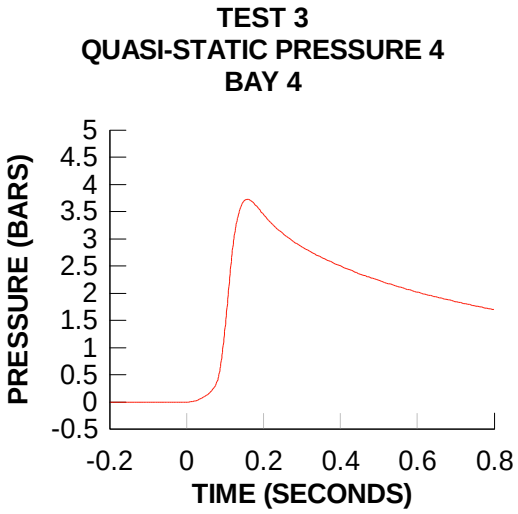
TEST 3
QUASI-STATIC PRESSURE 4
BAY 4
PRESSURE (BARS)
TIME (SECONDS)

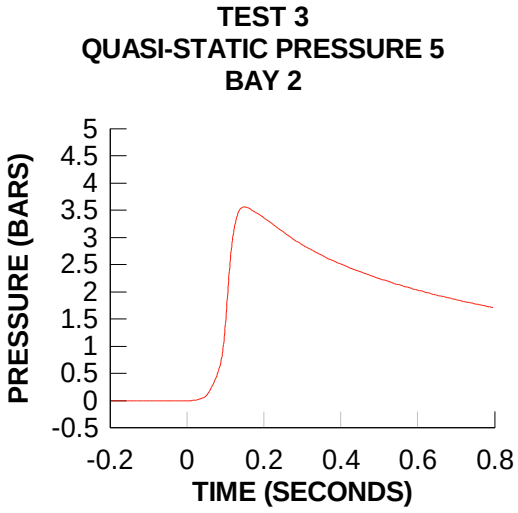
TEST 3
QUASI-STATIC PRESSURE 5
BAY 2
PRESSURE (BARS)
TIME (SECONDS)

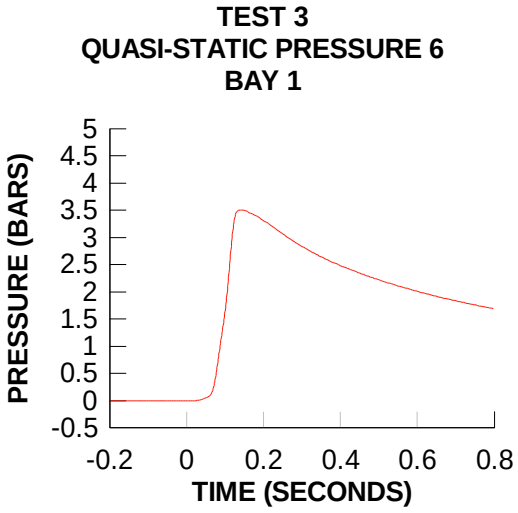
TEST 3
QUASI-STATIC PRESSURE 6
BAY 1
PRESSURE (BARS)
TIME (SECONDS)

TEST 4
QUASI-STATIC PRESSURE 1
BAY 5

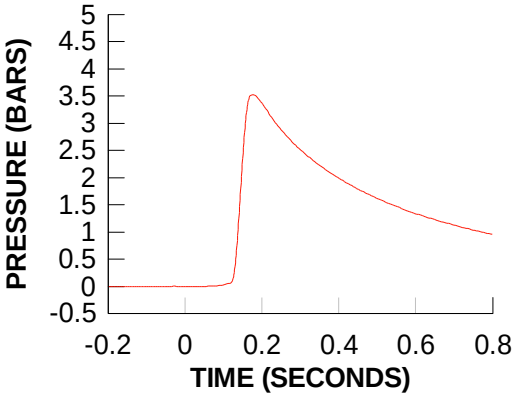

TEST 4
QUASI-STATIC PRESSURE 2
BAY 6

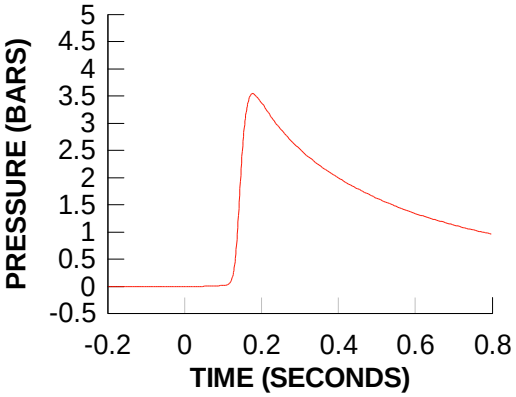

TEST 4
QUASI-STATIC PRESSURE 3
BAY 3

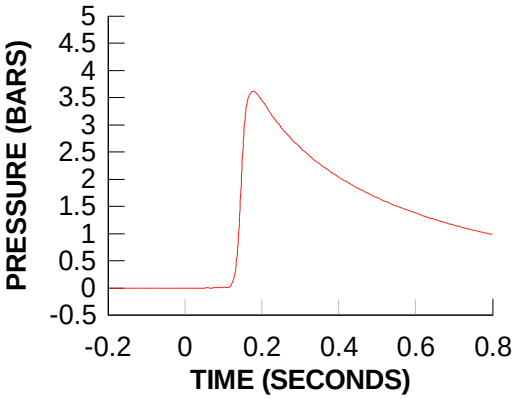

TEST 4
QUASI-STATIC PRESSURE 4
BAY 4

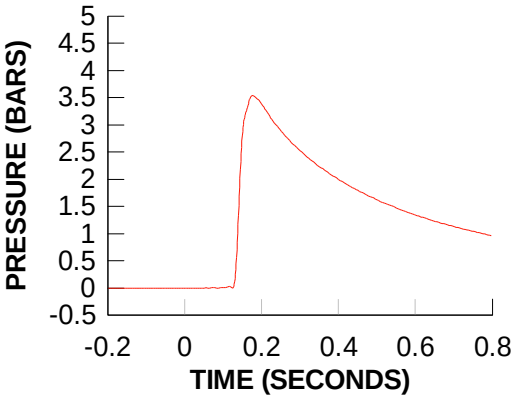

TEST 4
QUASI-STATIC PRESSURE 5
BAY 2

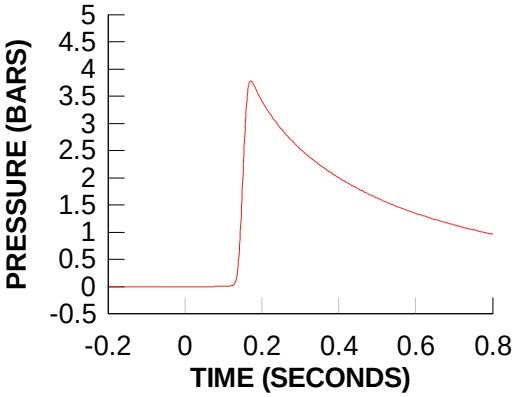

TEST 4
QUASI-STATIC PRESSURE 6
BAY 1

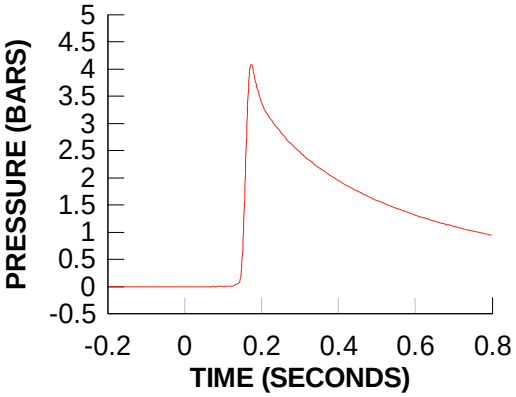

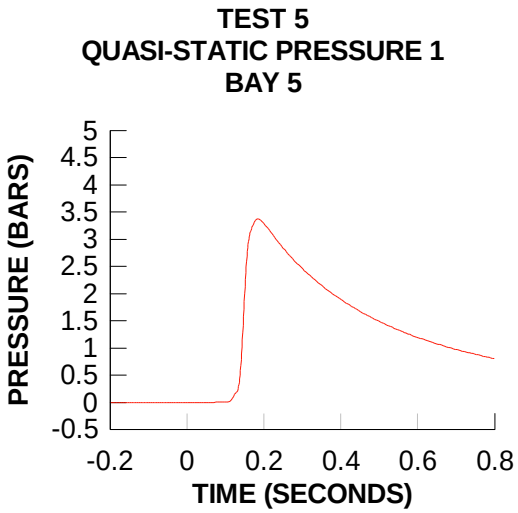
TEST 5
QUASI-STATIC PRESSURE 1
BAY 5
PRESSURE (BARS)
TIME (SECONDS)

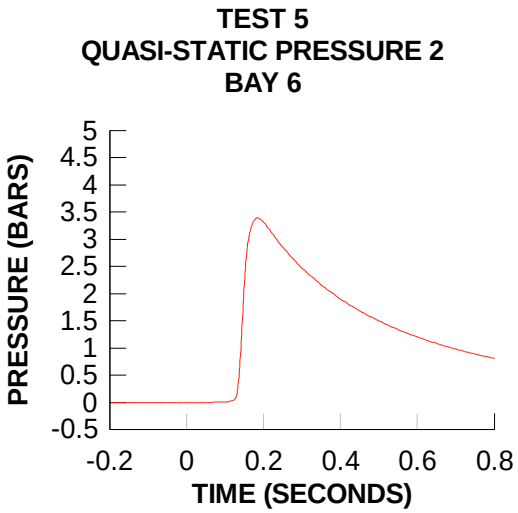
TEST 5
QUASI-STATIC PRESSURE 2
BAY 6
PRESSURE (BARS)
TIME (SECONDS)

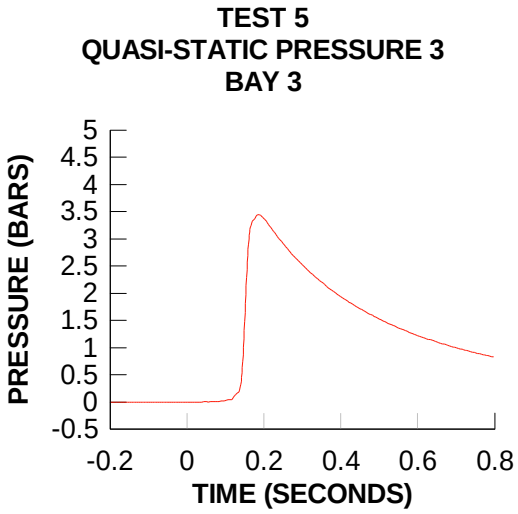
TEST 5
QUASI-STATIC PRESSURE 3
BAY 3
PRESSURE (BARS)
TIME (SECONDS)

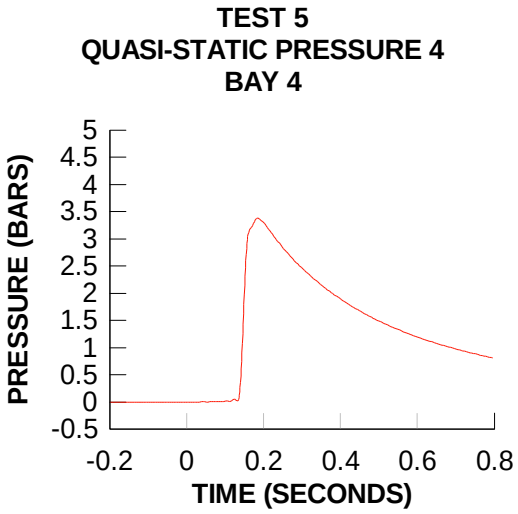
TEST 5
QUASI-STATIC PRESSURE 4
BAY 4
PRESSURE (BARS)
TIME (SECONDS)

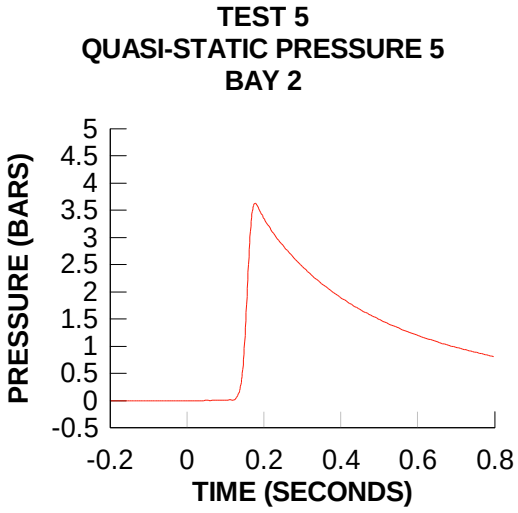
TEST 5
QUASI-STATIC PRESSURE 5
BAY 2
PRESSURE (BARS)
TIME (SECONDS)

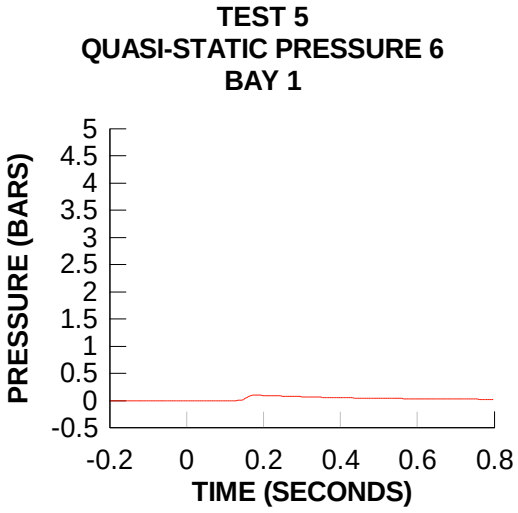
TEST 5
QUASI-STATIC PRESSURE 6
BAY 1
PRESSURE (BARS)
TIME (SECONDS)

TEST 6
QUASI-STATIC PRESSURE 1
BAY 5

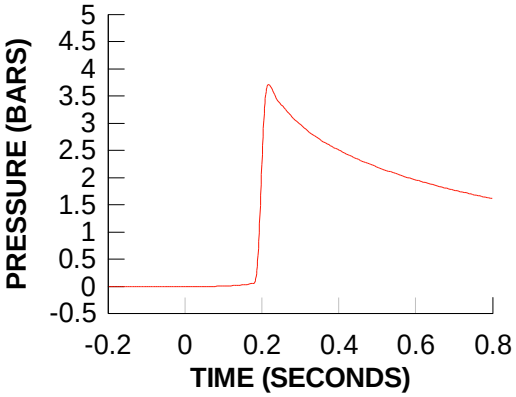

TEST 6
QUASI-STATIC PRESSURE 2
BAY 6

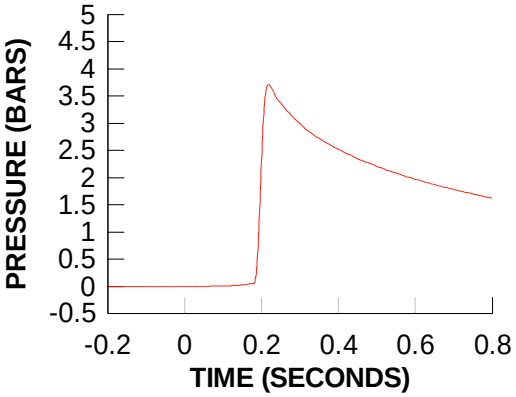

TEST 6
QUASI-STATIC PRESSURE 3
BAY 3

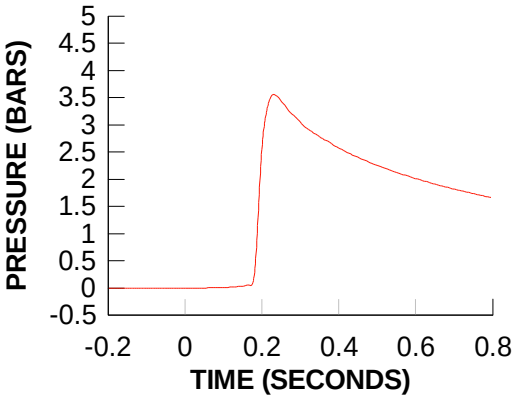

TEST 6
QUASI-STATIC PRESSURE 4
BAY 4

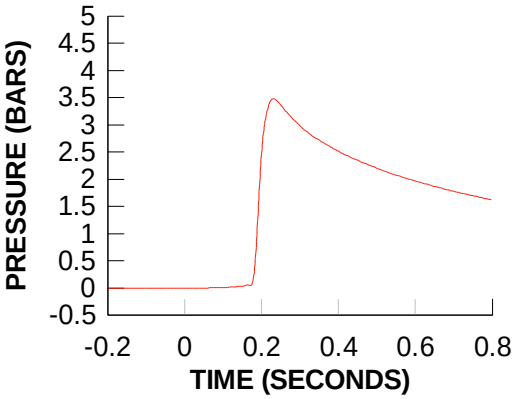

TEST 6
QUASI-STATIC PRESSURE 5
BAY 2

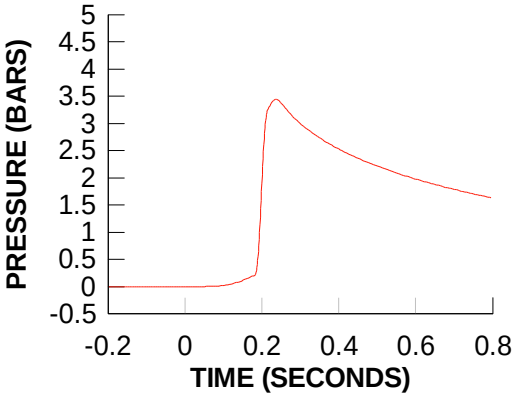

TEST 6
QUASI-STATIC PRESSURE 6
BAY 1

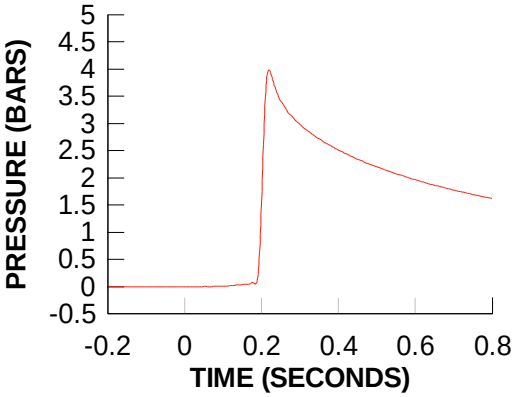

TEST 7
QUASI-STATIC PRESSURE 1
BAY 5

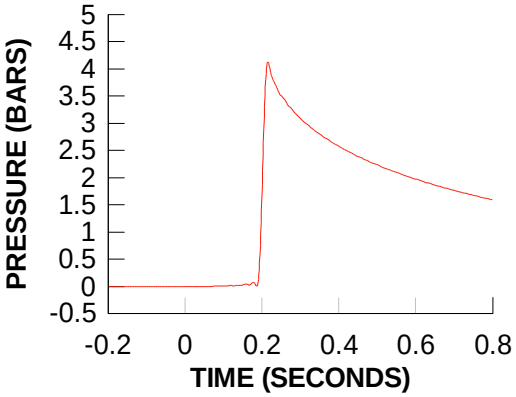

TEST 7
QUASI-STATIC PRESSURE 2
BAY 6

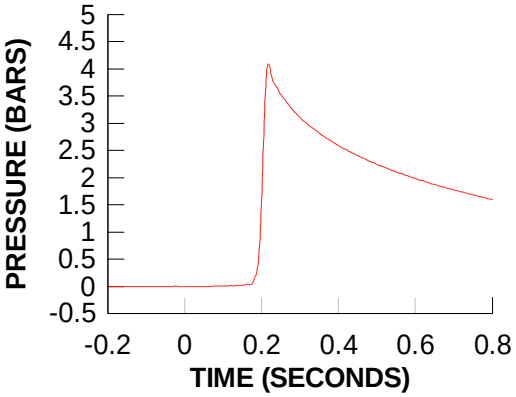

TEST 7
QUASI-STATIC PRESSURE 3
BAY 3

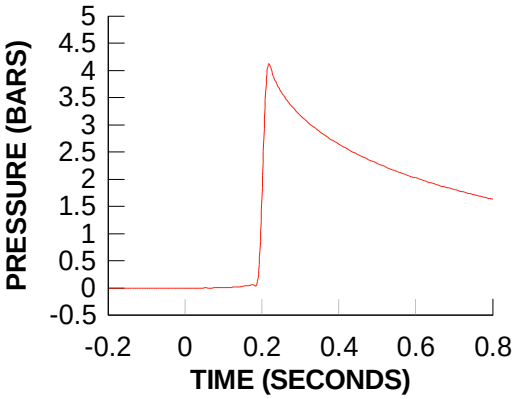

TEST 7
QUASI-STATIC PRESSURE 4
BAY 4

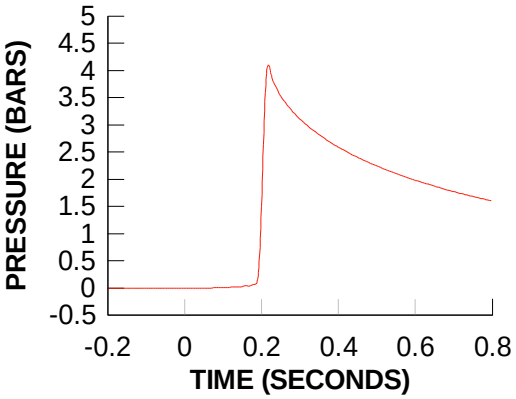

TEST 7
QUASI-STATIC PRESSURE 5
BAY 2

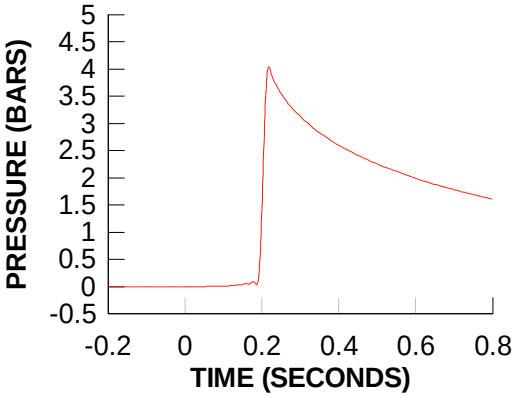

TEST 7
QUASI-STATIC PRESSURE 6
BAY 1

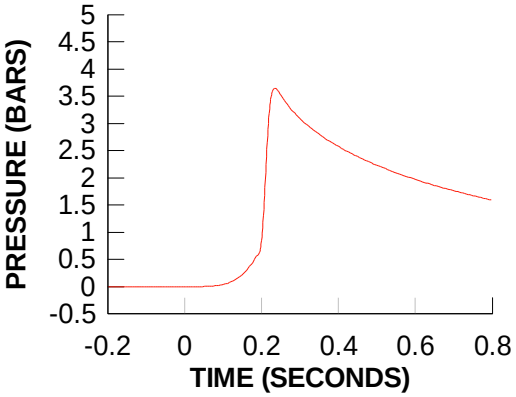

TEST 8
QUASI-STATIC PRESSURE 1
BAY 5

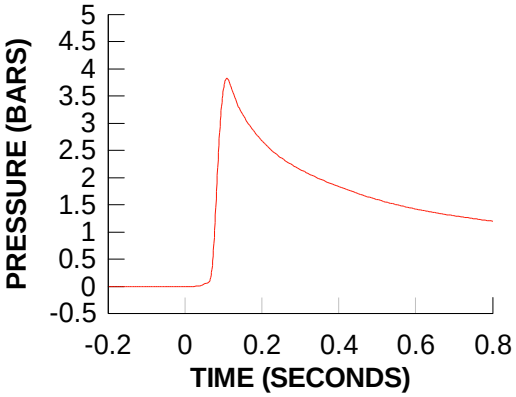

TEST 8
QUASI-STATIC PRESSURE 2
BAY 6

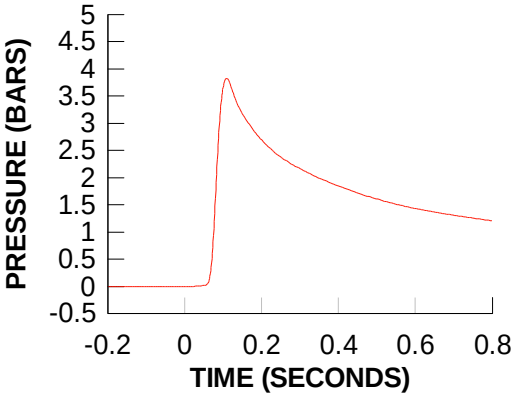

TEST 8
QUASI-STATIC PRESSURE 3
BAY 3

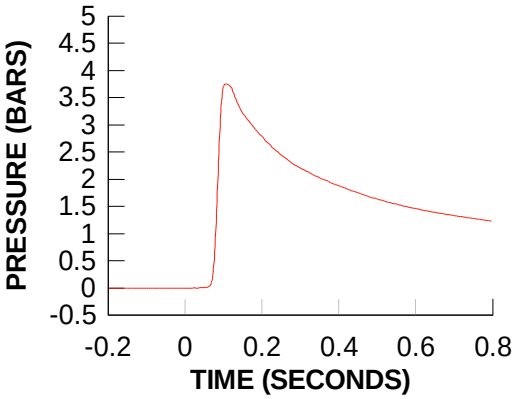

TEST 8
QUASI-STATIC PRESSURE 4
BAY 4

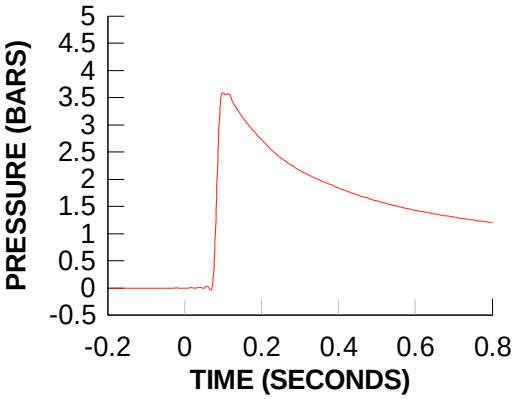

TEST 8
QUASI-STATIC PRESSURE 5
BAY 2

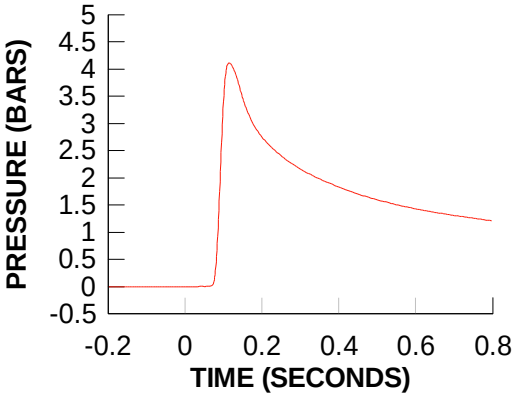

TEST 8
QUASI-STATIC PRESSURE 6
BAY 1

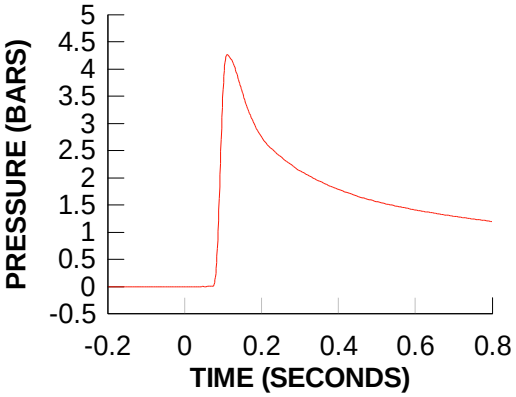

TEST 9
QUASI-STATIC PRESSURE 1
BAY 5

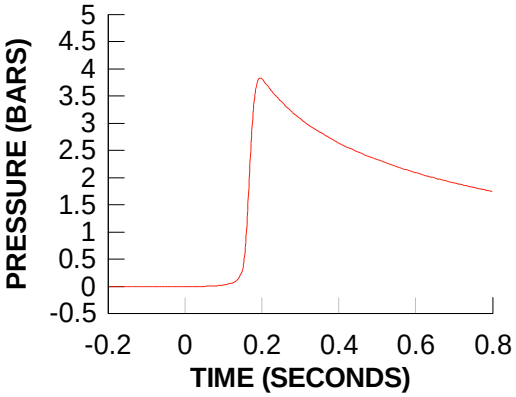

TEST 9
QUASI-STATIC PRESSURE 2
BAY 6

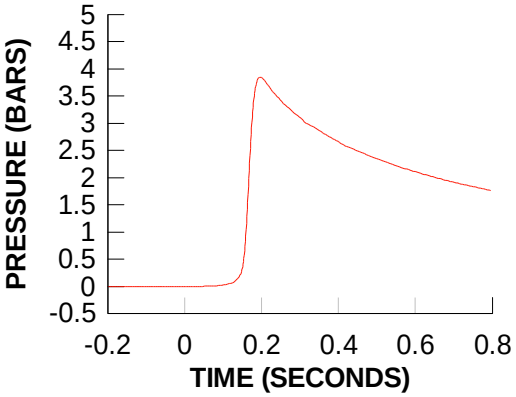

TEST 9
QUASI-STATIC PRESSURE 3
BAY 3

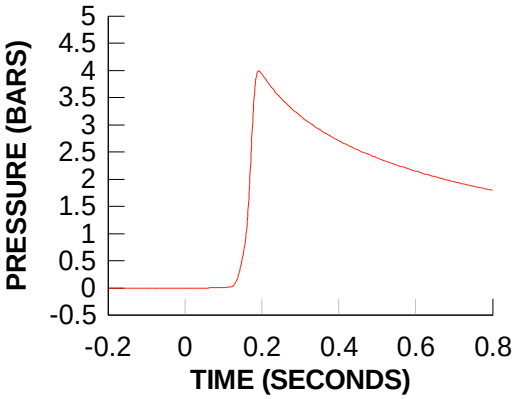

TEST 9
QUASI-STATIC PRESSURE 4
BAY 4

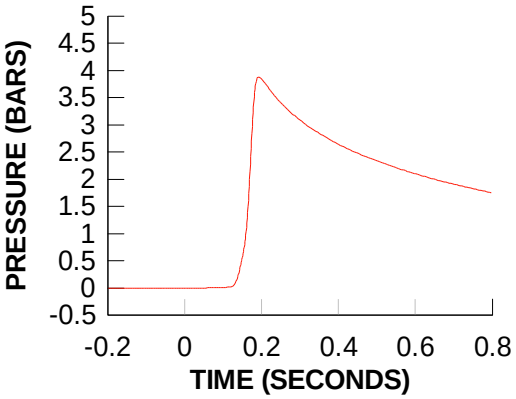

TEST 9
QUASI-STATIC PRESSURE 5
BAY 2

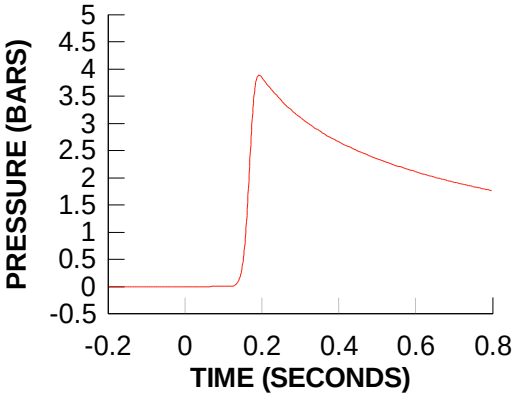

TEST 9
QUASI-STATIC PRESSURE 6
BAY 1

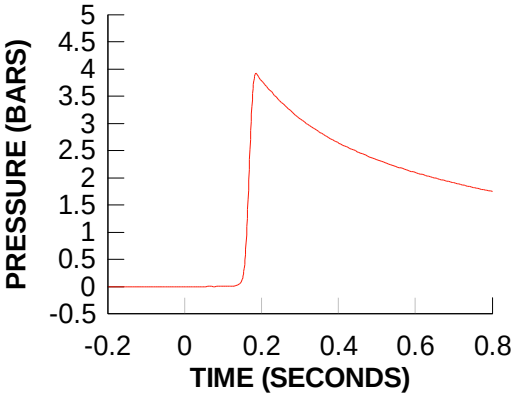

TEST 10
QUASI-STATIC PRESSURE 1
BAY 5

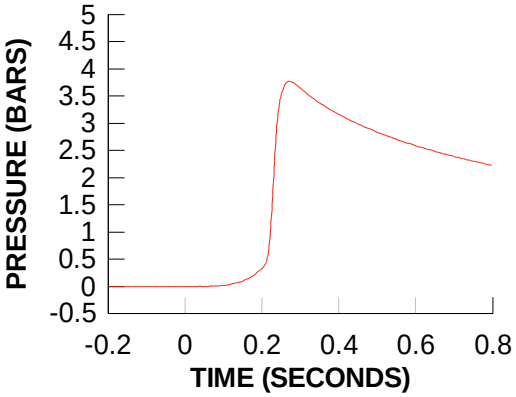

TEST 10
QUASI-STATIC PRESSURE 2
BAY 6

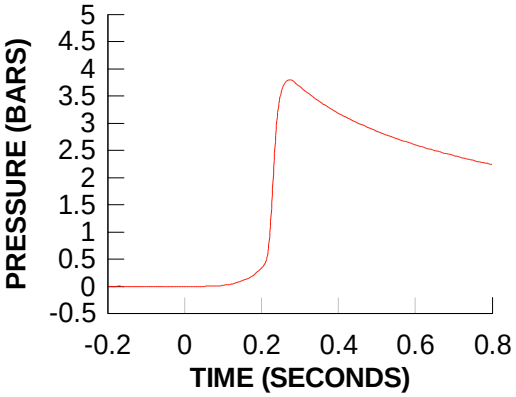

TEST 10
QUASI-STATIC PRESSURE 3
BAY 3

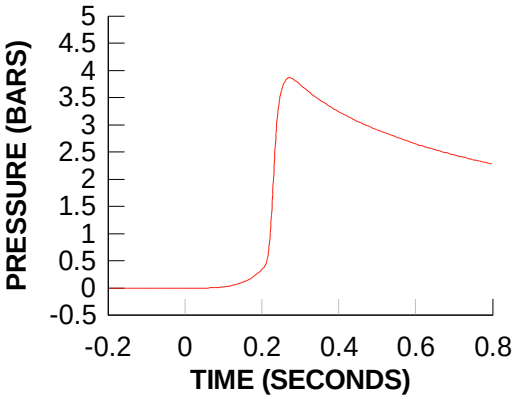

TEST 10
QUASI-STATIC PRESSURE 4
BAY 4

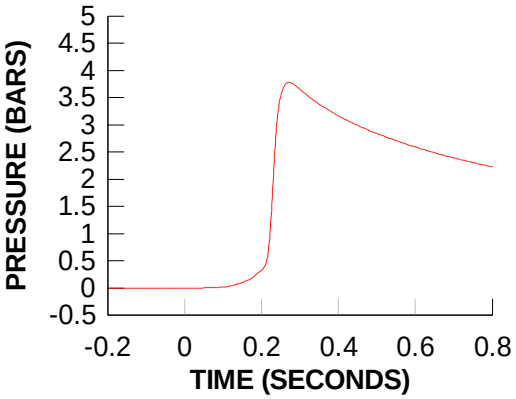

TEST 10
QUASI-STATIC PRESSURE 5
BAY 2

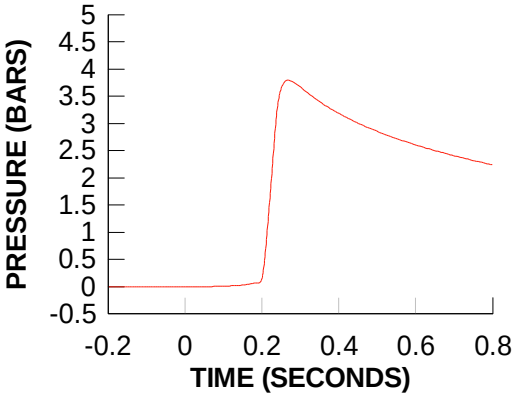

TEST 10
QUASI-STATIC PRESSURE 6
BAY 1

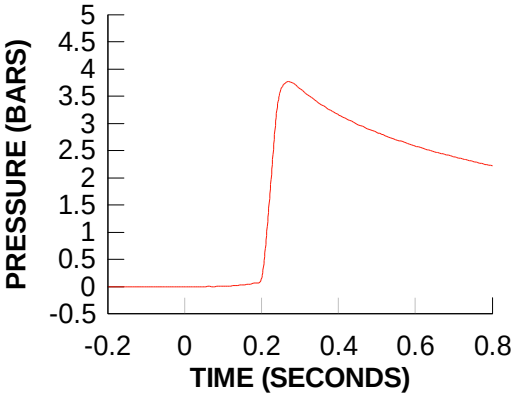

TEST 11
QUASI-STATIC PRESSURE 1
BAY 5

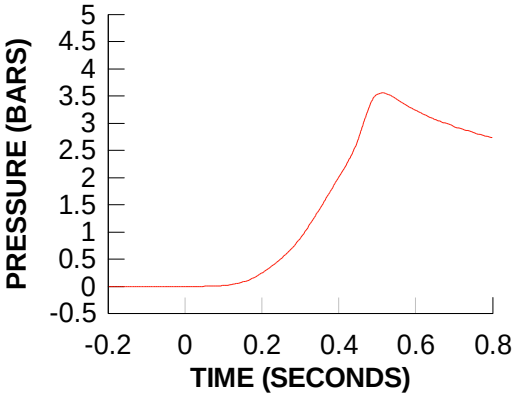

TEST 11
QUASI-STATIC PRESSURE 2
BAY 6

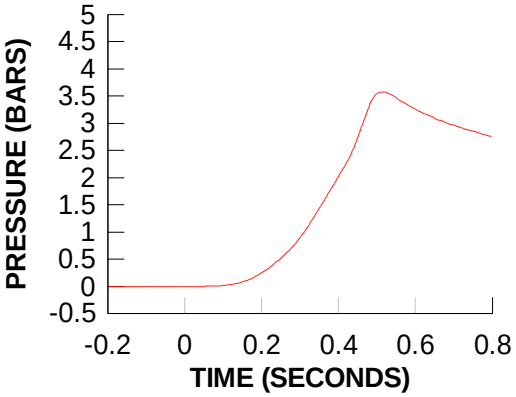

TEST 11
QUASI-STATIC PRESSURE 3
BAY 3

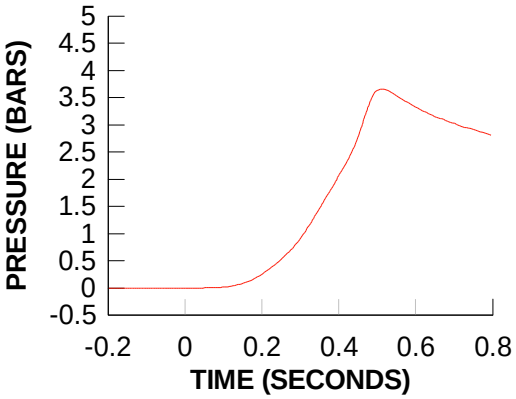

TEST 11
QUASI-STATIC PRESSURE 4
BAY 4

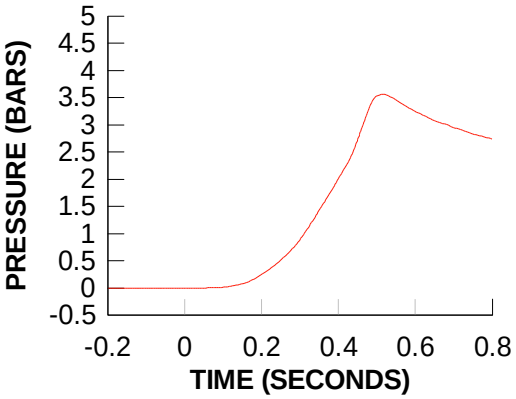

TEST 11
QUASI-STATIC PRESSURE 5
BAY 2

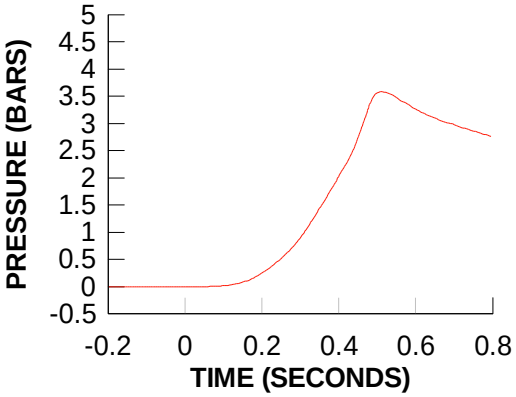

TEST 11
QUASI-STATIC PRESSURE 6
BAY 1

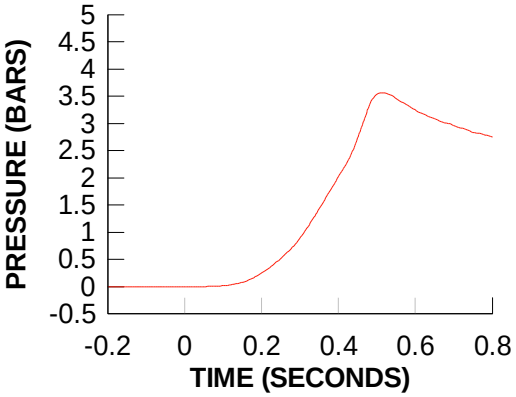

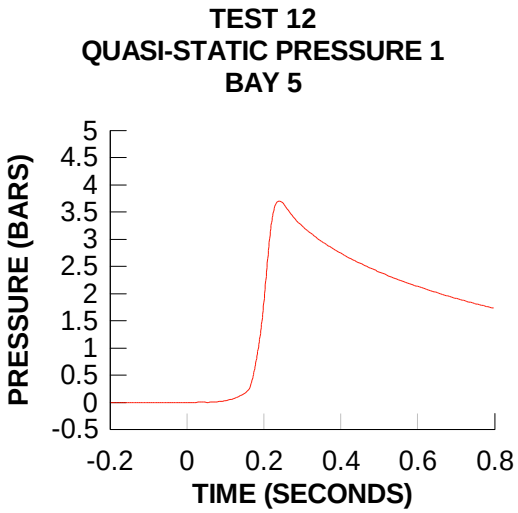
TEST 12
QUASI-STATIC PRESSURE 1
BAY 5
PRESSURE (BARS)
TIME (SECONDS)

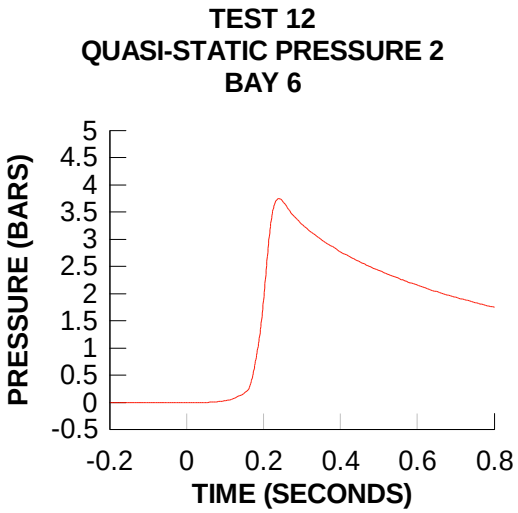
TEST 12
QUASI-STATIC PRESSURE 2
BAY 6
PRESSURE (BARS)
TIME (SECONDS)

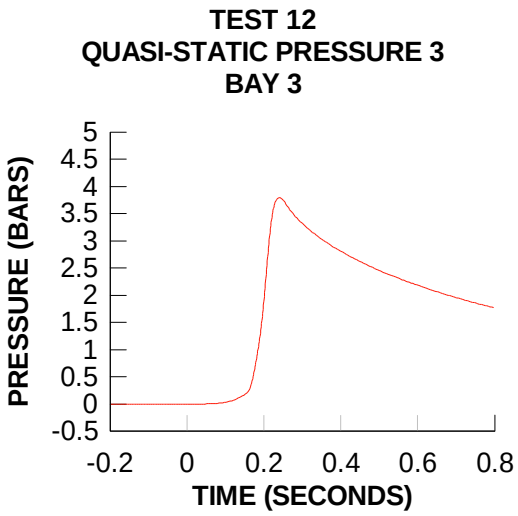
TEST 12
QUASI-STATIC PRESSURE 3
BAY 3
PRESSURE (BARS)
TIME (SECONDS)

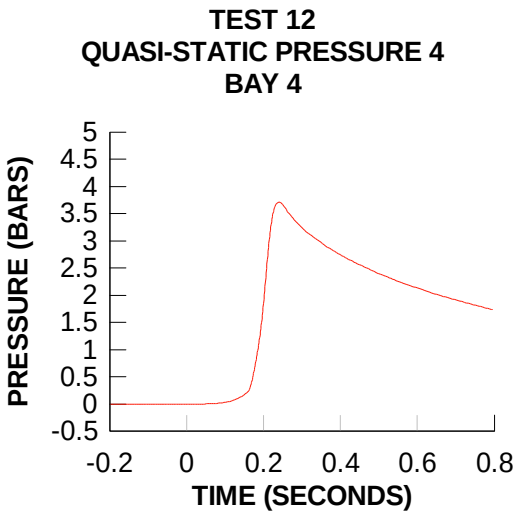
TEST 12
QUASI-STATIC PRESSURE 4
BAY 4
PRESSURE (BARS)
TIME (SECONDS)

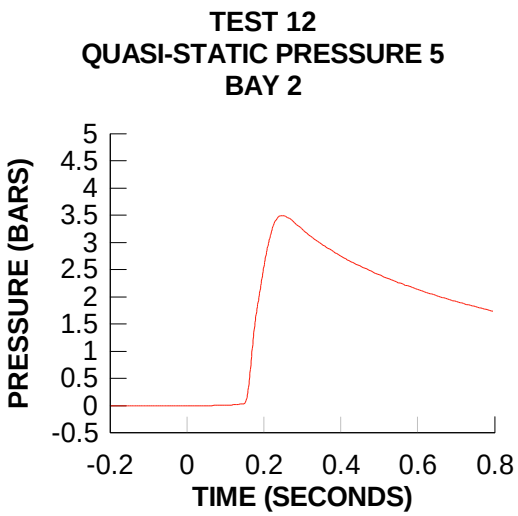
TEST 12
QUASI-STATIC PRESSURE 5
BAY 2
PRESSURE (BARS)
TIME (SECONDS)

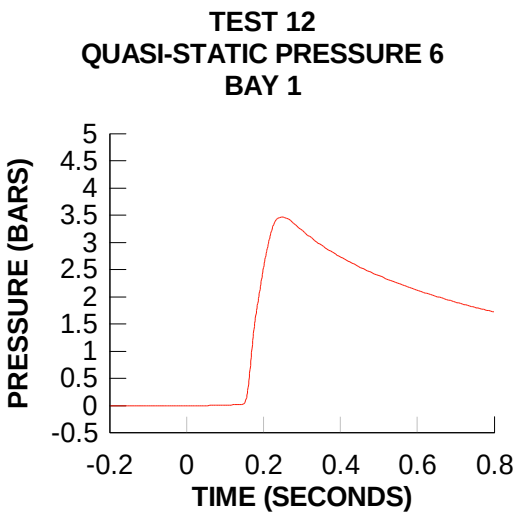
TEST 12
QUASI-STATIC PRESSURE 6
BAY 1
PRESSURE (BARS)
TIME (SECONDS)

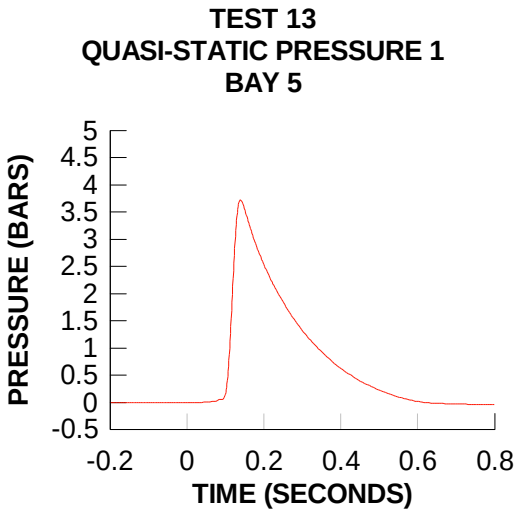
TEST 13
QUASI-STATIC PRESSURE 1
BAY 5
PRESSURE (BARS)
TIME (SECONDS)

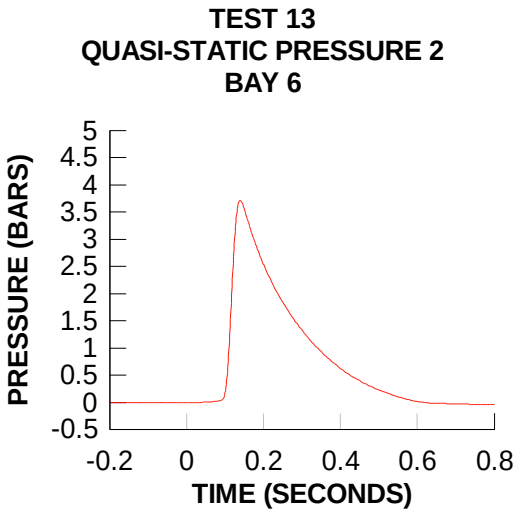
TEST 13
QUASI-STATIC PRESSURE 2
BAY 6
PRESSURE (BARS)
TIME (SECONDS)

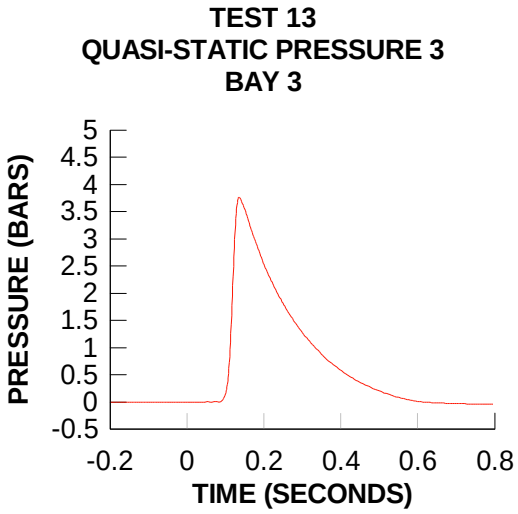
TEST 13
QUASI-STATIC PRESSURE 3
BAY 3
PRESSURE (BARS)
TIME (SECONDS)

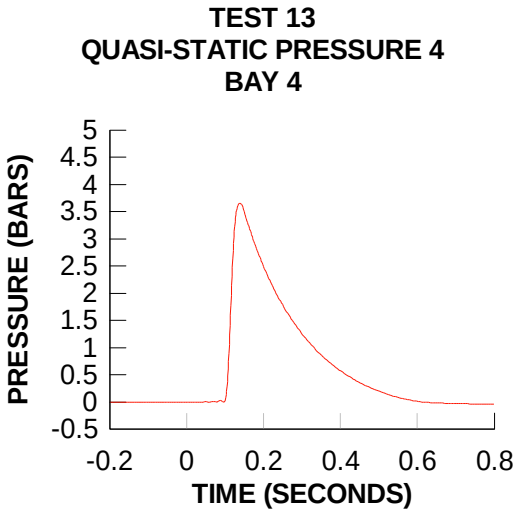
TEST 13
QUASI-STATIC PRESSURE 4
BAY 4
PRESSURE (BARS)
TIME (SECONDS)

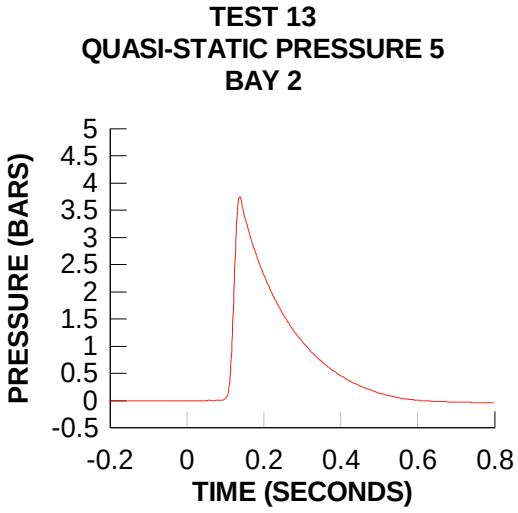
TEST 13
QUASI-STATIC PRESSURE 5
BAY 2
PRESSURE (BARS)
TIME (SECONDS)

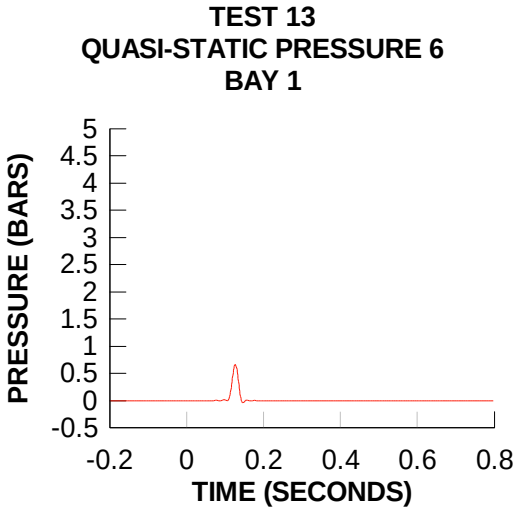
TEST 13
QUASI-STATIC PRESSURE 6
BAY 1
PRESSURE (BARS)
TIME (SECONDS)

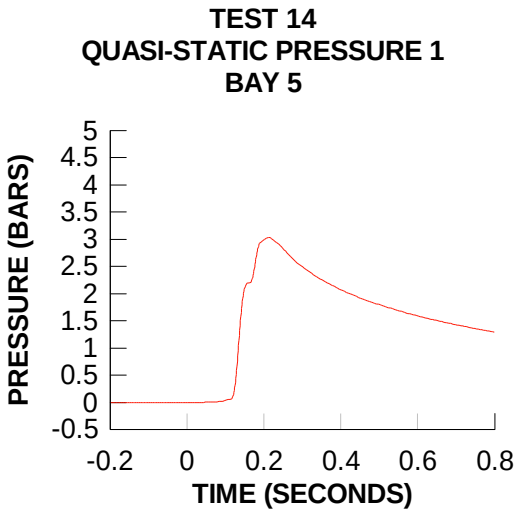
TEST 14
QUASI-STATIC PRESSURE 1
BAY 5
PRESSURE (BARS)
TIME (SECONDS)

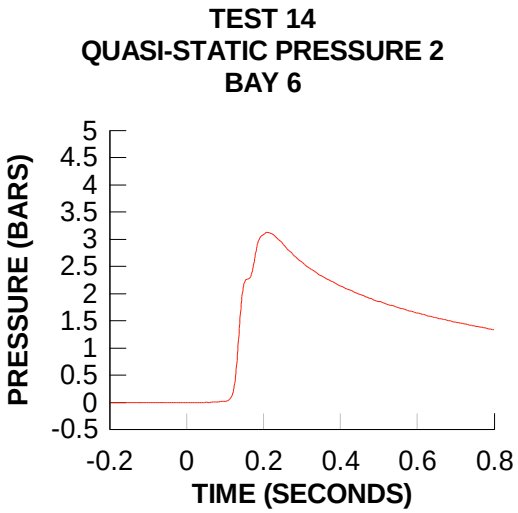
TEST 14
QUASI-STATIC PRESSURE 2
BAY 6
PRESSURE (BARS)
TIME (SECONDS)

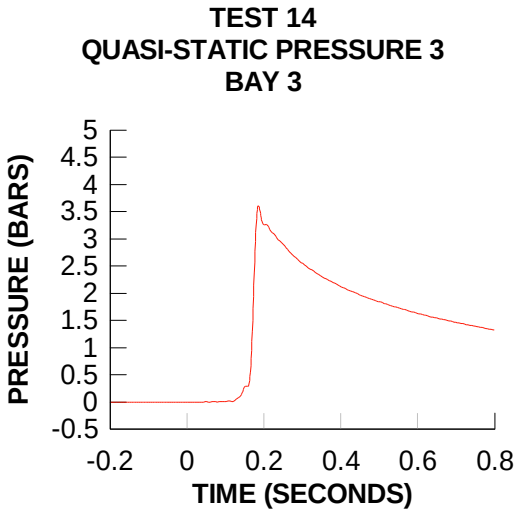
TEST 14
QUASI-STATIC PRESSURE 3
BAY 3
PRESSURE (BARS)
TIME (SECONDS)

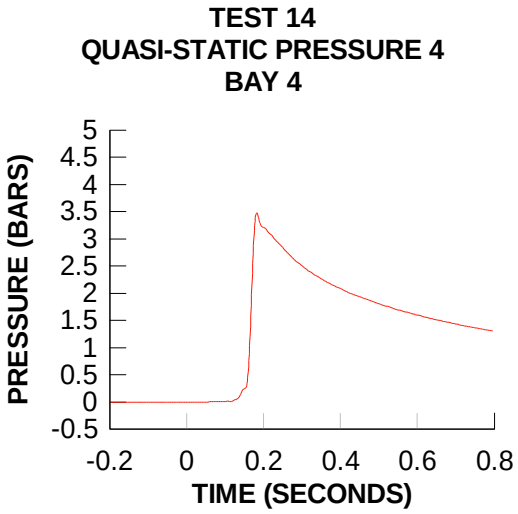
TEST 14
QUASI-STATIC PRESSURE 4
BAY 4
PRESSURE (BARS)
TIME (SECONDS)

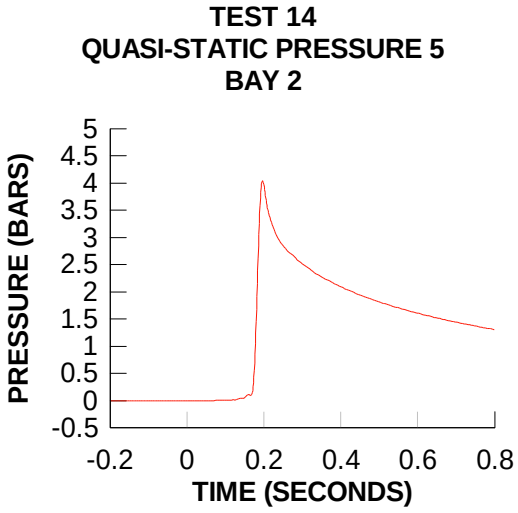
TEST 14
QUASI-STATIC PRESSURE 5
BAY 2
PRESSURE (BARS)
TIME (SECONDS)

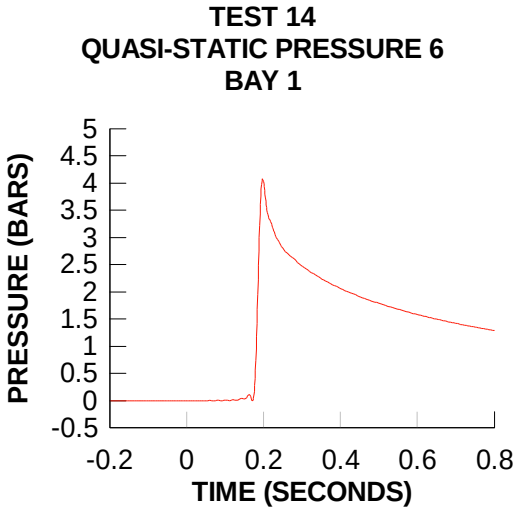
TEST 14
QUASI-STATIC PRESSURE 6
BAY 1
PRESSURE (BARS)
TIME (SECONDS)

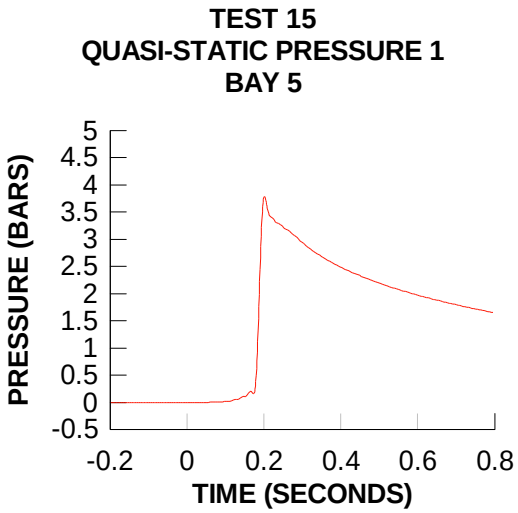
TEST 15
QUASI-STATIC PRESSURE 1
BAY 5
PRESSURE (BARS)
TIME (SECONDS)

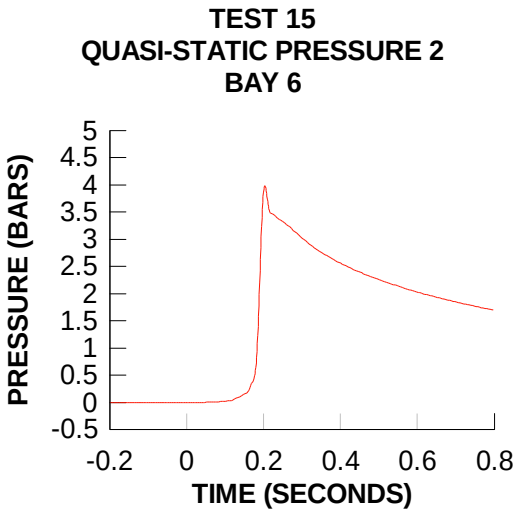
TEST 15
QUASI-STATIC PRESSURE 2
BAY 6
PRESSURE (BARS)
TIME (SECONDS)

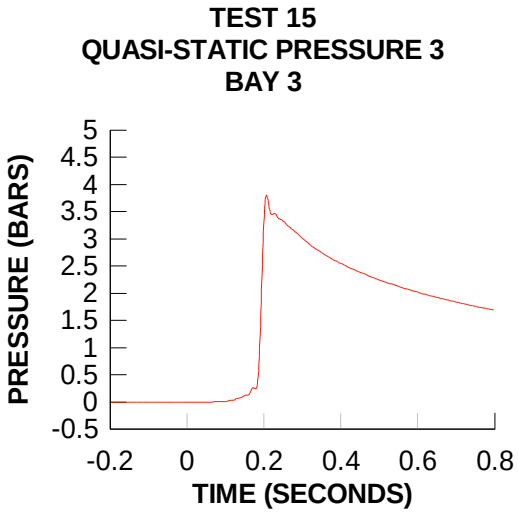
TEST 15
QUASI-STATIC PRESSURE 3
BAY 3
PRESSURE (BARS)
TIME (SECONDS)

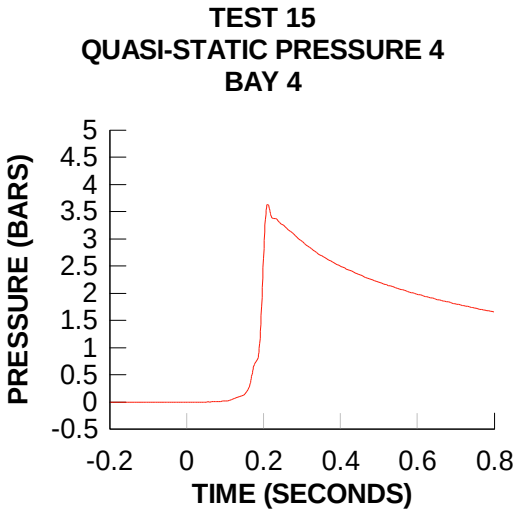
TEST 15
QUASI-STATIC PRESSURE 4
BAY 4
PRESSURE (BARS)
TIME (SECONDS)

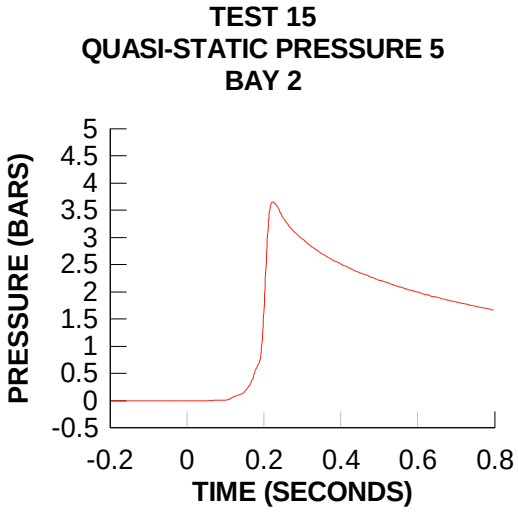
TEST 15
QUASI-STATIC PRESSURE 5
BAY 2
PRESSURE (BARS)
TIME (SECONDS)

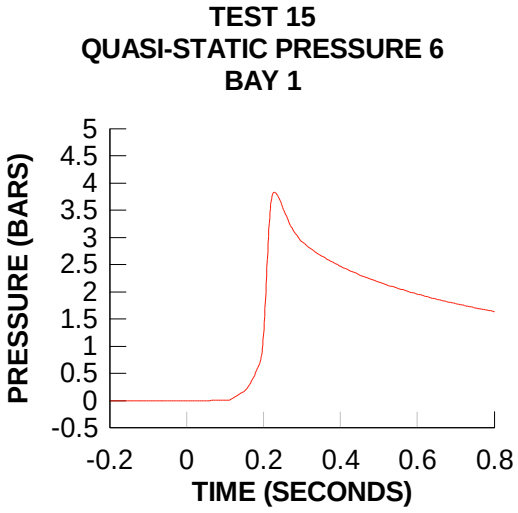
TEST 15
QUASI-STATIC PRESSURE 6
BAY 1
PRESSURE (BARS)
TIME (SECONDS)

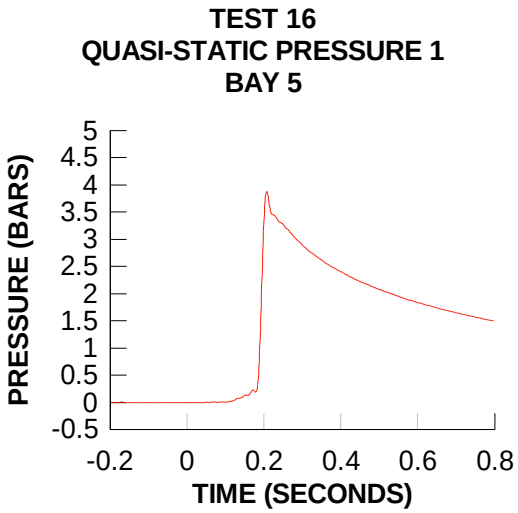
TEST 16
QUASI-STATIC PRESSURE 1
BAY 5
PRESSURE (BARS)
TIME (SECONDS)

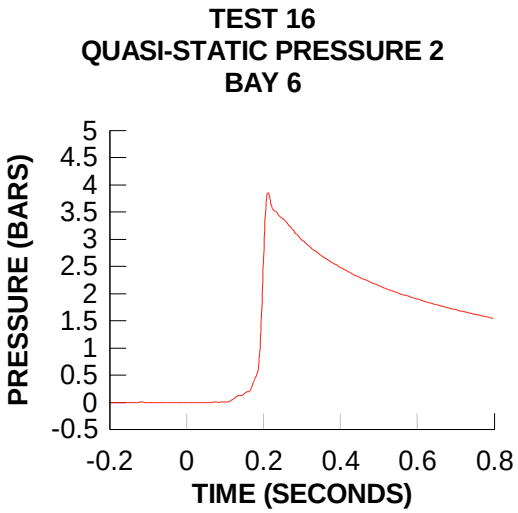
TEST 16
QUASI-STATIC PRESSURE 2
BAY 6
PRESSURE (BARS)
TIME (SECONDS)

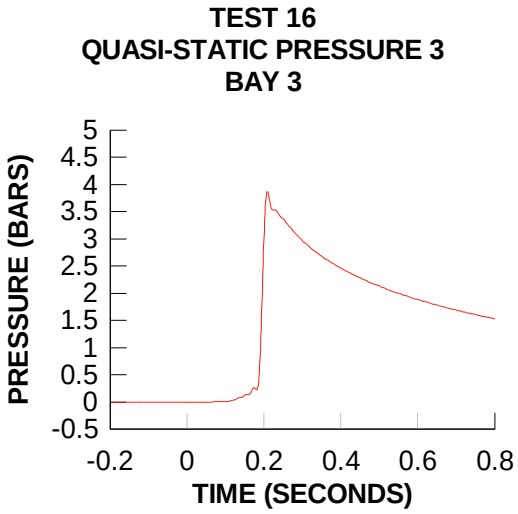
TEST 16
QUASI-STATIC PRESSURE 3
BAY 3
PRESSURE (BARS)
TIME (SECONDS)

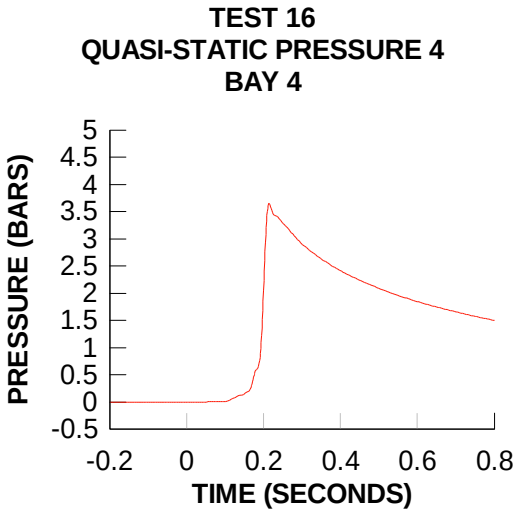
TEST 16
QUASI-STATIC PRESSURE 4
BAY 4
PRESSURE (BARS)
TIME (SECONDS)

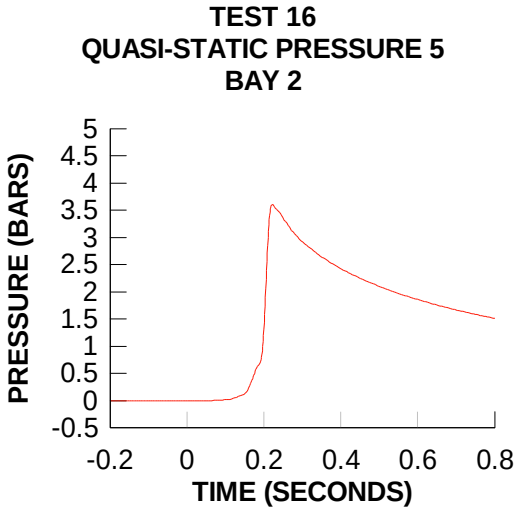
TEST 16
QUASI-STATIC PRESSURE 5
BAY 2
PRESSURE (BARS)
TIME (SECONDS)

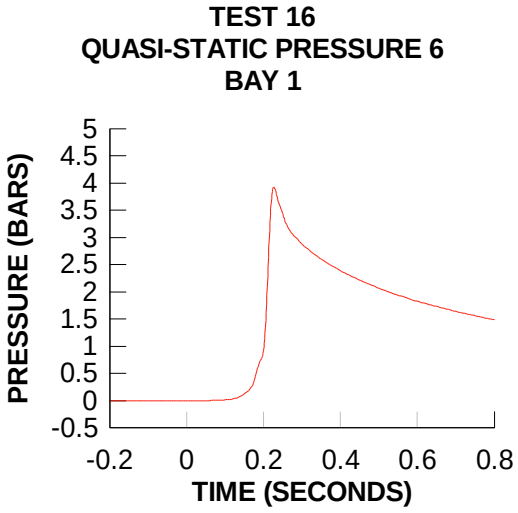
TEST 16
QUASI-STATIC PRESSURE 6
BAY 1
PRESSURE (BARS)
TIME (SECONDS)

TEST 17
QUASI-STATIC PRESSURE 1
BAY 5

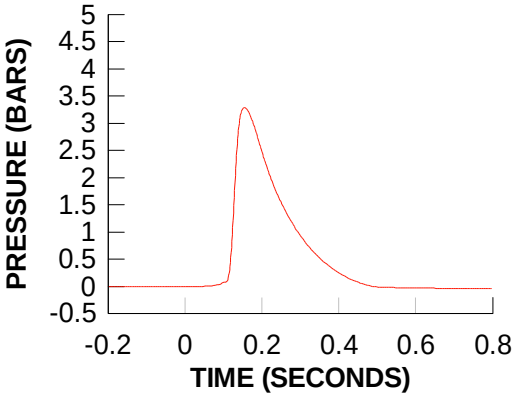

TEST 17
QUASI-STATIC PRESSURE 2
BAY 6

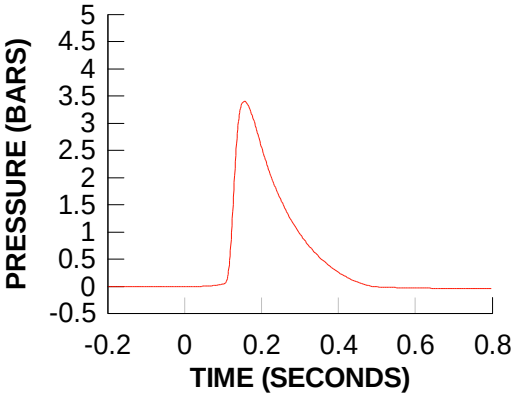

TEST 17
QUASI-STATIC PRESSURE 3
BAY 3

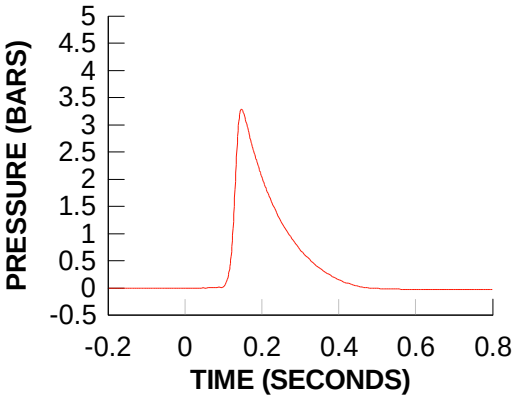

TEST 17
QUASI-STATIC PRESSURE 4
BAY 4

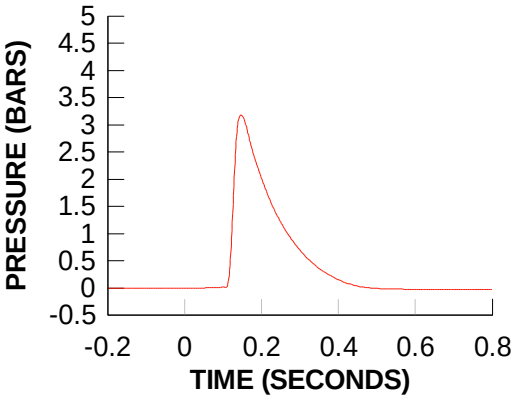

TEST 17
QUASI-STATIC PRESSURE 5
BAY 2

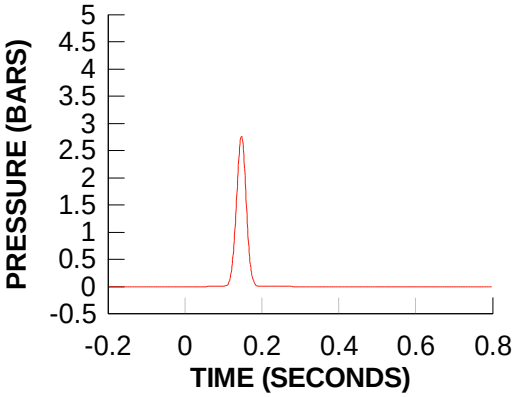

TEST 17
QUASI-STATIC PRESSURE 6
BAY 1

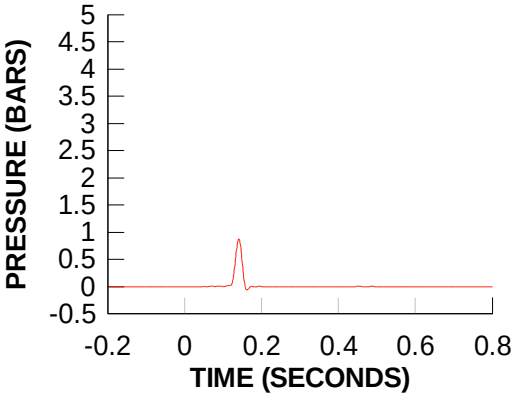

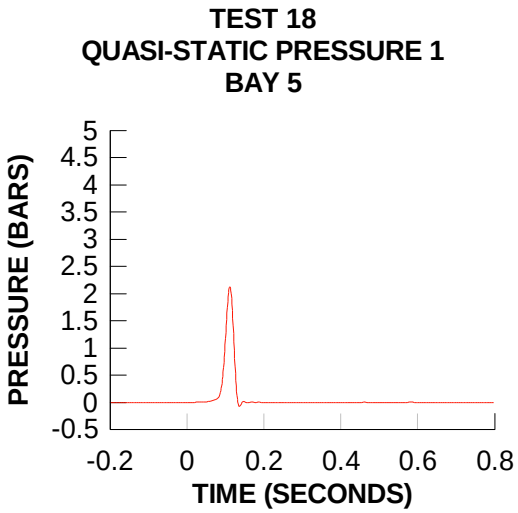
TEST 18
QUASI-STATIC PRESSURE 1
BAY 5
PRESSURE (BARS)
TIME (SECONDS)

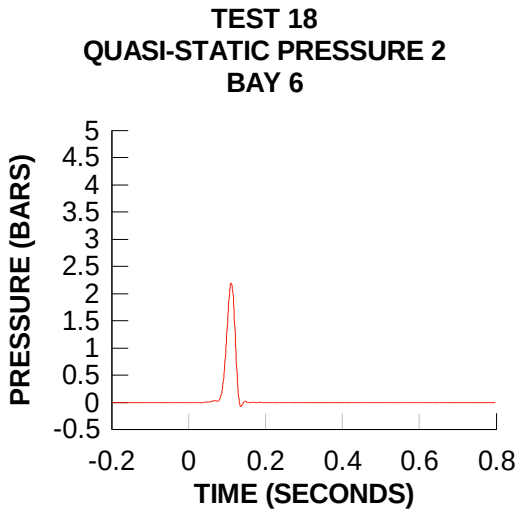
TEST 18
QUASI-STATIC PRESSURE 2
BAY 6
PRESSURE (BARS)
TIME (SECONDS)

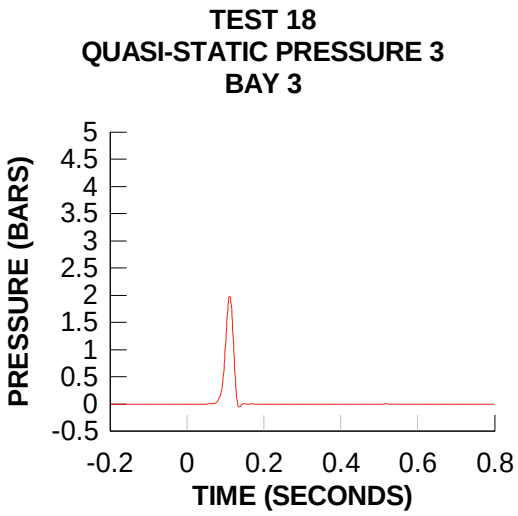
TEST 18
QUASI-STATIC PRESSURE 3
BAY 3
PRESSURE (BARS)
TIME (SECONDS)

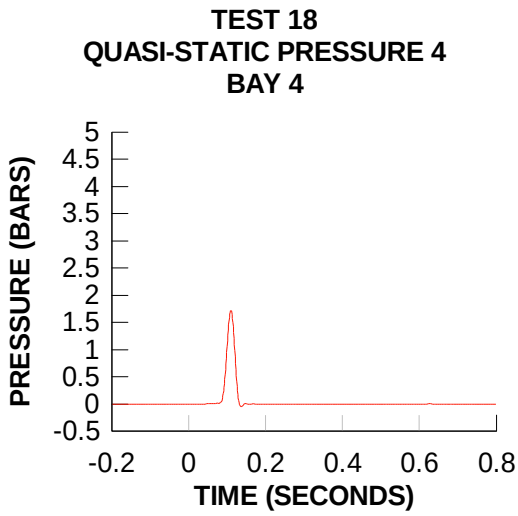
TEST 18
QUASI-STATIC PRESSURE 4
BAY 4
PRESSURE (BARS)
TIME (SECONDS)

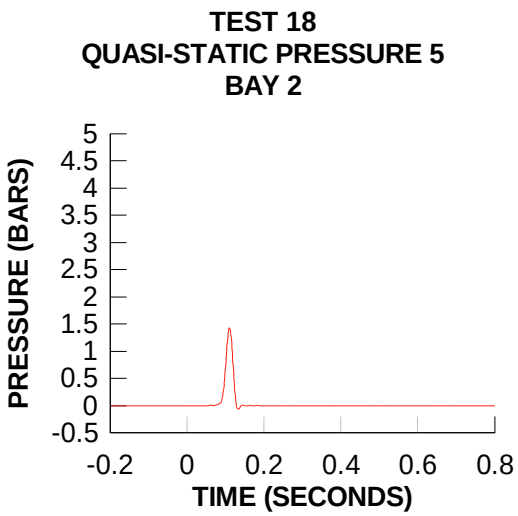
TEST 18
QUASI-STATIC PRESSURE 5
BAY 2
PRESSURE (BARS)
TIME (SECONDS)

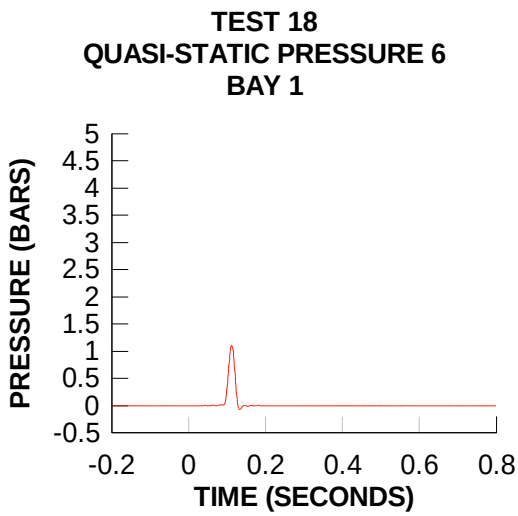
TEST 18
QUASI-STATIC PRESSURE 6
BAY 1
PRESSURE (BARS)
TIME (SECONDS)

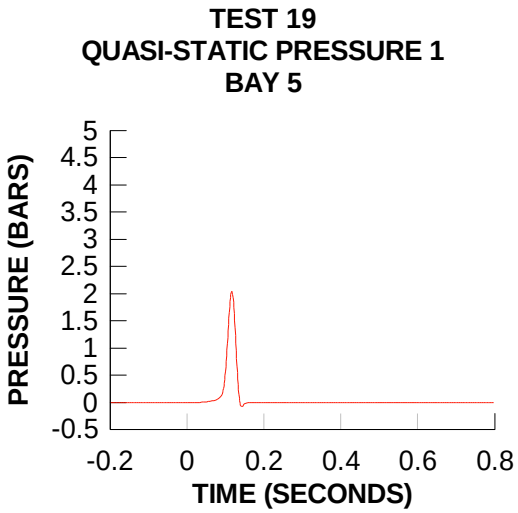
TEST 19
QUASI-STATIC PRESSURE 1
BAY 5
PRESSURE (BARS)
TIME (SECONDS)

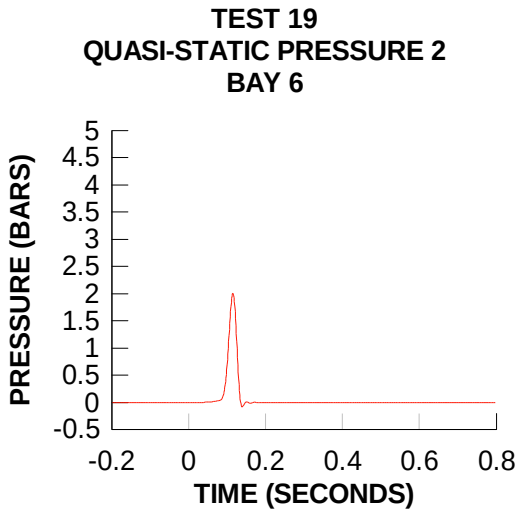
TEST 19
QUASI-STATIC PRESSURE 2
BAY 6
PRESSURE (BARS)
TIME (SECONDS)

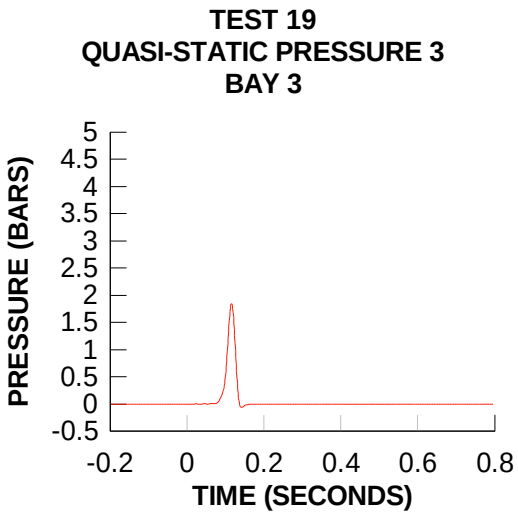
TEST 19
QUASI-STATIC PRESSURE 3
BAY 3
PRESSURE (BARS)
TIME (SECONDS)

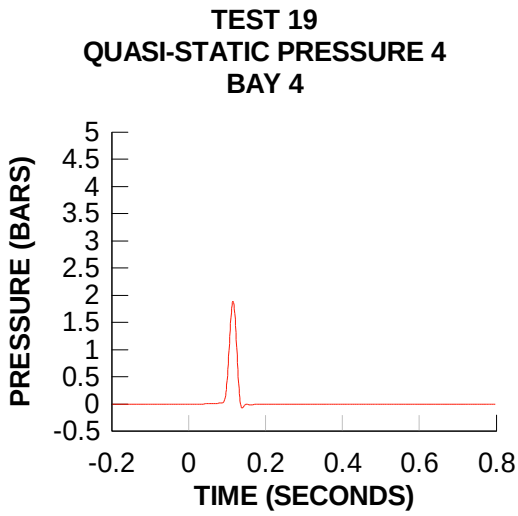
TEST 19
QUASI-STATIC PRESSURE 4
BAY 4
PRESSURE (BARS)
TIME (SECONDS)

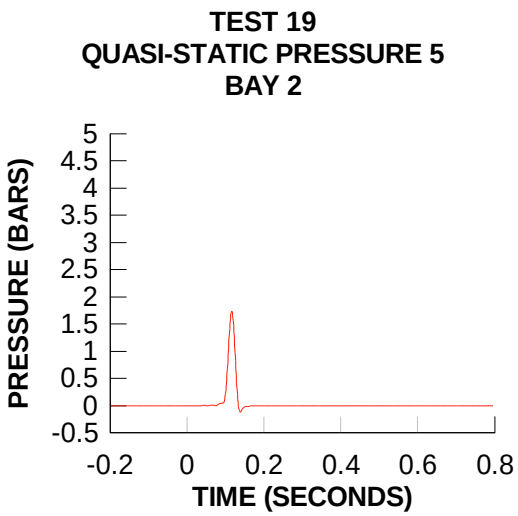
TEST 19
QUASI-STATIC PRESSURE 5
BAY 2
PRESSURE (BARS)
TIME (SECONDS)

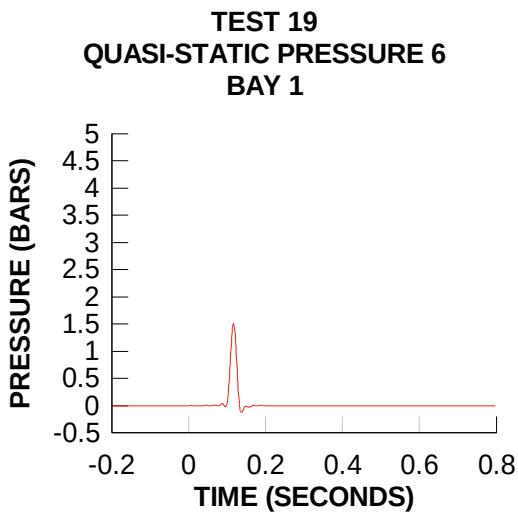
TEST 19
QUASI-STATIC PRESSURE 6
BAY 1
PRESSURE (BARS)
TIME (SECONDS)

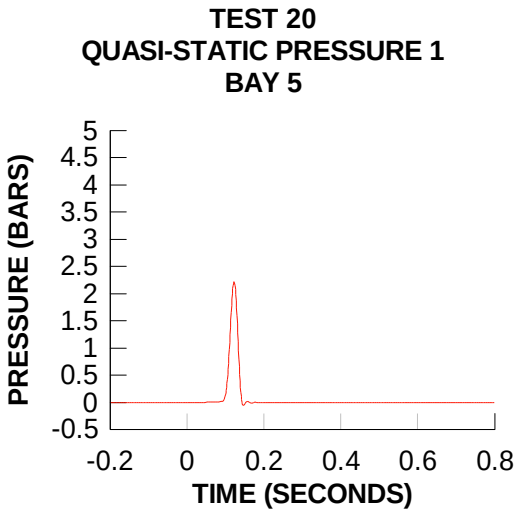
TEST 20
QUASI-STATIC PRESSURE 1
BAY 5
PRESSURE (BARS)
TIME (SECONDS)

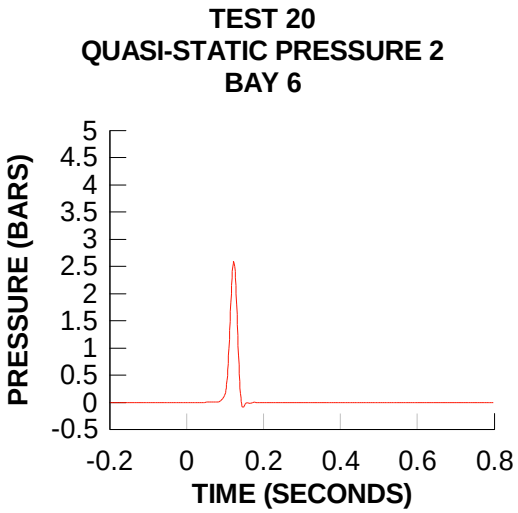
TEST 20
QUASI-STATIC PRESSURE 2
BAY 6
PRESSURE (BARS)
TIME (SECONDS)

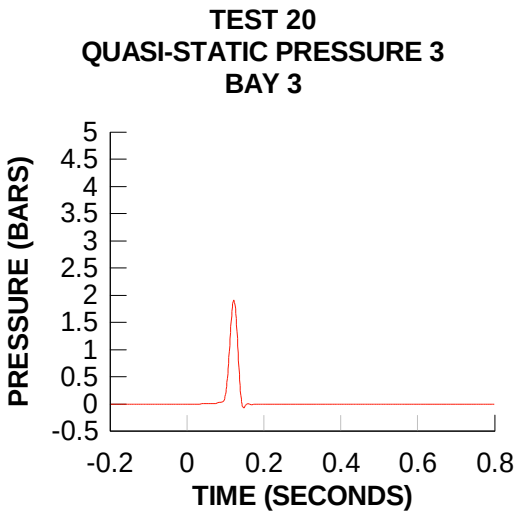
TEST 20
QUASI-STATIC PRESSURE 3
BAY 3
PRESSURE (BARS)
TIME (SECONDS)

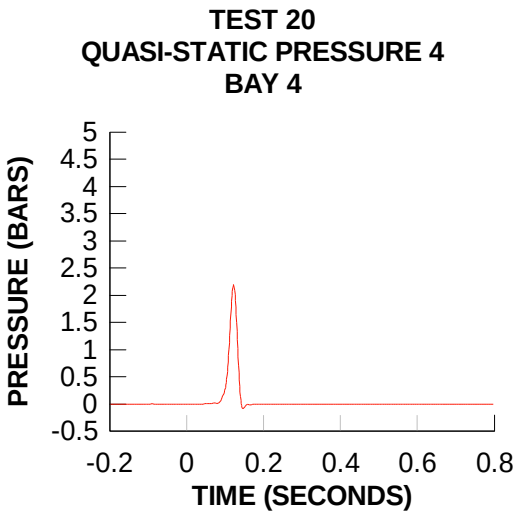
TEST 20
QUASI-STATIC PRESSURE 4
BAY 4
PRESSURE (BARS)
TIME (SECONDS)

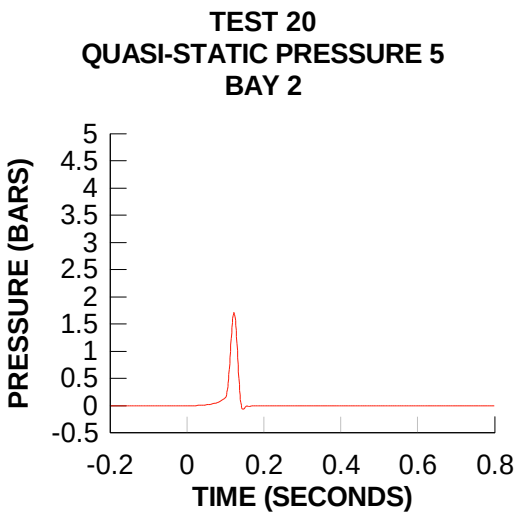
TEST 20
QUASI-STATIC PRESSURE 5
BAY 2
PRESSURE (BARS)
TIME (SECONDS)

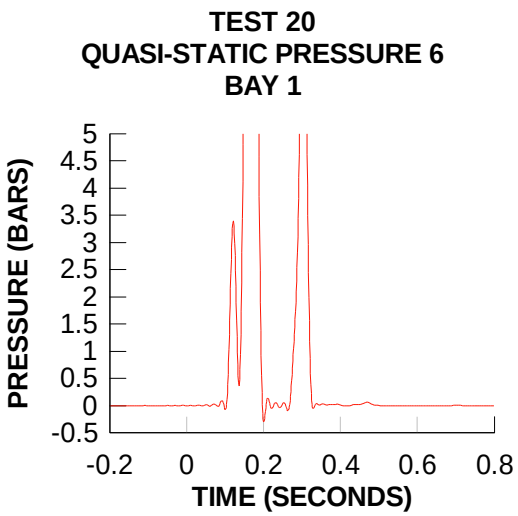
TEST 20
QUASI-STATIC PRESSURE 6
BAY 1
PRESSURE (BARS)
TIME (SECONDS)

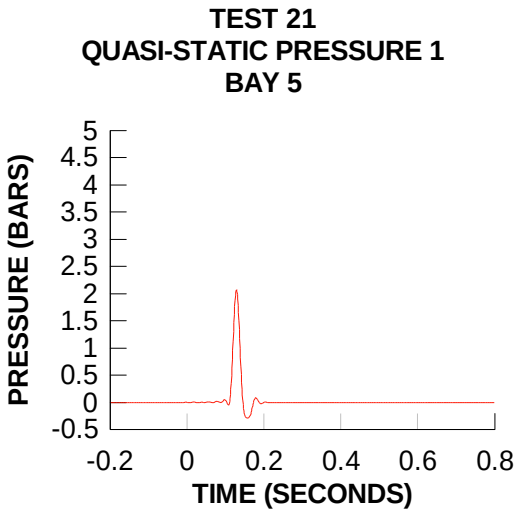
TEST 21
QUASI-STATIC PRESSURE 1
BAY 5
PRESSURE (BARS)
TIME (SECONDS)

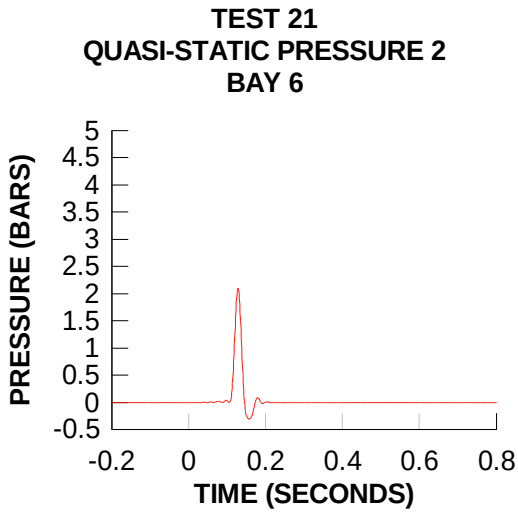
TEST 21
QUASI-STATIC PRESSURE 2
BAY 6
PRESSURE (BARS)
TIME (SECONDS)

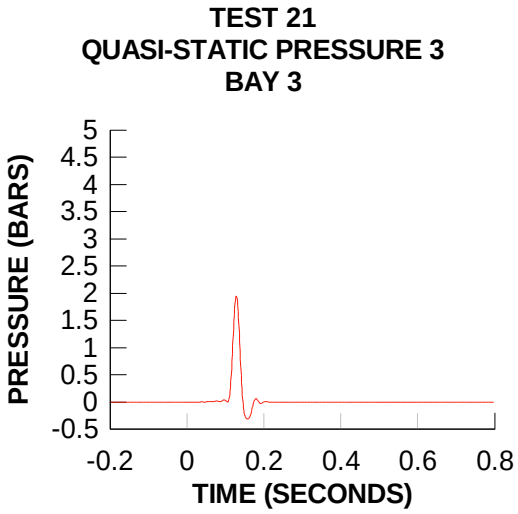
TEST 21
QUASI-STATIC PRESSURE 3
BAY 3
PRESSURE (BARS)
TIME (SECONDS)

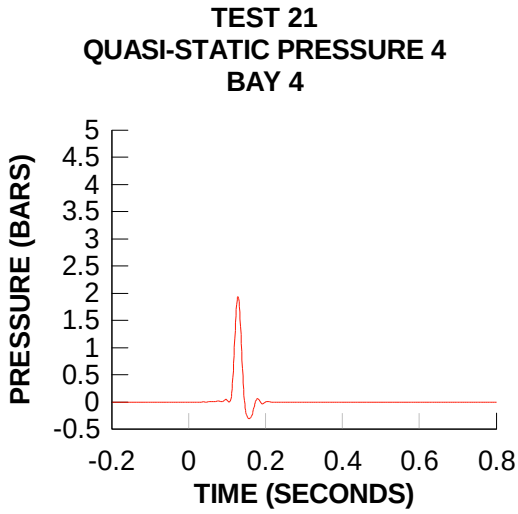
TEST 21
QUASI-STATIC PRESSURE 4
BAY 4
PRESSURE (BARS)
TIME (SECONDS)

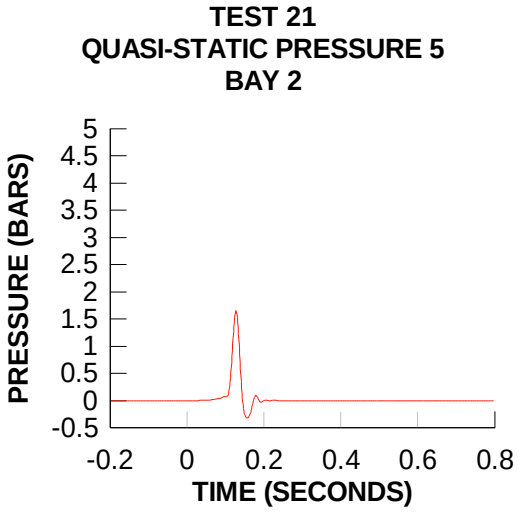
TEST 21
QUASI-STATIC PRESSURE 5
BAY 2
PRESSURE (BARS)
TIME (SECONDS)

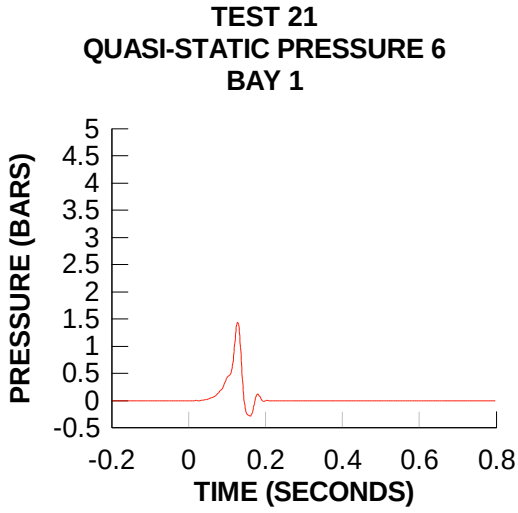
TEST 21
QUASI-STATIC PRESSURE 6
BAY 1
PRESSURE (BARS)
TIME (SECONDS)

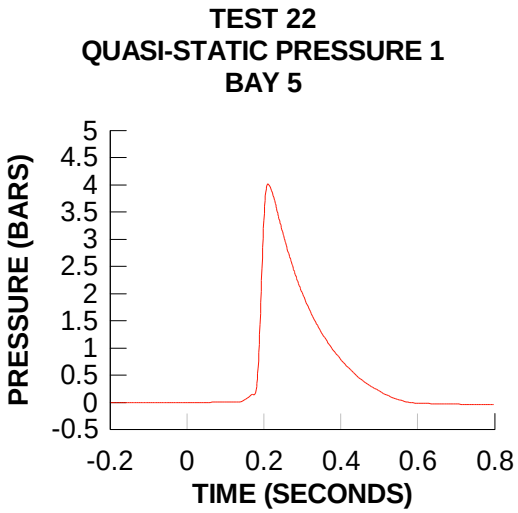
TEST 22
QUASI-STATIC PRESSURE 1
BAY 5
PRESSURE (BARS)
TIME (SECONDS)

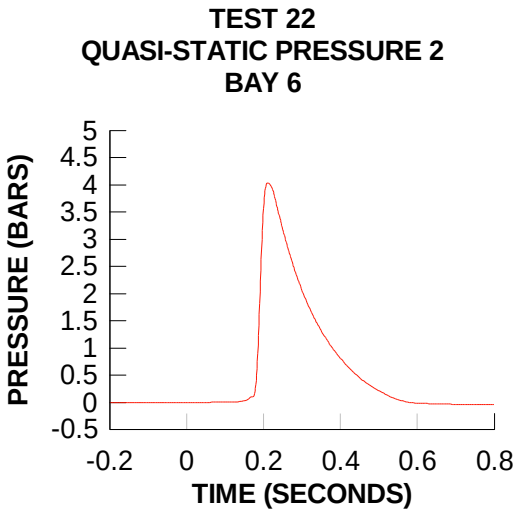
TEST 22
QUASI-STATIC PRESSURE 2
BAY 6
PRESSURE (BARS)
TIME (SECONDS)

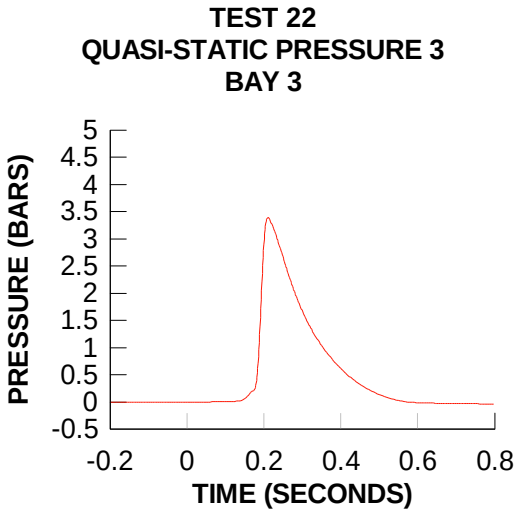
TEST 22
QUASI-STATIC PRESSURE 3
BAY 3
PRESSURE (BARS)
TIME (SECONDS)

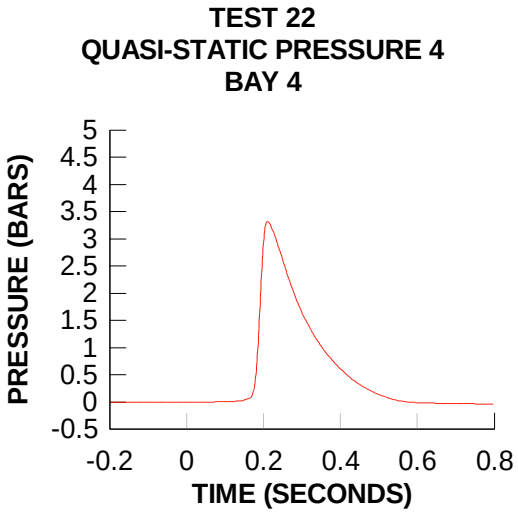
TEST 22
QUASI-STATIC PRESSURE 4
BAY 4
PRESSURE (BARS)
TIME (SECONDS)

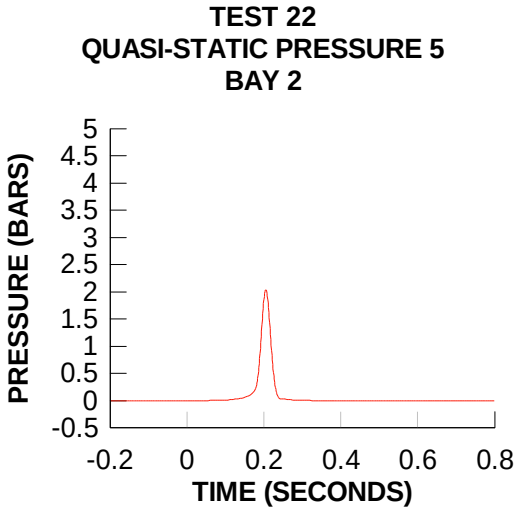
TEST 22
QUASI-STATIC PRESSURE 5
BAY 2
PRESSURE (BARS)
TIME (SECONDS)

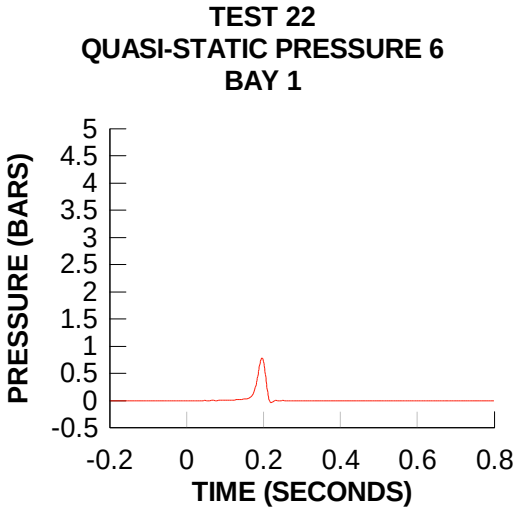
TEST 22
QUASI-STATIC PRESSURE 6
BAY 1
PRESSURE (BARS)
TIME (SECONDS)

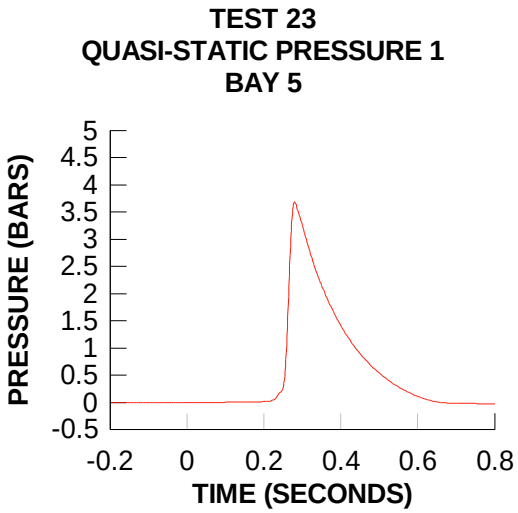
TEST 23
QUASI-STATIC PRESSURE 1
BAY 5
PRESSURE (BARS)
TIME (SECONDS)

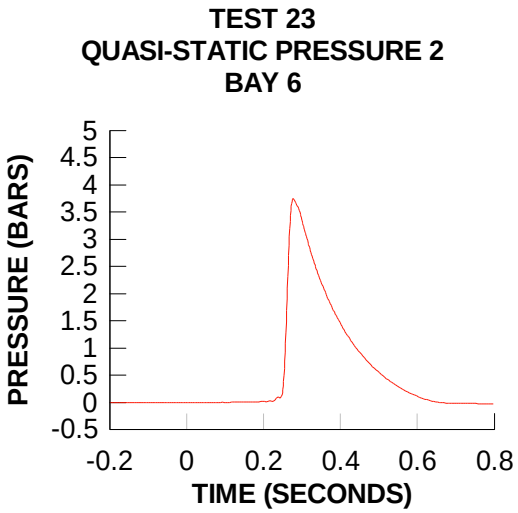
TEST 23
QUASI-STATIC PRESSURE 2
BAY 6
PRESSURE (BARS)
TIME (SECONDS)

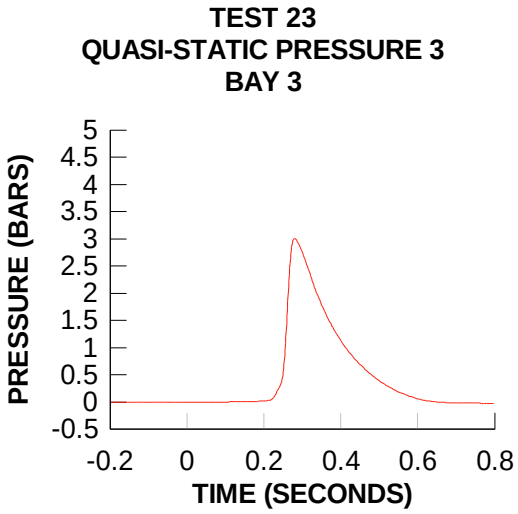
TEST 23
QUASI-STATIC PRESSURE 3
BAY 3
PRESSURE (BARS)
TIME (SECONDS)

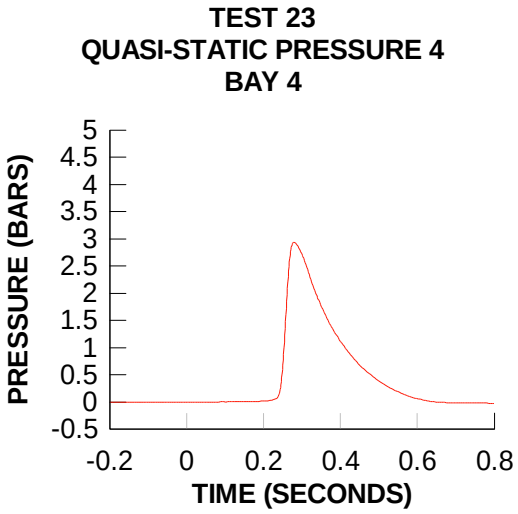
TEST 23
QUASI-STATIC PRESSURE 4
BAY 4
PRESSURE (BARS)
TIME (SECONDS)

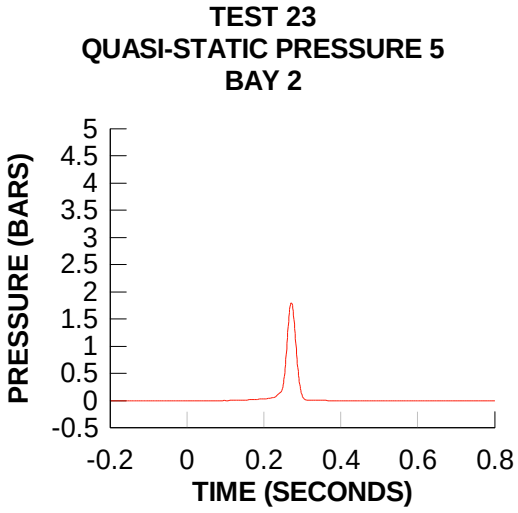
TEST 23
QUASI-STATIC PRESSURE 5
BAY 2
PRESSURE (BARS)
TIME (SECONDS)

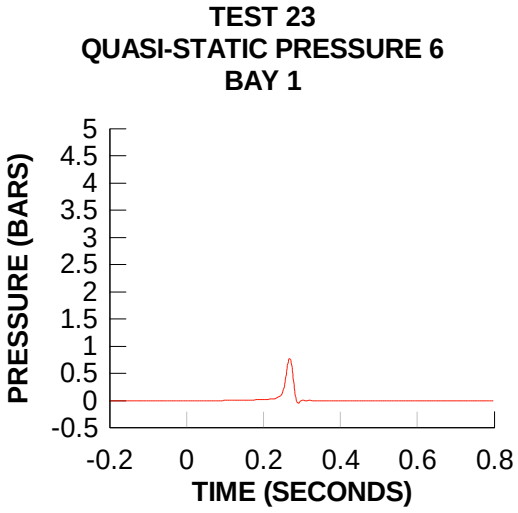
TEST 23
QUASI-STATIC PRESSURE 6
BAY 1
PRESSURE (BARS)
TIME (SECONDS)

TEST 24
QUASI-STATIC PRESSURE 1
BAY 5

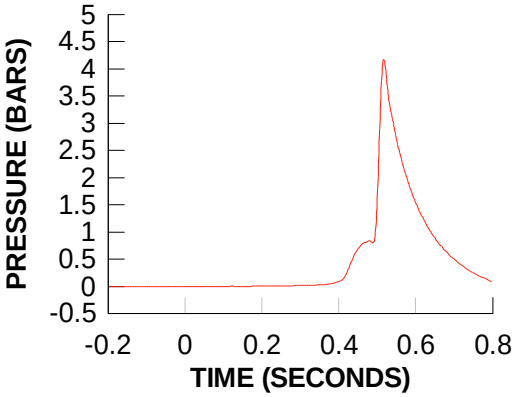

TEST 24
QUASI-STATIC PRESSURE 2
BAY 6

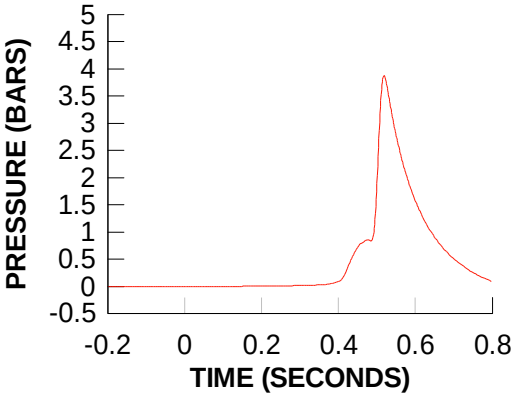

TEST 24
QUASI-STATIC PRESSURE 3
BAY 3

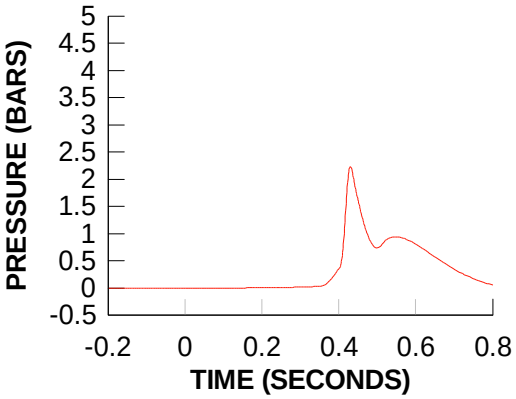

TEST 24
QUASI-STATIC PRESSURE 4
BAY 4

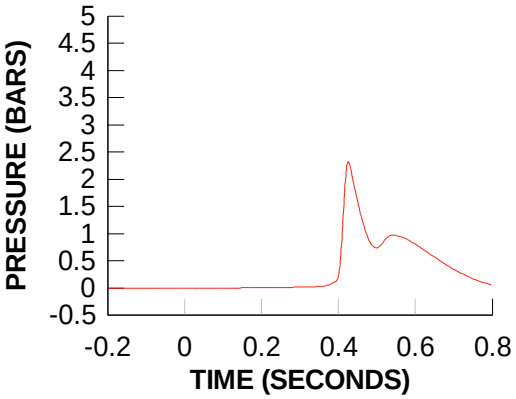

TEST 24
QUASI-STATIC PRESSURE 5
BAY 2

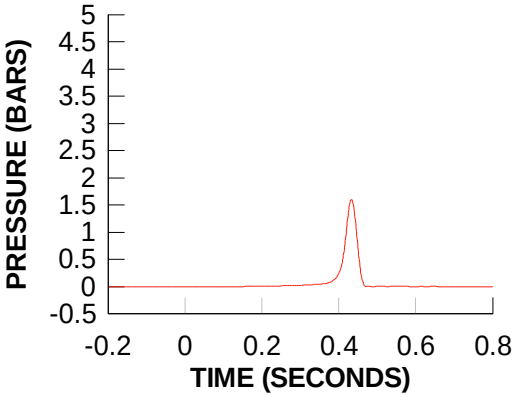

TEST 24
QUASI-STATIC PRESSURE 6
BAY 1

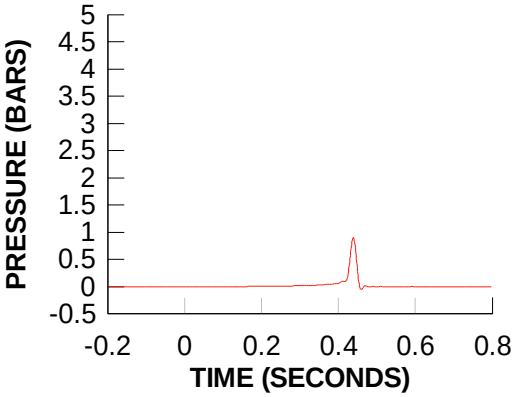

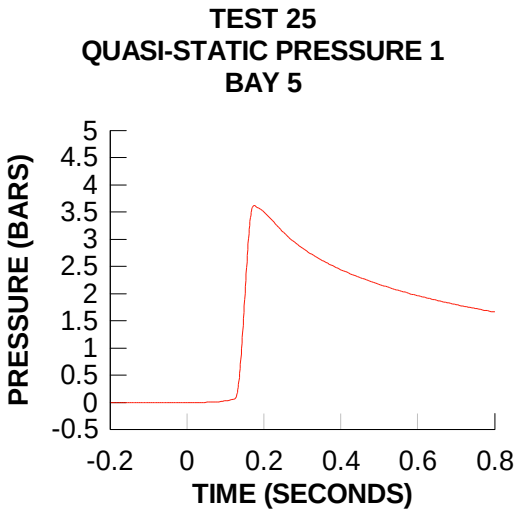
TEST 25
QUASI-STATIC PRESSURE 1
BAY 5
PRESSURE (BARS)
TIME (SECONDS)

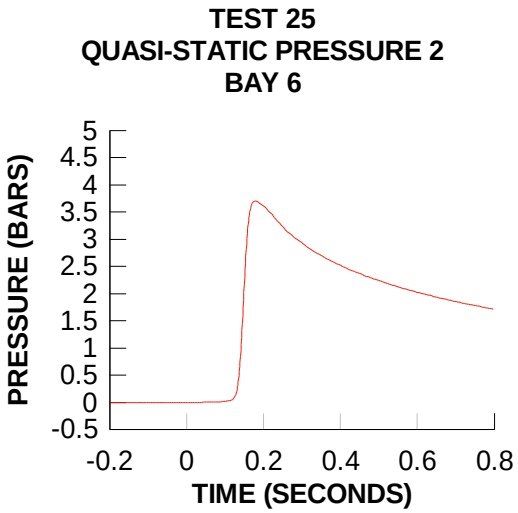
TEST 25
QUASI-STATIC PRESSURE 2
BAY 6
PRESSURE (BARS)
TIME (SECONDS)

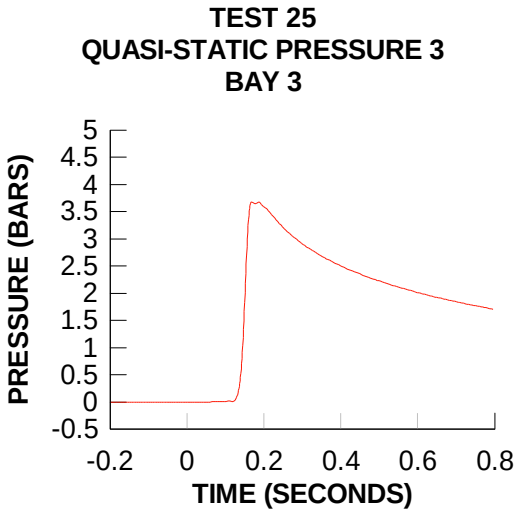
TEST 25
QUASI-STATIC PRESSURE 3
BAY 3
PRESSURE (BARS)
TIME (SECONDS)

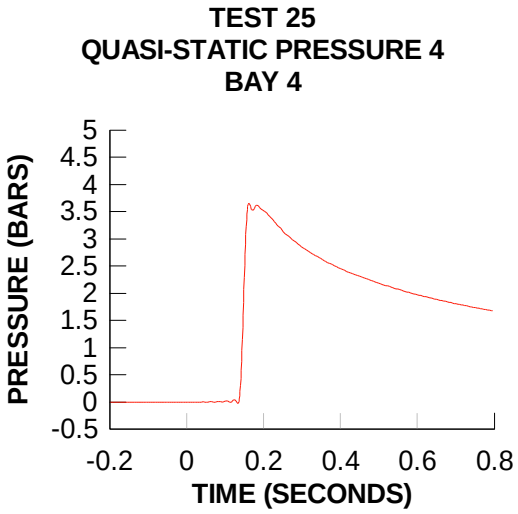
TEST 25
QUASI-STATIC PRESSURE 4
BAY 4
PRESSURE (BARS)
TIME (SECONDS)

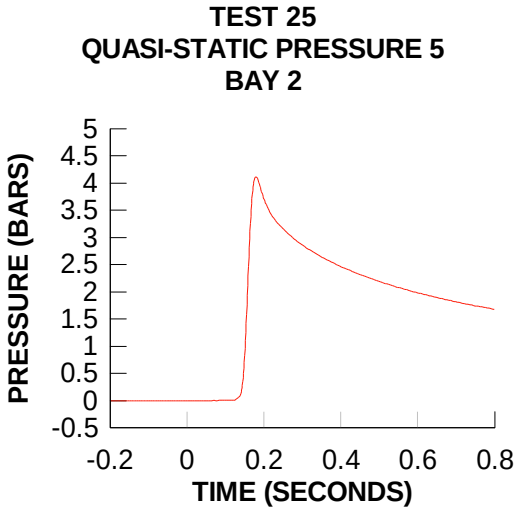
TEST 25
QUASI-STATIC PRESSURE 5
BAY 2
PRESSURE (BARS)
TIME (SECONDS)

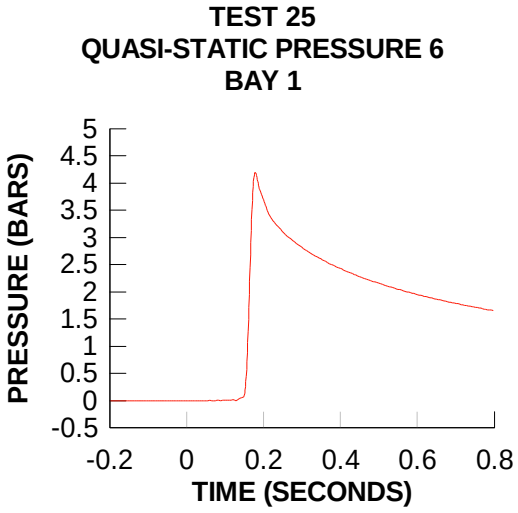
TEST 25
QUASI-STATIC PRESSURE 6
BAY 1
PRESSURE (BARS)
TIME (SECONDS)

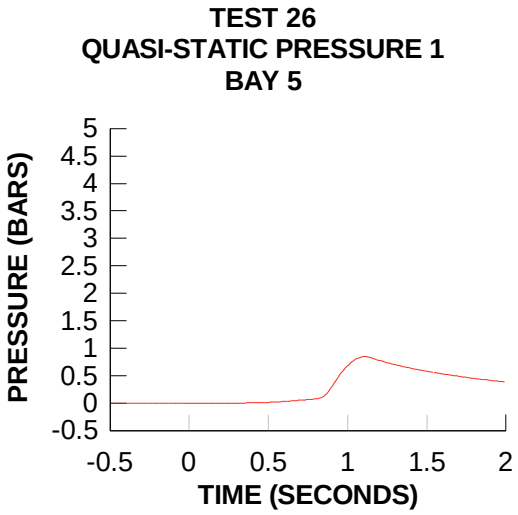
TEST 26
QUASI-STATIC PRESSURE 1
BAY 5
PRESSURE (BARS)
TIME (SECONDS)

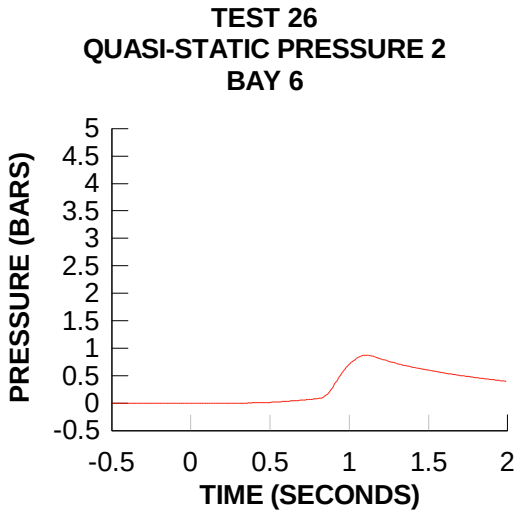
TEST 26
QUASI-STATIC PRESSURE 2
BAY 6
PRESSURE (BARS)
TIME (SECONDS)

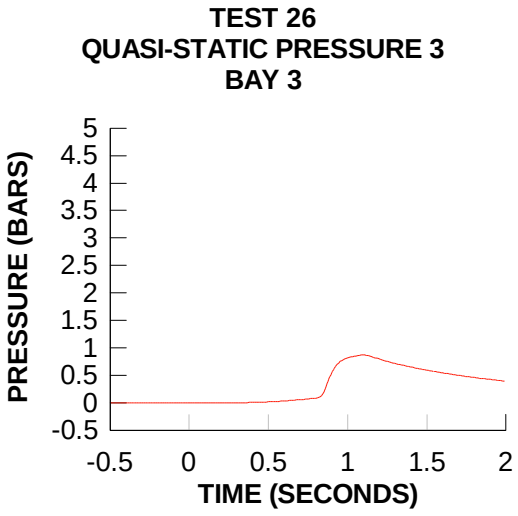
TEST 26
QUASI-STATIC PRESSURE 3
BAY 3
PRESSURE (BARS)
TIME (SECONDS)

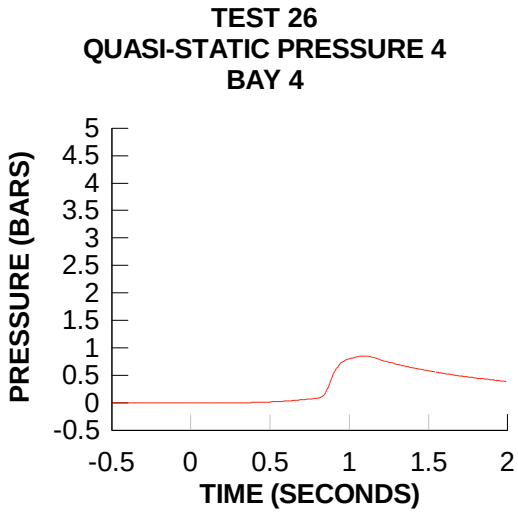
TEST 26
QUASI-STATIC PRESSURE 4
BAY 4
PRESSURE (BARS)
TIME (SECONDS)

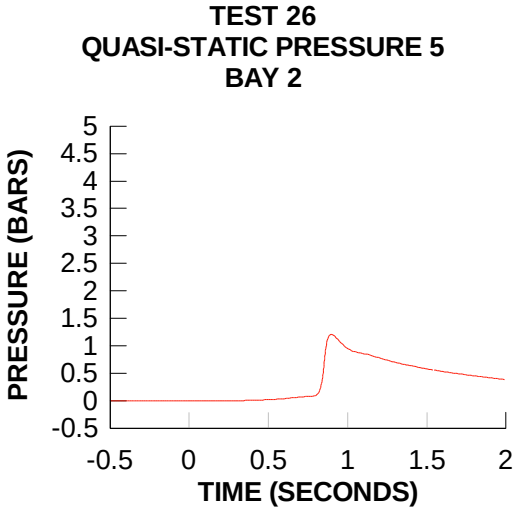
TEST 26
QUASI-STATIC PRESSURE 5
BAY 2
PRESSURE (BARS)
TIME (SECONDS)

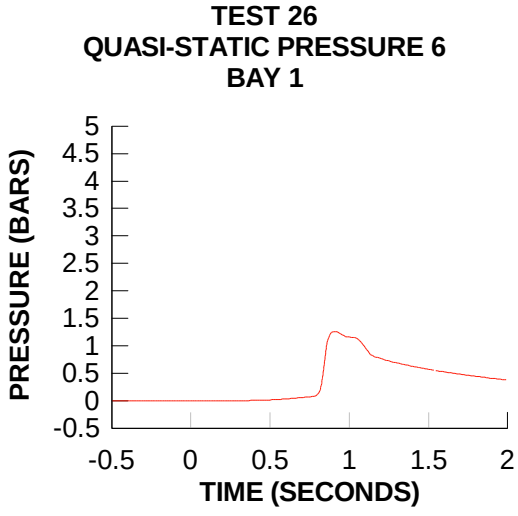
TEST 26
QUASI-STATIC PRESSURE 6
BAY 1
PRESSURE (BARS)
TIME (SECONDS)

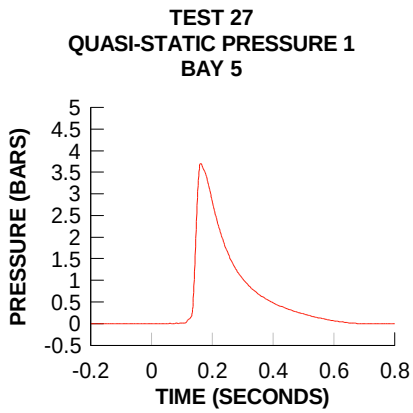
TEST 27
QUASI-STATIC PRESSURE 1
BAY 5
PRESSURE (BARS)
TIME (SECONDS)

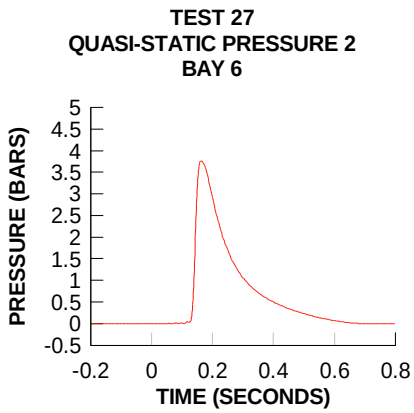
TEST 27
QUASI-STATIC PRESSURE 2
BAY 6
PRESSURE (BARS)
TIME (SECONDS)

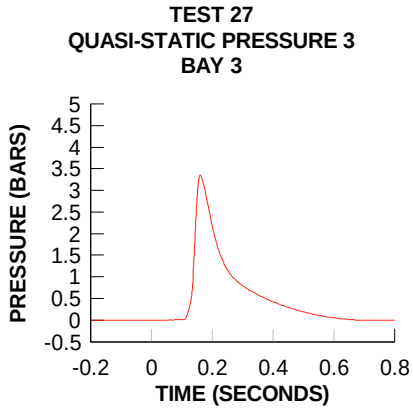
TEST 27
QUASI-STATIC PRESSURE 3
BAY 3
PRESSURE (BARS)
TIME (SECONDS)

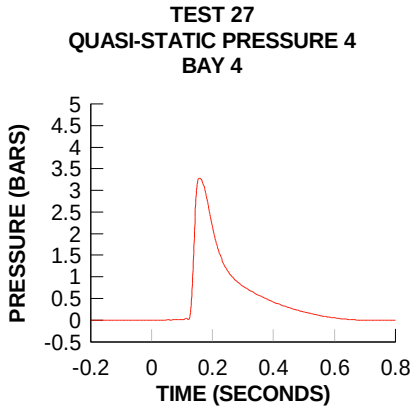
TEST 27
QUASI-STATIC PRESSURE 4
BAY 4
PRESSURE (BARS)
TIME (SECONDS)

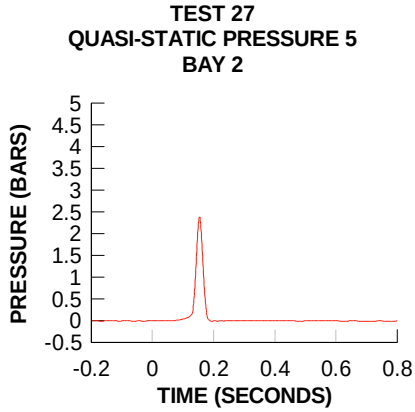
TEST 27
QUASI-STATIC PRESSURE 5
BAY 2
PRESSURE (BARS)
TIME (SECONDS)

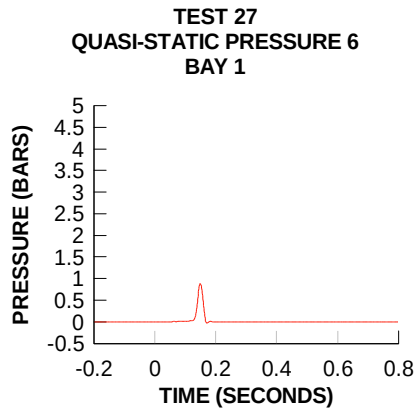
TEST 27
QUASI-STATIC PRESSURE 6
BAY 1
PRESSURE (BARS)
TIME (SECONDS)

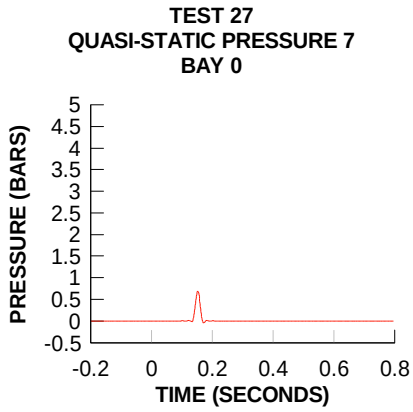
TEST 27
QUASI-STATIC PRESSURE 7
BAY 0
PRESSURE (BARS)
TIME (SECONDS)

TEST 28
QUASI-STATIC PRESSURE 1
BAY 5

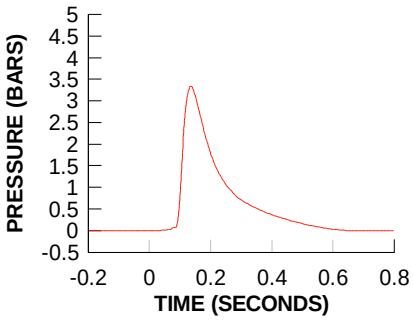

TEST 28
QUASI-STATIC PRESSURE 2
BAY 6

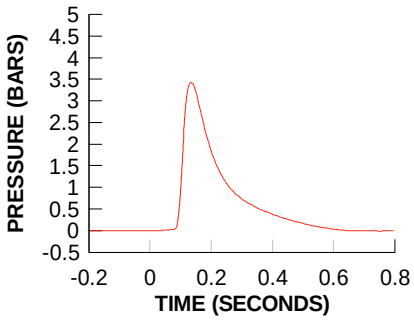

TEST 28
QUASI-STATIC PRESSURE 3
BAY 3

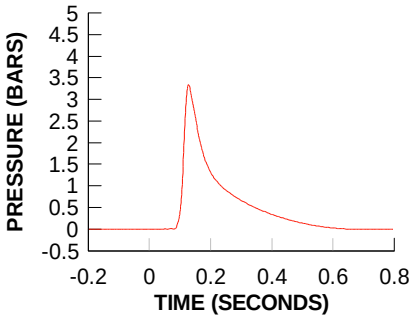

TEST 28
QUASI-STATIC PRESSURE 4
BAY 4

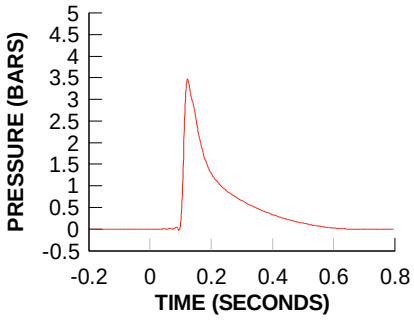

TEST 28
QUASI-STATIC PRESSURE 5
BAY 2

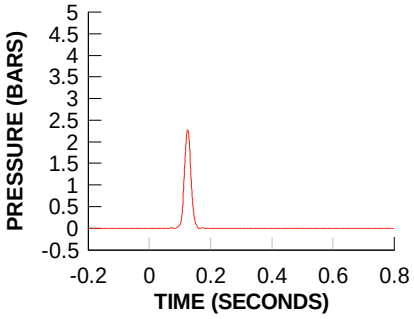

TEST 28
QUASI-STATIC PRESSURE 6
BAY 1

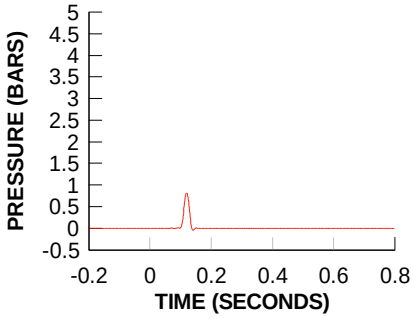

TEST 28
QUASI-STATIC PRESSURE 7
BAY 0

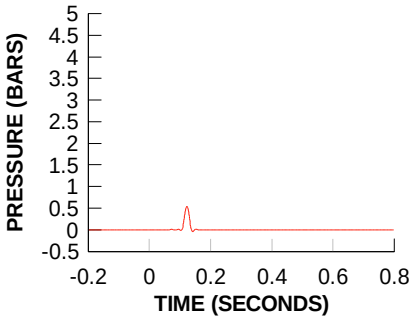

TEST 29
QUASI-STATIC PRESSURE 1
BAY 5

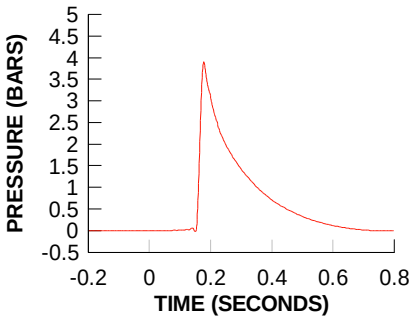

TEST 29
QUASI-STATIC PRESSURE 2
BAY 6

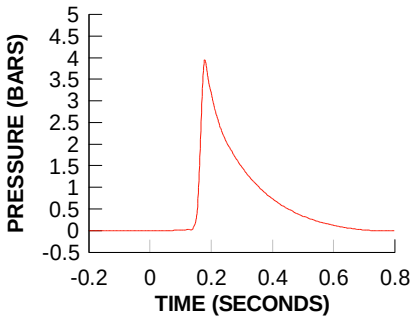

TEST 29
QUASI-STATIC PRESSURE 3
BAY 3

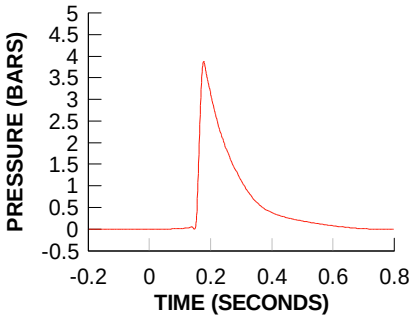

TEST 29
QUASI-STATIC PRESSURE 4
BAY 4

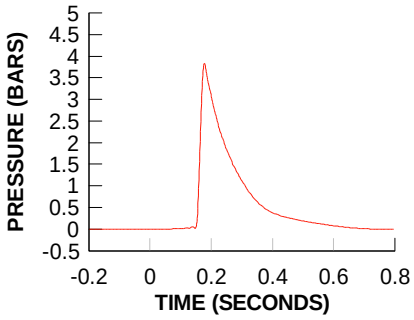

TEST 29
QUASI-STATIC PRESSURE 5
BAY 2

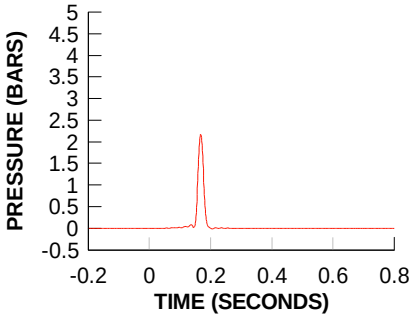

TEST 29
QUASI-STATIC PRESSURE 6
BAY 1

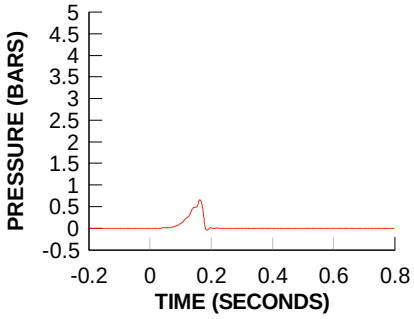

TEST 29
QUASI-STATIC PRESSURE 7
BAY 0

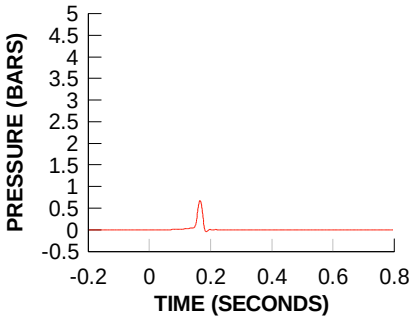

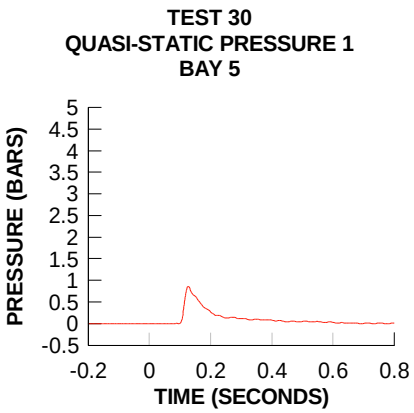
TEST 30
QUASI-STATIC PRESSURE 1
BAY 5
PRESSURE (BARS)
TIME (SECONDS)

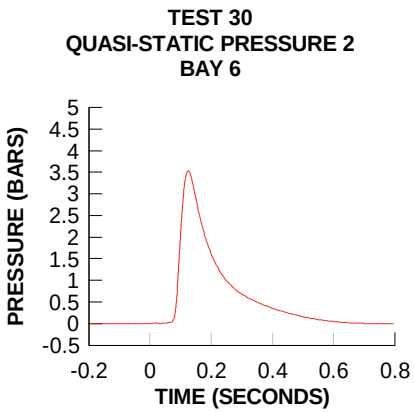
TEST 30
QUASI-STATIC PRESSURE 2
BAY 6
PRESSURE (BARS)
TIME (SECONDS)

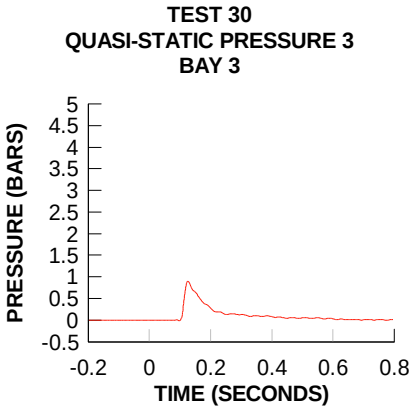
TEST 30
QUASI-STATIC PRESSURE 3
BAY 3
PRESSURE (BARS)
TIME (SECONDS)

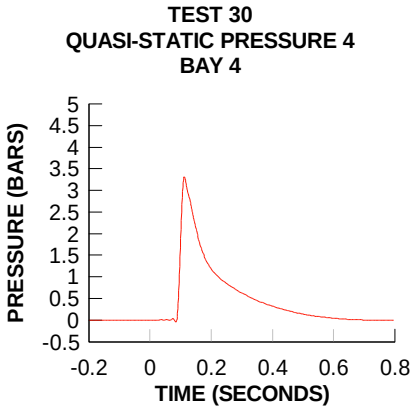
TEST 30
QUASI-STATIC PRESSURE 4
BAY 4
PRESSURE (BARS)
TIME (SECONDS)

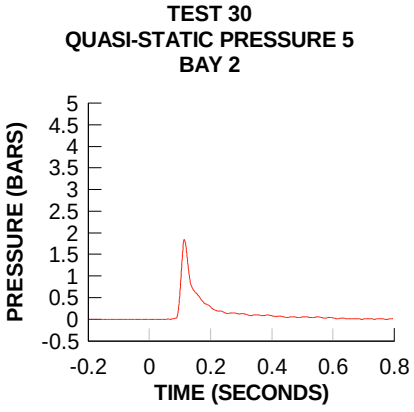
TEST 30
QUASI-STATIC PRESSURE 5
BAY 2
PRESSURE (BARS)
TIME (SECONDS)

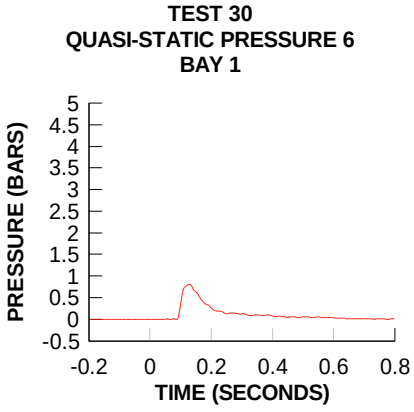
TEST 30
QUASI-STATIC PRESSURE 6
BAY 1
PRESSURE (BARS)
TIME (SECONDS)

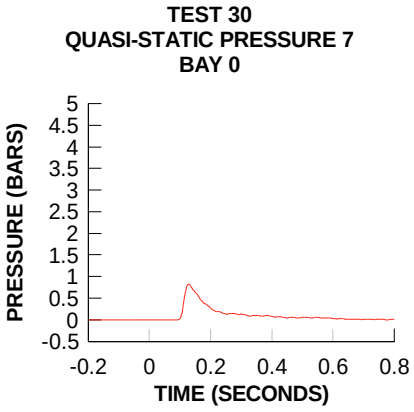
TEST 30
QUASI-STATIC PRESSURE 7
BAY 0
PRESSURE (BARS)
TIME (SECONDS)

D.5 PCB (Dynamic) Pressure

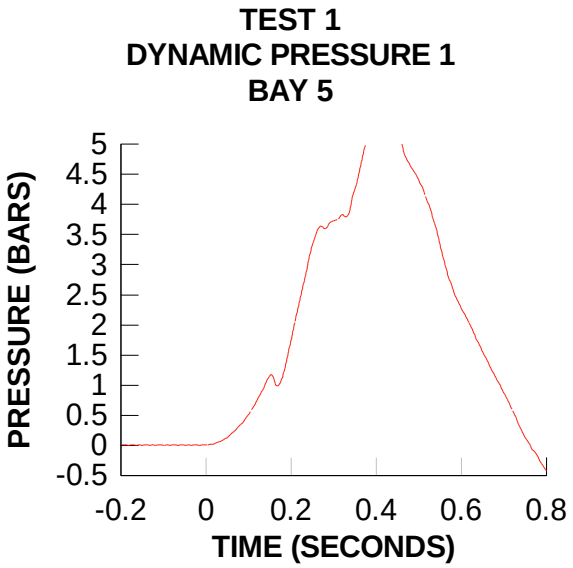
TEST 1
DYNAMIC PRESSURE 1
BAY 5
PRESSURE (BARS)
TIME (SECONDS)
5
4.5
4
3.5
3
2.5
2
1.5
1
0.5
0
-0.5
-0.2
0
0.2
0.4
0.6
0.8

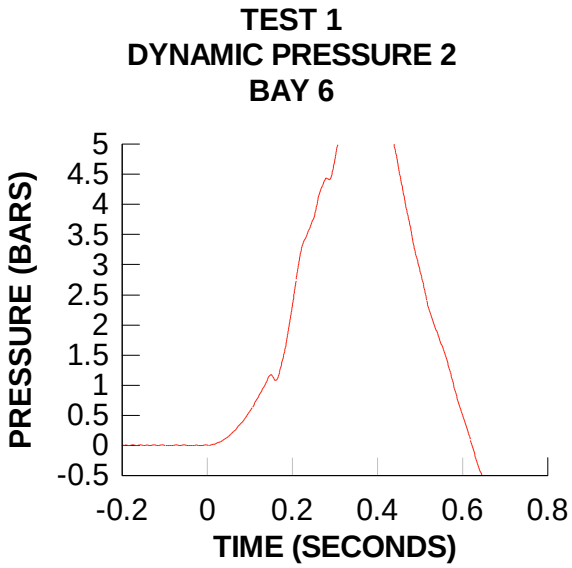
TEST 1
DYNAMIC PRESSURE 2
BAY 6
PRESSURE (BARS)
TIME (SECONDS)
5
4.5
4
3.5
3
2.5
2
1.5
1
0.5
0
-0.5
-0.2
0
0.2
0.4
0.6
0.8

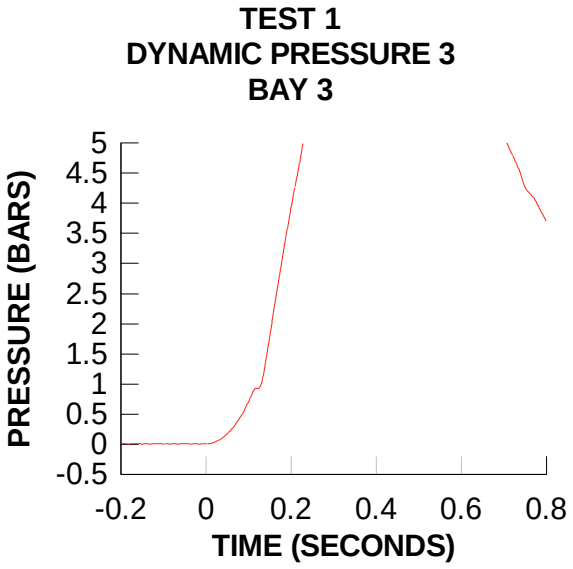
TEST 1
DYNAMIC PRESSURE 3
BAY 3
PRESSURE (BARS)
TIME (SECONDS)
5
4.5
4
3.5
3
2.5
2
1.5
1
0.5
0
-0.5
-0.2
0
0.2
0.4
0.6
0.8

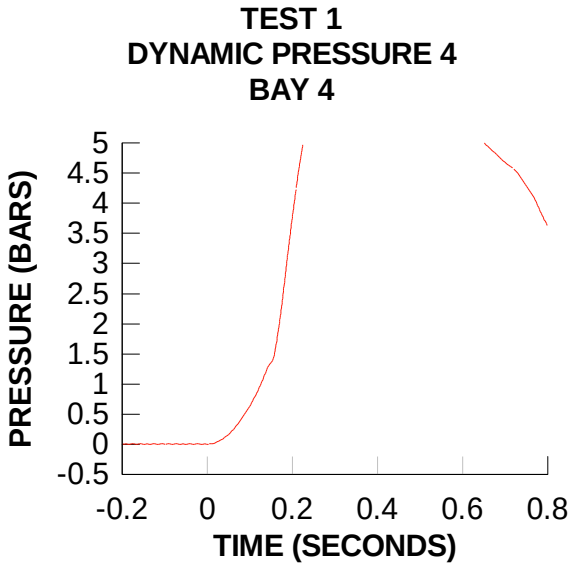
TEST 1
DYNAMIC PRESSURE 4
BAY 4
PRESSURE (BARS)
TIME (SECONDS)
5
4.5
4
3.5
3
2.5
2
1.5
1
0.5
0
-0.5
-0.2
0
0.2
0.4
0.6
0.8

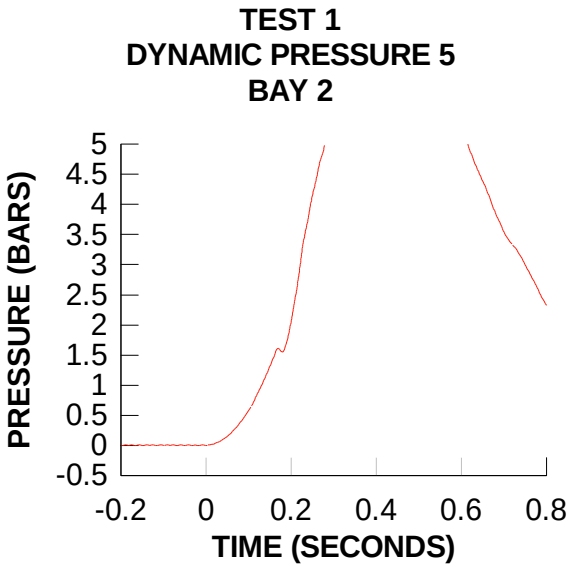
TEST 1
DYNAMIC PRESSURE 5
BAY 2
PRESSURE (BARS)
TIME (SECONDS)
5
4.5
4
3.5
3
2.5
2
1.5
1
0.5
0
-0.5
-0.2
0
0.2
0.4
0.6
0.8

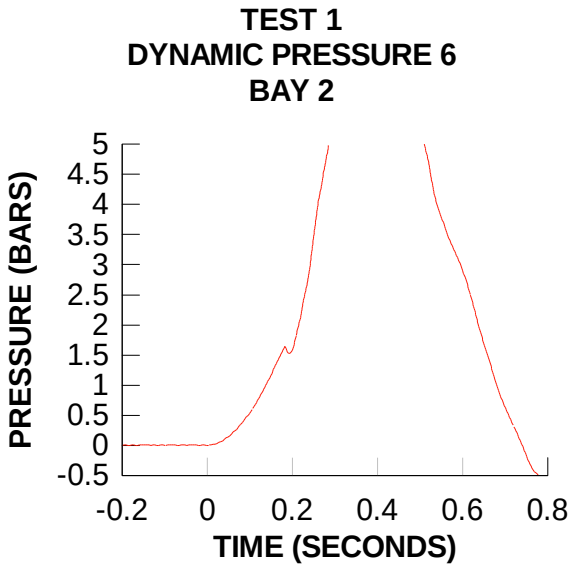
TEST 1
DYNAMIC PRESSURE 6
BAY 2
PRESSURE (BARS)
TIME (SECONDS)
5
4.5
4
3.5
3
2.5
2
1.5
1
0.5
0
-0.5
-0.2
0
0.2
0.4
0.6
0.8

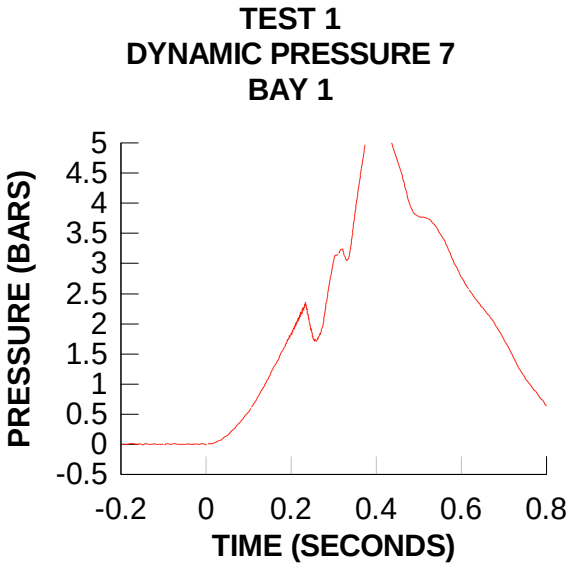
TEST 1
DYNAMIC PRESSURE 7
BAY 1
PRESSURE (BARS)
TIME (SECONDS)
5
4.5
4
3.5
3
2.5
2
1.5
1
0.5
0
-0.5
-0.2
0
0.2
0.4
0.6
0.8

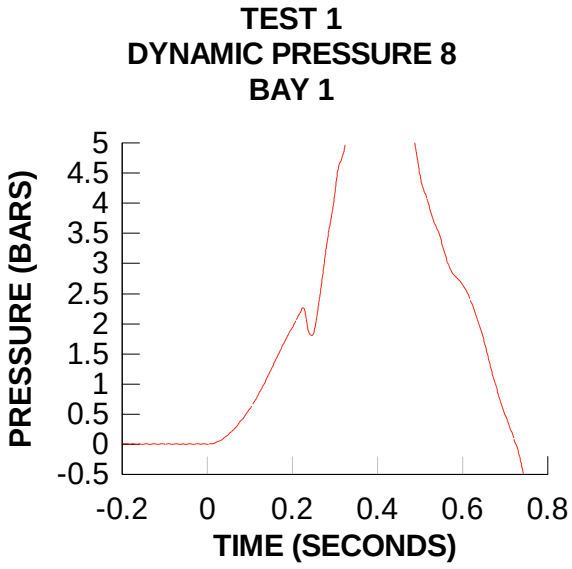
TEST 1
DYNAMIC PRESSURE 8
BAY 1
PRESSURE (BARS)
TIME (SECONDS)
5
4.5
4
3.5
3
2.5
2
1.5
1
0.5
0
-0.5
-0.2
0
0.2
0.4
0.6
0.8

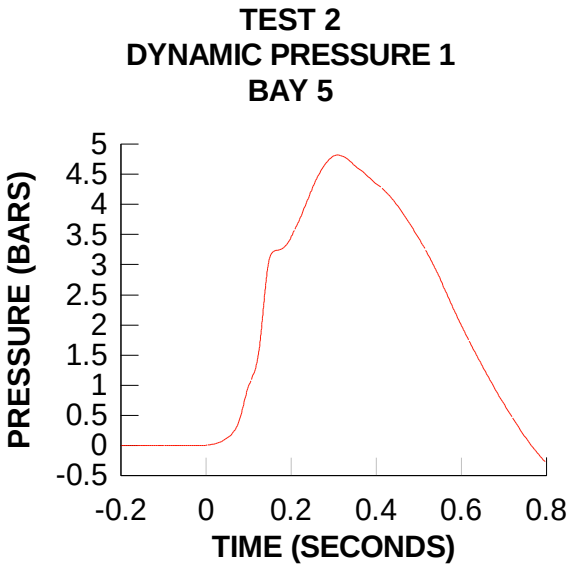
TEST 2
DYNAMIC PRESSURE 1
BAY 5
PRESSURE (BARS)
5
4.5
4
3.5
3
2.5
2
1.5
1
0.5
0
-0.5
-0.2
0
0.2
0.4
0.6
0.8
TIME (SECONDS)

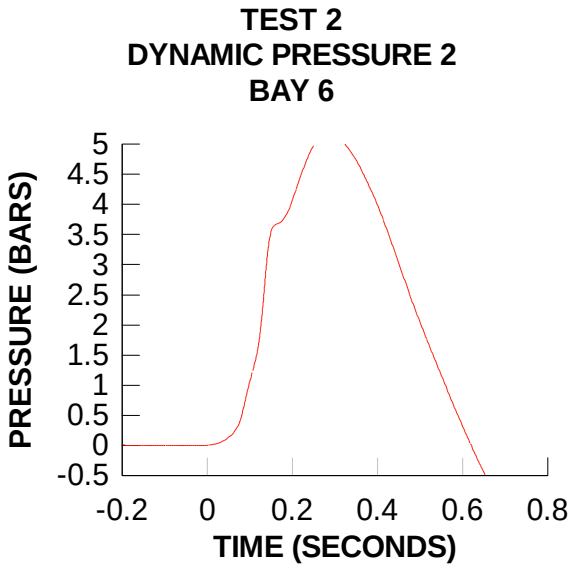
TEST 2
DYNAMIC PRESSURE 2
BAY 6
PRESSURE (BARS)
5
4.5
4
3.5
3
2.5
2
1.5
1
0.5
0
-0.5
-0.2
0
0.2
0.4
0.6
0.8
TIME (SECONDS)

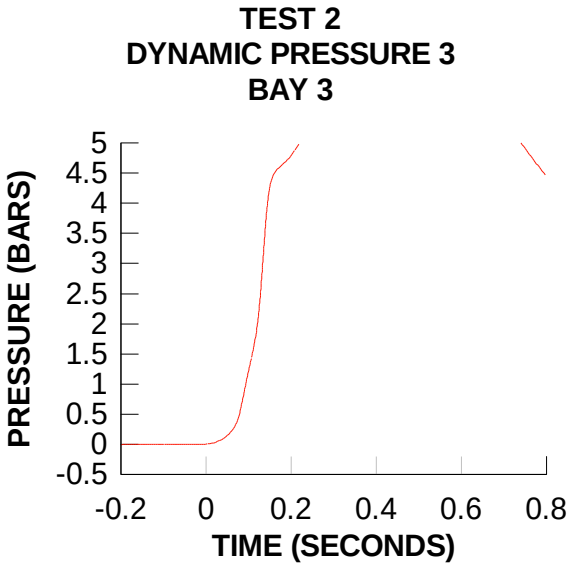
TEST 2
DYNAMIC PRESSURE 3
BAY 3
PRESSURE (BARS)
5
4.5
4
3.5
3
2.5
2
1.5
1
0.5
0
-0.5
-0.2
0
0.2
0.4
0.6
0.8
TIME (SECONDS)

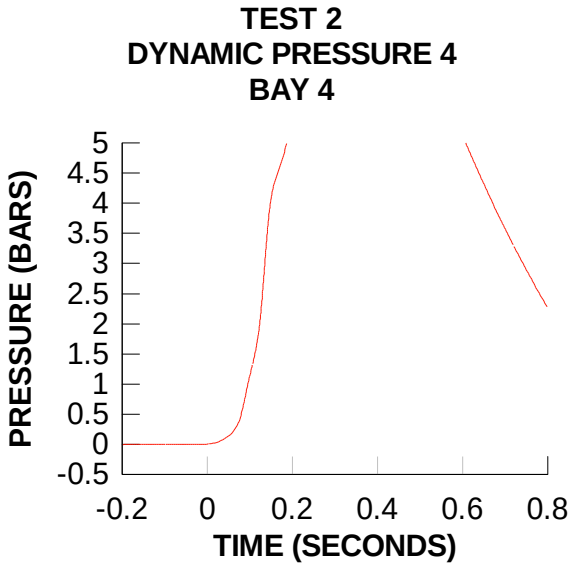
TEST 2
DYNAMIC PRESSURE 4
BAY 4
PRESSURE (BARS)
5
4.5
4
3.5
3
2.5
2
1.5
1
0.5
0
-0.5
-0.2
0
0.2
0.4
0.6
0.8
TIME (SECONDS)

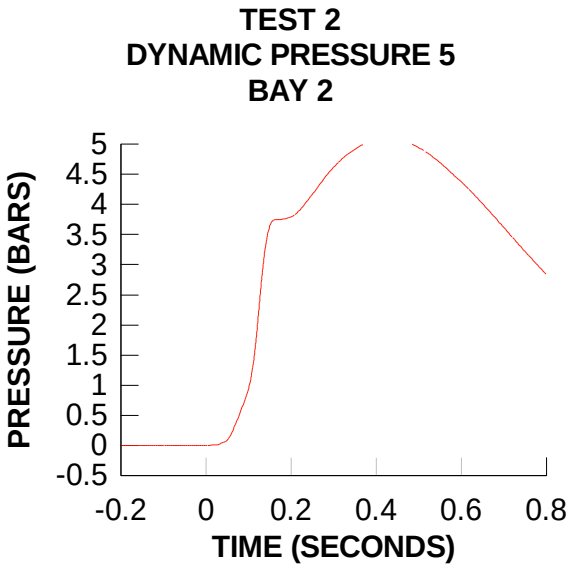
TEST 2
DYNAMIC PRESSURE 5
BAY 2
PRESSURE (BARS)
5
4.5
4
3.5
3
2.5
2
1.5
1
0.5
0
-0.5
-0.2
0
0.2
0.4
0.6
0.8
TIME (SECONDS)

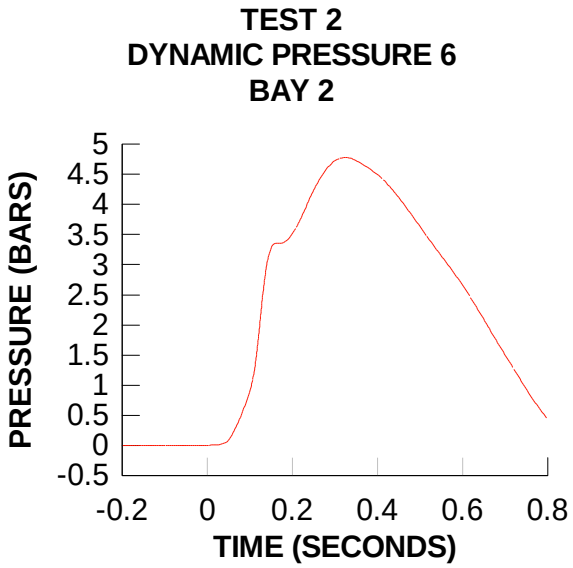
TEST 2
DYNAMIC PRESSURE 6
BAY 2
PRESSURE (BARS)
5
4.5
4
3.5
3
2.5
2
1.5
1
0.5
0
-0.5
-0.2
0
0.2
0.4
0.6
0.8
TIME (SECONDS)

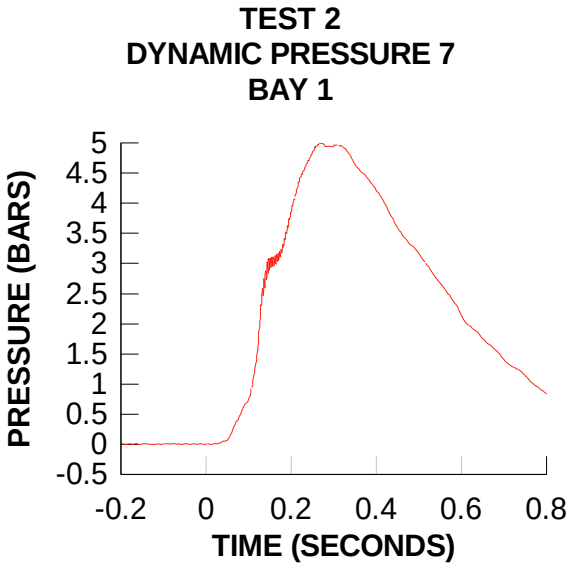
TEST 2
DYNAMIC PRESSURE 7
BAY 1
PRESSURE (BARS)
5
4.5
4
3.5
3
2.5
2
1.5
1
0.5
0
-0.5
-0.2
0
0.2
0.4
0.6
0.8
TIME (SECONDS)

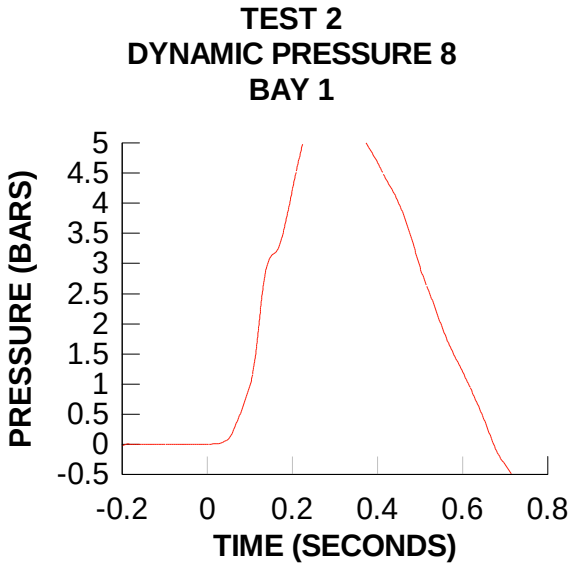
TEST 2
DYNAMIC PRESSURE 8
BAY 1
PRESSURE (BARS)
5
4.5
4
3.5
3
2.5
2
1.5
1
0.5
0
-0.5
-0.2
0
0.2
0.4
0.6
0.8
TIME (SECONDS)

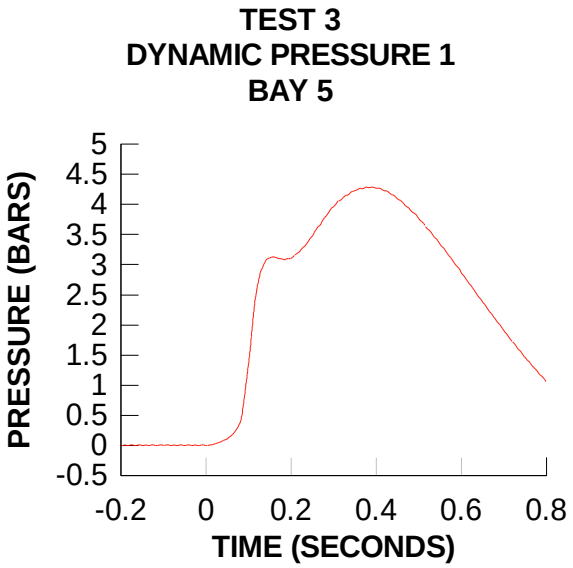
TEST 3
DYNAMIC PRESSURE 1
BAY 5
PRESSURE (BARS)
5
4.5
4
3.5
3
2.5
2
1.5
1
0.5
0
-0.5
-0.2
0
0.2
0.4
0.6
0.8
TIME (SECONDS)

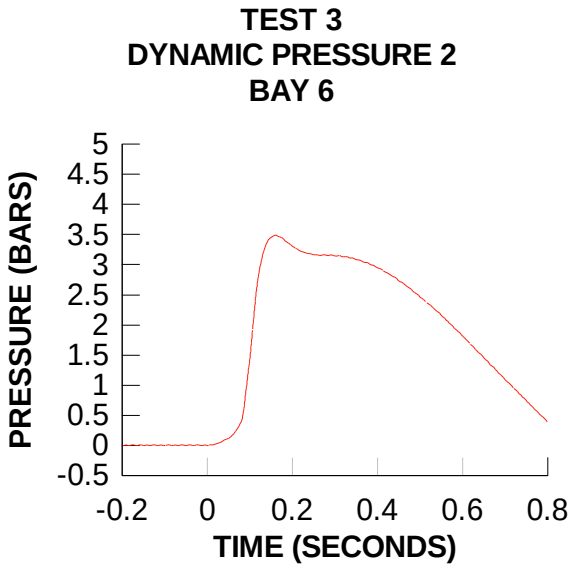
TEST 3
DYNAMIC PRESSURE 2
BAY 6
PRESSURE (BARS)
5
4.5
4
3.5
3
2.5
2
1.5
1
0.5
0
-0.5
-0.2
0
0.2
0.4
0.6
0.8
TIME (SECONDS)

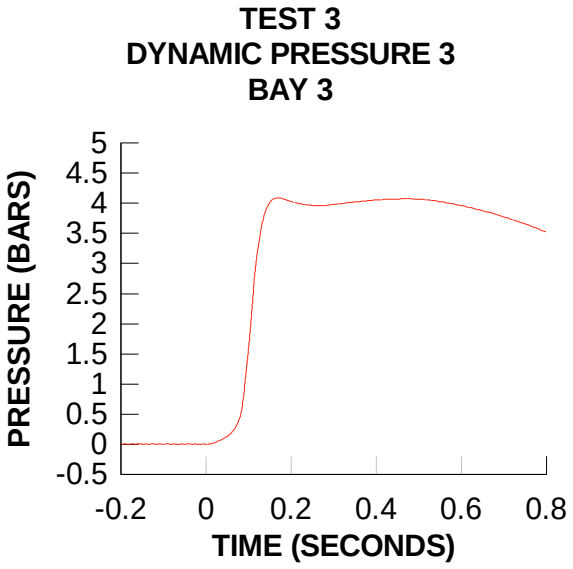
TEST 3
DYNAMIC PRESSURE 3
BAY 3
PRESSURE (BARS)
5
4.5
4
3.5
3
2.5
2
1.5
1
0.5
0
-0.5
-0.2
0
0.2
0.4
0.6
0.8
TIME (SECONDS)

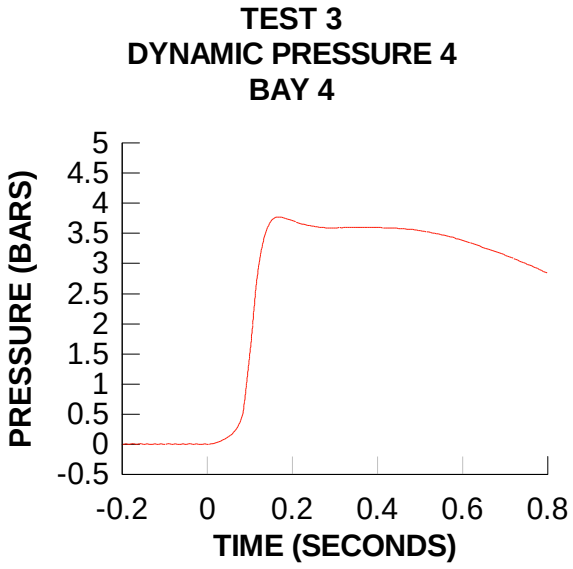
TEST 3
DYNAMIC PRESSURE 4
BAY 4
PRESSURE (BARS)
5
4.5
4
3.5
3
2.5
2
1.5
1
0.5
0
-0.5
-0.2
0
0.2
0.4
0.6
0.8
TIME (SECONDS)

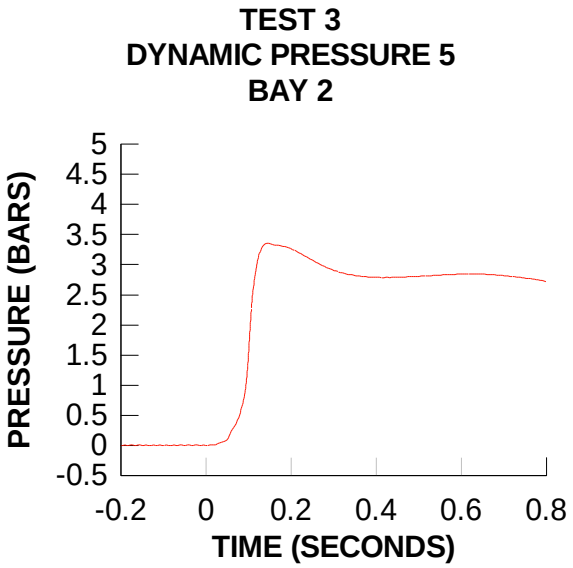
TEST 3
DYNAMIC PRESSURE 5
BAY 2
PRESSURE (BARS)
5
4.5
4
3.5
3
2.5
2
1.5
1
0.5
0
-0.5
-0.2
0
0.2
0.4
0.6
0.8
TIME (SECONDS)

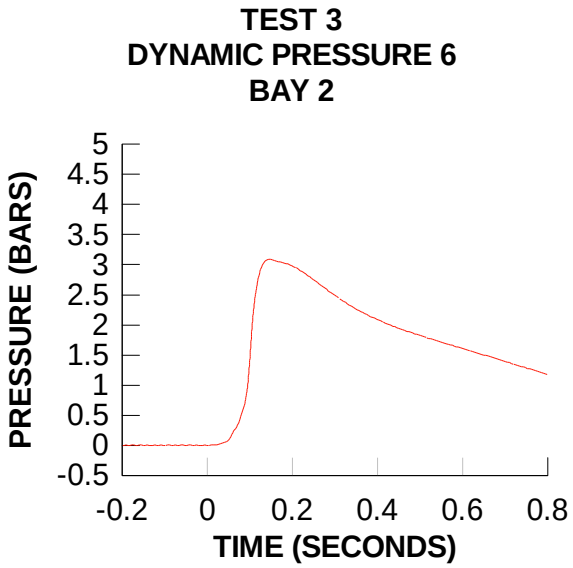
TEST 3
DYNAMIC PRESSURE 6
BAY 2
PRESSURE (BARS)
5
4.5
4
3.5
3
2.5
2
1.5
1
0.5
0
-0.5
-0.2
0
0.2
0.4
0.6
0.8
TIME (SECONDS)

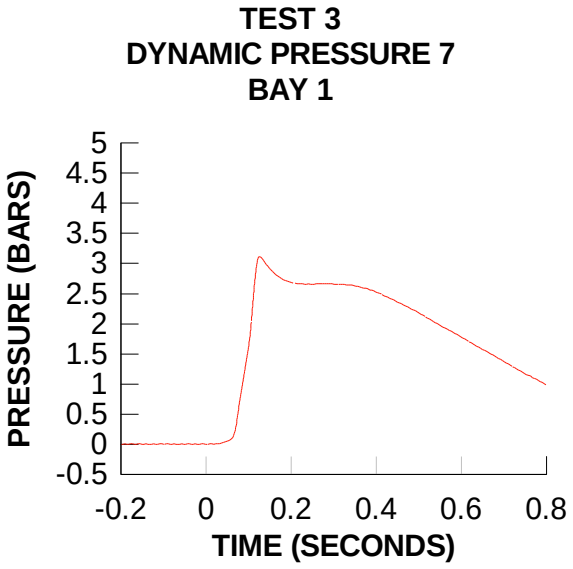
TEST 3
DYNAMIC PRESSURE 7
BAY 1
PRESSURE (BARS)
5
4.5
4
3.5
3
2.5
2
1.5
1
0.5
0
-0.5
-0.2
0
0.2
0.4
0.6
0.8
TIME (SECONDS)

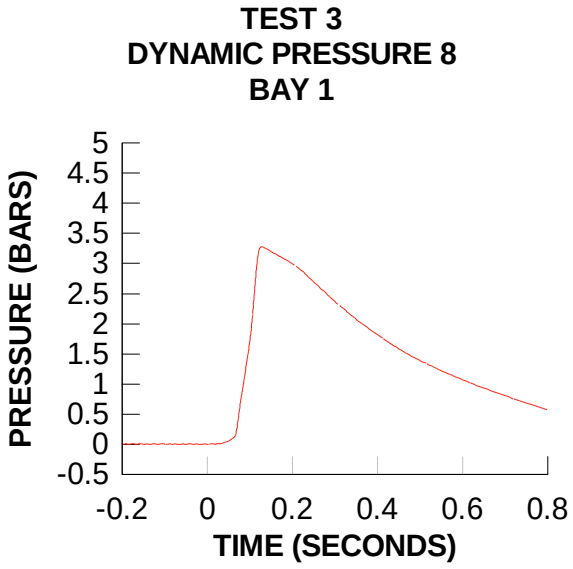
TEST 3
DYNAMIC PRESSURE 8
BAY 1
PRESSURE (BARS)
5
4.5
4
3.5
3
2.5
2
1.5
1
0.5
0
-0.5
-0.2
0
0.2
0.4
0.6
0.8
TIME (SECONDS)

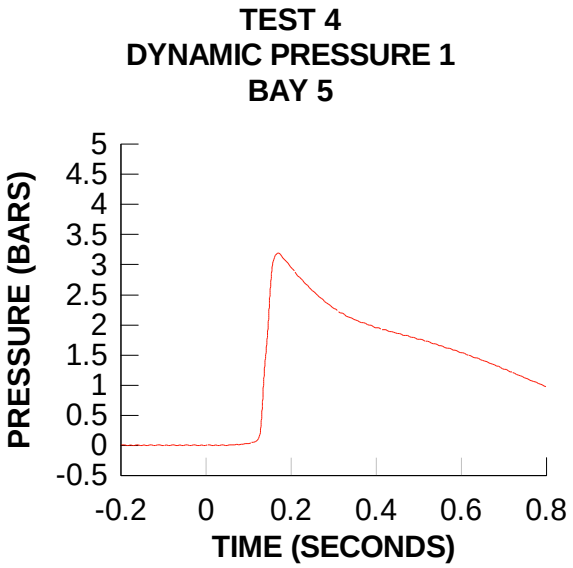
TEST 4
DYNAMIC PRESSURE 1
BAY 5
PRESSURE (BARS)
5
4.5
4
3.5
3
2.5
2
1.5
1
0.5
0
-0.5
-0.2
0
0.2
0.4
0.6
0.8
TIME (SECONDS)

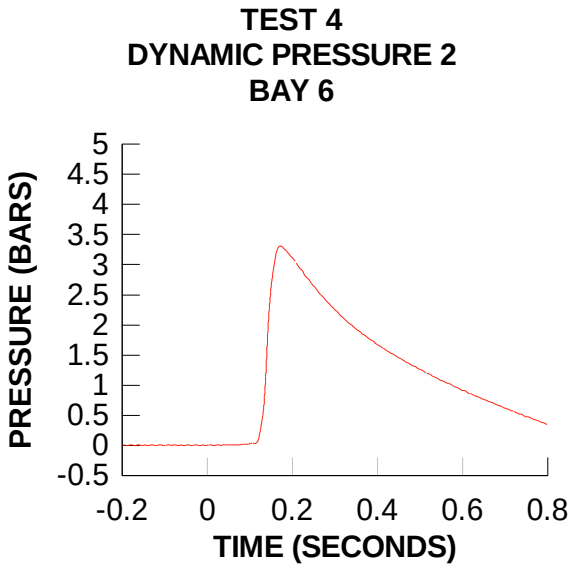
TEST 4
DYNAMIC PRESSURE 2
BAY 6
PRESSURE (BARS)
5
4.5
4
3.5
3
2.5
2
1.5
1
0.5
0
-0.5
-0.2
0
0.2
0.4
0.6
0.8
TIME (SECONDS)

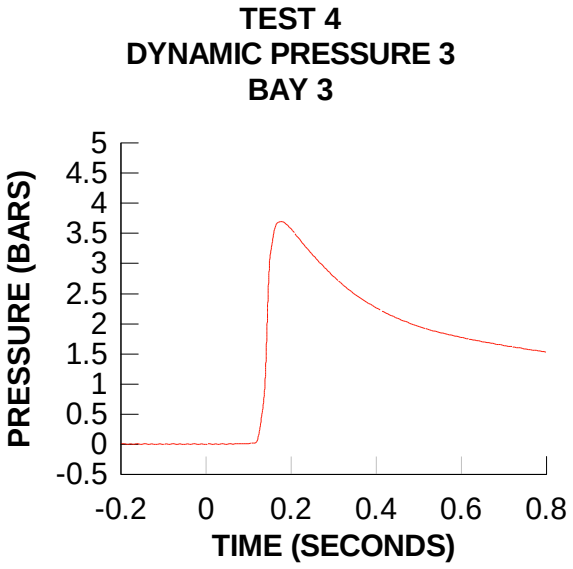
TEST 4
DYNAMIC PRESSURE 3
BAY 3
PRESSURE (BARS)
5
4.5
4
3.5
3
2.5
2
1.5
1
0.5
0
-0.5
-0.2
0
0.2
0.4
0.6
0.8
TIME (SECONDS)

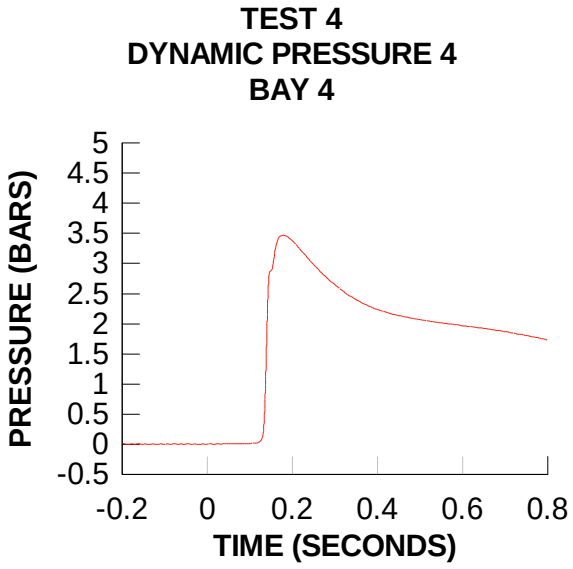
TEST 4
DYNAMIC PRESSURE 4
BAY 4
PRESSURE (BARS)
5
4.5
4
3.5
3
2.5
2
1.5
1
0.5
0
-0.5
-0.2
0
0.2
0.4
0.6
0.8
TIME (SECONDS)

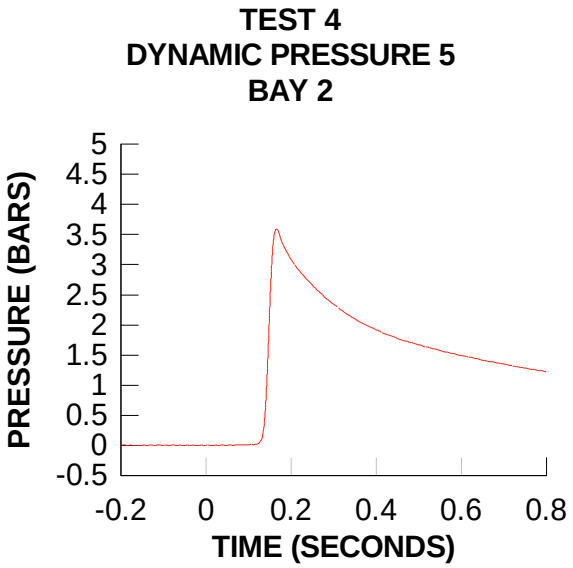
TEST 4
DYNAMIC PRESSURE 5
BAY 2
PRESSURE (BARS)
5
4.5
4
3.5
3
2.5
2
1.5
1
0.5
0
-0.5
-0.2
0
0.2
0.4
0.6
0.8
TIME (SECONDS)

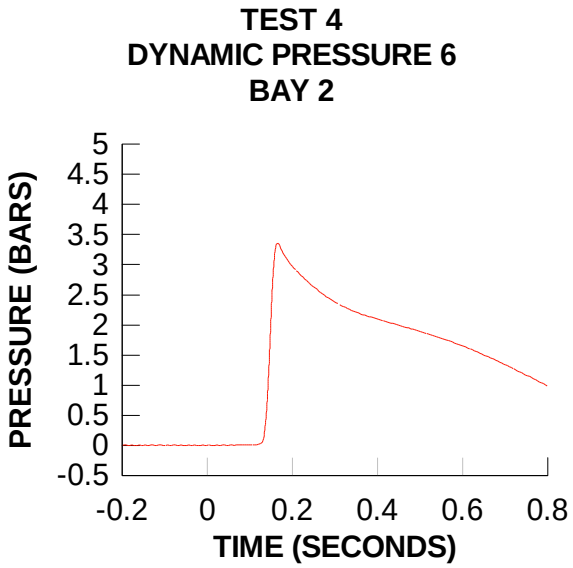
TEST 4
DYNAMIC PRESSURE 6
BAY 2
PRESSURE (BARS)
5
4.5
4
3.5
3
2.5
2
1.5
1
0.5
0
-0.5
-0.2
0
0.2
0.4
0.6
0.8
TIME (SECONDS)

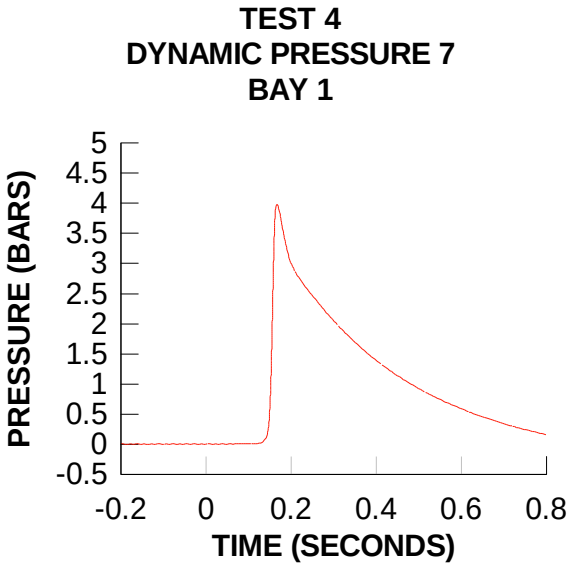
TEST 4
DYNAMIC PRESSURE 7
BAY 1
PRESSURE (BARS)
5
4.5
4
3.5
3
2.5
2
1.5
1
0.5
0
-0.5
-0.2
0
0.2
0.4
0.6
0.8
TIME (SECONDS)

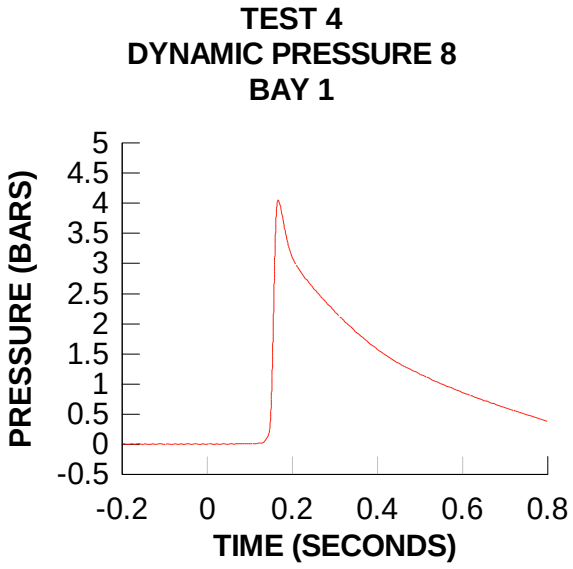
TEST 4
DYNAMIC PRESSURE 8
BAY 1
PRESSURE (BARS)
5
4.5
4
3.5
3
2.5
2
1.5
1
0.5
0
-0.5
-0.2
0
0.2
0.4
0.6
0.8
TIME (SECONDS)

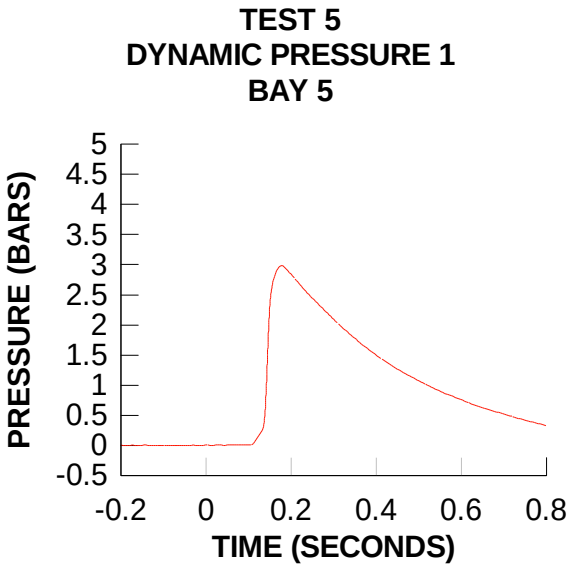
TEST 5
DYNAMIC PRESSURE 1
BAY 5
PRESSURE (BARS)
5
4.5
4
3.5
3
2.5
2
1.5
1
0.5
0
-0.5
-0.2
0
0.2
0.4
0.6
0.8
TIME (SECONDS)

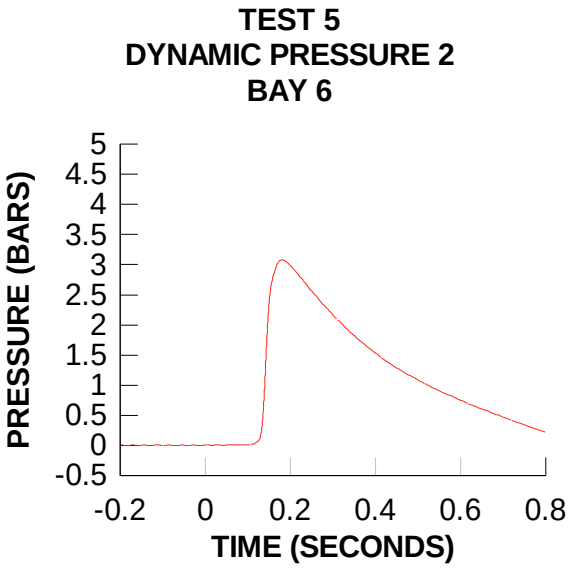
TEST 5
DYNAMIC PRESSURE 2
BAY 6
PRESSURE (BARS)
5
4.5
4
3.5
3
2.5
2
1.5
1
0.5
0
-0.5
-0.2
0
0.2
0.4
0.6
0.8
TIME (SECONDS)

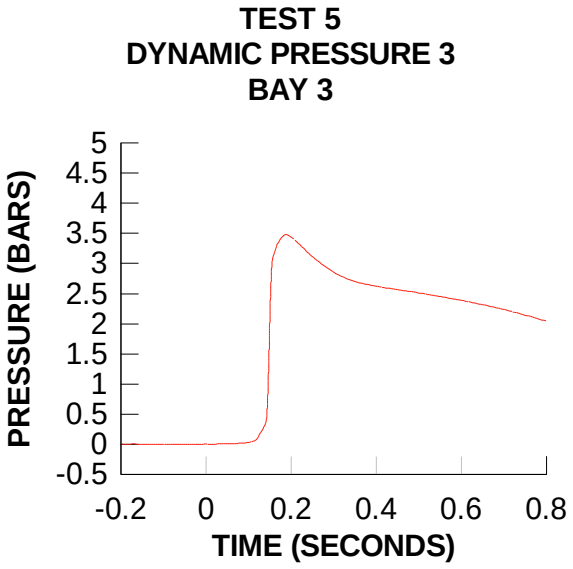
TEST 5
DYNAMIC PRESSURE 3
BAY 3
PRESSURE (BARS)
5
4.5
4
3.5
3
2.5
2
1.5
1
0.5
0
-0.5
-0.2
0
0.2
0.4
0.6
0.8
TIME (SECONDS)

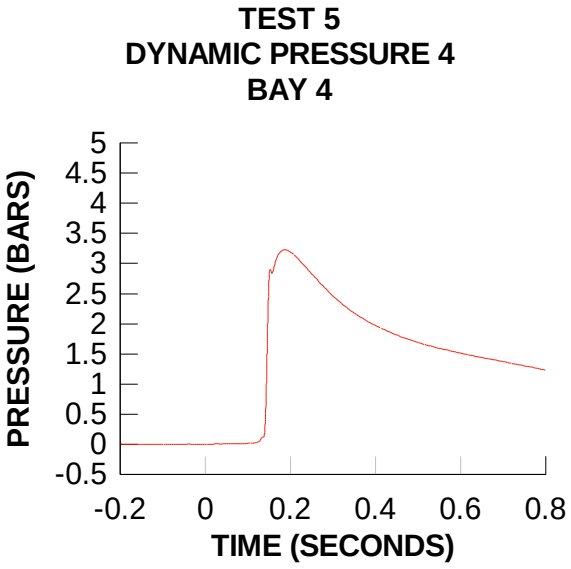
TEST 5
DYNAMIC PRESSURE 4
BAY 4
PRESSURE (BARS)
5
4.5
4
3.5
3
2.5
2
1.5
1
0.5
0
-0.5
-0.2
0
0.2
0.4
0.6
0.8
TIME (SECONDS)

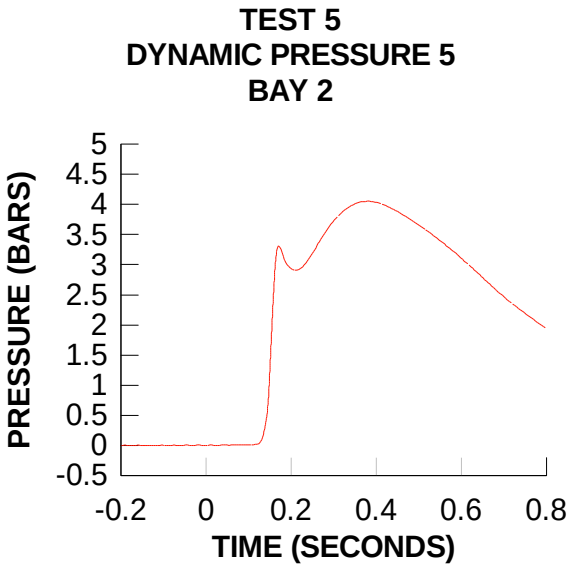
TEST 5
DYNAMIC PRESSURE 5
BAY 2
PRESSURE (BARS)
5
4.5
4
3.5
3
2.5
2
1.5
1
0.5
0
-0.5
-0.2
0
0.2
0.4
0.6
0.8
TIME (SECONDS)

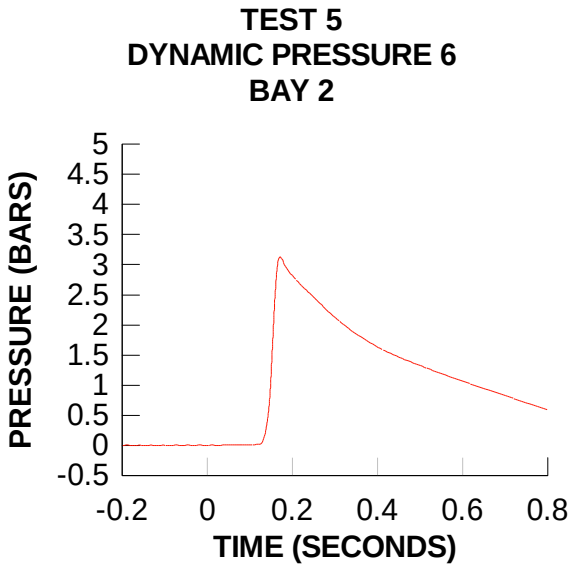
TEST 5
DYNAMIC PRESSURE 6
BAY 2
PRESSURE (BARS)
5
4.5
4
3.5
3
2.5
2
1.5
1
0.5
0
-0.5
-0.2
0
0.2
0.4
0.6
0.8
TIME (SECONDS)

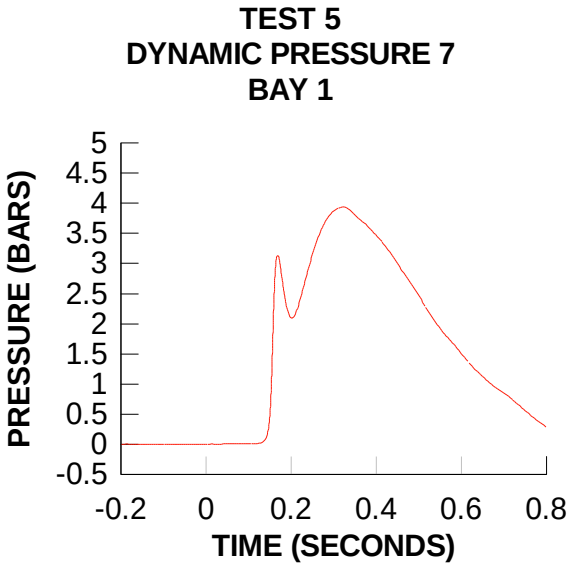
TEST 5
DYNAMIC PRESSURE 7
BAY 1
PRESSURE (BARS)
5
4.5
4
3.5
3
2.5
2
1.5
1
0.5
0
-0.5
-0.2
0
0.2
0.4
0.6
0.8
TIME (SECONDS)

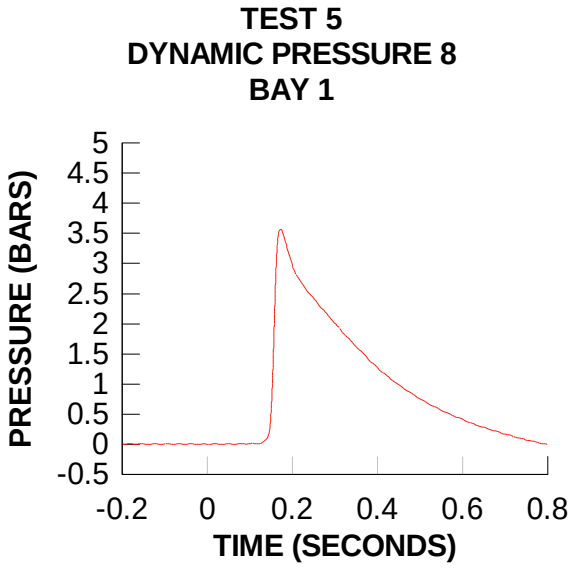
TEST 5
DYNAMIC PRESSURE 8
BAY 1
PRESSURE (BARS)
5
4.5
4
3.5
3
2.5
2
1.5
1
0.5
0
-0.5
-0.2
0
0.2
0.4
0.6
0.8
TIME (SECONDS)

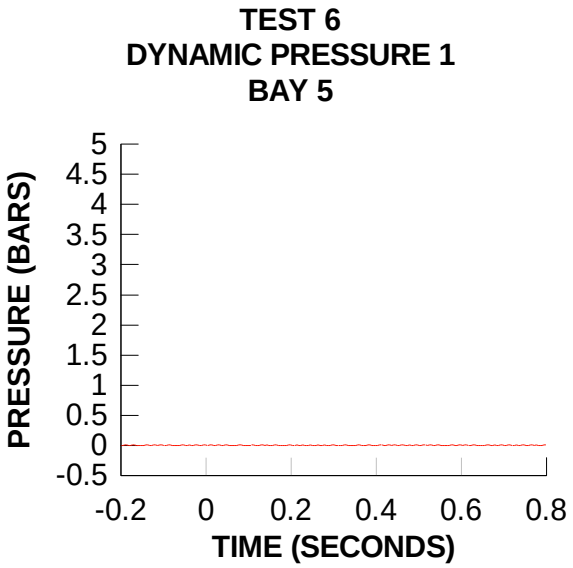
TEST 6
DYNAMIC PRESSURE 1
BAY 5
PRESSURE (BARS)
5
4.5
4
3.5
3
2.5
2
1.5
1
0.5
0
-0.5
-0.2
0
0.2
0.4
0.6
0.8
TIME (SECONDS)

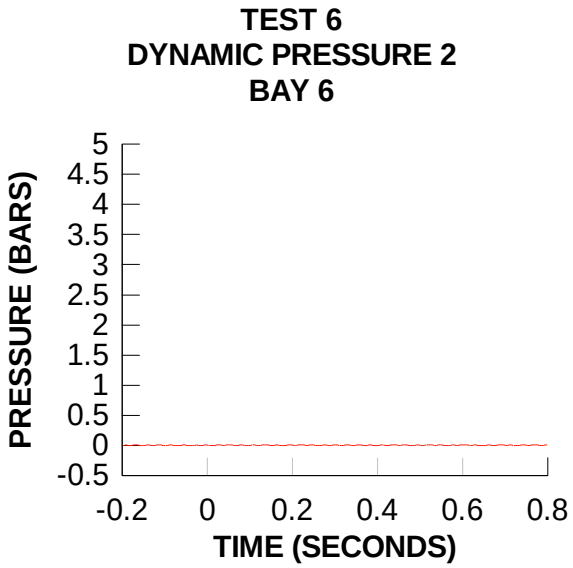
TEST 6
DYNAMIC PRESSURE 2
BAY 6
PRESSURE (BARS)
5
4.5
4
3.5
3
2.5
2
1.5
1
0.5
0
-0.5
-0.2
0
0.2
0.4
0.6
0.8
TIME (SECONDS)

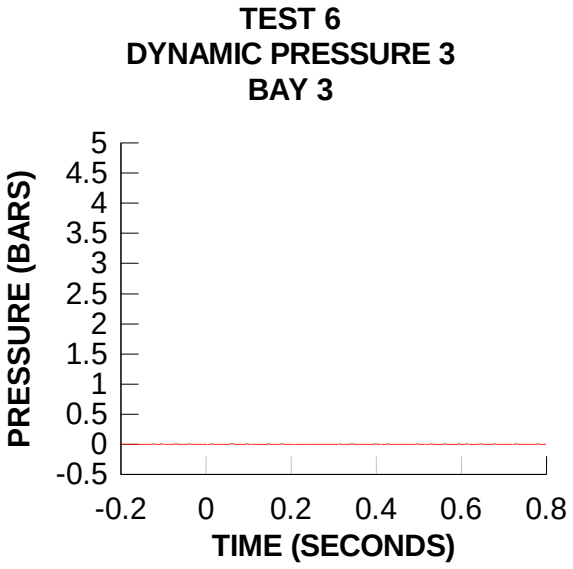
TEST 6
DYNAMIC PRESSURE 3
BAY 3
PRESSURE (BARS)
5
4.5
4
3.5
3
2.5
2
1.5
1
0.5
0
-0.5
-0.2
0
0.2
0.4
0.6
0.8
TIME (SECONDS)

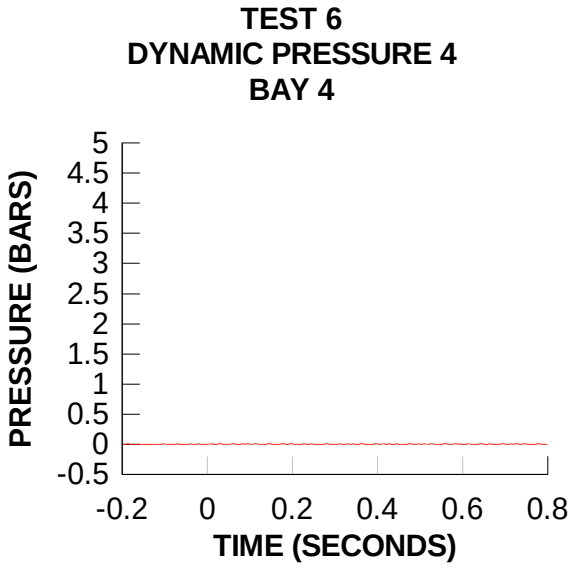
TEST 6
DYNAMIC PRESSURE 4
BAY 4
PRESSURE (BARS)
5
4.5
4
3.5
3
2.5
2
1.5
1
0.5
0
-0.5
-0.2
0
0.2
0.4
0.6
0.8
TIME (SECONDS)

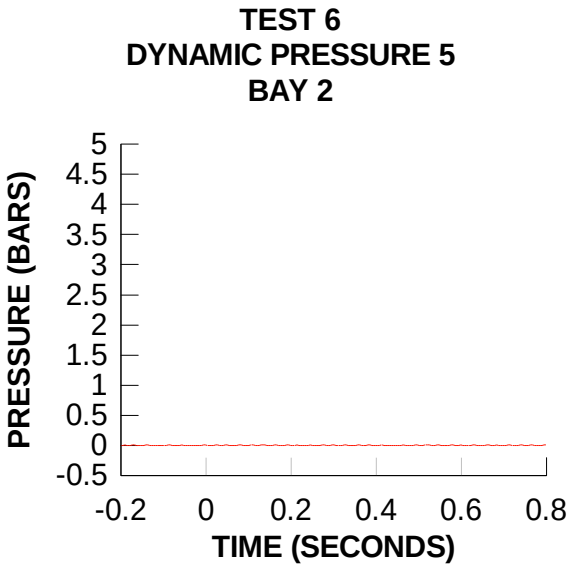
TEST 6
DYNAMIC PRESSURE 5
BAY 2
PRESSURE (BARS)
5
4.5
4
3.5
3
2.5
2
1.5
1
0.5
0
-0.5
-0.2
0
0.2
0.4
0.6
0.8
TIME (SECONDS)

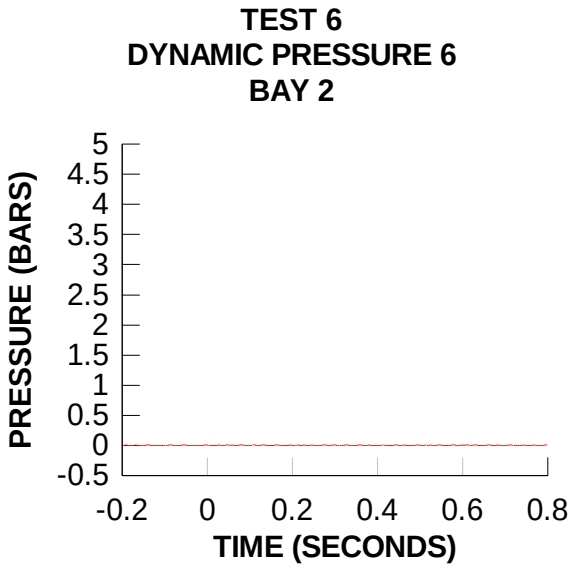
TEST 6
DYNAMIC PRESSURE 6
BAY 2
PRESSURE (BARS)
5
4.5
4
3.5
3
2.5
2
1.5
1
0.5
0
-0.5
-0.2
0
0.2
0.4
0.6
0.8
TIME (SECONDS)

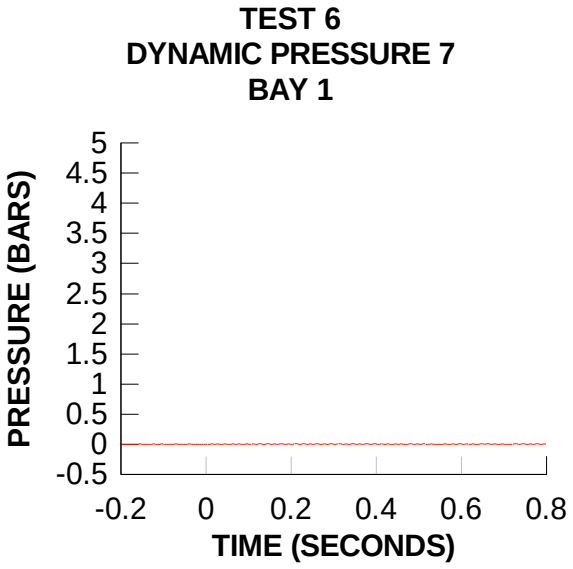
TEST 6
DYNAMIC PRESSURE 7
BAY 1
PRESSURE (BARS)
5
4.5
4
3.5
3
2.5
2
1.5
1
0.5
0
-0.5
-0.2
0
0.2
0.4
0.6
0.8
TIME (SECONDS)

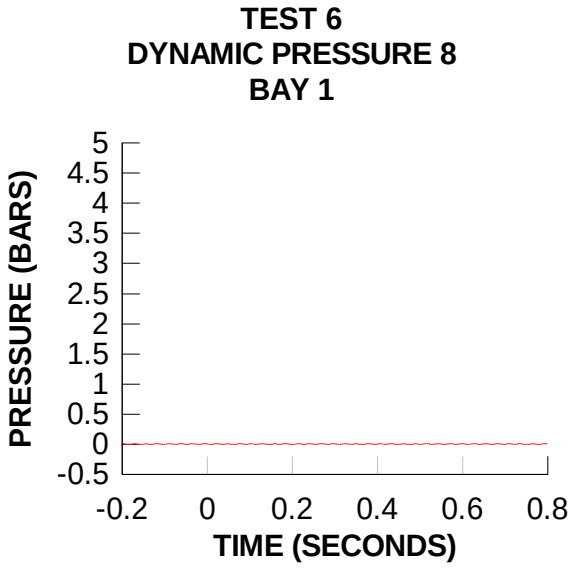
TEST 6
DYNAMIC PRESSURE 8
BAY 1
PRESSURE (BARS)
5
4.5
4
3.5
3
2.5
2
1.5
1
0.5
0
-0.5
-0.2
0
0.2
0.4
0.6
0.8
TIME (SECONDS)

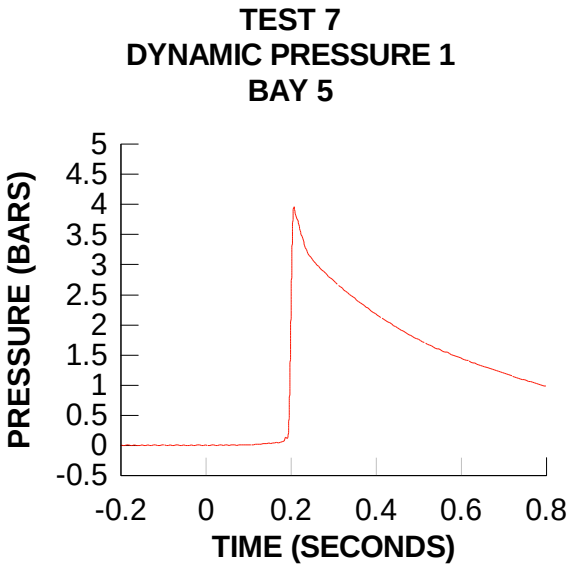
TEST 7
DYNAMIC PRESSURE 1
BAY 5
PRESSURE (BARS)
5
4.5
4
3.5
3
2.5
2
1.5
1
0.5
0
-0.5
-0.2
0
0.2
0.4
0.6
0.8
TIME (SECONDS)

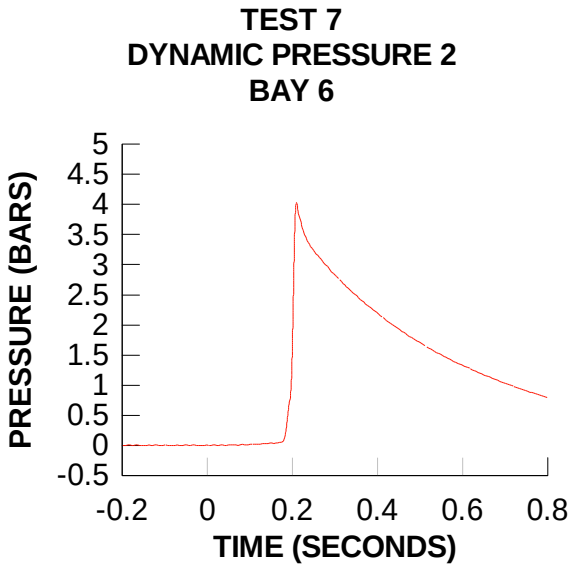
TEST 7
DYNAMIC PRESSURE 2
BAY 6
PRESSURE (BARS)
5
4.5
4
3.5
3
2.5
2
1.5
1
0.5
0
-0.5
-0.2
0
0.2
0.4
0.6
0.8
TIME (SECONDS)

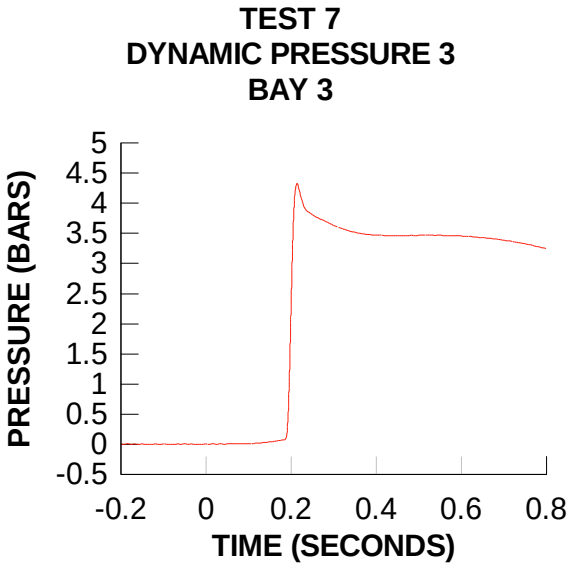
TEST 7
DYNAMIC PRESSURE 3
BAY 3
PRESSURE (BARS)
5
4.5
4
3.5
3
2.5
2
1.5
1
0.5
0
-0.5
-0.2
0
0.2
0.4
0.6
0.8
TIME (SECONDS)

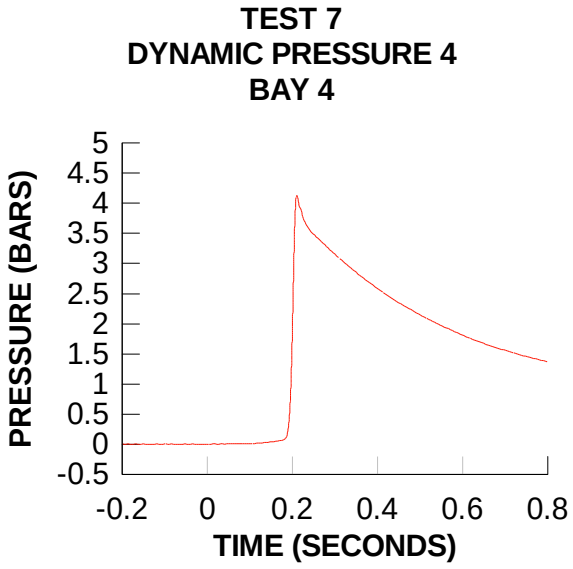
TEST 7
DYNAMIC PRESSURE 4
BAY 4
PRESSURE (BARS)
5
4.5
4
3.5
3
2.5
2
1.5
1
0.5
0
-0.5
-0.2
0
0.2
0.4
0.6
0.8
TIME (SECONDS)

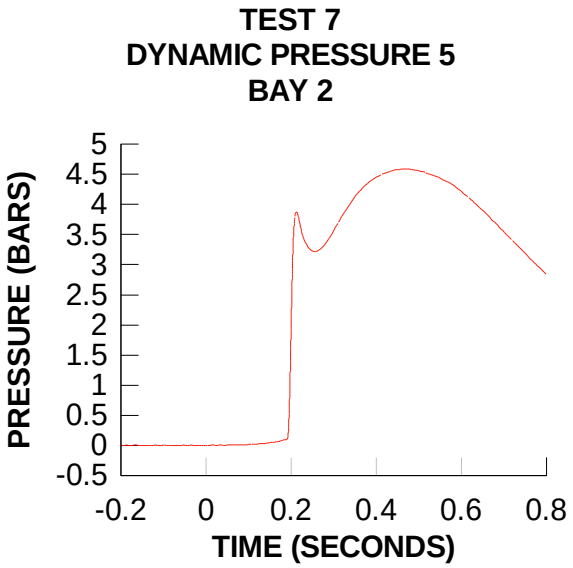
TEST 7
DYNAMIC PRESSURE 5
BAY 2
PRESSURE (BARS)
5
4.5
4
3.5
3
2.5
2
1.5
1
0.5
0
-0.5
-0.2
0
0.2
0.4
0.6
0.8
TIME (SECONDS)

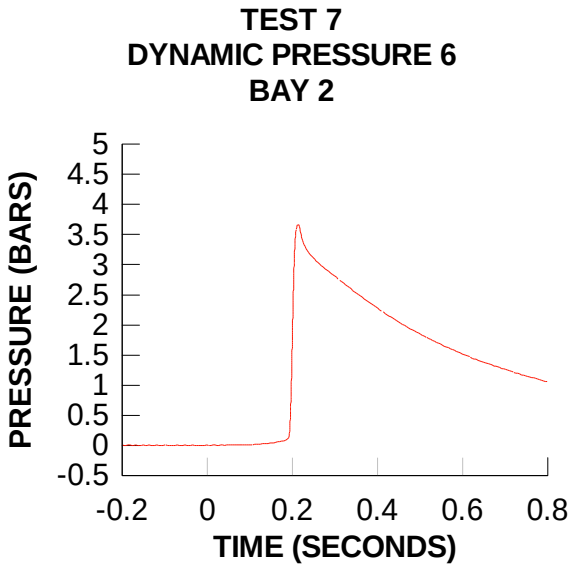
TEST 7
DYNAMIC PRESSURE 6
BAY 2
PRESSURE (BARS)
5
4.5
4
3.5
3
2.5
2
1.5
1
0.5
0
-0.5
-0.2
0
0.2
0.4
0.6
0.8
TIME (SECONDS)

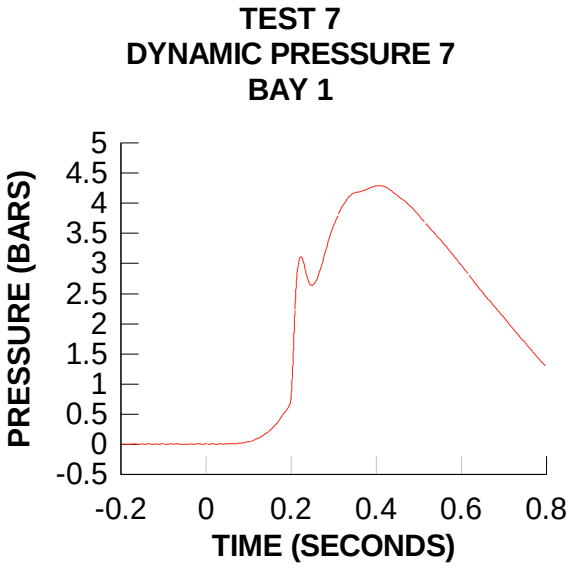
TEST 7
DYNAMIC PRESSURE 7
BAY 1
PRESSURE (BARS)
5
4.5
4
3.5
3
2.5
2
1.5
1
0.5
0
-0.5
-0.2
0
0.2
0.4
0.6
0.8
TIME (SECONDS)

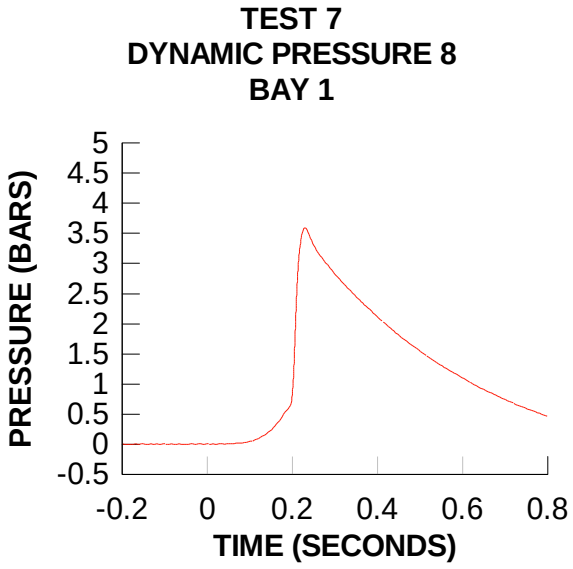
TEST 7
DYNAMIC PRESSURE 8
BAY 1
PRESSURE (BARS)
5
4.5
4
3.5
3
2.5
2
1.5
1
0.5
0
-0.5
-0.2
0
0.2
0.4
0.6
0.8
TIME (SECONDS)

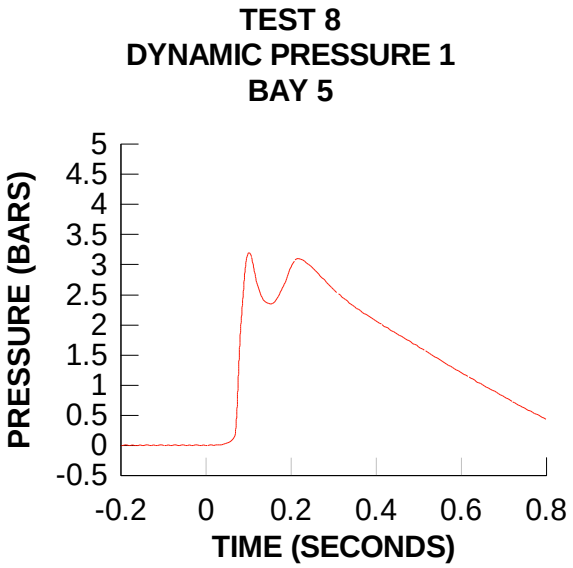
TEST 8
DYNAMIC PRESSURE 1
BAY 5
PRESSURE (BARS)
5
4.5
4
3.5
3
2.5
2
1.5
1
0.5
0
-0.5
-0.2
0
0.2
0.4
0.6
0.8
TIME (SECONDS)

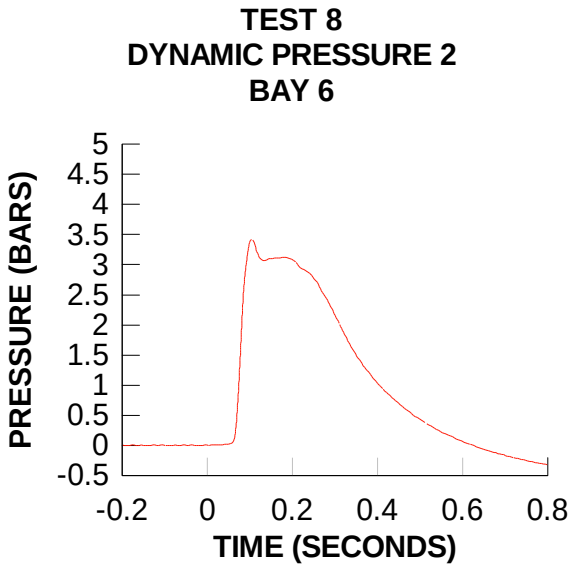
TEST 8
DYNAMIC PRESSURE 2
BAY 6
PRESSURE (BARS)
5
4.5
4
3.5
3
2.5
2
1.5
1
0.5
0
-0.5
-0.2
0
0.2
0.4
0.6
0.8
TIME (SECONDS)

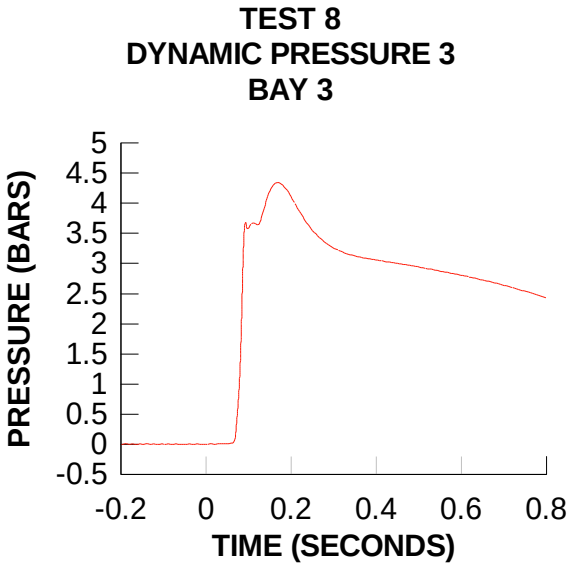
TEST 8
DYNAMIC PRESSURE 3
BAY 3
PRESSURE (BARS)
5
4.5
4
3.5
3
2.5
2
1.5
1
0.5
0
-0.5
-0.2
0
0.2
0.4
0.6
0.8
TIME (SECONDS)

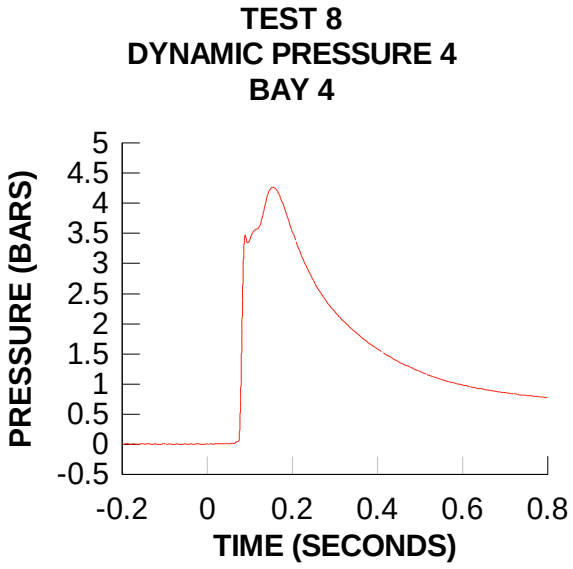
TEST 8
DYNAMIC PRESSURE 4
BAY 4
PRESSURE (BARS)
5
4.5
4
3.5
3
2.5
2
1.5
1
0.5
0
-0.5
-0.2
0
0.2
0.4
0.6
0.8
TIME (SECONDS)

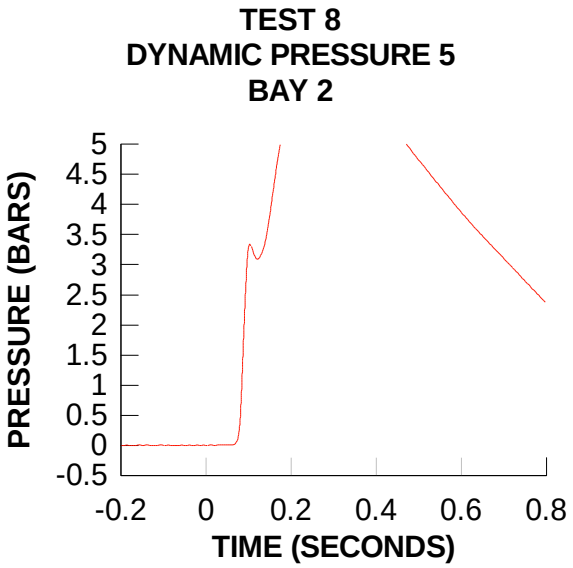
TEST 8
DYNAMIC PRESSURE 5
BAY 2
PRESSURE (BARS)
5
4.5
4
3.5
3
2.5
2
1.5
1
0.5
0
-0.5
-0.2
0
0.2
0.4
0.6
0.8
TIME (SECONDS)

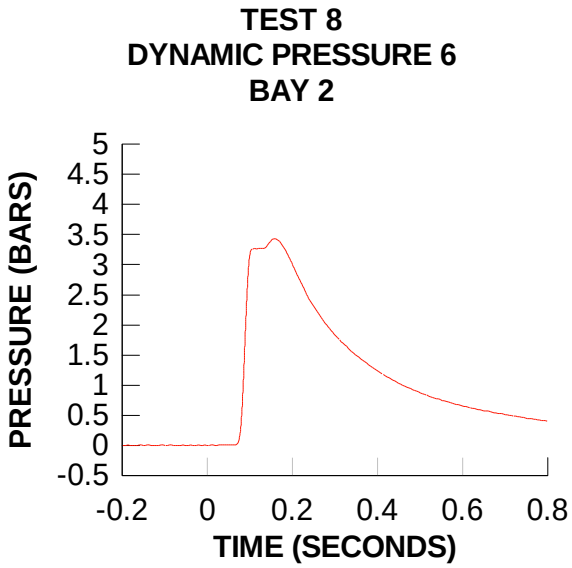
TEST 8
DYNAMIC PRESSURE 6
BAY 2
PRESSURE (BARS)
5
4.5
4
3.5
3
2.5
2
1.5
1
0.5
0
-0.5
-0.2
0
0.2
0.4
0.6
0.8
TIME (SECONDS)

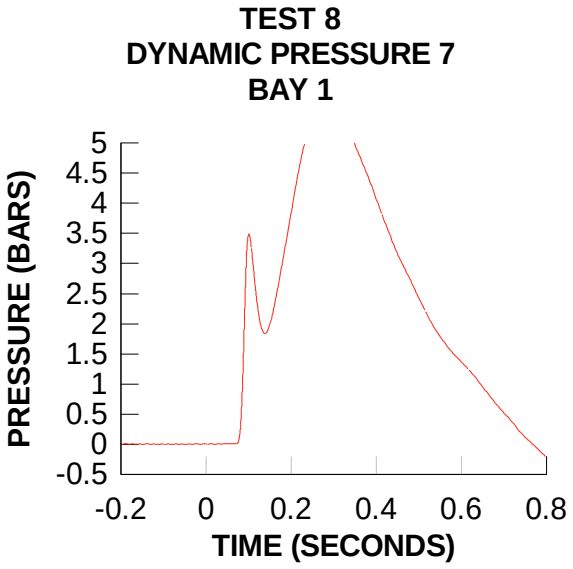
TEST 8
DYNAMIC PRESSURE 7
BAY 1
PRESSURE (BARS)
5
4.5
4
3.5
3
2.5
2
1.5
1
0.5
0
-0.5
-0.2
0
0.2
0.4
0.6
0.8
TIME (SECONDS)

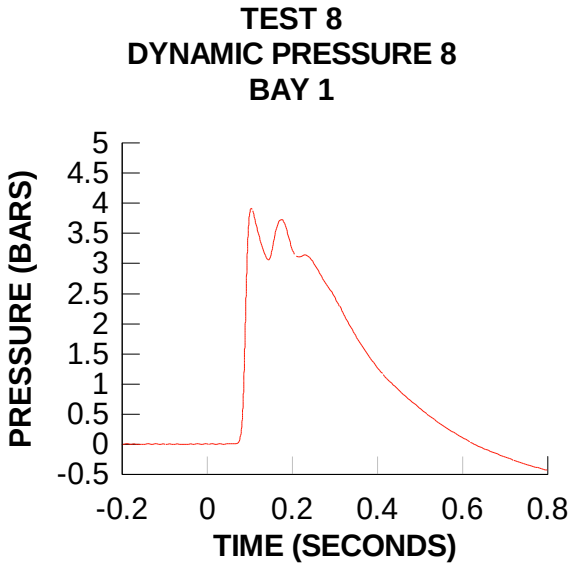
TEST 8
DYNAMIC PRESSURE 8
BAY 1
PRESSURE (BARS)
5
4.5
4
3.5
3
2.5
2
1.5
1
0.5
0
-0.5
-0.2
0
0.2
0.4
0.6
0.8
TIME (SECONDS)

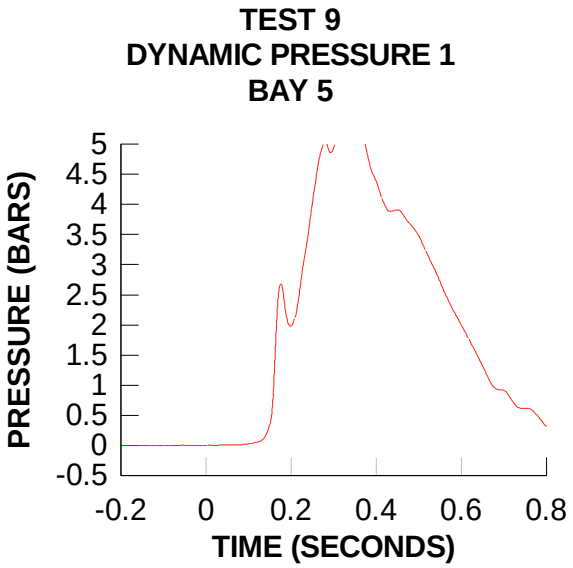
TEST 9
DYNAMIC PRESSURE 1
BAY 5
PRESSURE (BARS)
5
4.5
4
3.5
3
2.5
2
1.5
1
0.5
0
-0.5
-0.2
0
0.2
0.4
0.6
0.8
TIME (SECONDS)

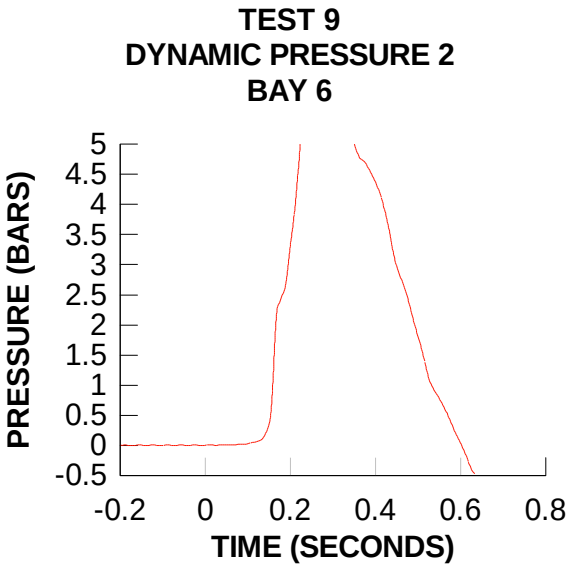
TEST 9
DYNAMIC PRESSURE 2
BAY 6
PRESSURE (BARS)
5
4.5
4
3.5
3
2.5
2
1.5
1
0.5
0
-0.5
-0.2
0
0.2
0.4
0.6
0.8
TIME (SECONDS)

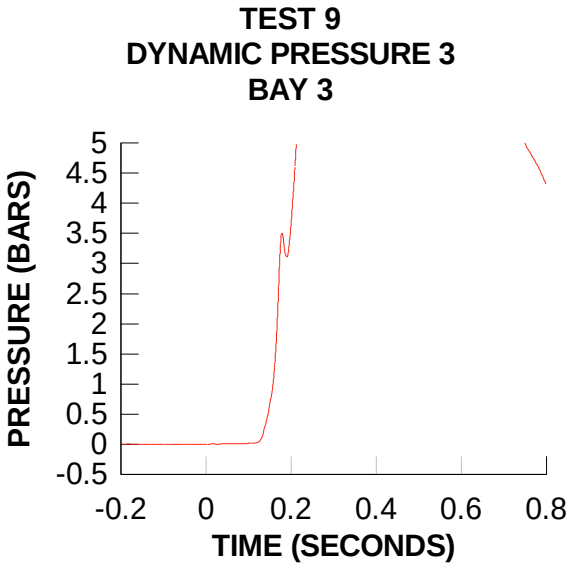
TEST 9
DYNAMIC PRESSURE 3
BAY 3
PRESSURE (BARS)
5
4.5
4
3.5
3
2.5
2
1.5
1
0.5
0
-0.5
-0.2
0
0.2
0.4
0.6
0.8
TIME (SECONDS)

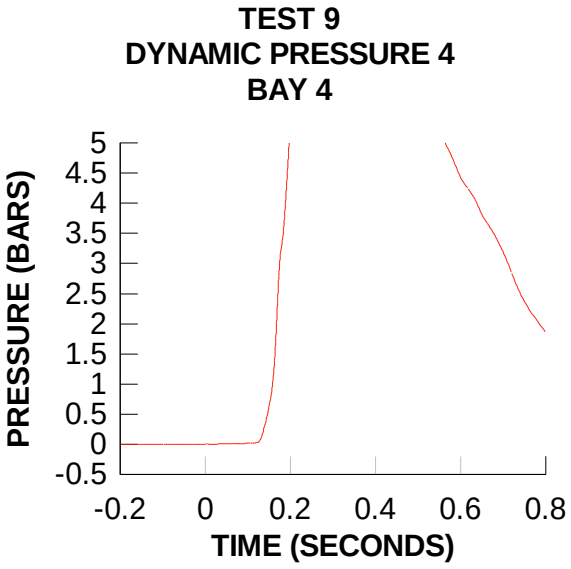
TEST 9
DYNAMIC PRESSURE 4
BAY 4
PRESSURE (BARS)
5
4.5
4
3.5
3
2.5
2
1.5
1
0.5
0
-0.5
-0.2
0
0.2
0.4
0.6
0.8
TIME (SECONDS)

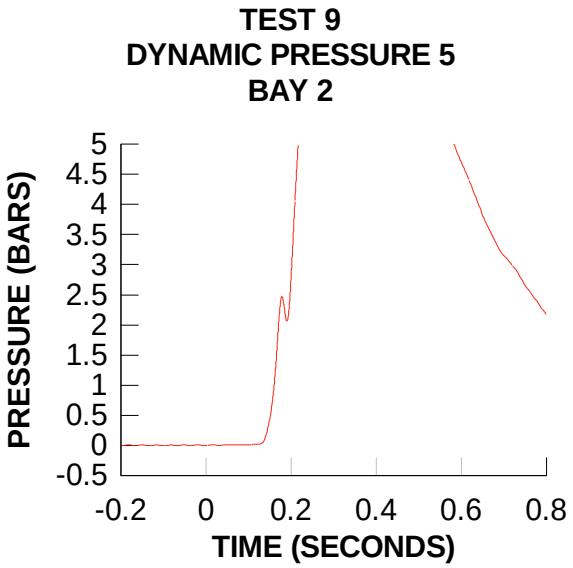
TEST 9
DYNAMIC PRESSURE 5
BAY 2
PRESSURE (BARS)
5
4.5
4
3.5
3
2.5
2
1.5
1
0.5
0
-0.5
-0.2
0
0.2
0.4
0.6
0.8
TIME (SECONDS)

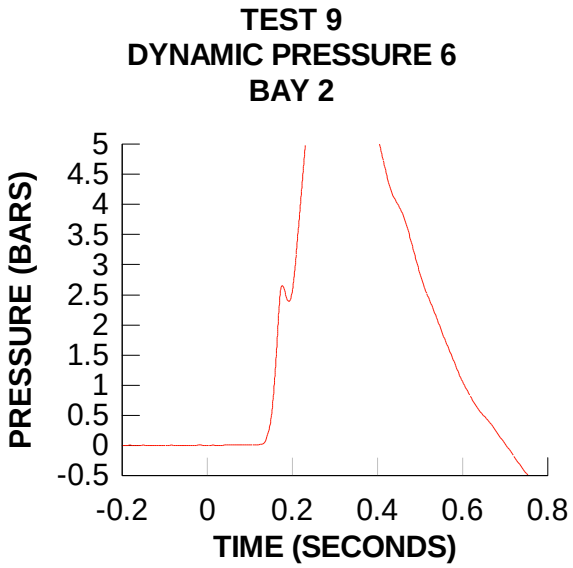
TEST 9
DYNAMIC PRESSURE 6
BAY 2
PRESSURE (BARS)
5
4.5
4
3.5
3
2.5
2
1.5
1
0.5
0
-0.5
-0.2
0
0.2
0.4
0.6
0.8
TIME (SECONDS)

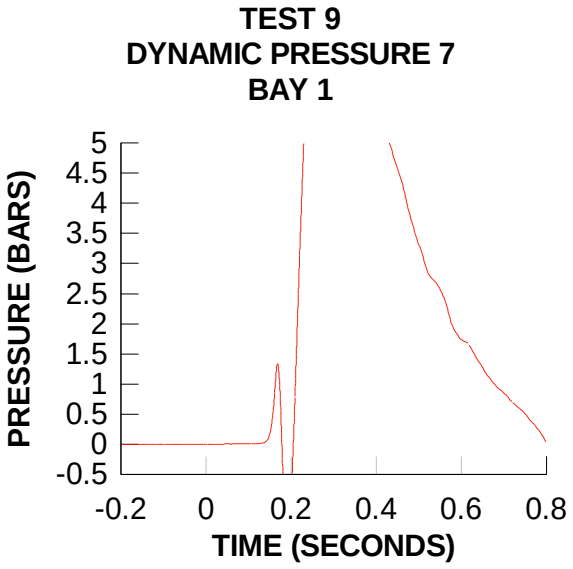
TEST 9
DYNAMIC PRESSURE 7
BAY 1
PRESSURE (BARS)
5
4.5
4
3.5
3
2.5
2
1.5
1
0.5
0
-0.5
-0.2
0
0.2
0.4
0.6
0.8
TIME (SECONDS)

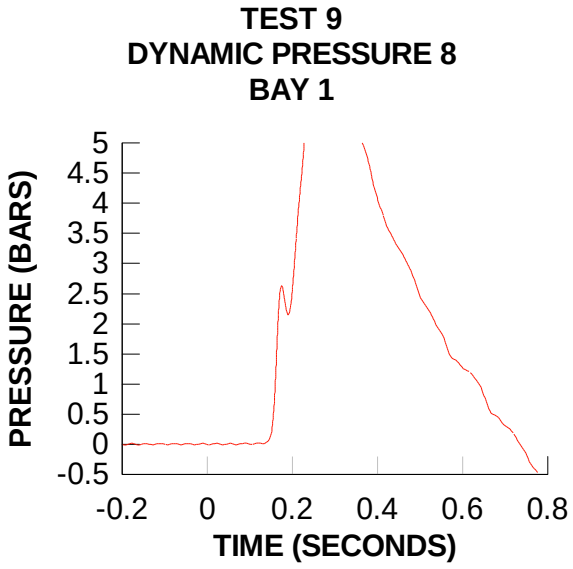
TEST 9
DYNAMIC PRESSURE 8
BAY 1
PRESSURE (BARS)
5
4.5
4
3.5
3
2.5
2
1.5
1
0.5
0
-0.5
-0.2
0
0.2
0.4
0.6
0.8
TIME (SECONDS)

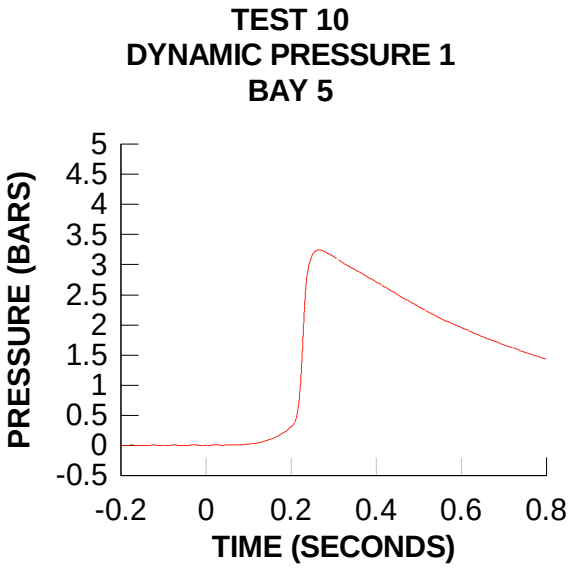
TEST 10
DYNAMIC PRESSURE 1
BAY 5
PRESSURE (BARS)
5
4.5
4
3.5
3
2.5
2
1.5
1
0.5
0
-0.5
-0.2
0
0.2
0.4
0.6
0.8
TIME (SECONDS)

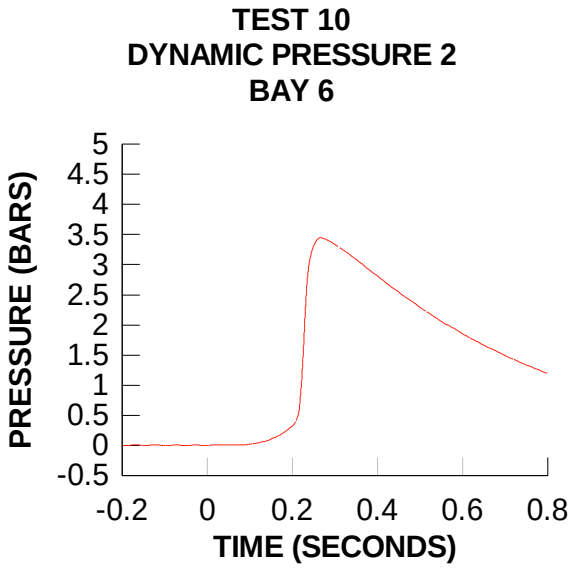
TEST 10
DYNAMIC PRESSURE 2
BAY 6
PRESSURE (BARS)
5
4.5
4
3.5
3
2.5
2
1.5
1
0.5
0
-0.5
-0.2
0
0.2
0.4
0.6
0.8
TIME (SECONDS)

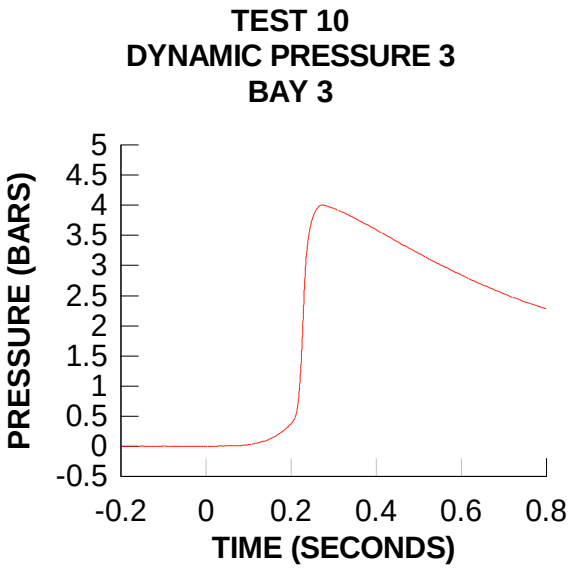
TEST 10
DYNAMIC PRESSURE 3
BAY 3
PRESSURE (BARS)
5
4.5
4
3.5
3
2.5
2
1.5
1
0.5
0
-0.5
-0.2
0
0.2
0.4
0.6
0.8
TIME (SECONDS)

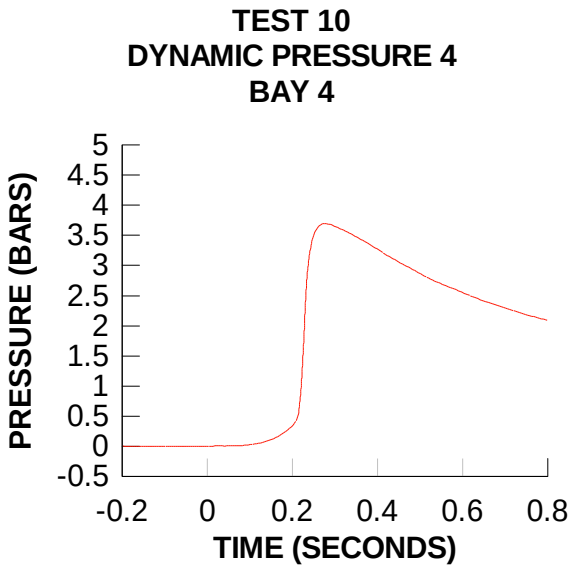
TEST 10
DYNAMIC PRESSURE 4
BAY 4
PRESSURE (BARS)
5
4.5
4
3.5
3
2.5
2
1.5
1
0.5
0
-0.5
-0.2
0
0.2
0.4
0.6
0.8
TIME (SECONDS)

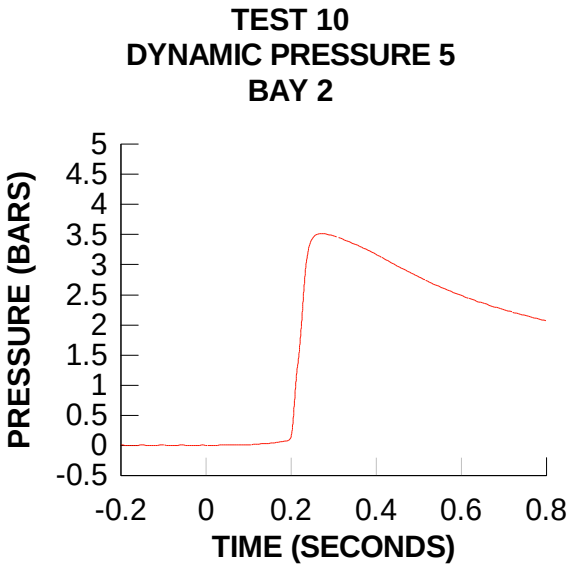
TEST 10
DYNAMIC PRESSURE 5
BAY 2
PRESSURE (BARS)
5
4.5
4
3.5
3
2.5
2
1.5
1
0.5
0
-0.5
-0.2
0
0.2
0.4
0.6
0.8
TIME (SECONDS)

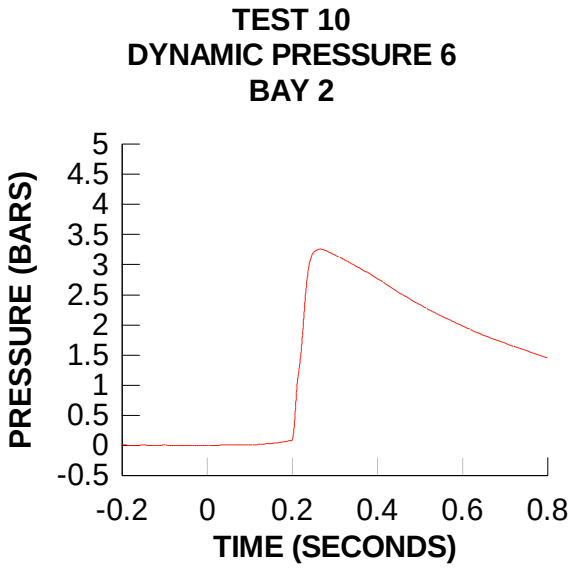
TEST 10
DYNAMIC PRESSURE 6
BAY 2
PRESSURE (BARS)
5
4.5
4
3.5
3
2.5
2
1.5
1
0.5
0
-0.5
-0.2
0
0.2
0.4
0.6
0.8
TIME (SECONDS)

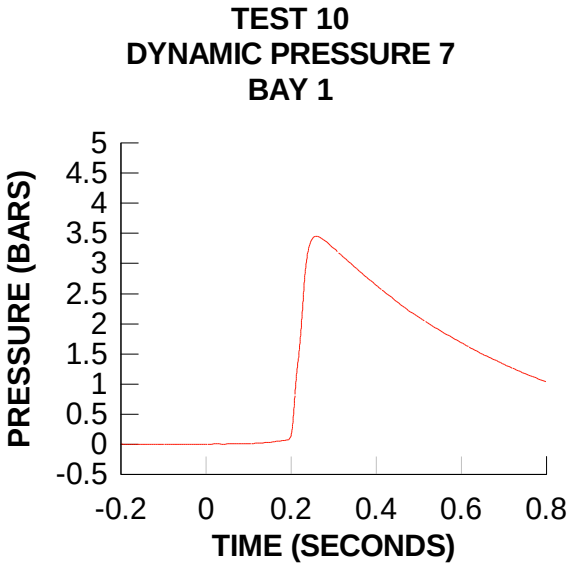
TEST 10
DYNAMIC PRESSURE 7
BAY 1
PRESSURE (BARS)
5
4.5
4
3.5
3
2.5
2
1.5
1
0.5
0
-0.5
-0.2
0
0.2
0.4
0.6
0.8
TIME (SECONDS)

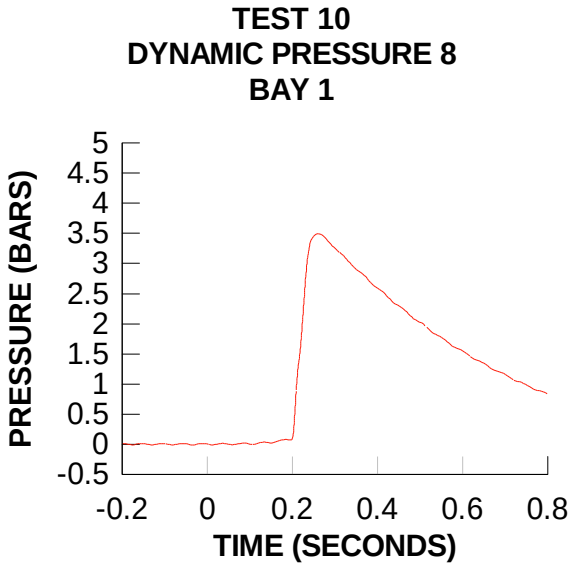
TEST 10
DYNAMIC PRESSURE 8
BAY 1
PRESSURE (BARS)
5
4.5
4
3.5
3
2.5
2
1.5
1
0.5
0
-0.5
-0.2
0
0.2
0.4
0.6
0.8
TIME (SECONDS)

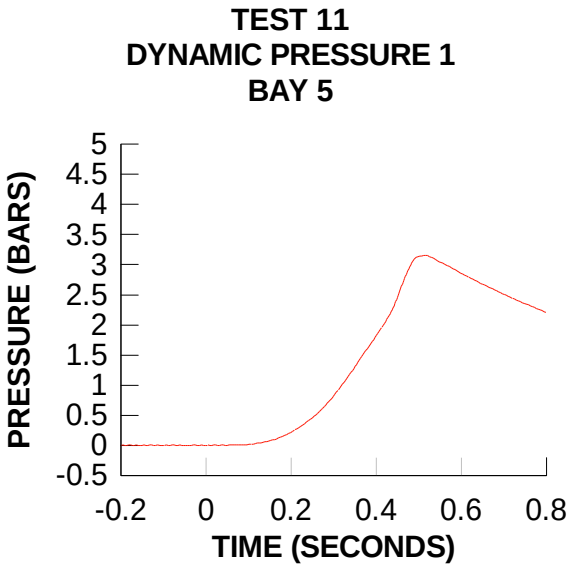
TEST 11
DYNAMIC PRESSURE 1
BAY 5
PRESSURE (BARS)
5
4.5
4
3.5
3
2.5
2
1.5
1
0.5
0
-0.5
-0.2
0
0.2
0.4
0.6
0.8
TIME (SECONDS)

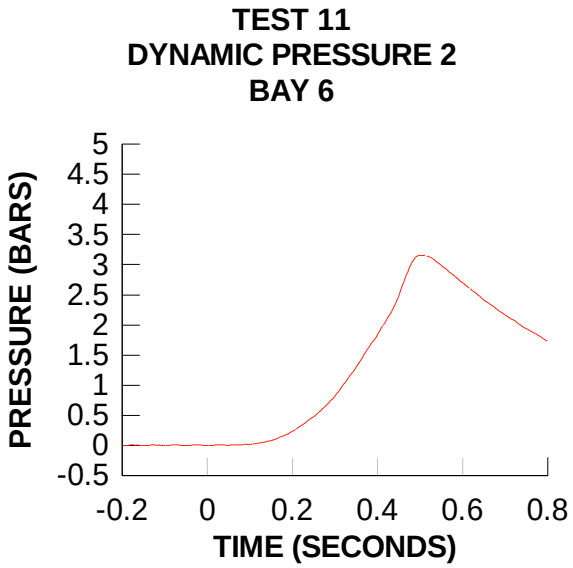
TEST 11
DYNAMIC PRESSURE 2
BAY 6
PRESSURE (BARS)
5
4.5
4
3.5
3
2.5
2
1.5
1
0.5
0
-0.5
-0.2
0
0.2
0.4
0.6
0.8
TIME (SECONDS)

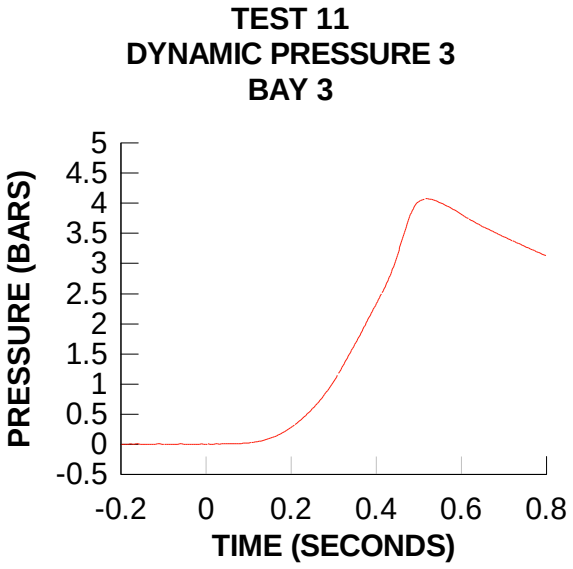
TEST 11
DYNAMIC PRESSURE 3
BAY 3
PRESSURE (BARS)
5
4.5
4
3.5
3
2.5
2
1.5
1
0.5
0
-0.5
-0.2
0
0.2
0.4
0.6
0.8
TIME (SECONDS)

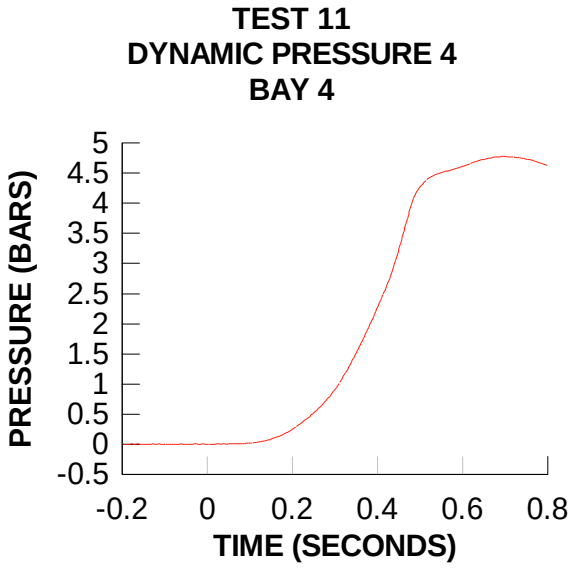
TEST 11
DYNAMIC PRESSURE 4
BAY 4
PRESSURE (BARS)
5
4.5
4
3.5
3
2.5
2
1.5
1
0.5
0
-0.5
-0.2
0
0.2
0.4
0.6
0.8
TIME (SECONDS)

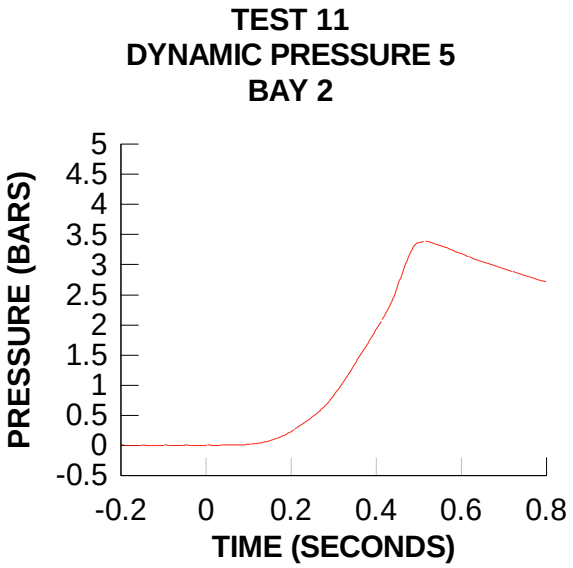
TEST 11
DYNAMIC PRESSURE 5
BAY 2
PRESSURE (BARS)
5
4.5
4
3.5
3
2.5
2
1.5
1
0.5
0
-0.5
-0.2
0
0.2
0.4
0.6
0.8
TIME (SECONDS)

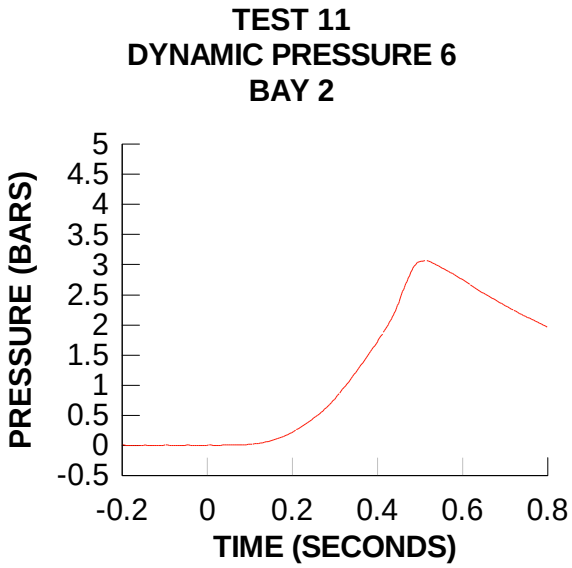
TEST 11
DYNAMIC PRESSURE 6
BAY 2
PRESSURE (BARS)
5
4.5
4
3.5
3
2.5
2
1.5
1
0.5
0
-0.5
-0.2
0
0.2
0.4
0.6
0.8
TIME (SECONDS)

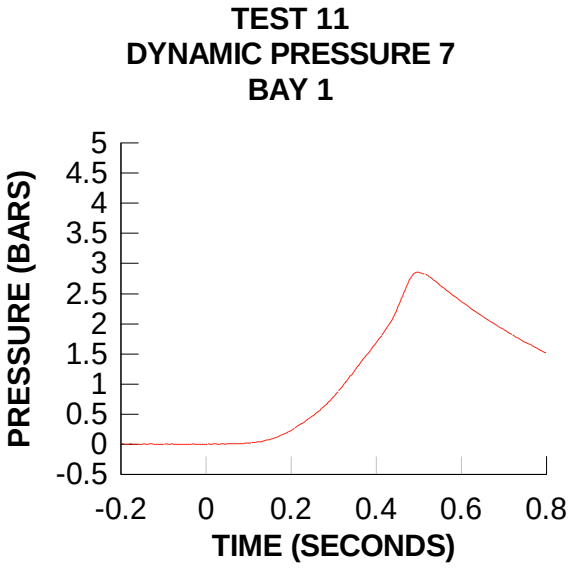
TEST 11
DYNAMIC PRESSURE 7
BAY 1
PRESSURE (BARS)
5
4.5
4
3.5
3
2.5
2
1.5
1
0.5
0
-0.5
-0.2
0
0.2
0.4
0.6
0.8
TIME (SECONDS)

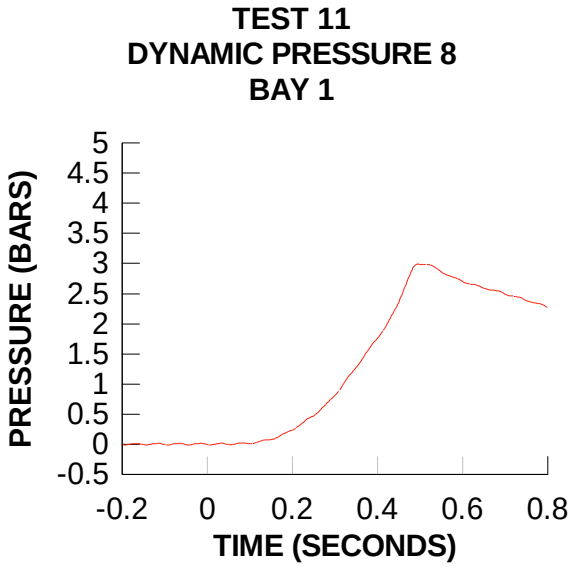
TEST 11
DYNAMIC PRESSURE 8
BAY 1
PRESSURE (BARS)
5
4.5
4
3.5
3
2.5
2
1.5
1
0.5
0
-0.5
-0.2
0
0.2
0.4
0.6
0.8
TIME (SECONDS)

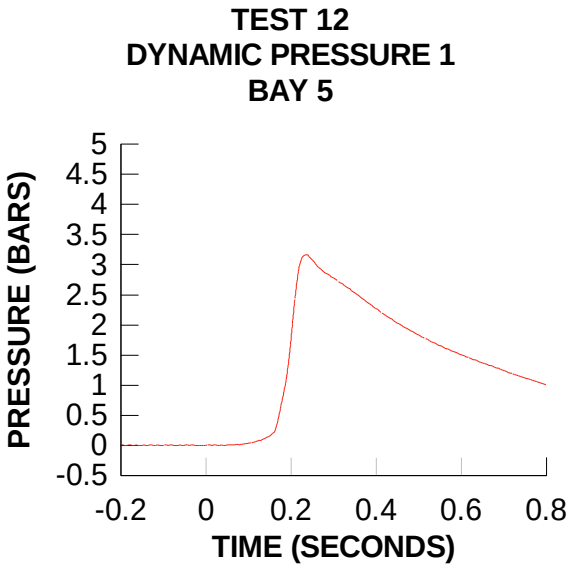
TEST 12
DYNAMIC PRESSURE 1
BAY 5
PRESSURE (BARS)
5
4.5
4
3.5
3
2.5
2
1.5
1
0.5
0
-0.5
-0.2
0
0.2
0.4
0.6
0.8
TIME (SECONDS)

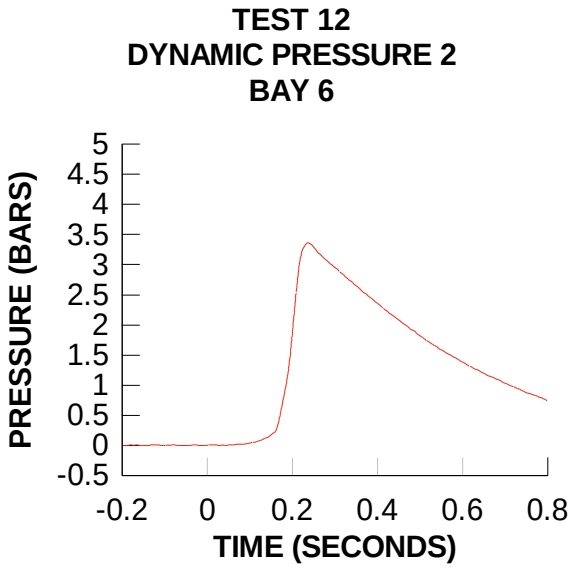
TEST 12
DYNAMIC PRESSURE 2
BAY 6
PRESSURE (BARS)
5
4.5
4
3.5
3
2.5
2
1.5
1
0.5
0
-0.5
-0.2
0
0.2
0.4
0.6
0.8
TIME (SECONDS)

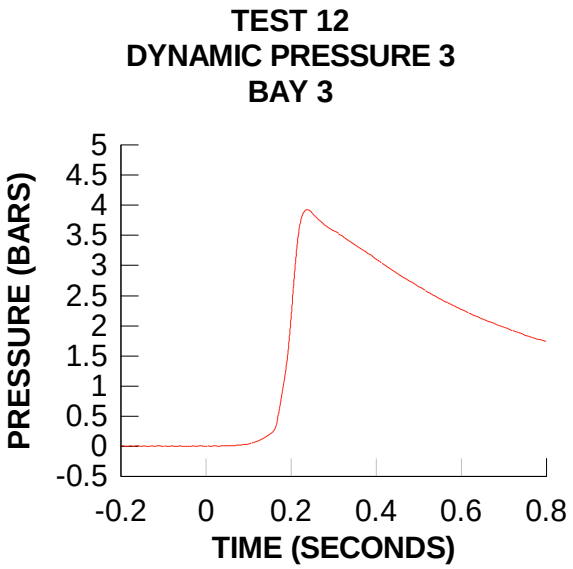
TEST 12
DYNAMIC PRESSURE 3
BAY 3
PRESSURE (BARS)
5
4.5
4
3.5
3
2.5
2
1.5
1
0.5
0
-0.5
-0.2
0
0.2
0.4
0.6
0.8
TIME (SECONDS)

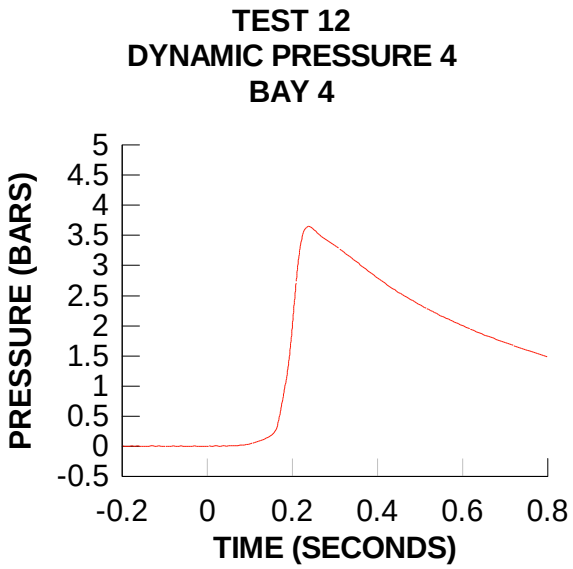
TEST 12
DYNAMIC PRESSURE 4
BAY 4
PRESSURE (BARS)
5
4.5
4
3.5
3
2.5
2
1.5
1
0.5
0
-0.5
-0.2
0
0.2
0.4
0.6
0.8
TIME (SECONDS)

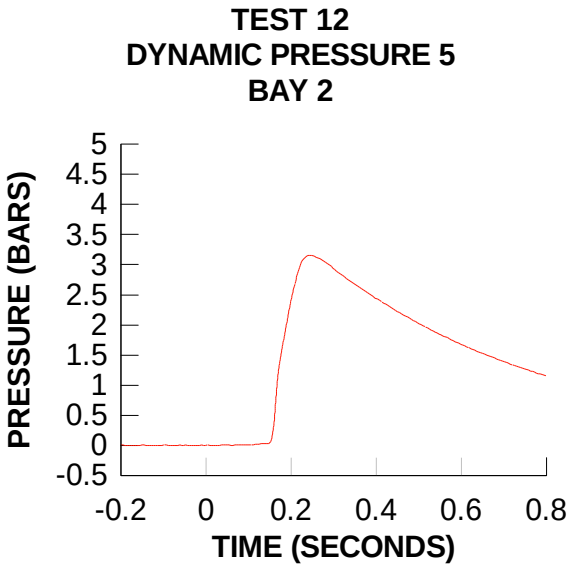
TEST 12
DYNAMIC PRESSURE 5
BAY 2
PRESSURE (BARS)
5
4.5
4
3.5
3
2.5
2
1.5
1
0.5
0
-0.5
-0.2
0
0.2
0.4
0.6
0.8
TIME (SECONDS)

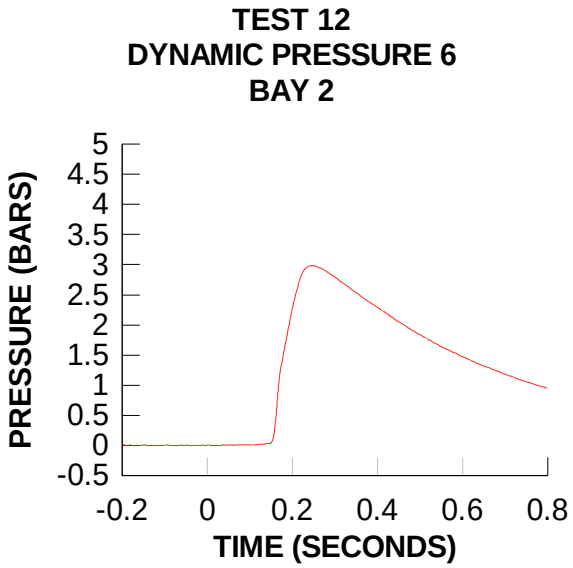
TEST 12
DYNAMIC PRESSURE 6
BAY 2
PRESSURE (BARS)
5
4.5
4
3.5
3
2.5
2
1.5
1
0.5
0
-0.5
-0.2
0
0.2
0.4
0.6
0.8
TIME (SECONDS)

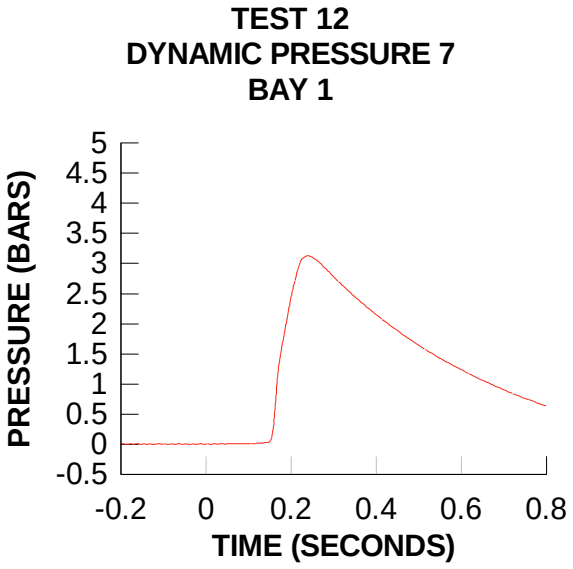
TEST 12
DYNAMIC PRESSURE 7
BAY 1
PRESSURE (BARS)
5
4.5
4
3.5
3
2.5
2
1.5
1
0.5
0
-0.5
-0.2
0
0.2
0.4
0.6
0.8
TIME (SECONDS)

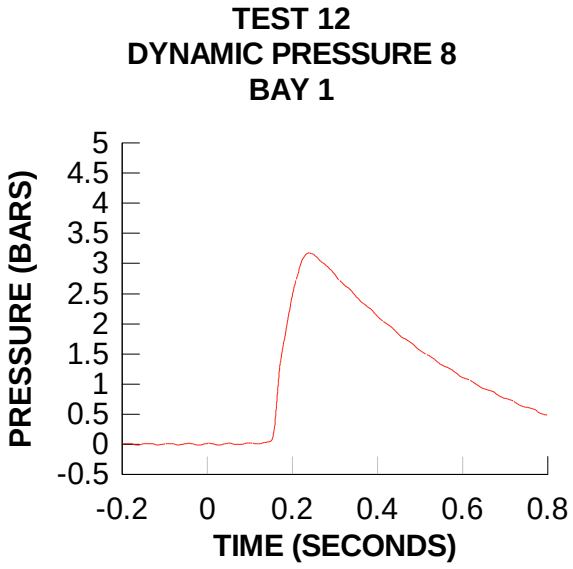
TEST 12
DYNAMIC PRESSURE 8
BAY 1
PRESSURE (BARS)
5
4.5
4
3.5
3
2.5
2
1.5
1
0.5
0
-0.5
-0.2
0
0.2
0.4
0.6
0.8
TIME (SECONDS)

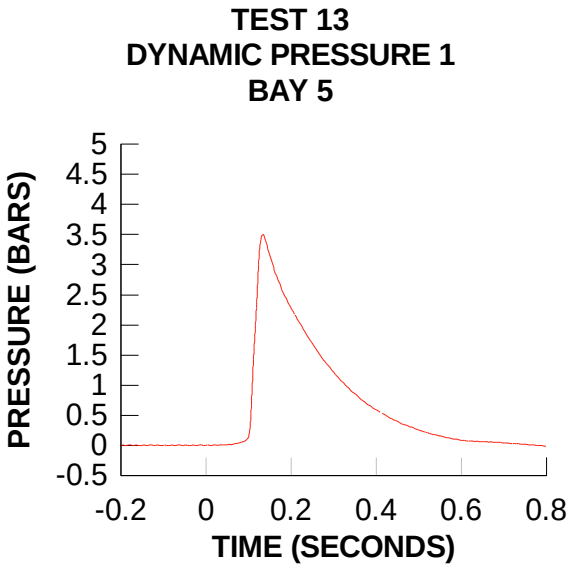
TEST 13
DYNAMIC PRESSURE 1
BAY 5
PRESSURE (BARS)
5
4.5
4
3.5
3
2.5
2
1.5
1
0.5
0
-0.5
-0.2
0
0.2
0.4
0.6
0.8
TIME (SECONDS)

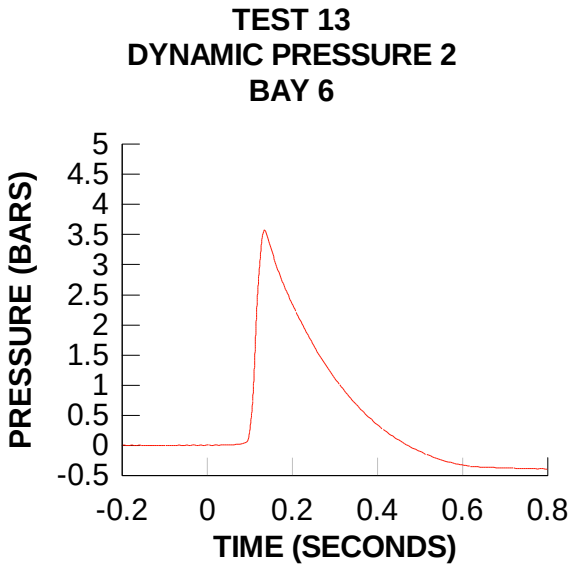
TEST 13
DYNAMIC PRESSURE 2
BAY 6
PRESSURE (BARS)
5
4.5
4
3.5
3
2.5
2
1.5
1
0.5
0
-0.5
-0.2
0
0.2
0.4
0.6
0.8
TIME (SECONDS)

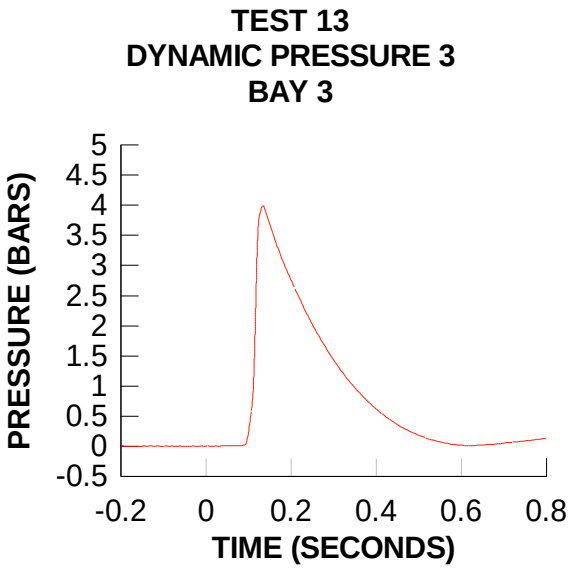
TEST 13
DYNAMIC PRESSURE 3
BAY 3
PRESSURE (BARS)
5
4.5
4
3.5
3
2.5
2
1.5
1
0.5
0
-0.5
-0.2
0
0.2
0.4
0.6
0.8
TIME (SECONDS)

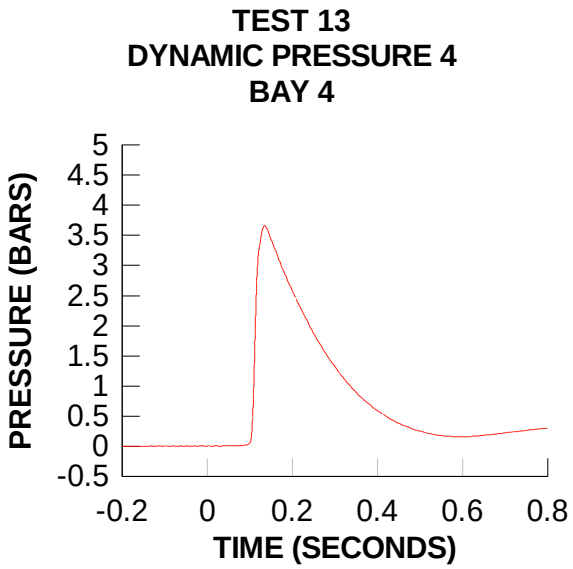
TEST 13
DYNAMIC PRESSURE 4
BAY 4
PRESSURE (BARS)
5
4.5
4
3.5
3
2.5
2
1.5
1
0.5
0
-0.5
-0.2
0
0.2
0.4
0.6
0.8
TIME (SECONDS)

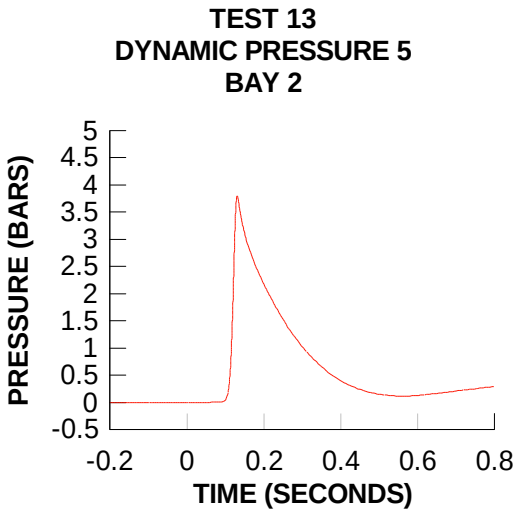
TEST 13
DYNAMIC PRESSURE 5
BAY 2
PRESSURE (BARS)
TIME (SECONDS)

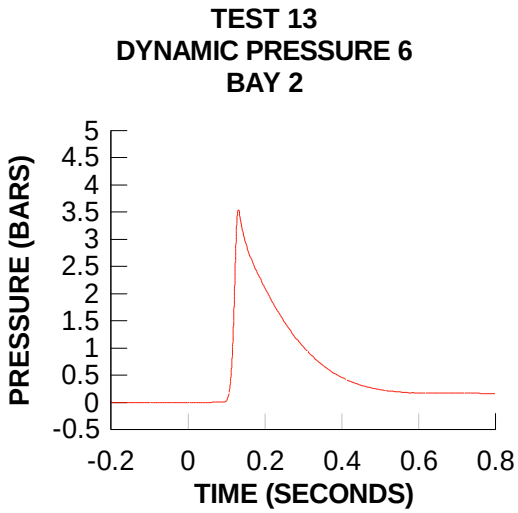
TEST 13
DYNAMIC PRESSURE 6
BAY 2
PRESSURE (BARS)
TIME (SECONDS)

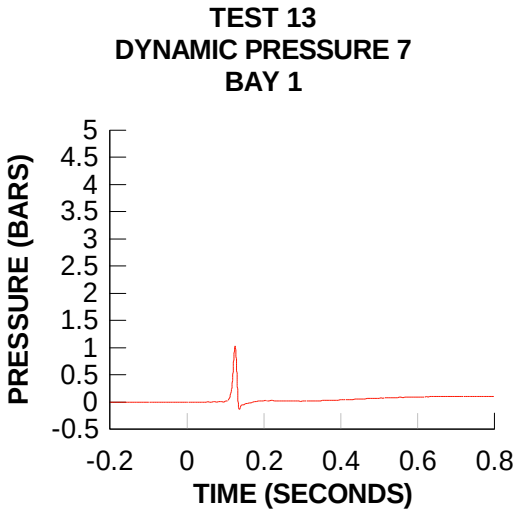
TEST 13
DYNAMIC PRESSURE 7
BAY 1
PRESSURE (BARS)
TIME (SECONDS)

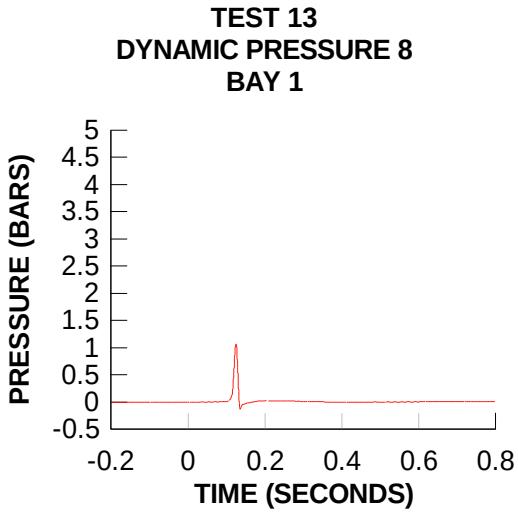
TEST 13
DYNAMIC PRESSURE 8
BAY 1
PRESSURE (BARS)
TIME (SECONDS)

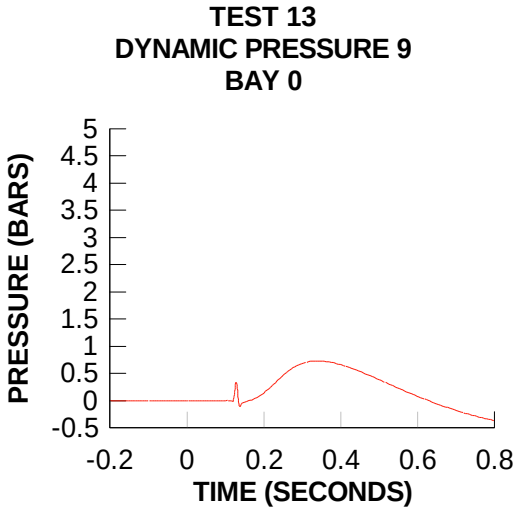
TEST 13
DYNAMIC PRESSURE 9
BAY 0
PRESSURE (BARS)
TIME (SECONDS)

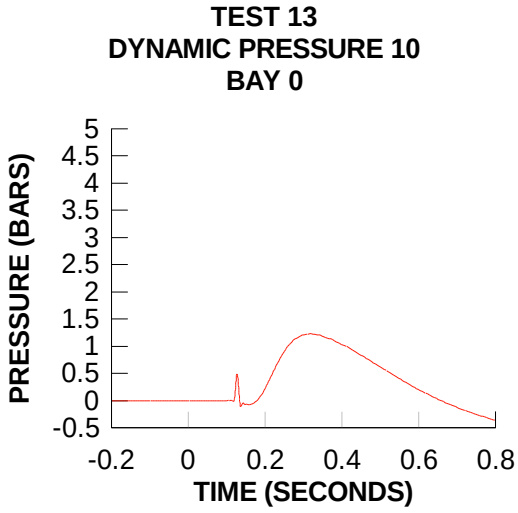
TEST 13
DYNAMIC PRESSURE 10
BAY 0
PRESSURE (BARS)
TIME (SECONDS)

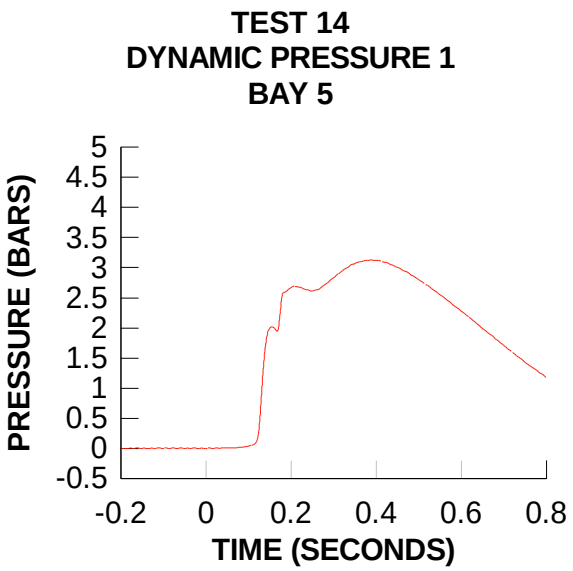
TEST 14
DYNAMIC PRESSURE 1
BAY 5
PRESSURE (BARS)
5
4.5
4
3.5
3
2.5
2
1.5
1
0.5
0
-0.5
-0.2
0
0.2
0.4
0.6
0.8
TIME (SECONDS)

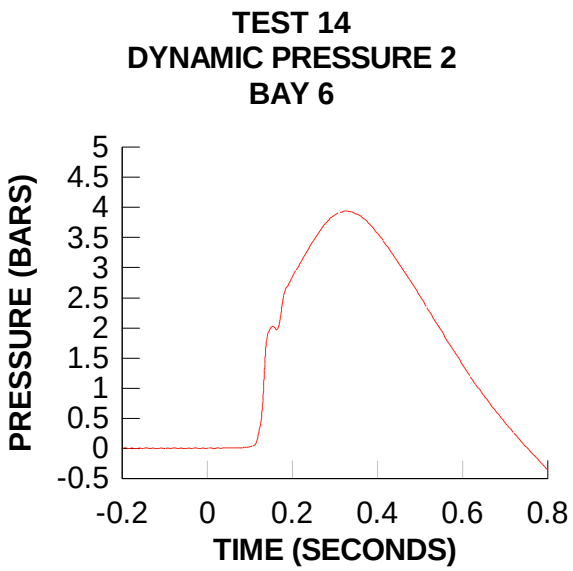
TEST 14
DYNAMIC PRESSURE 2
BAY 6
PRESSURE (BARS)
5
4.5
4
3.5
3
2.5
2
1.5
1
0.5
0
-0.5
-0.2
0
0.2
0.4
0.6
0.8
TIME (SECONDS)

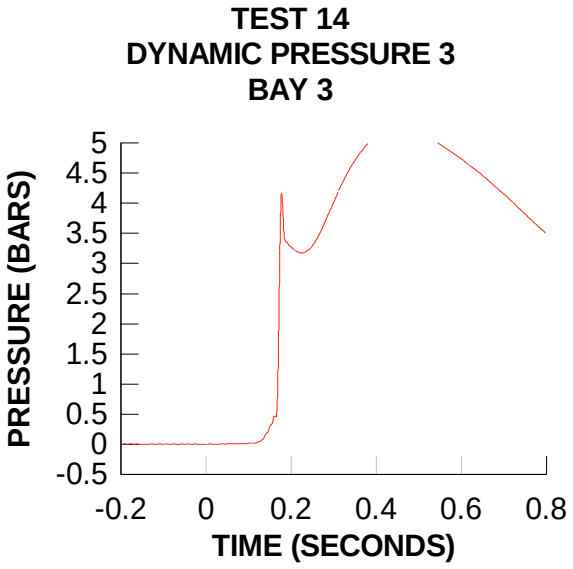
TEST 14
DYNAMIC PRESSURE 3
BAY 3
PRESSURE (BARS)
5
4.5
4
3.5
3
2.5
2
1.5
1
0.5
0
-0.5
-0.2
0
0.2
0.4
0.6
0.8
TIME (SECONDS)

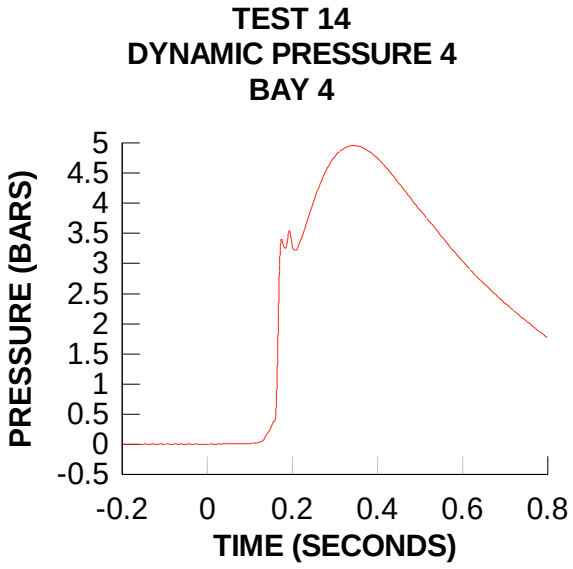
TEST 14
DYNAMIC PRESSURE 4
BAY 4
PRESSURE (BARS)
5
4.5
4
3.5
3
2.5
2
1.5
1
0.5
0
-0.5
-0.2
0
0.2
0.4
0.6
0.8
TIME (SECONDS)

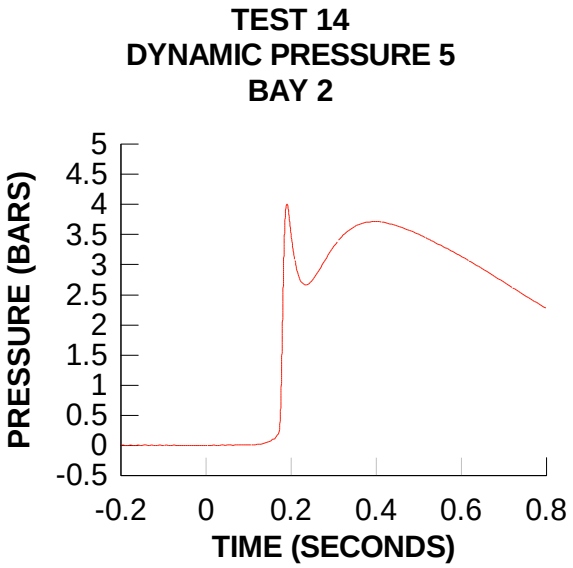
TEST 14
DYNAMIC PRESSURE 5
BAY 2
PRESSURE (BARS)
5
4.5
4
3.5
3
2.5
2
1.5
1
0.5
0
-0.5
-0.2
0
0.2
0.4
0.6
0.8
TIME (SECONDS)

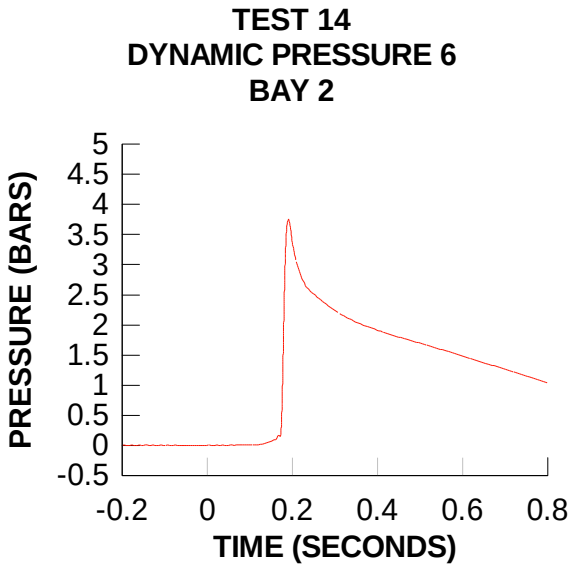
TEST 14
DYNAMIC PRESSURE 6
BAY 2
PRESSURE (BARS)
5
4.5
4
3.5
3
2.5
2
1.5
1
0.5
0
-0.5
-0.2
0
0.2
0.4
0.6
0.8
TIME (SECONDS)

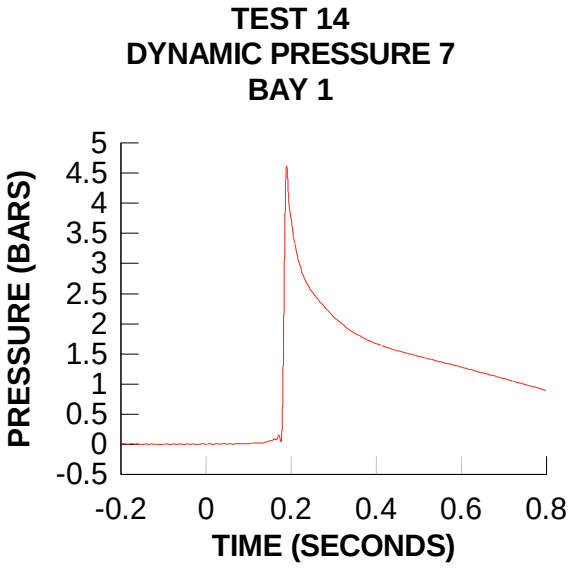
TEST 14
DYNAMIC PRESSURE 7
BAY 1
PRESSURE (BARS)
5
4.5
4
3.5
3
2.5
2
1.5
1
0.5
0
-0.5
-0.2
0
0.2
0.4
0.6
0.8
TIME (SECONDS)

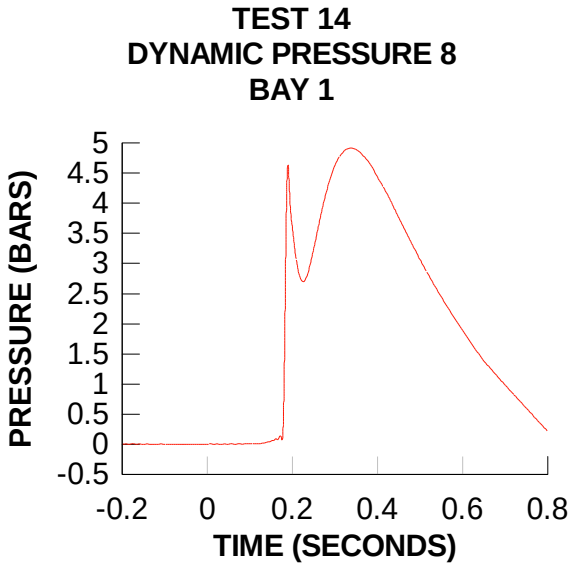
TEST 14
DYNAMIC PRESSURE 8
BAY 1
PRESSURE (BARS)
5
4.5
4
3.5
3
2.5
2
1.5
1
0.5
0
-0.5
-0.2
0
0.2
0.4
0.6
0.8
TIME (SECONDS)

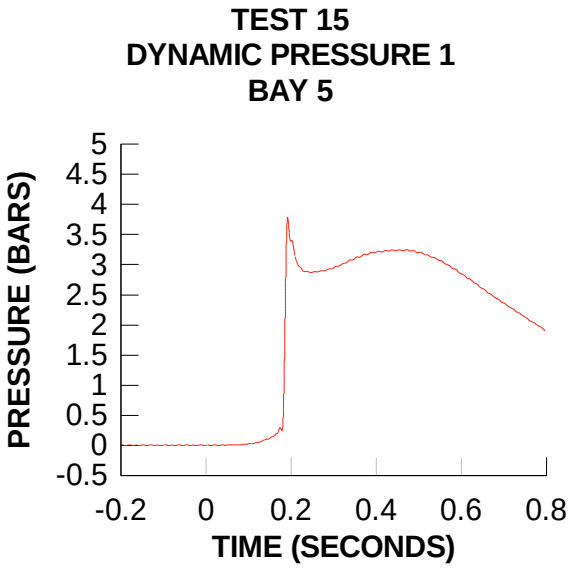
TEST 15
DYNAMIC PRESSURE 1
BAY 5
PRESSURE (BARS)
5
4.5
4
3.5
3
2.5
2
1.5
1
0.5
0
-0.5
-0.2
0
0.2
0.4
0.6
0.8
TIME (SECONDS)

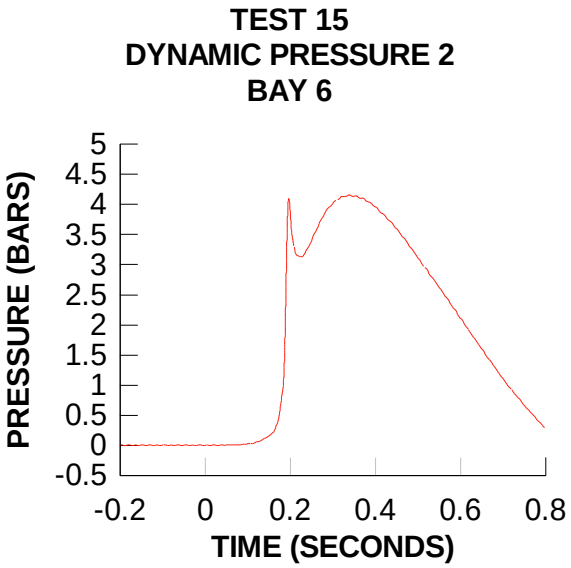
TEST 15
DYNAMIC PRESSURE 2
BAY 6
PRESSURE (BARS)
5
4.5
4
3.5
3
2.5
2
1.5
1
0.5
0
-0.5
-0.2
0
0.2
0.4
0.6
0.8
TIME (SECONDS)

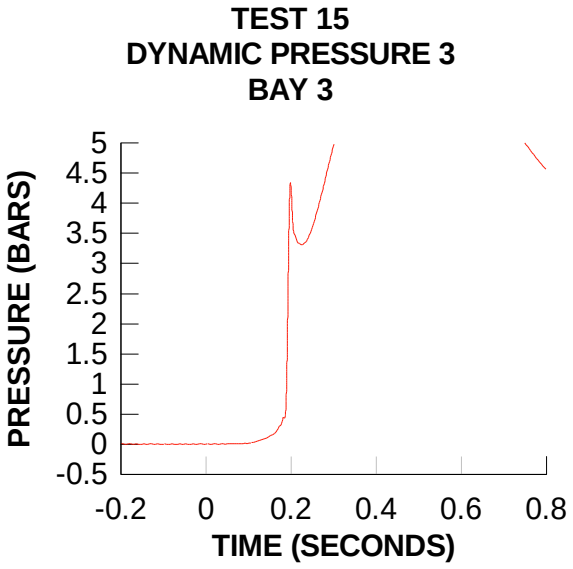
TEST 15
DYNAMIC PRESSURE 3
BAY 3
PRESSURE (BARS)
5
4.5
4
3.5
3
2.5
2
1.5
1
0.5
0
-0.5
-0.2
0
0.2
0.4
0.6
0.8
TIME (SECONDS)

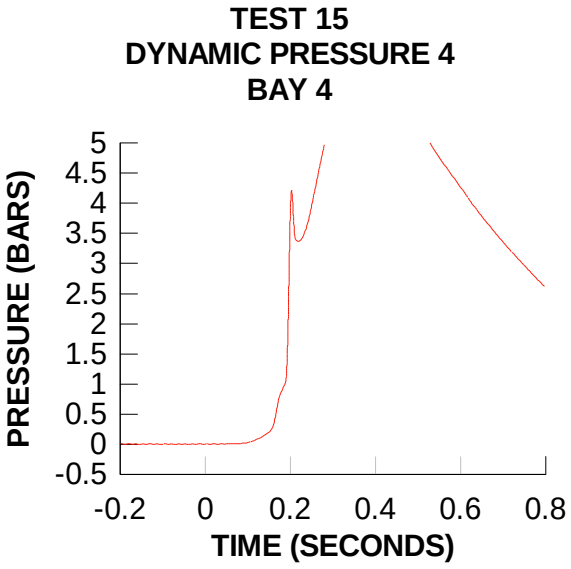
TEST 15
DYNAMIC PRESSURE 4
BAY 4
PRESSURE (BARS)
5
4.5
4
3.5
3
2.5
2
1.5
1
0.5
0
-0.5
-0.2
0
0.2
0.4
0.6
0.8
TIME (SECONDS)

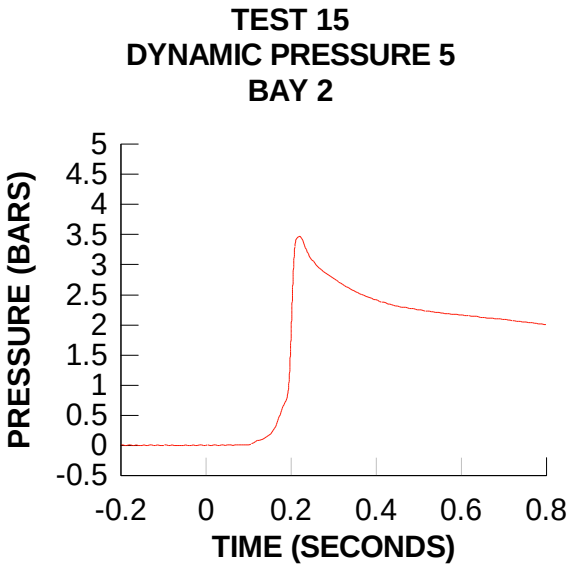
TEST 15
DYNAMIC PRESSURE 5
BAY 2
PRESSURE (BARS)
5
4.5
4
3.5
3
2.5
2
1.5
1
0.5
0
-0.5
-0.2
0
0.2
0.4
0.6
0.8
TIME (SECONDS)

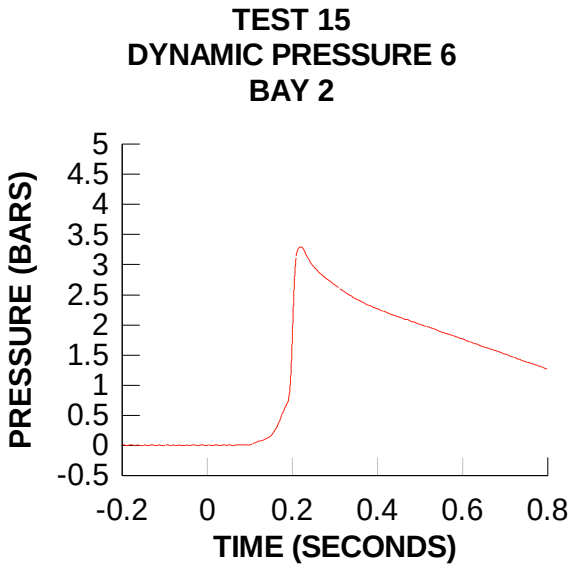
TEST 15
DYNAMIC PRESSURE 6
BAY 2
PRESSURE (BARS)
5
4.5
4
3.5
3
2.5
2
1.5
1
0.5
0
-0.5
-0.2
0
0.2
0.4
0.6
0.8
TIME (SECONDS)

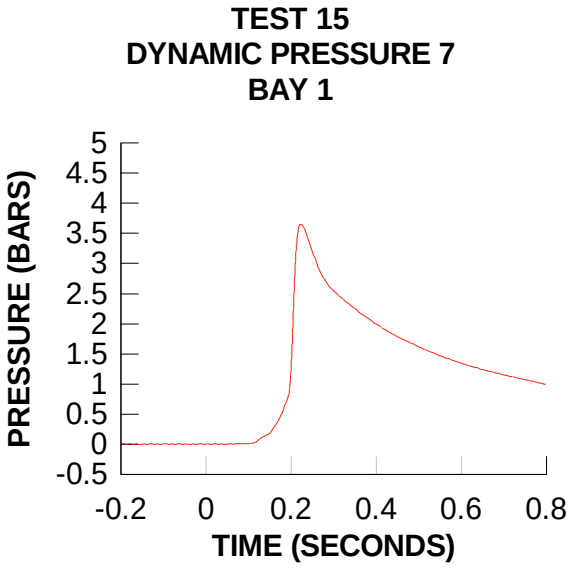
TEST 15
DYNAMIC PRESSURE 7
BAY 1
PRESSURE (BARS)
5
4.5
4
3.5
3
2.5
2
1.5
1
0.5
0
-0.5
-0.2
0
0.2
0.4
0.6
0.8
TIME (SECONDS)

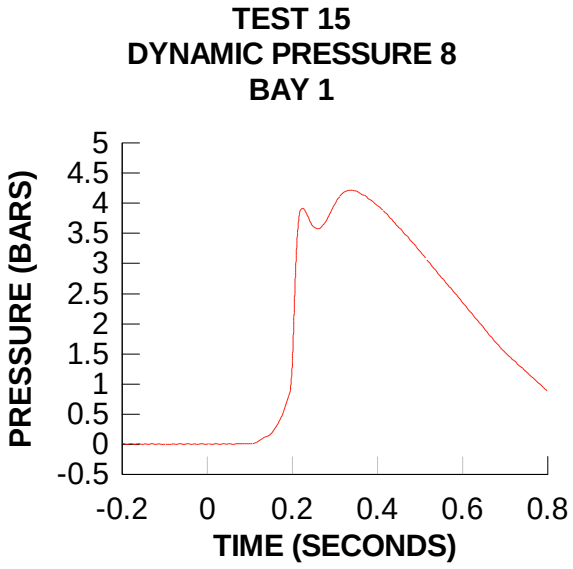
TEST 15
DYNAMIC PRESSURE 8
BAY 1
PRESSURE (BARS)
5
4.5
4
3.5
3
2.5
2
1.5
1
0.5
0
-0.5
-0.2
0
0.2
0.4
0.6
0.8
TIME (SECONDS)

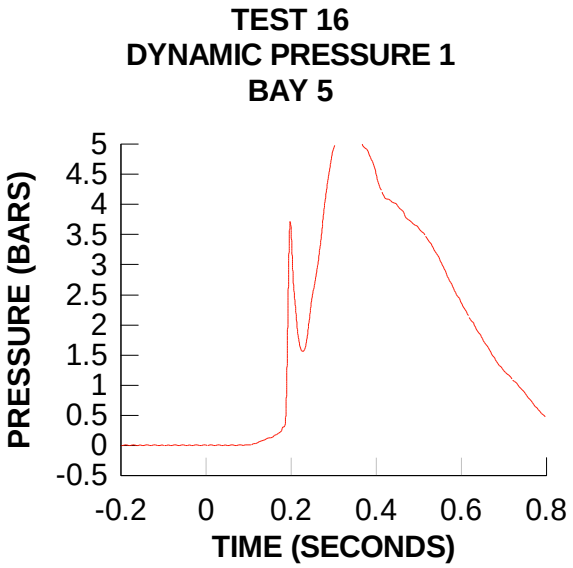
TEST 16
DYNAMIC PRESSURE 1
BAY 5
PRESSURE (BARS)
5
4.5
4
3.5
3
2.5
2
1.5
1
0.5
0
-0.5
-0.2
0
0.2
0.4
0.6
0.8
TIME (SECONDS)

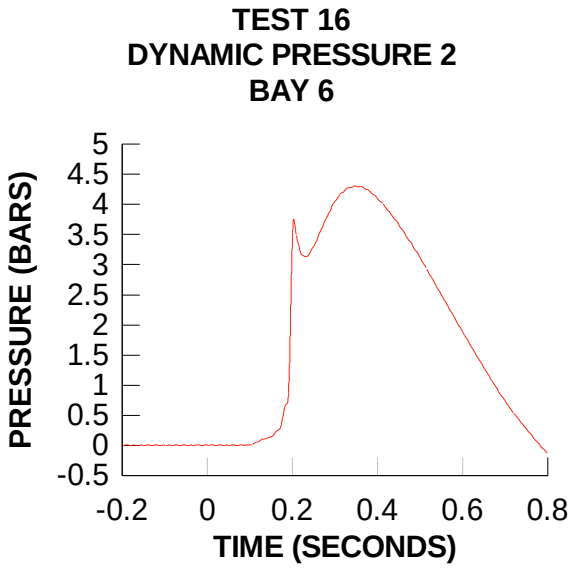
TEST 16
DYNAMIC PRESSURE 2
BAY 6
PRESSURE (BARS)
5
4.5
4
3.5
3
2.5
2
1.5
1
0.5
0
-0.5
-0.2
0
0.2
0.4
0.6
0.8
TIME (SECONDS)

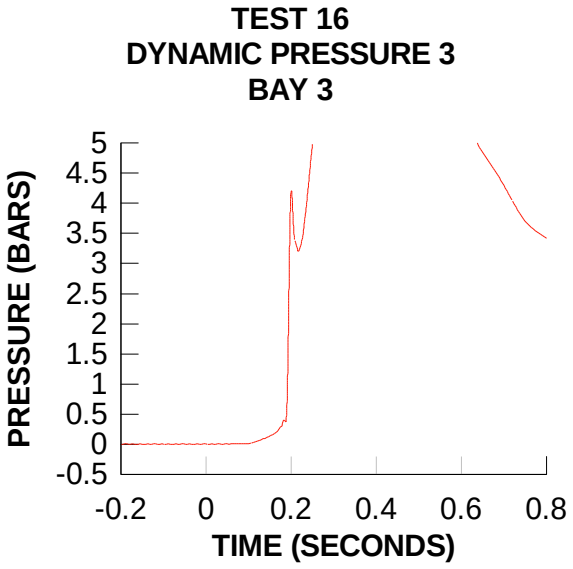
TEST 16
DYNAMIC PRESSURE 3
BAY 3
PRESSURE (BARS)
5
4.5
4
3.5
3
2.5
2
1.5
1
0.5
0
-0.5
-0.2
0
0.2
0.4
0.6
0.8
TIME (SECONDS)

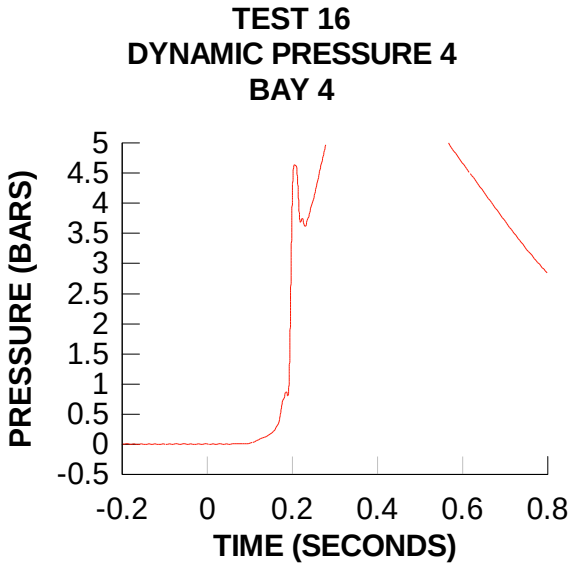
TEST 16
DYNAMIC PRESSURE 4
BAY 4
PRESSURE (BARS)
5
4.5
4
3.5
3
2.5
2
1.5
1
0.5
0
-0.5
-0.2
0
0.2
0.4
0.6
0.8
TIME (SECONDS)

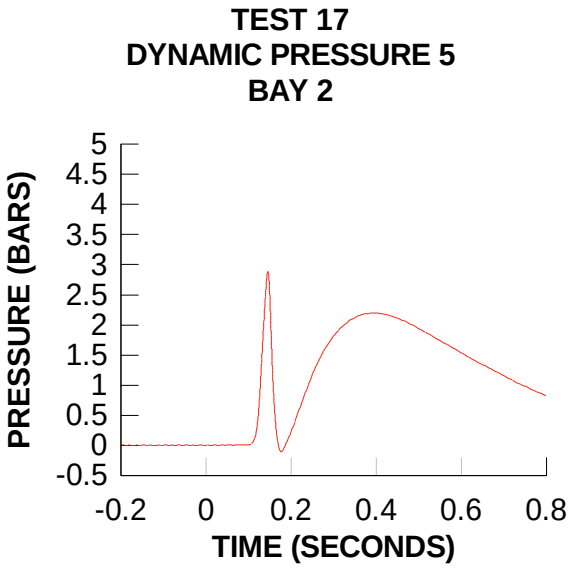
TEST 17
DYNAMIC PRESSURE 5
BAY 2
PRESSURE (BARS)
TIME (SECONDS)
5
4.5
4
3.5
3
2.5
2
1.5
1
0.5
0
-0.5
-0.2
0
0.2
0.4
0.6
0.8

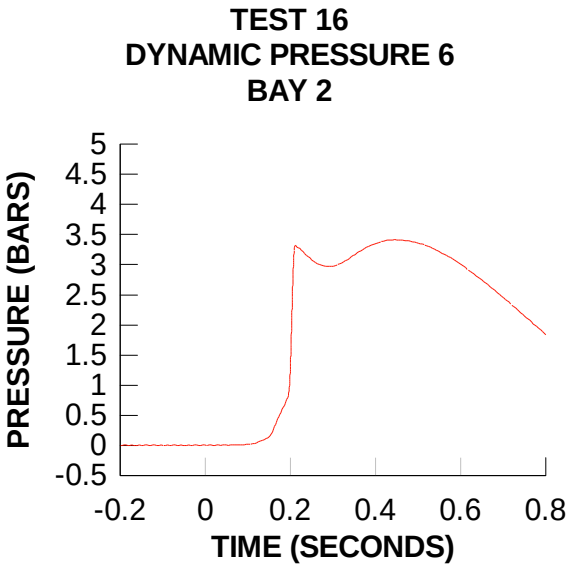
TEST 16
DYNAMIC PRESSURE 6
BAY 2
PRESSURE (BARS)
TIME (SECONDS)
5
4.5
4
3.5
3
2.5
2
1.5
1
0.5
0
-0.5
-0.2
0
0.2
0.4
0.6
0.8

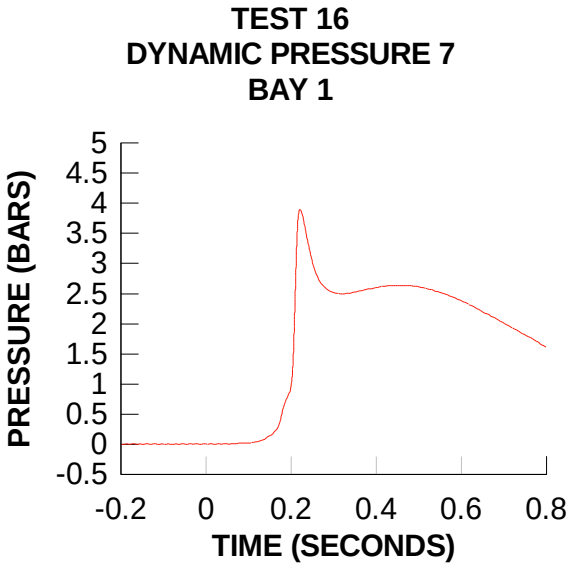
TEST 16
DYNAMIC PRESSURE 7
BAY 1
PRESSURE (BARS)
TIME (SECONDS)
5
4.5
4
3.5
3
2.5
2
1.5
1
0.5
0
-0.5
-0.2
0
0.2
0.4
0.6
0.8

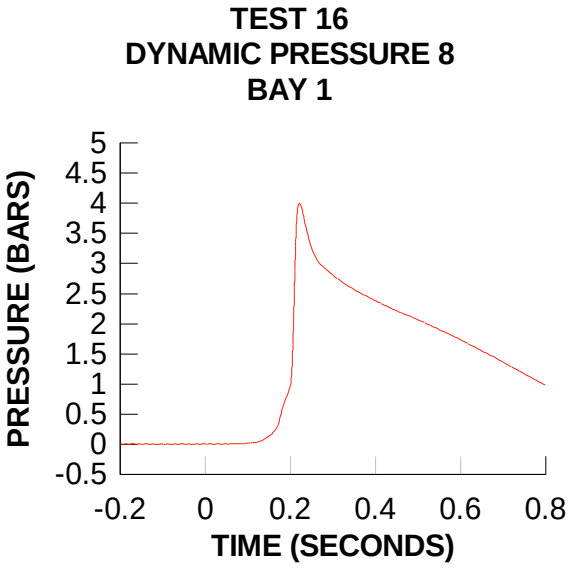
TEST 16
DYNAMIC PRESSURE 8
BAY 1
PRESSURE (BARS)
TIME (SECONDS)
5
4.5
4
3.5
3
2.5
2
1.5
1
0.5
0
-0.5
-0.2
0
0.2
0.4
0.6
0.8

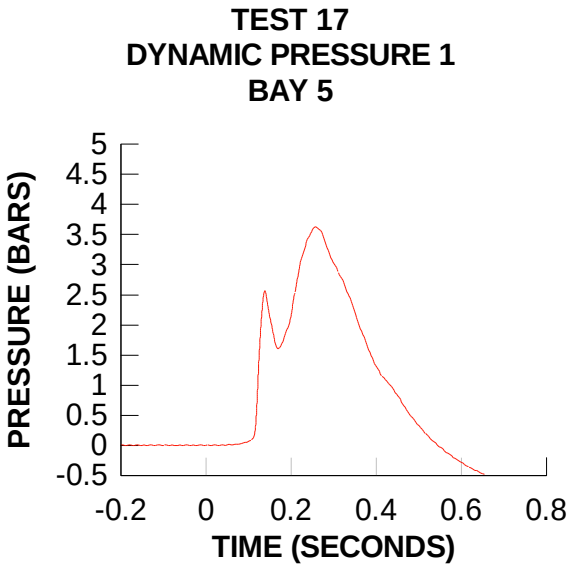
TEST 17
DYNAMIC PRESSURE 1
BAY 5
PRESSURE (BARS)
5
4.5
4
3.5
3
2.5
2
1.5
1
0.5
0
-0.5
-0.2
0
0.2
0.4
0.6
0.8
TIME (SECONDS)

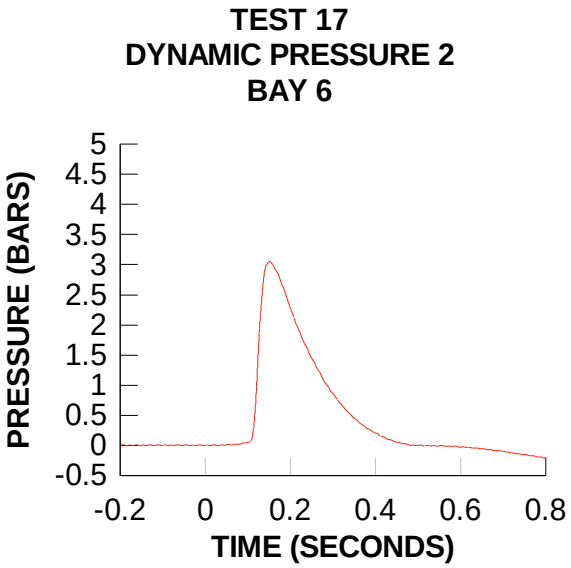
TEST 17
DYNAMIC PRESSURE 2
BAY 6
PRESSURE (BARS)
5
4.5
4
3.5
3
2.5
2
1.5
1
0.5
0
-0.5
-0.2
0
0.2
0.4
0.6
0.8
TIME (SECONDS)

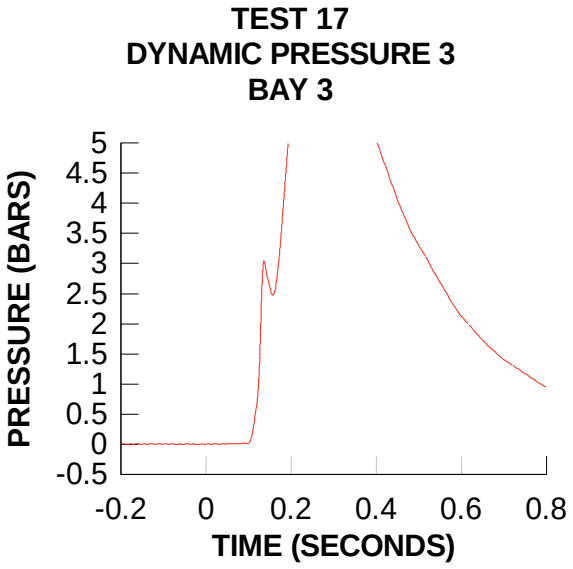
TEST 17
DYNAMIC PRESSURE 3
BAY 3
PRESSURE (BARS)
5
4.5
4
3.5
3
2.5
2
1.5
1
0.5
0
-0.5
-0.2
0
0.2
0.4
0.6
0.8
TIME (SECONDS)

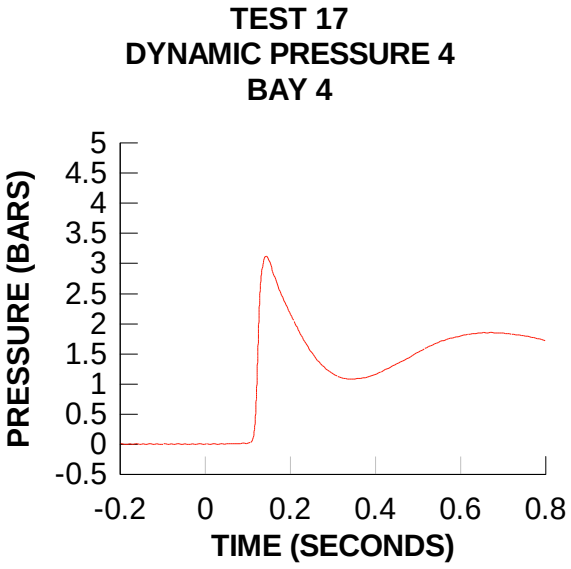
TEST 17
DYNAMIC PRESSURE 4
BAY 4
PRESSURE (BARS)
5
4.5
4
3.5
3
2.5
2
1.5
1
0.5
0
-0.5
-0.2
0
0.2
0.4
0.6
0.8
TIME (SECONDS)

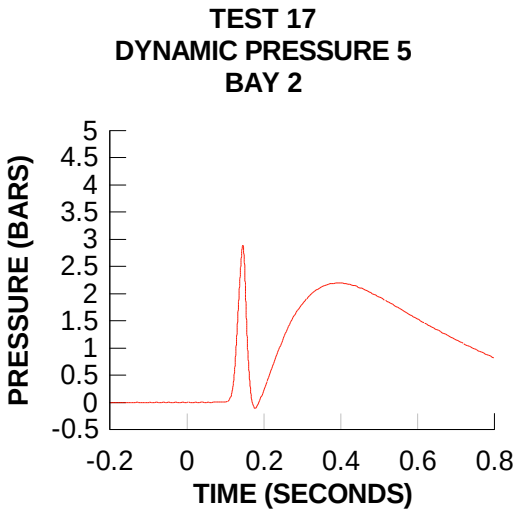
TEST 17
DYNAMIC PRESSURE 5
BAY 2
PRESSURE (BARS)
TIME (SECONDS)

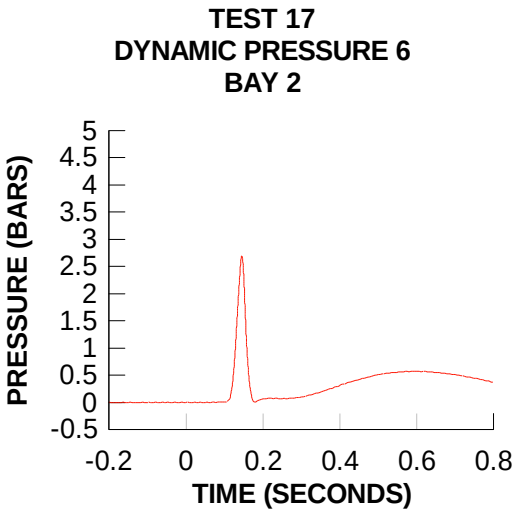
TEST 17
DYNAMIC PRESSURE 6
BAY 2
PRESSURE (BARS)
TIME (SECONDS)

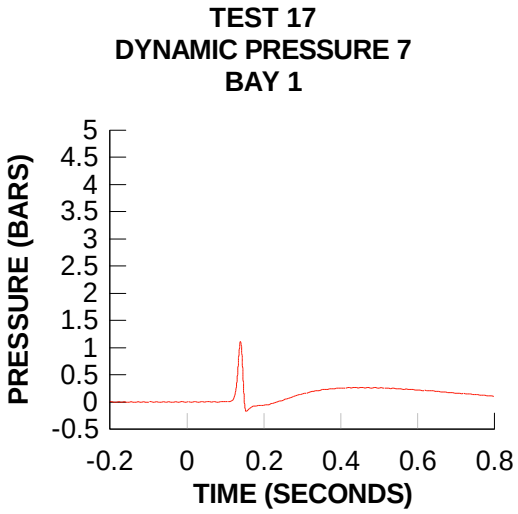
TEST 17
DYNAMIC PRESSURE 7
BAY 1
PRESSURE (BARS)
TIME (SECONDS)

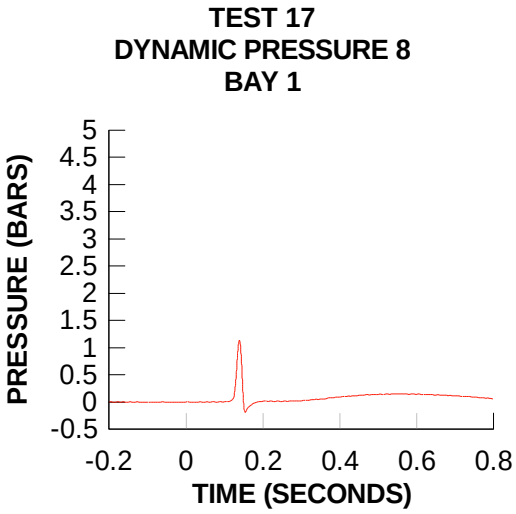
TEST 17
DYNAMIC PRESSURE 8
BAY 1
PRESSURE (BARS)
TIME (SECONDS)

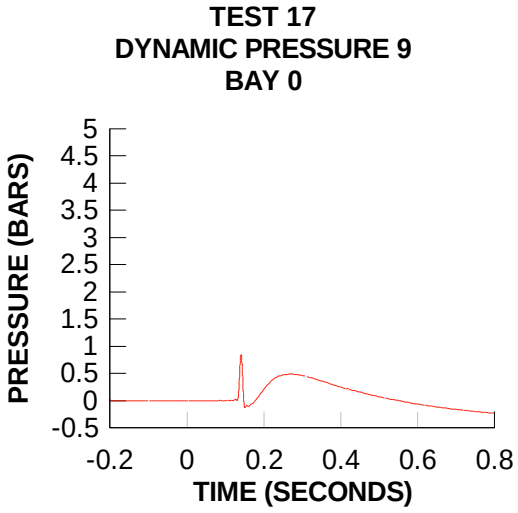
TEST 17
DYNAMIC PRESSURE 9
BAY 0
PRESSURE (BARS)
TIME (SECONDS)

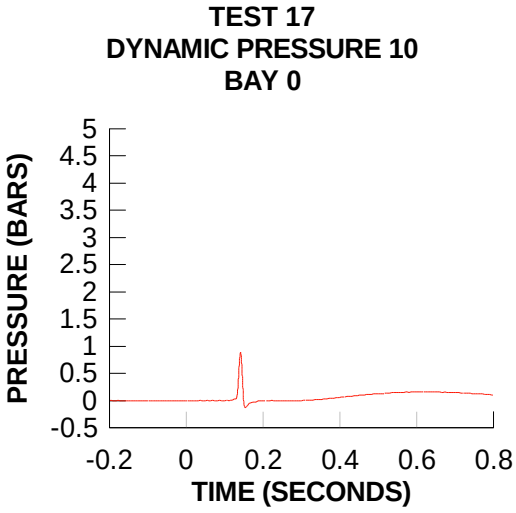
TEST 17
DYNAMIC PRESSURE 10
BAY 0
PRESSURE (BARS)
TIME (SECONDS)

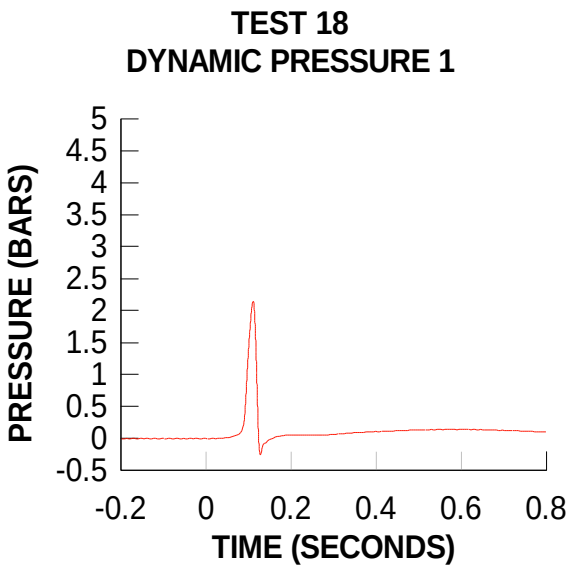
TEST 18
DYNAMIC PRESSURE 1
PRESSURE (BARS)
5
4.5
4
3.5
3
2.5
2
1.5
1
0.5
0
-0.5
-0.2
0
0.2
0.4
0.6
0.8
TIME (SECONDS)

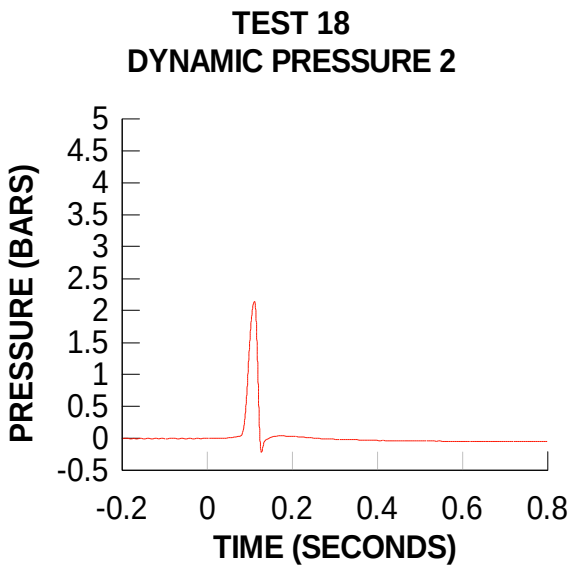
TEST 18
DYNAMIC PRESSURE 2
PRESSURE (BARS)
5
4.5
4
3.5
3
2.5
2
1.5
1
0.5
0
-0.5
-0.2
0
0.2
0.4
0.6
0.8
TIME (SECONDS)

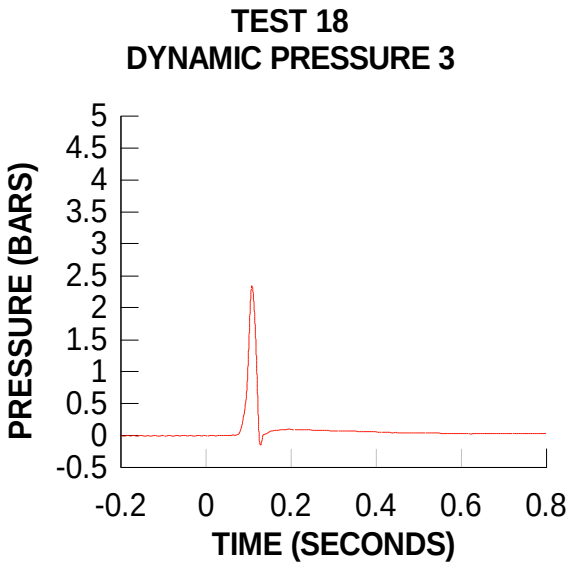
TEST 18
DYNAMIC PRESSURE 3
PRESSURE (BARS)
5
4.5
4
3.5
3
2.5
2
1.5
1
0.5
0
-0.5
-0.2
0
0.2
0.4
0.6
0.8
TIME (SECONDS)

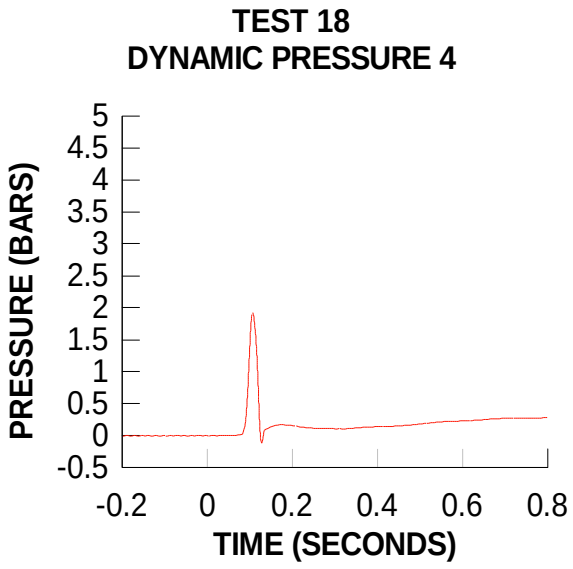
TEST 18
DYNAMIC PRESSURE 4
PRESSURE (BARS)
5
4.5
4
3.5
3
2.5
2
1.5
1
0.5
0
-0.5
-0.2
0
0.2
0.4
0.6
0.8
TIME (SECONDS)

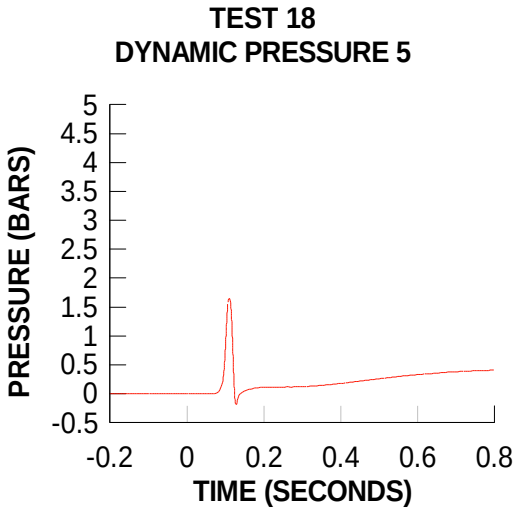
TEST 18
DYNAMIC PRESSURE 5
PRESSURE (BARS)
5
4.5
4
3.5
3
2.5
2
1.5
1
0.5
0
-0.5
-0.2
0
0.2
0.4
0.6
0.8
TIME (SECONDS)

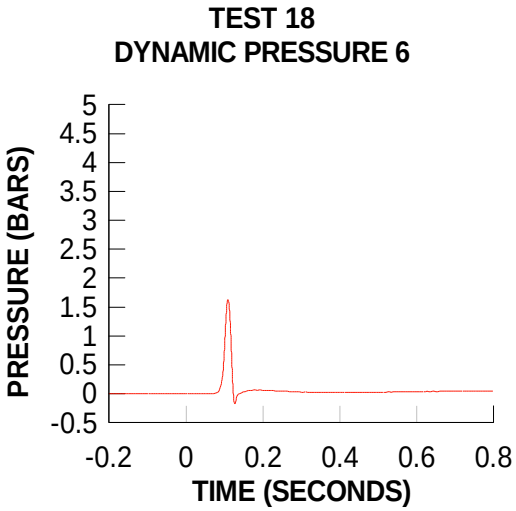
TEST 18
DYNAMIC PRESSURE 6
PRESSURE (BARS)
5
4.5
4
3.5
3
2.5
2
1.5
1
0.5
0
-0.5
-0.2
0
0.2
0.4
0.6
0.8
TIME (SECONDS)

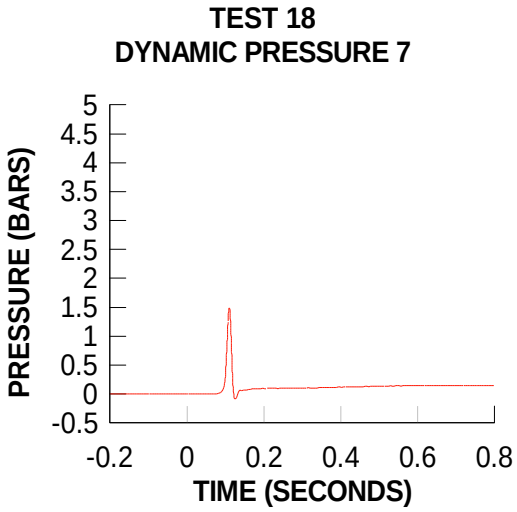
TEST 18
DYNAMIC PRESSURE 7
PRESSURE (BARS)
5
4.5
4
3.5
3
2.5
2
1.5
1
0.5
0
-0.5
-0.2
0
0.2
0.4
0.6
0.8
TIME (SECONDS)

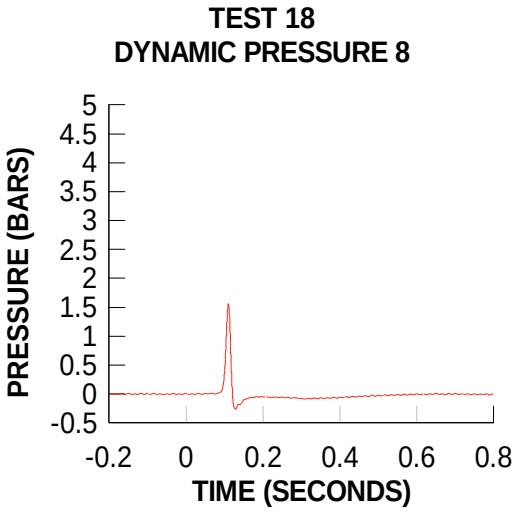
TEST 18
DYNAMIC PRESSURE 8
PRESSURE (BARS)
5
4.5
4
3.5
3
2.5
2
1.5
1
0.5
0
-0.5
-0.2
0
0.2
0.4
0.6
0.8
TIME (SECONDS)

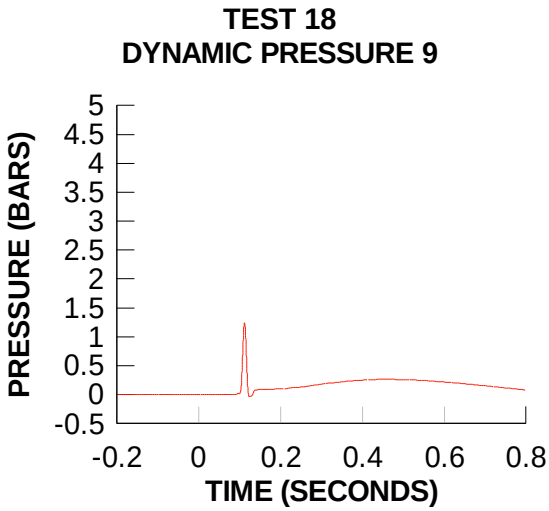
TEST 18
DYNAMIC PRESSURE 9
PRESSURE (BARS)
5
4.5
4
3.5
3
2.5
2
1.5
1
0.5
0
-0.5
-0.2
0
0.2
0.4
0.6
0.8
TIME (SECONDS)

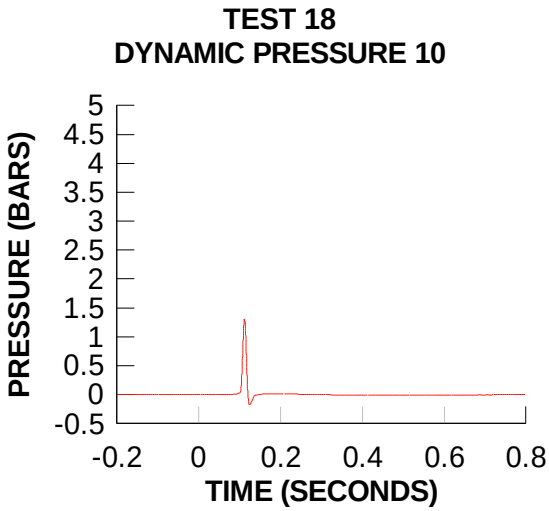
TEST 18
DYNAMIC PRESSURE 10
PRESSURE (BARS)
5
4.5
4
3.5
3
2.5
2
1.5
1
0.5
0
-0.5
-0.2
0
0.2
0.4
0.6
0.8
TIME (SECONDS)

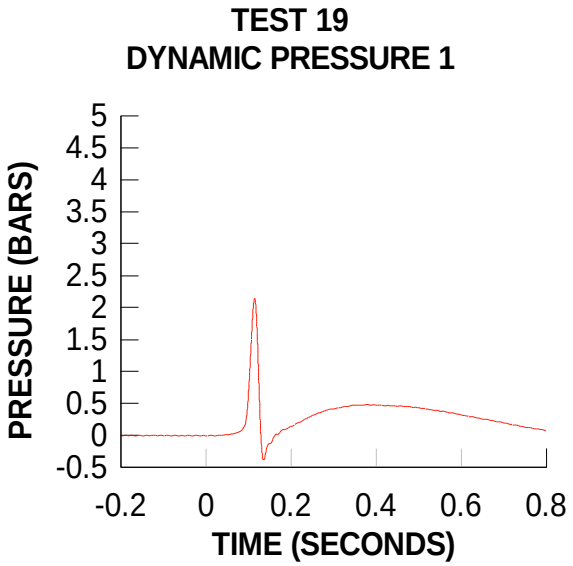
TEST 19
DYNAMIC PRESSURE 1
PRESSURE (BARS)
5
4.5
4
3.5
3
2.5
2
1.5
1
0.5
0
-0.5
-0.2
0
0.2
0.4
0.6
0.8
TIME (SECONDS)

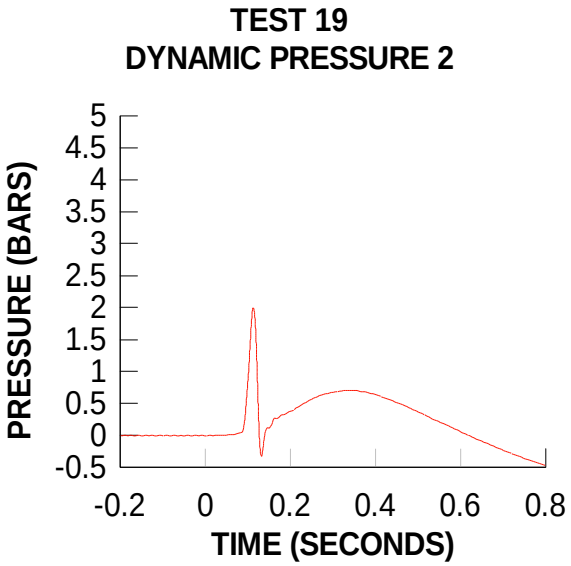
TEST 19
DYNAMIC PRESSURE 2
PRESSURE (BARS)
5
4.5
4
3.5
3
2.5
2
1.5
1
0.5
0
-0.5
-0.2
0
0.2
0.4
0.6
0.8
TIME (SECONDS)

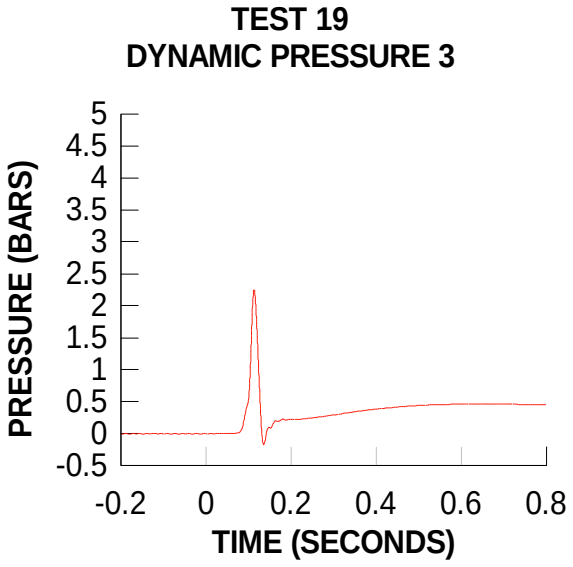
TEST 19
DYNAMIC PRESSURE 3
PRESSURE (BARS)
5
4.5
4
3.5
3
2.5
2
1.5
1
0.5
0
-0.5
-0.2
0
0.2
0.4
0.6
0.8
TIME (SECONDS)

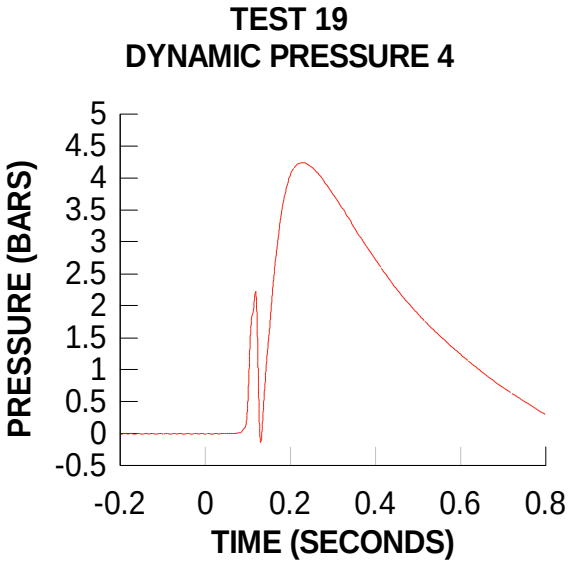
TEST 19
DYNAMIC PRESSURE 4
PRESSURE (BARS)
5
4.5
4
3.5
3
2.5
2
1.5
1
0.5
0
-0.5
-0.2
0
0.2
0.4
0.6
0.8
TIME (SECONDS)

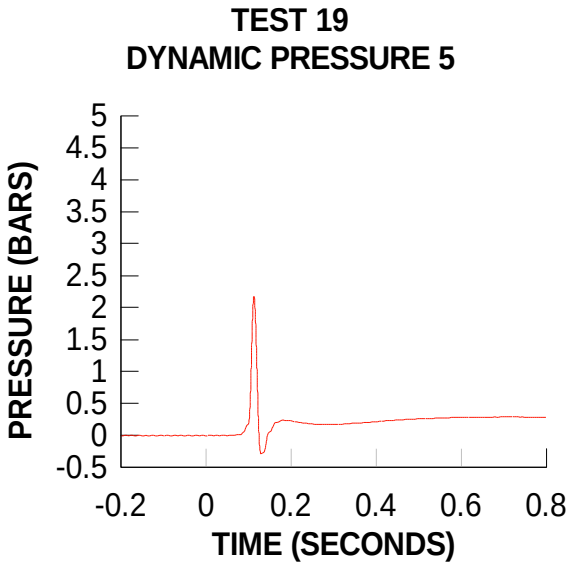
TEST 19
DYNAMIC PRESSURE 5
PRESSURE (BARS)
5
4.5
4
3.5
3
2.5
2
1.5
1
0.5
0
-0.5
-0.2
0
0.2
0.4
0.6
0.8
TIME (SECONDS)

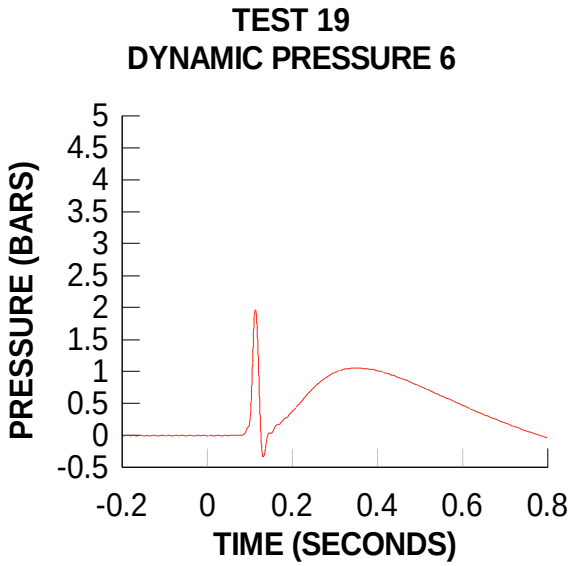
TEST 19
DYNAMIC PRESSURE 6
PRESSURE (BARS)
5
4.5
4
3.5
3
2.5
2
1.5
1
0.5
0
-0.5
-0.2
0
0.2
0.4
0.6
0.8
TIME (SECONDS)

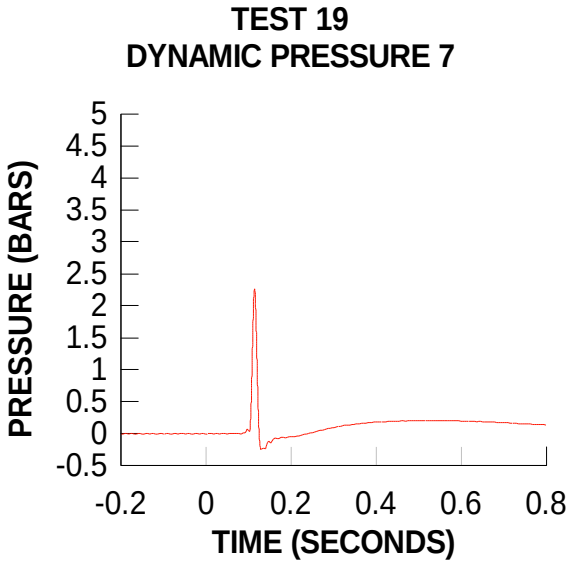
TEST 19
DYNAMIC PRESSURE 7
PRESSURE (BARS)
5
4.5
4
3.5
3
2.5
2
1.5
1
0.5
0
-0.5
-0.2
0
0.2
0.4
0.6
0.8
TIME (SECONDS)

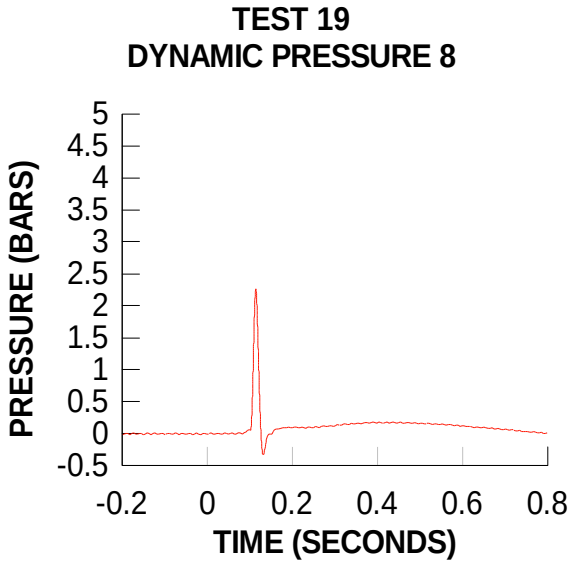
TEST 19
DYNAMIC PRESSURE 8
PRESSURE (BARS)
5
4.5
4
3.5
3
2.5
2
1.5
1
0.5
0
-0.5
-0.2
0
0.2
0.4
0.6
0.8
TIME (SECONDS)

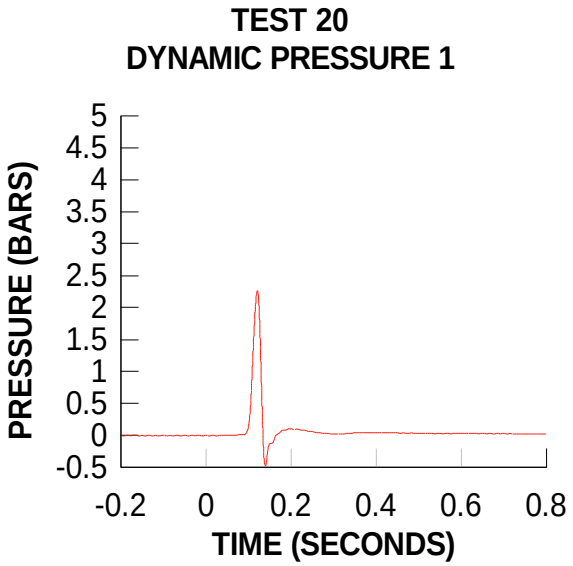
TEST 20
DYNAMIC PRESSURE 1
PRESSURE (BARS)
5
4.5
4
3.5
3
2.5
2
1.5
1
0.5
0
-0.5
-0.2
0
0.2
0.4
0.6
0.8
TIME (SECONDS)

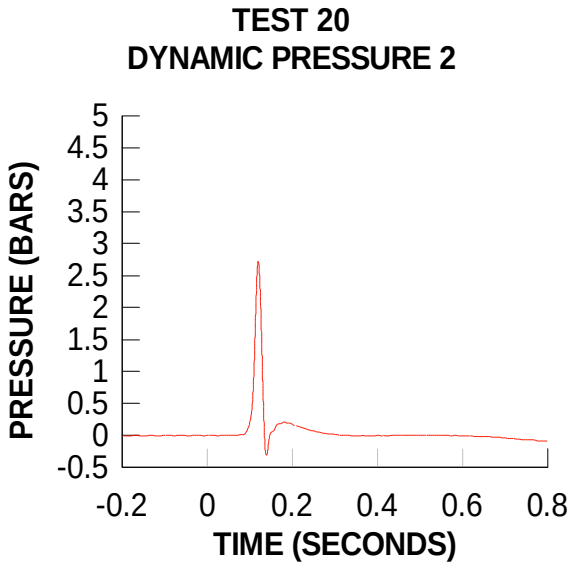
TEST 20
DYNAMIC PRESSURE 2
PRESSURE (BARS)
5
4.5
4
3.5
3
2.5
2
1.5
1
0.5
0
-0.5
-0.2
0
0.2
0.4
0.6
0.8
TIME (SECONDS)

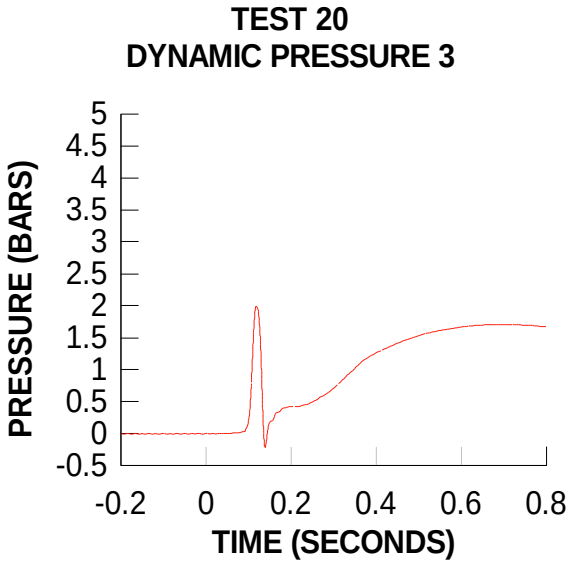
TEST 20
DYNAMIC PRESSURE 3
PRESSURE (BARS)
5
4.5
4
3.5
3
2.5
2
1.5
1
0.5
0
-0.5
-0.2
0
0.2
0.4
0.6
0.8
TIME (SECONDS)

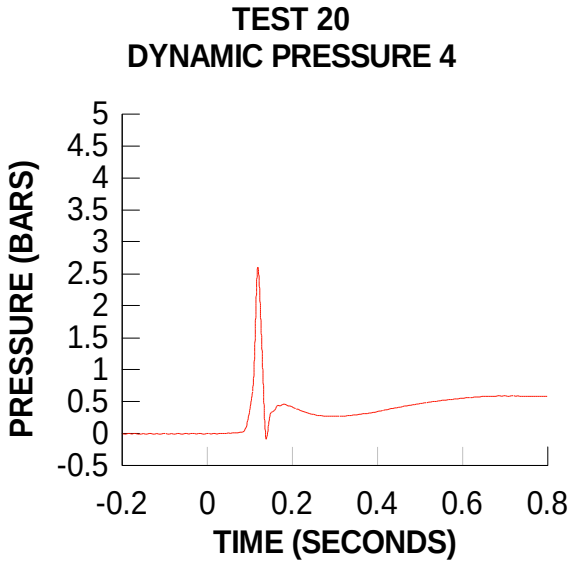
TEST 20
DYNAMIC PRESSURE 4
PRESSURE (BARS)
5
4.5
4
3.5
3
2.5
2
1.5
1
0.5
0
-0.5
-0.2
0
0.2
0.4
0.6
0.8
TIME (SECONDS)

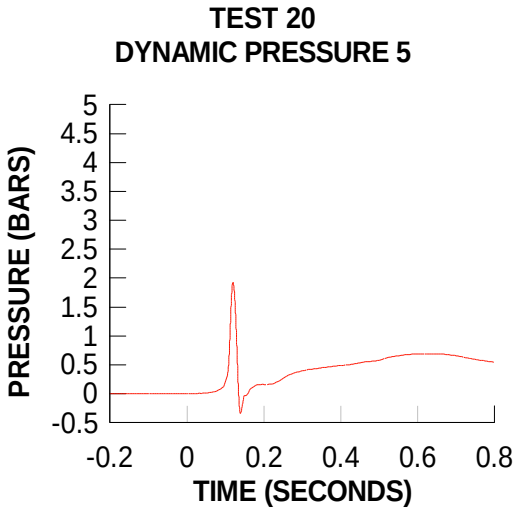
TEST 20
DYNAMIC PRESSURE 5
PRESSURE (BARS)
TIME (SECONDS)

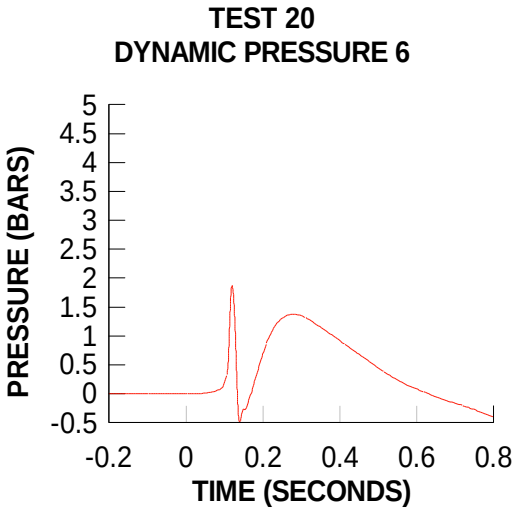
TEST 20
DYNAMIC PRESSURE 6
PRESSURE (BARS)
TIME (SECONDS)

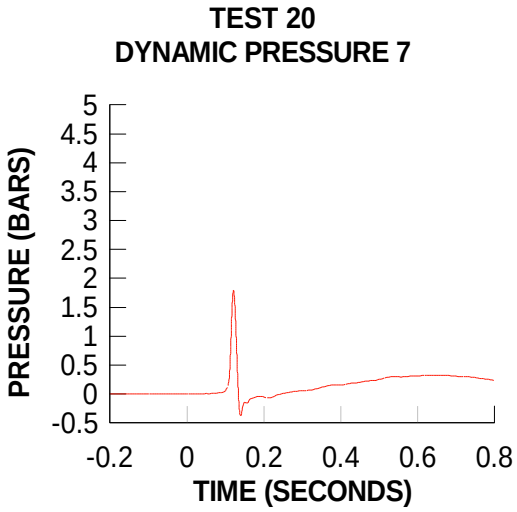
TEST 20
DYNAMIC PRESSURE 7
PRESSURE (BARS)
TIME (SECONDS)

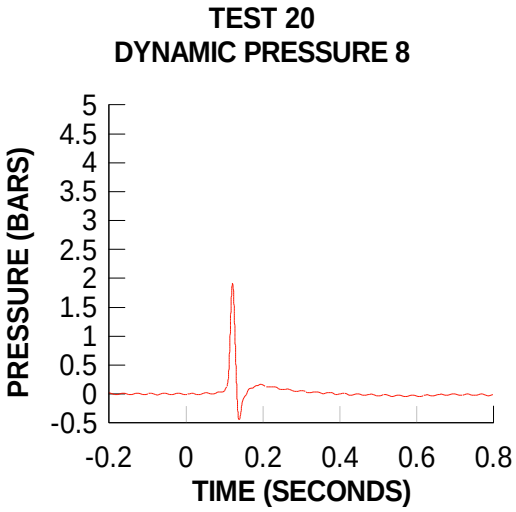
TEST 20
DYNAMIC PRESSURE 8
PRESSURE (BARS)
TIME (SECONDS)

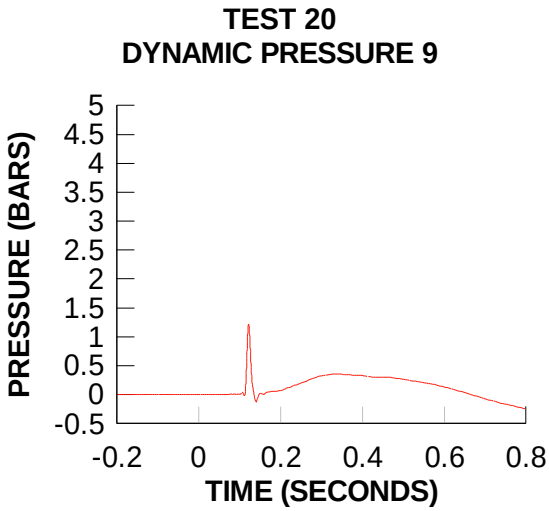
TEST 20
DYNAMIC PRESSURE 9
PRESSURE (BARS)
TIME (SECONDS)

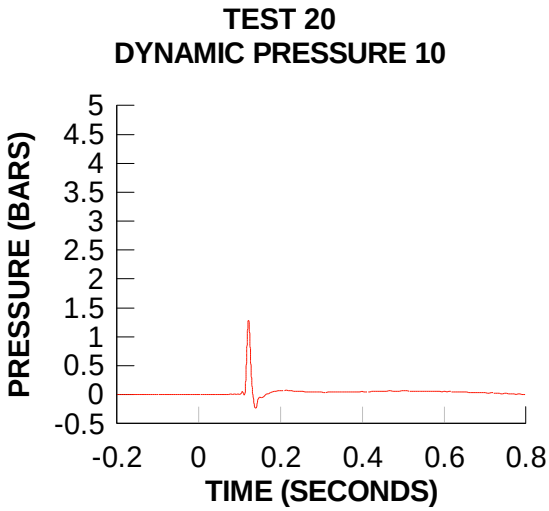
TEST 20
DYNAMIC PRESSURE 10
PRESSURE (BARS)
TIME (SECONDS)

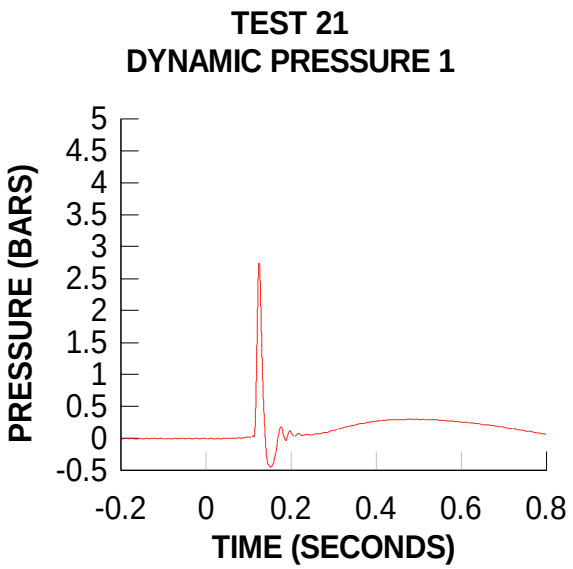
TEST 21
DYNAMIC PRESSURE 1
PRESSURE (BARS)
5
4.5
4
3.5
3
2.5
2
1.5
1
0.5
0
-0.5
-0.2
0
0.2
0.4
0.6
0.8
TIME (SECONDS)

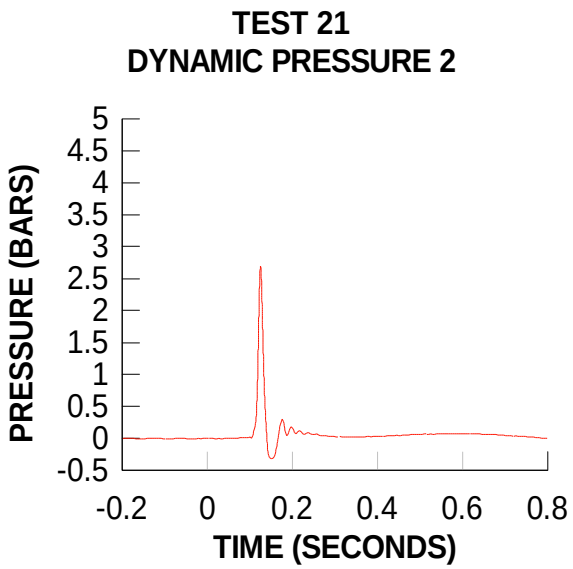
TEST 21
DYNAMIC PRESSURE 2
PRESSURE (BARS)
5
4.5
4
3.5
3
2.5
2
1.5
1
0.5
0
-0.5
-0.2
0
0.2
0.4
0.6
0.8
TIME (SECONDS)

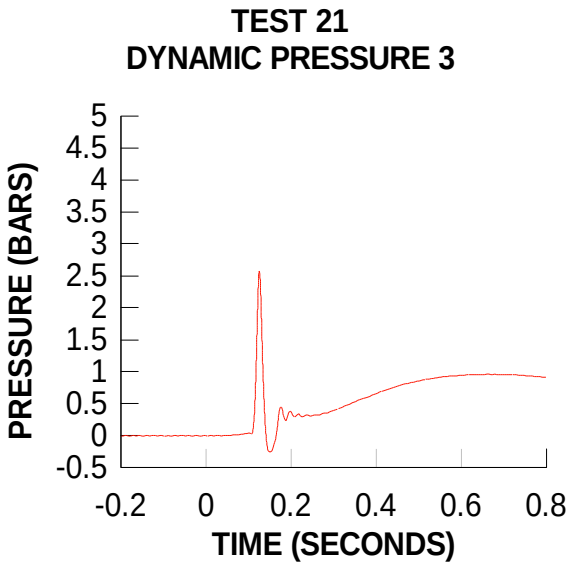
TEST 21
DYNAMIC PRESSURE 3
PRESSURE (BARS)
5
4.5
4
3.5
3
2.5
2
1.5
1
0.5
0
-0.5
-0.2
0
0.2
0.4
0.6
0.8
TIME (SECONDS)

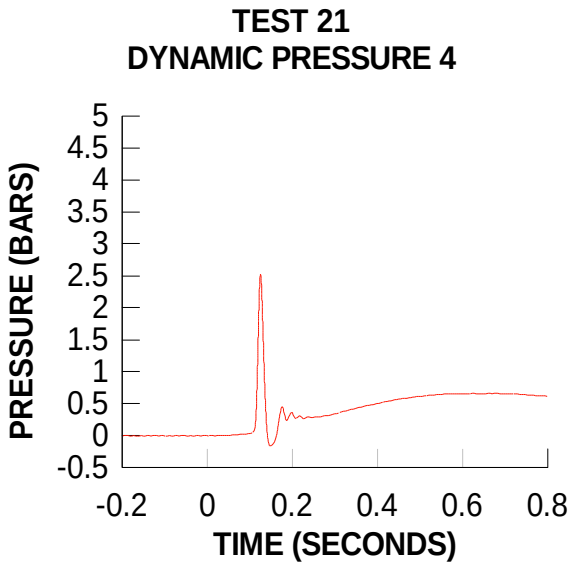
TEST 21
DYNAMIC PRESSURE 4
PRESSURE (BARS)
5
4.5
4
3.5
3
2.5
2
1.5
1
0.5
0
-0.5
-0.2
0
0.2
0.4
0.6
0.8
TIME (SECONDS)

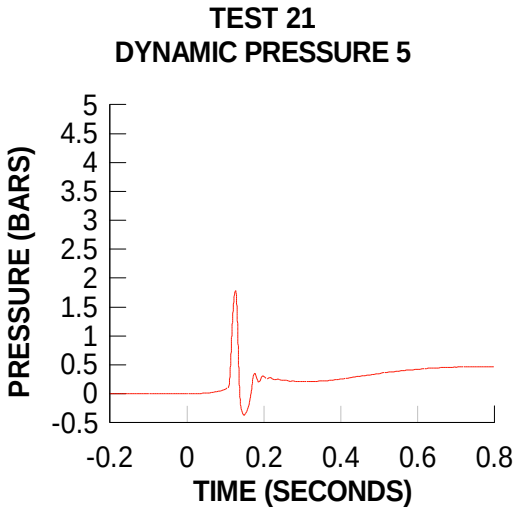
TEST 21
DYNAMIC PRESSURE 5
PRESSURE (BARS)
5
4.5
4
3.5
3
2.5
2
1.5
1
0.5
0
-0.5
-0.2
0
0.2
0.4
0.6
0.8
TIME (SECONDS)

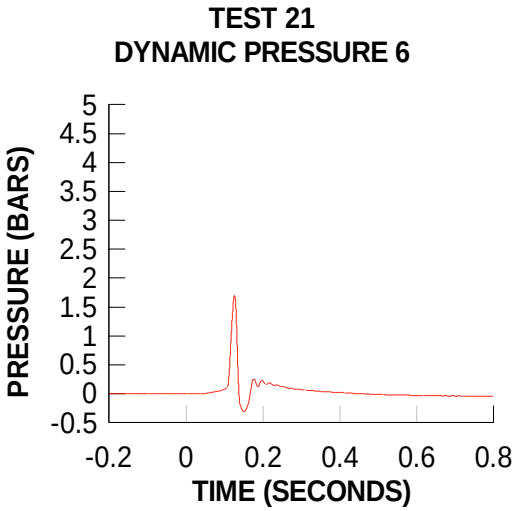
TEST 21
DYNAMIC PRESSURE 6
PRESSURE (BARS)
5
4.5
4
3.5
3
2.5
2
1.5
1
0.5
0
-0.5
-0.2
0
0.2
0.4
0.6
0.8
TIME (SECONDS)

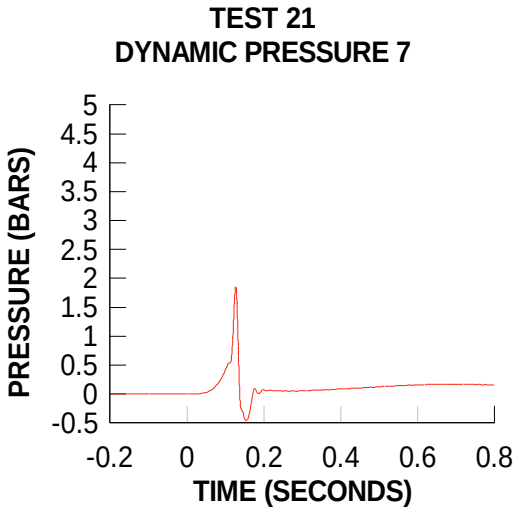
TEST 21
DYNAMIC PRESSURE 7
PRESSURE (BARS)
5
4.5
4
3.5
3
2.5
2
1.5
1
0.5
0
-0.5
-0.2
0
0.2
0.4
0.6
0.8
TIME (SECONDS)

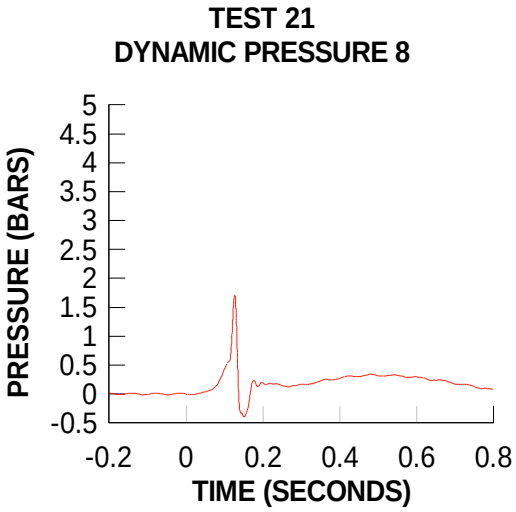
TEST 21
DYNAMIC PRESSURE 8
PRESSURE (BARS)
5
4.5
4
3.5
3
2.5
2
1.5
1
0.5
0
-0.5
-0.2
0
0.2
0.4
0.6
0.8
TIME (SECONDS)

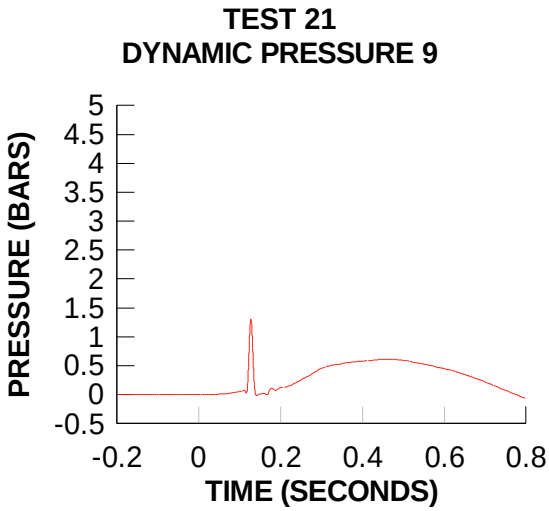
TEST 21
DYNAMIC PRESSURE 9
PRESSURE (BARS)
5
4.5
4
3.5
3
2.5
2
1.5
1
0.5
0
-0.5
-0.2
0
0.2
0.4
0.6
0.8
TIME (SECONDS)

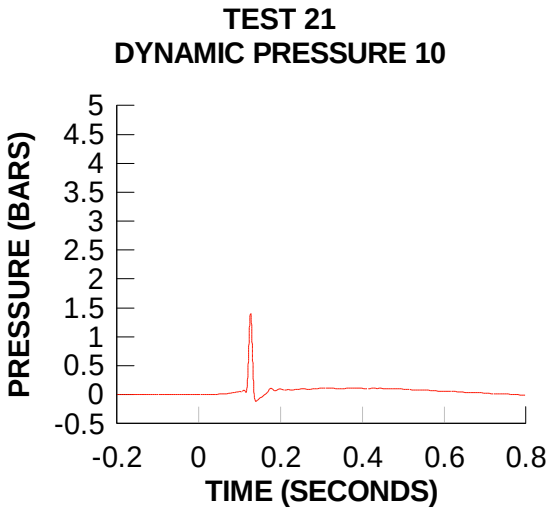
TEST 21
DYNAMIC PRESSURE 10
PRESSURE (BARS)
5
4.5
4
3.5
3
2.5
2
1.5
1
0.5
0
-0.5
-0.2
0
0.2
0.4
0.6
0.8
TIME (SECONDS)

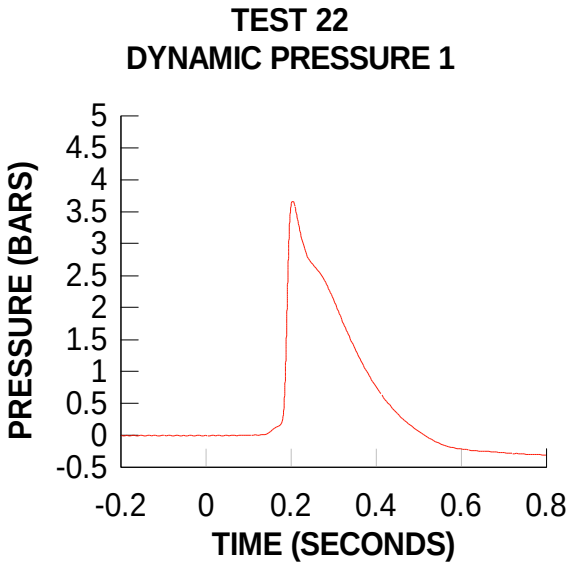
TEST 22
DYNAMIC PRESSURE 1
PRESSURE (BARS)
5
4.5
4
3.5
3
2.5
2
1.5
1
0.5
0
-0.5
-0.2
0
0.2
0.4
0.6
0.8
TIME (SECONDS)

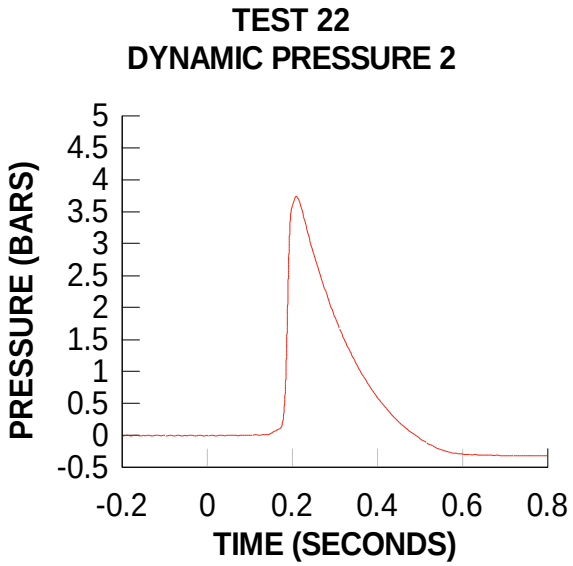
TEST 22
DYNAMIC PRESSURE 2
PRESSURE (BARS)
5
4.5
4
3.5
3
2.5
2
1.5
1
0.5
0
-0.5
-0.2
0
0.2
0.4
0.6
0.8
TIME (SECONDS)

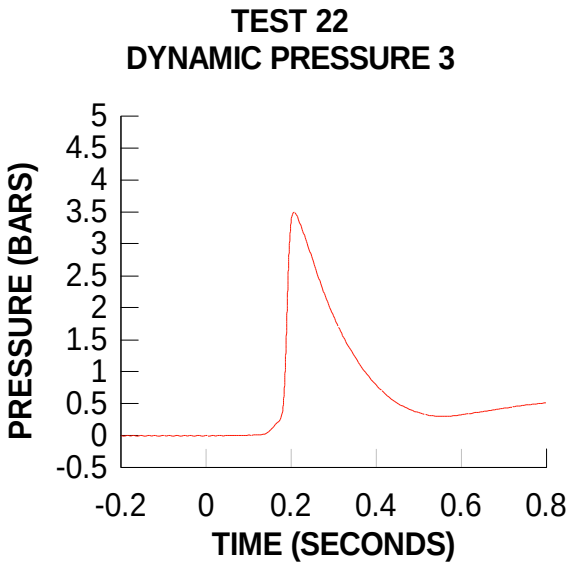
TEST 22
DYNAMIC PRESSURE 3
PRESSURE (BARS)
5
4.5
4
3.5
3
2.5
2
1.5
1
0.5
0
-0.5
-0.2
0
0.2
0.4
0.6
0.8
TIME (SECONDS)

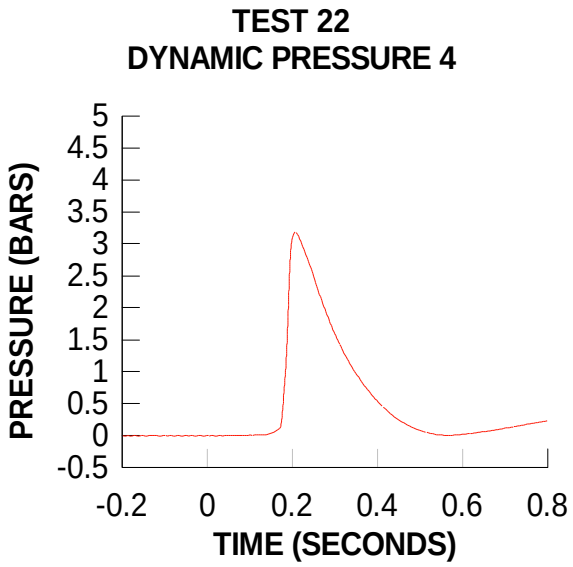
TEST 22
DYNAMIC PRESSURE 4
PRESSURE (BARS)
5
4.5
4
3.5
3
2.5
2
1.5
1
0.5
0
-0.5
-0.2
0
0.2
0.4
0.6
0.8
TIME (SECONDS)

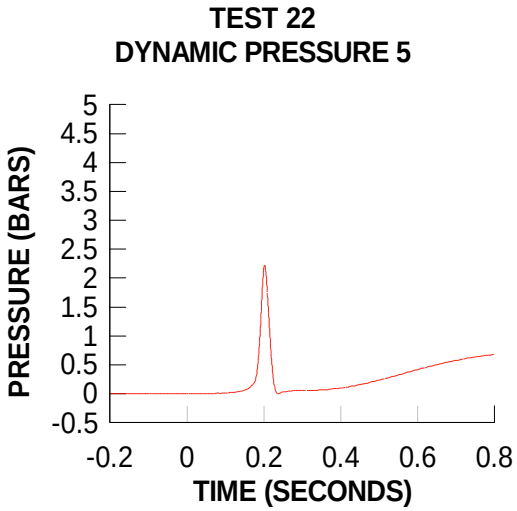
TEST 22
DYNAMIC PRESSURE 5
PRESSURE (BARS)
TIME (SECONDS)

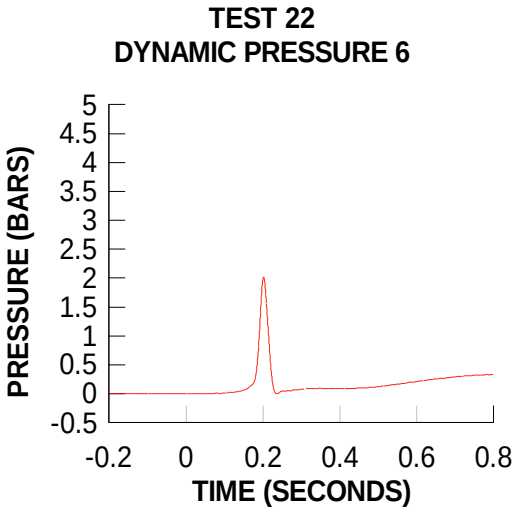
TEST 22
DYNAMIC PRESSURE 6
PRESSURE (BARS)
TIME (SECONDS)

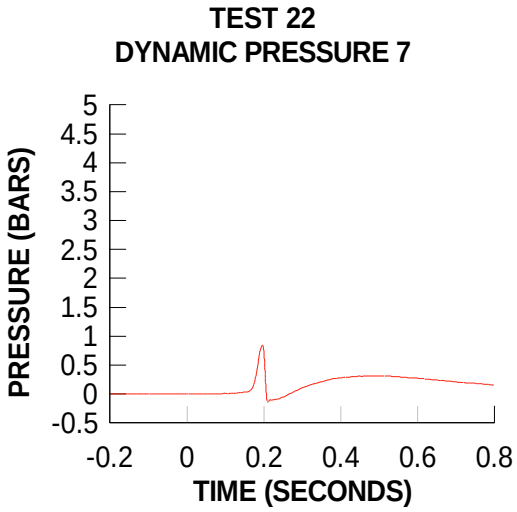
TEST 22
DYNAMIC PRESSURE 7
PRESSURE (BARS)
TIME (SECONDS)

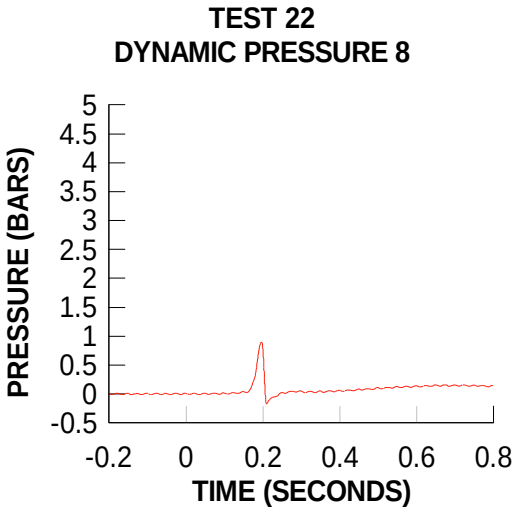
TEST 22
DYNAMIC PRESSURE 8
PRESSURE (BARS)
TIME (SECONDS)

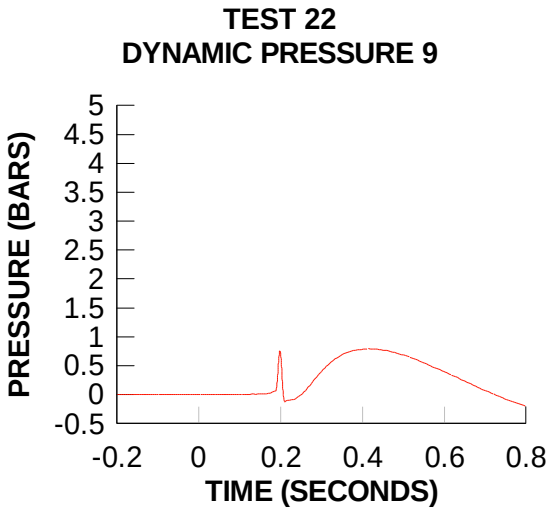
TEST 22
DYNAMIC PRESSURE 9
PRESSURE (BARS)
TIME (SECONDS)

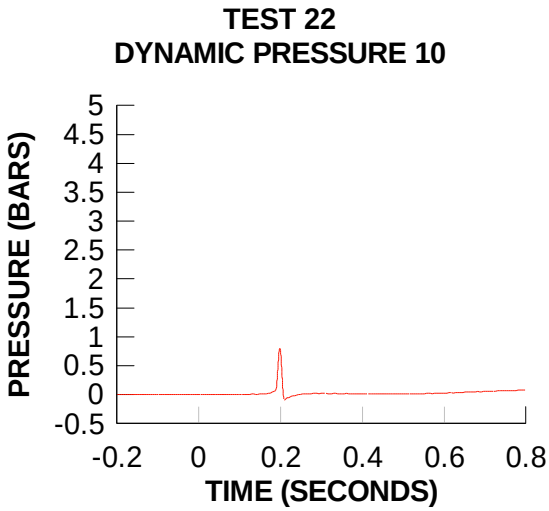
TEST 22
DYNAMIC PRESSURE 10
PRESSURE (BARS)
TIME (SECONDS)

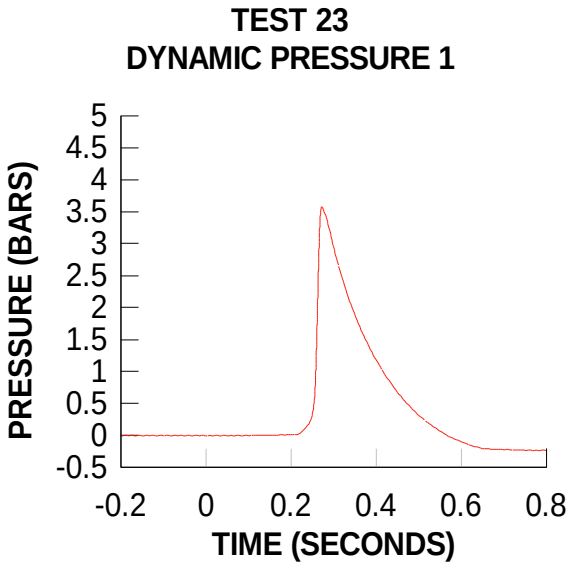
TEST 23
DYNAMIC PRESSURE 1
PRESSURE (BARS)
5
4.5
4
3.5
3
2.5
2
1.5
1
0.5
0
-0.5
-0.2
0
0.2
0.4
0.6
0.8
TIME (SECONDS)

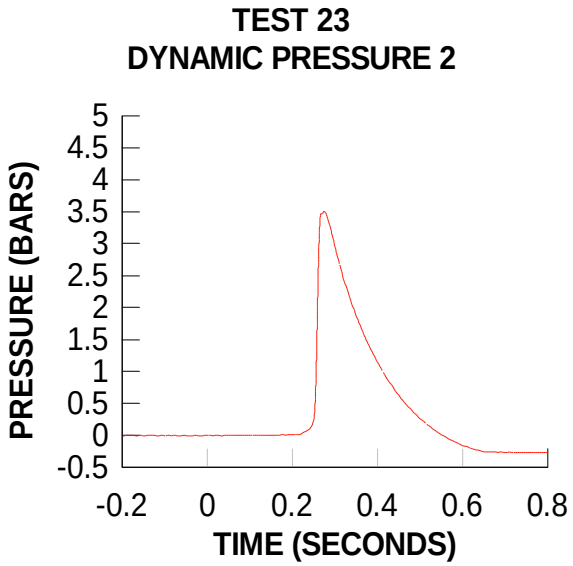
TEST 23
DYNAMIC PRESSURE 2
PRESSURE (BARS)
5
4.5
4
3.5
3
2.5
2
1.5
1
0.5
0
-0.5
-0.2
0
0.2
0.4
0.6
0.8
TIME (SECONDS)

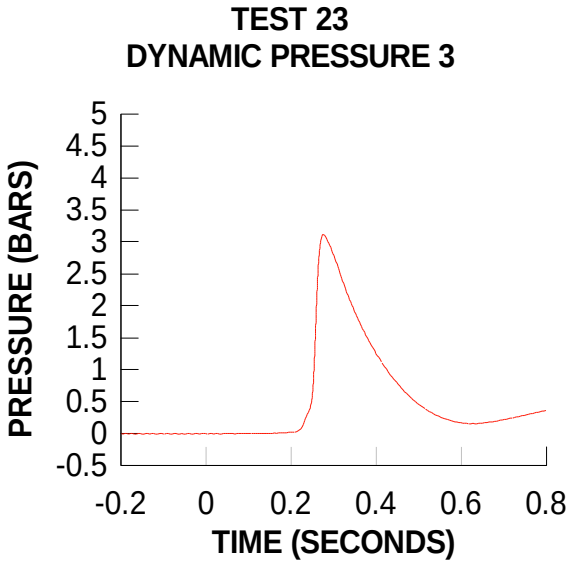
TEST 23
DYNAMIC PRESSURE 3
PRESSURE (BARS)
5
4.5
4
3.5
3
2.5
2
1.5
1
0.5
0
-0.5
-0.2
0
0.2
0.4
0.6
0.8
TIME (SECONDS)

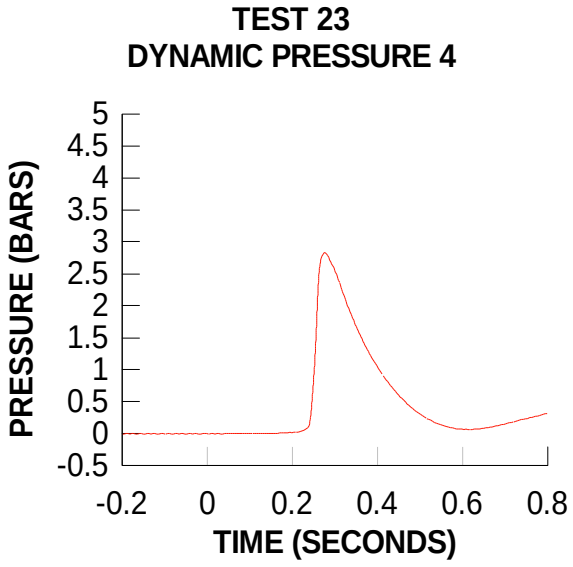
TEST 23
DYNAMIC PRESSURE 4
PRESSURE (BARS)
5
4.5
4
3.5
3
2.5
2
1.5
1
0.5
0
-0.5
-0.2
0
0.2
0.4
0.6
0.8
TIME (SECONDS)

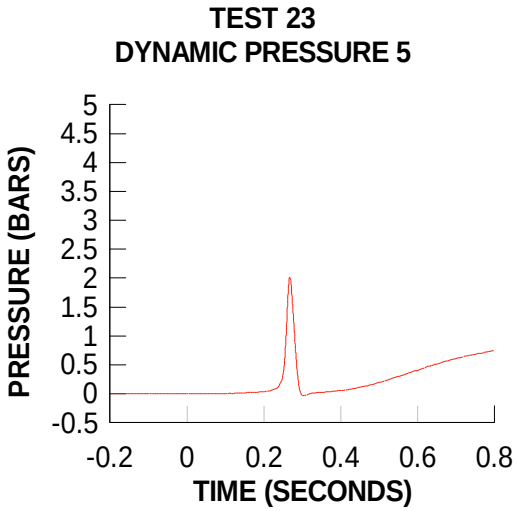
TEST 23
DYNAMIC PRESSURE 5
PRESSURE (BARS)
TIME (SECONDS)

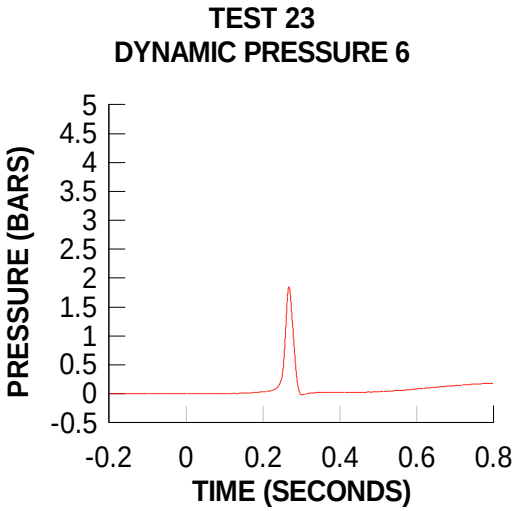
TEST 23
DYNAMIC PRESSURE 6
PRESSURE (BARS)
TIME (SECONDS)

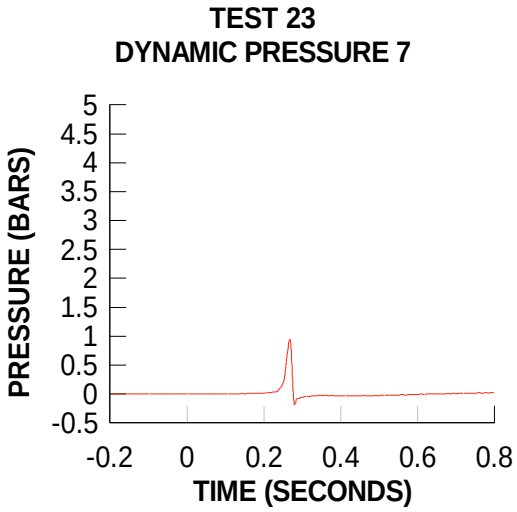
TEST 23
DYNAMIC PRESSURE 7
PRESSURE (BARS)
TIME (SECONDS)

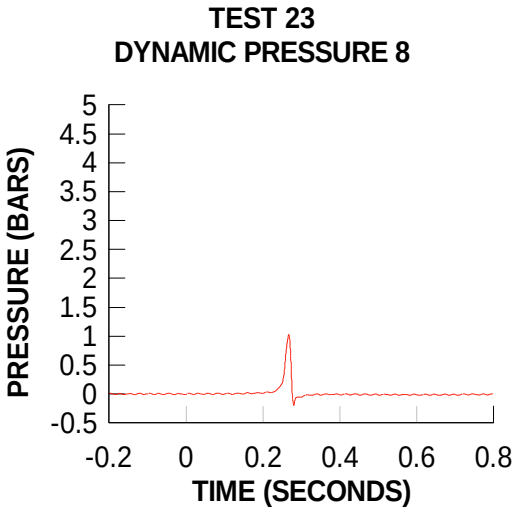
TEST 23
DYNAMIC PRESSURE 8
PRESSURE (BARS)
TIME (SECONDS)

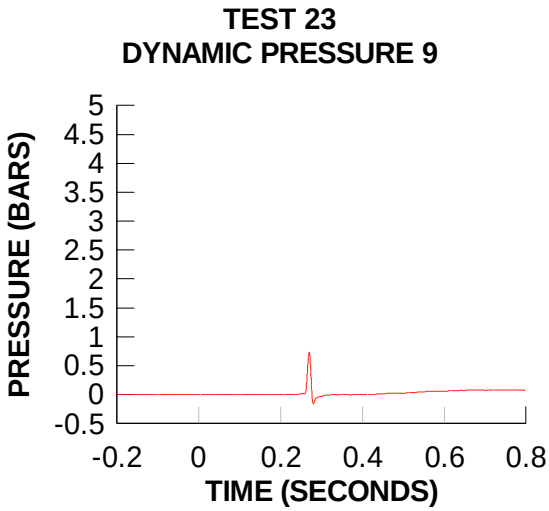
TEST 23
DYNAMIC PRESSURE 9
PRESSURE (BARS)
TIME (SECONDS)

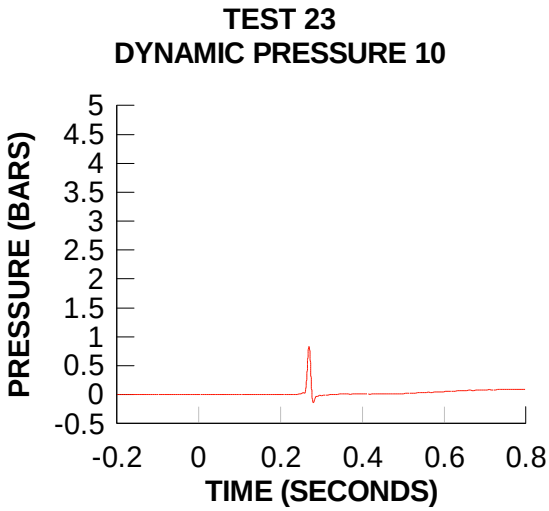
TEST 23
DYNAMIC PRESSURE 10
PRESSURE (BARS)
TIME (SECONDS)

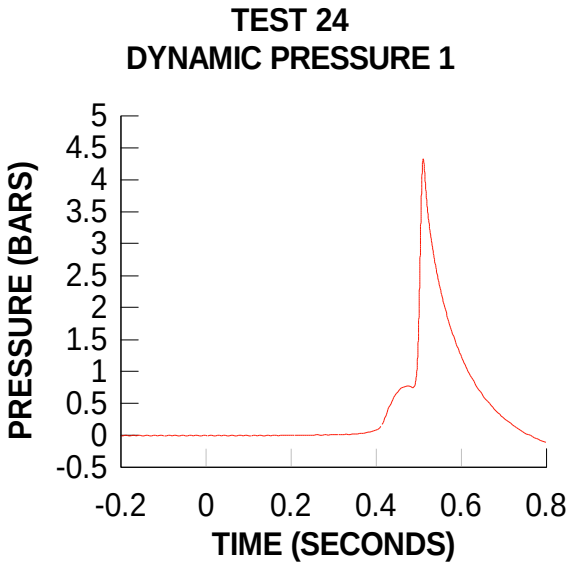
TEST 24
DYNAMIC PRESSURE 1
PRESSURE (BARS)
5
4.5
4
3.5
3
2.5
2
1.5
1
0.5
0
-0.5
-0.2
0
0.2
0.4
0.6
0.8
TIME (SECONDS)

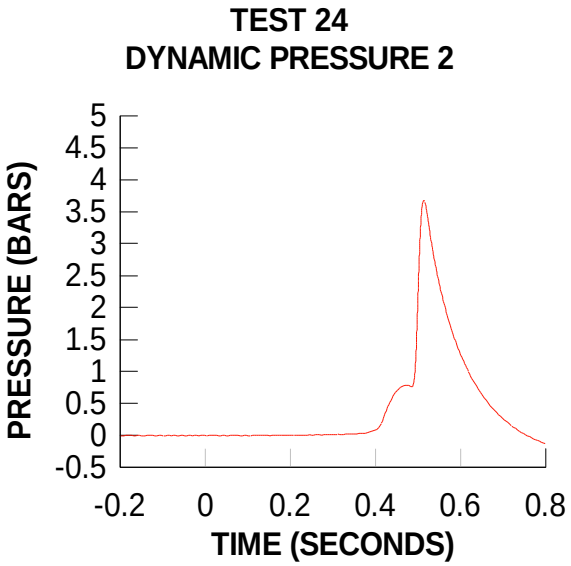
TEST 24
DYNAMIC PRESSURE 2
PRESSURE (BARS)
5
4.5
4
3.5
3
2.5
2
1.5
1
0.5
0
-0.5
-0.2
0
0.2
0.4
0.6
0.8
TIME (SECONDS)

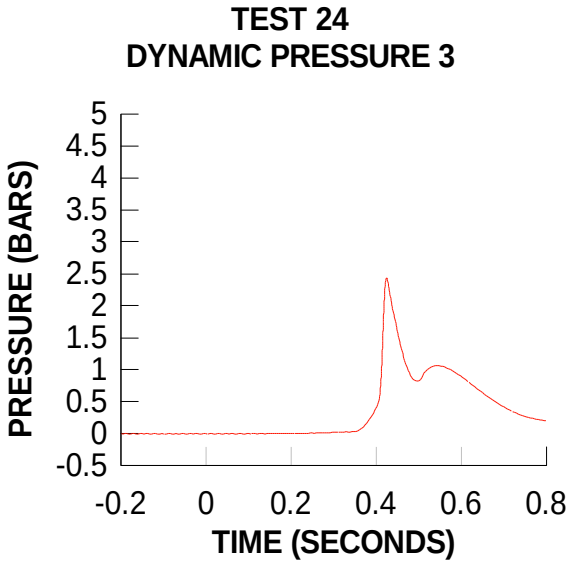
TEST 24
DYNAMIC PRESSURE 3
PRESSURE (BARS)
5
4.5
4
3.5
3
2.5
2
1.5
1
0.5
0
-0.5
-0.2
0
0.2
0.4
0.6
0.8
TIME (SECONDS)

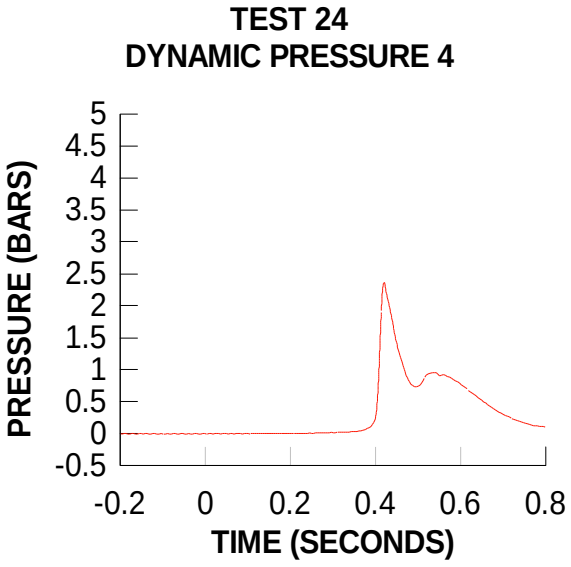
TEST 24
DYNAMIC PRESSURE 4
PRESSURE (BARS)
5
4.5
4
3.5
3
2.5
2
1.5
1
0.5
0
-0.5
-0.2
0
0.2
0.4
0.6
0.8
TIME (SECONDS)

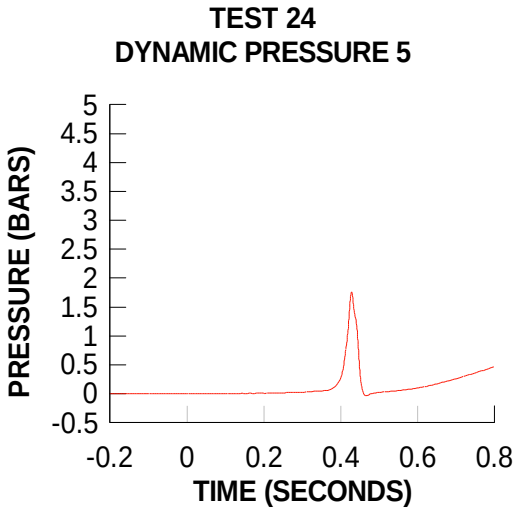
TEST 24
DYNAMIC PRESSURE 5
PRESSURE (BARS)
TIME (SECONDS)

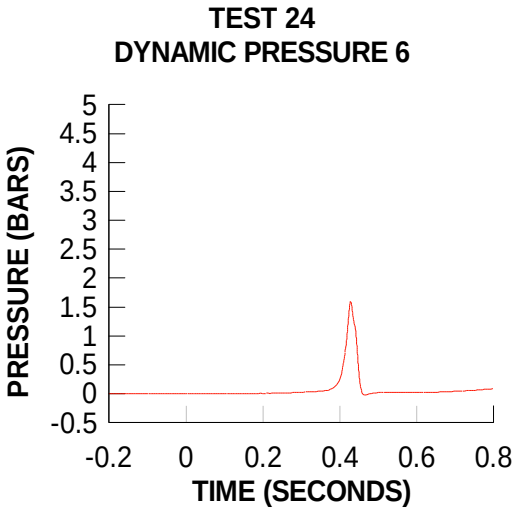
TEST 24
DYNAMIC PRESSURE 6
PRESSURE (BARS)
TIME (SECONDS)

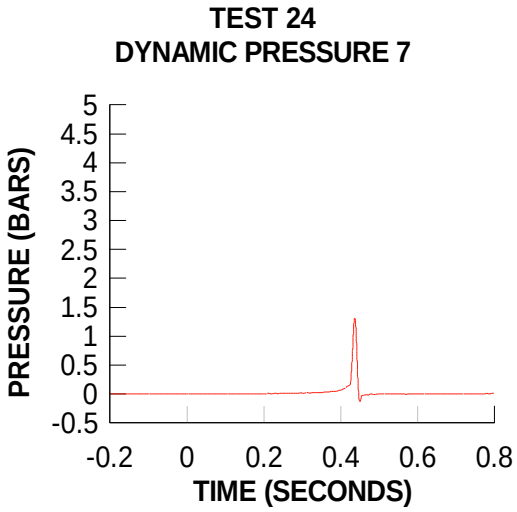
TEST 24
DYNAMIC PRESSURE 7
PRESSURE (BARS)
TIME (SECONDS)

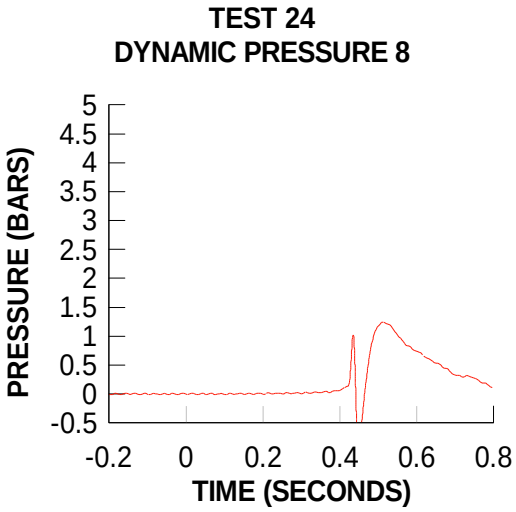
TEST 24
DYNAMIC PRESSURE 8
PRESSURE (BARS)
TIME (SECONDS)

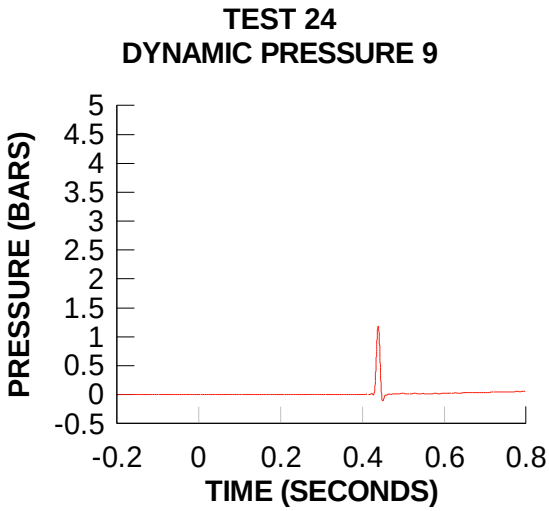
TEST 24
DYNAMIC PRESSURE 9
PRESSURE (BARS)
TIME (SECONDS)

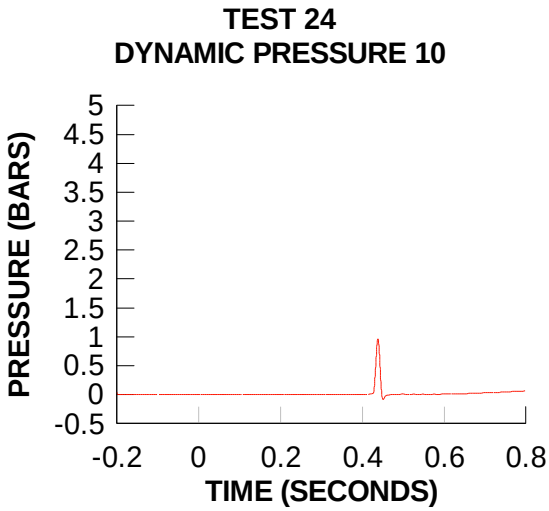
TEST 24
DYNAMIC PRESSURE 10
PRESSURE (BARS)
TIME (SECONDS)

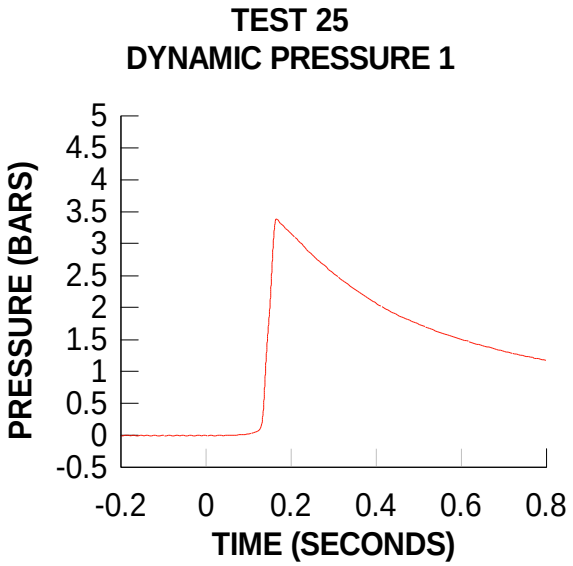
TEST 25
DYNAMIC PRESSURE 1
PRESSURE (BARS)
5
4.5
4
3.5
3
2.5
2
1.5
1
0.5
0
-0.5
-0.2
0
0.2
0.4
0.6
0.8
TIME (SECONDS)

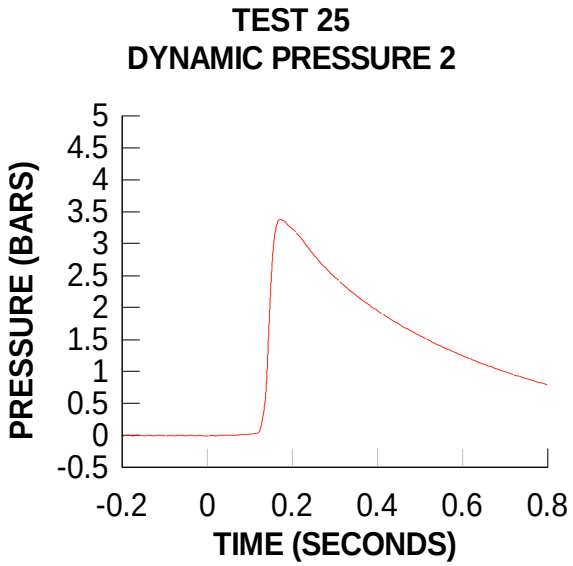
TEST 25
DYNAMIC PRESSURE 2
PRESSURE (BARS)
5
4.5
4
3.5
3
2.5
2
1.5
1
0.5
0
-0.5
-0.2
0
0.2
0.4
0.6
0.8
TIME (SECONDS)

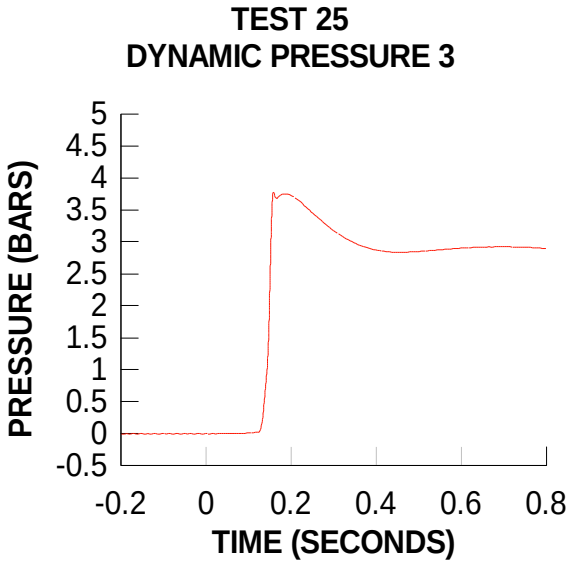
TEST 25
DYNAMIC PRESSURE 3
PRESSURE (BARS)
5
4.5
4
3.5
3
2.5
2
1.5
1
0.5
0
-0.5
-0.2
0
0.2
0.4
0.6
0.8
TIME (SECONDS)

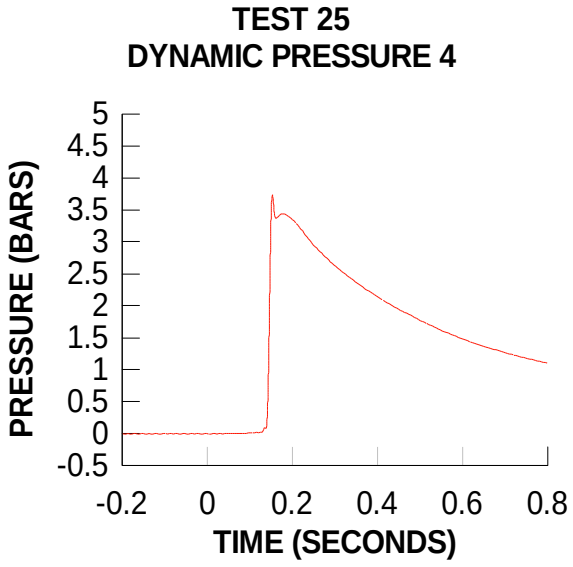
TEST 25
DYNAMIC PRESSURE 4
PRESSURE (BARS)
5
4.5
4
3.5
3
2.5
2
1.5
1
0.5
0
-0.5
-0.2
0
0.2
0.4
0.6
0.8
TIME (SECONDS)

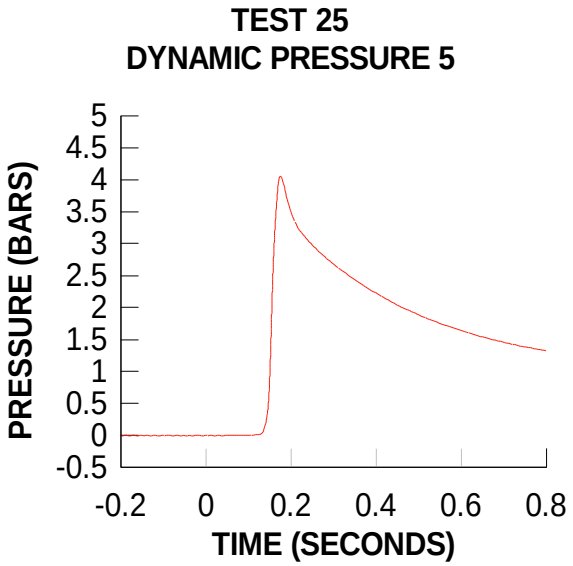
TEST 25
DYNAMIC PRESSURE 5
PRESSURE (BARS)
5
4.5
4
3.5
3
2.5
2
1.5
1
0.5
0
-0.5
-0.2
0
0.2
0.4
0.6
0.8
TIME (SECONDS)

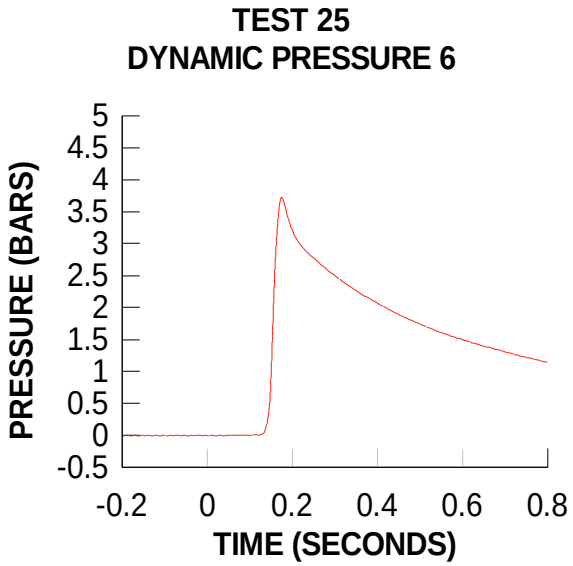
TEST 25
DYNAMIC PRESSURE 6
PRESSURE (BARS)
5
4.5
4
3.5
3
2.5
2
1.5
1
0.5
0
-0.5
-0.2
0
0.2
0.4
0.6
0.8
TIME (SECONDS)

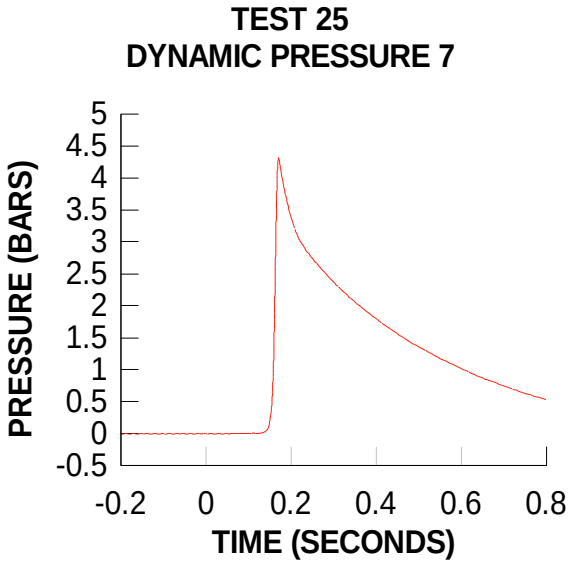
TEST 25
DYNAMIC PRESSURE 7
PRESSURE (BARS)
5
4.5
4
3.5
3
2.5
2
1.5
1
0.5
0
-0.5
-0.2
0
0.2
0.4
0.6
0.8
TIME (SECONDS)

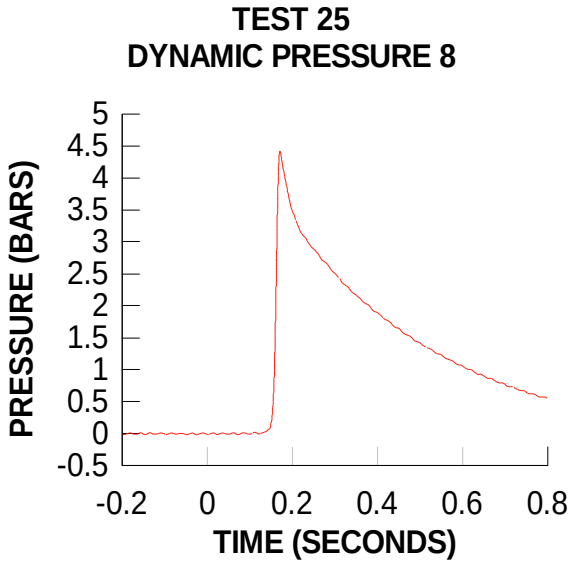
TEST 25
DYNAMIC PRESSURE 8
PRESSURE (BARS)
5
4.5
4
3.5
3
2.5
2
1.5
1
0.5
0
-0.5
-0.2
0
0.2
0.4
0.6
0.8
TIME (SECONDS)

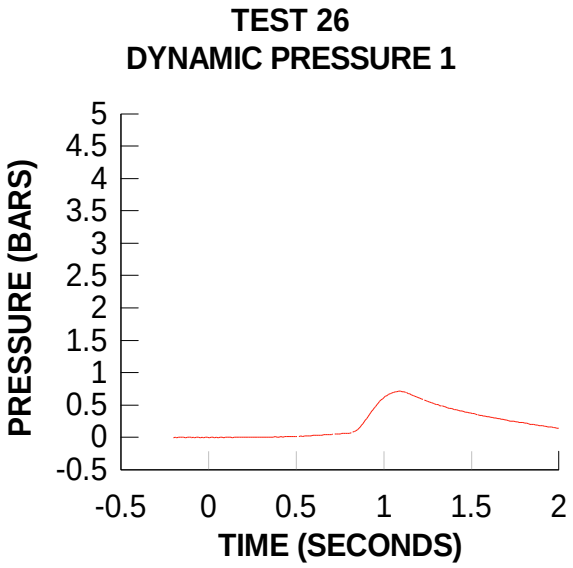
TEST 26
DYNAMIC PRESSURE 1
PRESSURE (BARS)
5
4.5
4
3.5
3
2.5
2
1.5
1
0.5
0
-0.5
-0.5
0
0.5
1
1.5
2
TIME (SECONDS)

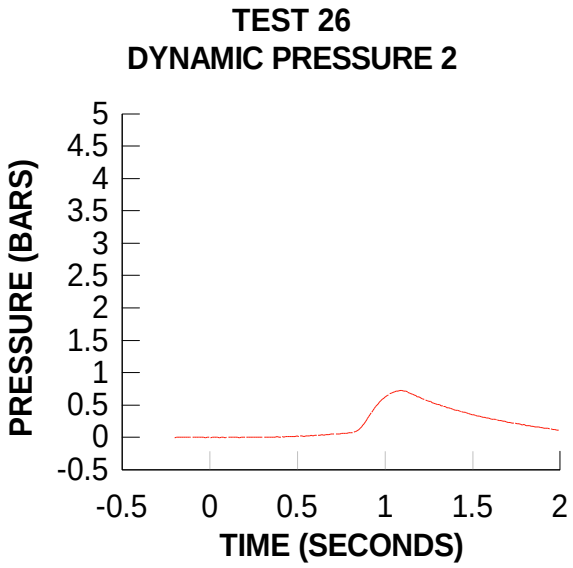
TEST 26
DYNAMIC PRESSURE 2
PRESSURE (BARS)
5
4.5
4
3.5
3
2.5
2
1.5
1
0.5
0
-0.5
-0.5
0
0.5
1
1.5
2
TIME (SECONDS)

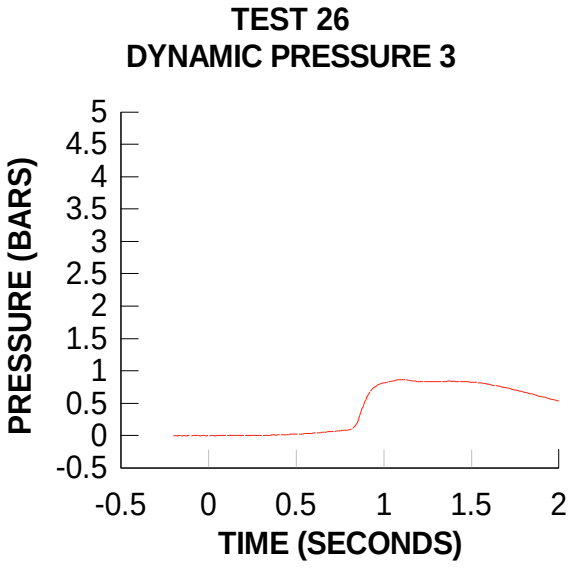
TEST 26
DYNAMIC PRESSURE 3
PRESSURE (BARS)
5
4.5
4
3.5
3
2.5
2
1.5
1
0.5
0
-0.5
-0.5
0
0.5
1
1.5
2
TIME (SECONDS)

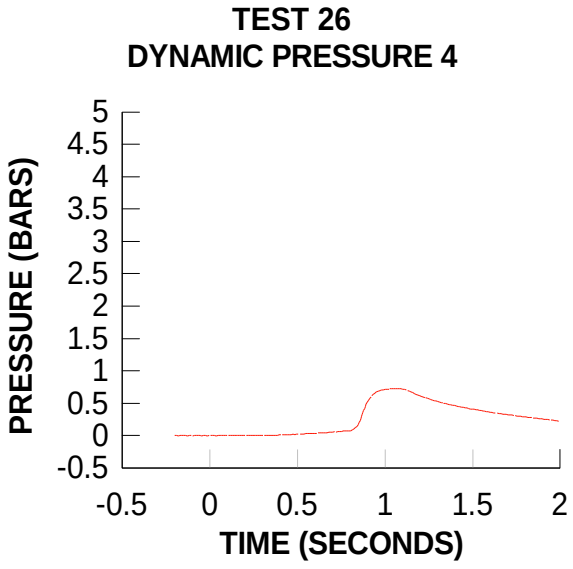
TEST 26
DYNAMIC PRESSURE 4
PRESSURE (BARS)
5
4.5
4
3.5
3
2.5
2
1.5
1
0.5
0
-0.5
-0.5
0
0.5
1
1.5
2
TIME (SECONDS)

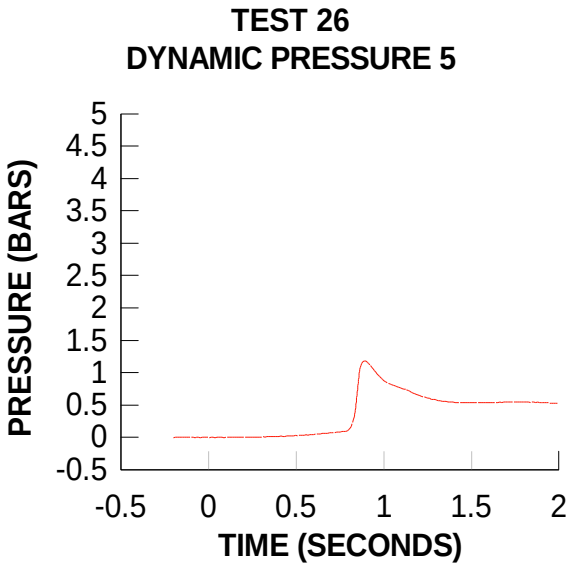
TEST 26
DYNAMIC PRESSURE 5
PRESSURE (BARS)
5
4.5
4
3.5
3
2.5
2
1.5
1
0.5
0
-0.5
-0.5
0
0.5
1
1.5
2
TIME (SECONDS)

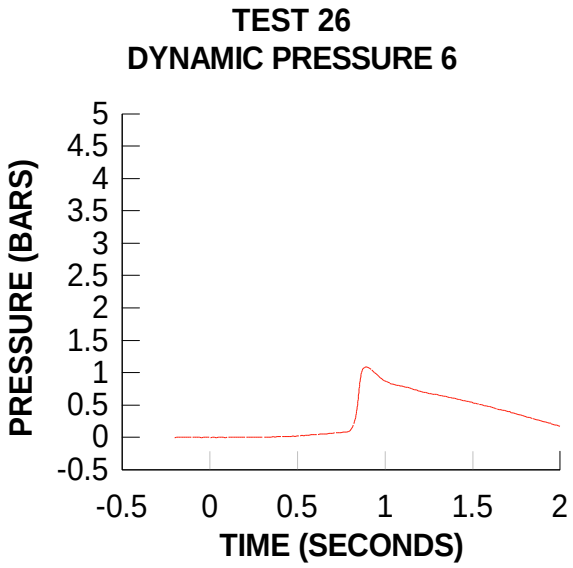
TEST 26
DYNAMIC PRESSURE 6
PRESSURE (BARS)
5
4.5
4
3.5
3
2.5
2
1.5
1
0.5
0
-0.5
-0.5
0
0.5
1
1.5
2
TIME (SECONDS)

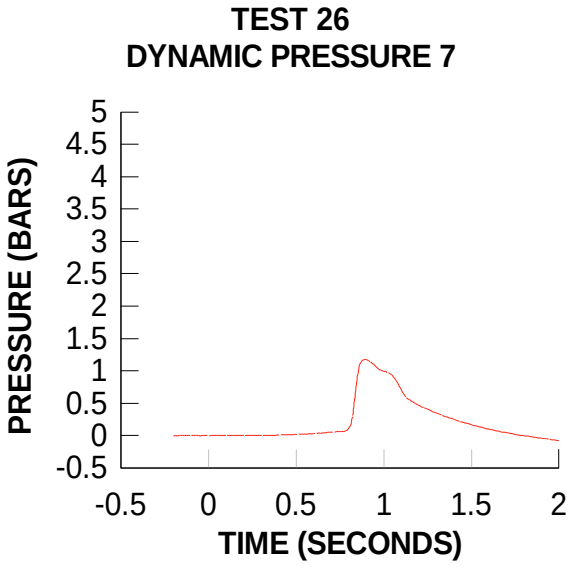
TEST 26
DYNAMIC PRESSURE 7
PRESSURE (BARS)
5
4.5
4
3.5
3
2.5
2
1.5
1
0.5
0
-0.5
-0.5
0
0.5
1
1.5
2
TIME (SECONDS)

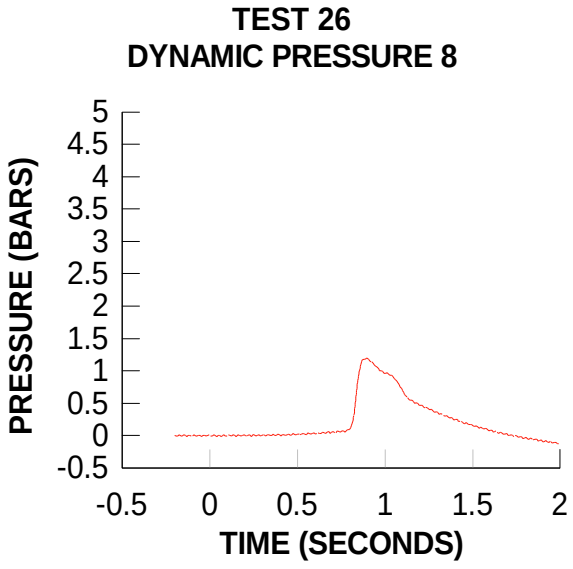
TEST 26
DYNAMIC PRESSURE 8
PRESSURE (BARS)
5
4.5
4
3.5
3
2.5
2
1.5
1
0.5
0
-0.5
-0.5
0
0.5
1
1.5
2
TIME (SECONDS)

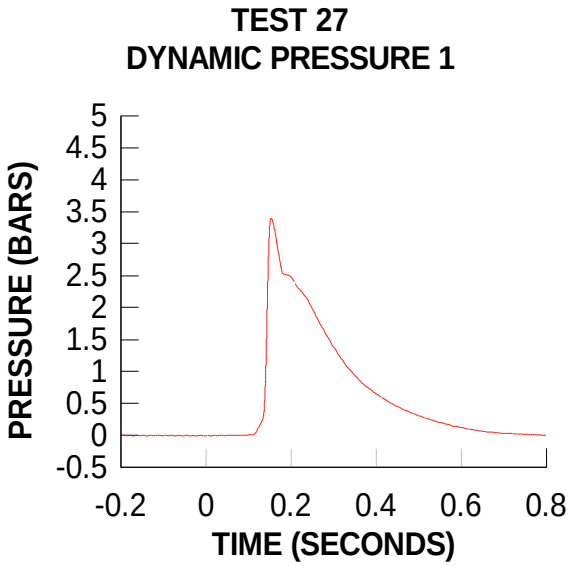
TEST 27
DYNAMIC PRESSURE 1
PRESSURE (BARS)
5
4.5
4
3.5
3
2.5
2
1.5
1
0.5
0
-0.5
-0.2
0
0.2
0.4
0.6
0.8
TIME (SECONDS)

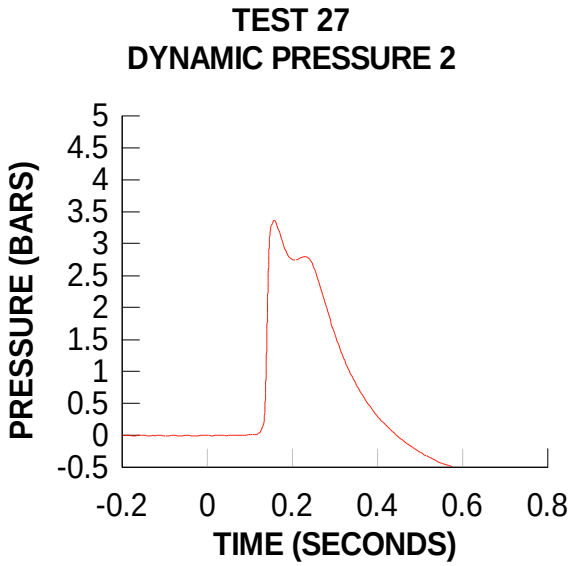
TEST 27
DYNAMIC PRESSURE 2
PRESSURE (BARS)
5
4.5
4
3.5
3
2.5
2
1.5
1
0.5
0
-0.5
-0.2
0
0.2
0.4
0.6
0.8
TIME (SECONDS)

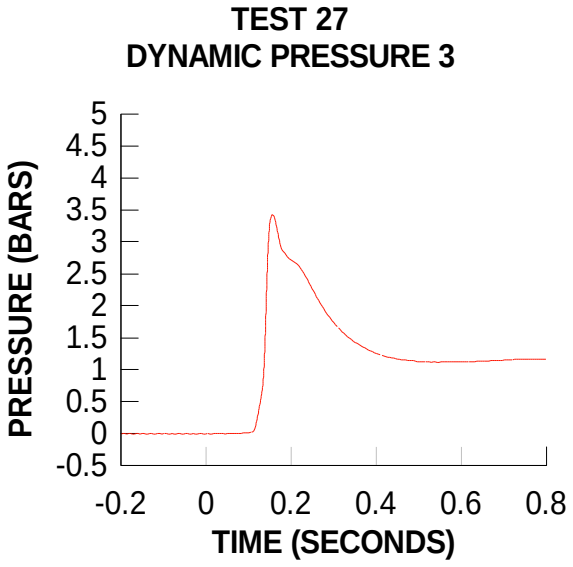
TEST 27
DYNAMIC PRESSURE 3
PRESSURE (BARS)
5
4.5
4
3.5
3
2.5
2
1.5
1
0.5
0
-0.5
-0.2
0
0.2
0.4
0.6
0.8
TIME (SECONDS)

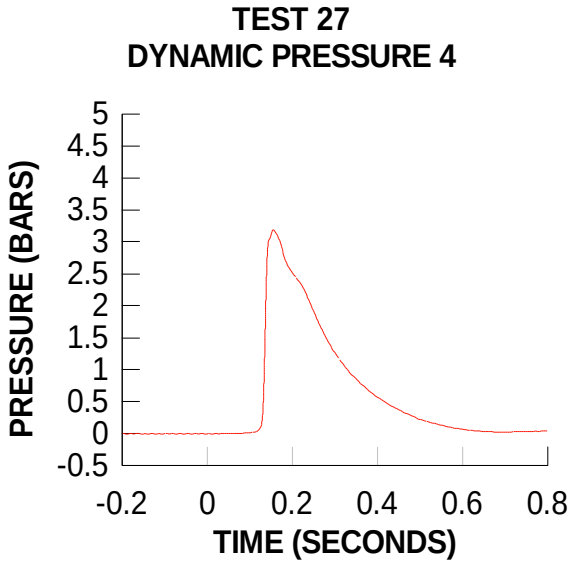
TEST 27
DYNAMIC PRESSURE 4
PRESSURE (BARS)
5
4.5
4
3.5
3
2.5
2
1.5
1
0.5
0
-0.5
-0.2
0
0.2
0.4
0.6
0.8
TIME (SECONDS)

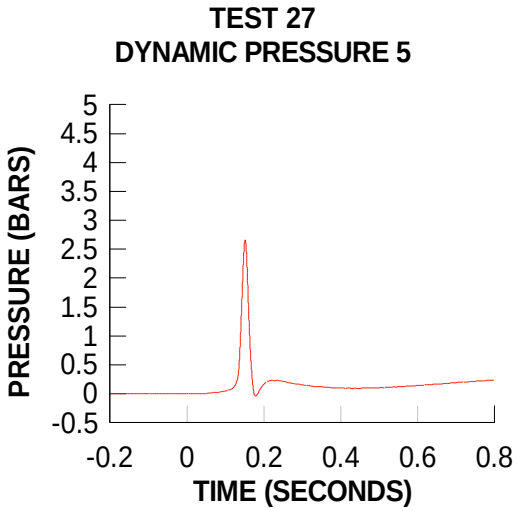
TEST 27
DYNAMIC PRESSURE 5
PRESSURE (BARS)
5
4.5
4
3.5
3
2.5
2
1.5
1
0.5
0
-0.5
-0.2
0
0.2
0.4
0.6
0.8
TIME (SECONDS)

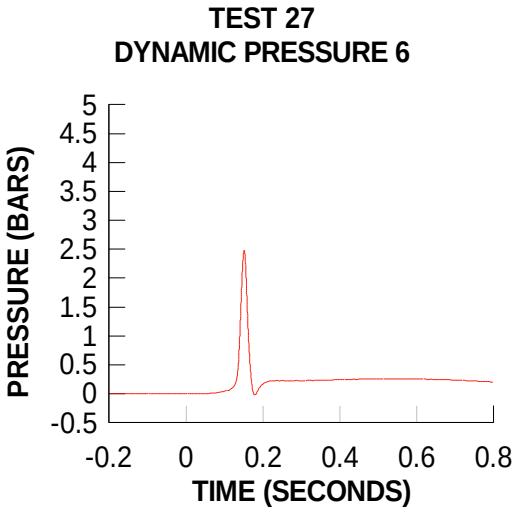
TEST 27
DYNAMIC PRESSURE 6
PRESSURE (BARS)
5
4.5
4
3.5
3
2.5
2
1.5
1
0.5
0
-0.5
-0.2
0
0.2
0.4
0.6
0.8
TIME (SECONDS)

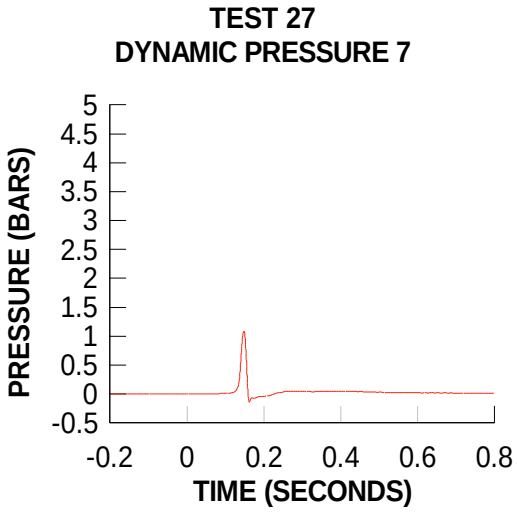
TEST 27
DYNAMIC PRESSURE 7
PRESSURE (BARS)
5
4.5
4
3.5
3
2.5
2
1.5
1
0.5
0
-0.5
-0.2
0
0.2
0.4
0.6
0.8
TIME (SECONDS)

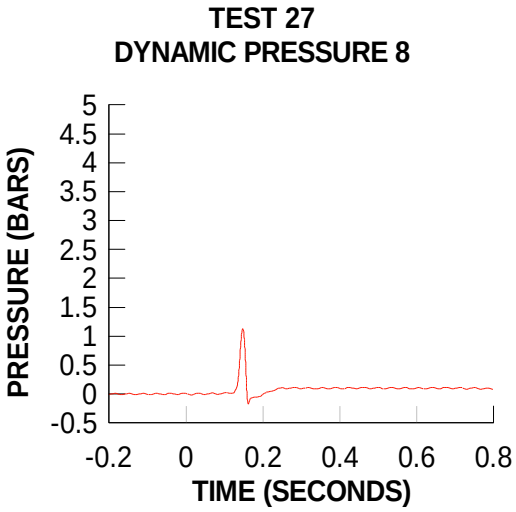
TEST 27
DYNAMIC PRESSURE 8
PRESSURE (BARS)
5
4.5
4
3.5
3
2.5
2
1.5
1
0.5
0
-0.5
-0.2
0
0.2
0.4
0.6
0.8
TIME (SECONDS)

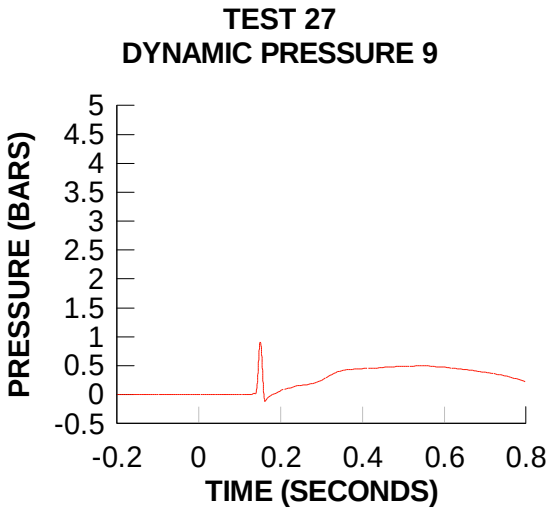
TEST 27
DYNAMIC PRESSURE 9
PRESSURE (BARS)
5
4.5
4
3.5
3
2.5
2
1.5
1
0.5
0
-0.5
-0.2
0
0.2
0.4
0.6
0.8
TIME (SECONDS)

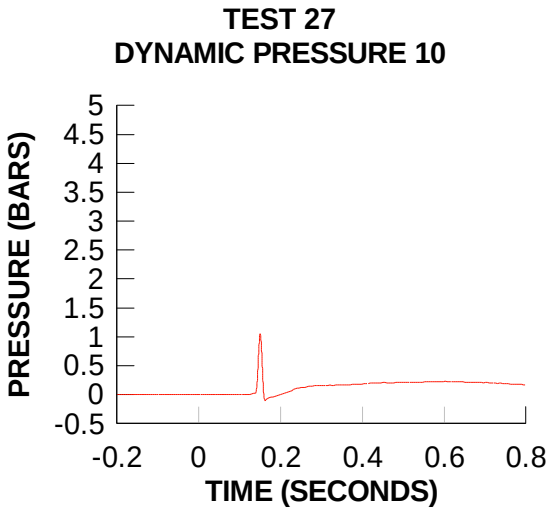
TEST 27
DYNAMIC PRESSURE 10
PRESSURE (BARS)
5
4.5
4
3.5
3
2.5
2
1.5
1
0.5
0
-0.5
-0.2
0
0.2
0.4
0.6
0.8
TIME (SECONDS)

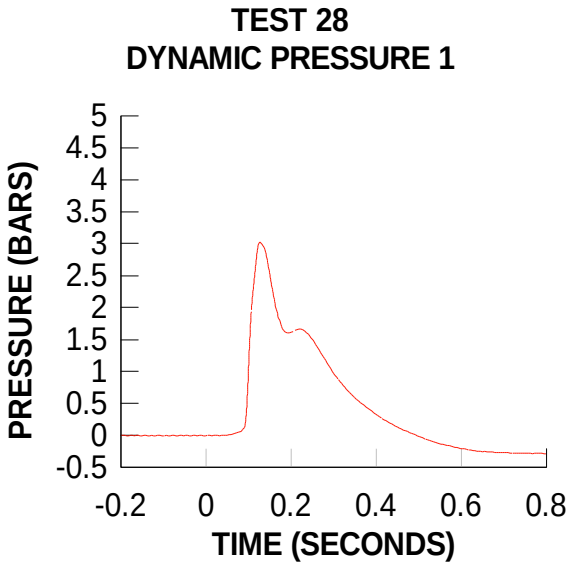
TEST 28
DYNAMIC PRESSURE 1
PRESSURE (BARS)
5
4.5
4
3.5
3
2.5
2
1.5
1
0.5
0
-0.5
-0.2
0
0.2
0.4
0.6
0.8
TIME (SECONDS)

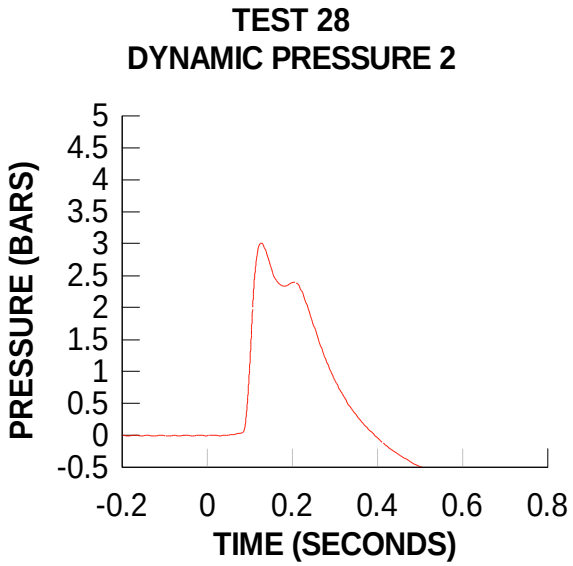
TEST 28
DYNAMIC PRESSURE 2
PRESSURE (BARS)
5
4.5
4
3.5
3
2.5
2
1.5
1
0.5
0
-0.5
-0.2
0
0.2
0.4
0.6
0.8
TIME (SECONDS)

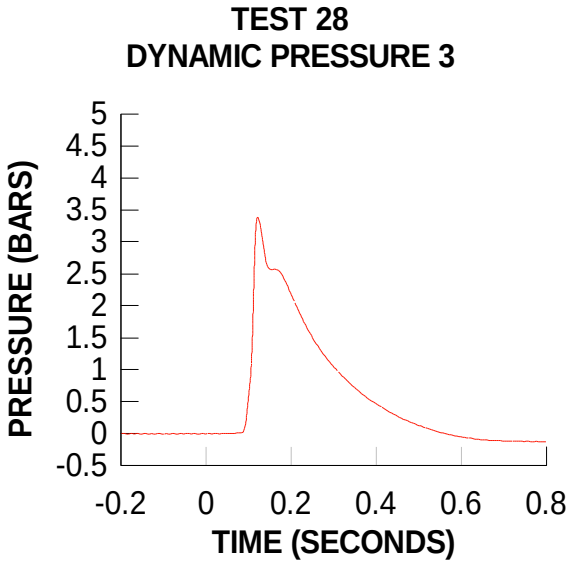
TEST 28
DYNAMIC PRESSURE 3
PRESSURE (BARS)
5
4.5
4
3.5
3
2.5
2
1.5
1
0.5
0
-0.5
-0.2
0
0.2
0.4
0.6
0.8
TIME (SECONDS)

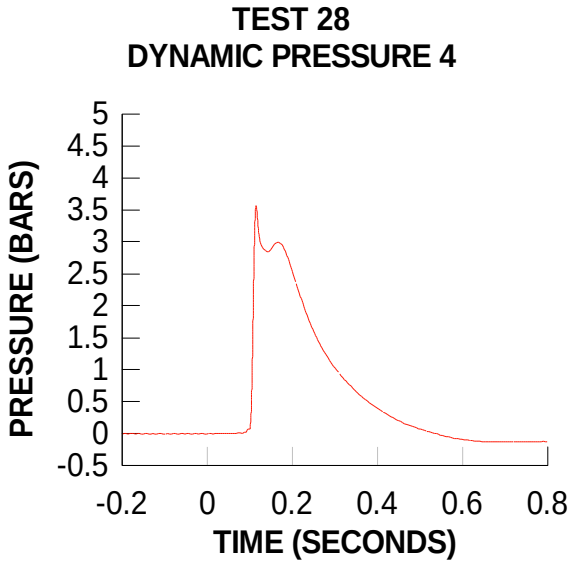
TEST 28
DYNAMIC PRESSURE 4
PRESSURE (BARS)
5
4.5
4
3.5
3
2.5
2
1.5
1
0.5
0
-0.5
-0.2
0
0.2
0.4
0.6
0.8
TIME (SECONDS)

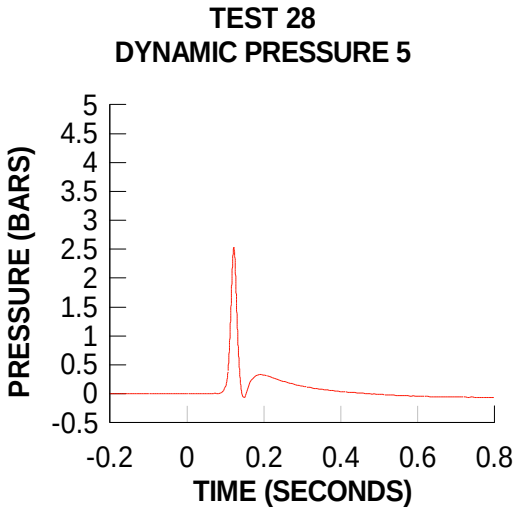
TEST 28
DYNAMIC PRESSURE 5
PRESSURE (BARS)
5
4.5
4
3.5
3
2.5
2
1.5
1
0.5
0
-0.5
-0.2
0
0.2
0.4
0.6
0.8
TIME (SECONDS)

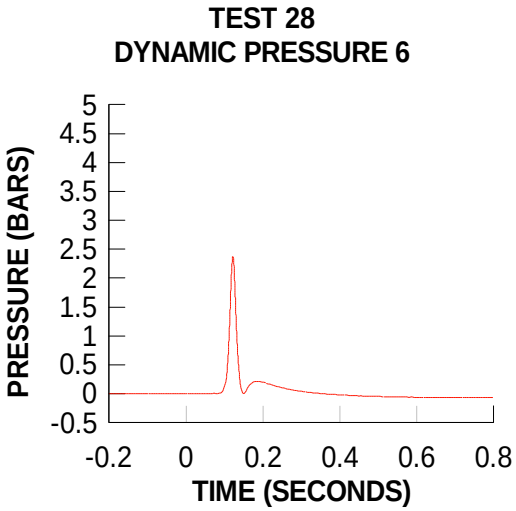
TEST 28
DYNAMIC PRESSURE 6
PRESSURE (BARS)
5
4.5
4
3.5
3
2.5
2
1.5
1
0.5
0
-0.5
-0.2
0
0.2
0.4
0.6
0.8
TIME (SECONDS)

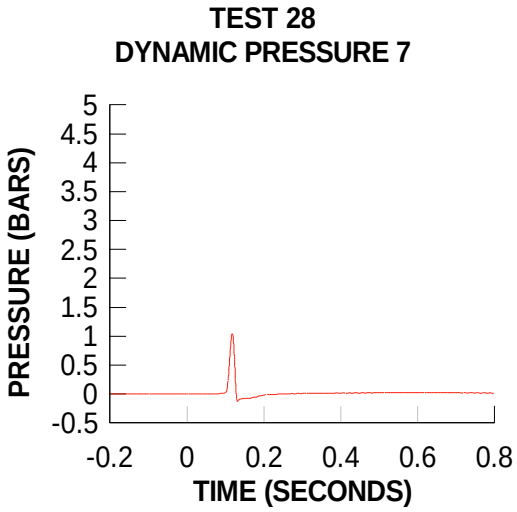
TEST 28
DYNAMIC PRESSURE 7
PRESSURE (BARS)
5
4.5
4
3.5
3
2.5
2
1.5
1
0.5
0
-0.5
-0.2
0
0.2
0.4
0.6
0.8
TIME (SECONDS)

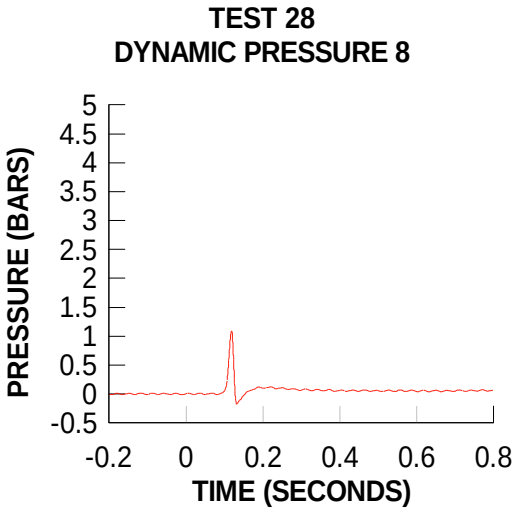
TEST 28
DYNAMIC PRESSURE 8
PRESSURE (BARS)
5
4.5
4
3.5
3
2.5
2
1.5
1
0.5
0
-0.5
-0.2
0
0.2
0.4
0.6
0.8
TIME (SECONDS)

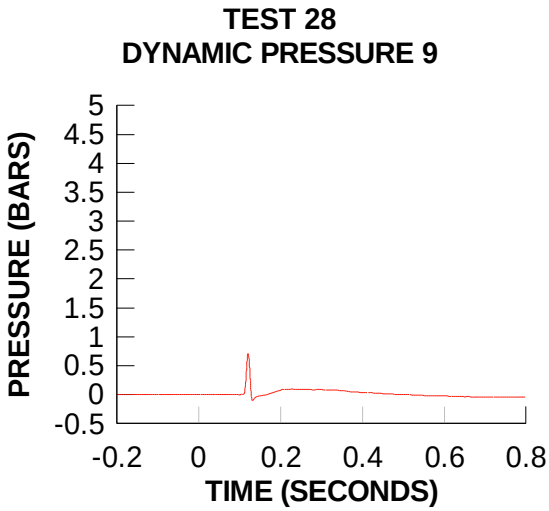
TEST 28
DYNAMIC PRESSURE 9
PRESSURE (BARS)
5
4.5
4
3.5
3
2.5
2
1.5
1
0.5
0
-0.5
-0.2
0
0.2
0.4
0.6
0.8
TIME (SECONDS)

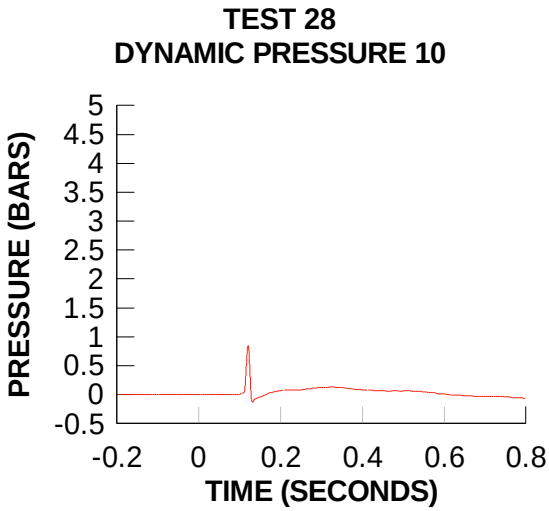
TEST 28
DYNAMIC PRESSURE 10
PRESSURE (BARS)
5
4.5
4
3.5
3
2.5
2
1.5
1
0.5
0
-0.5
-0.2
0
0.2
0.4
0.6
0.8
TIME (SECONDS)

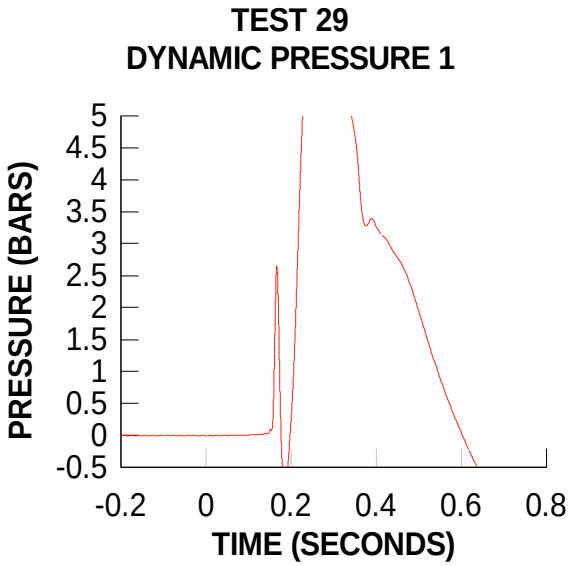
TEST 29
DYNAMIC PRESSURE 1
PRESSURE (BARS)
5
4.5
4
3.5
3
2.5
2
1.5
1
0.5
0
-0.5
-0.2
0
0.2
0.4
0.6
0.8
TIME (SECONDS)

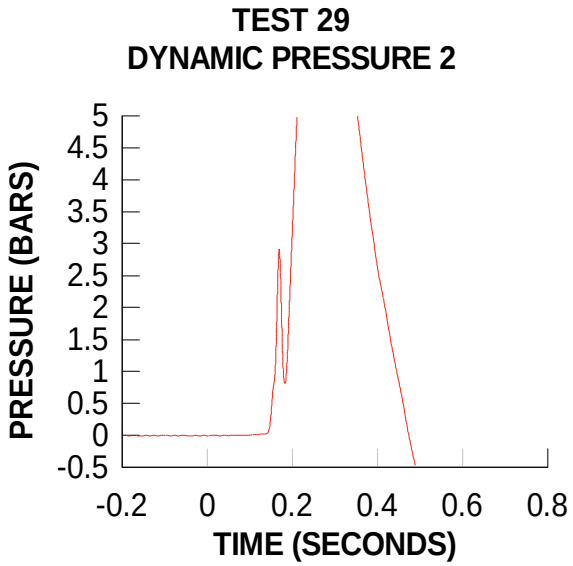
TEST 29
DYNAMIC PRESSURE 2
PRESSURE (BARS)
5
4.5
4
3.5
3
2.5
2
1.5
1
0.5
0
-0.5
-0.2
0
0.2
0.4
0.6
0.8
TIME (SECONDS)

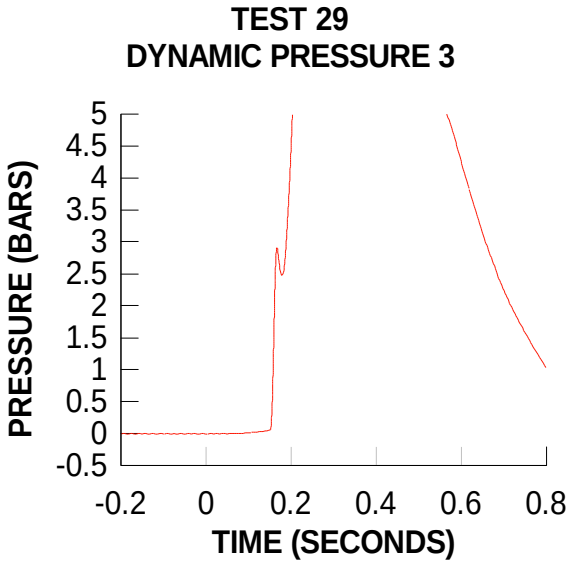
TEST 29
DYNAMIC PRESSURE 3
PRESSURE (BARS)
5
4.5
4
3.5
3
2.5
2
1.5
1
0.5
0
-0.5
-0.2
0
0.2
0.4
0.6
0.8
TIME (SECONDS)

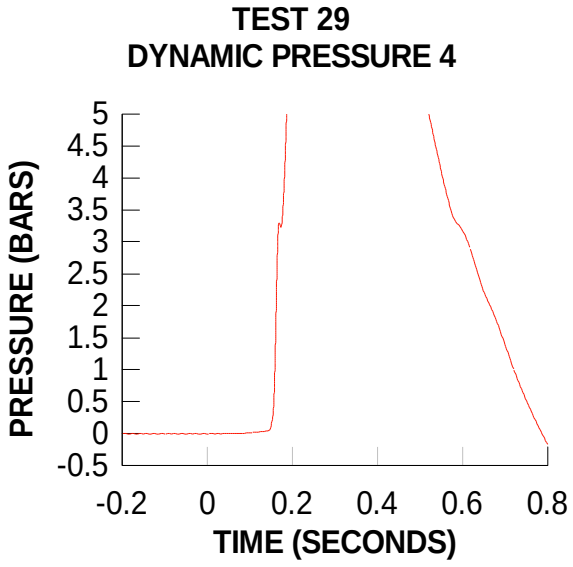
TEST 29
DYNAMIC PRESSURE 4
PRESSURE (BARS)
5
4.5
4
3.5
3
2.5
2
1.5
1
0.5
0
-0.5
-0.2
0
0.2
0.4
0.6
0.8
TIME (SECONDS)

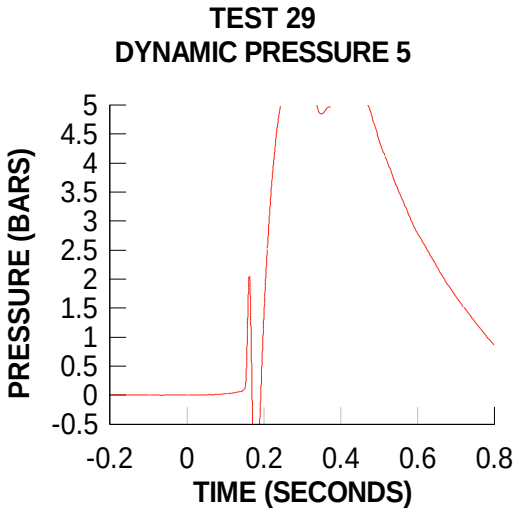
TEST 29
DYNAMIC PRESSURE 5
PRESSURE (BARS)
TIME (SECONDS)

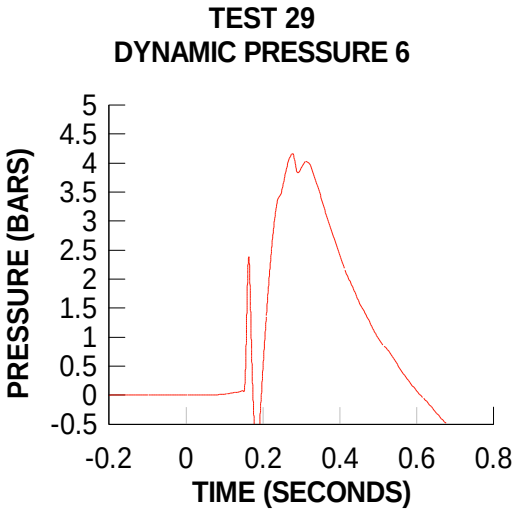
TEST 29
DYNAMIC PRESSURE 6
PRESSURE (BARS)
TIME (SECONDS)

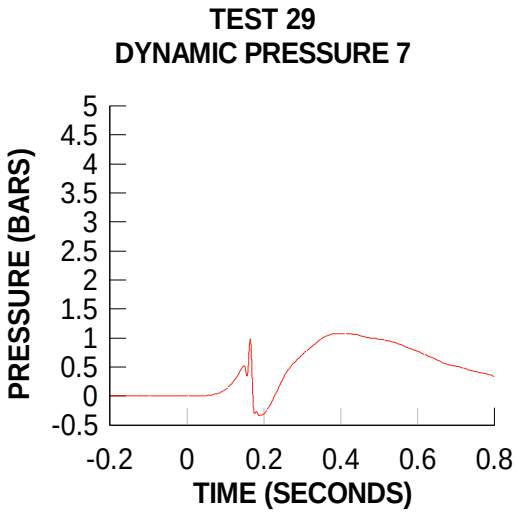
TEST 29
DYNAMIC PRESSURE 7
PRESSURE (BARS)
TIME (SECONDS)

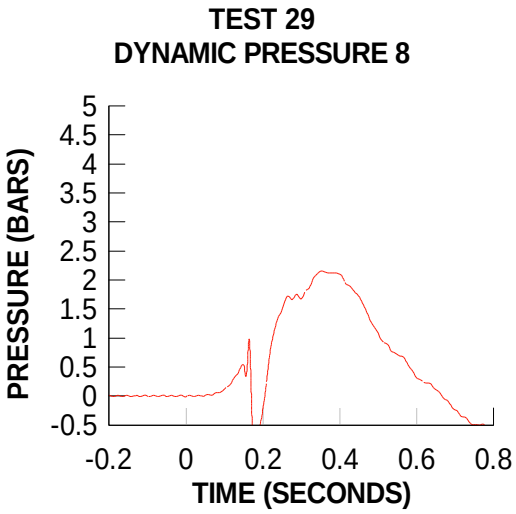
TEST 29
DYNAMIC PRESSURE 8
PRESSURE (BARS)
TIME (SECONDS)

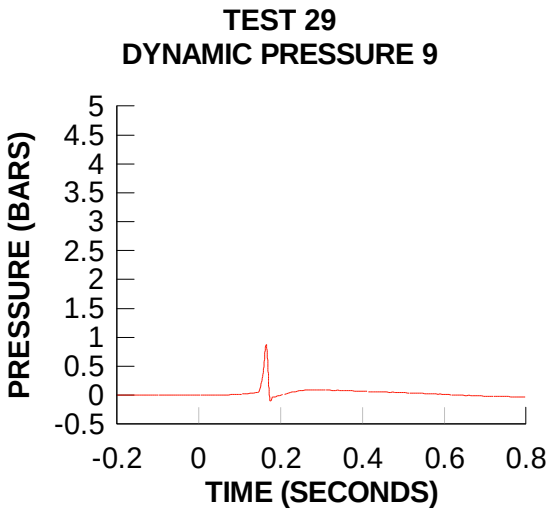
TEST 29
DYNAMIC PRESSURE 9
PRESSURE (BARS)
TIME (SECONDS)

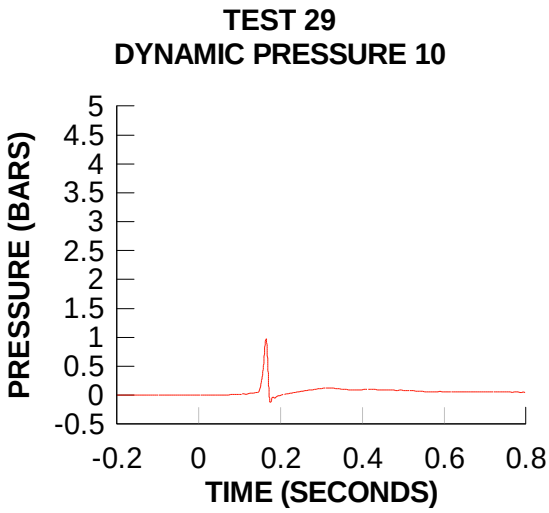
TEST 29
DYNAMIC PRESSURE 10
PRESSURE (BARS)
TIME (SECONDS)

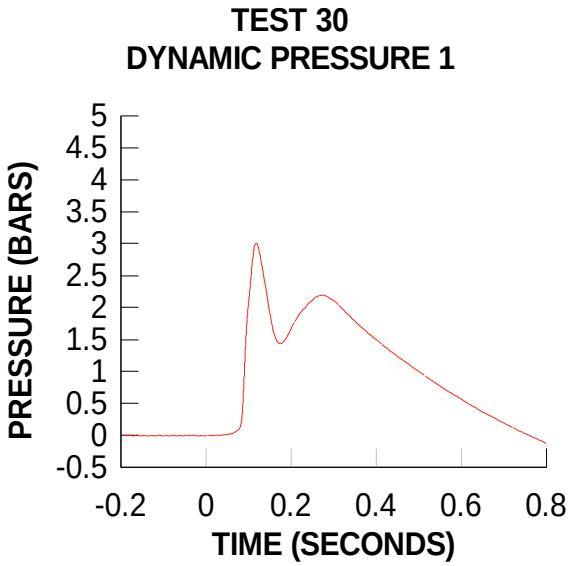
TEST 30
DYNAMIC PRESSURE 1
PRESSURE (BARS)
5
4.5
4
3.5
3
2.5
2
1.5
1
0.5
0
-0.5
-0.2
0
0.2
0.4
0.6
0.8
TIME (SECONDS)

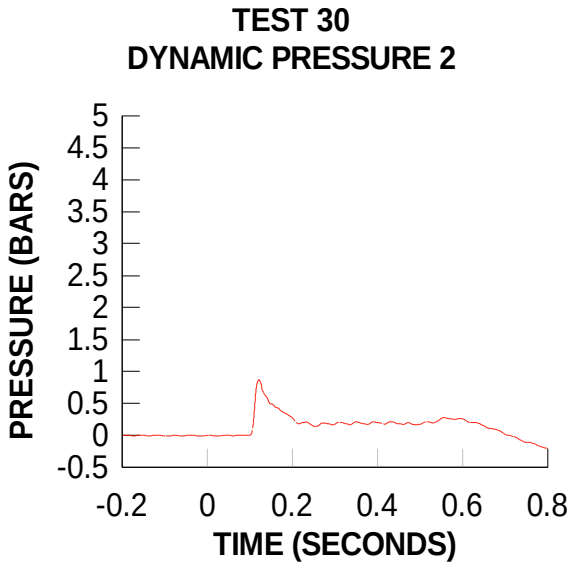
TEST 30
DYNAMIC PRESSURE 2
PRESSURE (BARS)
5
4.5
4
3.5
3
2.5
2
1.5
1
0.5
0
-0.5
-0.2
0
0.2
0.4
0.6
0.8
TIME (SECONDS)

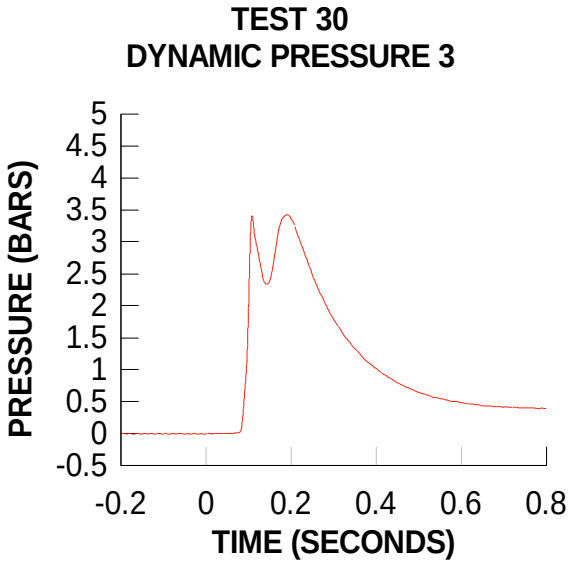
TEST 30
DYNAMIC PRESSURE 3
PRESSURE (BARS)
5
4.5
4
3.5
3
2.5
2
1.5
1
0.5
0
-0.5
-0.2
0
0.2
0.4
0.6
0.8
TIME (SECONDS)

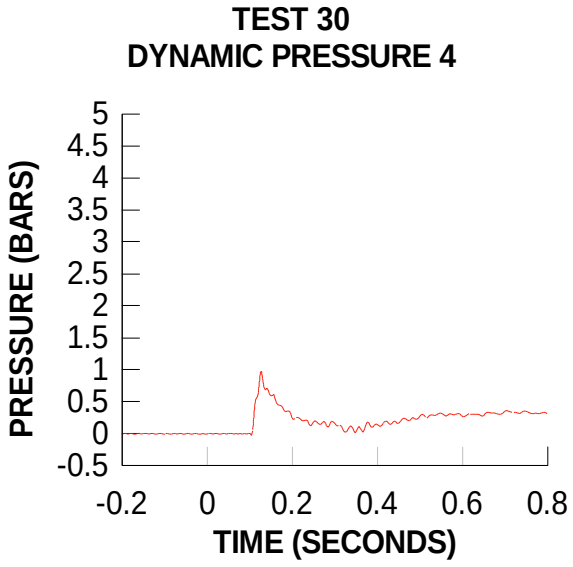
TEST 30
DYNAMIC PRESSURE 4
PRESSURE (BARS)
5
4.5
4
3.5
3
2.5
2
1.5
1
0.5
0
-0.5
-0.2
0
0.2
0.4
0.6
0.8
TIME (SECONDS)

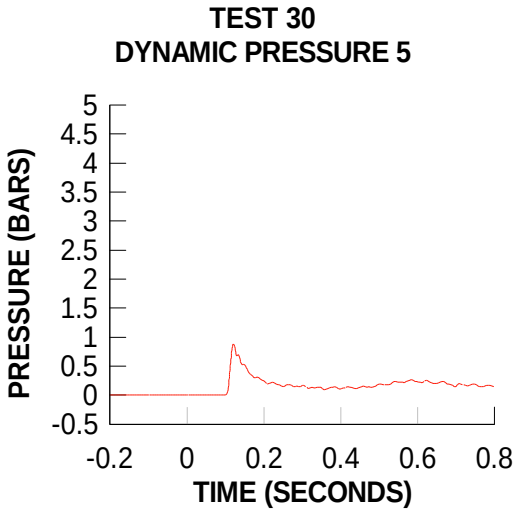
TEST 30
DYNAMIC PRESSURE 5
PRESSURE (BARS)
TIME (SECONDS)

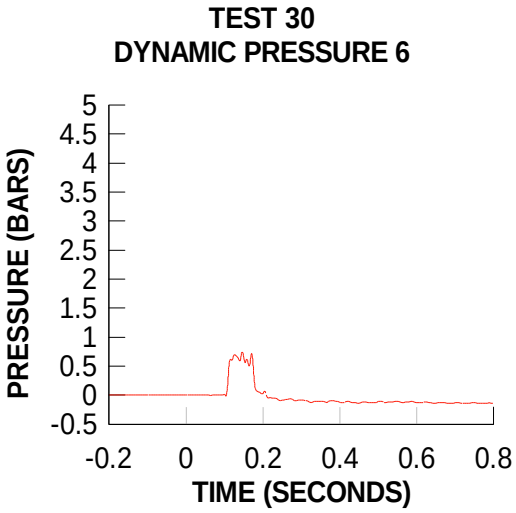
TEST 30
DYNAMIC PRESSURE 6
PRESSURE (BARS)
TIME (SECONDS)

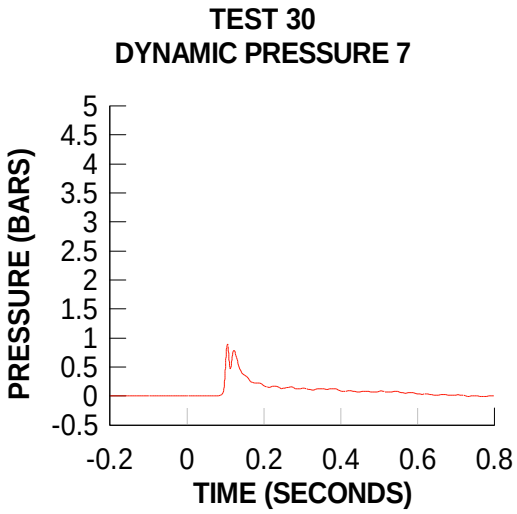
TEST 30
DYNAMIC PRESSURE 7
PRESSURE (BARS)
TIME (SECONDS)

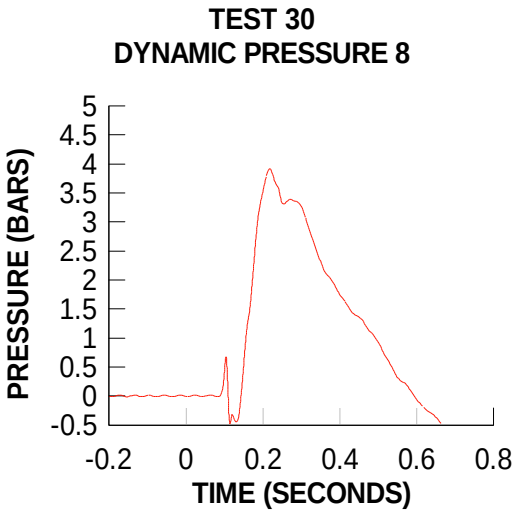
TEST 30
DYNAMIC PRESSURE 8
PRESSURE (BARS)
TIME (SECONDS)

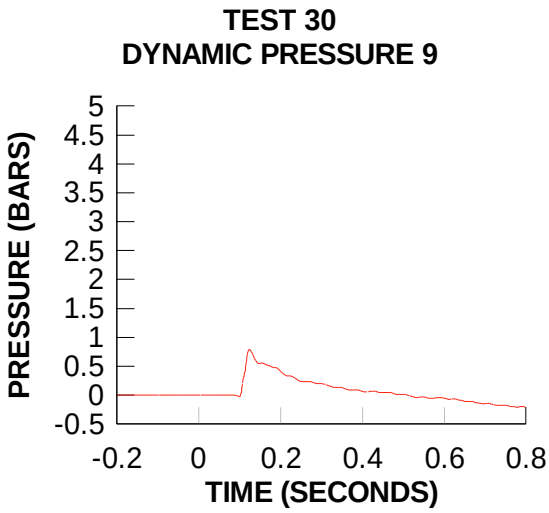
TEST 30
DYNAMIC PRESSURE 9
PRESSURE (BARS)
TIME (SECONDS)

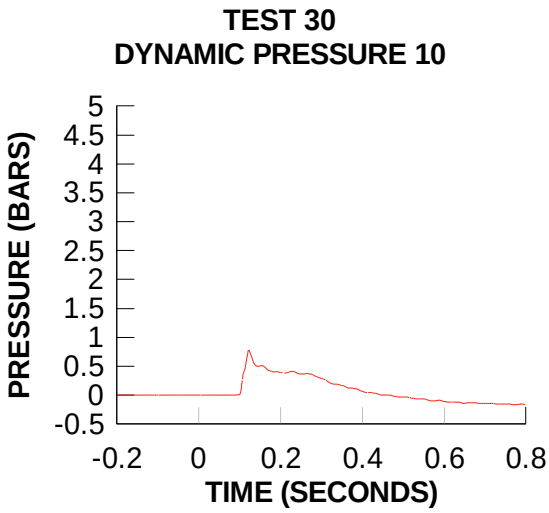
TEST 30
DYNAMIC PRESSURE 10
PRESSURE (BARS)
TIME (SECONDS)

D.6 Photodiodes

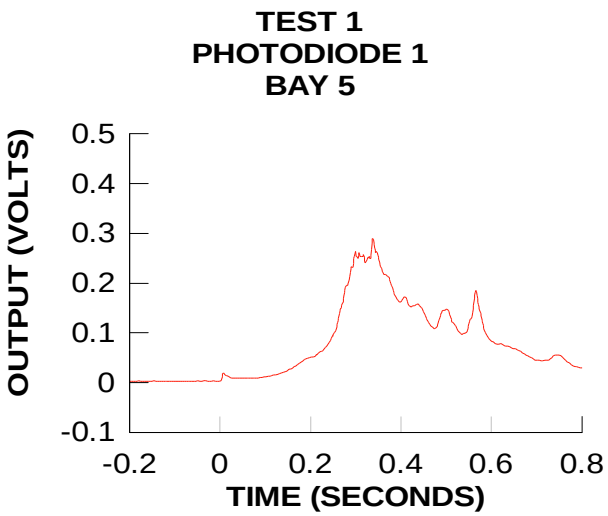
TEST 1
PHOTODIODE 1
BAY 5
OUTPUT (VOLTS)
0.5
0.4
0.3
0.2
0.1
0
-0.1
-0.2
0
0.2
0.4
0.6
0.8
TIME (SECONDS)

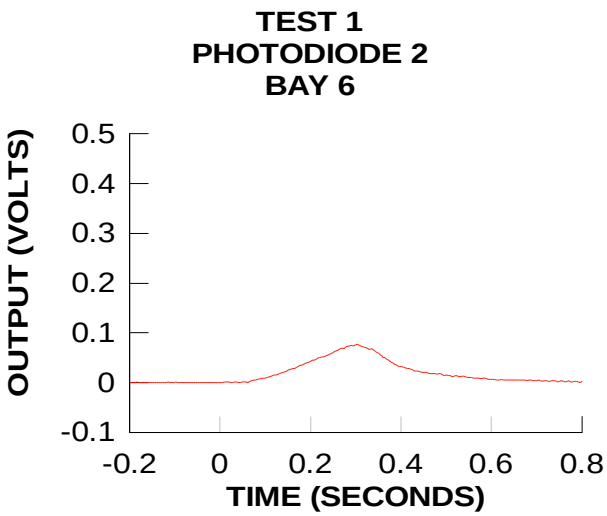
TEST 1
PHOTODIODE 2
BAY 6
OUTPUT (VOLTS)
0.5
0.4
0.3
0.2
0.1
0
-0.1
-0.2
0
0.2
0.4
0.6
0.8
TIME (SECONDS)

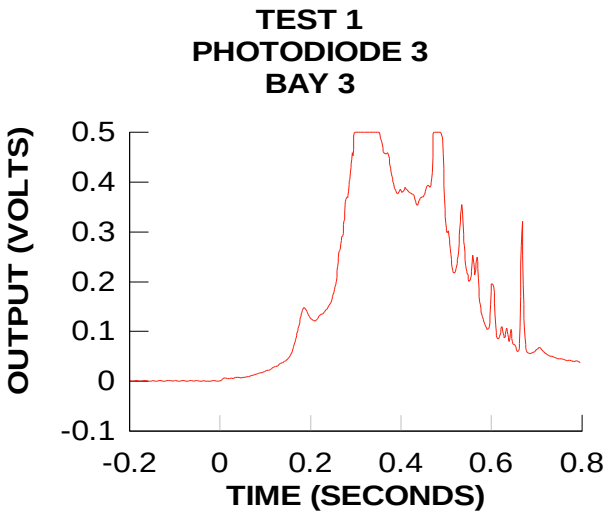
TEST 1
PHOTODIODE 3
BAY 3
OUTPUT (VOLTS)
0.5
0.4
0.3
0.2
0.1
0
-0.1
-0.2
0
0.2
0.4
0.6
0.8
TIME (SECONDS)

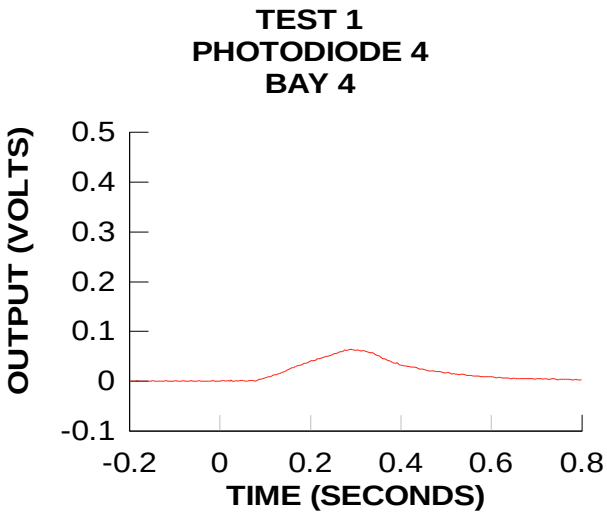
TEST 1
PHOTODIODE 4
BAY 4
OUTPUT (VOLTS)
0.5
0.4
0.3
0.2
0.1
0
-0.1
-0.2
0
0.2
0.4
0.6
0.8
TIME (SECONDS)

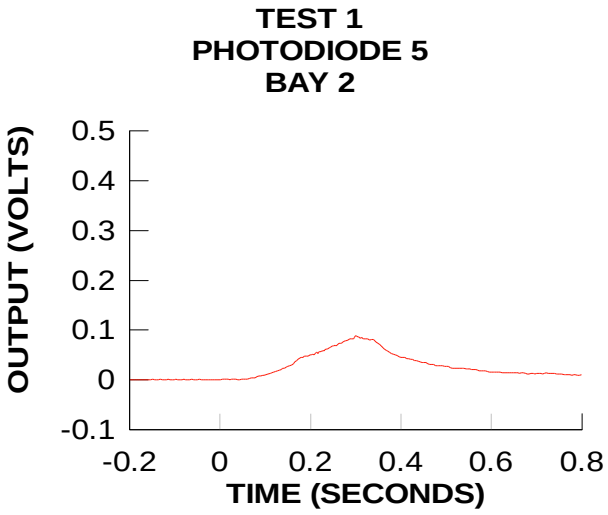
TEST 1
PHOTODIODE 5
BAY 2
OUTPUT (VOLTS)
0.5
0.4
0.3
0.2
0.1
0
-0.1
-0.2
0
0.2
0.4
0.6
0.8
TIME (SECONDS)

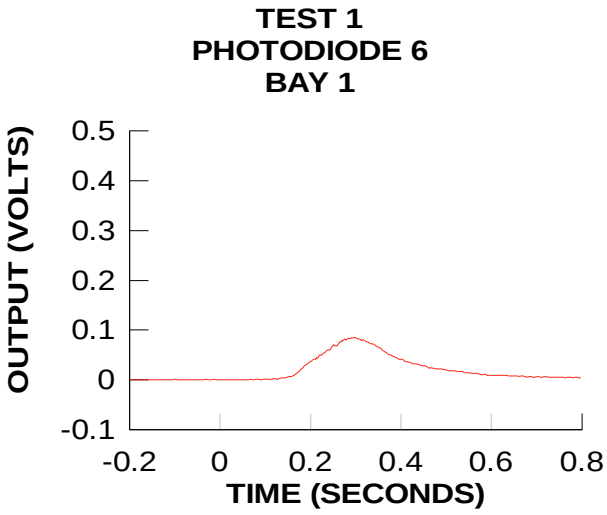
TEST 1
PHOTODIODE 6
BAY 1
OUTPUT (VOLTS)
0.5
0.4
0.3
0.2
0.1
0
-0.1
-0.2
0
0.2
0.4
0.6
0.8
TIME (SECONDS)

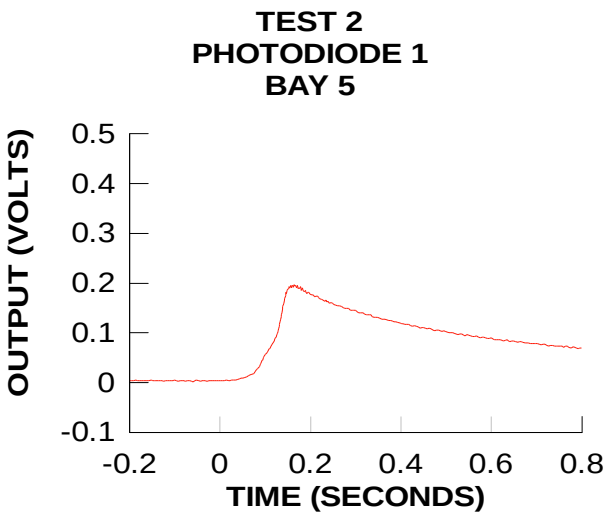
TEST 2
PHOTODIODE 1
BAY 5
OUTPUT (VOLTS)
0.5
0.4
0.3
0.2
0.1
0
-0.1
-0.2
0
0.2
0.4
0.6
0.8
TIME (SECONDS)

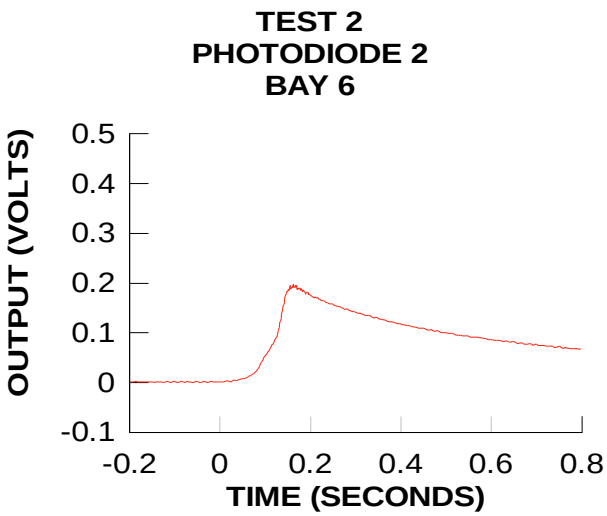
TEST 2
PHOTODIODE 2
BAY 6
OUTPUT (VOLTS)
0.5
0.4
0.3
0.2
0.1
0
-0.1
-0.2
0
0.2
0.4
0.6
0.8
TIME (SECONDS)

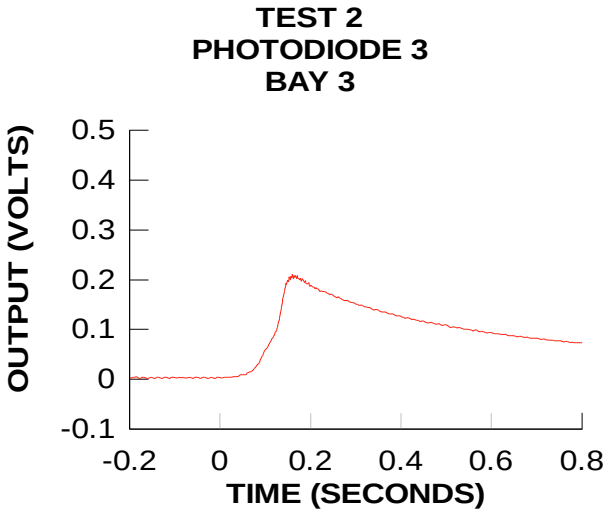
TEST 2
PHOTODIODE 3
BAY 3
OUTPUT (VOLTS)
0.5
0.4
0.3
0.2
0.1
0
-0.1
-0.2
0
0.2
0.4
0.6
0.8
TIME (SECONDS)

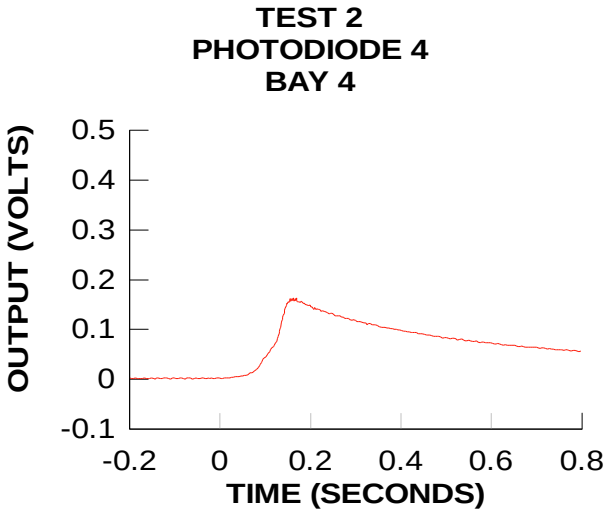
TEST 2
PHOTODIODE 4
BAY 4
OUTPUT (VOLTS)
0.5
0.4
0.3
0.2
0.1
0
-0.1
-0.2
0
0.2
0.4
0.6
0.8
TIME (SECONDS)

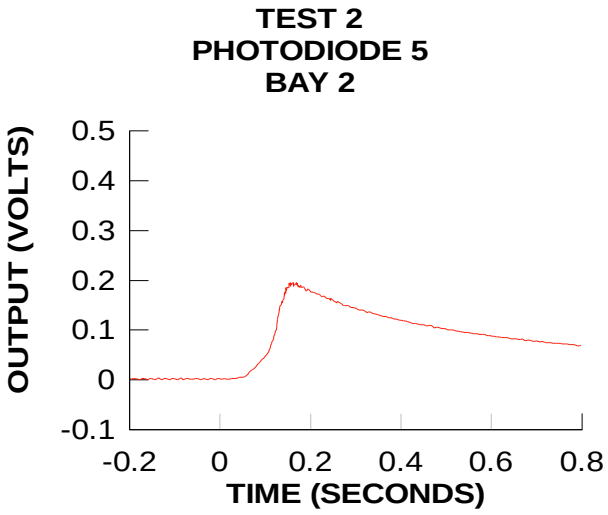
TEST 2
PHOTODIODE 5
BAY 2
OUTPUT (VOLTS)
0.5
0.4
0.3
0.2
0.1
0
-0.1
-0.2
0
0.2
0.4
0.6
0.8
TIME (SECONDS)

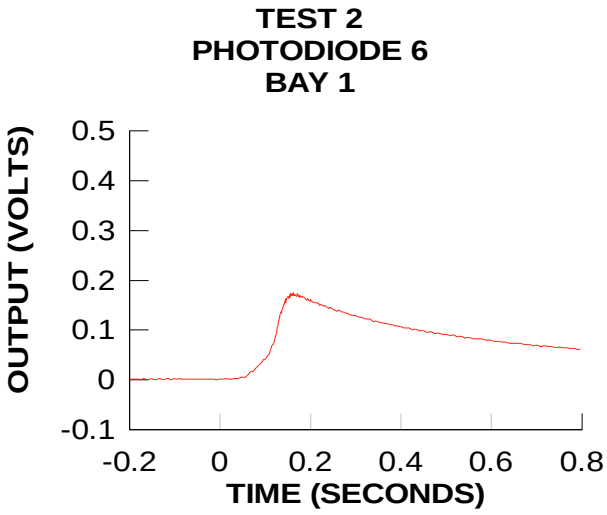
TEST 2
PHOTODIODE 6
BAY 1
OUTPUT (VOLTS)
0.5
0.4
0.3
0.2
0.1
0
-0.1
-0.2
0
0.2
0.4
0.6
0.8
TIME (SECONDS)

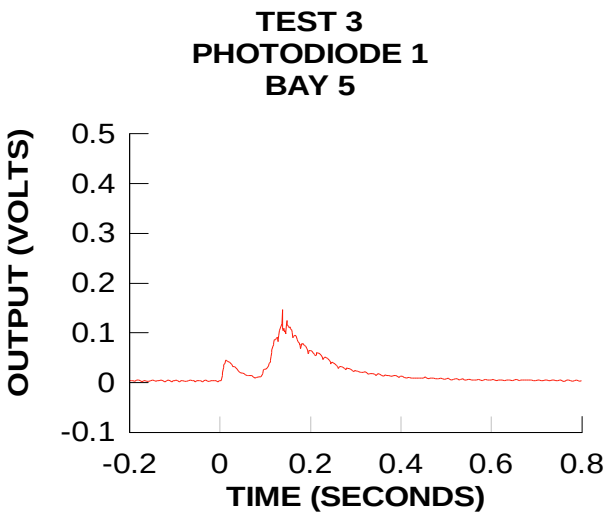
TEST 3
PHOTODIODE 1
BAY 5
OUTPUT (VOLTS)
0.5
0.4
0.3
0.2
0.1
0
-0.1
-0.2
0
0.2
0.4
0.6
0.8
TIME (SECONDS)

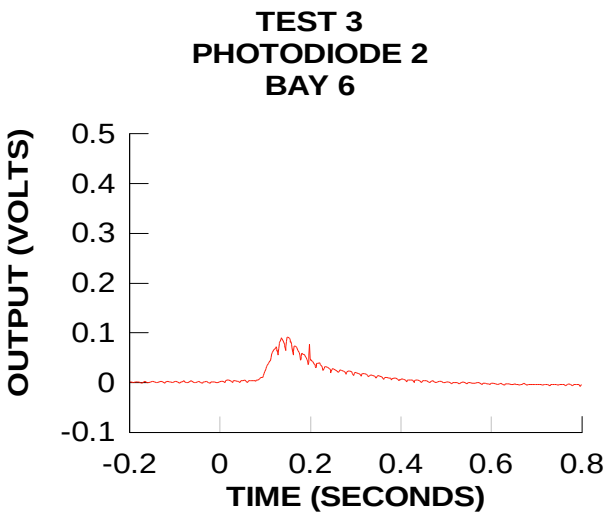
TEST 3
PHOTODIODE 2
BAY 6
OUTPUT (VOLTS)
0.5
0.4
0.3
0.2
0.1
0
-0.1
-0.2
0
0.2
0.4
0.6
0.8
TIME (SECONDS)

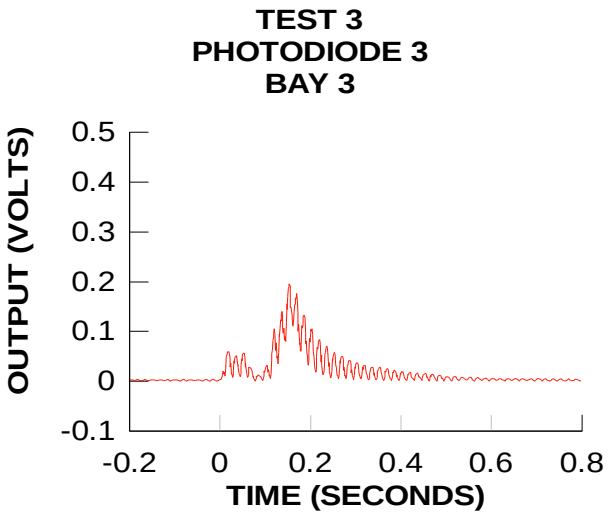
TEST 3
PHOTODIODE 3
BAY 3
OUTPUT (VOLTS)
0.5
0.4
0.3
0.2
0.1
0
-0.1
-0.2
0
0.2
0.4
0.6
0.8
TIME (SECONDS)

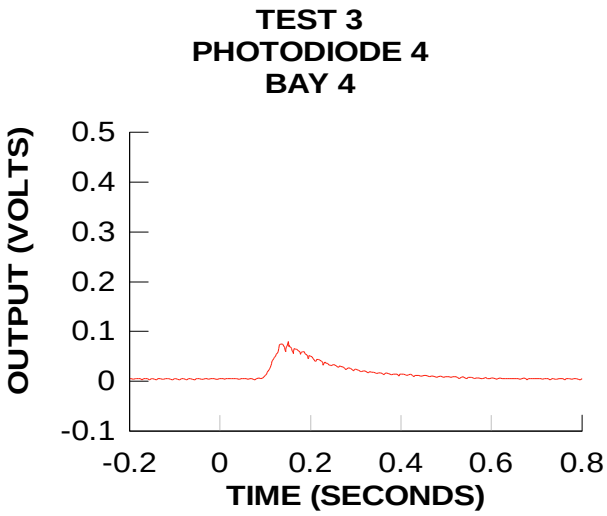
TEST 3
PHOTODIODE 4
BAY 4
OUTPUT (VOLTS)
0.5
0.4
0.3
0.2
0.1
0
-0.1
-0.2
0
0.2
0.4
0.6
0.8
TIME (SECONDS)

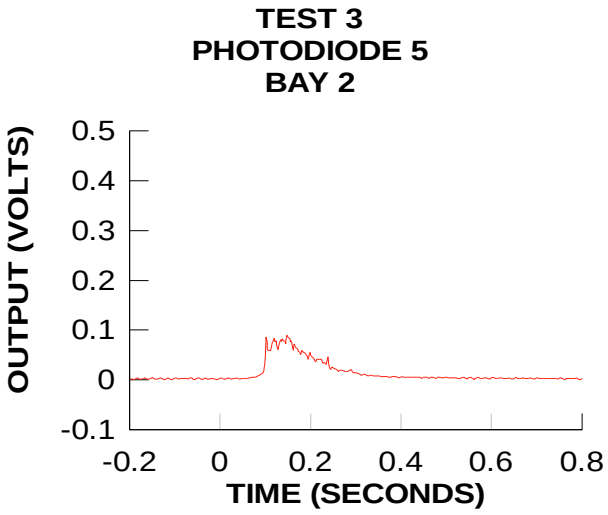
TEST 3
PHOTODIODE 5
BAY 2
OUTPUT (VOLTS)
0.5
0.4
0.3
0.2
0.1
0
-0.1
-0.2
0
0.2
0.4
0.6
0.8
TIME (SECONDS)

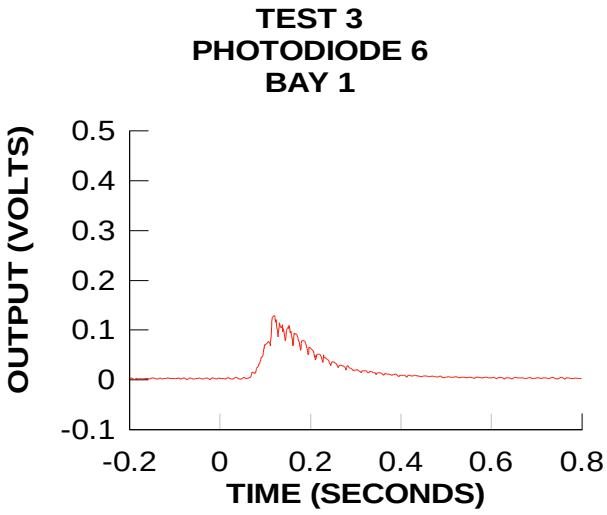
TEST 3
PHOTODIODE 6
BAY 1
OUTPUT (VOLTS)
0.5
0.4
0.3
0.2
0.1
0
-0.1
-0.2
0
0.2
0.4
0.6
0.8
TIME (SECONDS)

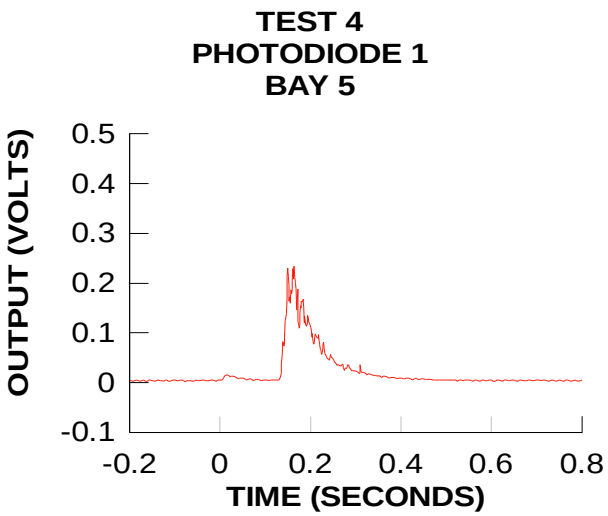
TEST 4
PHOTODIODE 1
BAY 5
OUTPUT (VOLTS)
0.5
0.4
0.3
0.2
0.1
0
-0.1
-0.2
0
0.2
0.4
0.6
0.8
TIME (SECONDS)

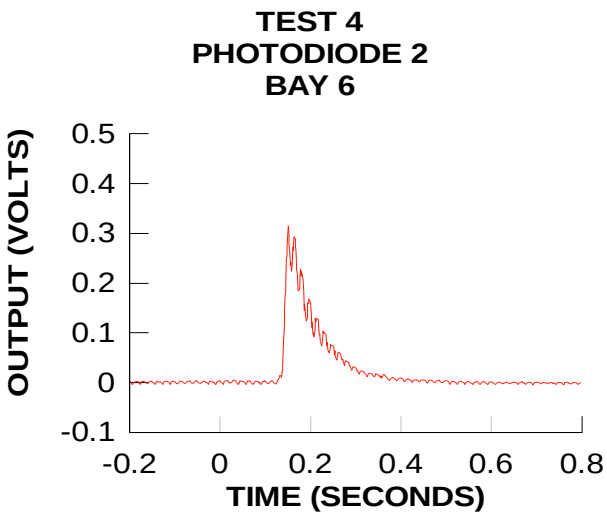
TEST 4
PHOTODIODE 2
BAY 6
OUTPUT (VOLTS)
0.5
0.4
0.3
0.2
0.1
0
-0.1
-0.2
0
0.2
0.4
0.6
0.8
TIME (SECONDS)

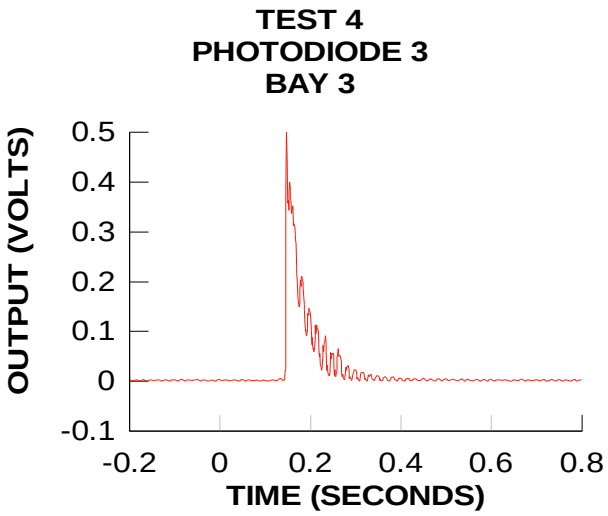
TEST 4
PHOTODIODE 3
BAY 3
OUTPUT (VOLTS)
0.5
0.4
0.3
0.2
0.1
0
-0.1
-0.2
0
0.2
0.4
0.6
0.8
TIME (SECONDS)

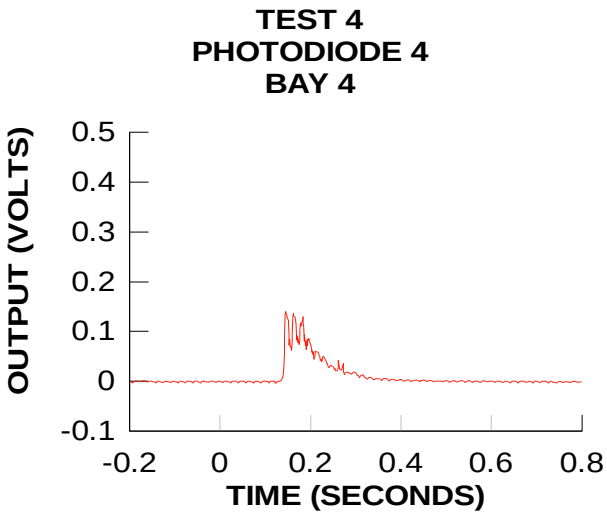
TEST 4
PHOTODIODE 4
BAY 4
OUTPUT (VOLTS)
0.5
0.4
0.3
0.2
0.1
0
-0.1
-0.2
0
0.2
0.4
0.6
0.8
TIME (SECONDS)

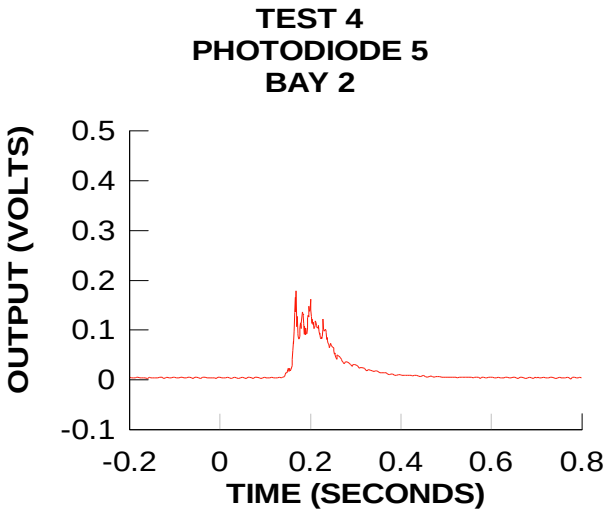
TEST 4
PHOTODIODE 5
BAY 2
OUTPUT (VOLTS)
0.5
0.4
0.3
0.2
0.1
0
-0.1
-0.2
0
0.2
0.4
0.6
0.8
TIME (SECONDS)

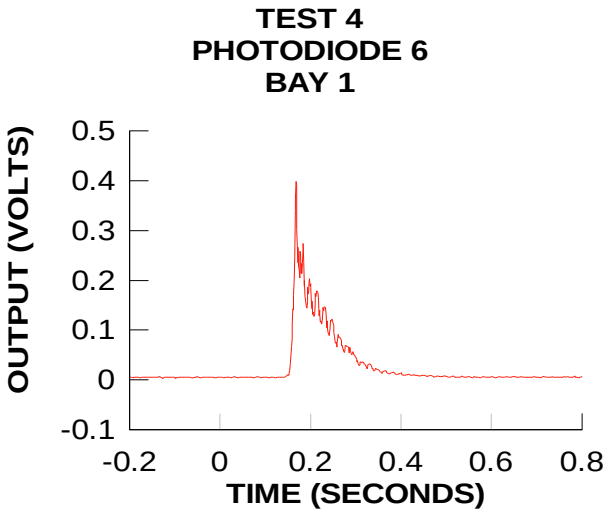
TEST 4
PHOTODIODE 6
BAY 1
OUTPUT (VOLTS)
0.5
0.4
0.3
0.2
0.1
0
-0.1
-0.2
0
0.2
0.4
0.6
0.8
TIME (SECONDS)

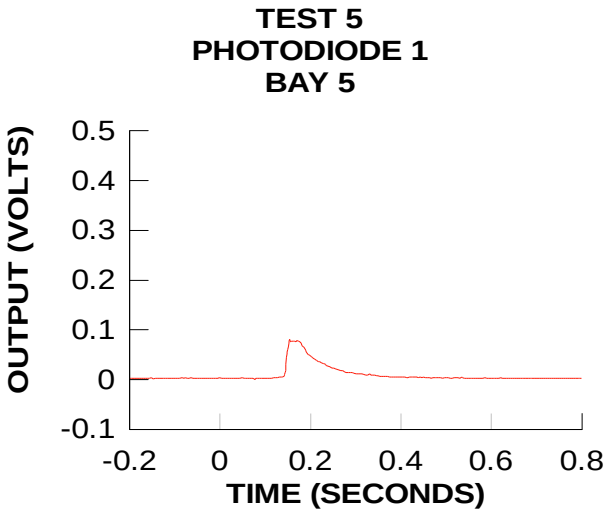
TEST 5
PHOTODIODE 1
BAY 5
OUTPUT (VOLTS)
0.5
0.4
0.3
0.2
0.1
0
-0.1
-0.2
0
0.2
0.4
0.6
0.8
TIME (SECONDS)

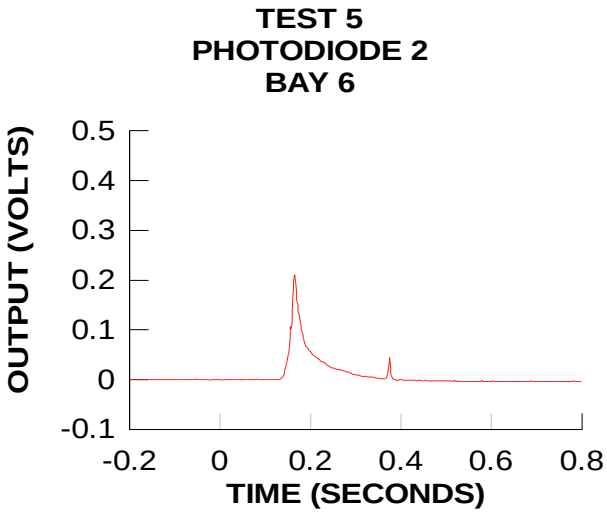
TEST 5
PHOTODIODE 2
BAY 6
OUTPUT (VOLTS)
0.5
0.4
0.3
0.2
0.1
0
-0.1
-0.2
0
0.2
0.4
0.6
0.8
TIME (SECONDS)

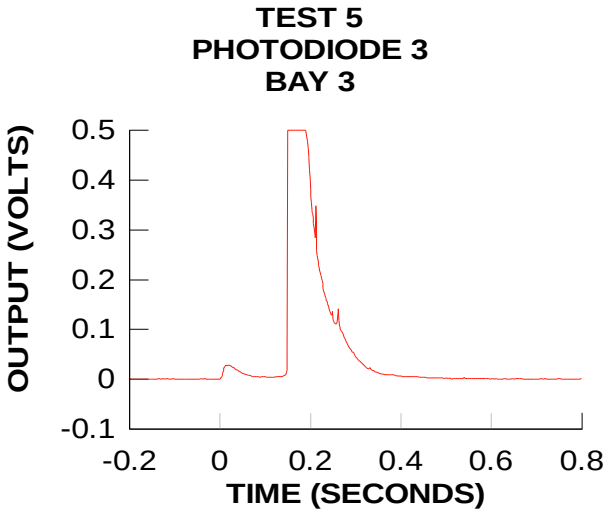
TEST 5
PHOTODIODE 3
BAY 3
OUTPUT (VOLTS)
0.5
0.4
0.3
0.2
0.1
0
-0.1
-0.2
0
0.2
0.4
0.6
0.8
TIME (SECONDS)

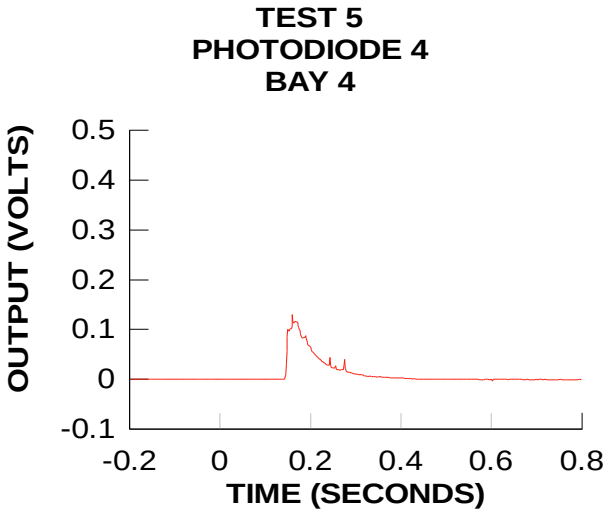
TEST 5
PHOTODIODE 4
BAY 4
OUTPUT (VOLTS)
0.5
0.4
0.3
0.2
0.1
0
-0.1
-0.2
0
0.2
0.4
0.6
0.8
TIME (SECONDS)

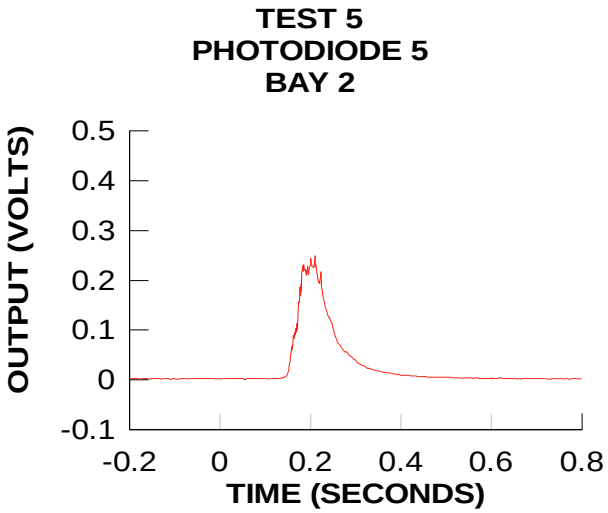
TEST 5
PHOTODIODE 5
BAY 2
OUTPUT (VOLTS)
0.5
0.4
0.3
0.2
0.1
0
-0.1
-0.2
0
0.2
0.4
0.6
0.8
TIME (SECONDS)

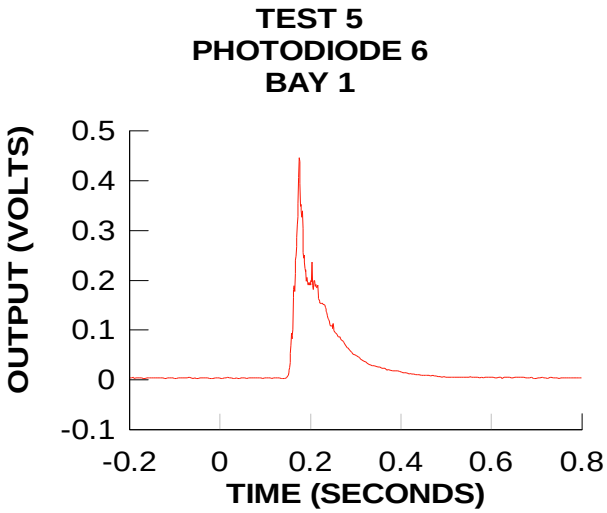
TEST 5
PHOTODIODE 6
BAY 1
OUTPUT (VOLTS)
0.5
0.4
0.3
0.2
0.1
0
-0.1
-0.2
0
0.2
0.4
0.6
0.8
TIME (SECONDS)

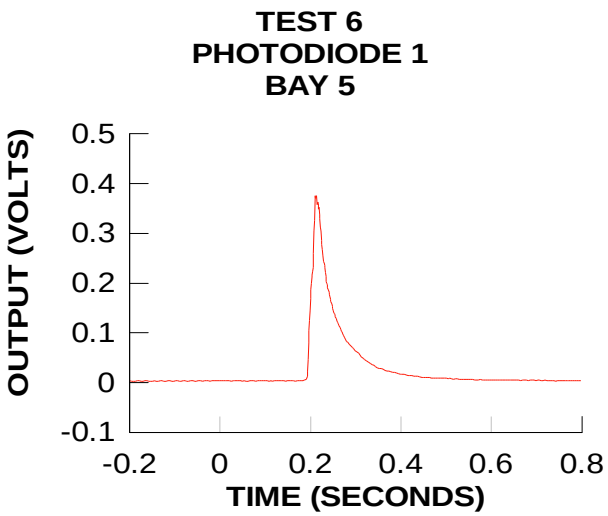
TEST 6
PHOTODIODE 1
BAY 5
OUTPUT (VOLTS)
0.5
0.4
0.3
0.2
0.1
0
-0.1
-0.2
0
0.2
0.4
0.6
0.8
TIME (SECONDS)

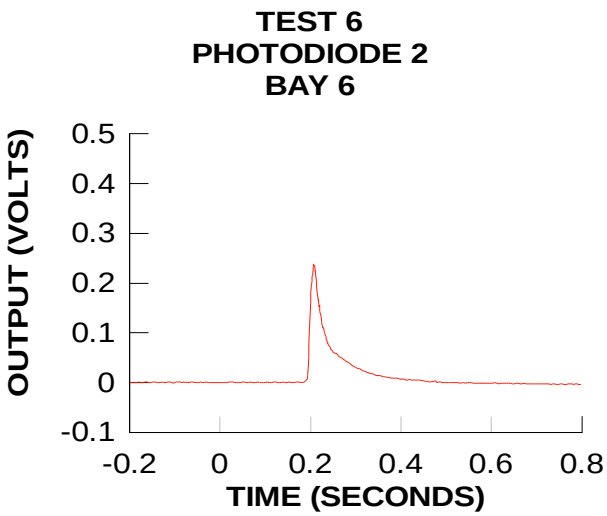
TEST 6
PHOTODIODE 2
BAY 6
OUTPUT (VOLTS)
0.5
0.4
0.3
0.2
0.1
0
-0.1
-0.2
0
0.2
0.4
0.6
0.8
TIME (SECONDS)

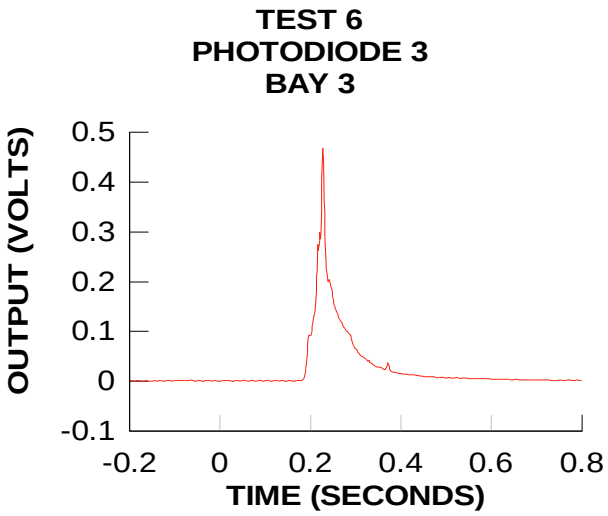
TEST 6
PHOTODIODE 3
BAY 3
OUTPUT (VOLTS)
0.5
0.4
0.3
0.2
0.1
0
-0.1
-0.2
0
0.2
0.4
0.6
0.8
TIME (SECONDS)

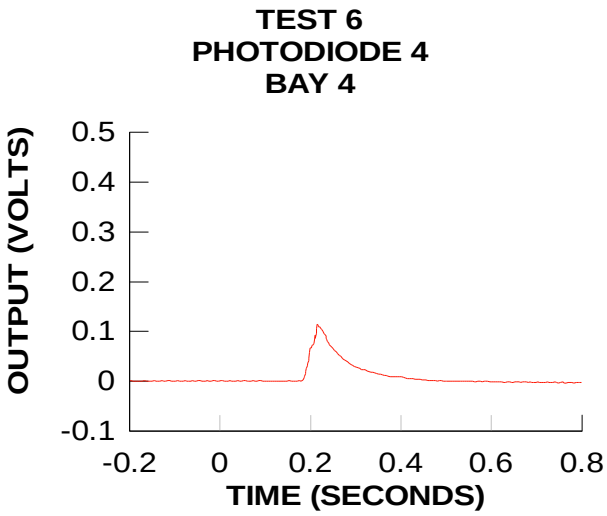
TEST 6
PHOTODIODE 4
BAY 4
OUTPUT (VOLTS)
0.5
0.4
0.3
0.2
0.1
0
-0.1
-0.2
0
0.2
0.4
0.6
0.8
TIME (SECONDS)

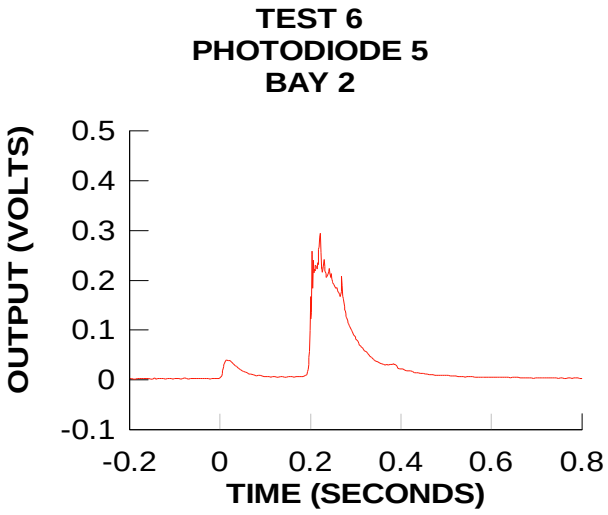
TEST 6
PHOTODIODE 5
BAY 2
OUTPUT (VOLTS)
0.5
0.4
0.3
0.2
0.1
0
-0.1
-0.2
0
0.2
0.4
0.6
0.8
TIME (SECONDS)

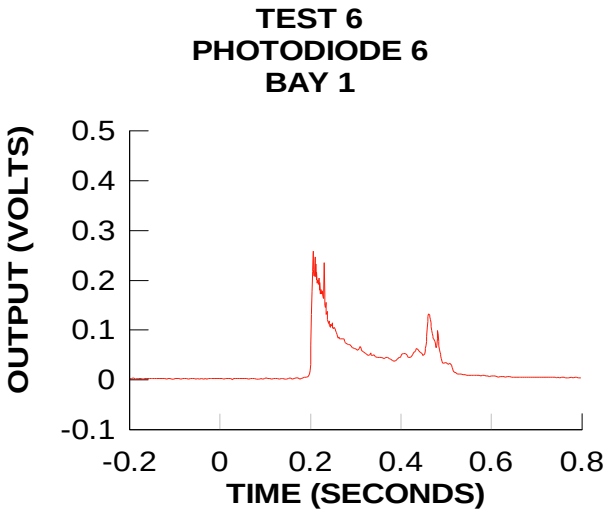
TEST 6
PHOTODIODE 6
BAY 1
OUTPUT (VOLTS)
0.5
0.4
0.3
0.2
0.1
0
-0.1
-0.2
0
0.2
0.4
0.6
0.8
TIME (SECONDS)

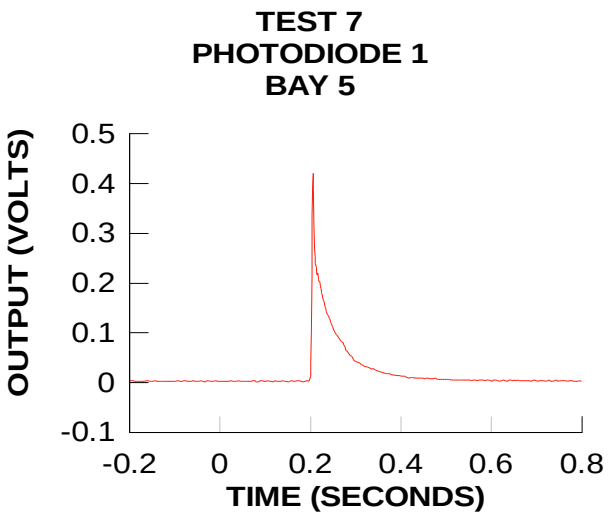
TEST 7
PHOTODIODE 1
BAY 5
OUTPUT (VOLTS)
0.5
0.4
0.3
0.2
0.1
0
-0.1
-0.2
0
0.2
0.4
0.6
0.8
TIME (SECONDS)

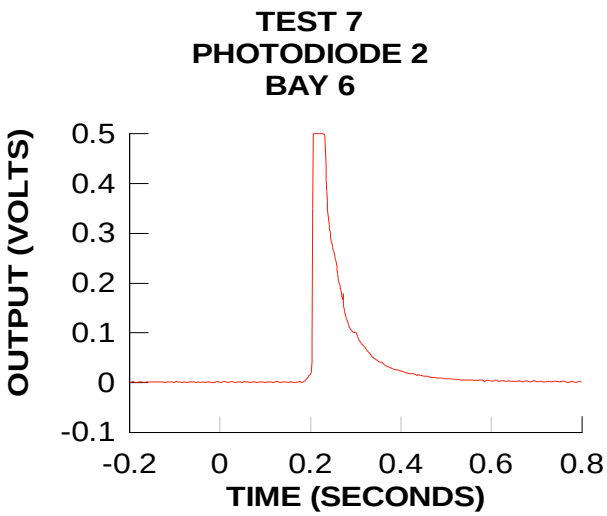
TEST 7
PHOTODIODE 2
BAY 6
OUTPUT (VOLTS)
0.5
0.4
0.3
0.2
0.1
0
-0.1
-0.2
0
0.2
0.4
0.6
0.8
TIME (SECONDS)

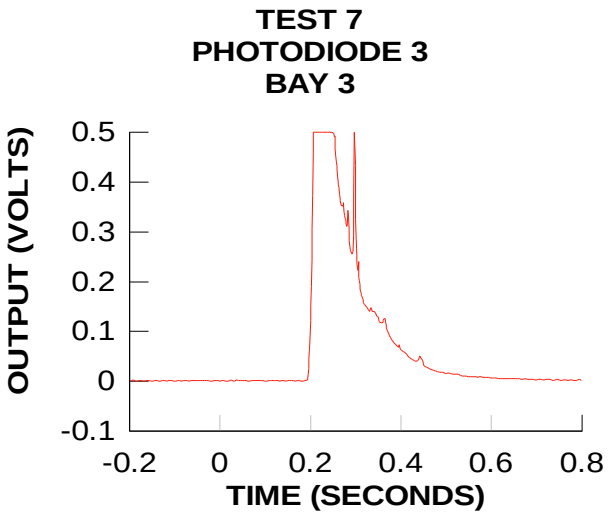
TEST 7
PHOTODIODE 3
BAY 3
OUTPUT (VOLTS)
0.5
0.4
0.3
0.2
0.1
0
-0.1
-0.2
0
0.2
0.4
0.6
0.8
TIME (SECONDS)

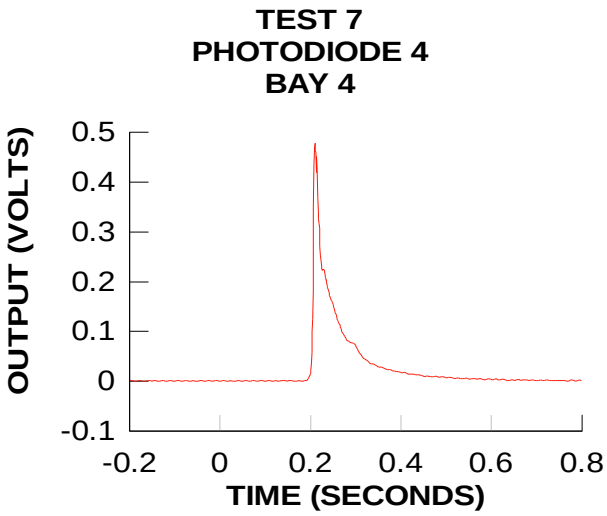
TEST 7
PHOTODIODE 4
BAY 4
OUTPUT (VOLTS)
0.5
0.4
0.3
0.2
0.1
0
-0.1
-0.2
0
0.2
0.4
0.6
0.8
TIME (SECONDS)

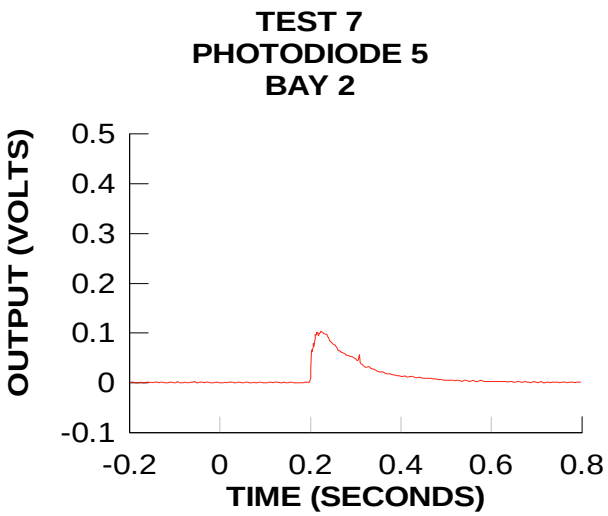
TEST 7
PHOTODIODE 5
BAY 2
OUTPUT (VOLTS)
0.5
0.4
0.3
0.2
0.1
0
-0.1
-0.2
0
0.2
0.4
0.6
0.8
TIME (SECONDS)

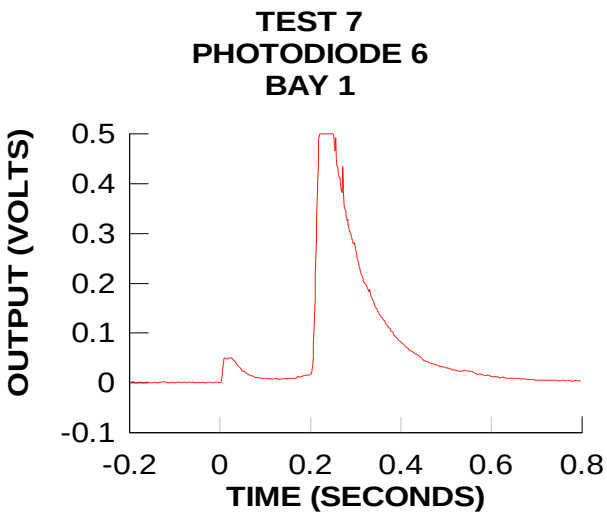
TEST 7
PHOTODIODE 6
BAY 1
OUTPUT (VOLTS)
0.5
0.4
0.3
0.2
0.1
0
-0.1
-0.2
0
0.2
0.4
0.6
0.8
TIME (SECONDS)

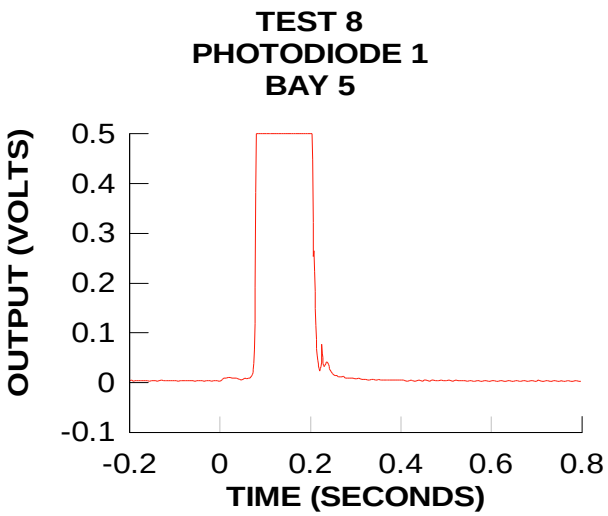
TEST 8
PHOTODIODE 1
BAY 5
OUTPUT (VOLTS)
0.5
0.4
0.3
0.2
0.1
0
-0.1
-0.2
0
0.2
0.4
0.6
0.8
TIME (SECONDS)

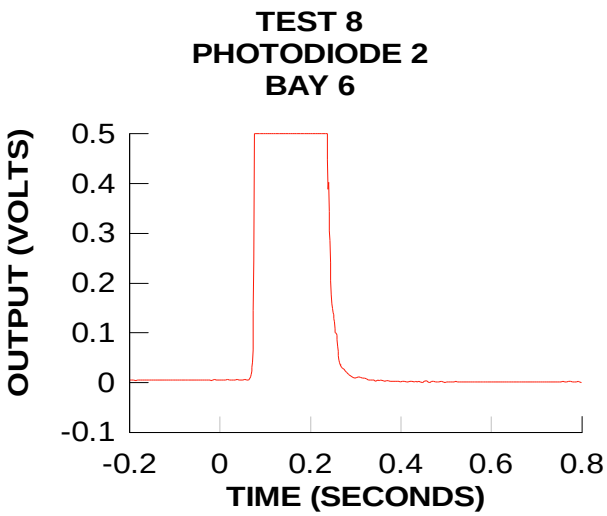
TEST 8
PHOTODIODE 2
BAY 6
OUTPUT (VOLTS)
0.5
0.4
0.3
0.2
0.1
0
-0.1
-0.2
0
0.2
0.4
0.6
0.8
TIME (SECONDS)

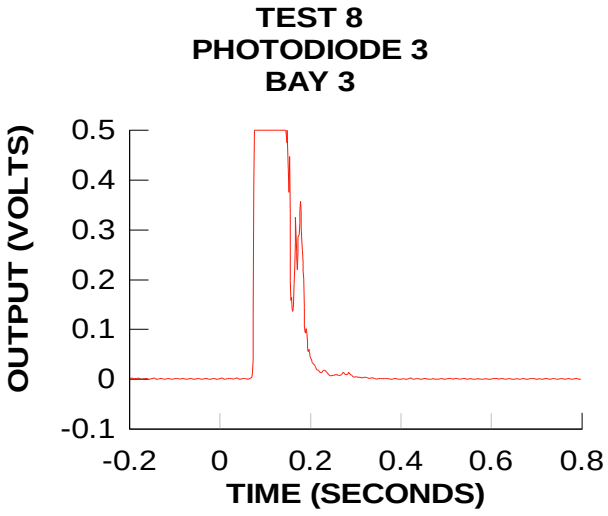
TEST 8
PHOTODIODE 3
BAY 3
OUTPUT (VOLTS)
0.5
0.4
0.3
0.2
0.1
0
-0.1
-0.2
0
0.2
0.4
0.6
0.8
TIME (SECONDS)

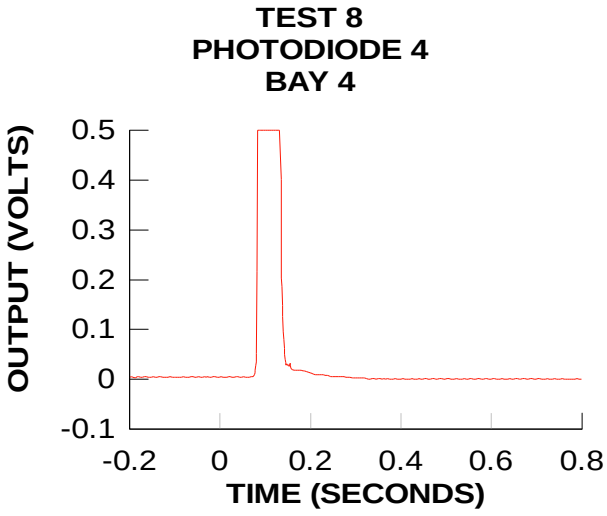
TEST 8
PHOTODIODE 4
BAY 4
OUTPUT (VOLTS)
0.5
0.4
0.3
0.2
0.1
0
-0.1
-0.2
0
0.2
0.4
0.6
0.8
TIME (SECONDS)

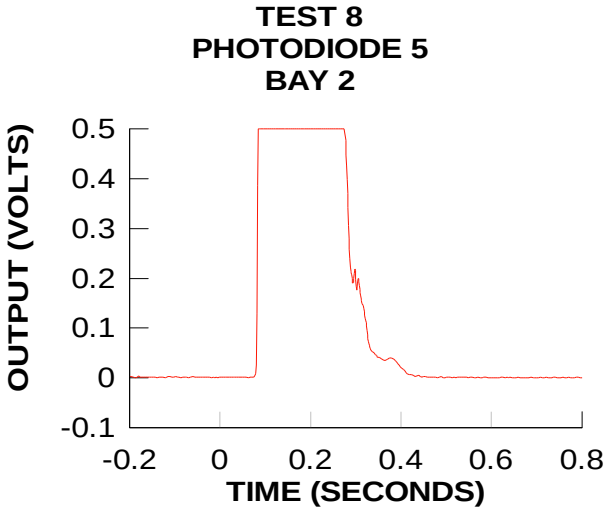
TEST 8
PHOTODIODE 5
BAY 2
OUTPUT (VOLTS)
0.5
0.4
0.3
0.2
0.1
0
-0.1
-0.2
0
0.2
0.4
0.6
0.8
TIME (SECONDS)

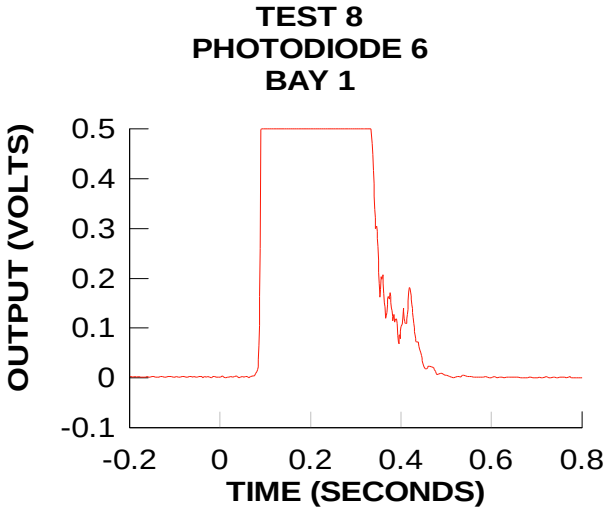
TEST 8
PHOTODIODE 6
BAY 1
OUTPUT (VOLTS)
0.5
0.4
0.3
0.2
0.1
0
-0.1
-0.2
0
0.2
0.4
0.6
0.8
TIME (SECONDS)

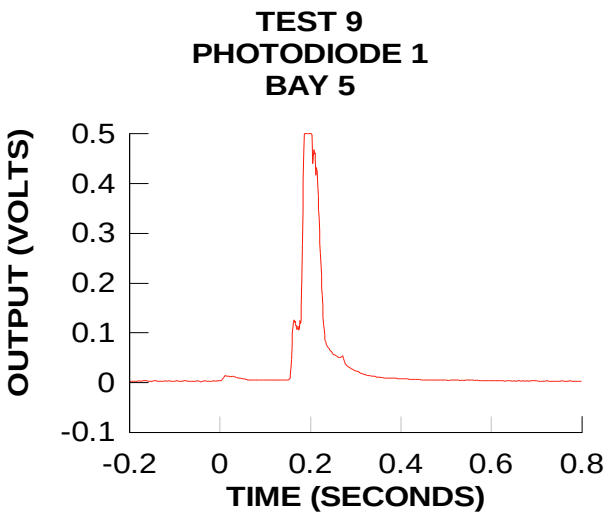
TEST 9
PHOTODIODE 1
BAY 5
OUTPUT (VOLTS)
0.5
0.4
0.3
0.2
0.1
0
-0.1
-0.2
0
0.2
0.4
0.6
0.8
TIME (SECONDS)

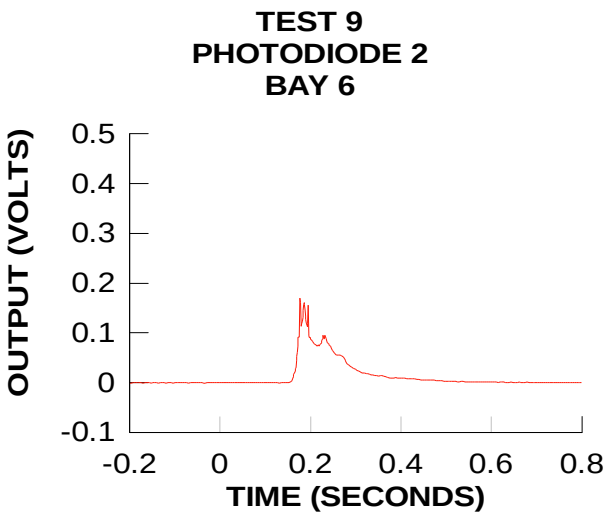
TEST 9
PHOTODIODE 2
BAY 6
OUTPUT (VOLTS)
0.5
0.4
0.3
0.2
0.1
0
-0.1
-0.2
0
0.2
0.4
0.6
0.8
TIME (SECONDS)

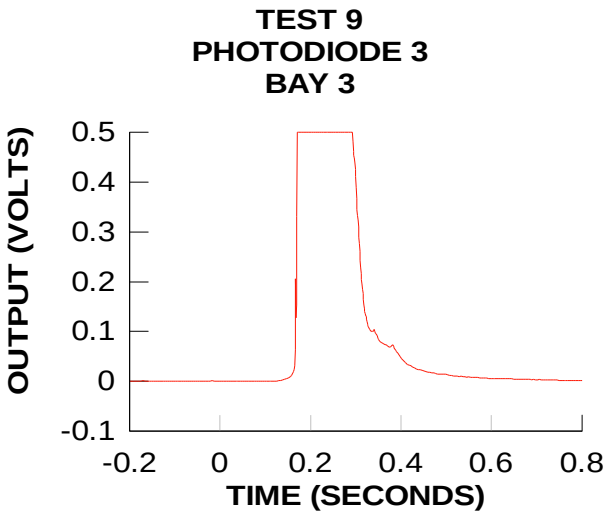
TEST 9
PHOTODIODE 3
BAY 3
OUTPUT (VOLTS)
0.5
0.4
0.3
0.2
0.1
0
-0.1
-0.2
0
0.2
0.4
0.6
0.8
TIME (SECONDS)

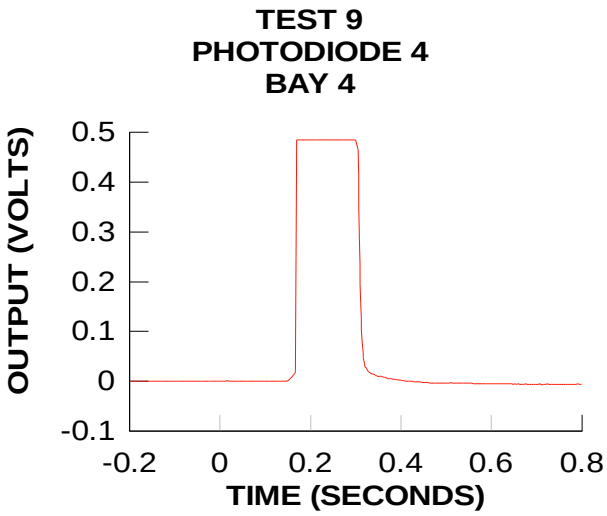
TEST 9
PHOTODIODE 4
BAY 4
OUTPUT (VOLTS)
0.5
0.4
0.3
0.2
0.1
0
-0.1
-0.2
0
0.2
0.4
0.6
0.8
TIME (SECONDS)

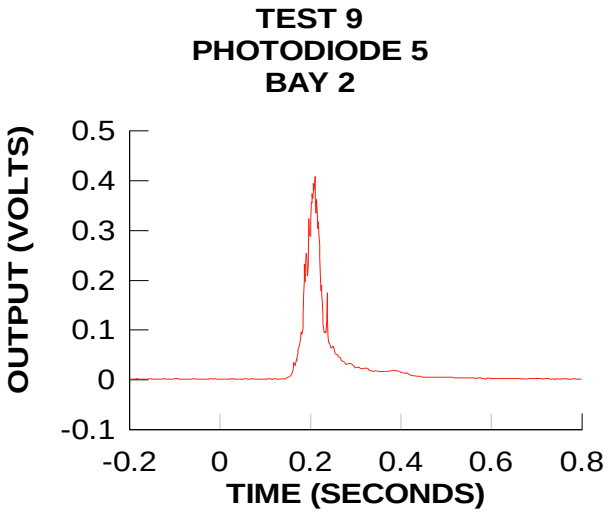
TEST 9
PHOTODIODE 5
BAY 2
OUTPUT (VOLTS)
0.5
0.4
0.3
0.2
0.1
0
-0.1
-0.2
0
0.2
0.4
0.6
0.8
TIME (SECONDS)

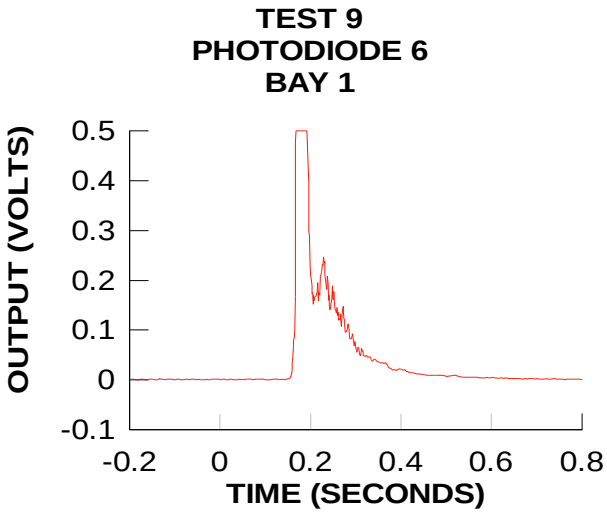
TEST 9
PHOTODIODE 6
BAY 1
OUTPUT (VOLTS)
0.5
0.4
0.3
0.2
0.1
0
-0.1
-0.2
0
0.2
0.4
0.6
0.8
TIME (SECONDS)

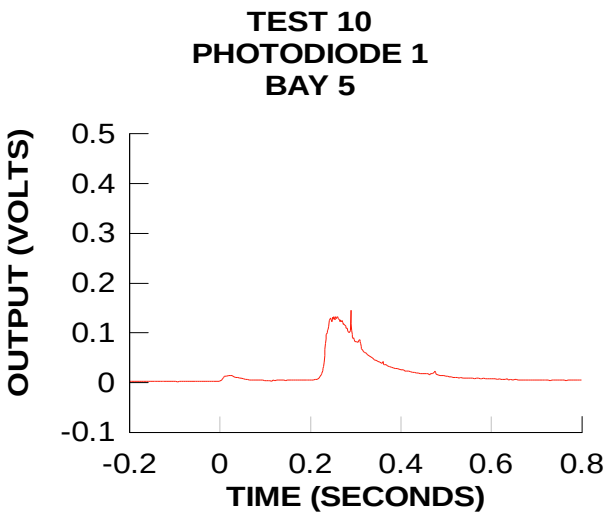
TEST 10
PHOTODIODE 1
BAY 5
OUTPUT (VOLTS)
0.5
0.4
0.3
0.2
0.1
0
-0.1
-0.2
0
0.2
0.4
0.6
0.8
TIME (SECONDS)

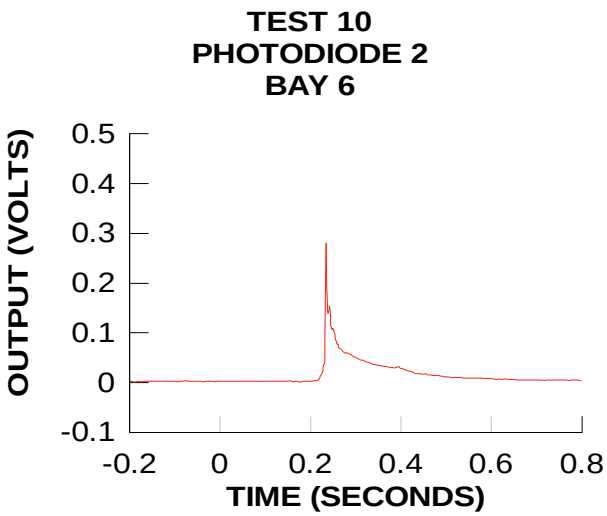
TEST 10
PHOTODIODE 2
BAY 6
OUTPUT (VOLTS)
0.5
0.4
0.3
0.2
0.1
0
-0.1
-0.2
0
0.2
0.4
0.6
0.8
TIME (SECONDS)

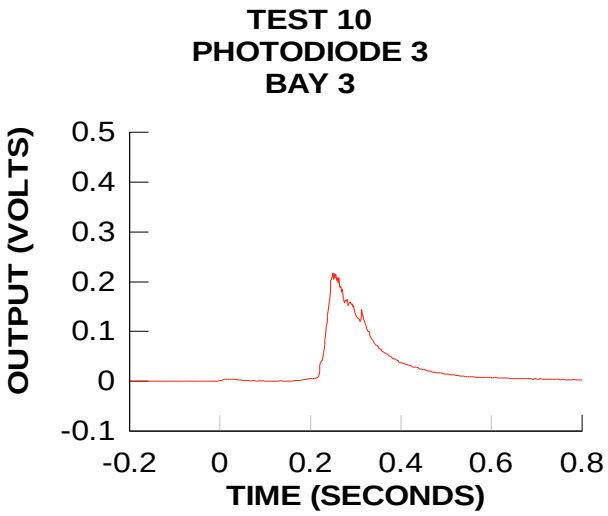
TEST 10
PHOTODIODE 3
BAY 3
OUTPUT (VOLTS)
0.5
0.4
0.3
0.2
0.1
0
-0.1
-0.2
0
0.2
0.4
0.6
0.8
TIME (SECONDS)

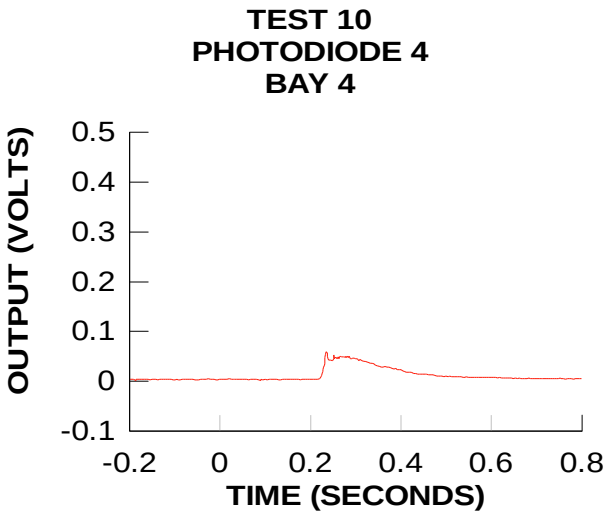
TEST 10
PHOTODIODE 4
BAY 4
OUTPUT (VOLTS)
0.5
0.4
0.3
0.2
0.1
0
-0.1
-0.2
0
0.2
0.4
0.6
0.8
TIME (SECONDS)

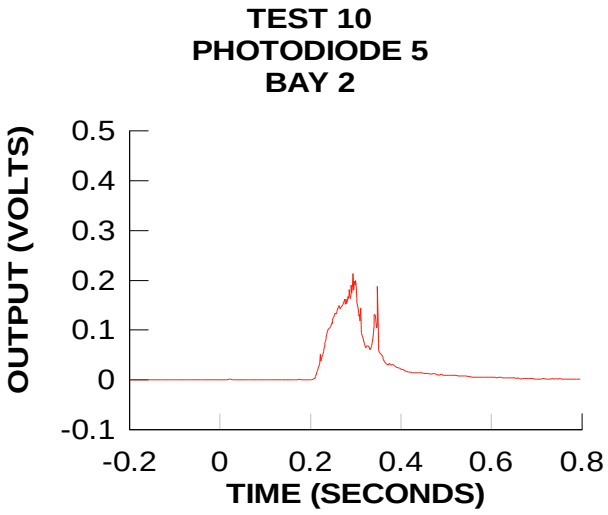
TEST 10
PHOTODIODE 5
BAY 2
OUTPUT (VOLTS)
0.5
0.4
0.3
0.2
0.1
0
-0.1
-0.2
0
0.2
0.4
0.6
0.8
TIME (SECONDS)

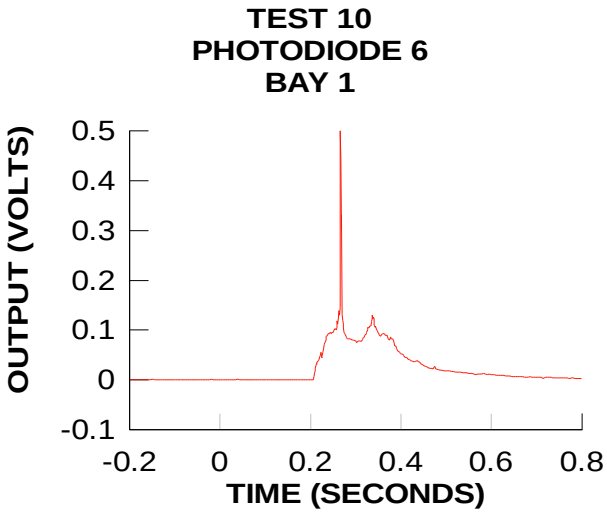
TEST 10
PHOTODIODE 6
BAY 1
OUTPUT (VOLTS)
0.5
0.4
0.3
0.2
0.1
0
-0.1
-0.2
0
0.2
0.4
0.6
0.8
TIME (SECONDS)

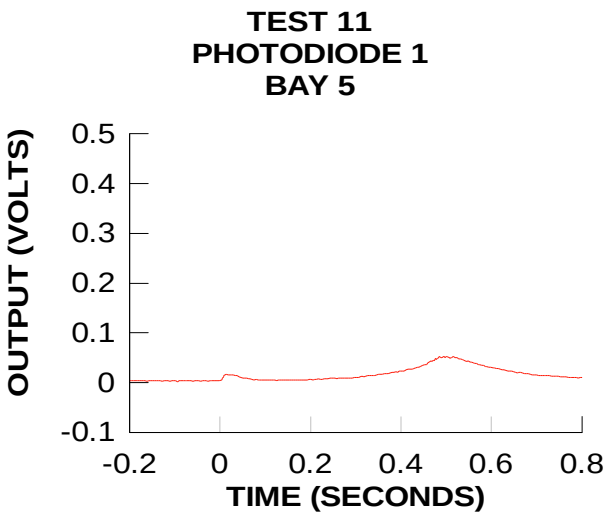
TEST 11
PHOTODIODE 1
BAY 5
OUTPUT (VOLTS)
0.5
0.4
0.3
0.2
0.1
0
-0.1
-0.2
0
0.2
0.4
0.6
0.8
TIME (SECONDS)

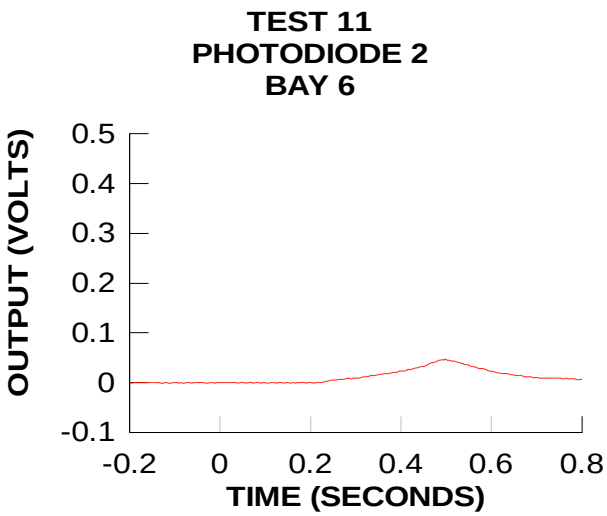
TEST 11
PHOTODIODE 2
BAY 6
OUTPUT (VOLTS)
0.5
0.4
0.3
0.2
0.1
0
-0.1
-0.2
0
0.2
0.4
0.6
0.8
TIME (SECONDS)

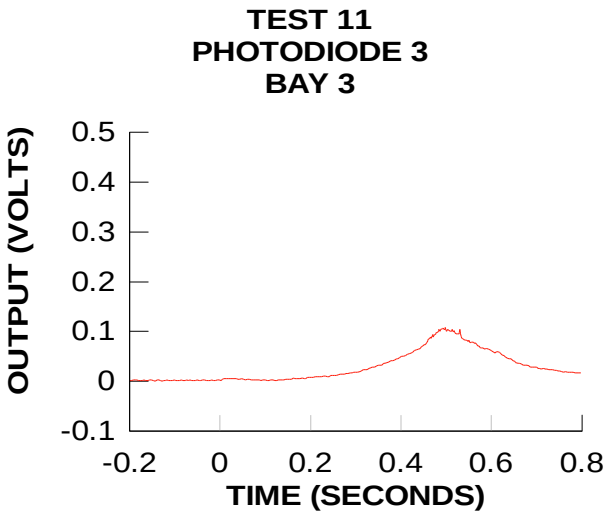
TEST 11
PHOTODIODE 3
BAY 3
OUTPUT (VOLTS)
0.5
0.4
0.3
0.2
0.1
0
-0.1
-0.2
0
0.2
0.4
0.6
0.8
TIME (SECONDS)

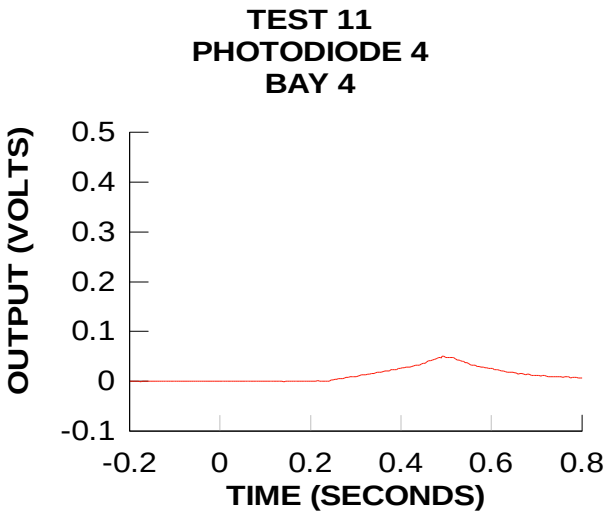
TEST 11
PHOTODIODE 4
BAY 4
OUTPUT (VOLTS)
0.5
0.4
0.3
0.2
0.1
0
-0.1
-0.2
0
0.2
0.4
0.6
0.8
TIME (SECONDS)

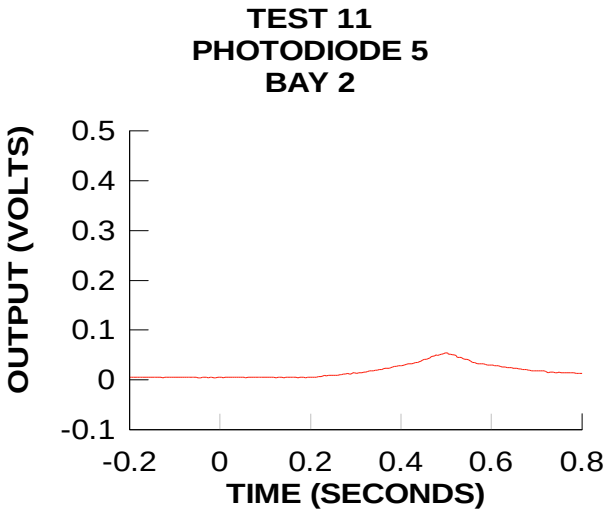
TEST 11
PHOTODIODE 5
BAY 2
OUTPUT (VOLTS)
0.5
0.4
0.3
0.2
0.1
0
-0.1
-0.2
0
0.2
0.4
0.6
0.8
TIME (SECONDS)

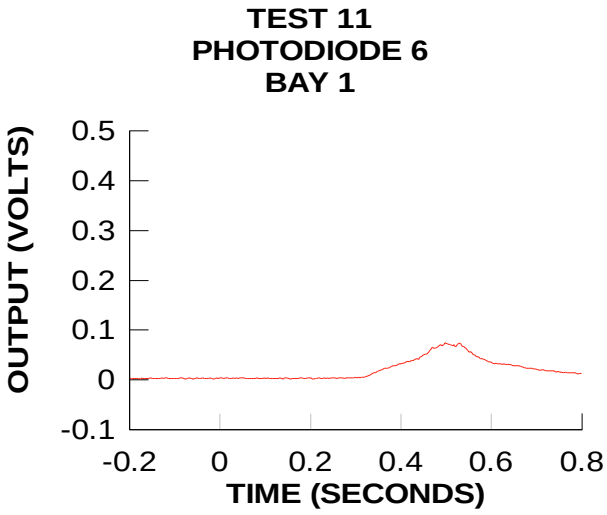
TEST 11
PHOTODIODE 6
BAY 1
OUTPUT (VOLTS)
0.5
0.4
0.3
0.2
0.1
0
-0.1
-0.2
0
0.2
0.4
0.6
0.8
TIME (SECONDS)

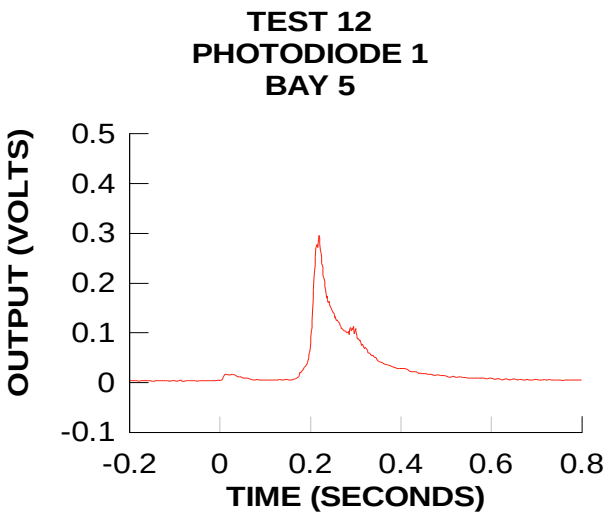
TEST 12
PHOTODIODE 1
BAY 5
OUTPUT (VOLTS)
0.5
0.4
0.3
0.2
0.1
0
-0.1
-0.2
0
0.2
0.4
0.6
0.8
TIME (SECONDS)

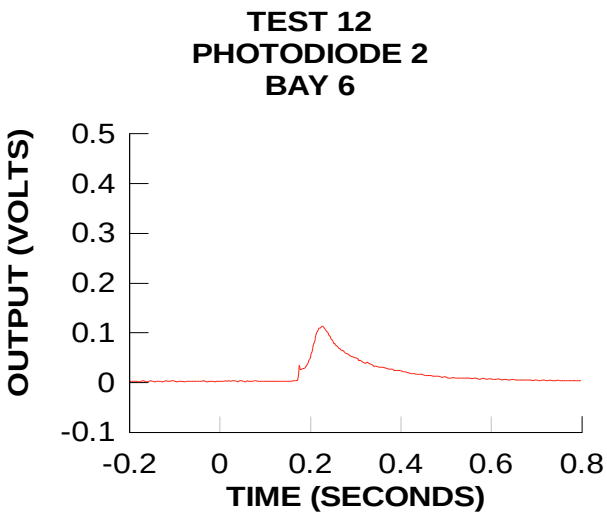
TEST 12
PHOTODIODE 2
BAY 6
OUTPUT (VOLTS)
0.5
0.4
0.3
0.2
0.1
0
-0.1
-0.2
0
0.2
0.4
0.6
0.8
TIME (SECONDS)

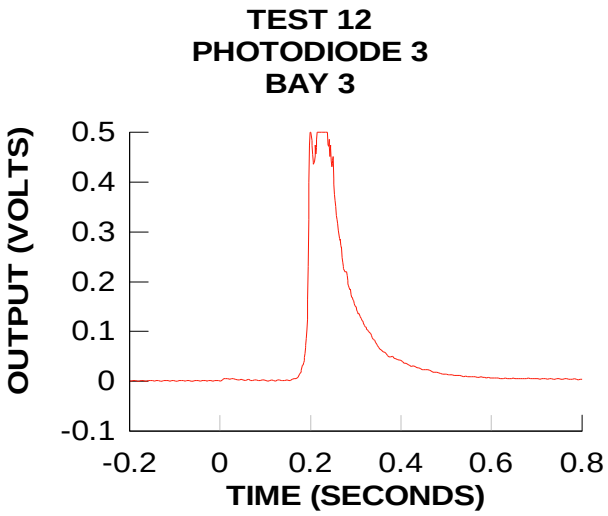
TEST 12
PHOTODIODE 3
BAY 3
OUTPUT (VOLTS)
0.5
0.4
0.3
0.2
0.1
0
-0.1
-0.2
0
0.2
0.4
0.6
0.8
TIME (SECONDS)

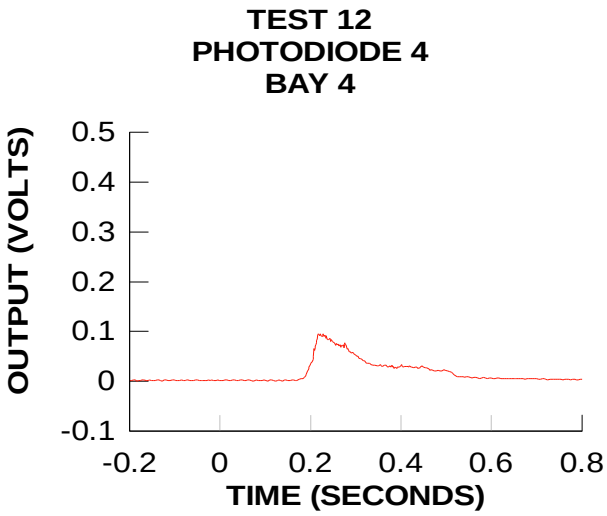
TEST 12
PHOTODIODE 4
BAY 4
OUTPUT (VOLTS)
0.5
0.4
0.3
0.2
0.1
0
-0.1
-0.2
0
0.2
0.4
0.6
0.8
TIME (SECONDS)

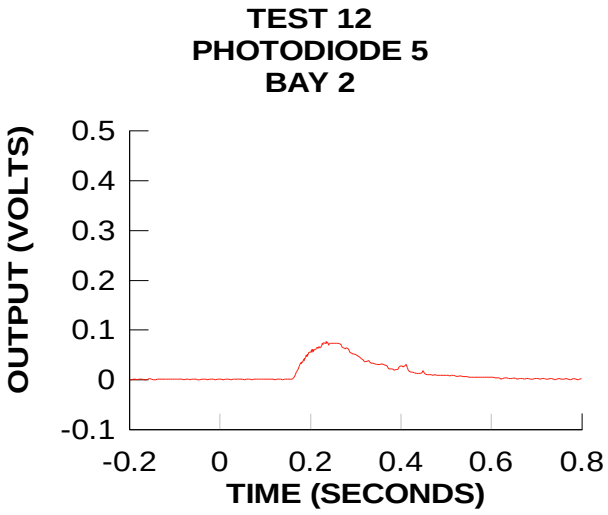
TEST 12
PHOTODIODE 5
BAY 2
OUTPUT (VOLTS)
0.5
0.4
0.3
0.2
0.1
0
-0.1
-0.2
0
0.2
0.4
0.6
0.8
TIME (SECONDS)

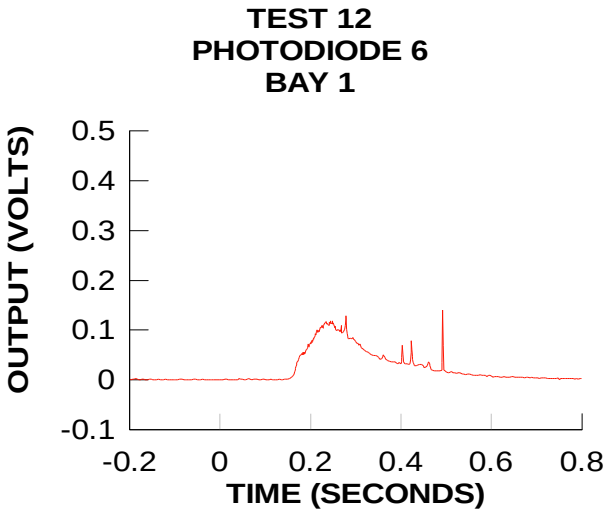
TEST 12
PHOTODIODE 6
BAY 1
OUTPUT (VOLTS)
0.5
0.4
0.3
0.2
0.1
0
-0.1
-0.2
0
0.2
0.4
0.6
0.8
TIME (SECONDS)

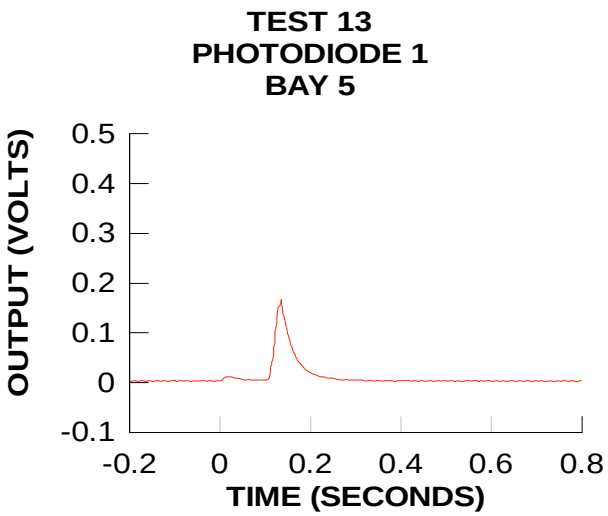
TEST 13
PHOTODIODE 1
BAY 5
OUTPUT (VOLTS)
0.5
0.4
0.3
0.2
0.1
0
-0.1
-0.2
0
0.2
0.4
0.6
0.8
TIME (SECONDS)

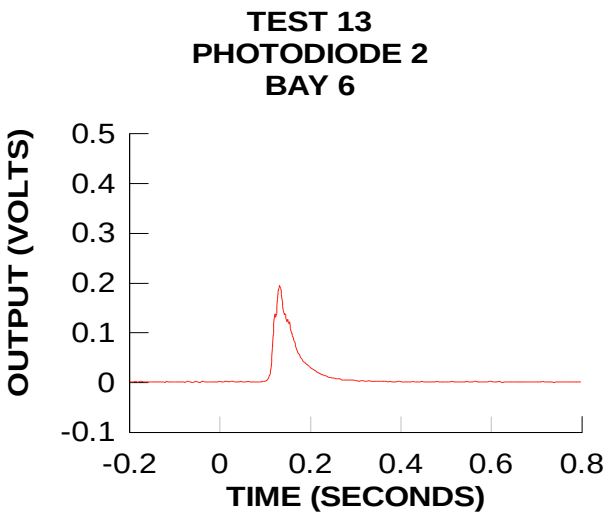
TEST 13
PHOTODIODE 2
BAY 6
OUTPUT (VOLTS)
0.5
0.4
0.3
0.2
0.1
0
-0.1
-0.2
0
0.2
0.4
0.6
0.8
TIME (SECONDS)

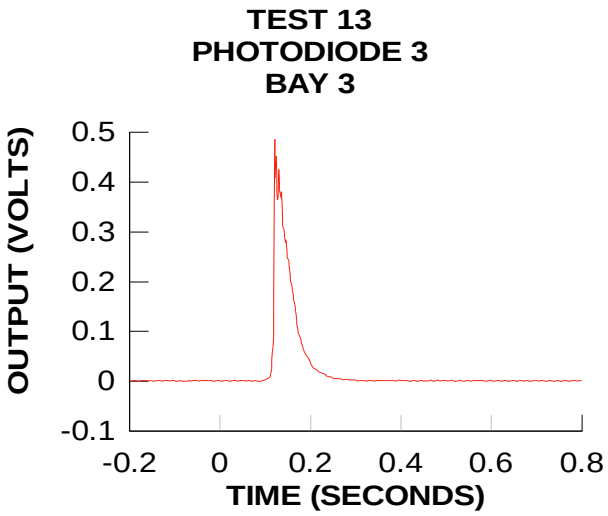
TEST 13
PHOTODIODE 3
BAY 3
OUTPUT (VOLTS)
0.5
0.4
0.3
0.2
0.1
0
-0.1
-0.2
0
0.2
0.4
0.6
0.8
TIME (SECONDS)

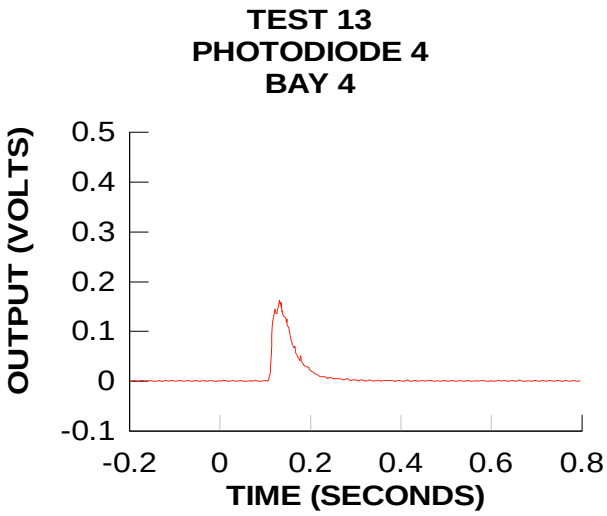
TEST 13
PHOTODIODE 4
BAY 4
OUTPUT (VOLTS)
0.5
0.4
0.3
0.2
0.1
0
-0.1
-0.2
0
0.2
0.4
0.6
0.8
TIME (SECONDS)

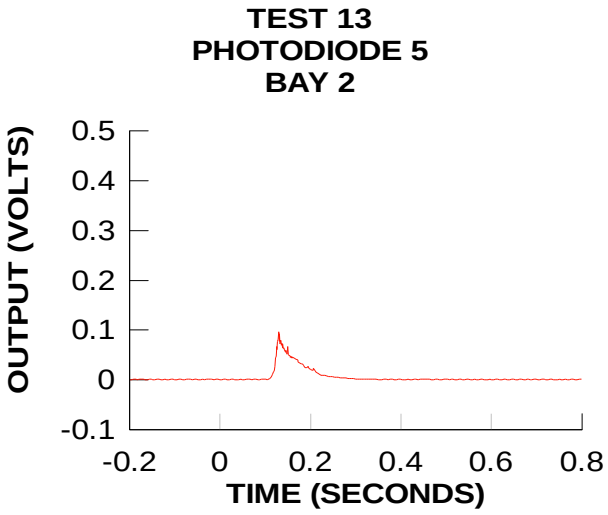
TEST 13
PHOTODIODE 5
BAY 2
OUTPUT (VOLTS)
0.5
0.4
0.3
0.2
0.1
0
-0.1
-0.2
0
0.2
0.4
0.6
0.8
TIME (SECONDS)

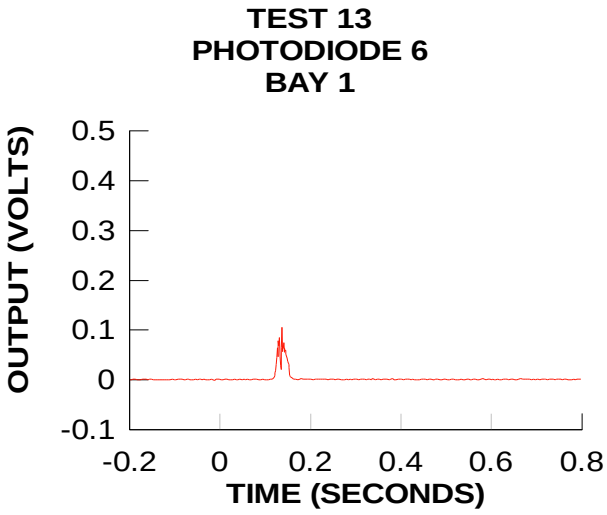
TEST 13
PHOTODIODE 6
BAY 1
OUTPUT (VOLTS)
0.5
0.4
0.3
0.2
0.1
0
-0.1
-0.2
0
0.2
0.4
0.6
0.8
TIME (SECONDS)

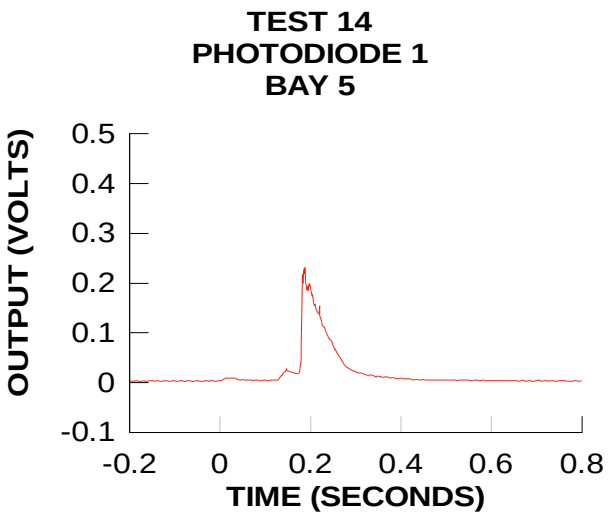
TEST 14
PHOTODIODE 1
BAY 5
OUTPUT (VOLTS)
0.5
0.4
0.3
0.2
0.1
0
-0.1
-0.2
0
0.2
0.4
0.6
0.8
TIME (SECONDS)

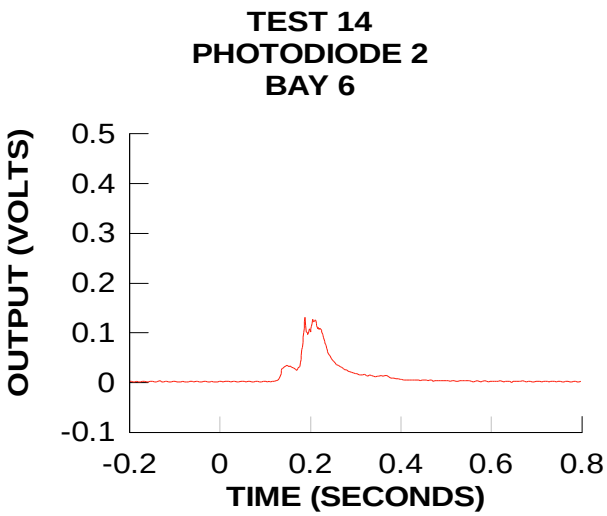
TEST 14
PHOTODIODE 2
BAY 6
OUTPUT (VOLTS)
0.5
0.4
0.3
0.2
0.1
0
-0.1
-0.2
0
0.2
0.4
0.6
0.8
TIME (SECONDS)

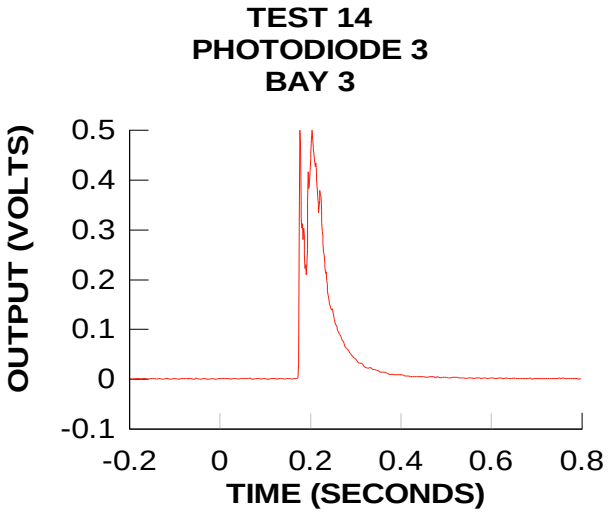
TEST 14
PHOTODIODE 3
BAY 3
OUTPUT (VOLTS)
0.5
0.4
0.3
0.2
0.1
0
-0.1
-0.2
0
0.2
0.4
0.6
0.8
TIME (SECONDS)

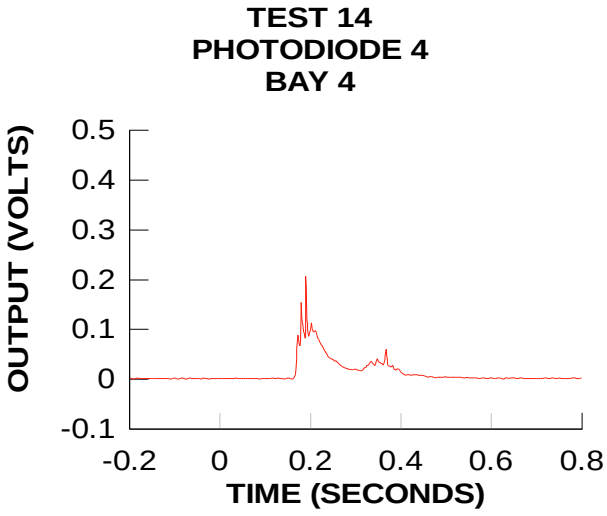
TEST 14
PHOTODIODE 4
BAY 4
OUTPUT (VOLTS)
0.5
0.4
0.3
0.2
0.1
0
-0.1
-0.2
0
0.2
0.4
0.6
0.8
TIME (SECONDS)

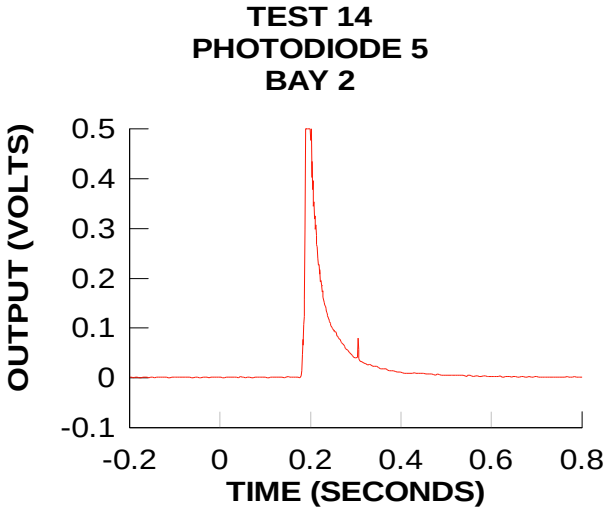
TEST 14
PHOTODIODE 5
BAY 2
OUTPUT (VOLTS)
0.5
0.4
0.3
0.2
0.1
0
-0.1
-0.2
0
0.2
0.4
0.6
0.8
TIME (SECONDS)

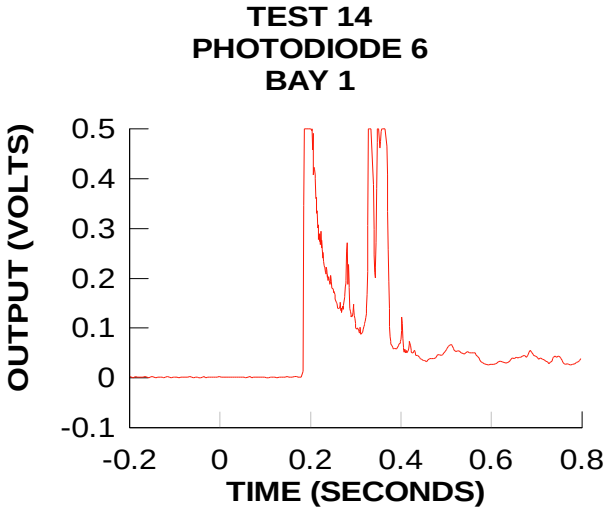
TEST 14
PHOTODIODE 6
BAY 1
OUTPUT (VOLTS)
0.5
0.4
0.3
0.2
0.1
0
-0.1
-0.2
0
0.2
0.4
0.6
0.8
TIME (SECONDS)

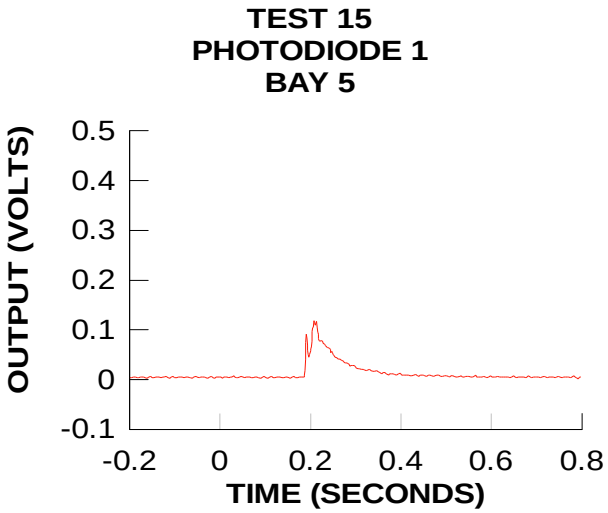
TEST 15
PHOTODIODE 1
BAY 5
OUTPUT (VOLTS)
0.5
0.4
0.3
0.2
0.1
0
-0.1
-0.2
0
0.2
0.4
0.6
0.8
TIME (SECONDS)

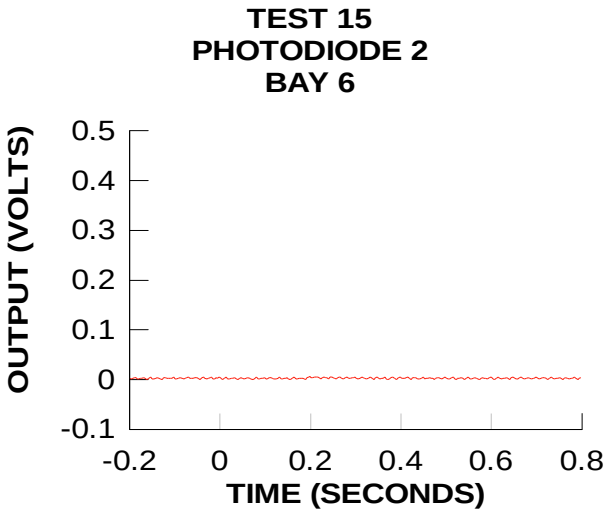
TEST 15
PHOTODIODE 2
BAY 6
OUTPUT (VOLTS)
0.5
0.4
0.3
0.2
0.1
0
-0.1
-0.2
0
0.2
0.4
0.6
0.8
TIME (SECONDS)

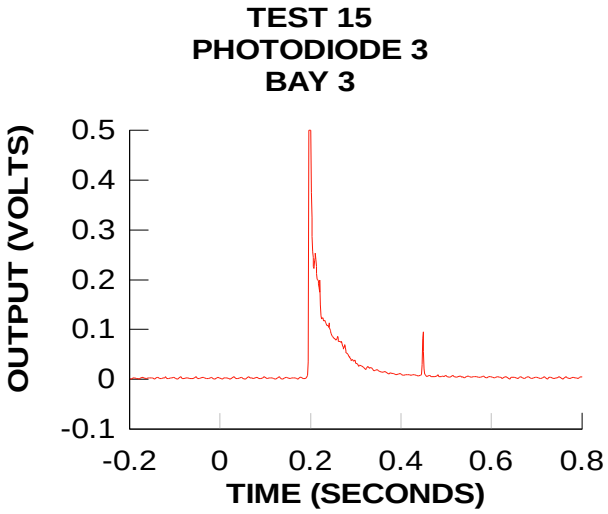
TEST 15
PHOTODIODE 3
BAY 3
OUTPUT (VOLTS)
0.5
0.4
0.3
0.2
0.1
0
-0.1
-0.2
0
0.2
0.4
0.6
0.8
TIME (SECONDS)

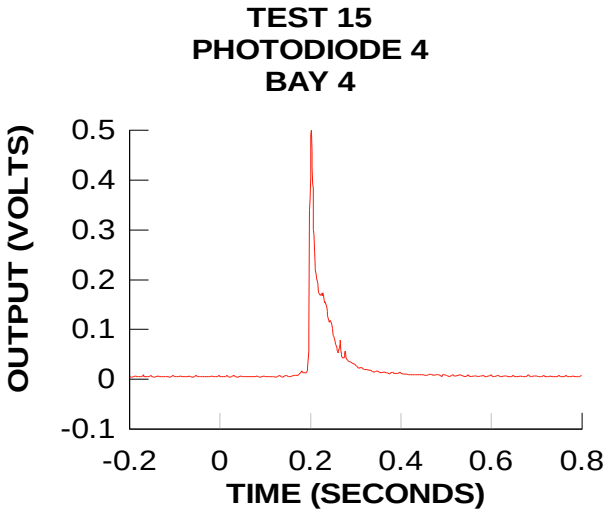
TEST 15
PHOTODIODE 4
BAY 4
OUTPUT (VOLTS)
0.5
0.4
0.3
0.2
0.1
0
-0.1
-0.2
0
0.2
0.4
0.6
0.8
TIME (SECONDS)

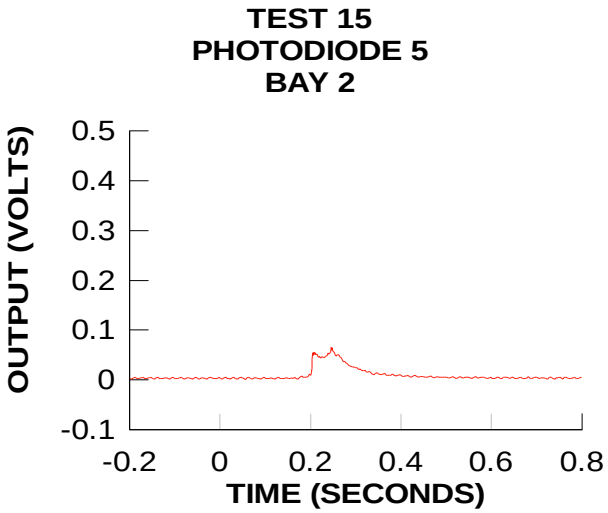
TEST 15
PHOTODIODE 5
BAY 2
OUTPUT (VOLTS)
0.5
0.4
0.3
0.2
0.1
0
-0.1
-0.2
0
0.2
0.4
0.6
0.8
TIME (SECONDS)

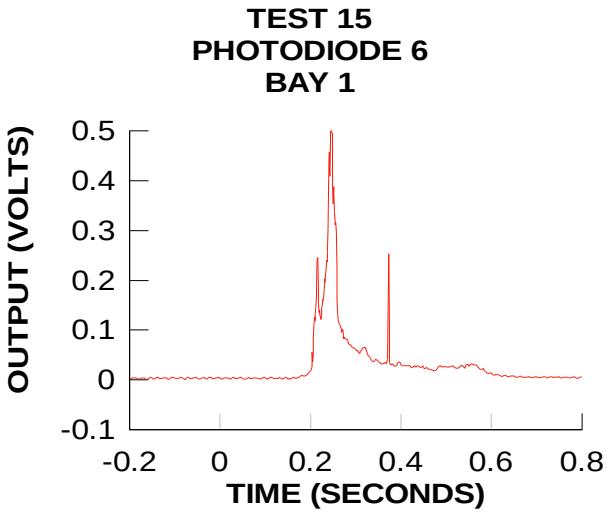
TEST 15
PHOTODIODE 6
BAY 1
OUTPUT (VOLTS)
0.5
0.4
0.3
0.2
0.1
0
-0.1
-0.2
0
0.2
0.4
0.6
0.8
TIME (SECONDS)

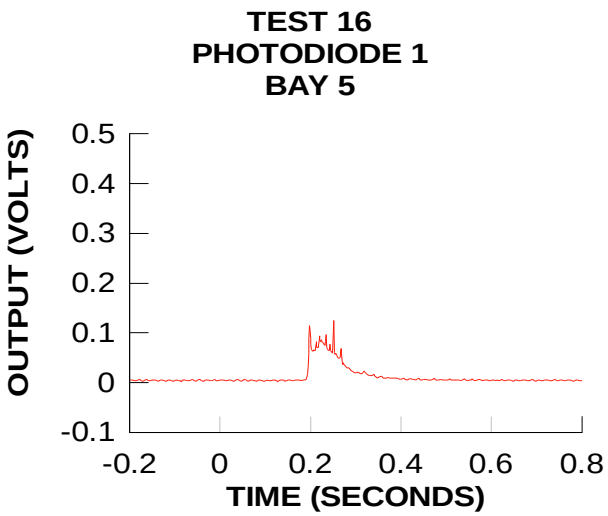
TEST 16
PHOTODIODE 1
BAY 5
OUTPUT (VOLTS)
0.5
0.4
0.3
0.2
0.1
0
-0.1
-0.2
0
0.2
0.4
0.6
0.8
TIME (SECONDS)

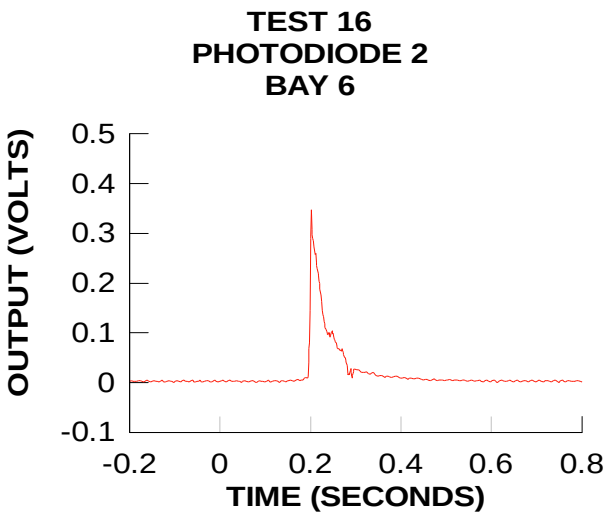
TEST 16
PHOTODIODE 2
BAY 6
OUTPUT (VOLTS)
0.5
0.4
0.3
0.2
0.1
0
-0.1
-0.2
0
0.2
0.4
0.6
0.8
TIME (SECONDS)

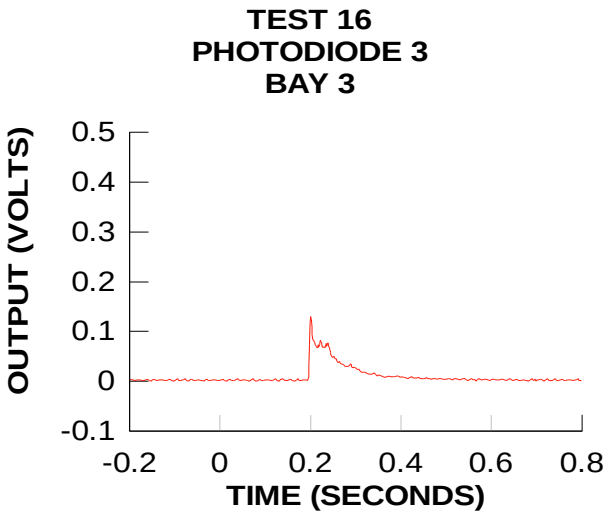
TEST 16
PHOTODIODE 3
BAY 3
OUTPUT (VOLTS)
0.5
0.4
0.3
0.2
0.1
0
-0.1
-0.2
0
0.2
0.4
0.6
0.8
TIME (SECONDS)

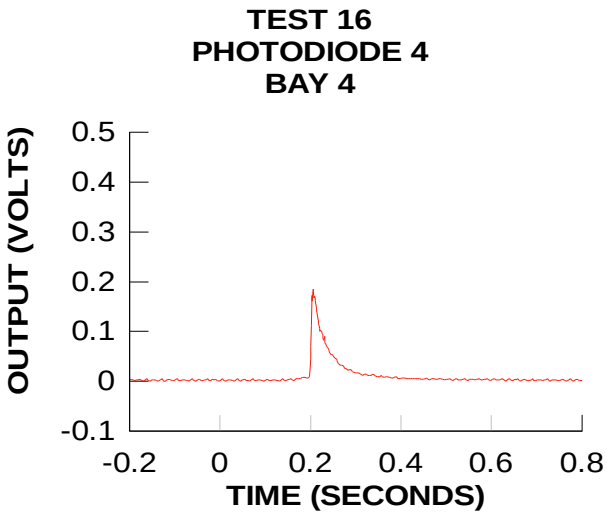
TEST 16
PHOTODIODE 4
BAY 4
OUTPUT (VOLTS)
0.5
0.4
0.3
0.2
0.1
0
-0.1
-0.2
0
0.2
0.4
0.6
0.8
TIME (SECONDS)

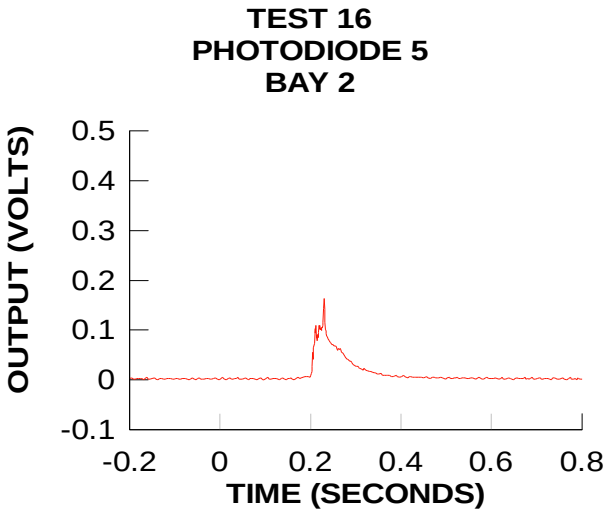
TEST 16
PHOTODIODE 5
BAY 2
OUTPUT (VOLTS)
0.5
0.4
0.3
0.2
0.1
0
-0.1
-0.2
0
0.2
0.4
0.6
0.8
TIME (SECONDS)

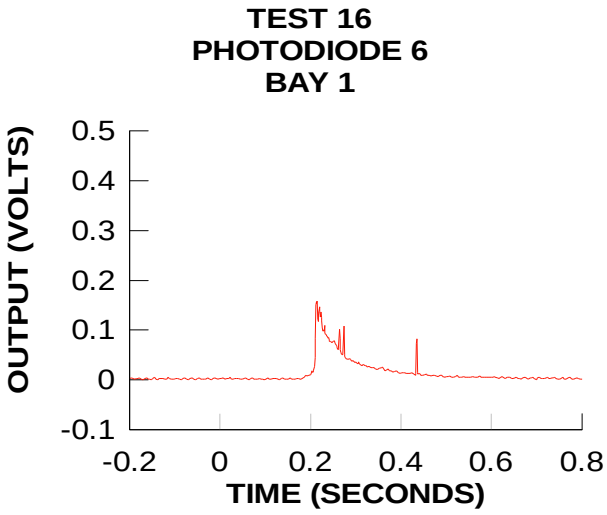
TEST 16
PHOTODIODE 6
BAY 1
OUTPUT (VOLTS)
0.5
0.4
0.3
0.2
0.1
0
-0.1
-0.2
0
0.2
0.4
0.6
0.8
TIME (SECONDS)

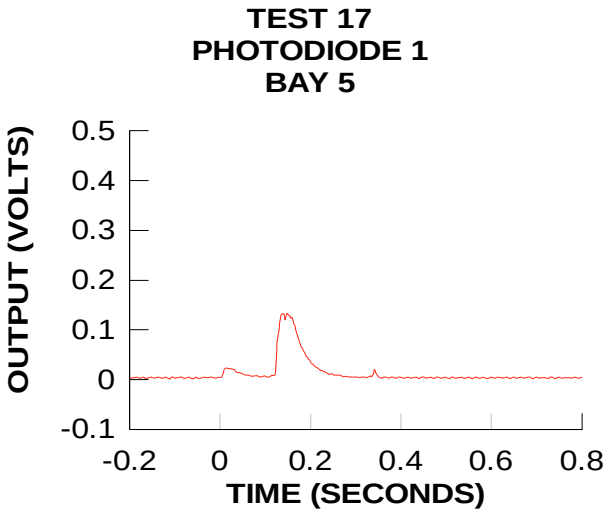
TEST 17
PHOTODIODE 1
BAY 5
OUTPUT (VOLTS)
0.5
0.4
0.3
0.2
0.1
0
-0.1
-0.2
0
0.2
0.4
0.6
0.8
TIME (SECONDS)

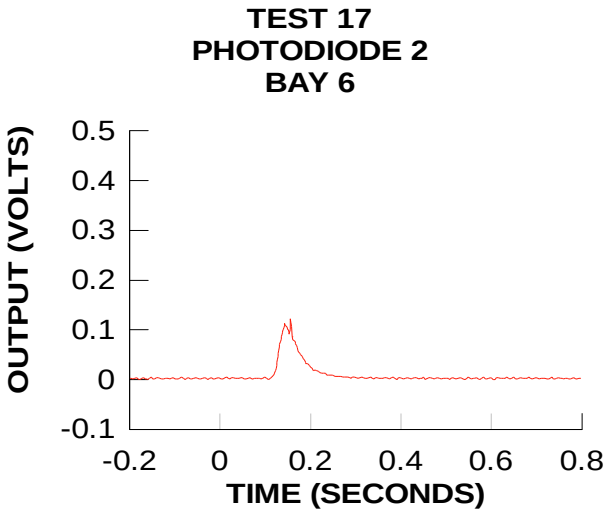
TEST 17
PHOTODIODE 2
BAY 6
OUTPUT (VOLTS)
0.5
0.4
0.3
0.2
0.1
0
-0.1
-0.2
0
0.2
0.4
0.6
0.8
TIME (SECONDS)

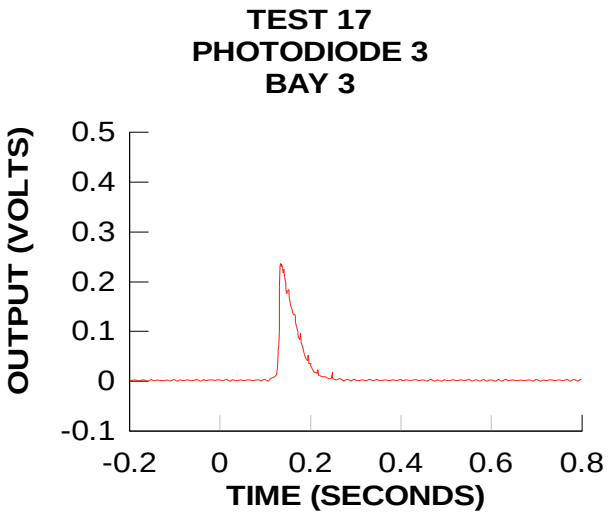
TEST 17
PHOTODIODE 3
BAY 3
OUTPUT (VOLTS)
0.5
0.4
0.3
0.2
0.1
0
-0.1
-0.2
0
0.2
0.4
0.6
0.8
TIME (SECONDS)

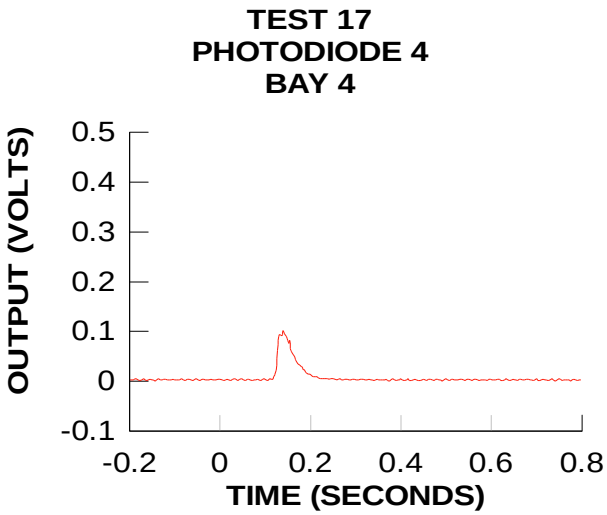
TEST 17
PHOTODIODE 4
BAY 4
OUTPUT (VOLTS)
0.5
0.4
0.3
0.2
0.1
0
-0.1
-0.2
0
0.2
0.4
0.6
0.8
TIME (SECONDS)

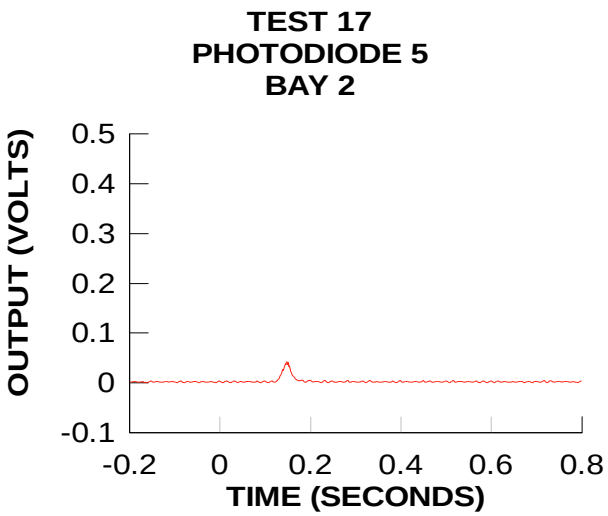
TEST 17
PHOTODIODE 5
BAY 2
OUTPUT (VOLTS)
0.5
0.4
0.3
0.2
0.1
0
-0.1
-0.2
0
0.2
0.4
0.6
0.8
TIME (SECONDS)

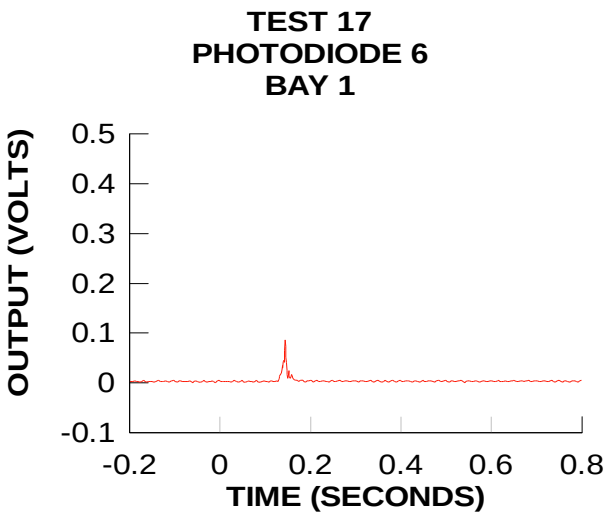
TEST 17
PHOTODIODE 6
BAY 1
OUTPUT (VOLTS)
0.5
0.4
0.3
0.2
0.1
0
-0.1
-0.2
0
0.2
0.4
0.6
0.8
TIME (SECONDS)

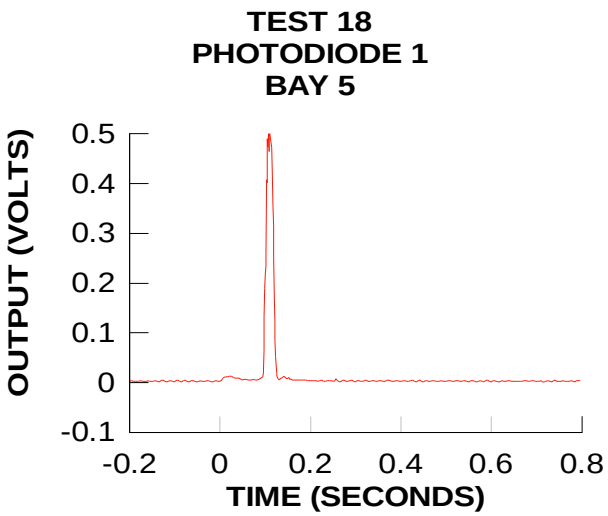
TEST 18
PHOTODIODE 1
BAY 5
OUTPUT (VOLTS)
0.5
0.4
0.3
0.2
0.1
0
-0.1
-0.2
0
0.2
0.4
0.6
0.8
TIME (SECONDS)

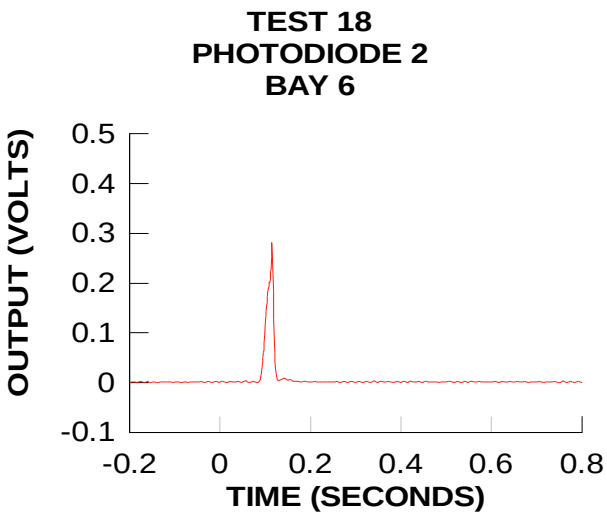
TEST 18
PHOTODIODE 2
BAY 6
OUTPUT (VOLTS)
0.5
0.4
0.3
0.2
0.1
0
-0.1
-0.2
0
0.2
0.4
0.6
0.8
TIME (SECONDS)

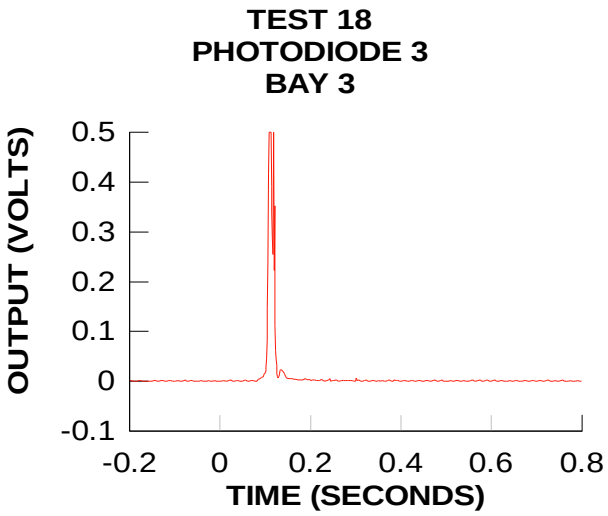
TEST 18
PHOTODIODE 3
BAY 3
OUTPUT (VOLTS)
0.5
0.4
0.3
0.2
0.1
0
-0.1
-0.2
0
0.2
0.4
0.6
0.8
TIME (SECONDS)

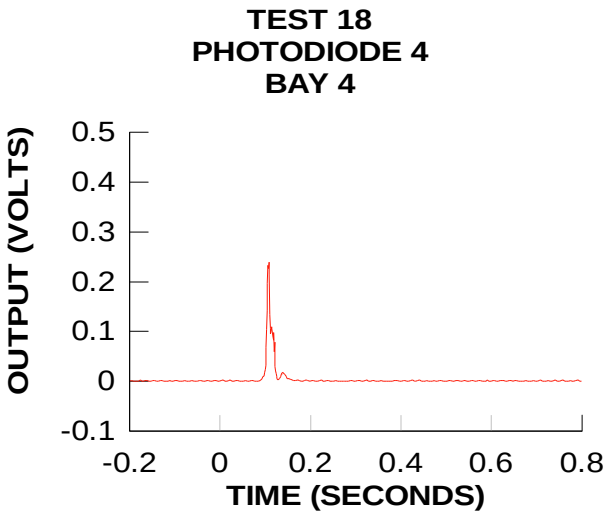
TEST 18
PHOTODIODE 4
BAY 4
OUTPUT (VOLTS)
0.5
0.4
0.3
0.2
0.1
0
-0.1
-0.2
0
0.2
0.4
0.6
0.8
TIME (SECONDS)

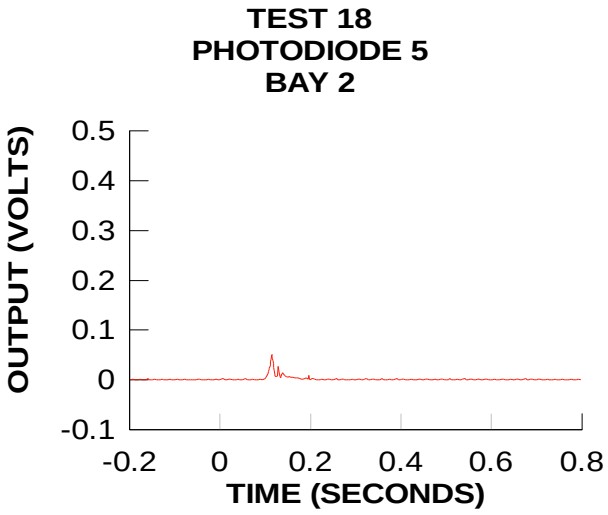
TEST 18
PHOTODIODE 5
BAY 2
OUTPUT (VOLTS)
0.5
0.4
0.3
0.2
0.1
0
-0.1
-0.2
0
0.2
0.4
0.6
0.8
TIME (SECONDS)

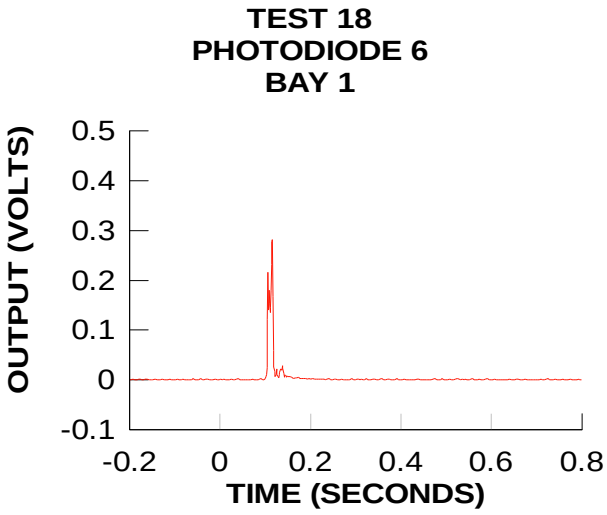
TEST 18
PHOTODIODE 6
BAY 1
OUTPUT (VOLTS)
0.5
0.4
0.3
0.2
0.1
0
-0.1
-0.2
0
0.2
0.4
0.6
0.8
TIME (SECONDS)

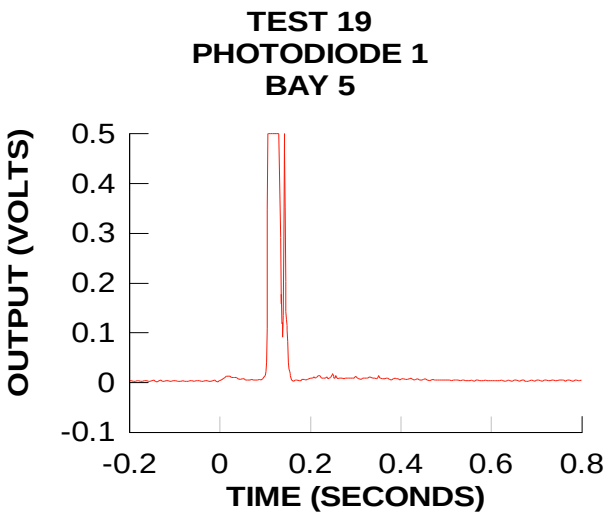
TEST 19
PHOTODIODE 1
BAY 5
OUTPUT (VOLTS)
0.5
0.4
0.3
0.2
0.1
0
-0.1
-0.2
0
0.2
0.4
0.6
0.8
TIME (SECONDS)

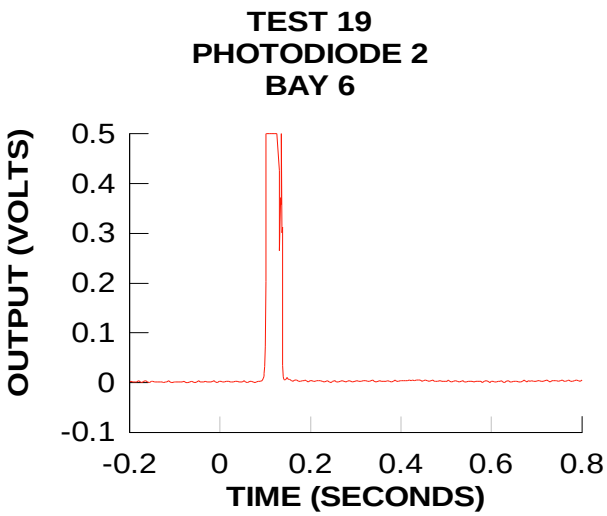
TEST 19
PHOTODIODE 2
BAY 6
OUTPUT (VOLTS)
0.5
0.4
0.3
0.2
0.1
0
-0.1
-0.2
0
0.2
0.4
0.6
0.8
TIME (SECONDS)

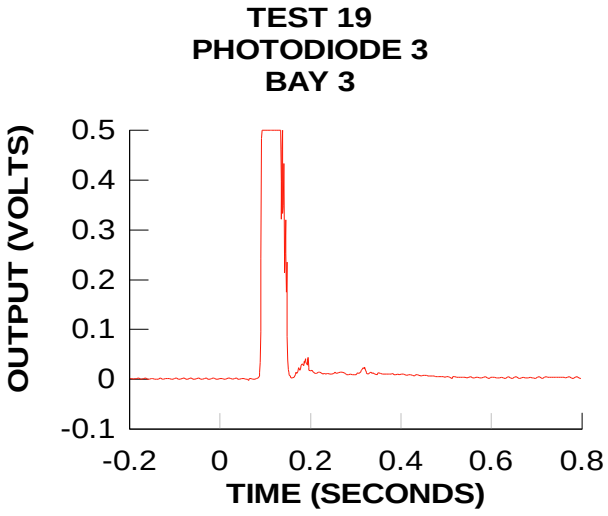
TEST 19
PHOTODIODE 3
BAY 3
OUTPUT (VOLTS)
0.5
0.4
0.3
0.2
0.1
0
-0.1
-0.2
0
0.2
0.4
0.6
0.8
TIME (SECONDS)

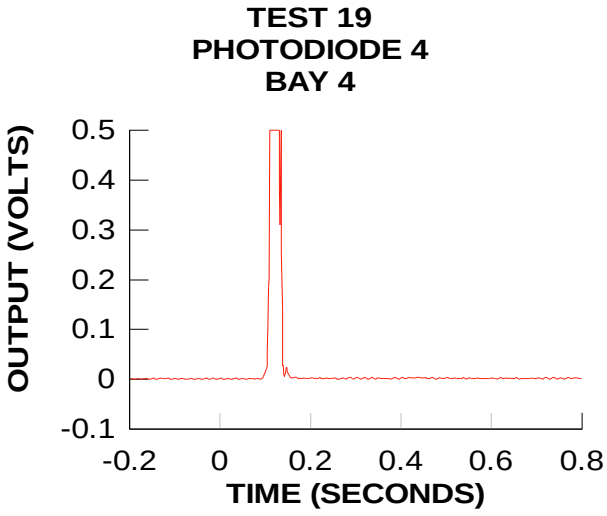
TEST 19
PHOTODIODE 4
BAY 4
OUTPUT (VOLTS)
0.5
0.4
0.3
0.2
0.1
0
-0.1
-0.2
0
0.2
0.4
0.6
0.8
TIME (SECONDS)

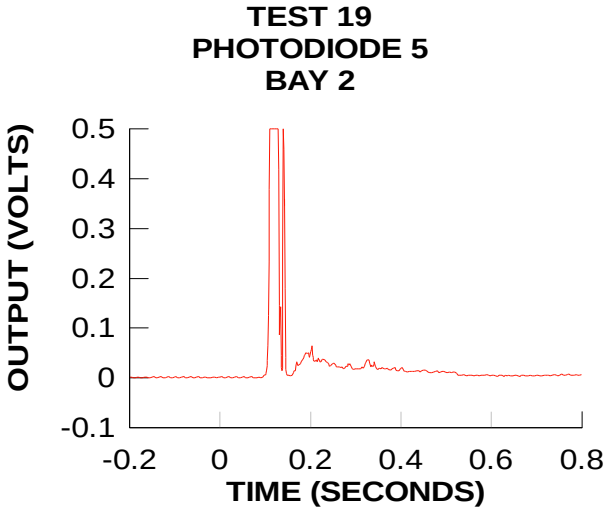
TEST 19
PHOTODIODE 5
BAY 2
OUTPUT (VOLTS)
0.5
0.4
0.3
0.2
0.1
0
-0.1
-0.2
0
0.2
0.4
0.6
0.8
TIME (SECONDS)

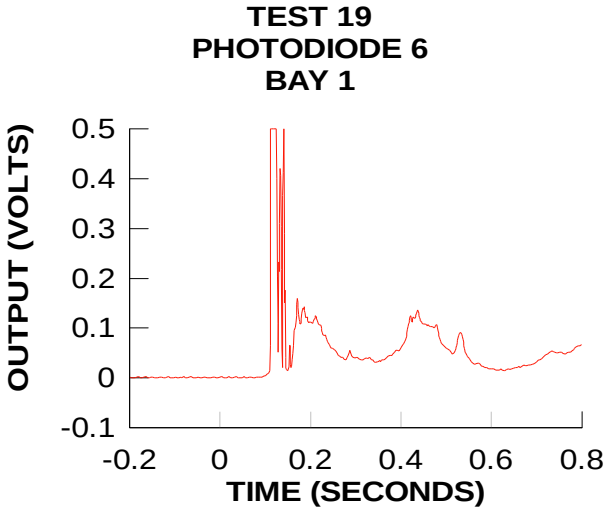
TEST 19
PHOTODIODE 6
BAY 1
OUTPUT (VOLTS)
0.5
0.4
0.3
0.2
0.1
0
-0.1
-0.2
0
0.2
0.4
0.6
0.8
TIME (SECONDS)

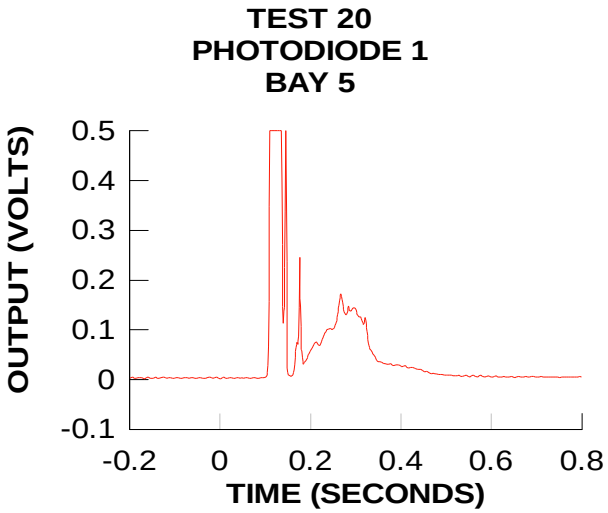
TEST 20
PHOTODIODE 1
BAY 5
OUTPUT (VOLTS)
0.5
0.4
0.3
0.2
0.1
0
-0.1
-0.2
0
0.2
0.4
0.6
0.8
TIME (SECONDS)

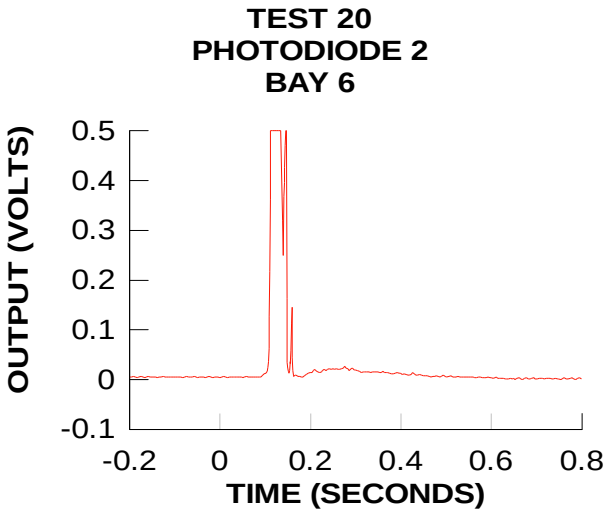
TEST 20
PHOTODIODE 2
BAY 6
OUTPUT (VOLTS)
0.5
0.4
0.3
0.2
0.1
0
-0.1
-0.2
0
0.2
0.4
0.6
0.8
TIME (SECONDS)

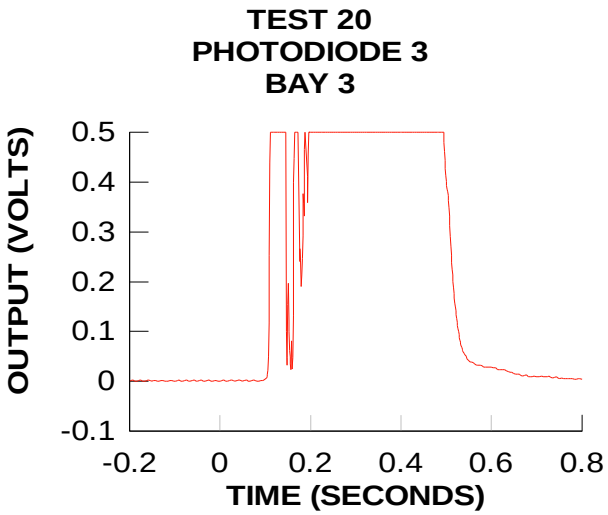
TEST 20
PHOTODIODE 3
BAY 3
OUTPUT (VOLTS)
0.5
0.4
0.3
0.2
0.1
0
-0.1
-0.2
0
0.2
0.4
0.6
0.8
TIME (SECONDS)

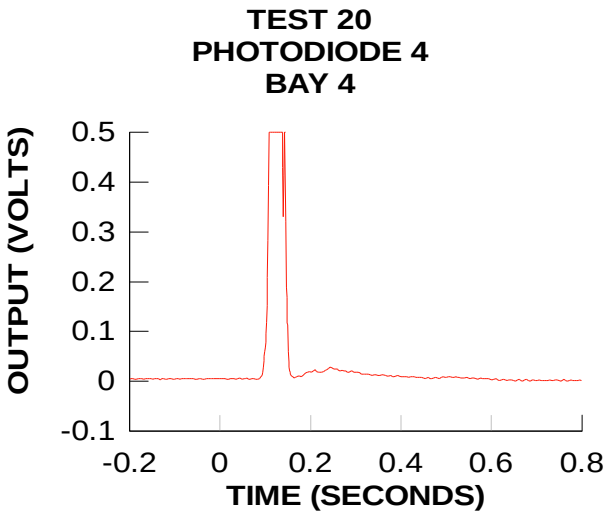
TEST 20
PHOTODIODE 4
BAY 4
OUTPUT (VOLTS)
0.5
0.4
0.3
0.2
0.1
0
-0.1
-0.2
0
0.2
0.4
0.6
0.8
TIME (SECONDS)

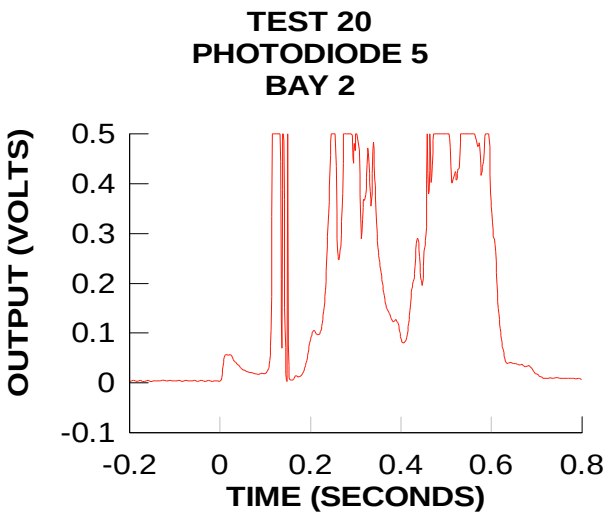
TEST 20
PHOTODIODE 5
BAY 2
OUTPUT (VOLTS)
0.5
0.4
0.3
0.2
0.1
0
-0.1
-0.2
0
0.2
0.4
0.6
0.8
TIME (SECONDS)

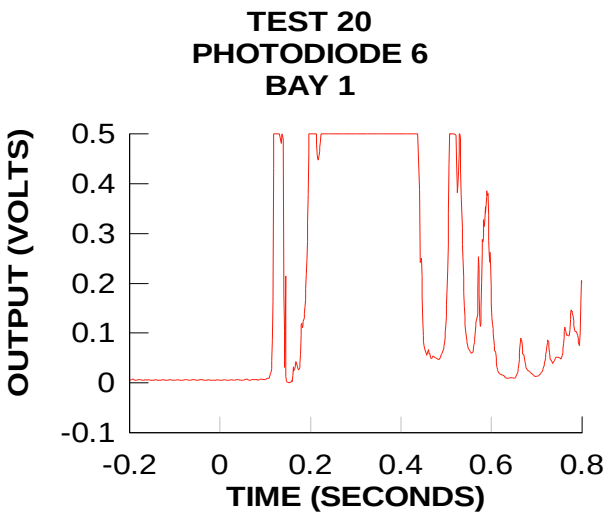
TEST 20
PHOTODIODE 6
BAY 1
OUTPUT (VOLTS)
0.5
0.4
0.3
0.2
0.1
0
-0.1
-0.2
0
0.2
0.4
0.6
0.8
TIME (SECONDS)

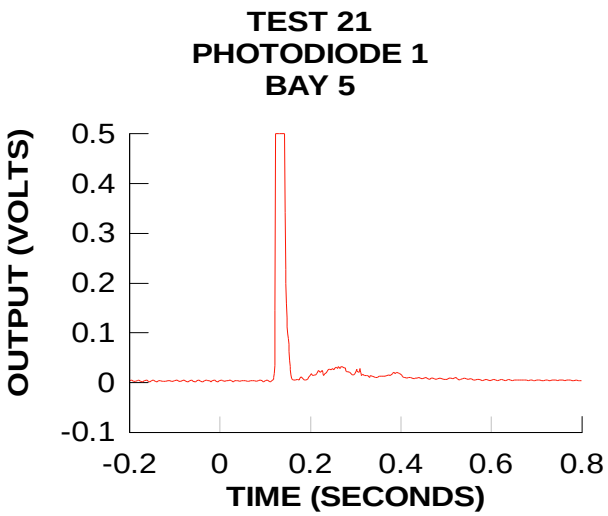
TEST 21
PHOTODIODE 1
BAY 5
OUTPUT (VOLTS)
0.5
0.4
0.3
0.2
0.1
0
-0.1
-0.2
0
0.2
0.4
0.6
0.8
TIME (SECONDS)

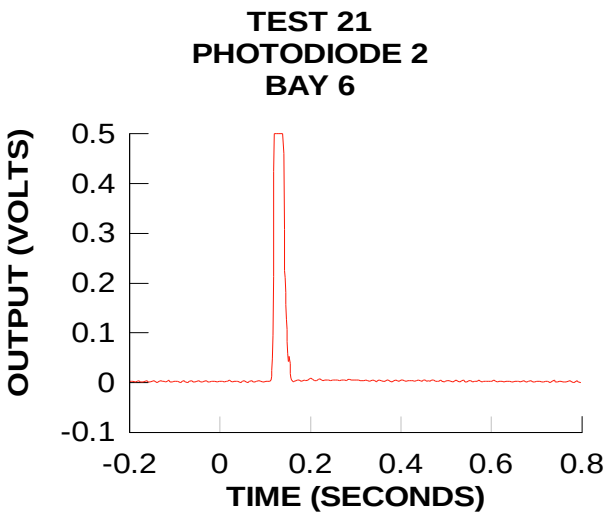
TEST 21
PHOTODIODE 2
BAY 6
OUTPUT (VOLTS)
0.5
0.4
0.3
0.2
0.1
0
-0.1
-0.2
0
0.2
0.4
0.6
0.8
TIME (SECONDS)

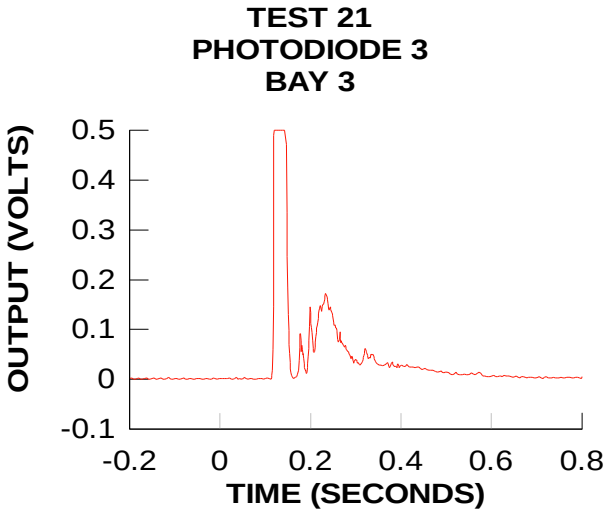
TEST 21
PHOTODIODE 3
BAY 3
OUTPUT (VOLTS)
0.5
0.4
0.3
0.2
0.1
0
-0.1
-0.2
0
0.2
0.4
0.6
0.8
TIME (SECONDS)

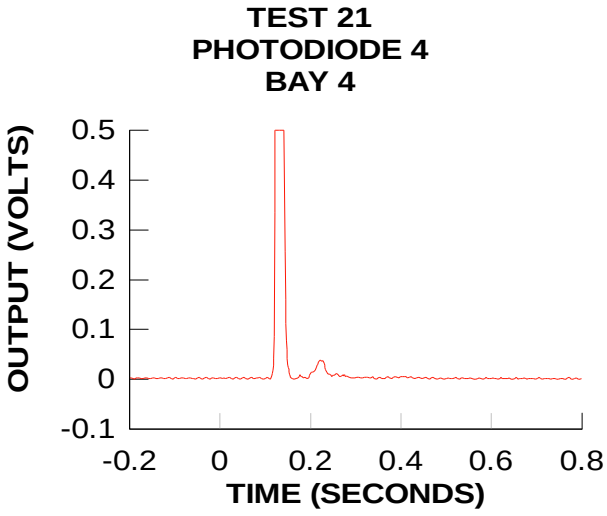
TEST 21
PHOTODIODE 4
BAY 4
OUTPUT (VOLTS)
0.5
0.4
0.3
0.2
0.1
0
-0.1
-0.2
0
0.2
0.4
0.6
0.8
TIME (SECONDS)

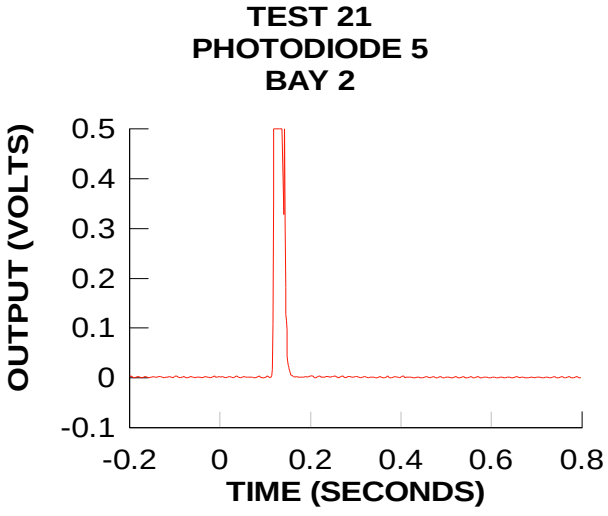
TEST 21
PHOTODIODE 5
BAY 2
OUTPUT (VOLTS)
0.5
0.4
0.3
0.2
0.1
0
-0.1
-0.2
0
0.2
0.4
0.6
0.8
TIME (SECONDS)

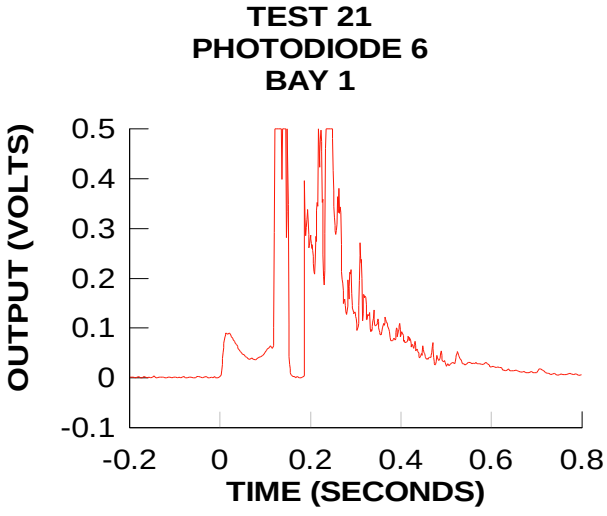
TEST 21
PHOTODIODE 6
BAY 1
OUTPUT (VOLTS)
0.5
0.4
0.3
0.2
0.1
0
-0.1
-0.2
0
0.2
0.4
0.6
0.8
TIME (SECONDS)

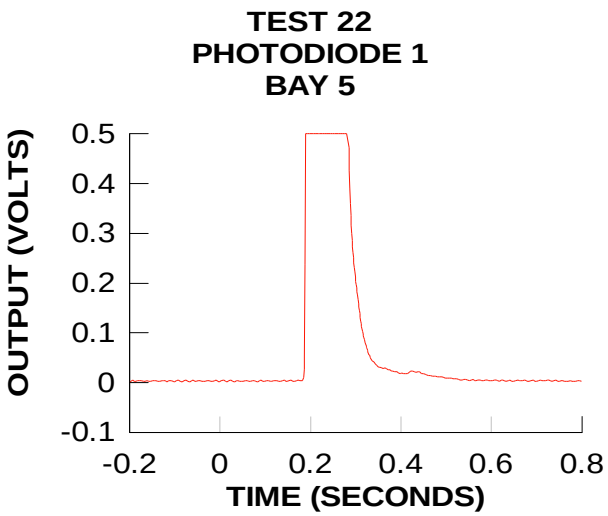
TEST 22
PHOTODIODE 1
BAY 5
OUTPUT (VOLTS)
0.5
0.4
0.3
0.2
0.1
0
-0.1
-0.2
0
0.2
0.4
0.6
0.8
TIME (SECONDS)

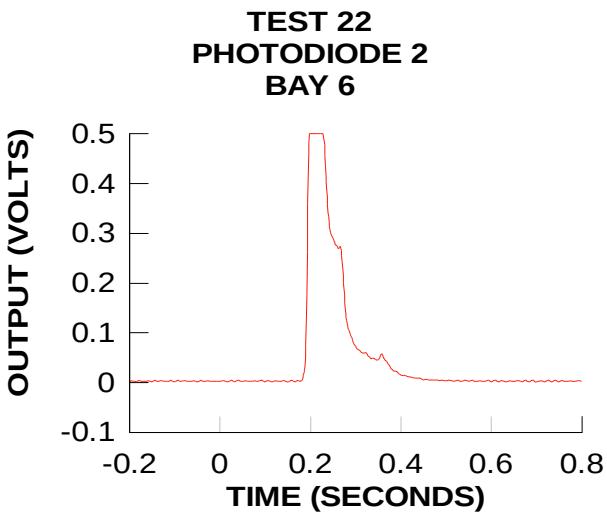
TEST 22
PHOTODIODE 2
BAY 6
OUTPUT (VOLTS)
0.5
0.4
0.3
0.2
0.1
0
-0.1
-0.2
0
0.2
0.4
0.6
0.8
TIME (SECONDS)

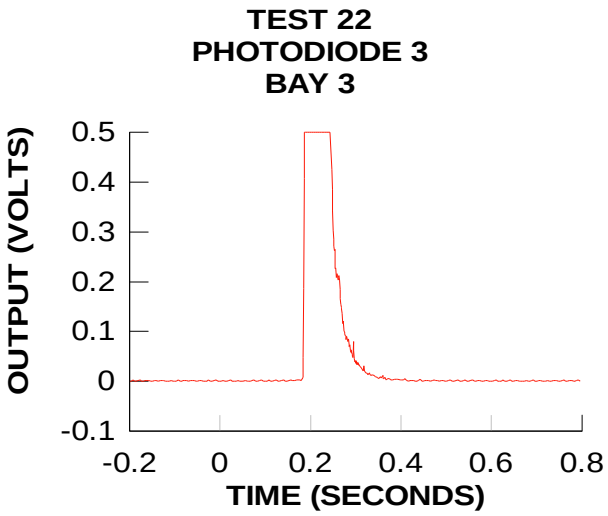
TEST 22
PHOTODIODE 3
BAY 3
OUTPUT (VOLTS)
0.5
0.4
0.3
0.2
0.1
0
-0.1
-0.2
0
0.2
0.4
0.6
0.8
TIME (SECONDS)

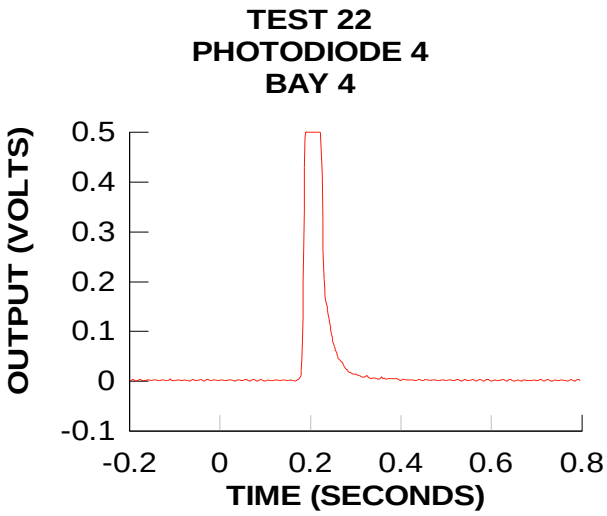
TEST 22
PHOTODIODE 4
BAY 4
OUTPUT (VOLTS)
0.5
0.4
0.3
0.2
0.1
0
-0.1
-0.2
0
0.2
0.4
0.6
0.8
TIME (SECONDS)

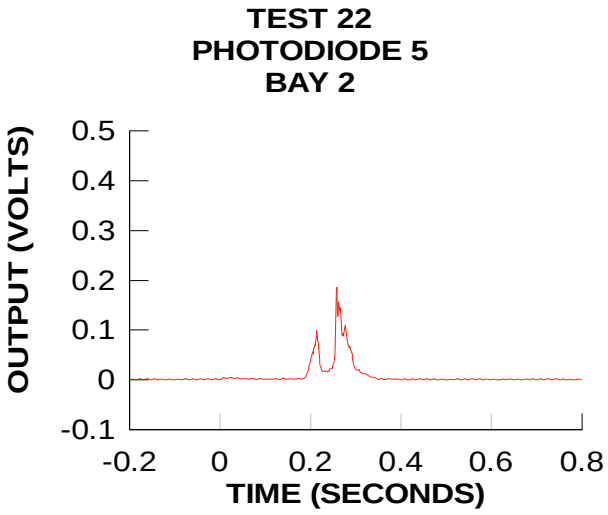
TEST 22
PHOTODIODE 5
BAY 2
OUTPUT (VOLTS)
0.5
0.4
0.3
0.2
0.1
0
-0.1
-0.2
0
0.2
0.4
0.6
0.8
TIME (SECONDS)

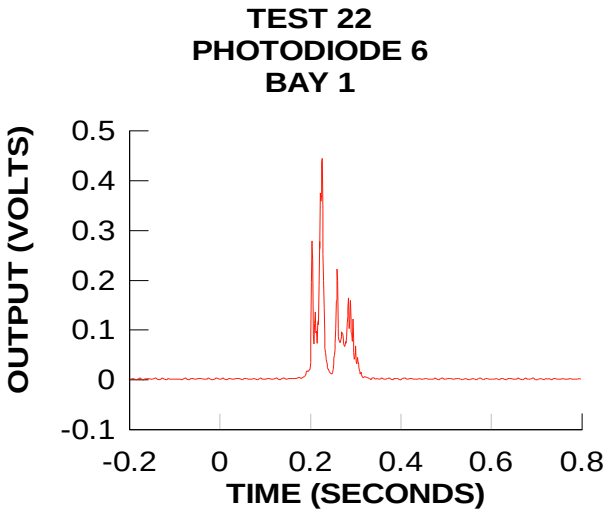
TEST 22
PHOTODIODE 6
BAY 1
OUTPUT (VOLTS)
0.5
0.4
0.3
0.2
0.1
0
-0.1
-0.2
0
0.2
0.4
0.6
0.8
TIME (SECONDS)

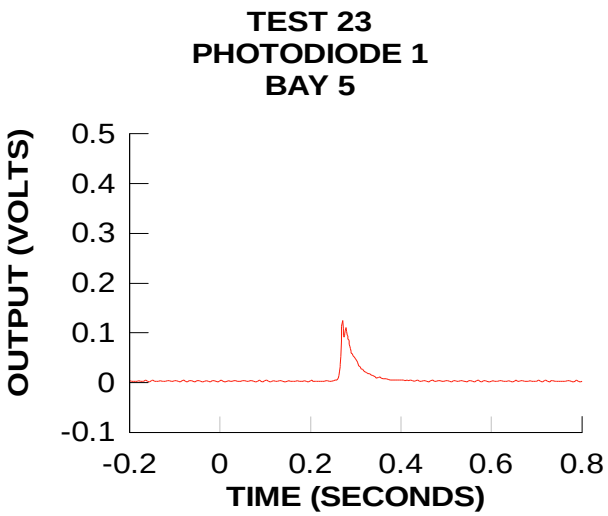
TEST 23
PHOTODIODE 1
BAY 5
OUTPUT (VOLTS)
0.5
0.4
0.3
0.2
0.1
0
-0.1
-0.2
0
0.2
0.4
0.6
0.8
TIME (SECONDS)

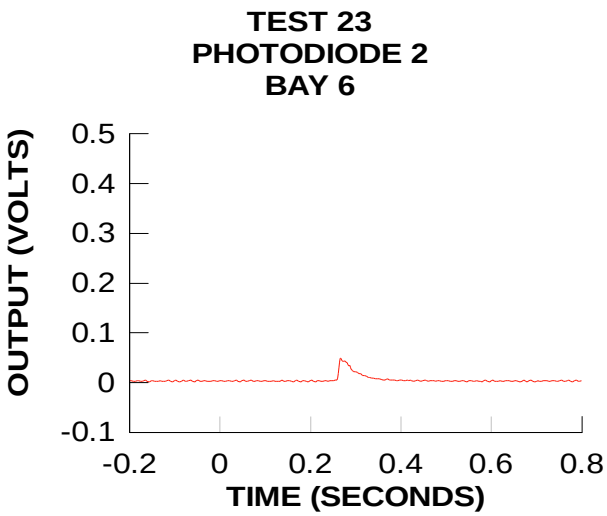
TEST 23
PHOTODIODE 2
BAY 6
OUTPUT (VOLTS)
0.5
0.4
0.3
0.2
0.1
0
-0.1
-0.2
0
0.2
0.4
0.6
0.8
TIME (SECONDS)

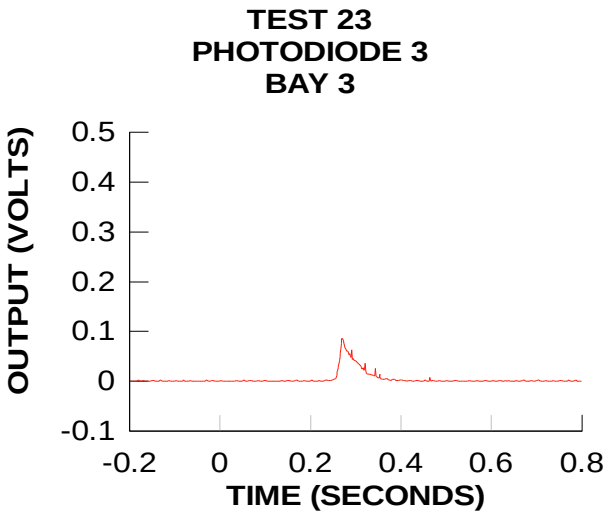
TEST 23
PHOTODIODE 3
BAY 3
OUTPUT (VOLTS)
0.5
0.4
0.3
0.2
0.1
0
-0.1
-0.2
0
0.2
0.4
0.6
0.8
TIME (SECONDS)

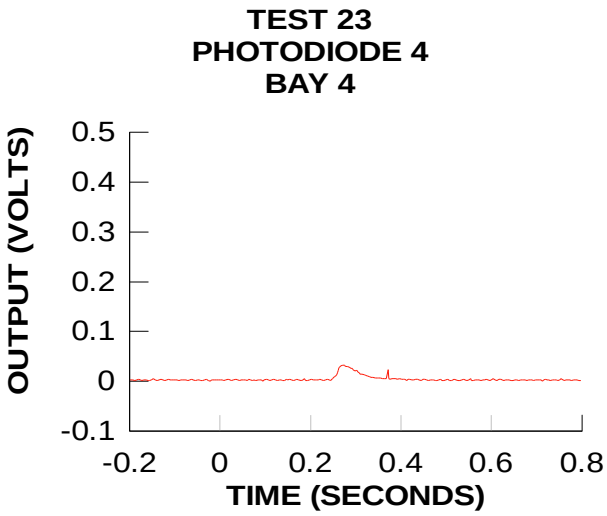
TEST 23
PHOTODIODE 4
BAY 4
OUTPUT (VOLTS)
0.5
0.4
0.3
0.2
0.1
0
-0.1
-0.2
0
0.2
0.4
0.6
0.8
TIME (SECONDS)

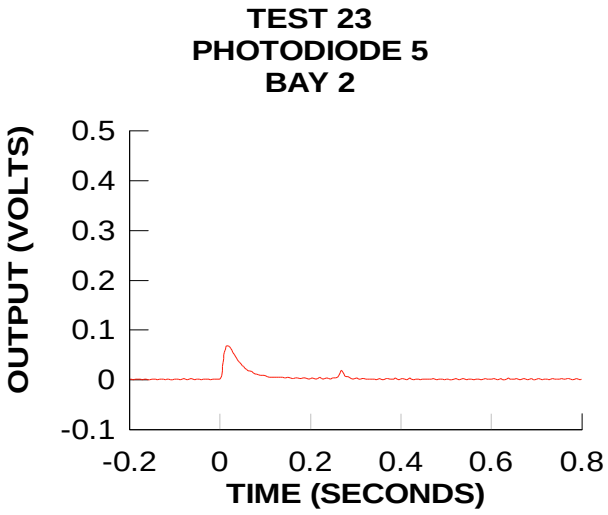
TEST 23
PHOTODIODE 5
BAY 2
OUTPUT (VOLTS)
0.5
0.4
0.3
0.2
0.1
0
-0.1
-0.2
0
0.2
0.4
0.6
0.8
TIME (SECONDS)

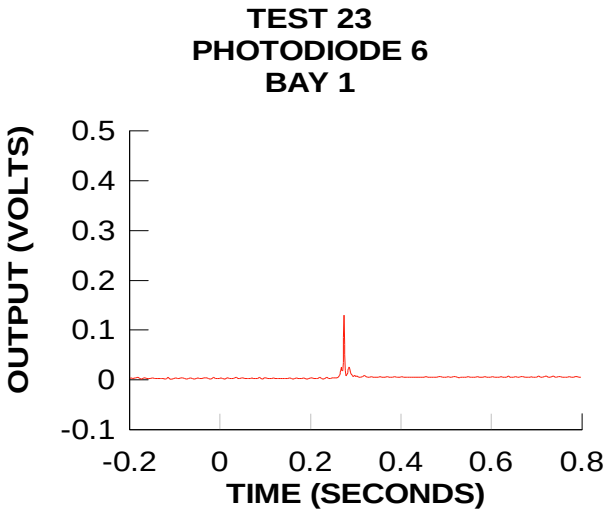
TEST 23
PHOTODIODE 6
BAY 1
OUTPUT (VOLTS)
0.5
0.4
0.3
0.2
0.1
0
-0.1
-0.2
0
0.2
0.4
0.6
0.8
TIME (SECONDS)

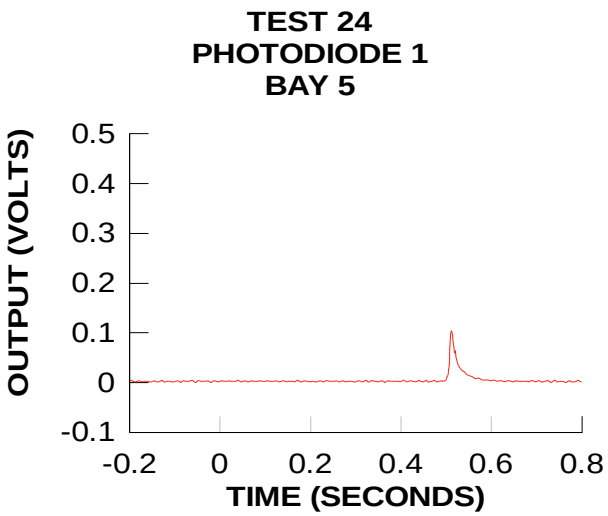
TEST 24
PHOTODIODE 1
BAY 5
OUTPUT (VOLTS)
0.5
0.4
0.3
0.2
0.1
0
-0.1
-0.2
0
0.2
0.4
0.6
0.8
TIME (SECONDS)

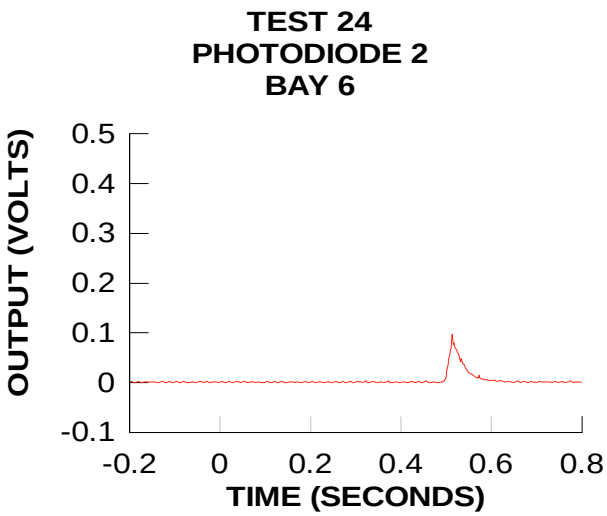
TEST 24
PHOTODIODE 2
BAY 6
OUTPUT (VOLTS)
0.5
0.4
0.3
0.2
0.1
0
-0.1
-0.2
0
0.2
0.4
0.6
0.8
TIME (SECONDS)

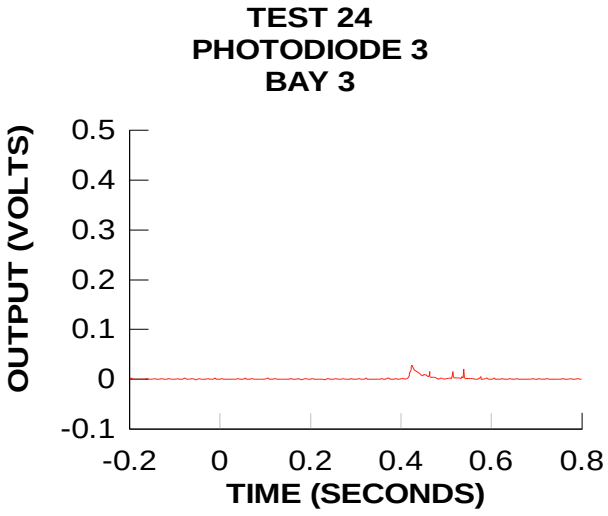
TEST 24
PHOTODIODE 3
BAY 3
OUTPUT (VOLTS)
0.5
0.4
0.3
0.2
0.1
0
-0.1
-0.2
0
0.2
0.4
0.6
0.8
TIME (SECONDS)

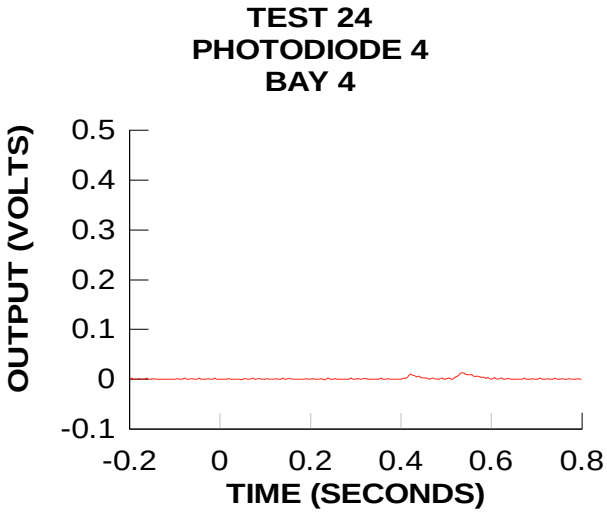
TEST 24
PHOTODIODE 4
BAY 4
OUTPUT (VOLTS)
0.5
0.4
0.3
0.2
0.1
0
-0.1
-0.2
0
0.2
0.4
0.6
0.8
TIME (SECONDS)

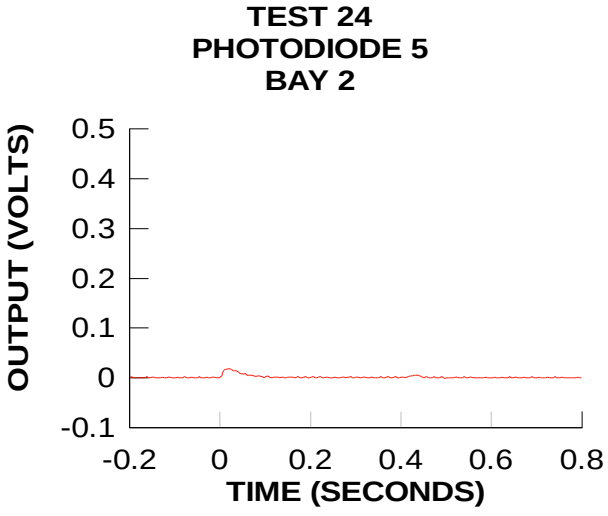
TEST 24
PHOTODIODE 5
BAY 2
OUTPUT (VOLTS)
0.5
0.4
0.3
0.2
0.1
0
-0.1
-0.2
0
0.2
0.4
0.6
0.8
TIME (SECONDS)

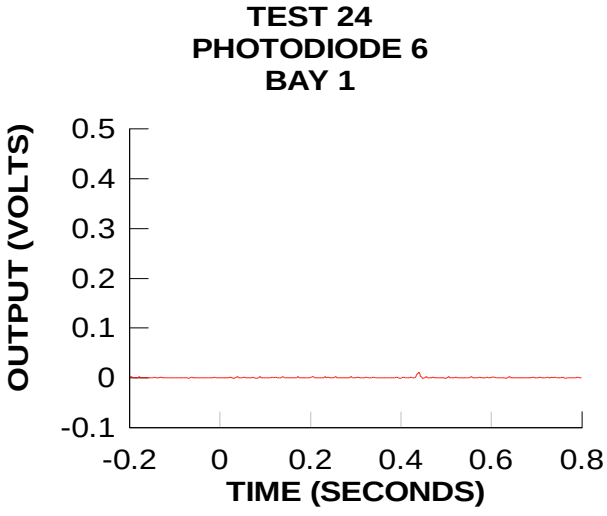
TEST 24
PHOTODIODE 6
BAY 1
OUTPUT (VOLTS)
0.5
0.4
0.3
0.2
0.1
0
-0.1
-0.2
0
0.2
0.4
0.6
0.8
TIME (SECONDS)

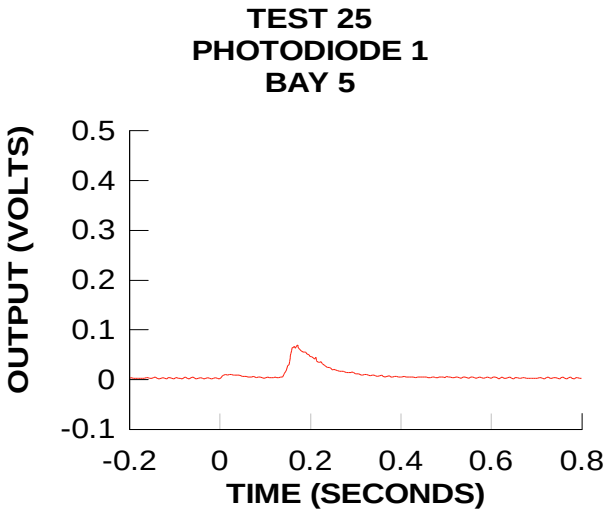
TEST 25
PHOTODIODE 1
BAY 5
OUTPUT (VOLTS)
0.5
0.4
0.3
0.2
0.1
0
-0.1
-0.2
0
0.2
0.4
0.6
0.8
TIME (SECONDS)

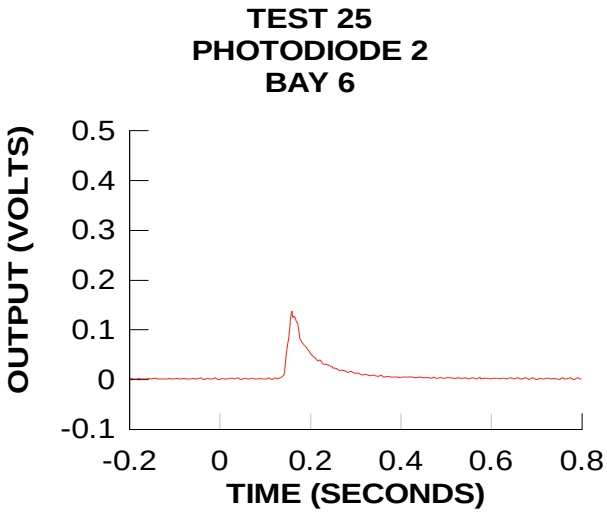
TEST 25
PHOTODIODE 2
BAY 6
OUTPUT (VOLTS)
0.5
0.4
0.3
0.2
0.1
0
-0.1
-0.2
0
0.2
0.4
0.6
0.8
TIME (SECONDS)

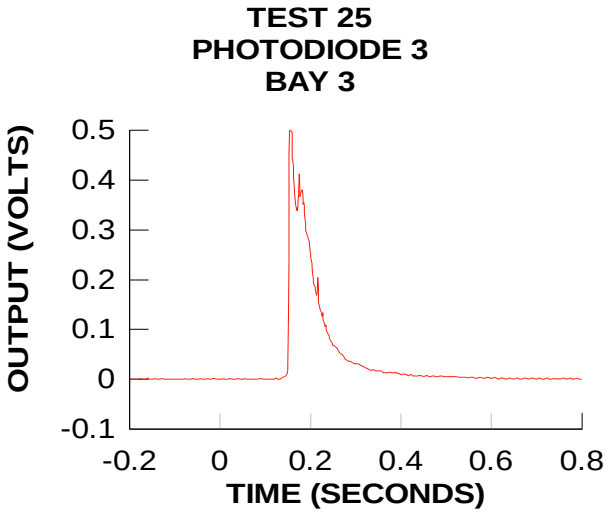
TEST 25
PHOTODIODE 3
BAY 3
OUTPUT (VOLTS)
0.5
0.4
0.3
0.2
0.1
0
-0.1
-0.2
0
0.2
0.4
0.6
0.8
TIME (SECONDS)

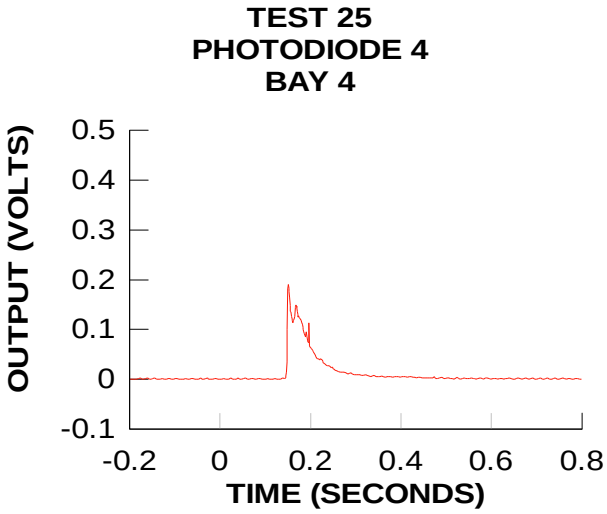
TEST 25
PHOTODIODE 4
BAY 4
OUTPUT (VOLTS)
0.5
0.4
0.3
0.2
0.1
0
-0.1
-0.2
0
0.2
0.4
0.6
0.8
TIME (SECONDS)

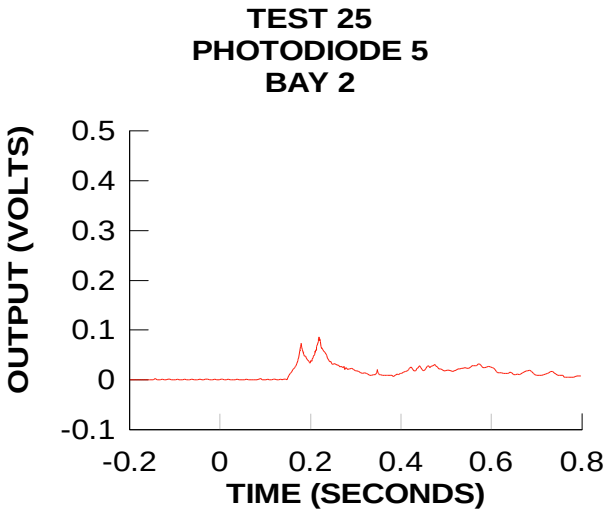
TEST 25
PHOTODIODE 5
BAY 2
OUTPUT (VOLTS)
0.5
0.4
0.3
0.2
0.1
0
-0.1
-0.2
0
0.2
0.4
0.6
0.8
TIME (SECONDS)

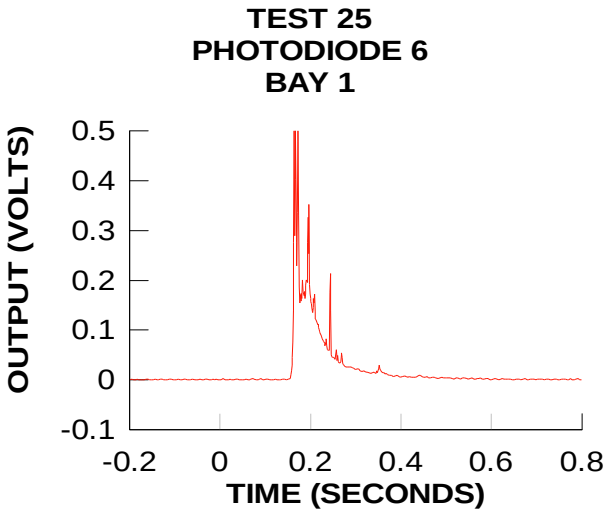
TEST 25
PHOTODIODE 6
BAY 1
OUTPUT (VOLTS)
0.5
0.4
0.3
0.2
0.1
0
-0.1
-0.2
0
0.2
0.4
0.6
0.8
TIME (SECONDS)

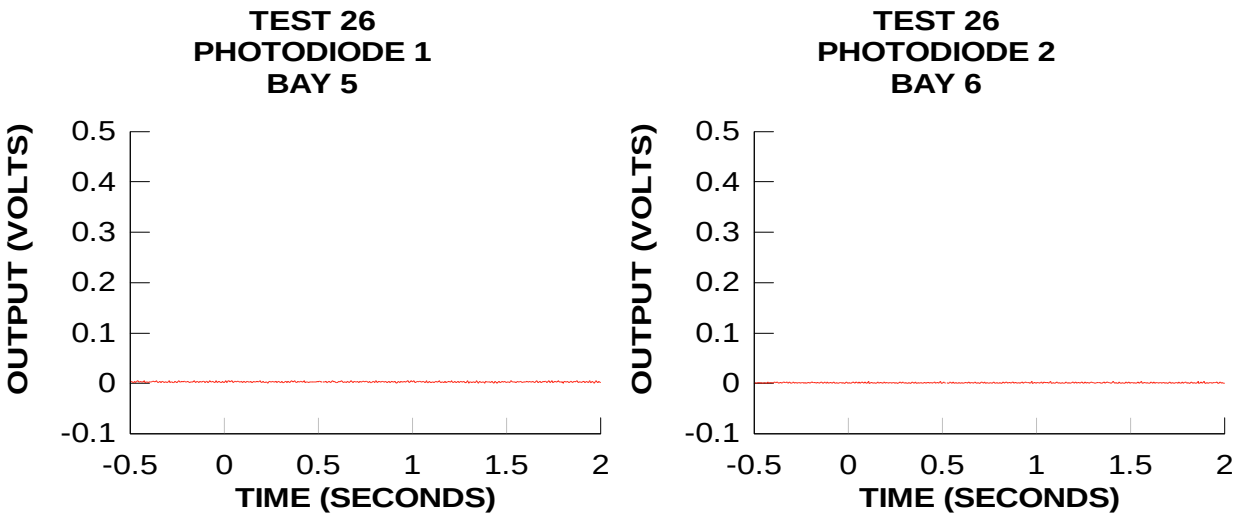
TEST 26
PHOTODIODE 1
BAY 5
OUTPUT (VOLTS)
0.5
0.4
0.3
0.2
0.1
0
-0.1
-0.5
0
0.5
1
1.5
2
TIME (SECONDS)

TEST 26
PHOTODIODE 2
BAY 6
OUTPUT (VOLTS)
0.5
0.4
0.3
0.2
0.1
0
-0.1
-0.5
0
0.5
1
1.5
2
TIME (SECONDS)

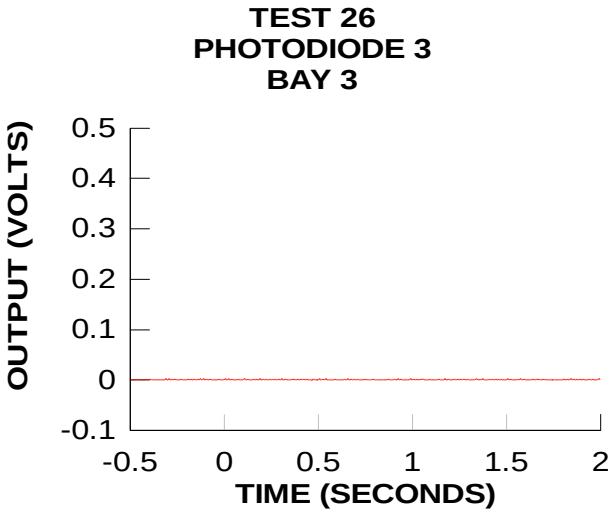
TEST 26
PHOTODIODE 3
BAY 3
OUTPUT (VOLTS)
0.5
0.4
0.3
0.2
0.1
0
-0.1
-0.5
0
0.5
1
1.5
2
TIME (SECONDS)

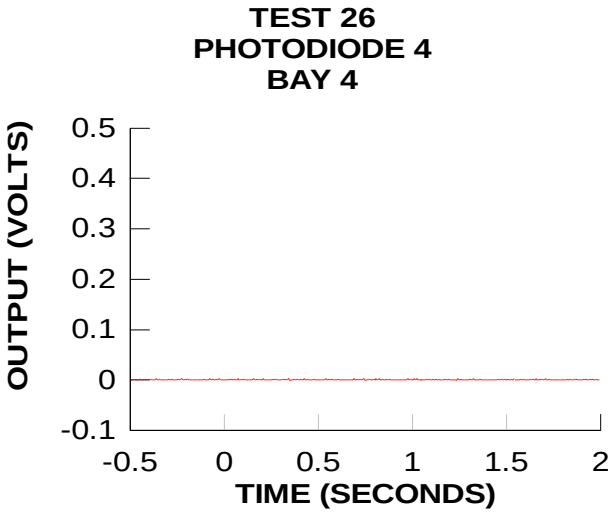
TEST 26
PHOTODIODE 4
BAY 4
OUTPUT (VOLTS)
0.5
0.4
0.3
0.2
0.1
0
-0.1
-0.5
0
0.5
1
1.5
2
TIME (SECONDS)

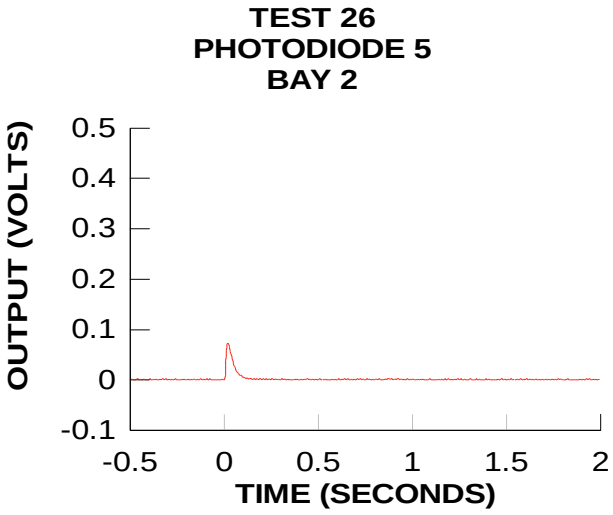
TEST 26
PHOTODIODE 5
BAY 2
OUTPUT (VOLTS)
0.5
0.4
0.3
0.2
0.1
0
-0.1
-0.5
0
0.5
1
1.5
2
TIME (SECONDS)

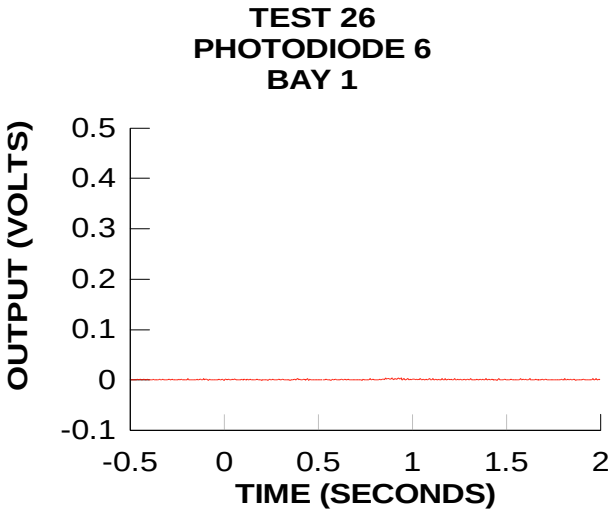
TEST 26
PHOTODIODE 6
BAY 1
OUTPUT (VOLTS)
0.5
0.4
0.3
0.2
0.1
0
-0.1
-0.5
0
0.5
1
1.5
2
TIME (SECONDS)

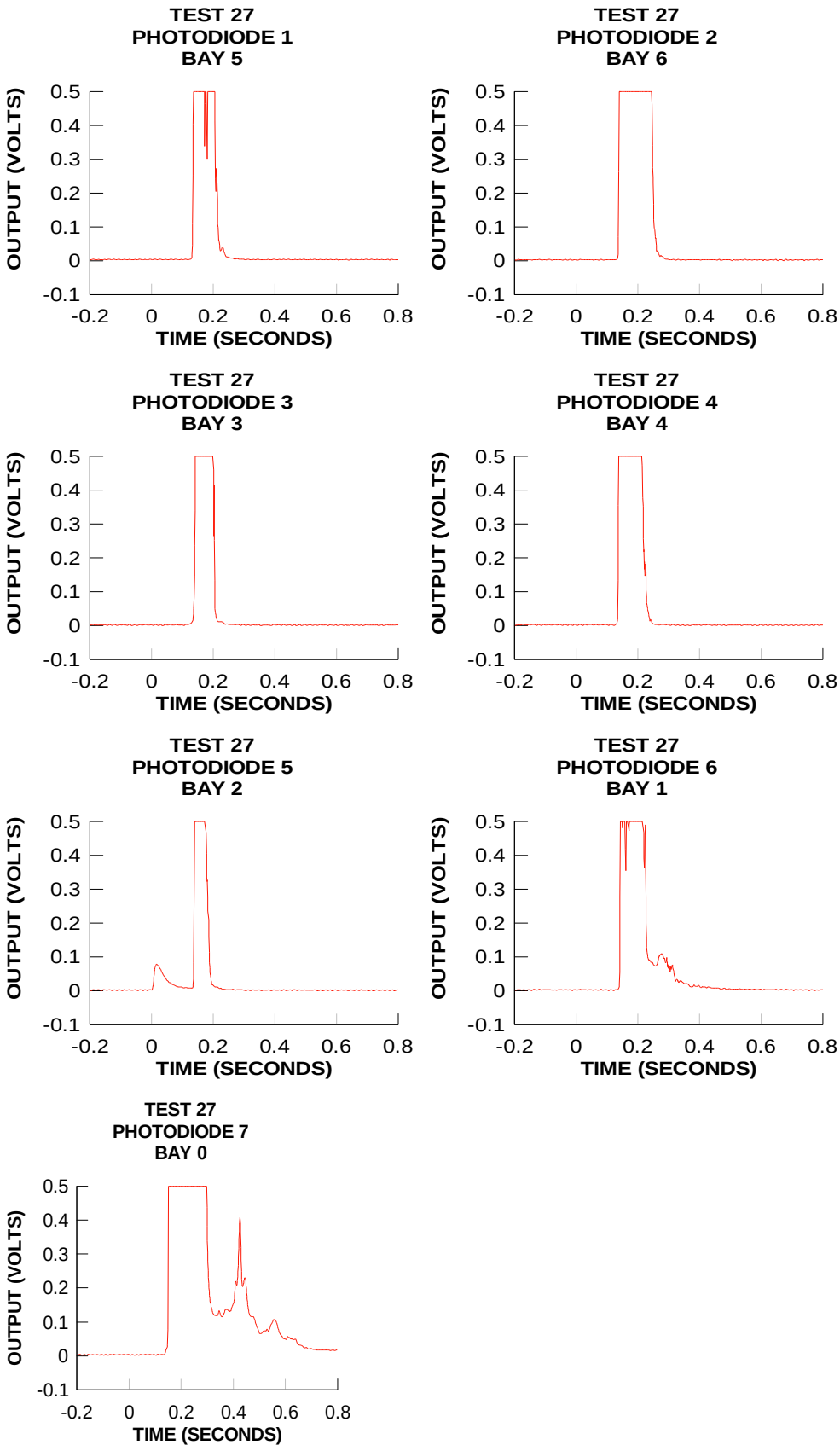
TEST 27
PHOTODIODE 1
BAY 5
TEST 27
PHOTODIODE 2
BAY 6
TEST 27
PHOTODIODE 3
BAY 3
TEST 27
PHOTODIODE 4
BAY 4
TEST 27
PHOTODIODE 5
BAY 2
TEST 27
PHOTODIODE 6
BAY 1
TEST 27
PHOTODIODE 7
BAY 0
OUTPUT (VOLTS)
TIME (SECONDS)
0.5
0.4
0.3
0.2
0.1
0
-0.1
-0.2
0.2
0.4
0.6
0.8

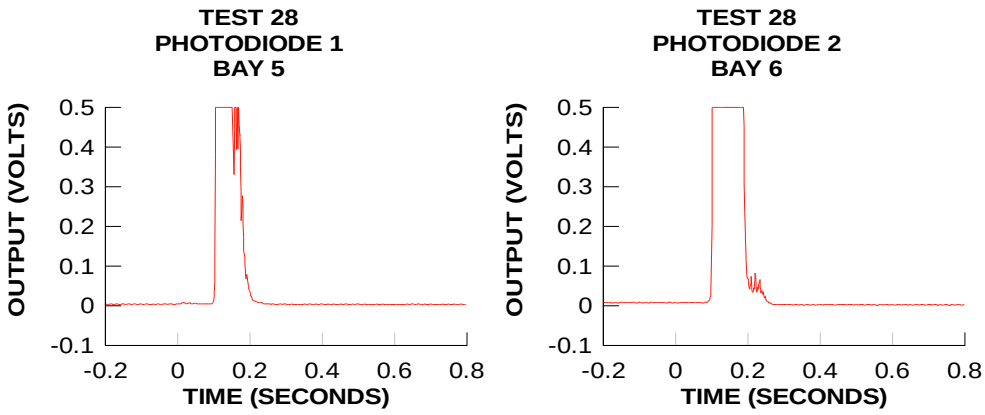
TEST 28
PHOTODIODE 1
BAY 5
OUTPUT (VOLTS)
TIME (SECONDS)

TEST 28
PHOTODIODE 2
BAY 6
OUTPUT (VOLTS)
TIME (SECONDS)

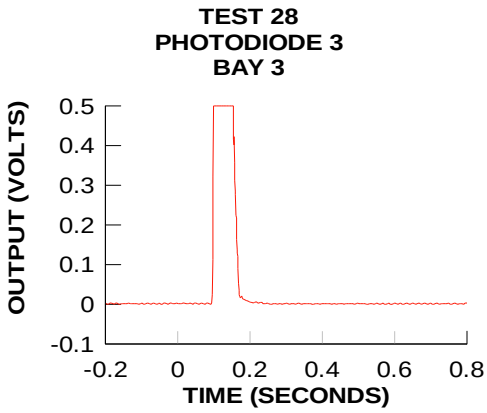
TEST 28
PHOTODIODE 3
BAY 3
OUTPUT (VOLTS)
TIME (SECONDS)

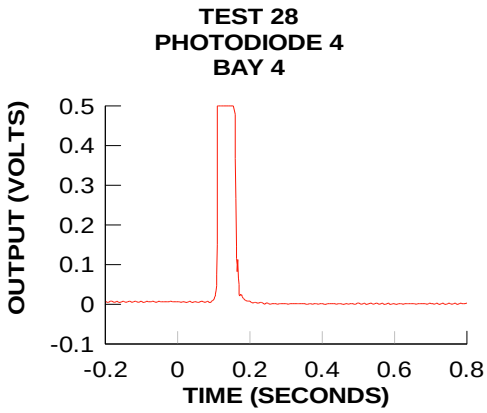
TEST 28
PHOTODIODE 4
BAY 4
OUTPUT (VOLTS)
TIME (SECONDS)

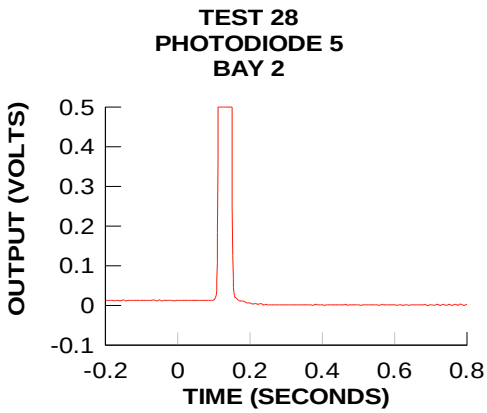
TEST 28
PHOTODIODE 5
BAY 2
OUTPUT (VOLTS)
TIME (SECONDS)

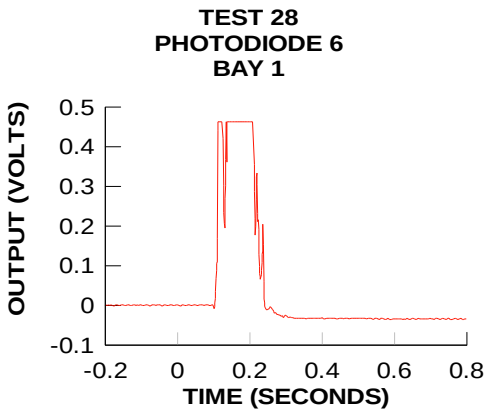
TEST 28
PHOTODIODE 6
BAY 1
OUTPUT (VOLTS)
TIME (SECONDS)

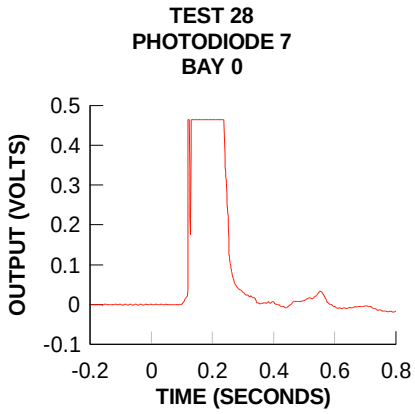
TEST 28
PHOTODIODE 7
BAY 0
OUTPUT (VOLTS)
TIME (SECONDS)

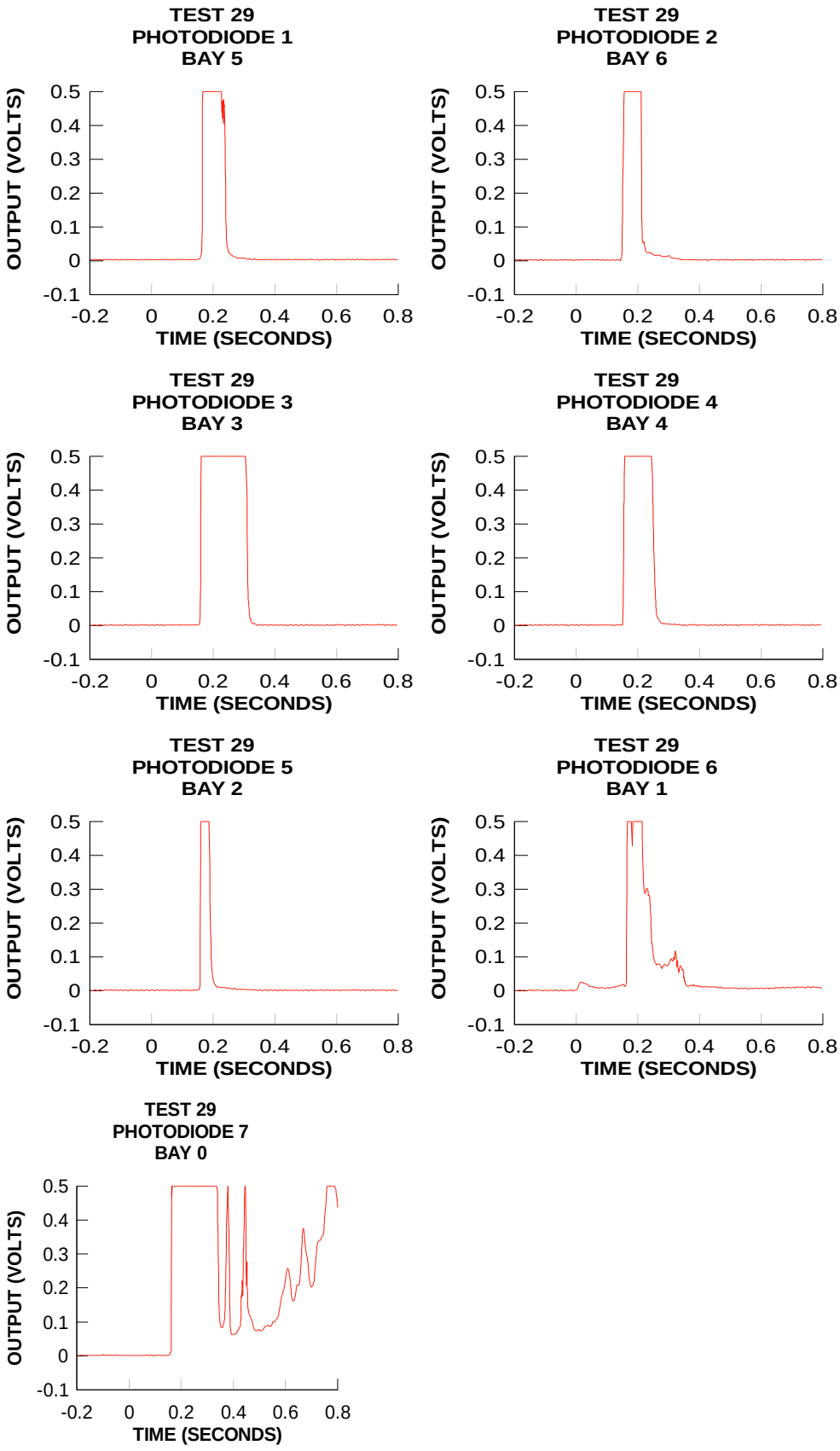
TEST 29
PHOTODIODE 1
BAY 5
TEST 29
PHOTODIODE 2
BAY 6
TEST 29
PHOTODIODE 3
BAY 3
TEST 29
PHOTODIODE 4
BAY 4
TEST 29
PHOTODIODE 5
BAY 2
TEST 29
PHOTODIODE 6
BAY 1
TEST 29
PHOTODIODE 7
BAY 0
OUTPUT (VOLTS)
TIME (SECONDS)
0.5
0.4
0.3
0.2
0.1
0
-0.1
-0.2
0.2
0.4
0.6
0.8

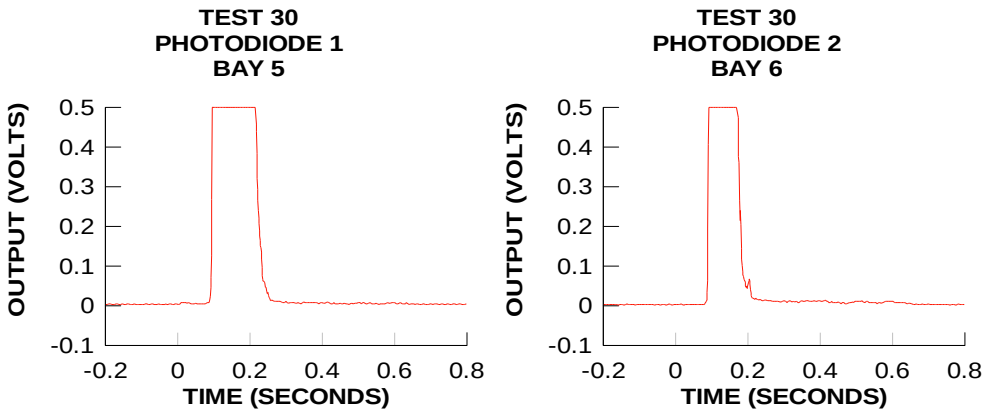
TEST 30
PHOTODIODE 1
BAY 5
OUTPUT (VOLTS)
TIME (SECONDS)

TEST 30
PHOTODIODE 2
BAY 6
OUTPUT (VOLTS)
TIME (SECONDS)

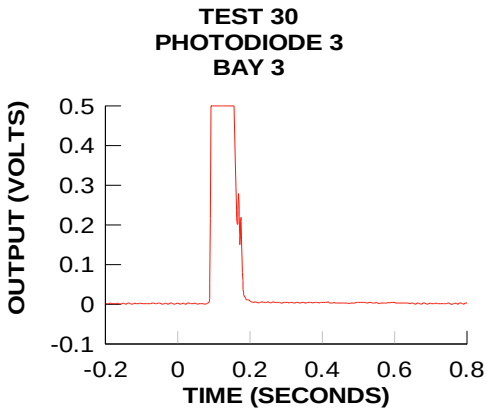
TEST 30
PHOTODIODE 3
BAY 3
OUTPUT (VOLTS)
TIME (SECONDS)

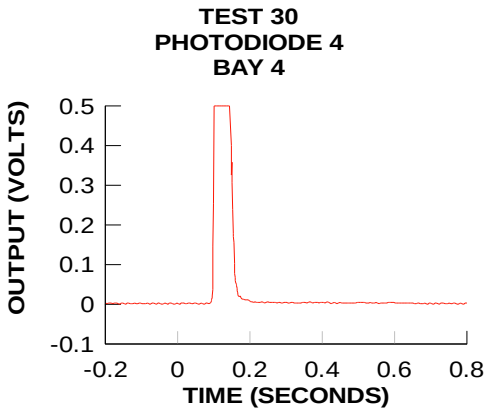
TEST 30
PHOTODIODE 4
BAY 4
OUTPUT (VOLTS)
TIME (SECONDS)

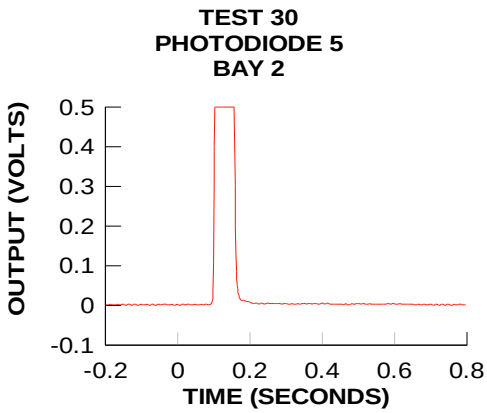
TEST 30
PHOTODIODE 5
BAY 2
OUTPUT (VOLTS)
TIME (SECONDS)

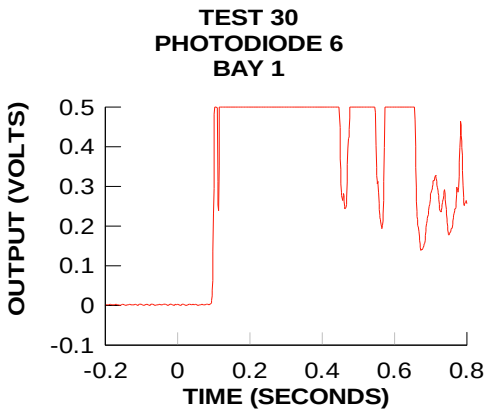
TEST 30
PHOTODIODE 6
BAY 1
OUTPUT (VOLTS)
TIME (SECONDS)

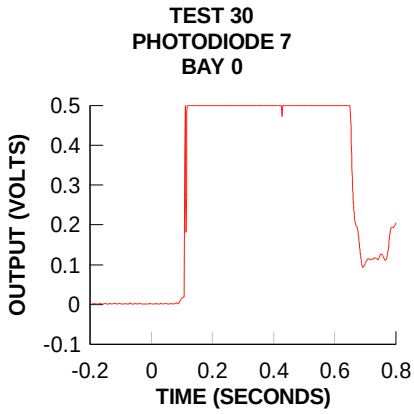
TEST 30
PHOTODIODE 7
BAY 0
OUTPUT (VOLTS)
TIME (SECONDS)